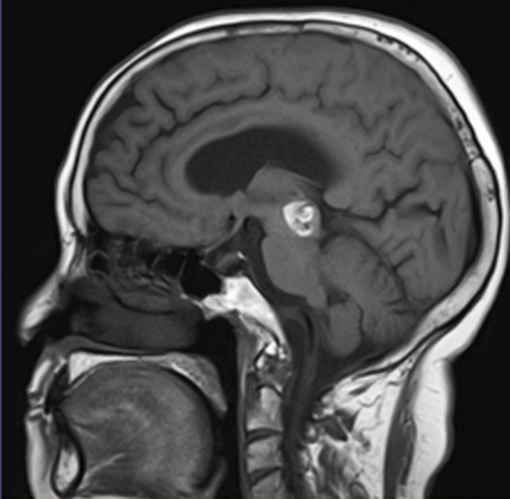
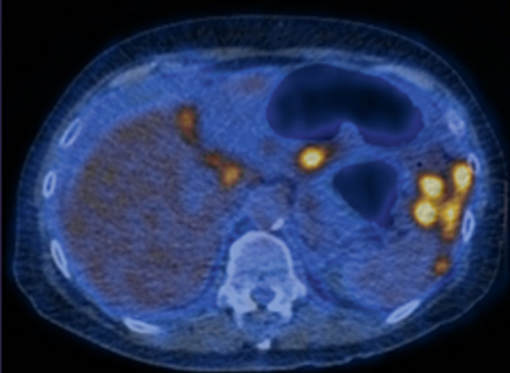


Andrea Rockall
Andrew Hatrick
Peter Armstrong
Martin Wastie



DIAGNOSTIC IMAGING

SEVENTH EDITION

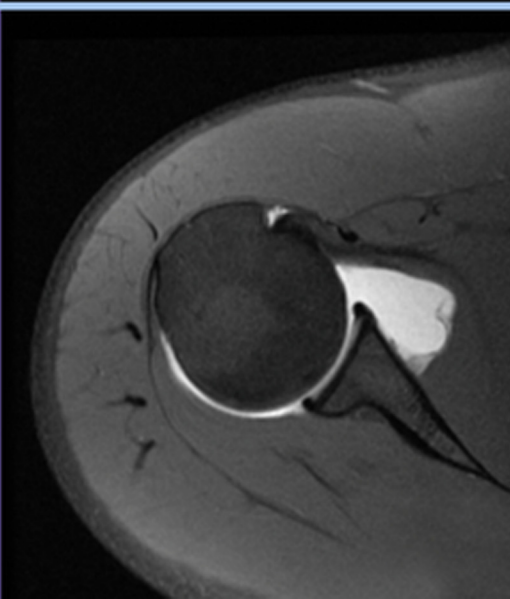


Wiley E-Text
Powered by VitalSource®

Available on
CourseSmart
Learn Smart. Choose Smart.



 **WILEY-BLACKWELL**



DIAGNOSTIC IMAGING

This new edition is also available as an e-book.

For more details, please see

www.wiley.com/buy/9780470658901

or scan this QR code:



Companion website

This book is accompanied by a companion website:

www.wileydiagnosticimaging.com

The website includes:

- Interactive multiple choice questions for each chapter
- Figures from the book in PowerPoint format

DIAGNOSTIC IMAGING

ANDREA ROCKALL

BSc, MBBS, MRCP, FRCR

Professor of Radiology

Imperial College, London, UK

ANDREW HATRICK

MA, MB BChir, MRCP, FRCR

Consultant General and Interventional Radiologist

Frimley Park Hospital NHS Foundation Trust

Frimley, UK

PETER ARMSTRONG

MBBS, FMed Sci, FRCP, FRCR

Formerly Professor of Radiology

Medical College of St Bartholomew's

and the Royal London Hospitals, London, UK

Formerly Professor and Vice-Chairman

Department of Radiology, University of Virginia

Charlottesville, Virginia, USA

MARTIN WASTIE

MB BChir, FRCP, FRCR

Formerly Professor of Radiology

University of Malaya Medical Centre

Kuala Lumpur, Malaysia

Formerly Consultant Radiologist

University Hospital, Nottingham, UK

SEVENTH EDITION

 **WILEY-BLACKWELL**

A John Wiley & Sons, Ltd., Publication

This edition first published 2013 © 2013 by A. Rockall, A. Hatrick, P. Armstrong, M. Wastie.
Previous editions published 1981 (as *X-ray Diagnosis*), 1987, 1992, 1998, 2004, 2009

Wiley-Blackwell is an imprint of John Wiley & Sons, formed by the merger of Wiley's global Scientific, Technical and Medical business with Blackwell Publishing.

Registered office: John Wiley & Sons, Ltd, The Atrium, Southern Gate, Chichester, West Sussex, PO19 8SQ, UK

Editorial offices: 9600 Garsington Road, Oxford, OX4 2DQ, UK
The Atrium, Southern Gate, Chichester, West Sussex, PO19 8SQ, UK
111 River Street, Hoboken, NJ 07030-5774, USA

For details of our global editorial offices, for customer services and for information about how to apply for permission to reuse the copyright material in this book please see our website at www.wiley.com/wiley-blackwell.

The right of the author to be identified as the author of this work has been asserted in accordance with the UK Copyright, Designs and Patents Act 1988.

All rights reserved. No part of this publication may be reproduced, stored in a retrieval system, or transmitted, in any form or by any means, electronic, mechanical, photocopying, recording or otherwise, except as permitted by the UK Copyright, Designs and Patents Act 1988, without the prior permission of the publisher.

Designations used by companies to distinguish their products are often claimed as trademarks. All brand names and product names used in this book are trade names, service marks, trademarks or registered trademarks of their respective owners. The publisher is not associated with any product or vendor mentioned in this book. This publication is designed to provide accurate and authoritative information in regard to the subject matter covered. It is sold on the understanding that the publisher is not engaged in rendering professional services. If professional advice or other expert assistance is required, the services of a competent professional should be sought.

Library of Congress Cataloging-in-Publication Data
Diagnostic imaging. — 7th ed. / Andrea G. Rockall ... [et al.].
p. ; cm.

Rev. ed. of: Diagnostic imaging / Peter Armstrong, Martin L. Wastie, Andrea G. Rockall. 6th ed. 2009.

Includes bibliographical references and index.

ISBN 978-0-470-65890-1 (pbk. : alk. paper)

I. Rockall, Andrea G. II. Armstrong, Peter, 1940– Diagnostic imaging.

[DNLM: 1. Diagnostic Imaging. WN 180]

616.07'54–dc23

201203

A catalogue record for this book is available from the British Library.

Wiley also publishes its books in a variety of electronic formats. Some content that appears in print may not be available in electronic books.

Cover image: © Andrea Rockall, Andrew Hatrick, Peter Armstrong, Martin Wastie
Cover design by Jim Smith

Set in 9/12 pt Palatino by Toppan Best-set Premedia Limited

Contents

Preface, vii	
Acknowledgements, viii	
List of Abbreviations, ix	
The Anytime, Anywhere Textbook, x	
1 Technical Considerations, 1	
2 Chest, 19	
3 Cardiac Disorders, 101	
<i>with the assistance of Dr Francesca Pugliese</i>	
4 Breast Imaging, 123	
<i>with the assistance of Dr Sarah Vinnicombe</i>	
5 Plain Abdomen, 129	
6 Gastrointestinal Tract, 141	
7 Hepatobiliary System, Spleen and Pancreas, 195	
8 Urinary Tract, 223	
9 Female Genital Tract, 273	
10 Peritoneal Cavity and Retroperitoneum, 291	
11 Bones, 309	
<i>with the assistance of Dr Kasthoori Jayarani</i>	
12 Joints, 347	
<i>with the assistance of Dr Kasthoori Jayarani</i>	
13 Spine, 369	
<i>with the assistance of Dr Rob Barker</i>	
14 Skeletal Trauma, 399	
<i>with the assistance of Dr Muaaze Ahmad</i>	
15 Brain, 427	
<i>with the assistance of Dr Rob Barker</i>	
16 Orbits, Head and Neck, 457	
<i>with the assistance of Dr Polly Richards</i>	
17 Vascular and Interventional Radiology, 471	
Appendix: Computed Tomography Anatomy of the Abdomen, 491	
Index, 497	

Preface

Medical imaging is central to many aspects of patient management. Medical students and junior doctors can be forgiven their bewilderment when faced with the daunting array of information which goes under the heading 'Diagnostic imaging'. Plain film examinations remain the most frequently requested imaging investigations that non-radiologists may be called on to interpret and we continue to give them due emphasis. However, the use of cross-sectional imaging techniques continues to increase and, in some situations, has taken over from the plain film. The growing use of ultrasound, computed tomography (CT), magnetic resonance imaging (MRI), radionuclide imaging, including positron emission tomography (PET), and interventional radiology is reflected in the new edition.

With the widespread availability of most of the various imaging techniques, there are often several ways of investigating the same condition. We have avoided being too prescriptive as practice varies depending on the available equipment as well as the preferences of the clinicians and radiologists. It is important, however, to appreciate not

only the advantages but also the limitations of modern medical imaging.

We have continued to try to meet the needs of the medical student and doctors in training by explaining the techniques used in diagnostic imaging and the indications for their use. We aim to help the reader understand the principles of interpretation of imaging investigations. New for this edition is the availability of online material, including multiple choice questions for each chapter, allowing readers to test their knowledge.

It is beyond the scope of a small book such as this one to describe fully the pathology responsible for the various imaging appearances and the role of imaging in clinical management. Consequently, we encourage our readers to study this book in association with the study of these other subjects.

Andrea Rockall
Andrew Hatrick
Peter Armstrong
Martin Wastie

Acknowledgements

It would not have been possible to prepare this edition without the help of the many radiologists who have given ideas, valuable comments and inspiration. We would like to thank particularly the staff of the Radiology Departments at St Bartholomew's Hospital, London, Frimley Park NHS Trust, University Hospital, Nottingham, University of Malaya Medical Centre, Kuala Lumpur and County Hospital, Lincoln for this and past edition illustrations. Our special thanks go to those radiologists who gave us their expert assistance, including Dr Rob Barker, Dr Francesca Pugliese, Dr Sarah Vinnicombe, Dr Muaaze Ahmad, Dr Polly Richards and Dr Kasthoori Jayarani.

The following kindly provided illustrations for this and previous editions: Lorenzo Biassoni, Nishat Bharwani, John Bowe, Paul Clark, Siew Chen Chua, Peter Jackson, Jill Jacobs, Ranjit Kaur, Priya Narayanan, Steven Oscroft, Niall Power, Shaun Preston, Ian Rothwell, Peter Twining, Caroline Westerhout and Bob Wilcox.

We would like to thank Julie Jessop for her superb secretarial help and we would like to express our gratitude to the staff of Wiley-Blackwell.

List of Abbreviations

ADC	apparent diffusion coefficient	HMPAO	hexamethylpropyleneamine oxime
AIDS	acquired immune deficiency syndrome	HOCM	hypertrophic obstructive cardiomyopathy
ALARA	'as low as reasonably achievable' principle	HRCT	high resolution computed tomography
AP	anteroposterior	¹²³ I	iodine-123
ARDS	adult respiratory distress syndrome	¹³¹ I	iodine-131
AVM	arteriovenous malformation	IPF	idiopathic pulmonary fibrosis
BBB	blood–brain barrier	IUCD	intrauterine contraceptive device
CFA	cryptogenic fibrosing alveolitis	IVC	inferior vena cava
CPPD	calcium pyrophosphate dihydrate	IVU	intravenous urography
CSF	cerebrospinal fluid	^{81m} Kr	krypton-81m
CT KUB	non-contrast computed tomography of the kidneys, ureters and bladder	MAG-3	mercaptoacetyl triglycine
CT	computed tomography	MDCT	multidetector CT
CTR	cardiothoracic ratio	MEN	multiple endocrine neoplasia
CXR	chest radiograph	MIBG	meta-iodobenzylguanidine
3D	three-dimensional	MIP	maximum intensity projection
DCE-MRI	dynamic contrast-enhanced magnetic resonance imaging	MRA	magnetic resonance angiography
DEXA	dual-energy x-ray absorption	MRCP	magnetic resonance cholangiopancreatography
DMSA	dimercaptosuccinic acid	MRI	magnetic resonance imaging
DTPA	diethylene triamine pentacetic acid	NHS	National Health Service
DWI	diffusion-weighted imaging	PA	posteroanterior
ERCP	endoscopic retrograde cholangiopancreatography	PEG	percutaneous endoscopic gastrostomy
EUS	endoscopic ultrasound	PET	positron emission tomography
EVAR	endovascular aneurysm repair	PTC	percutaneous transhepatic cholangiogram
FAST	focused assessment with sonography for trauma	PUJ	pelviureteric junction
FDG	F-18 fluorodeoxyglucose	RIG	radiologically inserted gastrostomy
FDG-PET	fluorodeoxyglucose positron emission tomography	SCIWORA	spinal cord injury without radiological abnormality
FLAIR	fluid attenuated inversion recovery	SPECT	single photon emission computed tomography
FNA	fine needle aspiration	^{99m} Tc	technetium-99m
GI	gastrointestinal	TCC	transitional cell carcinoma
GIST	gastrointestinal stromal tumour	TIPSS	transjugular intrahepatic portosystemic shunt
HCC	hepatocellular carcinoma	TRUS	transrectal ultrasound
		UIP	interstitial pneumonia

The Anytime, Anywhere Textbook

Wiley E-Text Powered by VitalSource®

For the first time, your textbook comes with free access to a **Wiley E-Text: Powered by VitalSource** – a digital, interactive version of this textbook which you own as soon as you download it.

Your **Wiley E-Text: Powered by VitalSource** allows you to:

Search: Save time by finding terms and topics instantly in your book, your notes, even your whole library (once you've downloaded more textbooks)

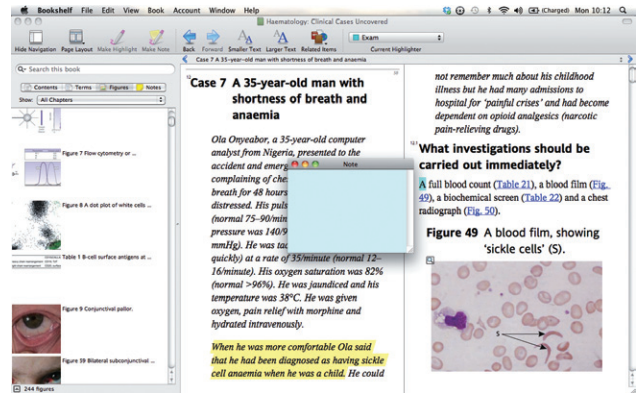
Note and Highlight: Colour code, highlight and make digital notes right in the text so you can find them quickly and easily

Organize: Keep books, notes and class materials organized in folders inside the application

Share: Exchange notes and highlights with friends, classmates and study groups

Upgrade: Your textbook can be transferred when you need to change or upgrade computers

Link: Link directly from the page of your interactive textbook to all of the material contained on the companion website



To access your Wiley E-Text: Powered by VitalSource:

- Find the redemption code on the inside front cover of this book and carefully scratch away the top coating of the label. Visit www.vitalsource.com/software/bookshelf/downloads to download the Bookshelf application to your computer, laptop or mobile device.
- If you have purchased this title as an e-book, access to your **Wiley E-Text: Powered by VitalSource** is available with proof of purchase within 90 days. Visit <http://support.wiley.com> to request a redemption code via the 'Live Chat' or 'Ask A Question' tabs.
- Open the Bookshelf application on your computer and register for an account.
- Follow the registration process and enter your redemption code to download your digital book.
- For full access instructions, visit www.wileydiagnosticimaging.com.

Available on
CourseSmart
Learn Smart. Choose Smart.



CourseSmart gives you instant access (via computer or mobile device) to this Wiley-Blackwell eTextbook and its extra electronic functionality, at 40% off the recommended retail print price. See all the benefits at www.coursesmart.com/students.

Instructors . . . receive your own digital desk copies!

It also offers instructors an immediate, efficient and environmentally-friendly way to review this textbook for your course.

For more information visit www.coursesmart.com/instructors.

With **CourseSmart**, you can create lecture notes quickly with copy and paste, and share pages and notes with your students. Access your Wiley **CourseSmart** digital textbook from your computer or mobile device instantly for evaluation, class preparation and as a teaching tool in the classroom.

Simply sign in at <http://instructors.coursesmart.com/bookshelf> to download your Bookshelf and get started. To request your desk copy, hit 'Request Online Copy' on your search results or book product page.

Companion website

This book is accompanied by a companion website:

www.wileydiagnosticimaging.com

The website includes:

- Interactive multiple choice questions for each chapter
- Figures from the book in PowerPoint format

Technical Considerations

Use of the imaging department

Good communication between clinicians and radiologists is vital because the radiology department needs to understand the clinical problem in order to carry out appropriate tests and to interpret the results in a meaningful way. Also, clinicians need to understand the strengths and limitations of the answers provided.

Sensible selection of imaging investigations is of great importance. There are two opposing philosophies. One approach is to request a battery of investigations, aimed in the direction of the patient's symptoms, in the hope that something will turn up. The other approach is 'trial and error': decide one or two likely diagnoses and carry out the appropriate test to support or refute these possibilities. We favour the selective approach as there is little doubt that the answers are usually obtained less expensively and with less distress to the patient. This approach depends on critical clinical evaluation; the more experienced the doctor, the more accurate he or she becomes in choosing appropriate tests.

Laying down precise guidelines for requesting imaging examinations is difficult because patients are managed differently in different centres. Box 1.1 provides important points when requesting imaging investigations.

Conventional radiography

X-rays are absorbed to a variable extent as they pass through the body. The visibility of both normal structures

Box 1.1 Best practice when requesting imaging investigations

- Only request an examination if it is likely to affect patient management
- The time interval between follow-up examinations should be appropriate and depends on the natural history of disease
- Localize the clinical problem as specifically as possible prior to imaging in order to reduce over-investigation and excess radiation exposure
- Careful consideration should be given to which imaging procedure is likely to give the relevant diagnostic information most easily
- Any investigations that have been requested but become unnecessary should be cancelled
- Examinations that minimize or avoid ionizing radiation should be chosen when possible
- Good communication with the radiologists is key to ensuring appropriate investigation pathways

and disease depends on this differential absorption. With conventional radiography there are four basic densities – gas, fat, all other soft tissues and calcified structures. X-rays that pass through air are least absorbed and, therefore, cause the most blackening of the radiograph, whereas calcium absorbs the most and so the bones and other calcified structures appear virtually white. The soft tissues, with the exception of fat, e.g. the solid viscera, muscle, blood, a variety of fluids, bowel wall, etc., all have similar absorptive capacity and appear the same shade of grey on conventional radiographs. Fat absorbs slightly fewer x-rays and, therefore, appears a little blacker than the other soft

tissues. Traditionally, images were produced using a silver-based photographic emulsion but now they are recorded digitally and viewed on computer screens in most centres.

Projections are usually described by the path of the x-ray beam. Thus, the term PA (posteroanterior) view designates that the beam passes from the back to the front, the standard projection for a routine chest film. An AP (anteroposterior) view is taken from the front. The term 'frontal' refers to either PA or AP projection. The image on an x-ray film is two-dimensional. All the structures along the path of the beam are projected on to the same portion of the film. Therefore, it is often necessary to take at least two views to gain information about the third dimension. These two views are usually at right angles to one another, e.g. the PA and lateral chest film. Sometimes two views at right angles are not appropriate and oblique views are substituted.

Portable x-ray machines can be used to take films of patients on the ward or in the operating theatre. Such machines have limitations on the exposures they can achieve. This usually means longer exposure times and poorer quality films. The positioning and radiation protection of patients in bed is often inferior to that which can be achieved within the x-ray department. Consequently, portable films should only be requested when the patient cannot be moved safely to the x-ray department.

Computed tomography

Computed tomography (CT) also relies on x-rays transmitted through the body. It differs from conventional radiography in that a more sensitive x-ray detection system is used, the images consist of sections (slices) through the body, and the data are manipulated by a computer. The x-ray tube and detectors rotate around the patient (Fig. 1.1). The outstanding feature of CT is that very small differences in x-ray absorption values can be visualized. Compared with conventional radiography, the range of densities recorded is increased approximately ten-fold. Not only can fat be distinguished from other soft tissues, but also gradations of density within soft tissues can be recognized, e.g. brain substance from cerebrospinal fluid, or tumour from surrounding normal tissues.

The patient lies with the body part to be examined within the gantry housing the x-ray tube and detectors. Although

other planes are sometimes practicable, axial sections are by far the most frequent. The operator selects the level and thickness to be imaged: the usual thickness is between 1.25 and 2 mm (often viewed by aggregating adjacent sections so they become 5 mm thick). The patient is moved past an array of detectors within the machine. In effect, the data at multiple adjacent levels are collected continuously, during which time the x-ray beam traces a spiral path to create a 'volume of data' within the computer memory. Multidetector (multislice) CT acquires multiple slices (64, 128, 256 or 320 depending on the machine) during one rotation of the x-ray tube. Multidetector CT enables the examination to be performed in a few seconds, thereby enabling hundreds of thin sections to be obtained in one breath-hold. A relatively new development is dual source (or dual energy) CT. This technique allows a virtual non-contrast CT image to be derived from CT acquired with intravenous iodinated contrast medium (see later in chapter) allowing a reduction in radiation dose in certain CT protocols.

The data obtained from the multislice CT exposures are reconstructed into an image by computer manipulation. The computer calculates the attenuation (absorption) value of each picture element (pixel). Each pixel is 0.25–0.6 mm in diameter, depending on the resolution of the machine, with a height corresponding to the chosen section thickness. The resulting images are displayed on a monitor and can be stored electronically. The attenuation values are expressed on an arbitrary scale (Hounsfield units) with water density being zero, air density being minus 1000 units and bone density being plus 1000 units (Fig. 1.2). The range and level of densities to be displayed can be selected by controls on the computer. The range of densities visualized on a particular image is known as the *window width* and the mean level as the *window level* or *window centre*. CT is usually performed in the axial plane, but because attenuation values for every pixel are present in the computer memory it is possible to reconstruct excellent images in other planes, e.g. coronal (Fig. 1.3), sagittal or oblique, and even three-dimensional (3D) images (Fig. 1.4).

The human eye can only appreciate a limited number of shades of grey. With a wide window all the structures are visible, but fine details of density difference cannot be appreciated. With a narrow window width, variations of just a few Hounsfield units can be seen, but much of the image is either totally black or totally white and in these

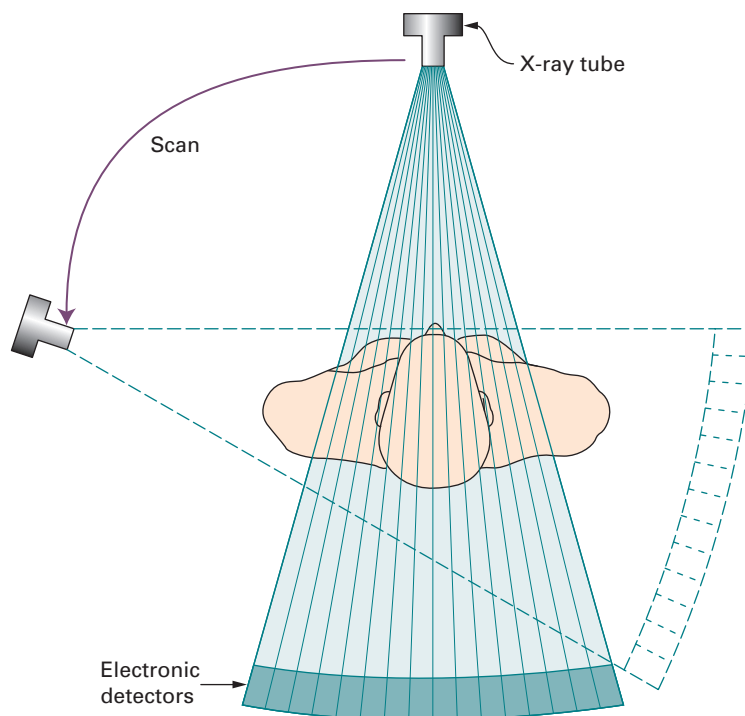


Fig. 1.1 Principle of CT. The x-ray tube and detectors move around the patient enabling a picture of x-ray absorption in different parts of the body to be built up.

areas no useful information is provided. The effects of varying window width and level are illustrated in Figs 1.5 and 2.6.

Computed tomography angiography

Rapid intravenous injections of contrast media result in significant opacification of blood vessels, which, with multiplanar or 3D reconstructions, can be exploited to produce angiograms. CT angiography, along with magnetic resonance angiography, is gradually replacing conventional diagnostic angiography.

Artefacts

There are numerous CT artefacts. The most frequent are those produced by movement and those from objects of very high density, such as barium in the bowel, metal

implants, dental fillings or surgical clips. Both types give rise to radiating linear streaks. The major problem is the resulting degradation of the image.

Contrast agents in conventional radiography and computed tomography

Radiographic contrast agents are used to visualize structures or disease processes that would otherwise be invisible or difficult to see. Barium is widely used to outline the gastrointestinal tract on conventional radiographic images; all the other radio-opaque media rely on iodine in solution to absorb x-rays. Iodine-containing solutions are used for urography, angiography and intravenous contrast enhancement at CT. Usually they are given in large doses, often with rapid rates of injection. As their only purpose is to produce opacification, ideally they should be pharmacologically inert. This has not yet been totally achieved,

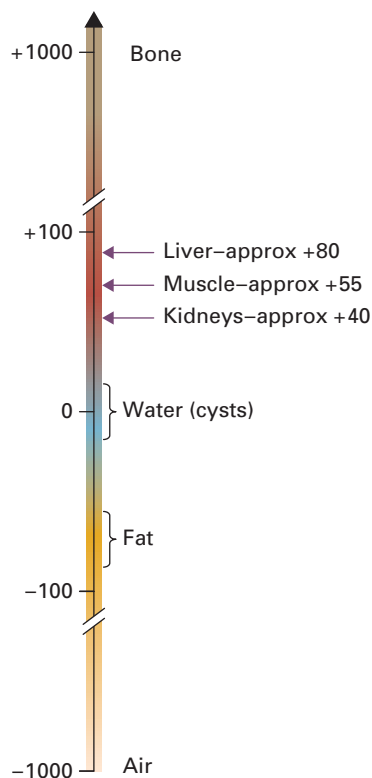


Fig. 1.2 Scale depicting the CT density (Hounsfield units) of various normal tissues in the body.

though the current low osmolality, non-ionic contrast media have exceedingly low complication rates.

Some patients experience a feeling of warmth spreading over the body as the iodinated contrast medium is injected. Contrast inadvertently injected outside the vein is painful and should be carefully guarded against. A few patients develop an urticarial rash, which usually subsides spontaneously.

Bronchospasm, laryngeal oedema or hypotension occasionally develop and may be so severe as to be life-threatening. It is therefore essential to be prepared for these dangerous reactions and to have available appropriate resuscitation equipment and drugs. Patients with known allergic manifestations, particularly asthma, are more likely to have an adverse reaction. Similarly, patients who have

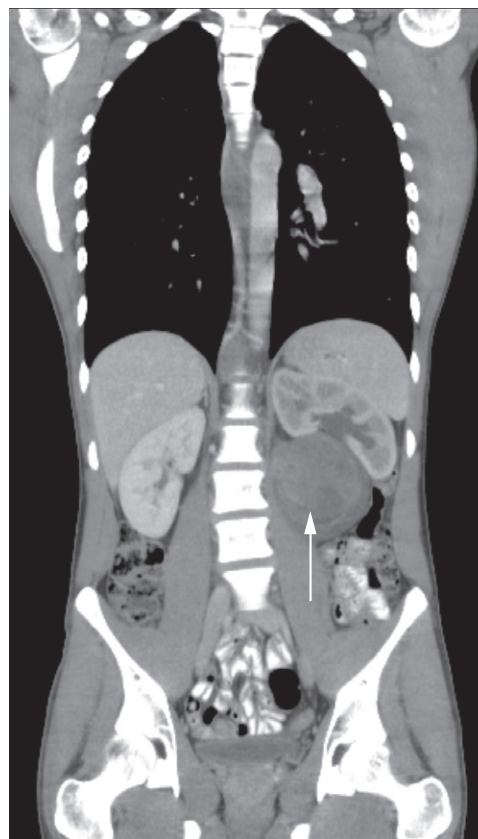


Fig. 1.3 Coronal reconstruction of CT of the chest, abdomen and pelvis. The images were obtained in the axial plane using very thin sections and then reconstructed into the desired plane – a coronal plane in this example. The illustrated section is through the posterior abdomen and shows the kidneys. There is a retroperitoneal mass (arrow) displacing the left kidney and causing hydronephrosis.

had a previous reaction to contrast agents have a higher than average risk of problems during the examination and an alternative method of imaging should be considered. Patients at higher risk are observed following the procedure. Intravenous contrast agents may have a deleterious effect on renal function in patients with impaired kidneys. Therefore, their use should be considered carefully on an individual basis and the patient should be well hydrated prior to injection.

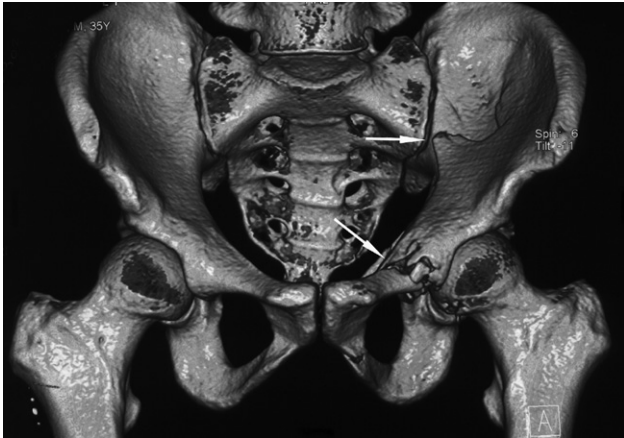


Fig. 1.4 Shaded surface 3D CT reconstruction. The images can be viewed in any desired projection and give a better appreciation of the pelvis. Two fractures are demonstrated in the left innominate bone (arrows), which were hard to diagnose on plain film.

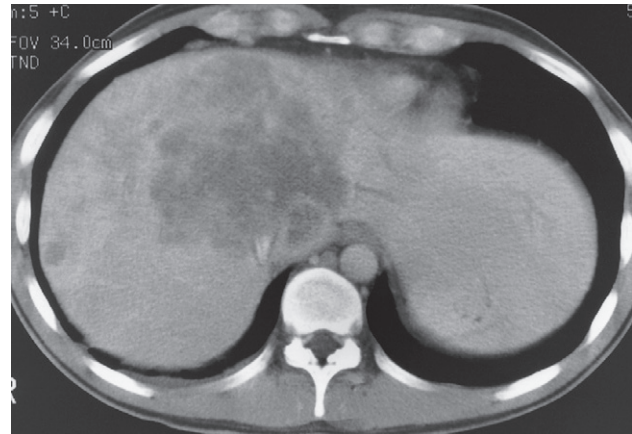
Ultrasound

In diagnostic ultrasound examinations, very high frequency sound is directed into the body from a transducer placed in contact with the skin. In order to make good acoustic contact, the skin is smeared with a jelly-like substance. As the sound travels through the body, it is reflected by the tissue interfaces to produce echoes which are picked up by the same transducer and converted into an electrical signal.

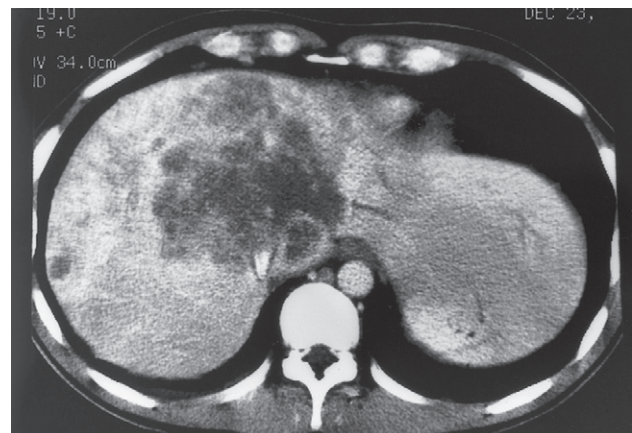
As air, bone and other heavily calcified materials absorb nearly all the ultrasound beam, ultrasound plays little part in the diagnosis of lung or bone disease. The information from abdominal examinations may be significantly impaired by gas in the bowel, which interferes with the transmission of sound.

Fluid is a good conductor of sound, and ultrasound is, therefore, a particularly good imaging modality for diagnosing cysts, examining fluid-filled structures such as the bladder and biliary system, and demonstrating the fetus in its amniotic sac. Ultrasound can also be used to demonstrate solid structures that have a different acoustic impedance to adjacent normal tissues, e.g. metastases.

Ultrasound is often used to determine whether a structure is solid or cystic (Fig. 1.6). Cysts or other fluid-filled



(a)



(b)

Fig. 1.5 Effect of varying window width on CT. In (a) and (b) the level has been kept constant at 65 Hounsfield units (HU). The window width in (a) is 500HU whereas in (b) it is only 150HU. Note that in the narrow window image (b), the metastases are better seen, but that structures other than the liver are better seen in (a).

structures produce echoes from their walls but no echoes from the fluid contained within them. Also, more echoes than usual are received from the tissues behind the cyst, an effect known as *acoustic enhancement*. Conversely, with a calcified structure, e.g. a gall stone (Fig. 1.7), there is a great reduction in the sound that will pass through, so a band of

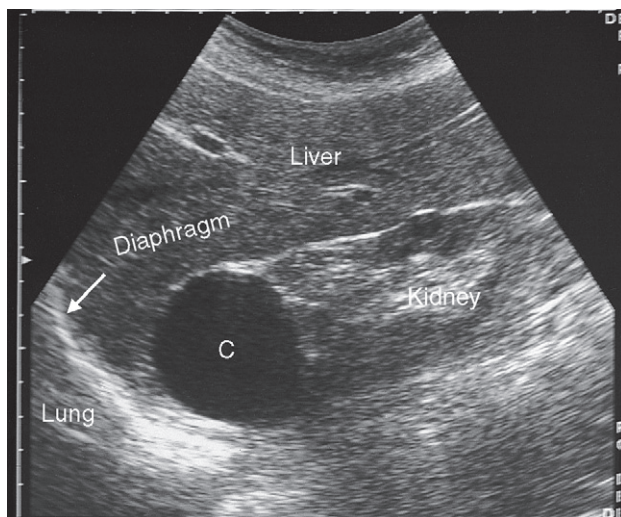


Fig. 1.6 Ultrasound scan of longitudinal section through the liver and right kidney. A cyst (C) is present in the upper pole of the kidney.

reduced echoes, referred to as an *acoustic shadow*, is seen behind the stone.

Ultrasound is produced by causing a special crystal to oscillate at a predetermined frequency. Very short pulses of sound lasting about a millionth of a second are transmitted approximately 500 times each second. The crystal not only transmits the pulses of sound but also 'listens' to the returning echoes, which are electronically amplified to be recorded as signals on a television monitor. Photographic or video reproductions of the image can provide a permanent record.

The time taken for each echo to return to the transducer is proportional to the distance travelled. Knowledge of the depth of the interface responsible for the echoes allows an image to be produced. Also, by knowing the velocity of sound in tissues, it is possible to measure the distance between interfaces. This is of great practical importance in obstetrics, for example, where the measurement of fetal anatomy has become the standard method of estimating fetal age.

During the scan, the ultrasound beam is electronically swept through the patient's body and a section of the internal anatomy is instantaneously displayed. The resulting image is a slice, so in order to obtain a 3D assessment a

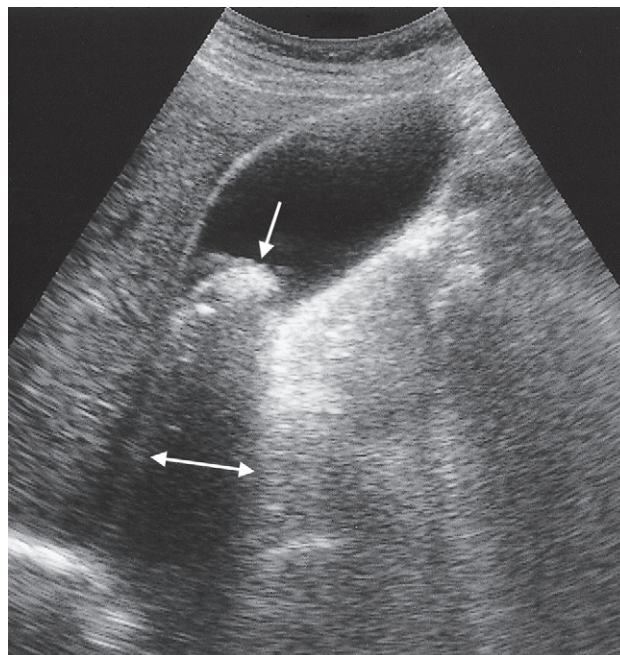


Fig. 1.7 Ultrasound scan of gall bladder showing a large stone in the neck of the gall bladder (downward pointing arrow). Note the acoustic shadow behind the stone (horizontal double-headed arrow).

number of slices must be created by moving or angling the transducer.

Unlike other imaging modalities, there are no fixed projections and the production of the images and their subsequent interpretation depend very much on the observations of the operator during the examination. Ultrasound images are capable of providing highly detailed information, e.g. very small lesions can be demonstrated (Fig. 1.8).

Small ultrasound probes, which may be placed very close to the region of interest, produce highly detailed images but with a limited range of a few centimetres. Examples are rectal probes for examining the prostate and transvaginal probes for the examination of the pelvic structures. Tiny ultrasound probes may be incorporated in the end of an endoscope. Lesions of the oesophagus, heart and aorta may be demonstrated with an endoscope placed in the oesophagus, and lesions of the pancreas may be detected with an endoscope passed into the stomach and duode-

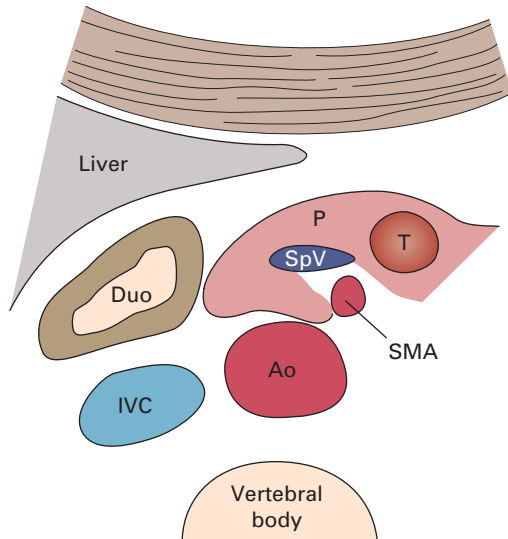


Fig. 1.8 Ultrasound scan of pancreas showing a 1 cm tumour (T) (an insulinoma) at the junction of the head and body of the pancreas. Ao, aorta; Duo, duodenum; IVC, inferior vena cava; P, pancreas; SMA, superior mesenteric artery; SpV, splenic vein.

num. Special ultrasound probes have also been developed that can be inserted into arteries to detect atheromatous disease.

Three-dimensional ultrasound has been recently developed and is used primarily in obstetrics to obtain 3D

images of the fetus. A conventional ultrasound transducer is used, which is moved slowly across the body recording simultaneously the location and ultrasound image. A 3D image can be constructed from the data received.

At the energies and doses currently used in diagnostic ultrasound, no harmful effects on any tissues have been demonstrated.

Ultrasound contrast agents have been developed. These agents contain microscopic air bubbles that enhance the echoes received by the probe. The air bubbles are held in a stabilized form, so they persist for the duration of the examination, and blood flow and perfusion to organs can be demonstrated. The technique is used to help characterize liver and renal abnormalities and in the investigation of cardiac disease.

Doppler effect

Sound reflected from a mobile structure shows a variation in frequency that corresponds to the speed of movement of the structure. This shift in frequency, which can be converted to an audible signal, is the principle underlying the Doppler probe used in obstetrics to listen to the fetal heart.

The Doppler effect can be exploited to image blood flowing through the heart or blood vessels. Here the sound is reflected from the blood cells flowing in the vessels (Fig. 1.9). If blood is flowing towards the transducer, the received signal is of higher frequency than the transmitted frequency, whilst the opposite pertains if blood is flowing away from the transducer. The difference in frequency between the sound transmitted and received is known as the Doppler frequency shift (Box 1.2). The direction of blood flow can readily be determined and flow towards the transducer is, by convention, coloured red, whereas blue indicates flow away from the transducer.

When a patient is being scanned, the Doppler information in colour is superimposed onto a standard ultrasound image (Fig. 1.10).

During the examination, the flow velocity waveform can be displayed and recorded. As the waveforms from specific arteries and veins have characteristic shapes, flow abnormalities can be detected. If the Doppler angle (Fig. 1.9) is known then the velocity of the flowing blood can be calculated, and blood flow can be calculated provided the diameter of the vessel is also known.

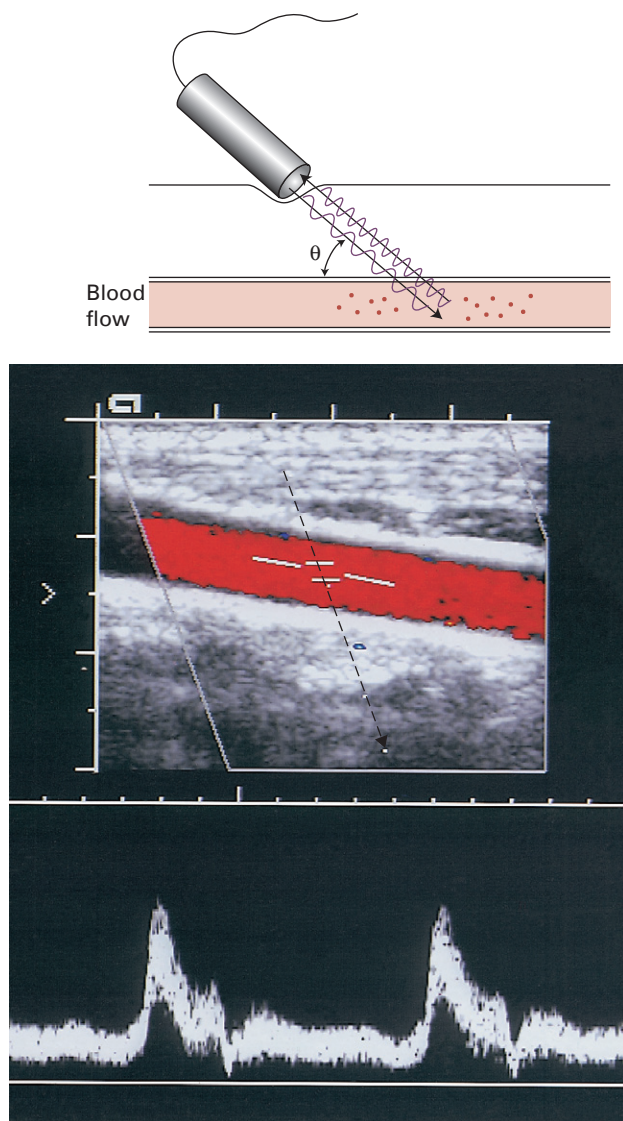


Fig. 1.9 Principle of Doppler ultrasound. In this example, flowing blood is detected in a normal carotid artery in the neck. With blood flowing away from the transducer, the frequency of the received sound is reduced, whereas with blood flowing towards the transducer, the frequency of the received sound is increased. For anatomical images, the flowing blood is colour coded according to the direction of flow. (θ is the angle between the vessel and the transmitted sound wave: an angle known as the Doppler angle. The angle of the beam is indicated by the fine zig-zag line across the image.) The flow-velocity waveform has been taken from the gate within the artery. The peaks represent systolic blood flow.

Box 1.2 Doppler frequency shift formula

$$\text{Frequency shift} = \frac{2Fi \times V \times \cos \theta}{c}$$

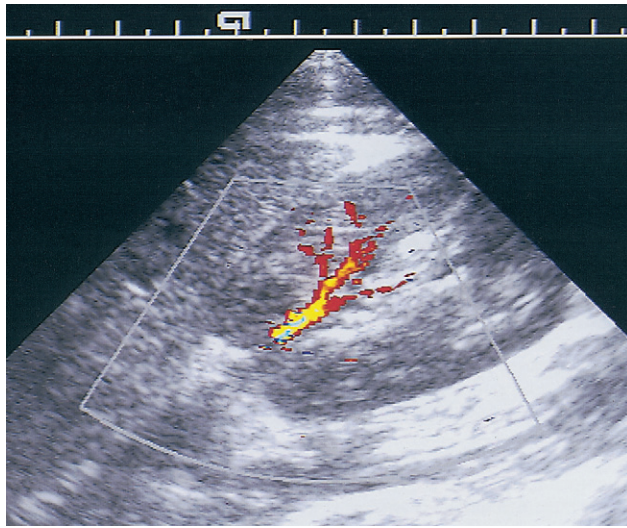
As c , the speed of sound in tissues, and Fi , the incident frequency of sound, are constant, and if θ , the Doppler angle, is kept constant, the frequency shift depends directly on the blood flow velocity V

Doppler studies are used to detect venous thrombosis, arterial stenosis and occlusion, particularly in the carotid arteries. In the abdomen, Doppler techniques can determine whether a structure is a blood vessel and can help in assessing tumour blood flow. In obstetrics, Doppler ultrasound is used particularly to determine fetal blood flow through the umbilical artery. With Doppler echocardiography it is possible to demonstrate regurgitation through incompetent valves and pressure gradients across valves can be calculated.

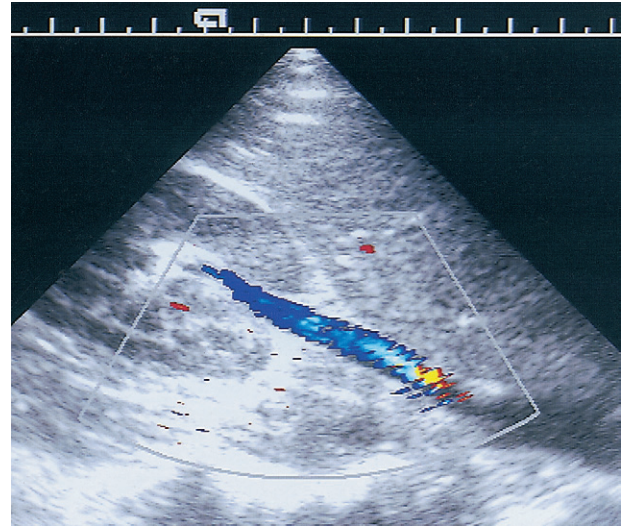
Radionuclide imaging

The radioactive isotopes used in diagnostic imaging emit gamma-rays as they decay. Gamma-rays are electromagnetic radiation, similar to x-rays, produced by radioactive decay of the nucleus. Many naturally occurring radioactive isotopes, e.g. potassium-40 and uranium-235, have half lives of hundreds of years and are, therefore, unsuitable for diagnostic imaging. The radioisotopes used in medical diagnosis are artificially produced and most have short half lives, usually a few hours or days. To keep the radiation dose to the patient at a minimum, the smallest possible dose of an isotope with a short half life should be used. Clearly, the radiopharmaceuticals should have no undesirable biological effects and should be rapidly excreted from the body following completion of the investigation.

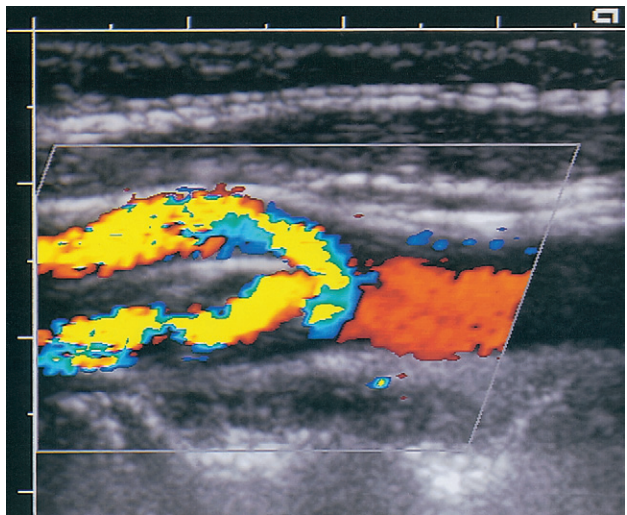
Radionuclides can be chemically tagged to certain substances that concentrate selectively in different parts of the body. Occasionally, the radionuclide in its ionic form will selectively concentrate in an organ, so there is no need to attach it to another compound. Such a radionuclide is technetium-99m (^{99m}Tc). It is readily prepared, has a convenient half life of 6 hours and emits gamma-radiation of a suitable energy for easy detection. Other radionuclides that are used include indium-111, gallium-67, iodine-123 and thallium-201.



(a)



(b)



(c)

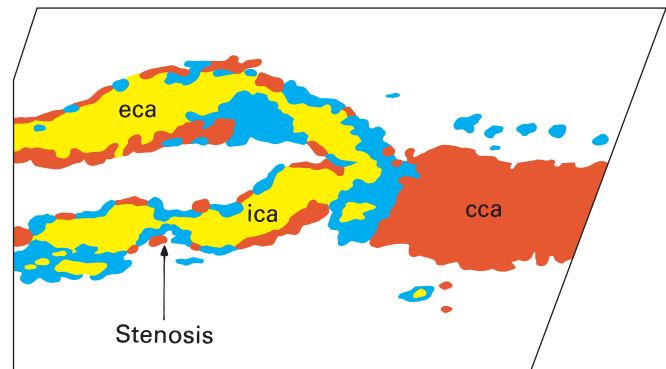


Fig. 1.10 Colour Doppler. (a) Normal renal artery. (b) Normal renal vein. (c) Bifurcation of the common carotid artery showing stenosis of the internal carotid artery. The flowing blood is revealed by colour. The precise colour depends on the speed and direction of the blood flow. cca, common carotid artery; eca, external carotid artery; ica, internal carotid artery.

Technetium-99m can be used in ionic form (as the pertechnetate) to detect ectopic gastric mucosa in Meckel's diverticulum, but it is usually tagged to other substances. For example, a complex organic phosphate labelled with ^{99m}Tc will be taken up by the bones and can be used to visu-

alize the skeleton (Fig. 1.11). Particles are used in lung perfusion images; macroaggregates of albumin with a particle size of 10–75 μm when injected intravenously are trapped in the pulmonary capillaries. If the macroaggregates are labelled with ^{99m}Tc , then the blood flow to the

lungs can be visualized. It is also possible to label the patient's own red blood cells with ^{99m}Tc to assess cardiac function, or the white cells with indium-111 or ^{99m}Tc for abscess detection. Small quantities of radioactive gases, such as xenon-133, xenon-127 or krypton-81m, can be inhaled to assess ventilation of the lungs. All these radiopharmaceuticals are free of side-effects.

The gamma-rays emitted by the isotope are detected by a gamma camera, enabling an image to be produced. A gamma camera consists of a large sodium iodide crystal, usually 40cm in diameter, coupled to a number of photomultiplier tubes. Light is produced when the gamma-rays strike and activate the sodium iodide crystal, and the light is then electronically amplified and converted to an electri-

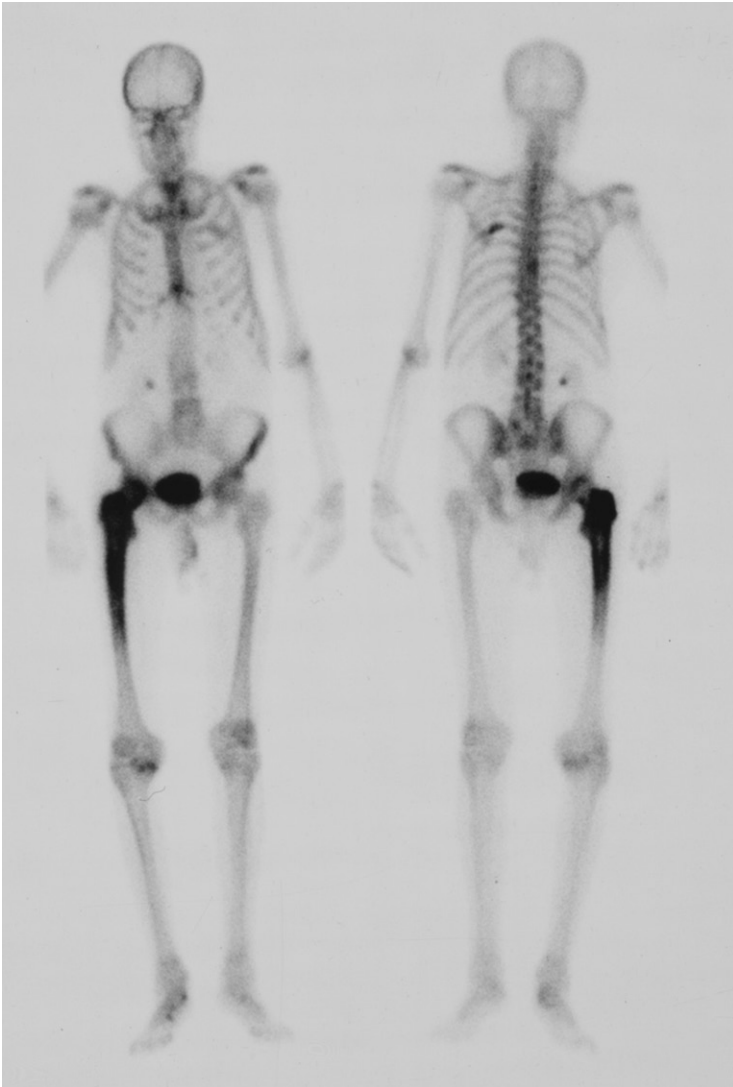


Fig. 1.11 Radionuclide bone scan. The patient has received an intravenous injection of a ^{99m}Tc -labelled bone-scanning agent (a complex organic phosphate). This agent is taken up by bone in proportion to bone turnover and blood flow. The increased uptake in the femur in this patient was due to Paget's disease.

cal pulse. The electrical pulse is further amplified and analyzed by a processing unit so that a recording can be made. Invariably, some form of computer is linked to the gamma camera to enable rapid serial images to be taken and to perform computer enhancement of the images when relevant.

In selected cases emission tomography is performed. In this technique, the gamma camera moves around the patient. A computer can analyze the information and produce sectional images similar to CT. Emission tomography can detect lesions not visible on the standard views. Because only one usable photon for each disintegration is emitted, this technique is also known as single photon emission computed tomography (SPECT).

Nuclear medicine techniques are used to measure function and to produce anatomical images. Even the anatomical images are dependent on function; for example, a bone scan depends on bone turnover. The anatomical informa-

tion they provide, however, is limited by the relatively poor spatial resolution of the gamma camera compared with other imaging modalities.

Positron emission tomography

Positron emission tomography (PET) uses short-lived positron-emitting isotopes, which are produced by a cyclotron immediately before use. Two gamma-rays are produced from the annihilation of each positron and can be detected by a specialized gamma camera. The resulting images reflect the distribution of the isotope (Fig. 1.12a). By using isotopes of biologically important elements such as carbon or oxygen, PET can be used to study physiological processes such as blood perfusion of tissues, and metabolism of substances such as glucose, as well as complex biochemical pathways such as neurotransmitter storage and binding. The most commonly used agent is

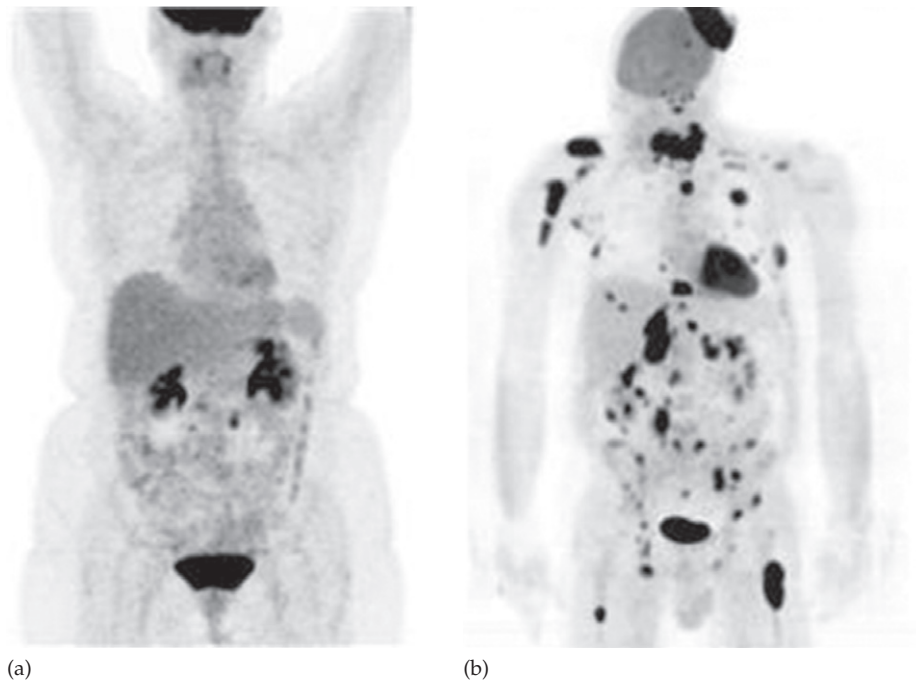


Fig. 1.12 FDG-PET scans, maximum intensity projections. (a) Normal isotope distribution. There is intense uptake in the brain and the neck uptake is in the tonsils. The FDG is excreted by the kidneys. (b) Lymphoma, showing multiple visceral, nodal, bone and scalp deposits.

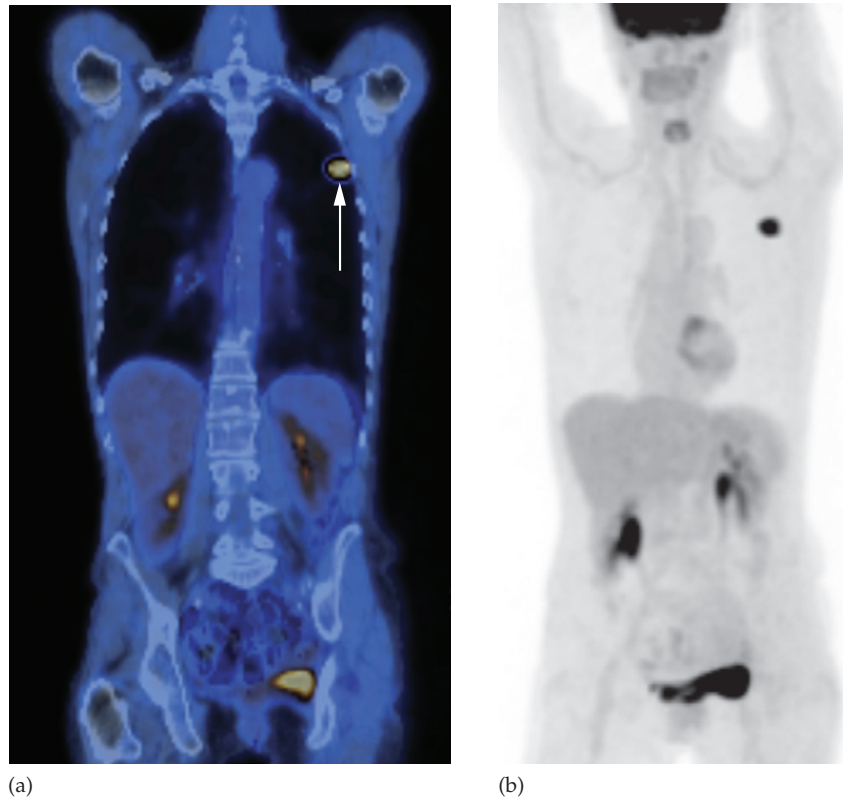


Fig. 1.13 FDG-PET/CT of lung cancer. (a) Coronal fused image and (b) maximum intensity projection, demonstrating a small left lung cancer (arrowed in (a)). The remainder of the FDG uptake is physiological.

F-18 fluorodeoxyglucose (FDG). This is an analogue of glucose and is taken up by cells in proportion to glucose metabolism, which is usually increased in tumour cells. Because muscle activity results in the uptake of FDG, the patient should rest quietly in the interval between injection of the FDG and scanning.

The images must be interpreted carefully as non-cancerous conditions may show uptake resembling cancer. PET using FDG is the most sensitive technique for staging solid tumours, such as bronchial carcinoma (Fig. 1.13), and in the follow-up of malignancies, particularly lymphoma (Fig. 1.12b), where other imaging techniques may be unable to distinguish active disease from residual fibrosis.

Positron emission tomography is also used in the evaluation of ischaemic heart disease and in brain disorders such as dementia, epilepsy and Parkinson's disease.

Positron emission tomography demonstrates biological function while CT gives anatomical information. If PET and CT are fused, the lesions detected by PET can be precisely localized by CT (Fig. 1.13). Modern equipment allows both PET and CT to be performed sequentially on the same machine.

Magnetic resonance imaging

The basic principles of magnetic resonance imaging (MRI) depend on the fact that the nuclei of certain elements align with the magnetic force when placed in a strong magnetic field. At the field strengths currently used in medical imaging, hydrogen nuclei (protons) in water molecules and lipids are responsible for producing anatomical images. If a radiofrequency pulse at the resonant frequency of hydro-

gen is applied, a proportion of the protons change alignment, flipping through a preset angle, and rotate in phase with one another. Following this radiofrequency pulse, the protons return (realign) to their original positions. As the protons realign (relax), they induce a signal which, although very weak, can be detected and localized by copper coils placed around the patient. An image representing the distribution of the hydrogen protons can be built up (Fig. 1.14). The strength of the signal depends not only on proton density but also on two relaxation times, T1 and T2; T1 depends on the time the protons take to return to the axis of the magnetic field, and T2 depends on the time the protons take to dephase (also known as T2 decay). A T1-weighted image is one in which the contrast between tissues is due mainly to their T1 relaxation properties, while in a T2-weighted image the contrast is due to the T2 relaxation properties (Table 1.1). Some sequences produce images that approximate mainly to proton density. Most pathological processes show increased T1 and T2 relaxation times and, therefore, these processes appear lower in signal (black) on a T1-weighted scan and higher in signal intensity (whiter) on a T2-weighted image than the normal surrounding tissues. The T1- and T2-weighting of an image can be selected by appropriately altering the timing and sequence of radiofrequency pulses.

There are many other sequences with a bewildering variety of names and acronyms. They are designed to highlight different tissue characteristics, for example to demonstrate water content (HASTE sequence), diminish the signal from fat and so highlight pathology or contrast enhancement (fat suppression or STIR sequence, see Fig. 6.43), or demonstrate the combination of water and lipid content in

the same voxel (chemical shift imaging, see Fig. 10.17). Dynamic contrast-enhanced images (DCE-MRI) using gadolinium contrast medium (see below) may be used to demonstrate the anatomy of the large vessels as well as the enhancement characteristics of tumour angiogenesis (Fig. 1.14c). More recent developments include diffusion-weighted imaging and magnetic resonance spectroscopy, which can further characterize tissues and are often used in tumour assessment (Fig. 1.15).

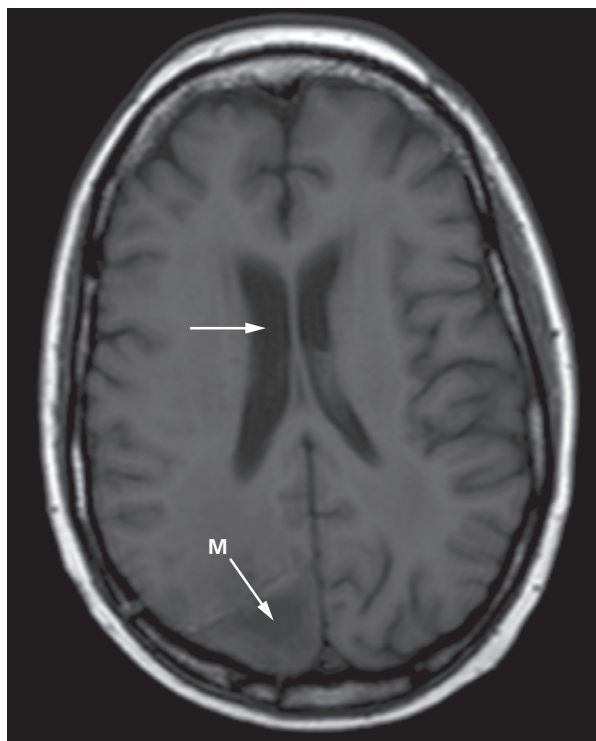
A typical MRI scanner (Fig. 1.16) consists of a large circular magnet. Inside the magnet are the radiofrequency transmitter and receiver coils, as well as gradient coils to allow spatial localization of the MRI signal. Ancillary equipment converts the signals into a digital form, which the computer can manipulate to create an image. One advantage of MRI over CT is that the information can be directly imaged in any plane. In most instances, MRI requires a longer scan time (often several minutes) compared with CT, with the disadvantage that the patient has to keep still during the scanning procedure. Unavoidable movements from breathing, cardiac pulsation and peristalsis often degrade the image. Techniques to speed up scan times and limit the effect of motion by the use of various electronic methods have been introduced. Cardiac gating and breath-hold sequences are now readily available.

Magnetic resonance imaging gives very different information to CT. The earliest successful application was for scanning the brain and spinal cord, where MRI has significant advantages over CT and few disadvantages. MRI is now also an established technique for imaging the spine, bones, joints, pelvic organs, liver, biliary system, urinary tract and heart. At first sight it may seem rather surprising that MRI provides valuable information in skeletal disease as calcified tissues do not generate any signal during the procedure. This seeming paradox is explained by the fact that MRI provides images of the bone marrow and the soft tissues inside and surrounding joints (Fig. 1.17).

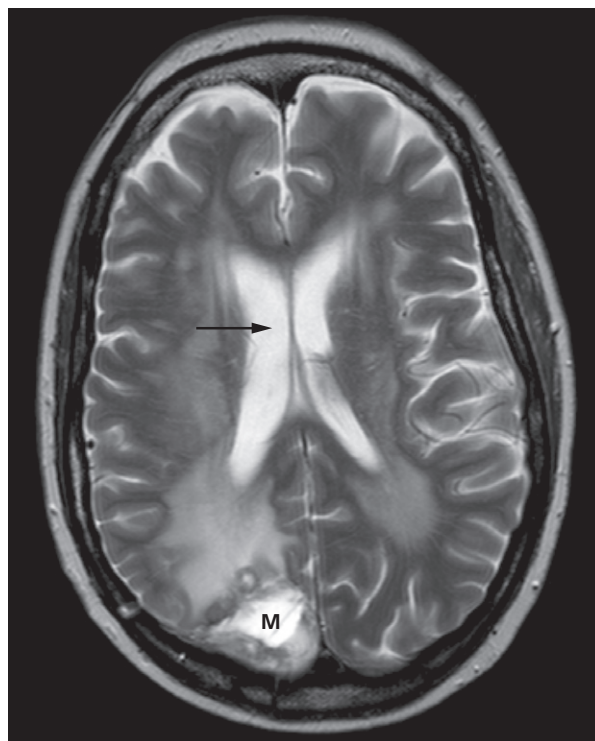
The physical basis of imaging blood vessels with MRI is complicated and beyond the scope of this book. Suffice it to say that, with some sequences, fast-flowing blood produces no signal (Fig. 1.18), whereas with others it produces a bright signal. This ‘motion effect’ can be exploited to image blood vessels. Such flow-sensitive sequences are mostly used for head and neck imaging, for example intracranial arteriovenous malformations and stenoses of the

Table 1.1 Appearance of water and fat on different magnetic resonance sequences

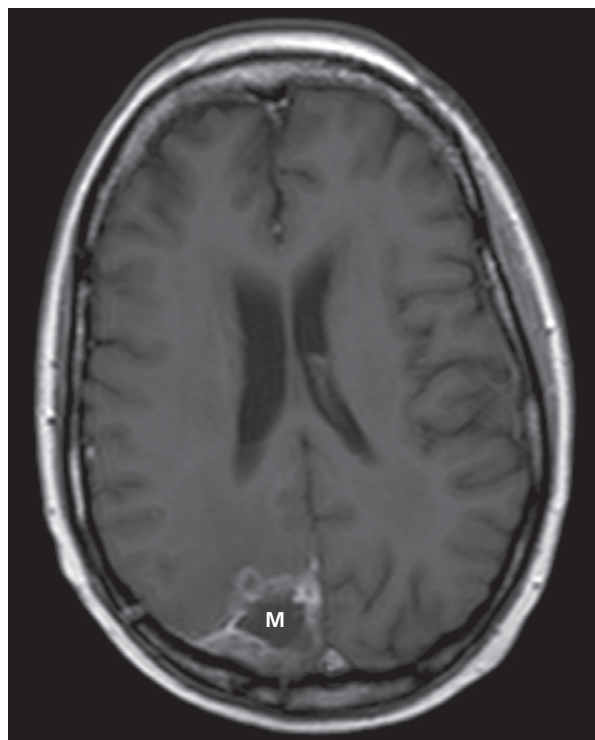
Sequence	Water signal intensity	Fat signal intensity
T1-weighted	Low	High
T2-weighted	High	High
T1 with fat saturation	Low	Low
T2 with fat saturation	High	Low



(a)



(b)



(c)

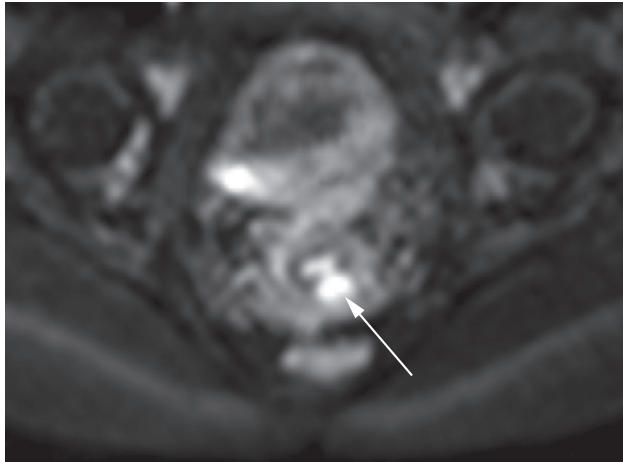
Fig. 1.14 MRI of brain. (a) Axial T1-weighted image. (b) Axial T2-weighted image. (c) Axial T1-weighted image following gadolinium. Note that the cerebrospinal fluid within the lateral ventricles is of low signal intensity on T1- and high signal intensity on T2-weighted images (arrows in (a) and (b)). Note also that the intensity of the white and grey matter of the brain differs on the two images. There is a metastasis from a breast carcinoma (M) in the right occipital pole, showing oedema around the mass on the T2-weighted image and enhancement on the post contrast image.

carotid arteries can be readily demonstrated without contrast media. The resulting images resemble a conventional angiogram (Fig. 1.19).

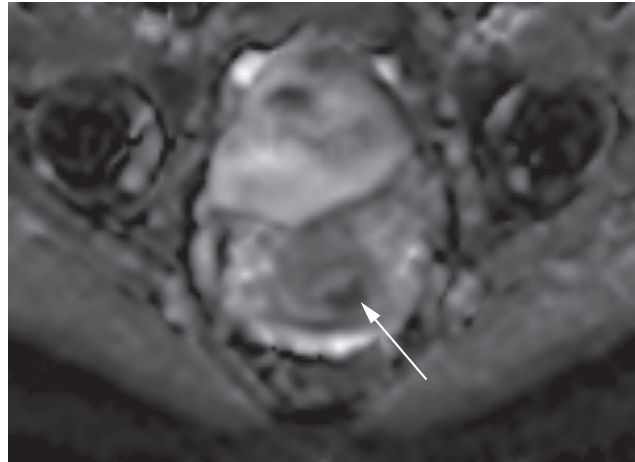
Magnetic resonance imaging of the heart uses electronic gating to obtain images during a specific portion of the cardiac cycle. With this technique it is possible to limit the degradation of the image by cardiac motion and demonstrate the cardiac chambers, valves and myocardium.

Alternatively, the beating heart can be directly visualized as a cine image.

One of the advantages of MRI is that it involves no ionizing radiation. The strong magnetic fields, however, mean that it is at present contraindicated in patients with certain implantable devices, including cardiac pacemakers, certain types of aneurysm clip and intraocular metallic foreign bodies.



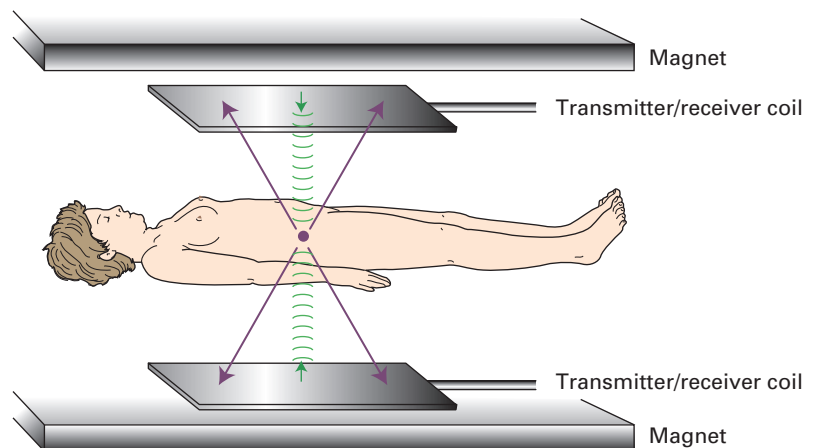
(a)



(b)

Fig. 1.15 Diffusion-weighted imaging. (a) A diffusion-weighted image with b value 750 demonstrating a small cervix cancer with high signal intensity (arrow). (b) The corresponding apparent diffusion coefficient (ADC) map demonstrates low signal intensity at the same position (arrow). This combination of high signal intensity on the high b value image and low signal intensity on the ADC map is consistent with restricted water diffusion, a characteristic feature of many cancers.

Fig. 1.16 Diagram of an MRI machine. The patient lies within a strong magnet (usually a cylindrical magnet). The radiofrequency transmitter coils send radiowaves into the patient and the same coils receive signals from within the patient. The intensity and source of these signals can be calculated and displayed as an image.



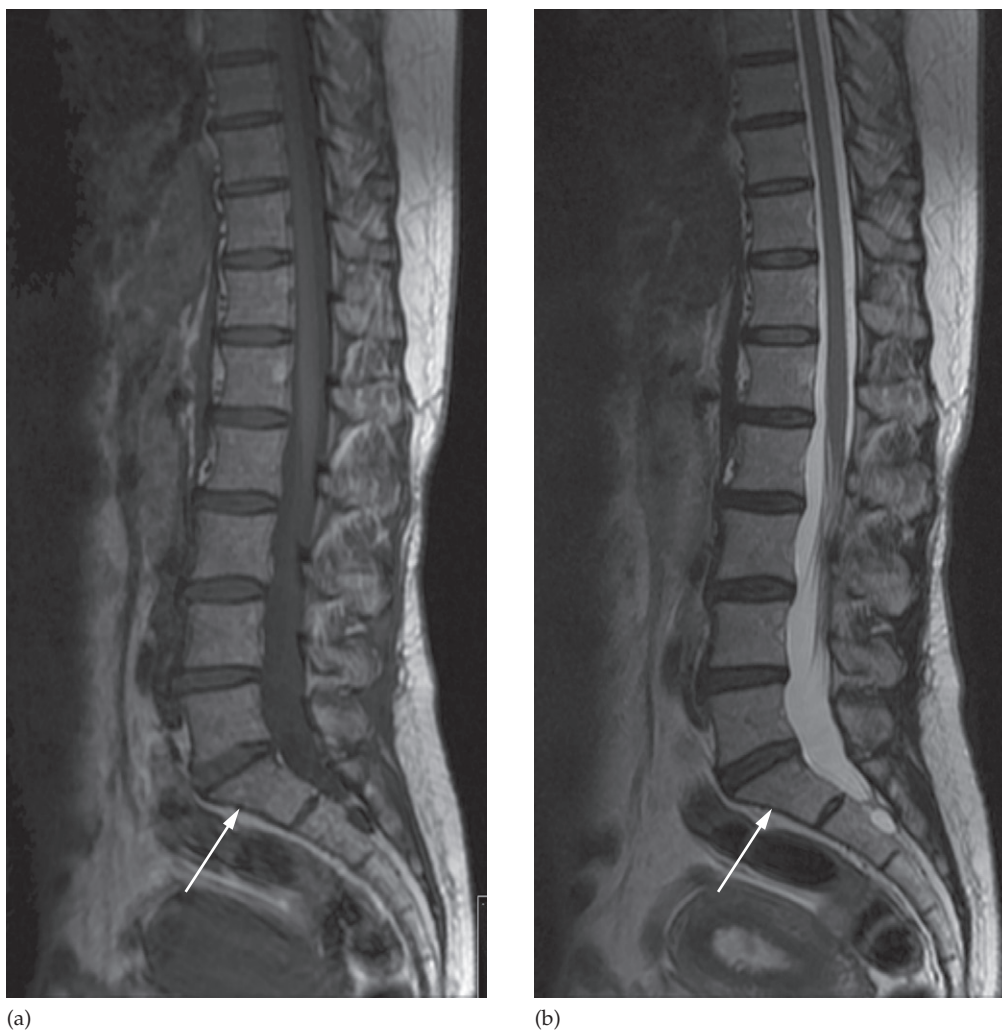


Fig. 1.17 MRI of a sagittal section of lumbar spine. (a) On this T1 sequence, the spinal cord is grey, cerebrospinal fluid (CSF) is nearly black and subcutaneous fat is white. (b) T2-weighted sequence. Here the CSF is white. Cortical bone (arrows) returns no signal and appears as a black line on both sequences. The fat in the bone marrow produces a signal that enables the vertebrae to be visualized.

Contrast agents for magnetic resonance imaging

Just as contrast media have been of great value in CT, magnetic contrast materials are providing useful diagnostic information with MRI. The most widely used agents are gadolinium compounds which only cross the blood–brain barrier when it is damaged by disease (see Fig. 1.14c), and which concentrate in tissues and disease processes with a

high blood supply. Tissues that concentrate the agent show very high signal intensity (i.e. they appear white) on T1-weighted images. Tissue-specific media, such as hepatocyte-specific agents and iron oxide agents for reticuloendothelial cell imaging, are also used. A particular application of contrast-enhanced MRI is magnetic resonance angiography, which along with CT angiography is gradually replacing conventional diagnostic angiography.

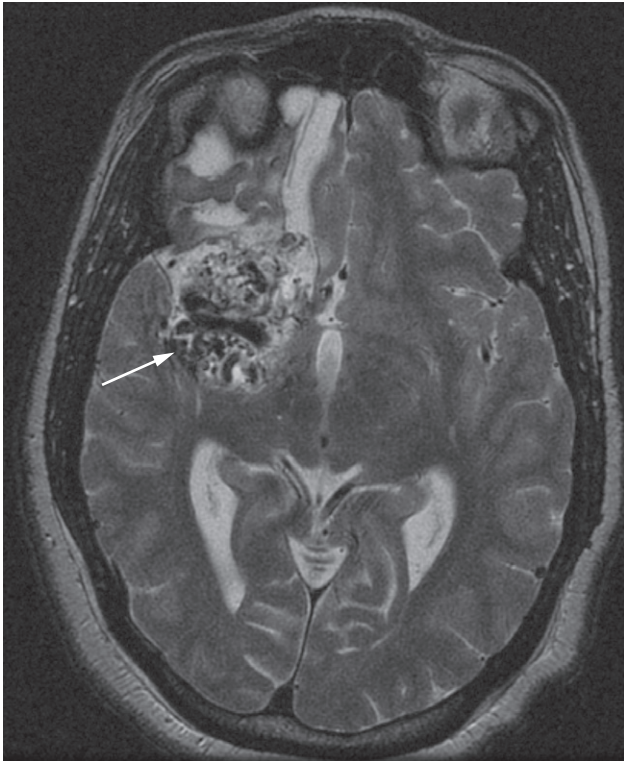


Fig. 1.18 MRI of brain showing an arteriovenous malformation (arrow) in the right cerebral hemisphere. The fast-flowing blood in the malformation is responsible for the absence of signal (signal void). The image is a T2-weighted image, and is normal apart from the arteriovenous malformation and its consequences.

Gadolinium-based contrast agents are generally very safe and anaphylactic reactions are rare. They are contraindicated in pregnancy. Also, it has recently been recognized that patients in renal failure, on dialysis or awaiting liver transplantation are at risk of developing nephrogenic systemic fibrosis, which can be fatal. In these patients, the magnetic resonance scan is done without the use of gadolinium-based contrast agents.

Picture archiving and communication systems

Digital recording has developed dramatically over the past two decades. CT, ultrasound, MRI, nuclear medicine and angiography are nowadays all digital techniques. Con-

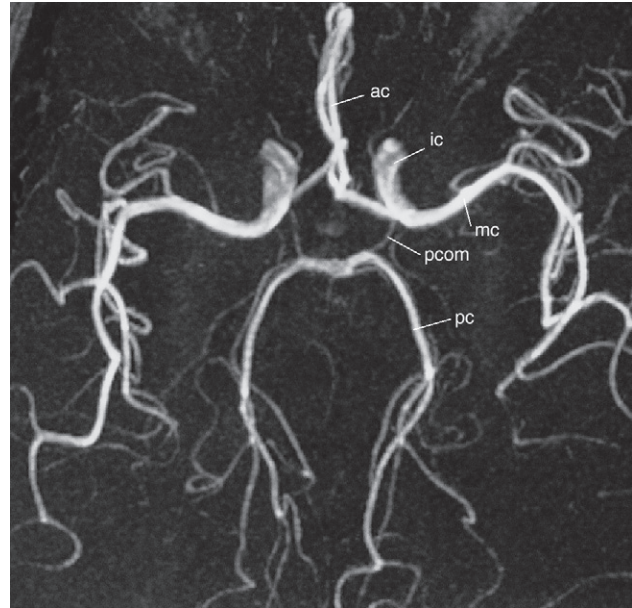


Fig. 1.19 Magnetic resonance angiogram of the intracranial arteries. No contrast medium was used to obtain this image. ac, anterior cerebral; ic, internal cerebral; mc, middle cerebral; pc, posterior cerebral; pcom, posterior communicating artery.

ventional radiographs are now predominantly in digital format.

Digital data can be processed by a computer, which allows electronic transmission of images between buildings, towns and countries, and most importantly allows computer storage. A fully digital department obviates the need for x-ray films; it enables radiologists to report from images displayed on high definition screens and the images as well as their reports to be readily viewed by clinicians on computers in their clinic.

Radiation hazards

X-rays used in conventional radiography and CT, as well as gamma-rays and other radionuclide emissions, are harmful. Natural radiation from the sun and radioactivity in the environment, together with atmospheric radioactivity from nuclear bombs and other man-made ionizing radiations, contribute a genetic risk over which an individual doctor has no control. However, ionizing radiation

for medical purposes is of several times greater magnitude than all other sources of man-made radiation and is under the control of doctors. It is their responsibility to limit the use of x-rays and other ionizing radiations to those situations where the benefit clearly outbalances the risks. Unnecessary radiation is to be deplored. The principle to be used is the so-called ALARA principle: 'as low as reasonably achievable'. This is achieved by the use of appropriate equipment and good technique – limiting the size of the x-ray beam to the required areas, limiting the number of films to those that are necessary, keeping repeat examinations to a minimum and ensuring that the examination has not already been performed. Just as important as these factors, all of which are really the province of those who work in the x-ray department, is the avoidance of unnecessary requests for x-ray examinations, particularly those that involve high radiation exposure such as lumbar spine x-rays and CT examinations. If possible, alternative techniques such as ultrasound or MRI should be considered. In other words, the imaging examination being requested must be justified.

Radiation is particularly harmful to dividing cells. Genetically adverse mutations may occur following radia-

tion of the gonads, resulting in congenital malformations and a genetic risk to the population. There is no threshold for the mutation rate, hence there is no such thing as a safe radiation dose.

Radiation to the developing fetus can have catastrophic effects. As well as the increased incidence of malformations induced in the developing fetus, it has been shown that the frequency with which leukaemia and other malignant neoplasms develop within the first 10 years of life is increased in children exposed to diagnostic x-rays while *in utero*, probably by about 40% compared with the normal population. Performing an x-ray that includes a fetus in the field of view should, therefore, be avoided where possible and exposure should be kept to the absolute minimum.

Radiation-induced cancer is of general concern. It is not known whether exposures of the magnitude used for individual diagnostic examinations induce cancers, but recent estimates suggest that a standard CT examination might be associated with a risk of cancer induction of 1 in 2000. If all radiation-reducing methods were followed, including the elimination of unnecessary examinations, then in the UK it might be possible to reduce the number of cancer fatalities by over 100 cases per year.

2

Chest

THORACIC DISEASE

Imaging techniques

Plain chest radiograph

A routine chest radiograph (CXR) consists of a posteroanterior (PA) view, also known as a frontal view, with the optional addition of a lateral view (Fig. 2.1). Both should be exposed on full inspiration with the patient in the upright position. Films taken on expiration are difficult to interpret, because in expiration the lung bases appear hazy and the heart opacity increases in size (Fig. 2.2).

Even though chest films are the commonest x-ray examinations performed, they are amongst the most difficult to interpret. In developing your interpretation technique, a routine is necessary in order to avoid overlooking valuable radiological signs. The order in which one looks at the structures is unimportant; what matters is to follow a routine, otherwise significant abnormalities will be missed. One approach to examining the frontal and lateral chest films is presented below.

Trace the diaphragm

The upper surfaces of the diaphragm should be clearly visible from one costophrenic angle to the other, except where the heart and mediastinum are in contact with the diaphragm. On a good inspiratory film, the dome of the right hemidiaphragm is at the level of the anterior end of the sixth rib, the right hemidiaphragm being up to 2.5 cm higher than the left.

Check the size and shape of the heart

See Figures 2.1 and 2.3 and Chapter 3 for details.

Check the position of the heart and mediastinum

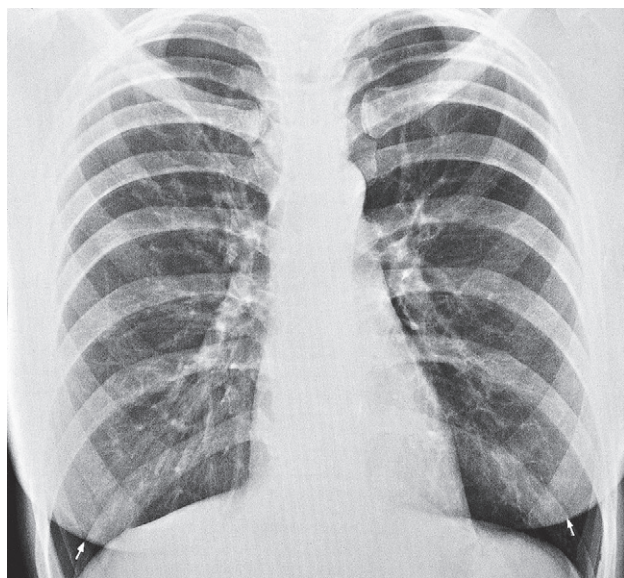
Normally, the trachea lies midway, or slightly to the right of the midpoint, between the medial ends of the clavicles. The position of the heart is variable; on average one-third lies to the right of the midline.

Look at the mediastinum

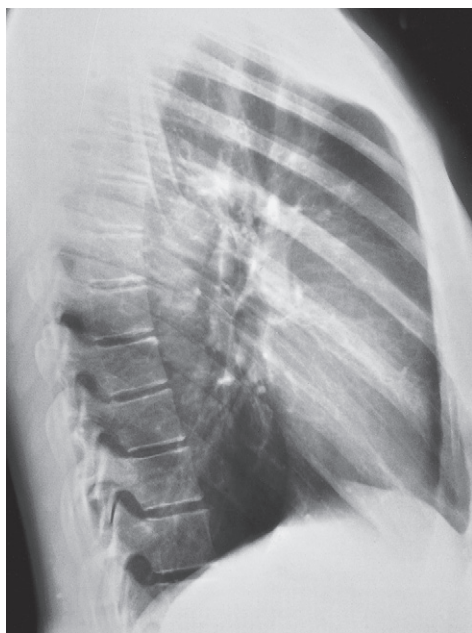
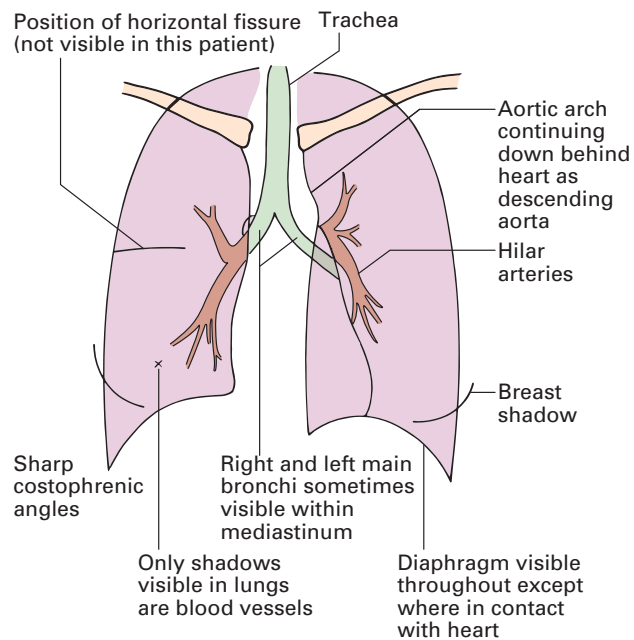
The outline of the mediastinum and heart should be clearly seen, except where the heart lies in contact with the diaphragm. The right superior mediastinal border is usually straight or slightly curved as it passes downwards to merge with the right heart border. The left superior mediastinal border is ill-defined above the aortic arch. With increasing age, the aorta elongates. Elongation necessarily involves unfolding, because the aorta is fixed at the aortic valve and at the diaphragm. This unfolding results in the ascending aorta deviating to the right and the descending aorta to the left. In young children, the normal thymus is often clearly visualized. It may be very large and should not be mistaken for disease (Fig. 2.3).

Examine the hilar structures

The hila represent the pulmonary arteries and veins. Air within the major bronchi can be recognized, but the walls of the bronchi are not usually visible. The hilar lymph nodes in the normal patient are too small to recognize as



(a)



(b)

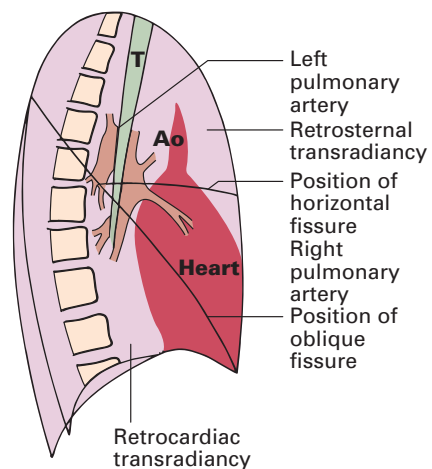
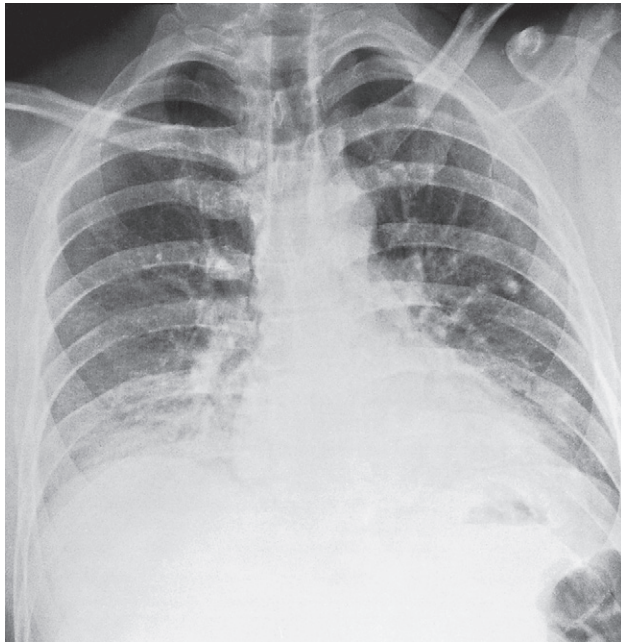
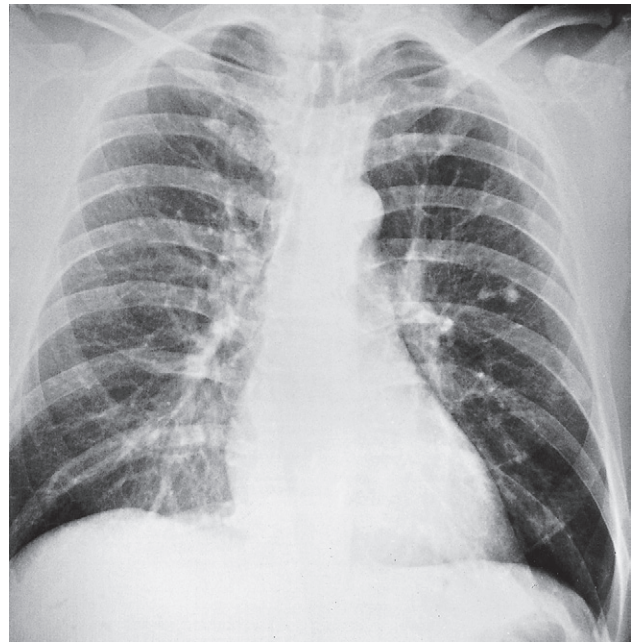


Fig. 2.1 Normal chest. (a) Posteroanterior view. The arrows point to the breast opacities of this female patient. (b) Lateral view. The vertebrae are more transradiant (i.e. blacker) as the eye travels down the spine, until the diaphragm is reached. Ao, aorta; T, trachea.



(a)



(b)

Fig. 2.2 Effect of expiration on chest films showing two films of the same patient taken one after the other. (a) Expiration. (b) Inspiration. On expiration the heart appears larger and the lung bases are hazy.

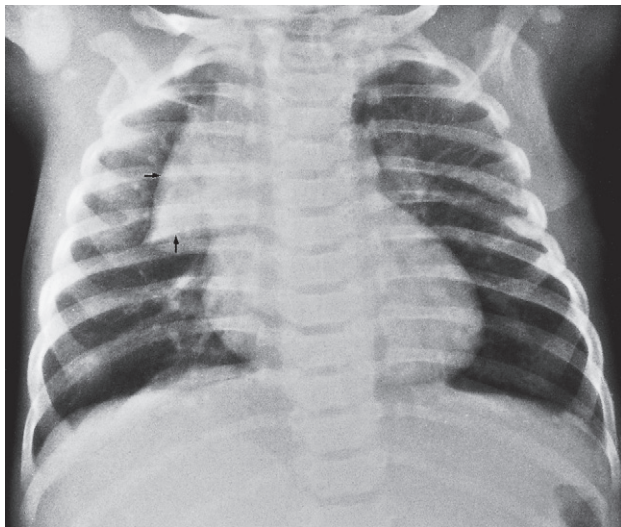


Fig. 2.3 Normal but prominent thymus in a child aged 3 months. The thymus shows the characteristic 'sail shape' projecting to the right of the mediastinum (arrows). This appearance should not be confused with right upper lobe consolidation or collapse.

discrete opacities. The left hilum is usually slightly higher in position than the right.

Examine the lungs

The only structures that can be identified within normal lungs are the blood vessels, the interlobar fissures and the walls of certain larger bronchi seen end-on. The fissures can only be seen if they lie along the line of the x-ray beam; they are, after all, composed of just two layers of pleura. Usually, only the horizontal fissure is visible in the frontal projection, running from the right hilum to the sixth rib in the axilla. There is no equivalent to the horizontal fissure on the left. The oblique fissures are only visible on the lateral view. The fissures form the boundaries of the lobes, so knowing their position is essential for an appreciation of lobar anatomy (Fig. 2.4). In about 1% of people there is an extra fissure visible in the frontal view – the so-called azygos lobe fissure (Fig. 2.5).

Look for abnormal pulmonary opacities or translucencies. Do not mistake the pectoral muscles, breasts (see

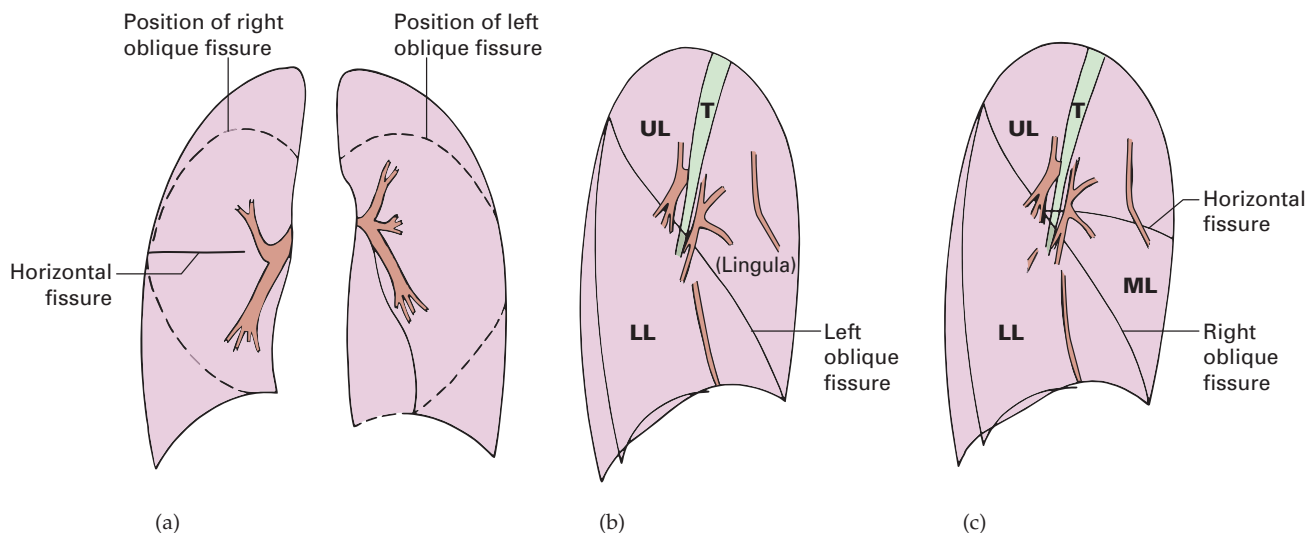
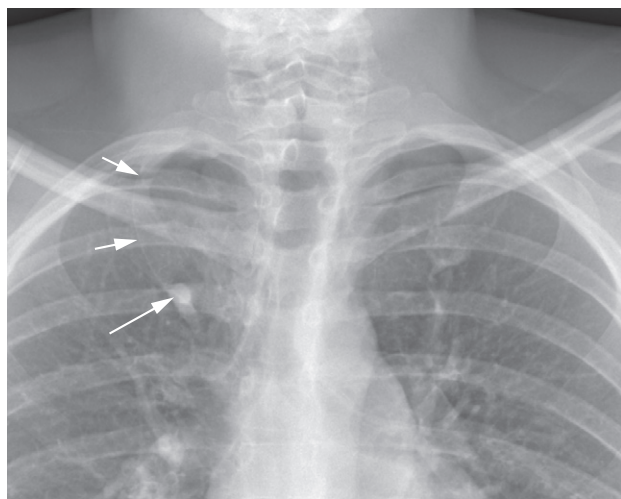
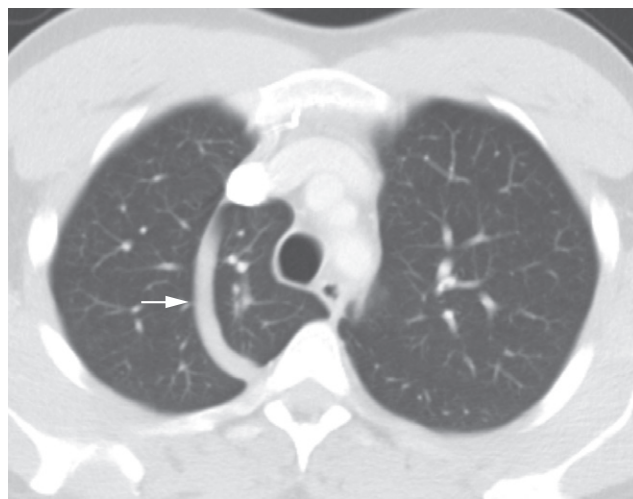


Fig. 2.4 Position of the lobes and fissures. (a) The oblique (major) fissure is similar on the two sides. The oblique fissures are not visible on the frontal view; their position is indicated by dashed lines. (b) In the left lung the oblique fissure separates the upper lobe (UL) and lower lobe (LL). (c) In the right lung, there is an extra fissure – the horizontal (minor) fissure, which separates the upper lobe (UL) and middle lobe (ML). (The lingular segments of the upper lobe are analogous to the segments of the middle lobe.) T, trachea.



(a)



(b)

Fig. 2.5 The azygos lobe fissure. During normal intrauterine development the azygos vein migrates through the lung from the chest wall to lie within the mediastinum. (a) CXR in a patient with an azygos 'lobe', the vein (large arrow) fails to reach the tracheobronchial angle and, therefore, lies in the lower end of the azygos fissure (small arrows). (b) CT in the same patient. The azygos fissure can be clearly seen (small arrow). This variant is of no clinical significance.

Fig. 2.1) or plaits of hair for pulmonary opacities. Skin lumps or the nipples may mimic pulmonary nodules. The nipples are usually in the fifth anterior rib space, but they are, in practice, rarely misdiagnosed because, in general, if one nipple is visible the other should also be seen.

A good method of finding subtle opacities on the frontal film is to compare one lung with the other, zone by zone. Detecting ill-defined opacities on the lateral view can be difficult.

Check the integrity of the ribs, clavicles and spine and examine the soft tissues

The bones of the chest should be checked for fractures and metastases. Any rib notching should be noted as it may indicate coarctation of the aorta. In females, check that both breasts are present. Following mastectomy the breast opacity cannot be defined. The reduction in the soft tissue bulk leads to an increased transradiancy of that side of the chest, which should not be confused with pulmonary disease.

Assess the technical quality of the film

Technical factors are important as incorrect exposure may hide disease, and faulty centring or projection may mimic pathology. The correctly exposed routine PA chest film is one in which the ribs and spine behind the heart can be identified but the lungs are not overexposed. Unless one can see through the heart, lower lobe lesions may be completely missed. A straight film is one where the medial ends of the clavicles are equidistant from the thoracic vertebrae.

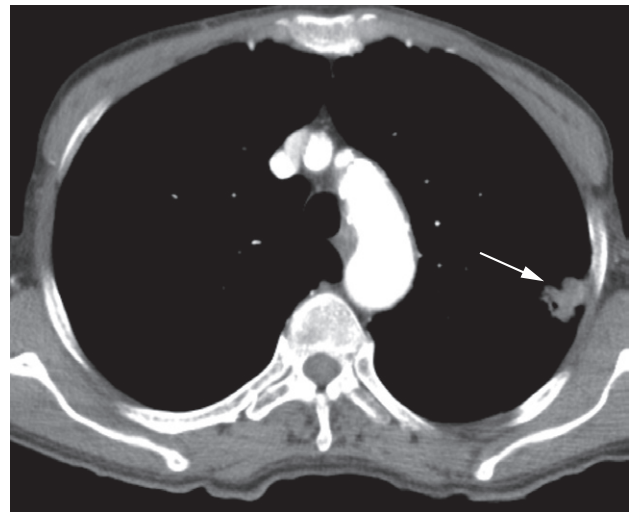
Computed tomography

Technique

A routine chest computed tomography (CT) examination consists of contiguous sections. Intravenous contrast medium is given in many cases, particularly when the purpose of the examination is to visualize the mediastinum, the hila or the pulmonary blood vessels. The images are usually viewed at both lung and mediastinal and bone window settings (Fig. 2.6) (see Fig. 1.2 for an explanation of CT windows and levels).



(a)



(b)

Fig. 2.6 Chest CT illustrating the different window centres (levels) used for the lungs and mediastinum. (a) Lung settings. A negative centre (minus 700 Hounsfield units [HU]) and a wide window width (1000 HU) shows the lungs to advantage, but there is no detail of mediastinal structures, the mediastinum being uniformly white. In this example, the lung vessels are the only identifiable opacities originating from within the lung. Note the peripheral left lung cancer (arrow). (b) Mediastinal settings. A centre close to average soft tissue density (40 HU) and a narrow window width (400 HU) shows the structures within the mediastinum clearly, but the lungs are blacked out. The lung cancer is arrowed.

Thin sections can be used to produce images with higher spatial resolution – so-called high resolution CT (HRCT). HRCT better demonstrates pulmonary parenchymal disease and bronchiectasis.

Indications

There are many indications for CT in chest disease, notably:

- Evaluating abnormalities on a CXR.
- Investigating causes of breathlessness:
 - acute, e.g. ?pulmonary embolus
 - chronic, e.g. interstitial lung disease.
- Staging of cancer.
- Evaluation of vascular anatomy, e.g. thoracic aortic aneurysms/dissection (Fig. 2.7).
- Performing CT-guided biopsy of a lung/pleural/mediastinal mass.

Normal images

Just as on CXRs, the only structures seen on CT within the normal lungs are blood vessels, pleural fissures and the walls of bronchi. Vessels within the lung are recognized by their shape rather than by contrast opacification (see Fig. 2.6a) and are distinguished from small lung nodules by their branching morphology and continuity observed during scrolling through the images on the workstation. Any uncertainty is usually resolved by review in the sagittal or coronal reformat or with the use of thick maximum intensity projections (MIPs), which enhances the three-dimensional nature of the nodules and helps differentiate them from pulmonary bronchi and vessels (Fig. 2.8).

The fissures may be seen as a line, or their position may be recognizable only as a relatively avascular zone within the lung. The CT appearances of the normal mediastinum and hilar are discussed later in this chapter.

Magnetic resonance imaging

Magnetic resonance imaging (MRI) has only a very small role in the management of pulmonary, pleural or mediastinal disease, although it is playing an increasingly large part in the diagnosis of cardiac and aortic diseases. MRI can be useful in selected patients with lung cancers, particularly apical tumours, when the relevant questions cannot

be answered by CT and MRI can show the intraspinal extent of mediastinal neural tumours.

Radionuclide lung scanning

There are two major types of radionuclide lung scan: perfusion and ventilation scans.

Perfusion scans use small particles, approximately 30 µm in diameter, labelled with technetium-99m (^{99m}Tc), injected intravenously. These particles become trapped in the pulmonary capillaries; the distribution of radioactivity, when imaged by a gamma camera, accurately reflects blood flow (Fig. 2.9a).

For ventilation scans, the patient inhales a radioactive gas such as xenon-133, xenon-127 or krypton-81m (^{81m}Kr) and the distribution of radioactive gas is imaged using a gamma camera (Fig. 2.9b).

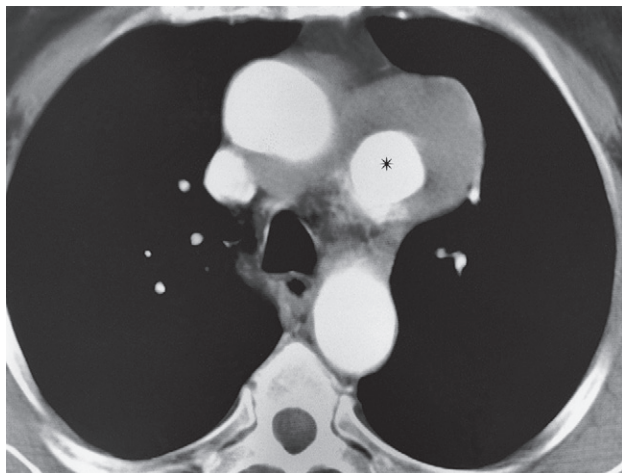
The major indication for radionuclide lung scanning is to diagnose or exclude pulmonary embolism, but this indication has been superseded by CT pulmonary angiography.

Positron emission tomography

See Chapter 1 for a technical description of fluorodeoxyglucose positron emission tomography (FDG-PET)/CT. FDG is taken up by a number of tumours, notably primary lung cancers, metastases and active lymphomatous tissue. FDG-PET/CT (Fig. 2.10) is used to stage lung cancer or lymphoma and to diagnose recurrent lung cancer. It is also increasingly used to diagnose the malignant nature of a solitary pulmonary nodule as well as pleural disease. Unfortunately, inflammatory conditions also concentrate FDG, so the appearances are not entirely specific for neoplastic tissue.

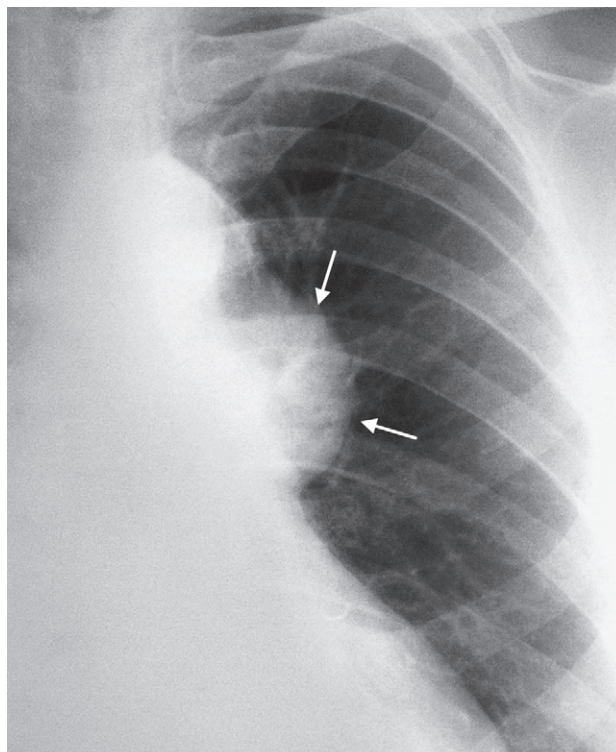
Ultrasound

The use of thoracic ultrasound, as opposed to cardiac ultrasound (see Chapter 3), is confined to processes in contact with the chest wall, notably pleural effusions, pleural masses and selected mediastinal masses. It can be very useful for guiding a needle to sample or drain loculated pleural fluid collections and for needle biopsy/aspiration cytology of masses in contact with the chest wall. As ultra-

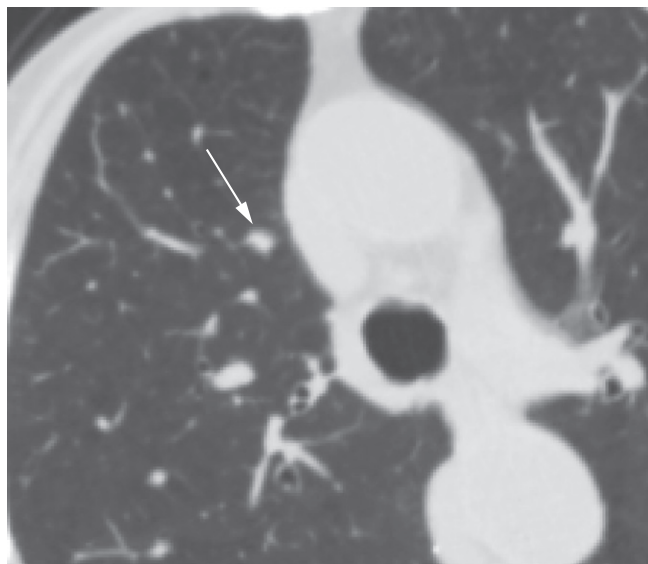


(a)

Fig. 2.7 Aortic aneurysm. (a) Example of the use of contrast-enhanced CT to diagnose an aortic aneurysm. The lumen of the aneurysm (*) enhances brightly. Much of the aneurysm is lined by clot. (b) The CXR shows a mass (arrows), but the precise diagnosis of aortic aneurysm cannot be made.



(b)



(a)



(b)

Fig. 2.8 Lung nodule (arrow) on (a) thin (0.6 mm) and (b) thick (11 mm) maximum intensity projection (MIP) images. On the thick MIP image, the nodule can clearly be identified separate from the adjacent branching vessels.

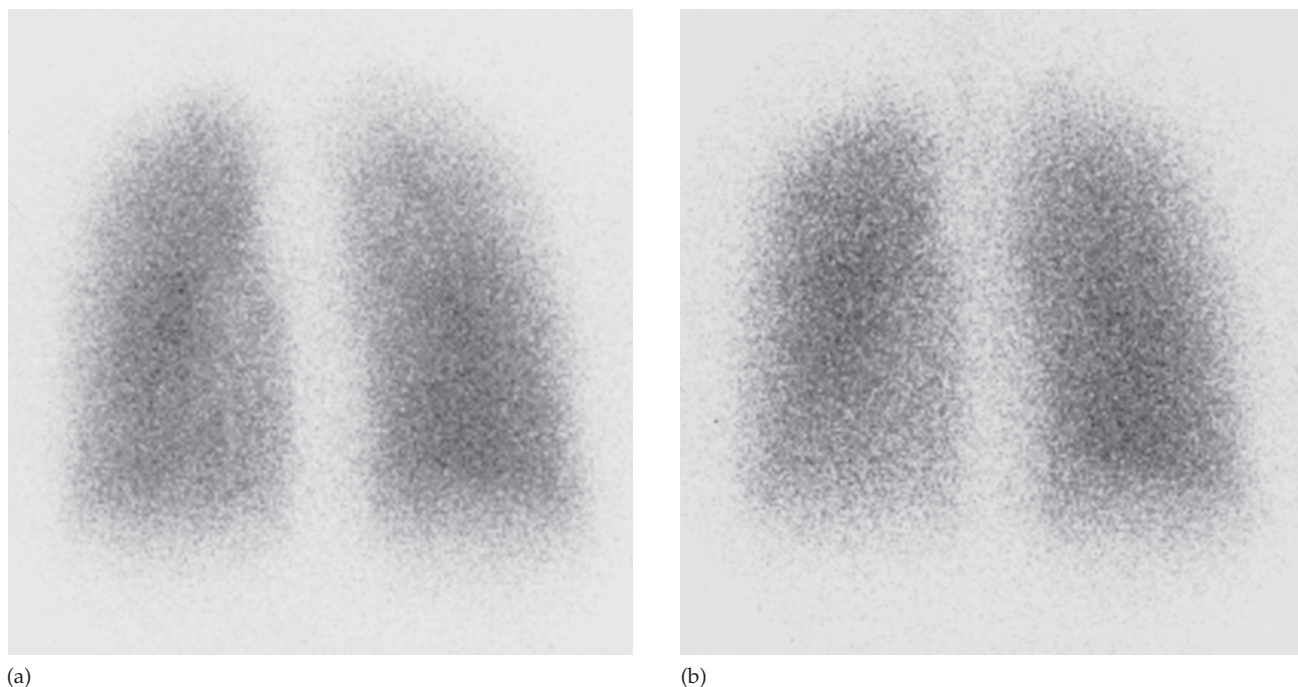


Fig. 2.9 (a) Normal radionuclide perfusion scan (posterior view) using ^{99m}Tc -labelled macroaggregates of albumin. (b) Normal radionuclide ^{81m}Kr ventilation scan (posterior view).

sound is absorbed by air in the lung, ultrasound cannot be used to evaluate processes that lie deep to aerated lung tissue.

It is possible to pass a small ultrasound probe through an endoscope in either the oesophagus or bronchus to visualize structures immediately adjacent to the oesophagus, e.g. para-oesophageal nodes and the descending aorta (see Figs 2.70 and 2.71).

Diseases of the chest with a normal chest radiograph

Serious respiratory disease may exist in patients who have a normal chest radiograph. Sometimes it is only possible to detect abnormality by comparison with previous or later examinations, e.g. subtle pulmonary opacities from infec-

tion or pulmonary fibrosis. Chest disease with a normal chest radiograph occurs in the following situations.

Obstructive airways disease

Asthma and acute bronchiolitis may produce overinflation of the lungs, but in many cases the chest film is normal. Emphysema, when severe, gives rise to the signs described in the section 'Diseases of the airways' later in this chapter, but, when the disease is moderate, the chest radiograph may be normal or very nearly so. Uncomplicated acute or chronic bronchitis does not usually produce any radiological signs, so if a patient with chronic bronchitis has an abnormal film some other disease or a complication has developed, e.g. pneumonia or cor pulmonale. Many patients with productive cough due to bronchiectasis show no plain film abnormality.

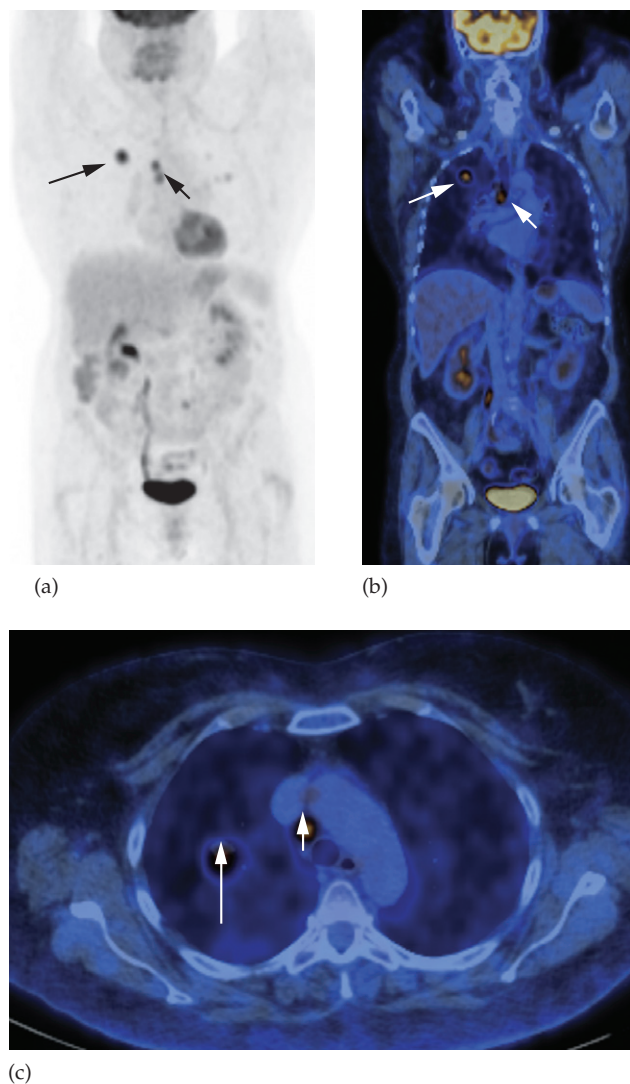


Fig. 2.10 FDG-PET scan of the chest and abdomen showing a focus of high activity in a lung cancer (large arrow) and mediastinal lymph node metastasis (small arrow). (a) Maximum intensity projection (MIP). (b) Coronal fused PET/CT. (c) Axial fused PET/CT. No other abnormality is seen on any of the images. High activity in the myocardium, kidneys and bladder is normal.

Small lesions

It is usually impossible to see solitary lung masses or consolidations of less than 1 cm in diameter. Even 2–3 cm lung cancers may be very difficult to identify on routine films if they are hidden by ribs or clavicles or if they lie behind the heart or diaphragm.

Endobronchial lesions, such as carcinoma, cannot be diagnosed on routine films unless they cause collapse/consolidation.

Pulmonary emboli without infarction

The chest radiograph is often normal even when life-threatening emboli are present.

Infections

Most patients with acute bacterial pneumonia present with recognizable consolidation, but in other infections, notably *Pneumocystis carinii* pneumonia, obvious pulmonary consolidation may only develop after the onset of symptoms. Patients with miliary tuberculosis may initially have a normal chest film.

Diffuse pulmonary fibrosis

Widespread pulmonary fibrosis may be responsible for breathlessness with substantial alteration in lung function tests before any clear-cut abnormalities are evident on chest radiographs.

Pleural abnormality

Dry pleurisy does not produce any radiological findings and small amounts of pleural fluid may be impossible to recognize on standard chest films.

Mediastinal masses

Plain chest radiography is very insensitive for the diagnosis of mediastinal masses, lymph node enlargement and mediastinal fluid collections.

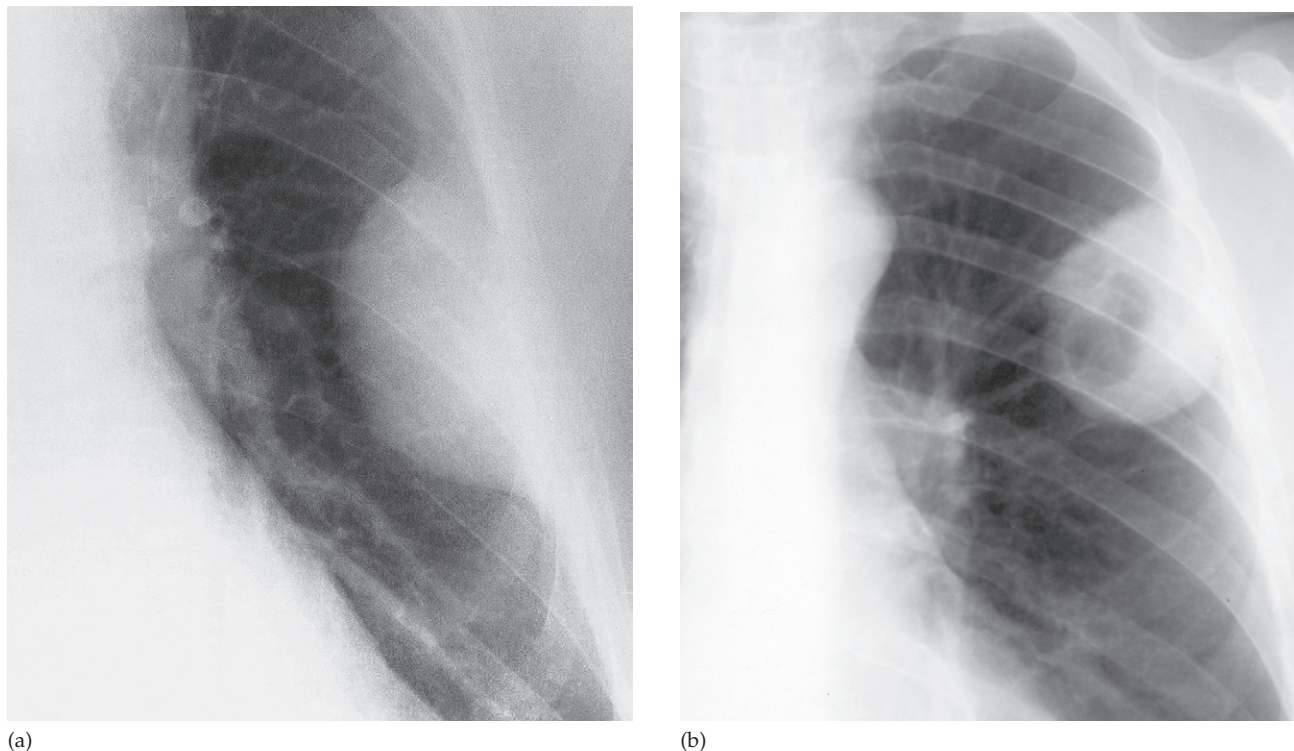


Fig. 2.11 (a) Extrapleural mass. The mass has a smooth convex border with a wide base on the chest wall (a myeloma lesion arising in a rib). This shape is quite different from a peripherally located pulmonary mass such as a primary carcinoma of the lung (b).

Abnormal chest signs

When viewing an abnormal examination of the chest, be it a plain film, CT or MRI, the first questions to ask are ‘Where is the abnormality?’ and ‘How extensive is it?’. Only then can the question ‘What is it?’ be answered, because the differential diagnosis for pulmonary lesions is clearly quite different from that for mediastinal, pleural or chest wall disease.

The first step is to examine all available films. Usually, the location of a lesion will be obvious. If the abnormality is surrounded on all sides by aerated lung it must arise within the lung. Similarly, many masses are clearly within the mediastinum. However, when a lesion is in contact with the pleura or mediastinum it may be difficult to decide its origin.

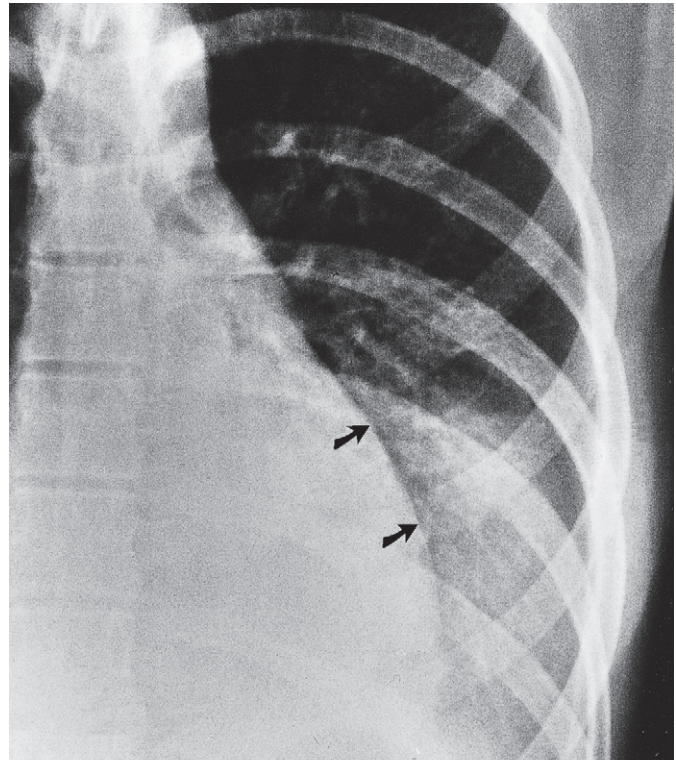
If the opacity has a broad base with smooth convex borders projecting into the lung and a well-defined outline it is likely to be pleural, extrapleural or mediastinal in origin (Fig. 2.11).

Silhouette sign

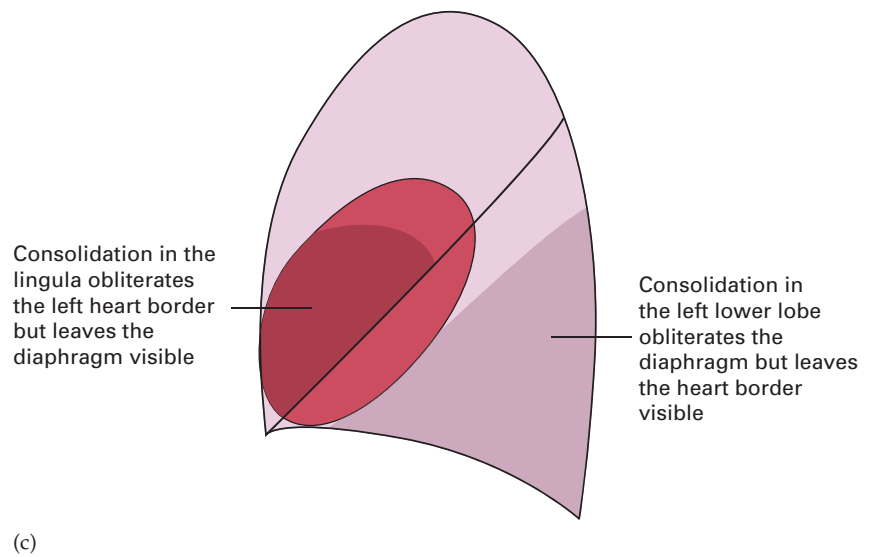
The silhouette sign (Fig. 2.12) is an invaluable sign for localizing disease from on the CXR. The information on a CXR is largely dependent on the contrast between air in the lungs compared with the opacity of the heart, blood vessels, mediastinum and diaphragm. An intrathoracic lesion touching the heart, aorta or diaphragm obliterates the border of the structure in question. This sign is known as the silhouette sign and has two important applications:



(a)



(b)



(c)

Fig. 2.12 The silhouette sign. (a) The left heart border is invisible because it is in contact with consolidation in the adjacent lingula. (b) The left heart border can be seen because the consolidation is in the left lower lobe and air in the lingula preserves the visibility of the cardiac silhouette (arrows). Note that now it is the diaphragm outline that is invisible. (c) A side view diagram of the lung explaining the relationship of the lingula and lower lobes to the heart and diaphragm.

1 It is often possible to localize an opacity by observing which borders are lost, e.g. loss of the heart border means that the opacity lies in the anterior half of the chest. Alternatively, loss of part of the diaphragm outline indicates disease of the pleura or of the lung in direct contact with the diaphragm, usually the lower lobes.

2 The silhouette sign makes it possible, on occasion, to diagnose disorders such as pulmonary consolidation or collapse even when the presence of an opacity is uncertain. It is a surprising fact that a wedge- or lens-shaped opacity may be very difficult to see because of the way it fades out at its margins, but if such a lesion is in contact with the mediastinum or diaphragm these will lose their normally sharp outlines.

Radiological signs of lung disease

It is helpful to try and place any abnormal intrapulmonary opacities into one or more of the broad categories shown in Box 2.1.

Air-space opacification

Air-space opacification means the replacement of air in the alveoli by fluid or other materials (e.g. pus or blood). The fluid can be either an exudate (often called 'consolidation') or a transudate (pulmonary oedema – a topic discussed later in this chapter). The signs of consolidation are:

- An opacity with ill-defined borders (Fig. 2.13), except where the opacity is in contact with a fissure, in which case the opacity has a well-defined edge.
- An air bronchogram (Fig. 2.14). Normally, it is not possible to identify air in bronchi within normally aerated lung, because the walls of the normal bronchi are too thin and air-filled bronchi are surrounded by air in the alveoli. However, if the alveoli are filled with fluid, the air in the

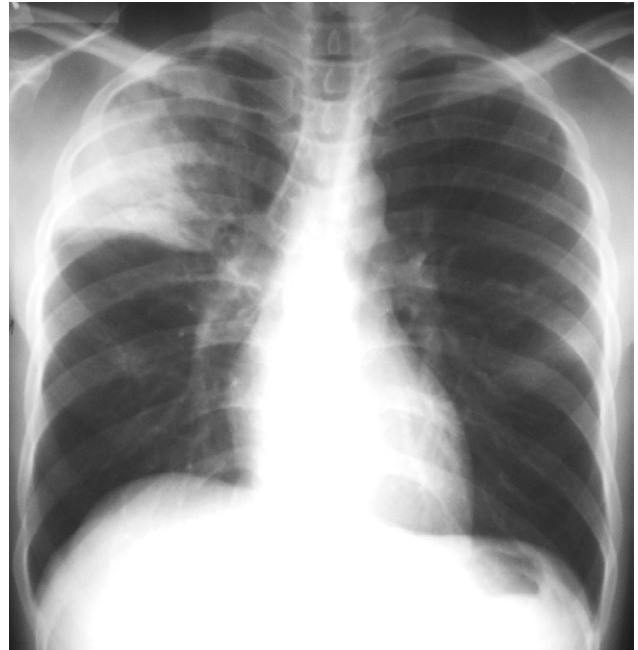


Fig. 2.13 Air-space filling. In this case, the consolidation in the right upper lobe is due to pneumonia.

bronchi contrasts with the fluid in the adjacent lung. This sign is seen to great advantage on CT (Fig. 2.15).

- The silhouette sign, namely loss of visualization of the adjacent mediastinal or diaphragm outline (see above for an explanation of this sign).

Consolidation of a whole lobe, or the majority of a lobe, is virtually diagnostic of bacterial pneumonia. The diagnosis of lobar consolidation requires an appreciation of the radiological anatomy of the lobes (see Fig. 2.4). Lobar consolidation produces an opaque lobe, except for air bronchograms. Because of the silhouette sign, the boundary between the affected lung and the adjacent heart, mediastinum and diaphragm is invisible. Figure 2.16 shows an example of lobar consolidation.

Patchy consolidation, i.e. one or more patches of ill-defined opacifying (Fig. 2.17), is usually due to:

- pneumonia
- infarction
- contusion
- immunological disorders.

Box 2.1 Radiological signs of lung disease

- Air-space opacification
 - Pulmonary collapse (atelectasis)
 - Spherical/nodular opacities
 - Linear opacities
 - Widespread small opacities
- The presence of cavitation or calcification should be noted

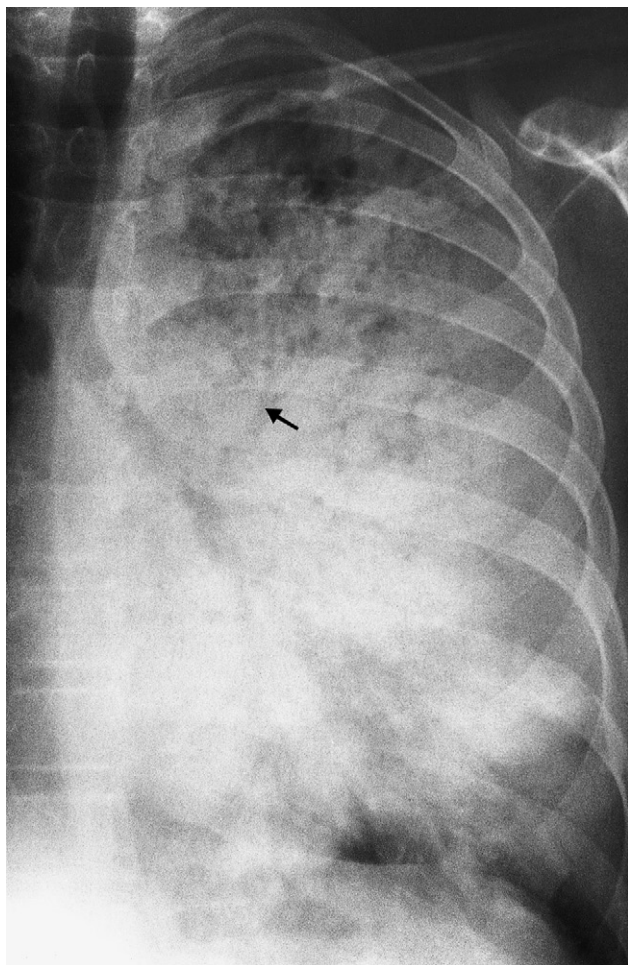


Fig. 2.14 The air bronchogram sign. An extensive air bronchogram is seen in this patient with pneumonia. The arrow points to a bronchus that is particularly well seen.

There is no reliable way of telling from either CXR or CT which of these possibilities is the cause. In most instances the clinical and laboratory findings point to one or other cause.

Cavitation (abscess formation) within consolidated areas in the lung may occur with many bacterial and fungal infections (Fig. 2.18). Abscess formation is only recognizable once there is communication with the bronchial tree, allowing the liquid centre of the abscess to be coughed up

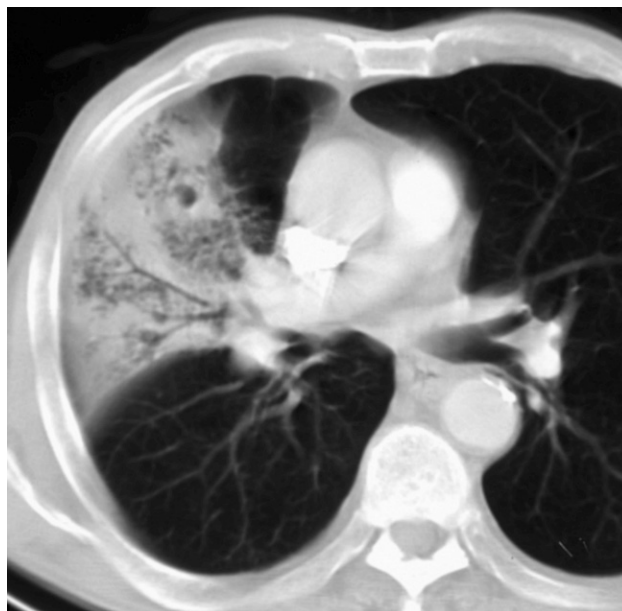


Fig. 2.15 The air bronchogram sign. CT showing an air bronchogram in an area of pulmonary consolidation from pneumonia.

and replaced by air. The air is then seen as a transradiancy within the consolidation and an air–fluid level may be present (Fig. 2.19). Cavitation is occasionally seen in other forms of pulmonary consolidation, e.g. infarction and Wegener’s granulomatosis. CT is better and more sensitive than CXR for demonstrating cavitation (Fig. 2.20).

Pulmonary collapse (atelectasis)

The common causes of pulmonary collapse (loss of volume of a lobe or lung) are:

- bronchial obstruction
- pneumothorax or pleural effusion
- linear atelectasis.

Collapse caused by bronchial obstruction

Collapse caused by bronchial obstruction occurs because air cannot get into the lung in sufficient quantities to replace the air absorbed from the alveoli. The signs of lobar collapse are:



(a)



(b)

Fig. 2.16 Consolidation of the right lower lobe. Note the application of the silhouette sign here. (a) Posteroanterior view. The heart border and the medial half of the right hemidiaphragm are visible, whereas the lateral half is invisible. (b) On the lateral view, the oblique fissure forms a well-defined anterior boundary and the right hemidiaphragm is ill defined. Only the left hemidiaphragm is seen clearly.

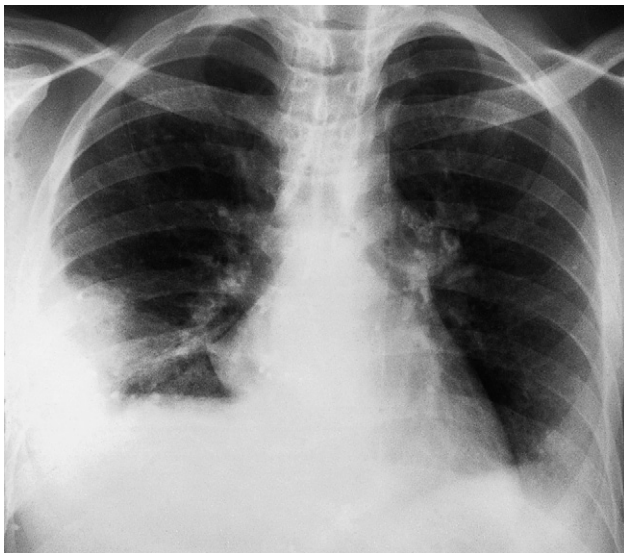
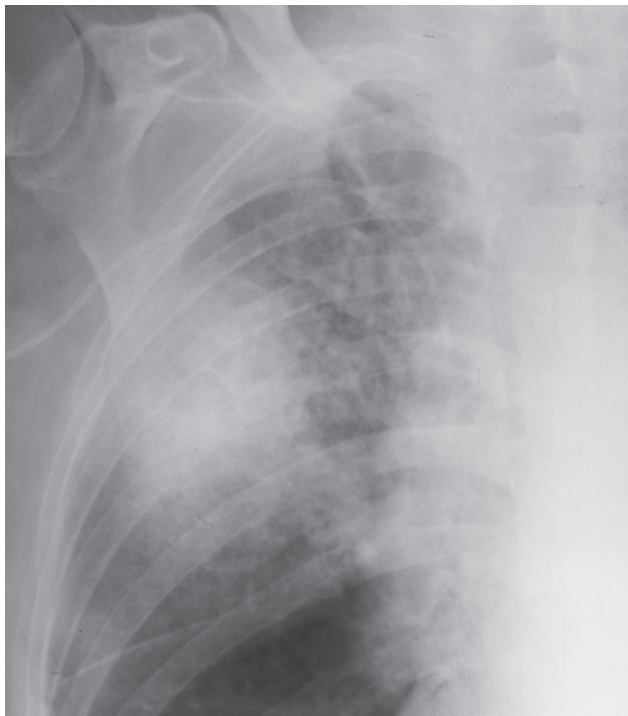
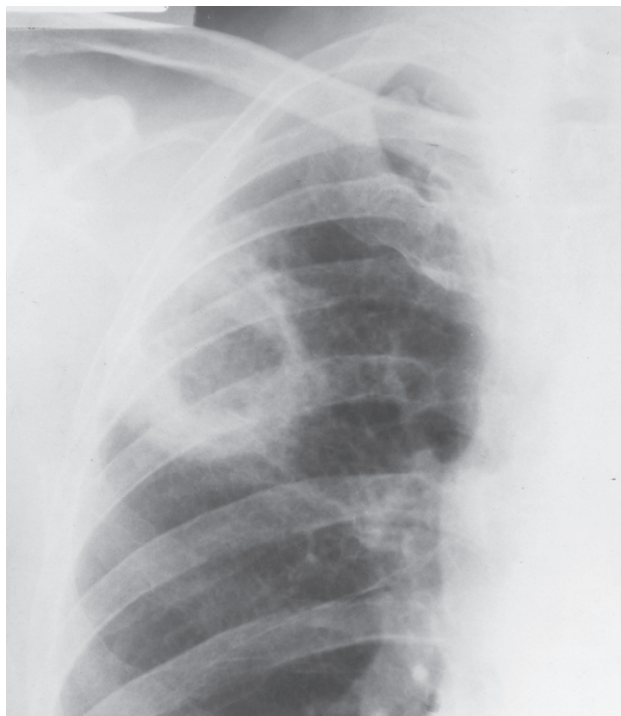


Fig. 2.17 Patchy consolidation in both lower lobes in a patient with bronchopneumonia.



(a)



(b)

Fig. 2.18 Cavitation in staphylococcal pneumonia. (a) A round area of consolidation which, 7 days later (b) shows central translucency due to the development of cavitation.

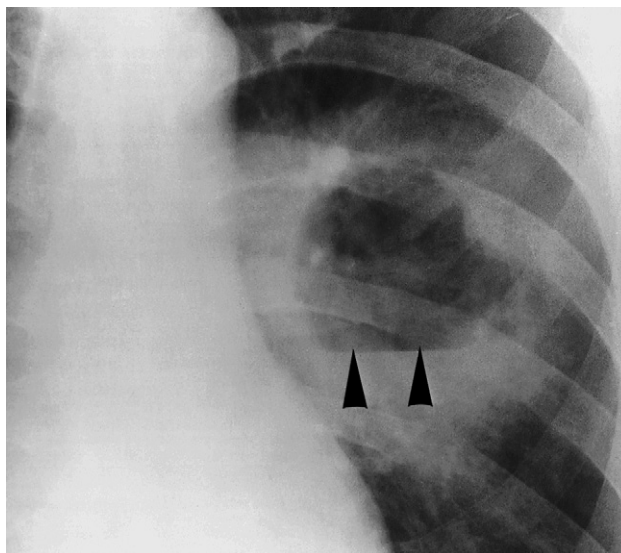


Fig. 2.19 Fluid level (arrowheads) in a lung abscess. Fluid levels are only visible if the chest radiograph is taken with a horizontal x-ray beam.

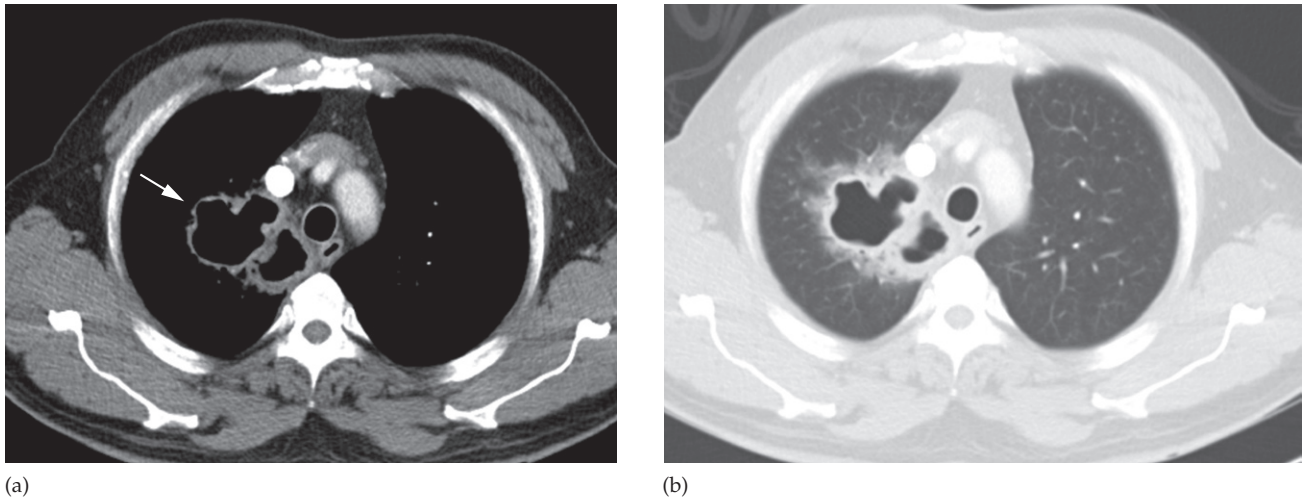


Fig. 2.20 Bacterial lung abscess shown by CT on (a) mediastinal and (b) lung windows. Note the thick-walled, air-filled cavity. The abscess is arrowed in (a).

- Displacement of mediastinal structures.
- Opacification of the collapsed lobe
- The silhouette sign. This not only helps diagnose lobar collapse when the resulting opacity is difficult to appreciate, but also helps to decide which lobe is collapsed. Collapse of the anteriorly located lobes (upper and middle) obliterates portions of the mediastinal and heart outlines, whereas collapse of the lower lobes obscures the outline of the adjacent diaphragm and descending aorta.

The commoner causes of lobar collapse are:

- Bronchial wall lesions, usually primary carcinoma, but occasionally other bronchial tumours such as carcinoid tumours.
- Intraluminal occlusion, usually foreign body or retained mucus plugs, particularly in postoperative, asthmatic or unconscious patients, or in patients on artificial ventilation.
- Invasion or compression by an adjacent malignant tumour or rarely by enlarged lymph nodes.

When a lobe collapses, the unobstructed lobe(s) on the side of the collapse undergoes compensatory expansion. The mediastinum and diaphragm may move towards the collapsed lobe.

As lobar collapse is such an important and often difficult diagnosis to make on CXR, it is worth devoting time to study the appearance of collapse of each of the lobes

(Figs 2.21–2.25). CT shows lobar collapse very well (Fig. 2.26), but is rarely necessary simply to diagnose a collapsed lobe.

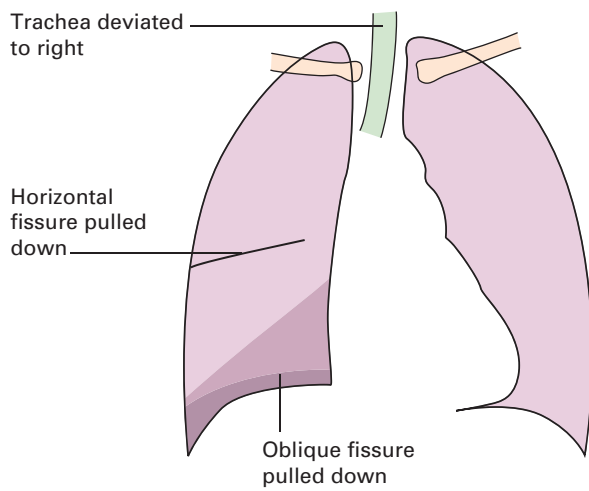
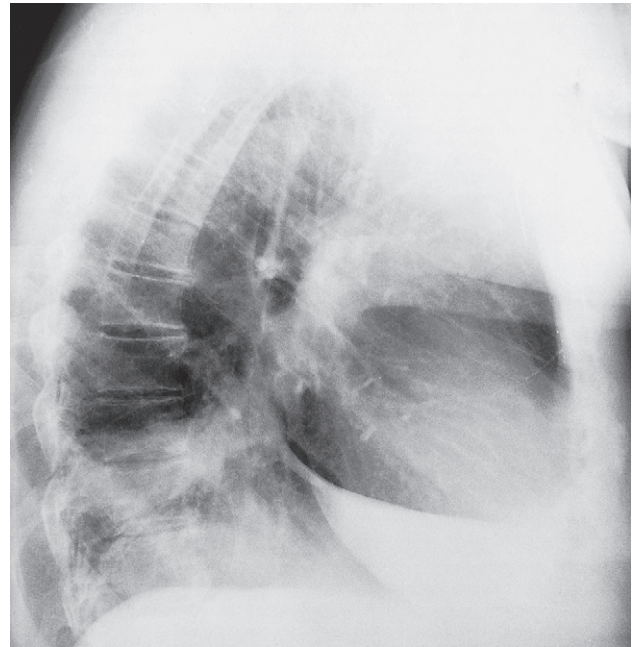
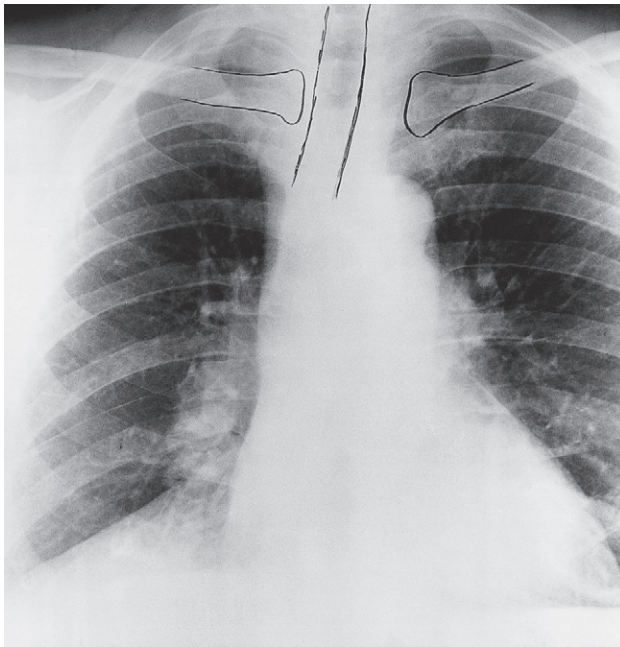
With collapse of the whole of one lung, the entire hemithorax is opaque and there is substantial mediastinal and tracheal shift (Fig. 2.27).

Collapse in association with pneumothorax or pleural effusion

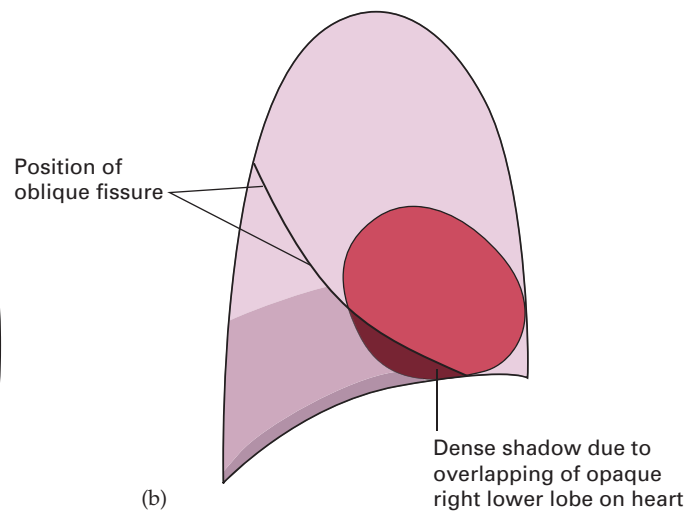
The presence of air or fluid in the pleural cavity allows the lung to collapse. In pneumothorax, the diagnosis is obvious but if there is a large pleural effusion with underlying pulmonary collapse it may be difficult to diagnose the presence of the collapse on a CXR. This problem does not arise with CT where it is easy to recognize pulmonary collapse despite the presence of a pleural effusion (Fig. 2.28). If lobar collapse is identified, it can be difficult to tell whether the collapse is due to pleural fluid or whether both the collapse and the effusion are due to the same process, e.g. carcinoma of the bronchus.

Linear atelectasis

Linear atelectasis is not secondary to bronchial obstruction, it is due to hypoventilation – the commonest cause of which is postoperative or post-traumatic pain. The result

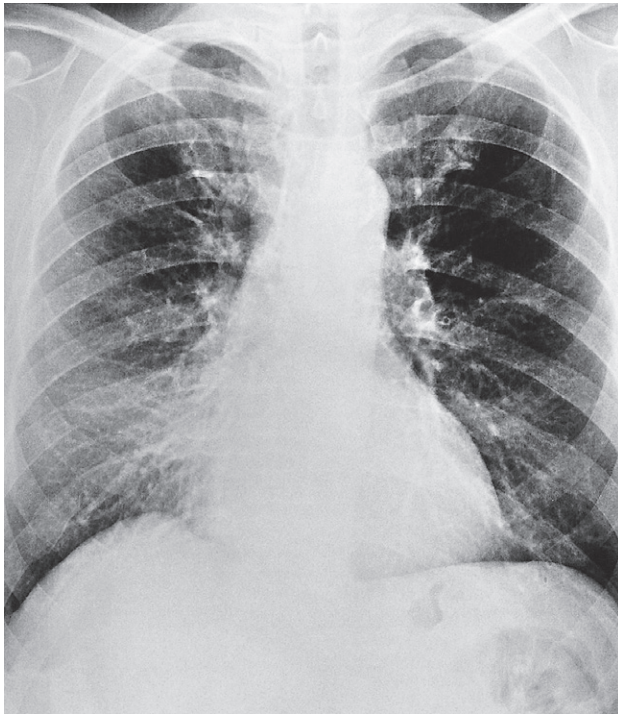


(a)

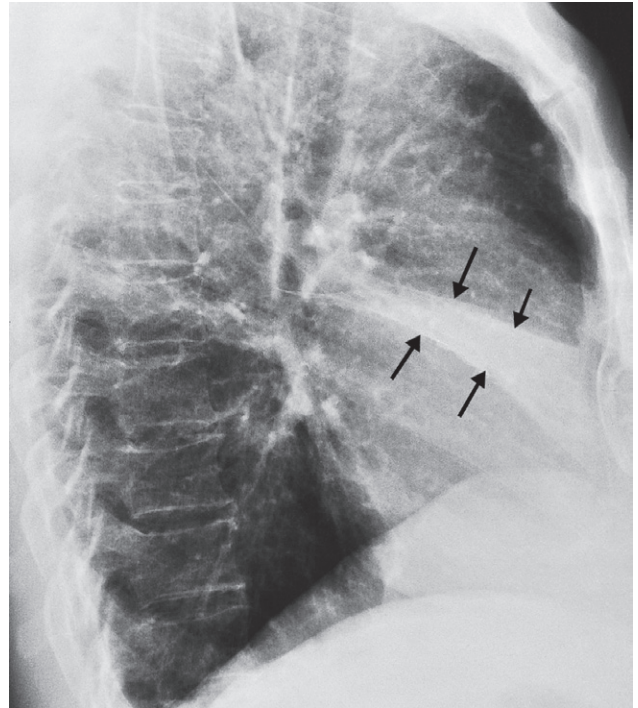


(b)

Fig. 2.21 Collapse of the right lower lobe. (a) Posteroanterior and (b) lateral views. In this example the apical segment is relatively well aerated.



(a)



(b)

Fig. 2.22 Collapse of the middle lobe. (a) Posteroanterior and (b) lateral views. The collapsed lobe is most obvious on the lateral view (arrows). Note the silhouette sign obliterating the lower right heart border.

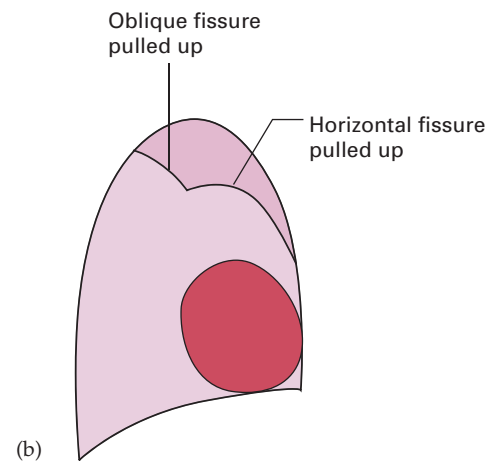
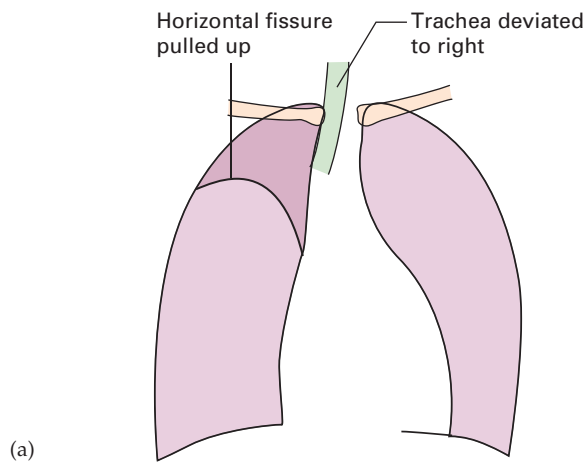
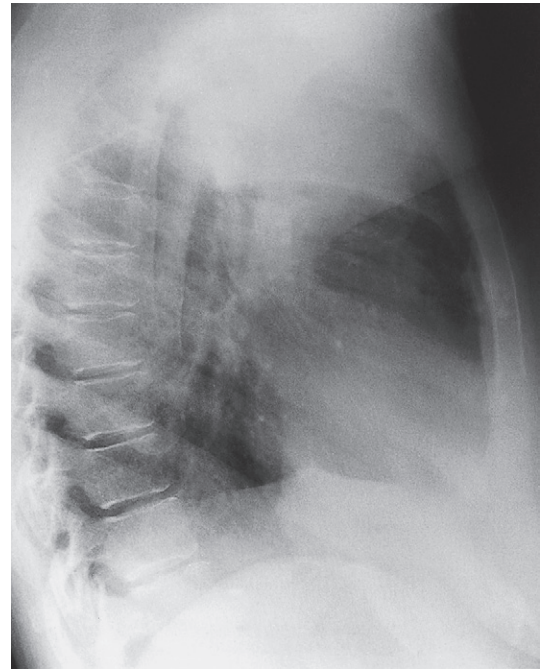
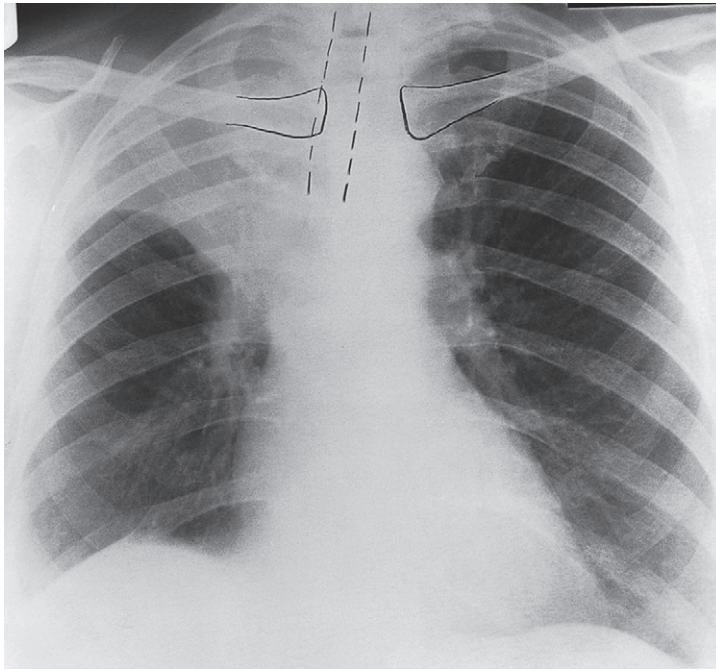
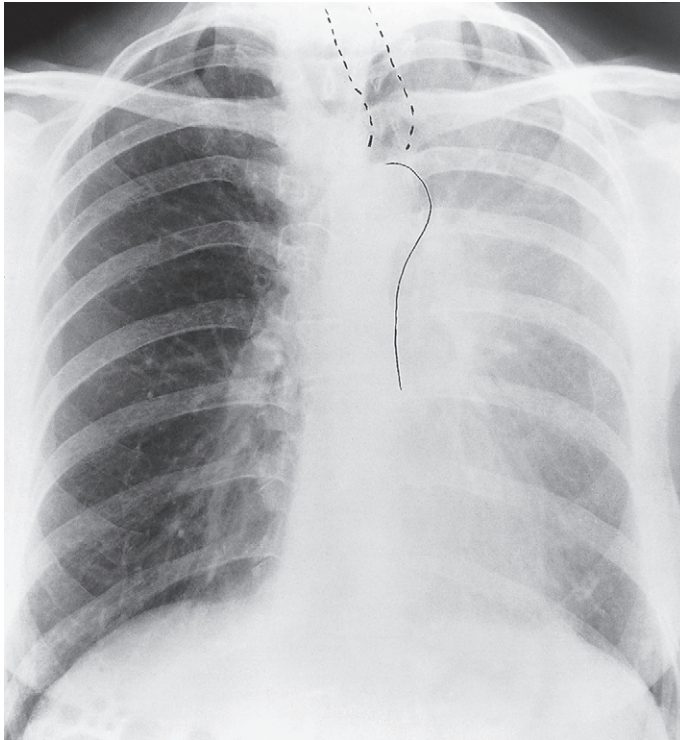
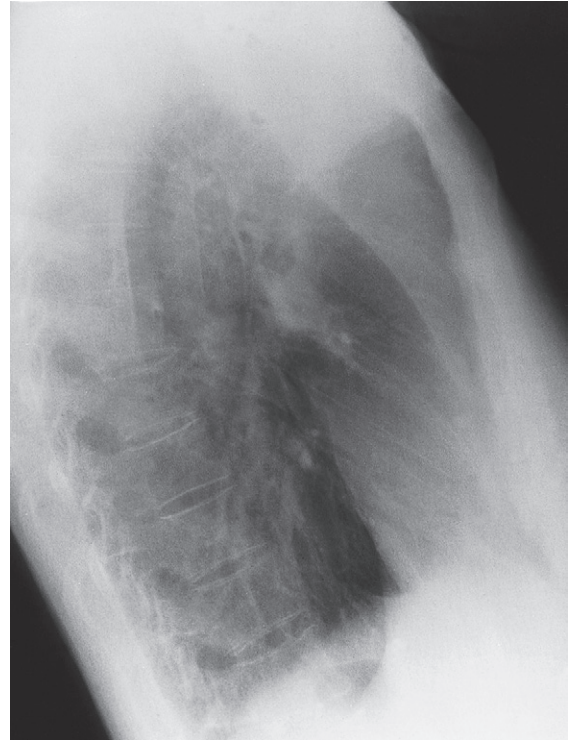


Fig. 2.23 Collapse of the right upper lobe. (a) Posteroanterior and (b) lateral views. Note the opacification in the right apex and elevated horizontal fissure.

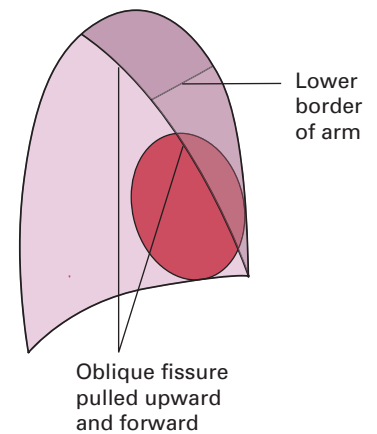


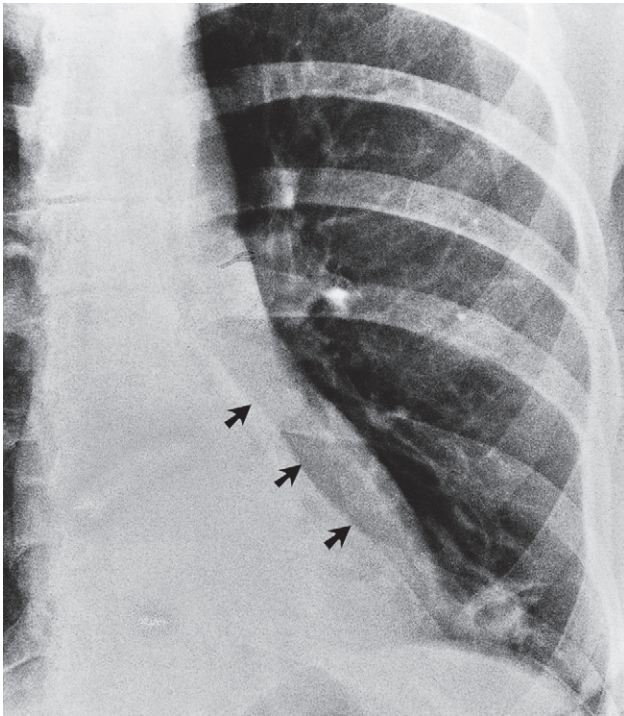
(a)



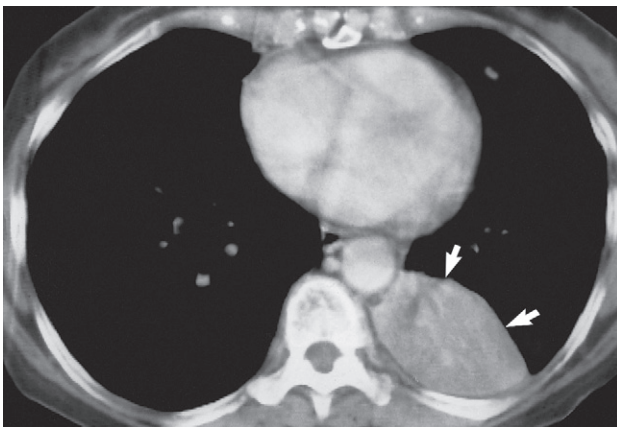
(b)

Fig. 2.24 Collapse of the left upper lobe. (a) Posteroanterior and (b) lateral views. Note the veil-like opacity of the left hemithorax on the PA view. The lower border of the collapsed lobe is ill defined. The upper two-thirds of the left mediastinal and heart borders are invisible, but the aortic knuckle and descending aorta are identifiable. The visible portions of the aorta have been drawn in for greater clarity. On the lateral view, the upper lobe can be seen collapsed anteriorly.





(a)



(b)

Fig. 2.25 Collapse of the left lower lobe. (a) Chest radiograph. The triangular opacity of the collapsed lobe is seen through the heart. Its lateral border is formed by the displaced oblique fissure (arrows). (b) CT. The collapsed lobe is seen lying posteriorly in the left thorax. The well-defined anterior margin is due to the displaced oblique fissure (arrows).

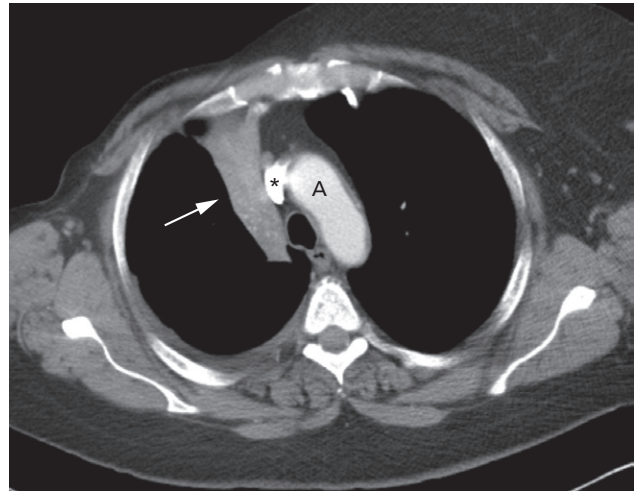


Fig. 2.26 CT of a severely collapsed right upper lobe. Note the smooth lateral border of the collapsed lobe formed by the displaced oblique (major) fissure (arrow). The scan shows compensatory overexpansion of the left upper lobe, which has crossed the midline anterior to the aortic arch (A). The superior vena cava is highlighted with an asterisk.

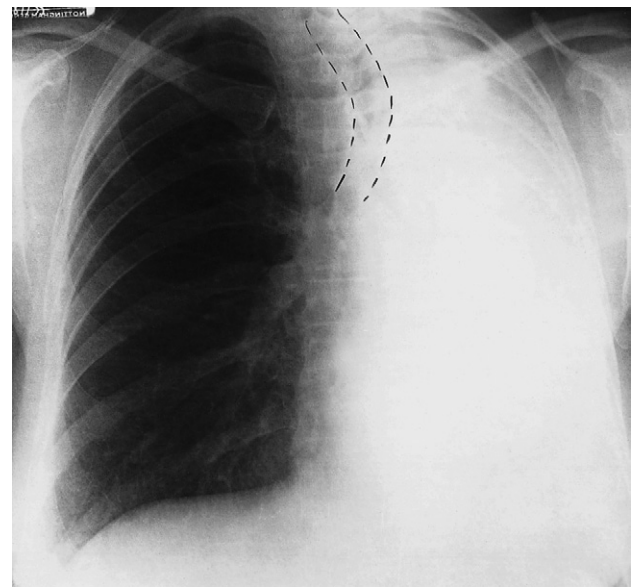


Fig. 2.27 Collapse of the left lung showing tracheal and mediastinal displacement.

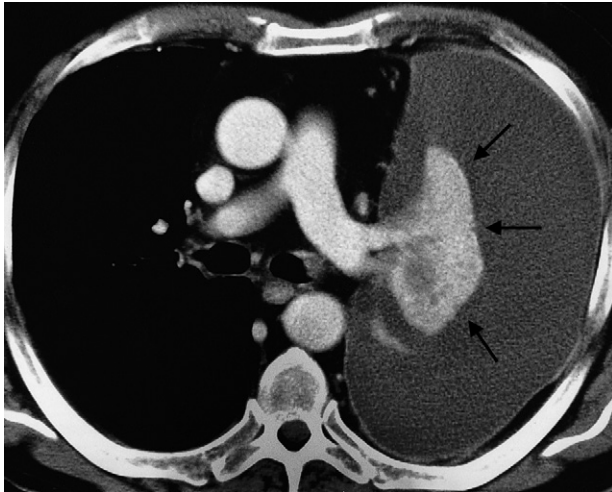


Fig. 2.28 CT showing pleural effusion and pulmonary collapse. The collapsed lobe (arrows) can be clearly seen beneath the large left pleural effusion.

is a horizontally orientated band or disc of collapse (see Fig. 2.37).

Spherical opacities (lung mass, lung nodule)

The diagnosis of a solitary spherical opacity in the lung (solitary pulmonary nodule) (Fig. 2.29) is a common problem (Box 2.2).

When a nodule is discovered in a patient who is over 50 and a smoker, bronchial carcinoma becomes the major consideration. In a patient less than 35 years old, primary carcinoma is highly unlikely. The patient's symptoms may be

Box 2.2 Causes of a solitary pulmonary nodule

- Bronchial carcinoma/bronchial carcinoid (neuroendocrine tumour)
- Benign tumour of the lung, hamartoma being the most common
- Infective granuloma, tuberculoma being the most common in the UK and fungal granuloma the most frequent in the USA
- Metastasis
- Lung abscess
- Rarely, spherical (round) pneumonia

helpful (e.g. obvious symptoms of chest infection in a patient with a lung abscess), but often there are no relevant symptoms even in patients with lung carcinoma. Metastasis is very unlikely in a patient without a known extrathoracic primary malignant tumour, but is an important consideration in those who are known to have such a tumour.

The possible diagnoses for a solitary pulmonary nodule listed in Box 2.2 include lesions that require very different forms of management. Hamartomas and granulomas are best left alone, whereas bronchial carcinoma, active tuberculosis and lung abscess require specific treatment. Further investigation with CT, FDG-PET/CT or biopsy may be necessary for further evaluation. Careful consideration of the following may help in making the diagnosis.

Comparison with previous films

Assessing the rate of growth of a spherical lesion in the lung is one of the most important factors in determining the correct management of the patient. Failure to grow over a period of 18 months or more is a strong pointer to either a benign tumour or an inactive granuloma. An enlarging mass is highly likely to be a bronchial carcinoma or a metastasis.

Calcification

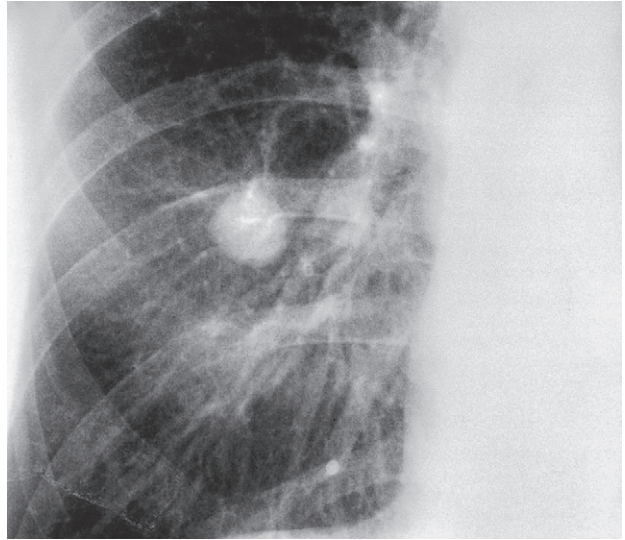
The presence of calcification is the other vital observation, because substantial calcification virtually rules out the diagnosis of a malignant lesion. Calcification is a common finding in hamartomas, tuberculomas and fungal granulomas. In hamartomas it is often of the 'popcorn' type (Fig. 2.30). Calcification can be difficult to recognize on CXR. CT is of great value in detecting calcification in a solitary pulmonary nodule. If benign patterns of calcification are seen at CT (uniform calcification throughout the nodule, concentric ring calcification or popcorn calcifications) then carcinoma of the lung can be excluded from the differential diagnosis (Fig. 2.31).

Involvement of the adjacent chest wall

Destruction of the adjacent ribs is virtually diagnostic of invasion by carcinoma. Tumours of the lung apex are particularly liable to invade the chest wall and adjacent bones (Pancoast's tumour). CT or a bone scan may be indicated to demonstrate this invasion (Fig. 2.32).



(a)



(b)



(c)

Fig. 2.29 Solitary spherical opacity. (a) The large size and the irregular infiltrating edge are important diagnostic features suggesting primary carcinoma of the lung. (b) The small size and relatively smooth border leads to a wider differential diagnosis. In this case the diagnosis was bronchial carcinoid. (c) Typical bronchial carcinoma on CT showing an infiltrating edge.

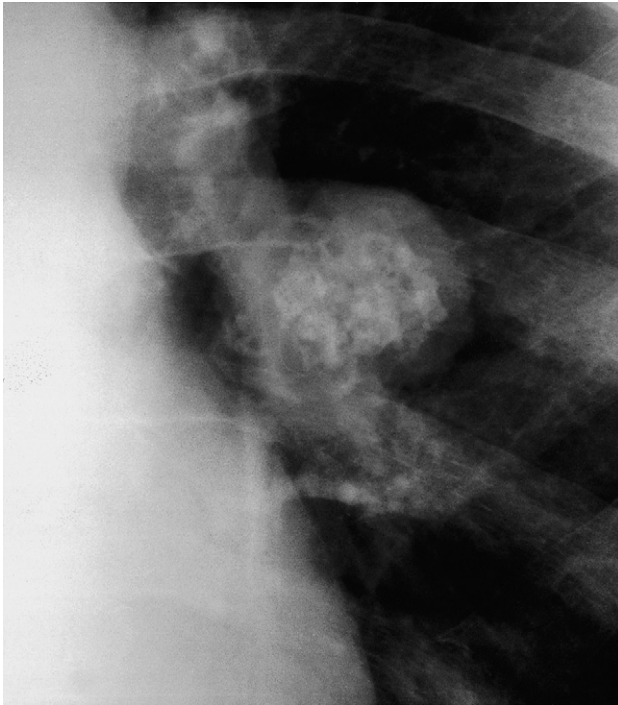


Fig. 2.30 Calcification in a pulmonary hamartoma. The central flocculant ('popcorn') calcification is typical of that seen in hamartomas.

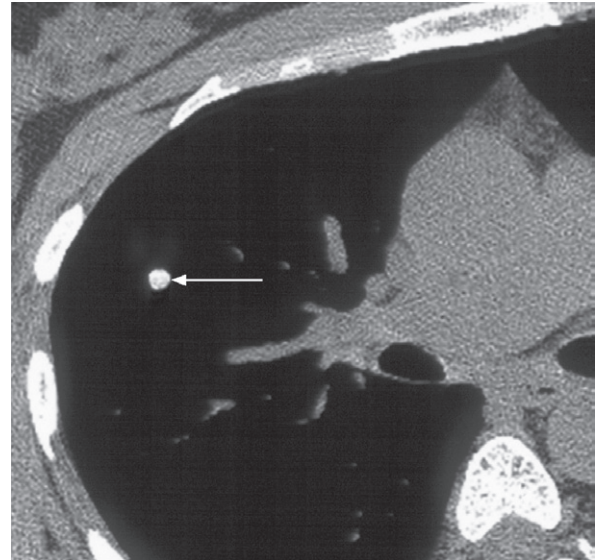
Shape of the opacity

Primary carcinomas are nearly always rounded with a lobulated, notched or infiltrating outline (Figs 2.29 and 2.33). Even if only one small portion of a round lesion has an irregular or lobular edge, the diagnosis of primary carcinoma should be seriously considered.

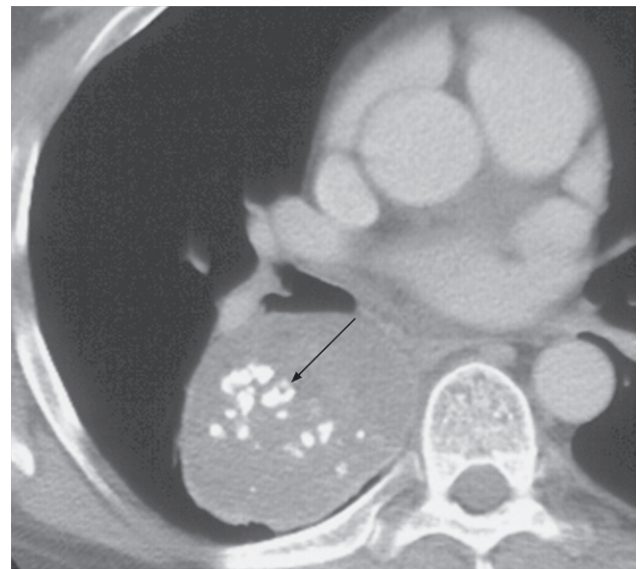
The shape may be obvious from plain films but CT can be used to confirm the rounded shape. Sometimes a lesion that is round and mass-like on CXR is shown to be linear or band-like on CT, in which case the diagnosis is likely to be a focal pulmonary scar of no significance.

Cavitation

If the centre of the mass undergoes necrosis, air is seen within the mass. An air–fluid level may be visible on an erect CXR. These features, which may be difficult to appreciate on plain films, are seen particularly well at CT.



(a)



(b)

Fig. 2.31 Benign patterns of calcification. (a) A small calcified nodule (arrow). The calcific density of this fungal granuloma is clearly shown by CT. (b) 'Popcorn' calcification (arrow) in an unusually large hamartoma. The calcification was difficult to appreciate on CXR.

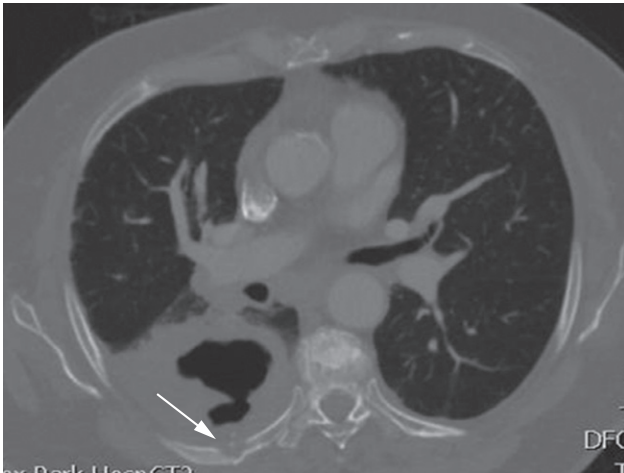


Fig. 2.32 CT showing a cavitating lung cancer with local invasion of the chest wall and erosion of the cortex of the adjacent rib (arrow).

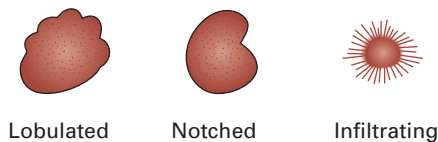


Fig. 2.33 Outlines of different primary carcinomas of the lung.

Cavitation almost always indicates a significant lesion. It is very common in lung abscesses (see Figs 2.18–2.20), relatively common in primary carcinomas (Fig. 2.34) and occasionally seen with metastases (especially squamous cell carcinoma) and pulmonary infarcts. It does not occur in benign tumours or inactive tuberculomas.

The distinction between cavitating neoplasms and lung abscesses can be very difficult and sometimes impossible, particularly if the walls are smooth. If, however, either the inner or outer walls are irregular, the diagnosis of carcinoma is highly likely.

Size

A solitary mass over 4 cm in diameter that does not contain calcium is nearly always either a primary carcinoma, a lung abscess or, rarely, round pneumonia. Lung abscesses of this size, however, virtually always show cavitation and round



Fig. 2.34 CT of cavitating primary carcinoma of the lung. The variable thickness of the cavity wall is a striking feature. The air–fluid level is also well seen (arrow).

pneumonias cause obvious clinical features of acute pneumonia.

Other lesions

The rest of the film should be checked carefully after a single lung mass has been found. Metastases are the common cause of multiple nodules.

Role of computed tomography

The role of CT in patients with a solitary pulmonary nodule is primarily to characterize the nodule using the following steps.

- 1 To demonstrate calcification in the nodule; however CT is not worth doing if the nodule is clearly calcified on plain films. As mentioned above, extensive calcification of a nodule effectively excludes primary carcinoma of the lung (see Fig. 2.31).
- 2 To establish whether or not the nodule is solitary or multiple, when the lesion in question is likely to be a metastasis or when surgical resection of the mass is being considered.
- 3 To localize the nodule accurately prior to bronchoscopic or percutaneous needle biopsy in cases where the position of the nodule is difficult to define on conventional films.

Table 2.1 Recommendations for follow-up and management of nodules smaller than 8mm detected incidentally at non-screening CT: Fleischner guidelines

Nodule size	Low risk patients*	High risk patients*
≤4mm	No follow-up needed	Follow-up at 12 months. If no change, no further imaging needed
>4 to 6 mm	Follow-up at 12 months. If no change, no further imaging needed	Initial follow-up CT at 6–12 months and then at 18–24 months if no change
>6 to 8 mm	Initial follow-up CT at 6–12 months and then at 18–24 months if no change	Initial follow-up CT at 3–6 months and then at 9–12 and 24 months if no change
>8mm	Follow-up CTs at around 3, 9 and 24 months. Dynamic contrast-enhanced CT, PET and/or biopsy	Same as for low risk patients

* Low risk patients: minimal or absent history of smoking and of other known risk factors. High risk patients: history of smoking or of other known risk factors.
CT, computed tomography; PET, positron emission tomography.

- 4 To stage the extent of disease in those cases where the nodule is likely to be a primary carcinoma.
- 5 Follow-up of an incidental asymptomatic nodule if it is thought to be benign (Table 2.1).

Role of positron emission tomography

Most lung cancers concentrate the PET agent FDG (Fig. 2.35) and all patients will have PET/CT as part of their staging if the CT suggests a curative treatment option. Only a small proportion, notably very small tumours (<1 cm) and slow-growing cancers, do not show increased uptake. A negative PET/CT scan is useful evidence in favour of a benign lesion or a very slow-growing tumour that can be reassessed after an interval. A positive PET scan does not necessarily give a diagnosis of lung cancer, as active inflammatory disease may also demonstrate increased uptake of FDG. The combination of a mass on CT that has characteristics suggestive of lung cancer and a positive FDG uptake provides good evidence of lung cancer.

Role of needle biopsy

Transthoracic needle biopsy, using either fine needle aspiration or cutting needles to obtain samples, is usually performed under CT control. If the sample yields lung cancer cells, then the diagnosis is established. However, failure to find malignant cells does not exclude the diagnosis of a malignant neoplasm, so the technique should only be used

when establishing the diagnosis of malignancy will affect the management plan, e.g. ensuring a diagnosis of lung cancer prior to radiotherapy, chemotherapy or in some cases prior to surgery.

Multiple pulmonary nodules

Multiple, well-defined spherical opacities in the lungs are virtually diagnostic of metastases (see Fig. 2.115). Occasionally, this pattern is seen with abscesses, other neoplasms or with granulomas caused by fungal infection, tuberculosis or collagen vascular disorders.

Line or band-like opacities

All line opacities within the lungs, except fissures and the walls of the large central bronchi, are abnormal. Septal lines are by far the most important.

Septal lines

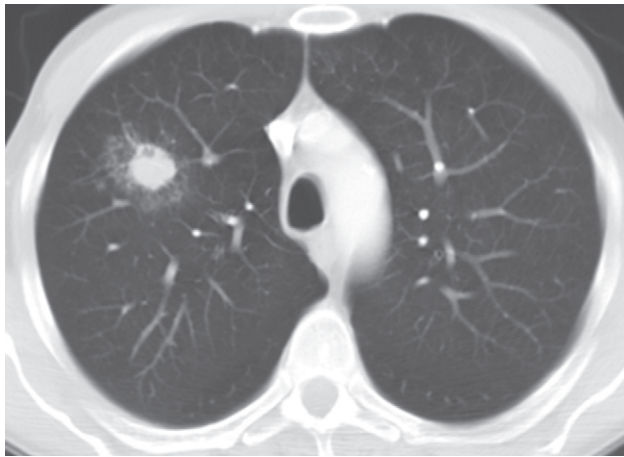
The interlobular septa within the lung are connective tissue planes containing lymph vessels. They are normally invisible. Only greatly thickened septa can be seen on a CXR. Septal lines are much thinner than the pulmonary blood vessels. On CXRs, septal lines are seen as so-called Kerley B lines (Fig. 2.36), namely horizontal lines, never more than 2 cm in length, best seen at the periphery of the lung. Unlike the blood vessels they often reach the edge of the lung. On



(a)



(c)



(b)

Fig. 2.35 FDG-PET imaging in a solitary pulmonary nodule. (a) The chest radiograph shows an ill-defined nodule. (b) CT shows a rounded nodule with a spiculated outline. (c) The PET scan shows substantial activity in the nodule (the myocardial activity is normal). The diagnosis was bronchial carcinoma.

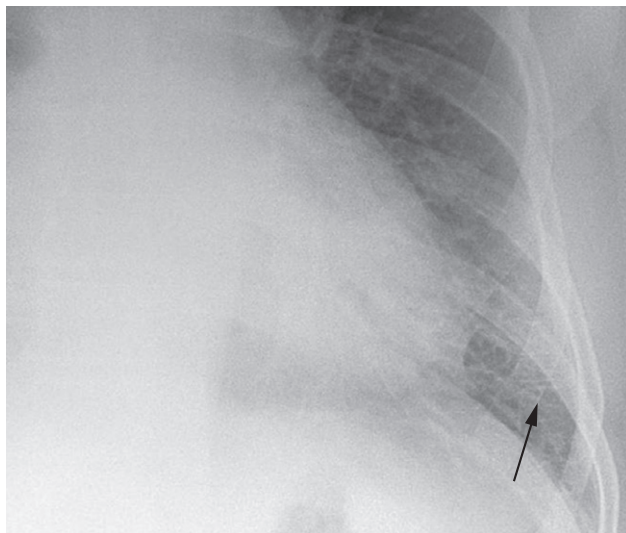


Fig. 2.36 Septal (Kerley B) lines in a patient with pulmonary oedema. The septal lines (arrow) are seen in the outer centimetre of lung where blood vessels are invisible or very difficult to identify.

CT, even mild thickening of interlobular pulmonary septa can be readily identified. There are two important causes of thickened interlobular septa:

- interstitial pulmonary oedema
- lymphangitis carcinomatosa.

Pleuropulmonary scars and linear (discoid) atelectasis

These two conditions are common causes of line or band-like opacities and are somewhat similar in appearance. Neither is of clinical significance. Linear scars are due to previous infection or infarction; they usually reach the pleura and are often associated with visible pleural thickening. Linear (discoid) atelectasis results in bands or discs of collapse (Fig. 2.37).

Emphysematous bullae

Bullae may be bounded and traversed by thin line opacities. Bullae have few, if any, normal vessels within them, which makes the interpretation easy (Fig. 2.38).

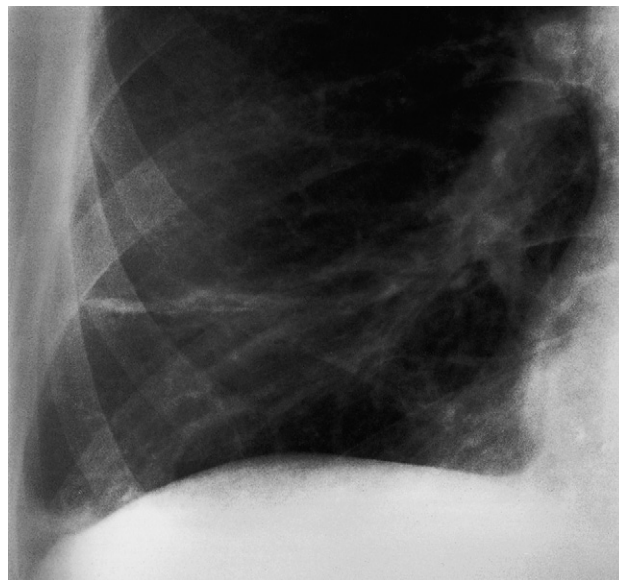


Fig. 2.37 Band-like opacity in the right lower lobe caused by discoid atelectasis.

Pleural edge in a pneumothorax

The pleural edge in a pneumothorax is seen as a line approximately parallel with the chest wall. No lung vessels can be seen beyond the pleural line. Once the line is spotted the diagnosis is rarely in doubt (see Fig. 2.53).

Widespread small pulmonary opacities

Chest radiographs with widespread, small (2–3 mm) pulmonary opacities often present a diagnostic problem. With few exceptions it is only possible to give a differential diagnosis when faced with such a film. A final diagnosis can rarely be made without knowledge of the patient's symptoms, signs and laboratory results.

Many descriptive terms have been applied to these opacities. In this book we will use three basic terms: (i) 'nodular', to signify discrete, small, round opacities (Fig. 2.39); (ii) 'reticular', to describe a net-like pattern of small lines; and (iii) 'reticulonodular', when both patterns are present (Fig. 2.40).

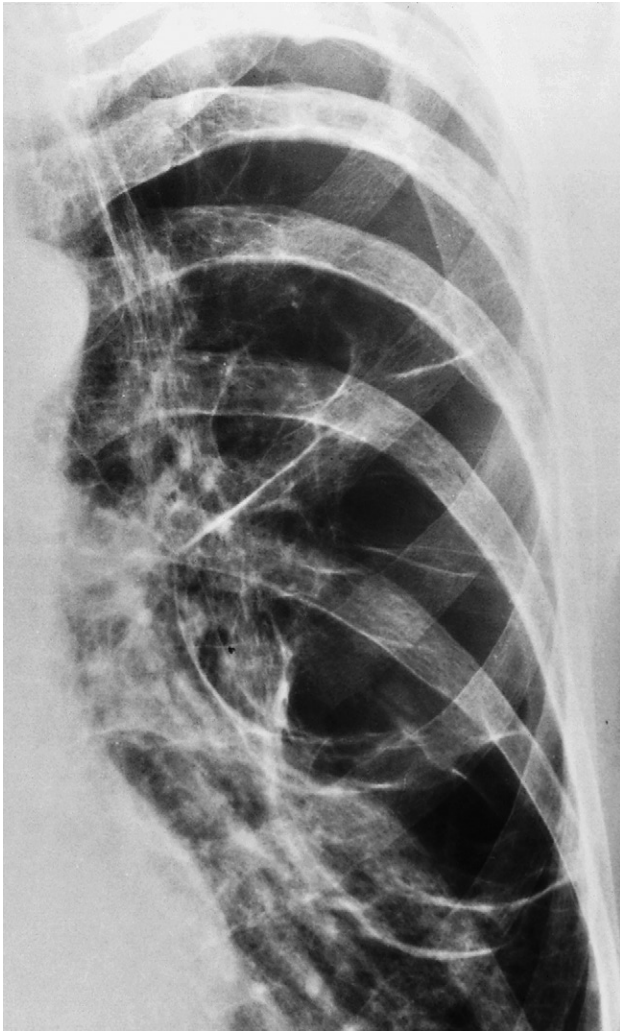


Fig. 2.38 Linear opacities caused by walls of bullae (blebs). The bullae are air-spaces devoid of blood vessels.

All three patterns are due to very small lesions in the lungs, no more than 1 or 2mm in size. Individual lesions of this size are invisible on a CXR. That these very small lesions are seen at all is explained by the phenomenon of superimposition; when myriads of tiny lesions are present in the lungs it is inevitable that many will lie in line with one another.

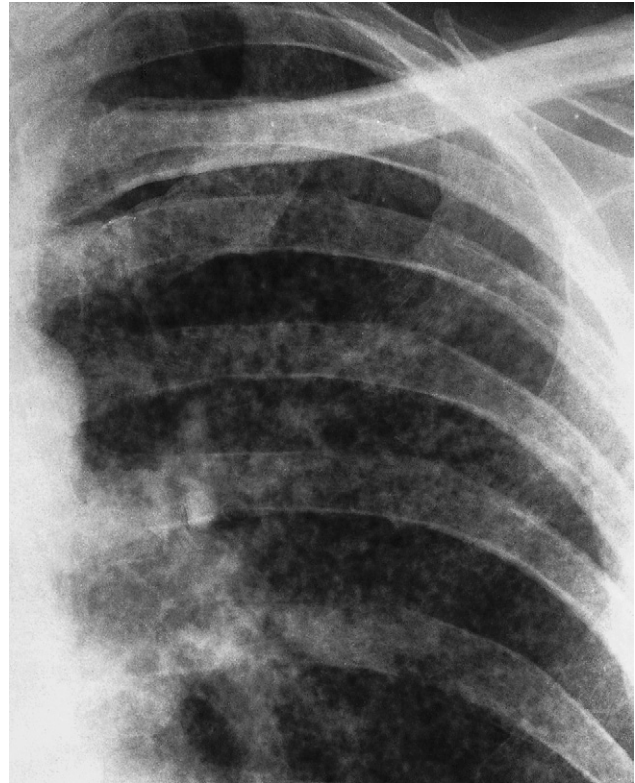


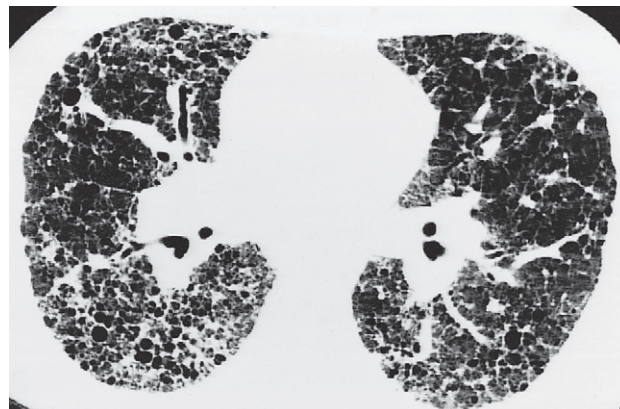
Fig. 2.39 Nodular opacifying in the lung of a patient with miliary tuberculosis.

How to decide whether or not multiple, small pulmonary opacities are present on a chest radiograph

Often, the greatest problem is to decide whether widespread abnormal opacification is present at all, as normal blood vessels can appear as nodules and interconnecting lines. To be confident involves looking carefully at many hundreds of normal films to establish the range of normal in one's mind. Look particularly at the areas between the ribs where the lungs are free of overlying opacities. The normal vessel pattern is a branching system that connects up in an orderly way. The vessels are larger centrally and become smaller as they travel to the periphery. Vessels seen end-on appear as small nodules, but these nodules are no bigger than vessels seen in the immediate vicinity and their number corresponds to the expected number of vessels in



(a)



(b)

Fig. 2.40 (a) Reticulonodular opacifying in the lung of a patient with fibrosing alveolitis. (b) HRCT of a different patient with cryptogenic (idiopathic) fibrosing alveolitis showing the honeycomb pattern to advantage.

that area. There are no visible vessels in the outer 1–2 cm of the lung. An important sign is that abnormal opacities obscure the adjacent vessels, and the borders of the mediastinum and diaphragm may be less sharp than normal.

High resolution computed tomography

When abnormal diffuse opacification is present or suspected, the next step is to obtain a HRCT to determine the precise pattern and distribution, in particular whether the disease process is distributed uniformly, whether it is more severe in one or other zone, and whether it extends outward from the hila or is peripherally predominant. Other abnormalities within the chest should then be sought. Once these observations have been made it is possible to produce the differential diagnoses shown in Table 2.2. A few conditions have quite specific appearances, e.g. lymphangitis carcinomatosa and interstitial pulmonary fibrosis, although the

precise cause of pulmonary fibrosis cannot be ascertained by CT.

Multiple ring opacities of 1 cm or larger

Multiple ring opacities larger than 1 cm are diagnostic of bronchiectasis (Fig. 2.41). The opacities represent dilated thick-walled bronchi.

Widespread small pulmonary calcifications

Widespread small pulmonary calcifications may occur following pulmonary infection with tuberculosis, histoplasmosis, chickenpox or pulmonary haemosiderosis.

Increased transradiancy of the lungs

Generalized increased transradiancy of the lungs is one of the signs of emphysema. The other signs are discussed later in this chapter.

Table 2.2 Commoner causes of nodular and reticular shadowing on chest radiographs and high resolution computed tomography (HRCT)

Diagnosis	Radiographic/HRCT pattern	Distribution of shadows	Other features that may be seen	Value of HRCT
Miliary tuberculosis	Small nodules of uniform size	Uniform	Mediastinal/hilar lymph nodes. One or more patches of consolidation	Only necessary in cases of clinical uncertainty
Sarcoidosis	Usually reticulonodular, but may show small nodules of uniform size very similar to miliary tuberculosis	Usual reticulonodular pattern radiates from hila (miliary pattern is usually uniform in distribution)	Hilar and middle mediastinal lymph node enlargement	Usually unnecessary. Characteristic pattern of pulmonary involvement and shows lymphadenopathy when doubtful on chest radiograph
Asbestosis	Fine reticulonodular	Predominant in peripheral portions of lungs, notably in lower zones	Pleural plaques which may be calcified. Pleural thickening which may be extensive (diffuse pleural thickening)	HRCT very useful to quantify interstitial lung fibrosis and diffuse pleural thickening
Interstitial pulmonary fibrosis (usual interstitial pneumonia, UIP)	Reticulonodular	Usually predominant in periphery of lobes and in lower zones	Diaphragm often high and indistinct	HRCT very useful to quantify interstitial pulmonary fibrosis and to assess potential responsiveness to steroids
Lymphangitis carcinomatosa	Reticulonodular. Septal lines	No predominant distribution	Bronchial wall thickening hilar adenopathy. Other signs of carcinoma	HRCT very useful in any doubtful cases as the HRCT features are usually reasonably characteristic

When only one hemithorax appears more transradiant than normal the following should be considered.

- Compensatory emphysema occurs when a lobe or lung is collapsed or has been excised and the remaining lung expands to fill the space.
- Pneumothorax. The diagnosis of pneumothorax depends on visualization of the lung edge with air peripheral to it, and checking that the space in question does not contain any vessels (see Figs 2.53 and 2.54).
- Reduction in the chest wall soft tissues, e.g. mastectomy.
- Air-trapping due to central obstruction (Fig. 2.42). Most obstructing lesions in a major bronchus lead to lobar collapse. Occasionally, particularly with an inhaled foreign body, a check-valve mechanism may lead to air-trapping. Inhaled foreign bodies are commonest in children; they usually lodge in a major bronchus. Often the CXR is normal,

but sometimes the affected lung becomes abnormally transradiant and the heart is displaced to the opposite side on expiration.

PLEURA

Pleural effusion

Pleural effusions may lie free within the pleural cavity, in which case the fluid falls to the most dependent portion of the pleura and assumes a shape dependent on the thoracic cage and the shape of the underlying lung (Figs 2.43–2.46), or it may become loculated by pleural adhesions (Figs 2.47–2.49). Although loculation occurs in all types of effusion, it is a particular feature of empyema. Such loculations may either be at the periphery of the lung or within the

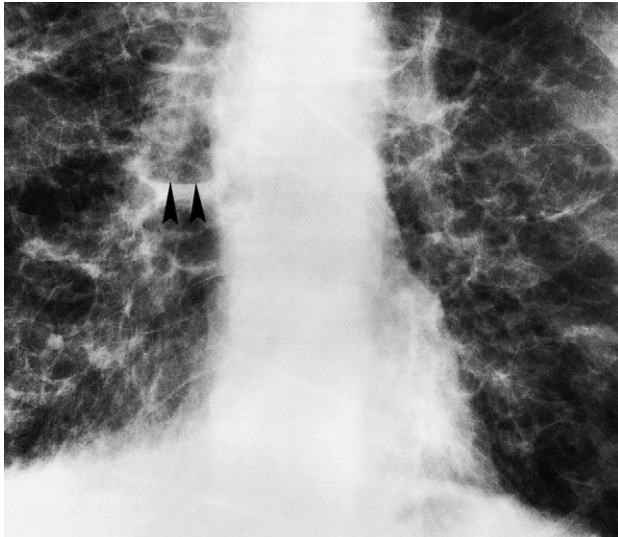


Fig. 2.41 Ring opacities in bronchiectasis. Each ring opacity represents a dilated bronchus. A fluid level in one of the dilated bronchi is arrowed.

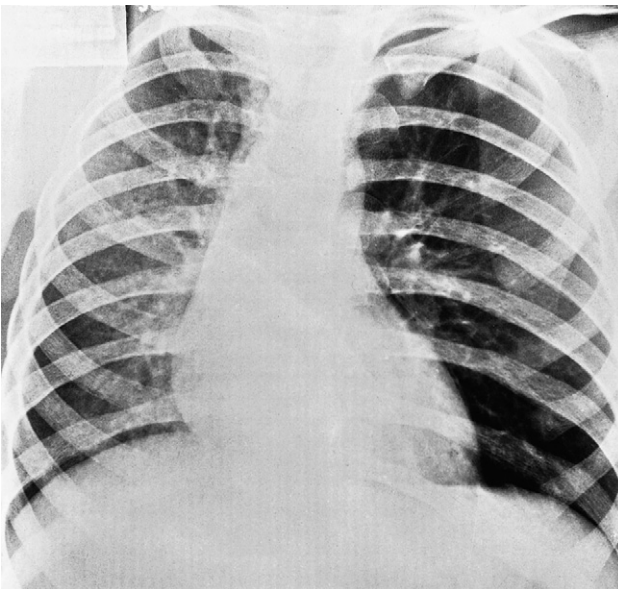


Fig. 2.42 Inhaled foreign body causing check valve obstruction of the left main bronchus. Note the increased transradiancy of the left lung, and the slight displacement of the heart to the right. (The film was exposed in expiration.)

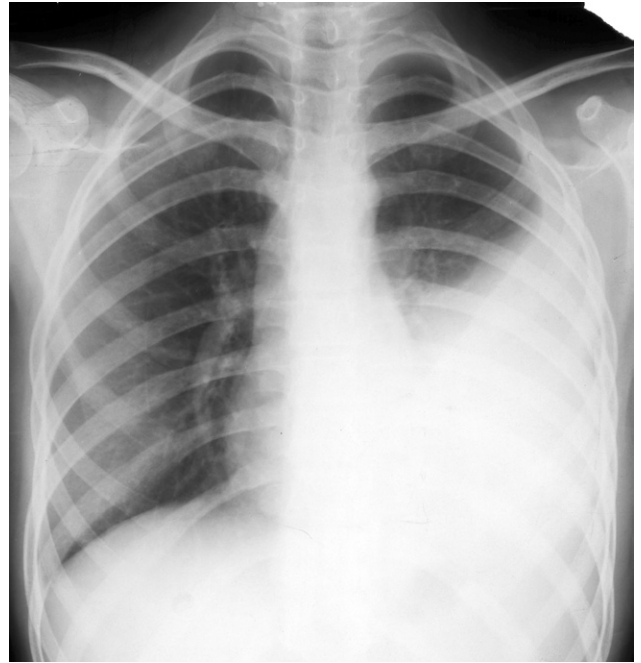


Fig. 2.43 Large left pleural effusion. The opacity of the pleural fluid is entirely homogeneous and lies outside the lung edge. The fluid appears higher laterally than medially, a point that can be useful in differentiating pleural fluid from pulmonary opacities. The trachea and heart are slightly displaced to the right.

fissures between the lobes. A loculated effusion may simulate a lung tumour on CXRs.

There are a number of notable causes of pleural effusion.

- *Infection.* Pleural effusions due to pneumonia are, on the whole, small and the pneumonia is usually the dominant feature on the chest film. Large loculated effusions in association with pneumonia often indicate empyema formation (Figs 2.47–2.49). In some cases of tuberculosis the effusion is the only visible abnormality and the effusion may be large.
- *Subphrenic abscess,* which is nearly always accompanied by a pleural effusion.
- *Malignant neoplasm.* Effusions occur with pleural metastases, but it is unusual to see the pleural deposits themselves on CXRs. Pleural metastases are occasionally seen on CT, MRI or ultrasound as nodular or mass-like pleural

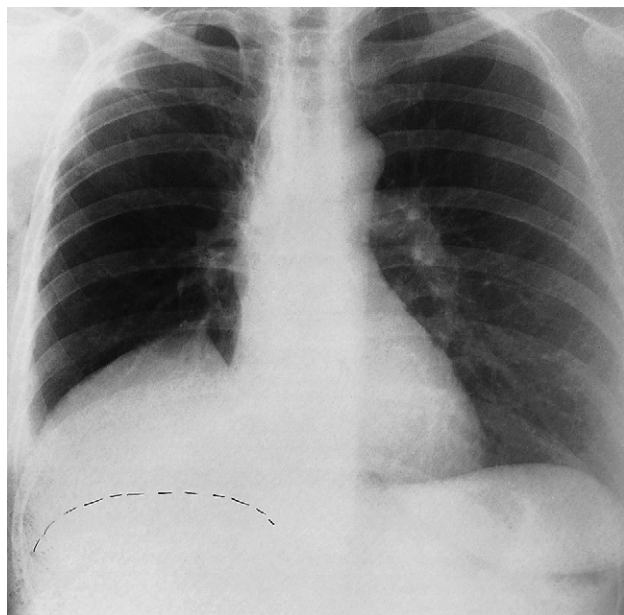


Fig. 2.44 Large right subpulmonary effusion (the patient has had a right mastectomy). Almost all the fluid is between the lung and the diaphragm. The right hemidiaphragm cannot be seen, but its estimated position has been pencilled in.

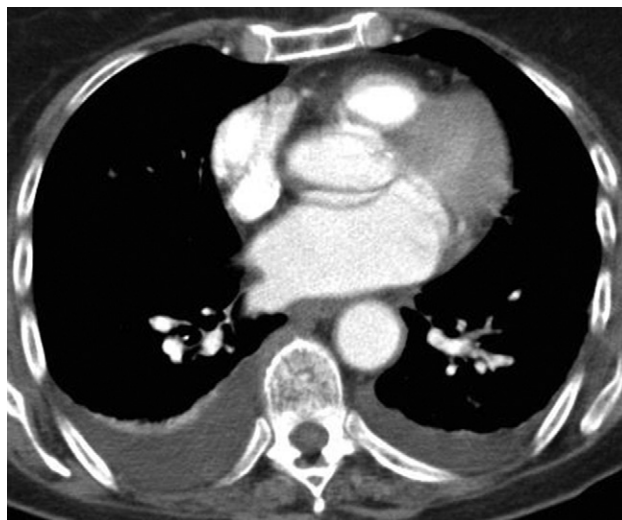


Fig. 2.45 CT of pleural fluid. The bilateral pleural effusions are of homogeneous density, with a CT number between zero and soft tissue. The well-defined meniscus-shaped border with the adjacent lung is typical. The right-sided effusion is causing a little compression collapse of the underlying lung (which shows contrast enhancement).

thickening. Malignant effusions are frequently large. If the effusion is due to bronchogenic carcinoma or malignant mesothelioma, other signs of the primary tumour are usually, but not always, evident.

- *Cardiac failure.* Small bilateral pleural effusions are seen frequently in acute left ventricular failure. Larger pleural effusions may be present in longstanding congestive cardiac failure. The effusions are usually bilateral, often larger on the right than the left. Other signs of cardiac failure – such as alteration in the size or shape of the heart, pulmonary oedema or the signs of pulmonary venous hypertension – are usually visible.

- *Pulmonary infarction.* Pulmonary emboli that result in pulmonary infarction may cause pleural effusion. Such effusions are usually small and accompanied by a lung opacity caused by the pulmonary infarct.

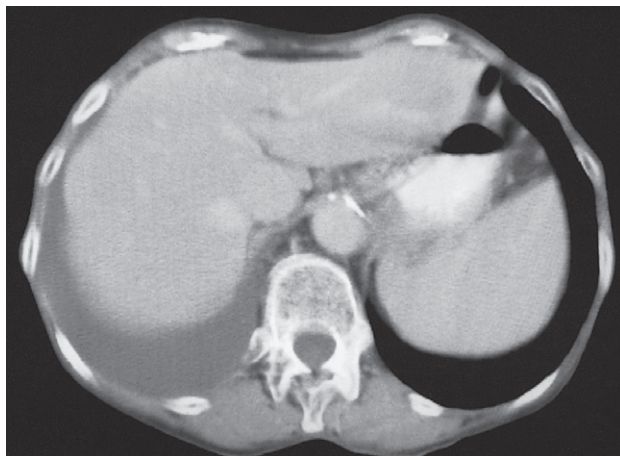
- *Collagen vascular diseases.* Pleural effusions, either unilateral or bilateral, are relatively common in various collagen vascular diseases. They may be the only abnormal features on chest imaging.

- *Nephrotic syndrome, renal failure and ascites* are all associated with pleural effusion.

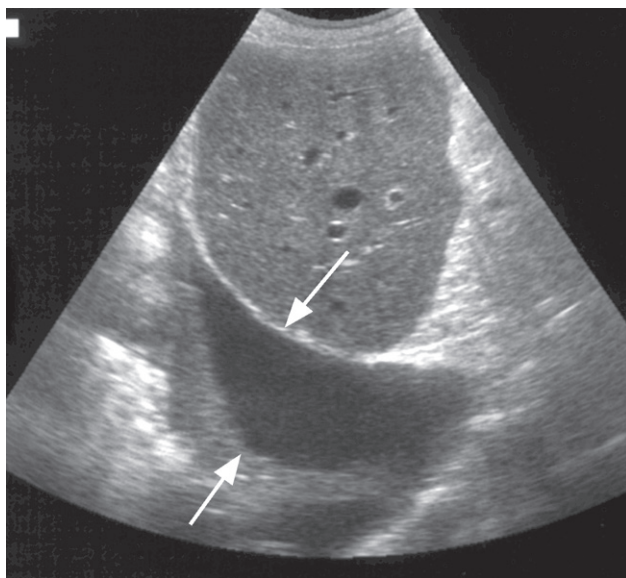
Plain radiographic findings

The radiographic appearances of fluid in the pleural cavity are the same regardless of whether the fluid is a transudate, an exudate, pus or blood (see Figs 2.43, 2.44, 2.47 and 2.48). Free fluid collects in the most dependent portion of the pleural cavity and always fills in the costophrenic angles. Usually the fluid surrounds the lung and is higher laterally than medially. Very large effusions run over the top of the lung. The smooth edge between the lung and the fluid can be recognized on an adequately penetrated film, providing the underlying lung is aerated. It is worth remembering that a large effusion may hide an abnormality in the underlying lung.

Sometimes, even with a large effusion, little or no fluid is seen running up the chest wall. The fluid is then known as a 'subpulmonary effusion' (see Fig. 2.44). The upper



(a)



(b)

Fig. 2.46 Pleural effusion. (a) CT. The section is taken through the lowermost portion of the pleural cavity and at this level the distinction from ascites is a potential problem because the diaphragm itself is not visible. Pleural fluid, as here, is not affected by the peritoneal reflections of the bare area (see Fig. 10.1). (b) Ultrasound, sagittal image. The pleural effusion is seen as a transonic area between the diaphragm (downward pointing arrow) and adjacent lung (upward pointing arrow).

border of the fluid is much the same shape as the normal diaphragm, and as the true diaphragm is obscured by the fluid it may be very difficult, or even impossible, to tell from the standard erect film if any fluid is present at all.

Ultrasound

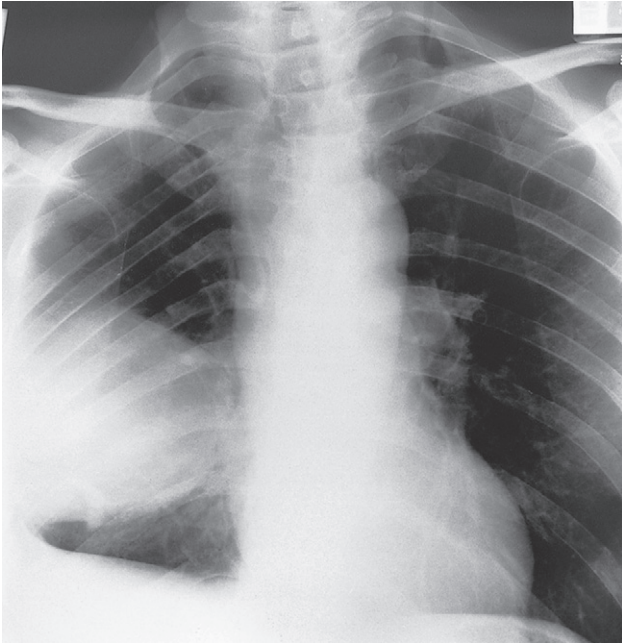
Ultrasound is a simple method of determining whether pleural fluid is present. Pleural fluid can be recognized as a hypoechoic area between the lung and diaphragm or between the chest wall and the lung (see Fig. 2.46b). It is only rarely possible to determine the nature of the fluid, e.g. in empyema multiple echoes may be seen due to the pus in the fluid. Ultrasound is particularly useful in defining the presence, size and shape of any pleural collection loculated against the chest wall (see Fig. 2.48b) or diaphragm, and is a convenient method of imaging control to guide procedures such as pleural fluid aspiration or drainage.

Computed tomography

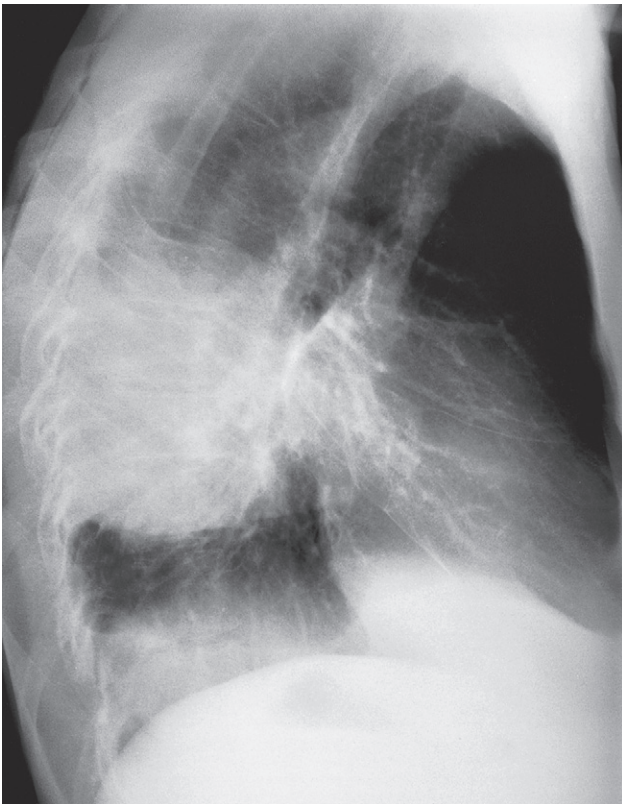
Pleural effusions are usually seen as an area of homogeneous fluid density between the chest wall and lung (see Figs 2.45 and 2.46). CT is particularly useful for showing loculated pleural effusions (see Fig. 2.48). If the fluid is due to recent haemorrhage it will show the high density of blood, otherwise it is not possible to determine the nature of the fluid. Free pleural fluid moves to the dependent portion of the chest (see Fig. 2.45) CT can be used to distinguish between lung abscess and empyema (see Figs 2.48c and 2.49). Like ultrasound, CT can be used to direct the placement of drainage tubes.

Pleural thickening (pleural fibrosis)

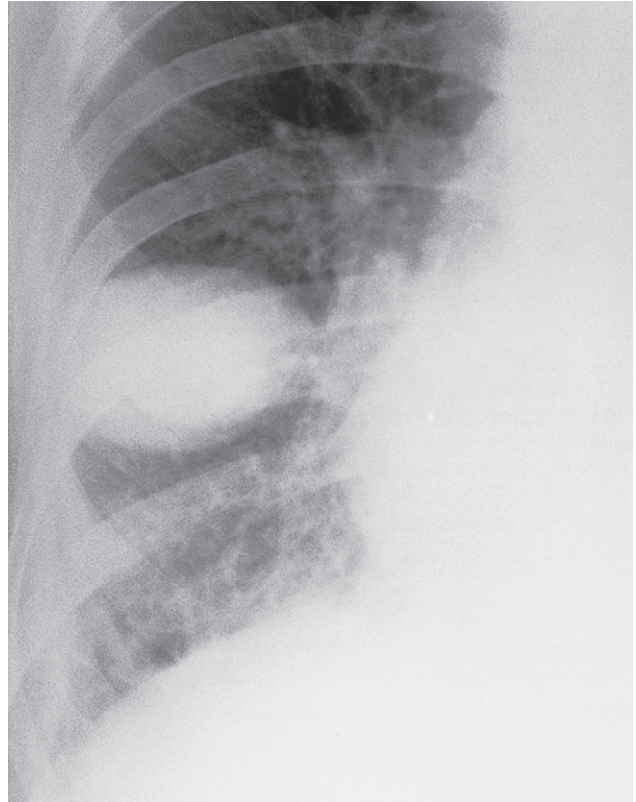
Fibrotic pleural thickening (scarring), especially in the costophrenic angles, may follow resolution of a pleural effusion, particularly following pleural infection or haemorrhage, or be due to asbestos exposure (Fig. 2.50). It is sometimes impossible to distinguish pleural fluid from pleural thickening on a CXR, especially if comparison with previous films is not possible. Ultrasound or CT can usually resolve the problem. Localized plaques of pleural thickening along the lateral chest wall commonly indicate asbestos exposure. Such plaques may show irregular calcification.



(a)

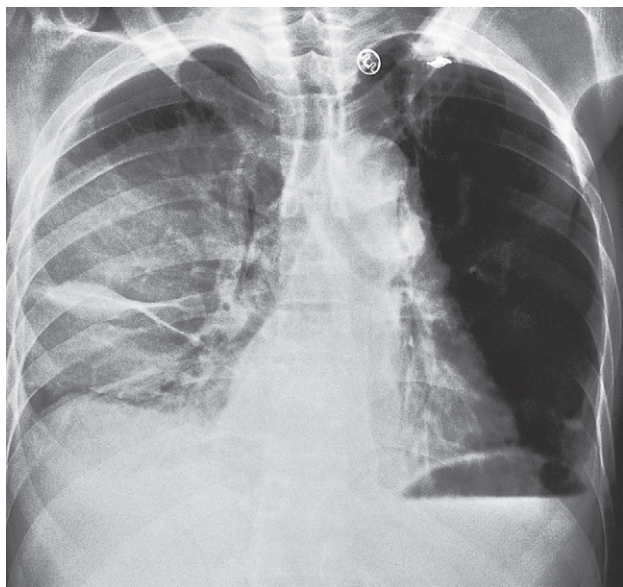


(b)

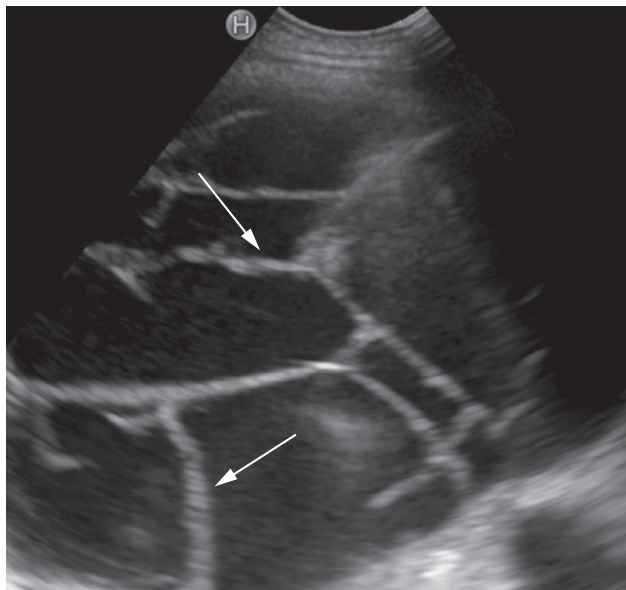


(c)

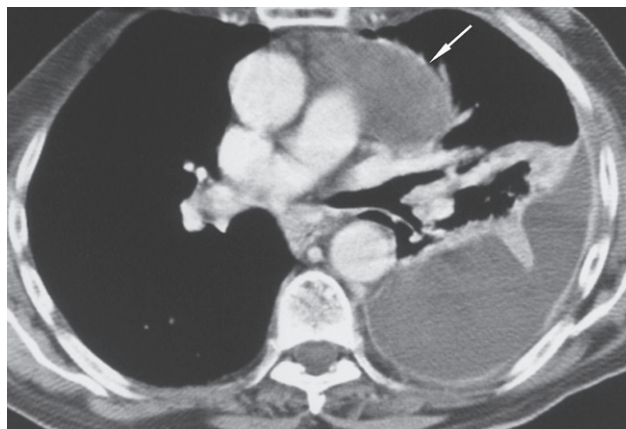
Fig. 2.47 Loculated pleural fluid. (a) Posteroanterior and (b) lateral views showing an empyema loculated against the posterior chest wall. (c) Fluid loculated in the horizontal (minor) fissure in another patient. Both these fluid collections could be confused with an intrapulmonary mass.



(a)

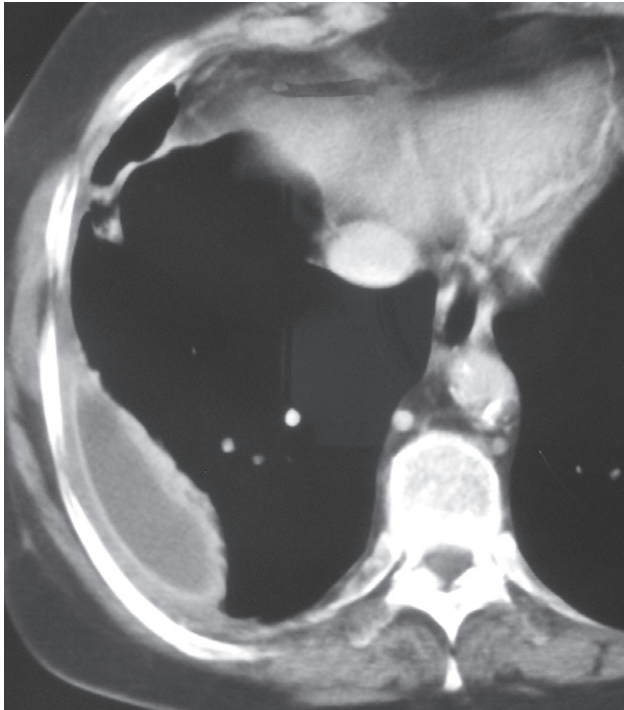


(b)

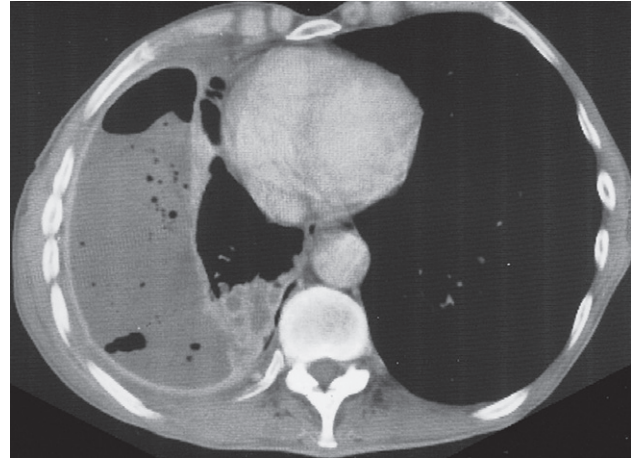


(c)

Fig. 2.48 Loculated pleural fluid (empyema). (a) Plain chest film showing the fluid loculated in the horizontal (minor) fissure. (b) Chest ultrasound in a different patient, demonstrating multiple septations (arrows) within the pleural fluid. (c) CT scan in a similar patient clearly shows the characteristic shape and location of two loculated pleural fluid collections (larger one posteriorly and a smaller one anteriorly [arrow]).



(a)



(b)

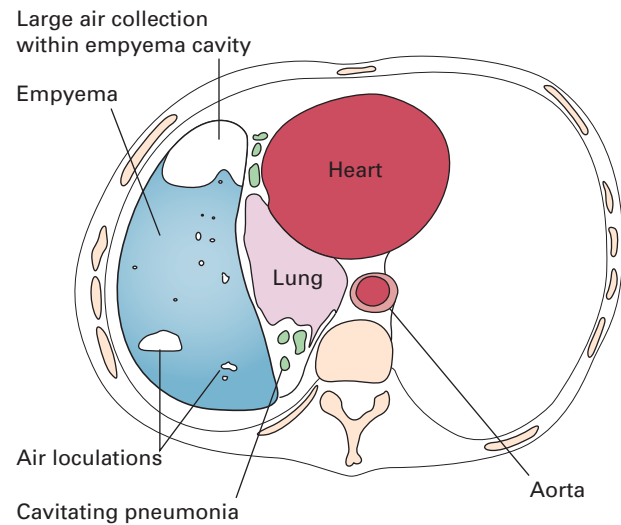


Fig. 2.49 Empyema. (a) CT showing a typical lens-shaped pleural fluid collection with a clearly marginated wall consisting of thickened pleura. (b) CT showing multiple loculated air collections within the pus.

Pleural tumours

The commonest pleural tumours are metastatic carcinomas (Fig. 2.51). Primary pleural tumours, such as mesotheliomas, are relatively uncommon. Many patients with malignant mesotheliomas give a history of asbestos exposure and may show the other features of asbestos-related dis-

ease. Pleural tumours produce lobulated masses based on the pleura. Malignant pleural tumours, both primary (malignant mesothelioma) and secondary, frequently cause pleural effusions which may obscure the tumour itself. The predominant feature of metastatic pleural tumours and some malignant mesotheliomas is a pleural effusion with no visible mass on imaging examinations.

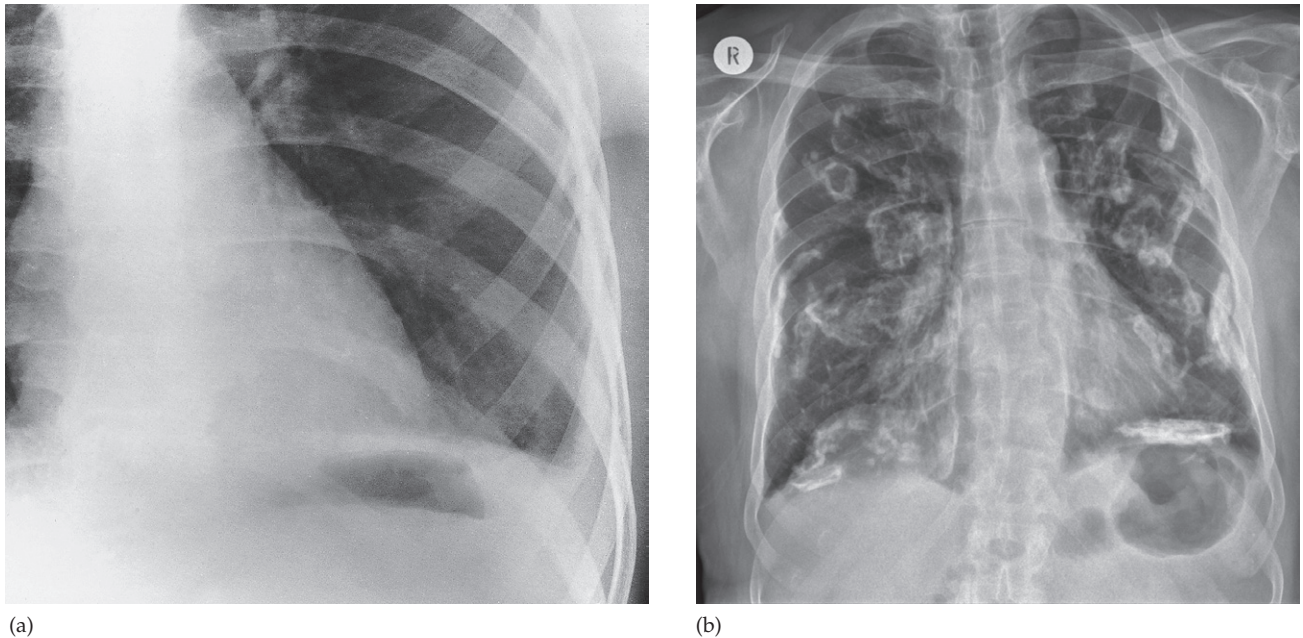


Fig. 2.50 Pleural thickening. (a) CXR in a patient who been treated for a tuberculous pleural effusion that had resolved leaving pleural thickening, which obliterated the left costophrenic angle. (b) CXR showing calcified pleural plaques in a different patient with previous asbestos exposure. The extensive calcification is usually best appreciated along the lateral chest wall or over the diaphragms. When seen on an AP film, the *en face* plaques are said to have a 'holly-leaf pattern' of calcification.

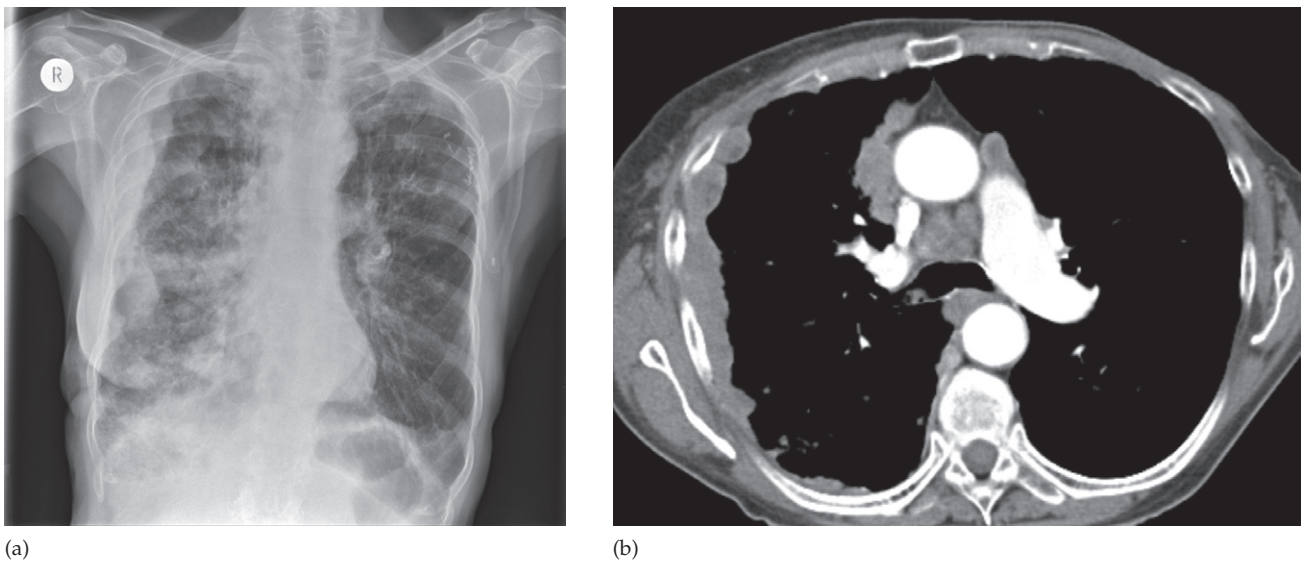


Fig. 2.51 Metastatic disease of the pleura. (a) CXR and (b) CT in a patient with breast cancer showing diffuse thickening of the pleura on the right, secondary to metastatic disease. Note the absence of the left breast shadow due to a previous mastectomy on the CXR.

Pleural calcification

Irregular plaques of calcium may be seen with or without accompanying pleural thickening. When unilateral they are likely to be due to either an old empyema, usually tuberculous (Fig. 2.52), or an old haemothorax. Bilateral pleural calcification is often related to asbestos exposure (see Fig. 2.50b). Sometimes no cause for pleural calcification can be found.

Pneumothorax

The majority of pneumothoraces occur in young people with no recognizable lung disease (Fig. 2.53). These patients have small blebs or bullae at the periphery of their lungs which burst. Occasionally pneumothorax can be due to:

- emphysema
- trauma



Fig. 2.52 Unilateral pleural calcifications from old tuberculous empyema.

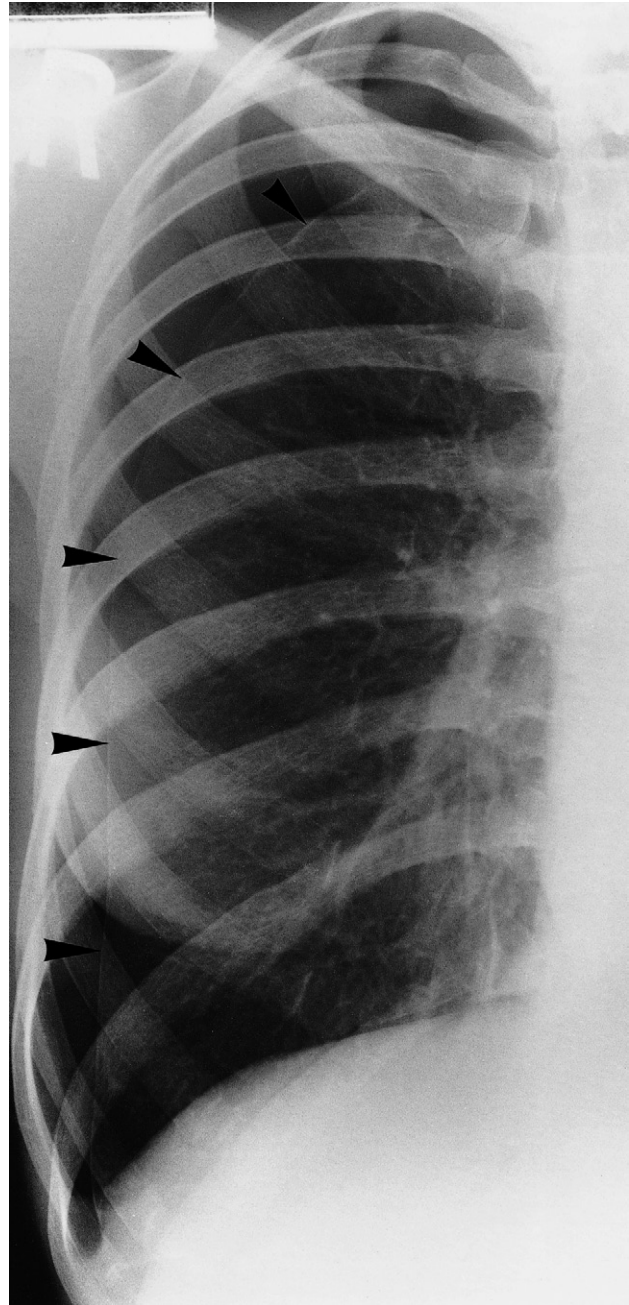


Fig. 2.53 Pneumothorax. The pleural edge is arrowed. The diagnosis of pneumothorax requires the identification of this edge and a clear space beyond it.

- certain forms of interstitial pulmonary disease
- *pneumocystis carinii* pneumonia
- metastases, rarely.

The diagnosis of pneumothorax depends on recognizing the following.

- A line of pleura due to the lung edge being separated from the chest wall, mediastinum or diaphragm by air.
- The absence of vessel opacities outside this line (lack of vessel opacities alone is insufficient evidence on which to make the diagnosis, as there may be few, or no, visible vessels in emphysematous bullae).
- If the pneumothorax is very large, there may be an appreciable increase in the density of the underlying collapsed lung (Fig. 2.54).

The detection of a small pneumothorax can be very difficult. The ribs may take a similar course to the line of the

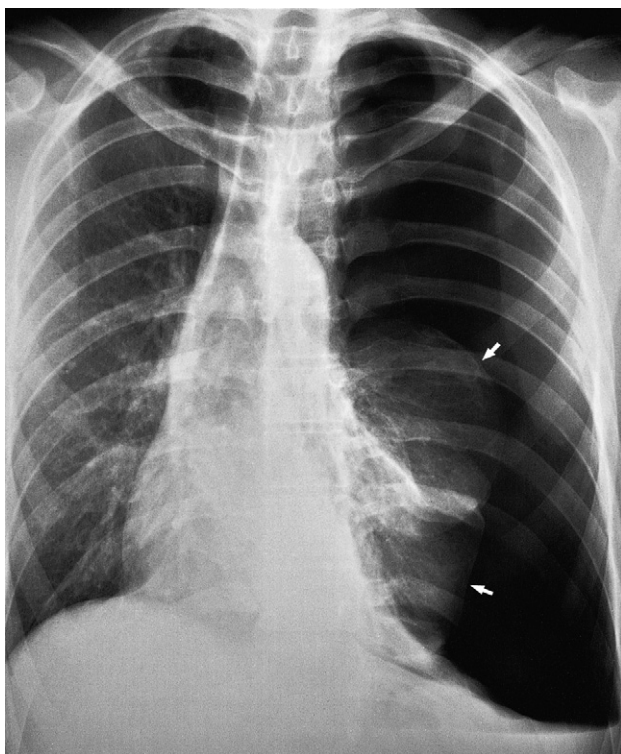


Fig. 2.54 Tension pneumothorax. The left hemidiaphragm is depressed and the mediastinum is shifted to the right. The left lung (arrows) is substantially collapsed and demonstrates increased density.

pleural edge, so the abnormality may not strike the casual observer. Sometimes a pneumothorax is more obvious on a film taken in expiration.

Once the presence of a pneumothorax has been noted, the next step is to decide whether or not it is under tension. This is easy if there is mediastinal shift and flattening or inversion of the hemidiaphragm (Fig. 2.54). Most tension pneumothoraces are large because the underlying lung collapses due to increased pressure in the pleural space, but small pneumothoraces can cause serious symptoms if the underlying pulmonary reserve is poor.

Hydropneumothorax, haemopneumothorax and pyopneumothorax

Fluid in the pleural cavity, whether it be a pleural effusion, blood or pus, assumes a different shape in the presence of a pneumothorax. The diagnostic feature is the air–fluid level (Fig. 2.55).

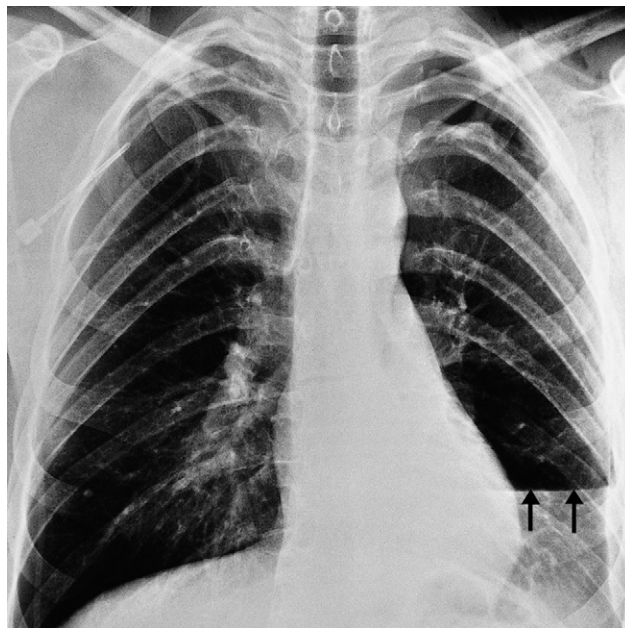


Fig. 2.55 Hydropneumothorax. The arrows point to the air–fluid level in the pleural space. In this case, the edge of the lung is difficult to see on the PA view; most of the fluid and air were loculated posteriorly.

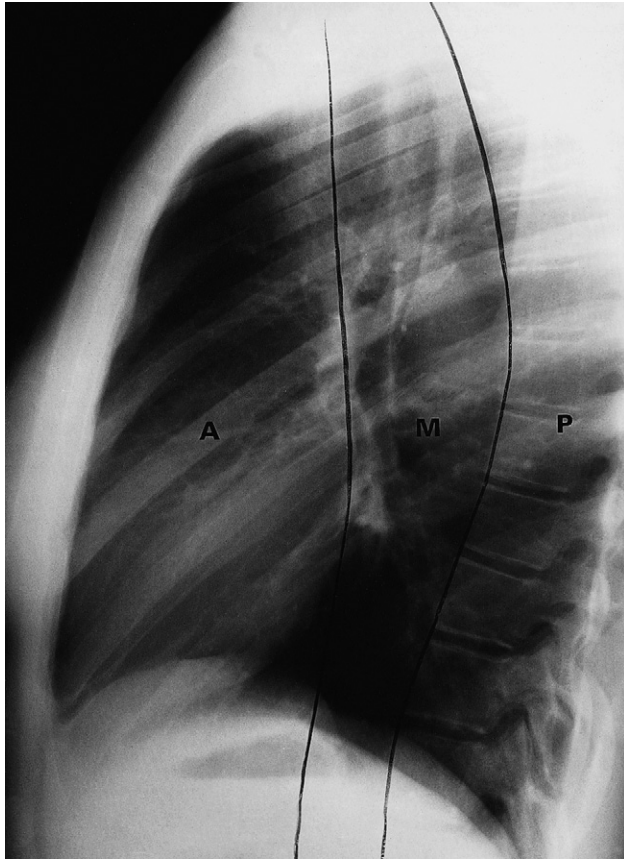
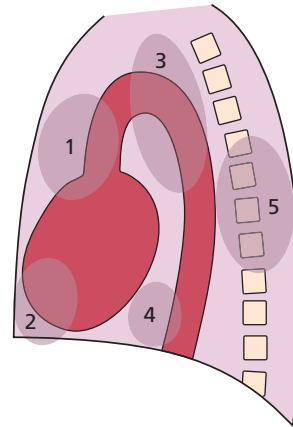


Fig. 2.56 The anterior (A), middle (M) and posterior (P) compartments of the mediastinum. The divisions are arbitrary and do not correspond to those used by anatomists. The anterior mediastinum refers to the structures anterior to the trachea and the major bronchi. The posterior mediastinum refers to structures posterior to a line joining the anterior boundary of the vertebral bodies.

Some fluid is present in the pleural cavity in most patients with pneumothorax. In spontaneous pneumothorax, the amount is usually small.

Mediastinum

The mediastinum is divided into anterior, middle and posterior divisions for descriptive purposes (Fig. 2.56). However, masses often cross from one compartment to the other. Mediastinal widening can be due to many different



ANTERIOR

1. Thyroid tumour
Thymic tumour or cyst
Teratoma/Dermoid cyst
Lymphadenopathy
Aortic aneurysm

2. Pericardial cyst
Fat pad
Morgagni hernia

MIDDLE

3. Thyroid tumour
Lymphadenopathy
Bronchogenic cyst
Aortic aneurysm

4. Hiatus hernia

POSTERIOR

5. Neurogenic tumours
Soft tissue mass of infection or neoplasm
Lymphadenopathy
Aortic aneurysm

Fig. 2.57 The causes of mediastinal masses divided according to location. Note that both lymphadenopathy and aortic aneurysms occur in all three major compartments.

pathological processes. These are usually classified according to their position in the mediastinum (Fig. 2.57). This can be demonstrated on a lateral CXR (Fig. 2.58) but is usually performed with CT.

Computed tomography and magnetic resonance imaging of the normal mediastinum

Computed tomography is the standard method for imaging the mediastinum. MRI is used only occasionally. The cross-sectional display and the ability to distinguish between fat, various soft tissues and blood vessels are major advantages of both techniques. The normal appearances are illustrated in Figs 2.59 and 2.60. The features to note while viewing these images are as follow.

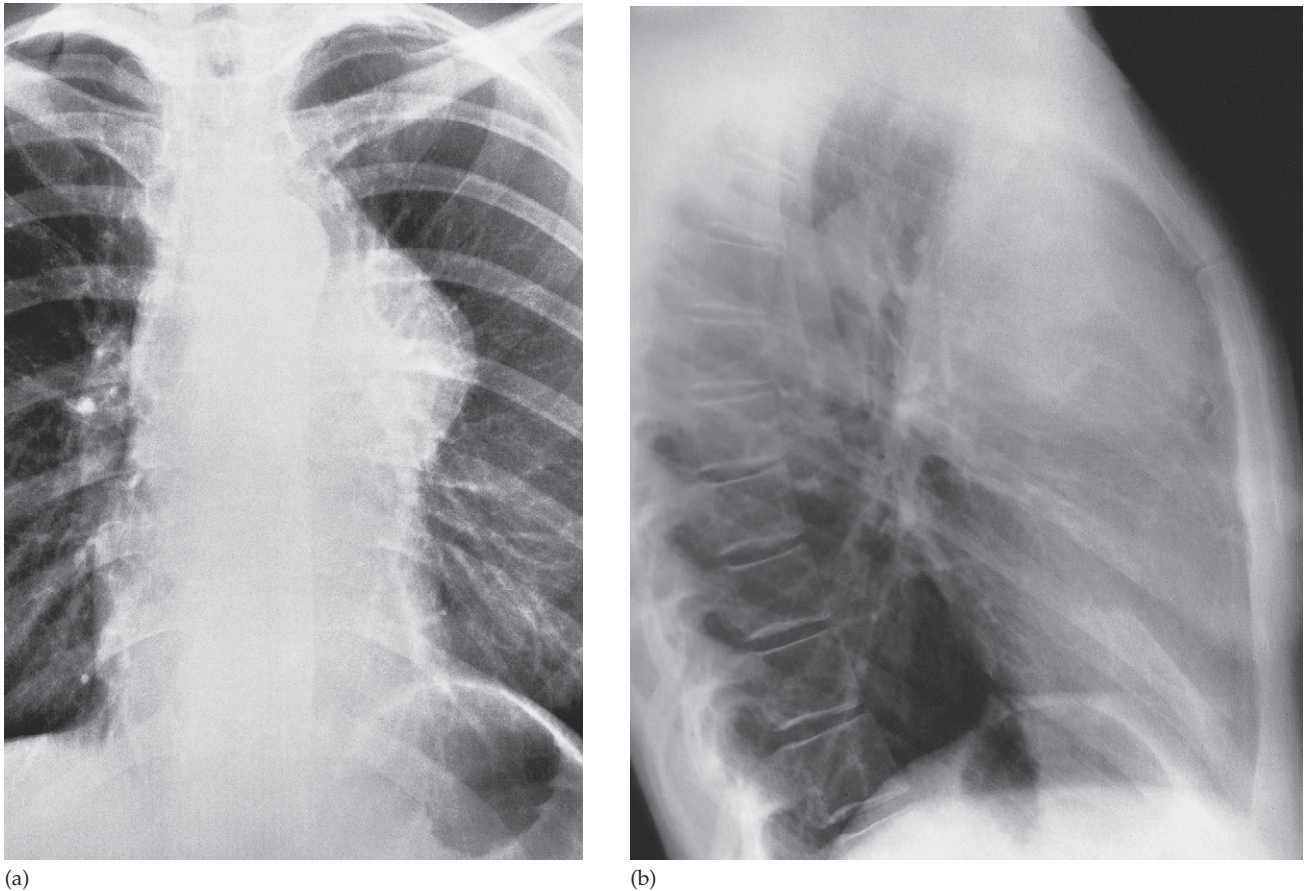


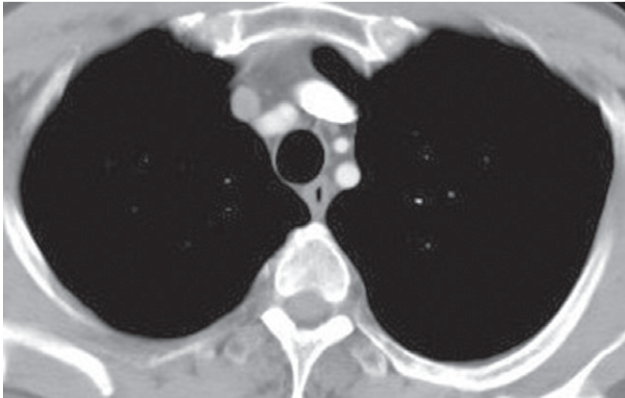
Fig. 2.58 Anterior mediastinal mass. (a) Posteroanterior and (b) lateral views. There is a large mass situated anteriorly in the mediastinum projecting to the left side which was due to a mass of lymph nodes involved by malignant lymphoma. Diagnosing the anterior location of the mass depends on noting the density of the retrosternal areas. This area should normally have the same density as the retrocardiac area.

- The mediastinum is composed predominantly of blood vessels. Visualization and differentiation from other soft tissue structures is aided with the use of intravenous contrast medium. At MRI, the larger vessels are readily seen without contrast agent.
- The only other normal structures of appreciable size are the thymus, oesophagus, trachea and bronchi.
- Normal lymph nodes are small, usually less than 6 mm in diameter (maximum 10 mm), and many are not visible.
- The mediastinal structures are surrounded by fat (low density on CT), this enables visualization of other small soft tissue masses which are generally of increased density.

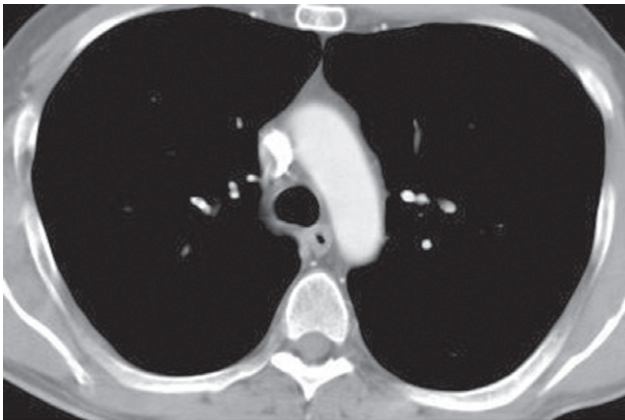
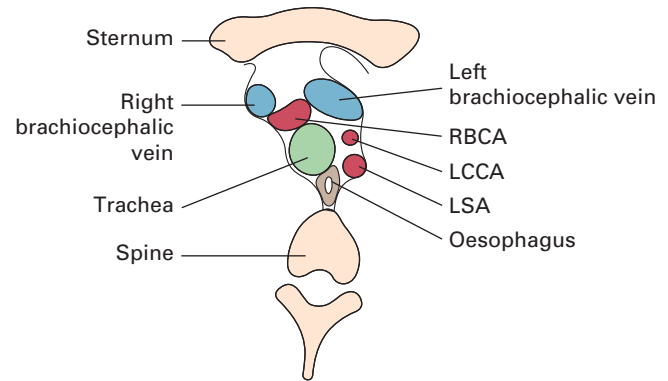
Mediastinal masses

Plain chest films

- Intrathoracic thyroid masses (goitres) are the most frequent cause of a superior mediastinal mass (Fig. 2.61). The characteristic feature is that the mass extends from the superior mediastinum into the neck and almost invariably compresses or displaces the trachea.
- A bronchogenic cyst (Fig. 2.62) is usually an incidental finding seen on CXR and confirmed on CT.
- Lymphadenopathy is the next most frequent cause of a mediastinal swelling. Lymphadenopathy may occur in any



(a)



(b)

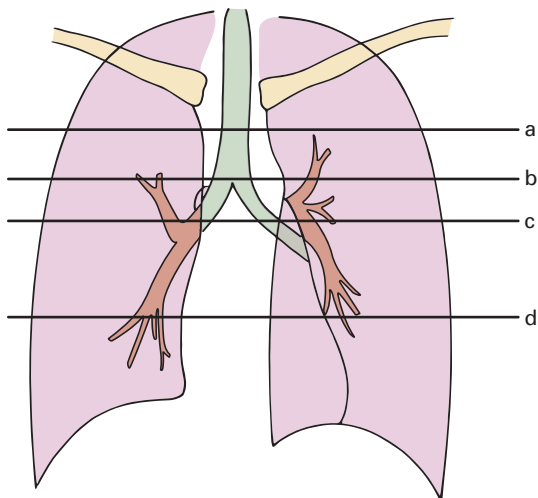
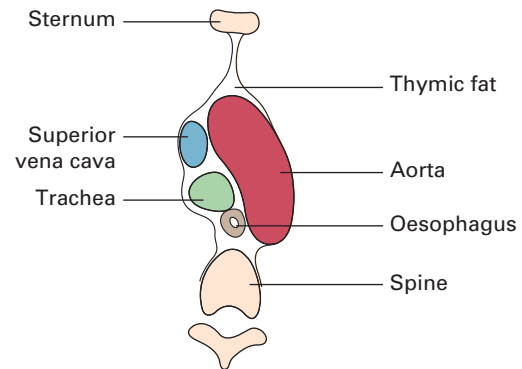
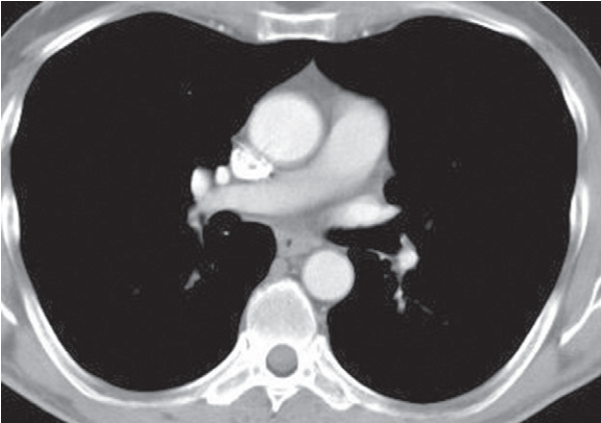
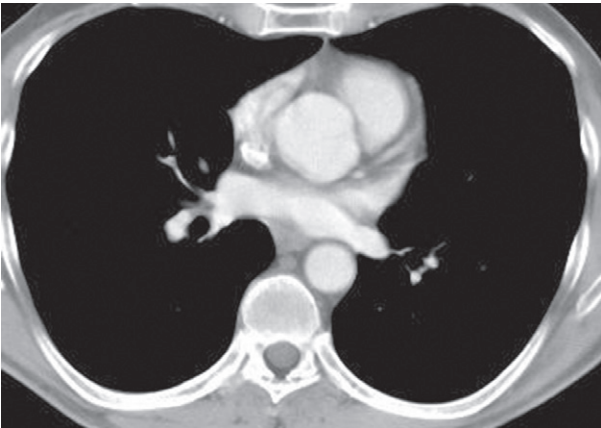


Fig. 2.59 CT of the normal mediastinum and corresponding line drawings. The levels at which the four selected levels were taken are shown in the diagrams below. Intravenous contrast has been given; it is particularly concentrated in the right brachiocephalic vein and superior vena cava. Air is present in the oesophagus, which can be a normal finding. LCCA, left common carotid artery; LMB, left main bronchus; LSA, left subclavian artery; RBCA, right brachiocephalic (innominate) artery; RMB, right main bronchus.

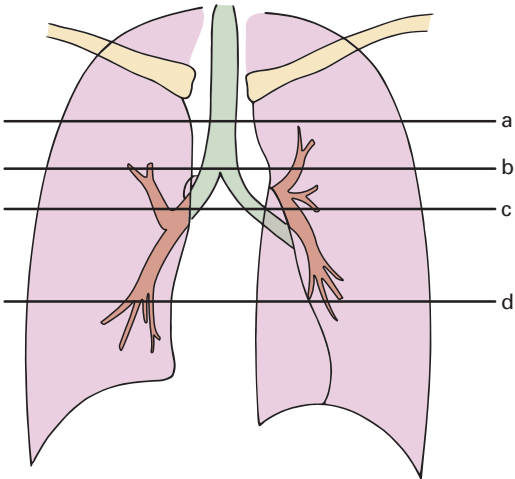
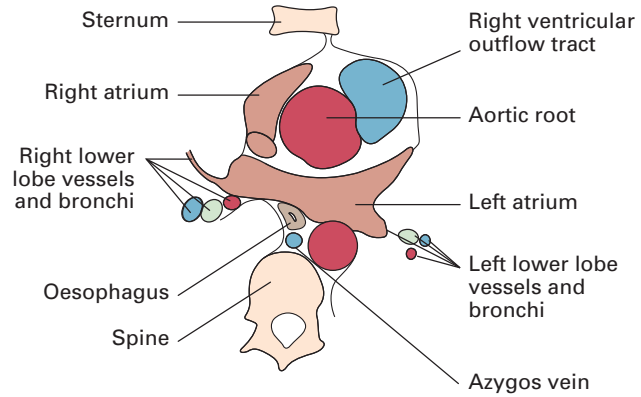
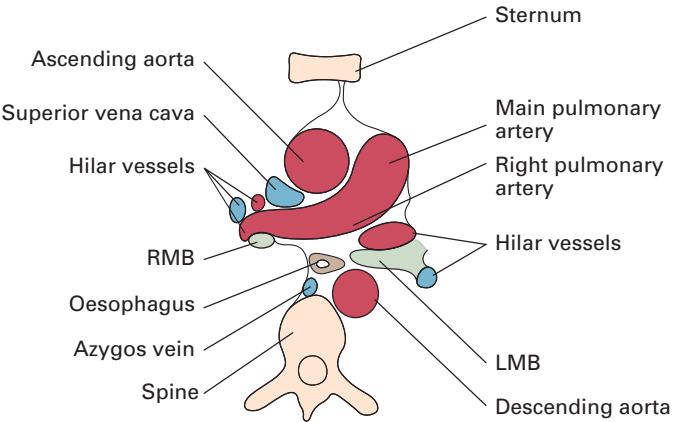


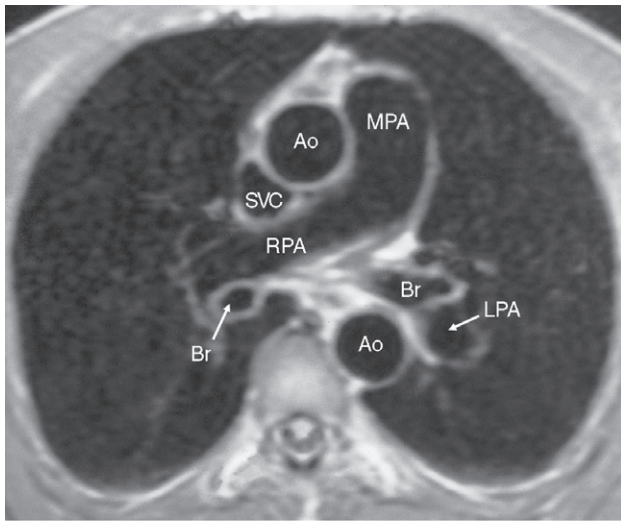
(c)



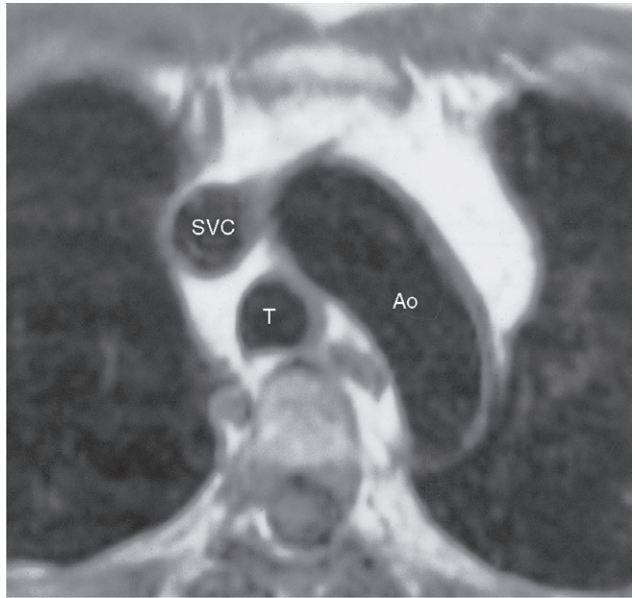
(d)

Fig. 2.59 (Continued)

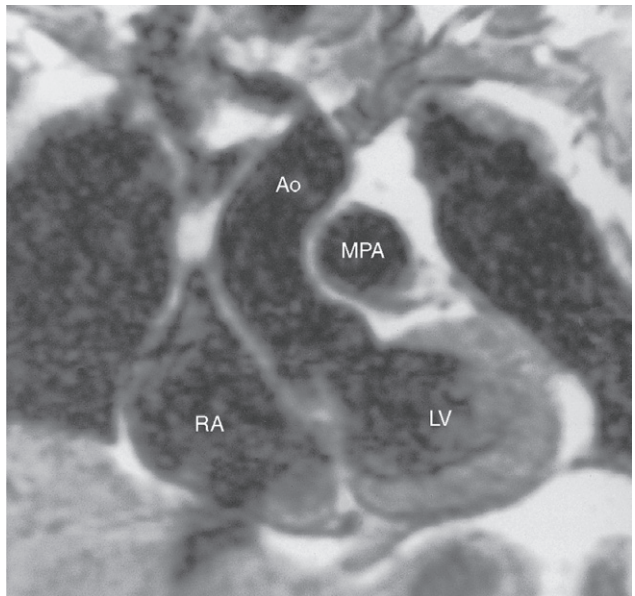




(a)

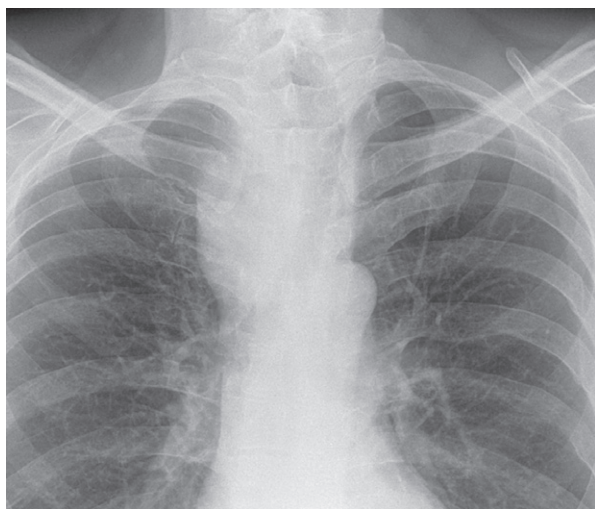


(b)

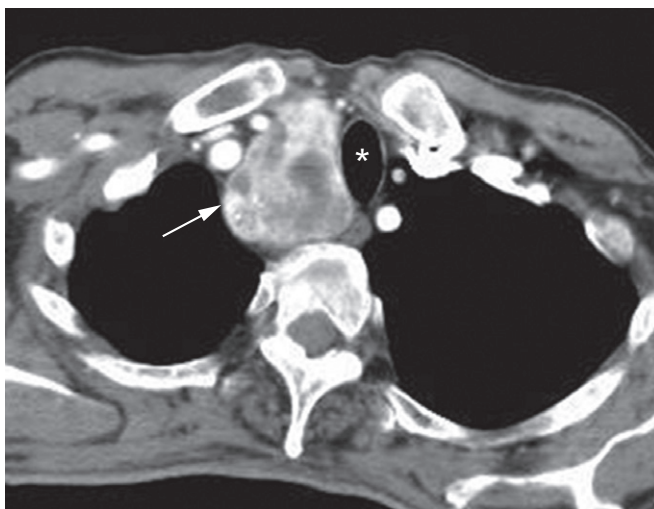


(c)

Fig. 2.60 MRI of the normal mediastinum (T1-weighted, cardiac gated). (a) Axial scan through the level of the pulmonary hila. (b) Higher axial section through the level of the aortic arch. (c) Coronal scan. Ao, aorta; Br, bronchi; LPA, left pulmonary artery; LV, left ventricle; MPA, main pulmonary artery; RA, right atrium; RPA, right pulmonary artery; SVC, superior vena cava; T, trachea.

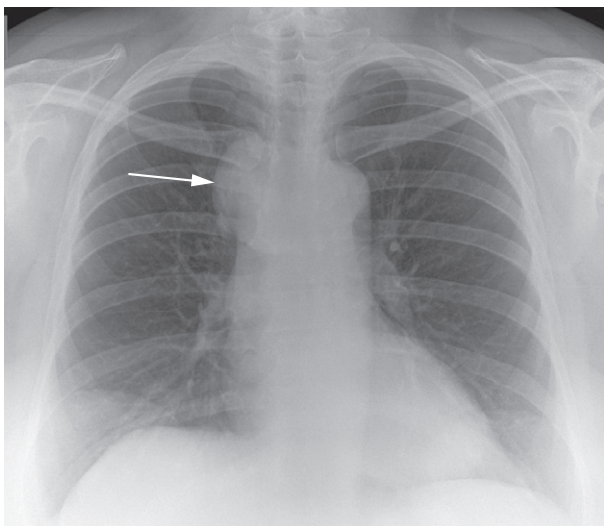


(a)

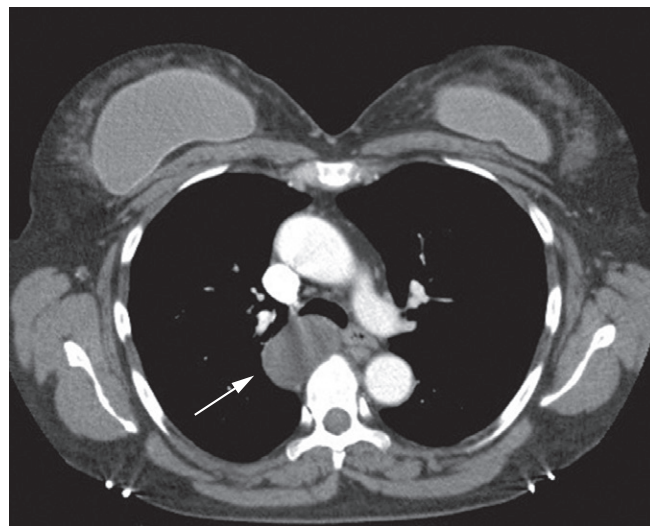


(b)

Fig. 2.61 Retrosternal goitre. (a) CXR showing a large, right-sided, superior mediastinal mass displacing the trachea. (b) CT in the same patient showing the heterogeneously enhancing mass (arrow) to the right of the trachea (*).



(a)



(b)

Fig. 2.62 (a) CXR and (b) CT in a patient with an incidental mediastinal mass, shown to represent a bronchogenic cyst (arrow). Note the bilateral breast implants on the CT.

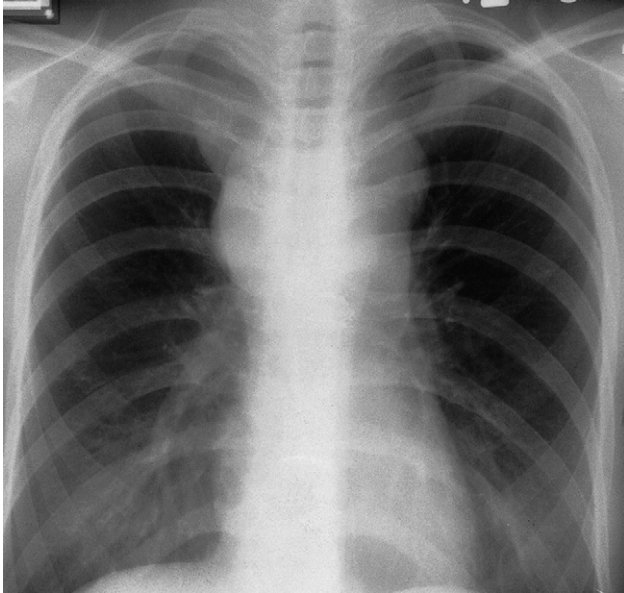
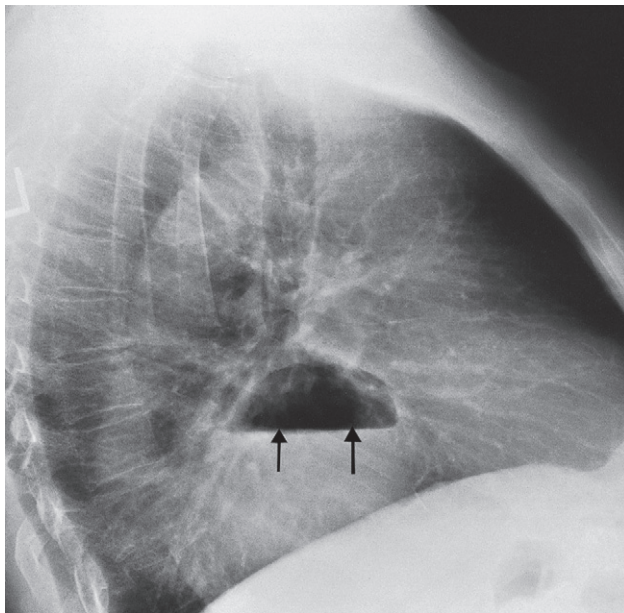


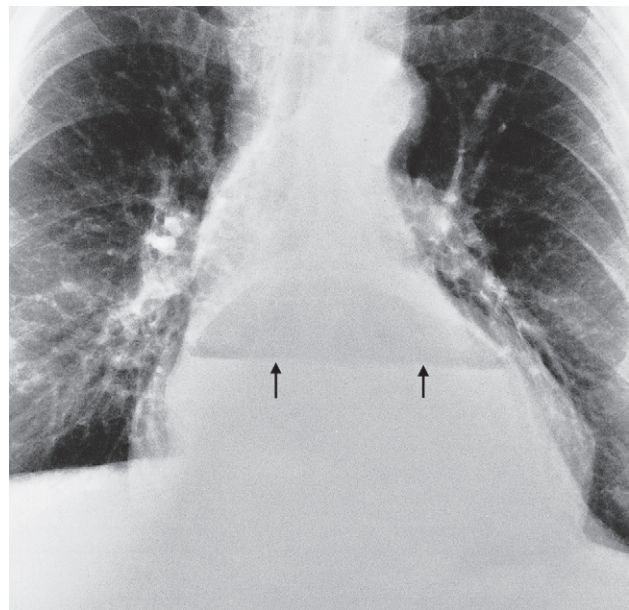
Fig. 2.63 Superior mediastinal mass. CXR showing lymph node enlargement. Note the bilateral lobular masses.

of the three compartments and it is often possible to diagnose enlarged lymph nodes from their lobulated outlines and the multiple locations involved (Fig. 2.63).

- Neurogenic tumours are by far the commonest cause of posterior mediastinal masses. Pressure deformity of the adjacent ribs and thoracic spine is often visible.
- Certain tumours, such as dermoid cysts and thymomas, are, for practical purposes, confined to the anterior mediastinum.
- Calcification occurs in many conditions, but almost never in malignant lymphadenopathy. Occasionally, the calcification is characteristic in appearance, e.g. curvilinear in vascular wall calcification.
- A mediastinal mass due to a hiatus hernia is usually easy to diagnose on plain films because it often contains air and may have a fluid level, best seen on the lateral view (Fig. 2.64).
- Masses in the right cardiophrenic angle anteriorly are usually all either large fat pads, benign pericardial cysts, or hernias through the foramen of Morgagni (Fig. 2.65).



(a)



(b)

Fig. 2.64 Hiatus hernia. (a) Lateral and (b) posteroanterior chest films showing characteristic retrocardiac density containing an air-fluid level (arrows).

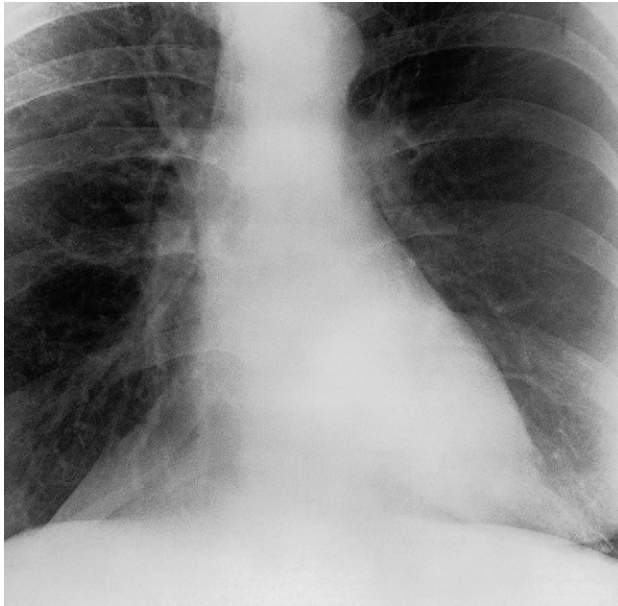


Fig. 2.65 Fat pads in both cardiophrenic angles. Note the loss of clarity of the adjacent cardiac outline – an example of the silhouette sign. The anterior location was confirmed on the lateral view.

Computed tomography

Computed tomography provides much more information than CXRs; occasionally, a specific diagnosis can be made. MRI is used only in highly selected cases, e.g. where CT contrast agents are contraindicated or in demonstrating the relationship of a posterior mass to the spinal canal (Fig. 2.66). There are two main advantages of CT.

1 Abnormalities can be accurately localized. Knowledge of the precise shape, position and size of a mediastinal mass frequently narrows the differential diagnosis. For instance, contiguity of the mass with the thyroid in the neck suggests a goitre (see Fig. 2.61), and multiple oval-shaped masses suggest lymphadenopathy (Fig. 2.67). Solid masses in the anterior mediastinum (Fig. 2.68) have a limited number of possibilities.

2 Occasionally, the density of the abnormality reveals its nature:

- Fat can be recognized as such, which is useful in distinguishing large cardiophrenic angle fat pads or unusual mediastinal fat collections from tumours, e.g. in

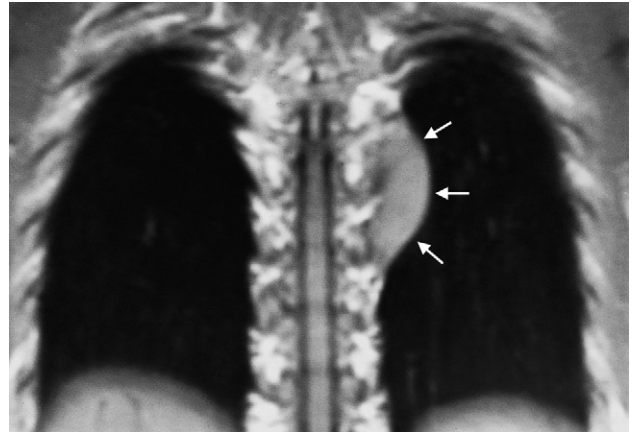


Fig. 2.66 Neurofibroma in the posterior mediastinum. MRI showing the neurofibroma (arrows) lying against the spine, but not growing into the spinal canal.

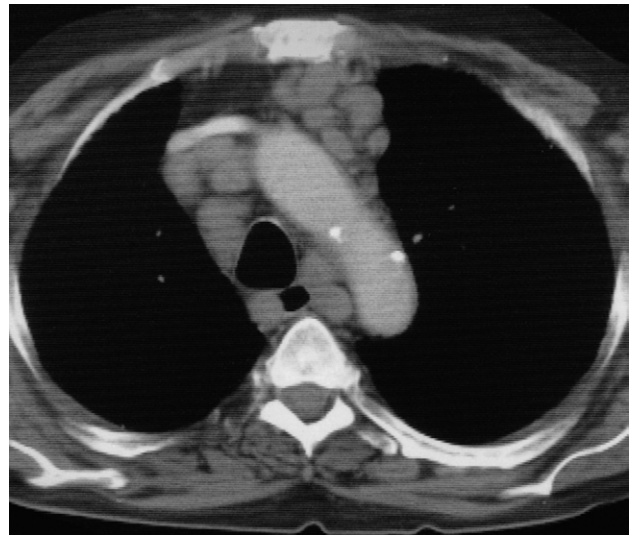


Fig. 2.67 Extensive mediastinal lymphadenopathy (caused by lymphoma) shown by CT.

Cushing's disease. Cystic teratomas (dermoid cysts) may contain recognizable fat.

- Because of its high iodine content, thyroid tissue is of higher attenuation than muscle prior to contrast medium administration. After contrast, it enhances brightly (see Fig. 2.61b).

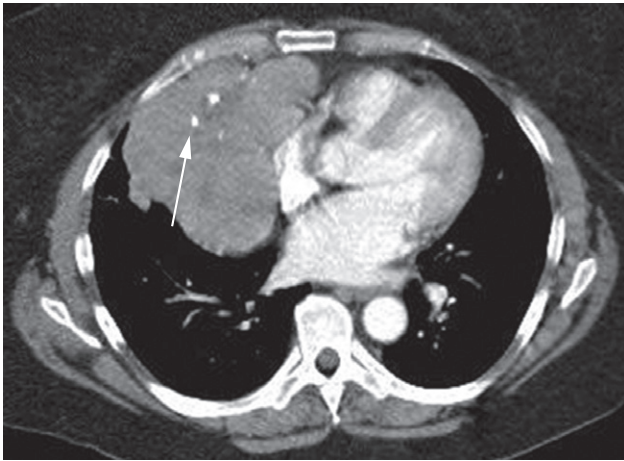


Fig. 2.68 Thymoma. CT showing a large, lobulated, anterior mediastinal mass with punctuate calcification (arrow), which proved on resection to be a thymic tumour.

- Intravenous contrast enhancement permits delineation of aneurysms (see below) and anomalous blood vessels from other masses.
- Calcification is readily seen. The presence of calcification in a mass is frequently seen in benign conditions.
- Cysts containing clear fluid, e.g. pericardial cysts and some bronchogenic cysts (see Fig. 2.62b), can be recognized by a CT number close to water (0 Hounsfield units).

Aortic aneurysm

Dilatation of the *ascending aorta* may be due to aneurysm formation or secondary to aortic regurgitation, aortic stenosis or systemic hypertension. Substantial dilatation of the ascending aorta is needed before a bulge of the right mediastinal border can be recognized; aortic unfolding is a commoner cause of a bulge of the right superior mediastinum than ascending aortic aneurysm.

The two common causes of aneurysm of the *descending aorta* are atheroma and aortic dissection. A rarer cause is previous trauma, usually following a severe deceleration injury. Descending aortic aneurysms are often visible on CXRs and atheromatous aneurysms usually show calcification in their walls.

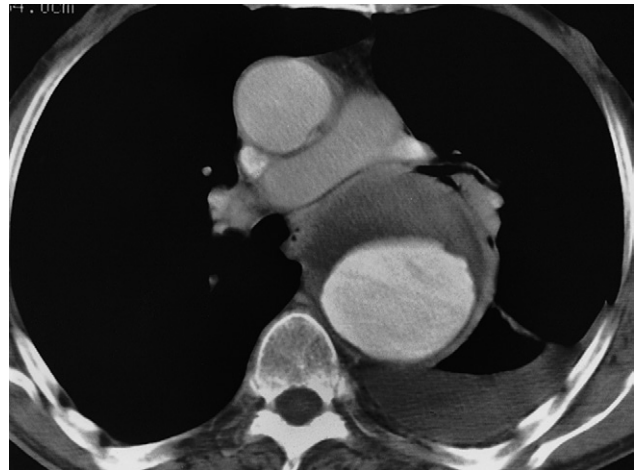


Fig. 2.69 CT showing an aneurysm of the descending aorta. The lumen has been opacified by intravenous contrast enhancement. The unopacified component is clot lining the aneurysm.

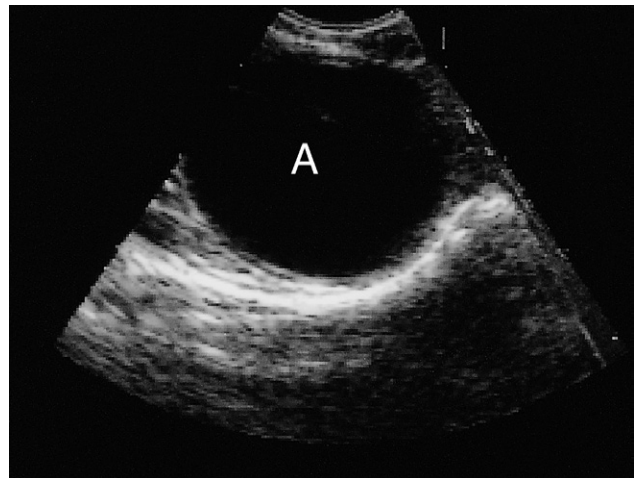
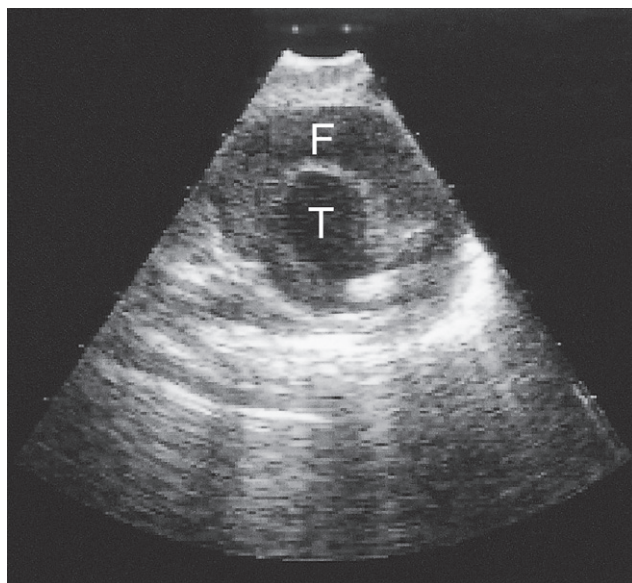


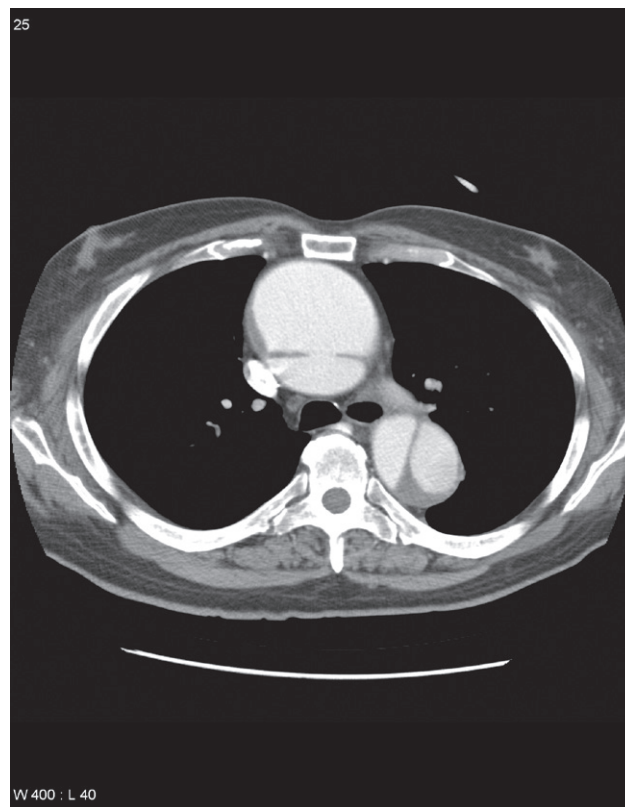
Fig. 2.70 Normal transoesophageal echocardiogram showing a normal descending aorta (A).

Computed tomography with intravenous contrast enhancement, magnetic resonance angiography (MRA) and/or echocardiography are very useful when aortic aneurysms are assessed (Figs 2.69–2.71). It is important to know the extent of aortic dissections because those involving the ascending aorta are treated surgically, while those confined to the descending aorta are usually treated by an



(a)

Fig. 2.71 (a) Transoesophageal echocardiogram showing the true (T) and false (F) lumina in the descending aorta. (b) CT showing the displaced intima separating the true and false lumina in the ascending and descending aorta.



(b)

endovascular approach if conservative management is not appropriate.

Standard echocardiography shows dissection of the aortic root, but transoesophageal echocardiography shows dissections distal to the aortic root and in the descending aorta as well. Aortic dissections can also be shown with CT (and MRI) and these non-invasive techniques have, in practice, replaced aortography.

Pneumomediastinum

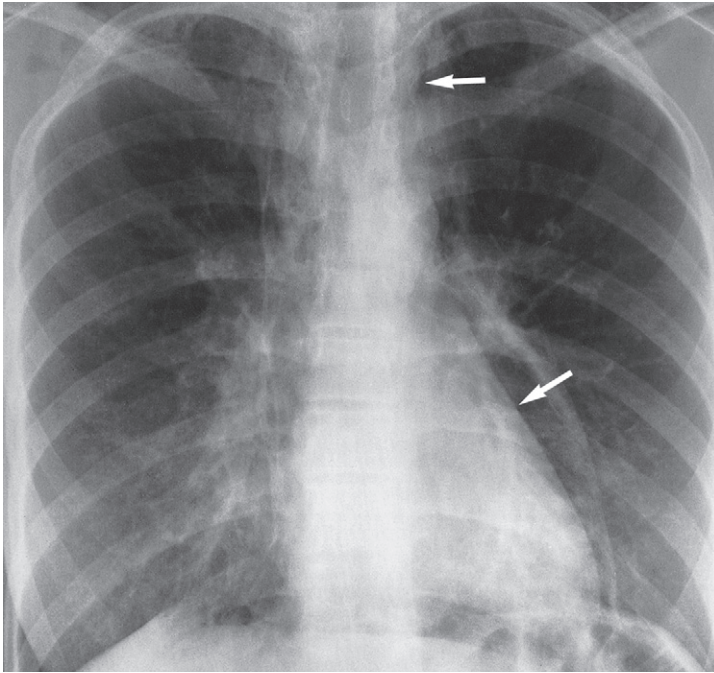
Air in the mediastinum indicates a tear in the oesophagus or an air leak from a bronchus (provided the air has not tracked into the mediastinum from the root of the neck, adjacent chest wall or retroperitoneum). These tears may be spontaneous or follow trauma, most commonly from endoscopy, following forceful vomiting (Boerhaave's syndrome) or the ingestion of sharp foreign bodies.

Spontaneous leakage from small bronchi in the lungs is most commonly seen in patients with asthma. The air, which tracks through the interstitial tissues of the lung into the mediastinum, is seen as fine streaks of transradiancy within the mediastinum, often extending upward into the neck (Fig. 2.72).

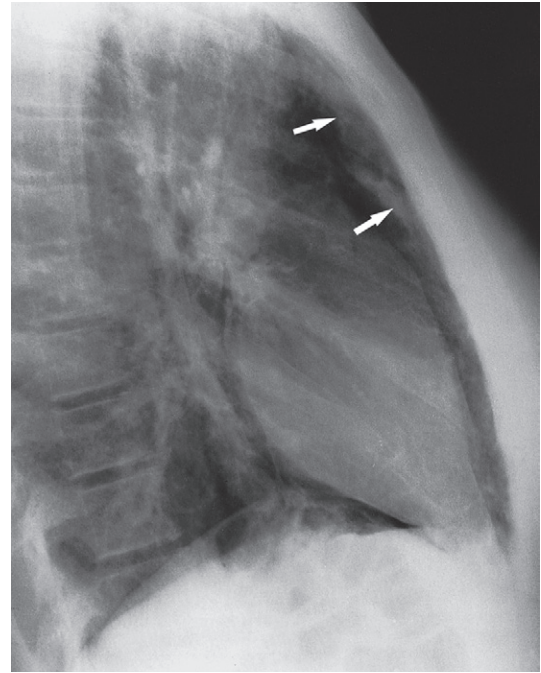
Hilar enlargement

The normal hilar opacities are composed of pulmonary arteries and veins. The main lower lobe arteries are typically 9–16 mm in diameter. Hilar lymph nodes cannot be identified as separate opacities on CXR and the walls of the central bronchi are too thin to contribute to any extent to the bulk of the hilar structures.

Hilar enlargement (Figs 2.73 and 2.74) raises two questions. Firstly, is the enlarged hilum due entirely to large blood vessels or to a mass? Vascular enlargement often



(a)



(b)

Fig. 2.72 Pneumomediastinum showing air (arrows) in the mediastinum extending up into the neck. (a) Posteroanterior and (b) lateral views.

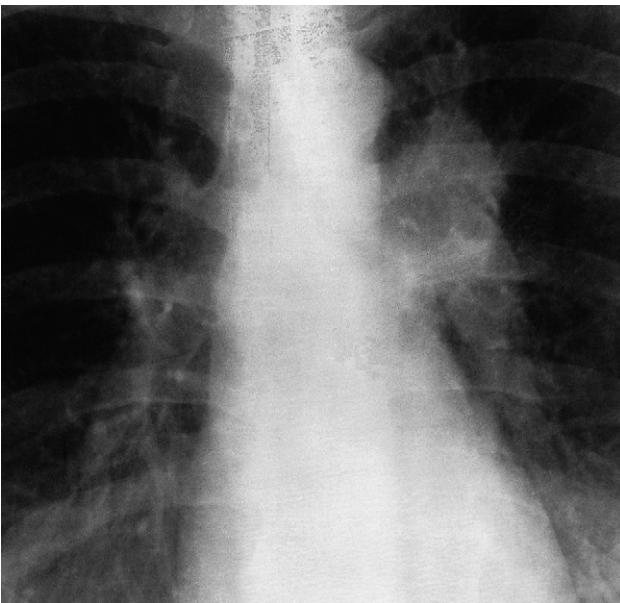


Fig. 2.73 Lobulated mass at the left hilum from enlarged lymph nodes. The right hilum is normal. The lymphadenopathy in this case was due to metastases from a bronchial carcinoma (not visible on this image) in the left lower lobe.

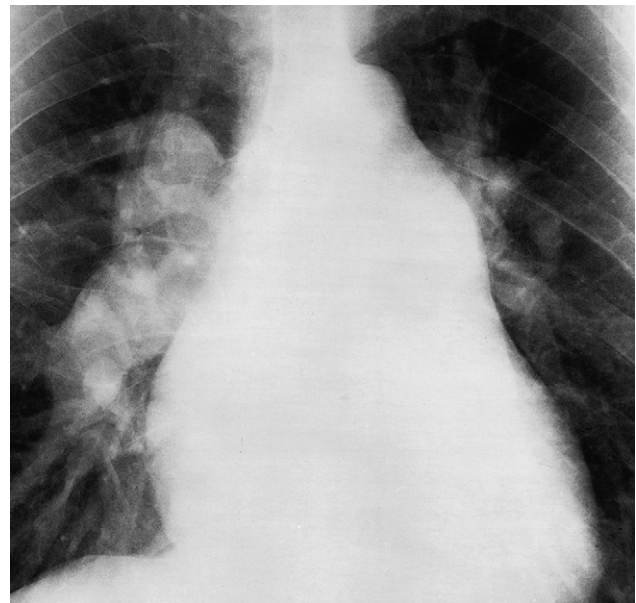


Fig. 2.74 Enlargement of the hilar arteries in a patient with severe pulmonary hypertension. Note that the heart and the main pulmonary artery are also enlarged and that the hilar opacities branch in the manner expected of arteries.



Fig. 2.75 Bilateral hilar adenopathy. The enlarged hila are lobular in outline and dense. The diagnosis in this patient was sarcoidosis.

demonstrates a branching pattern, is typically bilateral and may be accompanied by cardiac enlargement. Secondly, if a hilar mass is present, what is its nature? Hilar masses are nearly always due to either lymph node enlargement or carcinoma of the bronchus. In practice, if there is any clinical doubt the patient will have CT for further evaluation.

Lymph node enlargement

Usually more than one hilar node is enlarged, so in patients with lymphadenopathy the hilum appears lobulated in outline (Fig. 2.75). The adjacent bronchi are normal or very slightly narrowed. The causes of hilar enlargement are summarized in Box 2.3.

Box 2.3 Causes of hilar enlargement

- Metastases from carcinoma of the bronchus
- Lymphoma
- Infections: tuberculosis, histoplasmosis, fungal
- Sarcoidosis

Unilateral enlargement of hilar lymph nodes may be due to the following:

- Metastases from carcinoma of the bronchus (see Fig. 2.73), in which case the primary tumour is often visible; metastases from other primary sites are rare.
- Malignant lymphoma.
- Infections, particularly tuberculosis, and histoplasmosis in endemic areas. Tuberculosis is the commonest cause of unilateral hilar adenopathy in children.

Bilateral enlargement of hilar nodes occurs in:

- Sarcoidosis, which is far and away the commonest cause. The diagnosis is almost certain if the hilar enlargement is symmetrical and if the patient is asymptomatic, or has either erythema nodosum or iridocyclitis (see Figs 2.75 and Fig. 2.87). Simultaneous enlargement of the right paratracheal nodes is common. Lung changes are sometimes visible.
- Malignant lymphoma.
- Tuberculosis. African and Asian races show this form of the disease in which substantial nodal enlargement can be a feature. It is rare to see bilateral hilar enlargement due to tuberculosis in Caucasians.
- Fungal diseases, which are rare causes of bilateral hilar enlargement.

Neoplasm

Primary carcinoma of the bronchus frequently presents as a hilar mass. If lobar collapse/consolidation or narrowing of the adjacent bronchus is visible the diagnosis of carcinoma is virtually certain.

Diaphragm

Elevation of the diaphragm may be bilateral or unilateral, and secondary to abdominal distension/pathology (such as an abdominal mass or a subphrenic abscess), volume loss in the adjacent lung or a phrenic nerve palsy. It should always be borne in mind that subpulmonary effusion may mimic elevation of a hemidiaphragm (see Fig. 2.44). It is also important to realize that minor elevation of a hemidiaphragm is a relatively common incidental finding of no significance.

Marked elevation of one hemidiaphragm with no other visible abnormality suggests either paralysis or eventra-

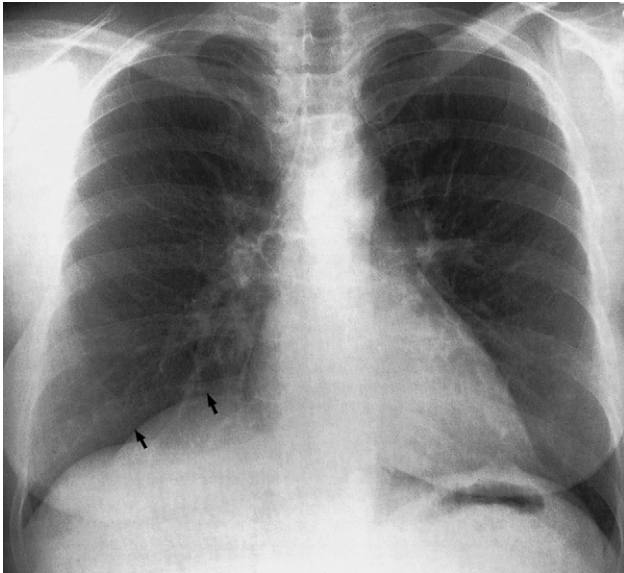


Fig. 2.76 Localized eventration of the diaphragm. There is a smooth localized elevation of the medial half of the right hemidiaphragm (arrows). On the lateral view, the eventration involved the anterior half of the right hemidiaphragm.

tion. Paralysis results from disorders of the phrenic nerves, e.g. invasion by carcinoma of the bronchus or damage following thoracic surgery. The signs are elevation of one hemidiaphragm, which on fluoroscopy or ultrasound shows paradoxical movement, i.e. it moves upward on inspiration. Eventration of the diaphragm is a congenital condition in which the diaphragm lacks muscle and becomes a thin membranous sheet. Except in the neonatal period it is almost always an incidental finding and does not cause symptoms. Eventration may involve all (usually the left) or part of one hemidiaphragm, resulting in a smooth 'hump' (Fig. 2.76).

Rupture of the diaphragm is discussed later in this chapter.

Chest wall

The chest wall should be examined for evidence of soft tissue swelling or rib abnormality. Because ribs are curved structures, some portions are always foreshortened on CXRs. Therefore, if a rib abnormality is suspected, CT

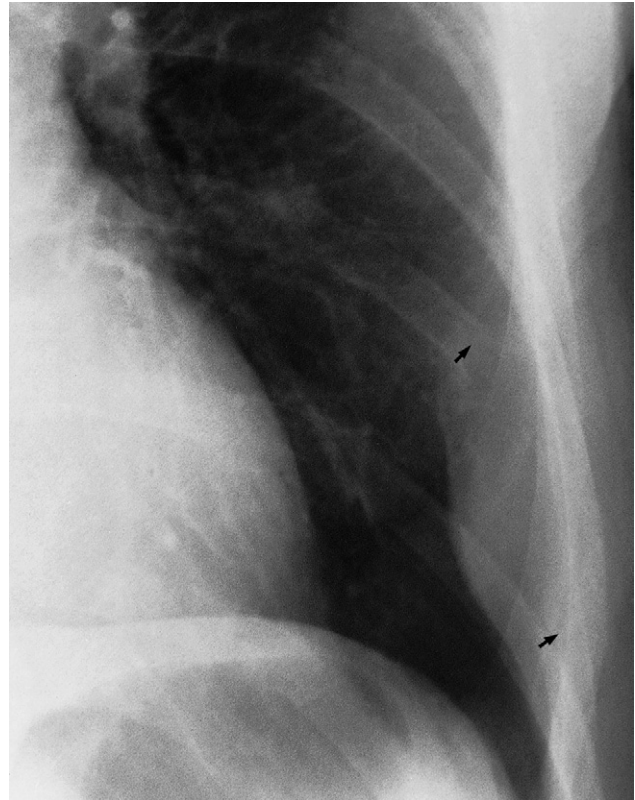


Fig. 2.77 Soft tissue swelling associated with a rib lesion. In this patient with myeloma in a rib, the soft tissue swelling is more obvious than the rib destruction. The bone between the two arrows has been destroyed. This important sign could be easily overlooked unless special attention is paid to identifying rib destruction in the region of soft tissue swelling.

oblique views should be obtained for further clarification. Soft tissue swelling occurs with a number of rib lesions: fractures, infections and neoplasms (Fig. 2.77). The soft tissue swelling may be more obvious than the rib lesion. Congenital abnormalities of the ribs are common, but rarely of clinical significance. It is important not to mistake bifid ribs or fused ribs for lung opacities on plain films.

SPECIFIC DISORDERS

The following section is devoted to specific thoracic disorders.

Bacterial pneumonia

The major purpose of CXR in patients with suspected chest infection is to establish whether or not pneumonia is present. Diagnosing the responsible infectious agent is rarely possible on radiological grounds as there is considerable overlap in the appearance of various bacterial pneumonias, and there is even overlap in the appearance of bacterial, fungal and viral pneumonias.

The basic radiological feature of pneumonia is one or more areas of consolidation, varying from a small, ill-defined opacity to a large opacity involving the whole of one or more lobes (see Fig. 2.16). Consolidation may be accompanied by loss of volume of the affected lobe – a feature that is particularly common in children. Cavitation may occur within the consolidated areas. Cavitation is a particular feature of infections with staphylococci, Gram-negative and anaerobic bacteria and tuberculosis.

The differentiation between pneumonia and pulmonary oedema or pulmonary infarction may, at times, be difficult or impossible radiographically. The clinical features usually decide the issue.

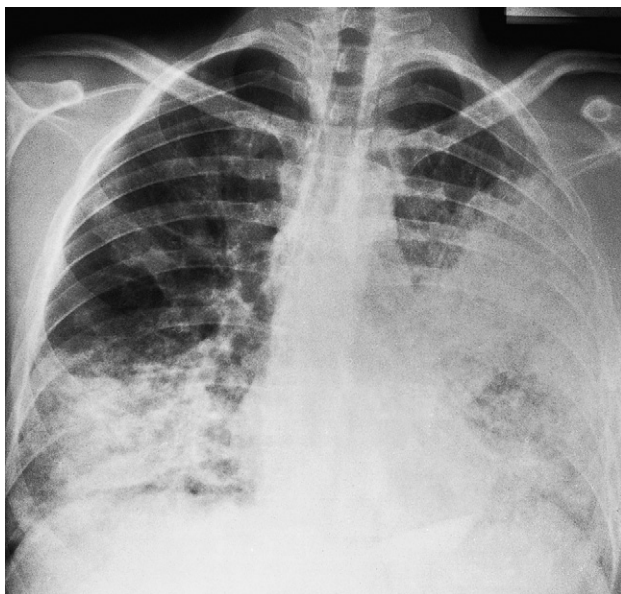


Fig. 2.78 Bilateral bronchopneumonia. There is widespread bilateral patchy consolidation.

A common infecting organism in community-acquired lobar pneumonia is *Streptococcus pneumoniae* (pneumococcal pneumonia). In pneumococcal pneumonia, there is usually dense consolidation of a considerable portion of one lobe, usually without loss of volume. There may be an associated pleural effusion.

When the consolidation is patchy, involving one or more lobes, it is commonly referred to as bronchopneumonia (Fig. 2.78). The most frequent causes of community-acquired bronchopneumonia are *Staphylococcus aureus*, various Gram-negative and anaerobic bacteria and *Mycoplasma pneumoniae*.

Pneumonia may be secondary to obstruction of a major bronchus, carcinoma being a common cause of obstruction. Bronchial obstruction should always be considered in any patient presenting with consolidation of one lobe, or of two lobes supplied by a common bronchus (e.g. the right middle and lower lobes), particularly if there is associated loss of volume.

See also the section 'Pulmonary tuberculosis' below.

Viral and mycoplasma pneumonia

Viral pneumonia and pneumonia due to *Mycoplasma pneumoniae* may produce widespread ill-defined consolidation (Fig. 2.79) and loss of clarity of the vascular markings, which on occasion may resemble pulmonary oedema. Alternatively, only a localized area of consolidation may be seen. Pleural effusions are rare. The radiological abnormality may persist for many weeks after clinical recovery.

Lung abscess

A lung abscess is a localized suppurative lesion of the lung parenchyma. The most frequent causes are:

- Aspiration of food or secretions. Such abscesses are usually in the apical (superior) segments of the lower lobes or in the posterior segments of the upper lobes.
- Infection beyond an obstructing lesion in the bronchus.
- Infected emboli, particularly in drug addicts.

A lung abscess is usually seen as a spherical opacity containing a central lucency due to air within the cavity (see Fig. 2.20). An air–fluid level may be present. It can be difficult or impossible to distinguish an infective lung

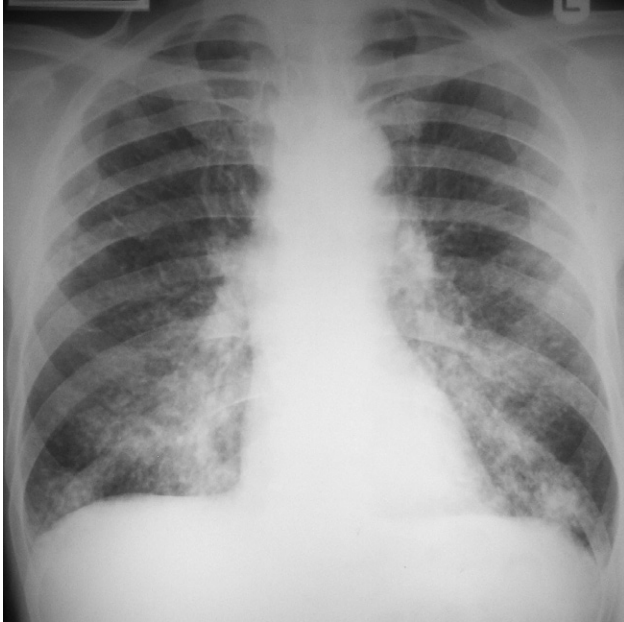


Fig. 2.79 Viral pneumonia, showing widespread, ill-defined, small areas of consolidation in both lungs.

abscess from a cavitating lung neoplasm or cavitation in Wegener's granulomatosis.

Pulmonary tuberculosis

Pulmonary tuberculosis is usually divided into primary and postprimary forms even though these divisions are not clear-cut. Primary tuberculosis is the result of the first infection with *Mycobacterium tuberculosis* and usually occurs in childhood. Postprimary tuberculosis, the usual form in adults, is believed to be re-infection, the patient having developed relative immunity following the primary infection. Tuberculosis (and atypical mycobacterial infections) is seen commonly in patients with acquired immune deficiency syndrome (AIDS).

Primary tuberculosis

In primary tuberculosis, an area of consolidation, known as the Ghon focus, develops in the periphery of the lung – usually in the mid or upper zones. Usually, the pulmonary opacity is small, but it may occasionally involve most

of the lobe. Sometimes the pulmonary consolidation is so small that it is invisible. The consolidation is often accompanied by visibly enlarged hilar or mediastinal lymph nodes (Fig. 2.80a). This combination of pulmonary consolidation and lymphadenopathy is known as the *primary complex*. The clinical features of the primary complex vary. The majority of patients have few, if any, symptoms; the remainder have fever, cough and malaise.

In most cases, whether treated or not, the primary complex heals and often calcifies. A calcified primary complex often remains visible throughout life.

Spread of primary tuberculous infection may occur via two routes:

- 1 The bronchial tree, leading to tuberculous bronchopneumonia. This appears radiologically as patchy or lobar consolidation; it often involves more than one lobe, may be bilateral and frequently cavitates.

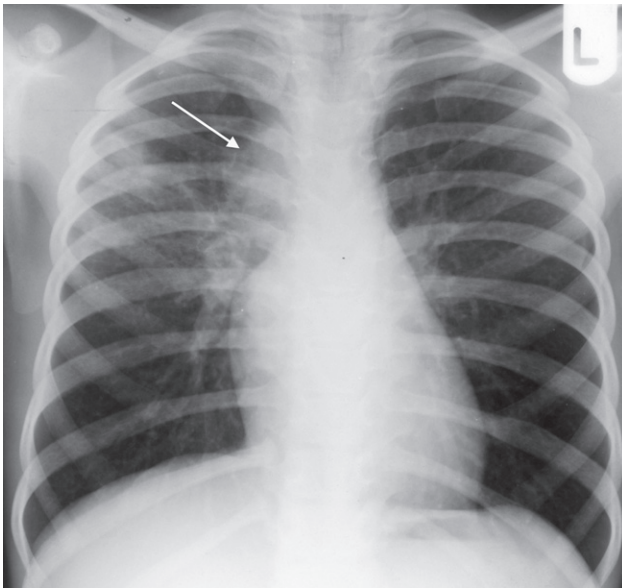
- 2 The blood stream, resulting in *miliary tuberculosis* (Fig. 2.80b) in which there are innumerable small nodules in the lungs, all much the same size and fairly evenly distributed. Usually, the nodules are well defined but in severe cases they become relatively confluent so that the individual nodules are difficult to appreciate. A pleural effusion may be present. It is important to note that the chest film may be normal in the early stages of miliary tuberculosis.

Primary tuberculosis may present with a pleural effusion. Occasionally the primary complex is also visible, but more often the effusion is the only visible abnormality.

Postprimary tuberculosis

Postprimary tuberculosis usually presents with cough, haemoptysis, weight loss, night sweats or malaise. Occasionally, the disease is discovered on a routine chest film. Postprimary tuberculosis is usually confined to the apical and posterior segments of the upper lobes and the apical segments of the lower lobes, though may present as a lower or middle lobe bronchopneumonia. The initial lesions are multiple small areas of consolidation (Fig. 2.81a) and are often bilateral. Pleural effusions are frequent and may be the only radiographic abnormality. The predominant or sole feature, particularly in non-Caucasians, may be mediastinal and/or hilar lymphadenopathy (Fig. 2.82).

If the infection progresses, any areas of consolidation may enlarge and frequently undergo cavitation. Cavities



(a)

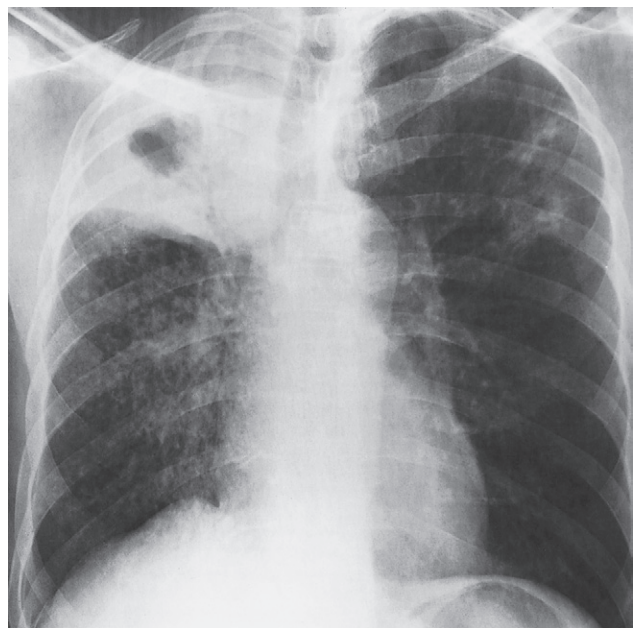


(b)

Fig. 2.80 Tuberculosis. (a) The primary complex. This 7-year-old child shows ill-defined consolidation in the right lung together with enlargement of the draining lymph nodes (arrow). (b) Miliary tuberculosis. The innumerable small nodular opacities uniformly distributed throughout the lungs in this young child are typical of miliary tuberculosis. In this instance, no primary focus of infection is visible.



(a)



(b)

Fig. 2.81 Postprimary tuberculosis. (a) There are ill-defined consolidations scattered in both upper lobes; their size and distribution should suggest the diagnosis of postprimary tuberculosis. (b) The right upper lobe is consolidated and contains a large central cavity. Patchy consolidation from tuberculous bronchopneumonia is seen in the right mid and lower zones and in the left upper zone.

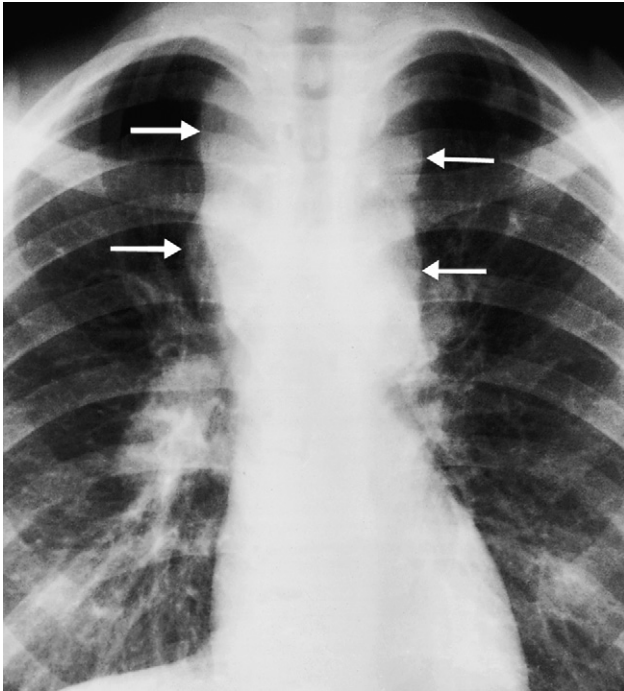


Fig. 2.82 Mediastinal lymphadenopathy (arrows) caused by tuberculosis.

are seen as rounded air-spaces (translucencies) completely surrounded by pulmonary opacification (Fig. 2.81b). As with the primary form, postprimary tuberculosis may spread to give widespread bronchopneumonia or miliary tuberculosis.

The infection may undergo partial or complete healing at any stage. Healing occurs by fibrosis, often with calcification (Fig. 2.83), but both fibrosis and calcification may be seen in the presence of continuing activity. Pleural effusions often leave permanent pleural thickening which may, on occasion, calcify.

Tuberculoma

The term tuberculoma refers to a tuberculous granuloma in the form of a spherical mass, usually less than a centimetre or two in diameter, and mostly much smaller. The edge is usually sharply defined and the lesions are often partly calcified. CT may be needed to demonstrate the

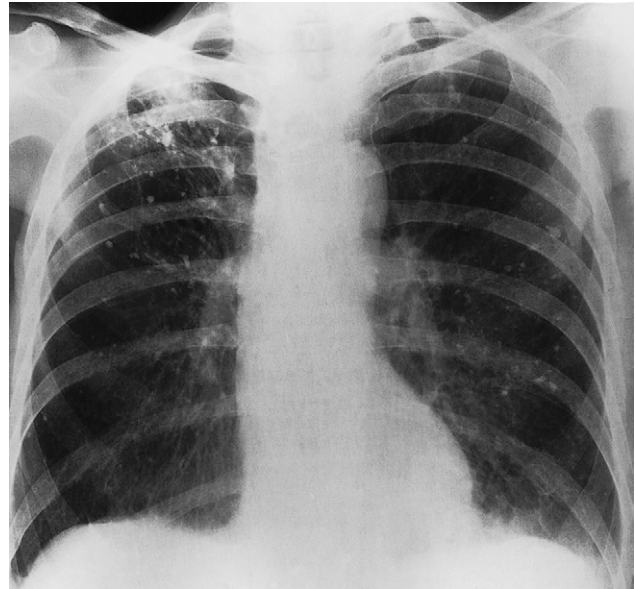


Fig. 2.83 Old calcified tuberculous disease. There are numerous foci of calcification in both lungs. The right upper lobe shows extensive fibrosis and bullae. There was no evidence in this patient that active infection was present. However, given this film in isolation, active disease could not be excluded.

calcification. Tuberculomas are almost invariably inactive even though viable tubercle bacilli may be present deep within the lesions.

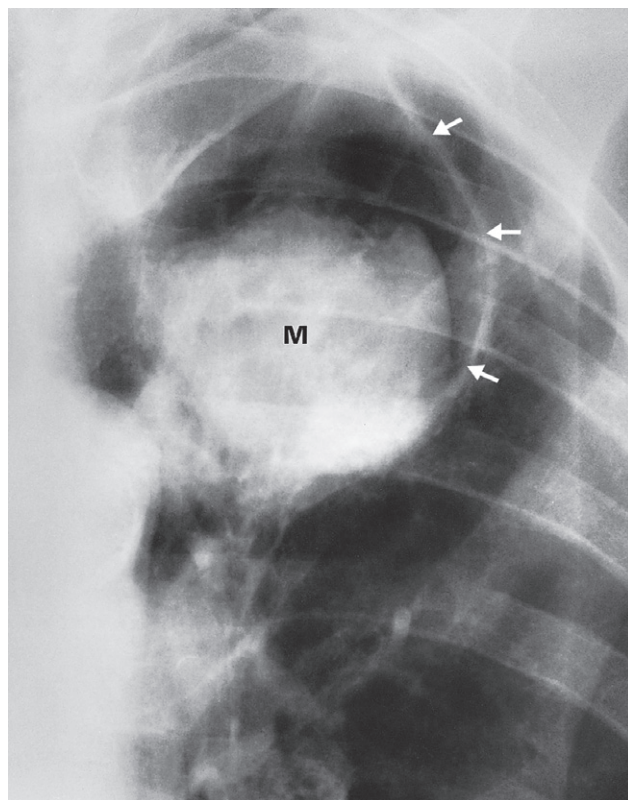
Mycetoma

The fungus *Aspergillus fumigatus* may colonize old tuberculous cavities to produce a ball of fungus (mycetoma) lying free within the cavity (Fig. 2.84). Air is seen between the mycetoma and the wall of the cavity. Cavities containing mycetomas are usually surrounded by other evidence of old tuberculous infection, particularly fibrosis and calcification of the adjacent lung. CT often allows a specific diagnosis of mycetoma to be made.

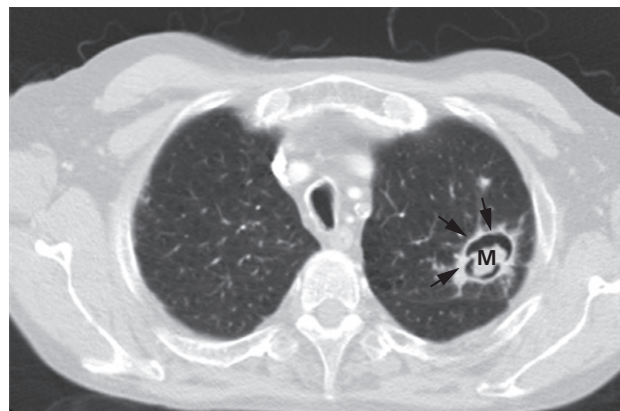
Is the tuberculosis active?

Valuable diagnostic signs of activity are:

- development of new lesions on serial films
- demonstration of cavities.



(a)



(b)

Fig. 2.84 Mycetoma. (a) Plain film in a pre-existing old tuberculous cavity, the wall of which is arrowed. The fungus ball moved around the cavity when the patient was placed on his side. (b) CT in a pre-existing old tuberculous cavity. M, mycetoma.

Lack of change over a period of years is useful evidence against activity, but the progression on serial chest films may be subtle, even with active disease. Many routine chest films in asymptomatic patients show evidence of previous tuberculosis. In a few, the diagnosis of active disease is readily apparent by the presence of cavities or by comparison with previous films. In the remainder it can be a considerable problem to decide which patients to investigate further and which to accept as having old inactive disease. The better defined the opacities and the greater the degree of calcification, the less the likelihood of activity. The presence of ill-defined opacities, even if partially calcified, is suggestive of active disease. However, the decision is often largely based on the clinical findings and the results of sputum examination for tubercle bacilli. It is important to realize that there is no way of excluding activity radiologi-

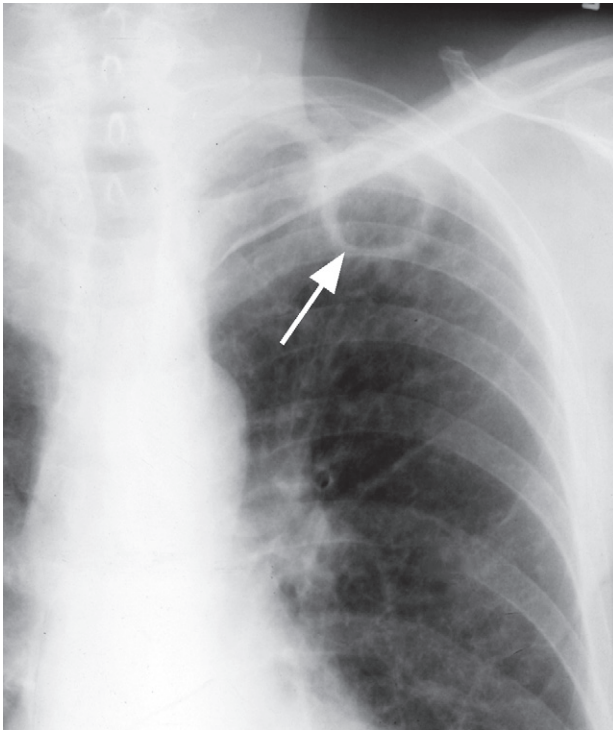
cally unless serial films show no change in the appearances over a prolonged period of time.

Fungal and parasitic diseases

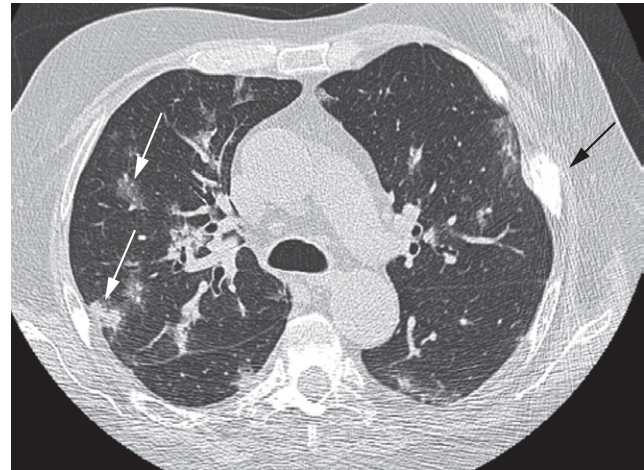
When fungi are inhaled they may produce lung infection. The radiological appearances vary with the particular fungus, but two broad divisions can be made:

1 Infection of an otherwise normal patient. Organisms such as histoplasmosis, coccidioidomycosis and blastomycosis (Fig. 2.85), which are found chiefly in North America, produce lung lesions that are very similar and often identical to tuberculosis. Cavitation is a particular feature. Healing by fibrosis and calcification is frequent.

2 Infection in an immunocompromised host. With impaired immunity, fungi such as *Candida albicans* and *Aspergillus*



(a)



(b)

Fig. 2.85 Fungus infection. (a) CXR in a patient from southeast USA. The cavity (arrow) was due to North American blastomycosis. Note the similarity to tuberculosis. Other fungi, e.g. histoplasmosis, can give an identical appearance. (b) CT (lung windows) in an immunocompromised patient following chemotherapy for metastatic prostate cancer. The CT shows a more diffuse pattern of fungal infiltration in the lungs (white arrows). Note the sclerotic bone metastasis (black arrow).

fumigatus, as well as several of the fungi native to North America, may cause widespread pneumonia. It is not possible to predict the infecting organism from the chest film although recognized signs on HRCT include multiple nodularities with surrounding ground glass appearances (Fig. 2.85b).

Aspergillus fumigatus affects the lung in three ways: (i) it may colonize a pre-existing cavity forming a fungus ball (mycetoma) (see Fig. 2.84); (ii) it may infect the lung in an immunocompromised patient causing severe pneumonia (see below); or (iii) it may be responsible for allergic bronchopulmonary aspergillosis.

Hydatid disease

Pulmonary infection with *Echinococcus granulosus* may result in cysts in the lung or pleural cavity. These cysts may be solitary or multiple and are seen as spherical opacities

with very well-defined borders. Hydatid cysts occasionally rupture to produce complex cavities.

Pneumonia in the immunocompromised host

Patients who are immunocompromised are not only more susceptible to pulmonary infection, often with unusual organisms, but also the pattern of the resulting pneumonia frequently shows an atypical radiographic appearance. Pneumonia in these patients may be due to the usual pathogens, but often it is due to opportunistic fungi, tuberculosis or *Pneumocystis carinii*.

Pneumonia in immunocompromised patients usually causes widespread non-specific pulmonary opacification. It may not even be possible to say whether the opacification is due to infection or to such conditions as pulmonary oedema, pulmonary haemorrhage or neoplastic disease.

The predilection of people with AIDS to develop *P. carinii* pneumonia means that widespread, uniformly distributed pulmonary opacification in a patient with AIDS is usually due to this organism (Fig. 2.86). AIDS patients are also prone to tuberculous infection and the development of

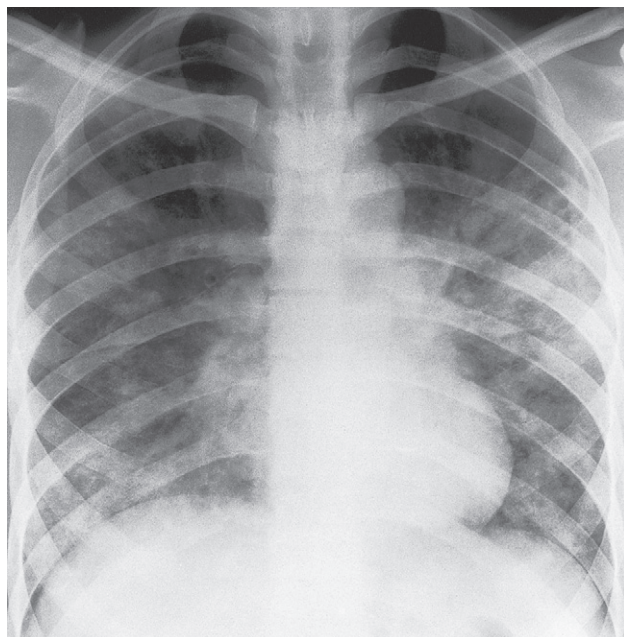
extensive Kaposi's sarcoma, both of which can appear similar to *P. carinii* pneumonia on plain chest radiography.

Sarcoidosis

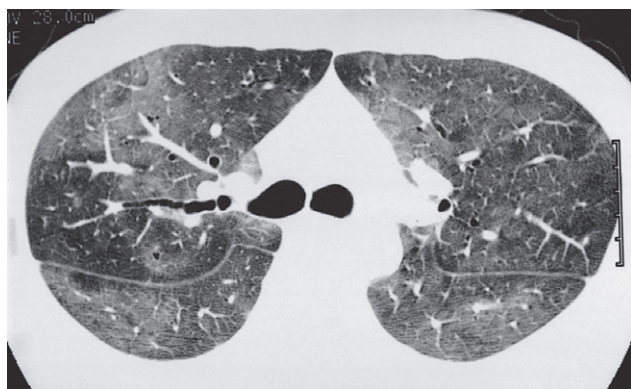
Sarcoidosis is characterized pathologically by non-caseating granulomas in many organs including lung, liver, spleen, lymph nodes, skin and bone. The aetiology is unknown and the diagnosis depends on correlating the clinical, pathological and radiological manifestations.

The radiological manifestations are largely confined to the chest. The features on CXR and CT are:

- Hilar and paratracheal lymphadenopathy. When hilar lymphadenopathy is present it is almost invariably bilateral and is usually symmetrical (see Fig. 2.75). Mediastinal adenopathy is common and the nodes are large enough to be visible on a CXR in about half the patients. Mediastinal lymphadenopathy is most readily recognized in the right paratracheal region. On chest CT (Fig. 2.87), the widespread distribution of the mediastinal lymphadenopathy is readily apparent. Unlike lymphoma, the lymph node enlargement is never predominant in the anterior mediastinum.
- Reticulonodular opacities in the lungs. The pattern varies from uniform small nodular opacities, which may clear on steroid therapy, to coarse reticular opacities maximal in the mid and upper zones, which represent pul-



(a)



(b)

Fig. 2.86 *Pneumocystis carinii* pneumonia in AIDS. (a) Chest x-ray showing typical widespread, low density air-space opacity. (b) HRCT in another patient with similar but less advanced changes.

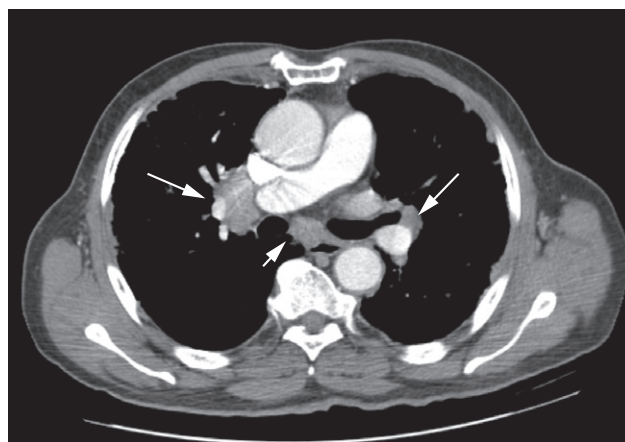


Fig. 2.87 Sarcoidosis. CT scan showing bilateral hilar (long arrows) and subcarinal (short arrow) lymphadenopathy.

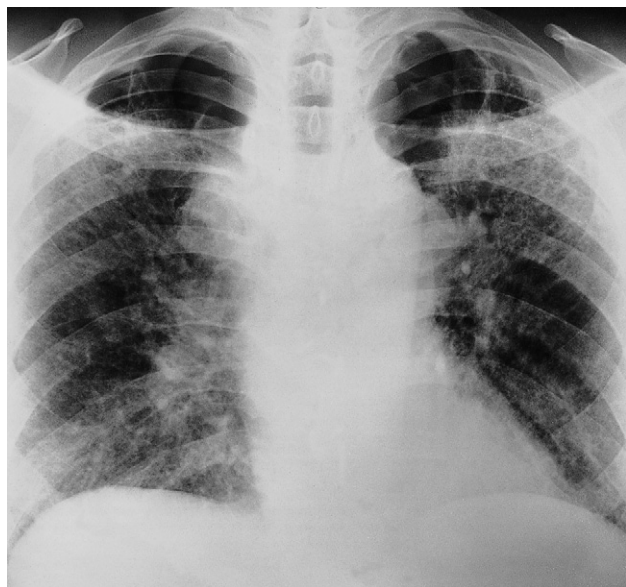


Fig. 2.88 Late fibrotic stage of sarcoidosis. The dense reticulonodular opacifying radiates outwards from the hila, maximally in the mid and upper zones. Enlarged lymph nodes are still visible at the hila and in the right paratracheal region. Many patients with this degree of pulmonary fibrosis from sarcoidosis do not have visibly enlarged lymph nodes.

monary fibrosis (Fig. 2.88). At this stage, the pulmonary disease is often irreversible.

The majority of patients with sarcoidosis of the chest have lymphadenopathy only, which clears without treatment and does not progress to pulmonary involvement. Many are discovered on a routine CXR and have no symptoms. Some present with iridocyclitis, some with erythema nodosum and fever, and a few with polyarthritis.

Approximately 10% of patients with sarcoidosis develop a significant degree of lung involvement; some have visibly enlarged lymph nodes at this stage. Often the lymph nodes get smaller and may return to normal, even though the lung fibrosis persists.

Diffuse interstitial pulmonary fibrosis

The known causes of diffuse interstitial pulmonary fibrosis include: extrinsic allergic alveolitis, collagen vascular diseases (notably rheumatoid arthritis), drug-induced fibrosis, pneumoconiosis and sarcoidosis. However, a substantial

proportion of cases are idiopathic in origin. Several names are given to the most common idiopathic form of diffuse interstitial fibrosis, notably usual interstitial pneumonia (UIP), idiopathic pulmonary fibrosis (IPF) and idiopathic or cryptogenic fibrosing alveolitis (CFA).

Usual interstitial pneumonia (cryptogenic fibrosing alveolitis, idiopathic pulmonary fibrosis)

In UIP there is thickening of the alveolar walls with fibrosis and desquamation. As the disease progresses, the alveolar walls break down and small, rounded air-spaces develop. At this stage, the appearances are known by the descriptive term 'honeycomb lung'. It causes a restrictive ventilation defect with severe reduction in gas transfer across the alveolar walls. The imaging features are:

- Hazy opacifying at the lung bases leading to a lack of clarity of the vessel outlines. Later, ill-defined nodules with connecting lines become discernible, which may contain circular lucencies (honeycomb lung) (Fig. 2.89).
- Decreased lung volume, often marked (Fig. 2.89).
- Eventually, the heart and pulmonary arteries enlarge due to increasingly severe pulmonary hypertension.

These signs are seen on both CXRs and HRCT. HRCT is more sensitive for detecting the changes, particularly areas of ground glass opacifying and honeycombing, and demonstrates the distribution and severity of disease (Fig. 2.89b).

Determining the cause of diffuse pulmonary fibrosis

The distribution of pulmonary opacities may give a clue to its aetiology. In UIP, the lung opacification is often maximal at the bases and at the lung periphery, although it may be fairly uniformly distributed in advanced cases (Fig. 2.89). Scleroderma and rheumatoid arthritis give an identical picture.

The combination of pulmonary fibrosis with certain other signs may lead to a specific diagnosis:

- Substantial past or present hilar/mediastinal adenopathy suggests sarcoidosis (see Fig. 2.88).
- Coexistent conglomerate masses in the mid and upper zones are virtually diagnostic of silicosis or coal miners' pneumoconiosis (see Fig. 2.92).
- Coexistent bilateral pleural thickening and calcification are highly suggestive of asbestosis.

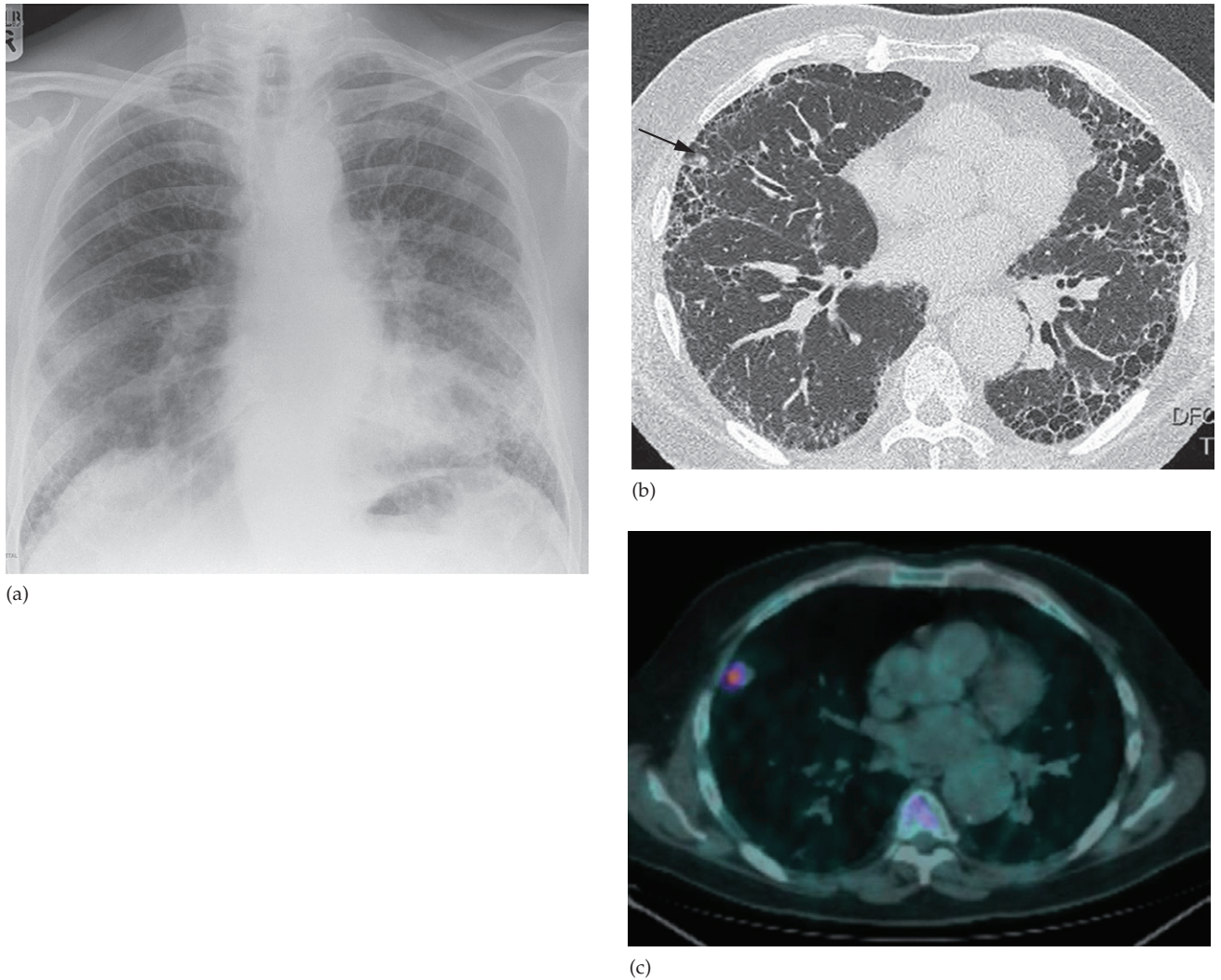


Fig. 2.89 Idiopathic UIP. (a) CXR showing reticulonodular opacifying (honeycomb lung) with basal predominance. Scleroderma, rheumatoid arthritis and drug-induced interstitial fibrosis give a similar picture. (b) HRCT showing the typically subpleural honeycomb distribution in the lungs. (c) Note also the small peripheral nodule in the right lung (arrow), which on FDG-PET/CT was confirmed to represent a lung cancer, which has a higher incidence in these patients.

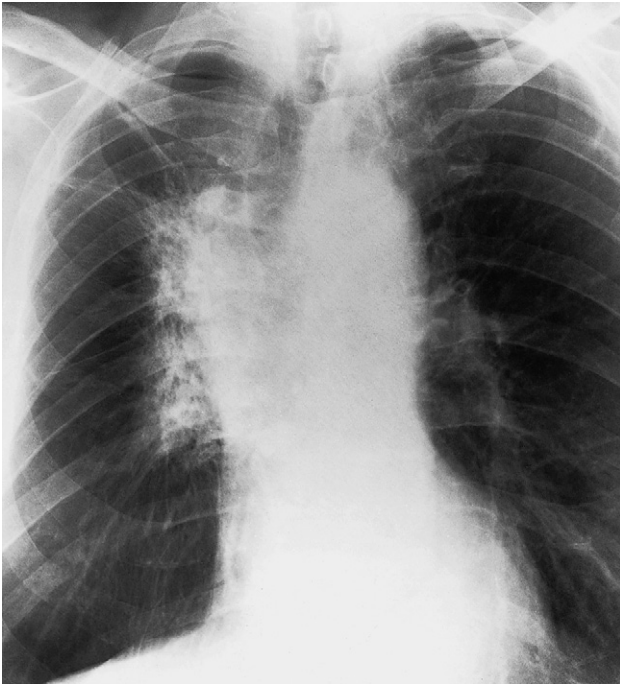


Fig. 2.90 Postradiation fibrosis. The patient had received radiation therapy for a carcinoma in the right upper lobe. Notice the geometric outline to the opacifying corresponding to the radiation field, the resulting mediastinal deviation and distortion of the pulmonary vessels.

- Past or present pleural effusions are highly suggestive of rheumatoid arthritis.

Radiation pneumonitis

Radiation pneumonitis may occur following radiotherapy for intrathoracic neoplasms and breast carcinoma (Figs 2.90 and 2.91). The response of the lung to radiation varies from patient to patient. Initially, there is no radiological change, but within a few weeks ill-defined, small opacities, indistinguishable from infective consolidation, are seen within the radiation field. If the inflammatory change goes on to fibrosis, there is dense, coarse opacification that may be sharply demarcated from the normal lung in a geometric fashion, conforming to the field of radiation but ignoring the lobar boundaries of the lung. There is loss of volume in the fibrosed areas. Extensive pleural thickening is also sometimes seen.

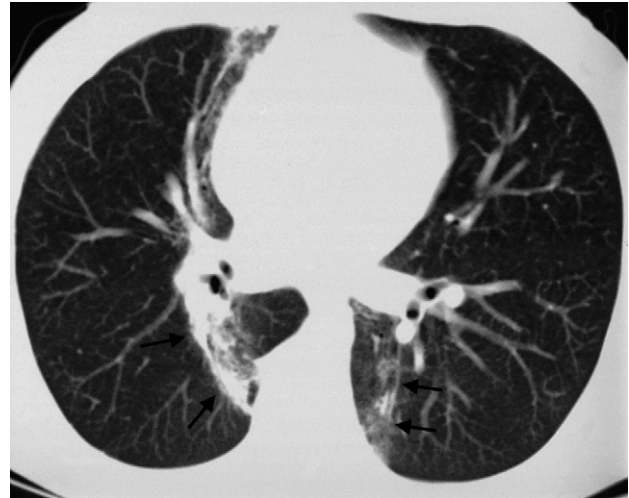


Fig. 2.91 CT in a patient treated with radiation therapy for lymphoma. Note the linear fibrosis (arrows) in the lungs on either side of the mediastinum.

Collagen vascular diseases

This group of diseases includes rheumatoid arthritis, systemic lupus erythematosus, polyarteritis nodosa, systemic sclerosis, dermatomyositis and Wegener's granulomatosis. Various radiological signs occur.

Rheumatoid lung

The most common finding in the chest is pleural effusion. Pulmonary fibrosis, indistinguishable from that seen in idiopathic pulmonary fibrosis, is another important feature.

An interesting sign of pulmonary involvement in rheumatoid arthritis is the development of rounded granulomas in the periphery of the lung, histologically similar to the subcutaneous nodules seen in this disease. These spherical nodules, which may be single or multiple, rarely exceed 3 cm in size. Eventually, many cavitate and then go on to resolve.

Systemic lupus erythematosus

The CXR is usually normal. The commonest abnormalities are pleural effusion and cardiac enlargement due to pericardial effusion. Patchy consolidation in the lungs is occasionally seen.

Scleroderma and dermatomyositis

The cardinal feature is basal reticulonodular opacities from pulmonary fibrosis, similar to that seen in idiopathic pulmonary fibrosis. Pleural effusion is rare. Widening of the oesophagus is a feature of scleroderma that may be visible on the CXR.

Wegener's granulomatosis

The lungs may show one or more well-defined consolidations or masses, usually in the mid zones, which may cavitate. These lesions are often difficult to distinguish from bronchogenic carcinoma, when single, or metastases, when multiple, on radiographic grounds alone.

Pneumoconiosis

The pneumoconioses consist of a group of conditions caused by the inhalation of a variety of dusts related to people's work.

Coal workers' pneumoconiosis

Coal workers' pneumoconiosis is now very uncommon, following the introduction of preventative measures. Simple pneumoconiosis is due to dust retention in the lungs with minor fibrosis. It does not give rise to symptoms, but radiologically it causes many small nodules similar in appearance to miliary tuberculosis. For reasons that are not entirely clear, progressive massive fibrosis may supervene. Progressive massive fibrosis causes homogeneous, rounded opacities in the upper halves of the lungs. The opacities may be unilateral or bilateral and there is usually nodular opacification in the rest of the lungs (Fig. 2.92).

Asbestos-related disease

Inhalation of asbestos fibres may lead to:

- *Pleural plaques.* Localized plaques of pleural thickening, some of which are calcified, are seen along the lateral chest wall and diaphragm. The plaques in themselves are harmless, but they are a useful pointer to previous asbestos exposure (Fig. 2.93, and see Fig. 2.50b).
- *Diffuse pleural thickening,* which may encase one or both lungs, and cause restrictive reduction in pulmonary function.



Fig. 2.92 Progressive massive fibrosis. Note the large oval opacities in the upper halves of both lungs. A nodular pattern is present elsewhere in the lung fields.

- *Pulmonary fibrosis.* Unlike the pleural plaques, which may be seen following minor exposure to asbestos, pulmonary fibrosis (asbestosis) only follows significant exposure. Pulmonary fibrosis in asbestosis is symmetrically bilateral and maximal at the bases, similar to UIP.
- *Development of malignant neoplasms.* Malignant mesothelioma and bronchial carcinoma are both seen with far higher frequency in asbestos-exposed patients than in the general population.

Diseases of the airways

Asthma

The chest film in asthma is usually normal or shows only air-trapping with flattening of the diaphragm. Bronchial



Fig. 2.93 CT showing extensive calcified pleural plaques in both hemithoraces, circumferentially around both lower lobes.

wall thickening may be seen. The main purpose of the CXR in asthma is:

- to determine complications, e.g. atelectasis
- to detect associated pneumonia
- to exclude other causes of acute dyspnoea, e.g. pulmonary oedema, pneumothorax or, rarely, tracheal obstruction.

A CXR should only be undertaken when one or more of the above conditions are a realistic possibility.

Allergic bronchopulmonary aspergillosis results from hypersensitivity to *Aspergillus fumigatus*. Asthma is the cardinal clinical feature of this disease. The radiological signs are allergic consolidations in the lung and proximal bronchiectasis, particularly in the mid and upper zones. The thickened walls of the dilated bronchi may be visible on a CXR.

Bronchiolitis

Severe bronchiolitis in young children, even when life-threatening, may show surprisingly little change on a CXR. The major sign is overinflation of the lungs, leading to a low position of the diaphragm. Some children show widespread, small, ill-defined areas of consolidation, but in many the lungs are clear.

Acute bronchitis

Acute bronchitis in adults and older children does not produce any radiological abnormality unless complicated by pneumonia.

Chronic obstructive pulmonary disease

Chronic obstructive pulmonary disease is an imprecise, but convenient, term that includes several common diseases, including chronic bronchitis and emphysema, and bronchiectasis.

Chronic bronchitis and emphysema

Chronic bronchitis and emphysema often coexist though pure forms of each are seen.

Chronic bronchitis is a clinical diagnosis based on productive cough for at least three consecutive months in two successive years. Pathologically, there is hypertrophy of the mucous glands throughout the bronchial tree. The CXR in uncomplicated chronic bronchitis is normal. If the film is abnormal, a complication such as emphysema, pneumonia or cor pulmonale has occurred, and the radiological features are then those of the complication in question.

Emphysema is defined pathologically as an increase beyond normal size of air-spaces distal to the terminal bronchiole with destructive changes in their walls. The radiological signs of emphysema (Fig. 2.94) are:

- Increased lung volume. The lungs increase in volume because of the combined effect of airways obstruction on abnormally compliant lungs. The diaphragm is pushed down and becomes low and flat. The heart is elongated and narrowed. The ribs are widely spaced and more lung lies in front of the heart and mediastinum. (Overinflation of the lungs can be said to be present if the hemidiaphragms at their midpoint are below the seventh rib anteriorly or the 12th rib posteriorly.)
- Attenuation of the vessels. The reduction in size and number of the pulmonary blood vessels can be generalized or localized. If severe, the involved area is called a bulla. The edge of a bulla is usually sharply demarcated. In some cases, the normal lung adjacent to the bulla is compressed and appears opaque.

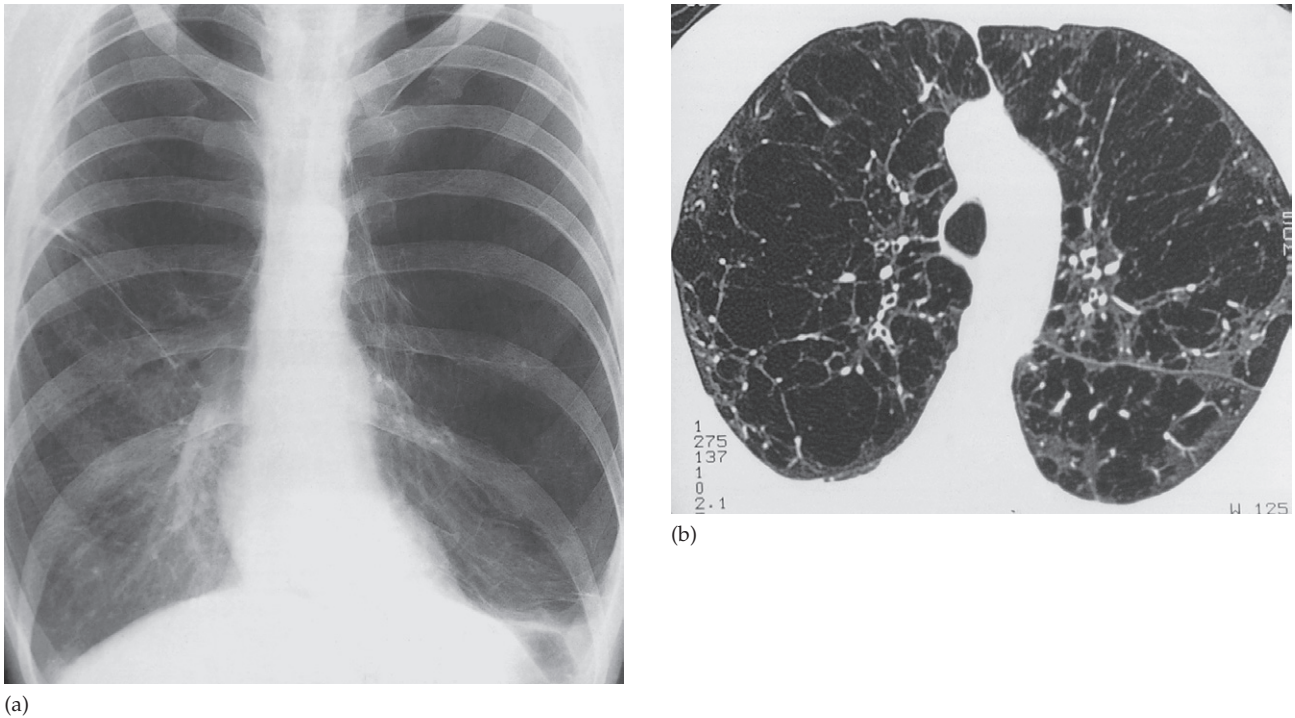


Fig. 2.94 Panacinar emphysema. (a) The diaphragm is low and flat and the ribs are widely spaced, indicating overinflation of the lungs. The peripheral vessels in most of the left lung and the upper half of the right lung are small and attenuated, indicating lung destruction. (b) CT showing innumerable bullae.

Bronchiectasis

Bronchiectasis is defined as irreversible dilatation of the bronchi, often accompanied by impairment of drainage of bronchial secretions leading to persistent infection.

Conditions that cause bronchiectasis include pulmonary infection in childhood, cystic fibrosis and longstanding bronchial obstruction.

The radiological features (Fig. 2.95) are:

- Visibly dilated bronchi. If they contain air, the thickened walls of the dilated bronchi may be seen as tubular or ring opacities. If filled with fluid, the dilated bronchi are either opaque or contain air–fluid levels. As these fluid levels are very short, they have to be looked for very carefully.
- Loss of volume of the affected lobe or lobes is almost invariable.
- A proportion of patients with symptomatic bronchiectasis have a normal CXR.

High resolution CT is very useful both to diagnose bronchiectasis and to assess its extent (Fig. 2.96).

Cystic fibrosis

Cystic fibrosis is an inherited disorder of exocrine glands resulting in secretion of viscid mucus. In cystic fibrosis, the small airways become blocked and secondary infections supervene. The finding of a high sodium chloride concentration in the sweat is diagnostic of the condition.

The radiological findings (Fig. 2.97) are:

- Small, ill-defined consolidations, maximal in the upper zones, some of which show cavitation.
- Bronchial wall thickening and the signs of bronchiectasis, both usually maximal in the upper zones.
- Evidence of airway obstruction. The diaphragm is low and flat and the heart is narrow and vertical, until cor pulmonale develops when cardiac enlargement may occur.

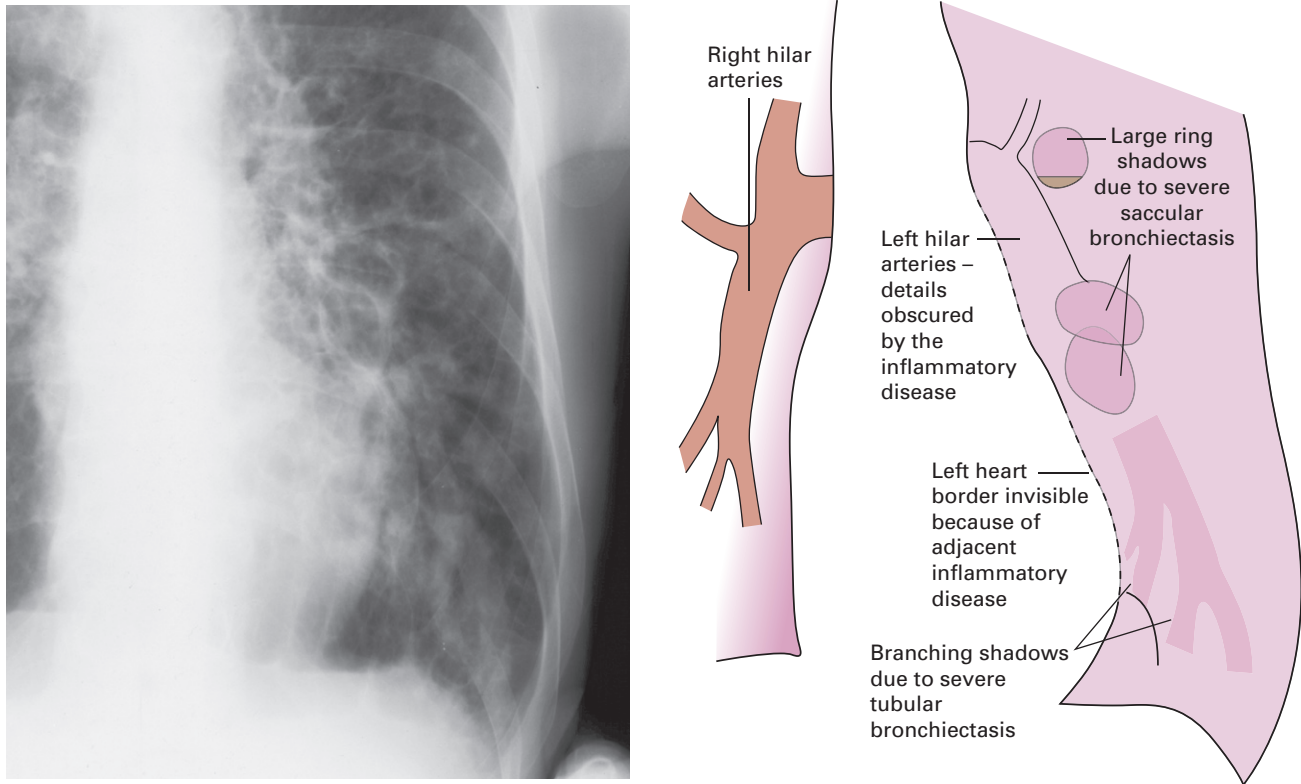


Fig. 2.95 Bronchiectasis. Plain film showing a mixture of saccular and tubular bronchiectasis. The branching ectatic bronchi resemble large blood vessels but should not be confused with them.

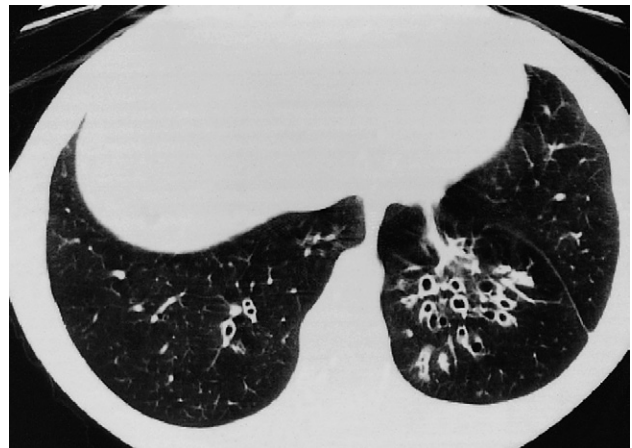


Fig. 2.96 Bronchiectasis. HRCT showing thick-walled, dilated bronchi crowded together in the left lower lobe. The normal appearance is seen in the right lower lobe.



Fig. 2.97 Cystic fibrosis in a 14-year-old child. There is bronchial wall thickening, ring opacities of bronchiectasis and widespread ill-defined opacifying. All these phenomena tend to be maximal in the mid and upper zones. The diaphragm is somewhat low from obstructive airways disease.

Respiratory distress in the newborn

There are many causes of respiratory distress in the first few days of life. Abnormalities are visible on the CXR in the majority; only two conditions are discussed here.

Hyaline membrane disease is one of the commonest abnormalities. It is a disease of the premature infant and is due to deficiency of surfactant in the lungs. Consequently, the alveoli collapse, so preventing gas exchange. The CXR appearance is one of the most important criteria in making the diagnosis.

The basic signs are widespread, very small pulmonary opacities and visible air bronchograms (Fig. 2.98). Air bronchograms are visible because the bronchi are surrounded by airless alveoli. In the milder forms, the nodules are small and the air bronchograms may be the most obvious and easily recognized sign. In the more severe forms, the pul-

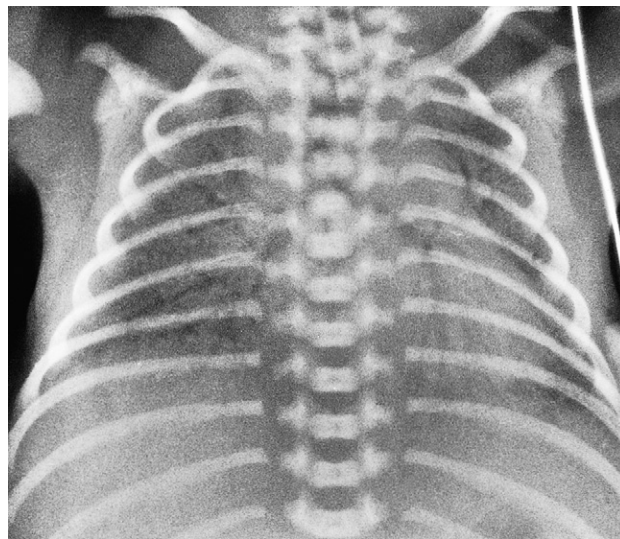


Fig. 2.98 Neonatal respiratory distress syndrome (hyaline membrane disease). Posteroanterior film showing the general granular opacity of the lungs typical of hyaline membrane disease. The vessels, the heart borders and the diaphragm outlines are indistinct and air bronchograms are visible. Note the uniformity of distribution of the changes in the lungs – an important diagnostic feature of hyaline membrane disease.

monary opacities become more obvious and may be confluent; the lungs then appear almost opaque, except for air bronchograms. The changes are nearly always uniform in distribution.

Meconium aspiration (Fig. 2.99). In meconium aspiration, the pulmonary opacification is usually patchy and distinctly streaky. Air bronchograms are not an obvious feature. The diaphragm is often lower than normal due to airways obstruction associated with sticky meconium in the bronchi.

Complications of therapy. In addition to establishing the initial diagnosis in neonates with various causes of respiratory distress, the CXR is vital in detecting complications of therapy. These include pneumothorax, lobar collapse and pneumomediastinum.

Adult respiratory distress syndrome

Adult respiratory distress syndrome (ARDS) is the name given to a syndrome in which the pulmonary capillaries

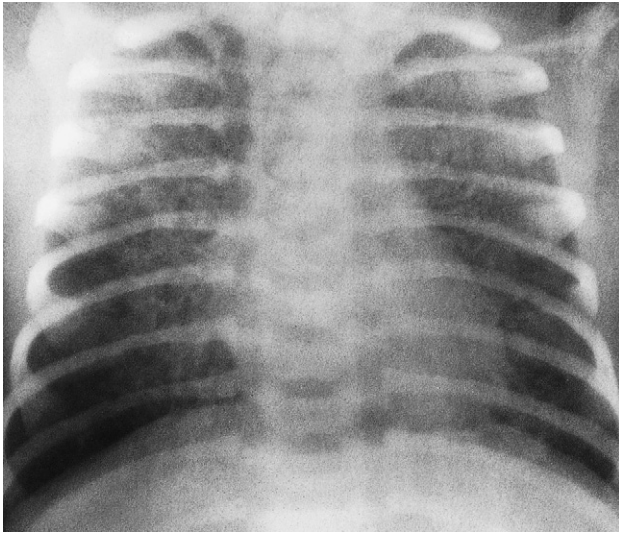


Fig. 2.99 Meconium aspiration. This baby born at term had fetal distress during delivery and was born through meconium-stained liquor. The film shows patchy consolidations rather than the uniform changes seen in hyaline membrane disease. The diaphragm is lower than normal in position, which is another differentiation from hyaline membrane disease.

leak proteinaceous fluid into the surrounding pulmonary interstitium and alveoli. The condition is also known as 'non-cardiogenic pulmonary oedema'. There are many precipitating causes including severe trauma, significant hypotension, septicaemia and fat embolism. It is believed that these insults produce a cascade of events, the nature of which has yet to be fully elucidated, leading to capillary damage, and hence to increased capillary permeability. The patients become increasingly short of breath and hypoxic, requiring mechanical ventilation to stay alive. The mortality, even with intense therapy and assisted ventilation, can be high. There is no specific treatment.

Chest radiographs show widespread pulmonary opacification (Fig. 2.100) resembling cardiogenic pulmonary oedema at first, but the pulmonary opacification becomes more widespread and more uniform over the ensuing 24–48 hours. The radiological abnormality may only develop 12–24 hours after the onset of tachypnoea, dyspnoea or hypoxaemia. As patients with ARDS require assisted ventilation, the chest film is used to detect the complications of ventilator therapy, notably pneumothorax and pneumomediastinum.

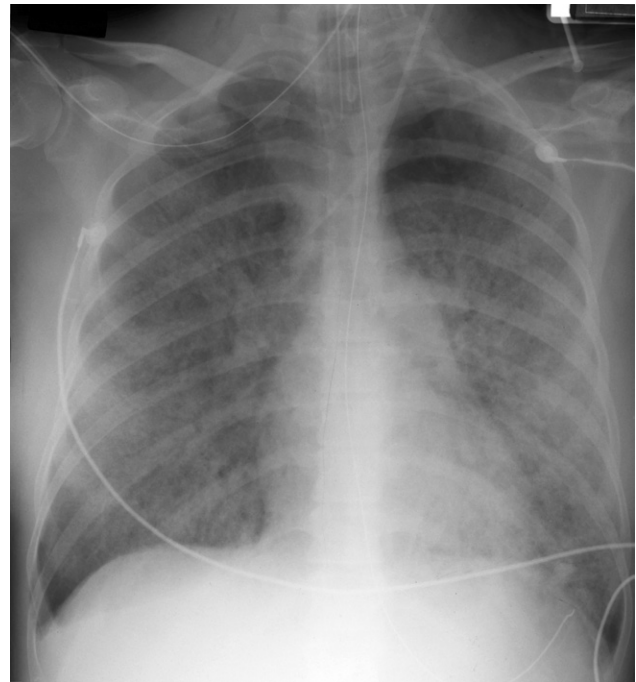


Fig. 2.100 Adult respiratory distress syndrome. There is widespread air-space opacity in the lungs.

Pulmonary emboli and infarction

Pulmonary emboli from thrombi originating in the veins of the legs and pelvis are very common in patients confined to bed, particularly those with heart disease and those who have had major surgery. Small emboli occurring over a long period of time may cause pulmonary hypertension.

Radionuclide lung scans can be performed to confirm or exclude the diagnosis of pulmonary emboli, but CT pulmonary angiography has become the investigation of choice.

Plain film abnormalities

In most cases, even with massive pulmonary embolism, CXRs show no abnormalities due to the emboli. However, in some patients, particularly those with heart disease, infarction occurs. Radiologically, infarcts cause one or more areas of consolidation based on the pleura and the diaphragm. They often affect both lungs and are indistinguishable from pneumonia. The differentiation between

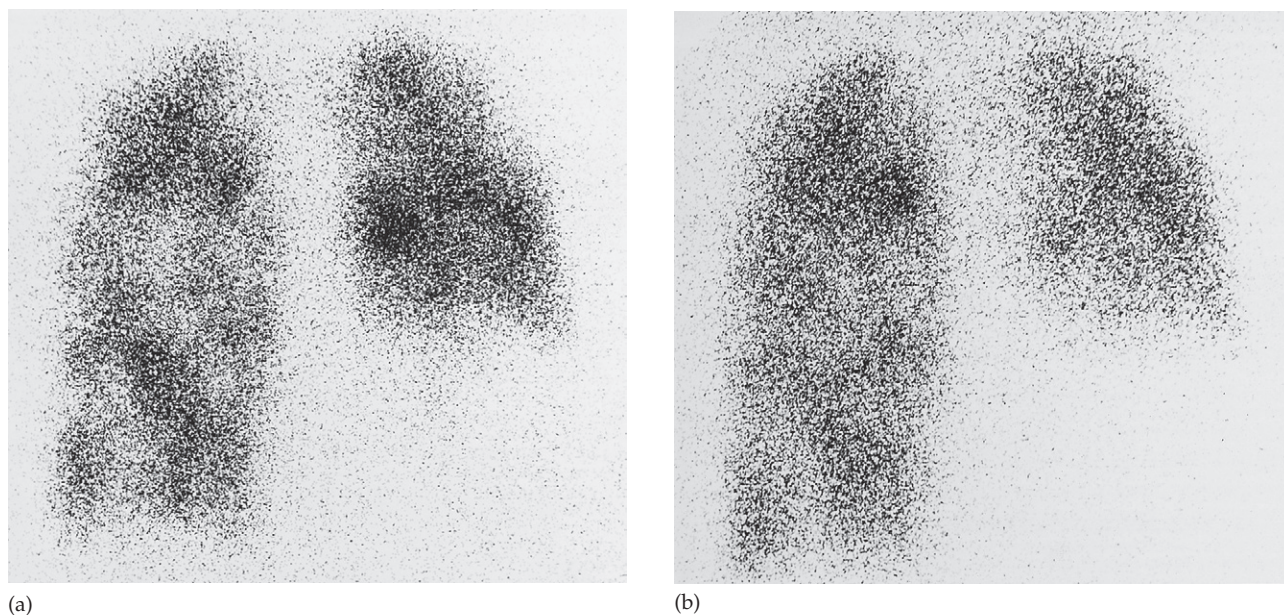


Fig. 2.101 Matched ventilation/perfusion defects. ^{99m}Tc macroaggregate perfusion scan (a) showing matched defects when compared to the ^{81m}Kr ventilation scan (b). Both are anterior scans. The patient had widespread emphysema.

pneumonia and pulmonary infarction depends on clinical rather than radiological factors.

Radionuclide lung scans

Radionuclide lung scans for diagnosing pulmonary embolism have largely been replaced by CT angiography. The diagnosis on radionuclide lung scanning depends on observing the distribution of radionuclide particles in the lungs following intravenous injection. The radionuclide particles do not reach the underperfused portions of the lungs, and, therefore, one or more defects are seen in the perfusion scan. A normal perfusion scan for practical purposes excludes pulmonary embolism.

A ventilation scan is also required in patients with perfusion defects in order to differentiate between the various other causes of perfusion defects, which include pneumonia, pulmonary oedema, tumours, bronchiectasis and emphysema. The ventilation and perfusion scans are compared. If similar defects of the same size and position are present on both scans, they are regarded as matched (Fig.

2.101), and, therefore, due to pneumonia, pulmonary oedema or airways disease; if not, the defects are mismatched (Fig. 2.102) and are likely to be due to pulmonary emboli. Unfortunately, many radionuclide scans are indeterminate and, therefore, unhelpful.

Computed tomography pulmonary angiography

Computed tomography pulmonary angiography involves imaging the pulmonary arteries during a rapid injection of intravenous contrast agent (see Fig. 2.102c). It shows the emboli as filling defects within the lumen of the opacified pulmonary arteries. The technique can demonstrate emboli in large and medium-sized pulmonary vessels, but is less reliable for excluding pulmonary emboli in the more distal, smaller pulmonary arteries.

Trauma to the chest

In major trauma CT is often needed, but a CXR is usually sufficient following minor trauma. A rib fracture can be

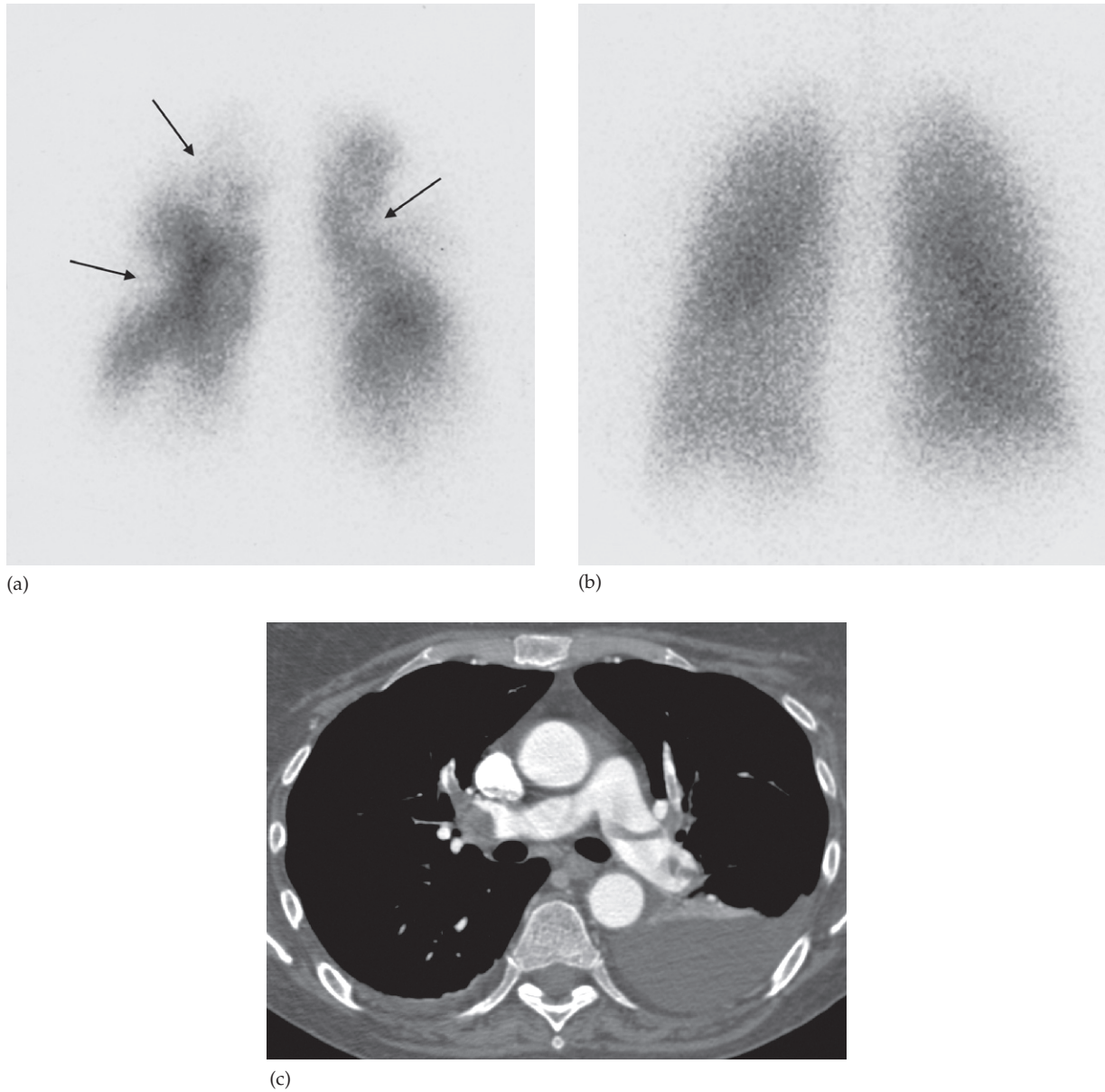


Fig. 2.102 Pulmonary emboli. (a) ^{99m}Tc macroaggregate perfusion scan (posterior view) showing multiple wedge-shaped defects. The more obvious ones have been arrowed. (b) The ventilation scan, using ^{81m}Kr (also a posterior view), is normal. (c) CT pulmonary angiogram showing bilateral filling defects due to emboli in the central pulmonary arteries (arrow).

diagnosed by noting a break or step in the cortex of a rib. Special views of the ribs may be necessary, as rib fractures are often invisible in the standard projections, particularly if the fracture lies below the diaphragm. Extrapleural soft tissue swelling from bruising, or frank haematoma, may be visible and guide the observer toward the site of the fracture. Rib fractures are frequently multiple and may result in a flail segment. Pleural effusion often accompanies rib fractures, the fluid frequently being blood. The following features should be looked for.

- *Pneumothorax* may occur if the lung is punctured by direct injury or by the sharp edge of a rib fracture. An air-fluid level in the pleural cavity due to the associated haemorrhage is common in such situations.
- *Surgical emphysema of the chest wall* may indicate the escape of air from the lungs. The presence of mediastinal emphysema in the absence of chest wall emphysema may indicate rupture of a bronchus, which is a rare event.
- *Pulmonary contusion*. Localized traumatic alveolar haemorrhage and oedema (Fig. 2.103) may be seen whether or not a rib fracture can be identified. The resulting pulmonary opacity is indistinguishable from other forms of pul-

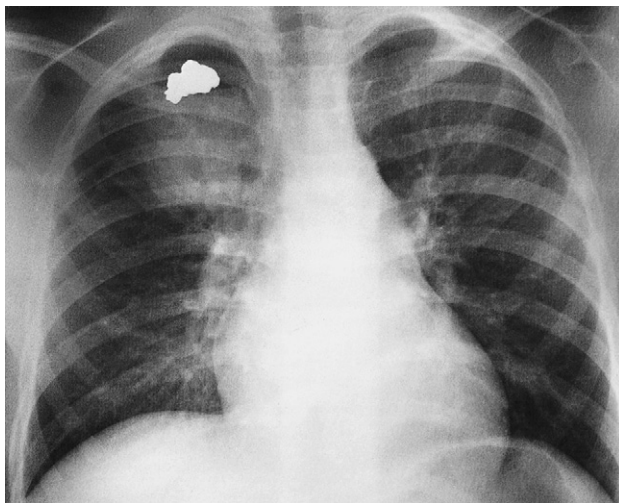


Fig. 2.103 Pulmonary contusion from a gunshot wound. The ill-defined consolidation represents haemorrhage and oedema in the right upper lobe. The deformed metallic fragments of the bullet are clearly visible.

monary consolidation, the relationship to the injury being important in establishing the diagnosis.

- *Adult respiratory distress syndrome* may follow severe trauma to any part of the body. Fat embolism is a specific subtype of ARDS, but its radiographic manifestations are identical to those of the other causes of ARDS.
- *Rupture of the diaphragm* is due to penetrating injury or compression of the abdomen and may permit herniation of the stomach or intestine into the chest. Such herniation is much commoner on the left than the right. Gas lucencies of the stomach or intestine are seen above the presumed position of the diaphragm, the diaphragm itself often being invisible due to an associated pleural effusion. CT may be indicated to establish the diagnosis (Fig. 2.104).
- *Rupture of the aorta* is a particularly serious consequence of rapid deceleration injuries. In patients that survive, the injury to the aorta is usually at the level of the ligamentum arteriosum. Ruptured aorta is a surgical emergency and is best diagnosed by CT angiography.

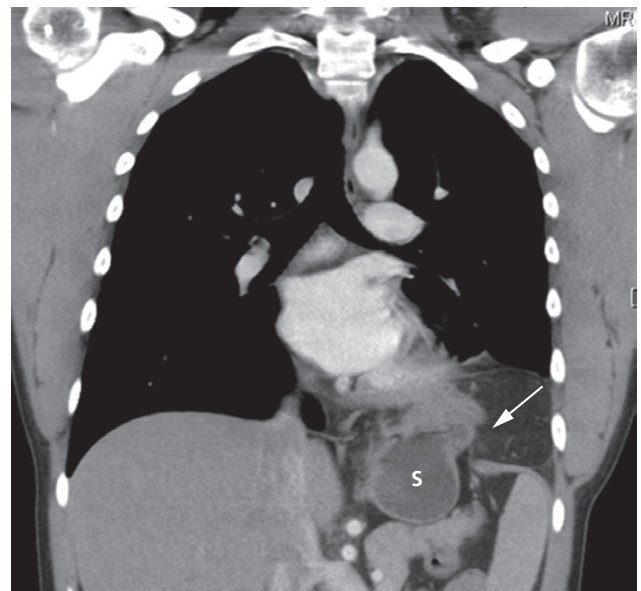


Fig. 2.104 Rupture of the diaphragm. Coronal reformatted CT showing rupture of the left hemidiaphragm and resultant herniation of the stomach (S) and abdominal fat into the chest (arrow).

Mediastinal widening due to bleeding, with or without pleural fluid, is the plain film sign of a ruptured aorta, but mediastinal widening is a difficult sign to assess. It may be due to excess mediastinal fat, or it may be artefactual due to the portable anteroposterior (AP) films that are often the only films that can be taken in these severely injured patients. CT may be used to confirm or exclude blood in the mediastinum. When blood is identified, it may be due to bleeding from the aortic rupture or to bleeding from other vessels – either arterial or venous. Although fractures of the ribs or sternum are usually present, there are many cases of aortic rupture on record without visible damage to the thoracic cage.

In some patients the diagnosis of aortic rupture is only made several months or years after the injury, when the development of an aneurysm is noted.

- *Rupture of the tracheobronchial tree* only occurs with major chest trauma. The cardinal signs are pneumomediastinum or pneumothorax that does not respond to a chest drain even on suction. The main complication is subsequent bronchostenosis.

Carcinoma of the bronchus

Carcinoma of the bronchus is one of the most common primary malignant tumours. It has a clear association with cigarette smoking. It is convenient to consider the radiological features of central and peripheral tumours separately.

Signs of a central tumour

The signs of a central tumour are:

- The tumour itself may present as a hilar mass (Fig. 2.105) with or without narrowing of the adjacent major bronchus.
- Collapse and/or consolidation of lung beyond the tumour (see Fig. 2.110). Lung collapse occurs because air is absorbed beyond the obstructed bronchus and cannot be replaced, whereas consolidation is the consequence of retained secretions and secondary infection.

Signs of a peripheral tumour

A peripheral tumour (Fig. 2.106) usually presents as a solitary pulmonary nodule/mass on plain films or chest CT. It

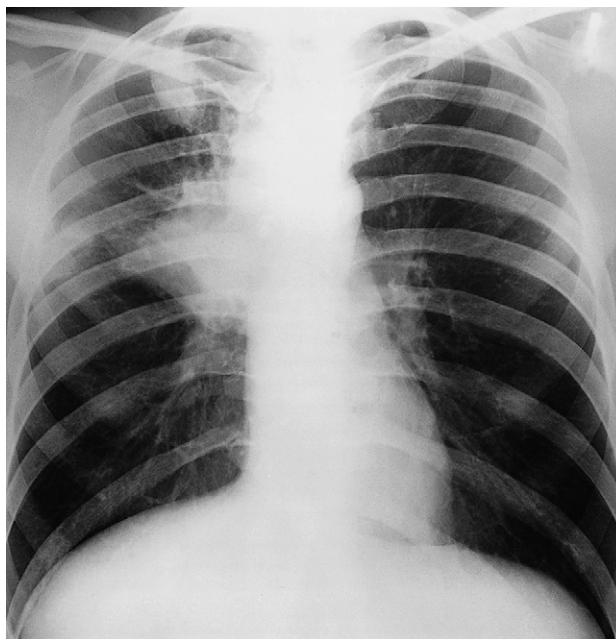


Fig. 2.105 Right hilar mass due to carcinoma of the bronchus. There is also a patch of consolidation in the right upper lobe laterally, from the central obstruction.

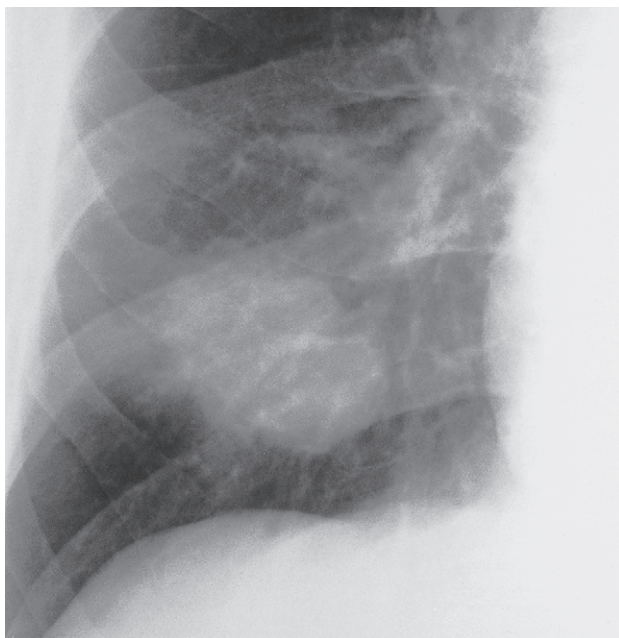
is very unusual to see a lung carcinoma of less than 1 cm in diameter on a CXR. Much smaller cancers, some even as small as a few millimetres may be discovered on CT (Fig. 2.107, and see Fig. 2.89).

The signs of a peripheral primary carcinoma are:

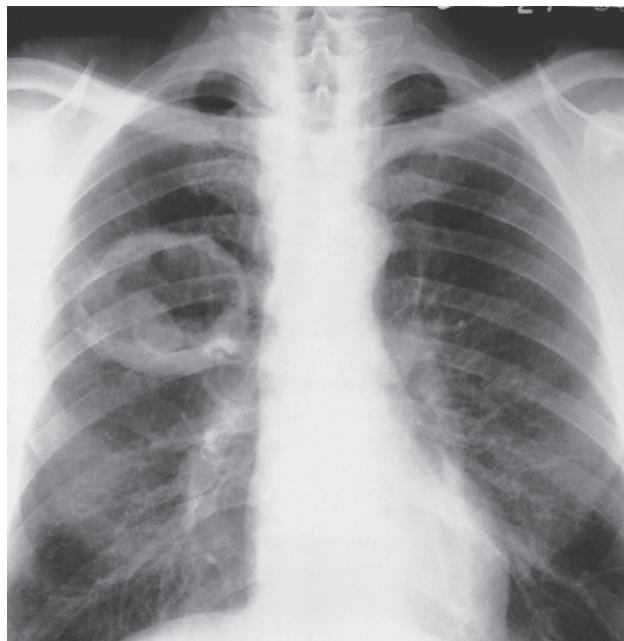
- A rounded opacity with an irregular border. Lobulation, notching and infiltrating edges are the common patterns.
- Cavitation within the mass. The walls of the cavity are classically thick and irregular, but thin-walled, smooth cavities due to carcinoma do occur.

Spread of bronchial carcinoma

Evidence of the spread of bronchial carcinoma may be visible on plain chest radiography, but CT has made a major contribution to the staging of lung cancer. FDG-PET/CT scanning is now used routinely to stage potentially operable tumours. MRI is only used for highly specific indications. The following features should be looked for.



(a)



(b)



(c)

Fig. 2.106 Appearance of peripheral lung carcinoma. A lobulated mass (a) and a cavitating mass (b) are shown on plain films. (c) A spiculated mass is shown on CT.

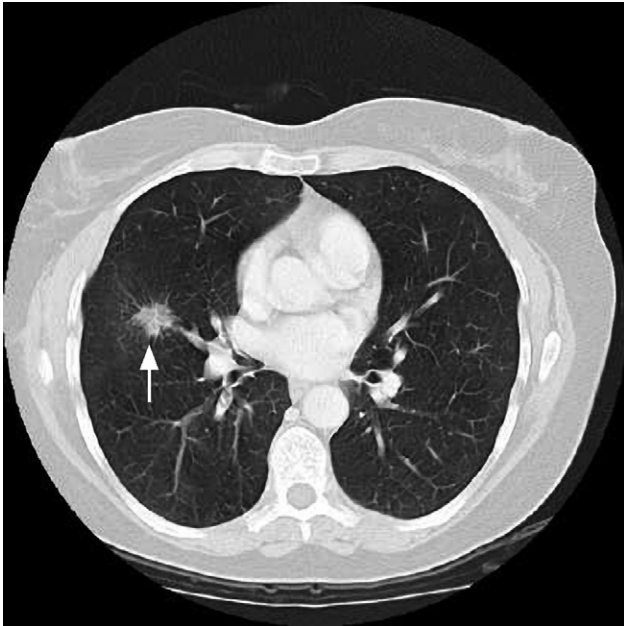


Fig. 2.107 Typical appearance and small size of a carcinoma of the bronchus discovered incidentally at CT.

- *Hilar and mediastinal lymph node enlargement* due to lymphatic spread of tumour. Only greatly enlarged lymph nodes can be recognized on plain CXRs. CT, on the other hand, has the ability to show even mildly enlarged nodes, which are not identifiable on plain film. Enlargement of lymph nodes does not necessarily mean metastatic involvement because reactive hyperplasia to the tumour or associated infection can be responsible for nodal enlargement, as can pre-existing disease – notably previous granulomatous infection. FDG-PET/CT (see Fig. 2.10) is used to identify neoplastic nodes although false-positive scans are obtained in patients with incidental and often unimportant inflammatory changes in the lymph nodes and false negatives can be seen in nodes below 1 cm in diameter. If there is any doubt on imaging, prior to resection of the primary tumour, biopsies can be obtained via mediastinoscopy or endobronchial ultrasound. It should be borne in mind, however, that nodes of 2 cm or greater in short axis diameter (Figs 2.108 and 2.109), which are PET positive in a patient with a bronchial carcinoma, almost invariably contain metastatic neoplasm.

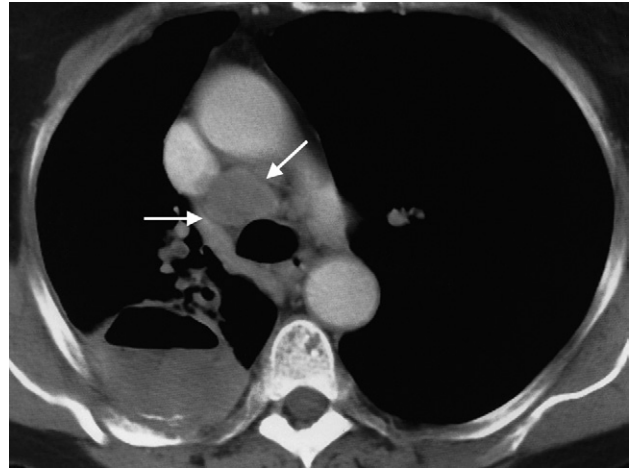


Fig. 2.108 CT scan of a greatly enlarged lymph node (arrows). Note that the primary tumour lying posteriorly in the right lung has invaded the chest wall and partially destroyed the adjacent rib.

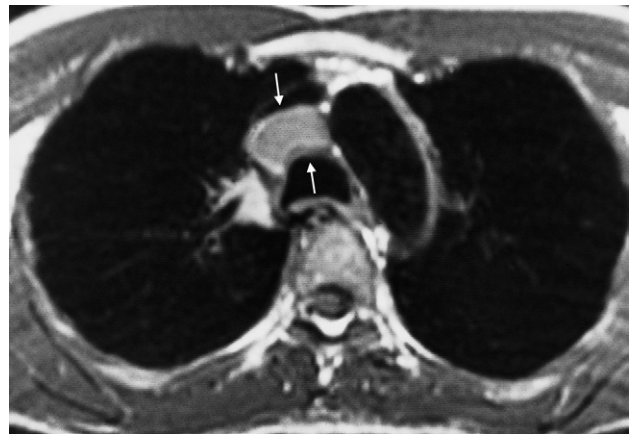


Fig. 2.109 MRI (T1-weighted) showing enlarged node (arrows) which stands out clearly against the background of no signal in the lung, trachea and aorta.

- *Pleural effusion* in a patient with lung cancer is usually due to malignant involvement of the pleura, but it may be secondary to associated infection of the lung or coincidental, as in heart failure.
- *Invasion of the mediastinum* is best assessed by CT because the neoplasm is directly visualized and the detailed anatomy is displayed (Fig. 2.110).

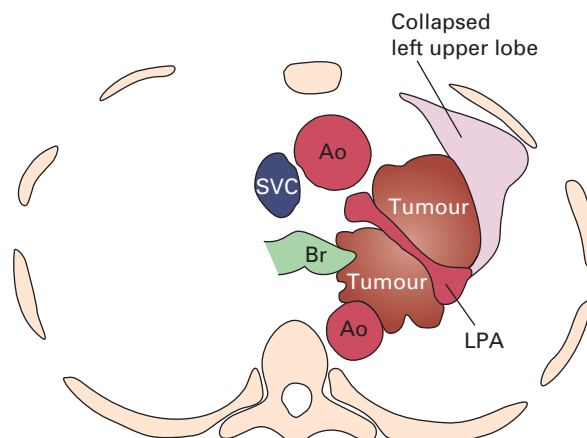
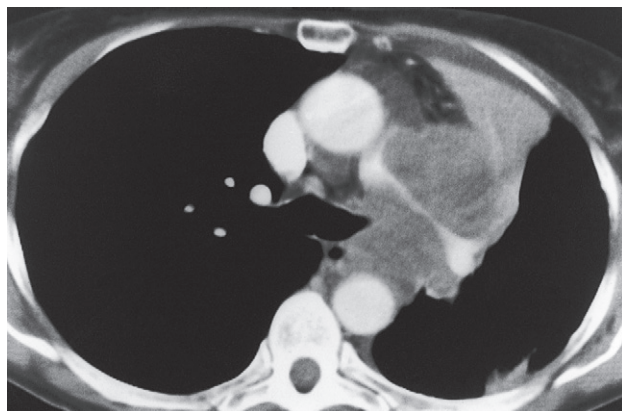


Fig. 2.110 Mediastinal invasion. Contrast-enhanced CT showing extensive tumour in the mediastinum, compressing the left pulmonary artery and causing left upper lobe collapse. Ao, aorta; Br, bronchus; LPA, left pulmonary artery; SVC, superior vena cava.

- *Invasion of the chest wall.* Destruction of a rib immediately adjacent to a pulmonary opacity is virtually diagnostic of bronchial carcinoma with chest wall invasion (Fig. 2.111). Recognizing the rib destruction can be difficult. It is important, therefore, to make a conscious effort to look directly at the ribs adjacent to the tumour. CT (and MRI) can demonstrate rib and soft tissue invasion when the bone is not visibly eroded on plain films (Fig. 2.112). Imaging techniques, even CT and MRI, may not always be reliable for determining chest wall invasion, and local chest wall pain remains an important indication that the tumour has crossed the pleura.

- *Rib metastases.* Carcinoma of the lung frequently metastasizes to the ribs, where it produces bone destruction. Sclerotic secondary deposits from lung carcinoma are rare.

- *Pulmonary metastases.* Primary lung carcinoma may metastasize to other parts of the lungs. The rounded opacities that result are similar to secondary deposits from other primary tumours.

- *Lymphangitis carcinomatosa* is the term applied to blockage of the pulmonary lymphatics by carcinomatous tissue. Lymphangitis carcinomatosa can be due to spread from abdominal and breast cancers as well as from carcinoma of the lung. The lymphatic vessels become grossly distended and the lungs become oedematous. The signs (Fig. 2.113) can be identical to those seen in interstitial pulmonary

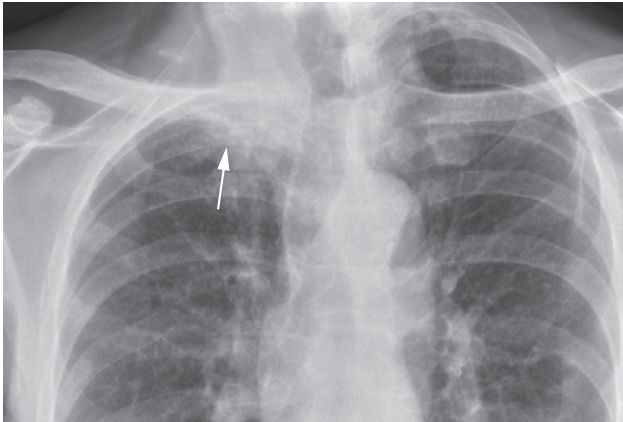
oedema (septal lines, loss of vessel clarity and peribronchial thickening), but if the heart is normal in size and there is hilar adenopathy and/or lobar consolidation, the diagnosis of lymphangitis carcinomatosa becomes more certain. The clinical story is very helpful: if the changes are due to pulmonary oedema, the patient usually complains of sudden onset of breathlessness, whereas the patient with lymphangitis carcinomatosa gives a story of slowly increasing dyspnoea over the preceding weeks or months. CT, particularly HRCT, has proven very valuable in demonstrating lymphangitis carcinomatosa because the appearances, in the correct clinical circumstances, are specific enough to obviate the need for biopsy (Fig. 2.114).

Metastatic neoplasms

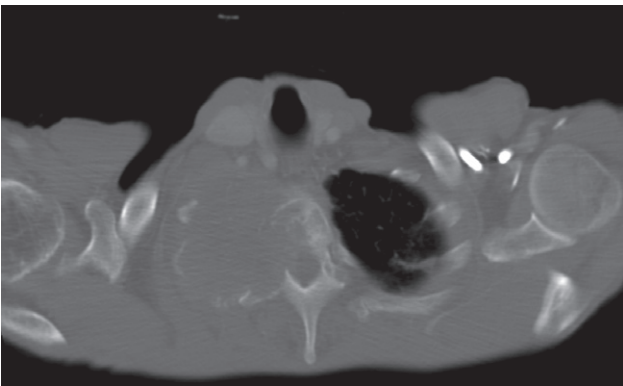
Metastases from extrathoracic primary tumours may be seen in the lungs, the pleura or the bones of the thoracic cage or, very rarely, in hilar and mediastinal lymph nodes.

Pulmonary metastases

Pulmonary metastases are, typically, spherical and well defined (Fig. 2.115), although irregular borders are occasionally seen. Usually, they are multiple and vary in size. Metastases have to be almost a centimetre in diameter, or



(a)



(b)

Fig. 2.111 Pancoast's tumour. (a) CXR showing a carcinoma arising at the apex of the right lung (arrow) that has invaded and destroyed the adjacent ribs and spine. (b) CT scan in the same patient demonstrating the bony invasion far more clearly.

larger, to be visible on a CXR. CT can demonstrate metastases as small as 3–6 mm. There is, however, a disadvantage attached to the excellent sensitivity of CT. Some small nodules are not metastases, but are benign processes such as tuberculomas or fungal granulomas. This is a major diagnostic problem in many parts of the United States, where fungal granulomas are very common and follow-up of indeterminate pulmonary nodules is undertaken according to the Fleischner guidelines (see Table 2.1).



Fig. 2.112 Pancoast's tumour. The carcinoma of the lung can be seen invading the root of the neck on this coronal MRI T1-weighted scan.

Pleural metastases

Pleural metastases usually give rise to pleural effusion; but metastatic adenocarcinoma can present with diffuse thickening of the pleura (see Fig. 2.51).

Metastases to ribs

Rib metastases are common with those primary tumours that metastasize to bone, notably bronchus, breast, kidney, thyroid and prostate (Fig. 2.116). All except prostatic and breast cancers produce mainly or exclusively lytic metastases.

With lytic metastases, the most reliable sign is destruction of the cortex, particularly of the upper border of a rib. One should be wary of diagnosing destruction of the lower borders of the posterior portions of the ribs, as these regions are often ill defined even under normal conditions. When in doubt, it is always wise to compare with the opposite side. Another pitfall in the diagnosis of rib metastases is that blood vessels in the lungs may cause confusing opacities. This confusion cannot arise at the edges of the chest

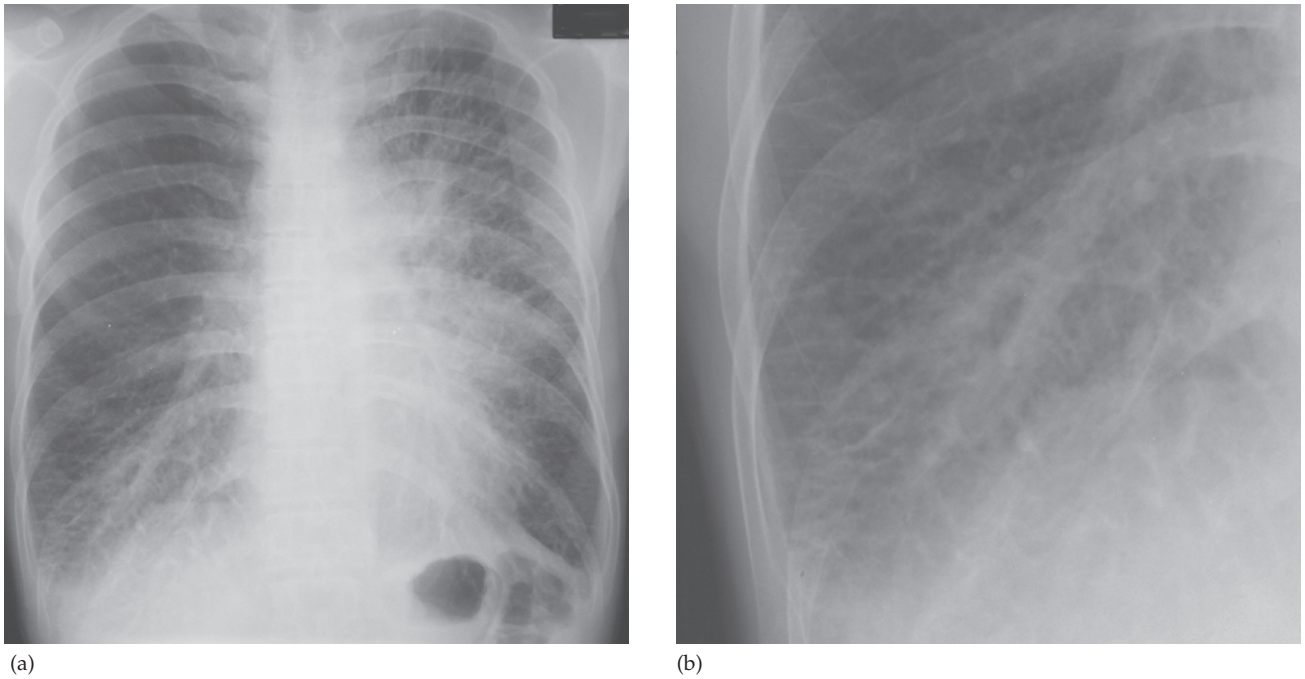


Fig. 2.113 Lymphangitis carcinomatosa. (a) There is widespread, ill-defined pulmonary opacifying with numerous septal lines. (b) The magnified view of the right lung base shows the septal (Kerley B) lines to advantage.

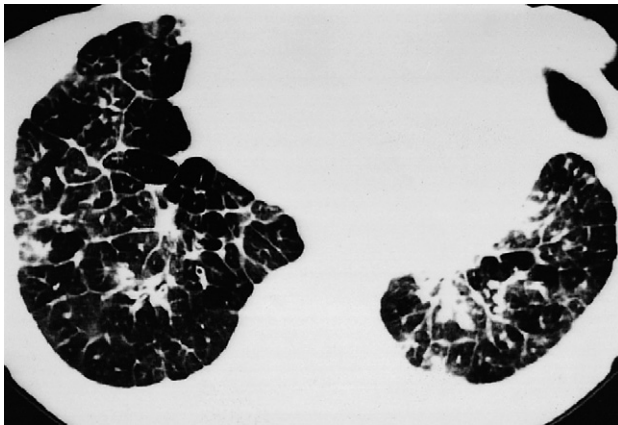
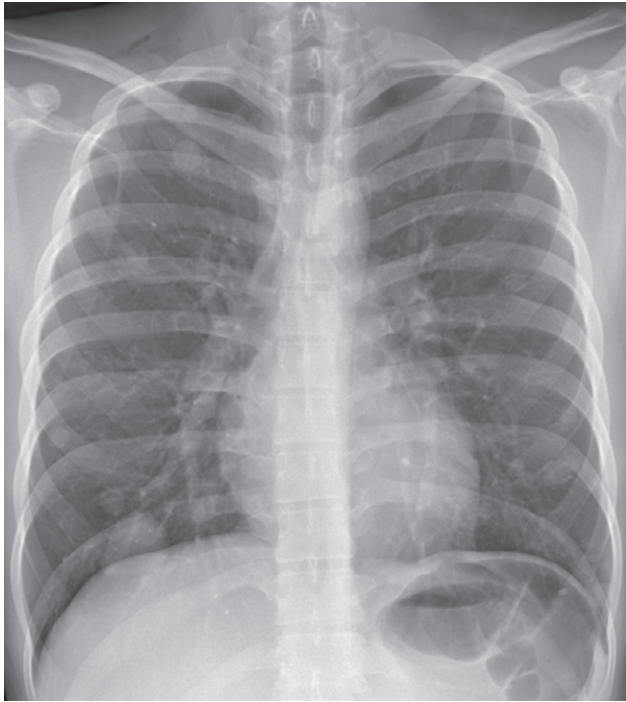
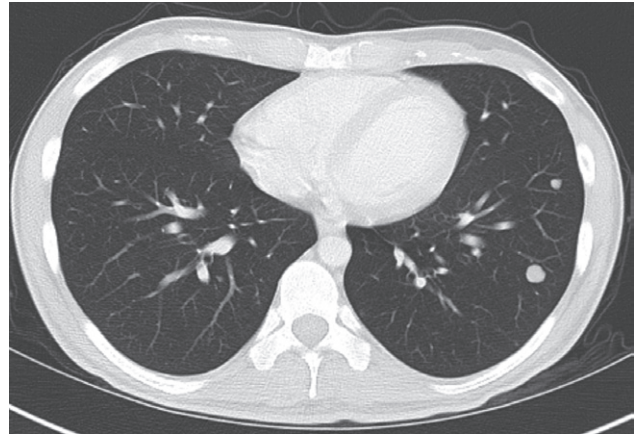


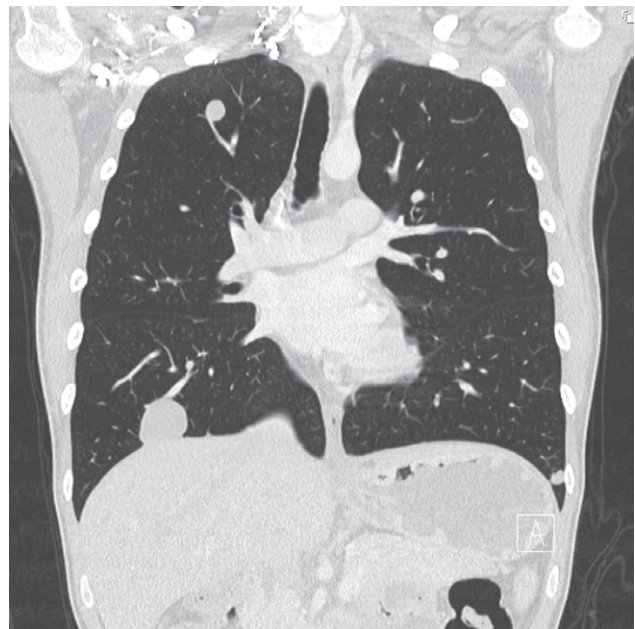
Fig. 2.114 Lymphangitis carcinomatosa. The widespread connecting lines representing irregularly thickened interlobular septa are very well shown by HRCT. This appearance is virtually pathognomonic of lymphangitis carcinomatosa.



(a)



(b)



(c)

Fig. 2.115 Pulmonary metastases. (a) There are numerous rounded opacities of varying sizes in both lungs. (b) Axial and (c) coronal reformatted CT in the same patient demonstrating the well-defined metastases, in this case from a testicular tumour.

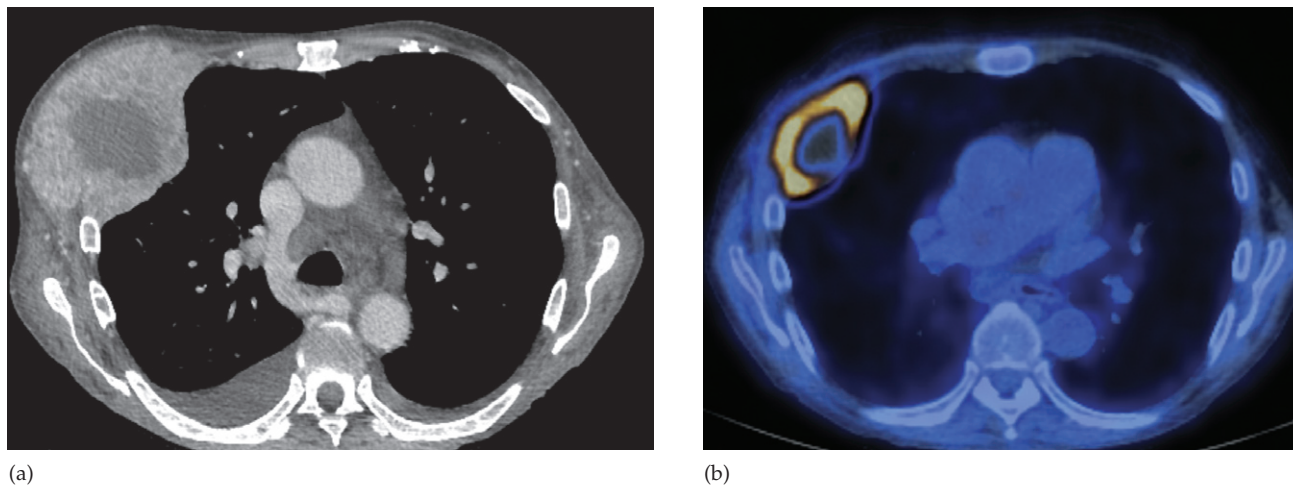


Fig. 2.116 (a) CT in a patient with metastatic renal cancer, and (b) FDG-PET/CT in a different patient, demonstrating a large focal pleural deposit.

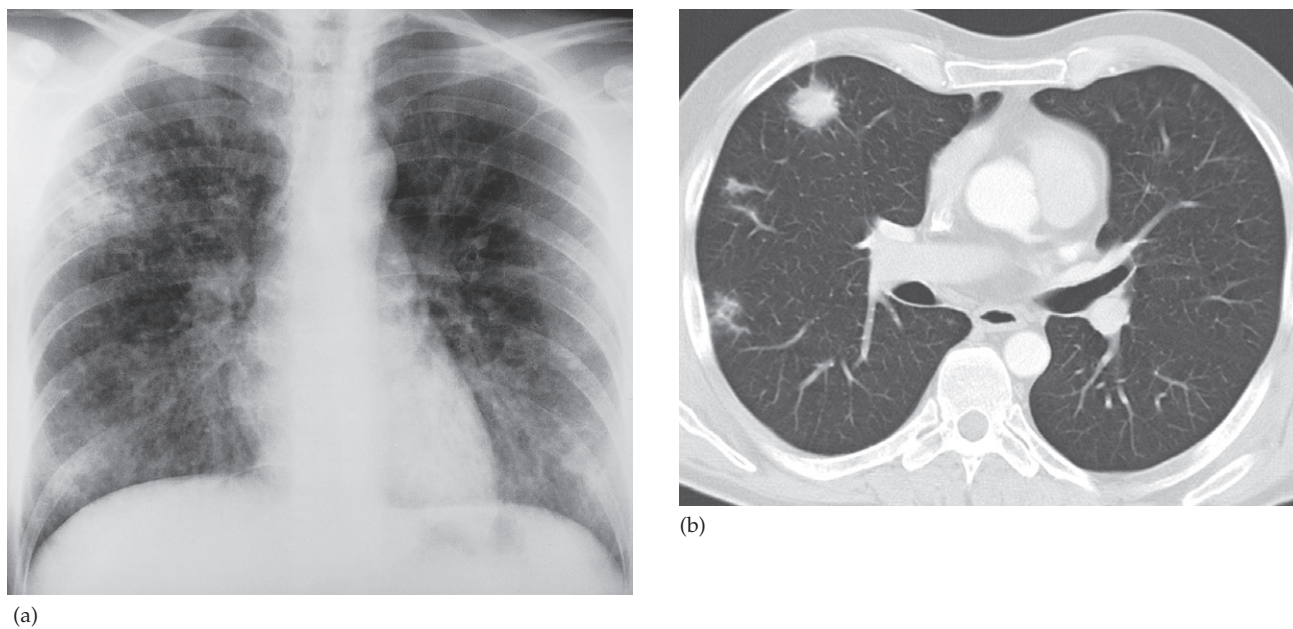


Fig. 2.117 (a) Lymphoma involving the lung. The extensive pulmonary consolidations were due to neoplastic involvement. Pneumonia can give a similar appearance. (b) CT in a patient with primary pulmonary lymphoma showing more nodular opacities.

where there is no lung projected over the ribs, so the extreme edge of the chest is a useful place to look for rib destruction. Soft tissue swelling is frequently seen adjacent to the rib deposit, so it is a good rule to look at the outer margin of the lung for soft tissue swelling as a clue to the presence of rib metastases (see Fig. 2.77).

Lymphoma

The common manifestations of intrathoracic malignant lymphoma are mediastinal and hilar adenopathy, and pleural effusion. These features can often be seen on plain

films, but CT is much the best method of confirming or excluding intrathoracic lymph node enlargement. Pulmonary involvement by lymphoma is unusual. It may take the form of large areas of infiltration of the lung parenchyma, resembling pulmonary pneumonia (Fig. 2.117a). As pulmonary infection is a common complication in patients with malignant lymphoma, it may be impossible to decide on radiological grounds whether the pulmonary consolidation is due to lymphomatous tissue or to infection. Occasionally, pulmonary lymphoma is seen as one or more mass lesions (Fig. 2.117b), which may cavitate. Pleural masses are a rare feature.

Cardiac Disorders

Imaging techniques

Cardiac imaging has become highly specialized and imaging techniques contribute to the diagnosis of cardiac diseases by providing a wide variety of diagnostic information (Box 3.1). Posteroanterior (PA) chest radiographs (CXR), sometimes supplemented by lateral chest films, are useful for assessing the effects of cardiac disease on the lungs and pleural cavities and measuring overall heart size, but the evaluation of specific chambers is unreliable. Echocardiography is widely used for morphological as well as functional information about the heart. It is excellent for looking at the heart valves, assessing chamber morphology and volume, determining the thickness of the ventricular wall and diagnosing intraluminal masses. Doppler ultrasound is used to determine the velocity and direction of blood flow through the heart valves and within cardiac chambers. Radionuclide examinations are used to assess myocardial blood flow and ventricular contractility, but provide little anatomical detail. Cardiac computed tomography (CT) and magnetic resonance imaging (MRI) are now becoming

more widely available, providing both functional and anatomical information in specific indications.

Plain chest radiography

Plain chest radiographic evidence of heart disease may be given by the size and shape of the heart together with any cardiac calcification, and by the size of pulmonary vessels and the presence of pulmonary oedema.

Heart size and shape

The standard plain films for the evaluation of cardiac disease are the PA view and a lateral chest film (Fig. 3.1). The cardiothoracic ratio (CTR) is a widely used, but crude, method of measuring heart size. The transverse diameter of the heart is normally less than half the internal diameter of the chest when measured on erect PA films (Fig. 3.2). Anteroposterior views magnify the heart, and films taken in supine or semi-erect positions lead to cardiac enlargement. Knowing whether or not the heart has increased in size compared with previous films is often more useful than the CTR in isolation. It should, however, be realized that the transverse cardiac diameter varies with the phase of respiration and, to some extent, with the cardiac cycle. Thus, changes in transverse diameter of less than 1.5 cm should be interpreted with caution. An overall increase in heart size may be due to dilatation of one or more cardiac chambers and/or to pericardial effusion. A potential pitfall is a patient with a severely *depressed sternum* (pectus excavatum) in whom the cardiac outline may appear enlarged

Box 3.1 Diagnostic information provided by cardiac imaging

- The structure and mechanical function of the cardiac chambers and valves
- Myocardial tissue characteristics, e.g. presence of myocardial scar and/or oedema
- Presence of stress-induced, reversible or irreversible perfusion defects in the myocardium
- Patency of the coronary arteries

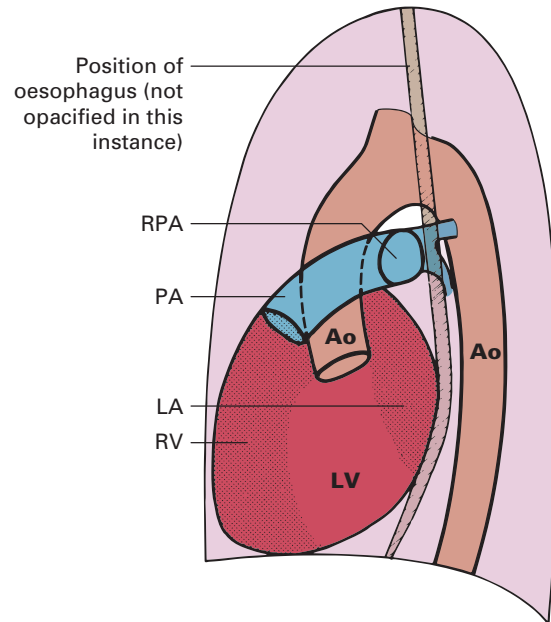
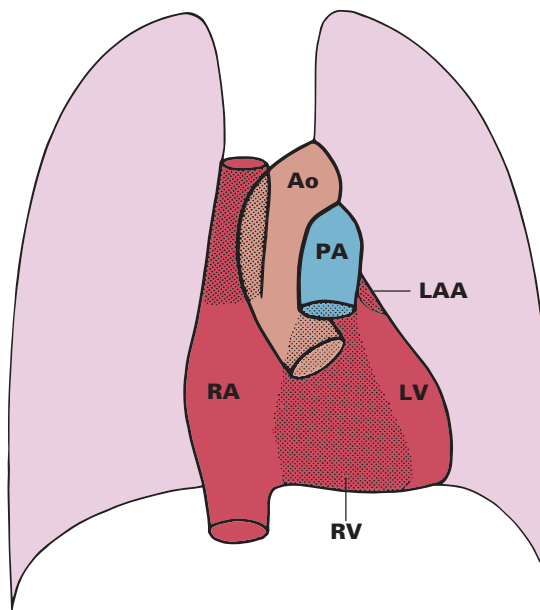
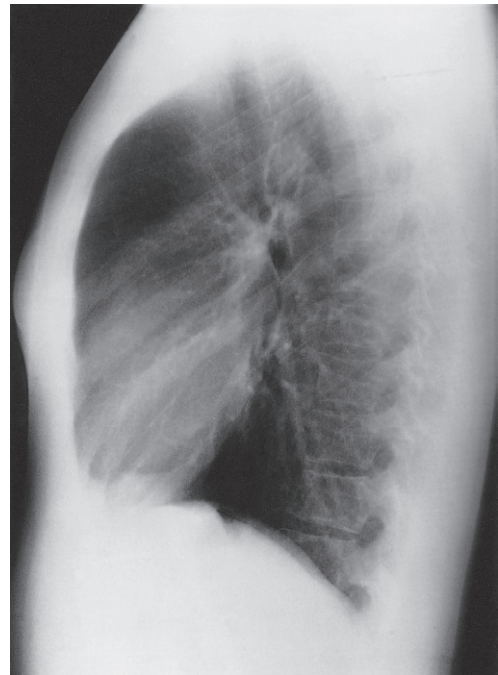
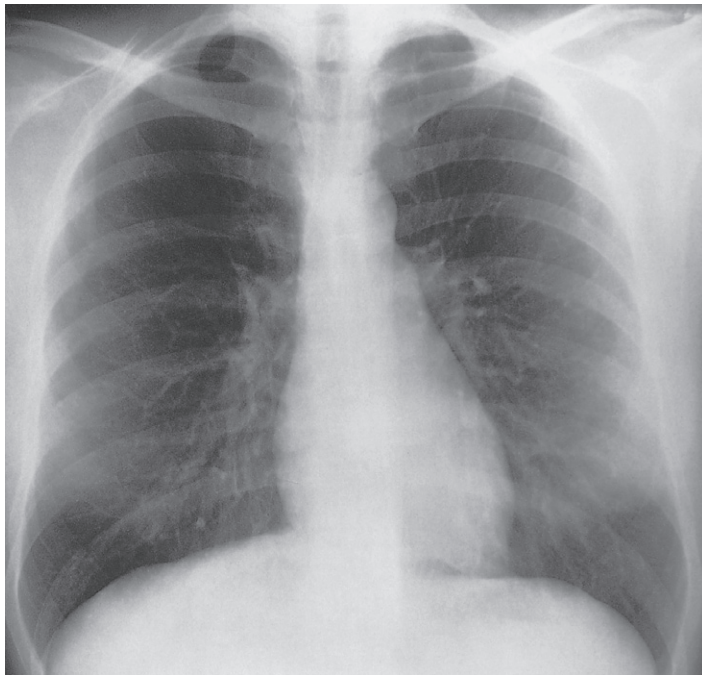


Fig. 3.1 Outline of the heart in posteroanterior and lateral views. Ao, aorta; LA, left atrium; LAA, left atrial appendage; LV, left ventricle; PA, pulmonary artery; RA, right atrium; RPA, right pulmonary artery; RV, right ventricle.

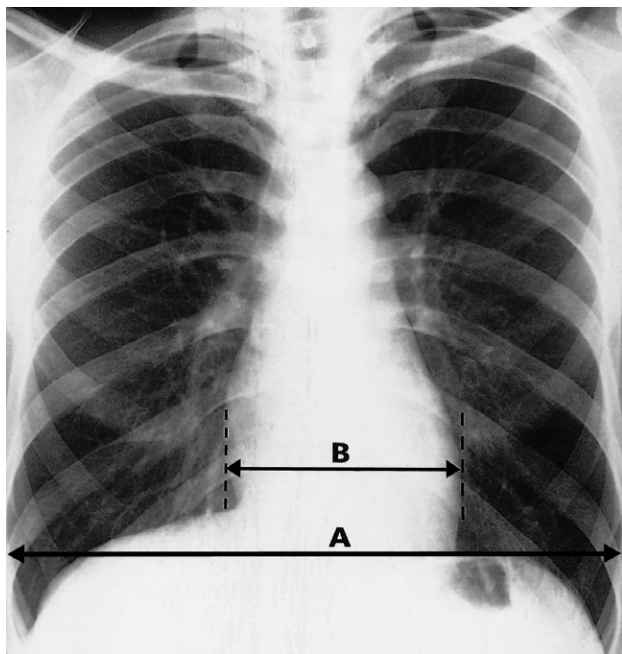


Fig. 3.2 Measurement of heart size. The transverse diameter of the heart is the distance between the two vertical tangents to the heart outline. When the cardiothoracic ratio (CTR) is calculated, the transverse diameter of the heart (B) is divided by the maximum internal diameter of the chest (A).

and altered in shape from simple rotation and displacement (Fig. 3.3).

Diagnosing specific chamber enlargement on plain films, with the possible exception of dilatation of the left atrium, is fraught with problems. It is rarely possible to distinguish ventricular hypertrophy from dilatation by looking at the external contours of the heart. Ventricular dilatation is recognized only as an overall increase in transverse cardiac diameter. Assessment of atrial size on the CXR, particularly left atrial enlargement (Fig. 3.4), is easier: the right border of an enlarged left atrium is visible as a double contour adjacent to the right heart border, usually within the main cardiac shadow. The left atrial appendage, when dilated, is seen as a bulge below the main pulmonary artery on the PA view. Right atrial enlargement causes an increase in the curvature of the right heart border and is often accompanied by enlargement of the superior vena cava.

The only plain film information directly relating to morphology of the valves is calcification, which is best evaluated at echocardiography. Calcification of the mitral valve ring is occasionally seen on CXRs in the elderly, and is often associated with mild mitral regurgitation.

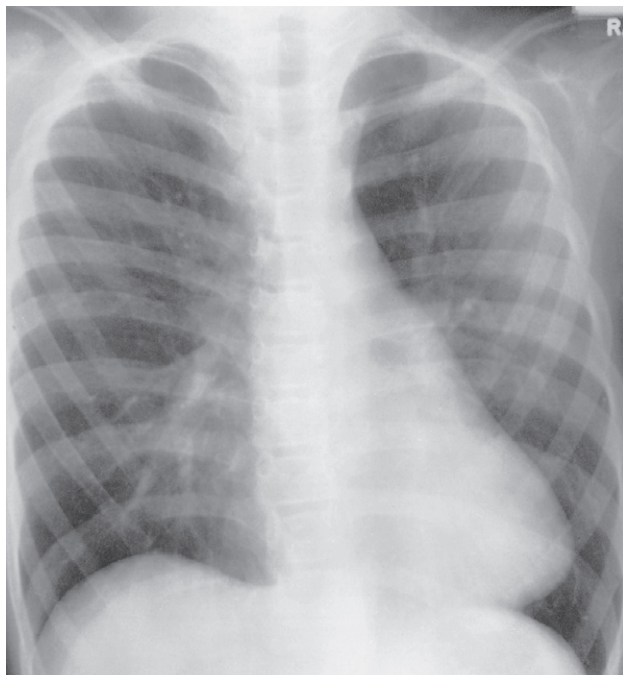
It is unusual to be able to diagnose a pericardial effusion from the plain CXR. Indeed, a patient may have sufficient pericardial fluid to cause life-threatening tamponade, but only have mild cardiac enlargement with an otherwise normal contour. A marked increase in the transverse cardiac diameter within a week or two, particularly if no pulmonary oedema occurs, is virtually diagnostic of the condition. Pericardial effusion should also be considered when the heart is greatly enlarged and there are no features to suggest specific chamber enlargement (Fig. 3.5). Extensive *pericardial calcification* is seen in patients with constrictive pericarditis.

Main pulmonary artery and pulmonary vasculature

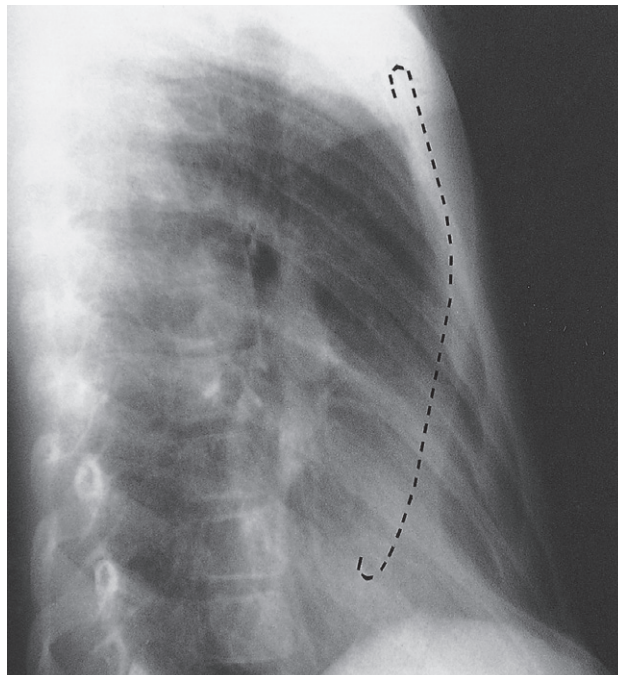
The CXR provides a simple method of assessing the size of the main pulmonary artery and the pulmonary vasculature. Even though it is not possible to measure the true diameter of the main pulmonary artery on plain film, there are degrees of bulging that permit one to say that it is indeed enlarged (Fig. 3.6). The assessment of the hilar vessels can be more objective since the diameter of the right lower lobe artery can be measured: the diameter at its mid-point is normally between 9 and 16mm. The size of the vessels within the lungs reflects pulmonary blood flow. There are no generally accepted measurements of normality, so the diagnosis is based on experience with normal films. By observing the size of these various vessels it may be possible to diagnose one of the following haemodynamic patterns.

Increased pulmonary blood flow due to left to right shunts

Atrial septal defect, ventricular septal defect (Fig. 3.7) and patent ductus arteriosus are the common anomalies in which there is shunting of blood from the systemic to the pulmonary circuits (so-called left to right shunts), thereby increasing pulmonary blood flow. In patients with a haemodynamically significant left to right shunt (2:1 or more), all the vessels from the main pulmonary artery to



(a)



(b)

Fig. 3.3 Pectus excavatum. (a) Posteroanterior view. Note how the heart is displaced and altered in shape by the depressed sternum. (b) Lateral film. The edge of the sternum has been traced in on this film. There was no cardiac disease in this patient.

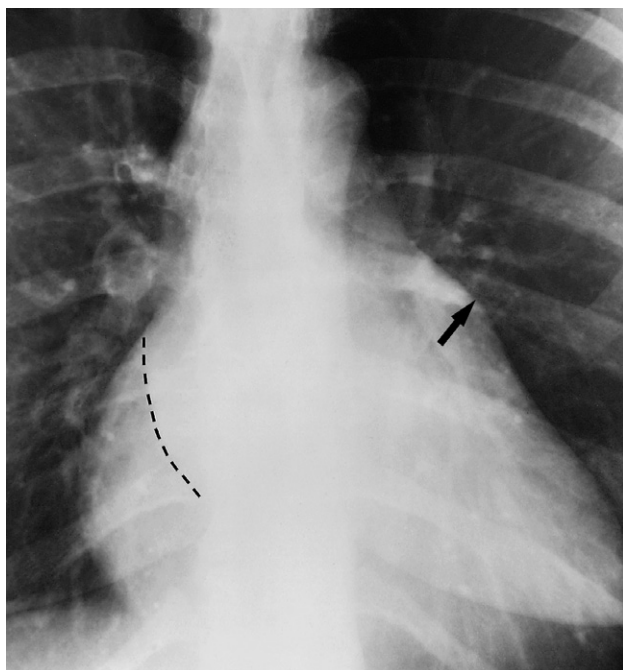


Fig. 3.4 Left atrial enlargement in a patient with mitral valve disease showing the 'double contour sign' (the left atrial border has been drawn in) and dilatation of the left atrial appendage (arrow).

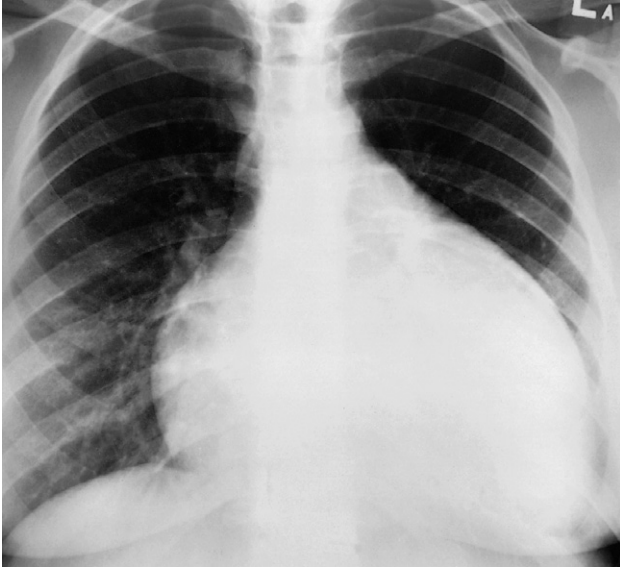


Fig. 3.5 Pericardial effusion. The heart is greatly enlarged. (Three weeks before, the heart had been normal in shape and size.) The outline is well defined and the shape globular. The lungs are normal. The cause in this case was a viral pericarditis. This appearance of the heart, though highly suggestive of pericardial effusion is not specific to it – a similar appearance can be seen with other causes of cardiac enlargement, e.g. cardiomyopathy.

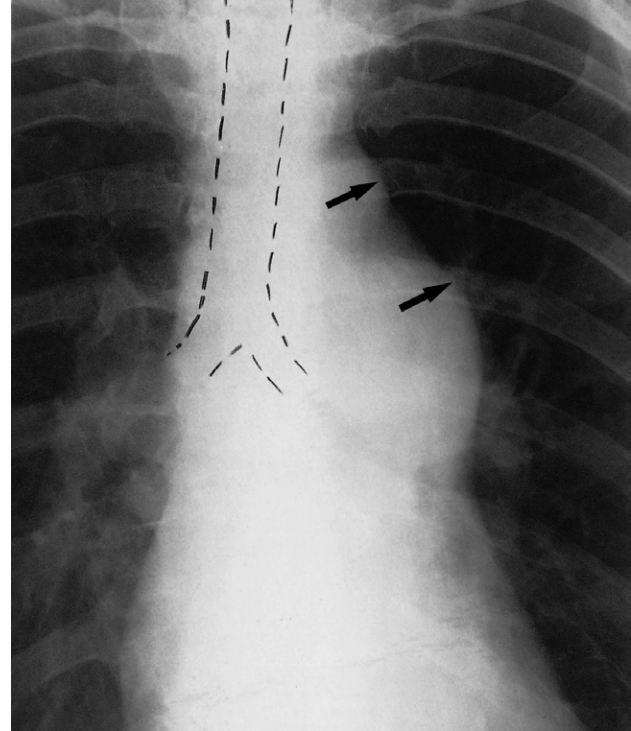
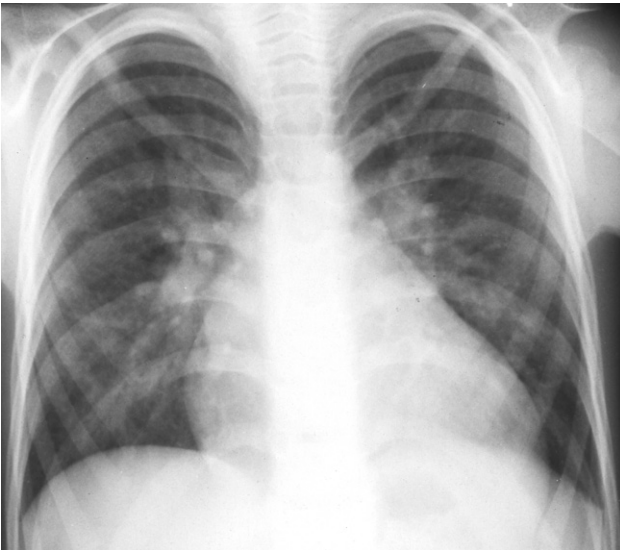


Fig. 3.6 Enlarged main pulmonary artery in a patient with pulmonary valve stenosis. The bulge of the main pulmonary artery (lower arrow) is clearly greater than normal and at first glance one might be deceived into diagnosing enlargement of the aorta. However, the aortic knuckle is the first 'bump' on the left mediastinal border (upper arrow). It projects 2.5–3 cm lateral to the trachea. The pulmonary artery forms the segment immediately below the aortic knuckle.

Fig. 3.7 Ventricular septal defect in a child. The heart is enlarged and there is obvious enlargement of the pulmonary vessels. The left to right shunt in this case was 3:1.

Box 3.2 Causes of pulmonary arterial hypertension

- Various lung diseases (e.g. cor pulmonale)
- Pulmonary emboli
- Mitral valve disease
- Left to right shunts
- Idiopathic pulmonary hypertension

the periphery of the lungs are large. This radiographic appearance is sometimes called pulmonary plethora.

Pulmonary arterial hypertension

The conditions that cause significant pulmonary arterial hypertension (Box 3.2) all increase the resistance of blood flow through the lungs.

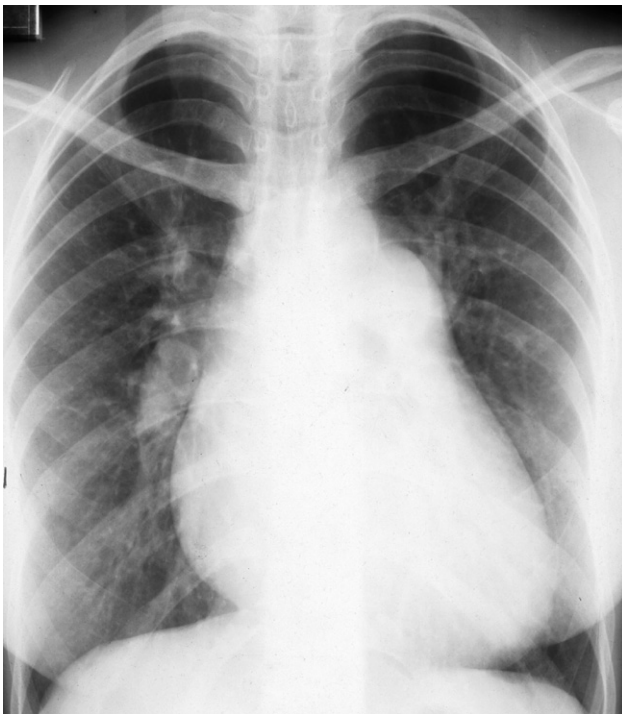


Fig. 3.8 Right ventricular enlargement in an adult with primary pulmonary hypertension. The heart is enlarged with the apex of the heart somewhat lifted off the diaphragm. Note also the features of pulmonary arterial hypertension – enlargement of the main pulmonary artery and hilar arteries with normal vessels within the lungs.

Pulmonary arterial hypertension (Fig. 3.8) has to be severe before it can be diagnosed on plain films. The CXR features are enlargement of the pulmonary artery and hilar arteries, the vessels within the lung being normal or small. The reason for pulmonary arterial hypertension may be visible on CXR, such as radiologically visible lung disease in cor pulmonale.

Pulmonary venous hypertension

Mitral valve disease (Fig. 3.9) and left ventricular failure are the common causes of elevated pulmonary venous pressure. In the normal upright person, the lower zone vessels are larger than those in the upper zones. In raised pulmonary venous pressure, the upper zone vessels enlarge and in severe cases become larger than those in the lower

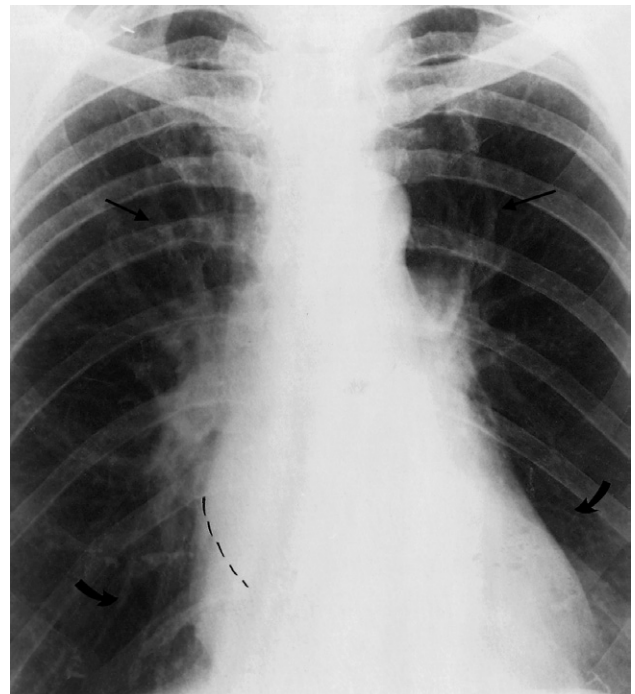


Fig. 3.9 Pulmonary venous hypertension in a patient with mitral valve disease. The upper zone vessels (straight arrows) are larger than the equivalent vessels in the lower zones (curved arrows). This is the reverse of the normal situation. (The left atrial border has been drawn in.)

zones. Eventually, pulmonary oedema will supervene and may obscure the blood vessels.

Pulmonary oedema

There are two radiographic patterns of cardiogenic pulmonary oedema: alveolar and interstitial. As oedema initially collects in the interstitial tissues of the lungs, all patients with alveolar oedema also have interstitial oedema.

Interstitial oedema (Fig. 3.10). There are many septa in the lungs which are invisible on the normal CXR because they consist of little more than a sheet of connective tissue containing very small blood and lymph vessels. When thickened by oedema, the peripherally located septa may be seen as lines, known as Kerley B lines, named after the radiologist who first described them. They are horizontal

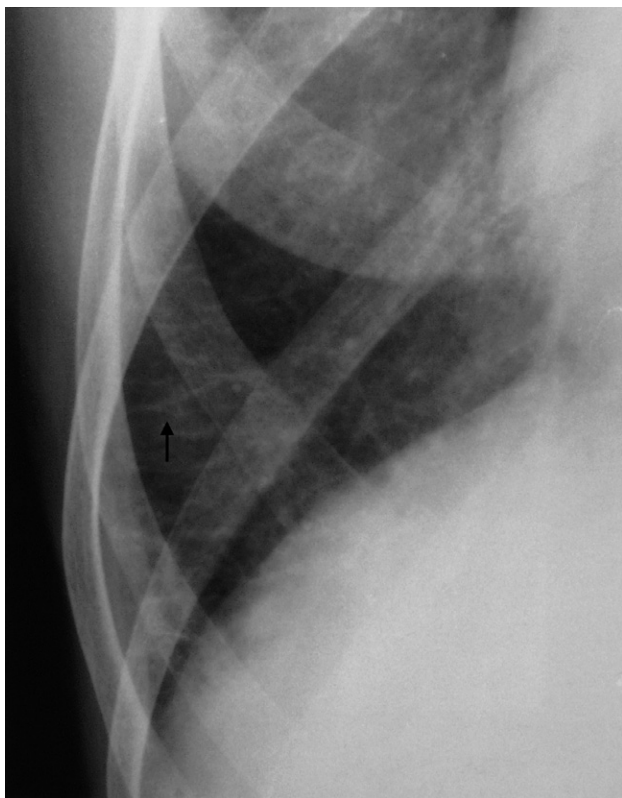


Fig. 3.10 Septal lines known as Kerley B lines in a patient with mitral stenosis. Note that these oedematous septa are horizontal, non-branching lines that reach the pleura. One such line in the right costophrenic angle is arrowed.

lines, never more than 2 cm long, seen laterally in the lower zones. They reach the lung edge and are, therefore, readily distinguished from blood vessels, which never extend into the outer centimetre of the lung. Another sign of interstitial oedema is that the outline of the blood vessels may become indistinct owing to oedema collecting around them. Fissures may appear thickened because oedema may collect against them.

Alveolar oedema (Fig. 3.11) is a more severe form of oedema in which the fluid collects in the alveoli. It is almost always bilateral, involving all the lobes. The pulmonary opacification is usually maximal close to the hila and fades out peripherally, leaving a relatively clear zone peripherally that may contain septal lines. This pattern of oedema is sometimes referred to as the 'butterfly' or 'bat's wing' pattern.

Echocardiography

Standard two-dimensional echocardiography (Fig. 3.12) demonstrates fan-shaped sections of the pericardial space,

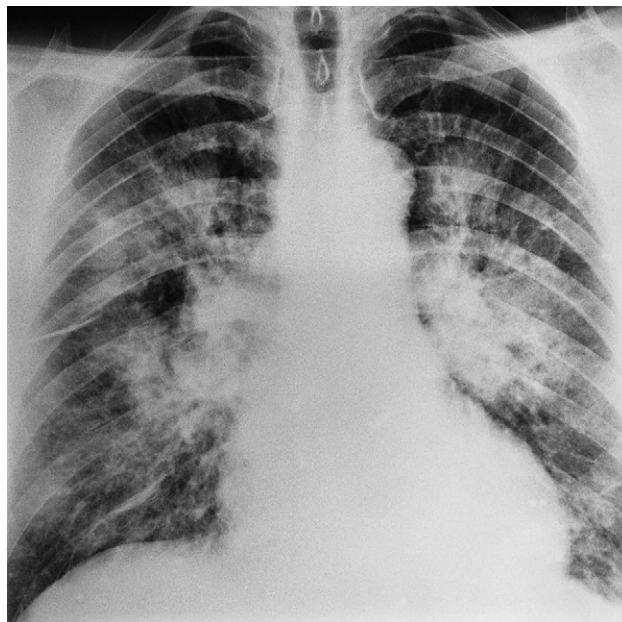


Fig. 3.11 Alveolar oedema in a patient with acute left ventricular failure following a myocardial infarction. The oedema fluid is concentrated in the more central portion of the lungs leaving a relatively clear zone peripherally. Note that all the lobes are fairly equally involved.

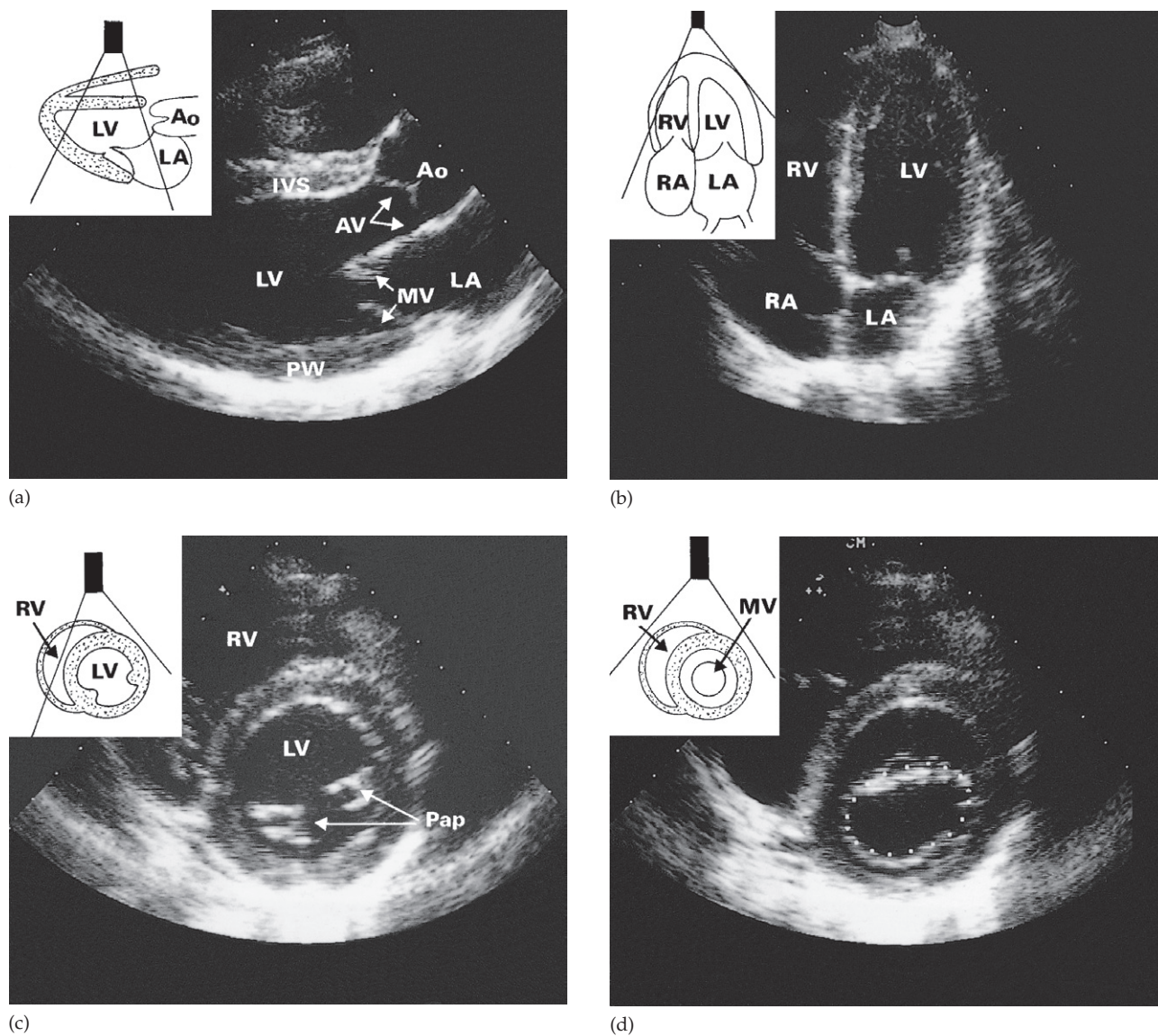


Fig. 3.12 Normal two-dimensional echocardiogram. (a) Parasternal long axis view. (b) Apical four-chamber view. (c) Parasternal short axis view at the level of the papillary muscles. (d) Similar view to (c) but at the level of the mitral valve. The dots indicate the area of the open valve. Ao, aorta; AV, aortic valve; IVS, interventricular septum; LA, left atrium; LV, left ventricle; MV, mitral valve; Pap, papillary muscles; PW, posterior wall of LV; RA, right atrium; RV, right ventricle. Courtesy of Andrew A. McLeod and Mark J. Monaghan.

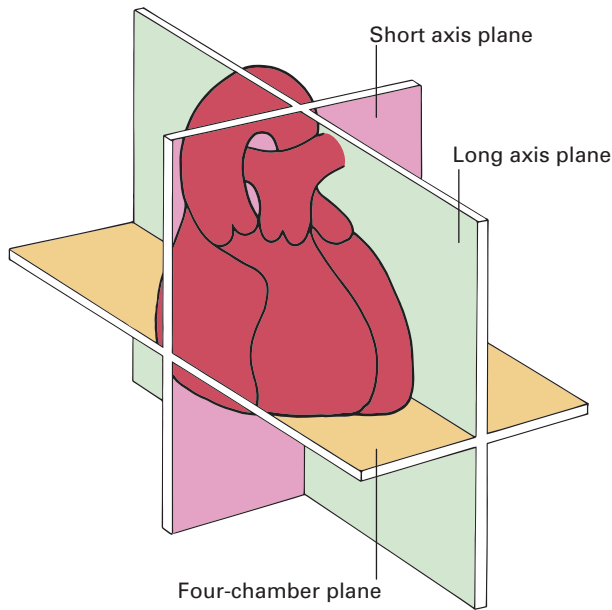


Fig. 3.13 Diagram illustrating the three orthogonal imaging planes used to demonstrate the heart with two-dimensional echocardiography. Ao, aorta; LV, left ventricle; PA, pulmonary artery; RA, right atrium; RV, right ventricle.

and individual cardiac chambers and valves in motion, by placing the transducer on the anterior chest wall in an intercostal or subcostal position (Fig. 3.13). It is also possible to place the ultrasound probe in the oesophagus or stomach to look at the cardiac structures from behind the heart (transoesophageal echocardiography).

Normally, all parts of the ventricular wall show equal movement and the left ventricular ejection fraction should be greater than 50%. Segments of ventricular wall with reduced movement or aneurysm formation can be demonstrated. Increased contractility of the left ventricle indicates hypertrophy, which can be primary (hypertrophic cardiomyopathy) or secondary to conditions such as aortic stenosis or systemic hypertension. The dimensions of each chamber can be readily assessed. Echocardiography also provides accurate estimates of wall thickness. Valve motion can be observed. Normally, the leaflets of all the valves are thin and give rise to clearly defined echoes with characteristic opening and closing motions.

Echocardiography can be performed after exercise or with a pharmacologically induced tachycardia to dem-

onstrate dyskinetic areas of ventricular muscle due to underlying coronary artery disease. Fluids containing tiny bubbles that reflect ultrasound can be injected intravenously and act as intravascular contrast agents.

Doppler echocardiography

As discussed in Chapter 1, when sound waves are reflected from a moving object, the frequency of the reflected waves is altered, depending on the velocity of the reflecting surface. With the Doppler technique, red blood cells can be used as reflecting surfaces and the velocity of blood flow in a given direction can be calculated and/or colour coded. The accuracy of the technique depends on the angle of flow with respect to the ultrasound beam, flow directly in line with the beam being the most accurately measured.

Doppler flow measurements/colour coding are used to:

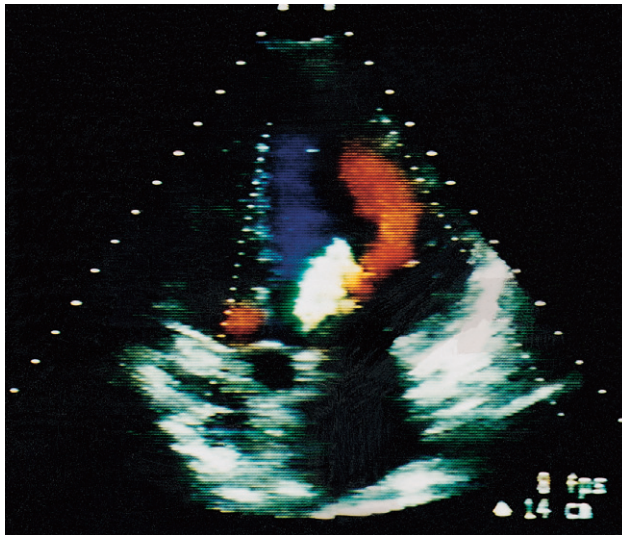
- Quantify pressure gradients across stenotic valves (derived from formulae that convert velocity across a valve into a pressure gradient).
- Detect and quantify flow, notably valvular regurgitation (Fig. 3.14), cardiac output and left to right shunts (Fig. 3.15).

Radionuclide studies

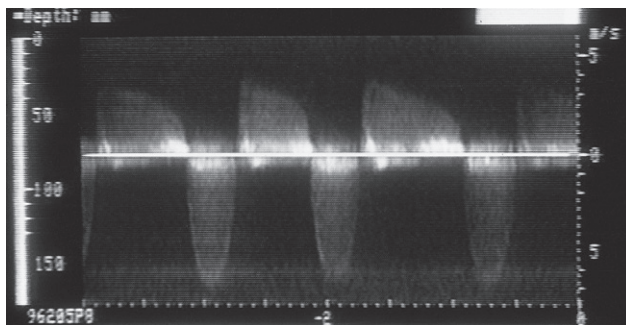
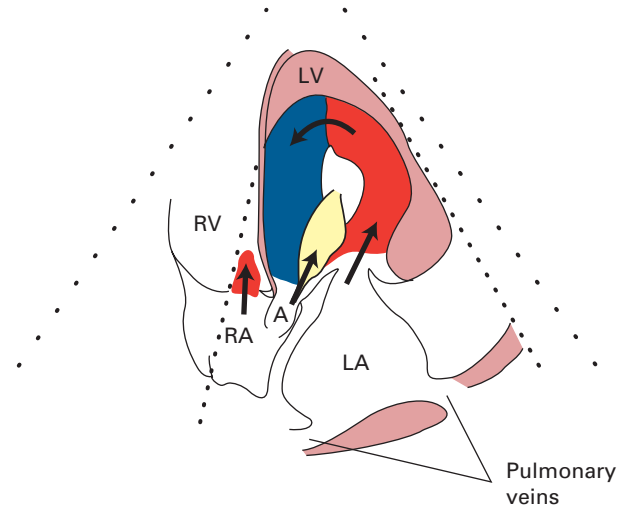
Nuclear medicine techniques are non-invasive and can be readily repeated. They give information on cardiac function and metabolism, but provide only limited anatomical detail. The two main radionuclide investigations in cardiology are myocardial perfusion scintigraphy and positron emission tomography (PET).

Myocardial perfusion scintigraphy

Myocardial perfusion scintigraphy uses radionuclide tracers that are taken up by the myocardium in proportion to blood flow, so regions of reduced perfusion appear as areas of reduced uptake. Myocardial perfusion imaging is used in patients with known or suspected ischaemic chest pain. As many patients only show impaired myocardial perfusion on exercise, the radionuclide is injected during actual or pharmacologically induced exercise. The images are repeated after the patient has rested for 3–4 hours. The sites and sizes of ischaemic areas can be assessed and a distinction between ischaemic and infarcted regions can be made by comparing peak exercise and resting images (Fig. 3.16).



(a)



(b)

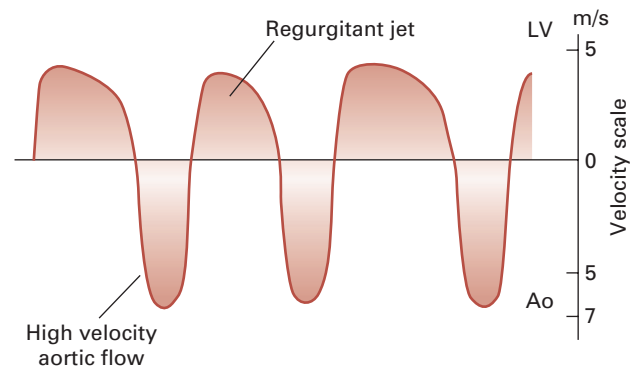


Fig. 3.14 Aortic valve disease. (a) Colour flow Doppler in a patient with aortic regurgitation. Apical four-chamber view showing turbulent jet (white) of regurgitant blood impinging on the anterior leaflet of the mitral valve to mix with the stream (red) passing from the left atrium (LA) to the left ventricle (LV). Note the change in colour to blue as the stream is directed by the ventricular apex towards the aortic valve. A small portion of right atrial to right ventricular flow is depicted in red. A, aorta; RA, right atrium; RV, right ventricle. (b) Continuous wave Doppler from the apical position in a patient with aortic stenosis and regurgitation showing a high velocity (7 m/s) jet into the aorta (Ao). There is immediate diastolic flow back into the LV, representing aortic regurgitation.

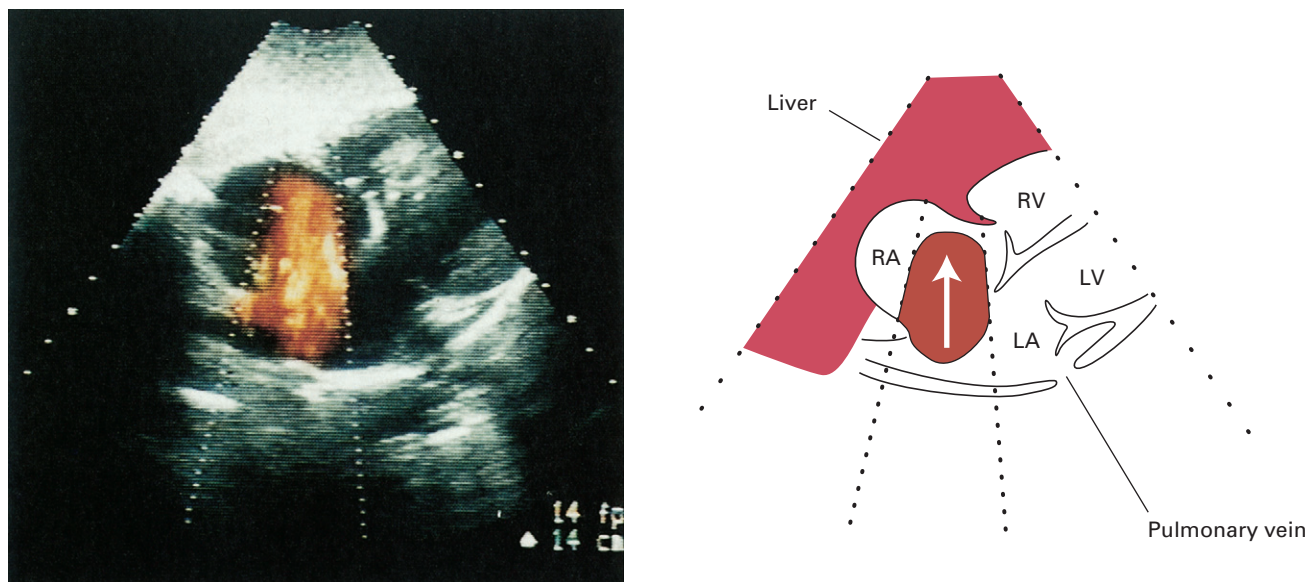


Fig. 3.15 Atrial septal defect. Colour flow Doppler in the subcostal four-chamber view showing substantial flow (red) passing from the left to right atrium. LA, left atrium; LV, left ventricle; RA, right atrium; RV, right ventricle.

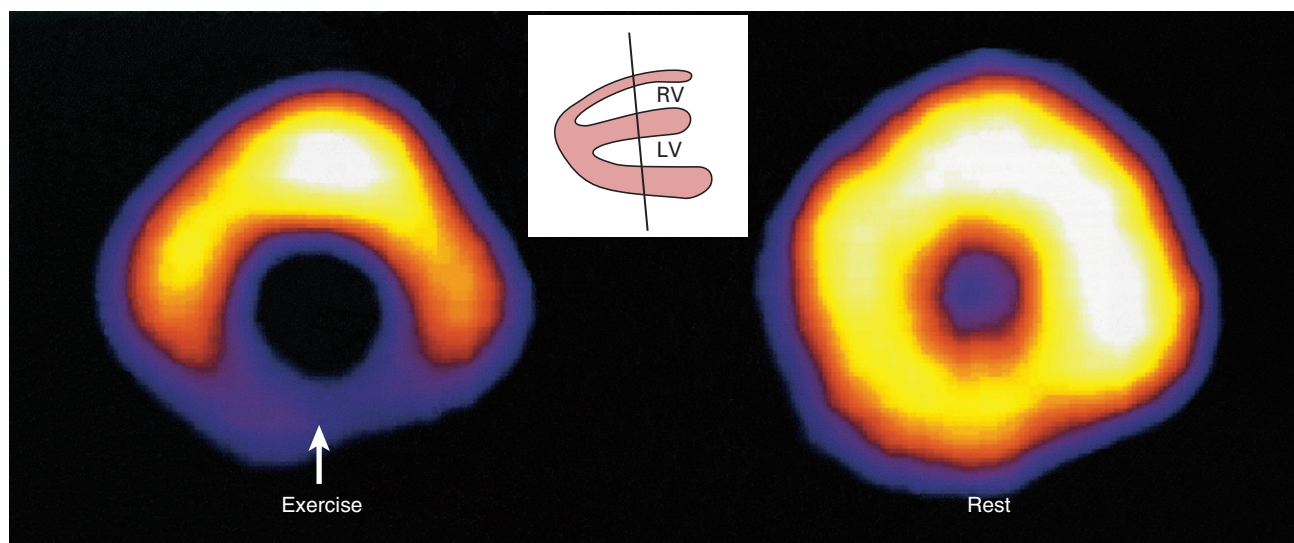


Fig. 3.16 Thallium-201 myocardial perfusion scans. On the exercise scan there is a large area of very reduced uptake in the inferior wall of the left ventricle (LV; arrow), with normal redistribution of the thallium on the rest scan indicating an area of ischaemia. Only the left ventricular wall is demonstrated as there is too little uptake of thallium by the normal right ventricle (RV).

Positron emission tomography

Positron emission tomography can provide cross-sectional images of the patient's anatomy after injection of either a flow tracer or a radionuclide, which is an analogue of glucose (18F-fluorodeoxyglucose), thus providing information on the myocardial metabolism. PET can identify areas of viable, non-viable and hibernating myocardium.

Computed tomography

Standard CT plays little part in the management of intracardiac disorders. Pericardial effusions and cardiac tumours are recognizable, but they are usually equally well or better seen at ultrasound. Modern multidetector CT scanners can produce high resolution images of the coronary arteries by applying electrocardiographic gating (cardiac CT). In general a cardiac CT study includes two scans:

- 1 A non-contrast scan for the measurement of coronary calcification (coronary artery calcium score). The amount of calcification can be used to determine who should receive prophylactic treatment for atheroma in the hope of preventing future cardiac events.
- 2 A contrast-enhanced scan (coronary CT angiography) for the study of the coronary arterial tree, cardiac chambers and valves together with the great vessels (see Fig. 3.20). The main focus of coronary CT angiography is the non-invasive identification of coronary artery stenosis in patients with suspected ischaemic chest pain.

Magnetic resonance imaging

Gating of the standard MRI sequences using an electrocardiogram provides an immense amount of unique information (Box 3.3). Myocardial perfusion may be evaluated after injection of a contrast agent (gadolinium) as regions of reduced perfusion. The ability to characterize tissues allows the identification of myocardial scar tissue, shown as areas where gadolinium accumulates on delayed imaging due a damaged capillary network.

Cardiac catheterization and angiography

Contrast can be injected through catheters which have been introduced under fluoroscopic control into the various

Box 3.3 Information available from cardiac gated MRI

- Anatomy of complex congenital heart disease
- Details of myocardial thickness, morphology and function
- Myocardial perfusion
- Tissue characterization
- Myocardial oedema
- Valve disease
- Pericardial disease
- Intracardiac tumours, which can be shown with great precision, better in many cases than with ultrasound

chambers of the heart and into vessels that lead in and out of these chambers. Coronary angiography (see Fig. 3.21), which provides detailed information about coronary artery stenoses, occlusions and collateral or anomalous vessels, is widely practiced in patients with acute myocardial infarction with a view to performing primary angioplasty and in patients being considered for coronary artery bypass grafting. Catheters can be introduced into the femoral artery or the radial artery and passed selectively into the orifices of each coronary artery.

Specific cardiac diseases

Heart failure

One or more of the following signs of heart failure may be seen on CXR (Fig. 3.17):

- Cardiac enlargement.
- Evidence of raised pulmonary venous pressure, namely enlargement of the vessels in the upper zones of the lung.
- Evidence of pulmonary oedema.
- Pleural effusions, which are usually bilateral, often larger on the right than the left, and if unilateral are almost always right-sided. (In acute left ventricular failure, small effusions are seen in the costophrenic angles running up the lateral chest wall.)

Cardiac ultrasound allows ventricular volumes and ejection fractions to be measured with considerable accuracy, as well as enabling valve gradients and degrees of regurgitation to be assessed. It is, therefore, an excellent diagnostic tool in evaluating heart failure. Cardiac MRI plays an important role in the diagnosis and characterization of

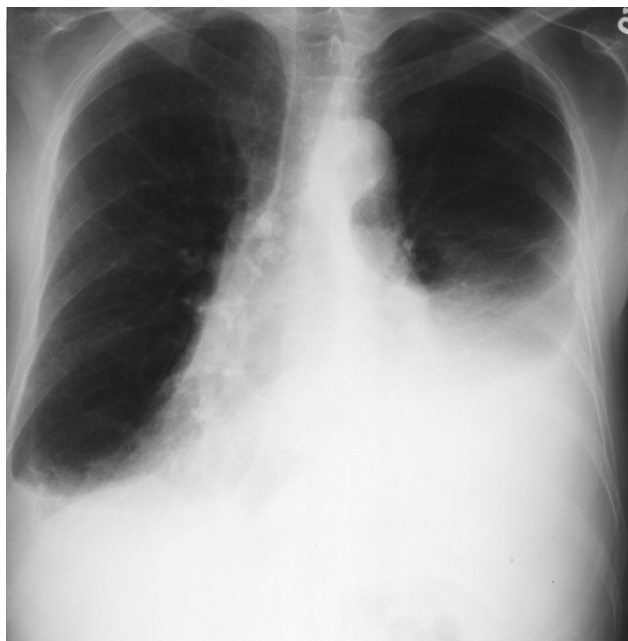


Fig. 3.17 Congestive cardiac failure. There are large bilateral pleural effusions. The heart is enlarged although it is difficult to measure it precisely because the pleural fluid obscures its borders.

heart failure. MRI shows cardiac morphology, function and viability. Acute tissue and perfusion injuries (like oedema and necrosis) can be detected. MRI gives important information in non-ischaemic heart failure by demonstrating scarring or infiltrative myocardial disease.

Ischaemic heart disease

Most patients with angina have a normal CXR and a normal echocardiogram. Patients with previous or new myocardial infarction may have a normal echocardiogram, but usually show evidence of reduced wall movement in the region of infarction, or dilatation of the whole of the left ventricle. *Stress echocardiography* can be used to attempt to differentiate infarcted viable but 'lethargic' myocardial muscle. A major use of echocardiography is to show aneurysms, which appear as outwardly bulging thin areas of the myocardium, although the apex not be explorable depending

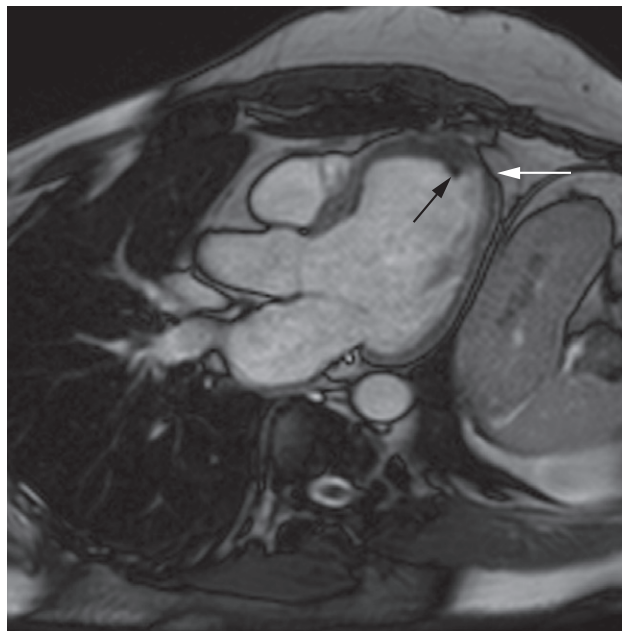


Fig. 3.18 Left ventricular aneurysm due to ischaemic damage. The three-chamber view, T2-weighted image shows a dilated left ventricle with a thin wall, particularly at the apex (white arrows). There is a hypointense intracavitary thrombus (black arrow) due to marked reduction of apical contraction.

on the chest wall morphology, in which case CT or MRI may be used (Fig. 3.18). Blood clots contained within an aneurysm can be recognized as numerous constant echoes in the cavity of the aneurysm. Sometimes there is mitral regurgitation due to papillary muscle infarction or dilatation of the mitral valve ring.

Most patients with myocardial infarction have a normal CXR, but severe ischaemic damage to the myocardium may result in one or more of the following signs:

- Cardiac enlargement and aneurysm formation.
- Signs of raised pulmonary venous pressure and pulmonary oedema.

Myocardial perfusion scintigraphy allows one to determine areas of myocardial ischaemia, and from their location it is sometimes possible to predict which of the coronary arteries is compromised. This technique not only enables a diagnosis of ischaemia to be made, but it can also help distinguish ischaemic muscle from scar due to infarction.

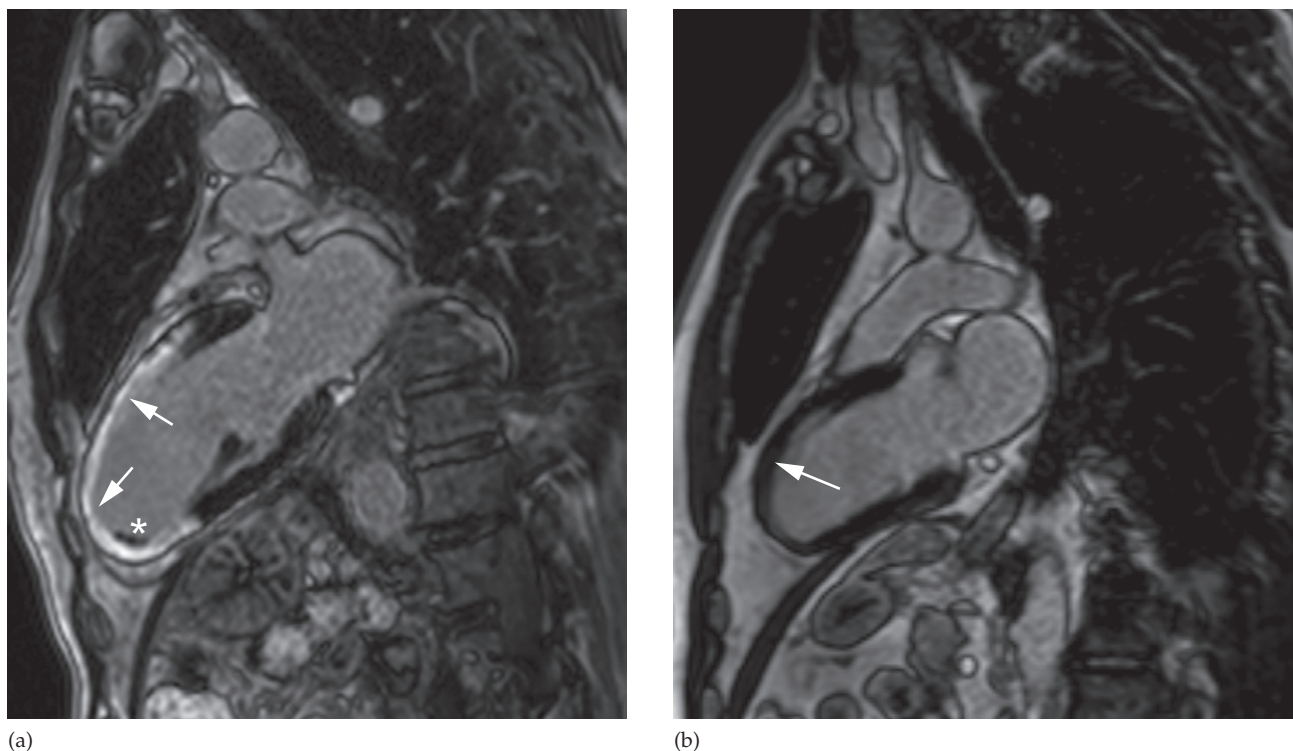


Fig. 3.19 Myocardial infarction on MRI. T1-weighted inversion recovery image acquired at 15 minutes after injection of gadolinium (late gadolinium enhancement). (a) There is a large area of hyperintensity (due to slow clearance of gadolinium) in the anterior wall and apex (arrows) consistent with scar tissue, suggesting transmural myocardial infarction. Also note an apical thrombus (*). (b) In a different patient, the normal myocardium demonstrates uniform low signal intensity (arrow).

Ischaemic areas seen on the exercise scan as regions of reduced uptake show normal activity on the resting scan (see Fig. 3.16). Infarcted areas in which there is little, if any, remaining viable myocardium will show a persistent defect on the resting scan. On cardiac MRI, ischaemic areas are seen on the stress scan as areas of reduced contrast uptake after injection of gadolinium. Infarcted areas will show accumulation of gadolinium on delayed images due to damage of the intramyocardial capillary bed and consequent reduced clearance of the contrast (Fig. 3.19). This ability to distinguish ischaemia and infarction may be useful when planning cardiac surgery.

The state of the coronary arteries can be determined by coronary CT angiography (Fig. 3.20) or conventional coro-

nary angiography (Fig. 3.21). Coronary CT angiography is preferred in patients with a low probability of disease based on clinical findings (e.g. chest pain with atypical features, lack of cardiovascular risk factors). In these circumstances, a non-invasive test is preferable in order to rule out the presence of coronary stenoses. In patients with a high probability of ischaemic heart disease (e.g. symptoms typically related to exercise) or with acute myocardial infarction, conventional coronary angiography is preferred with a view to performing coronary angioplasty. In conventional angiography, each artery is examined separately by multiple views to determine the extent of coronary artery occlusions and stenoses (Fig. 3.21). From this information, the appropriate treatment can be decided; this may be angi-

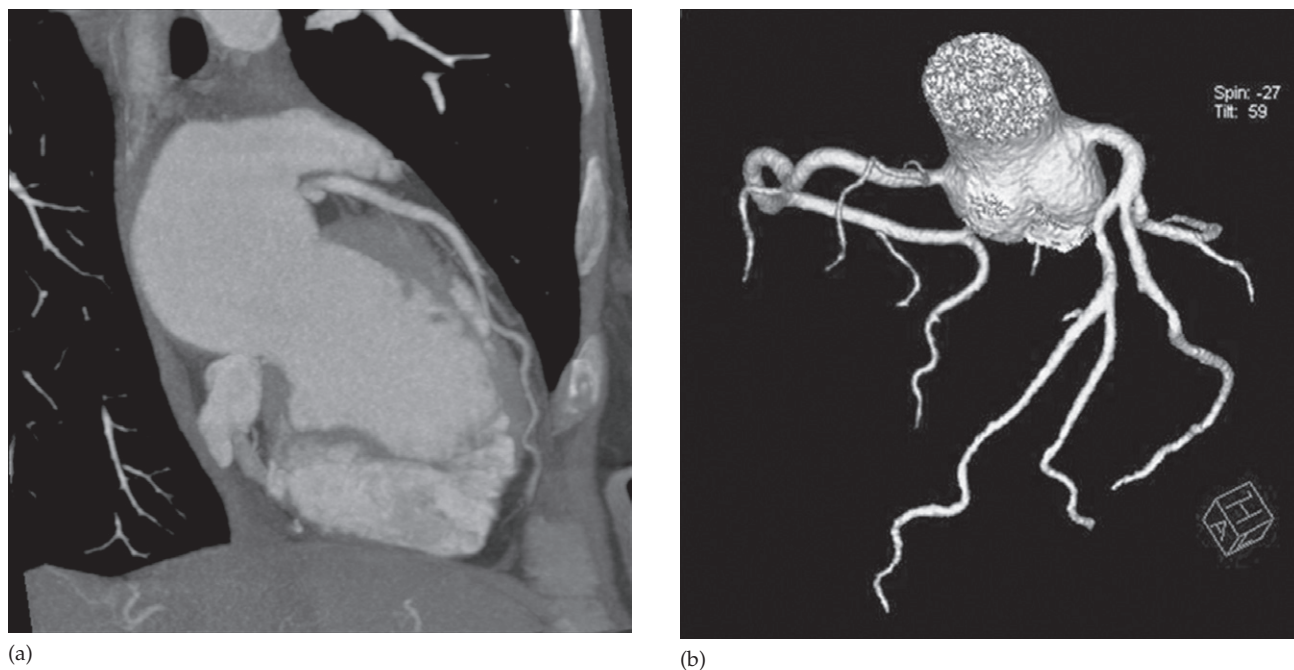


Fig. 3.20 CT coronary angiography showing haemodynamically insignificant coronary artery disease. (a) Oblique coronal reconstruction showing the left coronary artery on the posterior surface of the heart. (b) Three-dimensional reconstruction of the aortic root and both coronary arteries.

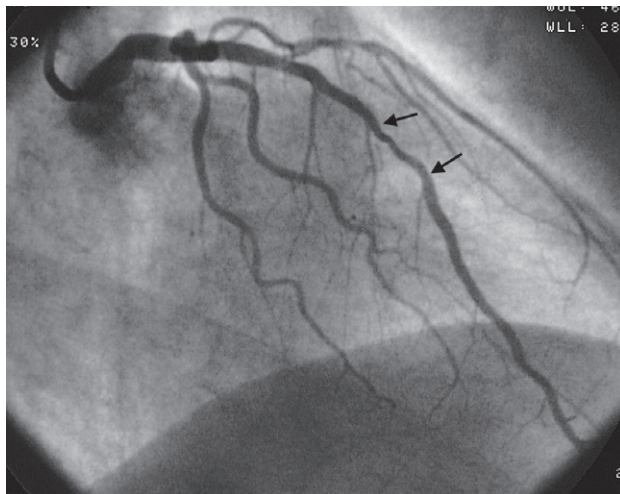
oplasty with stenting, bypass surgery or medical treatment. Coronary arteriography is usually combined with a left ventricular angiogram which shows the contractility of the left ventricle and any concomitant mitral regurgitation.

Hypertensive heart disease and other myocardial diseases

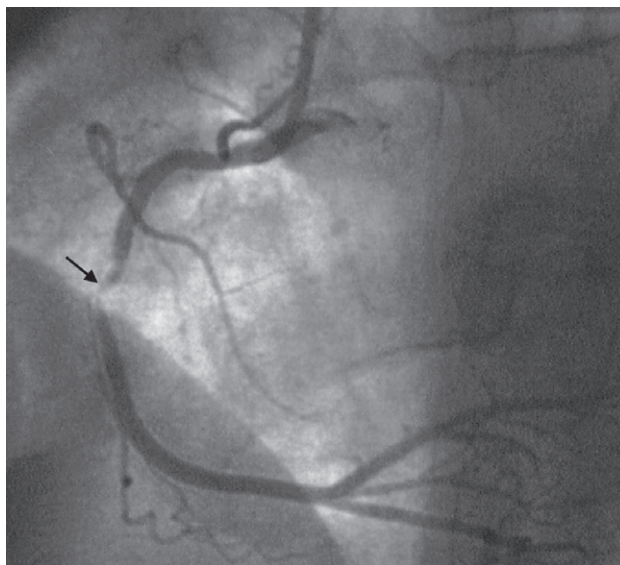
Ventricular hypertrophy without dilatation does not cause recognizable abnormality on a CXR. Therefore, in systemic hypertension and various forms of cardiomyopathy, the CXR only becomes abnormal once ventricular dilatation has taken place. If there is a rise in left ventricular end-diastolic pressure, moderate left atrial enlargement and signs of elevation of pulmonary venous pressure may be seen. The shape of the heart is the same regardless of the cause of the myocardial disorder. However, the aorta may enlarge in systemic hypertension.

Echocardiography and cardiac MRI in systemic hypertension show symmetrical increase in the thickness of the left ventricular wall with a normal aortic valve. Once decompensation occurs, the cavity will enlarge. The pattern of hypertrophy may be difficult to differentiate from that of idiopathic hypertrophic cardiomyopathy (also known as hypertrophic obstructive cardiomyopathy or HOCM). HOCM is a genetically transmitted primary myocardial disease (primary cardiomyopathy) which increases the risk of cardiac arrhythmia and sudden death. In HOCM, the hypertrophy is much greater in the ventricular septum than in the free wall. This asymmetrical septal hypertrophy is diagnostic of the condition (Fig. 3.22). Other primary cardiomyopathies include dilated cardiomyopathy, restrictive cardiomyopathy and arrhythmogenic cardiomyopathy.

Myocarditis is an inflammatory myocardial disease that may have infectious and non-infectious causes. The symptoms of acute and subacute myocarditis resemble those



(a)



(b)

Fig. 3.21 Coronary artery disease. (a) Left coronary artery injection showing a moderate stenosis between the arrows in the mid left anterior descending artery. (b) Right coronary artery injection showing tight stenosis (arrow) of the mid right coronary artery.

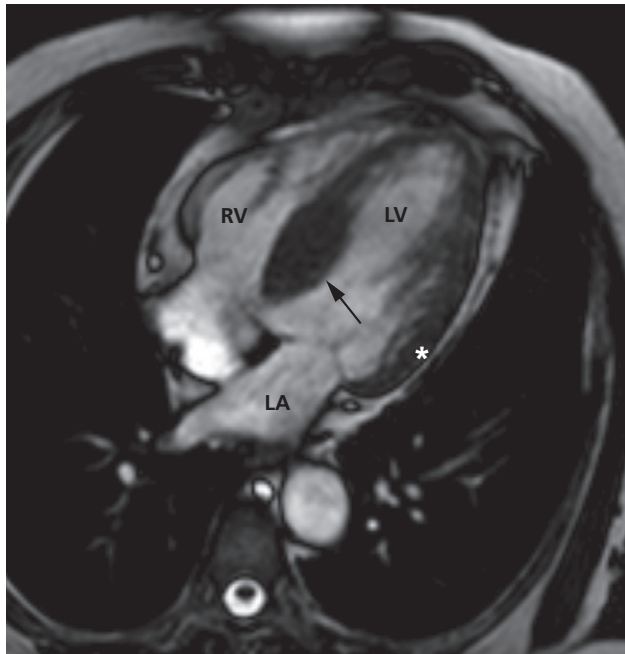
of an acute coronary syndrome characterized by chest pain and troponin rise. Acute ischaemia is therefore an important differential diagnosis. In clinically suspected myocarditis, cardiac MRI plays a pivotal role in confirming the diagnosis and determining the extent of involvement shown by myocardial oedema and possibly necrosis (scar) (Fig. 3.23). Coronary artery disease can be ruled out by conventional angiography or coronary CT angiography.

Valvular heart disease

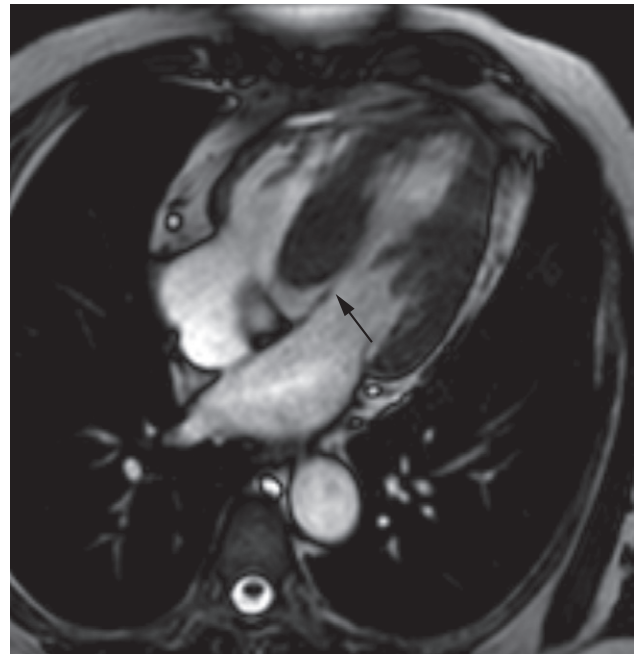
Valve stenosis and incompetence are readily diagnosed and quantified by echocardiography. Cardiac MRI is often the second line investigation. The role of the CXR (see Fig. 3.4) is minor, demonstrating cardiac size, presence of left atrial enlargement and severe calcification of the mitral or aortic valves. It can also show evidence of raised pulmonary venous pressure and any pulmonary oedema.

The important echocardiographic features of mitral stenosis are enlargement of the left atrium, thickening and calcification of the valve leaflets, restriction of valve movement and narrowing of the orifice (Fig. 3.24). Calcification is often present and is seen as a multiplicity of bright echoes arising within the leaflets. The gradient across the mitral valve can be calculated and the orifice of the mitral valve during diastole can be measured; a valve area of less than 1 cm^2 is classified as 'severe' stenosis. The left atrial cavity should be routinely examined for thrombi. Right ventricular hypertrophy and dilatation may be present in patients whose mitral stenosis has resulted in pulmonary arterial hypertension. In mitral regurgitation, echocardiography can quantify the size of the left atrium and left ventricle, and Doppler techniques can be used to grade the severity of regurgitation. The echocardiographic hallmark of aortic stenosis is thickening of the aortic valve leaflets with narrowing of the orifice: a valve area of less than 1 cm^2 indicates 'severe' stenosis. Doppler ultrasound can be used to quantify the gradient. Echocardiography can demonstrate the regurgitant jet in aortic regurgitation (see Fig. 3.14a) and it is possible to grade the severity of regurgitation using Doppler techniques (see Fig. 3.14b). Another major use of echocardiography in aortic regurgitation is to document left ventricular volume and ejection fraction.

Tricuspid stenosis and regurgitation. Both of these conditions give rise to enlargement of the right atrium and supe-



(a)

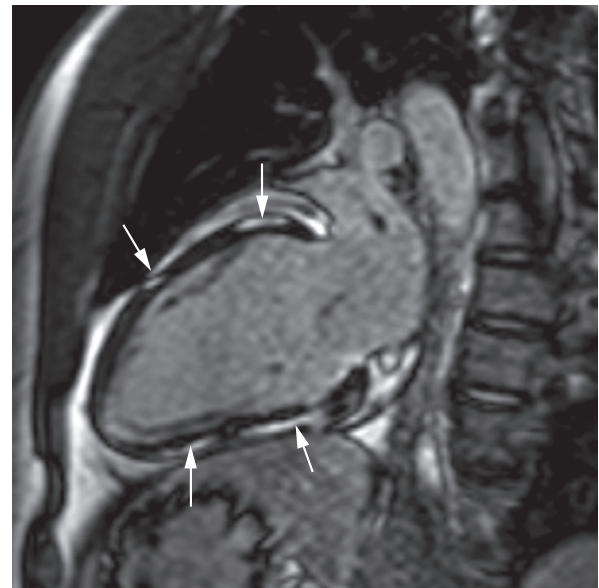


(b)

Fig. 3.22 Hypertrophic obstructive cardiomyopathy (HOCM). Axial T2-weighted MRI demonstrating the four-chamber view. (a) There is an asymmetrical focal hypertrophy of the septum to 2.5cm (arrow) and a normal lateral ventricular wall (*).LA, left atrium; LV, left ventricle; RV, right ventricle. (b) The anterior cusp of the mitral valve (arrow) contacts the septum during diastole – a diagnostic feature of this condition.

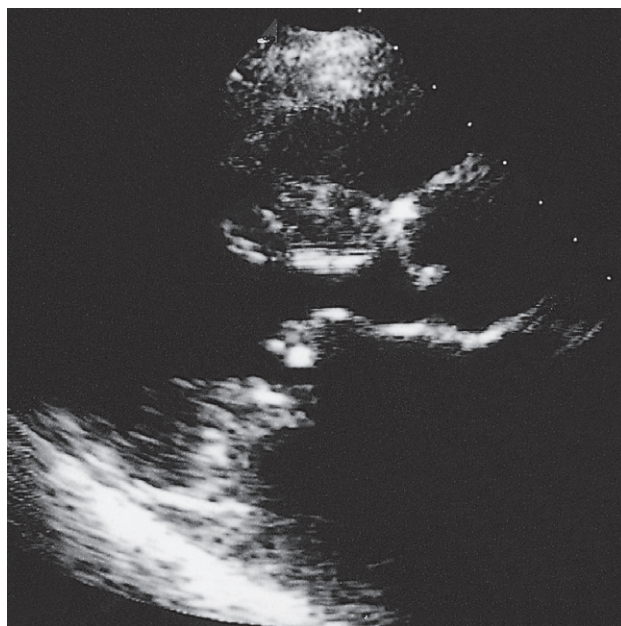


(a)

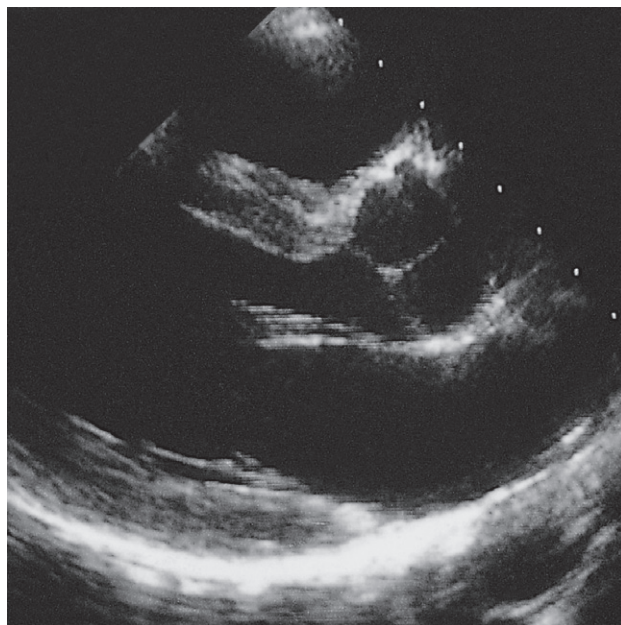


(b)

Fig. 3.23 Subacute myocarditis on MRI. (a) T2-weighted image with fat suppression showing diffuse hyperintensity of the left ventricular wall (arrows) suggesting myocardial oedema, in keeping with myocarditis. (b) Delayed post contrast T1-weighted image showing areas of hyperintensity (arrows) with a patchy subepicardial pattern indicative of myocardial damage.



(a)



(b)

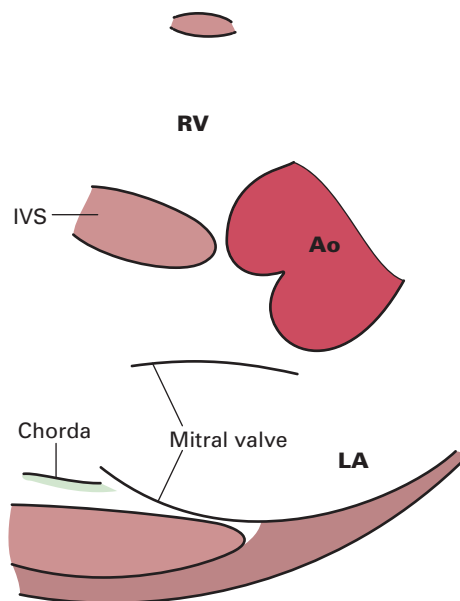
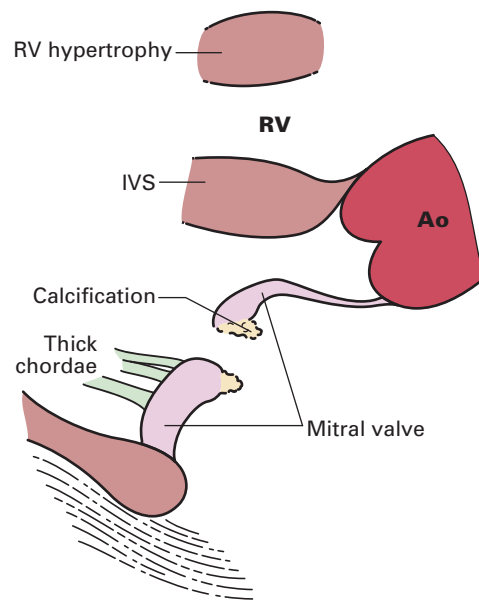
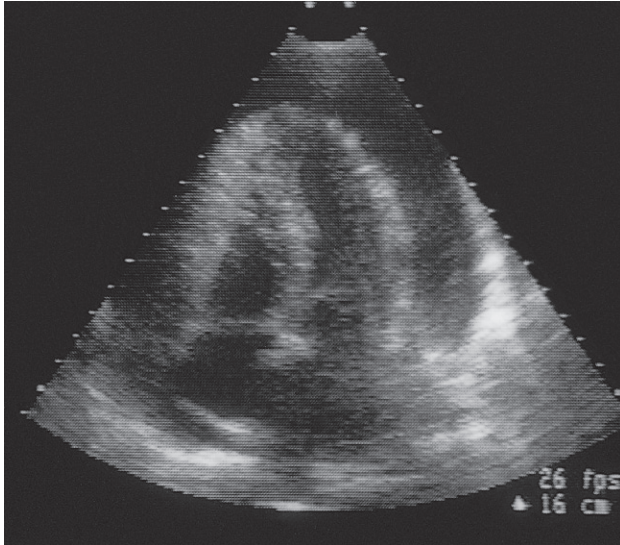


Fig. 3.24 Mitral stenosis on two-dimensional echocardiogram, parasternal long axis view. (a) The mitral valve is markedly thickened and shows calcification. The image is during diastole when the valve should be open, but in this case the orifice is narrowed and opening is impaired. (b) Normal image for comparison. Ao, aorta; IVS, interventricular septum; LA, left atrium; RV, right ventricle. Courtesy of Andrew A. McLeod and Mark J. Managhan.

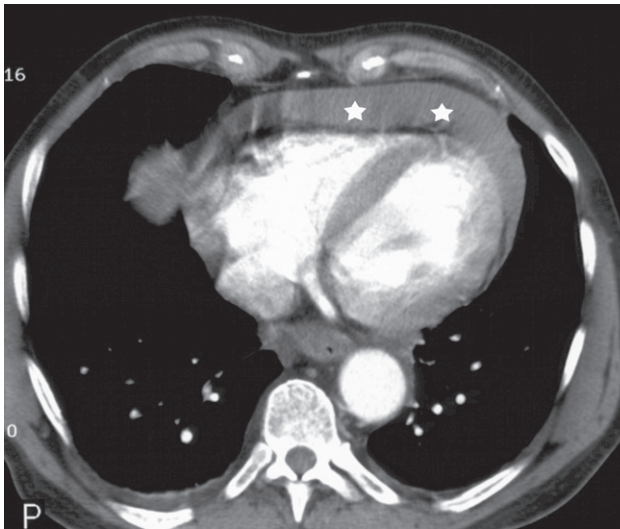
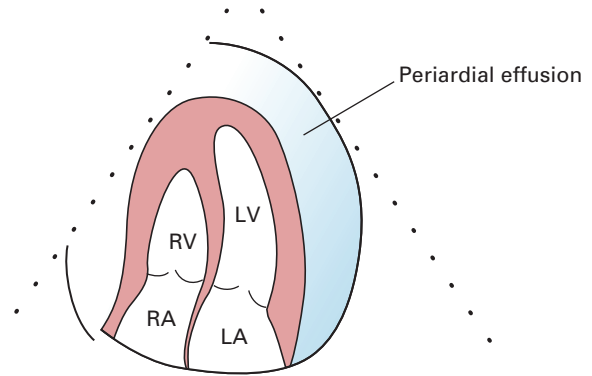
rior vena cava. They are almost never seen as isolated abnormalities and the features of coexistent mitral valve disease or pulmonary hypertension often dominate the picture. The echocardiographic features are similar in principle to those seen in mitral valve disease.

Pericardial effusion

Pericardial effusion is recognized on echocardiography as an echo-free space between the walls of the cardiac chambers and the pericardium (Fig. 3.25a). Quantities as small



(a)



(b)

Fig. 3.25 (a) Large pericardial effusion on an apical four-chamber view echocardiogram. LA, left atrium; LV, left ventricle; RA, right atrium; RV, right ventricle. (b) CT scan showing fluid density (stars) in the pericardium.

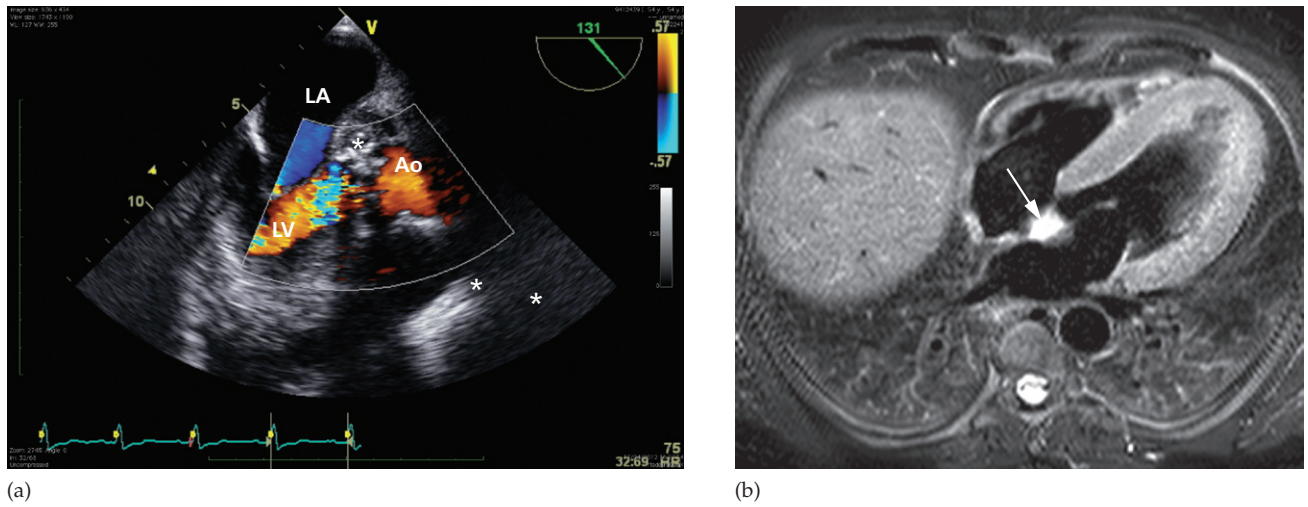


Fig. 3.26 Periaortic root abscess. (a) Transoesophageal echocardiogram (TOE) with Doppler showing a nearly 3 cm hyperechoic mass (*) adjacent to the aorta (Ao). Note that the mass is bulging into the left atrium (LA). LV, left ventricle. (b) T2-weighted axial MRI with fat suppression showing hyperintensity of the periaortic tissue in keeping with an abscess (arrow).

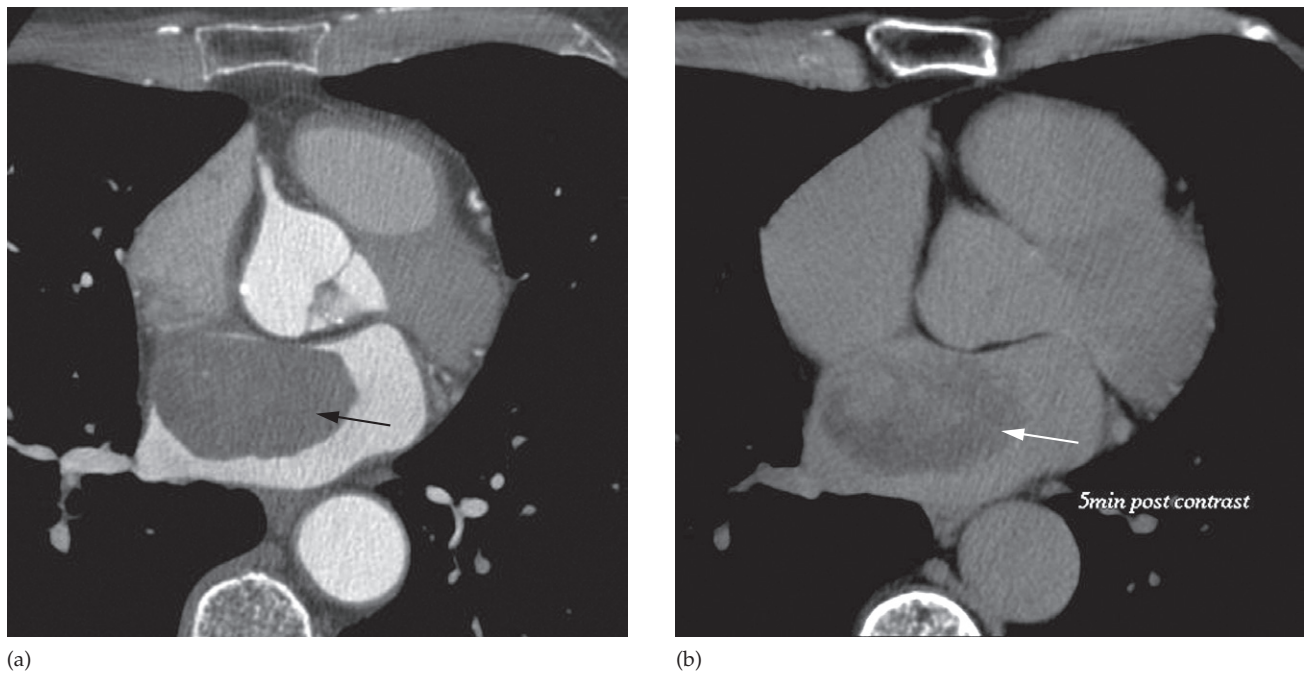


Fig. 3.27 Left atrial myxoma. (a) Axial CT image in the arterial phase post contrast medium injection showing a smooth mass (approximately 4.5cm) in the left atrium (arrow). (b) Repeat scan 5 minutes post contrast injection revealing inhomogenous inner enhancement, which is typical in myxoma (arrow), although may also rarely be seen in thrombi.

as 20–50 mL of pericardial fluid can be diagnosed by ultrasound. CT also readily demonstrates pericardial fluid (Fig. 3.25b). The nature of the fluid cannot usually be ascertained, and needle aspiration of the fluid may be necessary; such aspiration is best performed under ultrasound guidance.

Subacute bacterial endocarditis

Infective vegetations of the endocardial surfaces, particularly on the valves, as well as any adjacent abscess formation (Fig. 3.26) can be shown on echocardiography, cardiac MRI and cardiac CT. Vegetations on prosthetic valves are more difficult to identify. The valvular regurgitation often associated with endocarditis can be best shown on echocardiography and cardiac MRI.

Left atrial myxoma and other intracardiac masses

Intracardiac tumours are rare: left atrial myxoma is the most frequently encountered. It is a benign tumour that

usually arises in the interatrial septum or in the wall of the left atrium. As it enlarges, it becomes pedunculated to float in the left atrial cavity. The myxoma may, therefore, interfere with the function of the mitral valve and mimic mitral stenosis or regurgitation. Echocardiography has proved to be an excellent tool for its diagnosis by showing a mass of echoes in the cavity of the left atrium, which usually prolapses into the mitral valve orifice during diastole. Cardiac MRI and CT have also proved to be excellent methods of demonstrating left atrial myxoma (Fig. 3.27) and other intracardiac tumours.

Congenital heart disease

There are a large number of congenital malformations of the heart and great vessels. Frequently, they are multiple. Some conditions may be detected antenatally. Echocardiography, MRI, angiography and, to a much lesser extent, CXRs, are usually necessary for their elucidation. The topic is beyond the scope of this book.

Breast Imaging

Mammography is the mainstay of breast imaging in women aged over 50 years and is the only method of population-based screening that has been shown to result in a mortality reduction. In women under 40 years, high resolution ultrasound is the initial modality of choice, though mammography may also be indicated. Breast magnetic resonance imaging (MRI) is the most sensitive method of detecting breast cancer, but its clinical role has yet to be fully defined.

Mammography

Mammography is a low dose x-ray examination of the breast obtained using a dedicated x-ray unit designed to maximize the contrast between the various soft tissues of the breast. Normal mammographic appearances vary widely, with a variable proportion of low density adipose tissue and higher density fibroglandular parenchyma and stroma. With increasing age the glandular parenchyma involutes, resulting in increased conspicuity of abnormalities and greater mammographic sensitivity for breast cancer detection. Full field digital units are replacing conventional x-ray units and have been demonstrated to be more sensitive for breast cancer detection in women with dense breast tissue.

Mammography is used to investigate women over the age of 40 years presenting with breast symptoms, and as a screening test both for women at increased risk (often in conjunction with breast MRI) and for those women aged 50 or above at population risk.

The main abnormal mammographic findings are: masses, microcalcifications, distortions and parenchymal asymme-

Box 4.1 Key mammographic signs of breast cancer

- Ill-defined, irregular or spiculated mass or masses
- Pleomorphic microcalcifications, often with a linear or ductal distribution and with or without an associated mass or soft tissue density
- Associated features include:
 - architectural distortion
 - skin thickening
 - axillary lymph node enlargement

try. Key features of malignancy are listed in Box 4.1 and illustrated in Fig 4.1.

Benign masses are usually well defined and ovoid or spherical (Fig. 4.2). They may contain calcifications, but these are generally large and coarse in appearance.

Breast ultrasound

Breast ultrasound is the first line investigation in symptomatic women under 40 years, in whom the breast tissues are generally dense and in whom it is desirable to avoid irradiation of the breast tissue. It is also extremely useful in characterizing mammographic findings in older women since these are often indeterminate. It can differentiate between cystic and solid masses and usually between benign and malignant solid masses. Benign masses are generally round or ovoid, with well-defined borders, a homogeneous internal echo pattern, and either absent or peripheral internal vascularity on colour Doppler interrogation (Fig. 4.3). Malignant masses are generally irregular, poorly defined, interrupt the normal fascial planes of the breast and have abnormal internal vascularity (Fig. 4.4).

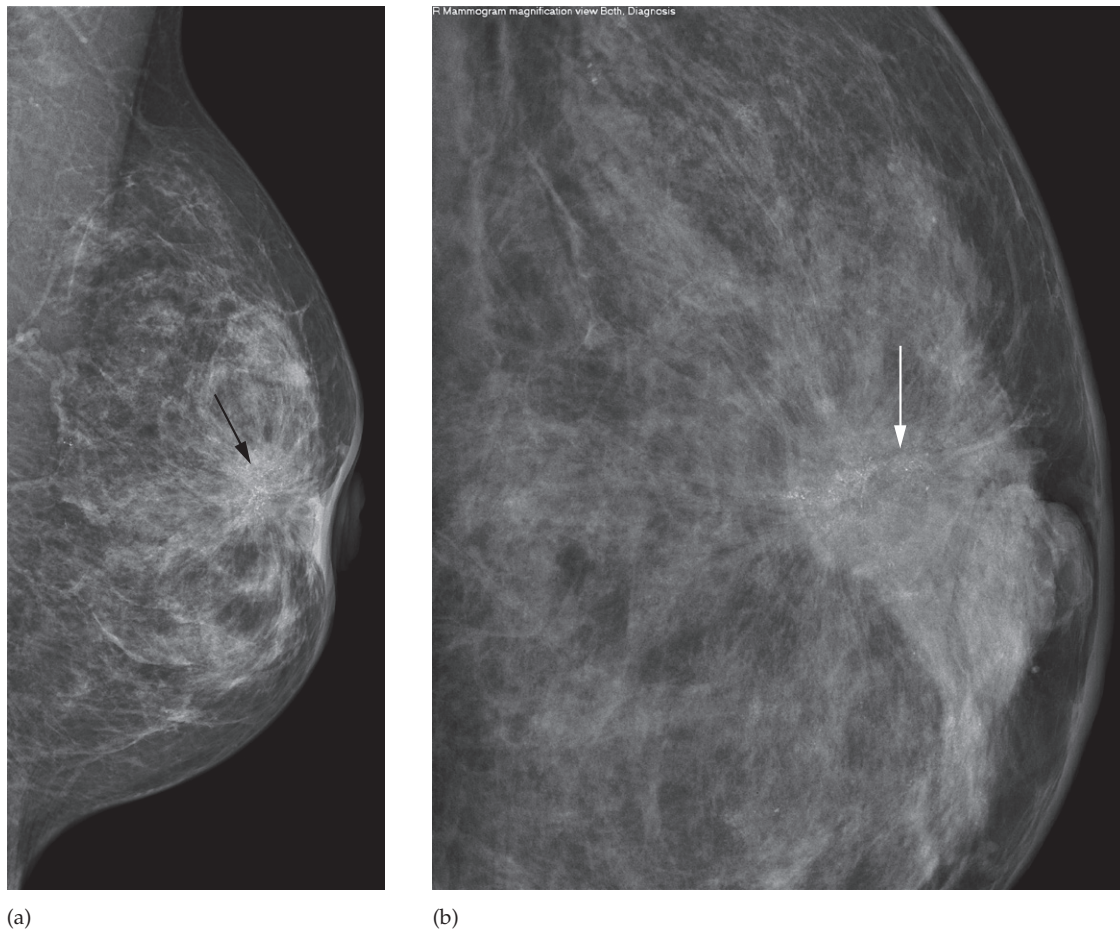


Fig. 4.1 Mammographic images of breast cancer. (a) Left mediolateral oblique and (b) compressed magnified left craniocaudal views of an irregular spiculated mass (black arrow) with associated pleomorphic microcalcification (white arrow) behind the nipple with associated architectural distortion and nipple retraction.

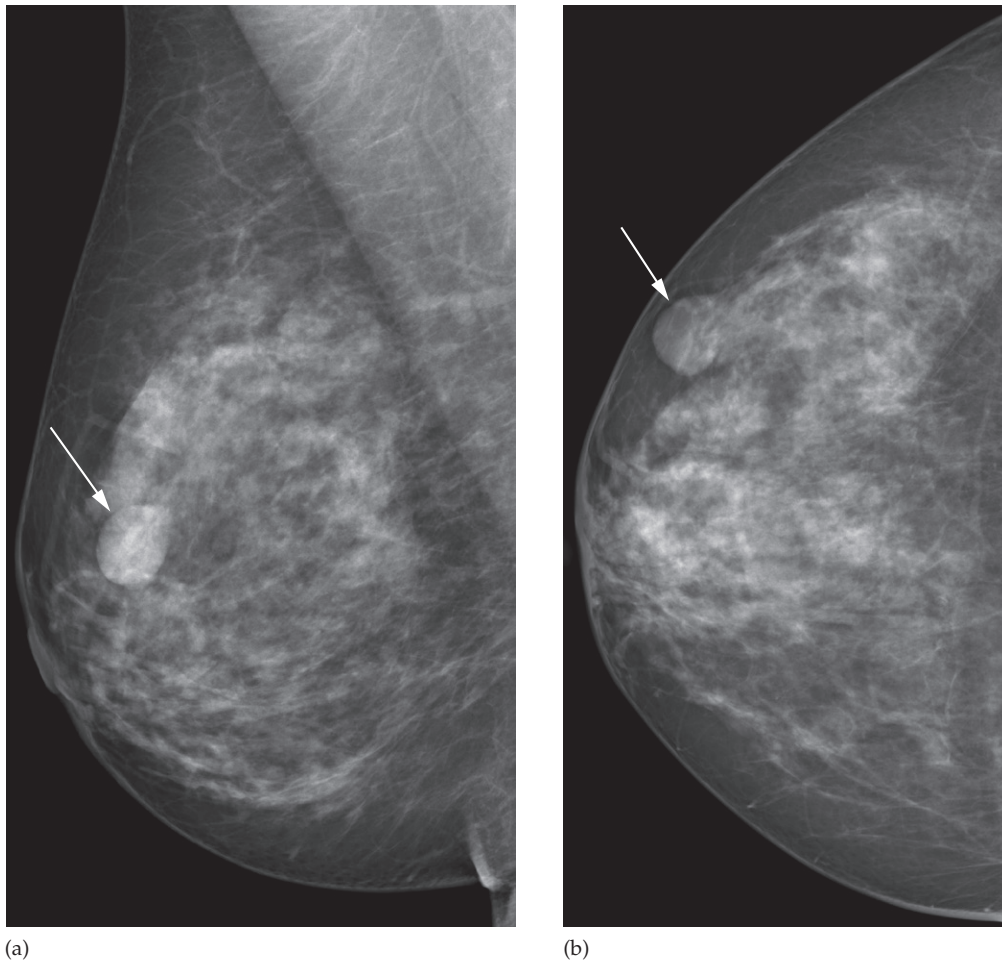


Fig. 4.2 Mammographic image of a benign breast lesion. (a) Right mediolateral oblique and (b) craniocaudal views of the right breast demonstrating a very well-defined ovoid mass in the upper outer quadrant of the breast (arrow).

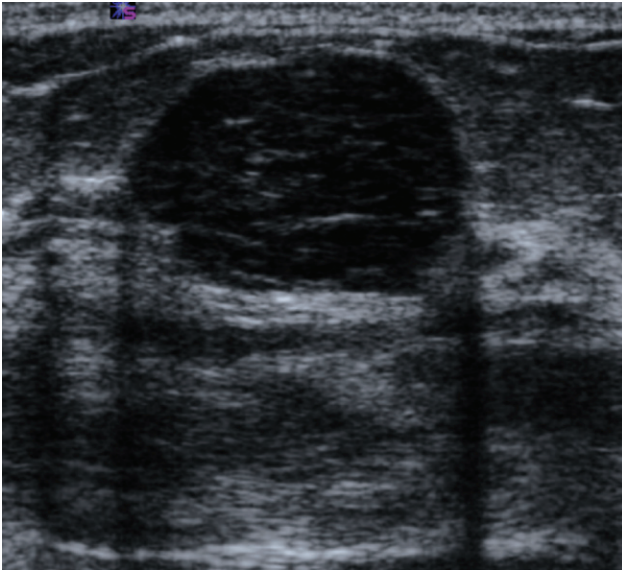
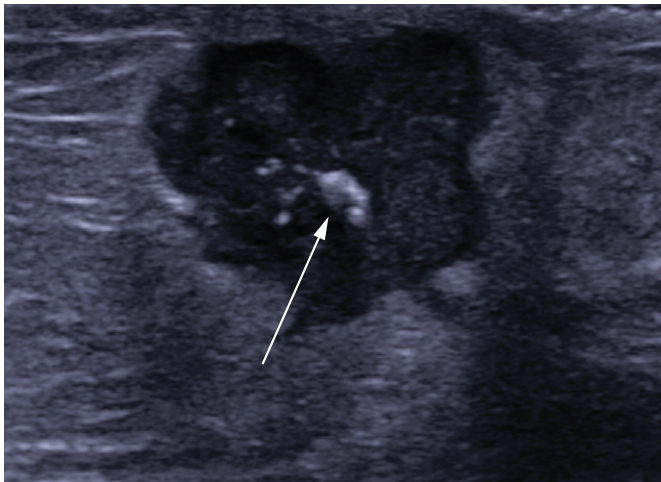
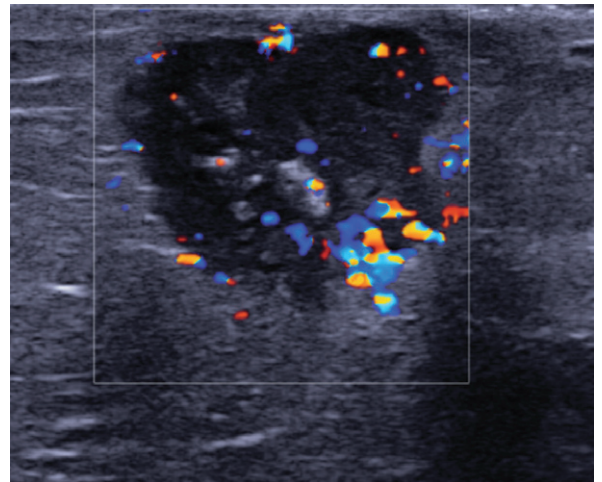


Fig. 4.3 Ultrasound image of a benign breast lesion. There is a very well-defined hypoechoic ovoid mass typical of a benign fibroadenoma. This is the same patient as in Fig. 4.2.



(a)



(b)

Fig. 4.4 Ultrasound of a breast cancer. (a) An irregular spiculated heterogenous mass containing hyperechoic microcalcification (arrow). (b) On Doppler interrogation, there is intense malignant vascularity. This is the same patient as in Fig. 4.1.

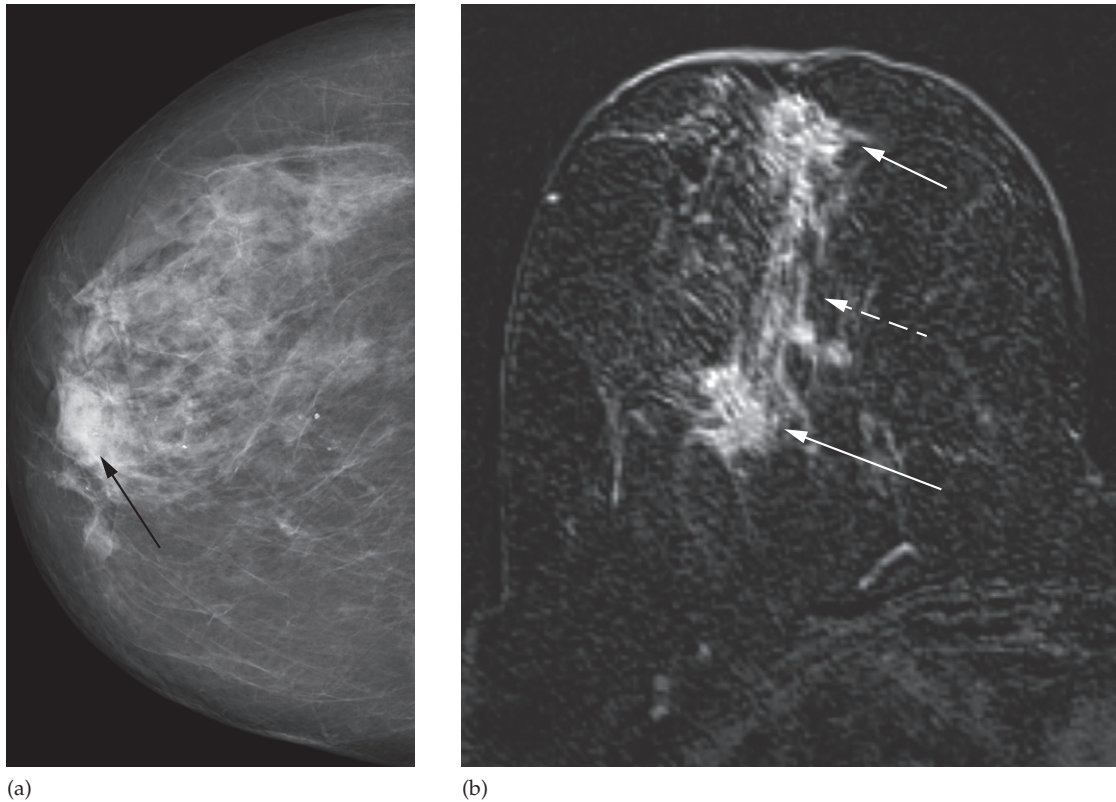


Fig. 4.5 Breast cancer with ductal carcinoma in situ. (a) Mammography demonstrates an irregular malignant mass (black arrow) with some associated microcalcification. (b) Axial contrast-enhanced subtracted MRI reveals the enhancing index mass (short arrow) and an additional unsuspected malignancy posteriorly (long arrow) with intervening linear and nodular enhancement typical of ductal carcinoma in situ (dashed arrow).

Ultrasound-guided fine needle aspiration or biopsy of breast masses is used to obtain histology in indeterminate or suspicious masses.

Breast magnetic resonance imaging

When the breast is difficult to evaluate with conventional imaging, breast MRI can depict the precise extent of malignant disease with very high sensitivity and moderate specificity (Fig. 4.5), which in turn may aid treatment planning. Unlike mammography, it does not utilize ionizing radiation

and its accuracy is unaffected by breast density, but there are issues around cost and timely access.

Breast screening

In the Western world breast cancer will affect as many as one in nine women in their lifetime and it is the most common cancer in women, representing a significant health problem. The UK National Health Service (NHS) Breast Screening Programme was set up in 1989 to tackle this

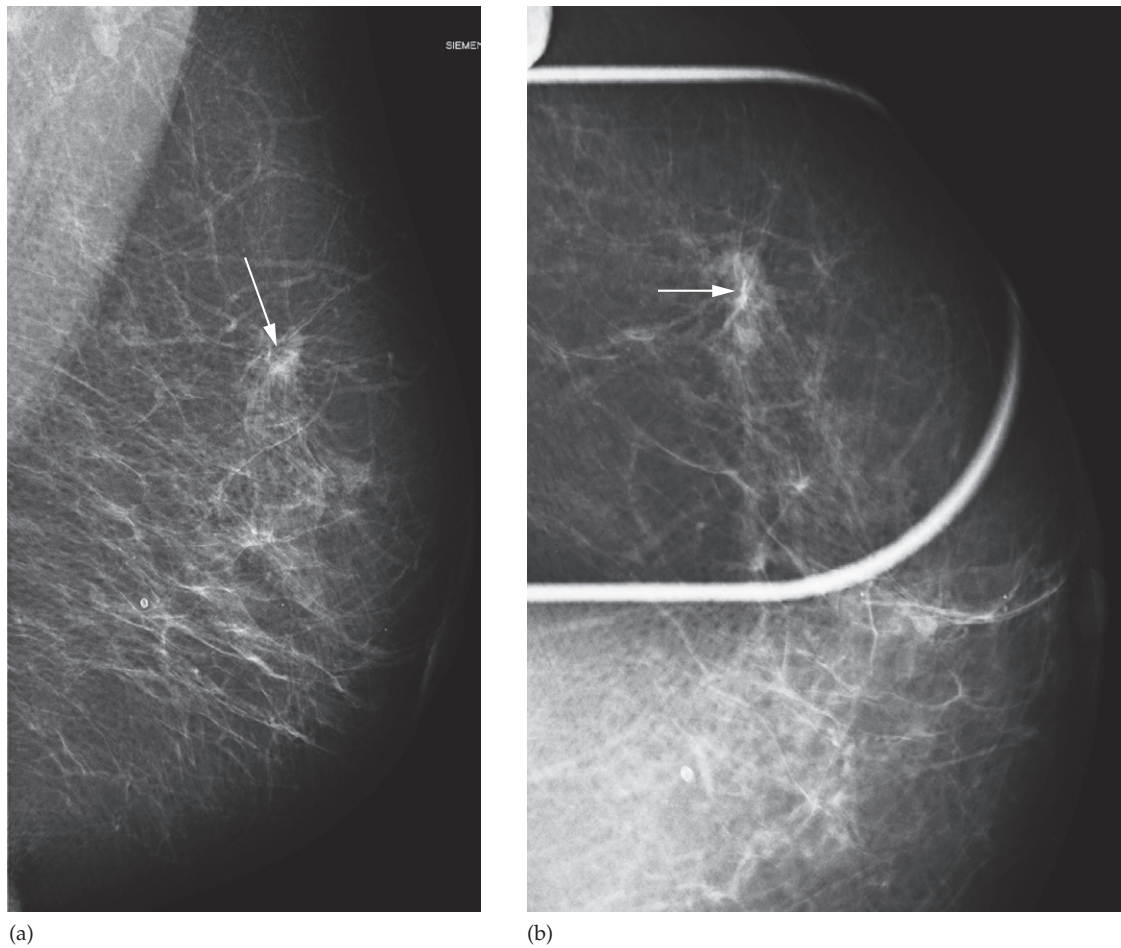


Fig. 4.6 Early breast cancer detected at screening mammography. (a) Left mediolateral oblique mammogram and (b) compressed craniocaudal view demonstrating a very small impalpable cancer (arrow).

issue. It offers 3-yearly mammography to women from 50 to 70 years. Mammography can detect early stage breast cancer before there is any clinical abnormality (Fig. 4.6). Numerous randomized controlled trials have demonstrated beyond doubt that good quality population-based screening can reduce breast cancer mortality.

In women at greatly increased risk of breast cancer, many of whom have genetic mutations such as the BRCA-1 and -2 mutations, MRI has been shown to be a more effective screening tool than mammography. However, it is as yet unknown whether this early detection will translate into a mortality reduction.

Plain Abdomen

The standard plain film of the abdomen is a supine antero-posterior (AP) view (Fig. 5.1). Erect films offer little further diagnostic information at the expense of increased radiation exposure to the patient. Free intraperitoneal air can be seen on an erect chest radiograph (CXR), which is usually performed at the time of the abdominal x-ray. Rarely, in patients who are unable to sit or stand, a lateral decubitus view (i.e. an AP film with the patient lying on his or her side) is performed using a horizontal x-ray beam as a means of detecting free intraperitoneal air.

There are a number of points to be considered when looking at a plain abdominal film:

- Analyze the intestinal gas pattern and identify any dilated portion of the gastrointestinal tract.
- Look for gas outside the lumen of the bowel.
- Look for ascites and soft tissue masses in the abdomen and pelvis.
- If there are any calcifications, try to locate exactly where they lie.
- Assess the size of the liver and spleen.

Intestinal gas pattern

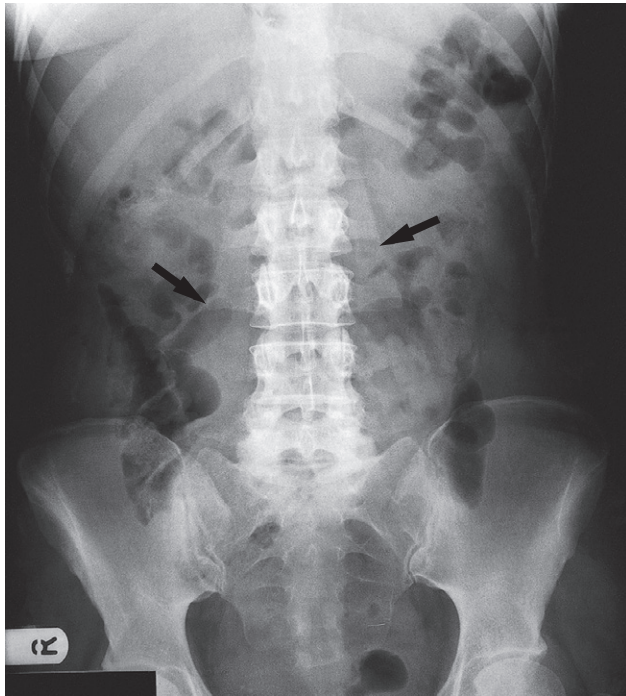
Relatively large amounts of gas are usually present in the stomach and colon in a normal patient. The stomach can be readily identified by its location above the transverse colon, by the band-like shadows of the gastric rugae in the supine view. The duodenum often contains air and there may be some gas in the normal small bowel, but it is rarely sufficient to outline the whole of a loop. If the bowel is

dilated it is important to try and decide which portion is involved.

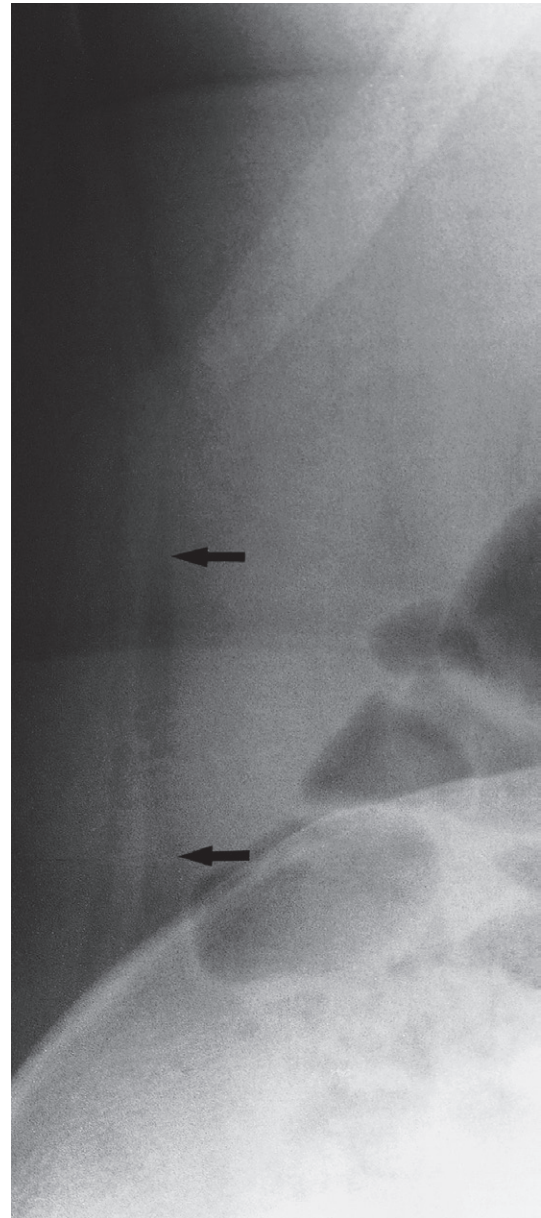
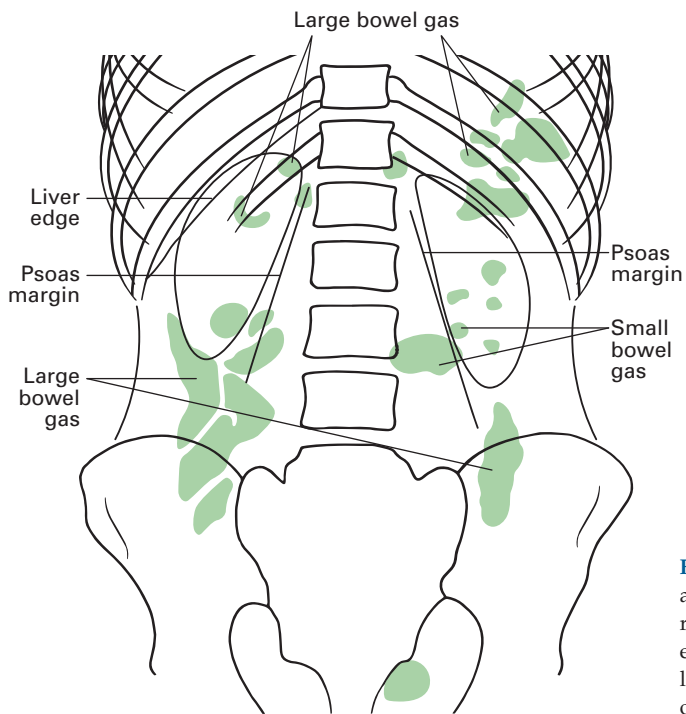
Dilatation of the bowel

The initial diagnosis of *intestinal obstruction* is usually made on clinical examination with the help of plain abdominal films. Dilatation of the bowel is the cardinal plain film sign of intestinal obstruction, and the pattern of dilatation is the key to the radiological distinction between small and large bowel obstruction. In small bowel obstruction, the small intestine is dilated down to the point of obstruction and the bowel beyond this point is either empty or of reduced calibre. In large bowel obstruction, the large bowel is dilated down to the level of obstruction. If the ileocaecal valve, where the ileum joins the colon, is incompetent, there will also be small bowel dilatation. Making the distinction between large and small bowel obstruction depends on the ability to recognize which portions of bowel are dilated.

Dilated small bowel usually lies in the centre of the abdomen within the 'frame' of the large bowel (but the sigmoid and transverse colon may be redundant and may also lie in the centre of the abdomen, particularly when dilated). When the proximal and mid small intestine are dilated, the valvulae conniventes (plica circulares) can be identified. The valvulae conniventes are always closer together and cross the width of the bowel (the colonic haustra do not), often giving rise to an appearance known



(a)



(b)

Fig. 5.1 Normal plain abdominal film. (a) Normal abdomen. The arrows point to the lateral borders of the psoas muscles. The renal outlines are obscured by the overlying colon. (b) Normal extraperitoneal fat stripe. Part of the right flank showing the layer of extraperitoneal fat (arrows), which indicates the position of the peritoneum.

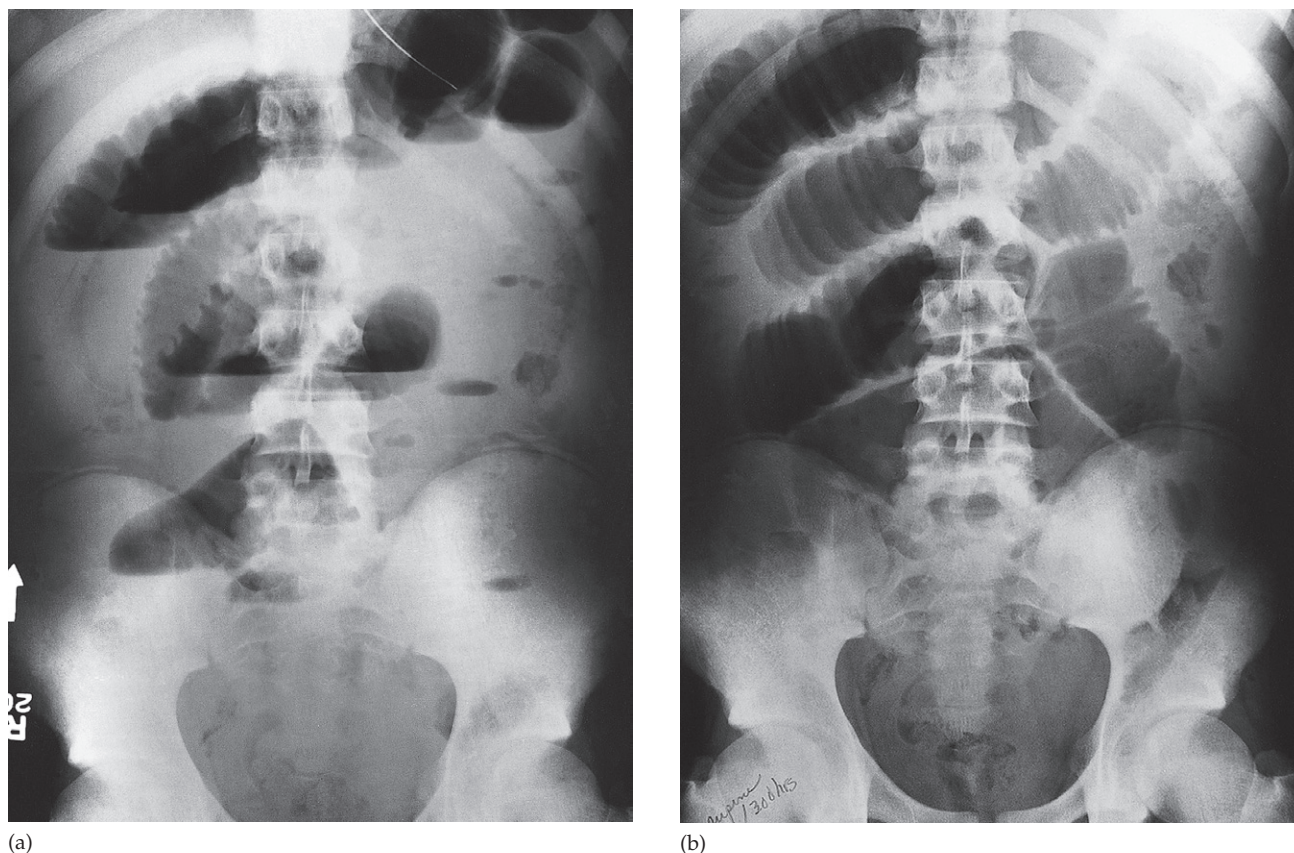


Fig. 5.2 Small bowel obstruction due to adhesions. (a) The jejunal loops are markedly dilated and show air–fluid levels in the erect film. The jejunum is recognized by the presence of valvulae conniventes. (b) The ‘stack of coins’ appearance is well demonstrated in the supine film. Note the large bowel contains less gas than normal.

as a ‘stack of coins’ (Fig. 5.2). The distal small intestine has a relatively smooth outline and it may be difficult to distinguish the lower ileum and the sigmoid colon because both may be smooth in outline. The radius of curvature of the loops is sometimes helpful: the tighter the curve, the more likely the loop is to be dilated small bowel.

The colon is recognized by its haustra, which usually form incomplete bands across the colonic gas shadows. Haustra are always present in the ascending and transverse colon, but may be absent distal to the splenic flexure. The presence of solid faeces is a useful and reliable indication of the position of the colon. The number of dilated loops is another valuable distinguishing feature between small and

large bowel dilatation, because even with a very redundant colon the numerous layered loops that are so often seen with small bowel dilatation are not present.

If the cause or site of the obstruction is not evident from plain films, and immediate exploratory surgery is not indicated, then computed tomography (CT) or a contrast study (either a follow-through for small bowel obstruction or instant enema for large bowel obstruction) is helpful. CT can demonstrate the site of obstruction by showing the location of the transition from dilated to collapsed bowel, and can confirm or exclude a mass at the site of obstruction (Fig. 5.3). With the increasing availability of CT, contrast follow-throughs are performed less frequently.

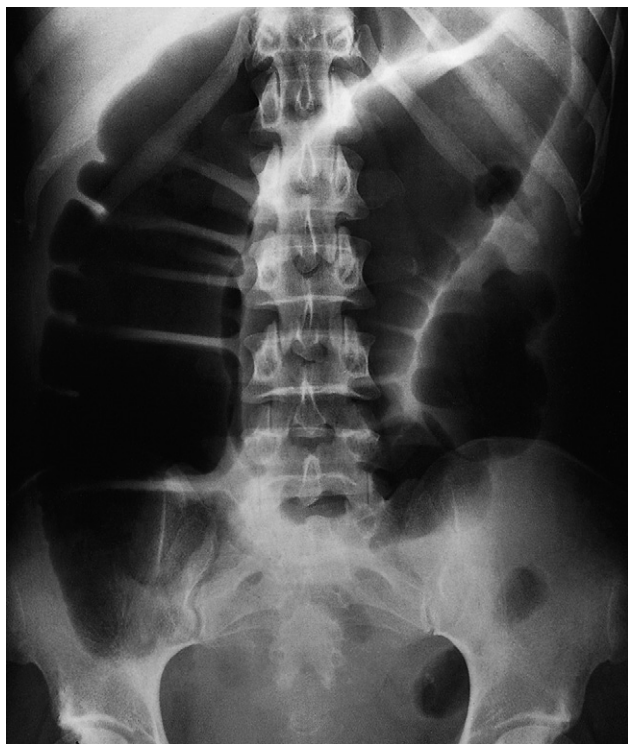


Fig. 5.3 Large bowel obstruction due to carcinoma at the splenic flexure. There is marked dilatation of the large bowel from the caecum to the splenic flexure.

Dilatation of the bowel occurs in a number of conditions. In remembering causes of mechanical bowel obstruction it is often easiest to think of conditions that: (i) obstruct the lumen (e.g. gall stone ileus); (ii) affect the bowel wall and cause a narrowing (e.g. Crohn's disease; or (iii) cause extrinsic compression of the bowel (e.g. adhesions). Bowel dilatation, however, occurs in conditions other than mechanical bowel obstruction, notably: paralytic ileus, acute ischaemia and inflammatory bowel disease. The radiological diagnosis of these phenomena depends mainly on the pattern of distribution of the dilated loops (Table 5.1).

Pneumoperitoneum

The radiological diagnosis of perforation of the gastrointestinal tract is based on recognizing free gas in the peritoneal

cavity (pneumoperitoneum) (Fig. 5.7). The most common cause of spontaneous pneumoperitoneum is a perforated peptic ulcer and two-thirds of such cases are recognizable radiologically. The largest quantities of free gas are seen after colonic perforation, and the smallest amounts with leakage from the small bowel. A pneumoperitoneum is very rare in acute appendicitis even if the appendix has perforated.

Free intraperitoneal air is a normal finding after laparotomy or laparoscopy. In adults, all the air is usually absorbed within 7 days. In children, the air absorbs much faster, usually within 24 hours. An increase in the amount of air on successive films indicates continuing leakage of air.

Pneumoperitoneum under the right hemidiaphragm is usually easy to recognize on an erect CXR as a curvilinear collection of gas between the line of the diaphragm and the opacity of the liver. Free gas under the left hemidiaphragm is more difficult to identify because of the overlapping gas shadows of the stomach and the splenic flexure of the colon. Gas in these organs may mimic free intraperitoneal air when none is present.

Gas in an abscess

Gas in an abdominal (Fig. 5.8) or pelvic abscess produces a very variable pattern on plain films. It may form either small bubbles or larger collections of air, both of which could be confused with gas within the bowel. Fluid levels in abscesses may be seen on a horizontal x-ray film. As abscesses are mass lesions, they displace the adjacent structures; for example, the diaphragm is elevated with a subphrenic abscess, and the bowel is displaced by pericolic and pancreatic abscesses. A pleural effusion or pulmonary collapse/consolidation are very common in association with subphrenic abscess. Ultrasound and CT are extensively used to evaluate abdominal abscesses (see Chapter 10).

Gas in the wall of the bowel

Numerous spherical or oval bubbles of gas are seen in the wall of the large bowel in adults in the benign condition known as *pneumatosis coli*. Linear streaks of intramural gas have a more sinister significance as they usually indicate infarction of the bowel wall. Gas in the wall of the bowel in the neonatal period, whatever its shape, is diagnostic of

Table 5.1 Patterns of bowel dilatation in gastrointestinal conditions

Diagnosis	Pattern of bowel dilatation
Mechanical obstruction of the small bowel (Fig. 5.2)	Small bowel dilatation, but colon is normal or reduced in calibre. Computed tomography may also show any responsible tumour or inflammatory mass
Mechanical obstruction of the large bowel (Fig. 5.3)	Dilatation of the colon down to the point of obstruction. May be accompanied by small bowel dilatation if the ileocaecal valve becomes incompetent
Generalized paralytic ileus (Fig. 5.4)	Both the large and the small bowel are dilated. The dilatation often extends down into the sigmoid colon and gas may be present in the rectum. It may be difficult to differentiate from low large bowel obstruction
Localized peritonitis	Often causes dilatation of the bowel loops adjacent to the inflammatory process (which may be specifically visible on computed tomography), giving rise to the so-called sentinel loops seen, for example, in appendicitis and pancreatitis
Gastroenteritis	Variable pattern. Some patients have a normal film and some show excess fluid levels without dilatation, whereas some mimic paralytic ileus and others mimic small bowel obstruction
Small bowel infarction	May mimic obstruction of the small bowel or obstruction of the large bowel depending on the distribution of the ischaemia
Closed loop obstruction (Fig. 5.5)	The diagnosis depends on whether the loop in question contains air. If it does, as for example in a caecal or sigmoid volvulus, the dilated loop is seen filled with gas in a characteristic shape. If the closed loop is filled with fluid – the common situation in most obstructed hernias – it may not be visible
Toxic dilatation of the colon (Fig. 5.6)	Usually, the dilatation is maximal in the transverse colon; indeed, the descending colon may be narrower than normal. The haustra are lost or grossly abnormal and the swollen islands of mucosa between the ulcers can be recognized as polypoid shadows. If the transverse colon is more than 6cm in diameter in a patient with colitis, toxic dilatation should be strongly suspected



Fig. 5.4 Paralytic ileus. There is considerable dilatation of the whole of the large bowel extending well down into the pelvis. Small bowel dilatation is also seen.

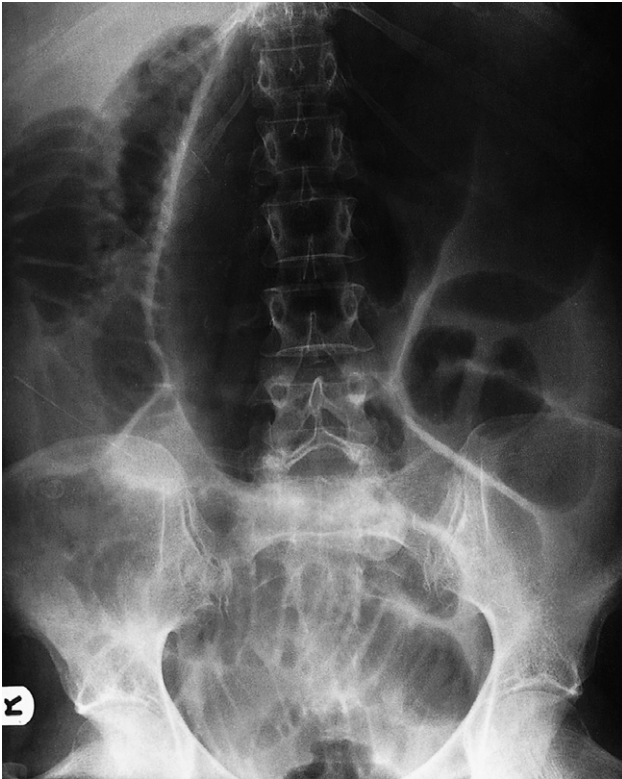


Fig. 5.5 Volvulus of the caecum. The twisted obstructed caecum and ascending colon now lie on the left side of the abdomen and appear as a large gas shadow. There is also extensive small bowel dilatation from obstruction by the volvulus.

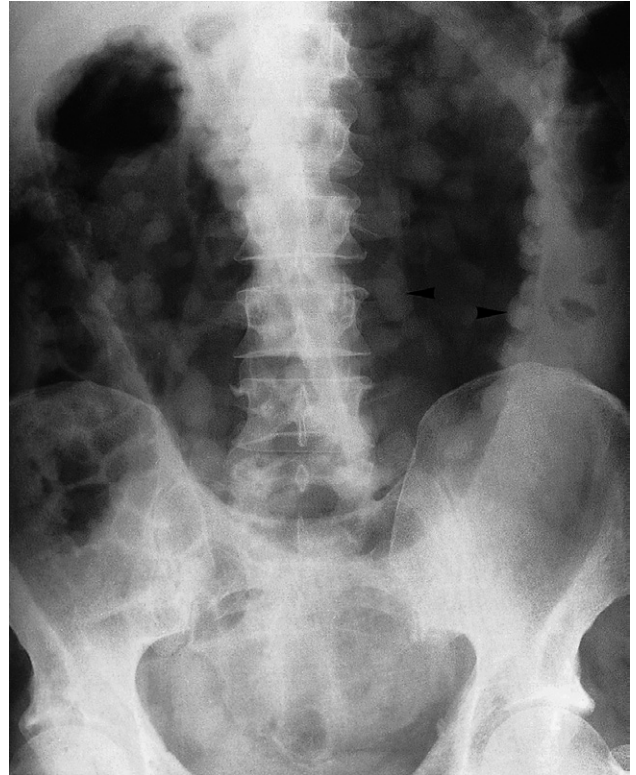


Fig. 5.6 Toxic dilatation of the large bowel from ulcerative colitis. The dilatation is maximal in the transverse colon. Note the loss of haustra and islands of hypertrophied mucosa. Two of these pseudopolyps are arrowed.

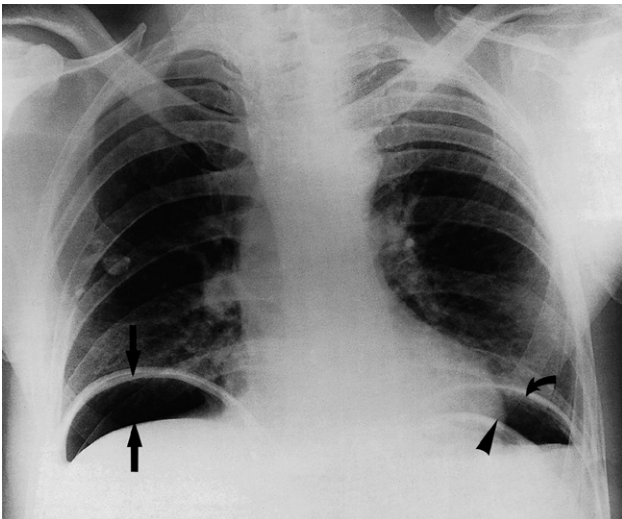


Fig. 5.7 Free gas in the peritoneal cavity. On this chest radiograph, air can be seen under the domes of both hemidiaphragms. The curved arrow points to the left hemidiaphragm and the arrow head to the wall of the stomach. The two vertical arrows point to the diaphragm and upper border of the liver.

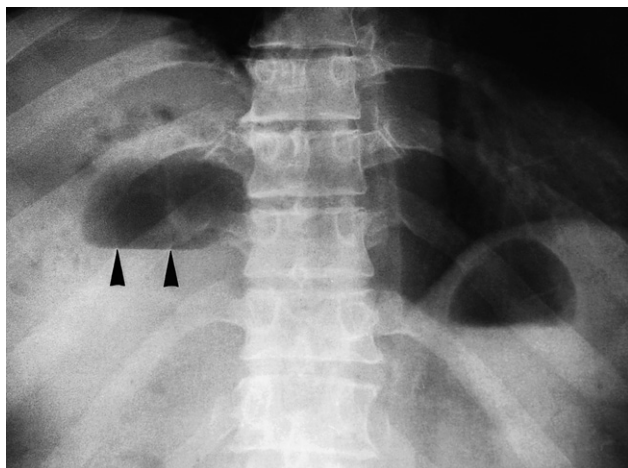


Fig. 5.8 Gas in a right subphrenic abscess. There are several collections of gas within the abscess. The largest of these contains a fluid level (arrowheads). The air–fluid level under the left hemidiaphragm is normal. It is in the stomach.

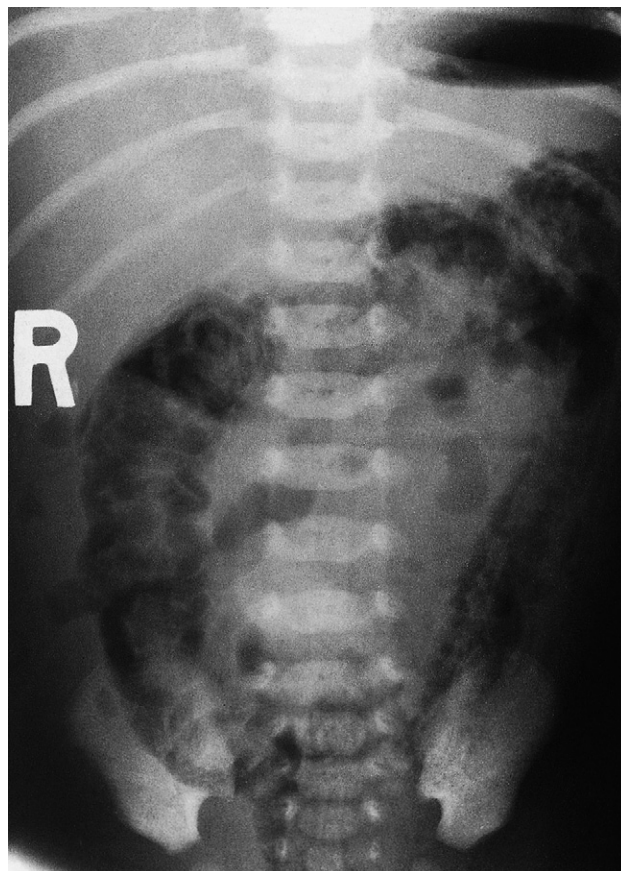


Fig. 5.9 Necrotizing enterocolitis in a neonate. There is intramural gas throughout the colon.

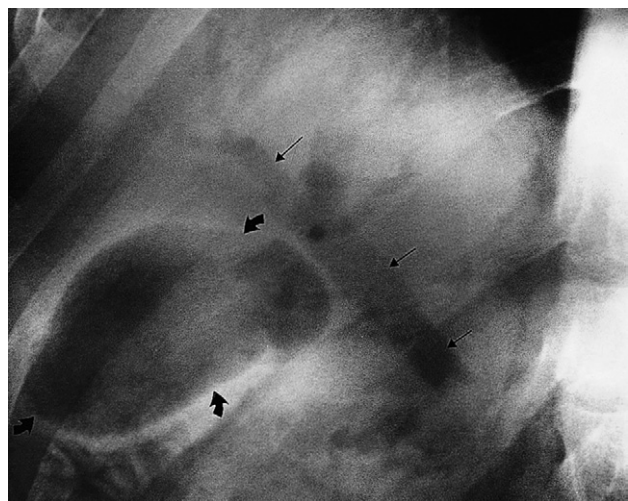


Fig. 5.10 Gas in the biliary tree. The gall bladder (curved arrows) and the duct system (straight arrows) have been outlined with air. The patient had an anastomosis of the common bile duct to the bowel.

necrotizing enterocolitis (Fig. 5.9), a disease that is fairly common in premature babies with respiratory problems.

Gas in the biliary system

Gas in the biliary system is seen on plain films following sphincterotomy or anastomosis of the common bile duct to the bowel (Fig. 5.10). It is also seen with a fistula from erosion of a gall stone into the duodenum or colon, or following penetration of a duodenal ulcer into the common bile duct.



Fig. 5.11 Ascites. Note how the gas in the ascending and descending colon (arrows) is displaced by the fluid away from the side walls of the abdomen.

Gas may be seen, very occasionally, in the wall or lumen of the gall bladder in acute cholecystitis from gas-forming organisms.

Ascites

Small amounts of ascites cannot be detected on plain films. Larger quantities separate the loops of bowel from one another and displace the ascending and descending colon from the fat stripes, which indicate the position of the peritoneum along the lateral abdominal walls (see Fig. 5.1). The loops of small bowel float to the centre of the abdomen (Fig. 5.11).

In practice, plain films are of very limited value in the diagnosis of ascites as the signs are so difficult to interpret confidently except when a large amounts of ascites is present. Ascites is readily recognized at ultrasound or CT (see Chapter 10).

Abdominal calcification

An attempt should always be made to determine the nature of any abdominal calcification. The first essential is to localize the calcification, as once the organ of origin is known the pattern or shape of the calcification will usually limit the diagnosis to just one or two choices (Box 5.1).

The most common calcifications are of little or no significance to the patient; most are phleboliths, calcified lymph nodes, costal cartilages and arterial calcification. Calcifications in the abdomen are likely to be one of the following:

- *Pelvic vein phleboliths* (Fig. 5.12) are very common; they may cause diagnostic confusion in that they may be mistaken for urinary calculi and faecoliths.
- *Calcified mesenteric lymph nodes* (Fig. 5.13) caused by old tuberculosis are important only in that they may be difficult to differentiate from other calcifications. Their pattern is often specific: they are irregular in outline and very dense, and because they lie in the mesentery they are often mobile. It is usually possible to see that they are composed of a conglomeration of smaller, rounded calcifications.
- *Vascular calcification* occurs in association with atheroma, and generally has a curvilinear appearance. There is no useful correlation with the haemodynamic severity of the vascular disease. Calcification is frequently present in the walls of *abdominal aortic aneurysms* (Fig. 5.14) and, if suspected, further evaluation should be undertaken with ultrasound.
- *Uterine fibroids* (Fig. 5.15) may contain numerous irregularly shaped, well-defined calcifications conforming to the

Box 5.1 Causes of abdominal calcification

- Pelvic vein phleboliths
- Calcified mesenteric lymph nodes
- Vascular calcification
- Uterine fibroids
- Soft tissue calcification
- Ovarian masses
- Adrenal calcification
- Liver calcification
- Gall stones
- Splenic calcification
- Pancreatic calcification
- Faecoliths
- Renal stones and other calcifications of the urinary tract

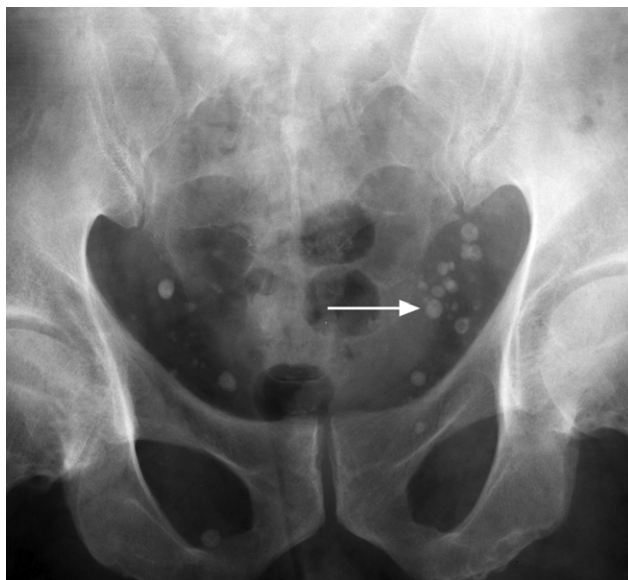


Fig. 5.12 Calcified phleboliths in the pelvis. The arrow points to one of the phleboliths.

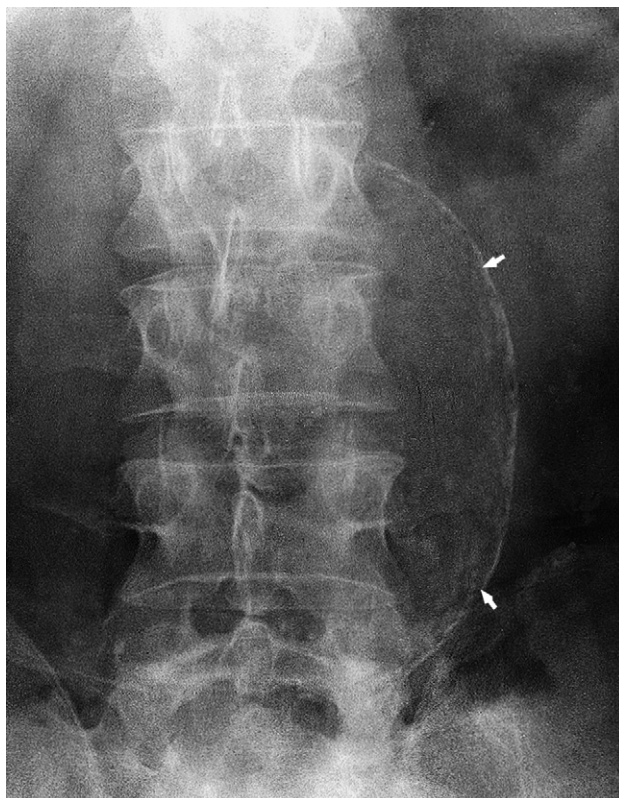


Fig. 5.14 Calcified abdominal aortic aneurysm (arrows). The aneurysm measured 8 cm in diameter on the lateral view.



Fig. 5.13 Calcified mesenteric lymph nodes from old tuberculosis (arrows).

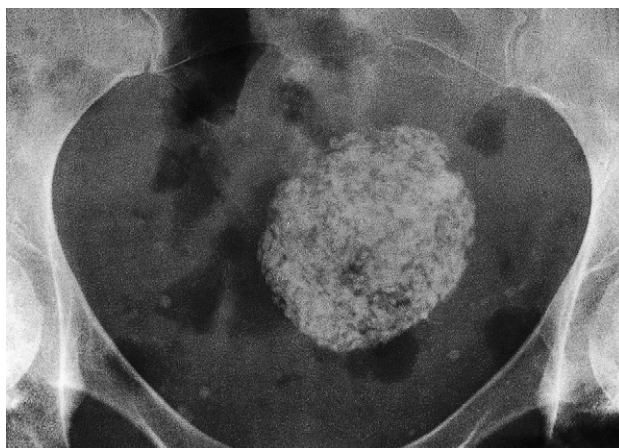


Fig. 5.15 Calcification in a large uterine fibroid.



Fig. 5.16 Adrenal calcification (arrow).

spherical outline of fibroids. Again, the calcification is by itself of no significance to the patient.

- *Soft tissue calcification* in the buttocks may be seen following injection of certain medicines. These shadows can at times be confused with intra-abdominal calcifications.
- *Malignant ovarian masses* occasionally contain visible calcium. The only benign ovarian lesion that is visibly calcified is the *dermoid cyst*, which may contain various calcified components, of which teeth are the commonest (see Fig. 9.10b).
- *Adrenal calcification* (Fig. 5.16) occurs after adrenal haemorrhage, after tuberculosis and occasionally in adrenal tumours. However, the majority of patients with adrenal calcification are asymptomatic healthy people in whom the cause of the calcification is unclear. Only a minority of patients with Addison's disease have adrenal calcification.



Fig. 5.17 Pancreatic calcification.

- *Liver calcification* occurs in hepatomas and rarely in other liver tumours. Hydatid cysts, abscesses and tuberculosis may also calcify over time.
- *Gall stones* are discussed in Chapter 7.
- *Splenic calcification* is rarely of clinical significance. It is seen in cysts, infarcts, old haematomas and following tuberculosis.
- *Pancreatic calcification* occurs in chronic pancreatitis. The calcifications are mainly small calculi within the pancreas. The position of the calcification usually enables the diagnosis to be made without difficulty (Fig. 5.17).
- *Faecoliths*. Calcified faecoliths may be seen in diverticula of the colon or in the appendix (Fig. 5.18). Appendiceal faecoliths are an important radiological observation, as the presence of an appendolith is a strong indication that the patient has acute appendicitis, often with gangrene and perforation. However, only a small proportion of patients with appendicitis have a radiologically visible appendolith.
- *Renal stones and other calcifications of the urinary tract* are discussed in Chapter 8.

Liver and spleen

Substantial enlargement of the liver has to occur before it can be recognized on a plain abdominal film. As the liver enlarges it extends well below the costal margin, displacing the hepatic flexure, transverse colon and right kidney downwards and displacing the stomach to the left. The diaphragm may also be elevated.

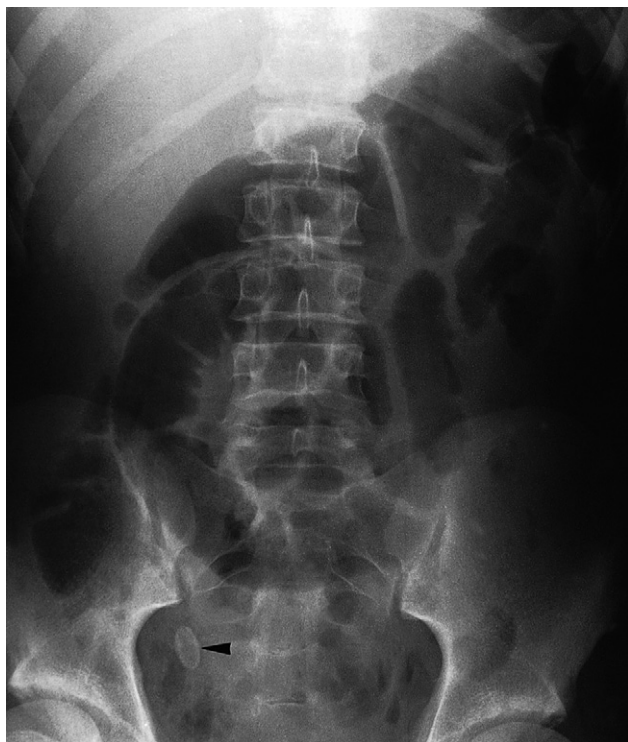


Fig. 5.18 Appendolith. The oval calcified shadow (arrowhead) is a faecolith in the appendix. The patient had perforated appendicitis. Note the dilated loops of small bowel in the centre of the abdomen due to peritonitis – the so-called sentinel loops.

Occasionally, there is a tongue-like extension of the right lobe into the right iliac fossa. This is a normal variant known as a *Reidl's lobe* and should not be confused with generalized liver enlargement.

As the spleen enlarges, the tip becomes visible in the left upper quadrant below the lower ribs. Eventually, it may fill the left side of the abdomen and even extend across the midline into the right lower quadrant. The splenic flexure of the colon and the left kidney are displaced downwards and medially, and the stomach is displaced to the right.

Abdominal and pelvic masses

Attempting to diagnose the nature of an abdominal mass on a plain film is notoriously difficult, and ultrasound, CT or magnetic resonance imaging (MRI) are the appropriate imaging modalities. The site of the mass, the displacement

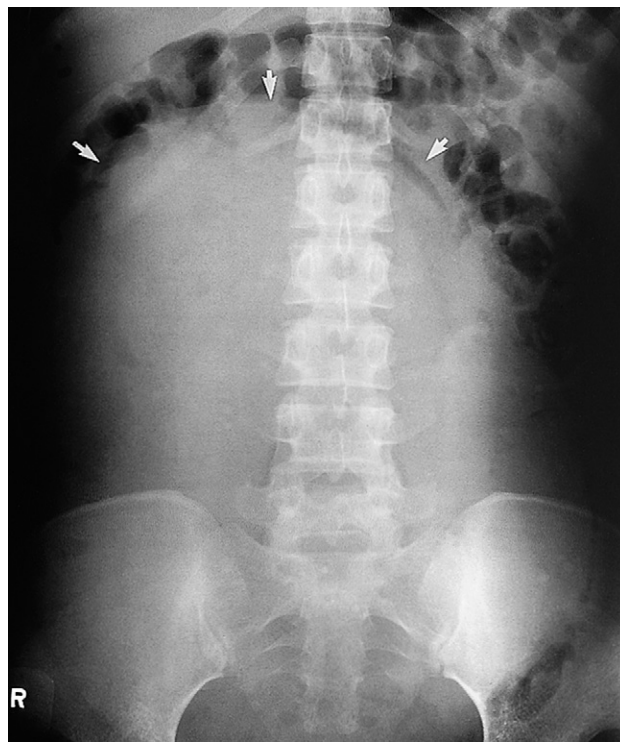


Fig. 5.19 Mass arising out of the pelvis (arrows) displacing bowel to the sides of the abdomen. The mass was a large cystadenocarcinoma of the ovary.

of adjacent structures and the presence of calcification are important diagnostic signs but plain films are unable to distinguish between solid and cystic masses.

An enlarged bladder can be seen as a mass arising from the pelvis, displacing loops of bowel. In females, uterine and ovarian enlargements also appear as masses arising from the pelvis. Ovarian cysts can become very large, almost filling the abdomen and displacing the bowel to the sides of the abdomen (Fig. 5.19). An ovarian dermoid cyst can be readily identified on a plain film due to its content of low attenuation fat and often the presence of other mesenchymal structures within it, such as teeth.

Retroperitoneal tumours and lymph nodes, when large, become visible on plain films. Renal masses, especially cysts and hydronephrosis, can become large and appear as masses in the flank. With retroperitoneal masses the outline of the psoas muscle may become invisible.

Gastrointestinal Tract

The previous chapter discussed plain films in detail, but for most intestinal disorders some form of endoscopy or imaging examination is necessary.

Endoscopy is often the first investigation because it shows mucosal lesions directly and also allows biopsy material to be obtained. Imaging is pivotal for showing processes that cannot be diagnosed or assessed endoscopically, for example to visualize the bowel beyond a stricture that cannot be traversed by an endoscope. The indications for barium examinations have dramatically reduced as endoscopy services have developed. Computed tomography (CT) techniques such as CT pneumocolon and virtual colonoscopy have now been widely taken up, and magnetic resonance imaging (MRI) is now used routinely for the local staging of rectal carcinoma and increasingly for imaging the small bowel. Fluorodeoxyglucose positron emission tomography (FDG-PET)/CT is used to identify sites of metastatic disease in selected patients with a primary carcinoma of the gastrointestinal (GI) tract.

Imaging techniques: general principles

Contrast examinations

Barium sulphate is the best contrast medium for demonstrating the GI tract on conventional radiographic studies, e.g. fluoroscopy (screening). It produces excellent opacification, good coating of the mucosa and is completely inert. Its disadvantages are that the barium may solidify and impact proximal to a colonic or rectal stricture, and it may

cause a severe inflammatory peritonitis if there is a barium leak from the bowel. In addition, patients must be reasonably mobile in order to undertake a complete barium study. A water-soluble contrast medium, such as Gastrografin, is predominantly used when perforations or anastomotic leaks are suspected (as it does not cause inflammatory peritonitis), in cases where small bowel obstruction is suspected and in specific circumstances in paediatric patients. Given rectally, it can demonstrate and confirm the site of hold up in suspected large bowel obstruction. It has several disadvantages: it is hypertonic and soon becomes diluted; it is an irritant should it inadvertently enter the lungs; and it is less radio-opaque than barium. Increasingly, CT is used as not only can it delineate the level of obstruction, but often the cause can also be illicit.

Most barium and Gastrografin examinations are carried out under fluoroscopic control so that the passage of contrast can be observed on a television monitor and the radiologist can position the patient to demonstrate and record clearly any abnormality. One of the values of fluoroscopy is to ensure that an abnormality has a constant appearance. Peristaltic waves are transitory and so can be easily distinguished from a true narrowing, which is constant.

Barium examinations of the stomach and colon (and in some cases small bowel) are usually undertaken using a double-contrast technique: the mucosa is initially coated with barium and then the lumen is distended by introducing air or some other gas, often in combination with an injection of a short-acting smooth muscle relaxant.

Computed tomography

Unlike conventional barium examinations and endoscopic procedures, CT can show the full width of the wall of the structures in question as well as the surrounding fat. Modern multidetector CT scanners with 64 detectors or more allow very rapid acquisition of high resolution images, which may be reformatted in the sagittal or coronal plane. In addition, the lumen of the gastrointestinal tract may be evaluated using either Gastrografin as the contrast agent (e.g. standard abdominal CT), air as the contrast agent (e.g. CT pneumocolon and virtual colonoscopy; see later in this chapter) or water as a negative contrast agent especially in the staging of upper GI malignancies, which enables better visibility of the bowel wall. CT is therefore useful for diagnosing and staging GI tumours, as well as for assessing the complications of treatment such as surgery and chemotherapy. It can be used in elderly or infirm patients, because a CT examination is much less demanding for the patient than either a barium enema or colonoscopy. CT can be used to diagnose appendicitis and is useful in patients with intestinal obstruction and suspected damage to the bowel wall following trauma.

Ultrasound examinations

Ultrasound can detect intra-abdominal fluid and assess the bowel wall in certain situations, but gives limited information about the bowel mucosa. Ultrasound is used for the diagnosis of infantile pyloric stenosis, intussusception and in cases of suspected appendicitis when the diagnosis is not obvious clinically (see Fig. 6.65). The use of endoscopic ultrasound is a specialized procedure that has a variety of uses, notably assessing the depth of invasion of tumours in the oesophagus, gastric or rectal wall and diagnosing small tumours in the pancreas and wall of the duodenum.

Magnetic resonance imaging

Magnetic resonance imaging of the GI tract can be limited, due to artefacts caused by peristalsis of the bowel. It is routinely used for assessing the local spread of rectal carcinoma prior to surgical resection, and for assessing perianal fistula and abscess formation (see Fig. 6.43). It is also developing an increasing role in the imaging of the small

bowel using newly developed fast magnetic resonance sequences and specific oral contrast media. The role in the assessment of oesophageal cancer is currently under development

Nuclear medicine

Nuclear medicine studies are used for assessing bowel transit, particularly gastric emptying. Labelled white cells can detect sites of inflammatory bowel disease and sepsis and certain radiopharmaceuticals can localize neuroendocrine tumours in the GI tract. FDG-PET/CT is used to demonstrate metastases in patients with a malignancy of the gastrointestinal tract (see Fig. 6.11).

Basic descriptive terms

A number of basic terms are used to describe the appearances on imaging studies of the gastrointestinal tract.

- *Mucosal pattern.* The normal mucosa of the stomach and small bowel is thrown into folds, which are exaggerated by peristaltic contractions, whereas the mucosa of the distended colon and rectum is smooth. Diseased mucosa may be abnormally smooth or abnormally irregular.
- *Ulceration.* An ulcer is a breach of a mucosal surface that becomes visible when the crater contains barium (Fig. 6.1).
- *Filling defect* is a term used to describe any process that prevents the normal filling of the lumen. There are three types of filling defects: (i) intraluminal filling defects (e.g. food), which are surrounded by barium (Fig. 6.2a); (ii)

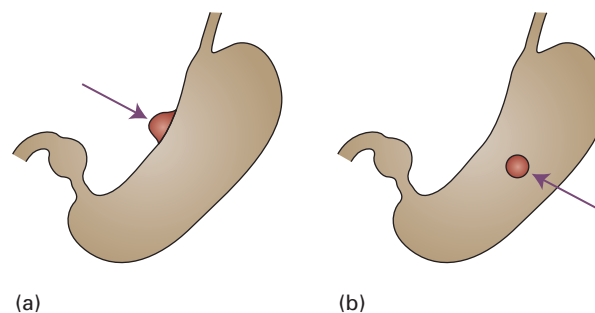


Fig. 6.1 Ulceration. (a) In profile the ulcer is seen as an outward projection (arrow). (b) *En face* the ulcer appears rounded (arrow).

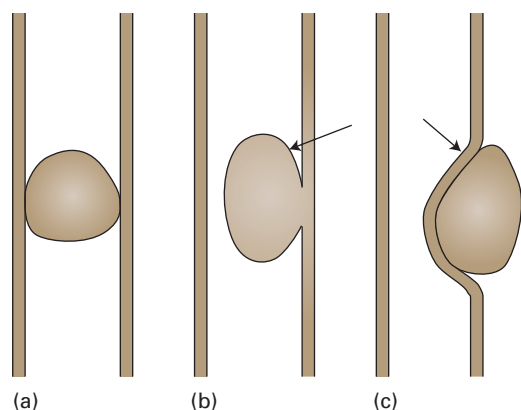


Fig. 6.2 Filling defects in the bowel. (a) Intraluminal. (b) Intramural; note the sharp angle (arrow) made with the wall. (c) Extramural; there is a shallow angle (arrow) with the wall of the bowel.

intramural filling defects (e.g. a carcinoma or leiomyoma), which cause an indentation on the lumen and are not completely surrounded by barium (Fig. 6.2b); and (iii) extramural filling defects compressing the lumen from the outside (e.g. enlarged pancreas or lymph nodes), in which the mucosa is preserved but is stretched over the filling defect (Fig. 6.2c).

- A *stricture* is a circumferential narrowing. A stricture must be differentiated from the transient narrowing which occurs with normal peristalsis. A stricture may have tapering ends (Fig. 6.3a) or it may end abruptly and have overhanging edges giving an appearance known as 'shouldering' (Fig. 6.3b). Shouldering is an important radiological sign of malignancy.

OESOPHAGUS

Imaging techniques

Plain films

Plain films do not normally show the oesophagus unless it is very dilated (e.g. achalasia), but they are of use in demonstrating an opaque foreign body such as a bone lodged in the oesophagus (Fig. 6.4a). Plain films are also used to check the position of a nasogastric tube, to ensure that the

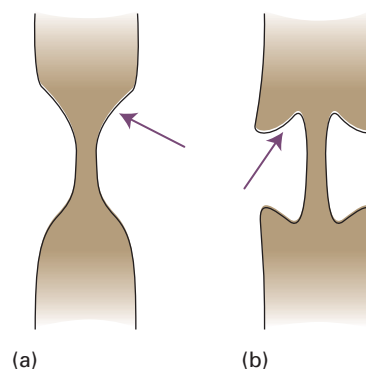


Fig. 6.3 Stricture. (a) Tapering ends (arrow). (b) Overhanging edges or shouldering (arrow).

tube travels down through the oesophagus and into the stomach, rather than down into one of the main bronchi or an oesophageal pouch (Fig. 6.4b, c).

The barium swallow is the standard contrast examination employed to visualize the oesophagus. The use of CT and endoscopic ultrasound is limited to the assessment of oesophageal carcinoma.

Barium swallow examination

The patient swallows a gas-producing agent to distend the oesophagus, followed by barium, and its passage down the oesophagus is observed on a television monitor. Films are taken with the oesophagus both full of barium to show the outline, and following the passage of the barium to show the mucosal pattern.

The oesophagus has a smooth outline when full of barium. When empty and contracted, barium normally lies in between the folds of mucosa, which appear as three or four long, straight, parallel lines (Fig. 6.5).

Peristaltic waves can be observed during fluoroscopy. They move smoothly along the oesophagus to propel the barium rapidly into the stomach. It is important not to confuse a contraction wave with a true narrowing: a narrowing is constant whereas a contraction wave is transitory. Sometimes the contraction waves do not occur in an orderly fashion but are pronounced and prolonged, giving the oesophagus an undulated appearance (Fig. 6.6). These so-called tertiary contractions usually occur in the elderly, and

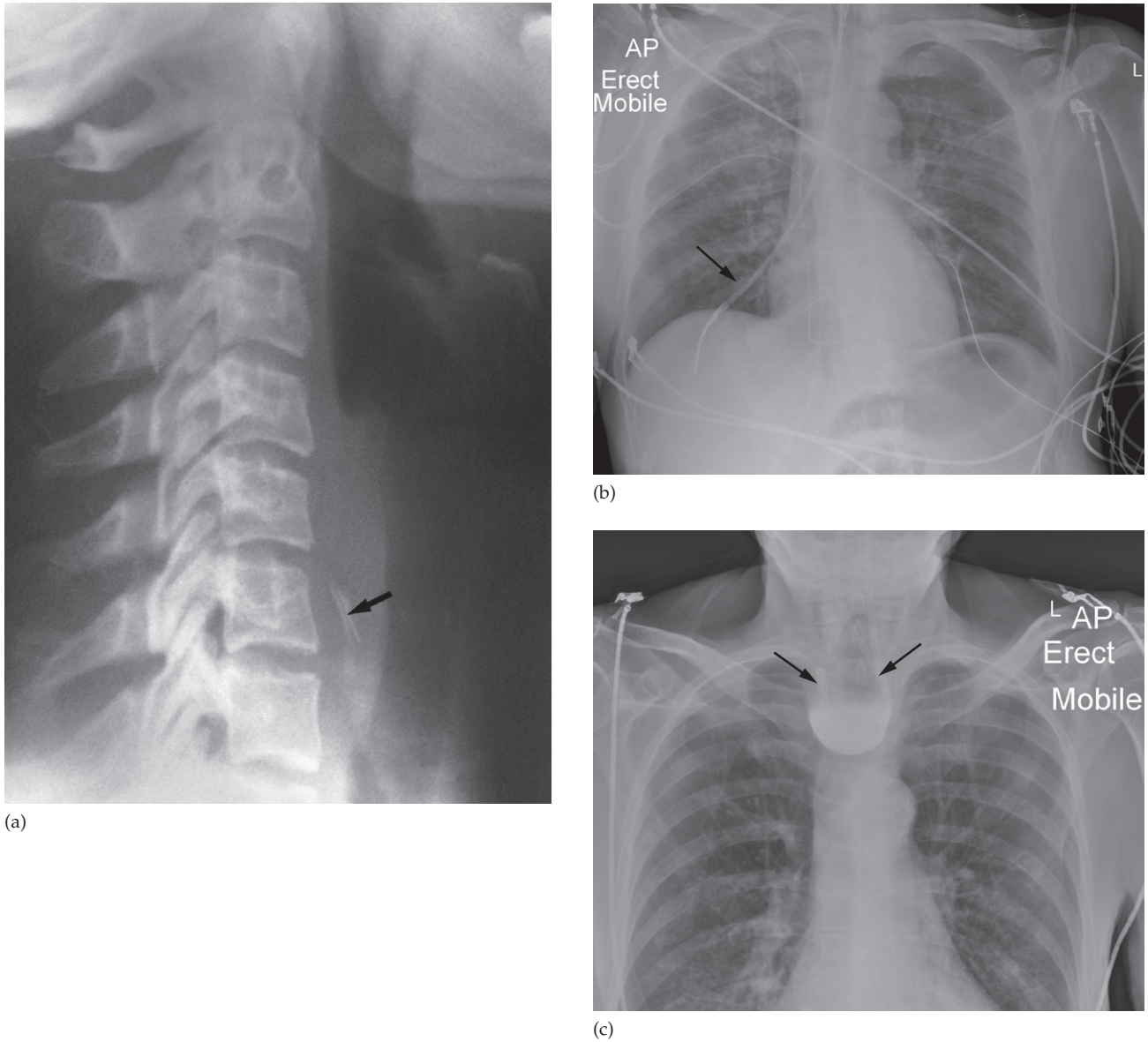


Fig. 6.4 (a) Foreign body in the oesophagus. Lateral view of the neck showing a chicken bone (arrow) lodged in the upper end of the oesophagus. (b) A nasogastric tube has been placed down the right main bronchus (arrow). (c) A nasogastric tube has coiled within an oesophageal pouch (arrows). Note that barium has been used to demonstrate the pouch.

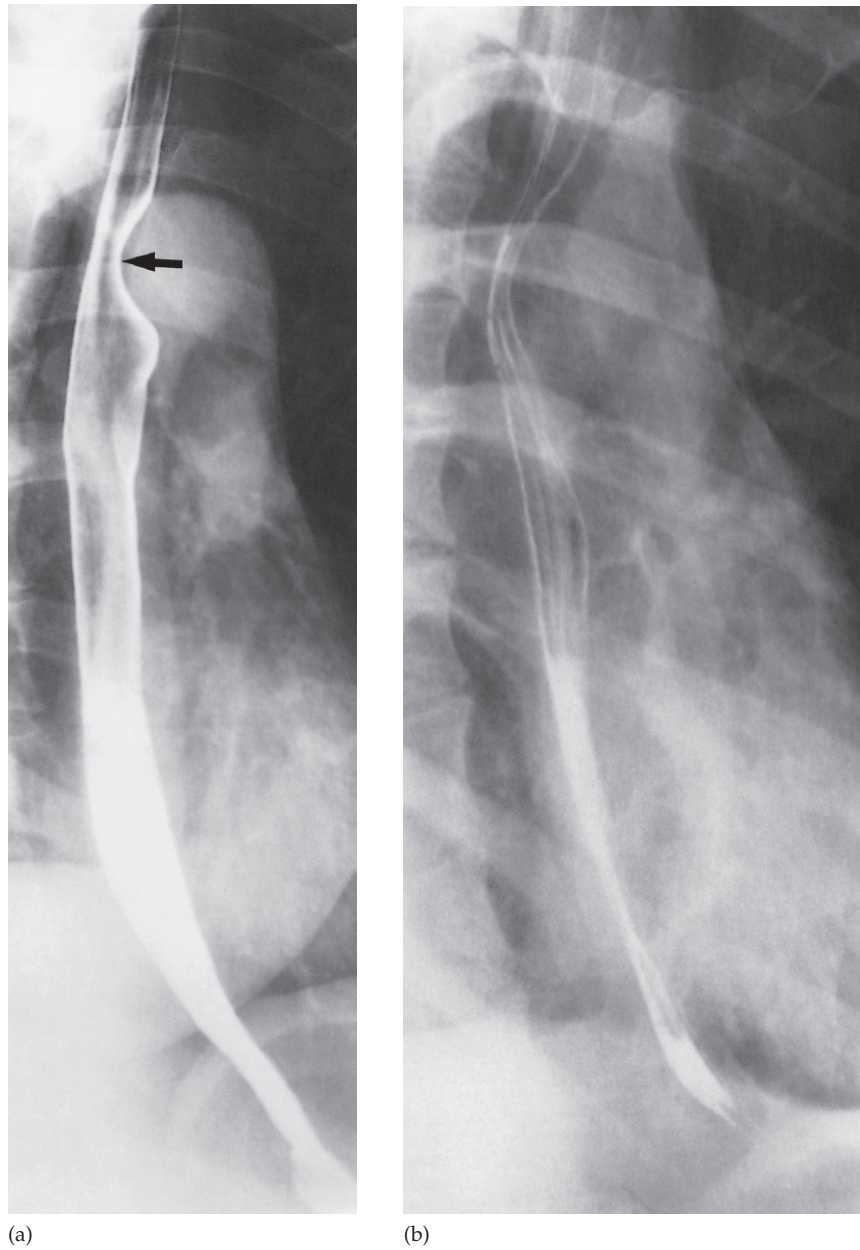


Fig. 6.5 Normal oesophagus. (a) Full of barium to show the smooth outline and indentation made by the aortic arch (arrow). (b) Film taken after the main volume of barium has passed, to show the parallel mucosal folds.

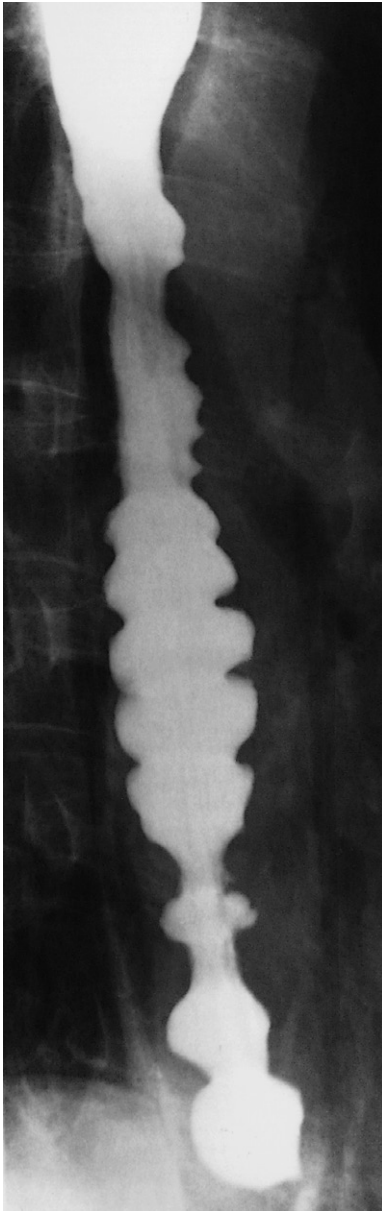


Fig. 6.6 Tertiary contractions (corkscrew esophagus) giving the oesophagus an undulated appearance.

Box 6.1 Indications for contrast studies of the oesophagus

- Swallowing disorders, including confirming or excluding a pharyngeal pouch
- Determining the length of oesophageal strictures
- Assessing possible mild gastro-oesophageal reflux. (although usually done by manometry)
- Assessing the integrity of an oesophageal anastomosis
- Following obesity reduction surgery and anti-reflux surgery
- Demonstrating an oesophagobronchial or pleural fistula

in most instances they do not give rise to symptoms. Occasionally, tertiary contractions cause dysphagia.

Endoscopy is the primary investigation in patients with dysphagia. In centres where expert endoscopy is readily available, the indications for barium or water-soluble contrast studies are shown in Box 6.1.

Computed tomography

Computed tomography is used in the staging of carcinoma of the oesophagus. The primary function of CT is to detect distant disease (e.g. lung, liver or bone metastases), and although it does give information on local staging, this is more accurately performed by endoscopic ultrasound

Fluorodeoxyglucose positron emission tomography/computed tomography

In patients with oesophageal carcinoma who have potentially curable disease, an FDG-PET/CT study (see Fig. 6.11) is performed to identify any occult metastases prior to undertaking either surgery or definitive chemoradiotherapy.

Oesophageal abnormalities

Strictures of the oesophagus

Causes of strictures of the oesophagus are shown in Box 6.2.

Oesophageal carcinoma

Oesophageal carcinoma is usually first diagnosed at upper GI endoscopy and confirmed by biopsy. Carcinomas usu-

Box 6.2 Causes of strictures or narrowing of the oesophagus

- Oesophageal cancer
- Peptic strictures
- Achalasia
- Corrosive strictures
- Benign tumours (leiomyomas)
- Other mediastinal masses
- Anomalous right subclavian artery



Fig. 6.7 Oesophageal carcinoma. There is an irregular stricture with shouldering (arrow) at the upper end.

ally involve the full circumference of the oesophagus to form a stricture, which can be readily demonstrated at barium swallow examination. It may occur anywhere in the oesophagus, shows an irregular lumen with shouldered edges and is often several centimetres in length (Fig. 6.7). A soft tissue mass may be visible.

Assessing the extent of the tumour is carried out by endoscopic ultrasound and CT examination. *Endoscopic ultrasound* (EUS) is able to demonstrate the layers of the oesophageal wall and the surrounding lymph nodes. Oesophageal cancer is seen as a hypoechoic mass and the depth of invasion of the tumour into the oesophageal wall may be assessed (Fig. 6.8). EUS is also used to assess and, if necessary, biopsy, regional lymph nodes to detect potential metastatic disease that might place the patient in a palliative rather than curative pathway. On CT the tumour is seen as a thickening of the oesophageal wall and the length of the tumour can usually be assessed (Fig. 6.9). CT may also show invasion of the mediastinum or adjacent structures, evidence of metastatic spread to lymph nodes, liver or lungs (Fig. 6.10). *FDG-PET/CT* is used to exclude the presence of occult metastatic disease in patients who are considered potentially curable (either by surgery or

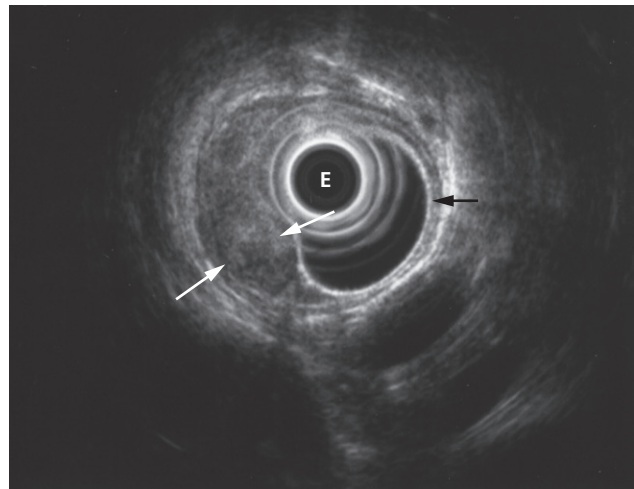


Fig. 6.8 EUS of oesophageal carcinoma. Note the thickening of the oesophageal mucosa (between the white arrows). A normal part of the oesophagus is indicated by the black arrow. E, endoscope.

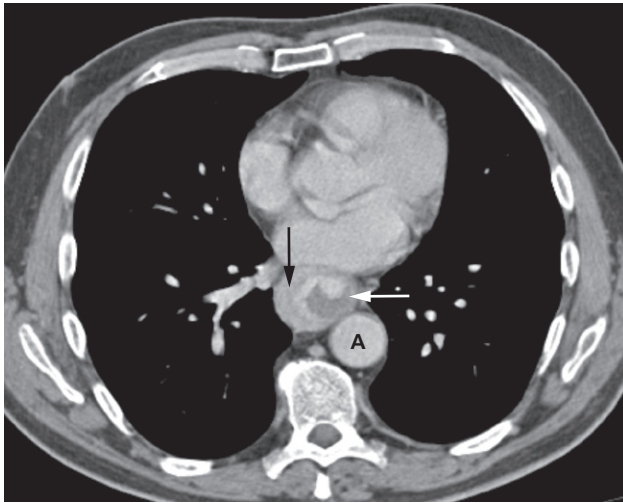


Fig. 6.9 Oesophageal cancer on CT. There is thickening and enhancement of the right lateral oesophageal wall (black arrow). In this case, the left wall of the oesophagus is relatively normal (white arrow). A, aorta.

radical chemoradiotherapy) after initial evaluation with CT and EUS (Fig. 6.11). Assessment of response to treatment and follow-up of patients with carcinoma of the oesophagus is usually done with CT and endoscopy. FDG-PET/CT is increasingly being used to assess the response of the tumour to chemotherapy or radiotherapy, allowing an early change in therapy in patients who are non-responders.

Peptic strictures

Peptic strictures can be demonstrated at barium swallow. They are found at the lower end of the oesophagus and are almost invariably associated with a hiatus hernia and gastro-oesophageal reflux and, therefore, the stricture may be some distance above the diaphragm. Peptic strictures are characteristically short and have smooth outlines with tapering ends (Fig. 6.12).

Achalasia

Achalasia is a neuromuscular abnormality resulting in failure of relaxation at the cardiac sphincter, which presents at barium swallow examination as a smooth, tapered narrowing, always at the lower end of the oesophagus (Fig.

6.13). There is associated dilatation of the oesophagus, which often shows absent peristalsis. The dilated oesophagus usually contains food residue and may be visible on the plain chest radiograph. The lungs may show consolidation and bronchiectasis from aspiration of the oesophageal contents. The stomach gas bubble is usually absent because the oesophageal contents act as a water seal, but this sign is not diagnostic of achalasia as it is seen in other causes of oesophageal obstruction and can occasionally be observed in healthy people.

Corrosive strictures

Corrosive strictures are the result of swallowing corrosives such as acids or alkalis. They are long strictures that begin at the level of the aortic arch. As with other benign strictures, they are usually smooth with tapered ends on barium swallow examinations, but may be irregular (Fig. 6.14).

Benign tumours

Leiomyomas cause a smooth, rounded indentation into the lumen of the oesophagus. A soft tissue mass may be seen in the mediastinum indicating extraluminal extension.

Other mediastinal masses

Mediastinal masses (e.g. lymphadenopathy secondary to lymphoma or lung cancer) can cause extrinsic compression and narrowing of the oesophagus.

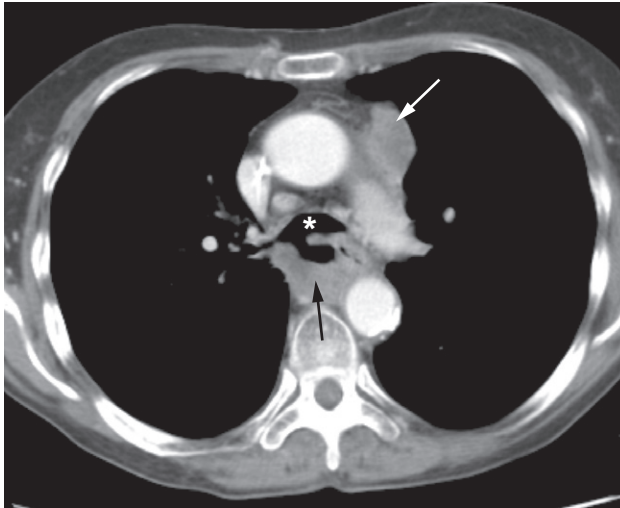
Anomalous right subclavian artery

An anomalous right subclavian artery, which, instead of coming from the innominate artery, arises as the last major branch from the aortic arch, gives rise to a characteristic short, smooth narrowing as it crosses behind the upper oesophagus (Fig. 6.15).

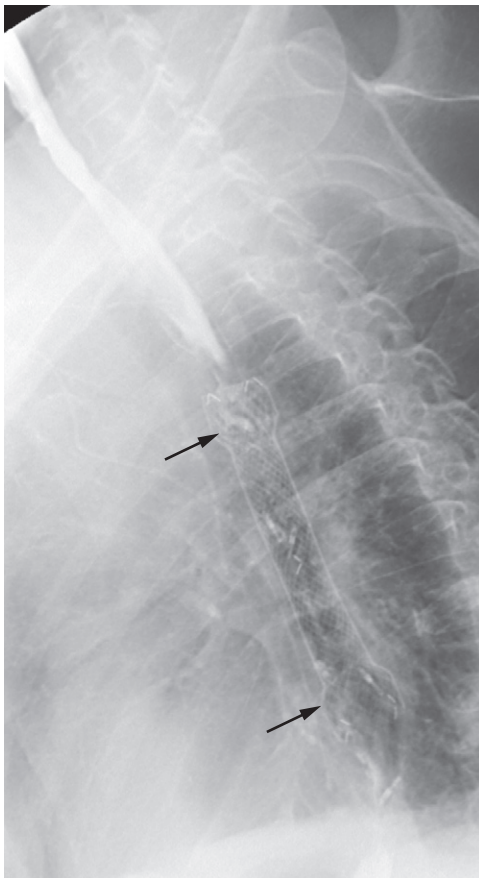
Dilatation of the oesophagus

There are two main types of oesophageal dilatation – obstructive and non-obstructive:

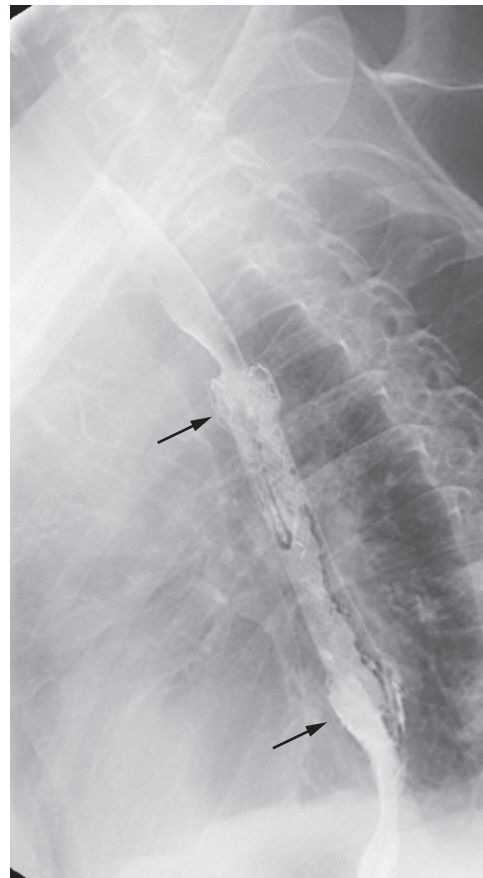
- Dilatation due to obstruction is associated with a visible stricture. The patient with a carcinoma usually presents with dysphagia before the oesophagus becomes very dilated. On the other hand, a markedly dilated oesophagus



(a)



(b)



(c)

Fig. 6.10 (a) Extensive oesophageal cancer (black arrow) has eroded into the posterior aspect of the carina (*) forming a fistula. Enlarged lymph nodes are present in the anterior mediastinum (white arrow). (b) A stent has been placed across the fistula (arrows). (c) Barium swallow confirms occlusion of the fistula, with no leakage of barium into the bronchial tree.



Fig. 6.11 FDG-PET/CT in a patient with oesophageal carcinoma. The PET component of the study demonstrates the primary tumour (T) at the lower oesophagus. In addition, there is a hot spot over the liver (long arrow).

indicates a very longstanding condition, usually achalasia or occasionally a benign stricture.

- Dilatation without obstruction occurs in scleroderma. The disease involves the oesophageal muscle, resulting in dilatation of the oesophagus, which resembles an inert tube with no peristaltic movement so that barium does not flow from the oesophagus into the stomach unless the patient stands upright.

Other abnormalities of the oesophagus

An *oesophageal web* is a thin, shelf-like projection arising from the anterior wall of the cervical portion of the oesophagus

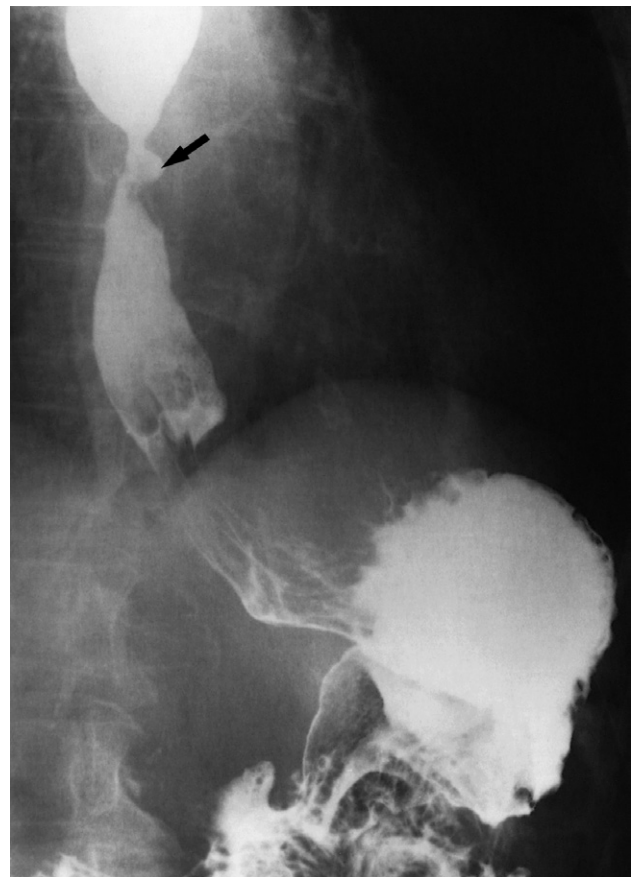


Fig. 6.12 Peptic stricture due to gastro-oesophageal reflux in a patient with a hiatus hernia. There is a short smooth stricture at the oesophagogastric junction with an ulcer crater within the stricture (arrow).

and can only be seen when the oesophagus is full of barium (Fig. 6.16). A web may be an isolated finding, but the combination of a web, dysphagia and iron deficiency anaemia is known as Plummer–Vinson syndrome.

Oesophageal diverticula are saccular outpouchings, which are often seen as chance findings, in the intrathoracic portion of the oesophagus. One type of diverticulum, the pharyngeal pouch or Zenker's diverticulum (Fig. 6.17) is important as it may give rise to symptoms caused by retention of food and pressure upon the oesophagus. A pharyngeal pouch arises through a congenital weakness in the inferior constrictor muscle of the pharynx and comes to lie

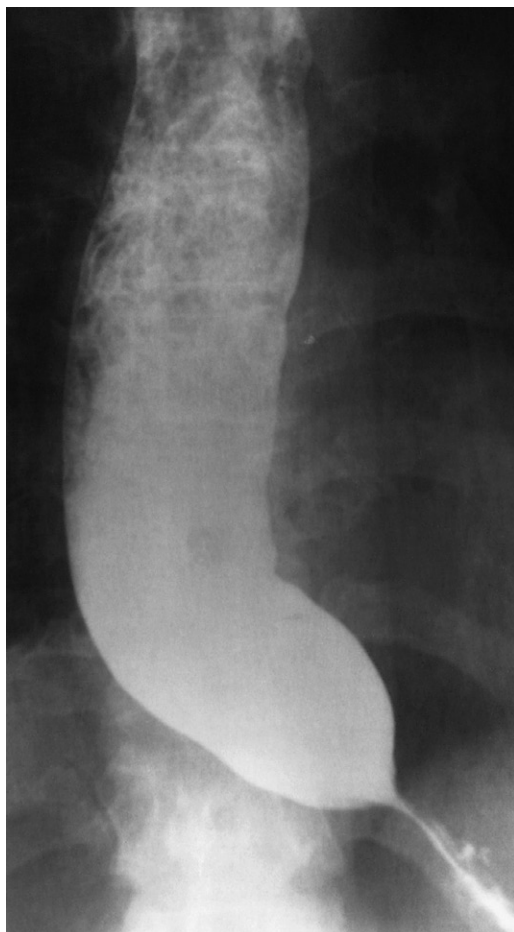


Fig. 6.13 Achalasia. The very dilated oesophagus containing food residues shows a smooth narrowing at its lower end.

behind the oesophagus near the midline. It may reach a very large size and can cause displacement and compression of the oesophagus.

In *oesophageal atresia*, the oesophagus ends as a blind pouch in the upper mediastinum. Several different types exist (Fig. 6.18), but the most frequent is for the upper part of the oesophagus to be a blind sac with a fistula between the lower segment of the oesophagus and the tracheobronchial tree. A plain abdominal film will show air in the bowel if a fistula is present between the tracheobronchial tree and the oesophagus distal to the atretic segment.



Fig. 6.14 Corrosive stricture.

The diagnosis of oesophageal atresia is made by passing a soft tube into the oesophagus and showing that the tube holds up or coils in the blind-ending pouch. The use of contrast agents is potentially dangerous because the contrast may cause respiratory problems if it spills over into the trachea.

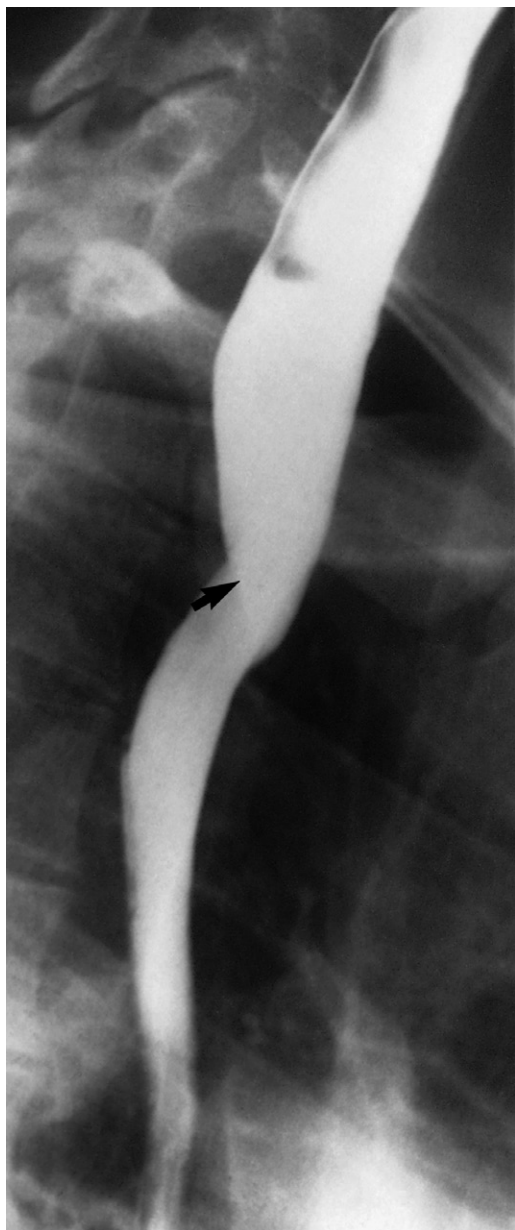


Fig. 6.15 Anomalous right subclavian artery. There is a localized indentation caused by the anomalous artery as it passes behind the oesophagus (arrow).



Fig. 6.16 Oesophageal web. There is a shelf-like indentation (arrow) from the anterior wall of the upper oesophagus.

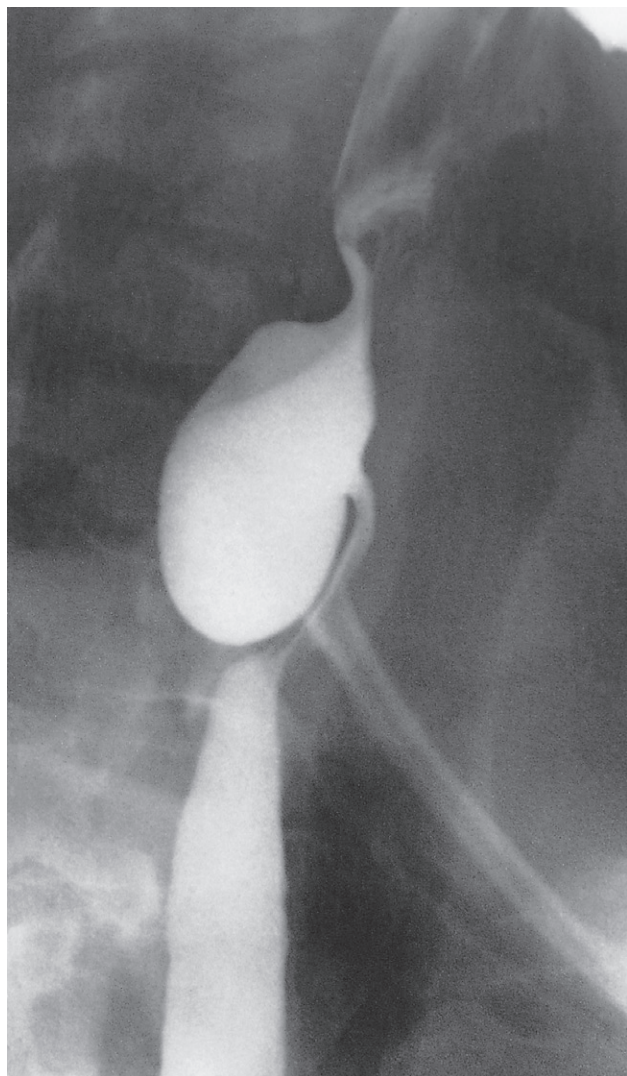


Fig. 6.17 Pharyngeal pouch (Zenker's diverticulum). The pouch lies behind the oesophagus, which is displaced forward.

STOMACH AND DUODENUM

Imaging techniques

Barium meal examination

Barium meal examination is now rarely performed as it has been superseded by endoscopy. The usual technique

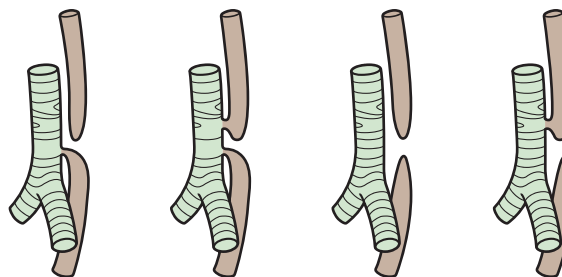


Fig. 6.18 Diagram of the various types of oesophageal atresia. The first two types also have an oesophagotracheal fistula distal to the atretic segment and will show air in the stomach.

involves instructing the patient to fast for at least 6 hours prior to the examination. The stomach is distended with a gas-producing agent, and an intravenous injection of a short-acting smooth muscle relaxant is often given. The patient drinks about 200 mL of barium. Films are taken in various positions with the patient both erect and lying flat, so that each part of the stomach and duodenum is shown distended by barium and also distended with air but coated with barium to show the mucosal pattern (Fig. 6.19). The duodenal cap or bulb arises just beyond the short pyloric canal, and the duodenum forms a loop around the head of the pancreas to reach the duodenojejunal flexure. Diverticula arising beyond the first part of duodenum are a common finding and are usually without clinical significance (Fig. 6.20).

Although contrast studies are now less useful in the diagnosis of mucosal abnormalities, they still have an important role in functional studies of the upper GI tract or to evaluate any potential anastomotic leak (Box 6.3). For this reason it is usually water-soluble contrast agents that are used, which are more rapidly resorbed than barium and importantly will allow timely subsequent imaging with CT. A patient who has undergone an upper GI study with barium will probably have to wait for at least 2 weeks for the barium to clear from the bowel before proceeding to CT, in order to avoid artifact.

Computed tomography

Accurate assessment of the stomach on CT requires good patient preparation and fastidious technique. Firstly, the



Fig. 6.19 Normal stomach and duodenum on double-contrast barium meal. On this supine view, barium collects in the fundus of the stomach. The body and the antrum of the stomach together with the duodenal cap and loop are coated with barium and distended with gas. Note how the fourth part of the duodenum and duodenojejunal flexure are superimposed on the body of the stomach.

Box 6.3 Indications for contrast studies of the stomach and duodenum

- Failed gastroscopy
- Assessment of duodenal strictures that cannot be characterized or navigated on endoscopy
- Assessment of functional patency/gastric emptying following gastroenterostomy or anti-obesity surgery
- To confirm or rule out anastomotic leak following gastric surgery (a water-soluble contrast agent)

patient must not eat for 6 hours prior to the CT to ensure that no food residues remain in the stomach, which could obscure or mimic disease. The patient is usually given about 100mL of tap water to drink (acting as a negative contrast) as well as a smooth muscle relaxant, in order to

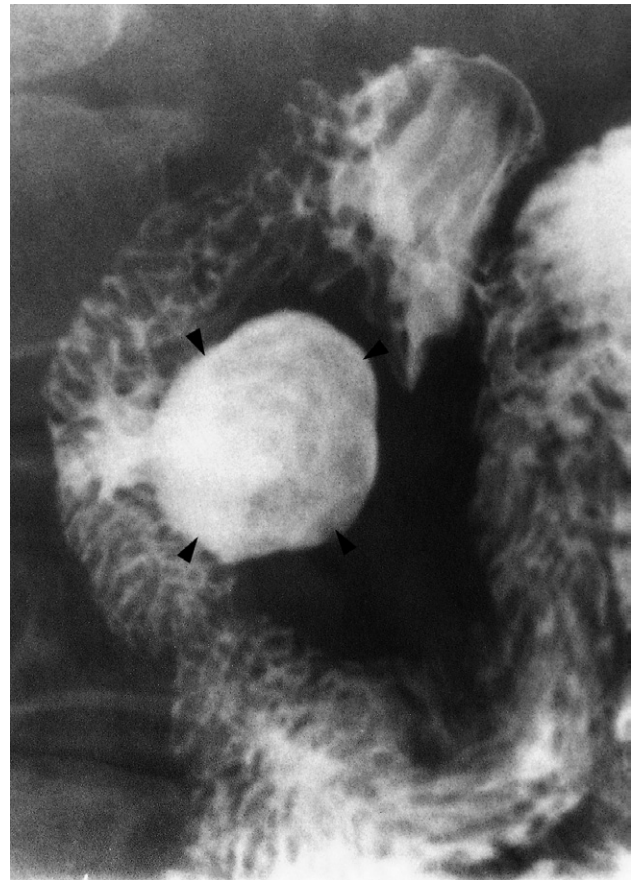


Fig. 6.20 Duodenal diverticulum arising from the second part of the duodenum (arrowheads).

distend the stomach and duodenum (Fig. 6.21). If the stomach is not distended during the scan, any thickening of the gastric wall could be misinterpreted as being a mass. During the scan, intravenous iodinated contrast medium is injected to demonstrate enhancement of both the normal structures as well as to distinguish the enhancement characteristics of any abnormality.

Upper GI endoscopy is widely used as the initial investigation in patients with possible disease of the stomach and duodenum. It enables the mucosa of the stomach and duodenum to be directly inspected and biopsied. The main indications for its use are summarized in Box 6.4.

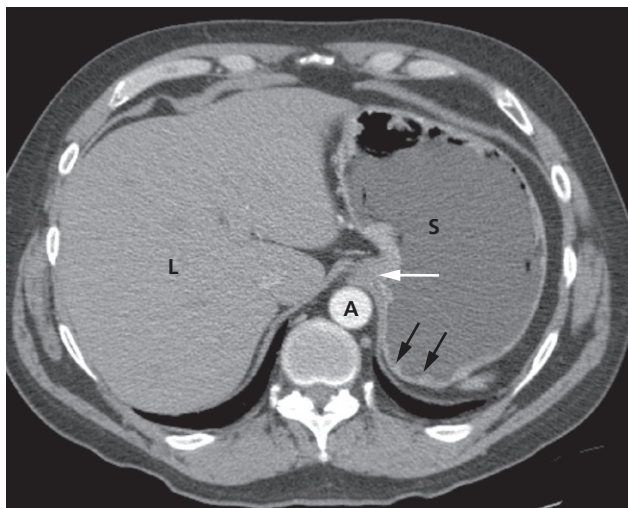


Fig. 6.21 CT of a normal stomach. The stomach has been distended by oral water contrast and the use of an intravenous smooth muscle relaxant. Some normal rugal folds are still visible (black arrows). Note the gastro-oesophageal junction (white arrow). A, aorta L, liver; S, stomach.

Box 6.4 Indications for upper gastrointestinal (GI) endoscopy

Diagnosis and follow-up

- Peptic ulcer disease
- Haematemesis and melaena
- Dyspepsia and dysphagia
- Barrett's oesophagus

Biopsies

- Coeliac disease
- Confirmation and follow-up of malignant tumours

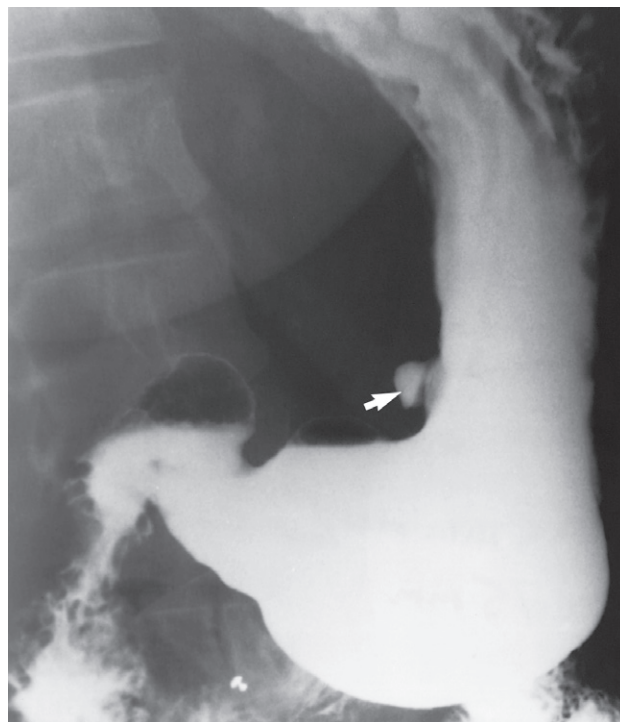
Therapeutic

- Injection/clipping/banding to stop bleeding from ulcers or oesophageal varices
- Removal of ingested foreign bodies
- Stenting of upper GI strictures
- Feeding tube placement

Specific diseases of the stomach and duodenum

Peptic ulcer

Gastric ulcers may be benign (Fig. 6.22) or malignant so confirmation at gastroscopy is routinely undertaken,



(a)



(b)

Fig. 6.22 Benign ulcer. (a) In profile, the ulcer (arrow) projects from the lesser curve of the stomach. (b) *En face* the ulcer (arrow) is seen as a rounded collection of barium.



Fig. 6.23 Gastric carcinoma on barium study. There are a number of large filling defects in the antrum and body of the stomach.

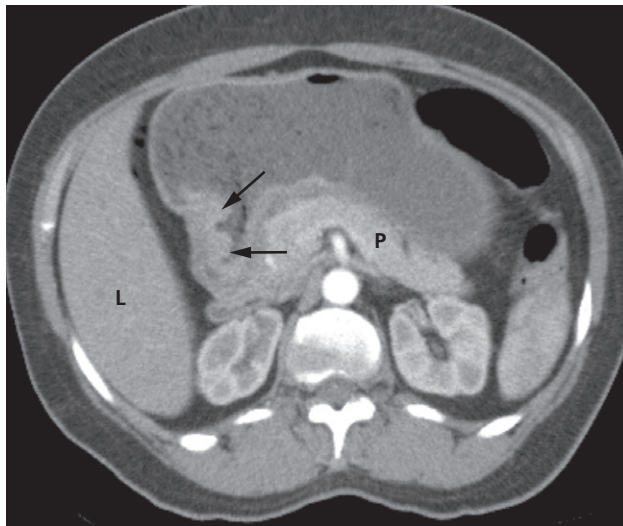
whereas duodenal ulcers are almost invariably benign. Ulcers are identified as projections of barium beyond the mucosal profile. With duodenal ulceration, the duodenal cap (bulb) may be very deformed by scarring.

Gastric carcinoma

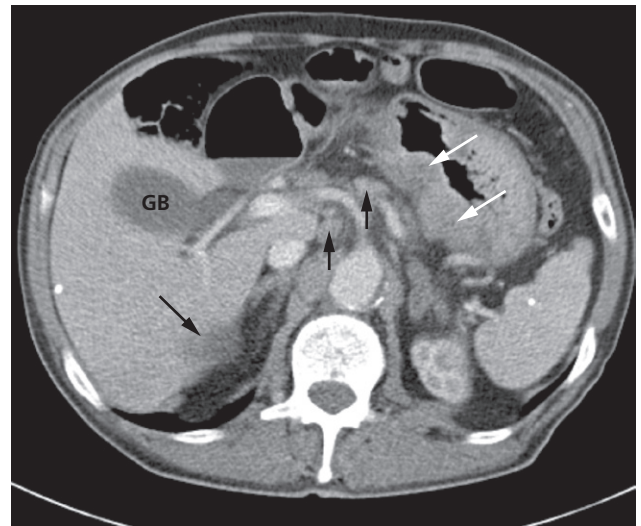
Emphasis is placed on the diagnosis of early gastric cancer, which is confined to the mucosa, as early treatment has a much better prognosis. In the past, high quality barium meal examination has been used as a screening tool in some countries to detect early gastric carcinoma. However, gastroscopy has now almost completely taken over this role.

At barium examination, gastric carcinoma typically produces an irregular filling defect with alteration of the normal mucosal pattern (Fig. 6.23).

Computed tomography is the main imaging modality for the preoperative staging of patients with gastric cancer as it can show the extent of the primary tumour but also any distant disease (Fig. 6.24). EUS may be used in some cases for local staging and patients will undergo staging lapor-



(a)



(b)

Fig. 6.24 Gastric carcinoma on CT. (a) A focal ulcer is seen arising in the antrum (arrows). (b) In a different patient, there is diffuse thickening of the wall of the stomach (white arrows). Several lymph nodes (short black arrows) and a liver metastasis (long black arrow) are also seen. GB, gall bladder; L, liver; P, pancreas.

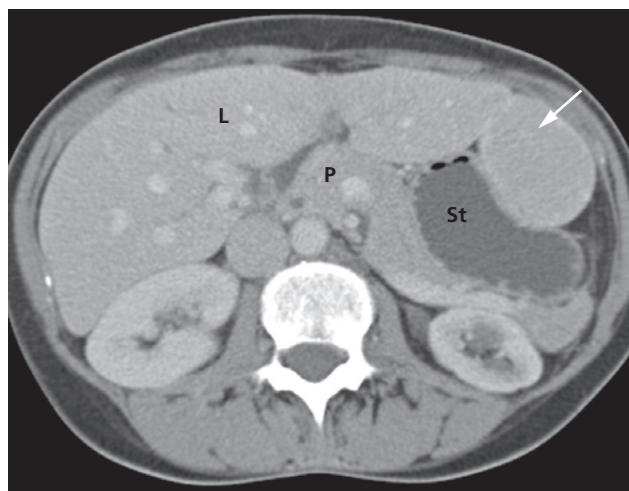


Fig. 6.25 Gastrointestinal stromal tumour on CT. There is a smooth ovoid mass arising from the anterior wall of the stomach (arrow). This causes an indentation of the stomach. L, liver; P, pancreas; St, stomach.

oscopy prior to curative surgery. FDG-PET/CT does not have a clear role in the primary staging of gastric cancer due to the normal uptake of FDG by the gastric mucosa.

Other gastric tumours

Gastrointestinal stromal tumours (GISTs) arise from the wall of the stomach resulting in a smooth, round, submucosal filling defect, which may ulcerate as the tumour enlarges (Fig. 6.25). GISTs are a group of tumours that are usually benign and well differentiated; they may occur anywhere in the GI tract but 60–70% occur in the stomach.

A *leiomyoma* is a submucosal tumour which, as well as projecting into the lumen of the stomach, may have a large extraluminal extension that can be easily recognized at CT.

Neuroendocrine tumours of the stomach and duodenum include gastric carcinoid tumours and gastrinomas. Gastrointestinal carcinoid tumours can be found anywhere in the GI tract, particularly the appendix, but can be found incidentally in the stomach often as multiple small (<1 cm) tumours on a background of pernicious anaemia/chronic atrophic gastritis. Occasionally they are seen in association



Fig. 6.26 Duodenal gastrinoma. The duodenum has been distended using a smooth muscle relaxant and oral water. The tiny gastrinoma is seen as a brightly enhancing lesion in the wall of the duodenum (arrow), on the arterial phase of enhancement. A, aorta; D, duodenal lumen; K, kidney.

with MEN (multiple endocrine neoplasia) type 1 in association with other endocrine tumours, or as a solitary larger tumour (>3 cm) where they can cause local symptoms of abdominal pain and bleeding as well as the carcinoid syndrome. Gastrinomas usually secrete gastrin, resulting in increased gastric acidity and peptic ulceration. Gastrinomas are often very small and typically enhance brightly in the arterial phase (Fig. 6.26).

Gastric polyps

Gastric polyps may be single or multiple. They may be sessile or have a stalk. Even with high quality radiographs it is often impossible to distinguish benign from malignant polyps. For this reason, gastroscopy with biopsy or operative removal is invariably carried out on all suspected polyps. Other *intraluminal defects* within the stomach include food or blood following a haematemesis. Sometimes ingested fibrous material, such as hair, may intertwine forming a ball or bezoar (Fig. 6.27).

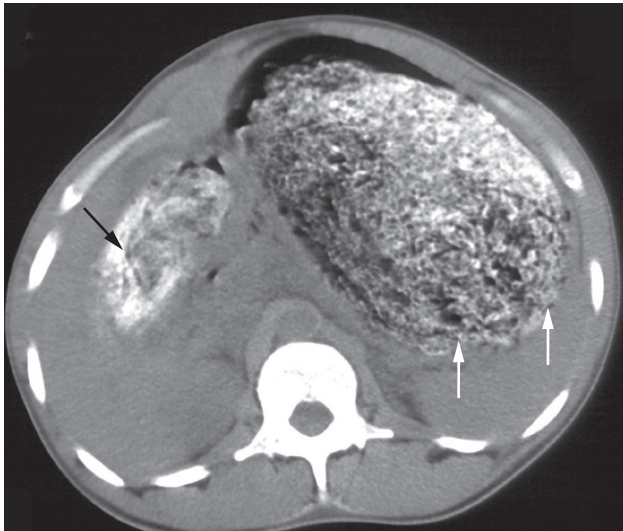


Fig. 6.27 CT of a bezoar. The stomach is distended by a large mass of hair mixed with oral contrast (white arrows). The antrum is also distended by the ingested material (black arrow).

Lymphoma

The stomach is the most frequent site of lymphoma involving the GI tract, either as primary disease or by infiltration from adjacent nodes. The appearance of primary gastric lymphoma is typically of an extensive area of diffuse thickening of the gastric wall (Fig. 6.28). There may be extensive, bulky lymphadenopathy adjacent to the tumour. The appearance may mimic gastric carcinoma.

Gastric outlet obstruction

In most patients, contrast leaves the stomach within a few minutes of the smooth muscle relaxant wearing off, but in others this only occurs after the patient has been lying on the right side for some time. Prolonged delay in a patient with a dilated stomach containing food residues needs to be explained. In adults, the causes of gastric outlet obstruction are listed in Box 6.5.

In infants, pyloric stenosis is by far the commonest cause of gastric outlet obstruction. Often, the diagnosis is made clinically and can be confirmed with ultrasound, which has superseded barium meal. Ultrasound shows a thickened, elongated pyloric canal (Fig. 6.29).

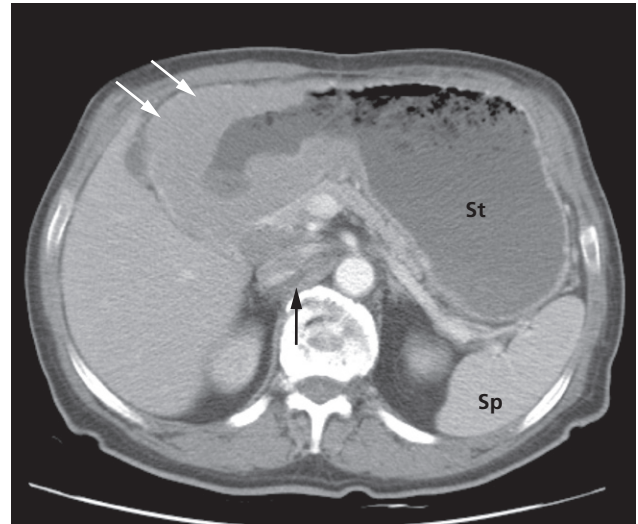


Fig. 6.28 Gastric lymphoma in the antrum, demonstrated on CT (white arrows). Lymphadenopathy surrounds the inferior vena cava (black arrow). St, stomach; Sp, spleen.

Box 6.5 Causes of gastric outlet obstruction

- Chronic duodenal ulceration: the diagnosis depends on demonstrating a very deformed, stenosed duodenal cap. It may or may not be possible to identify an actual ulcer crater
- Carcinoma of the antrum
- Duodenal, ampullary and pancreatic carcinoma
- Acute or chronic pancreatitis, including pseudocyst formation
- Poor functional patency of a gastroenterostomy
- Pyloric stenosis in infants

Hiatus hernia

A hiatus hernia is a herniation of the stomach into the mediastinum through the oesophageal hiatus in the diaphragm. It is a common finding. Two main types of hiatus hernia exist: sliding and rolling. An alternative name for a rolling hernia is 'para-oesophageal' (Fig. 6.30).

The commoner type is the sliding hiatus hernia, where the gastro-oesophageal junction and a portion of the stomach are situated above the diaphragm (Fig. 6.31). The cardiac sphincter is usually incompetent, so reflux from the stomach to the oesophagus occurs readily and this may

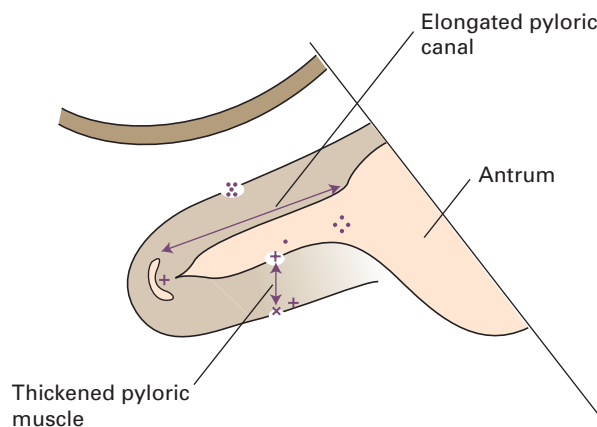
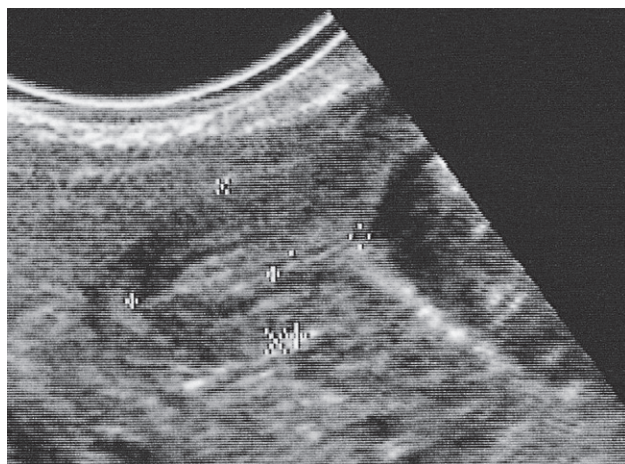
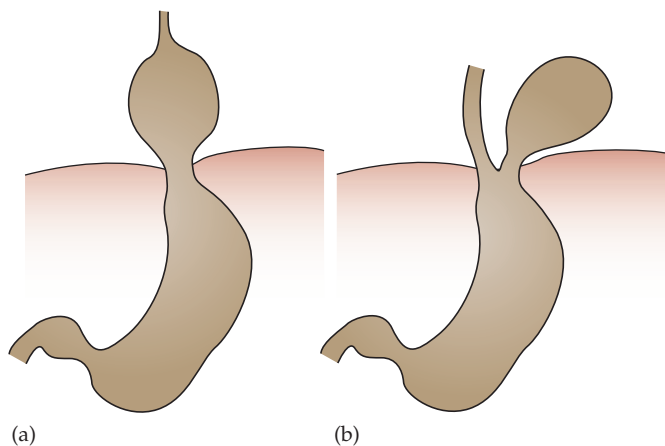


Fig. 6.29 Pyloric stenosis. Ultrasound scan in a neonate showing a thickened, elongated pyloric canal.

Fig. 6.30 Hiatus hernia. (a) Sliding: a portion of the stomach and the gastro-oesophageal junction are situated above the diaphragm. (b) Rolling or para-oesophageal: the gastro-oesophageal junction is below the diaphragm.



cause oesophagitis, ulceration or peptic stricture. A small sliding hernia may be demonstrated in most people during a barium meal examination, provided that enough manoeuvres have been undertaken to increase intra-abdominal pressure. It is, therefore, difficult to assess the significance of a small hernia with little or no reflux.

In a rolling or para-oesophageal hernia, the fundus of the stomach herniates through the diaphragm, but the oesophagogastric junction often remains competent below the diaphragm.

A large hernia, particularly one of the para-oesophageal type, may not be reduced when the patient is in the erect position. In these instances the hiatus hernia will be seen on chest films and on CT (Fig. 6.32).

SMALL INTESTINE

The small bowel remains one of the most difficult organs to evaluate. Unlike the stomach and duodenum, fiberoptic

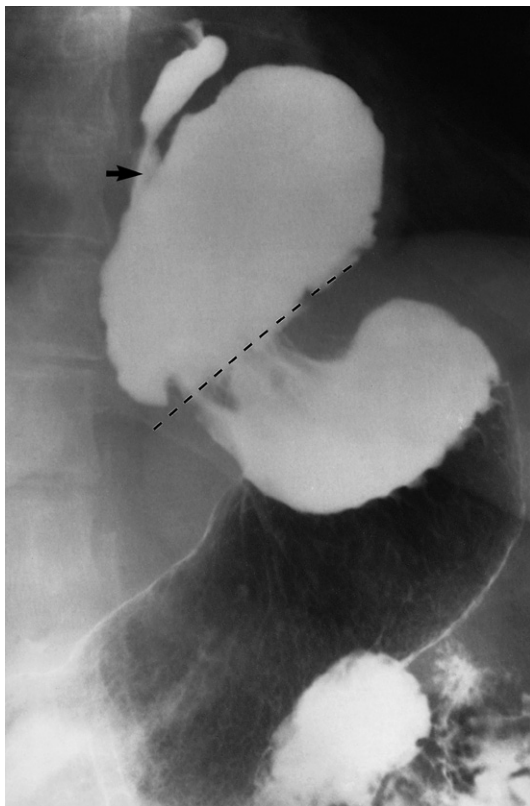
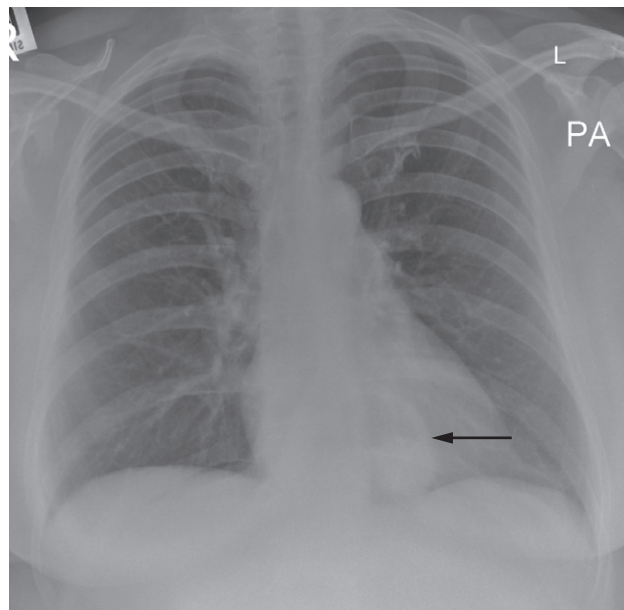
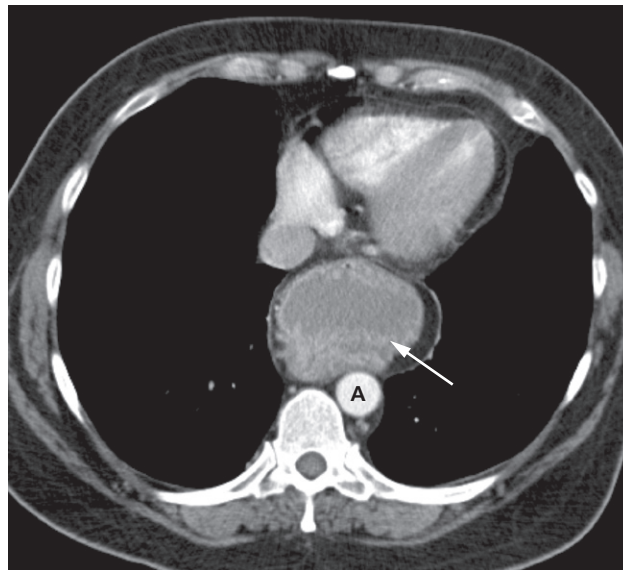


Fig. 6.31 Sliding hiatus hernia. The fundus of the stomach and the gastro-oesophageal junction (arrow) have herniated through the oesophageal hiatus and lie above the diaphragm (dotted line).

endoscopy is difficult to perform due to the long and tortuous nature of the small intestine. Imaging studies (contrast studies, CT, MRI) therefore play a pivotal role in the evaluation of the small bowel. Capsule endoscopy, which requires the patient to ingest a tiny capsule containing a camera, may be helpful in some cases (Fig. 6.33). The capsule is ultimately passed with the faeces and may provide information concerning luminal or mural abnormalities of the small bowel. Small bowel endoscopy (enteroscopy) is becoming increasingly available but is still only used in very specific circumstances.



(a)



(b)

Fig. 6.32 Hiatus hernia. (a) Chest x-ray demonstrating a rounded mass (arrow) with an air-fluid level projected behind the heart shadow. (b) CT in the same patient demonstrating the fundus of the stomach extending up into the posterior mediastinum (arrow). A, aorta.

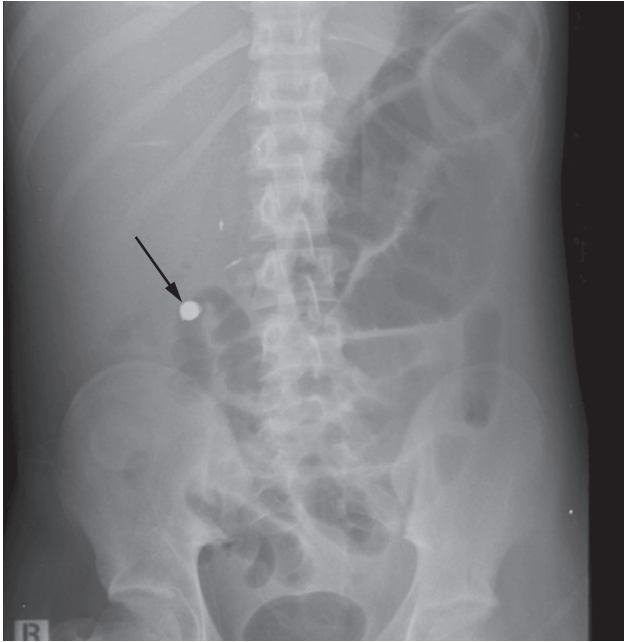


Fig. 6.33 A capsule endoscope within a loop of small bowel (arrow). A nasogastric tube is also present, projected over the left upper quadrant.

Imaging techniques

Standard imaging techniques and their indications are:

- *Small bowel follow-through (small bowel meal)* (Fig. 6.34). The patient drinks about 200–300 mL of barium and its passage through the small intestine is observed by taking films at regular intervals until the barium reaches the colon. This can be a time-consuming procedure and usually takes 2–3 hours, but the transit time is very variable. The indications for a barium examination of the small bowel are listed in Box 6.6.
- *Enteroclysis (small bowel enema)* (Fig. 6.35) distends the bowel and gives excellent mucosal detail, and is an alternative to a small bowel follow-through. The disadvantage is that it requires intubation with a nasoduodenal tube, which is passed to the duodenojejunal flexure, usually resulting in an increased radiation dose. Barium is injected through the tube followed by water or methyl cellulose to propel the barium through the small bowel, allowing distension of bowel and a double-contrast effect.

- *Computed tomography* has a role in the assessment of small bowel disease as it can show thickening of the bowel wall, an important sign of inflammatory bowel disease and lymphoma, and occasionally mucosal irregularity and small bowel neoplasms. The patient fasts for 4–6 hours prior to the procedure and then may be given oral Gastrografin or water to delineate the small bowel. In some cases, an intravenous bowel relaxant is injected. CT enteroclysis may also be performed with contrast being infused into the small bowel via a nasoduodenal tube, followed by CT. Intravenous iodinated contrast medium is injected to demonstrate vessels and enhancing structures.
- *Ultrasound* has a developing role in the investigation of small bowel pathology. In some cases, it can demonstrate small bowel thickening and free fluid associated with inflammatory conditions, and can demonstrate a thickened appendix suggestive of appendicitis and occasionally the presence of an intussusception.
- *Magnetic resonance imaging* for assessment of the small bowel is becoming increasingly utilized. Fast breath-hold sequences and smooth muscle relaxants are used to reduce movement artefacts and improve the clarity of the image.
- *Nuclear medicine techniques*, using meta-iodobenzylguanidine (MIBG) or octreotide, may be used in cases of suspected neuroendocrine or carcinoid tumours. Technetium-99m (^{99m}Tc) may be used to detect Meckel's diverticulum.

Normal appearances of the small bowel

The normal small intestine (see Fig. 6.34) occupies the central and lower abdomen, usually framed by the colon. The terminal portion of the ileum enters the medial aspect of the caecum through the ileocaecal valve. As the terminal ileum may be the first site of disease, this region is often fluoroscoped and observed on a television monitor so that peristalsis can be seen and films can be taken with the terminal ileum unobscured by other loops of small intestine.

The barium forms a continuous column defining the diameter of the small bowel, which is normally not more than 25 mm unless enteroclysis has been performed. Transverse folds of mucous membrane project into the lumen of the bowel and barium lies between these folds, which appear as lucent filling defects of about 2–3 mm in

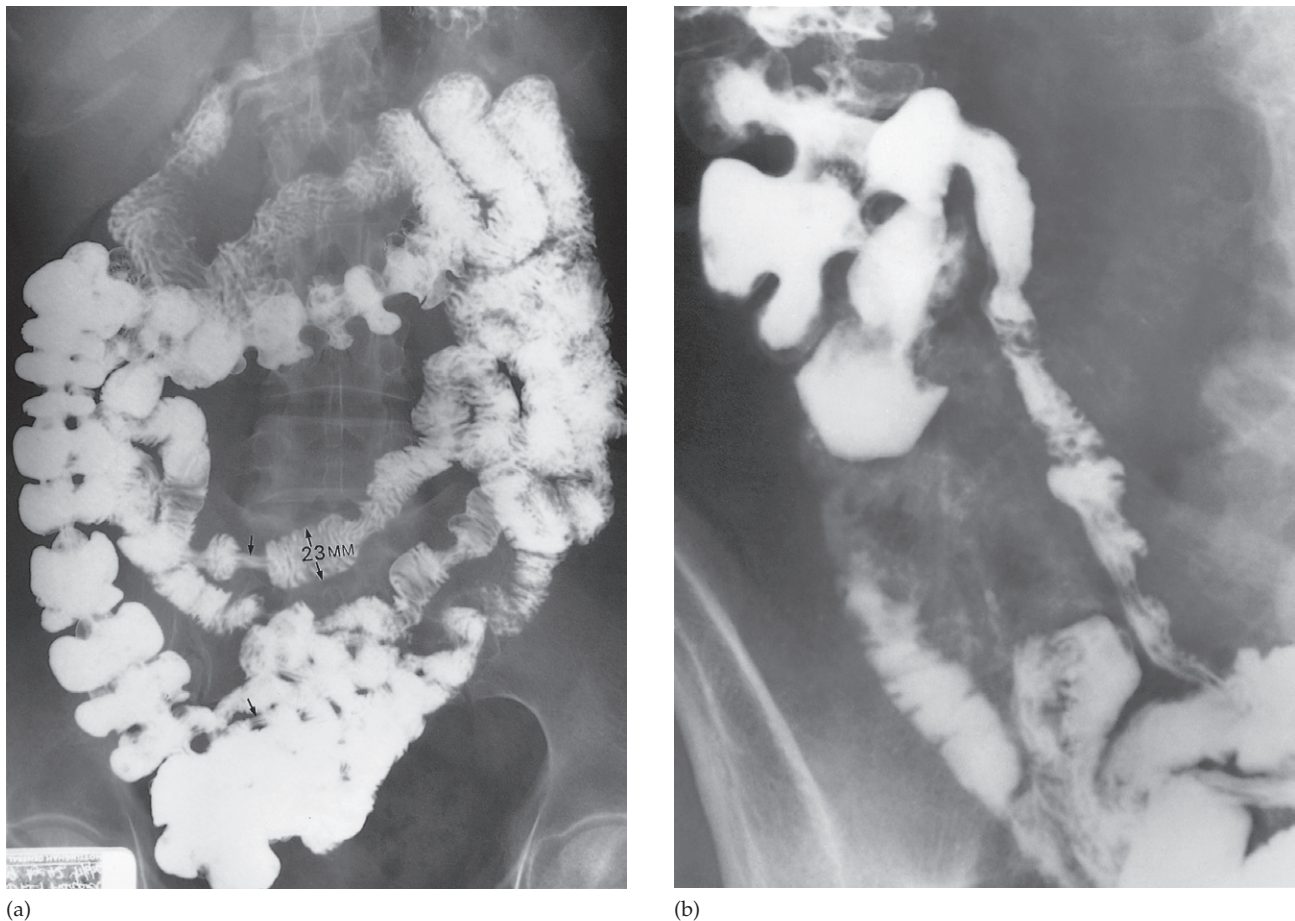


Fig. 6.34 (a) Normal barium follow-through. The small intestine, ascending and transverse colon are filled with barium. The jejunum in the left side of the abdomen has a much more marked mucosal fold pattern than the ileum, which is lying in the pelvis. When a peristaltic wave contracts the bowel, the mucosal folds lie longitudinally (arrows). Note the way of measuring the diameter of the bowel. In the pelvis the loops overlap and details of the bowel become hidden. (b) Normal terminal ileum.

Box 6.6 Indications for small bowel follow-through

- Inflammatory bowel disease (Crohn's disease)
- Suspected stricture
- Malabsorption
- Enterocutaneous fistulae
- Post small bowel resection, to assess small bowel length, in short bowel syndrome
- Malrotation

width. The appearance of the mucosal folds depends upon the diameter of the bowel. When distended, the folds are seen as lines traversing the barium column known as valvulae conniventes. When the small bowel is contracted the folds lie longitudinally, and when it is relaxed the folds assume an appearance described as feathery. The mucosal folds are largest and most numerous in the jejunum and tend to disappear in the lower part of the ileum.



Fig. 6.35 Normal enteroclysis (small bowel enema). This technique gives good mucosal detail. The arrow points to the terminal ileum. Note that a tube has been passed through the stomach into the jejunum.

On CT, the small bowel is seen as multiple loops usually containing oral water or contrast medium. The lumen of each loop should not exceed 25 mm (Fig. 6.36). The wall of the small bowel may not be properly assessed unless the small bowel is distended. Images may be reformatted to review the appearance of the bowel wall in coronal or sagittal planes.

Imaging signs of disease of the small intestine

Dilatation

Dilatation usually indicates malabsorption, paralytic ileus or small bowel obstruction (Fig. 6.37). A diameter over 30 mm is definitely abnormal, but it is important to make sure that two overlapping loops are not being measured.

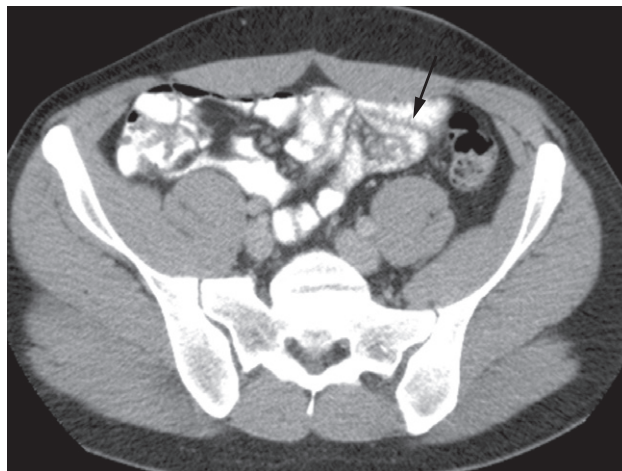


Fig. 6.36 Normal CT of the small bowel. The small bowel contains Gastrografin contrast medium. Note the feathery appearance of the jejunal loops (arrow).

Mucosal abnormality

The mucosal folds become thickened in many conditions (e.g. malabsorption states, oedema or haemorrhage in the bowel wall) and when inflamed or infiltrated (Fig. 6.38). As mucosal fold thickening occurs in many diseases, it is not possible to make a particular diagnosis unless other more specific features are present.

Narrowing

The only normal narrowings are those caused by peristaltic waves. They are smooth, concentric and transient, with normal mucosal folds traversing them and normal bowel proximally. The common causes of strictures are Crohn's disease (Fig. 6.39), tuberculosis and lymphoma. Strictures do not contain normal mucosal folds and usually result in dilatation of the bowel proximally.

Ulceration

The outline of the small bowel should be smooth apart from the indentation caused by normal mucosal folds. Ulcers appear as spikes projecting outwards, which may



Fig. 6.37 Dilatation from small bowel obstruction. The diameter of the bowel is greatly increased. The feathery mucosal pattern is lost and the folds appear as thin lines traversing the bowel, known as valvulae conniventes (arrows).

be shallow or deep (Fig. 6.40). Ulceration is seen in Crohn's disease, tuberculosis and lymphoma. When there is a combination of fine ulceration and mucosal oedema, a 'cobblestone' appearance may be seen.

Specific diseases of the small intestine

Crohn's disease

Crohn's disease is a disease of unknown aetiology characterized by localized areas of non-specific chronic granulomatous inflammation, which nearly always affects the

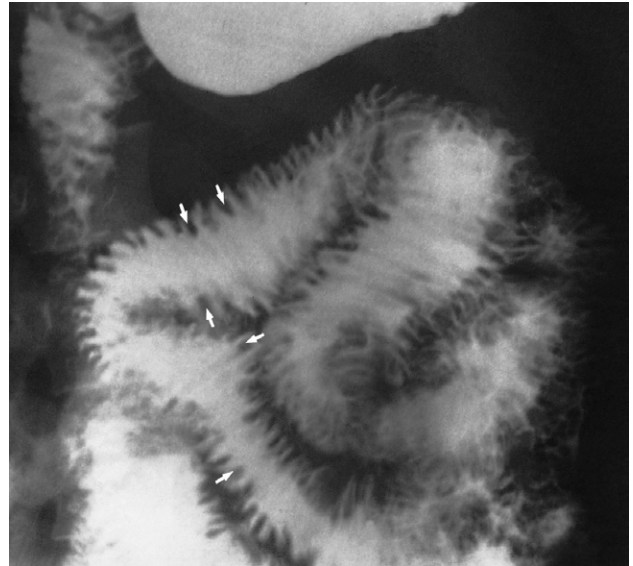
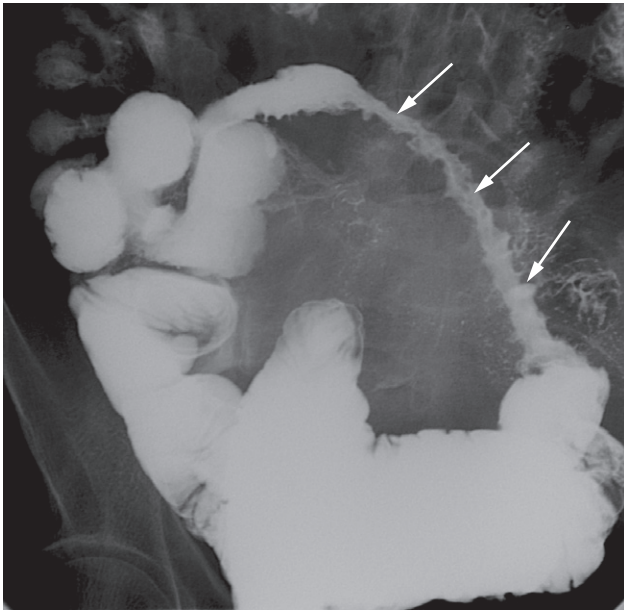


Fig. 6.38 Mucosal abnormality with infiltration of the bowel, in this case from oedema. The mucosal folds become thickened (some are arrowed).

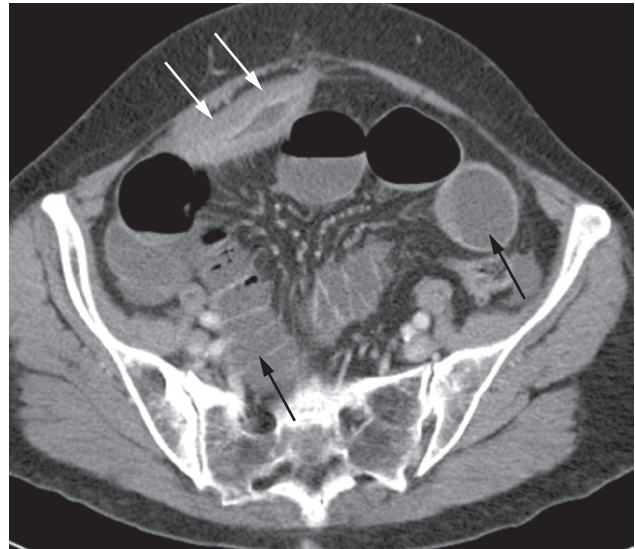
terminal ileum. In addition, it may cause disease in several different parts of the small and large intestine, often leaving normal intervening bowel, the affected parts being known as skip lesions.

The major signs on barium examinations and cross-sectional imaging (Figs 6.39–6.41) that may be seen in isolation or combination include:

- Strictures, which are extremely variable in length. Sometimes a loop of bowel is so narrow, either from spasm or oedema and fibrosis in the bowel wall, that its appearance has been called the 'string sign'.
- Contraction of the caecum, which may be seen particularly when there is visible disease in the terminal ileum.
- Dilatation of the bowel, which may be seen proximal to narrowed areas.
- Ulcers; these are sometimes quite deep. Fine ulceration combined with mucosal oedema gives rise to the so-called 'cobblestone' appearance.
- Thickening, distortion or effacement of mucosal folds.
- Separation of loops of bowel, due to bowel wall thickening or an inflammatory mass.



(a)



(b)

Fig. 6.39 Narrowing. (a) There is a long stricture (arrows) in the ileum due to Crohn's disease and an abnormal mucosal pattern. There is also separation of the abnormal segment from other loops of the bowel. (b) CT in the same patient demonstrating marked thickening of the abnormal loop of small bowel, with a narrowed lumen (white arrows). Several dilated loops of small bowel are also seen (black arrows), due to some obstruction at the level of the stricture.



Fig. 6.40 Ulceration. Abnormal loops of bowel in Crohn's disease showing the ulcers as outward projections (arrows).

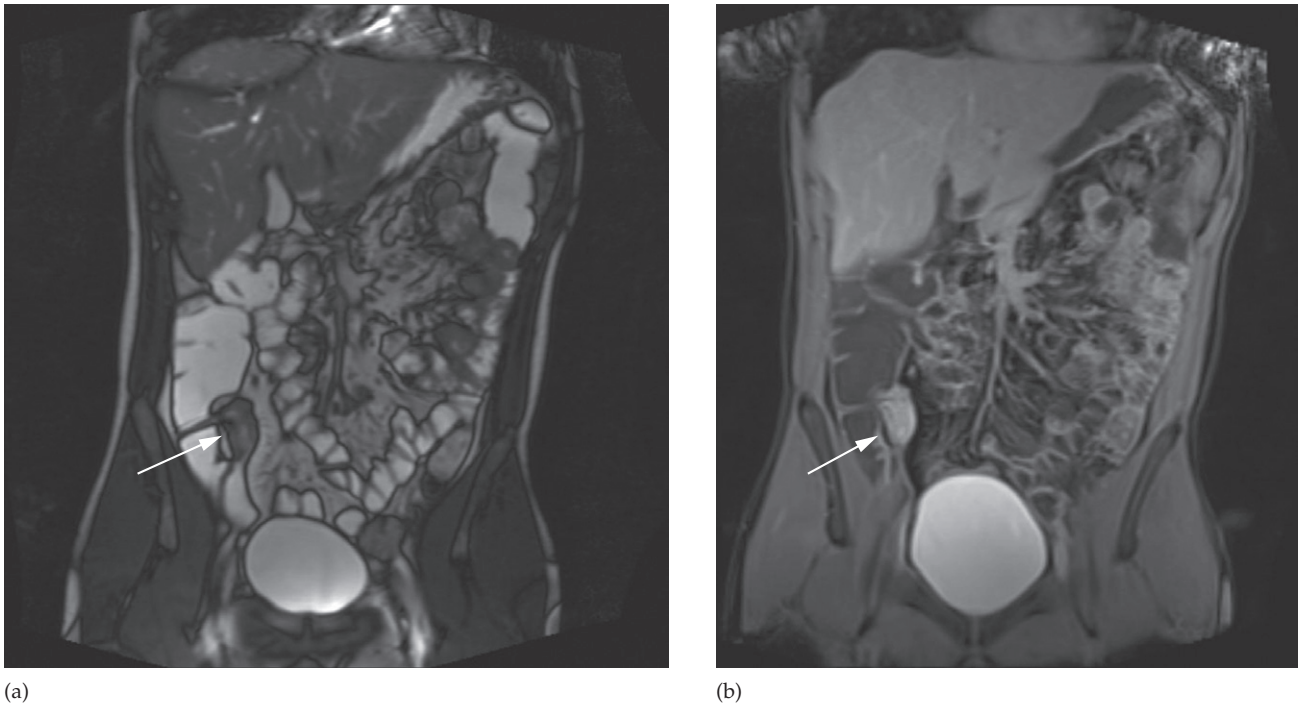


Fig. 6.41 MRI of Crohn's disease. (a) Coronal T2 and (b) coronal T1 post contrast images demonstrating mucosal thickening and enhancement involving the terminal ileum (arrows), characteristic of Crohn's disease.

- Fistulae to other small bowel loops, colon, bladder or vagina (Fig. 6.42). When the fistula is between adjacent loops of small intestine it can be difficult to detect.
- Signs of malabsorption (see below).

Ultrasound may be helpful in identifying thickened loops of bowel, as well as abscess collections in the lower abdomen although these are usually better delineated at CT. Involved loops of bowel, on CT, have a thick-walled appearance with streaky, high density of the surrounding mesenteric fat due to surrounding oedema and inflammatory change. When Crohn's disease affects the anal canal, a perianal fistula often results. MRI is often used to demonstrate the position and extent of the fistula. In particular, MRI is used in suspected complex fistulae, where there may be extension into the pelvis above the levator plate or extension through the sphincter into the ischiorectal fossae (Fig. 6.43).

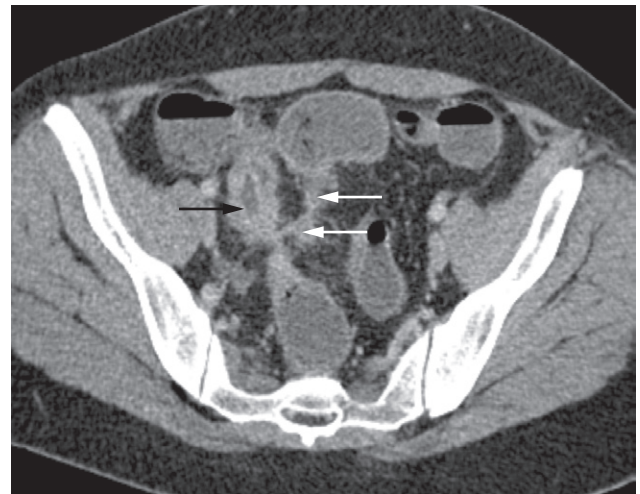


Fig. 6.42 CT of a fistula (white arrows) between the ileum and the sigmoid colon in a patient with Crohn's disease. Note the thickened and inflamed loop of ileum (black arrow).

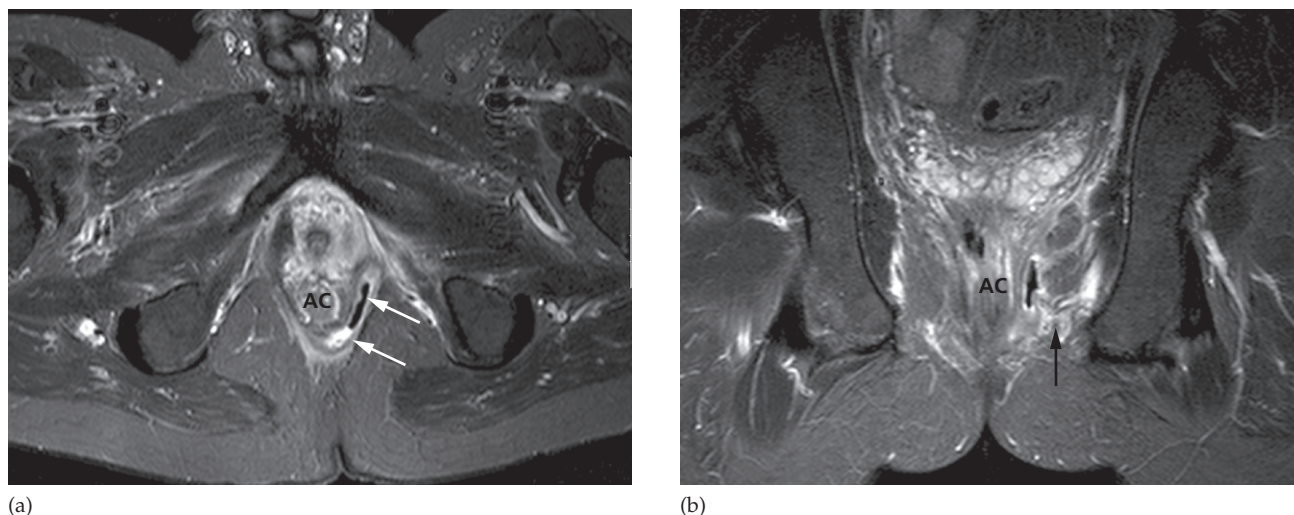


Fig. 6.43 Perianal fistula in Crohn's disease on MRI. (a) Axial MRI using a specialized sequence which is T2-weighted with fat saturation (STIR sequence) demonstrating air and fluid within a cavity that runs in the left intersphincteric space, involving the external sphincter (arrows). (b) Coronal STIR demonstrating air within the fistula as well as bright inflammatory change in the ischiorectal fat (arrow). AC, anal canal.

Small bowel ischaemia

Intestinal infarction, a serious life-threatening condition, is caused by occlusion of the superior mesenteric artery, either due to a thrombosis or an embolus (Fig. 6.44). There may be thickening and oedema of the wall of the small bowel, and gas may be seen within the bowel wall. Perforation may occur, with free gas seen within the peritoneal cavity. There may be air within the superior mesenteric vein or portal vein system in severe cases. These features are best demonstrated on a post contrast CT, performed in the arterial and portal venous phase, which will also demonstrate the arterial anatomy.

Tuberculosis

Tuberculosis of the small bowel is indistinguishable from Crohn's disease on barium examination. It commonly affects the ileocaecal region and also causes contraction of the caecum. On CT, there may be signs of diffuse peritoneal involvement, with ascites, thickening of the omentum, peritoneal and serosal nodules, and lymph node enlargement. These appearances may be indistinguishable from a

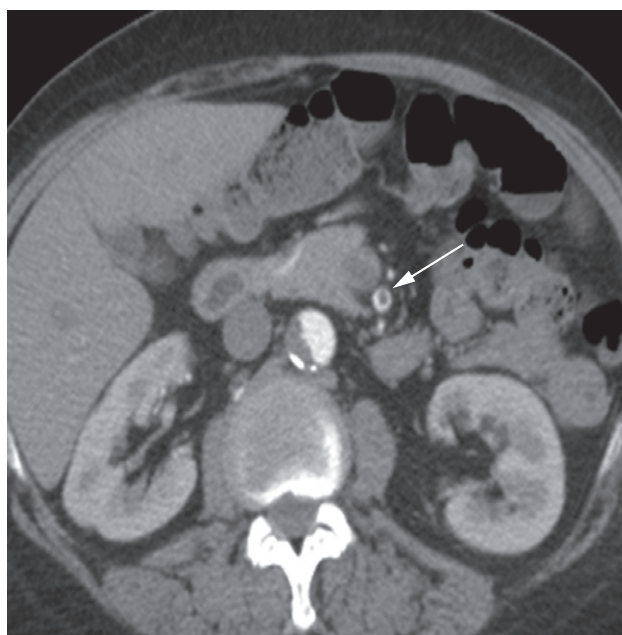


Fig. 6.44 Axial CT showing a thrombus in the superior mesenteric artery (arrow).



Fig. 6.45 Lymphoma. Lymphomatous infiltration has occurred in the lower loops of the bowel causing thickening of the mucosal folds (small arrows) and discrete filling defects due to tumour nodules (curved arrows).

disseminated intraperitoneal malignancy and ultrasound or CT-guided biopsy is usually required to establish the diagnosis.

Lymphoma

The infiltration in the wall of the bowel with lymphoma gives an appearance that is often extremely difficult to distinguish from Crohn's disease. Features that may help differentiate the two conditions on barium examinations are small mucosal filling defects due to tumour nodules (Fig. 6.45) and displacement of loops caused by enlarged mesenteric lymph nodes. Enlargement of the liver and spleen may also be present. CT and ultrasound can show very marked thickening of the bowel wall (Fig. 6.46), which can help differentiate between Crohn's disease and lymphoma. CT can also demonstrate mesenteric and para-



Fig. 6.46 Lymphoma. CT with the bowel opacified by contrast agent. The wall of all the bowel loops is considerably thickened. The arrows point to a portion of bowel which is particularly involved by lymphoma.

aortic lymphadenopathy and lymphomatous deposits in the liver and spleen.

Malabsorption

A number of disorders result in defective absorption of foodstuffs, minerals or vitamins. The definitive test for malabsorption is jejunal biopsy.

The following imaging signs may occur with any of the causes of malabsorption (Fig. 6.47):

- Small bowel dilatation, the jejunum being affected more than the ileum.
- Thickening of mucosal folds.
- The barium may be diluted by the excessive fluid in the small bowel and so appears less dense.

The use of barium follow-through in malabsorption is mainly confined to demonstrating a structural abnormality causing the malabsorption, notably:

- Crohn's disease.
- Lymphoma.
- Anatomical abnormalities, e.g. decreased length of small bowel available for absorption, such as surgical resection or a fistula short-circuiting a length of small bowel.



Fig. 6.47 Malabsorption. The bowel is dilated and the mucosal folds thickened. In the lower loops the barium appears less dense due to it becoming diluted. No specific cause for the malabsorption can be detected, which in this case was due to gluten enteropathy.

- Stagnation of bowel contents, allowing bacterial overgrowth, which utilizes nutrients from the bowel lumen, caused by:
 - multiple small bowel diverticula (Fig. 6.48)
 - a dilated loop cut off from the main stream of the bowel in which there is delayed filling and emptying (blind loop)
 - a dilated loop proximal to a stricture (stagnant loop).

Acute small bowel obstruction

Acute small bowel obstruction can be due to a variety of causes, notably peritoneal adhesions (usually postopera-



Fig. 6.48 Diverticulosis. A number of diverticula of varying size can be seen arising from the small bowel (some are arrowed).

tively or following previous peritoneal inflammation), obstruction in hernial orifices, Crohn's disease, at the site of twisting in volvulus, or occasionally due to metastatic carcinoma, lymphoma or even primary small bowel tumours. A barium examination is not carried out in most cases of obstruction as the diagnosis is usually made on clinical history and examination with the help of plain abdominal films. If the cause of small bowel obstruction is evident clinically (e.g. in a patient with a strangulated hernia or known widespread malignancy), further imaging is rarely required. However, if the cause of the obstruction is not evident, then a contrast follow-through study may be helpful. Water-soluble contrast is used in preference to barium. If the contrast is seen within the large bowel at 24 hours, conservative management is likely to be successful because the degree of obstruction is likely to be minor. If there is mechanical obstruction in the proximal small bowel, then the contrast will remain in the dilated stomach and proximal small bowel at 24 hours.

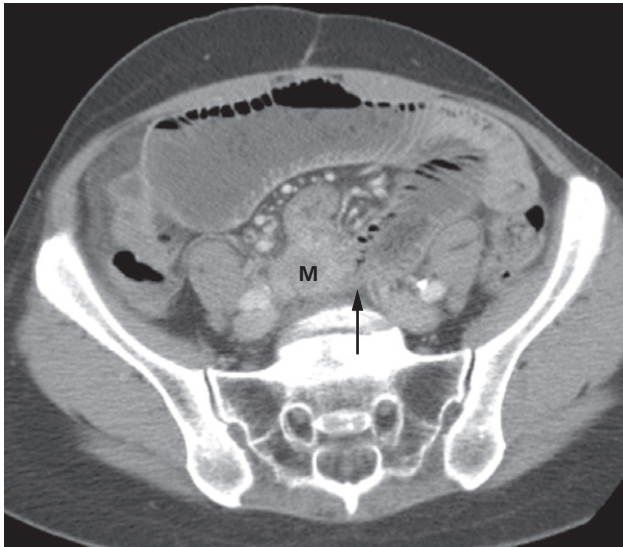


Fig. 6.49 CT of small bowel obstruction in a patient with recurrent ovarian cancer. There is an abrupt change in calibre of the dilated small bowel lumen (arrow) where a mass (M) is infiltrating the bowel wall.

Computed tomography is an increasingly useful technique to demonstrate the site of obstruction by showing the transition zone from dilated to collapsed small bowel, and also to confirm or exclude a mass at the site of obstruction (Fig. 6.49). No imaging technique can directly demonstrate adhesions, the commonest cause of small bowel obstruction.

Malrotation

During intrauterine life, the bowel undergoes a series of rotations. Failure of the normal rotation may result in the small bowel being situated in the right side of the abdomen and the colon on the left side. However, in children it is important to recognize even minor degrees of malrotation as the condition predisposes to intestinal volvulus, which is often a surgical emergency. Malrotation is diagnosed when the duodenojejunal flexure is displaced downwards and to the right of its normal position, which should be level with the duodenal cap and to the left of the spine.



Fig. 6.50 Worm infestation. Several long, tubular filling defects (arrows) can be seen due to roundworms (*Ascaris*) in the small bowel.

Worm infestation

Roundworms (*Ascaris*) are commonly encountered worms, large enough to be seen as filling defects in the lumen of the bowel (they may grow up to 35 cm long) (Fig. 6.50). The worms themselves may ingest the barium to have their own barium meal and barium may be seen in their digestive tracts.

LARGE INTESTINE

Imaging techniques

Colonoscopy

Colonoscopy is now the gold standard for examining the colonic mucosa. The technique allows direct inspection of

the mucosal surface of the bowel and may be used for diagnostic or therapeutic biopsy or resection of mucosal lesions. Colonoscopy may fail for several reasons:

- incomplete colonic evaluation
- impassable stricture
- patient intolerance
- increased risk of perforation, e.g. in extensive or severe acute colitis.

If colonoscopy fails to reach the caecum, the large bowel may be investigated by performing either a barium enema or, increasingly frequently, a CT pneumocolon which can often be performed on the same day as the bowel has already been prepared.

Barium enema

Firstly, the bowel is prepared by means of aperients or washout to rid the colon of faecal material, which might otherwise mask small lesions and cause confusion by simulating polyps. Barium is run into the colon under gravity through a tube inserted into the rectum. Air is then blown in to push the barium around the colon with the result that the colon is distended with air and the mucosa coated with barium, giving the 'double-contrast' effect. Films are taken in various projections so that all the loops of colon are unravelled.

Although diverticular disease and colonic carcinoma are well demonstrated at barium enema, CT pneumocolon is increasingly being used following failed colonoscopy. Instant enemas (water-soluble contrast) are still used in suspected large bowel obstruction to confirm the diagnosis and also to delineate the level of obstruction in a patient who may be considered for bowel decompression with a colonic stent, prior to surgery (see Chapter 17, Fig.17.20)

Computed tomography pneumocolon

Computed tomography pneumocolon has superseded barium enema as the method of choice for identifying malignant tumours of the colon when colonoscopy has failed as it has the advantage of allowing not only the diagnosis of the tumour but also the demonstration of metastatic disease.. The technique is also used in patients who are frail and with poor mobility, in which case colonoscopy (and barium enema) would be difficult to undertake.

The patient is given a purgative to clean the colon prior to the CT examination and a smooth muscle relaxant is given by injection. A rectal tube is inserted and the colon is distended with gas (carbon dioxide or air) and intravenous contrast is given to enhance any tumours that may be present. Neither barium nor Gastrografin is used. One scan is obtained with the patient supine, followed by a second scan with the patient prone. In some centres, as an alternative for frail and immobile patients, avoiding the use of aperients, the colon is filled with contrast by giving oral contrast some time before the examination and a CT of the abdomen is then performed.

With multidetector CT and the appropriate software, the CT pneumocolon images can be viewed as sectional images in any desired plane. They can also be reconstructed to a three-dimensional display and viewed as *virtual colonoscopy* (see Fig. 6.75b). Virtual colonoscopy requires a substantial amount of time and training to interpret.

Sigmoidoscopy is performed in almost every patient in whom a barium enema or CT pneumocolon is requested, because lesions in the rectum, especially mucosal abnormalities, may be missed.

Magnetic resonance imaging

Magnetic resonance imaging of the colon is challenging due to movement artefacts from bowel peristalsis. This can be overcome to some extent by using a smooth muscle relaxant and rapid sequences. MRI is mainly used to evaluate the rectum and anal canal, where movement artefacts are minimal. No specific patient preparation is required.

Nuclear medicine studies

Intestinal transit time may be evaluated using an oral radiopharmaceutical in patients with chronic constipation. The presence of inflammation may be assessed using indium-111 or technetium hexamethylpropyleneamine oxime (HMPAO)-labelled white cells in patients with ulcerative colitis.

Normal appearance of the colon

The radiological anatomy of the normal colon is shown in Fig. 6.51. Certain features are worth emphasizing.

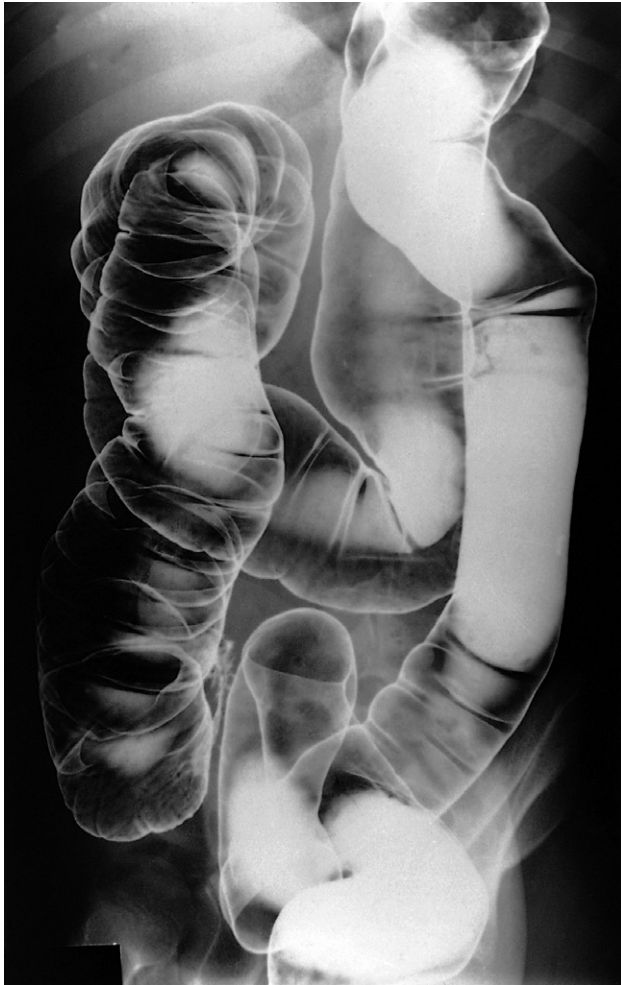


Fig. 6.51 Normal double-contrast barium enema.

The length of the colon is very variable and sometimes there are redundant loops, particularly in the sigmoid and transverse colon. The calibre decreases from the caecum to the sigmoid colon.

The caecum is usually situated in the right iliac fossa, but it may be seen under the right lobe of the liver or even in the centre of the abdomen if it possesses a long mesentery. The lips of the ileocaecal valve may project into the caecum and cause a filling defect, which must not be mistaken for a tumour. Filling of the terminal ileum and appendix with

rectal contrast may occur, but if they do not fill no significance can be attached to this.

Haustra can usually be recognized in the whole of the colon, although they may be absent in the descending and sigmoid regions. The outline of the descending colon, apart from the haustra, is smooth.

Imaging signs of disease of the large intestine

Narrowing of the lumen

Narrowing of the colon may be due pathology:

- inside the lumen of the bowel (e.g. impacted faeces)
- inside the bowel wall (may be due to physiological spasm)
- outside the bowel wall due to compression by an extrinsic mass.

Spasm is often seen in normal patients and, providing it is an isolated finding, it can be ignored. Spasm is also seen in conjunction with diverticular disease and various inflammatory disorders.

The main causes of *stricture* formation in the bowel wall are listed in Box 6.7.

When attempting to diagnose the nature of a stricture in the colon the following points should be borne in mind:

- *Neoplastic strictures* have shouldered edges, an irregular lumen and are rarely more than 6 cm in length (Fig. 6.52), whereas benign strictures classically have tapered ends, a relatively smooth outline and may be of any length.
- *Ulceration* may be seen in strictures due to Crohn's disease, and sacculcation of the colon is a feature of ischaemic strictures.

Box 6.7 Causes of narrowing of the colonic lumen

- Carcinoma
- Diverticular disease
- Crohn's disease
- Ischaemic colitis
- Rarer causes:
- Tuberculosis:
 - lymphogranuloma venereum
 - amoebiasis
 - radiation fibrosis

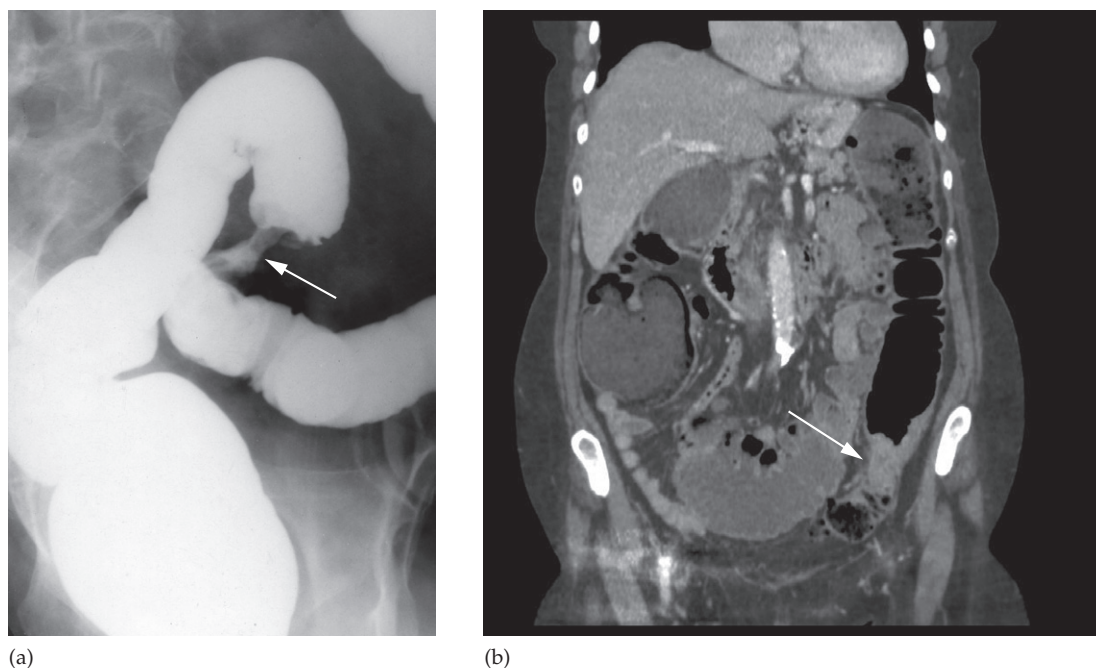


Fig. 6.52 Stricture. (a) Barium enema and (b) coronal CT showing a short, circumferential narrowing in the sigmoid colon (arrows) from a carcinoma.

- *Narrowing due to diverticular disease* is usually accompanied by other signs of diverticular disease. It is sometimes impossible to distinguish a stricture due to a carcinoma in an area of diverticular disease from a stricture due to diverticular disease.

- The site of the stricture can help in limiting the differential diagnosis. Strictures due to diverticular disease are almost always confined to the sigmoid colon. Ischaemic strictures are usually centred somewhere between the splenic flexure and the sigmoid colon. Crohn's disease and tuberculosis have a predilection for the caecum.

Extrinsic compression by a mass arising outside the wall of the bowel causes a smooth narrowing of the colon at barium enema examination, frequently from one side only, and often displaces the colon, e.g. ovarian and uterine masses. Extrinsic compression causing a smooth indentation on the caecum may be seen with a mucocele of the appendix, appendix abscess or an inflammatory mass in Crohn's disease.

Dilatation

Dilatation of the colon is difficult to assess. Double-contrast barium enema and CT pneumocolon examinations both involve distending the colon, so that its diameter is partly dependent on the amount of barium and air introduced.

The causes of dilatation of the colon are:

- *Obstruction*. Here the important consideration is not the dilatation itself but the nature of the obstructing lesion. In complete obstruction, colonoscopy and barium enema examinations may only show one end of the stricture, whereas CT will usually demonstrate the cause of the obstruction.

- *Paralytic ileus*. This diagnosis is usually made on clinical grounds with the help of plain films of the abdomen. A water-soluble contrast enema is occasionally undertaken when it proves difficult to distinguish paralytic ileus (also called 'pseudo-obstruction') from mechanical obstruction to the distal colon. The contrast study will show a

dilated, but otherwise normal, colon in the case of paralytic ileus.

- *Volvulus*.
- *Ulcerative colitis* with toxic dilatation (see Fig. 5.6).
- *Hirschsprung's disease* and *megacolon*.

Filling defects

Filling defects in the colon, as elsewhere in the GI tract, may be intraluminal, arise from the wall or be due to pressure from an extrinsic mass.

A localized filling defect is likely to be a polyp or a neoplasm. Faeces cause a filling defect which can be very difficult to distinguish from a polyp or tumour (Fig. 6.53). Therefore, whenever possible, all imaging examinations of the colon should be made with a clean colon in order to avoid misdiagnosing polyps that are in fact faeces. Faeces have no attachment to the wall of the bowel, are completely surrounded by barium or air, and move according to the position of the patient, usually lying in the dependent part of the bowel.

Intramural haemorrhage, oedema or air in the wall of the colon (pneumatosis coli) all cause multiple, smooth filling defects arising from the wall of the bowel.

A unique type of filling defect is seen in intussusceptions.

Diverticula and muscle hypertrophy

These are seen with diverticular disease (Fig. 6.54) and are discussed later in this chapter.

Ulceration

Ulcers of the colonic mucosa can be recognized on barium enema as small projections from the lumen into the wall of the bowel, causing the normally smooth outline of the colon to have a fuzzy or shaggy appearance (Fig. 6.55). The two major causes of ulceration are ulcerative colitis and Crohn's disease. Rarer causes include tuberculosis and amoebic and bacillary dysentery.

Specific diseases of the colon

Inflammatory bowel disease

Although classic changes are described for both ulcerative colitis and Crohn's disease, it is sometimes difficult to dis-

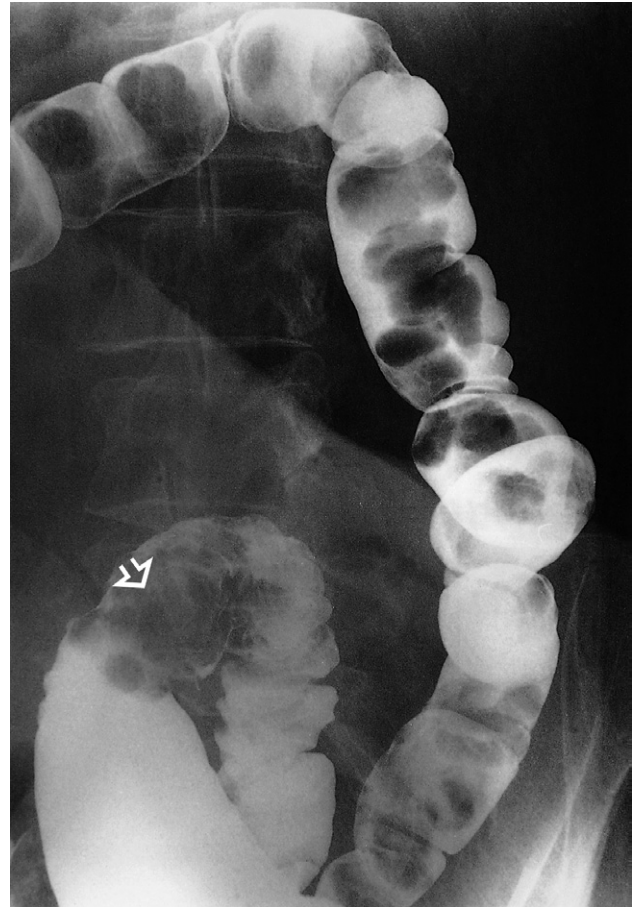
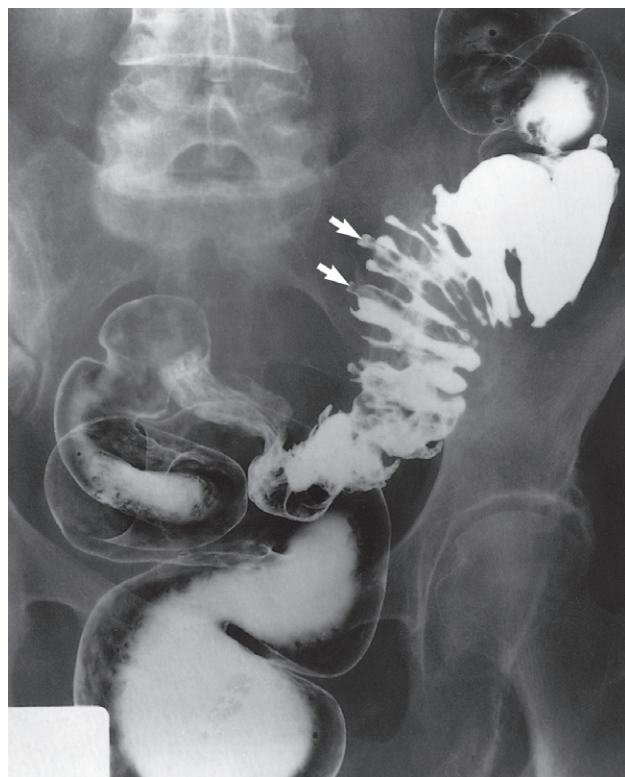


Fig. 6.53 Filling defects. Lumps of faeces have caused smooth filling defects surrounded by barium. However, in the sigmoid colon there is a large filling defect with ill-defined edges (arrow); this is a carcinoma. A clean colon is essential for a satisfactory barium enema.

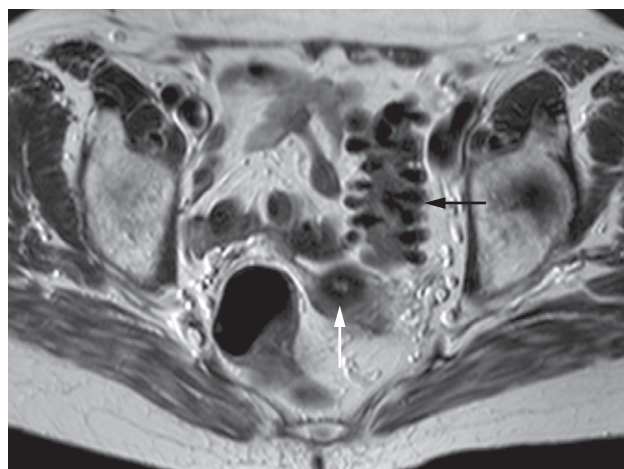
tinguish between the two conditions (which, therefore, are often both referred to as inflammatory bowel disease). Imaging can be important not only for diagnosis, but also to assess the extent and severity of the disease and to detect complications.

Ulcerative colitis

Ulcerative colitis is a disease of unknown aetiology characterized by inflammation and ulceration of the colon. The



(a)



(b)

Fig. 6.54 (a) Muscle hypertrophy and diverticula. Muscle hypertrophy gives the sigmoid colon a serrated appearance. Two small diverticula are arrowed. (b) Axial T2-weighted MRI in a different patient demonstrating multiple air-filled diverticula in the sigmoid colon (black arrow). Note the normal low signal intensity of the cervix (white arrow).

disease always involves the rectum. When more extensive it extends in continuity around the colon, sometimes affecting the whole colon.

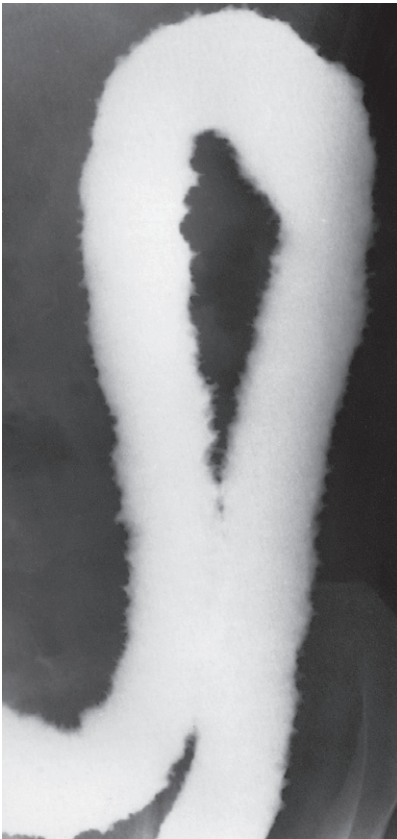
The cardinal radiological sign is widespread ulceration (see Fig. 6.55). The ulcers are usually shallow, but in severe cases may be quite deep. In all but the milder cases, there is loss of the normal colonic haustra in the affected portions of the colon. Oedema of the perirectal tissues causes widening of the space between the sacrum and the rectum. Narrowing and shortening of the colon, giving the appearance of a rigid tube (Fig. 6.56), and pseudopolyps are seen in advanced disease. Pseudopolyps are small filling defects projecting into the lumen of the bowel, formed by swollen mucosa in between the areas of ulceration. The swelling of these islands of inflamed mucosa makes it difficult to assess the true depth of the ulceration.

Strictures are rare, and, when present, are likely to be due to carcinoma; the incidence of colonic carcinoma in long-standing ulcerative colitis is significantly increased.

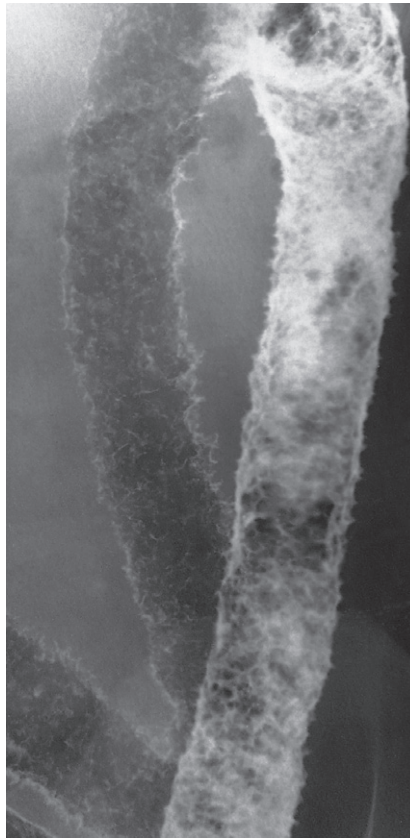
On CT, the bowel wall may be thickened up to 5–8 mm, in continuity from the rectum to the proximal extent of disease. The mucosa enhances brightly. In chronic ulcerative colitis there is visible fatty infiltration in the submucosa, resulting in a 'target sign' appearance (Fig. 6.57).

When the whole colon is involved, the terminal ileum may become dilated. As the ileocaecal valve in this situation is incompetent, the abnormal terminal ileum is usually demonstrated at barium enema.

Toxic dilatation (toxic megacolon) is a serious complication (Fig. 6.58). The diagnosis is made on clinical grounds and on examination of the plain abdominal film or standard CT. Barium enema and CT pneumocolon should be



(a)

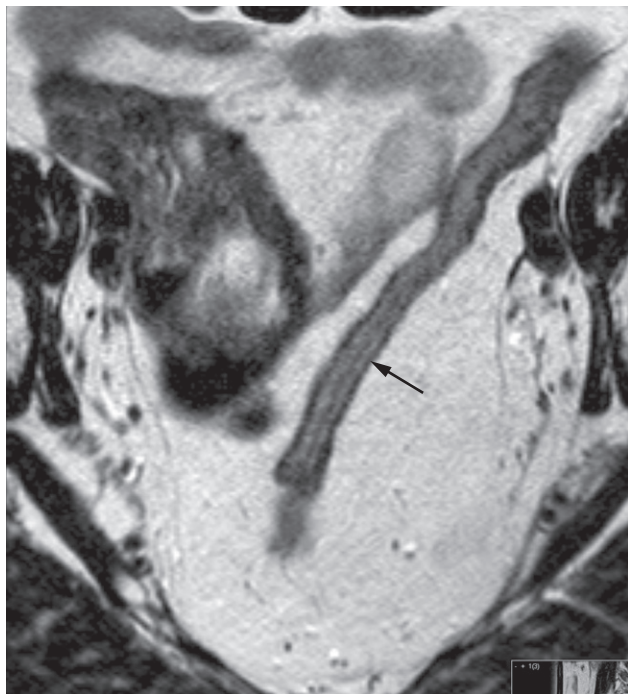


(b)

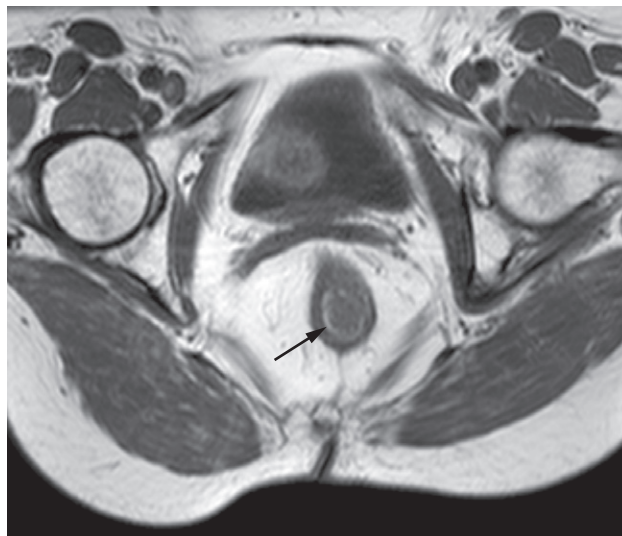
Fig. 6.55 Ulceration. (a) Single contrast. (b) Double contrast. In this case of ulcerative colitis, the ulceration causes the normally smooth outline of the colon to be irregular.



Fig. 6.56 Ulcerative colitis. With longstanding disease, the haustra are lost and the colon becomes narrowed and shortened, coming to resemble a rigid tube. Reflux into the ileum through an incompetent ileocaecal valve has occurred.



(a)



(b)

Fig. 6.57 MRI of chronic ulcerative colitis. (a) Axial T2-weighted image demonstrating a complete loss of haustra in the sigmoid colon (arrow). (b) Axial T1-weighted image demonstrating increased submucosal fibro-fatty changes in the rectum, which is of high signal intensity on T1 (arrow).

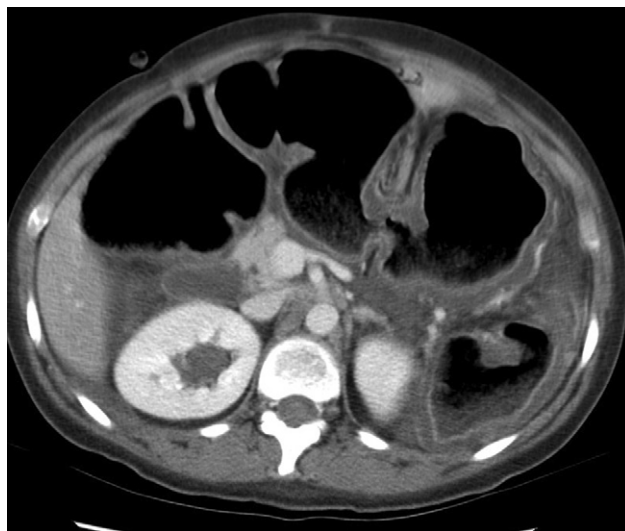


Fig. 6.58 Toxic megacolon demonstrated on CT. The transverse and descending colon are thick-walled and inflamed with enhancement of the mucosa and marked dilatation of the lumen.

avoided in the presence of toxic dilatation owing to the risk of perforating the colon, a contraindication that also applies to colonoscopy.

Crohn's disease

Crohn's disease is a chronic granulomatous condition of unknown aetiology, which may affect any part of the GI tract, but most frequently involves the lower ileum and the colon. The colon may be the only part of the alimentary tract to be involved, but usually the disease affects the small bowel if the colon is involved.

At an early stage in the disease, the findings at barium enema are loss of haustration, narrowing of the lumen of the bowel and shallow ulceration. This criss-crossing ulceration combined with mucosal oedema may give rise to a 'cobblestone' appearance of the mucosa (Fig. 6.59). Later, the ulcers become deeper and may track in the submucosa (Fig. 6.60). The ulcers may be very deep, penetrating into the muscle layer, when they are described as 'rose-thorn ulcers' or deep fissures. The deep ulceration in Crohn's disease may lead to the formation of intra- and extramural abscesses. Fistulae are an important complication. The additional features visible at CT are thickening of the bowel wall, strands in the surrounding fat, fistulae and extracolonic fluid collections.

Strictures are a common finding in Crohn's disease (Fig. 6.61). The strictures are smooth and have tapered ends. When the caecum is involved it is usually markedly contracted. Ulcers may or may not be present in the strictured area. The disease is not always circumferential; one of the features that distinguish it from ulcerative colitis is that it may involve only one portion of the circumference of the bowel.

Another important diagnostic feature is the presence of the so-called 'skip lesion' (Fig. 6.61), namely areas of disease with intervening normal bowel. Skip lesions are virtually diagnostic of Crohn's disease. However, the entire colon may be involved or the disease may be limited to just one segment. There is a predilection for the caecum and terminal ileum. The rectum is often spared – another important differentiating feature from ulcerative colitis. Fistulae may also occur between the colon and the small bowel, bladder or vagina, which may be demonstrated on water-soluble contrast studies or MRI (Fig. 6.62).

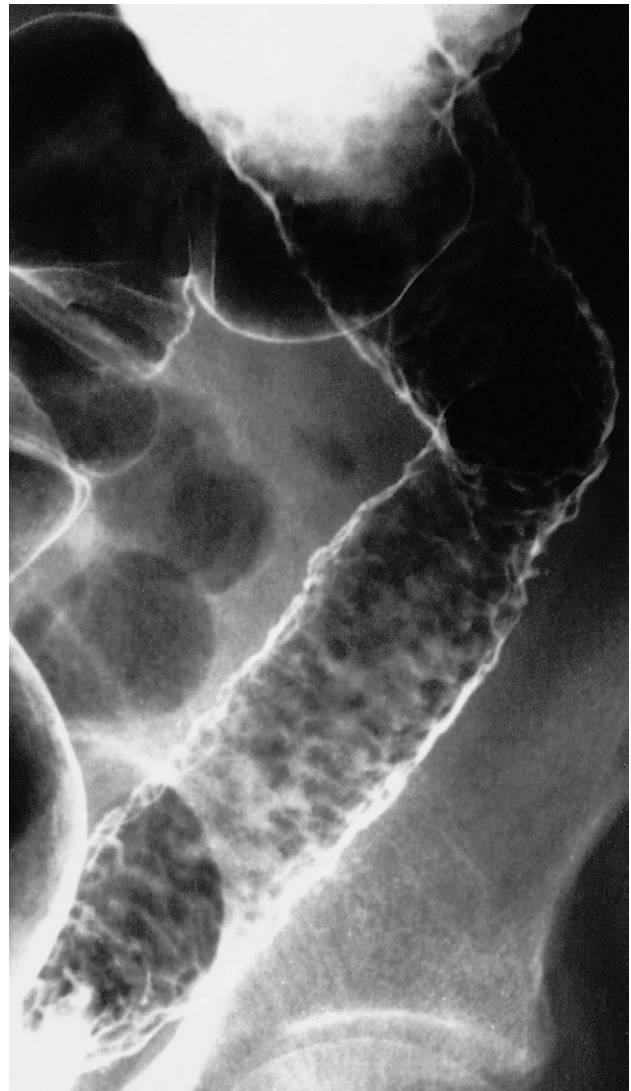


Fig. 6.59 Crohn's disease. The mucosal pattern has a 'cobblestone' appearance due to criss-crossing fine ulceration.

Diverticular disease

Diverticula are sac-like out-pouchings of mucosa through the muscular layer of the bowel wall. They are associated with hypertrophy of the muscle layer and are probably due to herniation of mucosa through areas of weakness where blood vessels penetrate the muscle. Diverticula are very



Fig. 6.60 Crohn's disease. Very deep ulcers are present; two examples of an ulcer tracking in the submucosa are arrowed.



Fig. 6.61 Strictures in Crohn's disease. A long stricture is present in the transverse colon (between the curved arrows) and a shorter one in the sigmoid colon (between the small arrows). In this case, the outline of the strictures is irregular due to ulceration. These two abnormal segments with normal intervening bowel are an example of 'skip lesions' – an important diagnostic feature of Crohn's disease.



Fig. 6.62 Rectovaginal fistula in Crohn's disease. During the barium enema, filling of the vagina with barium occurred. Note the ulceration in the rectum.

common, particularly in the elderly. They are seen in all parts of the colon, but are commonest in the sigmoid colon. The term diverticulitis is used when infection of the affected segment causes symptoms such as sepsis, diarrhoea or obstruction.

The diverticula, when filled with barium, are seen as spherical out-pouchings with a narrow neck (see Fig. 6.54). The colon may also show a 'saw-tooth' serrated appearance from hypertrophy of the muscle coats. Sometimes, the signs of muscle hypertrophy are seen in isolation. Some diverticula may not fill; this is particularly true when inflammation occludes the necks of the diverticula. On CT, the affected loop of bowel appears thick-walled and there is

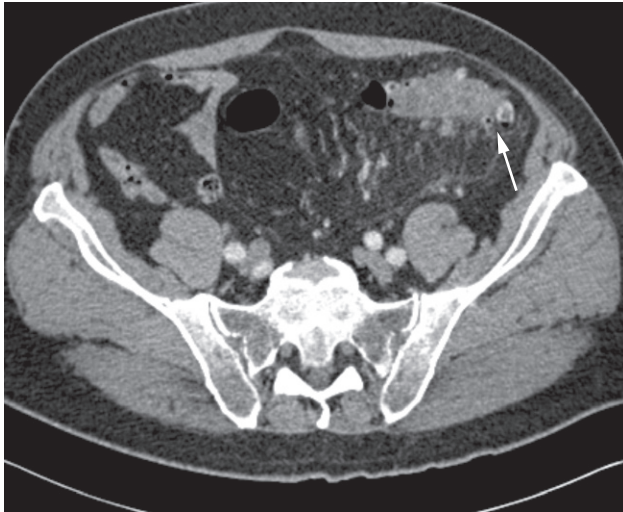


Fig. 6.63 Diverticular disease. Numerous diverticula are seen as out-pouchings from the sigmoid colon (arrow). There is marked stranding of the surrounding fat planes. In this case there is no associated abscess.

stranding of the surrounding fat due to oedema and inflammatory change (Fig. 6.63).

A diverticulum may perforate, resulting in a pericolic abscess or fistula into the bladder, small bowel or vagina. This is recognized by noting barium outside the colon, either in the pericolic region or within the structure to which the fistula has occurred. An abscess is most readily diagnosed with CT. Occasionally, diverticula perforate directly into the peritoneal cavity causing peritonitis, and free intraperitoneal air should be looked for on a plain abdominal film if necessary. A stricture with or without local abscess formation may occur (Fig. 6.64). Usually, this is clearly within an area of recognizable diverticular disease. It is, however, often impossible to differentiate such a stricture from a carcinoma occurring coincidentally in a patient with diverticular disease.

Appendicitis

In most cases, the diagnosis of appendicitis is obvious clinically and imaging is unnecessary. In cases of doubt the diagnosis can be made with ultrasound, which shows a distended, non-compressible appendix with a thickened

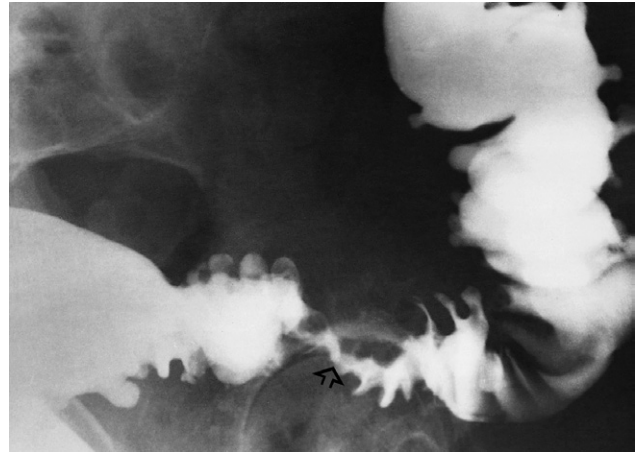


Fig. 6.64 Diverticular disease. A stricture is present (arrow). Although there is recognizable diverticular disease at both ends of the stricture, it is impossible to definitely exclude a carcinoma.

oedematous wall, often accompanied by free fluid within the pelvis (Fig. 6.65a). An appendicolith may be visible within the appendix as a hyperechoic area casting an acoustic shadow (Fig. 6.65b). Similar changes can be demonstrated with CT. An appendix abscess can be diagnosed with CT (Fig. 6.66) or ultrasound as a mass in the right iliac fossa.

Ischaemic colitis

Acute infarction of the large bowel is very rare. Ischaemia is usually a more chronic process giving rise, initially, to mucosal oedema and haemorrhage, which may resolve. Chronic mesenteric ischaemia is often a delayed diagnosis as patients may present with vague symptoms, and not the classic history of post-prandial pain. It occurs due to narrowing of the arteries supplying the bowel, and usually at least two of the three vessels (coeliac access, superior and inferior mesenteric arteries) will be affected. If suspected, a CT arteriogram is very helpful in not only demonstrating the presence of bowel abnormalities (e.g. strictures), but also demonstrating pathology in the mesenteric vessels, and helping determine whether revascularization can be undertaken by an endovascular or surgical approach. In the later stages, a stricture may form (Fig. 6.67a).

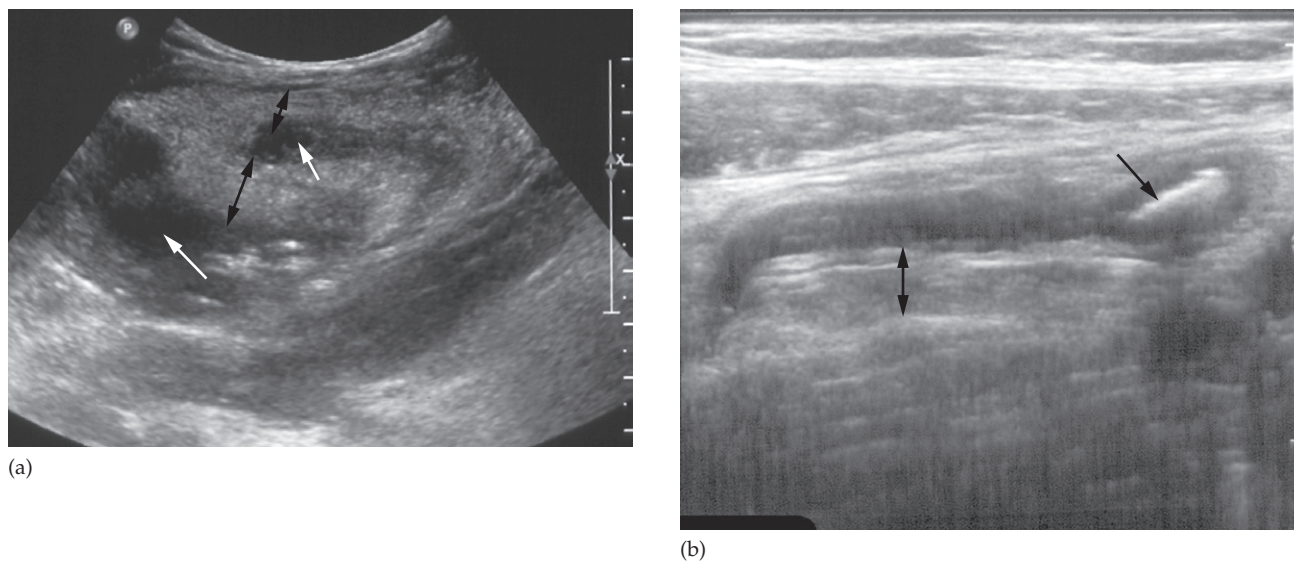


Fig. 6.65 Appendicitis. (a) Longitudinal ultrasound scan demonstrating marked thickening of the wall of the appendix (double head arrows). Fluid is seen within the lumen and surrounding the appendix (white arrows). (b) An appendicolith is seen in the tip of the appendix in a different patient (black arrow). A double-headed arrow again indicates thickening of the appendix wall.

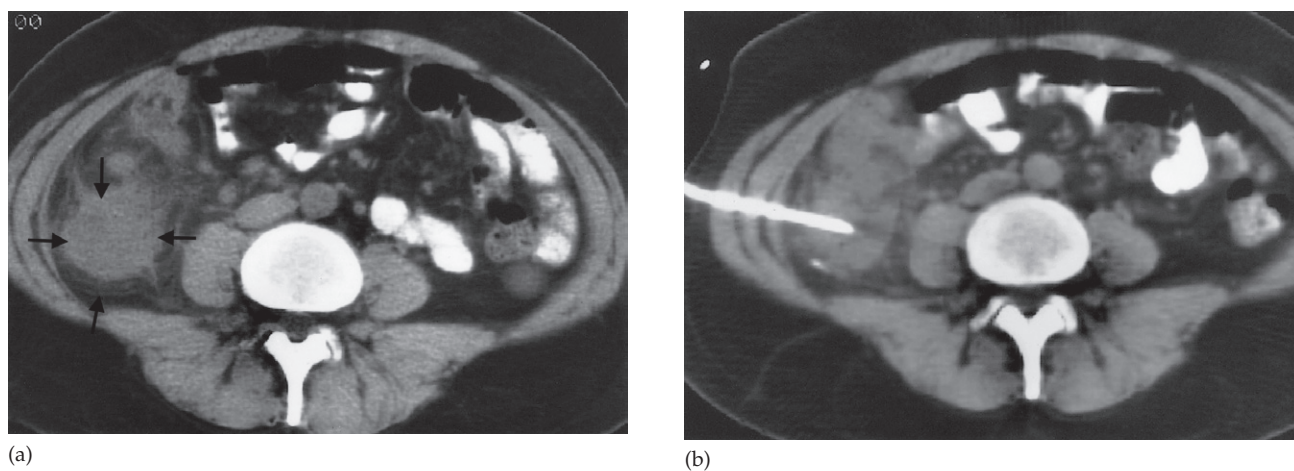
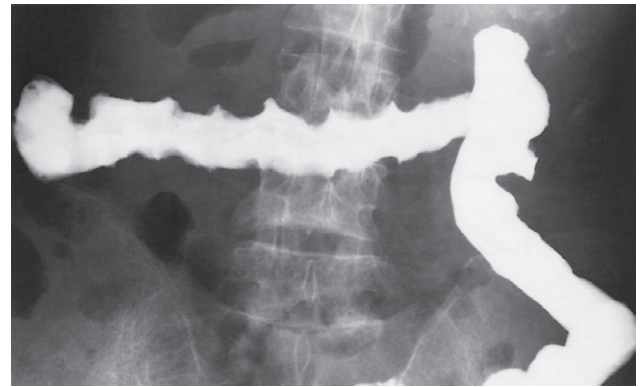


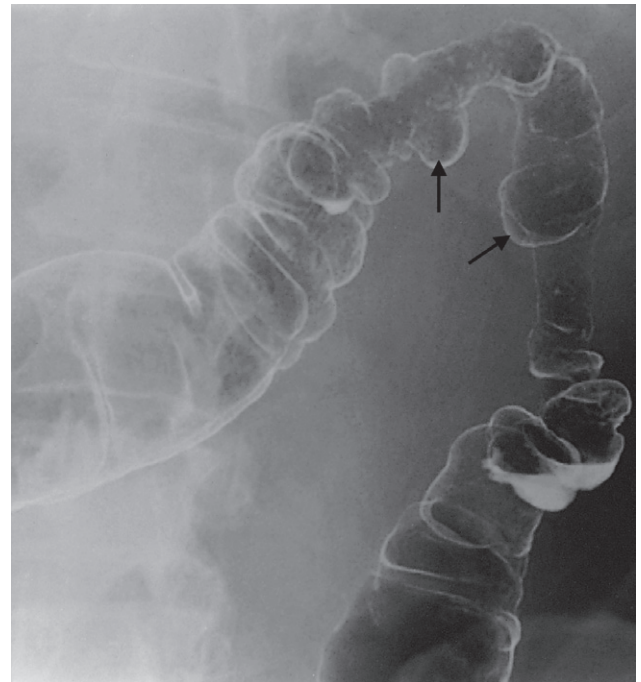
Fig. 6.66 Appendix abscess. (a) CT showing a mass (arrows) in the right iliac fossa. (b) The abscess was drained under CT guidance.



(a)



(b)



(c)

Fig. 6.67 Ischaemic colitis, in three different patients. (a) Coronal CT showing a stricture (arrow) and proximal bowel dilatation (*) which developed following thrombus in the superior mesenteric artery a few months previously (see Fig. 6.44). (b) Barium enema demonstrating mucosal haemorrhage and oedema that have caused indentations resembling thumb prints in the transverse colon. (c) A long smooth stricture involving the splenic flexure with sacculations arising from the colon (arrows).

On barium studies, mucosal haemorrhage and oedema may be recognized by observing multiple, smooth indentations into the lumen of the bowel, resembling thumb prints (Fig. 6.67b). If stricture formation occurs, the stricture will be smooth and have tapered ends. The site is usually,

but not always, centred between the splenic flexure and the sigmoid colon because these are the regions of the colon with the most vulnerable blood supply (Fig. 6.67c). Sacculations may be seen arising from one side of the stric-tured area.

Pneumatosis coli

In this unusual condition, gas-filled spaces are present in the wall of the bowel. These cyst-like spaces do not communicate with the lumen. They can be identified on a plain film of the abdomen, but the diagnosis is much easier with a barium enema where the cysts cause smooth, translucent filling defects projecting from the wall of the bowel (Fig. 6.68). The appearance could be confused with intramural haemorrhage and oedema, or with colitis if the presence of air within the cysts is not appreciated.

Volvulus

In a volvulus, a loop of bowel twists on its mesentery. This happens most frequently in the sigmoid colon, particularly when it is redundant, and less often in the caecum. The twisted loop becomes greatly distended and the bowel proximal to the volvulus is obstructed by the twist and may, therefore, also be dilated.

The diagnosis is usually made on plain abdominal films (see Chapter 5, Fig. 5.5), but a CT may be helpful in doubtful cases so that, if confirmed, non-operative reduction of the volvulus may be attempted. This will show a smooth, tapered narrowing from twisting of the colon (Fig. 6.69), with marked dilatation of the bowel proximal to the twist.

Intussusception

An intussusception is the invagination of one segment of the bowel into another. Infants and young children are much more liable to intussusception than adults.

By far the commonest type is an *ileocolic intussusception*, namely ileum invaginating into the colon. Other types are *colocolic*, when the colon invaginates into another part of the colon, and *ileo-ileal* when the ileum invaginates into a more distal segment of ileum.

The diagnosis of intussusception in children is often made using ultrasound, by diagnosing an abdominal mass often with a hyperechoic centre (Fig. 6.70). In infants and young children, in particular, the diagnosis is often confirmed by an enema with air or carbon dioxide as the contrast agent, and an attempt at reduction of the intussusception is made using the increased pressure of the introduced air or carbon dioxide. When gas is insufflated



Fig. 6.68 Pneumatosis coli. Part of the colon showing numerous translucencies in the colon wall owing to many gas-filled cysts.

per rectum under fluoroscopic or ultrasound control, the flow of gas will be obstructed by the leading edge of the intussusception and an attempt at pneumatic reduction can be made in order to avoid a laparotomy (Fig. 6.71). If such a reduction is to be safely carried out, the child should have no clinical signs of peritonitis. The longer the symptoms have been present, the greater the risk of perforating gangrenous bowel.

In adults, intussusception is almost always due to the presence of a neoplasm, typically in the submucosa, such



Fig. 6.69 Volvulus. A smooth narrowing is seen in the sigmoid colon where the colon has twisted (arrow). Note the dilated colon proximal to this.

as lymphomatous deposits or melanoma metastases. The diagnosis is usually made on CT. A sausage-shaped mass is demonstrated, which has mesenteric fat within the lumen of the intussusciens (Fig. 6.72). Surgical treatment is invariable.

Colorectal tumours

Polyps

The word 'polyp' means a small mass of tissue arising from the wall of the bowel projecting into the lumen. They are best investigated by endoscopy, but may be found at barium enema or CT pneumocolon. It is often impossible on radiological grounds to exclude frank malignancy in a

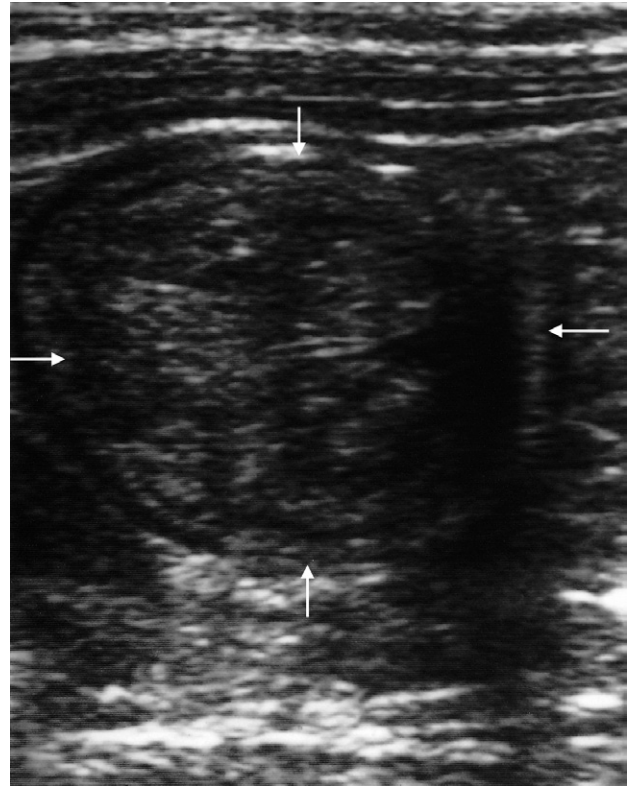
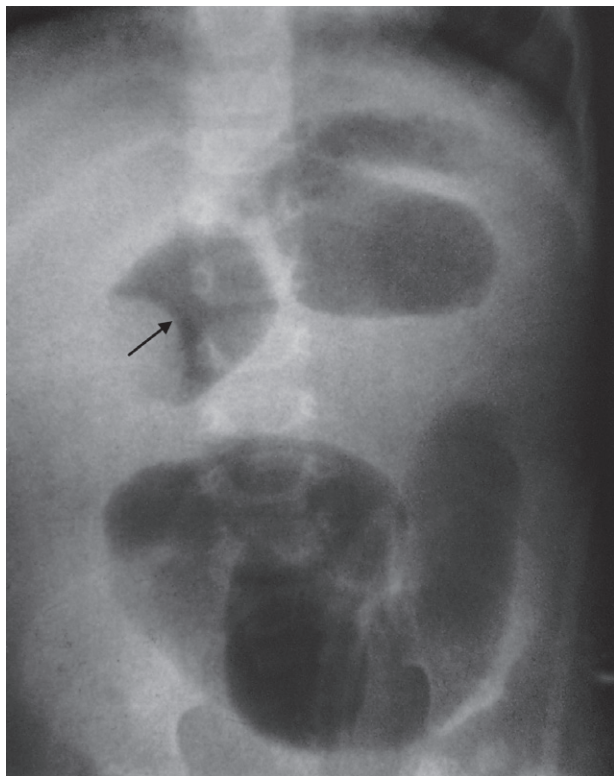


Fig. 6.70 Intussusception. Ultrasound of the upper abdomen showing the intussusception as a mass (arrows).

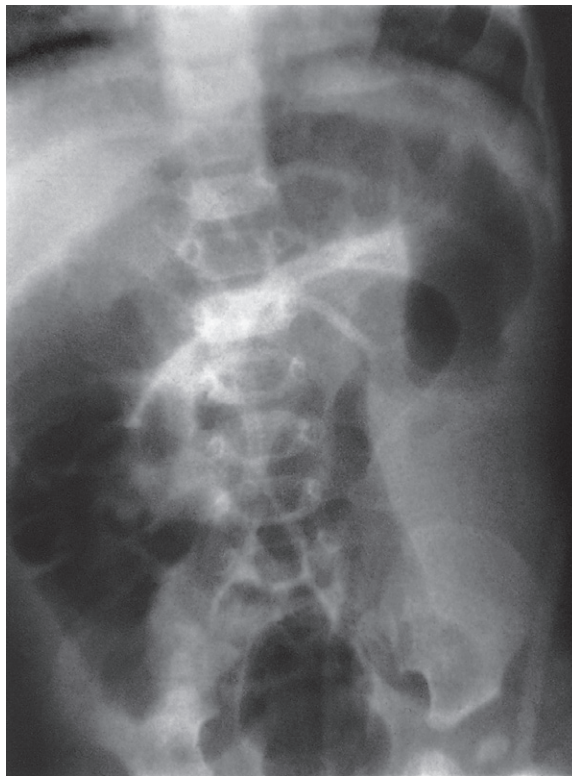
polyp in an adult. However, only a tiny minority of polyps less than 1cm in size, and very few less than 2cm, are cancers. The features that suggest malignancy are a diameter of more than 2cm, a short thick stalk or an irregular surface.

Polyps may be sessile or on a stalk, single or multiple. The common polyps are:

- *Adenomatous polyps* (Fig. 6.73) are benign neoplasms but have a predisposition to malignant change. They are, therefore, removed endoscopically when discovered, regardless of whether or not an individual polyp is believed to be responsible for symptoms. Polyps may first be discovered because of a positive faecal occult blood test or may present with overt bleeding. They may be single or multiple and are found most frequently in the rectosigmoid region. In



(a)



(b)

Fig. 6.71 Intussusception. (a) Film taken during reduction of the intussusception with air insufflated per rectum showing a filling defect in the transverse colon (arrow) owing to ileum invaginated into the colon. (b) Later film showing that the intussusception has been reduced, with air filling the caecum and entering the small bowel.



(a)



(b)

Fig. 6.72 Intussusception due to a tumour on CT. (a) Axial and (b) coronal reformat demonstrating a sausage-shaped mass in the right iliac fossa (arrows). Mesenteric fat and vessels are seen in the centre of the mass.

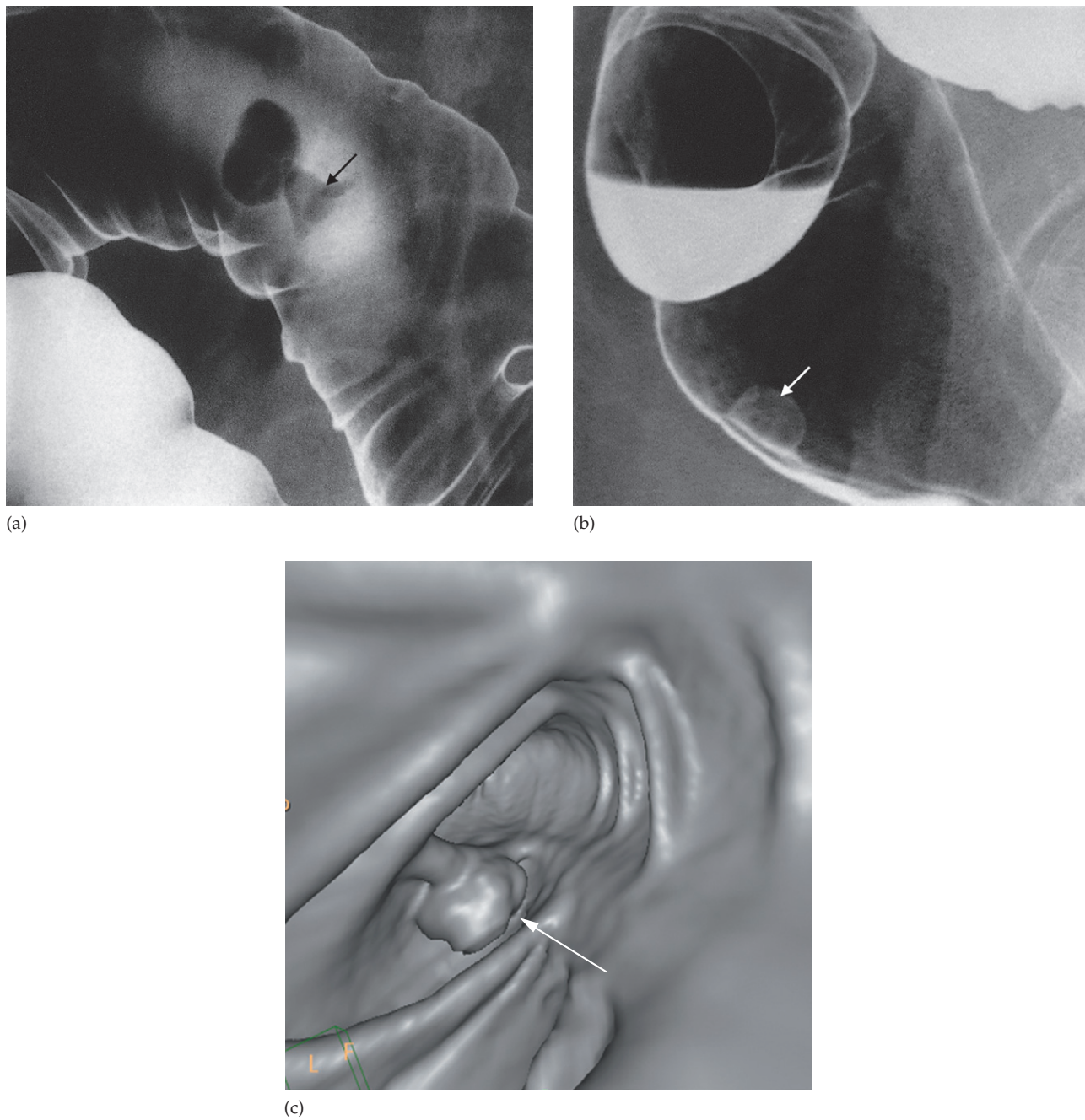


Fig. 6.73 Polyps. (a) Pedunculated polyp (arrow) outlined by barium in the sigmoid colon. (b) Sessile polyp (arrow) in the rectum. (c) CT pneumocolon of a sessile polyp (arrow) in large bowel.

familial polyposis they are numerous and one or more will, in time, undergo malignant change.

- *Villous adenomas* are benign sessile tumours showing a sponge-like appearance owing to barium trapped between the villous strands. They are usually large when first discovered and are frequently mistaken for faeces. The common sites are the rectum and caecum. There is a high incidence of malignant change.
- *Polypoid adenocarcinomas*.
- *Juvenile polyps*. Almost all isolated polyps in children are benign. They are probably developmental in origin.
- *Inflammatory polyps (pseudopolyps)* are seen in ulcerative colitis.
- *Hyperplastic or metaplastic polyps*.

Carcinoma

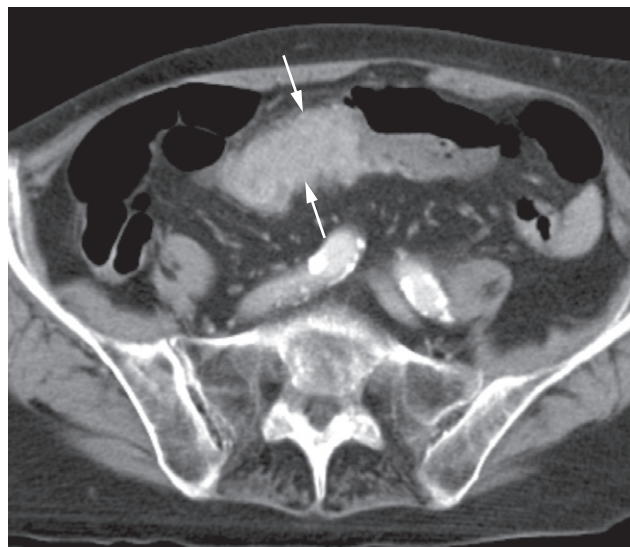
Carcinomas may arise anywhere in the colon and rectum but they are commonest in the rectosigmoid region and caecum. The appearance and behaviour of a carcinoma in

these two sites are usually quite different. The patient with a rectosigmoid carcinoma often has an annular stricture and presents with alteration in bowel habit and obstruction, whereas with a caecal carcinoma the tumour can become very large without obstructing the bowel, so anaemia and weight loss are the common presenting features.

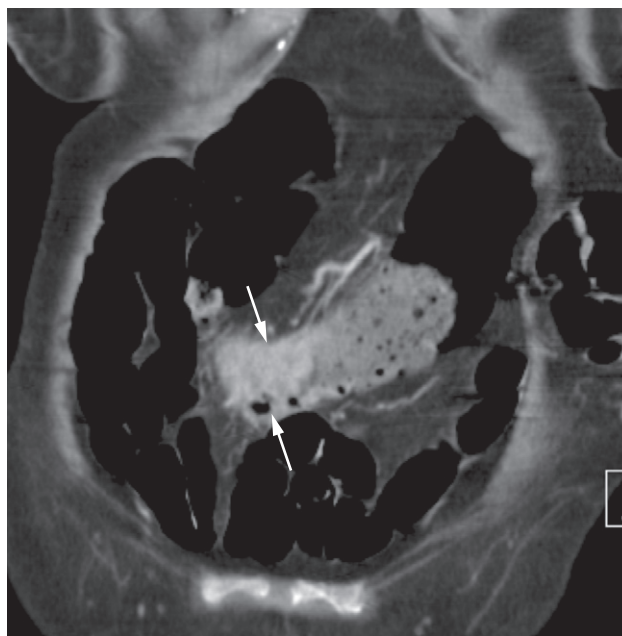
A barium enema shows annular carcinomas as an irregular stricture with shouldered edges (see Fig. 6.52). Such strictures are rarely more than 6 cm in length. The polypoid or fungating carcinoma causes an irregular filling defect projecting into the lumen of the bowel.

Multiple primary tumours must be excluded, as a patient with one carcinoma of the colon has a higher than normal risk of developing a second colonic cancer, which may be present simultaneously or after the first tumour has been removed.

Computed tomography (Fig. 6.74), particularly CT pneumocolon (Fig. 6.75), is an alternative examination to a barium enema for the diagnosis of colonic carcinoma. A



(a)



(b)

Fig. 6.74 Colon carcinoma. (a) Standard axial CT acquired on thin sections showing a tumour (arrows) in the transverse colon. (b) Coronal reformat of the same tumour (arrows).

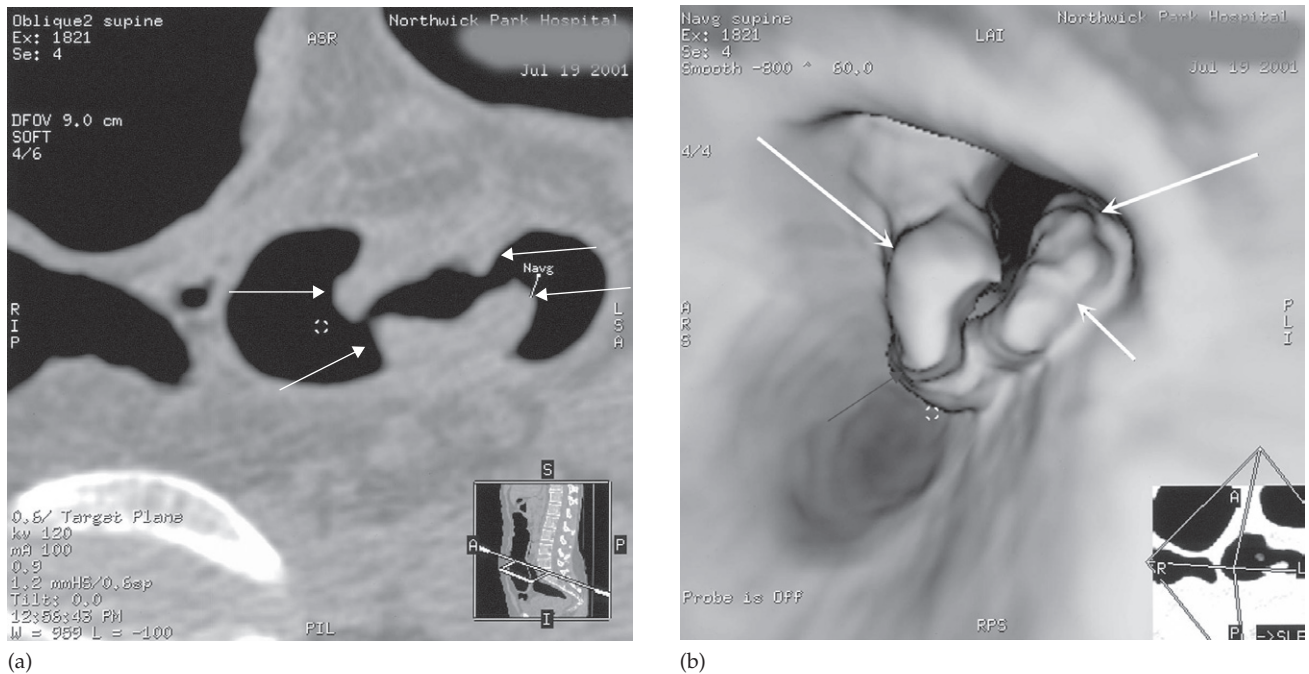


Fig. 6.75 Colon carcinoma shown by CT pneumocolon. (a) Oblique axial section showing a stricture with classic shouldered edges (arrows). (b) Virtual colonoscopy demonstrating the irregularly shaped tumour (arrows).

carcinoma can be recognized as thickening of the bowel wall and an irregular narrowing of the lumen of the colon.

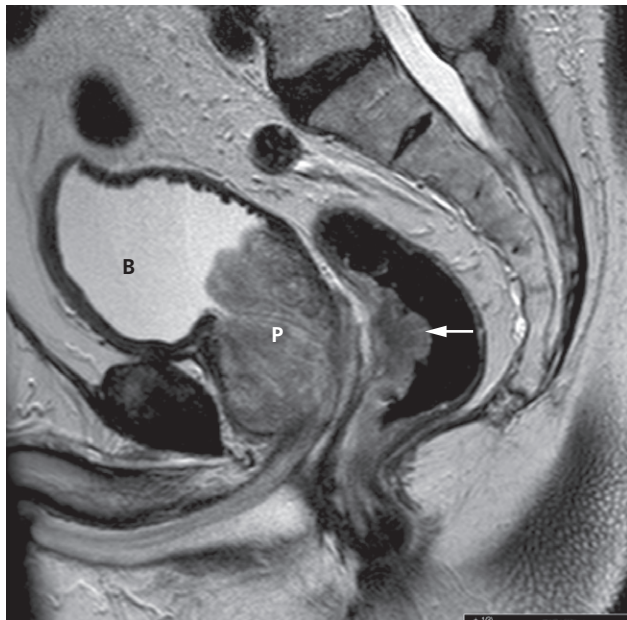
Magnetic resonance imaging is the method of choice for accurate preoperative assessment of the local extent of *rectal carcinoma*. High resolution T2-weighted images through the tumour can accurately delineate the rectum, as well as the mesorectal fat and mesorectal fascia, which surround the rectum (Fig. 6.76). The mesorectal fascia is an important anatomical landmark as it represents the surgical plane of dissection during rectal cancer surgery. The distance between tumour invading the mesorectal fat and the mesorectal fascia can be measured and the surgical resection margin safely predicted. The possibility of an involved surgical margin can be accurately anticipated (Fig. 6.77) and may significantly influence the treatment planning. The role of endoscopic ultrasound in rectal cancer is limited to very early stage disease as some tumours cannot be adequately evaluated.

Staging colorectal carcinoma. CT is used to demonstrate distant metastases to the liver or lungs and to identify para-

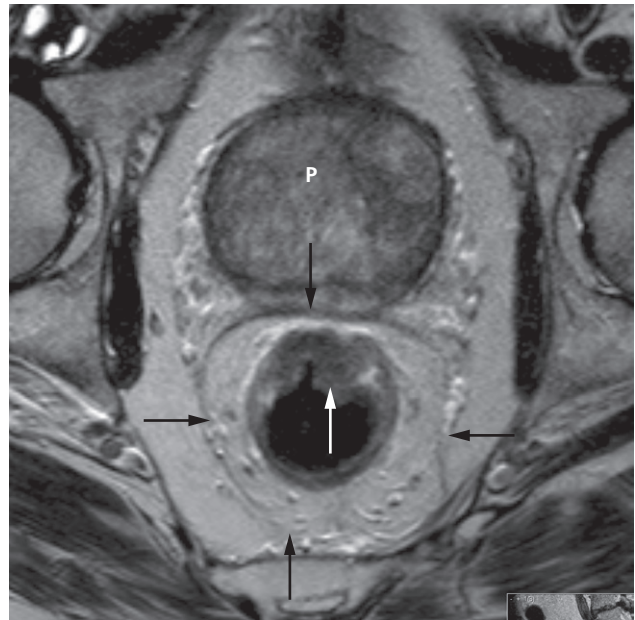
aortic nodal disease. CT can also inform on the local staging of a colonic tumour (e.g. infiltration into abdominal or pelvic organs) although the definitive extent of local disease may not be known until the time of surgery (Fig. 6.78). FDG-PET/CT is not currently used routinely for initial staging of colorectal cancer, but it is more sensitive than CT in the detection of metastatic sites of disease and is used in suspected recurrent disease in patients who are to be considered for potential curative surgery (e.g. hepatic resection for liver metastases) to ensure there are no other sites of recurrence.

Hirschsprung's disease (congenital aganglioneosis)

Hirschsprung's disease is due to the absence of ganglion cells beyond a certain level in the colon, usually in the sigmoid or rectosigmoid region. In time, the colon proximal to the aganglionic segment becomes grossly distended, but in those patients who present soon after birth the dilatation may not be obvious.



(a)



(b)

Fig. 6.76 MRI of rectal carcinoma. (a) Sagittal T2-weighted image demonstrating a polypoid growth (arrow) arising from the anterior wall of the rectum. Note the benign hyperplasia of the prostate (P) and a slightly trabeculated bladder (B). (b) Axial image of the same tumour (white arrow). Note the mesorectal fascia (black arrows) that encases the mesorectal fat and the rectum.

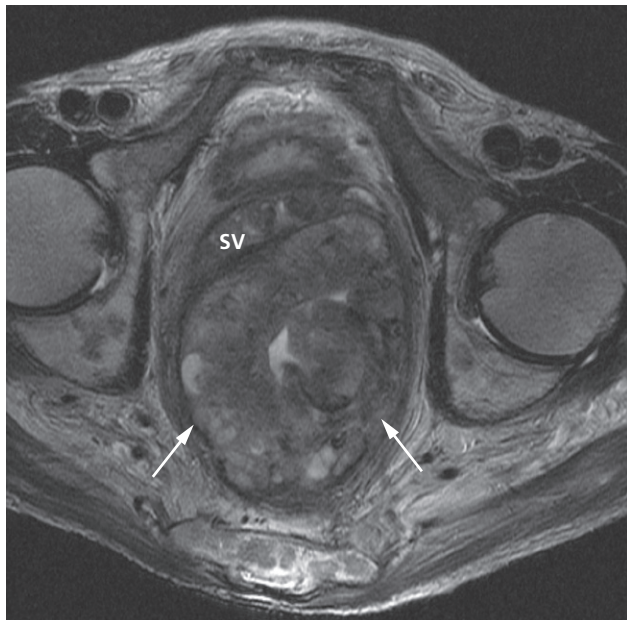


Fig. 6.77 MRI of advanced rectal carcinoma. The tumour (arrows) has completely invaded the perirectal fat and fascia and there is infiltration of the seminal vesicles (SV).

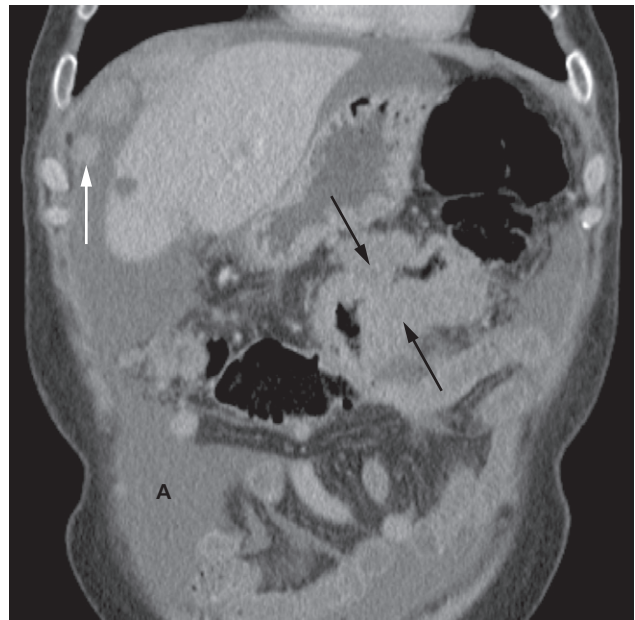


Fig. 6.78 Locally advanced cancer of the transverse colon (black arrows) on a CT coronal reformat. Multiple peritoneal metastases (white arrow) are seen beneath the diaphragm and there is ascites (A) consistent with metastatic disease.

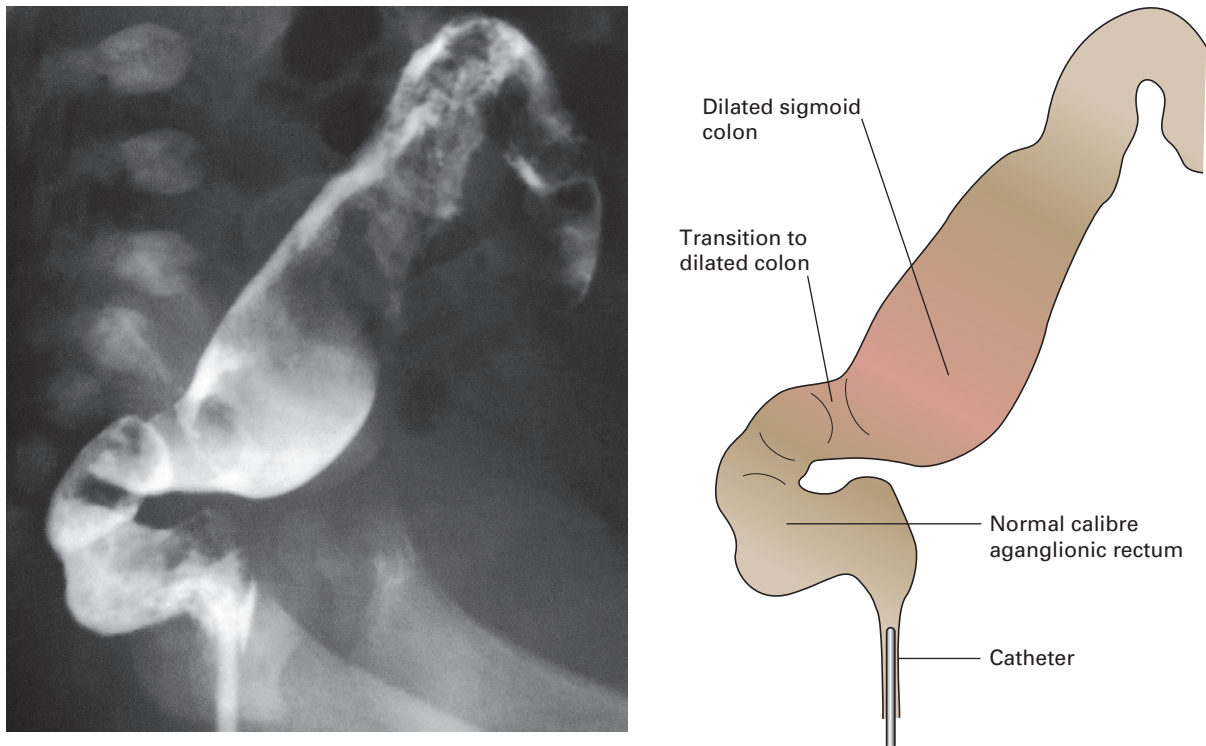


Fig. 6.79 Hirschsprung's disease. Note the transition between the normal calibre aganglionic rectum and the dilated sigmoid colon.

The aganglionic segment, usually the rectum, is either normal or small at barium enema and the diagnosis depends on recognizing the transition from the normal or reduced calibre colon to the dilated colon (Fig. 6.79). To prevent the danger of water intoxication from the dilated colon, the colon is not washed out before the barium enema. The barium introduced is usually limited to the amount required to show the zone of transition from aganglionic to dilated bowel.

Idiopathic megacolon (functional megacolon)

The cause of idiopathic megacolon is believed to be chronic constipation. Both the rectum and colon are dilated and contain a large amount of faeces. The large-sized rectum serves as a differentiating feature from Hirschsprung's disease.

Anal fistula and perianal abscess

Most anal fistulae are simple low tracks that can be assessed by clinical examination and do not require imaging. MRI is the best method of demonstrating the course of an anal fistula and in complex or recurrent cases is used to help plan the surgical approach (see Fig. 6.43).

SPECIFIC USES OF IMAGING IN THE GASTROINTESTINAL TRACT

Imaging investigation of the acute abdomen

The term 'acute abdomen' refers to the rapid onset of symptoms – such as pain, nausea and vomiting – which may indicate serious intra-abdominal pathology. The differential diagnosis is wide (Box 6.8).

Box 6.8 Common causes of acute abdomen

- Small bowel obstruction
- Large bowel obstruction
- Paralytic ileus
- Acute appendicitis/Meckel's diverticulum
- Peptic ulcer disease
- Diverticulitis
- Severe colitis
- Intra-abdominal abscess
- Gastroenteritis
- Acute intestinal ischaemia/infarction
- Acute cholecystitis
- Acute pancreatitis
- Ectopic pregnancy
- Pelvic inflammatory disease
- Leaking/ruptured abdominal aortic aneurysm
- Acute thoracic disease, e.g. myocardial infarction or pneumonia
- Renal tract pathology

A careful history and physical examination are always needed when evaluating a patient with suspected acute abdomen. The diagnostic imaging aspects of the specific conditions are discussed in the relevant sections of this and other chapters. The following discussion concentrates on the *role* of various imaging investigations in patients with an acute abdomen.

Plain films

The diagnosis of *perforation of the GI tract* is aided by demonstrating a spontaneous pneumoperitoneum on plain abdominal or chest films (see Chapter 5, Fig. 5.7). Erect chest x-rays are usually requested at the same time as an abdominal film to exclude acute pulmonary conditions that can cause acute abdominal pain, notably pneumonia close to the diaphragm. An upright chest x-ray is also a more sensitive method for detecting a pneumoperitoneum than an abdominal x-ray film, even when the abdominal film is taken in the upright position.

Dilatation of the bowel is the cardinal sign of *intestinal obstruction* on plain abdominal films, and the pattern of dilatation is the key to the radiological distinction between small and large bowel obstruction (see Chapter 5 for a description of plain film findings).

Barium or Gastrografin follow-through

If the cause or site of intestinal obstruction is not evident from clinical examination (e.g. strangulated hernia, previous surgery, widespread malignancy) and plain films, and providing immediate exploratory surgery is not indicated, a contrast follow-through study may be helpful. *Gastrografin* is used in preference to barium. If the contrast agent is seen within the large bowel at 24 hours, conservative management is likely to be successful. If there is mechanical obstruction in the proximal small bowel, then the contrast will remain in the dilated stomach and proximal small bowel at 24 hours. Unfortunately, in distal small bowel obstruction, the contrast becomes too diluted to determine the nature of any obstruction, but the absence of contrast in the large bowel does indicate that the obstruction is in the small bowel.

Ultrasound

Transabdominal ultrasound is an easily performed procedure in acutely ill patients, and can be a bedside procedure if necessary. It is, therefore, a useful test for a variety of acute abdominal conditions, particularly for imaging acute disease of the biliary, urinary and gynaecological tracts, and for imaging the acute abdomen in children, notably when looking for pyloric stenosis and intussusception. Ultrasound has the disadvantage that gas in the GI tract, which is often a particular feature in many acute abdominal conditions, creates substantial blind spots.

Computed tomography

Computed tomography provides similar information to ultrasound, but without blind spots, and is being increasingly used, often as the initial imaging examination. CT provides much more information than plain films because it shows not only the gas inside and outside the bowel more sensitively and in more detail than on plain film, but it also demonstrates the abdominal wall, the peritoneal cavity and the state of all the solid organs within the abdomen. CT is, therefore, the best overview technique to demonstrate ascites, bowel perforation or inflammation (Fig. 6.80), and many acute disorders of the liver, spleen, pancreas and

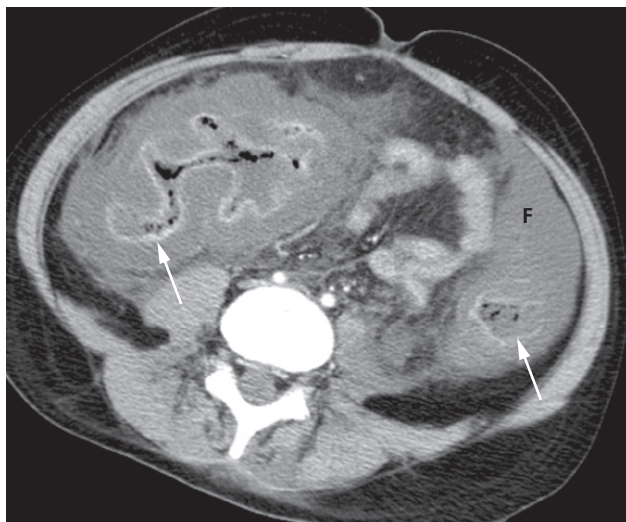


Fig. 6.80 Pseudomembranous colitis secondary to *Clostridium difficile* infection. There is gross thickening of the colonic wall, thickened enhancing mucosa (arrows) and inflammatory changes and free fluid (F) in the surrounding tissues.

kidneys. It can be a useful technique in selected cases of intestinal obstruction to demonstrate the site of obstruction by showing the location of the transition from dilated to collapsed bowel, and also to confirm or exclude a mass at the site of obstruction, although the commonest causes of small bowel obstruction, adhesions, are not usually visible. CT is also valuable for triaging patients with non-specific acute abdominal pain, particularly in patients with marked obesity, unclear ultrasound findings and possible bowel obstruction, and is the examination of choice in patients with palpable abdominal masses, suspected abdominal aortic aneurysm or retroperitoneal disease.

Imaging investigation of acute bleeding from the gastrointestinal tract

The gold standard investigation for acute GI haemorrhage is endoscopy. The source of haemorrhage in the upper GI tract (i.e. within the oesophagus, stomach or duodenum) can usually be diagnosed and treated at endoscopy.

In lower GI haemorrhage (including the small and large bowel), endoscopy is less helpful as the site and cause of

the bleeding can be obscured by the blood within the bowel. In most cases, the acute bleed resolves spontaneously, and then the bowel may be prepared with purgatives for diagnostic colonoscopy. If, however, there is uncontrolled lower GI haemorrhage, then CT arthrography is very helpful in identifying the source of the bleeding and any variant arterial anatomy that may be present prior to considering whether mesenteric embolization or surgery is the best management option (Fig. 6.81).

Nuclear medicine techniques may be employed to localize the bleeding but require a rate of more than 0.5 mL/min and have been superseded by more modern multislice CT scanners. They are occasionally used to investigate more chronic bleeding and require the patient's red blood cells to be labelled with ^{99m}Tc prior to imaging with a gamma camera, so that any blood collecting in the bowel will be visualized. Radionuclide imaging is very sensitive for identifying active bleeding, although localizing the exact site of bleeding can be difficult. Barium studies are never used in investigating acute GI haemorrhage, because the presence of barium may preclude other investigations.

Colonic bleeding in adults is most commonly due to diverticular disease, angiodysplasia, malignancy or inflammatory bowel disease (Crohn's disease and ulcerative colitis). Colonic diverticular disease is most common in the sigmoid colon. Angiodysplasia is a submucosal vascular lesion, usually found in the caecum or ascending colon, and is a fairly common cause of bleeding in elderly patients. Colonoscopy is usually performed but may be unrewarding as it is sometimes not possible to reach the right side of the colon. Even when the caecum is reached, angiodysplasia may not be visible through the colonoscope.

The causes of bleeding in the small bowel are all rare but include benign and malignant tumours, vascular malformations, jejunal diverticula, Meckel's diverticulum and inflammatory bowel disease. Meckel's diverticulum, if it contains ectopic gastric mucosa, may be responsible for unexplained bleeding, particularly in children. Meckel's diverticulum is very difficult to demonstrate on a barium follow-through, but may be visualized with radionuclide techniques. An intravenous injection of ^{99m}Tc (^{99m}Tc -pertechnetate) is given, which localizes in gastric mucosa. High uptake is seen in the stomach and in any gastric mucosa within a Meckel's diverticulum (Fig. 6.82).



(a)



(b)

Fig. 6.81 Acute lower GI bleed. (a) CT arteriogram demonstrating arterial blush at the site of bleeding in the transverse colon (arrow). (b) Digital subtraction arteriogram in the same patient showing active extravasation (arrow) from a branch of the inferior mesenteric artery, which was subsequently embolized.



Fig. 6.82 Meckel's diverticulum. ^{99m}Tc -pertechnetate scan showing an isolated area of uptake in the ectopic gastric mucosa in a Meckel's diverticulum (arrow). Normal uptake of radionuclide is seen in the stomach.

Imaging investigation of abdominal trauma

Initial imaging in cases of abdominal trauma is usually with plain x-ray in order to identify free gas, in addition to bony injuries. A very rapid assessment for intra-abdominal free fluid (which is usually blood in the trauma setting) can be undertaken with FAST ultrasound (see Chapter 7) and CT. Although ultrasound may be helpful in the detection of haemoperitoneum in the unstable patient, CT is used to detect injuries of the solid organs and the GI tract (see Figs 7.21 and 7.46). Vascular injuries may also be detected. CT is performed using intravenous contrast media in order to

assess the integrity of the major vessels and the vascular supply to the solid organs. Fracture of solid organs is associated with areas of low attenuation and disruption of the organ; in addition, there is adjacent haemorrhage. Perforation of the GI tract will be accompanied by free intraperitoneal air. Diaphragmatic rupture is well demonstrated by performing coronal reformats. Bone window settings must be reviewed to detect pelvic and vertebral fractures. Fractures may be displayed using reformatted coronal, sagittal and three-dimensional views, which may be helpful in surgical planning.

Hepatobiliary System, Spleen and Pancreas

Many different methods of imaging the hepatobiliary system and pancreas are available, notably ultrasound, computed tomography (CT), radionuclide imaging and magnetic resonance imaging (MRI). Invasive studies such as percutaneous or operative cholangiography and endoscopic retrograde cholangiopancreatography (ERCP) may be indicated. Every test has its own advantages and disadvantages. Ultrasound, for example, is particularly useful for diagnosing gall bladder disease, recognizing dilated bile ducts, diagnosing cysts and abscesses, and defining perihepatic fluid collections, whereas CT and MRI are particularly sensitive for detecting and characterizing mass lesions such as metastases and abscesses. Often the various methods complement each other, and, in practice, the imaging techniques used will depend on local expertise and may vary from centre to centre.

Although in clinical practice the liver and biliary tree are usually considered together, for the sake of clarity we will discuss them independently. Interventional techniques designed to treat or remove gall stones and to drain the biliary system are described in Chapter 17.

LIVER

Imaging techniques

Ultrasound

The *normal hepatic parenchyma* (Fig. 7.1) is of uniform echogenicity, composed of medium and low level echoes, interspersed with the bright echoes of the portal triads and

echo-free areas corresponding to large hepatic veins. The normal liver displays considerable variation in size and shape. The right hepatic lobe is much larger than the left, which may be small. The falciform ligament, which contains the ligamentum teres, lies between the medial and lateral segments of the left lobe. The ligamentum teres is often surrounded by fat; the resulting echo pattern should not be confused with a mass (Fig. 7.2).

The portal vein within the liver divides into the right and left branches. Running alongside the portal veins are the hepatic arteries and bile ducts, both of which are usually too small to be visualized within the liver. Surrounding these portal triads is an echo-reflective sheath of fibrous and fatty tissue. The hepatic veins run separately, increasing in diameter as they drain towards the inferior vena cava at the level of the diaphragm (Fig. 7.3).

Focal masses are recognized as alterations of the normal echo pattern. They can be divided into cysts, solid masses or complex combinations of the two. Cysts that are echo-free and have thin or invisible walls can be assumed to be benign (Fig. 7.4). Solid and complex masses (Figs 7.5 and 7.6) within the liver may be either benign or malignant in nature. Theoretically, most benign solid masses are well defined and should demonstrate a relatively sharp margin with the adjacent hepatic parenchyma, whereas malignant lesions may demonstrate a more irregular border. However, in practice it is often difficult to distinguish benign from malignant lesions unless the mass is clearly a simple cyst.

When multiple solid or complex masses are seen within the liver, metastatic disease is the likely diagnosis, especially in patients with a known primary tumour. The

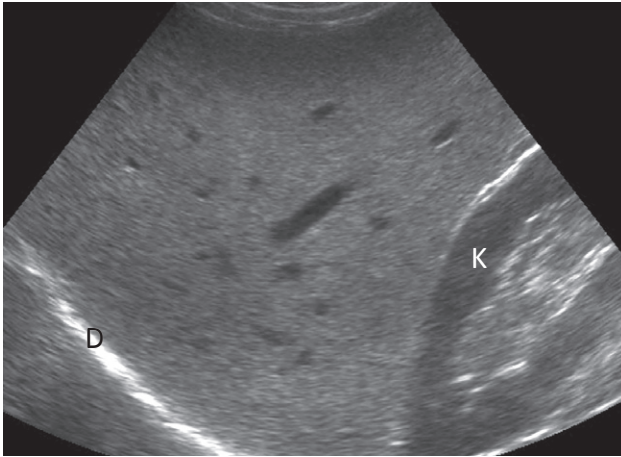


Fig. 7.1 Ultrasound of normal liver. Longitudinal scan showing a uniform echo pattern interspersed with bright echoes of portal triads and echo-free areas of hepatic and portal veins. D, diaphragm; K, right kidney.

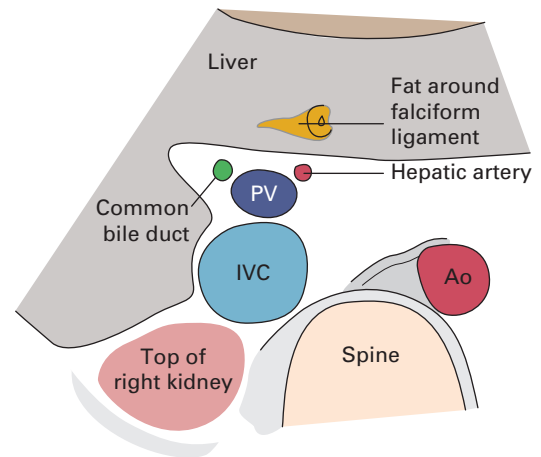
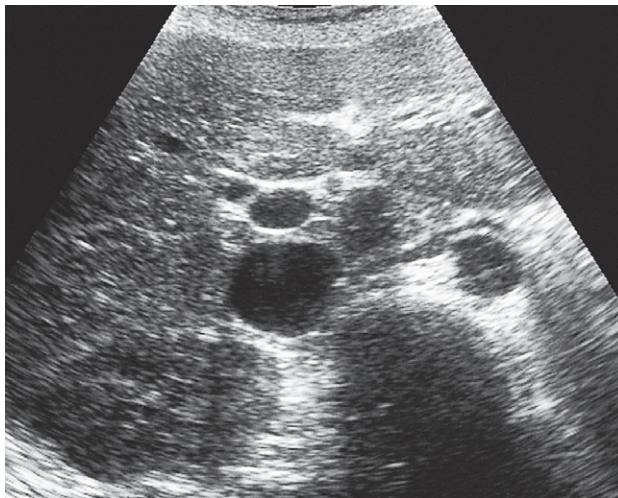


Fig. 7.2 Ultrasound of normal liver. Transverse scan across the porta hepatis. Ao, aorta; IVC, inferior vena cava; PV, portal vein.

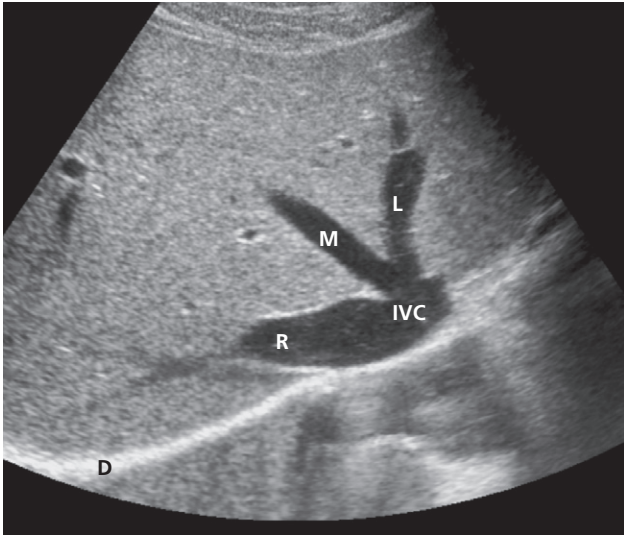


Fig. 7.3 Ultrasound of normal liver. Transverse scan through the superior portion of the liver showing the right (R), middle (M) and left (L) hepatic veins draining into the inferior vena cava (IVC) as it penetrates the diaphragm (D).

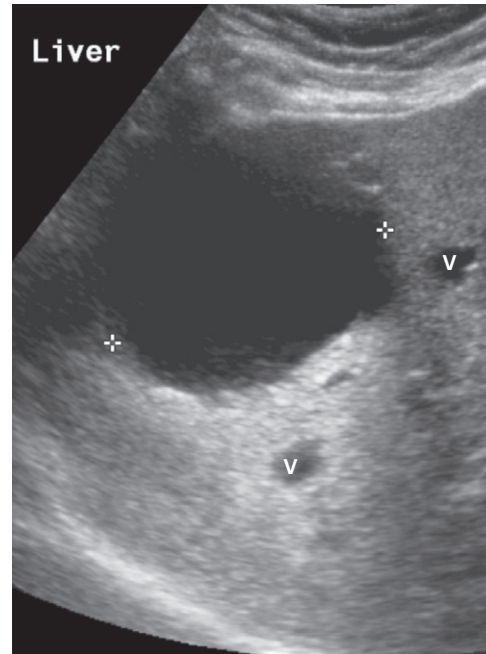


Fig. 7.4 Ultrasound of a benign cyst. Note the imperceptible wall and absence echoes within the cyst. There is also posterior acoustic enhancement (increased echogenicity of structures deep to the cyst) secondary to enhanced transmission of the ultrasound waves through the water density of the cyst. V, hepatic veins.

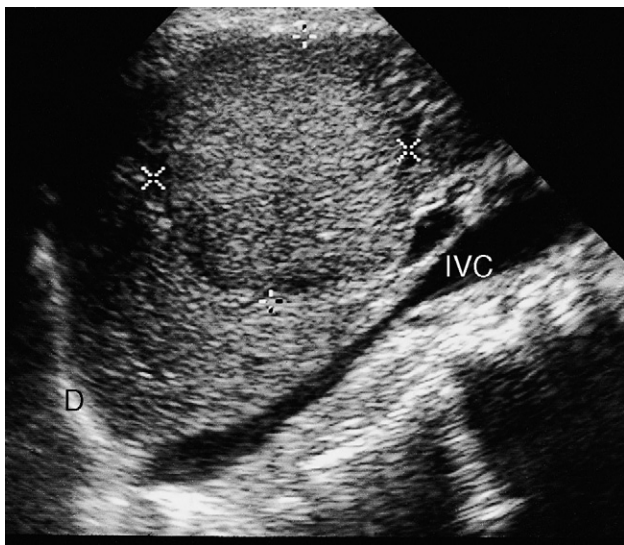


Fig. 7.5 Ultrasound of a solid mass. Longitudinal scan showing an echogenic mass (indicated by cursors), which proved to be a metastasis. D, diaphragm; IVC, inferior vena cava.

differential diagnoses of multiple masses are multiple abscesses, regenerating nodules in cirrhosis of the liver and multiple haemangiomas.

Diffuse parenchymal diseases such as diffuse chronic inflammation and diffuse neoplastic infiltration can cause a generalized increase in the intensity of echoes from the liver parenchyma, and are difficult to distinguish from one another.

Computed tomography

Intravenous contrast medium is usually given in order to increase the density of normal liver parenchyma and to emphasize the density difference between the normal parenchyma and lesions that enhance poorly, such as tumours or abscesses (Fig. 7.7). It is possible to visualize the different phases of liver opacification by taking scans



Fig. 7.6 Ultrasound of complex mass. Longitudinal scan of an abscess showing a spherical mass (arrows) with areas of echogenicity both greater and less than normal liver.

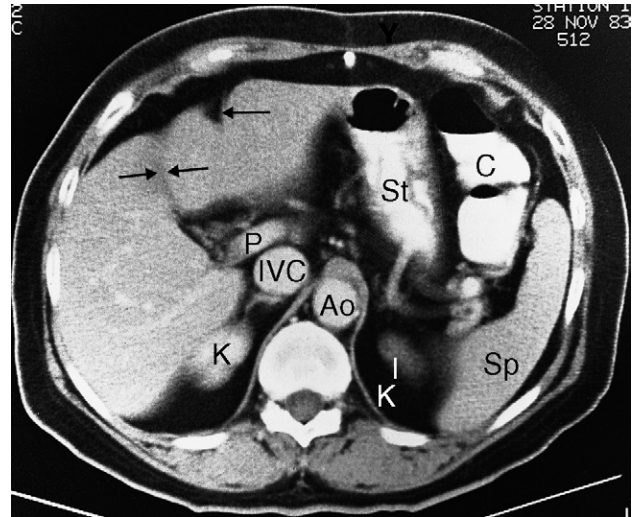


Fig. 7.7 CT scan of normal liver through the porta hepatis (enhanced scan). Ao, aorta; C, colon; IVC, inferior vena cava; K, kidney; P, portal vein; Sp, spleen; St, stomach. The single arrow indicates a fissure for the falciform ligament, and the double arrows a fissure for the gall bladder, which divides the liver into the right and left lobes.

at varying times after the injection of contrast. The liver has a dual blood supply from the hepatic artery and portal vein. Most metastases are best demonstrated as low attenuation areas during the portal venous phase on a scan taken 60–70 seconds after the injection of contrast. Scanning during the arterial phase, about 30 seconds after the injection of contrast, will show lesions such as haemangiomas and some neoplasms, particularly hepatomas and highly vascular metastases (e.g. carcinoid), as areas of greater enhancement than the surrounding parenchyma.

Anatomically, the liver is divided into eight functionally independent segments (Fig. 7.8). Each segment has its own hepatic artery and portal venous inflow, hepatic venous drainage and biliary drainage. This classification is important in hepatic surgery as each segment can be resected without damaging the remaining ones. For the liver to remain viable, resections must proceed along the vessels that define the peripheries of these segments. This means that resection lines run parallel to the hepatic veins. The

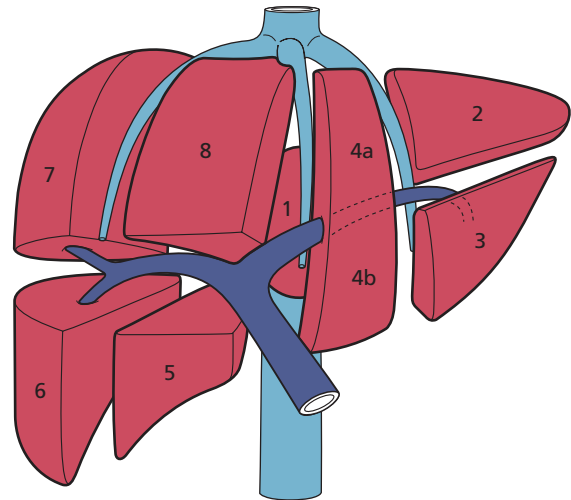


Fig. 7.8 The liver is divided anatomically into eight segments, each of which has its own independent vascular supply and biliary drainage.

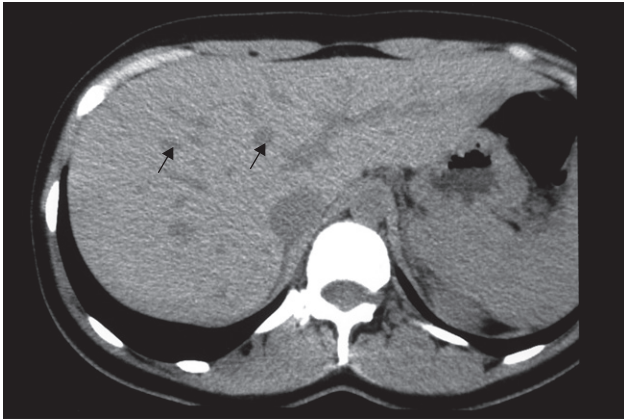


Fig. 7.9 CT scan of normal liver showing unopacified veins (arrows), which should not be confused with metastases.

fissure for the gall bladder divides the liver into the right and left lobes and the falciform ligament divides the left lobe into the medial and lateral segments.

The normal hepatic parenchyma has a relatively high density prior to contrast enhancement; higher than that of muscle and higher or equal in density to the spleen. On images taken without intravenous contrast medium, the hepatic veins and portal veins are seen as branching, low density structures coursing through the liver. As CT is a sectional technique, some of these branches may be seen as round or oval low density areas, which should not be confused with metastases (Fig. 7.9). After contrast enhancement, the veins opacify to become similar or higher in density than the surrounding parenchyma. Because the normal intrahepatic bile ducts are not visible and hepatic vessels opacify with the contrast medium, the normal hepatic parenchyma shows either uniform density or shows the veins clearly opacified against a background of uniform density. The region of the porta hepatis is recognizable as the entrance and exit points of the major vessels and bile ducts. The biliary system distal to the right and left hepatic ducts can be identified, but the smaller intrahepatic bile ducts are not visible in the normal patient.

Magnetic resonance imaging

Magnetic resonance imaging is used as a problem-solving technique to give additional information to ultrasound and

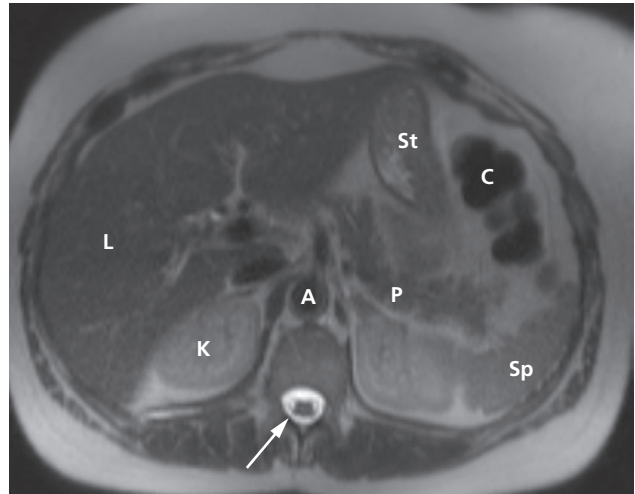


Fig. 7.10 Normal T2-weighted MRI scan of the upper abdomen. The liver parenchyma (L) shows intermediate signal intensity. The cerebral spinal fluid has high signal intensity (arrow). A, aorta; C, splenic flexure of colon; K, kidney; P, pancreas; Sp, spleen; St, stomach.

CT. It is, however, also an excellent technique for demonstrating primary and secondary tumours and is often used if hepatic surgery is contemplated. Axial sections give images akin to CT (Fig. 7.10), but images can also be obtained in the coronal and sagittal planes. Intravenous contrast is used to improve visualization and help characterize lesions. New liver-specific agents are being developed: some are taken up by hepatocytes and some by the reticuloendothelial cells. Malignant tumours do not normally possess hepatocytes or reticuloendothelial cells, so there is heightened contrast between the tumour and normal liver.

Liver masses

Ultrasound, CT and MRI are all good methods of deciding whether a mass is present (Box 7.1). Modern imaging techniques can go a long way to predicting the nature of the mass, though occasionally the definitive diagnosis depends on biopsy. This, however, should not be undertaken in a potentially resectable lesion without discussion with a hepatic surgeon as seeding along the biopsy tract may compromise the surgical field.

Box 7.1 Types of liver masses**Malignant**

- Metastases
- Hepatocellular carcinoma (HCC)
- Cholangiocarcinoma
- Fibrolamellar carcinoma
- Sarcomas (rare)

Benign

- Hepatic cysts
- Biliary hamartomas
- Haemangiomas
- Hepatic adenomas (can have malignant potential)
- Focal nodular hyperplasia
- Liver abscesses
- Regenerating nodules in cirrhotic liver

Malignant liver neoplasms

Metastases, notably from carcinoma of the stomach, colon, pancreas, lung and breast, are much more common than primary tumours (hepatoma and malignant lymphoma, both of which can be multifocal).

Metastases are often multiple, situated peripherally and of variable size. At ultrasound, they may show increased echogenicity (Fig. 7.11a) or, more usually, decreased echogenicity compared with the surrounding parenchyma (Fig. 7.11b). At times, they show a complex echo pattern and when they undergo central necrosis they may even resemble cysts. A metastasis may have an echogenic centre, giving an appearance described as a ‘target lesion’ (Fig. 7.11c). Some metastases have an echo pattern virtually identical to that of the surrounding parenchyma, which means they cannot be identified at sonography.

At CT, metastases are seen as rounded areas, usually lower in density than the contrast-enhanced surrounding parenchyma (Fig. 7.12a). Most are well demarcated from the adjacent parenchyma. Intense contrast enhancement is sometimes seen within the tumour, or immediately surrounding it – a useful differentiating feature, which is not seen with cysts. Some metastases, notably carcinoid, are hypervascular and appear as high density areas on arterial phase images (Fig. 7.12b).

Magnetic resonance imaging is an excellent method of demonstrating metastases, which typically have a signal lower than normal liver on a T1-weighted scan and a high

signal intensity on a T2-weighted scan (Fig. 7.13). Various intravenous contrast agents may be used to aid their visualization.

Primary carcinomas of the liver, which include hepatocellular carcinoma (HCC) and cholangiocarcinoma, are usually solitary but they may be multifocal. Their CT (Fig. 7.14), ultrasound and MRI features are similar to metastatic neoplasms. Fibrolamellar carcinoma is a rare tumour, often presenting in adolescents/young adults as a large mass, often with a central calcified scar.

Benign liver masses

Benign masses are encountered fairly frequently in the general population. Most are cysts, some are haemangiomas. Focal nodular hyperplasia and adenomas are rare but can closely resemble malignant masses. MRI can be very helpful in differentiating benign from malignant lesions. Interpretation of abnormalities seen in patients with established cirrhosis can be difficult as there is a spectrum of abnormalities ranging from benign regenerating nodules, through dysplastic nodules, to HCC.

Liver cysts

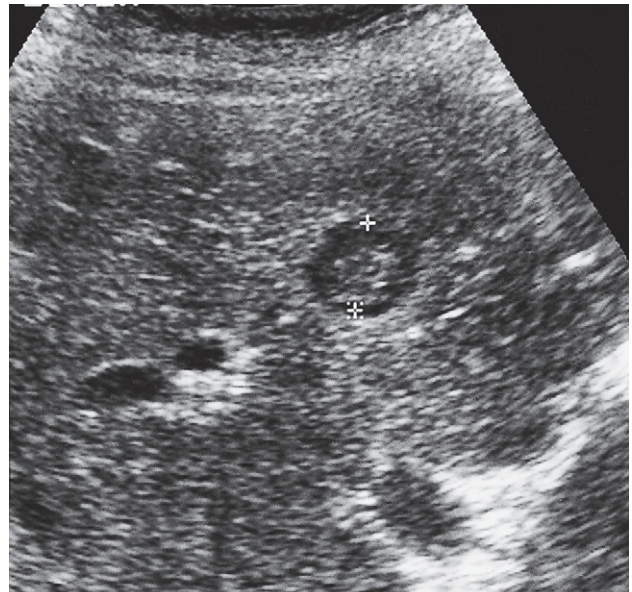
Simple cysts of the liver may be single or multiple, and are usually congenital in origin; some are due to infection. Multiple hepatic cysts occur in adult polycystic disease, which not only affects the kidneys but may also involve the liver and other organs. These cysts are variable in size and are scattered through the liver. Multiple biliary hamartomas are another rare cause of multiple small hepatic lesions. They represent disorganized clusters of dilated cystic bile ducts and have the imaging appearances of multiple small simple cysts.

At ultrasound, liver cysts show the typical features of cysts elsewhere in the body, namely a sharp margin, no echoes within the lesion, and intense echoes from the front and back walls with acoustic enhancement deep to the larger cysts (see Fig. 7.4).

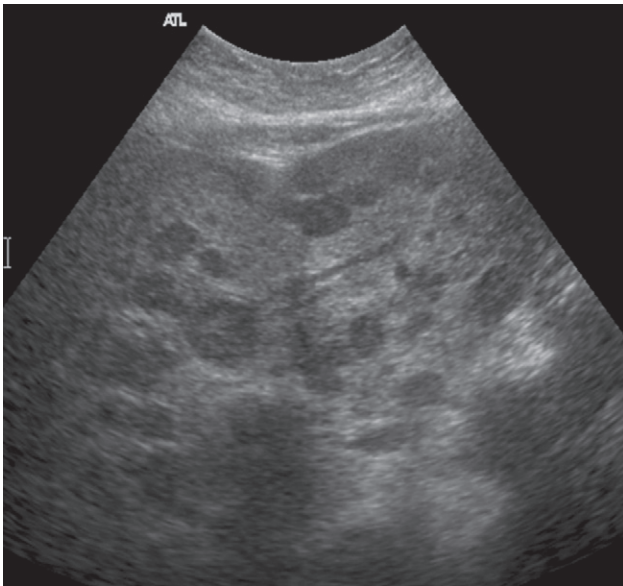
At CT, cysts show very well-defined margins and have attenuation values similar to that of water (Fig. 7.15a). It is often not possible to characterize small lesions, and with lesions below 1 cm in diameter it may be difficult to distinguish cyst from neoplasm.



(a)



(c)



(b)

Fig. 7.11 Ultrasound of liver metastases. (a) Multiple hyperechoic metastases scattered throughout the liver. (b) Multiple metastases appearing as well-defined, round, hypoechoic lesions scattered throughout the liver. (c) The cursors indicate a metastasis showing reduced echogenicity, but with an echogenic centre known as a target lesion.

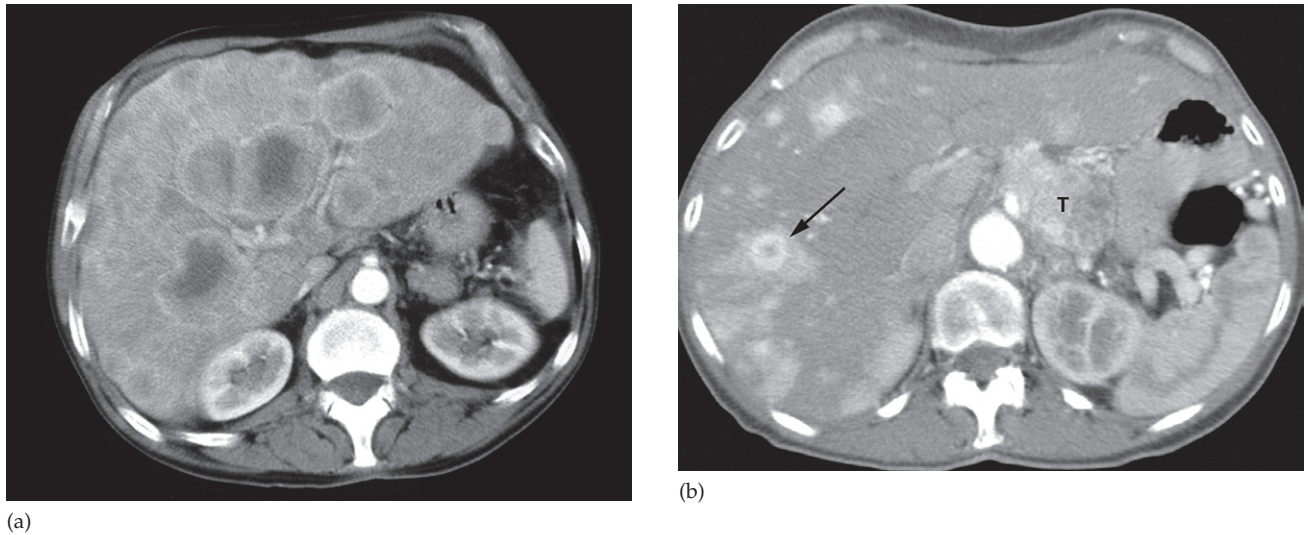


Fig. 7.12 CT scan of liver metastases. (a) There are a large number of low density lesions in both lobes of the liver, which show enhancement around their edges. The patient had carcinoma of the bronchus. (b) Vascular metastases (arrow) due to a carcinoid tumour (T) appearing as areas of high density on this arterial phase image.

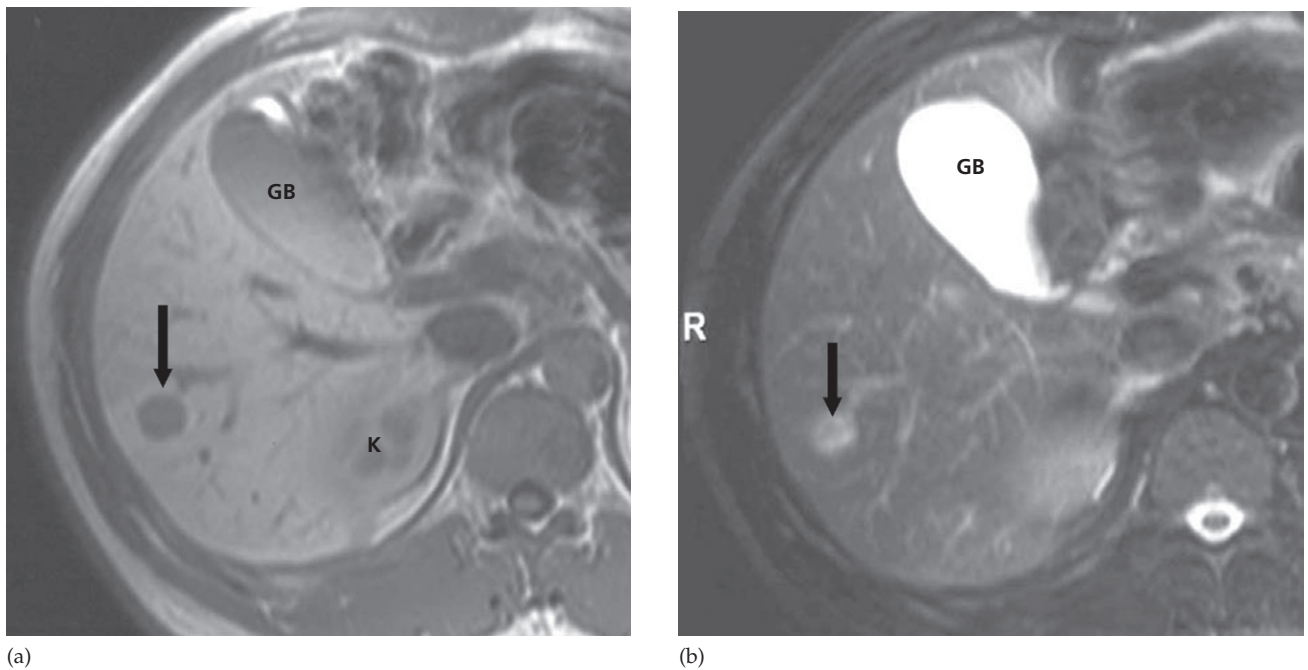


Fig. 7.13 Liver metastasis on MRI. (a) T1-weighted MRI scan showing a solitary low signal intensity focus in the liver (arrow). (b) T2-weighted MRI (with fat saturation) showing the same metastasis. This is of higher signal intensity than the normal liver parenchyma; however, the signal intensity is not as bright as a haemangioma or cyst. GB, gall bladder; K, kidney.

At MRI, the features are similar to those found at CT. Cysts have the expected signal intensity of water, namely low signal on a T1-weighted scan and high signal on a T2-weighted scan.

Cysts due to echinococcus (hydatid) disease may be single or multiple; a few show calcified walls. Daughter

cysts may be seen within a main cyst at both ultrasound and CT (Fig. 7.15b). Unless these features are present, hydatid cysts may prove indistinguishable from simple cysts at both ultrasound and CT.

Occasionally metastases can have a cystic appearance.

Haemangiomas of the liver

The detection of one or more haemangiomas of the liver is a common incidental finding and rarely requires treatment. Occasionally, they can cause significant haemorrhage, especially following trauma, and therefore percutaneous biopsy should be avoided if possible. Haemangiomas are typically well-defined, peripheral, echogenic masses at ultrasound (Fig. 7.16a). At CT, there is usually a characteristic enhancement pattern characterized by sequential contrast opacification, beginning as nodular or globular areas of enhancement at the periphery and proceeding toward the centre over time until the density increases to become similar to that of the surrounding liver (Fig. 7.16b).

Magnetic resonance imaging shows uniform very high intensity on T2-weighted images (Fig. 7.17), a characteristic that is shared with benign cysts, but which is very unusual with malignant neoplastic lesions.

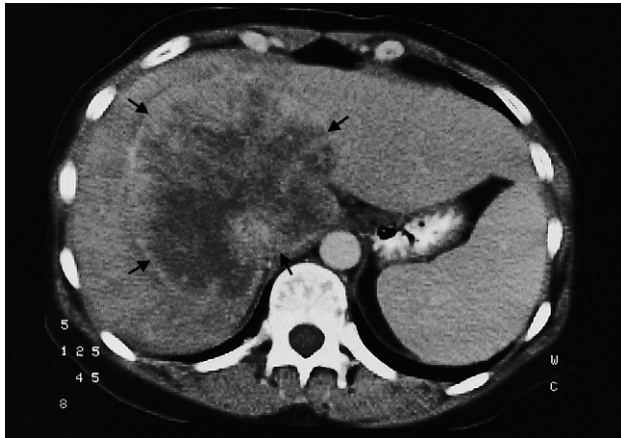
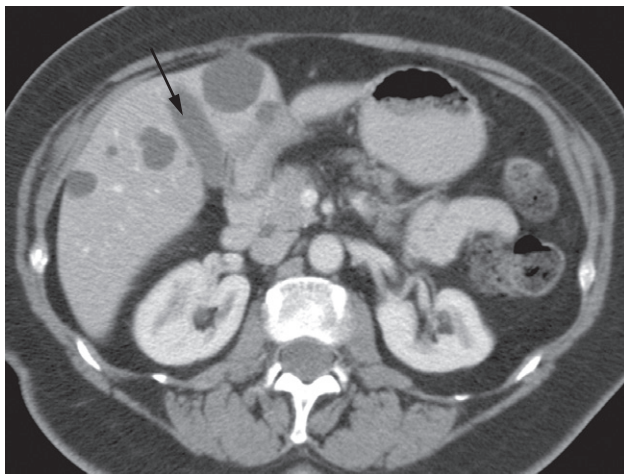
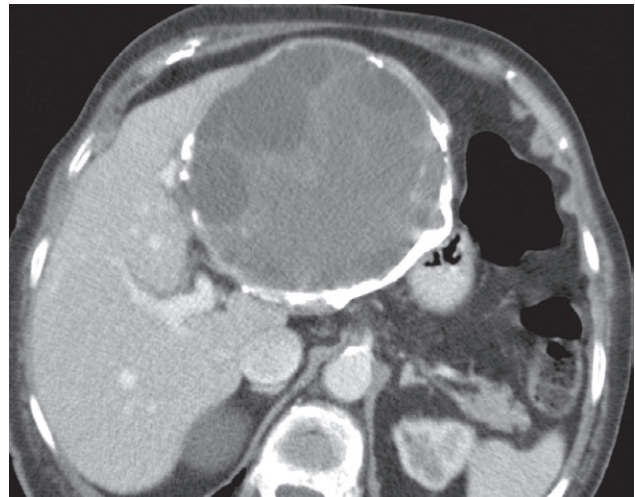


Fig. 7.14 CT scan of hepatoma showing a large mass of variable density (arrows).

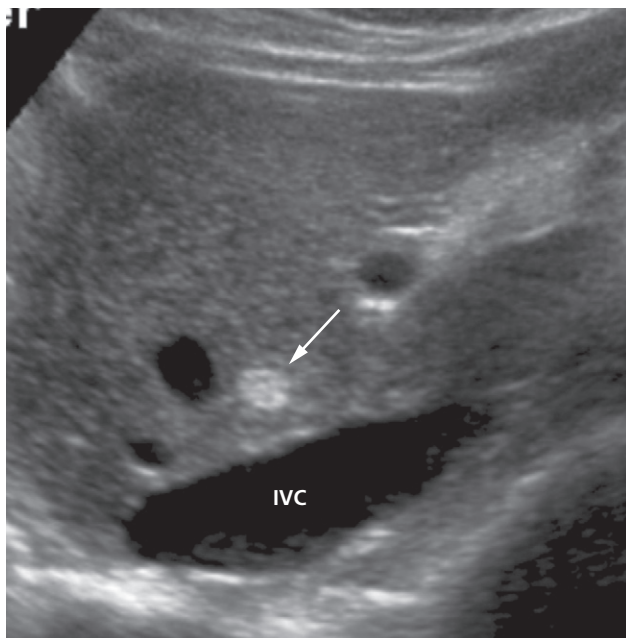


(a)

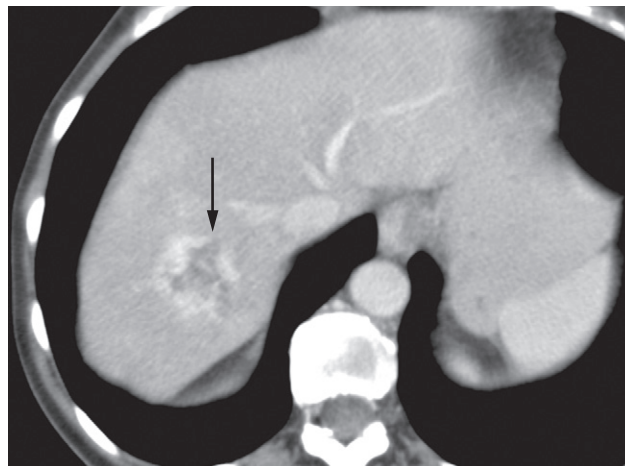


(b)

Fig. 7.15 CT scan of liver cysts. (a) Simple cysts. CT shows several well-defined, low attenuation lesions of near water density. Note their density is equivalent to the bile in the gall bladder (arrowed). (b) Complex cyst. CT scan showing a multilocular hydatid cyst with calcification in its wall.



(a)



(b)

Fig. 7.16 Haemangioma (incidental finding). (a) Ultrasound scan showing an echogenic mass in the right lobe of the liver (arrow). IVC, inferior vena cava. (b) CT scan, in another patient, after intravenous contrast enhancement showing a low density lesion in the right lobe of the liver (arrow) with peripheral nodular enhancement, characteristic of a haemangioma.

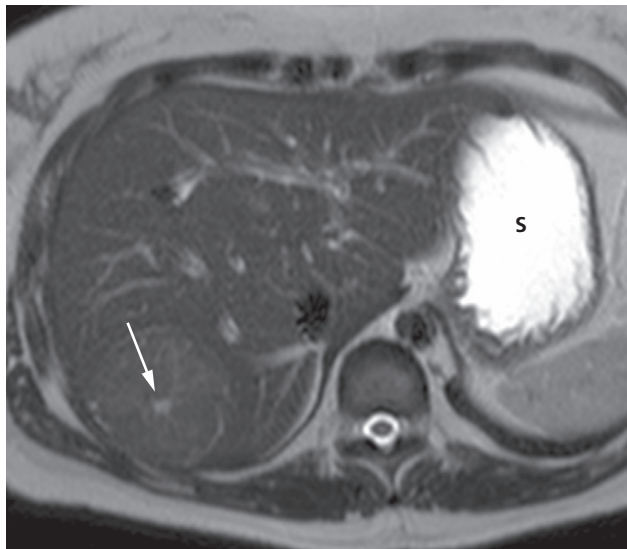


(a)

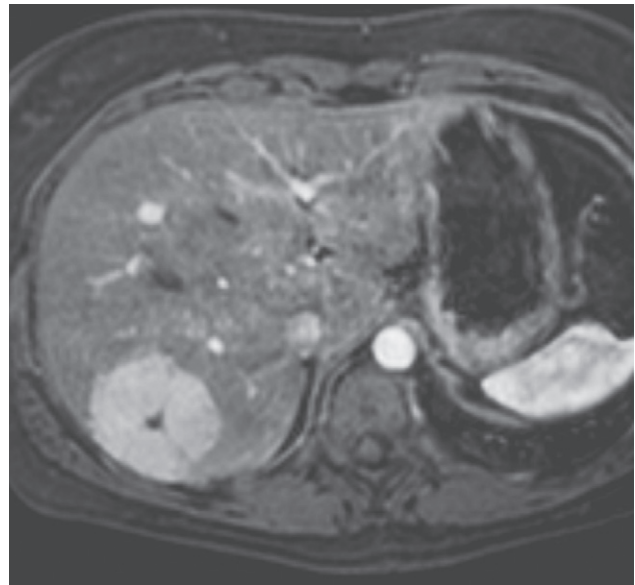


(b)

Fig. 7.17 MRI of a haemangioma. (a) Low signal intensity focus (arrow) on a coronal T1-weighted image. (b) High signal intensity focus (arrow) on a coronal T2-weighted image. L, right lung base; Sp, spleen.



(a)



(b)

Fig. 7.18 MRI of focal nodular hyperplasia. (a) Axial T2-weighted image demonstrating a mass in the right lobe of the liver that is isointense to normal liver with a hyperintense central scar (arrow). S, stomach. (b) An axial T1-weighted arterial phase image, post contrast, demonstrating avid enhancement of the mass with sparing of the central scar. These features are characteristic of focal nodular hyperplasia.

Adenoma and focal nodular hyperplasia

Both of these conditions appear as hypervascular masses on arterial phase, both on CT and MRI (Fig. 7.18).

Liver abscesses

Abscesses appear somewhat similar to cysts but usually they can be distinguished (Fig. 7.19). Hepatic abscesses tend to have fluid centres, with walls that are thicker, more irregular and more obvious than those of simple cysts. Although the CT attenuation values in the centre of an abscess may be the same as water, usually they are higher. At ultrasound, a layer of necrotic debris may be seen within the abscess. Occasionally, chronic abscesses calcify.

Abscesses cannot usually be distinguished from necrotic tumours at either ultrasound, CT or MRI, but the clinical situation should aid in making the distinction. Aspiration and drainage are invariably undertaken in any case of sus-

pected abscess and are conveniently performed under ultrasound guidance.

Cirrhosis of the liver and portal hypertension

In portal hypertension the pressure in the portal venous system is elevated due to obstruction of the flow of blood in the portal or hepatic venous systems. Cirrhosis of the liver is by far the most frequent cause. Other causes include occlusion of the hepatic veins (Budd–Chiari syndrome) and thrombosis of the portal vein, particularly following infection of the umbilical vein in the neonatal period or secondary to pancreatitis.

Because the portal venous pressure is raised, blood flows through anastomotic channels, known as portosystemic anastomoses, to enter the vena cava, bypassing the liver. These collateral channels may be found in various sites, but the most important are varices at the lower end of the

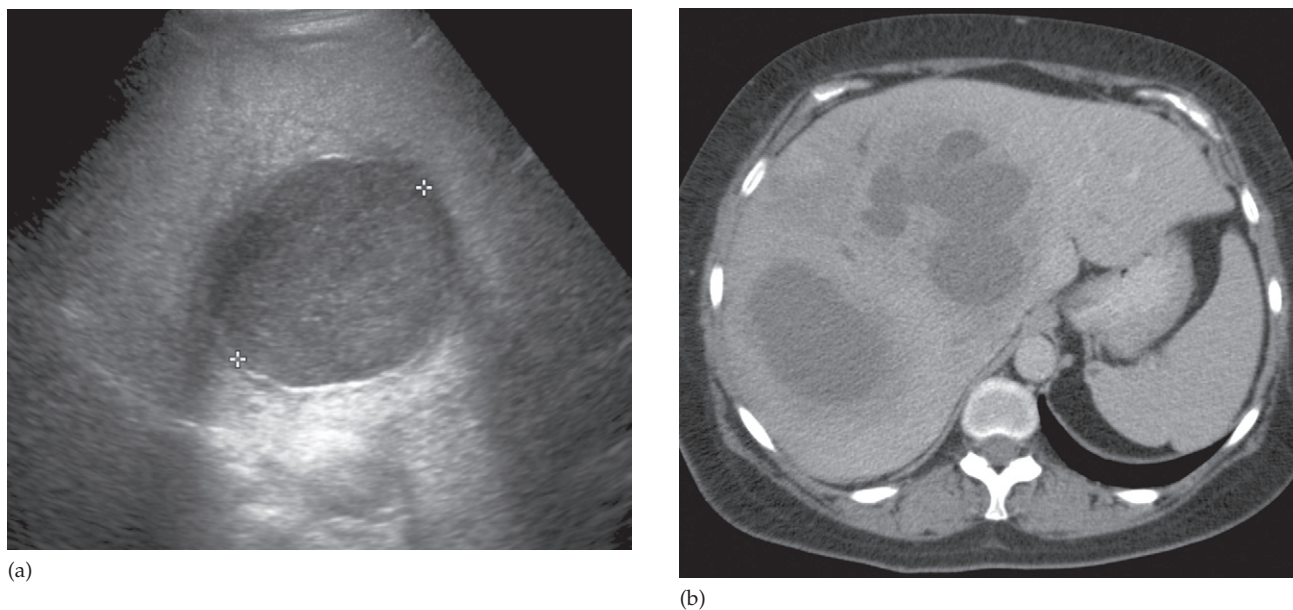


Fig. 7.19 Liver abscess. (a) Ultrasound scan showing an area of mixed echogenicity in the liver. (b) CT in another patient showing multifocal areas of low attenuation. Compared to liver cysts (see Fig. 7.15a), they are not nearly as well circumscribed.

oesophagus and in the upper abdomen (Fig. 7.20). The collateral channels can be shown with colour-flow Doppler ultrasound.

The signs of cirrhosis of the liver at CT and ultrasound are reduction in size of the right lobe of the liver and irregularity of the surface of the liver, together with splenomegaly. Ascites may be present as well. The texture of the liver at ultrasound may be diffusely abnormal; at CT, the parenchyma appears normal until late in the disease.

Patency of the splenic, portal and hepatic veins can be assessed with Doppler ultrasound, CT or MRI.

For persistent bleeding varices, the percutaneous procedure known as TIPSS (transjugular intrahepatic portosystemic shunt) can be undertaken. In this procedure, a connection between the portal and systemic venous system is created by placing a stent, to embolize the varices if required (see Chapter 17). This connects a large hepatic and portal vein within the liver, which effectively decreases the portal venous pressure and also allows access to the portal venous system.

Liver trauma

Trauma to the liver is the commonest abdominal injury that leads to death. Parenchymal lacerations are the most frequent injury and they are often accompanied by subcapsular and intrahepatic haematomas (Fig. 7.21). Ultrasound has become part of the standard assessment of patients who give a history of abdominal trauma and are hypotensive or unable to give an accurate history due to impaired consciousness. Focused assessment with sonography for trauma (FAST scan) is a rapid bedside examination that examines four areas for free fluid:

- perihepatic and hepatorenal space
- perisplenic space
- pelvis
- pericardium.

As a rapid, non-invasive, bedside test, ultrasound has significant advantages over diagnostic peritoneal lavage and CT scanning for the evaluation of free intraperitoneal fluid. The average time to perform a FAST scan in the

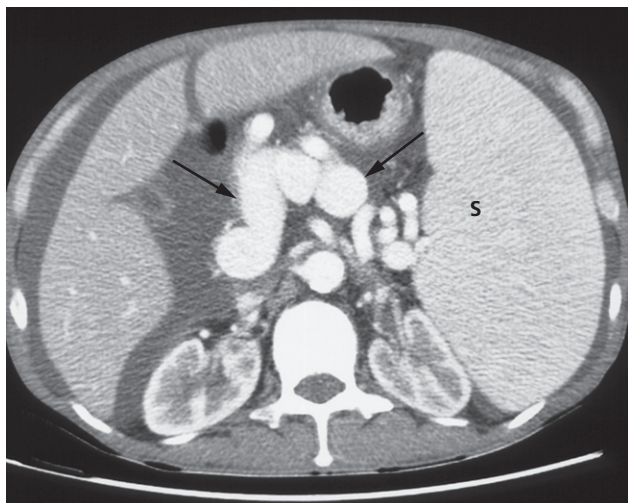


Fig. 7.20 Varices on CT due to portal hypertension. There is marked enhancement of multiple serpiginous vessels in the upper abdomen (arrows), extending into the splenic hilum. There is splenomegaly and ascites. S, spleen.

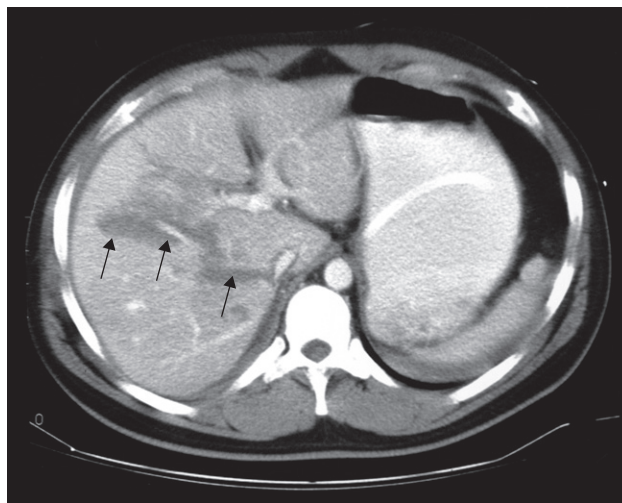


Fig. 7.21 Liver trauma. CT scan showing laceration in the right lobe of the liver (arrows). A nasogastric tube is present in the stomach.

hands of an experienced operator is 2–3 minutes. CT scanning, however, is more sensitive and specific, and lacerations and haematomas are recognized as low density areas relative to the contrast-enhanced parenchyma. Leakage of contrast indicates active bleeding.

Fatty infiltration of the liver

Fatty infiltration of the liver, whilst not normal, is a relatively frequent finding, particularly in those with hypercholesterolaemia, obesity or diabetes, patients on chemotherapy or in those who take alcohol to excess. Fatty infiltration may involve the whole liver, or it may just involve individual subsections. In some patients it is a benign process (non-alcoholic fatty liver disease), whilst in others it can proceed to cirrhosis (non-alcoholic steatohepatitis).

Fatty infiltration leads to a reduction in the attenuation of the affected parenchyma causing low density on CT scans (Fig. 7.22). The vessels are then seen as relatively high attenuation structures against a background of low density parenchyma, even on images taken without intravenous contrast medium. On ultrasound, the liver parenchyma shows increased echogenicity, the so-called 'bright liver',

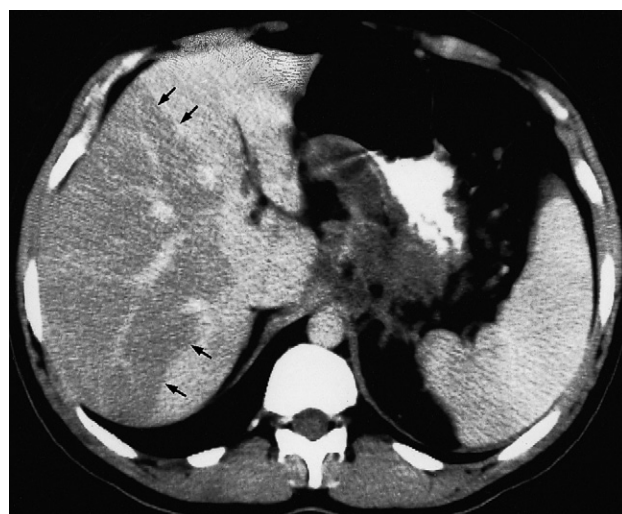


Fig. 7.22 Fatty degeneration of the liver shown by CT as a large focal area of reduced attenuation in the right lobe of the liver (arrows).

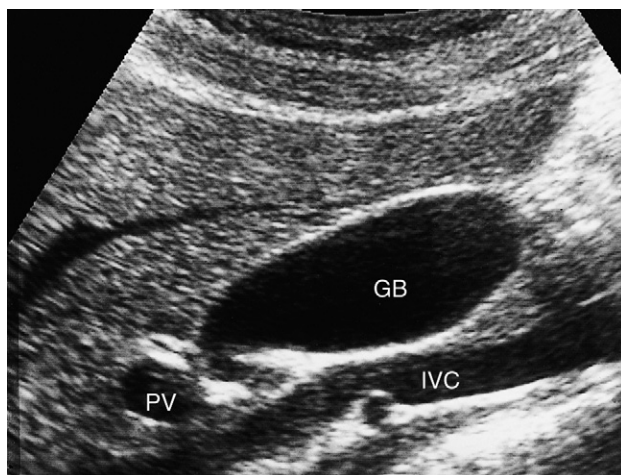


Fig. 7.23 Ultrasound of normal gall bladder. Note the thin wall and absence of echoes from within the gall bladder. GB, gall bladder; IVC, inferior vena cava; PV, portal vein.

in which the echogenicity of the liver is similar to that of the central echo complex of the kidney. MRI can be very helpful in problem cases because fat gives a characteristic set of signals.

BILIARY SYSTEM

The gall bladder and bile duct system can be demonstrated by a variety of imaging techniques. Ultrasound is the initial method of imaging because it is the simplest test for showing gall stones, diseases of the gall bladder and excluding bile duct dilatation. Occasionally, radionuclide imaging using hepatobiliary agents is used as a functional assessment to exclude biliary obstruction.

Gall stones, gall bladder wall thickening and dilatation of the common bile duct are also visible at CT, but as ultrasound provides better information it is used as the primary method of examination for these problems.

Imaging techniques

Ultrasound

As the gall bladder is a fluid-filled structure, it is particularly amenable to sonographic examination. Because it is

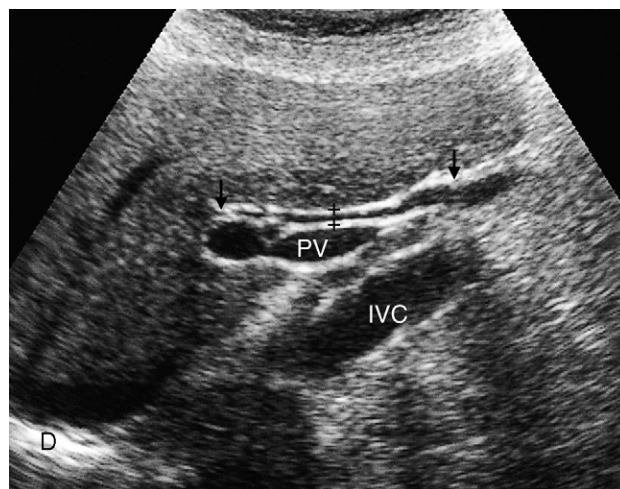


Fig. 7.24 Normal common bile duct. Longitudinal ultrasound scan showing the common bile duct, situated between the arrows, lying anterior to the portal vein. The common bile duct measures 4mm in diameter (crosses). D, diaphragm; IVC, inferior vena cava; PV, portal vein.

important that the gall bladder should be full of bile, the patient is asked to fast in order to prevent gall bladder contraction, but no other preparation is necessary. The normal gall bladder wall is so thin that it is sometimes barely perceptible (Fig. 7.23). *Gall bladder wall thickening* suggests either acute or chronic cholecystitis. *Gall stones* greater than 1 or 2mm in size can usually be identified at ultrasound examination. It is usually impossible to diagnose cystic duct obstruction with ultrasound; the cystic duct is too small to identify and the stones that impact in it are often too small to see.

Ultrasound is the initial investigation for demonstrating the *bile ducts*. The common hepatic or common bile duct can be visualized in almost all patients; it is seen as a small, tubular structure lying anterior to the portal vein in the porta hepatis and should not measure more than 7mm in diameter (Fig. 7.24) unless the patient has had a cholecystectomy, when it may be larger. The lower end of the common bile duct is often obscured by gas in the duodenum.

The normal intrahepatic biliary tree is of such small calibre that only small portions a few millimetres long may be seen at ultrasound.

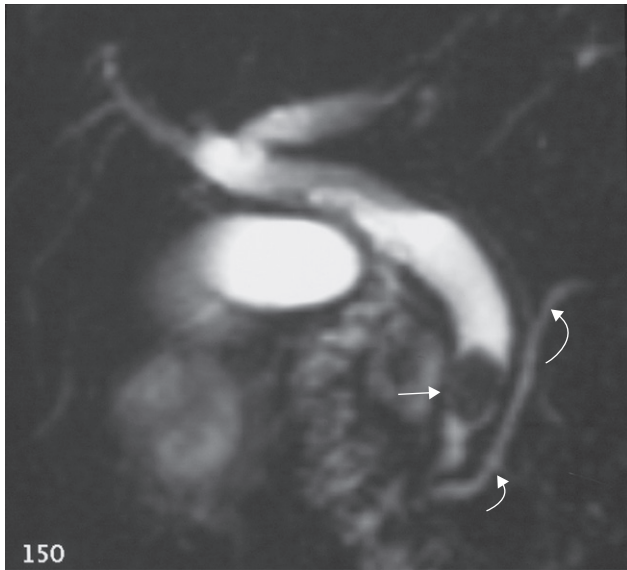


Fig. 7.25 MRCP. A stone is present in the common bile duct (arrow) with dilatation of the ducts above it. A normal pancreatic duct has also been demonstrated (curved arrows).

Magnetic resonance cholangiopancreatography

Magnetic resonance imaging uses special fluid-sensitive sequences to visualize the biliary and pancreatic ducts. The examination is non-invasive and no contrast agents are needed. Magnetic resonance cholangiopancreatography (MRCP) is replacing ERCP in many instances as a non-invasive investigation for biliary and pancreatic disorders (Fig. 7.25), although ERCP is necessary for any endoscopic biopsy or treatment.

Endoscopic retrograde cholangiopancreatography

Endoscopic retrograde cholangiopancreatography consists of injecting contrast material directly into the common bile duct through a catheter inserted into the papilla of Vater via an endoscope positioned in the duodenum (Fig. 7.26). In the case of stones in the common bile duct, sphincterotomy and endoscopic basket or balloon extraction may be employed. With obstruction due to tumour, biopsies or brushings can be obtained and the obstruction relieved with stents passed through the endoscope across the

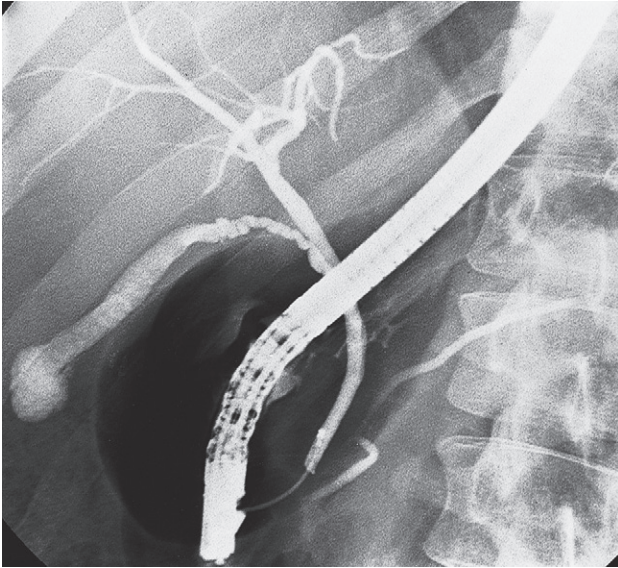
obstruction. It is still occasionally used for more detailed imaging of the intrahepatic biliary ducts as resolution is better than with MRCP (e.g. in sclerosing cholangitis). Pancreatitis is an occasional complication of ERCP.

Percutaneous transhepatic cholangiogram

Percutaneous transhepatic cholangiogram (PTC) can demonstrate the bile duct system in order to show the site and cause of obstruction and is generally performed if an ERCP is unsuccessful in treating a distal common bile duct obstruction or as the primary procedure in treating a more proximal hilar stricture. The procedure is carried out under local anaesthesia and, because it is far easier and safer to perform if the intrahepatic bile ducts are dilated, the patient is usually jaundiced at the time of examination. The examination consists of passing a fine needle (usually 22 or 23 gauge) through the abdominal wall into the liver and injecting contrast directly into an intrahepatic bile duct (see Chapter 17, Fig. 17.22). Haemorrhage is an occasional problem, as are septicaemia and biliary peritonitis. PTC is also used to introduce stents across an obstruction if this cannot be achieved endoscopically at ERCP.

Hepatobiliary radionuclide scanning

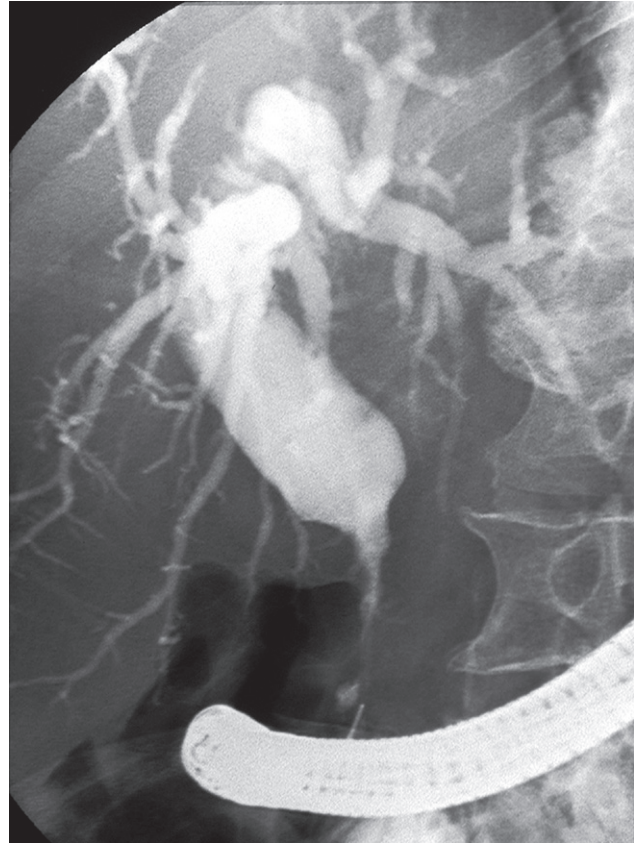
Iminodiacetic acid pharmaceuticals labelled with technetium-99m (^{99m}Tc) are excreted by the liver following intravenous injection and may be used for imaging the bile duct system. Hepatic excretion occurs despite relatively high serum bilirubin levels, and, therefore, these agents can be used when the patient is jaundiced, even with serum bilirubin levels of up to $250\mu\text{mol/L}$ (15mg%). All that is required is that the patient fasts for 4 hours prior to the injection of the radionuclide. Normally, the gall bladder, common bile duct, duodenum and small bowel are all seen within the first hour, confirming the patency and integrity of both the cystic duct and the common bile duct. The main use of this technique is in patients with suspected biliary leak following biliary surgery. Excretion of the radionuclide tracer from the biliary tree into the peritoneal cavity is diagnostic of a leak. The technique may also be used in acute cholecystitis (with non-filling of the gall bladder in cases of an impacted stone in the cystic duct; Fig. 7.27) or in children, when biliary atresia is suspected.



(a)



(b)



(c)

Fig. 7.26 ERCP.(a) A normal biliary system has been shown by injecting contrast through a catheter passed from the endoscope into the common bile duct. The pancreatic duct has also been filled. (b) A dilated ductal system with numerous large calculi in the hepatic and common bile ducts. (c) A stricture in the common bile duct from a cholangiocarcinoma is causing marked dilatation of the biliary system above it.

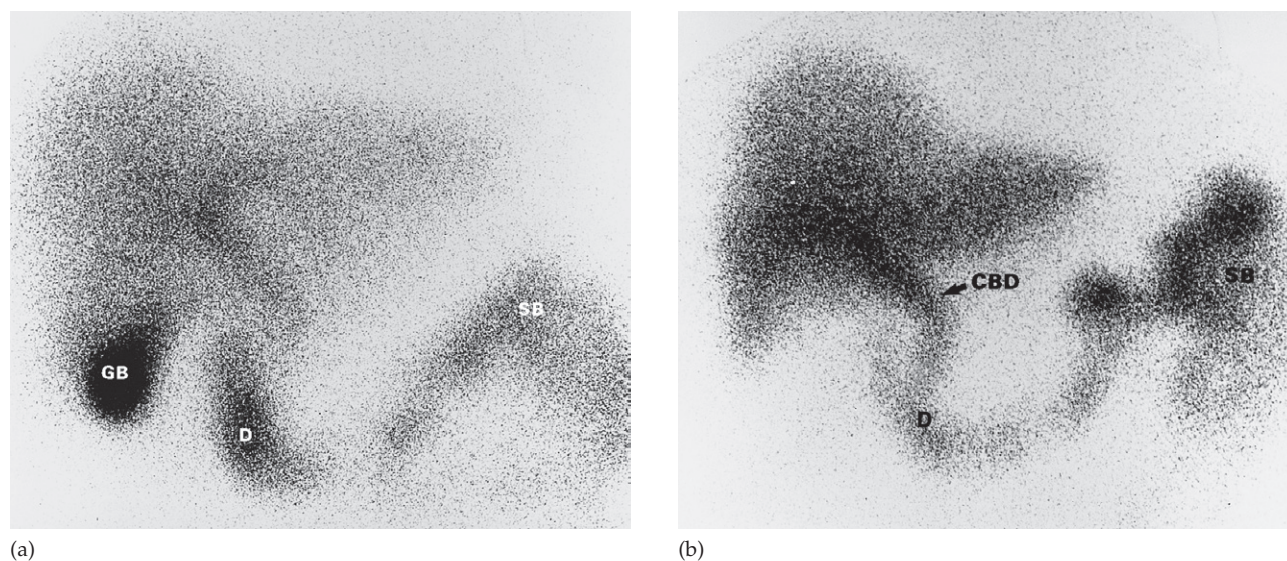


Fig. 7.27 Hepatobiliary scan. (a) Normal iminodiacetic acid (IDA) scan. There is obvious filling of the gall bladder (GB). Activity is also present in the duodenum and small bowel. (b) Cystic duct obstruction. The IDA scan in this patient with acute right upper quadrant pain shows the duct system but no filling of the gall bladder. CBD, common bile duct; D, duodenum; SB, small bowel.



Fig. 7.28 Radio-opaque gall stones. Plain film showing multifaceted stones with lucent centres.

Gall stones and cholecystitis

Gall stones are a frequent finding in adults, particularly middle-aged females. Together with accompanying chronic cholecystitis, they are a major cause of recurrent upper abdominal pain. The presence of stones within the gall bladder does not necessarily mean the patient's pain is due to gall stones. In the appropriate clinical setting, however, identification of gall stones may be sufficient for many surgeons to take action.

Some 20% of gall stones contain sufficient calcium to be visible on plain film (Fig. 7.28). They vary greatly in size and shape and, typically, have a dense outer rim with a more lucent centre. Calcified sludge within the gall bladder is also known as 'milk of calcium' bile.

At ultrasound, gall stones are seen as strongly echogenic foci within the dependent portion of the gall bladder. Acoustic shadows are usually seen behind stones because most of the ultrasound beam is reflected by the stones and only a little passes on through the patient (Fig. 7.29). The presence of an acoustic shadow is an important diagnostic feature for confirming stones in the gall bladder or common

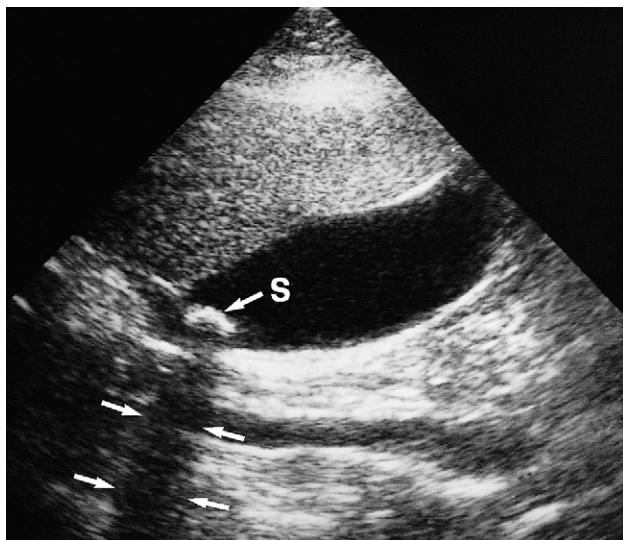


Fig. 7.29 Ultrasound of a gall stone showing a stone (S) in the gall bladder. The arrows point to the acoustic shadow behind the stone.

bile duct. Acoustic shadowing is not seen with polyps. The vast majority of polyps are small (Fig. 7.30), measuring only a few millimetres and are not neoplasms but aggregations of cholesterol.

Although ultrasound is very accurate at diagnosing gall stones, it is much less reliable for detecting stones in the common bile duct, which are better demonstrated with MRCP.

Cholecystitis

In acute cholecystitis ultrasound will usually detect gall stones, inflammatory debris, gall bladder wall thickening and a rim of fluid adjacent to the gall bladder (Fig. 7.31a). On CT, the gall bladder wall is thickened and there is surrounding inflammatory change seen as stranding in the adjacent fat (Fig. 7.31b). In acute cholecystitis, pain is often localized to the gall bladder. In chronic cholecystitis, the gall bladder is often contracted and thick-walled.

Jaundice

Clinical examination and biochemical tests often permit the cause of jaundice to be diagnosed. Imaging tests may, however, be required when there is doubt as to the nature

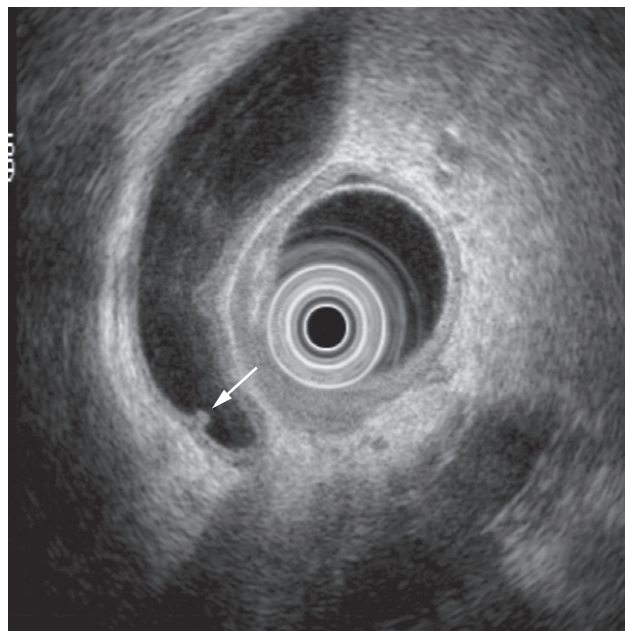


Fig. 7.30 Endoscopic ultrasound showing a small polyp in the gall bladder with no acoustic shadow (arrow).

of the jaundice. The basis of this distinction is that dilated biliary ducts are a feature of jaundice from biliary obstruction. Imaging is used to determine the site (e.g. distal common bile duct or hilar obstruction) and, if possible, the cause of obstruction (Box 7.2).

Dilatation of the intra- and extrahepatic biliary system can be identified at ultrasound (Fig. 7.32a), CT (Fig. 7.32b) and MRI. Ultrasound is the more available test and is usually the first test to be performed. Dilated intrahepatic biliary ducts are seen at ultrasound as serpentine structures paralleling the portal veins, a finding known as the 'double-channel sign'. The common bile duct lies just in front of the portal vein and is dilated when more than 7 mm in diameter. Ultrasound is good for demonstrating the level of obstruction and sometimes the specific cause for biliary

Box 7.2 Major causes of biliary obstruction

- Impacted stone in the common bile duct
- Carcinoma of the head of the pancreas
- Carcinoma of the ampulla of Vater
- Cholangiocarcinoma

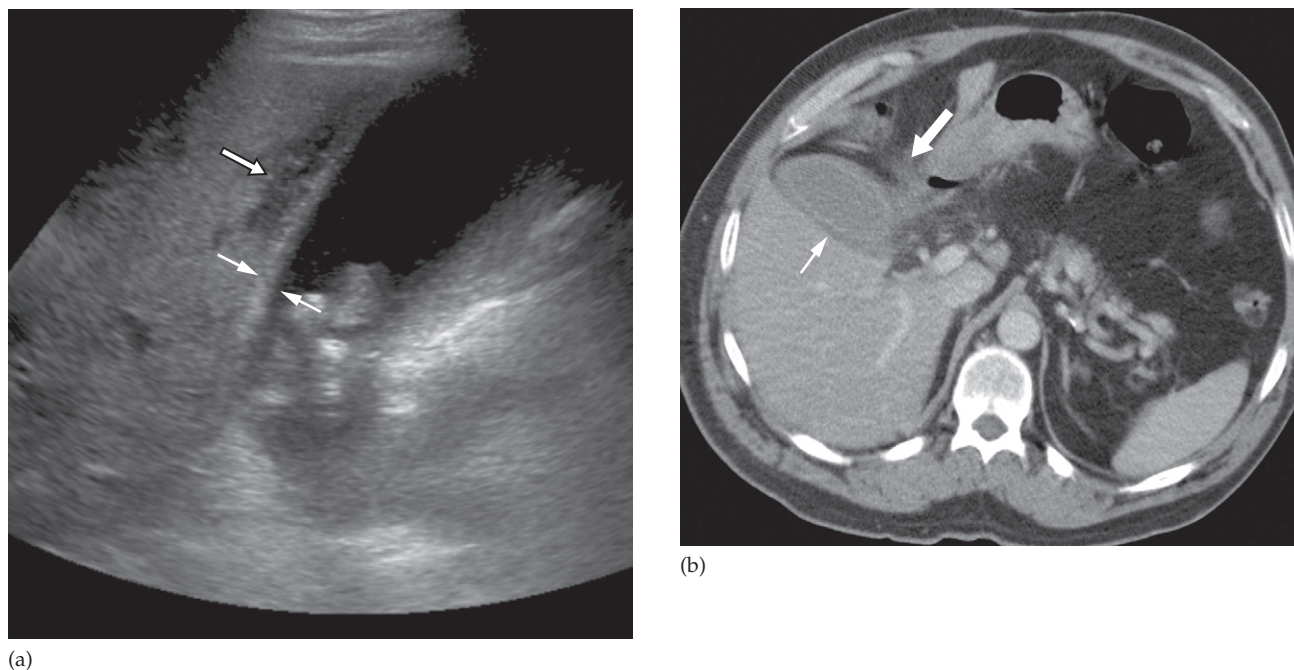


Fig. 7.31 Acute cholecystitis. (a) Ultrasound showing a thick, oedematous gall bladder wall indicated by the thin arrows. There is also evidence of fluid adjacent to the gall bladder indicative of acute inflammation (thick arrow). (b) CT scan of acute cholecystitis showing a thick-walled gall bladder with adjacent oedema and inflammatory change as evidenced by a surrounding low attenuation rim (thin arrow) and lack of clarity (stranding) in the adjacent fat (thick arrow).

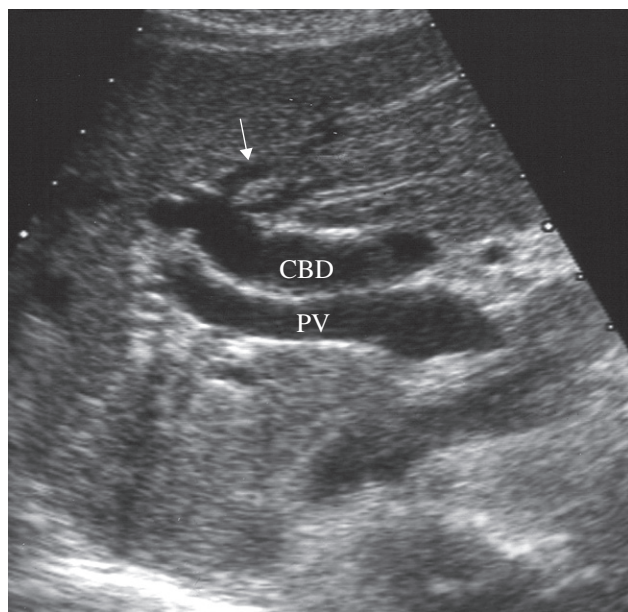
obstruction can be seen, e.g. a stone impacted within the common bile duct (Fig. 7.33) or a mass in the pancreatic head. More often, the cause cannot be seen, mainly because overlying gas in the duodenum obscures the lower end of the common bile duct and further imaging is required depending on the ultrasound findings. For suspected stone disease or a hilar stricture, MRCP is often more helpful than CT in delineating the biliary tree and, conversely, CT is more often used for further evaluation and staging of a distal obstruction secondary to an underlying pancreatic malignancy. Substantial dilatation of the common hepatic and common bile ducts may be present with only minimal dilatation of the intrahepatic ducts; the intrahepatic biliary tree may not dilate at all within the first 48 hours following obstruction.

Once a diagnosis has been established, the patient usually undergoes biliary decompression at ERCP. If this fails, or

there is a hilar stricture present, then decompression is performed at PTC. Occasionally, patients who are well enough may go straight to surgery to remove an underlying malignancy if it is thought that complete resection is possible and there is no metastatic disease.

PANCREAS

Computed tomography is now the mainstay for imaging the pancreas. A major advantage of CT over transabdominal ultrasound is that it can image the pancreas regardless of the amount of bowel adjacent to it, whereas the ultrasound beam is absorbed by gas in the gastrointestinal tract. This has led to the development of endoscopic ultrasound, which is routinely used in the diagnosis (including biopsy) of pancreatic disease and staging in patients with pancreatic cancer (e.g. involvement of the superior mesenteric



(a)



(b)

Fig. 7.32 Dilated biliary ducts. (a) Longitudinal ultrasound scan showing a dilated common bile duct (CBD) measuring 11 mm in diameter lying in front of the portal vein (PV). Normally the duct is much smaller than the accompanying vein. A dilated intrahepatic duct is arrowed. (b) CT scan showing dilated intrahepatic ducts (arrows) in the liver.

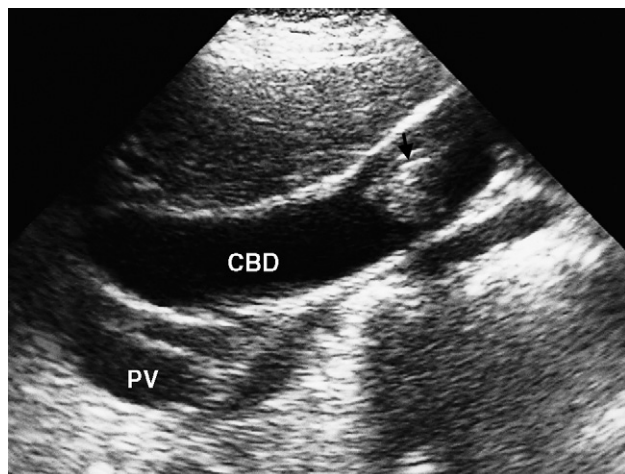


Fig. 7.33 Stones in the common bile duct (CBD). The common bile duct is dilated, measuring 2 cm in diameter, and a large stone (arrow) is seen in its lower portion. PV, section through the portal vein.

artery precludes a surgical cure) (Fig. 7.34). MRI, ERCP (Fig. 7.35) and arteriography are used in selected cases.

The normal pancreas is an elongated retroperitoneal organ surrounded by a variable amount of fat (Fig. 7.36). The head nestles in the duodenal loop (for CT scanning, the duodenum is opacified by an oral contrast agent) and the uncinate process folds behind the superior mesenteric artery and vein; these vessels form a useful landmark to help identify the head of the pancreas. The body of the pancreas lies in front of the superior mesenteric artery and vein, and passes behind the stomach, with the tail situated near the hilum of the spleen. The splenic vein, which can be a surprisingly large structure, is another very useful landmark. Lying behind the pancreas, it joins the superior mesenteric vein posterior to the neck of the pancreas to form the portal vein.

In most people, the pancreas runs obliquely across the retroperitoneum, being higher at the splenic end. Because of this oblique orientation, CT shows different portions

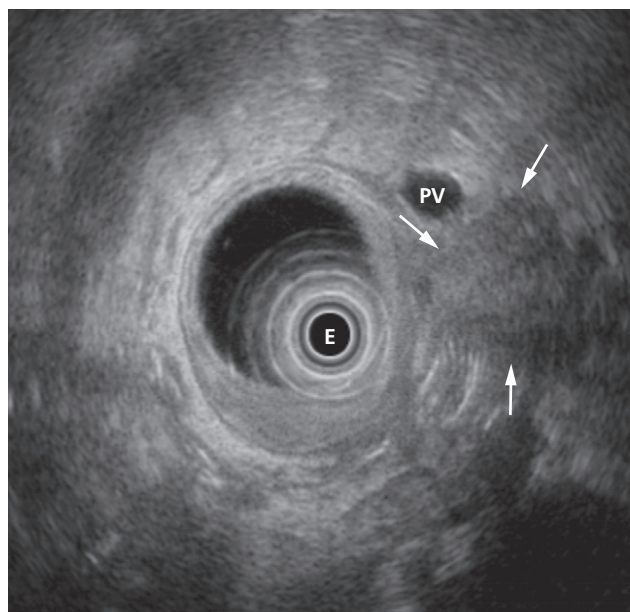
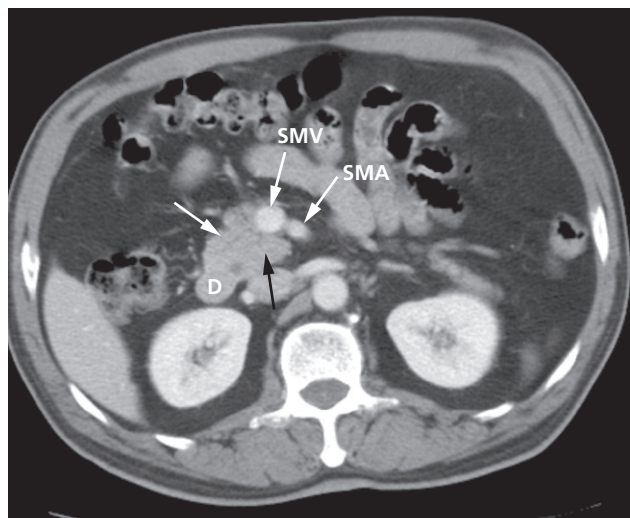


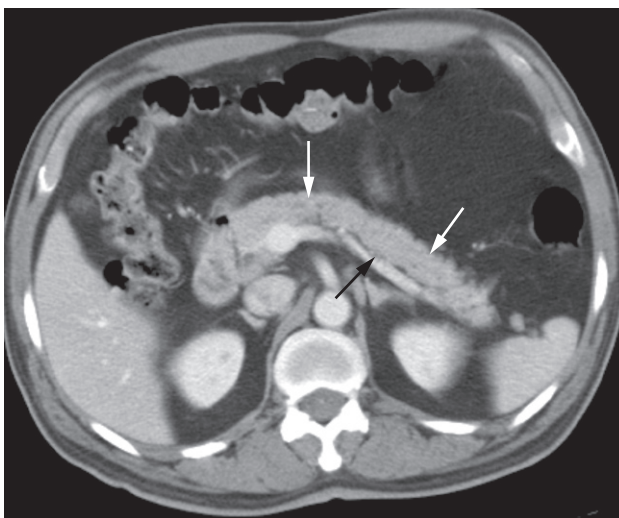
Fig. 7.34 Endoscopic ultrasound showing a mass in the pancreas (arrows) that involves the portal vein (PV). E, endoscope.



Fig. 7.35 Endoscopic retrograde pancreatography. The pancreatic duct has been cannulated from the endoscope in the duodenum and contrast injected to demonstrate a normal duct system.



(a)



(b)

Fig. 7.36 CT scan of normal pancreas. Note that several sections may be needed to display the pancreas. (a) The head of the pancreas (white arrow) nestling between the second part of the duodenum (D) and the superior mesenteric vessels (SMA and SMV). The uncinate process lies anterior to the inferior vena cava (black arrow). (b) CT scan taken 3 cm higher, showing the body and part of the tail (white arrows). Note the splenic vein (black arrow), which lies posterior to the body of the pancreas.

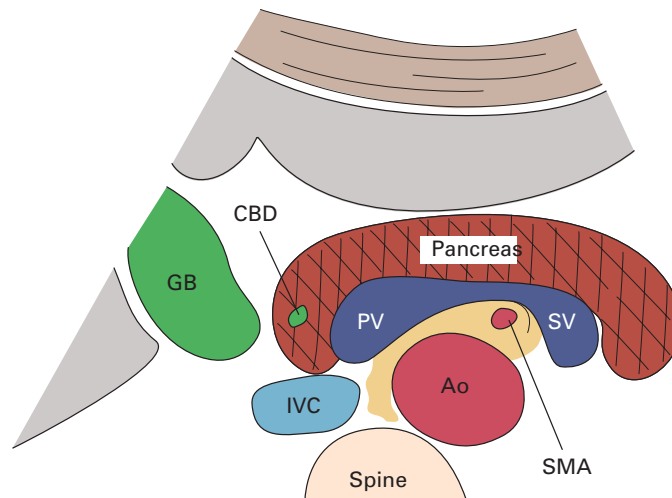


Fig. 7.37 Ultrasound of normal pancreas (transverse scan). Ao, aorta; CBD, common bile duct; GB, gall bladder; IVC, inferior vena cava; PV, portal vein; SMA, superior mesenteric artery; SV, splenic vein.

of the pancreas on the various sections. The normal pancreas shows a feathery texture, corresponding to pancreatic lobules interspersed with fat. Atrophy is a common feature of ageing. At ultrasound, the pancreas gives reasonably uniform echoes of medium to high level compared with the adjacent liver (Fig. 7.37). The pancreatic duct may be seen, with the normal lumen being no more than 2mm in diameter.

Pancreatic masses

The usual causes of masses in, or immediately adjacent to, the pancreas are: carcinoma of the pancreas (including cystic neoplasms), metastases to adjacent lymph nodes, focal pancreatitis, pancreatic abscess and pseudocyst formation (Box 7.3). Occasionally, congenital cysts may be seen.

Most neoplasms of the pancreas are *adenocarcinomas*, two-thirds of which occur in the head of the pancreas. Tumours arising in the head may obstruct the common bile duct, giving rise to jaundice, and are, therefore, sometimes diagnosed when relatively small. Tumours arising in the body and tail have to be fairly large to give rise to signs or symptoms, pain being the cardinal symptom. As the pancreas is so variable, measurements have not proved useful

Box 7.3 Major causes of pancreatic masses

Malignant causes

- Adenocarcinomas
- Lymph node metastases
- Metastases to body of pancreas (e.g. melanoma)

Malignant potential causes

- Neuroendocrine tumours:
 - insulinoma
 - gastrinoma
 - glucagonoma
 - VIPoma
- Mucinous cystadenomas
- Intraductal papillary mucinous neoplasm

Benign causes

- Serous cystadenomas
- Focal pancreatitis
- Pseudocysts

VIP, vasoactive intestinal peptide.

in diagnosing masses. The important sign of carcinoma of the pancreas at both CT and ultrasound is, therefore, a focal mass within or deforming the outline of the gland (Fig. 7.38). On contrast-enhanced CT, the tumour appears of lower density compared with the normal pancreatic tissue

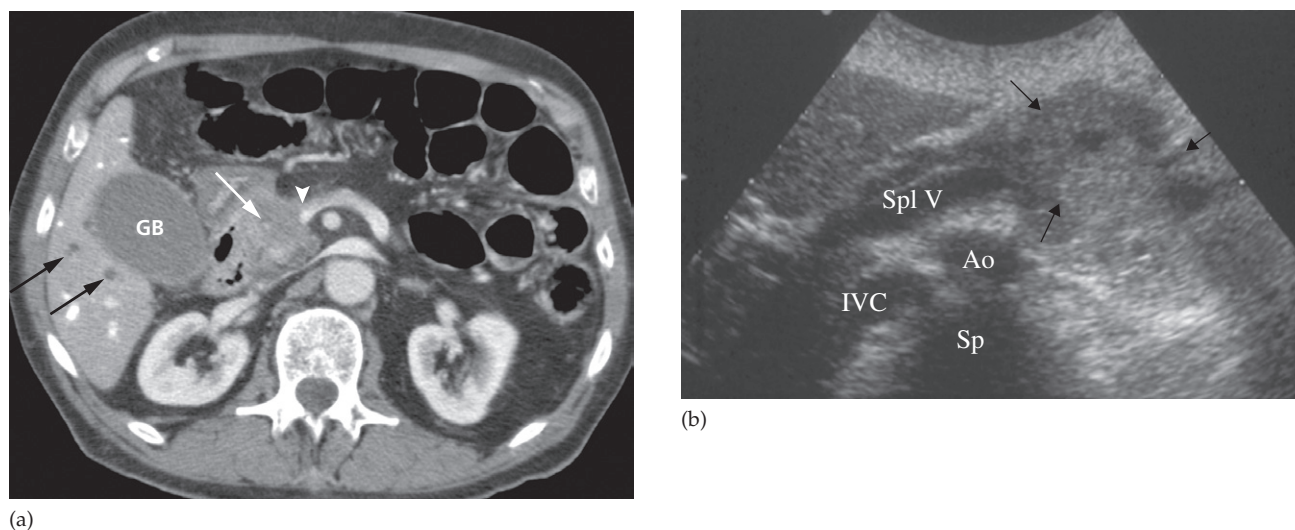


Fig. 7.38 Carcinoma of the pancreas. (a) CT scan showing a focal mass in the head of the pancreas (white arrow), which involves the portal/mesenteric vein confluence (arrow head) and may preclude curative surgery (compare with the endoscopic ultrasound image, Fig. 7.34, performed in the same patient). Note the dilated intrahepatic bile ducts (black arrows) and distended gall bladder (GB). (b) Transverse ultrasound scan showing a large mass in the body of the pancreas (arrows). Ao, aorta; IVC, inferior vena cava; Sp, spine; Spl V, splenic vein.

(Fig. 7.38a). The main pancreatic duct may be dilated distal to an obstructing tumour mass and can be identified on all imaging modalities.

Cystic tumours of the pancreas are less common than solid lesions and are often detected incidentally, but range from benign lesions (which can be observed) to highly malignant tumours (which should be resected). The aim of imaging is to try and differentiate between the two and it can be very difficult. It is important to correlate the imaging findings with the clinical history of the patient and the presence or absence of symptoms. In many cases an endoscopic ultrasound will be performed with aspiration of the cystic content. A high mucinous content with an elevated carcinoembryonic antigen level ≥ 200 ng/mL or atypical cytology is suggestive of a malignant (mucinous) neoplasm.

Staging investigations attempt to identify potentially resectable tumours. Most are irresectable at presentation: the presence of liver metastases, lymphadenopathy, retroperitoneal invasion, tumour encasement of arteries and veins are contraindications to surgery.

The presence of pancreatic *neuroendocrine tumours*, of which insulinoma is the commonest example, is suggested by clinical presentation and biochemical investigations. These tumours are difficult to detect as they are usually small and do not deform the pancreatic contour. They may be seen on ultrasound, CT or MRI as small round masses within the pancreas (Fig. 7.39a). Sometimes selective angiography is required, where they stand out from the rest of the pancreas by virtue of their hypervascularity (Fig. 7.39b). Special somatostatin receptor radionuclide scans (octreoscan) may also demonstrate the tumour and any metastases.

Acute pancreatitis

Acute pancreatitis causes abdominal pain, fever, vomiting and leucocytosis, together with elevation of the serum amylase. The findings at CT and ultrasound vary with the amount of necrosis, haemorrhage and suppuration (Fig. 7.40). The pancreas is usually enlarged, often diffusely, and may show irregularity of its outline, caused by extension

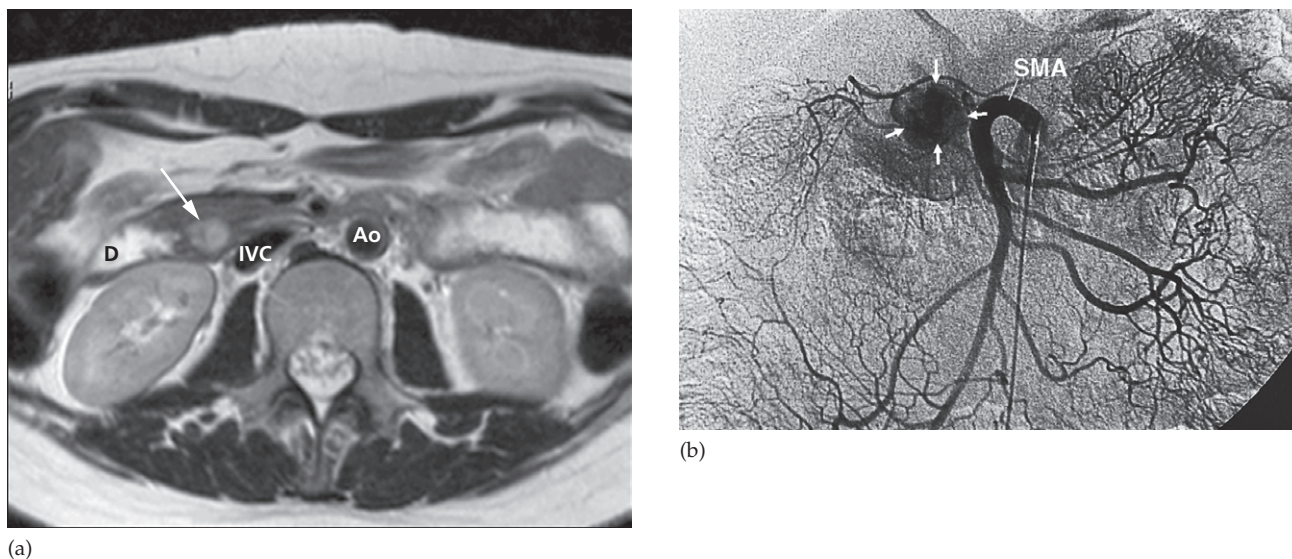


Fig. 7.39 Insulinoma. (a) Axial T2-weighted MRI demonstrating a 1.5 cm insulinoma in the uncinate process of the pancreas (arrow). (b) Selective superior mesenteric angiogram in another patient showing the tumour as a vascular blush (arrows). Ao, aorta; D, duodenum; IVC, inferior vena cava; SMA, superior mesenteric artery.

of the inflammatory process into the surrounding retroperitoneal fat – features that are well seen at CT. There may be low density areas at CT and echo-poor areas at sonography, representing oedema and focal necrosis within or adjacent to the pancreas.

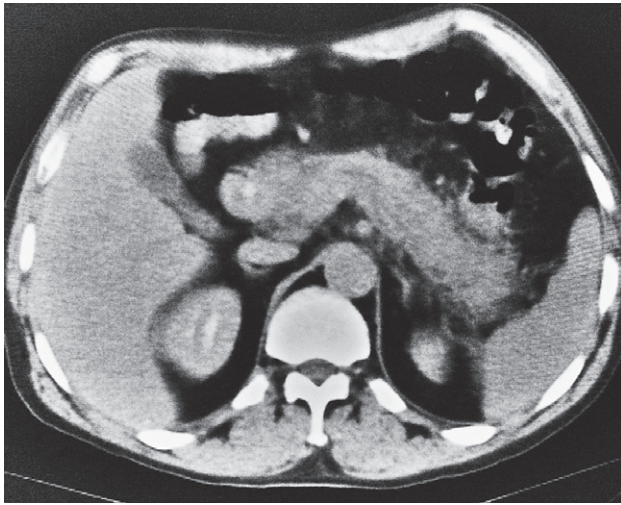
The diagnosis of pancreatitis is usually made on clinical and biochemical grounds; the purpose of imaging is to assess the severity of the disease and to demonstrate complications:

- The pancreas may be necrotic and non-viable if it does not enhance at CT after intravenous contrast.
- An abscess appears as a localized fluid collection, which may contain gas.
- Vascular complications are serious and these include splenic vein thrombosis, arterial erosion and the formation of a pseudoaneurysm.
- *Pseudocysts* are a complication of acute pancreatitis in which tissue necrosis leads to a leak of pancreatic secretions, which are then contained in a cyst-like manner within and adjacent to the pancreas. They can be well demonstrated by CT (or ultrasound) as thin- or thick-walled cysts

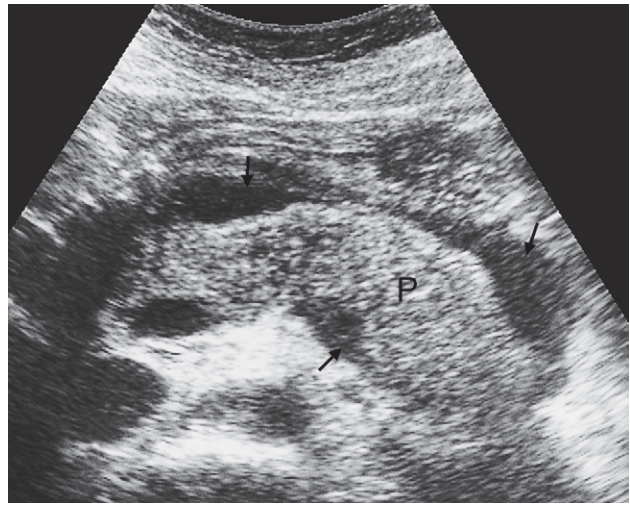
containing fluid (Fig. 7.41). They vary in size from very small to many centimetres in diameter. Many pseudocysts resolve in the weeks following an attack of acute pancreatitis. Some persist and may need surgical or percutaneous drainage. Both CT and ultrasound are excellent methods of following such cysts and determining the best approach to treatment.

Chronic pancreatitis

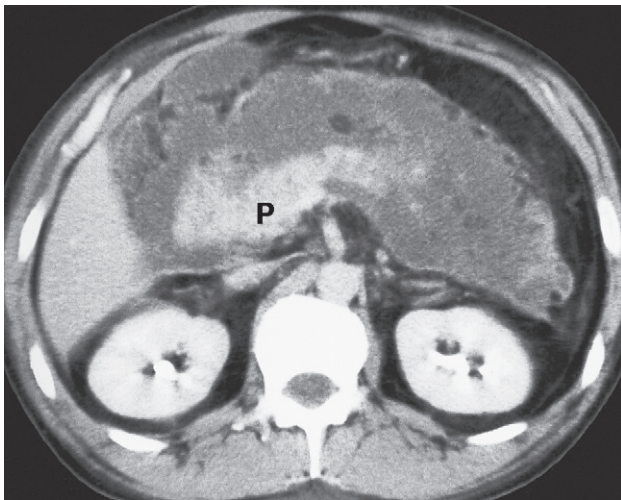
Chronic pancreatitis results in fibrosis, calcifications, and ductal stenoses and dilatations. Pseudocysts are seen with chronic pancreatitis just as they are in the acute form. The calcification in chronic pancreatitis is mainly due to small calculi within the pancreas; they are often recognizable on plain films (see Figs 5.17 and 7.42a) and ultrasound, but are particularly obvious at CT (Fig. 7.42a). The gland may enlarge generally or focally. Focal enlargement is rare and is then often indistinguishable from carcinoma. Conversely, the pancreas may atrophy focally or generally. Atrophy is a non-specific sign; it is frequently seen in normal elderly



(a)

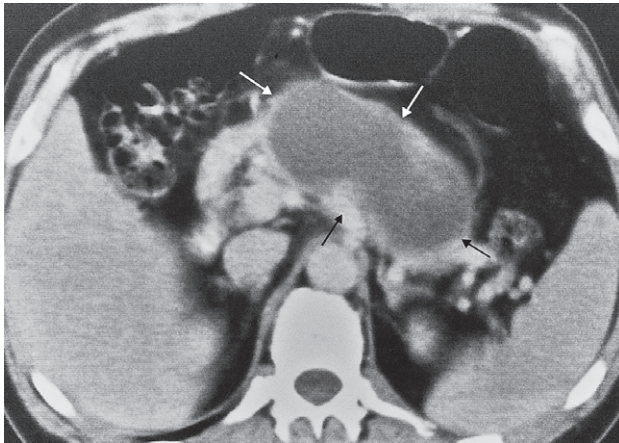


(c)

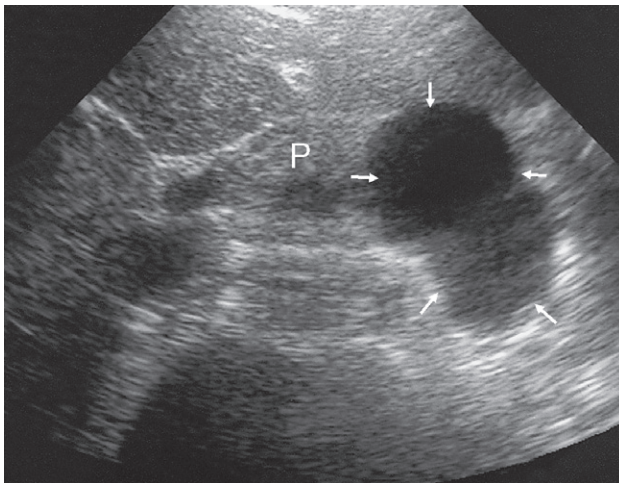


(b)

Fig. 7.40 Acute pancreatitis. (a) CT scan showing diffuse enlargement of the pancreas with ill-defined edges. (b) CT scan showing considerable inflammation around the pancreas (P). (c) Transverse ultrasound scan showing a swollen pancreas (P) with some fluid around the pancreas (arrows).



(a)

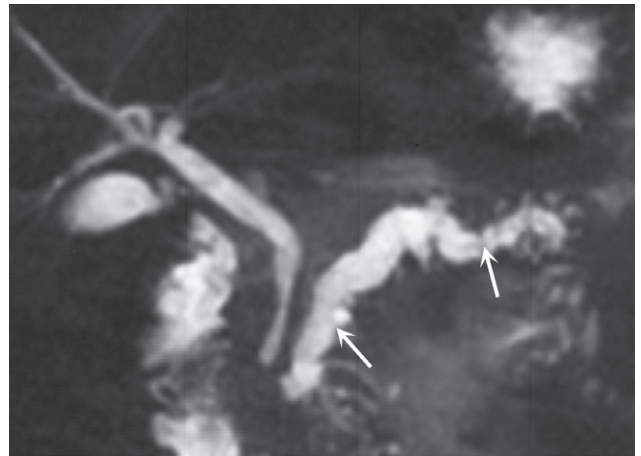


(b)

Fig. 7.41 Pancreatic pseudocyst. (a) CT scan showing a large cyst arising within the pancreas (arrows). (b) Transverse ultrasound scan. The arrows indicate a pseudocyst arising from the body of the pancreas (P). Same patient as Fig. 7.40c, 6 weeks later.



(a)



(b)

Fig. 7.42 Chronic pancreatitis. (a) CT scan showing numerous small areas of calcification within the pancreas (arrows). (b) MRCP showing a normal biliary duct system but irregular dilatation of the pancreatic duct (arrows).



Fig. 7.43 CT scan of a hydatid cyst (C) in the spleen with calcification in its walls.

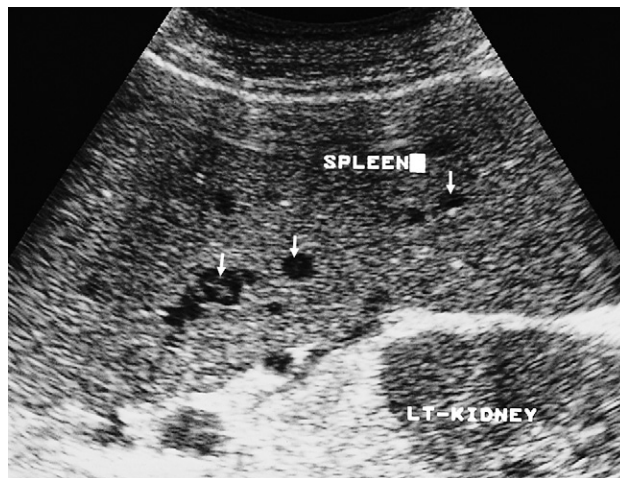


Fig. 7.44 Lymphoma. Ultrasound showing an enlarged spleen with several hypoechoic areas within it; some of these are arrowed.

people and also occurs distal to a carcinoma. The pancreatic duct may be enlarged and irregular, a feature that is visible at CT, and particularly striking at ultrasound.

Endoscopic retrograde cholangiopancreatography is occasionally used to try and document chronic pancreatitis and exclude carcinoma. The generalized irregular dilatation of the duct system seen with chronic pancreatitis is very well demonstrated. MRCP can be used as an alternative, non-invasive method (Fig. 7.42b).

Pancreatic trauma

Trauma to the pancreas is uncommon but serious. Injuries to other structures are frequent, so CT is the best method of investigation. In addition to lacerations and haematomas, the release of pancreatic enzymes into the surrounding tissues leads to traumatic pancreatitis and tissue necrosis. The features here are similar to other forms of acute pancreatitis (see above), including the subsequent development of pseudocysts.

SPLEEN

Imaging the spleen is, in many respects, similar to imaging the liver. At ultrasound, the spleen has a homogeneous

appearance with the same echo density as the liver. CT and MRI are excellent ways to examine the spleen; normal CT images are shown in the Appendix.

The commonly encountered splenic masses are cysts, including hydatid cysts (Fig. 7.43), abscesses and tumours. Lymphomas (Fig. 7.44) are much commoner than metastases, which are rare in the spleen.

Many conditions cause enlargement of the spleen but cause no change in splenic texture on ultrasound, or any change in density on a CT scan. These conditions include lymphoma, portal hypertension (see Fig. 7.20), chronic infection and various blood disorders, e.g. haemolytic anaemias and leukaemia. As the appearance of the enlarged spleen in all these conditions is similar, imaging does little except confirm the presence of splenomegaly.

Splenic infarction may occur secondary to severe pancreatitis, pancreatic carcinoma, sickle cell disease or trauma. It is well demonstrated on CT as either focal or complete loss of normal enhancement following intravenous contrast (Fig. 7.45).

Splenic trauma

The spleen is the most commonly injured organ in blunt abdominal trauma and lacerations, contusions or

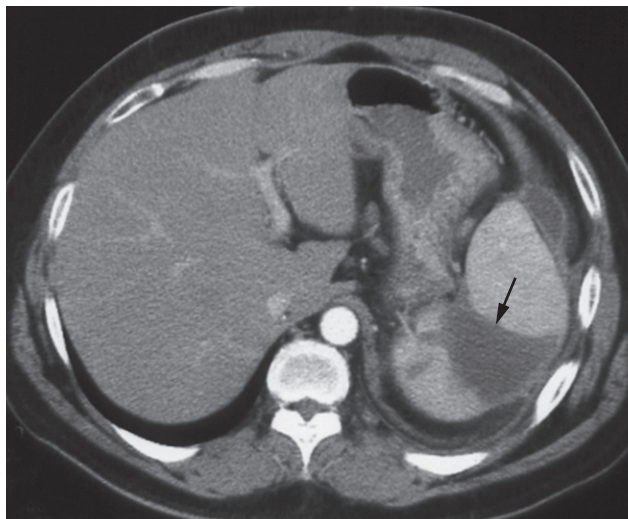


Fig. 7.45 Splenic infarction. CT with contrast demonstrating a wedge-shaped, non-enhancing segment of spleen (arrow) consistent with infarction.

haematomas may result. Rupture may be delayed until some time after the injury. *Splenic injury* may be detected by ultrasound, but CT is a superior method of investigation as not only does it demonstrate better the damage to the spleen, but it can also show intraperitoneal blood and visualize injuries to other abdominal organs, particularly the

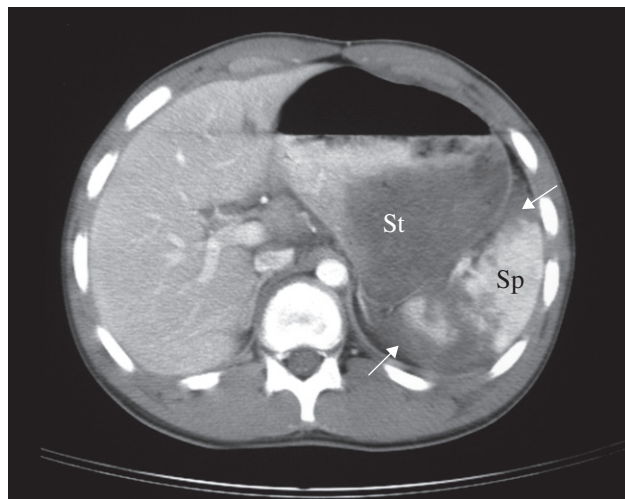


Fig. 7.46 Ruptured spleen on CT. The spleen is shattered with low density blood (arrows) adjacent to the fragments. Sp, spleen; St, stomach.

adjacent liver and left kidney (Fig. 7.46). In patients with splenic laceration, consideration should be given to selective arterial embolization. This may allow some preservation of splenic function, which would be lost if the patient underwent surgery and splenectomy.

Urinary Tract

The four basic examinations of the urinary tract are ultrasound, intravenous urography (IVU), computed tomography (CT) and radionuclide examinations. Magnetic resonance imaging (MRI), arteriography and studies requiring catheterization or direct puncture of the collecting systems are limited to selected patients. Fluorodeoxyglucose positron emission tomography (FDG-PET)/CT is still under investigation as an imaging tool in the urinary tract, as there are currently several limitations due to excretion of the tracer in the renal tract and poor uptake in many urological malignancies.

Ultrasound, CT and MRI are essentially used for anatomical information; the functional information they provide is limited. The converse is true of radionuclide examinations where functional information is paramount. IVU provides both functional and anatomical information.

Imaging techniques

Ultrasound

Ultrasound is the first line investigation in most patients, providing anatomical information without requiring ionizing radiation or the use of intravenous contrast medium. The following are the main uses of ultrasound:

- To investigate patients with symptoms thought to arise from the urinary tract.
- To demonstrate the size of the kidneys and exclude hydronephrosis in patients with renal failure.

- To diagnose hydronephrosis, renal tumours, abscesses and cysts including polycystic disease.
- To assess and follow-up renal size and scarring in children with urinary tract infections.
- To assess the bladder and prostate.

Normal renal ultrasound

At ultrasound, the kidneys should be smooth in outline. The parenchyma surrounds a central echo-dense region, known as the central echo complex (the renal sinus), consisting of the pelvicaliceal system, together with the surrounding fat and renal blood vessels (Fig. 8.1). In most instances, the normal pelvicaliceal system is not visible within the renal sinus. The renal cortex generates homogeneous echoes that are of equal reflectivity or less reflective than those of the adjacent liver or spleen, and the renal pyramids are seen as triangular hypoechoic areas adjacent to the renal sinus. During the first 2 months of life, cortical echoes are relatively more prominent and the renal pyramids are disproportionately large and strikingly hypoechoic.

The normal adult renal length, measured by ultrasound, is 9–12 cm. Renal length varies with age, being maximal in the young adult. There may be a difference between the two kidneys, normally of less than 1.5 cm. A kidney with a bifid collecting system is usually 1–2 cm larger than a kidney with a single pelvicaliceal system. Minor changes in size occur in many conditions (Tables 8.1 and 8.2).

Normal ureters are not usually visualized due to overlying bowel gas. The urinary bladder should be examined in the distended state: the walls should be sharply defined and barely perceptible (Fig. 8.2). The bladder may also be assessed following micturition, to measure the postmicturition residual volume of urine.

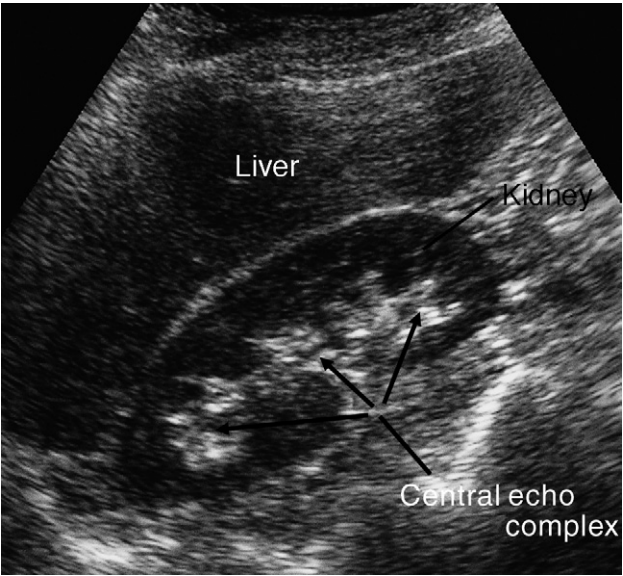


Fig. 8.1 Normal ultrasound of the right kidney.

Urography

Urography is the term used to describe the imaging of the renal tract using intravenous iodinated contrast medium. The traditional intravenous urogram has largely been replaced by a combination of ultrasound and CT urography. CT has the advantage of being highly sensitive for the detection of stones, including those that may be radiolucent on plain film, allows the characterization of renal lesions and the detection of ureteric lesions, and demonstrates the surrounding retroperitoneal and abdominal tissues. In addition, CT overcomes the overlap of superimposed tissues, which can cause difficulty when interpreting traditional IVU.

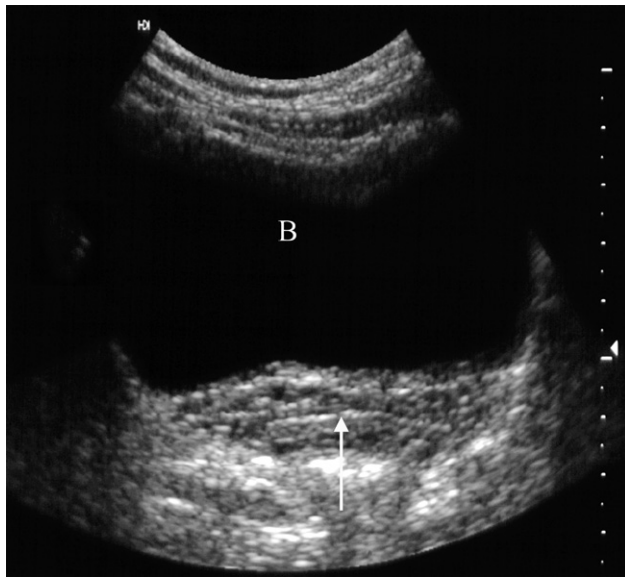
The principles of both techniques are similar. Firstly, ‘non-contrast’ imaging of the renal tract is required, in order to identify all renal tract calcifications. In some cases, where the clinical question relates to renal calculi, the non-contrast CT may be sufficient (known as the ‘CT KUB’). However, where a renal mass is suspected or a possible ureteric or bladder mass is suspected, the non-contrast study is followed by the injection of iodinated contrast medium. Images are obtained at specific time intervals in order to demonstrate the nephrogram (contrast within the kidneys) and the urogram (contrast within the ureters and bladder). CT IVU may be reformatted in the coronal plane in order to have a similar appearance to traditional

Table 8.1 Conditions associated with small kidneys

	Diagnosis	Imaging
Unilateral but may be bilateral	Chronic pyelonephritis	Focal scars and dilated calices
	Tuberculosis	See Fig. 8.42
	Obstructive atrophy	Dilatation of all calices with uniform loss of renal parenchyma
	Renal artery stenosis or occlusion	Outline may be smooth or scarred, but the calices appear normal
	Hypoplasia	Very rare; kidneys may be smooth or irregular in outline with fewer calices. Calices may be clubbed
Always bilateral	Radiation nephritis	Small in size but no distinguishing features
	Chronic glomerulonephritis of many types	Usually no distinguishing features. In all these conditions the kidneys may be small with smooth outlines and normal pelvicaliceal system
	Hypertensive nephropathy	
	Diabetes mellitus	
	Collagen vascular diseases	
	Analgesic nephropathy	Calices often abnormal

Table 8.2 Conditions associated with enlarged kidneys

	Diagnosis	Imaging
<i>Always unilateral May be unilateral or bilateral</i>	Compensatory hypertrophy	Opposite kidney small or absent
	Bifid collecting system	Diagnosis obvious from abnormalities of collecting systems
	Renal mass	Mass is seen
	Hydronephrosis	Visible distension of the renal collecting systems
	Lymphomatous infiltration	May show obvious masses; the kidneys may, however, be large but otherwise unremarkable
<i>Always bilateral</i>	Renal vein thrombosis	No Doppler signal is visible in the renal vein and thrombus may be evident
	Polycystic disease	Characteristic imaging appearance (see Fig. 8.52)
	Acute glomerulonephritis	Non-specific enlargement
	Amyloidosis	Non-specific enlargement (rare)

**Fig. 8.2** Normal ultrasound of the full bladder (B). Note the smooth thin bladder wall. The vagina lies posteriorly (arrow).

IVU. The main indications for urography are listed in Box 8.1.

Contrast medium and its excretion

Urographic contrast media are highly concentrated solutions of organically bound iodine. A large volume (e.g. 100 mL) is injected intravenously and is carried in the blood

Box 8.1 Main indications for urography

Intravenous urography or CT urography

- When detailed demonstration of the pelvicaliceal system and ureters are required
- In suspected ureteric injury, e.g. following pelvic surgery or trauma
- Assessment of acute ureteric colic

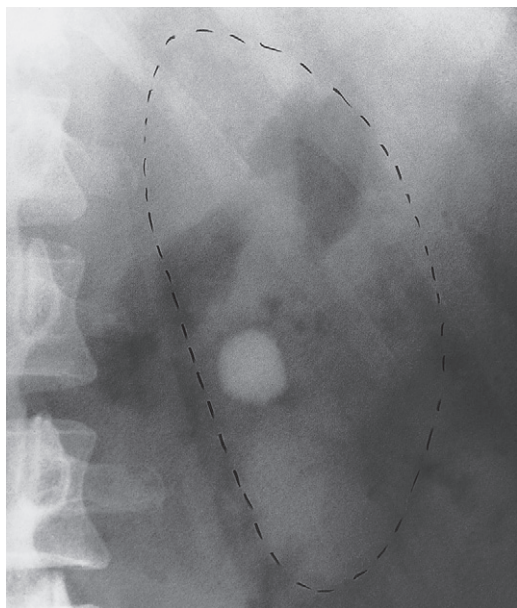
CT urography

- Investigation of renal calculi
- Investigation of haematuria
- Characterization of a renal mass
- Staging and follow-up of renal carcinoma
- To delineate renal vascular anatomy (e.g. suspected renal artery stenosis or prior to live related kidney donation)
- To diagnose or exclude renal trauma

to the kidneys, where it passes into the glomerular filtrate. The contrast medium within the glomerular filtrate is concentrated in the renal tubules and then passes into the pelvicaliceal systems.

Adverse reactions to intravenous contrast media are discussed in Chapter 1.

Patients are allowed to drink up to 500 mL of fluid in the 4 hours before IVU or CT but should not eat. It is particularly important not to fluid-restrict patients with impaired renal function before they are given contrast medium as this may predispose to contrast medium-induced nephrotoxicity.



(a)



(b)

Fig. 8.3 (a) A rounded calcification is seen overlying the left kidney in the anteroposterior plain film. (b) Post contrast film in the same patient. As the contrast medium and the calculus have the same radiographic density, the calculus is hidden by the contrast medium.

Plain film intravenous urogram

Identify all calcifications. Decide if they are in the kidneys by relating them to the renal outlines during inspiration and expiration or oblique views or tomograms where necessary. Calcifications seen in the line of the ureters or bladder must be reviewed with post contrast scans, to determine whether the calcification lies in the renal tract. Note that calcification can be obscured by contrast medium and stones are missed if no plain film is taken (Fig. 8.3). The major causes of urinary tract calcification include calculi, diffuse nephrocalcinosis, localized nephrocalcinosis (e.g. tuberculosis or tumours) and prostatic calcification.

Look at the other structures on the film. Include a review of the bones and other soft tissues, just as you would on any plain abdominal film.

Films taken after injection of contrast medium

Kidneys

- 1 Check that the kidneys are in their normal positions (Fig. 8.4). The left kidney is usually higher than the right.
- 2 Identify the whole of both renal outlines. If any indentations or bulges are present they must be explained.
 - Local indentations (Fig. 8.5). The renal parenchymal width should be uniform and symmetrical, between 2



Fig. 8.4 Normal IVU, full-length 15-minute film. Note that the bladder is well opacified. The whole of the right ureter and part of the left ureter are seen. Often, only a portion of the ureter is visualized owing to peristalsis emptying certain sections. The bladder outline is reasonably smooth. The roof of the bladder shows a shallow indentation from the uterus.

and 2.5cm. Minor indentations between normal calices are due to persistent fetal lobulations. All other local indentations are scars.

- *Local bulges of the renal outline.* A bulge of the renal outline may be due to a mass or a cyst, which often displaces and deforms the adjacent calices. An important normal variant causing a bulge of the outline is the so-called 'splenic hump' (Fig. 8.6).

3 Measure the renal lengths. The normal length of the adult kidney at IVU is between 10 and 16cm. These figures are higher than those for renal size measured on ultrasound mainly due to radiographic magnification of the image.

Calices

The calices should be evenly distributed and reasonably symmetrical. The shape of a normal calix is 'cupped' and when it is dilated it is described as 'clubbed' (Fig. 8.7). The normal 'cup' is due to the indentation of the papilla into the calix. Caliceal dilatation has two basic causes: destruction of the papilla or obstruction (Box 8.2).

Box 8.2 Causes of dilated calices

Due to obstruction, with dilatation down to a specific point of hold-up

Within the lumen

- Calculus
- Blood clot
- Sloughed papilla

Within the wall of the collecting system

- Intrinsic pelviureteric junction obstruction
- Transitional cell tumour
- Infective stricture (e.g. tuberculosis or schistosomiasis)

Extrinsic compression

- Retroperitoneal fibrosis
- Pelvic tumour, e.g. cervical, ovarian or rectal carcinoma
- Aberrant renal artery or retrocaval ureter

Due to papillary atrophy or destruction

- Reflux nephropathy
- Papillary necrosis
- Tuberculosis

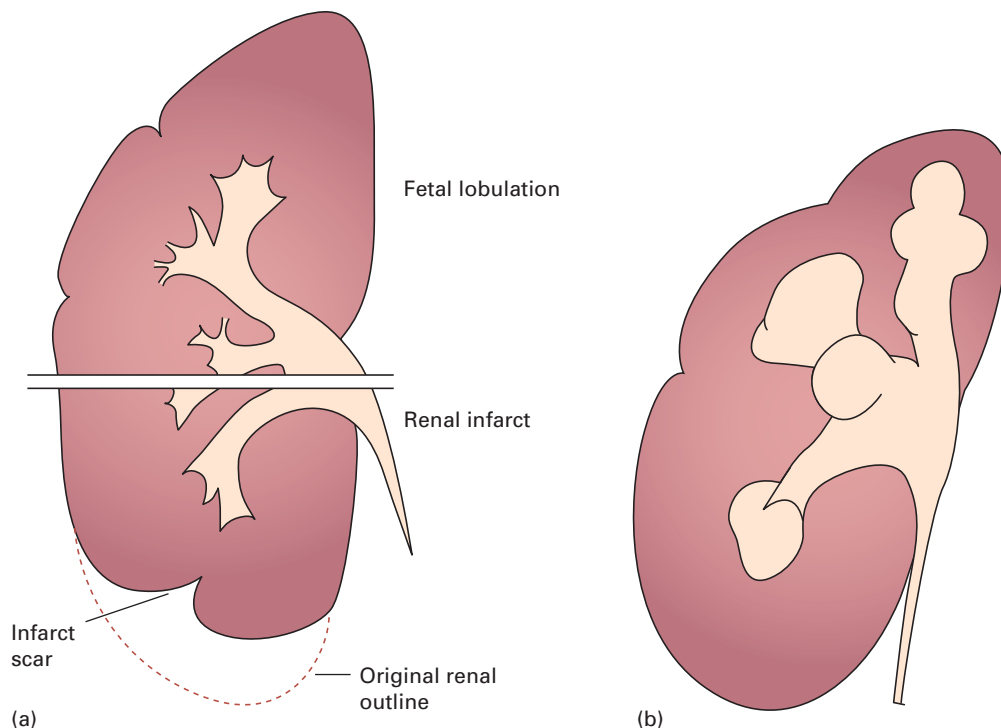


Fig. 8.5 (a) The distinction between fetal lobulation and renal infarction. With fetal lobulation, indentations in the renal outline are shallow and correspond to the lobules of the kidney, i.e. the indentations are between calices. With renal infarction, the maximal indentation is opposite a calix and there is usually extensive loss of renal parenchyma. (b) Scars in chronic pyelonephritis (drawing of Fig. 8.7b). The reductions in renal parenchymal width are opposite calices, and these calices are dilated. The overall kidney size is reduced, as is usual. Scars in tuberculosis have much the same appearance but are usually associated with other signs of tuberculosis.

Renal pelvis and ureters

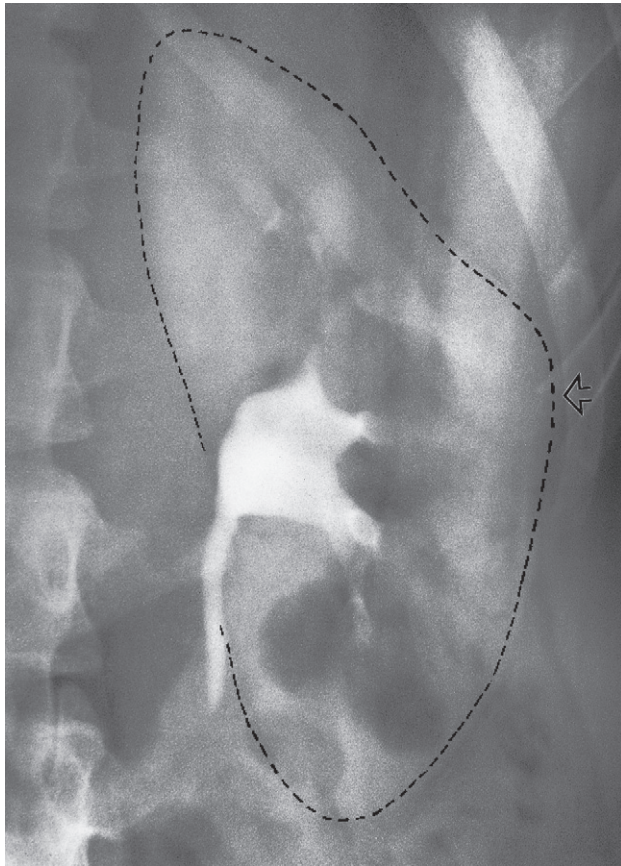
The normal renal pelvis and pelviureteric junction are funnel shaped. The ureters are usually seen in only part of their length on any one film of IVU because of obliteration of the lumen by peristalsis. Dilatation of the renal pelvis and ureter may be secondary to obstruction but there are other causes (e.g. congenital variant or secondary to vesicoureteric reflux). Filling defects within the pelvis and ureters should be identified. The three common causes are tumours, calculi or blood clots. Congenital variations of the renal collecting system are relatively common (see Fig. 8.49).

Bladder

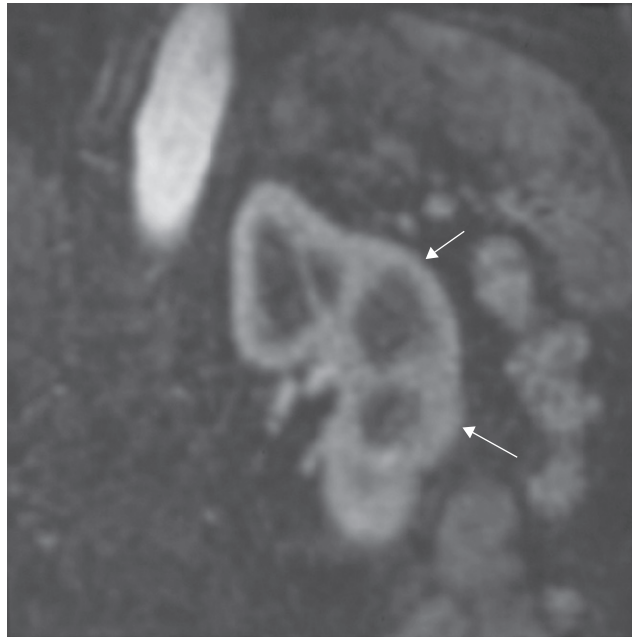
The bladder is a centrally located structure that should have a smooth outline. It often shows normal smooth indentations from above owing to the uterus or the sigmoid colon, and from below by muscles of the pelvic floor (see Fig. 8.4). After micturition the bladder should be empty, apart from a little contrast trapped in the folded mucosa.

Computed tomography urography

The technique varies depending on the indication. In almost all cases, CT is initially performed without intrave-



(a)



(b)

Fig. 8.6 The 'splenic hump'. (a) A bulge is present on the lateral aspect of the left kidney (arrow) but there is no displacement of the calices. This splenic hump is a normal variant. (b) Coronal MRI (with gadolinium) of a left splenic hump (arrows), in which normal corticomedullary anatomy is demonstrated.

nous contrast medium (non-contrast CT or 'CT KUB') to identify calcification (Figs 8.8 and 8.9). Images are then obtained following the administration of a rapid bolus of intravenous contrast medium. The time at which images are obtained following contrast administration depends on the indication and include: (i) the early renal cortical enhancement phase; (ii) the homogeneous nephrogram phase; and (iii) the delayed urographic phase, obtained several minutes later to demonstrate contrast within the collecting systems. With the multidetector CT (MDCT) systems, images may be reformatted in the coronal or sagittal plane for surgical planning (Fig. 8.10).

A 'split bolus' technique may be used in order to reduce the radiation dose to the patient: following the non-contrast

scan, a portion of the intravenous contrast dose is injected and the patient waits approximately 10 minutes, allowing the contrast to enter the ureters. Then, the patient is repositioned on the scanner and the remainder of the contrast medium is given as a rapid bolus with the scan obtained at the corticomedullary or nephrographic phase. This technique provides diagnostic images of both the kidneys and the ureters, whilst reducing the radiation to the patient.

Non-contrast 'CT KUB'

The position, size and Hounsfield unit of any renal calculi should be recorded. The line of the ureters is then followed down to the bladder in order to identify any ureteric stones.

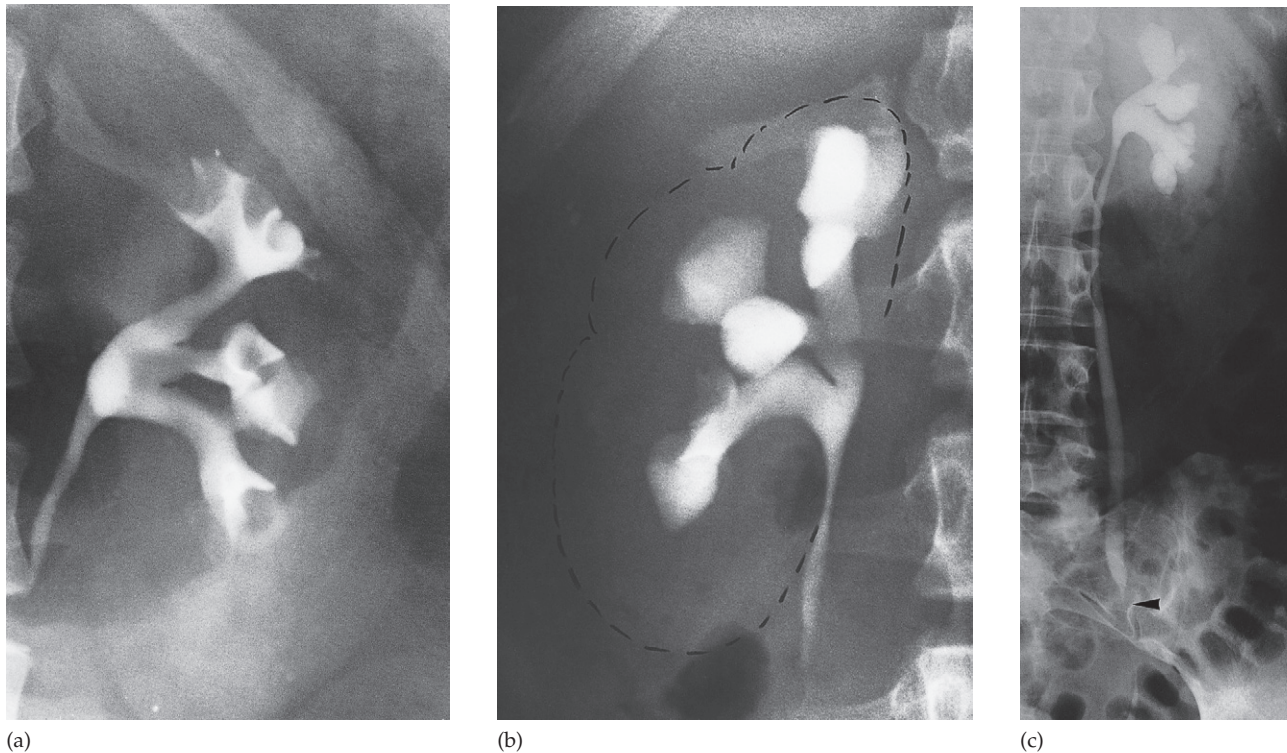


Fig. 8.7 Calices. (a) Normal calices. Each calix is cup-shaped. (b) Many of the calices are clubbed. There is scarring of the parenchyma of the upper half of the kidney indicating that the diagnosis is chronic pyelonephritis. (c) All the calices are dilated, the dilatation of the collecting system extending down to the point of obstruction (arrow), in this case owing to a malignant retroperitoneal lymph node.

Viewing coronal and sagittal thin section reformatted images increases the ability to detect very small stones (see Fig. 8.22). Occasionally, it may be difficult to differentiate a small calcified phlebolith from a non-obstructing ureteric stone, particularly if the ureter is not distended above the stone. In this case, correlation with post contrast CT IVU may be necessary. The appearance of the other organs and the bones should be assessed. In cases of suspected acute renal colic, alternative causes of pain should be sought, such as appendicitis.

Computed tomography after injection of contrast medium

Corticomedullary phase. At approximately 35–40 seconds following the start of the contrast injection, the only parts of

the renal tract that have enhanced are the renal arteries and renal cortex. Thus, there is a marked difference in the attenuation of the cortex and the medulla (see Fig. 8.8b). There is no contrast medium in the collecting system, which therefore has a low attenuation. This early stage of enhancement is particularly useful for evaluation of the renal arteries, which may be reformatted as a CT angiogram, as well as for the evaluation of highly vascular renal tumours.

Nephrographic phase. This occurs at approximately 90 seconds and demonstrates uniform opacification of the renal parenchyma. There is homogeneous opacification of the cortex and the medulla, the 'homogeneous nephrogram' phase, and some contrast medium is seen in the renal pelvis. There is usually a clearly visible difference in the density of normal renal tissue and a tumour.

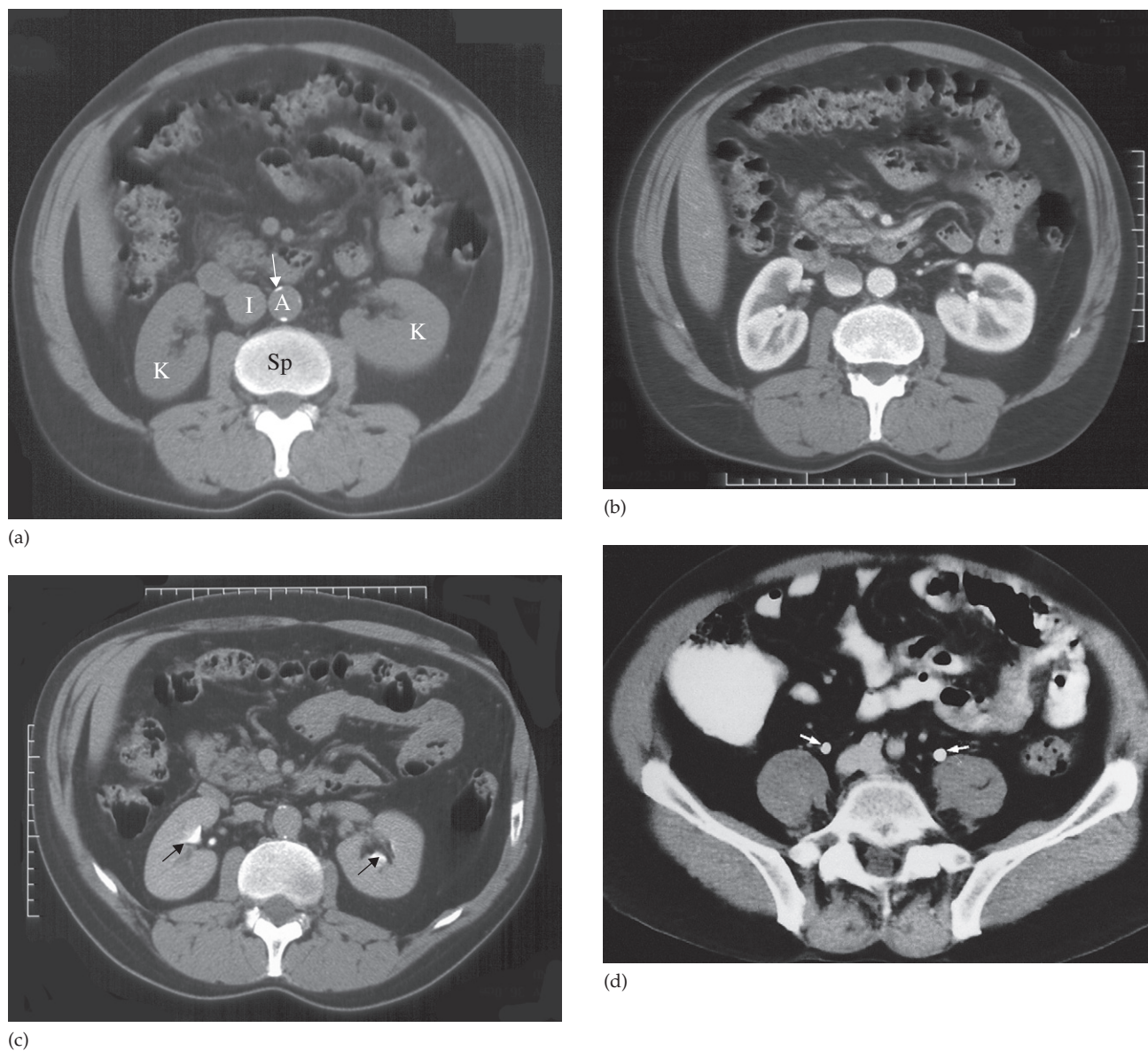


Fig. 8.8 Normal CT of kidneys and bladder, with (a–c) showing the same level through the renal hilum. (a) Before the intravenous contrast has been given. Note the calcification in the wall of the aorta (arrow). A, aorta; I, inferior vena cava; K, kidney; Sp, spine. (b) Forty seconds after intravenous contrast infusion, demonstrating the corticomedullary phase, with marked enhancement of the renal cortex. (c) Ten minutes following the contrast infusion, demonstrating homogeneous opacification of the parenchyma and dense opacification of the pelvicaliceal system (arrows). (d) Section through the pelvis showing the ureters (arrows) ten minutes after contrast has been given.

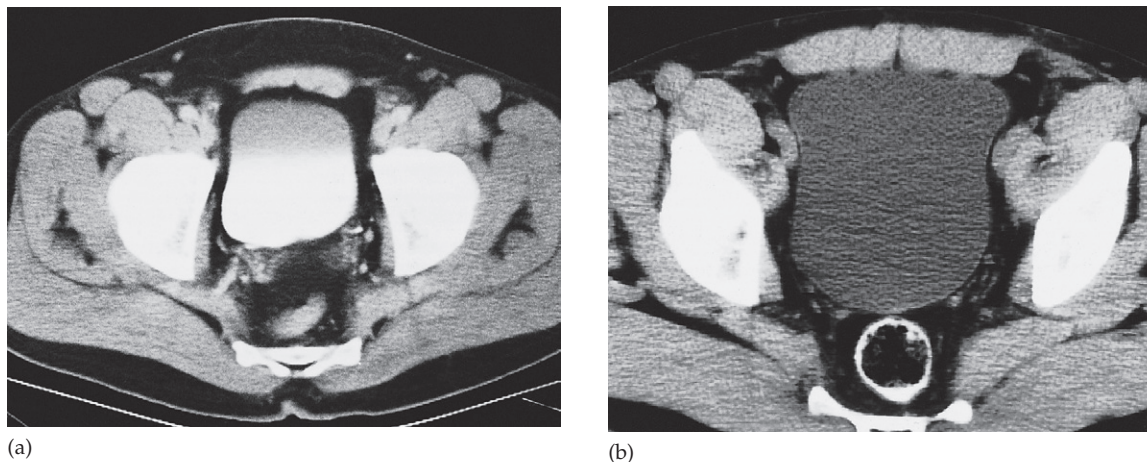


Fig. 8.9 (a) CT section through an opacified bladder in a male patient showing that the bladder wall is too thin to be seen. Note the layering of contrast medium. (b) Section through a bladder without contrast opacification. The bladder wall can be identified as a thin line.

Urographic phase. Obtained at approximately 10–15 minutes after contrast injection, during this phase the pelvicaliceal system, ureters and bladder should contain contrast. The pelvicaliceal system should show cupped calices with a uniform width of renal parenchyma from calix to renal edge, and the renal sinus fat that surrounds the pelvicaliceal system should be clearly visualized. The ureters are seen in cross-section as dots lying on the psoas muscles (see Fig. 8.8d). They will not necessarily be seen at all levels because peristalsis obliterates the lumen intermittently. The bladder has a smooth outline and stands out against the pelvic fat; its wall is thin and of reasonably uniform diameter. Contrast medium opacification of the urine in the bladder is variable depending on how much contrast medium has reached the bladder. The contrast medium is heavier than urine and, therefore, the dependent portion is usually more densely opacified (see Fig. 8.9). Curved reformats of the ureters may be used to display the urographic phase (see Fig. 8.10).

Magnetic resonance imaging

Magnetic resonance imaging gives similar anatomical information to CT, with the advantage of being able to obtain scans directly in multiple planes. It is generally used

in selected circumstances, e.g. to demonstrate renal artery stenosis or inferior vena caval extension of renal tumours, or to clarify problems not solved by ultrasound or CT. It is also used to assess the extent of bladder or prostate cancer prior to consideration for surgery. Calcification is not visible on MRI, which is one of the main disadvantages of the technique for renal tract imaging.

Normal magnetic resonance imaging

As with CT and ultrasound, the renal contours should be smooth. Corticomedullary differentiation is best seen on T1-weighted images and immediately following intravenous contrast enhancement with gadolinium (Fig. 8.11). The renal collecting systems, ureters and bladder are best seen on T2-weighted images, as the fluid returns a high signal intensity (Fig. 8.12). A heavily T2-weighted image may be used to acquire a magnetic resonance urogram. Some normal variants are well demonstrated on MRI: fetal lobulation is seen as an undulating renal contour but with uniform cortical thickness on coronal images (see Fig. 8.6b); a column of Bertin (which is normal renal parenchyma that may look mass-like) may be distinguished from a mass, as it has the same signal characteristics as the rest of the kidney on all sequences. The renal vasculature is best dem-



Fig. 8.10 CT reformat. This is the same patient as in Fig. 8.8a–c. The ureter (arrow) has been reformatted in the coronal plane. A, aorta; B, bladder; I, inferior vena cava; K, kidney.

onstrated following intravenous gadolinium and may be displayed in three dimensions (Fig. 8.13).

Radionuclide examination

Radionuclide techniques for studying the kidneys include:

- The renogram, which measures renal function.
- Scans of renal morphology (dimercaptosuccinic acid (DMSA) scan), although the advent of CT and ultrasound has reduced the need for such scans. They are now used mainly for evaluating renal scarring (see Fig. 8.43).
- The presence of reflux in children may be diagnosed using the technique of indirect voiding cystography. A radionuclide tracer is infused into the bladder via a catheter. The child then voids whilst being imaged by the gamma camera. The presence of reflux can be detected if tracer activity is seen to rise up into one or both of the ureters at the time of micturition (Fig. 8.14).

Renogram

If substances that pass into the urine are labelled with a radionuclide and injected intravenously, their passage through the kidney can be observed with a gamma camera (Fig. 8.15). The two agents of choice are technetium-99m (^{99m}Tc) diethylene triamine pentacetic acid (DTPA) and ^{99m}Tc mercaptoacetyl triglycine (MAG-3). DTPA is filtered by the glomeruli and is not absorbed or secreted by the tubules, whereas MAG-3 is both filtered by the glomeruli and secreted by the tubules.

The gamma camera is positioned posteriorly over the kidneys and a rapid injection of the radiopharmaceutical is given. Early images show the major blood vessels and both kidneys. Activity is then seen in the renal parenchyma and by 5 minutes the collecting systems should be visible. Serial images over 20 minutes show progressive excretion and clearance of activity from the kidneys. Computerized quantitative assessment enables a renogram curve to be produced and the relative function of each kidney to be calculated.

The main indications for a renogram are:

- Measurement of relative renal function in each kidney – this may help the surgeon decide between nephrectomy and more conservative surgery.

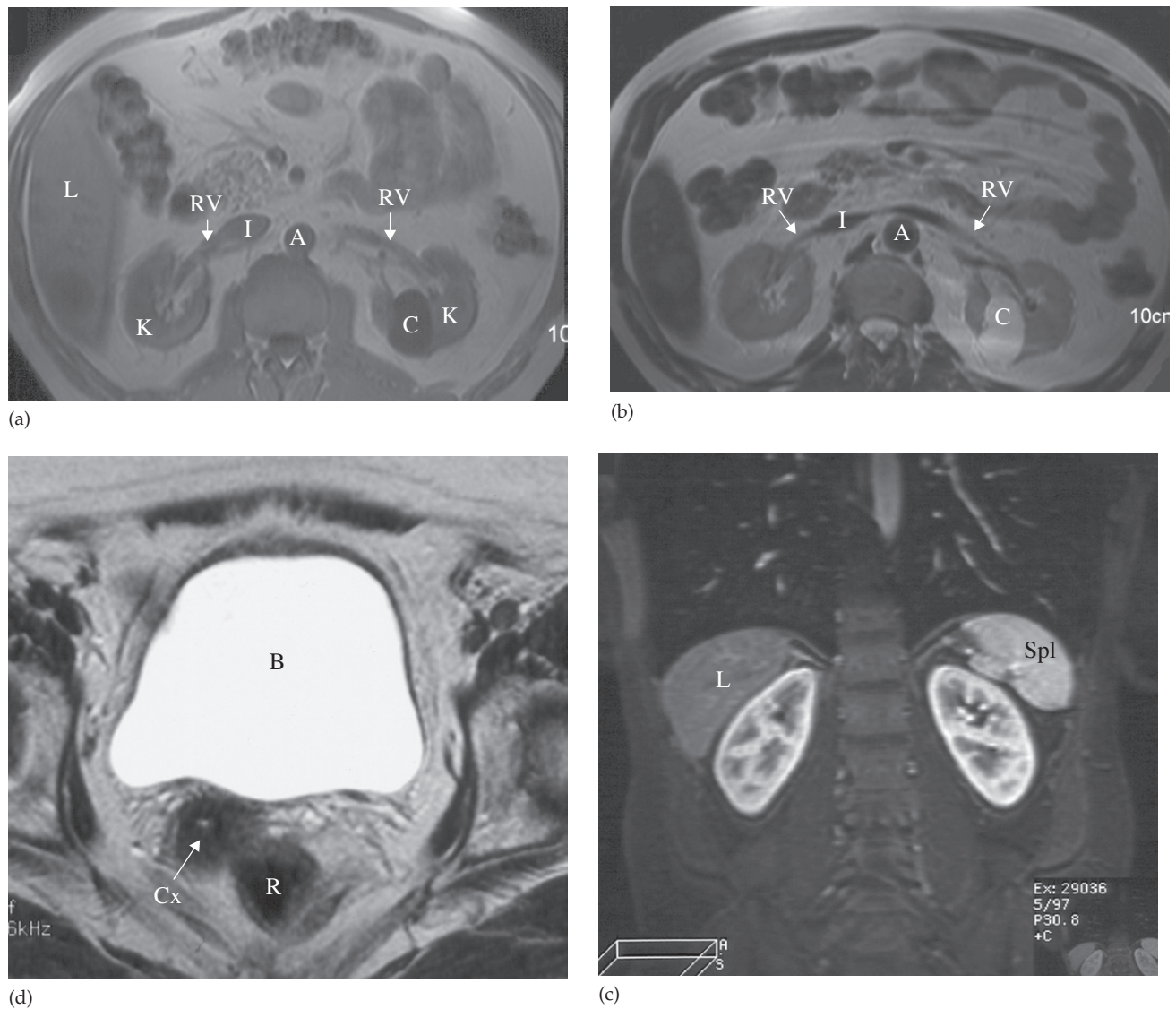


Fig. 8.11 MRI of the kidneys. (a) T1-weighted and (b) T2-weighted images in the axial plane at the level of the renal hila. Note the simple cyst (C) in the left kidney, which returns a low signal on T1- and a high signal on T2-weighted images. (c) Coronal image of the kidneys, in a different patient, following intravenous gadolinium infusion. (d) Normal bladder (B) on a T2-weighted image. The bladder wall is thin and smooth. A, aorta; Cx, cervix; I, inferior vena cava; K, kidney; L, liver; R, rectum; RV, renal vein; Spl, spleen.



Fig. 8.12 T2-weighted MRI showing a dilated ureter (arrow) due to obstruction by a pelvic mass (M).

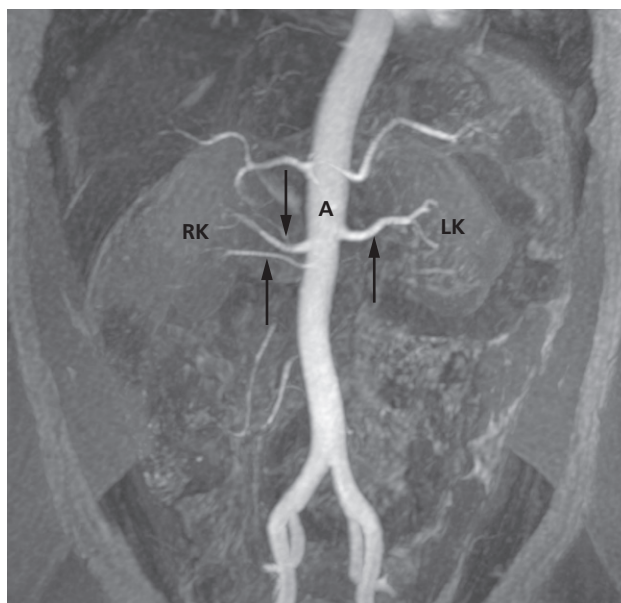


Fig. 8.13 Magnetic resonance angiogram of normal renal arteries, displayed coronally (arrows). There are two renal arteries supplying the right kidney (RK) and one supplying the left kidney (LK). A, aorta.

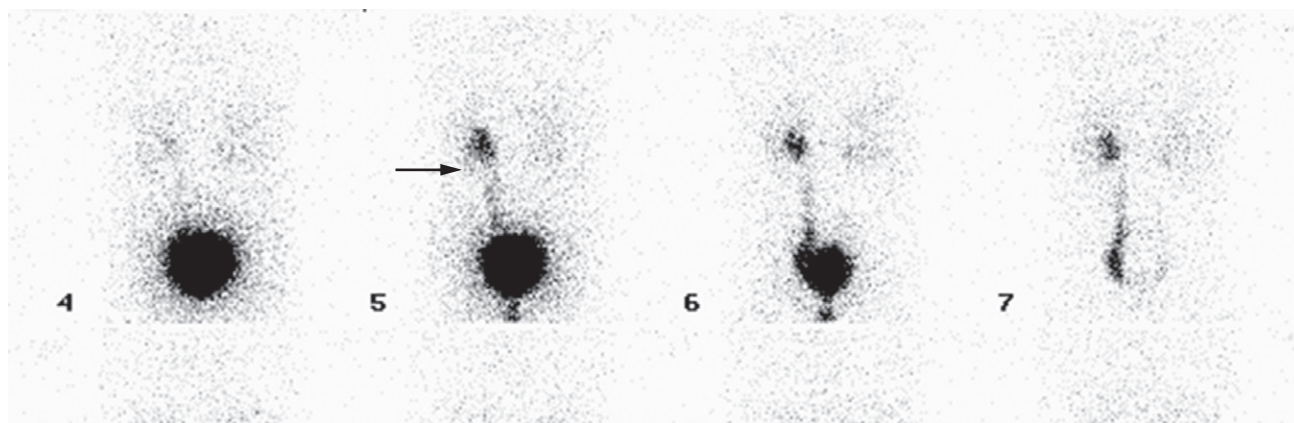


Fig. 8.14 Indirect voiding cystogram (posterior view) with tracer instilled into the bladder. Voiding is recorded on the gamma camera, starting at image 5. There is immediate reflux into the left ureter (arrow). The bladder is virtually empty on the final image, 7.

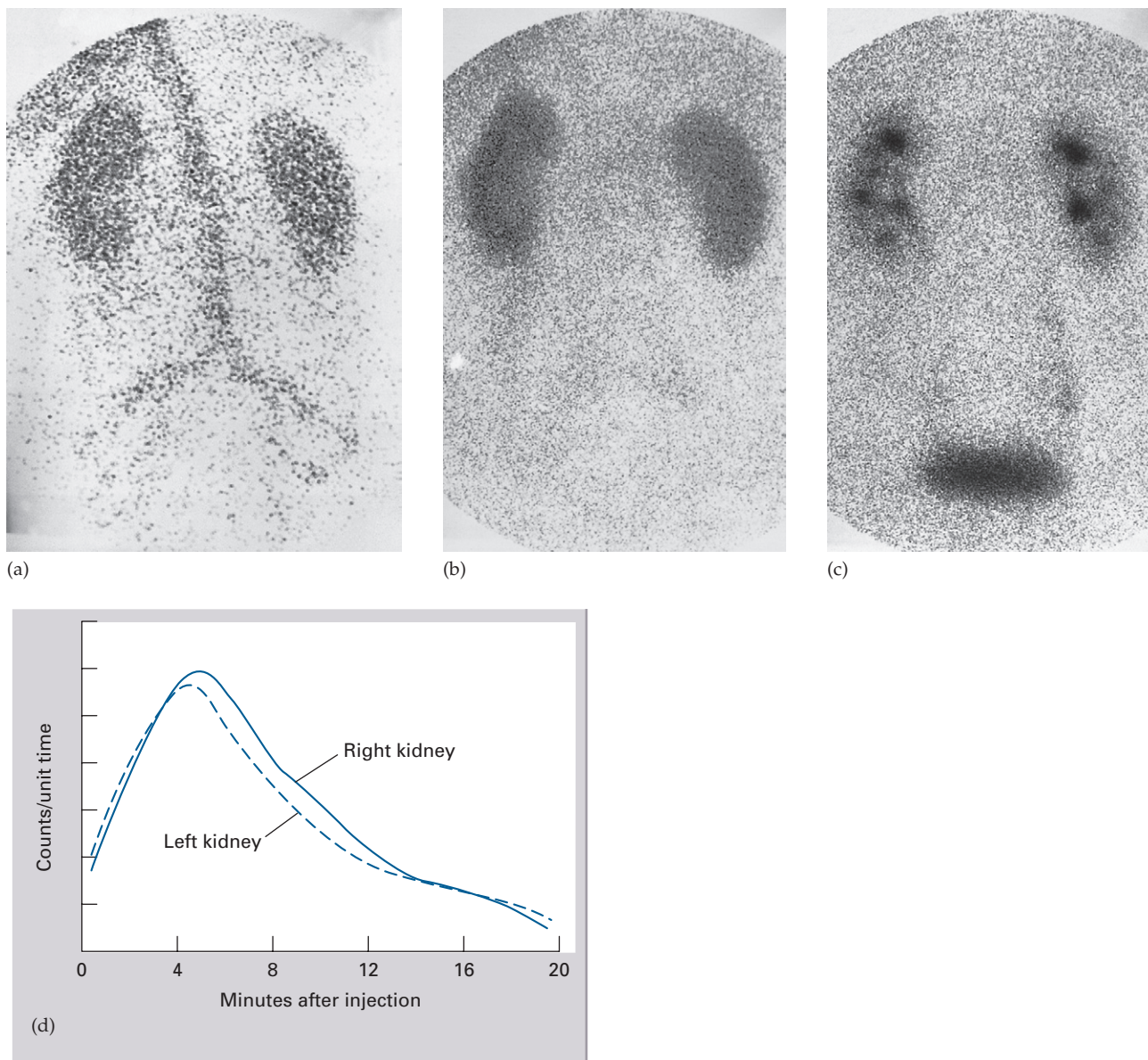


Fig. 8.15 ^{99m}Tc DTPA renogram, serial images. (a) Vascular phase. (b) Filtration phase. (c) Excretion phase. (d) The renogram curve.

- Investigation of urinary tract obstruction, particularly pelviureteric junction obstruction.
- Investigation of renal transplants.

Special techniques

Retrograde and antegrade pyelography

The techniques of retrograde and antegrade pyelography (the term pyelography means demonstrating the pelvicaliceal system and ureters) involve direct injection of contrast material into the pelvicaliceal system or ureters through catheters placed via cystoscopy (retrograde pyelography) or percutaneously into the kidney via the loin (antegrade pyelography). The indications are limited to those situations where the information cannot be achieved by less invasive means, e.g. IVU, CT or MRI to confirm a possible transitional cell carcinoma in the renal pelvis or ureter.

Voiding cystourethrogram (micturating cystogram) and videourodynamics

In voiding cystourethrography, the bladder is filled with iodinated contrast medium through a catheter and films are taken during voiding. The entire process is observed fluoroscopically to identify vesicoureteric reflux. The bladder and urethra can be assessed during voiding to demonstrate strictures or urethral valves (see Fig. 8.62).

Videourodynamic examination combines voiding cystourethrography with bladder pressure measurements, which necessitate bladder and rectal pressure lines. It is useful in the investigation of incontinence to distinguish detrusor instability from sphincter weakness (stress incontinence). The test is also helpful in patients with obstructive symptoms, mainly elderly men, to differentiate true obstruction from bladder instability, and in patients with a neurogenic bladder.

Urethrography

The urethra is visualized during voiding cystourethrography. For full visualization of the male urethra, however, an ascending urethrogram with contrast medium injection via the external urethral meatus is necessary (see Fig. 8.61). The usual indications for the examination are the identification of urethral strictures and to demonstrate extravasation from the urethra or bladder neck following trauma.

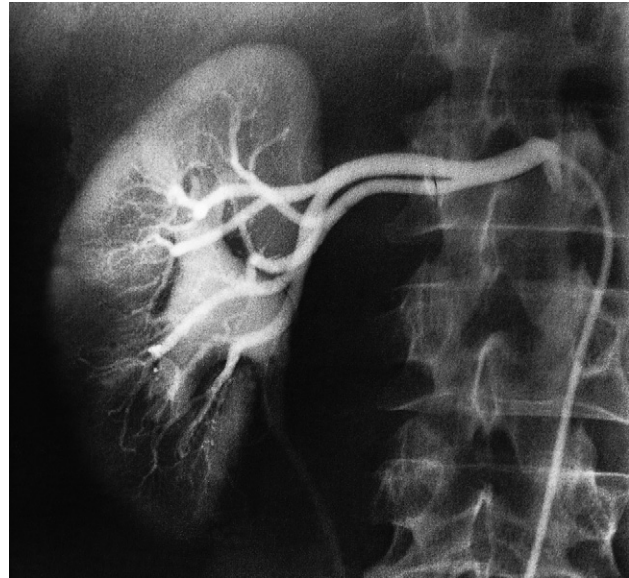


Fig. 8.16 Normal selective right renal arteriogram. Note that not only are the arteries well shown but there is also an excellent nephrogram. The renal pelvis and ureter are opacified because of a previous injection of contrast.

Renal arteriography

Renal arteriography is performed via a catheter introduced into the femoral artery by the Seldinger technique (see Chapter 17). Selective injections are made into one or both renal arteries (Fig. 8.16). It is mainly used to confirm the CT or MRI findings of vascular anatomy prior to renal surgery and to confirm renal artery stenosis prior to percutaneous balloon angioplasty.

Urinary tract disorders

Urinary calculi

Urinary calculi may be asymptomatic. The imaging of calculi causing urinary obstruction is described below.

Most urinary calculi are calcified and show varying density on x-ray examinations. Many are uniformly calcified but some, particularly bladder stones, may be laminated. Only pure uric acid and xanthine stones are radiolucent on plain radiography, but they can be identified at CT or ultrasound (Fig. 8.17).

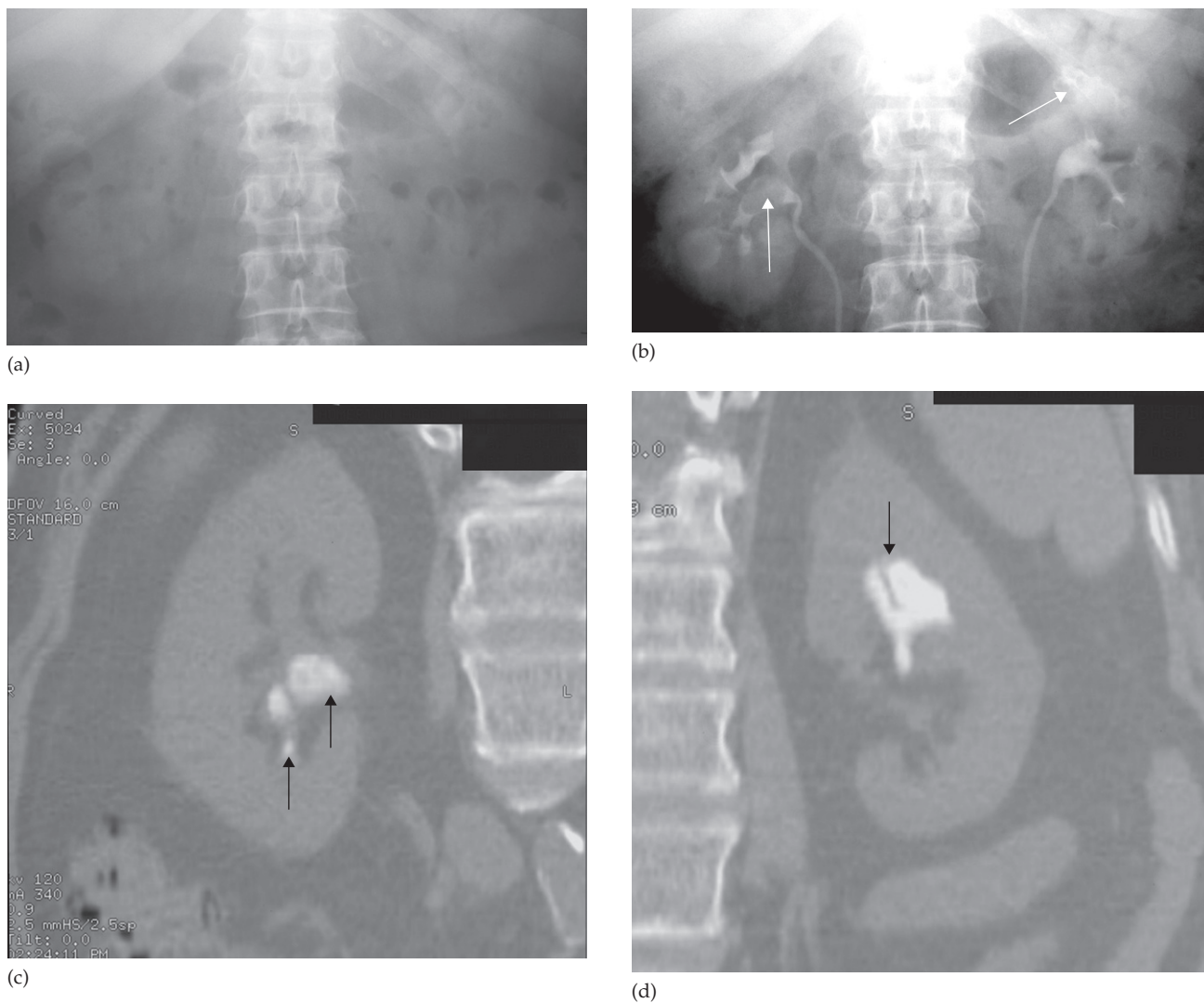


Fig. 8.17 (a) IVU control film. Renal stones are not visible on the right and are very poorly visualized on the left. (b) IVU following intravenous contrast. Filling defects are seen in the right lower calix and pelvis and in the left upper pole calices (arrows). (c, d) CT of the kidneys in the same patient with no contrast medium, reformatted in the coronal plane, demonstrating the renal stones in both the right (c) and left (d) kidneys (arrows).



Fig. 8.18 Plain film showing a calcified staghorn calculus in each kidney.

Small renal calculi are often round or oval; the larger ones frequently assume the shape of the pelvicaliceal system and are known as staghorn calculi (Fig. 8.18).

Plain film examination of the urinary tract is more sensitive than ultrasound for detecting opaque renal and ureteric calculi. It is essential to examine the preliminary film of an IVU carefully, because even large calculi can be completely hidden within the opacified collecting system once contrast medium has been given (see Fig. 8.3). Stones in the ureters may be partly obscured where they overlie the vertebral transverse processes or the sacrum.

Most renal calculi of more than 5 mm in size are readily seen at ultrasound, but smaller calculi may be missed, particularly if they are located within the renal sinus, where they may be obscured by echoes from the surrounding fat. Stones, regardless of their composition, produce intense echoes and cast acoustic shadows (Fig. 8.19). Staghorn calculi, filling the caliceal system, cast very large acoustic shadows, which may even mask an associated hydronephrosis. Stones in the ureters cannot be excluded on ultrasound, although stones lodged at the vesicouteric junction may be demonstrated (Fig. 8.20). Stones in the bladder, or in bladder diverticula, are well demonstrated on ultrasound.

Computed tomography without intravenous contrast medium is exquisitely sensitive for the detection of calculi. It is used in place of IVU for the detection and precise

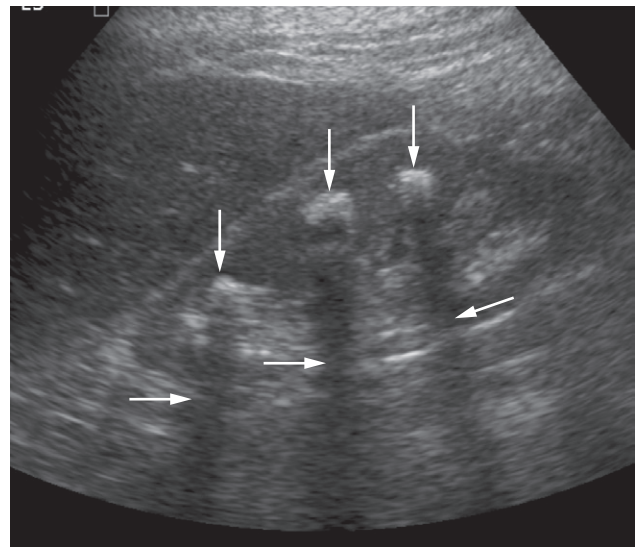


Fig. 8.19 Ultrasound of stones in the right kidney. The stones (vertical arrows) appear as bright echoes. Note the acoustic shadows behind the stones (horizontal arrows).

anatomical localization of stones prior to treatment in most centres (Figs 8.21 and 8.22). If a stone is obstructing a ureter, the dilated ureter can usually be followed down to the level of the stone, below which the ureter is undistended. In some cases, particularly if a small ureteric stone is not

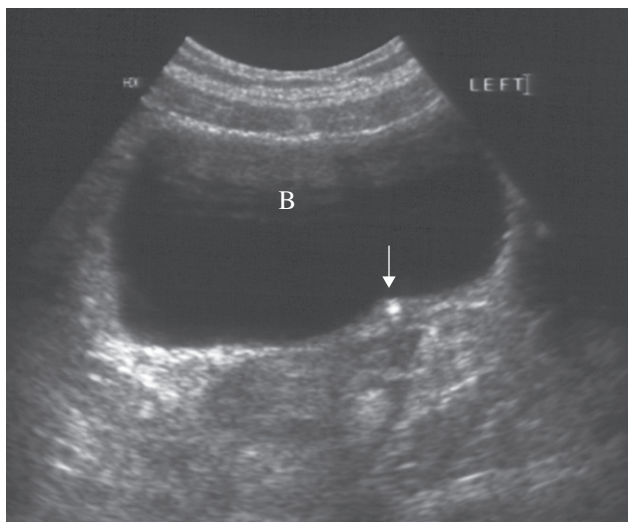


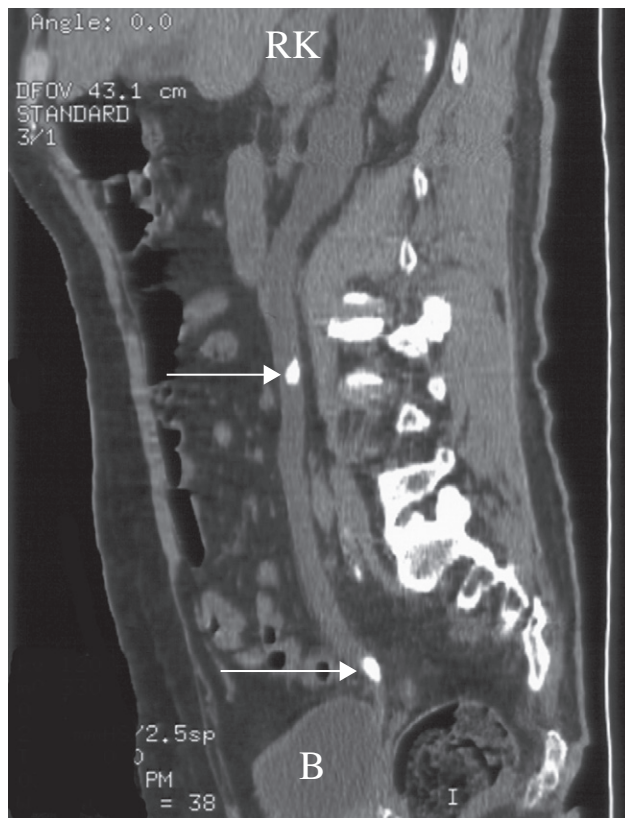
Fig. 8.20 Ultrasound of the bladder (B), demonstrating a stone lodged at the left vesicoureteric junction (arrow). In this case, no acoustic shadow was seen.



Fig. 8.21 Non-contrast enhanced CT in a patient with crossed fused ectopia, a renal anatomical variant (K). Multiple stones were demonstrated (arrows), allowing accurate planning of his lithotripsy treatment.



(a)



(b)

Fig. 8.22 Non-contrast-enhanced CT reformatted in the coronal plane (a) and sagittal plane (b), demonstrating a hydronephrotic right kidney (RK) and two stones in the dilated right ureter (long arrows). The patient also has kidney stones in the left pelvicaliceal system (short arrows). B, bladder.



(a)



(b)

Fig. 8.23 Nephrocalcinosis. (a) On plain film, there are numerous calcifications in the pyramids of both kidneys (the left kidney is not illustrated). (b) In a different patient, bilateral renal parenchymal calcifications are demonstrated on CT KUB. There is also one calculus lying within the right renal pelvis (arrow).

causing obstruction and the ureter is not dilated, it can be difficult to be certain if a calcification lies within or outside the ureter. In these cases, the use of intravenous contrast media and delayed phase imaging can be very helpful to delineate the line of the ureter.

Nephrocalcinosis

Nephrocalcinosis is the term used to describe focal or diffuse calcification within the renal parenchyma (Fig. 8.23). Diffuse nephrocalcinosis may be associated with the following:

- Hypercalcaemia and/or hypercalciuria, notably hyperparathyroidism and renal tubular acidosis.

- Widespread papillary necrosis and medullary sponge kidney (a congenital condition with dilated collecting tubules in which small calculi can form) in the presence of normal calcium metabolism.

Urinary tract obstruction

The principal feature of obstruction is dilatation of the pelvicaliceal system and ureter. All the affected calices are dilated to approximately the same degree; the degree depends on the chronicity, with more marked dilatation seen more often in longstanding obstruction. The obstructed collecting system is dilated down to the level of the obstructing pathology and demonstrating this level is a prime

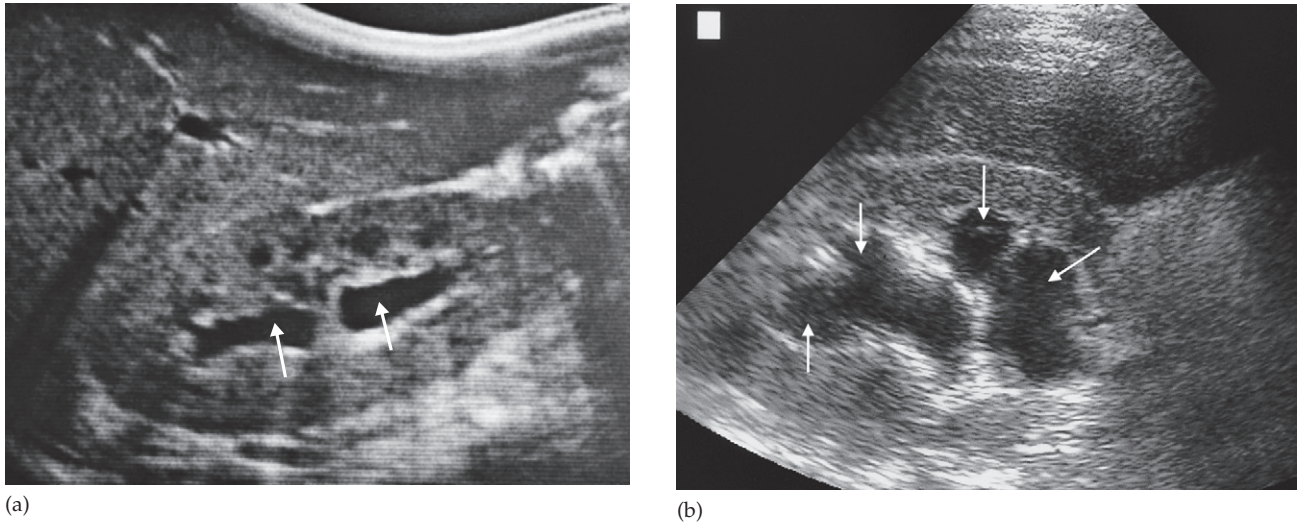


Fig. 8.24 Dilatation of the pelvicaliceal system. (a) Longitudinal ultrasound scan of the right kidney showing spreading of the central echo complex of the dilated collecting system (arrows). (b) Here the dilatation of the calices is greater (arrows).

objective of imaging (see Fig. 8.7c). Ultrasound and urographic examination play major roles when evaluating urinary tract obstruction, and CT urography has overtaken IVU for the investigation of obstruction (see Fig. 8.22). Radionuclide studies show typical changes, but are rarely the primary imaging procedures.

Ultrasound

Dilatation of the pelvicaliceal system is demonstrated sonographically as a multiloculate fluid collection in the central echo complex, caused by pooling of urine within the distended pelvis and calices (Fig. 8.24a). As the distension becomes more severe, the dilated calices can resemble multiple renal cysts, but dilated calices, unlike cysts, show continuity with the renal pelvis (Fig. 8.24b). With prolonged obstruction, thinning of the cortex due to atrophy will be seen.

Proximal ureteric dilatation can frequently be identified, but overlying bowel often obscures dilatation of the mid and distal ureter. If the obstruction is at the level of the vesicoureteric junction, the distal ureter can usually be visualized. It follows, therefore, that while some causes of obstruction are identifiable (e.g. carcinoma of the bladder or a stone at the vesicoureteric junction), it is often not pos-

sible to determine the cause of urinary tract obstruction at ultrasound examination. Ultrasound may demonstrate a pelvic mass, such as a uterine or ovarian mass, causing external compression of the collecting system.

Intravenous urogram

In some centres, IVU remains the primary imaging modality in patients with suspected acute obstruction, which is usually caused by a calculus. Plain films may demonstrate the calculus responsible for the obstruction. However, as parts of the ureter overlie the transverse processes of the vertebrae and the wings of the sacrum, the calculus may be impossible to see on plain film. Following injection of intravenous contrast medium, a film of the renal tract is taken at approximately 15 minutes. If the urogram is normal, with contrast seen in normal, undistended ureters bilaterally, then this effectively rules out ureteric colic as the cause of acute pain. If one of the ureters is obstructed, then a dense nephrogram will be seen and opacification of the pelvicaliceal system and ureter on the obstructed side takes much longer. Delayed films are, therefore, an essential part of any IVU where the level of obstruction is not shown on routine films. In time, the collecting system and the level of obstruction can usually be demonstrated (Fig. 8.25).

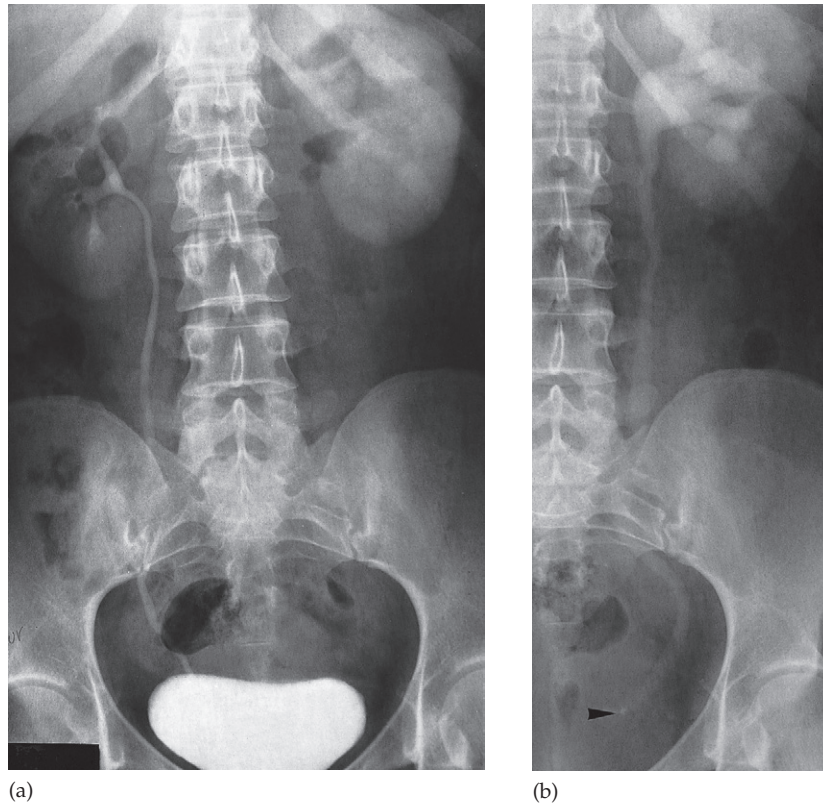


Fig. 8.25 Acute ureteric obstruction from a stone in the lower end of the left ureter. (a) A film taken 30 minutes after the injection of contrast medium. There is obvious delay in the appearance of the pyelogram on the left. The left kidney shows a very dense nephrogram which is characteristic of acute ureteric obstruction. (b) A film taken 23 hours later shows opacification of the obstructed collecting system down to the obstructing calculus (arrowhead).

Computed tomography

Computed tomography is now widely used to evaluate urinary tract obstruction (Fig. 8.26). In acute obstruction, non-contrast enhanced CT sensitively demonstrates calculi and the unopacified, dilated collecting system can frequently be traced down to the point of obstruction (see Fig. 8.22). Non-contrast CT is often used in acute ureteric colic, as an alternative to IVU, in patients with an allergy to intravenous contrast medium. CT also has the advantage of demonstrating possible alternative causes of acute abdominal pain, such as appendicitis. Chronic obstruction by tumour, either within the renal collecting system or by an external tumour causing compression, may be visual-

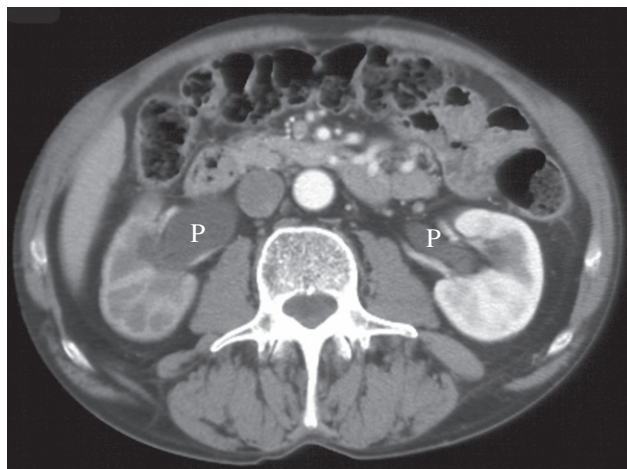
ized directly on CT or MRI and staging of the tumour can be performed during the same investigation.

Causes of obstruction to the ureters and pelvicaliceal systems

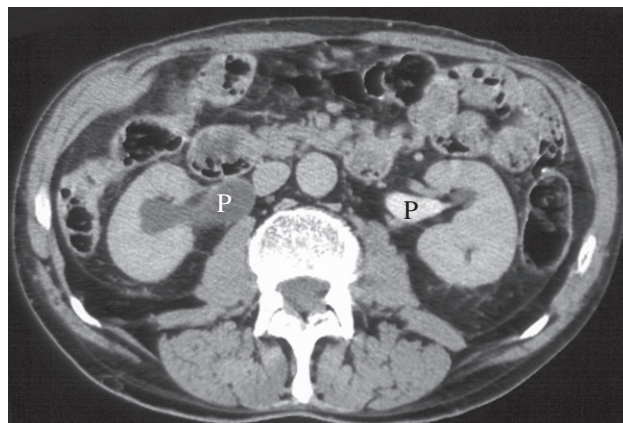
There are many causes of obstruction to the urinary tract, which may arise at any level from the pelvicaliceal system down to the urethra (see Box 8.2).

Causes within the lumen of the urinary tract

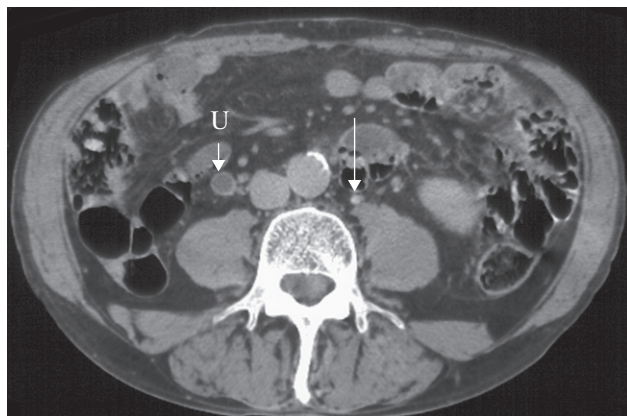
Calculi are by far the commonest cause of obstruction of the urinary tract. The imaging techniques are described above. A sloughed papilla in papillary necrosis is a rare



(a)



(b)



(c)

Fig. 8.26 (a) CT at the corticomedullary phase of enhancement. There is obstruction of the right kidney with dilatation of the pelvicaliceal system, reduced cortical enhancement and some loss of cortical thickness, suggesting that the obstruction may be longstanding. (b) CT at the delayed phase of enhancement. Intravenous contrast is seen in the left renal pelvis but not in the obstructed right renal pelvis. (c) CT through the dilated right ureter (U), in the same patient as (a) and (b). Note the normal left ureter (long arrow). P, renal pelvis.

cause of ureteric obstruction. The diagnosis can be suspected when other papillae still within the kidney show signs of papillary necrosis (see Fig. 8.44). Blood clot within the collecting system needs to be differentiated from other causes such as stones or a tumour (see Fig. 8.38).

Causes arising in the wall of the collecting system

A *transitional cell carcinoma* (TCC) (see Fig. 8.39) within the ureter or the bladder in the region of the vesicoureteric junction may cause obstruction (a TCC in the pelvicaliceal system rarely causes obstruction). Ureteric tumours may be

seen as a filling defect on IVU or as a point of obstruction with no visible mass. Ureteric TCCs are well demonstrated by pyelography, either retrograde or antegrade. CT, particularly MDCT, may also be used to demonstrate pelvicaliceal and ureteric tumours, particularly on the delayed 'urographic' images, when the pelvicaliceal system and ureter are filled with contrast medium. Carcinoma of the bladder causing ureteric obstruction can usually be identified on IVU, ultrasound, CT or MRI, though cystoscopy is the best method of establishing the diagnosis.

Infective strictures of the collecting systems are mostly due to tuberculosis or schistosomiasis. In the case of tuber-

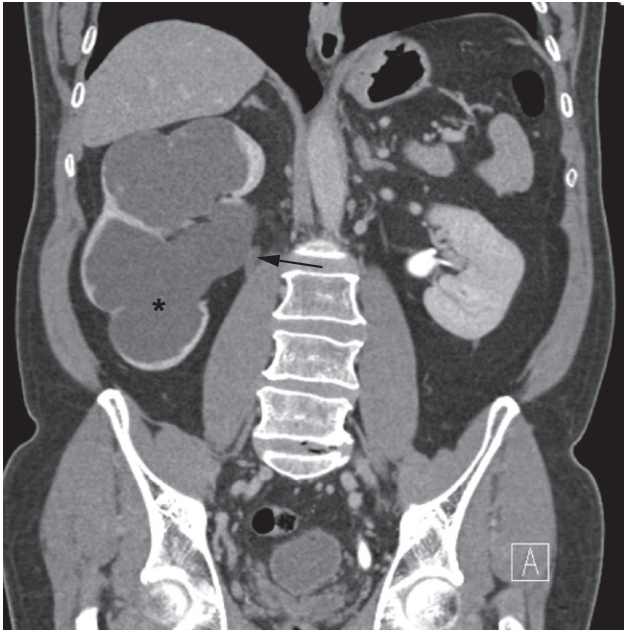


Fig. 8.27 Intrinsic PUV obstruction. The pelvicaliceal system is considerably dilated (*). There is an abrupt change in calibre at the level of the PUV (arrow) and the ureter from the PUV onward is normal in calibre.

culosis there is usually other imaging evidence to suggest the diagnosis (see Fig. 8.42).

Congenital intrinsic pelviureteric junction obstruction

In this disorder, peristalsis is not transmitted across the pelviureteric junction (PUJ). The disease may present at any age but it is usually discovered in children or young adults. The diagnosis depends on identifying dilatation of the renal pelvis and calices, with an abrupt change in calibre at the PUJ (Fig. 8.27). Often, the ureter cannot be identified at all; if it is seen, it will be either narrow or normal in size.

Pelviureteric junction obstruction can be difficult to distinguish on IVU from an otherwise normal, unobstructed, dilated renal pelvis – the so-called ‘baggy pelvis’. This distinction can be made by giving a diuretic intravenously. In PUJ obstruction, the induced diuresis causes further dilatation of the pelvicaliceal system and the patient develops loin pain, whereas a baggy system drains. Similarly, a diu-

retic can be given during a renogram (Fig. 8.28). If there is obstruction, the radionuclide accumulates within the kidney and renal pelvis, whereas with a baggy pelvis there is rapid washout of the radionuclide from the suspect kidney.

Extrinsic causes of obstruction

Tumours. Carcinoma of the cervix, ovary and rectosigmoid colon and malignant lymph node enlargement are frequent causes of ureteric obstruction. The ureters may be visibly deviated by the tumour but, frequently, the ureteric course is normal. Because some of these tumours originate in the midline or are bilateral, both ureters may be obstructed. CT is the ideal method of diagnosis because it shows the tumour mass as well as the level of obstruction.

Retroperitoneal fibrosis. In most cases, no cause can be found for this benign fibrotic condition, which encases the ureters and causes obstruction. When first seen, only one side may be obstructed but, eventually, the condition becomes bilateral. The obstruction is usually at the L4/5 level. Fibrosis may extend superiorly to surround the kidneys and inferiorly to involve the pelvic side walls. CT has become the diagnostic method of choice (Fig. 8.29).

Renal parenchymal masses

Most solitary masses arising within the renal parenchyma are either *malignant tumours* or *simple cysts*. In adults, a malignant tumour is almost certain to be a renal cell carcinoma, whereas in young children it is usually Wilms’ tumour. Other causes of a renal mass include: renal abscess, benign tumour (notably oncocytoma or angiomyolipoma), hydatid cyst and metastasis.

Occasionally, invagination of normal cortical tissue into the central part of the kidney (sometimes called a ‘renal pseudotumour’ or column of Bertin) may produce the signs of a localized mass at ultrasound. DMSA, CT or MRI can be used to exclude a true tumour.

Multiple renal masses include:

- multiple simple cysts
- polycystic disease
- malignant lymphoma
- metastases
- inflammatory masses.

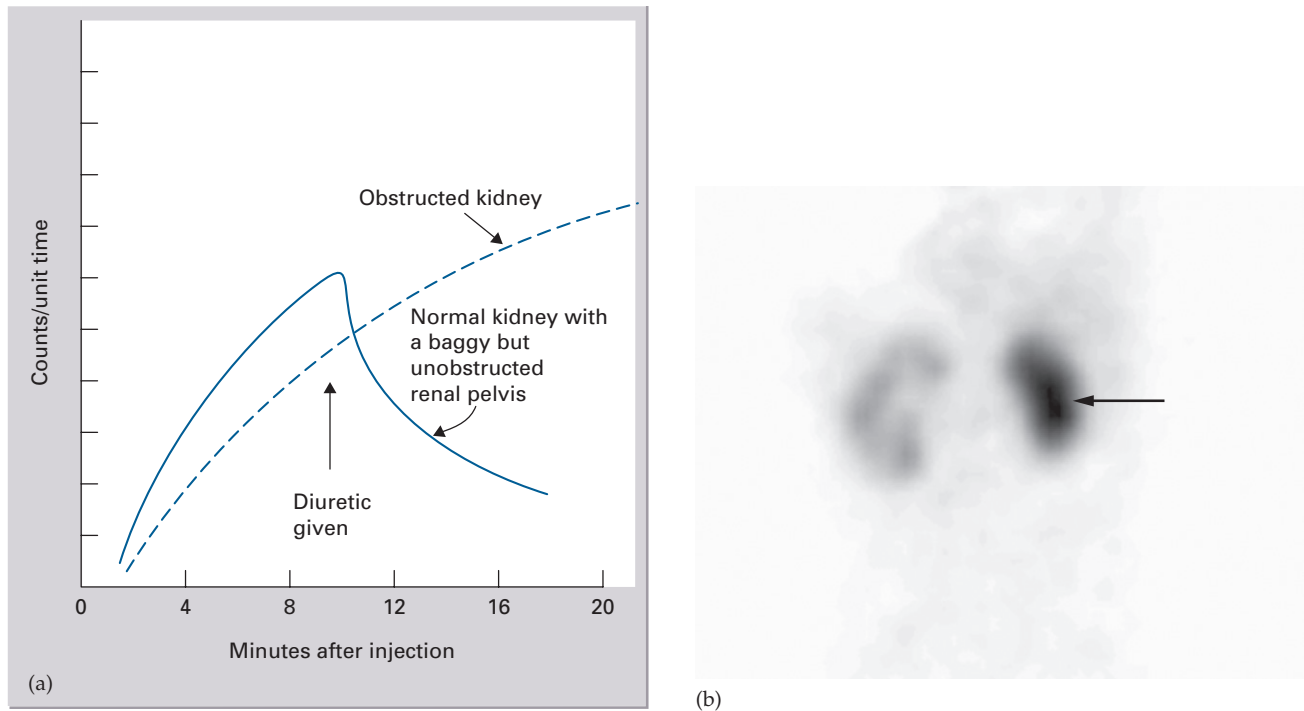


Fig. 8.28 (a) Diuretic renogram comparing PUJ obstruction (dashed line) with a 'baggy' but otherwise normal renal pelvis (continuous line). Frusemide was given at 10 minutes and in the case of the 'baggy' pelvis resulted in rapid washout of radioactivity from the kidney. (b) The post diuretic renogram image demonstrates washout of tracer on the unobstructed side and accumulation of tracer in the dilated renal pelvis on the obstructed side (arrow).

Ultrasound

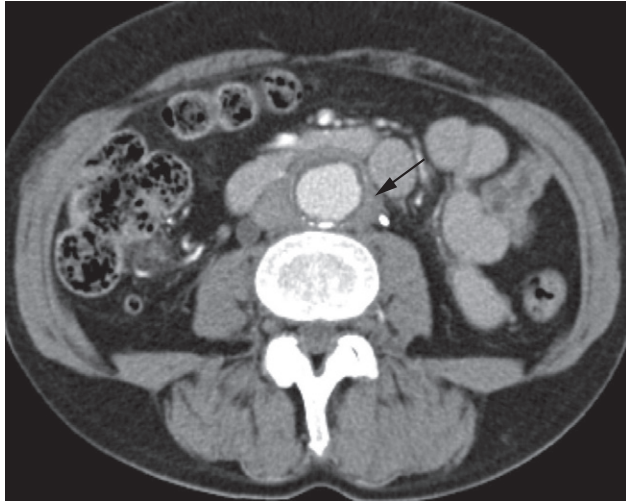
Renal masses are usually first detected at ultrasound examination (Fig. 8.30). Ultrasound can establish whether a mass is a simple cyst and can, therefore, be ignored, or whether the lesion is solid and, therefore, is likely to be a renal carcinoma. A mass with mixed cystic and solid features falls into the indeterminate category and could be a renal tumour, a renal abscess, or possibly a complex benign cyst or other benign condition.

Simple cysts are very common in the middle-aged and elderly. They are filled with clear fluid and thus demonstrate no echoes from within the cyst. They show obvious echoes from the front and back walls of the cyst and a column of increased echoes behind the cyst, because of increased through transmission of the sound, known as 'acoustic enhancement'. Most cysts are spherical in shape.

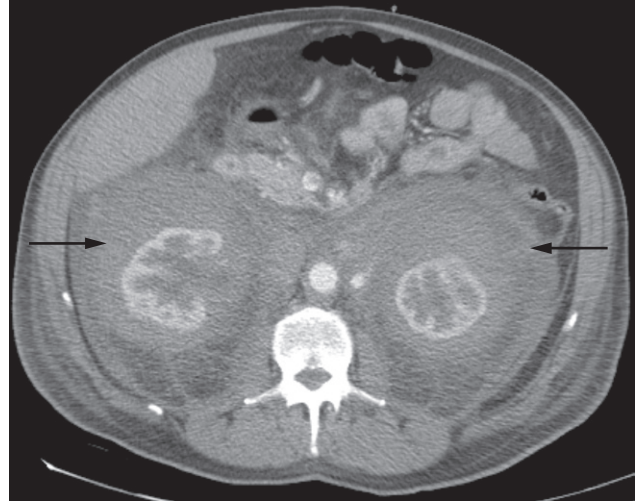
They may be solitary or multiple, unilocular or have septations. Some cysts contain low level echoes in their dependent portions, presumably due to previous haemorrhage. When the ultrasonographer is sure that the diagnosis is a simple cyst, no further investigation is needed. Indeterminate lesions with both cystic and solid components need further evaluation with CT.

Angiomyolipomas (Fig. 8.30d) are a fairly frequent incidental finding at ultrasound, appearing as small echogenic masses. CT or MRI may be used to confirm the diagnosis (see below).

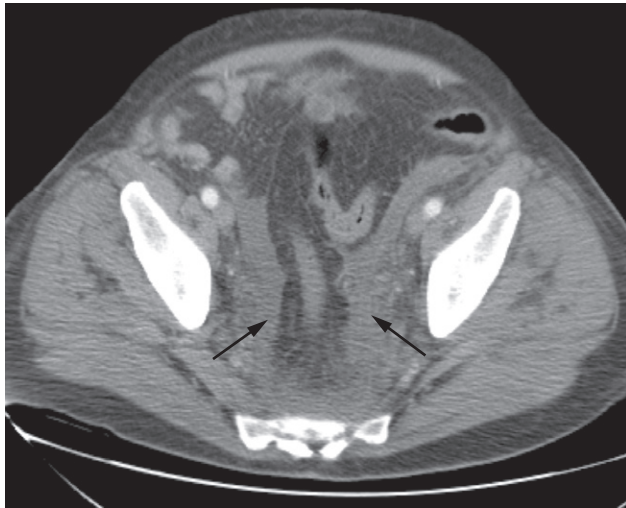
Solid renal masses have numerous internal echoes of varying intensity. Because sound is attenuated during its passage through a solid lesion, the back wall is not as sharp as that seen with a cyst, and there is often little or no acoustic enhancement deep to the mass. Solid masses may be irregular in outline and contain calcifications.



(a)



(b)



(c)

Fig. 8.29 Retroperitoneal fibrosis. (a) CT scan demonstrating a cuff of fibrous tissue surrounding the aorta (arrow). The retroperitoneal fibrosis extended down to the level of aortic bifurcation. (b) In a different patient, there is mild hydronephrosis on the right. Both kidneys are surrounded by dense fibrosis, infiltrating the perinephric fat (arrows). (c) The fibrosis extended down the aorta to the pelvis.

When a tumour is demonstrated, the ultrasonographer should also look for extension into the renal vein and inferior vena cava, check for liver and retroperitoneal metastases, and examine the opposite kidney.

Intravenous urography

The initial diagnosis of a renal mass is now rarely made on IVU as ultrasound and CT are the usual primary modal-

ities. The basic signs of a renal parenchymal mass on an IVU are:

- A rounded lucency in the nephrogram.
- Bulging of the renal outline. Sometimes, the outline is so indistinct that the bulge cannot be appreciated.
- Displacement and/or distortion of the major and minor calices.
- Calcification in a small proportion of renal carcinomas (Fig. 8.31).

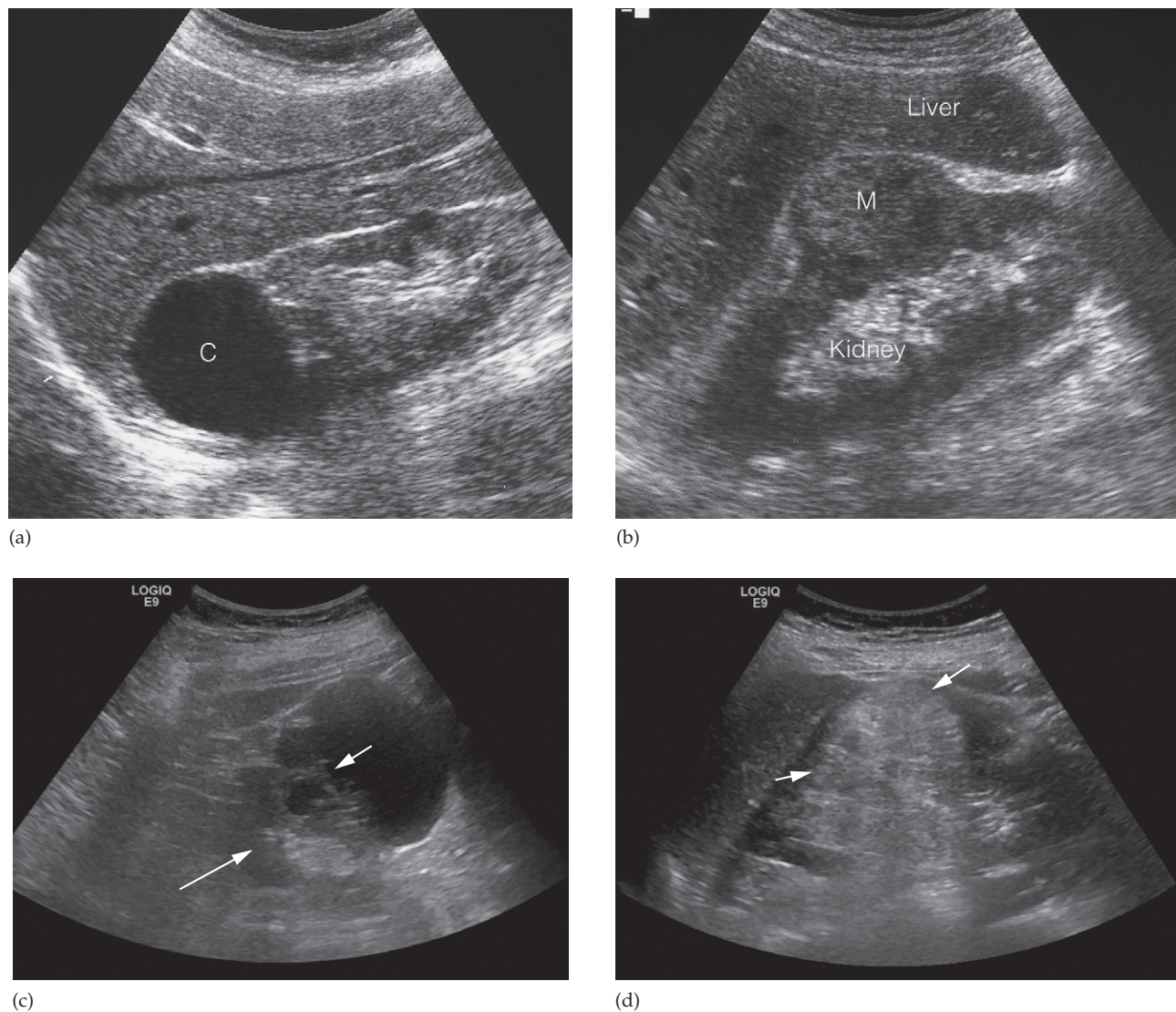


Fig. 8.30 Ultrasound in renal masses. (a) Simple cyst (C) showing sharp walls and no echoes arising within the cyst. Note the acoustic enhancement behind the cyst. (b) Tumour showing echoes within a solid mass (M). (c) Complex cystic mass which could be due to cystic renal cell carcinoma. The short arrow points to the irregular solid part of the mass. The adjacent normal renal parenchyma is shown with a long arrow. (d) Angiomyolipoma; this incidental finding shows the typical appearance of a well-defined echogenic mass (arrows). Same patient as in Fig. 8.32c.



Fig. 8.31 Plain radiograph of a partially calcified renal cell carcinoma.

Once a mass is seen or suspected at IVU, the next step is to diagnose its nature using ultrasound or CT. It should be noted that any solitary mass in a young child, or any mass that contains visible calcification, particularly if the calcification is more than just a thin line at the periphery, is likely to be a malignant tumour.

Computed tomography and magnetic resonance imaging

Increasingly, renal masses are detected incidentally as part of a CT scan undertaken for a different purpose. In addition, CT has proved very useful for characterizing indeterminate renal masses identified on ultrasound. CT may be used to differentiate cysts from tumours, to diagnose angiomyolipomas (Fig. 8.32) and to stage renal carcinoma. Renal masses may be characterized on MRI, but this is usually reserved for solving specific problems.

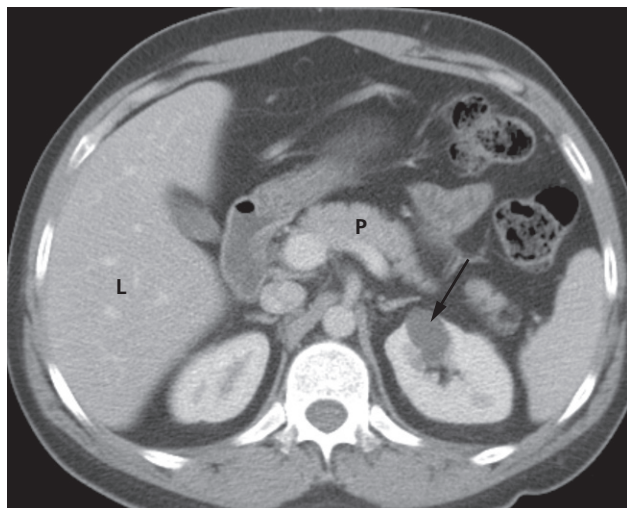
At CT, a typical *simple renal cyst* is a spherical mass with an imperceptible wall (Fig. 8.32a). The interior of the cyst is homogeneous with attenuation values similar to water. The margins between the cyst and the normal renal parenchyma are sharp. When all of these criteria are met, the diagnosis of simple cyst is certain and there is no need to proceed further. On MRI, a simple cyst appears as a well-defined, rounded mass with a homogeneous high signal intensity on T2-weighted images and low signal on T1-weighted images, with no post gadolinium enhancement (see Fig. 8.11).

Angiomyolipomas are usually incidental findings. They are benign tumours, which rarely cause problems, although, on occasion, they cause significant retroperitoneal haemorrhage. At CT and MRI, their fat content allows a confident diagnosis (Fig. 8.32b, c).

Renal cell carcinomas are approximately spherical and often lobulated (Fig. 8.33). The attenuation value of renal tumours on scans without intravenous contrast enhancement is often fairly close to that of normal renal parenchyma, but focal necrotic areas may result in areas of low density, and stippled calcification may be present in the interior of the mass as well as around the periphery. Following intravenous contrast administration, renal cell carcinomas enhance, but not to the same degree as the normal parenchyma, and they are inhomogeneous in their enhancement pattern. The CT diagnosis of renal carcinoma is usually sufficiently accurate so that preoperative biopsy is rarely performed.

Diagnostic difficulty arises with indeterminate cystic masses. The degree and appearance of any solid component within the cyst influences the risk of the lesion being malignant. Depending on the clinical circumstances and on the imaging appearances, the clinician may opt to follow up the lesion on imaging or may decide to proceed to surgery, on the assumption that the lesion is likely to be malignant. In some centres, indeterminate renal lesions are further evaluated with percutaneous biopsy under CT guidance.

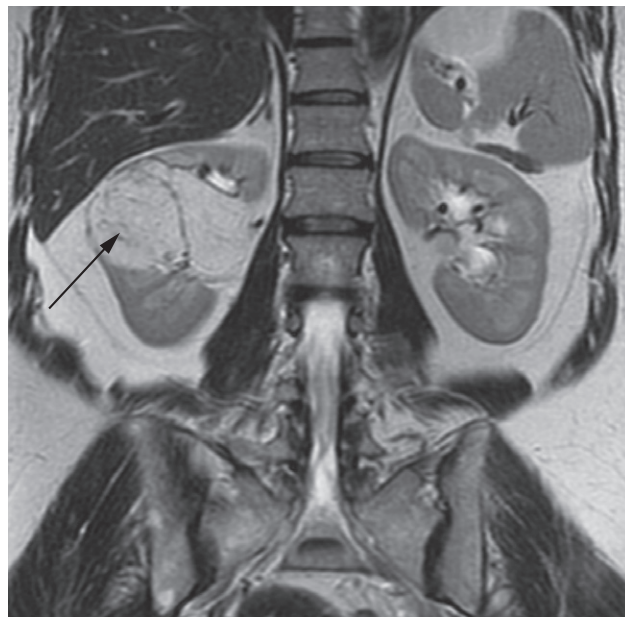
Staging of renal cell carcinoma is usually undertaken with CT, the current method of choice (Fig. 8.34). CT shows local direct spread, can demonstrate enlargement of draining lymph nodes in the retroperitoneum, can diagnose liver, adrenal and pancreatic metastases and can show tumour growing along the renal vein into the inferior vena cava.



(a)



(b)



(c)

Fig. 8.32 Benign renal masses. (a) Cyst in the left kidney (arrow) on CT showing a well-defined edge, imperceptible wall and uniform water density. The cyst shows no enhancement and was an incidental finding. L, liver; P, pancreas. (b) Angiomyolipoma seen as a well-defined mass (arrows) of fat density on CT. (c) Coronal T2-weighted MRI demonstrating a large angiomyolipoma in the central part of the right kidney (arrow).

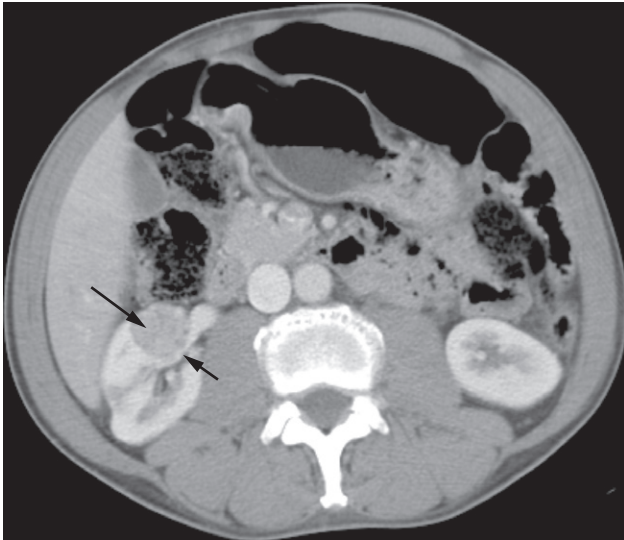


Fig. 8.33 Renal cell carcinoma. The mass in the right kidney (long arrow) shows substantial enhancement and is invading the anterior wall of the right renal vein (short arrow).

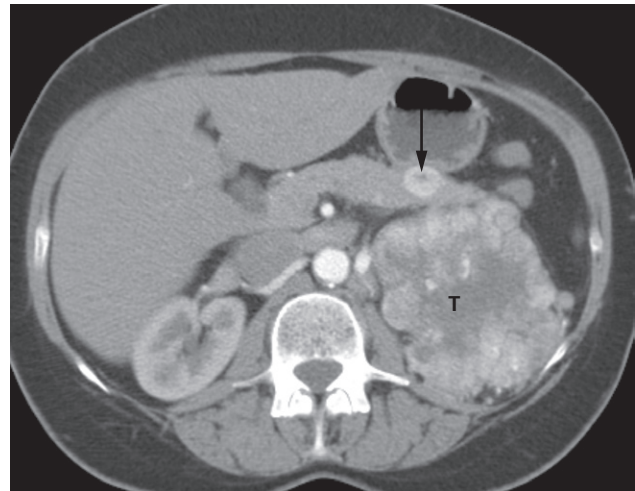
The renal vein and inferior vena cava are particularly well demonstrated on sagittal and coronal views on MRI (Fig. 8.35), as well as on sagittal and coronal reformats of MDCT images. These additional scan planes help to demonstrate the anatomical relations of the mass to the renal hilar vessels and may help in planning partial resections of the kidney.

Wilms' tumour is the likely diagnosis in a child with a renal mass (Fig. 8.36). These lesions are frequently large and may contain stippled calcifications.

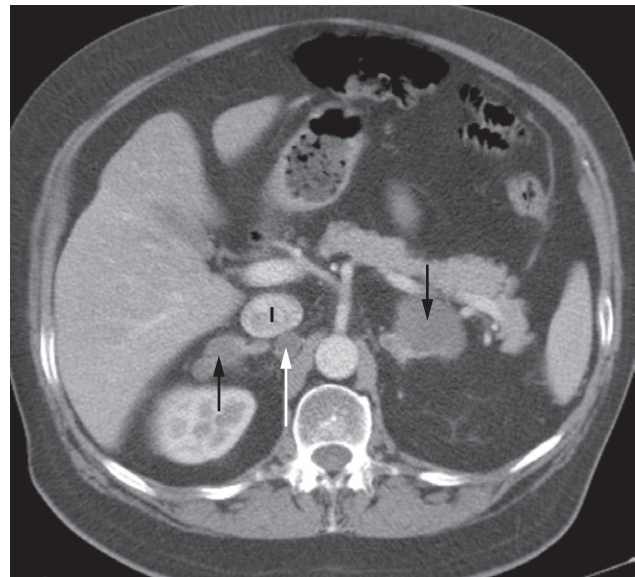
Urothelial tumours

Almost all tumours that arise within the collecting systems of the kidneys are *transitional cell carcinomas*. The tumours sometimes occur in multiple sites and, therefore, both the pelvicaliceal systems and ureters should be carefully scrutinized. Although bladder tumours may be demonstrated, these are better evaluated at cystoscopy.

Computed tomography has taken over from IVU in most centres for demonstrating the upper tracts (pelvicaliceal system and ureters). *Filling defects* within the renal pelvis



(a)



(b)

Fig. 8.34 Staging renal carcinoma. (a) CT scan showing a large tumour (T) in the left kidney from renal cell carcinoma and an enhancing metastasis (arrow) in the pancreas. (b) In another patient showing bilateral adrenal metastases (black arrows) and a nodal metastasis (white arrow). I, inferior vena cava.

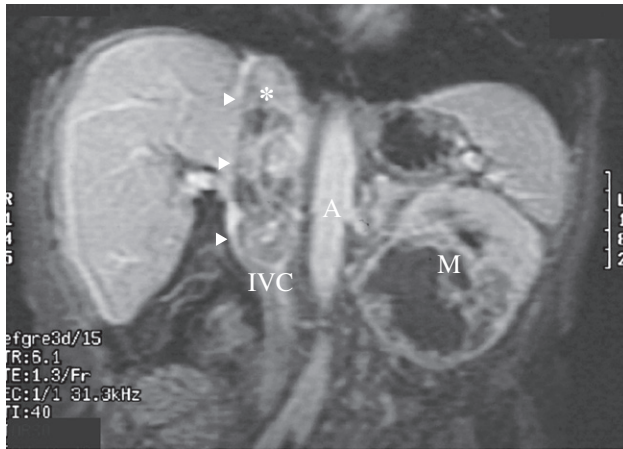


Fig. 8.35 Coronal MRI scan showing a huge left renal carcinoma (M) with tumour extending into the inferior vena cava (IVC) via the left renal vein (not seen on the view). The caval extension of tumour (arrowheads) extends to the top of the IVC (*). A, aorta.

and ureters should be looked for. In the pelvicaliceal system, TCCs are seen as lobulated or, very occasionally, as fronded filling defects projecting into the lumen (Fig. 8.37a). It is easy to confuse such tumours with overlying gas shadows on IVU, and ultrasound or CT may be required to solve the problem. The differential diagnosis of a filling defect in the collecting systems includes calculi and blood clot. Most urinary stones contain visible calcification, and virtually all calcified filling defects are stones. However, radiolucent calculi can cause a diagnostic problem on IVU, and CT plays an important role in confirming or ruling out radiolucent calculi (see Fig. 8.17). The diagnosis of blood clot as the cause of a filling defect rests on knowing that the patient has severe haematuria and noting the smooth outline of the filling defect (Fig. 8.38). Sometimes the distinction between tumour and clot is difficult. If clot is a possibility, then follow-up to check for resorption of the clot may be helpful.

At ultrasound, TCCs can be difficult to see because they blend with the renal sinus fat, although large tumours can usually be demonstrated as a central mass within the sinus (Fig. 8.37b). Ultrasound may help to differentiate between a radiolucent stone and tumour, as the calculus demonstrates acoustic shadowing.

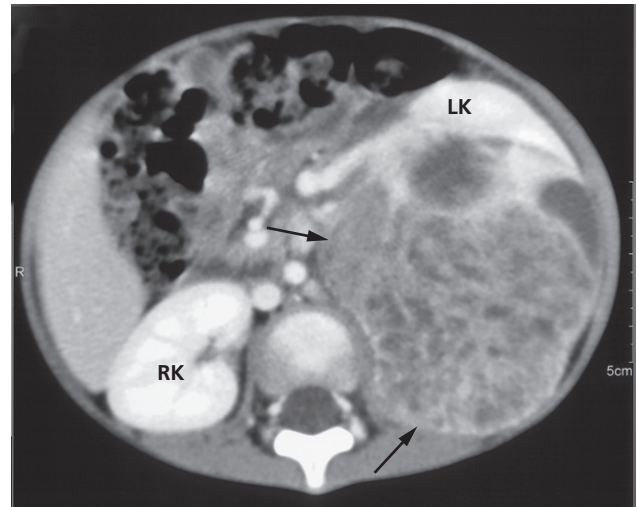


Fig. 8.36 Wilms' tumour. A large heterogeneously enhancing mass arises from the posterior aspect of the left kidney (arrows). The remainder of the left kidney (LK) parenchyma lies anteriorly. RK, right kidney.

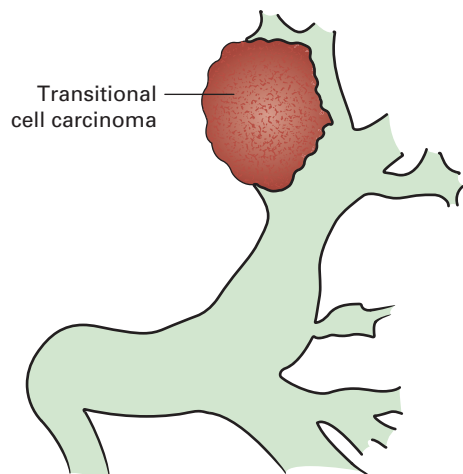
Computed tomography urography demonstrates thickening of the wall of the ureter at the site of a urothelial tumour. The ureter is often obstructed at the level of a TCC (Fig. 8.39). If this is the case, then no contrast may be seen in the ureter on the 10-minute delayed-phase CT images. Three-dimensional reformatting of the collecting system may be undertaken to demonstrate the location and extent of the tumour prior to surgery. Tumour staging may be done at the same time.

In some cases, where there is an equivocal appearance on CT urography, antegrade or retrograde pyelography may also be used to demonstrate the tumour.

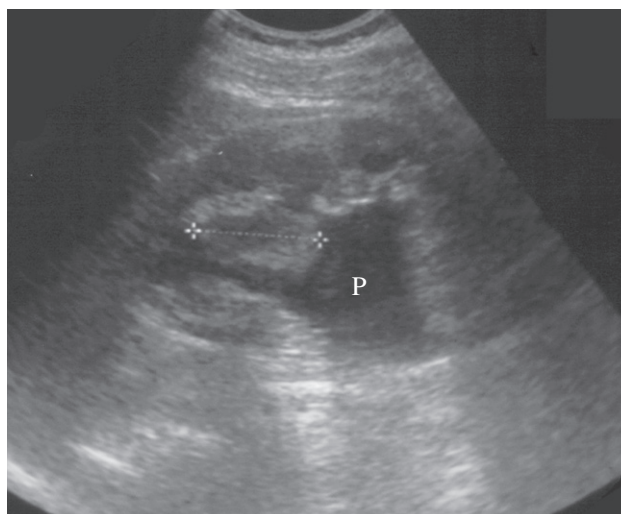
Acute infections of the upper urinary tracts

Acute pyelonephritis

Acute pyelonephritis is usually due to bacterial infection from organisms that enter the urinary system via the urethra. Anatomical abnormalities such as stones, duplex systems complicated by obstruction or reflux, obstructive



(a)



(b)

Fig. 8.37 (a) Filling defect in an upper calix due to transitional cell carcinoma. (b) Ultrasound, in a different patient, demonstrating a tumour mass (between the cursors) projecting into the renal pelvis (P).

lesions and conditions such as diabetes mellitus all predispose to infection. In adults, only selected patients require imaging.

Most patients with acute urinary tract infection do not require urgent imaging investigations. In patients presenting with signs of infection associated with pain, particu-

larly if the symptoms are not settling with antibiotics, ultrasound and plain films may diagnose underlying stones, obstruction or abscess formation. In acute pyelonephritis the ultrasound is either normal or demonstrates diffuse or focal swelling of the kidney, with diminished echoes due to cortical oedema. In some cases, if the pain is

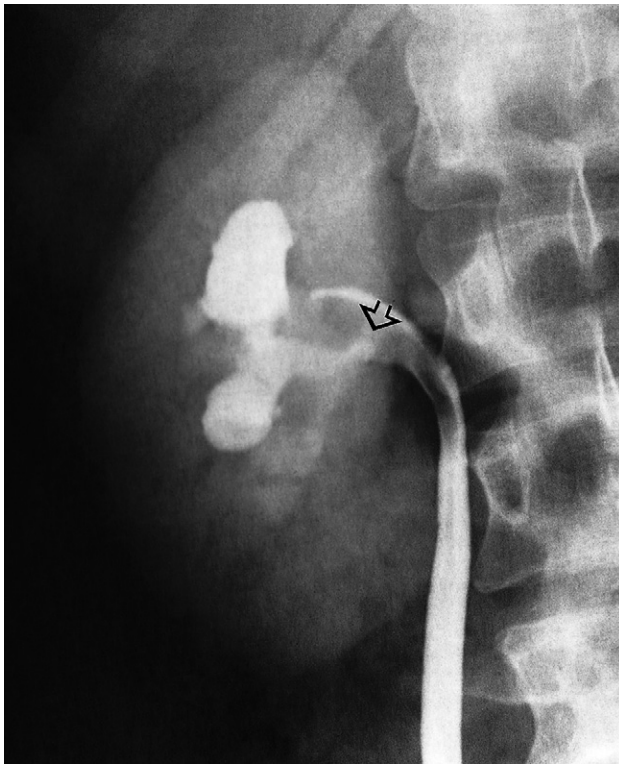
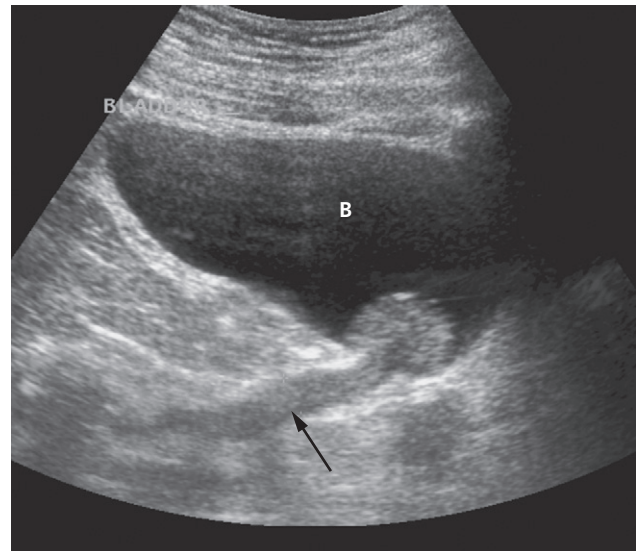


Fig. 8.38 Filling defect due to blood clot in the pelvis and upper ureter (arrow).

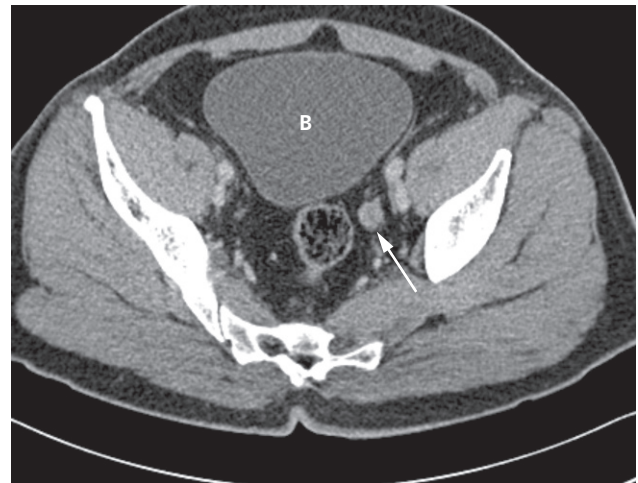
severe, IVU or CT KUB may be done to demonstrate or rule out acute ureteric colic.

Following resolution of the acute episode, imaging of the renal tract is undertaken in women with recurrent infections or after a single confirmed urinary tract infection in men. Ultrasound of the kidneys may demonstrate underlying obstruction or stones. The bladder is imaged while full, to rule out a bladder stone, and then following micturition in order to demonstrate residual urine, which could account for recurrent infection. Urography may be performed if there is a suspected duplex system complicated by obstruction or reflux.

Investigation of the renal tract is indicated in all children with a confirmed urinary tract infection. The aim is to identify an abnormality, such as reflux, which could lead to renal damage, if left untreated (see Fig. 8.14). Ultrasound



(a)



(b)

Fig. 8.39 Transitional cell carcinoma. (a) Ultrasound demonstrating a polypoid mass arising at the vesicoureteric junction in the bladder (B), extending up the ureter (arrow). (b) CT in the same patient demonstrating thickening and enhancement of the left ureter (arrow).

is used to measure the size of the kidneys, to identify any stones or scarring, and to demonstrate or rule out hydronephrosis or hydroureter. The bladder is assessed for post-micturition residual urine. Many hospitals do a DMSA radionuclide scan of the kidneys to demonstrate scarring.

Micturating cystography is performed in male (and in some female) children to look for vesicoureteric reflux and urethral valves.

Renal and perinephric abscesses

Ultrasound is the initial imaging investigation in most suspected renal abscesses, although in patients who are very unwell CT is often the first imaging investigation.

Intrarenal abscesses (Fig. 8.40) may have thick walls and show both cystic and solid components recognizable at both ultrasound and CT, but may just look like a simple cyst. With CT, it is possible to see enhancement of the wall of the abscess following intravenous contrast injection.

Simple cysts may become secondarily infected, in which case the ultrasound and CT features resemble those of a simple cyst, but the wall may be a little thicker and there will frequently be a layer of echogenic debris in the dependent portion of the cyst.

Perinephric abscesses may conform to the shape of the underlying kidney. The CT and sonographic characteristics are variable, usually showing both solid and cystic elements (Fig. 8.41). The cystic portions frequently contain internal echoes at ultrasound owing to debris. As most perinephric abscesses are secondary to an infective focus

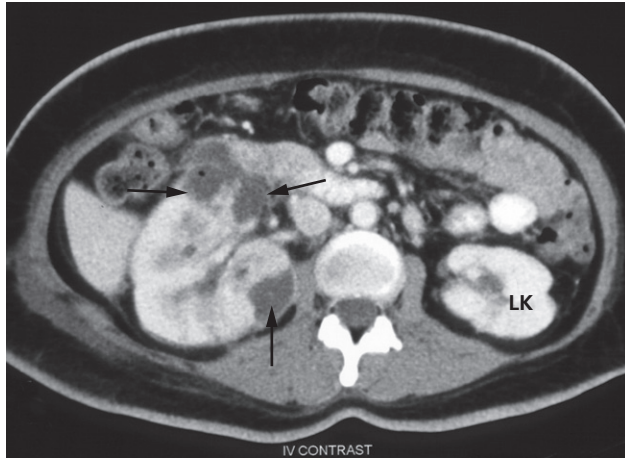
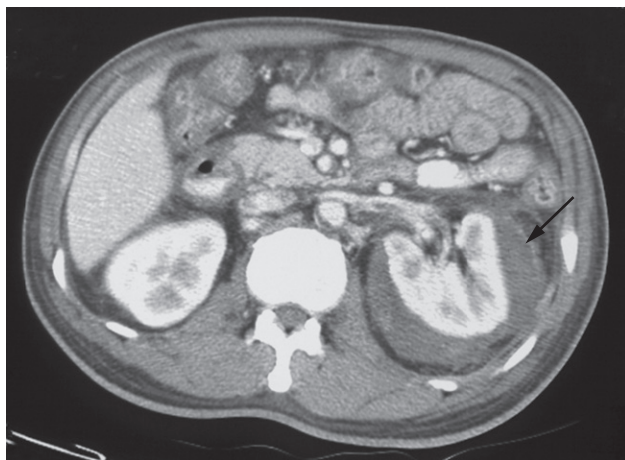
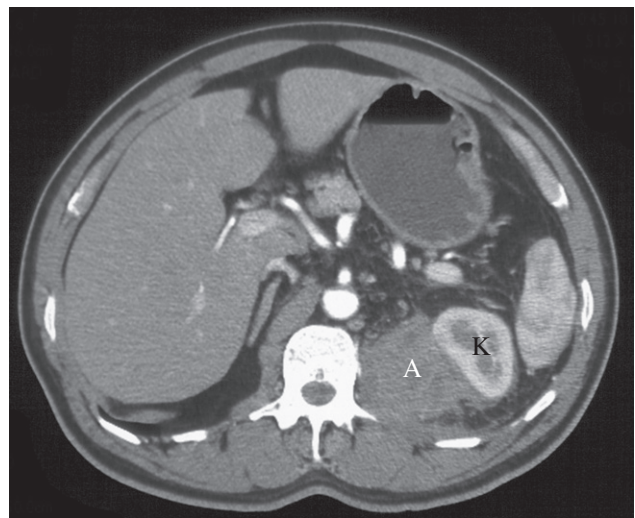


Fig. 8.40 CT scan with intravenous contrast demonstrating multiple low attenuation fluid collections in the right renal cortex, consistent with multiple renal abscesses (arrows). LK, left kidney.



(a)



(b)

Fig. 8.41 Perinephric abscess. (a) CT scan showing loculated fluid (arrow) with a thick enhancing wall surrounding the left kidney. (b) An abscess collection (A) lies posterior to the left kidney (K), with the enhancing kidney displaced anteriorly by the collection.

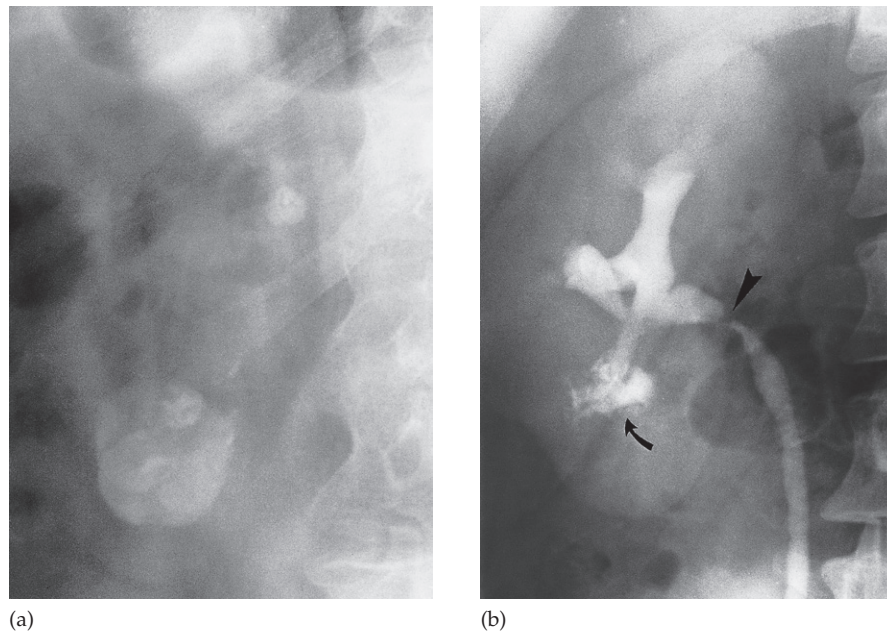


Fig. 8.42 (a) Renal parenchymal calcification from tuberculosis on plain film. (b) In another patient, after contrast, there is irregularity of the calices (curved arrow) and stricture formation of the pelvis (arrowhead).

within the kidney, an underlying renal abnormality is often demonstrable.

Pyonephrosis

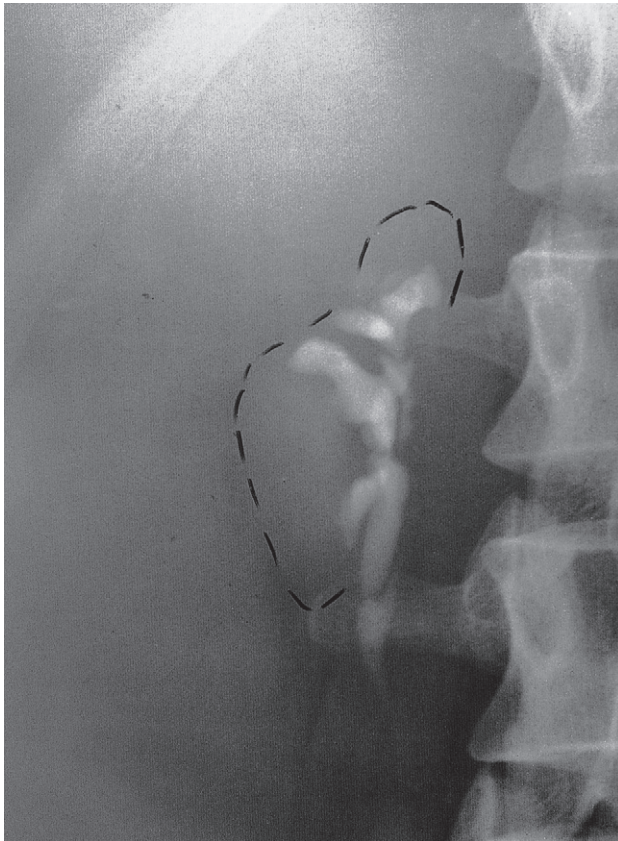
Pyonephrosis only occurs in collecting systems that are obstructed. Ultrasound is the most useful imaging modality for pyonephrosis. In addition to showing the dilated collecting system, it may demonstrate multiple echoes within the collecting system from infected debris.

Tuberculosis

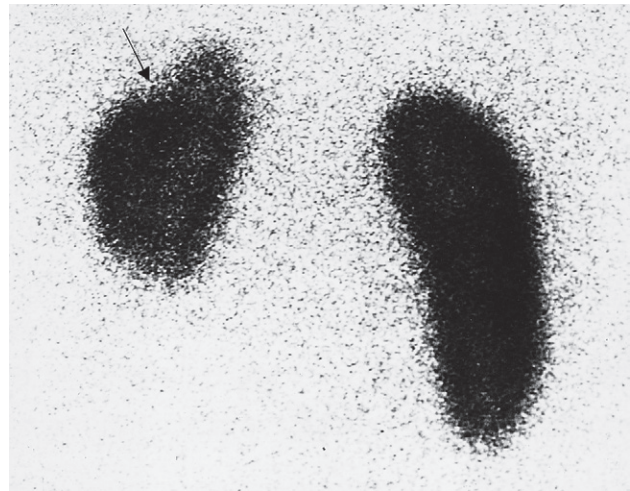
Urinary tuberculosis follows blood-borne spread of *Mycobacterium tuberculosis*, usually from a focus of infection in the lung. The tubercle bacilli infect the cortex of the kidneys and may cause tiny cortical granulomas, which rupture through capillaries into the renal tubules and involve other portions of the urinary and genital systems.

In the early stages of the disease, the ultrasound and IVU may be normal. There are various signs that develop in the later stages that are best seen on IVU:

- Calcification is common (Fig. 8.42). Usually, there are one or more foci of irregular calcification, but in advanced cases with longstanding tuberculous pyonephrosis the majority of the kidney and hydronephrotic collecting system may be calcified, leading to a so-called autonephrectomy. Calcification implies healing but does not mean that the disease is inactive.
- The earliest change on the post contrast films is irregularity of a calyx. Later, a definite contrast-filled cavity may be seen adjacent to the calyx.
- Strictures of any portion of the pelvicaliceal system or ureter may occur, producing dilatation of one or more calices (Fig. 8.42). The multiplicity of strictures is an important diagnostic feature.
- If the bladder is involved, the wall is irregular because of inflammatory oedema; advanced disease causes fibrosis



(a)



(b)

Fig. 8.43 Reflux nephropathy (chronic pyelonephritis). (a) IVU showing a severely shrunken kidney with multiple scars and clubbed calices. (b) DMSA scan (posterior view) showing a shrunken left kidney with a focal scar in the upper pole (arrow).

resulting in a thick-walled, small volume bladder. Multiple strictures may be seen in the urethra.

Ultrasound may demonstrate calcifications and pelvicaliceal dilatation and cavities, but the appearances are non-specific. CT can sensitively demonstrate early calcifications, small cavities and extrarenal spread.

Chronic pyelonephritis (reflux nephropathy)

Chronic pyelonephritis or reflux nephropathy refers to the late appearances of focal or diffuse scarring of the kidney, thought to be due to reflux of infected urine from the bladder into the kidneys, leading to destruction and scarring of the renal substance. Most damage occurs in the first years of life. The severity of reflux diminishes as the child

gets older and may have ceased by the time the diagnosis of reflux nephropathy is made (see Fig. 8.14). The condition is often bilateral and asymmetrical.

The signs of reflux nephropathy (Fig. 8.43) are:

- *Local reduction in renal parenchymal width (scar formation)*. The distance between the calix and the adjacent renal outline is usually substantially reduced and may be as little as 1 or 2mm. The upper and lower calices are the most susceptible to damage from reflux. IVU, DMSA radionuclide scans and ultrasound are all useful for demonstrating cortical scars.
- *Dilatation of the calices in the scarred areas*. The dilatation is the result of atrophy of the pyramids.
- *Overall reduction in renal size* partly from loss of renal substance and partly because the scarred areas do not grow.



Fig. 8.44 Papillary necrosis showing dilated calices from loss of the papillae. Some of the papillae have sloughed and appear as filling defects within the calices (lower arrow). The upper arrow points to a contrast-filled cavity within a papilla.

- *Dilatation of the affected collecting system* from reflux may be seen.
- *Vesicoureteric reflux* may be demonstrated at micturating (voiding) cystography.

Papillary necrosis

In papillary necrosis, part or all of the renal papilla sloughs and may fall into the pelvicaliceal system (Fig. 8.44). These necrotic papillae may remain within the pelvicaliceal system, sometimes causing obstruction, or they may be voided. There are a number of conditions with strong associations with papillary necrosis. The most frequent are:

- high analgesic intake
- diabetes mellitus
- sickle cell disease

- infection, but usually only with very severe infections or infection with obstruction.

Intravenous urography or CT urography are the modalities for demonstrating papillary necrosis. The pattern of destruction of the papilla takes many forms; the disease is usually patchy in distribution and severity. If the papilla is only partially necrotic, contrast can be seen tracking around or into it. If the papilla is totally sloughed, the calix appears spherical, having lost its papillary indentation. When sloughed, the papilla may then be seen as a filling defect in a spherical calix or it may have passed down the ureter, often causing obstruction as it does so.

The necrotic papilla can calcify prior to sloughing. A sloughed, calcified papilla within the collecting system may closely resemble a urinary calculus.

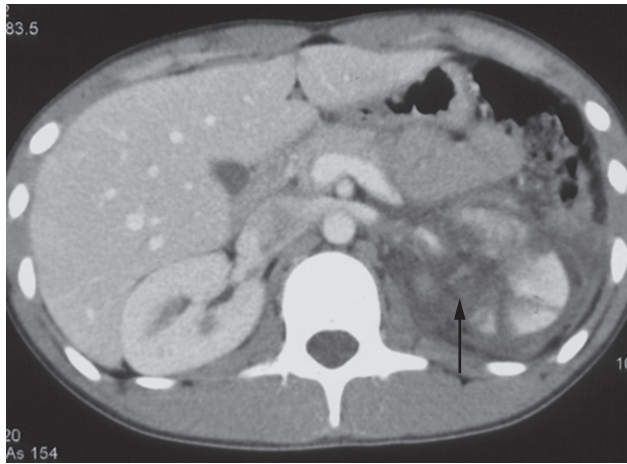
Renal trauma

The kidney and the spleen are the most frequent internal abdominal organs to be injured. Blunt trauma, particularly road traffic accidents and contact sports, are the mechanisms of injury in well over three-quarters of patients, the remainder being caused by penetrating injury. Loin pain and haematuria are the major presenting features.

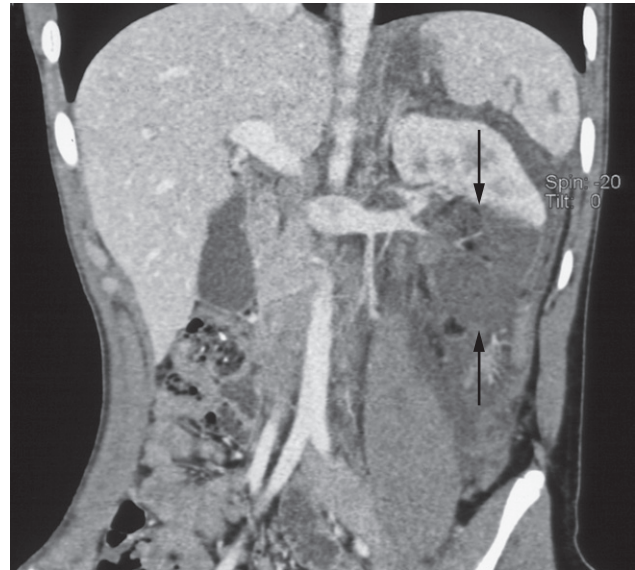
The indications for imaging tests depend on the clinical features and surgical approach. CT is the preferred investigation as it has the advantage that it can not only demonstrate the kidneys but can also show or exclude damage to other abdominal structures (Fig. 8.45). Computed tomography can demonstrate the following:

- The presence or absence of perfusion to the injured kidney.
- That the opposite kidney is normal (or not).
- The extent of renal parenchymal damage.
- Injuries to other organs, a feature of great importance in penetrating injury, where other organs are frequently lacerated.

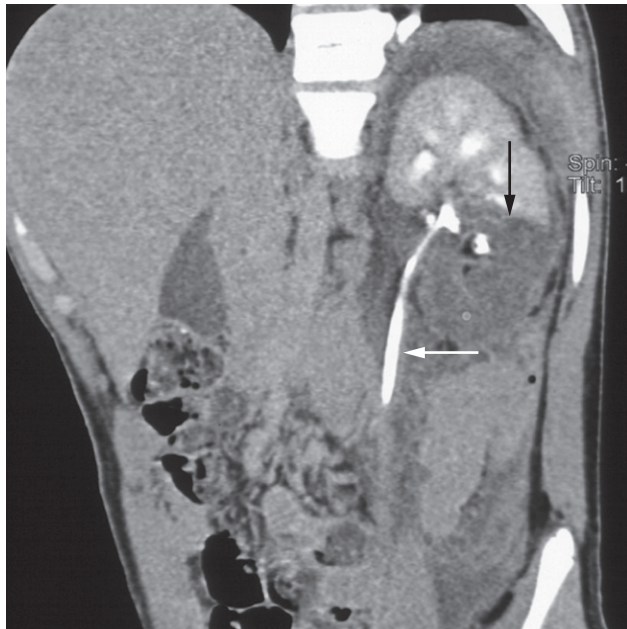
The appearances depend on the extent of injury. Minor injury (contusion and small capsular haematomas) produces swelling of the parenchyma, which compresses the calices. If the kidney substance is torn, the renal outline is irregular and the calices are separated. Large subcapsular and extracapsular blood collections may be present and extravasation of contrast may be seen. Retroperitoneal haemorrhage may displace the kidney. Fragmentation



(a)



(b)



(c)

Fig. 8.45 Renal trauma. (a) Axial CT demonstrating reduced perfusion in the midpole of the left kidney (arrow). Fluid is seen in the perinephric tissues. (b) Coronal reformat demonstrating a sharp cut-off of perfusion with complete loss of perfusion in the lower pole (black arrows). (c) Delayed oblique sagittal reformat demonstrating contrast in the collecting system (white arrow) and confirming no leak of contrast (black arrow).

of the kidney is a serious event, often, although by no means always, requiring nephrectomy or surgical repair. If thrombosis or rupture of the renal artery occurs, there will be no nephrogram. Renal infarction is a very serious condition demanding urgent restoration of blood flow or nephrectomy.

Hypertension in renal disease

Most patients with hypertension have essential, or primary, hypertension. However, renal disease may account for hypertension in a small percentage of patients. Renal conditions causing hypertension include renal artery stenosis,

chronic glomerulonephritis, chronic pyelonephritis, polycystic disease, polyarteritis nodosa and diabetic nephropathy. The common feature is a reduction in blood supply to all or part of the kidney.

Although *renal artery stenosis* may cause hypertension, it is also a frequent incidental finding at postmortem or angiographically in normotensive patients. The common cause is atheroma. Renal artery stenosis may be suspected at ultrasound if one kidney is smaller than the other. Doppler of the renal artery may diagnose the condition, although this is technically difficult. Radionuclide renography is used in some centres; this shows a delay in peak activity and a relative reduction of function on the affected side if renal artery stenosis is present. CT and magnetic resonance angiography are frequently used to diagnose renal artery stenosis non-invasively prior to undertaking intra-arterial angiography and balloon angioplasty (Fig. 8.46).

In *chronic pyelonephritis*, the artery supplying the diseased kidney may be smaller in size than that supplying the normal kidney (Fig. 8.47).



Fig. 8.46 Renal artery stenosis (arrow) demonstrated on a magnetic resonance angiogram. There is post-stenotic dilatation beyond the stenosis. The right kidney is small in size.

In *glomerulonephritis*, *polyarteritis nodosa* and *diabetic nephropathy*, there is usually bilateral uniform reduction in renal size without other specific features. Essential hypertension may cause identical changes at ultrasound and the decision as to whether the small kidneys are the cause or the result of hypertension cannot be made radiologically.

Nowadays, because of improved drug therapy, the search for a renal cause is largely limited to children with severe hypertension and those patients whose hypertension is inadequately controlled or who have clinical evidence of renal disease.

Renal failure

The main roles of imaging in patients with impaired renal function are to detect obstruction to the urinary tract and to determine renal size. Bilateral small kidneys suggest chronic, often irreversible, renal failure.

Renal failure from obstructive uropathy

The cardinal sign of obstructive uropathy is dilatation of the pelvicaliceal system. Ultrasound is the initial investigation to confirm or exclude obstruction (see Fig. 8.24).

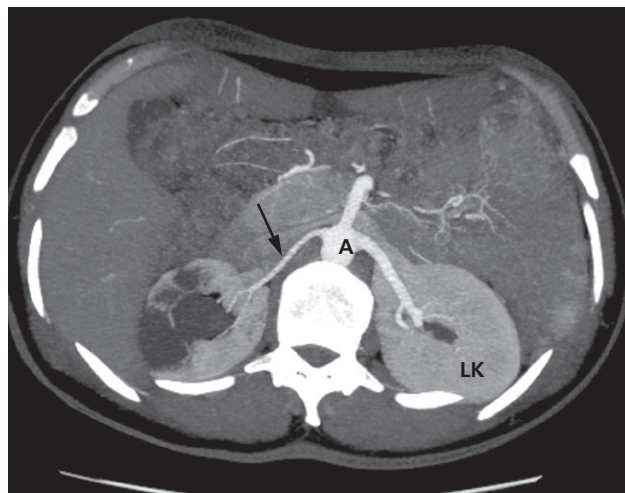


Fig. 8.47 Chronic pyelonephritis secondary to stones on CT angiography. The right kidney is smaller than the left and contains multiple cystic areas following chronic infection from stone disease. The right renal artery is small in calibre (arrow). A, aorta; LK, left kidney.

Investigations to identify urinary calculi should be undertaken in any patient with renal failure and hydronephrosis demonstrated by ultrasound. The demonstration of a normal pelvicaliceal system makes an obstructive cause for renal failure extremely unlikely.

Renal failure from intrinsic renal disease ('end-stage kidney')

Once obstruction and pre-renal conditions have been excluded, intrinsic renal disease is assumed to be responsible for the renal failure.

Chronic reflux nephropathy is the only specific diagnosis that can be made by imaging with any certainty. Most end-stage kidneys are small in size with a thin parenchyma, smooth outlines and normal calices. There are many causes for these appearances, notably chronic glomerulonephritis and diabetes (see Table 8.1). Increased parenchymal reflectivity may be demonstrated by ultrasound (Fig. 8.48) but the appearances are non-specific.

Acute tubular necrosis

In acute tubular necrosis, from whatever cause, the ultrasound scan shows kidneys that are normal or enlarged with

normal pelvicaliceal systems. The renal parenchyma may appear diffusely echogenic. If IVU or CT is performed, a dense nephrogram persists for up to 24 hours without visible caliceal filling.

Congenital anomalies of the urinary tract

Congenital variations in the anatomy of the urinary tract are frequent. Only the more common anomalies are discussed here (congenital PUJ obstruction is discussed earlier in this chapter).

Bifid collecting systems

Bifid collecting systems (Fig. 8.49) are the most frequent congenital variations. The condition may be unilateral or bilateral. The two ureters may join at any level between the renal hilum and the bladder or may insert separately into the bladder. Sometimes just the renal pelvis is bifid, an anomaly of no importance. At the other extreme, the two ureters may be separate throughout their length and have separate openings into the bladder. The ureter draining the upper moiety may drain outside the bladder, e.g. into the

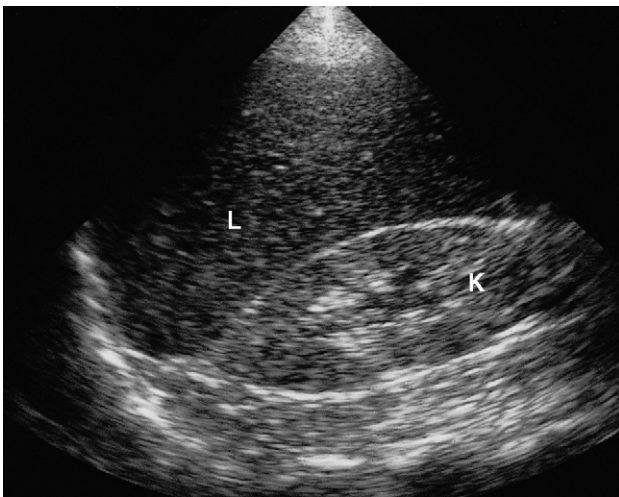


Fig. 8.48 Intrinsic renal disease. Ultrasound of right kidney (longitudinal scan). The kidney is small and the cortical echoes are increased and therefore the central echo is less obvious. Normally, the liver is more echo-reflective than the renal cortex. K, kidney; L, liver.



Fig. 8.49 Bifid collecting system. There is a bifid collecting system on the left with the two ureters joining at the level of the transverse process of L5. Note that the left kidney is larger than the right.

vagina or urethra, producing incontinence if the opening is beyond the urethral sphincter. Such ureters, known as *ectopic ureters*, are frequently obstructed (Fig. 8.50) and lead to dilatation of the entire moiety; the dilated lower ureter may prolapse into the bladder, forming a *ureterocele*. The ureterocele causes a smooth filling defect in the bladder on IVU, and on ultrasound may be seen as a cystic structure within the bladder at the position of the vesicoureteric junction.

Ectopic kidney

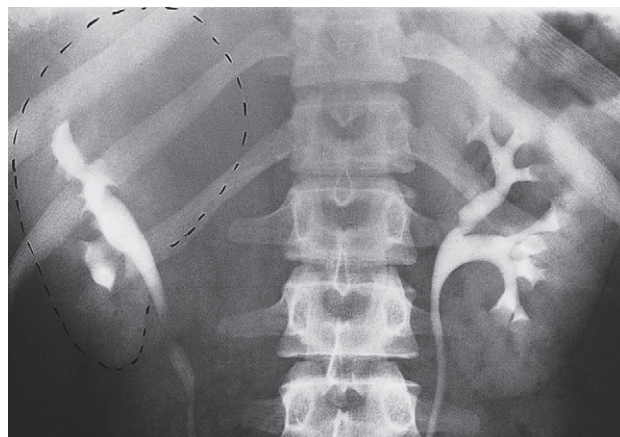
During fetal development the kidneys ascend within the abdomen. An ectopic kidney results if this ascent is halted. They are usually in the lower abdomen and rotated so that the pelvis of the kidney points forward. The ureter is short and travels directly to the bladder. In some cases, both kidneys lie on the same side of the pelvis and are fused (see Fig. 8.21). Chronic pyelonephritis, hydronephrosis and calculi are all more common in ectopic kidneys, but ectopic kidneys are often incidental findings of no consequence to the patient, except as a cause of diagnostic confusion with other causes of lower abdominal masses; the diagnosis can be made on ultrasound in most cases.

Horseshoe kidney

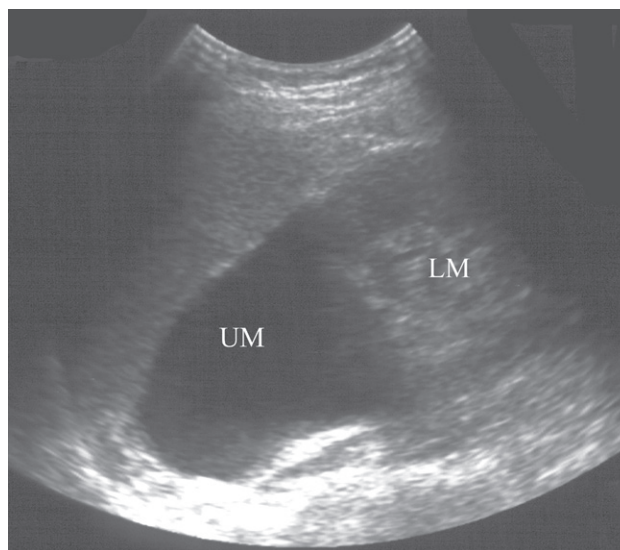
The kidneys may fail to separate, giving rise to a horseshoe kidney. Almost invariably it is the lower poles that remain fused (Fig. 8.51). The anomaly may be an incidental finding and of no significance, but PUJ obstruction to the collecting systems and calculi formation are both fairly common.

Inherited cystic disease of the kidneys

There are many varieties of cystic renal disease varying from simple cysts, which may be single or multiple, to complex renal dysplasias. The most frequent complex dysplasia encountered in clinical practice is autosomal dominant polycystic kidney disease. This is a familial disorder which, although inherited, usually presents between the ages of 35 and 55 years with hypertension, renal failure or haematuria, or following the discovery of bilaterally enlarged kidneys. The reason for the late presentation is that the cysts are initially small and do not cause trouble for a long time. The diagnosis is readily made at ultra-

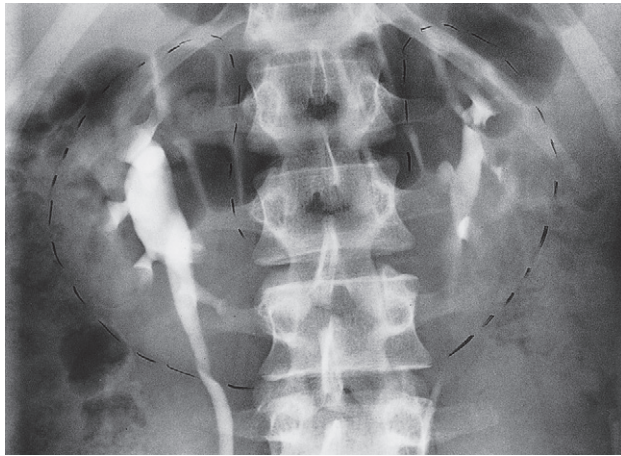


(a)

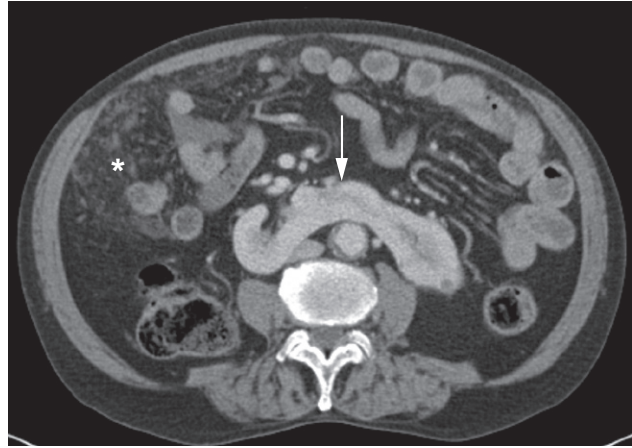


(b)

Fig. 8.50 (a) Obstructed ectopic ureter. There is a bifid collecting system on the right. The upper moiety is obstructed and dilated causing deformity of the lower moiety. The obstructed moiety does not opacify. (b) Ultrasound, in a different patient, showing a dilated upper moiety (UM), with no remaining renal parenchyma. The lower moiety (LM) appears normal.



(a)



(b)

Fig. 8.51 Horseshoe kidneys. (a) The two kidneys are fused at their lower poles. The striking feature is the alteration in the axis of the kidneys: the lower calices are closer to the spine than the upper calices. The kidneys are rotated so that their pelvises point forward and the lower calices point medially. The medial aspects of the lower poles cannot be identified. (b) CT scan of a different patient, following intravenous contrast enhancement, showing fusion of the lower poles of the kidneys. The patient had disseminated peritoneal metastatic disease from ovarian cancer (*).

sound, as well as on CT (Fig. 8.52). The liver and pancreas may also contain cysts and these organs are routinely examined in such patients. Early diagnosis of autosomal dominant polycystic kidney disease when only a few cysts are present is now possible using ultrasound. Ultrasound screening is usually offered at the age of 18 to the offspring of those with the disease.

Renal agenesis

In renal agenesis, the opposite kidney, providing it is normal, will show compensatory hypertrophy. Complete absence of blood flow and function on the affected side will be shown on radionuclide studies, and no renal tissue can be identified with ultrasound or CT examination.

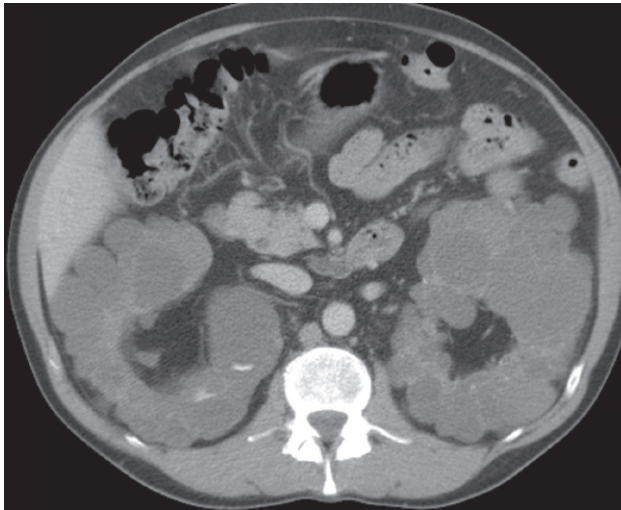
Bladder disorders

The bladder is well demonstrated on all imaging modalities. At ultrasound, the simplest routine method of imaging, the bladder lumen should be free of echogenic structures and its wall should be of uniform thickness (see Fig. 8.2). When the bladder is distended, the wall should be less than

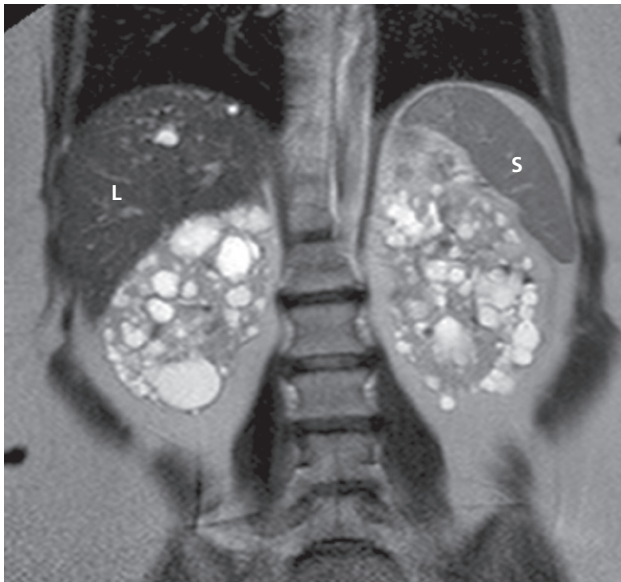
3mm thick. The volume of the bladder may be calculated by measuring the dimensions of the bladder.

Bladder tumours

The bladder is the most frequent site for neoplasms in the urinary tract (Fig. 8.53). Almost all are transitional cell carcinomas of varying degrees of malignancy. They vary in shape: some are delicate, fronded papillary lesions, some are sessile irregular masses, and others form flat, plaque-like growths that infiltrate widely. On ultrasound examination, bladder tumours are seen as soft tissue masses protruding into the fluid-filled bladder or as localized bladder wall thickening, but the technique is poor for detecting extravesical spread. IVU is less sensitive than ultrasound in detecting small bladder masses, but if the mass is large enough a filling defect in the bladder may be seen. Gas and faeces in the sigmoid colon or rectum, projected over the bladder outline on IVU, may closely resemble a bladder neoplasm. Ultrasound can be used to confirm an intravesical mass. On rare occasions, there is visible calcification on the surface of the tumour.



(a)



(b)

Fig. 8.52 Advanced polycystic disease in adults. (a) CT scan, taken after intravenous contrast enhancement, showing that both kidneys are greatly enlarged and almost entirely replaced by cysts of variable size. (b) Coronal T2-weighted MRI in another patient demonstrating multiple bilateral renal cysts as well as a few cysts in the liver (L). S, spleen.

The nature and extent of a tumour in the bladder is best observed at cystoscopy. The main role of urography is to demonstrate any other lesions in the upper tracts (pelvicaliceal systems and ureters), as transitional cell carcinomas are often multifocal.

On CT and MRI, a bladder tumour is seen as a soft tissue mass projecting from the wall or a focal thickening of the bladder wall (Fig. 8.53). As the diagnosis is best established by cystoscopy and biopsy, the roles of CT and MRI are to stage the tumour. No imaging technique is very reliable for assessing the depth of invasion within the muscle of the bladder, but CT and MRI can determine the spread of tumour beyond the bladder wall and assess lymph node involvement (Fig. 8.53d).

Bladder diverticula

Bladder diverticula (Fig. 8.54) may be congenital in origin but are usually the consequence of chronic obstruction to bladder outflow. Because of urinary stasis, diverticula predispose to infection and stone formation and tumours may, on occasion, arise within them. Most diverticula fill at urography and cystography. They are readily demonstrated at ultrasound, CT and MRI. When large, diverticula may deform the adjacent bladder or ureter.

Bladder calcification

Calculi are the most frequent cause of calcification in the bladder. Such calculi may be large and laminated. Calcification in the wall of the bladder is rare. When seen, it is usually due to schistosomiasis or bladder tumour.

Neurogenic bladder

There are two basic types of neurogenic bladder, although attempts to correlate these types with specific neurological lesions have not been satisfactory:

- 1 The large, atonic, smooth-walled bladder with poor or absent contractions and a large residual volume.
- 2 The hypertrophic type, which can be regarded as neurologically induced bladder outflow obstruction. In this condition, the bladder is of small volume, has a very thick, grossly trabeculated wall and shows marked sacculcation

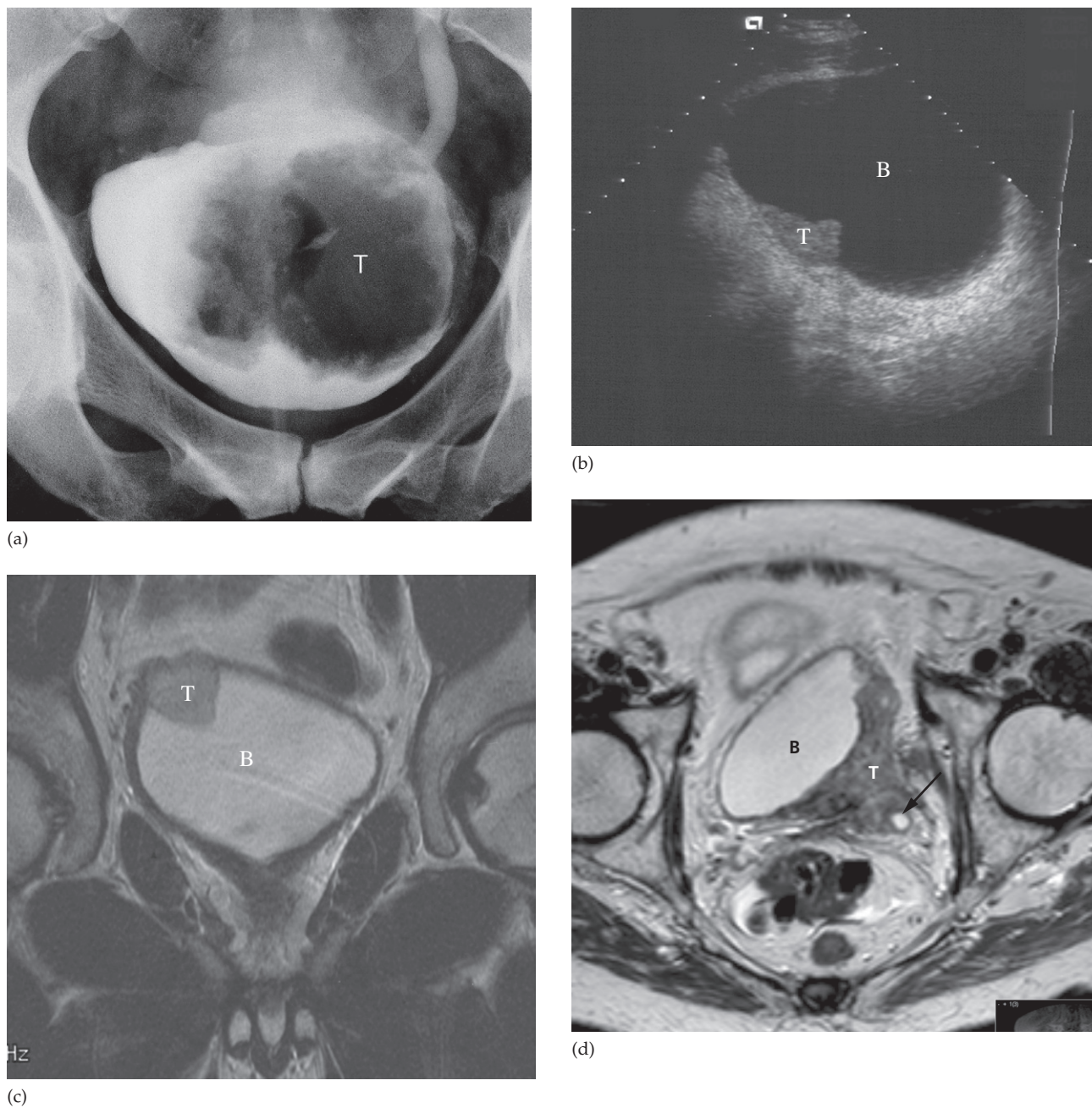


Fig. 8.53 Bladder neoplasm. (a) There is a large filling defect in the left side of the bladder from a transitional cell carcinoma. Note the obstructive dilatation of the left ureter. (b) Ultrasound scan from a different patient showing a small tumour within the bladder. (c) T2-weighted coronal MRI of the bladder tumour seen on ultrasound in (b). (d) Advanced stage bladder tumour arising from the left bladder wall and extending into the perivesical fat. Note the obstructed left ureter (arrow). B, bladder; T, tumour.

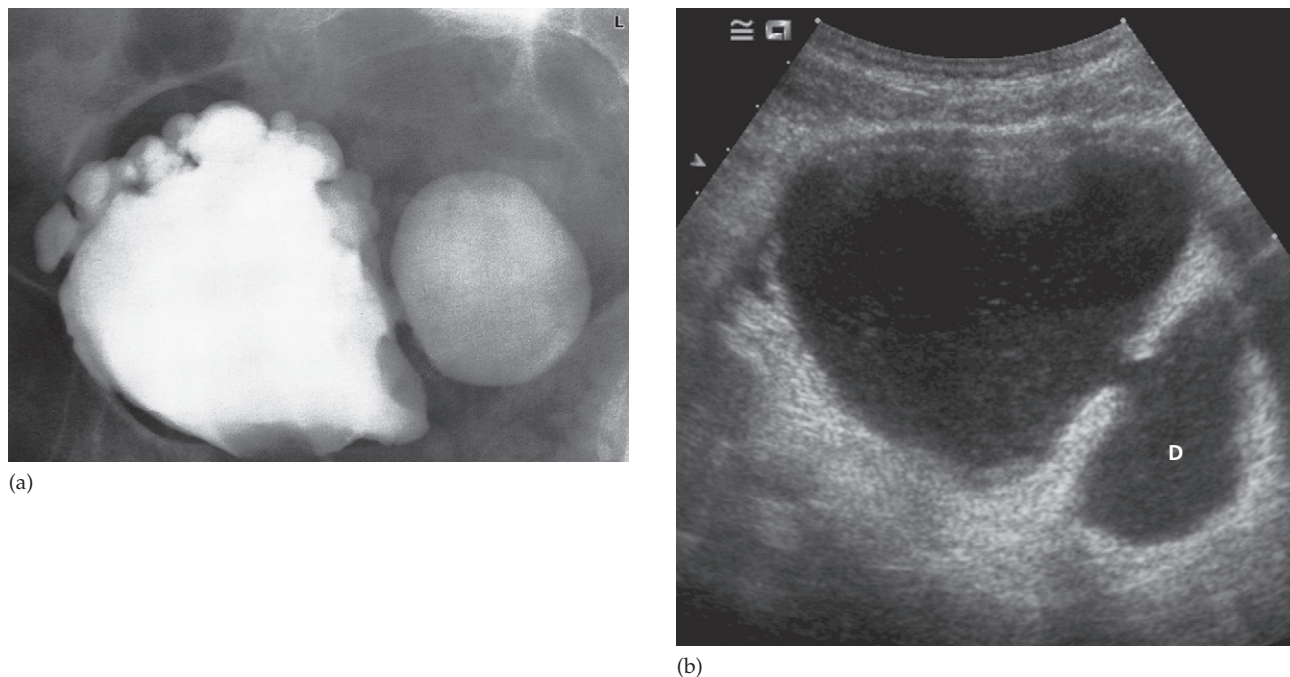


Fig. 8.54 Bladder diverticula. (a) Cystogram showing numerous outpouchings from the bladder with a very large diverticulum projecting to the left. (b) Ultrasound of a large diverticulum (D) in a different patient.

(Fig. 8.55). The ureters and pelvicaliceal systems may be dilated.

Full assessment of neuropathic bladder dysfunction requires voiding cystourethrography combined with pressure measurements, so-called videourodynamics.

Trauma to the bladder and urethra

A direct blow to the distended bladder may result in intraperitoneal bladder rupture: contrast introduced into the bladder will leak out into the peritoneal cavity.

Extraperitoneal rupture of the bladder may be part of an extensive injury such as occurs with fractures of the pelvis. A common site of rupture is at the bladder base, in which case the bladder shows elevation and compression from extravasated urine and haematoma.

Rupture of the bladder may be revealed sonographically by the presence of a perivesicular fluid collection but the actual site of a tear will not be seen.

Cystography remains the best way of demonstrating the actual site of leakage from the bladder (Fig. 8.56). If there is any suspicion of associated damage to the urethra, an ascending urethrogram with a water-soluble contrast medium may show rupture of the urethra with extravasation of contrast medium into the adjacent tissues. The urethrogram should be performed before passing the catheter into the bladder for the cystogram.

Computed tomography may demonstrate fresh haematomas within the pelvis (which are of high density) or urine collections (which are of low density). It also demonstrates the associated fractures, some of which may not be apparent on plain radiographs.



Fig. 8.55 Neurogenic bladder. The outline of the bladder is very irregular due to trabeculation of the bladder wall. The bladder has a small volume with an elongated shape; this appearance has been described as a 'Christmas tree bladder'. There is a balloon catheter in the dilated posterior urethra.



Fig. 8.56 Rupture of the base of the bladder. Cystogram showing extravasation of contrast into the extraperitoneal space on the left, and deformity of the bladder due to surrounding haematoma and urine. There is a fracture of the right pubic bone.

Prostate and urethra disorders

Prostatic enlargement

Prostatic enlargement is very common in elderly men. It is usually due to benign hypertrophy but may be due to carcinoma. The diagnosis of enlargement is made by digital rectal examination.

Prostatic ultrasound uses a transducer designed to be introduced into the rectum. Transrectal ultrasound (TRUS) can show the overall size of the prostate and can diagnose relatively small masses within its substance (Fig. 8.57). Unfortunately, ultrasound cannot distinguish benign from malignant disease when confined to the prostate, except on the basis that masses in the peripheral zone are likely to be malignant and those in the central zone are more likely to be benign.

Transrectal ultrasound-guided biopsy is used extensively for the diagnosis of prostatic carcinoma. Antibiotic prophylaxis is given prior to introducing the biopsy needle, which is positioned within a needle guide along the TRUS probe. Usually 10–12 biopsies are then obtained, one from each area of the gland, as well as from any suspicious areas.

Computed tomography does not demonstrate the internal structure of the prostate as well as TRUS or MRI. However, in cases of known prostatic carcinoma, it is helpful in determining the extent of local spread as well as lymph node metastases.

Magnetic resonance imaging is used to assess early stage prostate cancer in patients being considered for radical surgery or radiotherapy. Tumour in the peripheral zone is

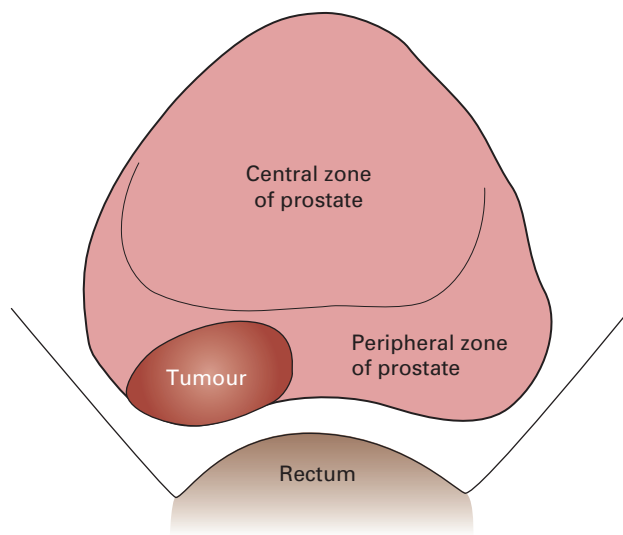
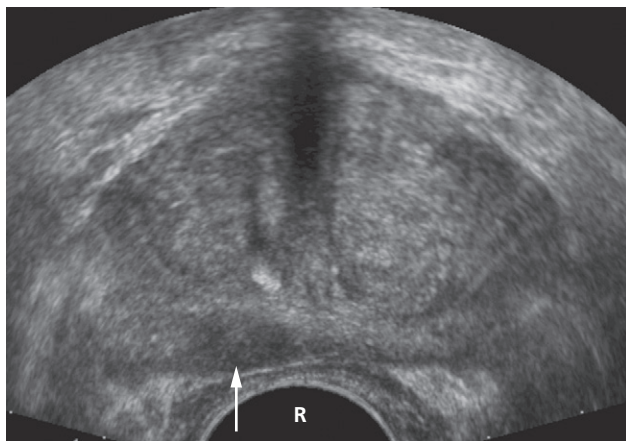


Fig. 8.57 Early prostate cancer. Prostate carcinoma shown by TRUS. The tumour (T) is seen as a low echogenic ovoid mass in the right peripheral zone (arrow). R, rectum.

seen as a relatively low signal mass within the normal high signal of the peripheral zone on T2-weighted images (Fig. 8.58a). Using a specialized sequence called diffusion-weighted imaging (DWI), together with the apparent diffusion coefficient (ADC) image, it is possible to assess restricted diffusivity of water molecules, a feature of prostate cancer. This is seen as a bright area on DWI and a dark

area on the ADC map (Fig. 8.58b, c). MRI is used to demonstrate extracapsular tumour spread, to show invasion of the seminal vesicles, and to demonstrate possible lymph node metastases (Fig. 8.59).

Prostatic calcification

Prostatic calcification is due to numerous prostatic calculi (Fig. 8.60). It is so common that it can be regarded as a normal finding in older men, and shows no correlation with the symptoms of prostatic hypertrophy nor any relation to prostatic carcinoma. Flecks of calcification of varying size, approximately symmetrical about the midline, are seen just inferior to the bladder.

Bladder outflow obstruction

The most frequent cause of bladder outflow obstruction is enlargement of the prostate. Other causes include bladder tumours, urethral strictures and, in male infants or boys, posterior urethral valves. As discussed above, patients with neurological deficit may have neurogenic obstruction to bladder emptying. Regardless of the cause, ultrasound can demonstrate all the imaging signs of bladder outflow obstruction:

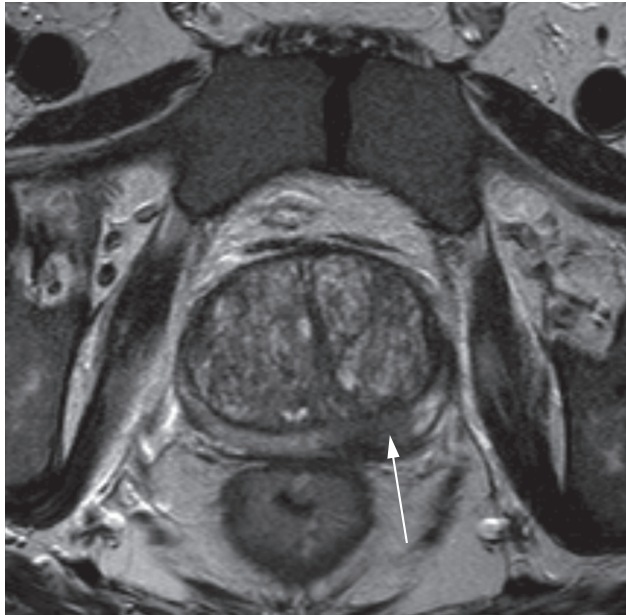
- Increased trabeculation and thickness of the bladder wall, often with diverticula formation.
- Residual urine in the bladder after micturition.
- Dilatation of the collecting systems.

Urethral stricture

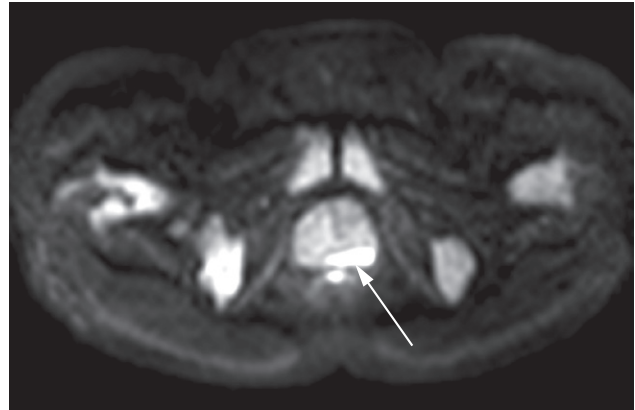
The majority of urethral strictures are due to previous trauma or infection. Post-traumatic strictures are usually in the proximal penile urethra – the most vulnerable portion of the urethra to external trauma. Such strictures are usually smooth in outline and relatively short. Inflammatory strictures, which are usually gonococcal in origin, may be seen in any portion of the urethra, but are usually found in the anterior urethra. Urethral strictures are imaged by urethrography (Fig. 8.61).

Posterior urethral valves

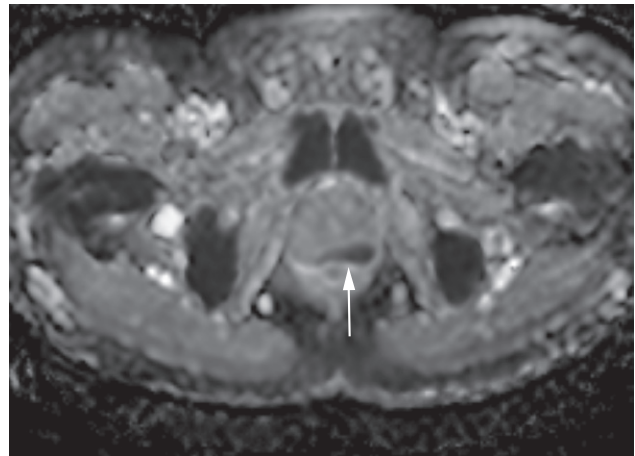
Congenital valves in the posterior urethra in boys are the commonest cause of bladder outflow obstruction in male



(a)



(b)



(c)

Fig. 8.58 MRI of early prostate cancer. (a) T2-weighted MRI demonstrating focal low signal intensity in the left peripheral zone (arrow). (b) The lesion (arrow) is of high signal intensity on b 1000 DWI. (c) The lesion is of low signal intensity on the ADC map, consistent with restricted water diffusivity which is characteristic of prostate cancer (arrow).

children. The diagnosis may be first suspected at antenatal ultrasound, when there is bilateral hydronephrosis. After birth, ultrasound confirms bilateral hydronephrosis and hydroureters and a thick-walled bladder. Urethral valves cannot be demonstrated by retrograde urethrography as there is no obstruction to retrograde flow. They are easily demonstrated at micturating cystourethrography, where substantial dilatation of the posterior urethra is seen, which terminates abruptly in a convex border formed by the valves (Fig. 8.62).

Scrotum and testes disorders

The scrotal contents are usually imaged with ultrasound, but MRI is occasionally used. The two main indications for scrotal ultrasound are scrotal swelling or scrotal pain.

In patients with *scrotal swelling*, it is essential to differentiate between an intratesticular cause, such as suspected testicular tumour, and an extratesticular cause, such as varicocele, hydrocele or infection (such as epididymitis or epididymo-orchitis) (Fig. 8.63). Benign epididymal cysts



Fig. 8.59 Coronal T2-weighted MRI of the prostate gland (P) demonstrating invasion of the right seminal vesicle by carcinoma of the prostate (white arrow). Note the normal left seminal vesicle (black arrow).



Fig. 8.60 Prostatic calcification. Numerous calculi just above the pubic symphysis are present in the prostate.

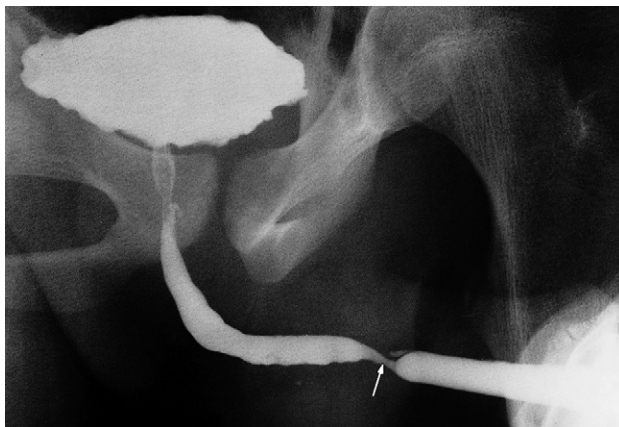


Fig. 8.61 Urethral stricture. An ascending urethrogram showing a stricture in the penile urethra (arrow). The patient had gonorrhoea.

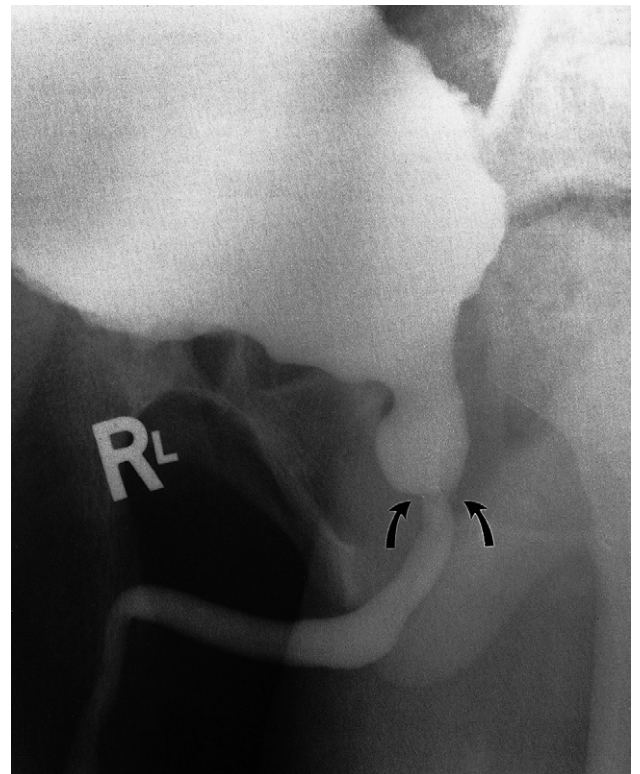
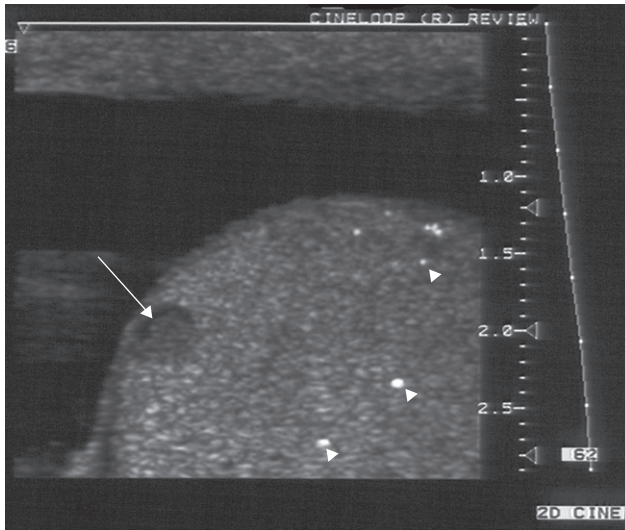
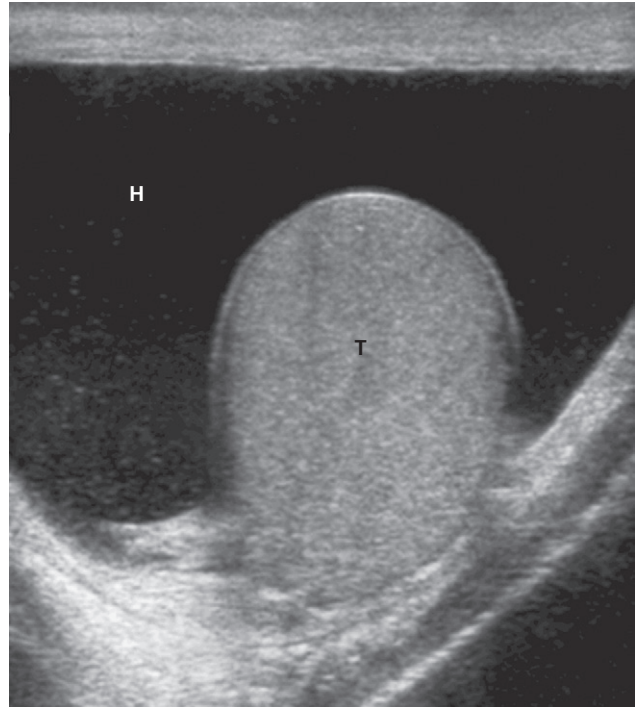


Fig. 8.62 Posterior urethral valves in a 6-year-old boy. On this micturating (voiding) cystogram, the site of the valves is recognized by dilatation of the posterior urethra. Note the irregular outline of the thick-walled bladder due to chronic obstruction.



(a)

Fig. 8.63 (a) Ultrasound of a testis demonstrating a small seminoma (arrow). Several very bright echogenic specks of microcalcification are seen (arrowheads). (b) A hydrocoele (H) is demonstrated surrounding an otherwise normal testis (T).



(b)

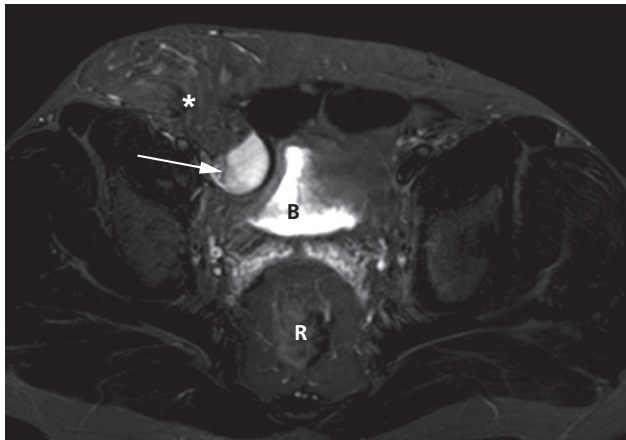


Fig. 8.64 MRI of an undescended right testis (arrow). The testis lies in the region of the right inguinal canal and appears of very high signal on the T2-weighted image with fat saturation. There is also a right inguinal hernia containing fat (*). B, bladder; R, rectum.

are common and can be readily distinguished from testicular tumours on ultrasound examination.

Doppler ultrasound can be used for patients with acute *testicular pain and/or swelling* to distinguish between testicular torsion, in which testicular perfusion is dramatically decreased, and acute epididymitis/orchitis, in which testicular perfusion is normal or increased.

Magnetic resonance imaging can produce highly detailed images of the scrotal contents but is only used in rare cases where ultrasound does not provide sufficient information.

Ectopic testis in the inguinal canal, the commonest site, can be diagnosed by ultrasound. In those few cases where the ectopic testis lies within the abdomen, or where the ultrasound is inconclusive, MRI is the investigation of choice (Fig. 8.64).

Female Genital Tract

Ultrasound, computed tomography (CT) and magnetic resonance imaging (MRI) have important roles to play in gynaecological disease. Because of its diagnostic ease and ready availability, ultrasound is usually the first and principal examination. Ultrasound is used extensively in obstetric practice and is a key aspect of antenatal care. MRI is now routinely used in the evaluation of several gynaecological malignancies and certain benign conditions, CT being reserved for staging the distant extent of malignant disease. Positron emission tomography (PET) may be used in the management of gynaecological malignancy. Conventional radiology plays almost no part – the major exception being hysterosalpingography.

Normal appearances

Ultrasound

Ultrasound of the pelvis can be carried out in two ways: either by scanning through the abdominal wall or transvaginally with a specialized ultrasound probe inserted into the vagina. With the transvaginal route the pelvic organs are nearer the ultrasound probe, so image quality is much improved. The patient is scanned with an empty bladder. When abdominal scanning is undertaken, it is essential for the patient to have a full bladder to act as an acoustic 'window' through which the pelvic structures can be seen. Scans are made in the longitudinal and transverse planes.

On a midline longitudinal or transverse scan the *vagina* can be recognized as a tubular structure, with a central linear echo arising from the opposing vaginal surfaces. The

uterus lies immediately behind the bladder, and the body of the uterus can be seen to be in continuity with the cervix and vagina (Fig. 9.1). The myometrium shows low level echoes, whereas the endometrial cavity gives an echogenic linear stripe (Fig. 9.2). The precise appearance of the uterus depends on the age and parity of the patient and also on the lie of the uterus. The normal *fallopian tubes* are too small to be visualized sonographically.

The *ovaries* are suspended from the broad ligament and usually lie lateral to the uterus near the pelvic side walls. During childbearing years, the ovaries measure 2.5–5 cm in greatest diameter, but after the menopause they atrophy. The endocrine changes occurring during the menstrual cycle have a great effect on the appearance of the ovaries. During the early phase, several cystic structures are seen, representing developing follicles (Fig. 9.2c). Around the eighth day of the cycle, one follicle becomes dominant and may reach 2–2.5 cm in diameter prior to ovulation. At ovulation, the follicle ruptures and immediately decreases in size giving rise to the corpus luteum, which degenerates if there is no intervening pregnancy. By observing these changes it is possible to determine whether an infertile woman is ovulating.

Computed tomography

Multislice CT of the pelvis may be optimized with the use of oral contrast (water or dilute iodine-based contrast) given 1 hour prior to pelvic imaging to aid the differentiation of bowel loops from adnexal structures. Intravenous contrast medium may help to differentiate between vessels

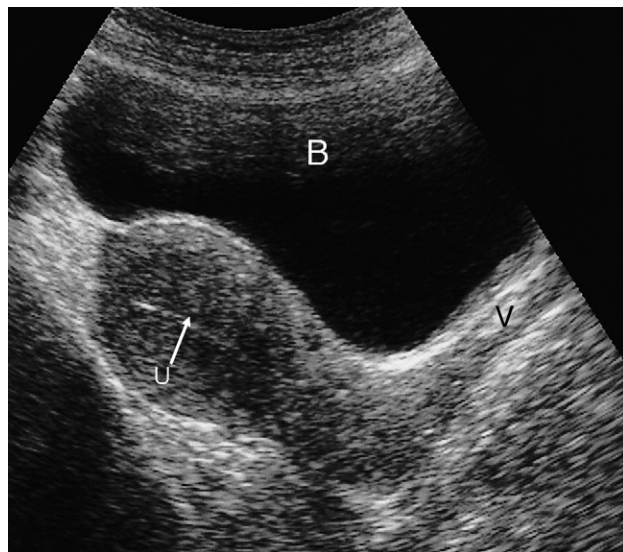


Fig. 9.1 Normal abdominal scan of the uterus and vagina (longitudinal section). The central echo of the uterus (U) corresponds to the endometrial cavity; the uterus itself has a homogeneous echo texture. B, bladder; V, vagina.

and lymph nodes, and to assess the enhancement pattern of a mass. Viewing on coronal and sagittal reformatted images is also helpful. The vagina is seen as a linear structure between the urethra and rectum. Immediately above the vagina, the *cervix* is seen as a rounded soft tissue structure approximately 3 cm in diameter. The body of the *uterus* (Fig. 9.3) merges with the cervix and its precise appearance depends on the lie of the uterus. The endometrial lining cannot be fully assessed on CT. The fallopian tubes and broad ligaments are usually not visible and the ovaries may not be identified. The parametrium is of fat density, the interface with the pelvic musculature being clearly visible. The uterus may be surrounded by loops of bowel.

Magnetic resonance imaging

Pelvic anatomy is very well demonstrated because of the excellent soft tissue contrast afforded by MRI. The patient may be given a muscle relaxant to reduce movement artefacts from the bowel. Images are usually taken in the

axial and sagittal planes but may be supplemented by oblique images, particularly for examination of the cervix or endometrium. Axial images give anatomical appearances similar to CT. T2-weighted sagittal images show the vagina and cervix in continuity with the body of the uterus. The zonal anatomy of the uterus is best demonstrated on T2-weighted images, with the endometrium having a high signal intensity, the adjacent inner myometrium (junctional zone) a low signal intensity, and the myometrium an intermediate signal intensity (Fig. 9.4). The cervix may be predominantly low in signal intensity. Variations of uterine anatomy are well delineated on MRI (Figs 9.5 and 9.6). The ovaries are of intermediate signal intensity and often contain multiple high signal follicles on T2-weighted images (Fig. 9.5). The broad ligaments can also be identified.

Positron emission tomography/computed tomography

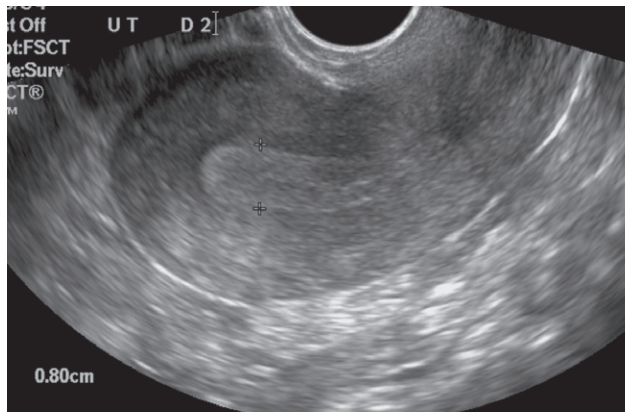
In selected cases, the extent and distribution of gynaecological cancer may be assessed using fluorodeoxyglucose positron emission tomography (FDG-PET)/CT. This technique is particularly helpful in detecting disease that has metastasized beyond the pelvis (see Fig. 9.9d). In addition, some centres are using the technique to assess response to chemotherapy.

Gynaecological pathology

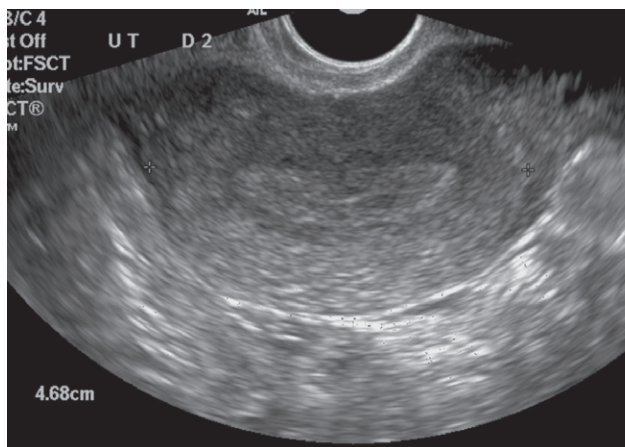
Patients attending for pelvic imaging may present with non-specific symptoms of lower abdominal discomfort or pain, a sensation of bloating, with abnormal vaginal bleeding or a pelvic mass. Pelvic imaging may also be undertaken for the investigation of infertility. Ultrasound is the initial investigation in most cases.

Pelvic masses

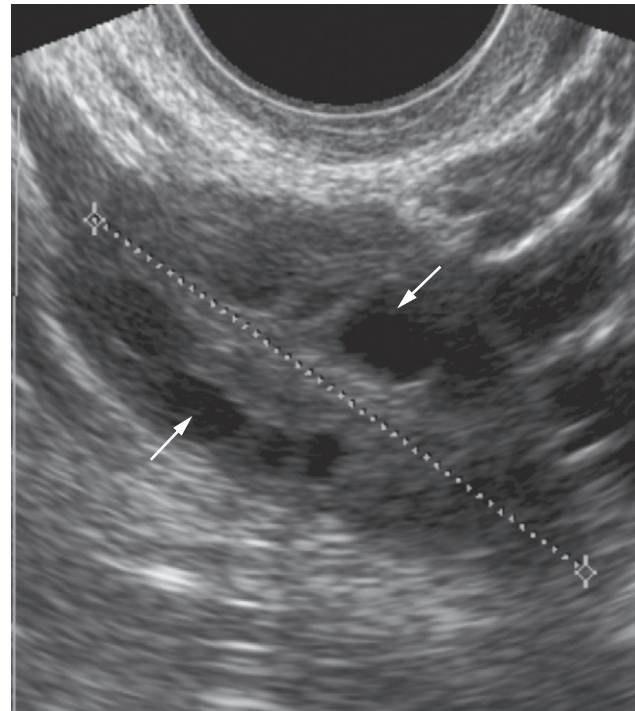
Ultrasound, CT and MRI will be abnormal in virtually any patient in whom a mass can be felt on physical examination. With ultrasound, it is possible to tell whether the mass is cystic or solid. In some cases, the characteristics of the adnexal cyst or mass may indicate whether the



(a)



(b)



(c)

Fig. 9.2 Normal transvaginal ultrasound scan. (a) Longitudinal section through the uterus. Note the echogenic endometrial stripe between the measurement calipers. (b) Transverse section through the uterus. (c) Normal ovary. Several normal follicles are seen (arrows).

lesion is benign in nature or likely to be malignant. However, in some cases, this distinction cannot be made on ultrasound alone and MRI may be helpful in further characterization. CT is predominantly used to demonstrate the extent of disease in the abdomen in cases of malignant disease. A limitation of imaging, particularly ultrasound and CT, is that sometimes it is not possible to determine from which organ the mass arises; an ovarian mass that lies in contact with the uterus may appear similar to a mass arising within the uterus and vice versa. MRI, which may be performed in any scan plane, may be used to help make the distinction.

Ovarian masses

Ovarian cysts

Sometimes a follicle or corpus luteum persists as a follicular or corpus luteum cyst, both of which are easily recognized by ultrasound, CT or MRI (Fig. 9.7). Follicular cysts are mostly asymptomatic and regress spontaneously. Corpus luteum cysts are most often seen in the first trimester of pregnancy; they usually resolve, but may rupture or twist. Haemorrhage into both types of cyst may occur and gives a characteristic appearance on ultrasound.

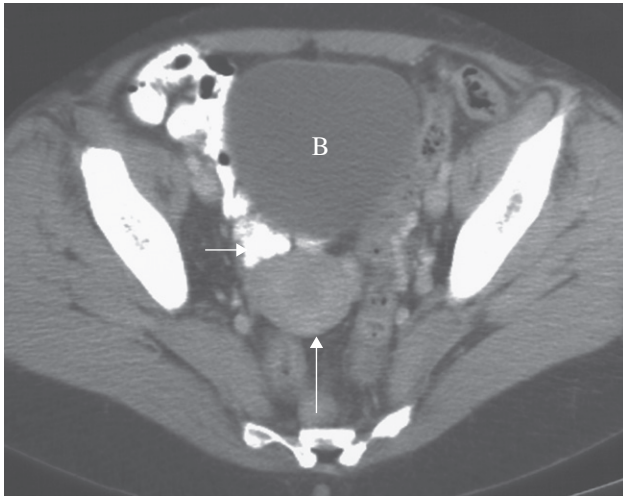


Fig. 9.3 Normal uterus (long arrow) in a 49-year-old patient, on CT, following intravenous contrast enhancement. Note the oral contrast medium within loops of the small bowel (short arrow). B, bladder.

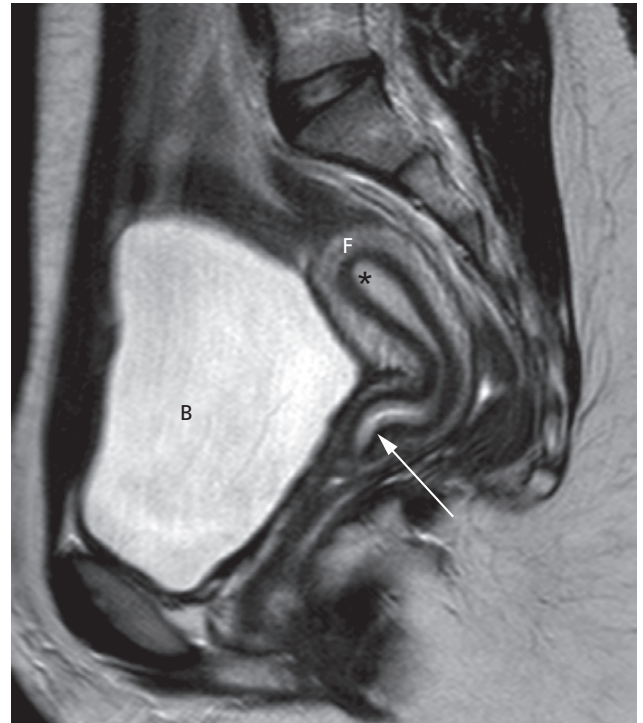


Fig. 9.4 Normal uterus on sagittal T2-weighted MRI. The endometrium (*) returns a high signal intensity. The cervix (white arrow) is in continuity with the lower uterine body. B, bladder; F, uterine fundus.

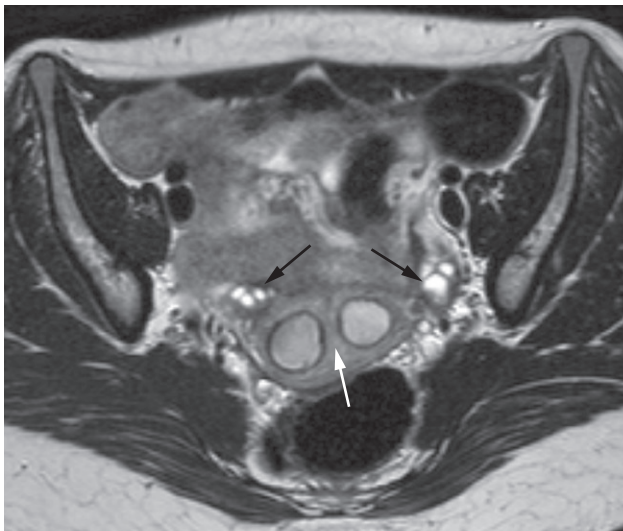


Fig. 9.5 Axial MRI of a septate uterus, an anatomical variant. The endometrial cavity is divided into two compartments by a septum of myometrium (white arrow). Note the normal ovaries bilaterally (black arrows).

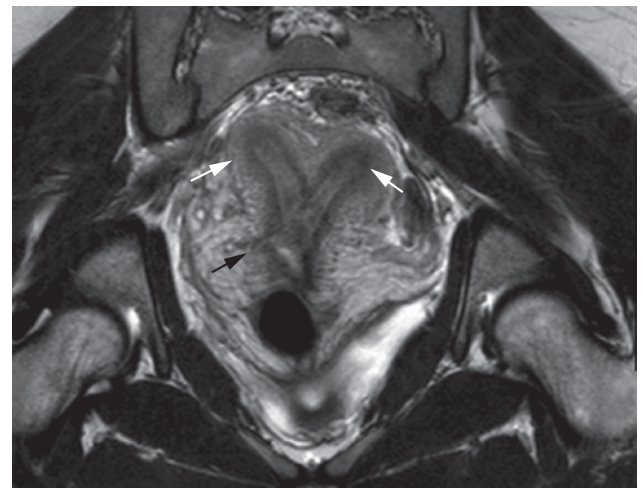
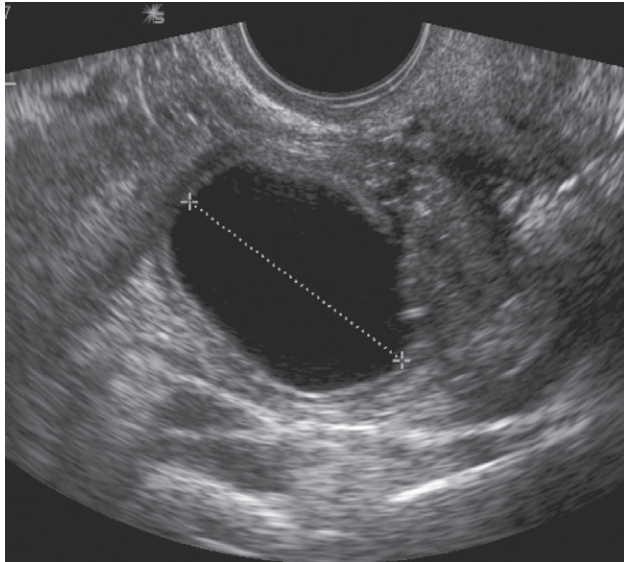
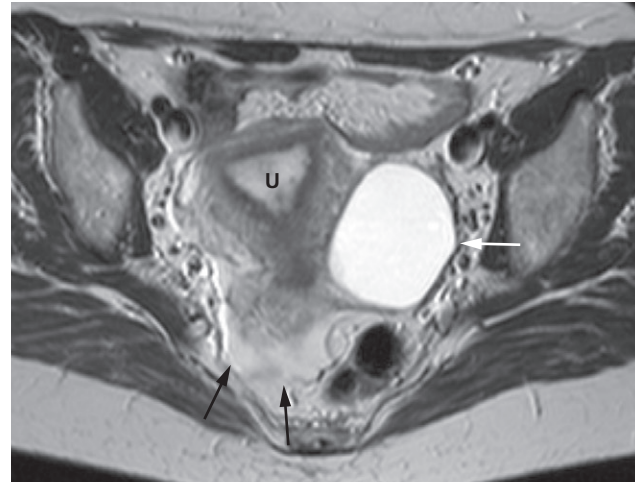


Fig. 9.6 Oblique coronal T2-weighted MRI of a bicornuate uterus, with two divergent cornu (white arrows). The scar from a previous caesarean section is also seen (black arrow).



(a)



(b)

Fig. 9.7 Ovarian cyst. (a) Longitudinal ultrasound scan to the right of midline showing a 5cm cyst in the right ovary with no internal echoes. (b) Axial T2-weighted MRI scan showing a left-sided ovarian cyst (white arrow) with benign features. There is a small volume of free fluid in the pouch of Douglas (black arrows). U, uterus.

The typical features of polycystic ovaries on ultrasound or MRI include large volume ovaries with multiple small follicles arranged around the periphery, forming the appearance of a 'string of pearls' (Fig. 9.8).

Ovarian tumours

The commonest ovarian tumours are the cystadenoma and the cystadenocarcinoma. Ovarian tumours can be predominantly cystic, solid or a mixture of the two (Fig. 9.9). Those that are cystic may be multilocular. On ultrasound, the recognized features of benign lesions and malignant lesions are listed in Box 9.1. In some cases it is not possible to say whether the mass is benign or malignant based on the ultrasound, unless there is evidence of local invasion or distant spread. MRI may be used to further characterize indeterminate masses as benign or malignant prior to deciding on patient management. With disseminated malignancy, deposits within the omentum and ascites may be visible (see Fig. 10.3), but small omental and peritoneal

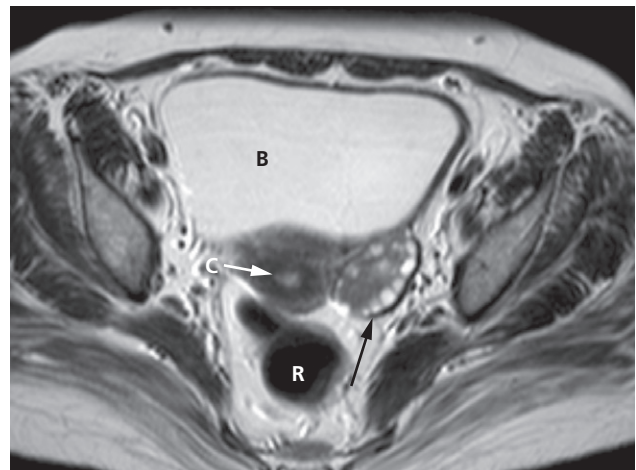


Fig. 9.8 Polycystic ovary. Axial T2-weighted MRI demonstrating a left ovary (black arrow) which is large in size and has multiple small cysts arranged around the periphery of the ovary, in a characteristic 'string of pearls' distribution. B, bladder; C, cervix; R, rectum.

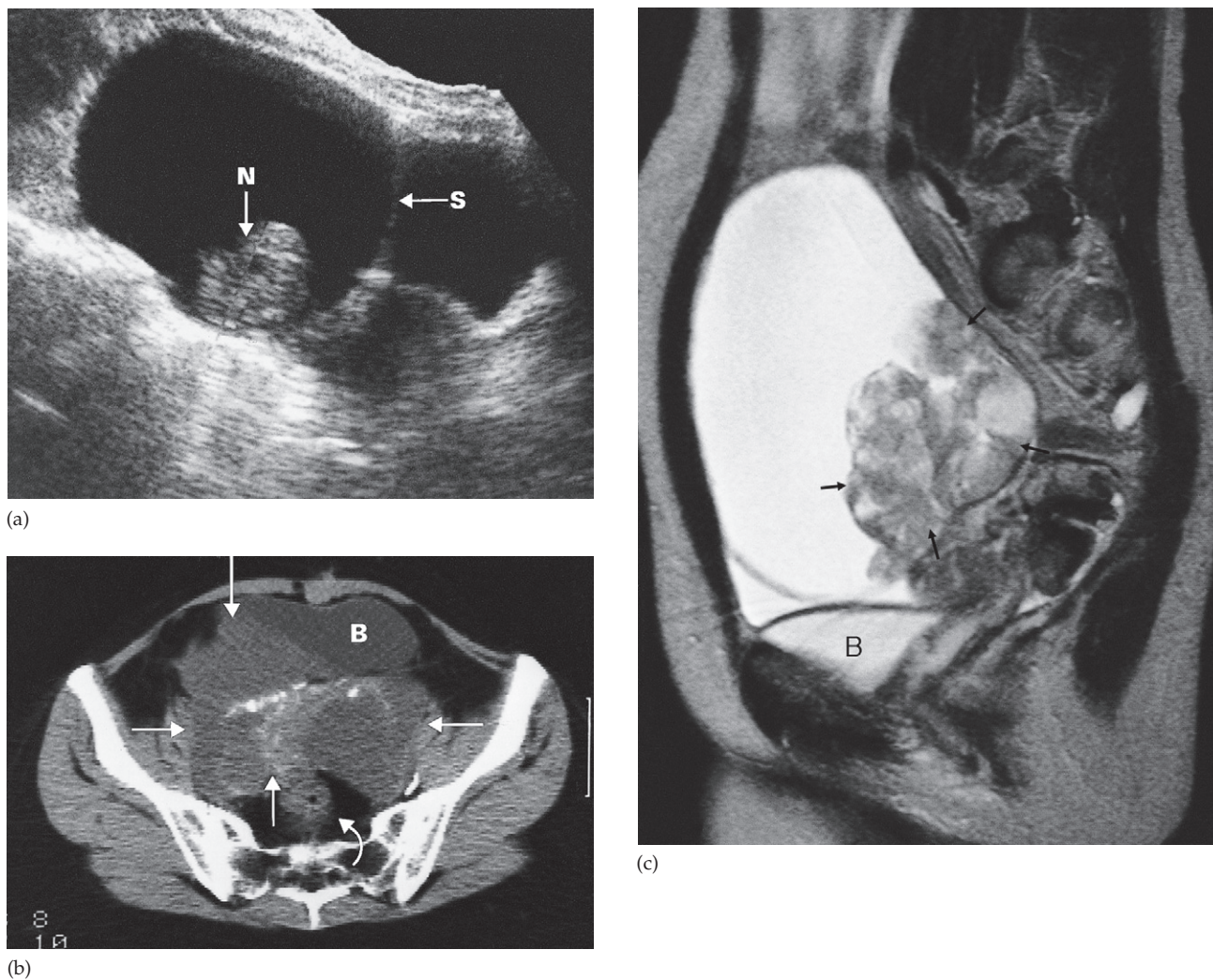
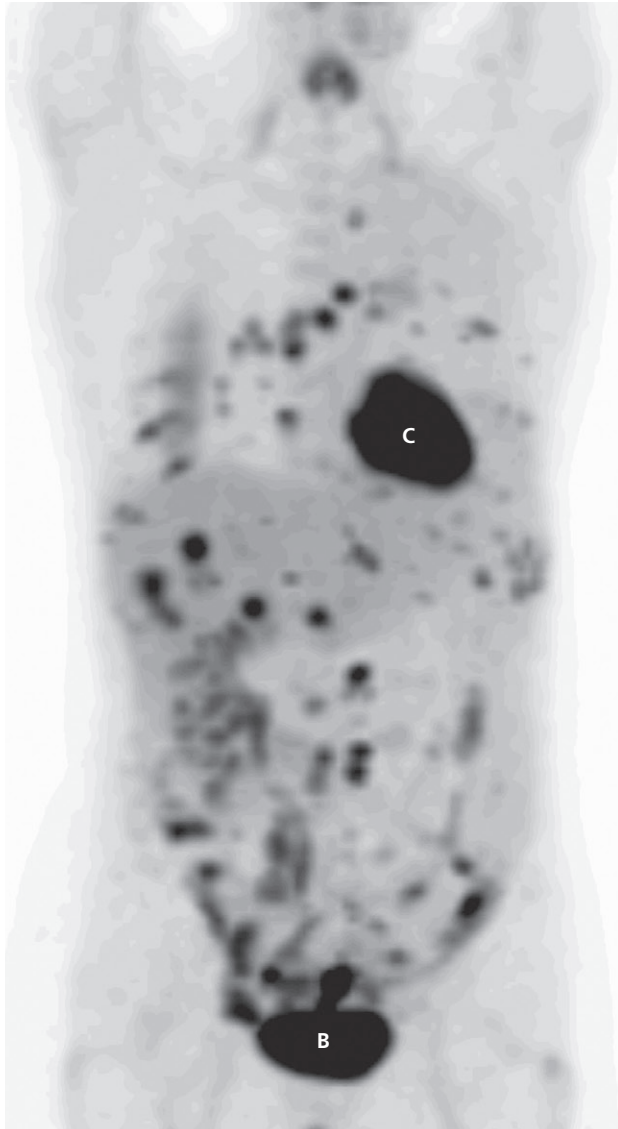


Fig. 9.9 Ovarian carcinoma. (a) Longitudinal ultrasound scan showing a very large multilocular cystic tumour containing septa (S) and solid nodules (N). The lesion was a cystadenocarcinoma. (b) CT scan showing a large partly cystic, partly solid ovarian carcinoma (arrows). The tumour, which contains irregular areas of calcification, has invaded the right side of the bladder (B). The rectum is indicated by a curved arrow. (c) MRI scan showing a partly solid (arrows) and partly cystic tumour. The cystic component is of high signal intensity on this T2-weighted image. (d) FDG-PET/CT in a patient with disseminated ovarian cancer. Abnormally increased activity is seen in the chest, liver and peritoneum. Normal cardiac (C) and bladder (B) activity is demonstrated.



(d)

Fig. 9.9 Continued

Box 9.1 Morphological features of benign and malignant ovarian masses

Benign ovarian masses

- Small simple cyst
- Thin cyst wall
- If septate, then thin and smooth septations
- No solid components
- If solid components are seen, then no vascularity is seen on Doppler

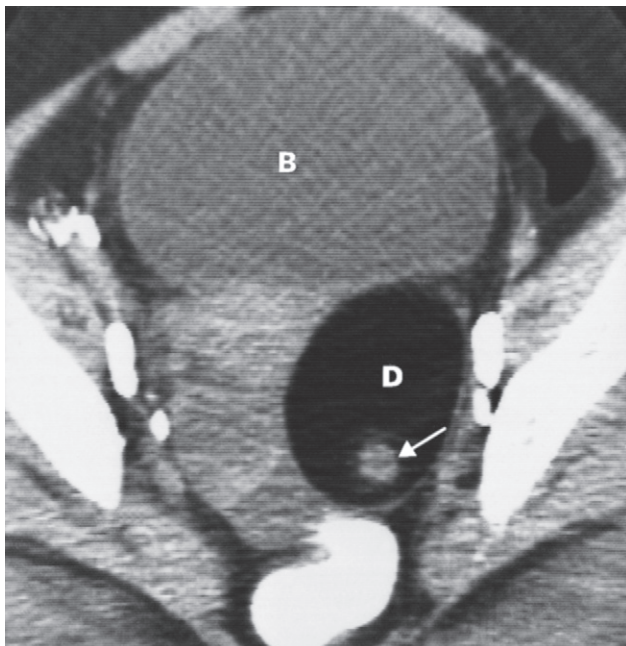
Malignant ovarian masses

- Mixed solid and cystic mass
- Vascularity within solid components on Doppler
- Thickened septations, >3 mm
- Large size
- Bilateral masses
- Associated ascites or peritoneal deposits

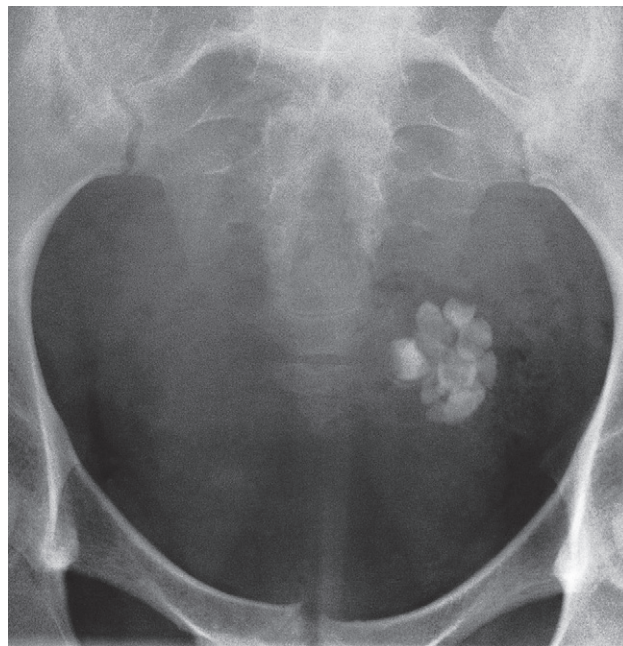
metastases are frequently difficult to detect. FDG-PET/CT may be used to demonstrate the extent of disseminated disease in order to aid treatment planning (Fig. 9.9d). Ultrasound, CT and MRI may show hydronephrosis from ureteric obstruction by the tumour and may also demonstrate enlarged lymph nodes, liver metastases or pleural effusions.

The optimal treatment of ovarian carcinoma is by hysterectomy, oophorectomy and surgical removal of all macroscopic tumour, and formal staging is usually carried out during surgery. Preoperative imaging may be used to provide the surgeon with information concerning the extent and distribution of macroscopic disease. Imaging, including FDG-PET/CT, is used in the detection of recurrent disease.

A *dermoid cyst* can usually be confidently diagnosed because of the fat within it, and it may contain various calcified components, of which teeth are the commonest. These ovarian tumours are predominantly benign and can usually be recognized on ultrasound but are also readily diagnosed on CT or MRI and sometimes on plain radiographs (Figs 9.10 and 9.11). Otherwise, only very large ovarian tumours are recognizable on plain abdominal radiographs as a soft tissue mass, occasionally containing calcium, arising from the pelvis.

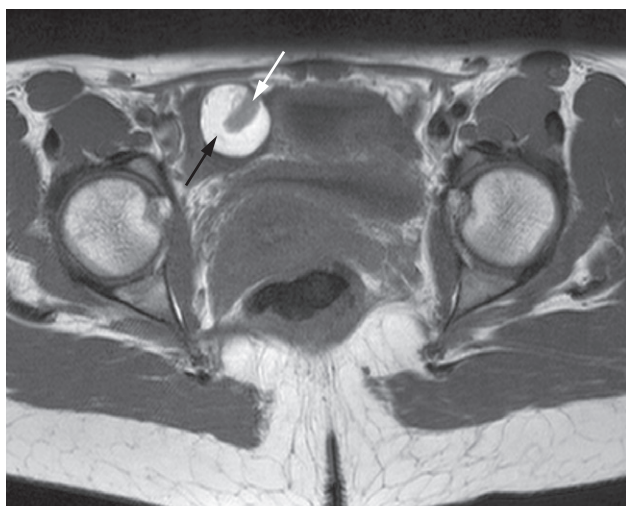


(a)

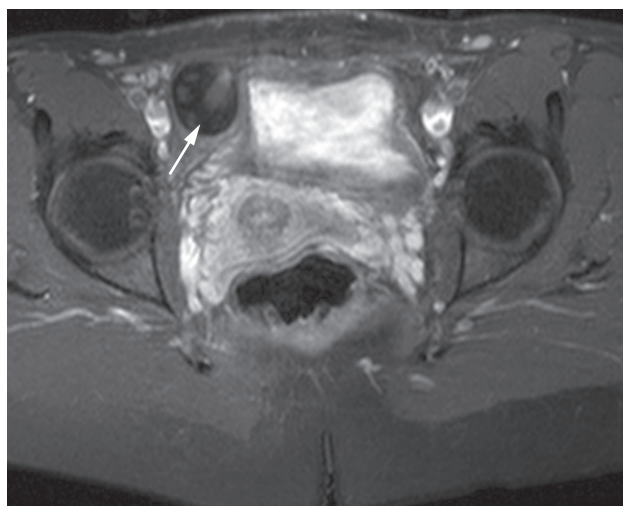


(b)

Fig. 9.10 Dermoid cyst. (a) CT scan showing the oval-shaped fat density of a dermoid cyst (D) containing calcified material (arrow). B, bladder. (b) Plain film of another patient showing well-developed teeth within the cyst.

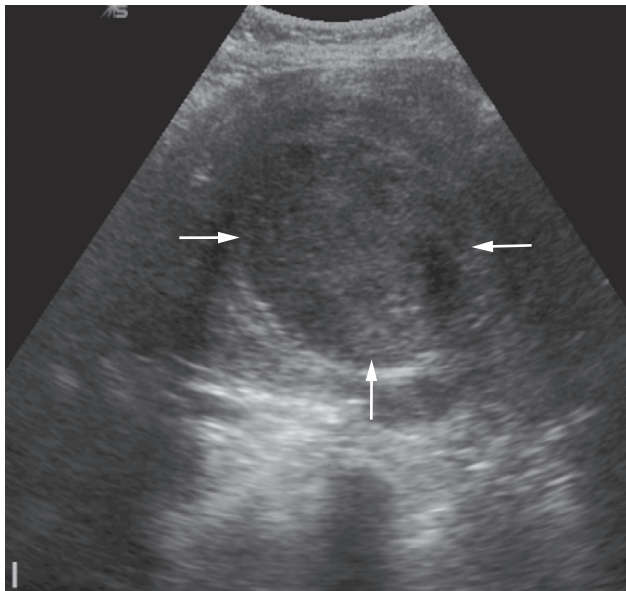


(a)

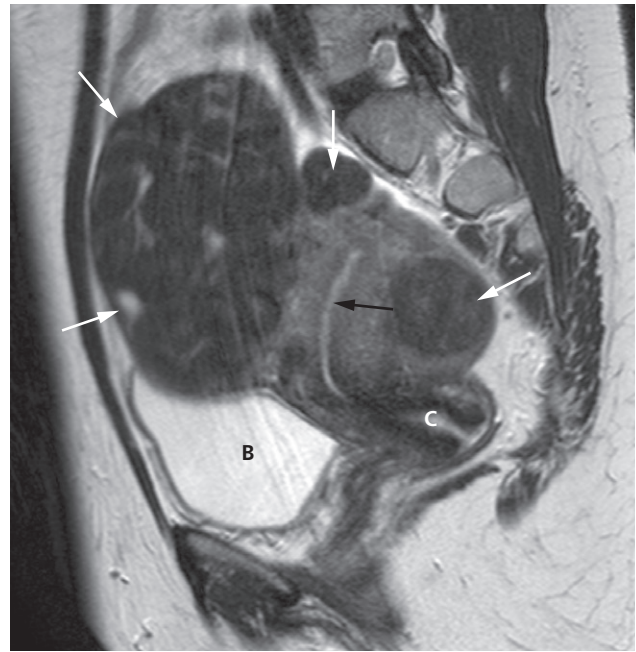


(b)

Fig. 9.11 Benign dermoid cyst. (a) Axial T1-weighted MRI demonstrating a complex cyst that contains high signal intensity material, indicating the possible presence of lipid (black arrow). An internal solid component is also seen (white arrow). (b) Axial T1-weighted image with fat saturation demonstrating an almost complete drop of signal intensity within the cyst, consistent with the presence of lipid (arrow). This confirms the diagnosis of a dermoid cyst. There was no enhancement of the internal solid component.



(a)



(b)

Fig. 9.12 (a) Transverse ultrasound scan showing a large fibroid in the uterus. Its extent is indicated by the arrows. (b) Sagittal T2-weighted MRI demonstrating several uterine fibroids (white arrows), which are of low signal intensity. The endometrial cavity is normal (black arrow). B, bladder; C, cervix.

Uterine masses

Fibroids

Leiomyomas (fibroids) are common in women over 30 years of age. They are often asymptomatic, but may cause menorrhagia or present as a palpable mass. When sufficiently large, a fibroid can be seen on a plain film as a mass in the pelvis and may show multiple irregular but well-defined calcifications (see Fig. 5.15). Ultrasound and CT both show a spherical or lobular uterine mass. At ultrasound, the mass may be either hypoechoic or echogenic (Fig. 9.12a), whereas at CT fibroids are usually the same density as the adjacent myometrium. MRI can readily identify fibroids as they typically have a different signal characteristic from the normal uterus (Fig. 9.12b).

Adenomyosis

Adenomyosis is a benign condition in which there is endometrial tissue within the myometrium. This results in

smooth muscle hypertrophy. Patients may present with dysmenorrhoea and abnormal uterine bleeding. The uterus is typically enlarged. On ultrasound, there is increased heterogeneity of the myometrium. On MRI, there is focal or diffuse thickening of the junctional zone and, in some cases, multiple bright projections are seen extending from the endometrium into the myometrium (Fig. 9.13).

Carcinoma of the cervix and body of the uterus

The diagnosis of carcinoma of the cervix is normally made by cytology or biopsy and physical examination. Endometrial carcinoma may be suspected on ultrasound when there is widening of the endometrial stripe, but confirmation of the diagnosis is based on histology.

Magnetic resonance imaging is useful to determine the extent of *carcinoma of the cervix* preoperatively, because the extent (or tumour stage) determines whether the patient is managed with surgery or with chemoradiotherapy. The observations to be made are whether the tumour is

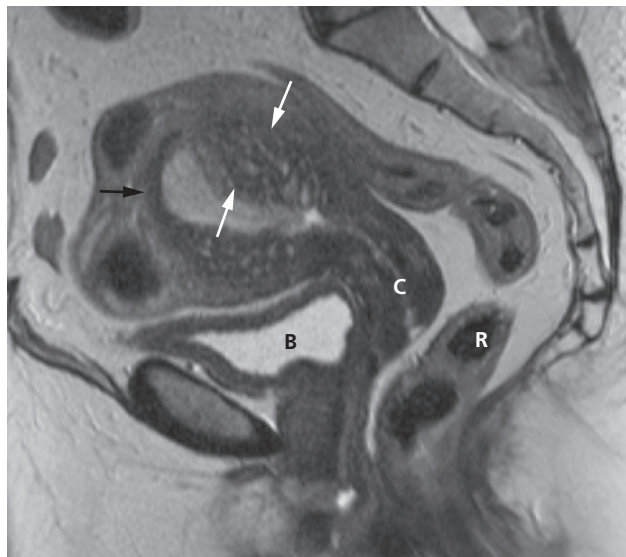


Fig. 9.13 Adenomyosis. Sagittal T2-weighted MRI demonstrating a markedly widened junctional zone containing small cysts (between the white arrows). A normal section of junctional zone is seen in the region of the uterine fundus (black arrow). Two low signal intensity ovoid fibroids are also present in the fundus. B, bladder; C, cervix; R, rectum.

confined to the cervix (Fig. 9.14) or whether it extends into the parametrium, lymph nodes, rectum, bladder or pelvic side walls (Fig. 9.15). MRI is very accurate in assessing the local extent of the tumour. CT and MRI also enable the detection of dilatation of the ureters in cases where the tumour has caused ureteric obstruction.

Endometrial carcinoma is usually treated by surgical removal of the uterus, ovaries and pelvic lymph nodes. MRI may be used preoperatively in order to guide the extent of surgery as it can predict the depth of myometrial invasion by tumour (Fig. 9.16) and demonstrate involvement of the cervix and nodal enlargement.

Pelvic inflammatory disease

Pelvic inflammatory disease may be due to venereal infection, commonly gonorrhoea, which in the acute stages gives rise to a tubo-ovarian abscess. Pelvic inflammation and abscess formation may also occur following pelvic surgery, childbirth or abortion and may be seen in associa-

tion with intrauterine contraceptive devices, appendicitis or diverticular disease. The usual imaging technique is ultrasound. Irrespective of the cause of the infection, ultrasound will show a hypoechoic or complex mass in the adnexal region or pouch of Douglas (cul-de-sac) (Fig. 9.17). Blockage of the fallopian tubes may cause a hydrosalpinx, which can be recognized as a hypoechoic adnexal mass, which is often tubular in shape.

The appearance of pelvic inflammatory disease on ultrasound may be indistinguishable from endometriosis and ectopic pregnancy, conditions that both occur in women of reproductive age. In some cases, the appearances may be indistinguishable from an ovarian malignancy.

Endometriosis

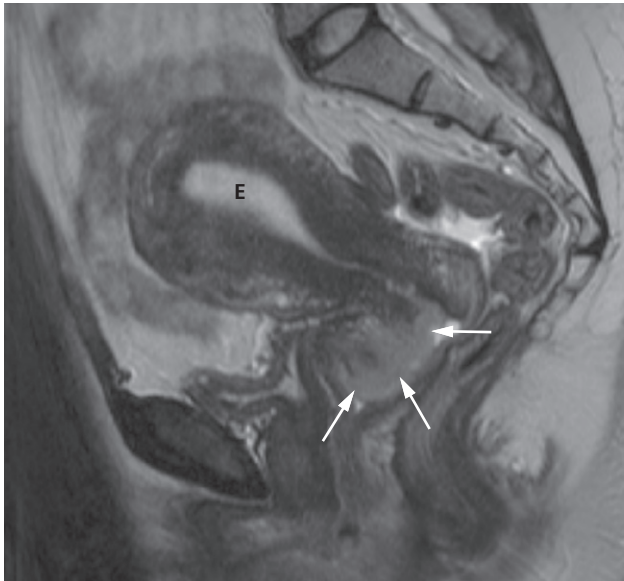
In endometriosis, there is endometrial tissue outside the uterus, most commonly confined to the pelvis. At ultrasound, endometriosis is usually seen as a cystic mass with homogeneous internal echogenicity in the adnexal region and/or pouch of Douglas corresponding to the chocolate cysts found on pathological examination (Fig. 9.18). There are characteristic appearances on MRI due to recurrent haemorrhage into endometriomas (Fig. 9.19) and there is often in-drawing of the rectum towards the pouch of Douglas due to the development of fibrous adhesions.

Detection of intrauterine contraceptive devices

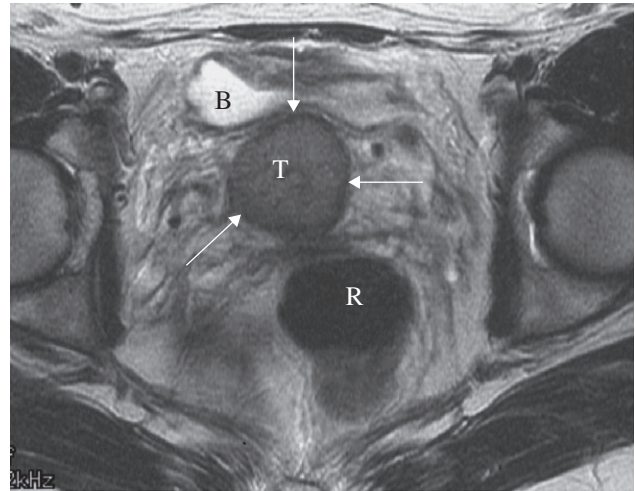
The lost intrauterine contraceptive device (IUCD) is a relatively common problem and ultrasound should be the first investigation. Different devices have characteristic appearances. They are seen as highly reflective structures and their relationship to the uterine cavity can be determined (Fig. 9.20). If the IUCD cannot be located in the pelvis, then a plain film of the abdomen should be taken in case the device has migrated through the uterus. If there is a coexisting pregnancy, it becomes very difficult to locate the IUCD by ultrasound after the first trimester.

Hysterosalpingography

Hysterosalpingography is performed in selected cases of infertility in order to assess the patency of the fallopian tubes. A catheter with a seal to prevent leakage from the

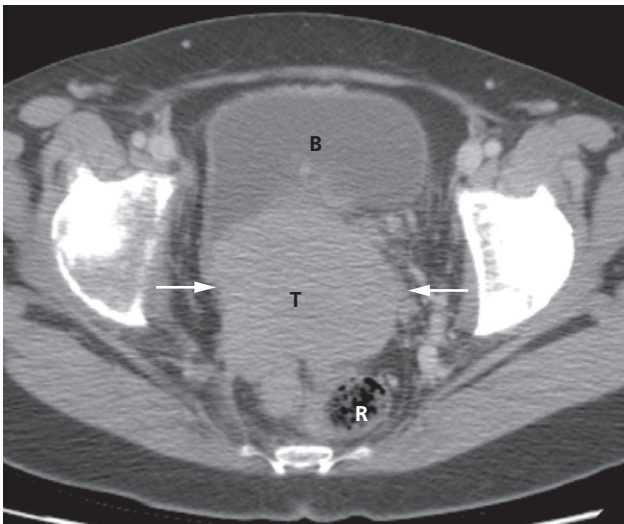


(a)



(b)

Fig. 9.14 Carcinoma of the cervix. (a) Sagittal T2-weighted MRI scan showing a tumour confined to the cervix (arrows). E, endometrium. (b) Axial T2-weighted MRI in a different patient demonstrating a cervical tumour (T), which is confined to the cervix, with a thin layer of normal, low signal cervical tissue surrounding the tumour (arrows). B, bladder; R, rectum.



(a)

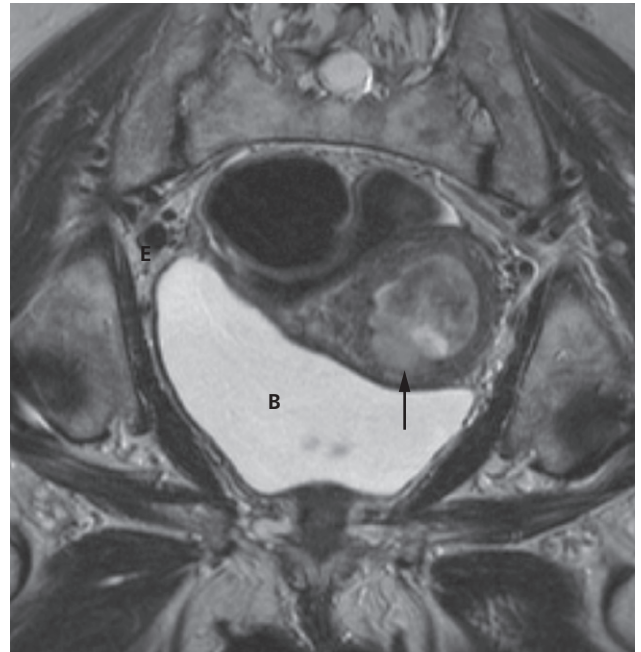


(b)

Fig. 9.15 Advanced carcinoma of the cervix. (a) CT scan showing a large tumour (T) of the cervix invading the parametrium (arrows) and extending into the rectum posteriorly. (b) Sagittal T2-weighted MRI of the same patient. Note the tumour (T) extending down the vagina. B, bladder; E, endometrium; R, rectum.



(a)



(b)

Fig. 9.16 Endometrial cancer. (a) Sagittal T2-weighted MRI demonstrating a polypoid tumour mass distending the endometrial cavity (arrow). (b) Oblique axial MRI in a different patient. The endometrial tumour mass is invading into the deep myometrium (arrow). B, bladder; C, cervix; V, vagina.

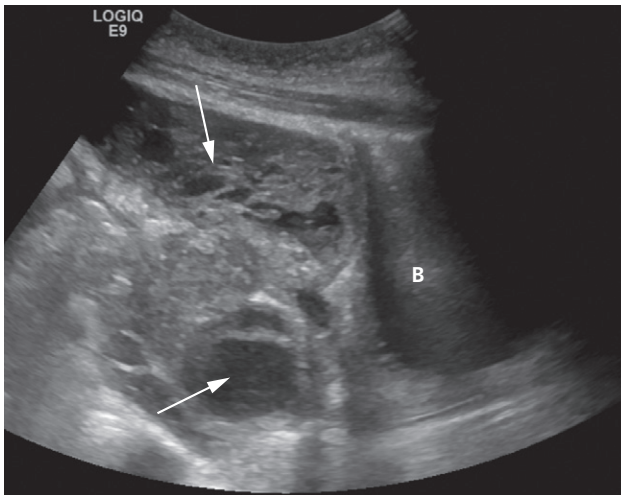


Fig. 9.17 Pelvic abscess. Ultrasound scan showing a highly complex cystic and solid hypoechoic mass with multiple locules (arrows) behind the bladder (B).

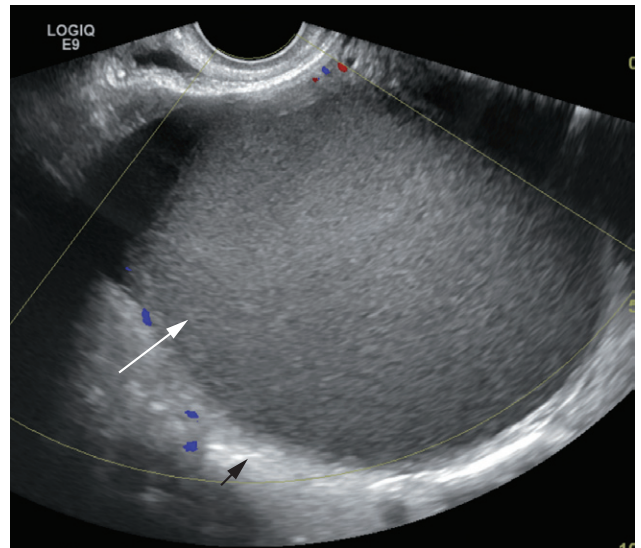
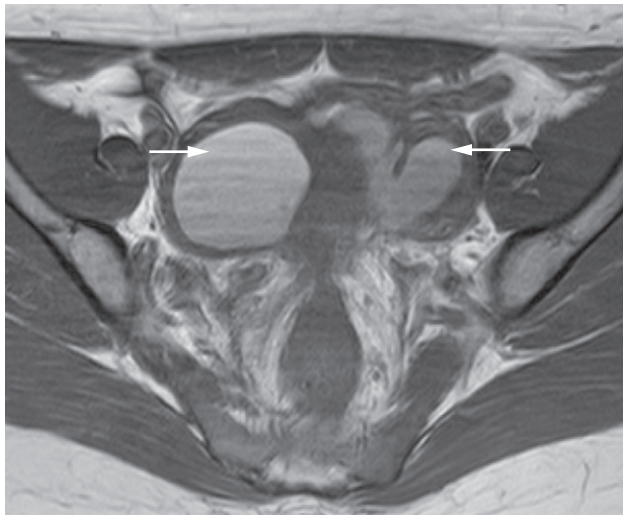
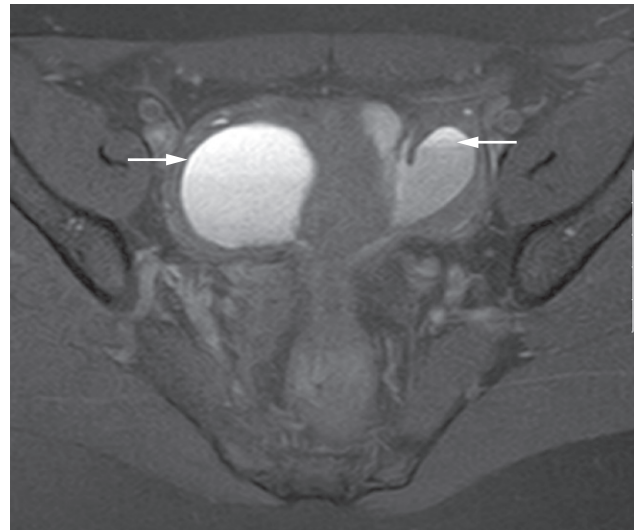


Fig. 9.18 Endometriotic cyst. Transvaginal Doppler ultrasound demonstrating an adnexal cyst that has homogeneous internal echogenicity (white arrow), increased through transmission of sound (black arrow) and no Doppler signal within the cyst.



(a)



(b)

Fig. 9.19 Bilateral endometriotic cysts. (a) Axial T1-weighted MRI showing haemorrhagic cysts in the pelvis (arrows), which have a relatively high signal on this sequence. (b) The cysts retain the high signal intensity on this fat-saturated T1 sequence, confirming the presence of blood. There is some variation in the signal intensity, a characteristic of endometriotic cysts.

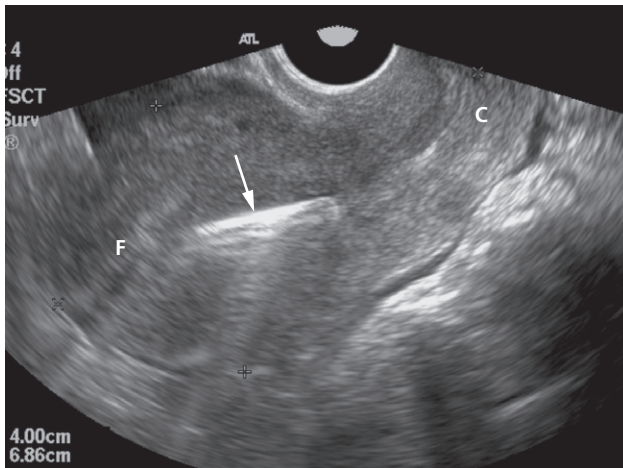


Fig. 9.20 Intrauterine contraceptive device (arrow) seen as a linear reflective echo within the uterine cavity, shown on a longitudinal ultrasound scan. C, cervix; F, uterine fundus.

external cervical os is inserted into the uterus. Sufficient iodinated contrast is then injected under fluoroscopic control to fill the uterus and fallopian tubes (Fig. 9.21). If the fallopian tubes are patent, there is free spill into the peritoneum, recognized by the demonstration of contrast between loops of bowel. Congenital variations in uterine morphology, which may prevent maintenance of pregnancy, can also be assessed.

Ultrasound hysterosalpingography may be performed to detect tubal patency. This technique, which avoids the use of ionizing radiation, involves injecting an ultrasound contrast agent into the uterus through a catheter and following the passage of contrast through the fallopian tubes with ultrasound.

Obstetric ultrasound

Ultrasound of the pregnant patient is simple to perform and has proved reliable in examining the fetus. No biological damage has yet been attributed to ultrasound examination as currently used in obstetric practice. No fetal abnormalities have been attributable to ultrasound during

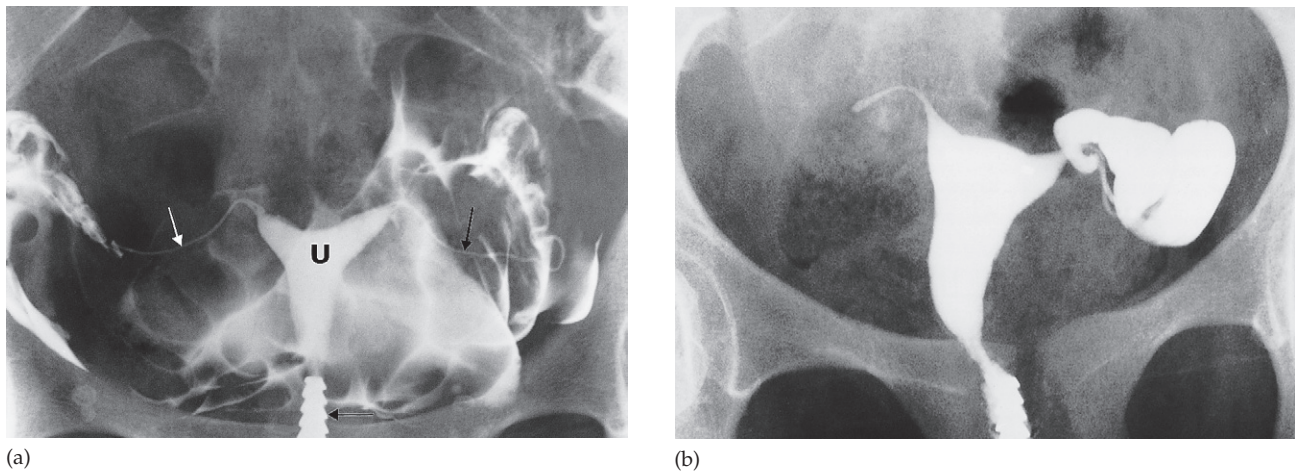


Fig. 9.21 Hysterosalpingogram. (a) Normal genital tract. Contrast has been injected to fill the uterus (U) and both fallopian tubes (vertical arrows). Free spill into the peritoneum has occurred to outline loops of bowel. Note the cannula in the cervical canal (horizontal arrow). (b) Hydrosalpinx. Both fallopian tubes are obstructed and dilated, the left one massively. There is no spill of contrast into the peritoneum.

pregnancy over the several decades that the technique has been in use. In addition to fetal evaluation, maternal disease, which may occur during the course of the pregnancy, or complications of pregnancy may also be safely investigated using ultrasound. In particular, diseases of the urinary tract, gall bladder or suspected deep venous thrombosis may be diagnosed. Following delivery, retained products of conception can be readily detected on ultrasound of the uterus.

Ultrasound in the first trimester

Ultrasound examination during early pregnancy may be undertaken transabdominally or transvaginally, although transvaginal examination provides higher resolution. The normal gestational sac is a small cystic structure lying within the uterine cavity, first seen at the fifth week of amenorrhea, following the last menstrual period. The developing fetus is seen by the sixth week and the fetal heart beat is visible by the seventh week. The pregnancy can be dated by measuring the length of the fetus, between the seventh and 12th weeks of pregnancy (Fig. 9.22). Multiple pregnancies can also be detected. Between 10 and 14 weeks, the nuchal translucency – fluid along the back of the fetal neck – may be measured. This technique can be



Fig. 9.22 Eleven-week-old fetus. The crown-rump length is indicated by the crosses. The fetus is seen in sagittal section and the head is clearly visible on the left and the body to the right.

used to detect Down's syndrome and some other chromosomal or fetal abnormalities.

Ultrasound in the second and third trimesters

After the first trimester, transabdominal ultrasound is used to assess fetal maturity by measuring both the biparietal diameter of the fetal head and the femur length, both of which can be precisely defined. By comparing the measurements with a standard growth chart, an estimate of gestational age can be obtained. Using this method, dating is most accurate between 18 and 20 weeks. This is also a suitable time to identify fetal abnormalities.

Placental imaging

The placenta is easily evaluated sonographically as well as on MRI (Fig. 9.23). By the ninth week, it is seen as a well-defined intrauterine structure lining the inner wall of a portion of the uterine cavity. Abnormalities related to the placenta may be diagnosed on ultrasound, including placental haemorrhage and placenta praevia, a condition in which the placenta remains positioned over the lower uterine segment after the 36th week of pregnancy.

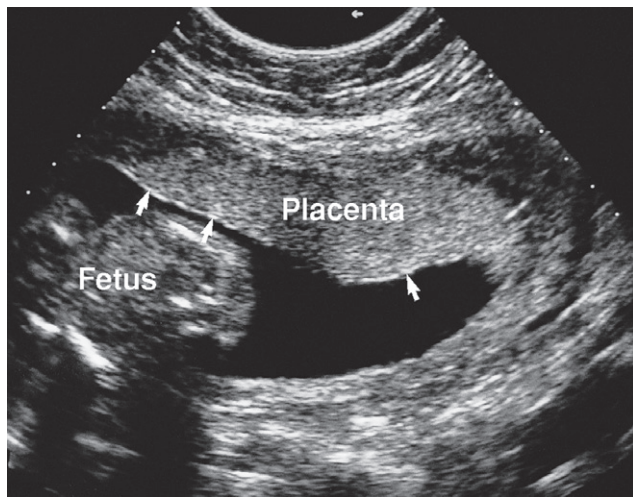
'Large for dates' uterus

A common problem in obstetric care is the patient whose uterus is larger than expected. The causes are listed in Box 9.2.

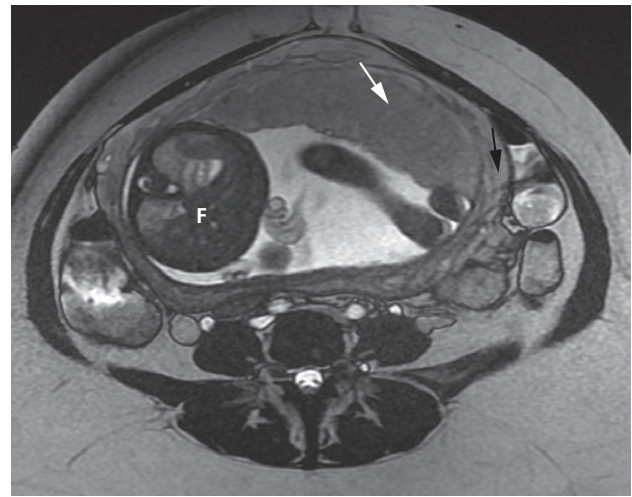
Polyhydramnios is associated with maternal abnormalities such as diabetes and with a number of fetal conditions. The fetal abnormalities include neural tube defects and obstruction of the alimentary tract, e.g. oesophageal or duodenal atresia, where the hydramnios is due to an impaired circulation of swallowed amniotic fluid. Polyhydramnios also occurs with normal multiple pregnancies.

Box 9.2 Causes of 'large for dates' uterus

- Inaccurate dating (the commonest cause)
- Multiparity
- Trophoblastic disease (such as benign hydatidiform mole or malignant choriocarcinoma)
- Associated ovarian or uterine tumours (such as fibroids), either of which may be mistaken for generalized enlargement of the uterus
- Polyhydramnios (defined as twice the volume of amniotic fluid expected for the stage of gestation)



(a)



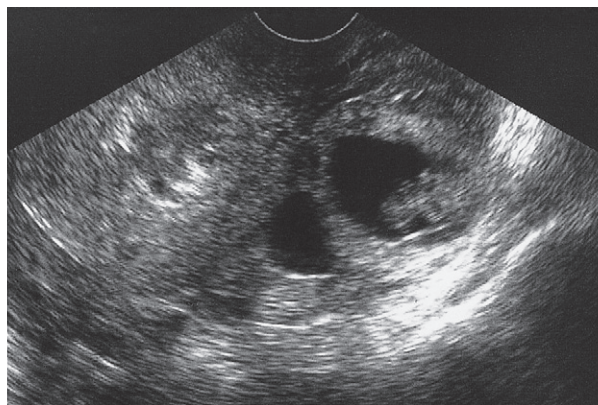
(b)

Fig. 9.23 Placental imaging. (a) Placenta seen on a longitudinal scan at 18 weeks' gestation. The chorionic plate is seen as a thin line of bright echoes (arrows). (b) Axial T2-weighted MRI through the placenta (white arrow); myometrium is indicated by the black arrow. F, fetus.

'Small for dates' uterus: intrauterine growth retardation

Ultrasound is used to assess intrauterine growth retardation, which carries a greatly increased risk of perinatal death and alters obstetric management. However, it is important not to misdiagnose a fetus as being small for dates because of an error in calculating the age from the menstrual history: hence the need for accurate dating early in pregnancy. Growth retardation may occur due to congenital abnormalities or intrauterine infection, resulting in symmetrical growth retardation of the head and body. Placental insufficiency or maternal disease such as hypertension or diabetes may cause asymmetrical growth retardation in the third trimester, with growth of the fetal body being affected to a greater degree than growth of the fetal head.

The uterine size may be small for dates due to a reduced volume of amniotic fluid. The fetal kidneys contribute significantly to the amniotic fluid volume. The presence of profound oligohydramnios, although most frequently due to premature rupture of the membranes, should raise the possibility of a renal abnormality. The commonest identifiable abnormalities are hydronephrosis and the dysplastic condition multicystic kidney. Chronic bladder outlet obstruction, which is usually caused by posterior urethral valves, can lead to bilateral hydronephrosis and hydroureters and a massively dilated, thick-walled bladder.



Ultrasound for karyotyping

Ultrasound may be used to guide a needle into the correct position to obtain a sample of amniotic fluid (amniocentesis), placental tissue (chorion villus sampling) or cord blood from the umbilical vein (cordocentesis). These types of tissues may be used for fetal karyotyping.

Fetal death

It is possible to see the heart beating and observe fetal movement on ultrasound from the seventh week of pregnancy onward. Failure to observe these phenomena suggests fetal death, but in the early stages of pregnancy one must be careful that the gestational age has been calculated correctly. It is, therefore, important to repeat the scan after a suitable interval if there is any doubt. After the ninth week, fetal death can be readily diagnosed by the absence of a visible heart beat.

Ectopic pregnancy

Ectopic pregnancy generally presents with sudden pain due to rupture of the ectopically placed gestational sac and should be managed as a medical emergency. The ruptured ectopic pregnancy itself is not always visible. When seen sonographically, it is identified as an adnexal mass having both solid and cystic characteristics, and occasionally a fetus can be seen within it (Fig. 9.24). There should be no

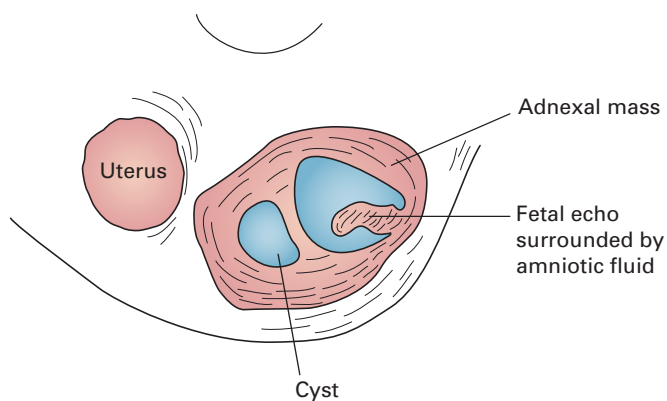


Fig. 9.24 Ectopic pregnancy. Transvaginal scan in the transverse plane in a patient whose pregnancy test was positive. The uterus is seen containing no gestational sac and there is a predominantly cystic adnexal mass containing a fetal echo surrounded by amniotic fluid.

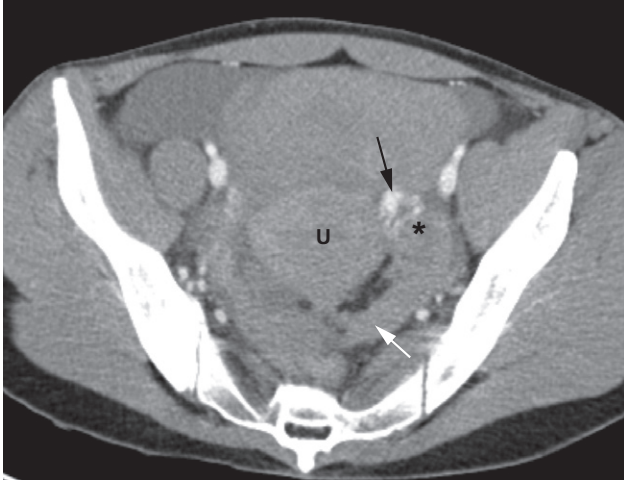


Fig. 9.25 Ruptured ectopic pregnancy on CT. There is a left adnexal mass (*) with leakage of intravenous iodinated contrast (black arrow) due to bleeding. There is high density fluid in the pelvis and pouch of Douglas (white arrow) consistent with haemorrhagic ascites. U, uterus.

intrauterine pregnancy. On CT, high density free fluid may be seen in the pouch of Douglas from haemorrhage (Fig. 9.25). These signs, by themselves, are not enough to make the diagnosis of ectopic gestation, as pelvic inflammatory disease, rupture of adnexal cysts and various neoplasms can appear identical.

In clinical practice, if the pregnancy test is positive and no intrauterine gestation can be identified, the obstetrician may assume that there is an ectopic pregnancy.

Peritoneal Cavity and Retroperitoneum

PERITONEAL CAVITY

The peritoneal cavity is the potential space encompassed by the visceral and parietal layers of the peritoneum. The cavity is divided into two main sections, the greater sac and the lesser sac, which lies posterior to the stomach.

Peritoneal cavity disorders

Ascites

Free peritoneal fluid collects in a predictable manner. With the patient supine, the fluid tends to fall to the most dependent portions of the peritoneal cavity: in the pelvis anterior to the upper rectum (known as the pouch of Douglas in females), in the space anterior to the right kidney (known as Morrison's pouch) and in the paracolic gutters. If larger amounts of fluid are present, fluid will be seen throughout the peritoneal cavity and the stomach and loops of bowel may be seen floating in the ascites.

Ultrasound, computed tomography (CT) and magnetic resonance imaging (MRI) can demonstrate very small amounts of ascites, far less than the amount needed for clinical detection. No imaging technique can reliably distinguish the nature of the fluid, e.g. pus or ascitic fluid.

At CT (Fig. 10.1), ascites is of lower density than the liver, spleen and kidney and these organs stand out clearly compared with the adjacent fluid. If there is a significant amount of blood within ascites due to intraperitoneal haemorrhage, the density of the fluid will be higher than simple serous

fluid (see Fig. 9.25). One of the easiest sites at which to recognize ascites on CT is adjacent to the liver. A uniform band of low density is readily identified between the liver and the diaphragm or abdominal wall. It is worth noting that ascites cannot collect posterior to the upper liver because of the peritoneal reflection forming the so-called bare area (Fig. 10.1b).

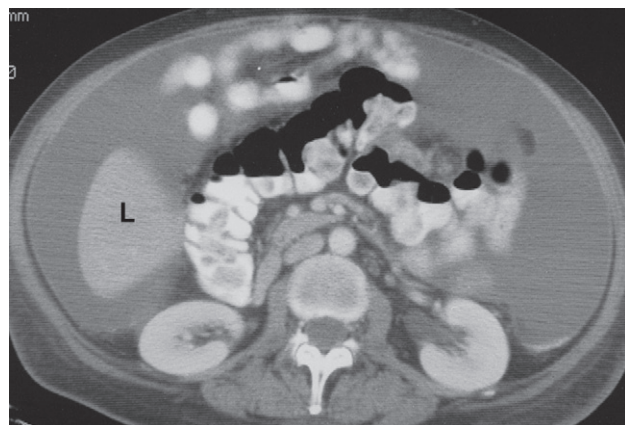
At ultrasound (Fig. 10.2), ascites is seen as echo-free regions with excellent transmission of sound. Ultrasound may be used to direct the insertion of a pigtail catheter into ascites in order to drain the fluid. When loculated, ascites is seen as discrete collections of fluid partly surrounded by bands of adhesions and partly by the edges of normal abdominal structures, e.g. bowel wall or liver edge. Loculated collections of ascites may not be distinguishable from fluid in abscesses because the density of infected and uninfected fluid can be identical.

Pseudomyxoma peritonei is a type of loculated intraperitoneal fluid of high viscosity, associated with mucinous tumours that have disseminated in the peritoneal cavity.

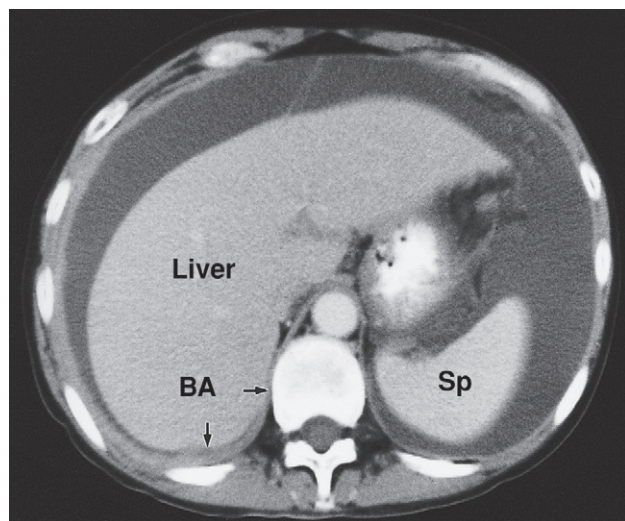
Plain film detection of ascites is discussed in Chapter 5.

Peritoneal tumours

By far the most frequent neoplastic disease of the peritoneum is metastases from an abdominal or pelvic tumour, particularly carcinoma of the ovary. The peritoneum may be studded with tiny nodules that are frequently too small to detect on imaging and, in these cases, ultrasound and CT may only show ascites. In other cases, peritoneal



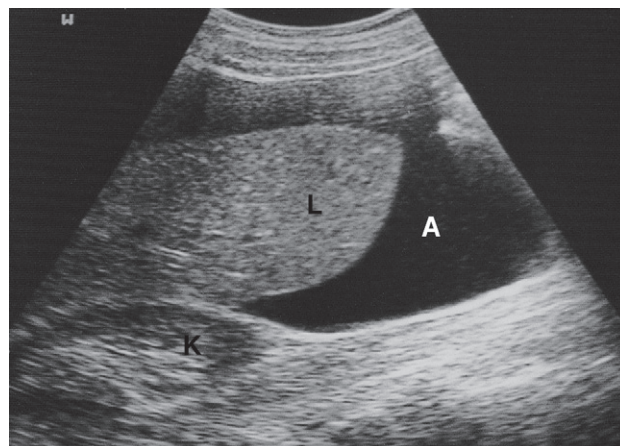
(a)



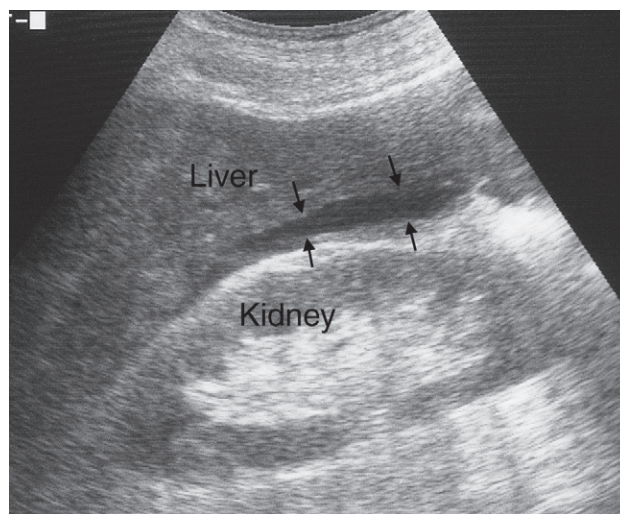
(b)

Fig. 10.1 CT scan of ascites. (a) At the level of the kidneys. The fluid is seen surrounding the lower portion of the liver (L) and the bowel loops. (b) At the level of the liver and spleen (Sp). Note that the ascites cannot collect posteromedial to the right lobe of the liver because of the peritoneal reflections of the bare area (BA).

nodules are clearly demonstrated on CT. Numerous metastatic nodules within the omental fat may coalesce to form what is known as an 'omental cake' (Fig. 10.3a). Peritoneal deposits may be seen on MRI, particularly using the diffusion-weighted sequence, in which deposits are typi-



(a)



(b)

Fig. 10.2 Ultrasound of ascites. (a) The ascites (A) appears as a transonic area. The liver is clearly seen surrounded by the ascitic fluid. K, right kidney; L, liver. (b) Only a very small amount of ascites is present in this patient. The ascites (arrows) lies between the liver and kidney in Morrison's pouch.

cally of high signal intensity on the high b value images (Fig. 10.3b). Fluorodeoxyglucose positron emission tomography (FDG-PET)/CT may also be used to demonstrate the extent of peritoneal disease in tumours that are highly metabolically active (Fig. 10.3c). Ultrasound or CT-guided

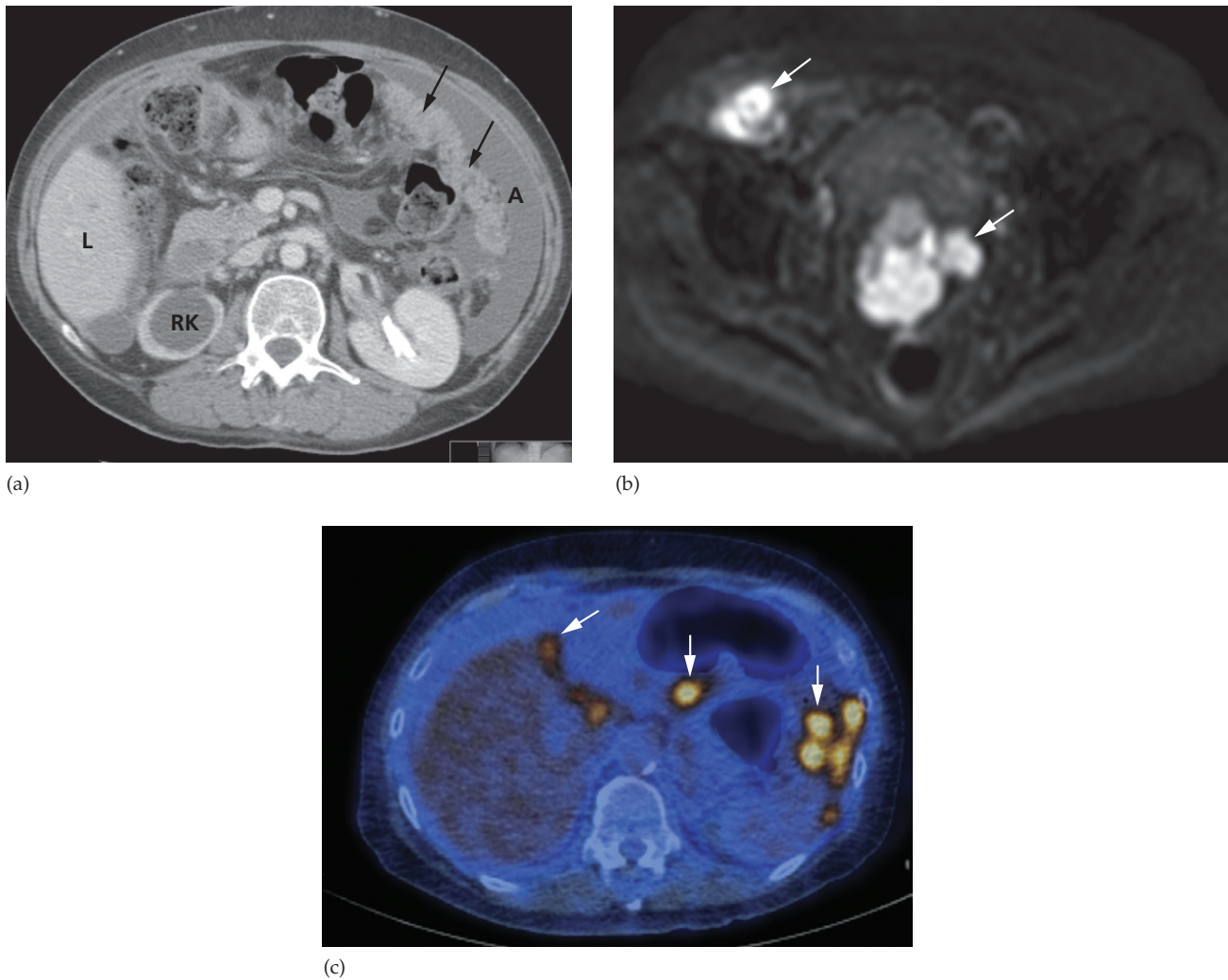


Fig. 10.3 Intraoperative spread of ovarian carcinoma in three different patients. (a) CT demonstrating ascites (A) and an 'omental cake' of tumour deposits (arrows). There is hydronephrosis of the right kidney (RK). L, liver. (b) Diffusion-weighted MRI, b 1000 image, demonstrating the high signal intensity of peritoneal deposits (arrows). (c) Fused FDG-PET/CT demonstrating multiple FDG-avid peritoneal deposits (arrows) in the upper abdomen.

biopsy of the omental cake may be performed in cases where a tissue diagnosis is required prior to treatment planning, particularly as several pathologies may mimic ovarian cancer (Box 10.1). Carcinoid tumours of the small bowel may metastasize to form a mesenteric mass (Fig. 10.4). These are often partially calcified and may cause a desmoplastic reaction in the surrounding mesentery.

Intraoperative abscesses

Intraoperative abscesses may follow a perforation of the bowel or biliary tract, either spontaneous or post-traumatic, particularly following surgery. In the case of bowel perforation, free intraoperative air may be detected in addition to the abscess. The common locations are subphrenic,

Box 10.1 Diseases that mimic disseminated carcinoma of the ovary

- Primary peritoneal malignancy
- Disseminated gastrointestinal malignancy (e.g. stomach or colon)
- Disseminated pancreatic cancer
- Disseminated breast cancer (usually lobular subtype)
- Tuberculosis

subhepatic, paracolic and pelvic. The expected site of the abscess depends on the site of perforation, e.g. duodenal leakage usually results in subhepatic or subphrenic abscesses, whereas a leak from the left colon often results in paracolic or pelvic abscesses. Multiple abscesses are not uncommon following a perforation. Ascites frequently accompanies abdominal and pelvic abscesses.

Computed tomography demonstrates most abscesses and rarely gives false-positive results. Ultrasound can be just as informative, provided it is positive, and may be preferred because it is quick and simple to perform, and may be done at the bedside in patients on intensive care.

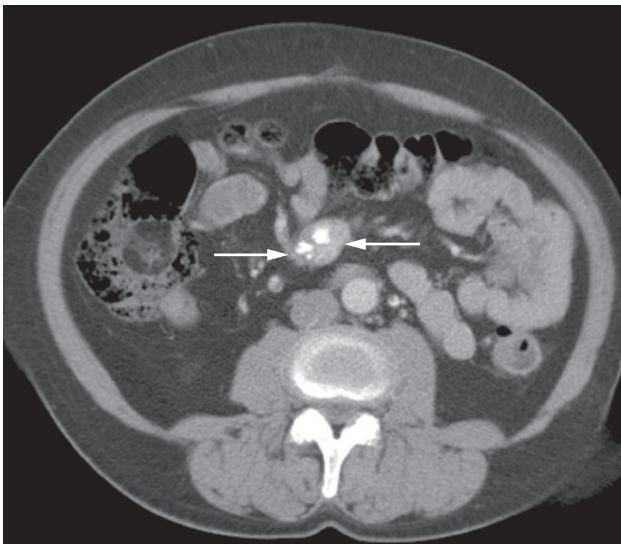


Fig. 10.4 CT demonstrating a mass in the small bowel mesentery (arrows), which contains several dense calcifications. This is a secondary deposit from an ileal carcinoid tumour.

The disadvantage of ultrasound is that gas in dilated loops of bowel can interfere with the images and, therefore, abscesses may be overlooked.

Ultrasound appearances

The ultrasonographer searches for any localized fluid collections lying outside the bowel. Abscesses assume many different configurations depending on the adjacent organs (Fig. 10.5). They often have slightly irregular walls and may contain internal echoes due to septations or debris. These internal echoes are not, however, specific for infection. Gas in an abscess appears echogenic and produces acoustic shadowing but it can be difficult to distinguish from gas within the bowel.

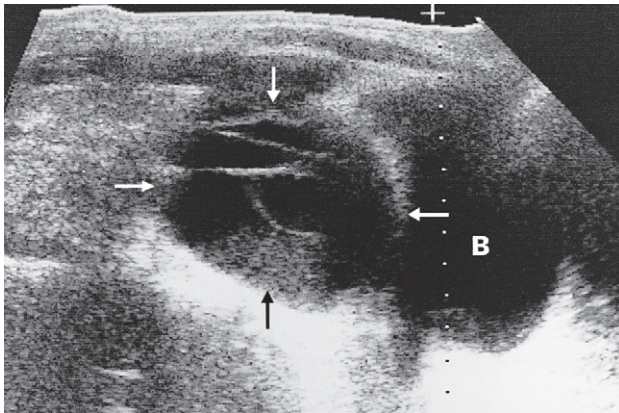
The major differential diagnosis is from loops of bowel and uninfected loculations of ascites, blood or lymph, all of which can occur postoperatively. The distinction may require needle aspiration of the fluid.

Computed tomography appearances

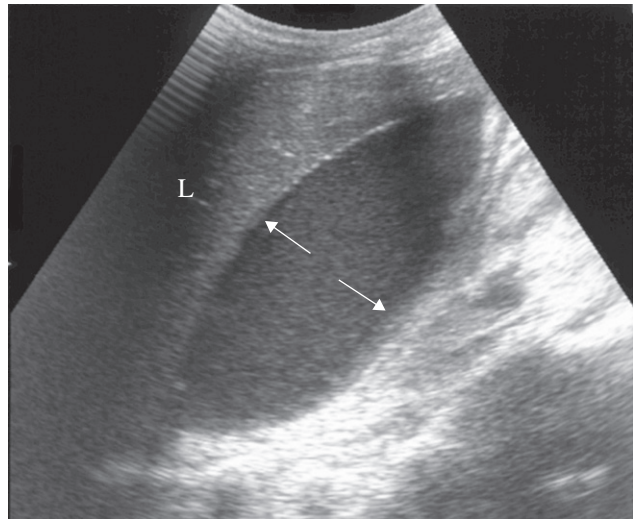
The basic principles are similar to those described for ultrasound. At CT, the fluid centre of the abscess is identified as a homogeneous density surrounded by a definite wall of soft tissue lying within the peritoneal cavity but outside the bowel (Fig. 10.6). Gas within the abscess is seen in approximately half the patients and is a very useful sign because it helps distinguish infected from uninfected fluid loculations. The gas may take the form of multiple small streaks or bubbles, or it may collect as one large bubble. Air–fluid levels may be present within larger collections. The wall of the abscess often shows enhancement following intravenous contrast administration. Subphrenic abscesses may be difficult to distinguish from pleural empyemas at CT; the peritoneal and pleural cavities are, after all, separated only by the diaphragm, a structure that can be difficult to identify at CT. In such cases, coronal or sagittal reformat of the CT or ultrasound will usually be very helpful because it can demonstrate the position of the abscess in relation to the diaphragm.

The major diagnostic problems are:

- Distinguishing between abscesses and distended or matted loops of bowel. The distinction at CT can usually be made by opacifying the bowel. With ultrasound, peristalsis of bowel loops can be observed directly.

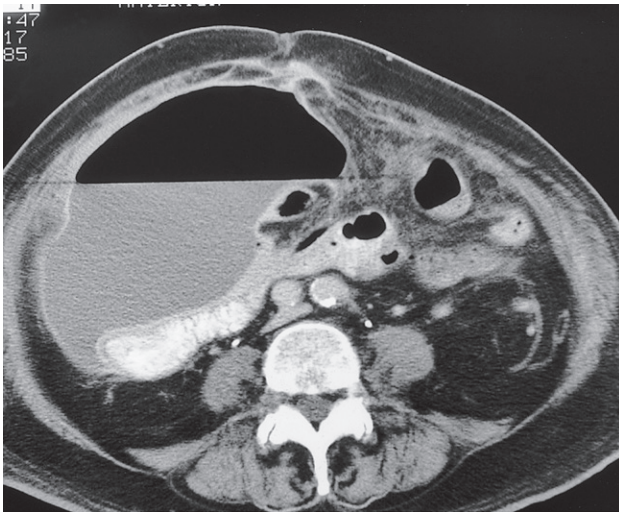


(a)



(b)

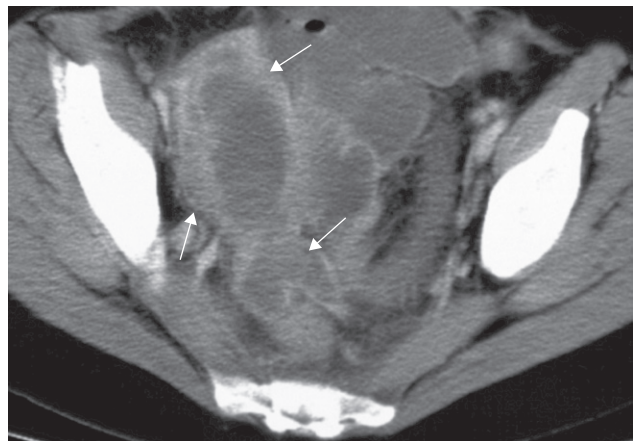
Fig. 10.5 Intraperitoneal abscess shown by ultrasound in two separate patients. (a) A large complex mass (arrows) just above the bladder (B). This young man had Crohn's disease. (b) A large abscess (arrows) lying directly beneath the liver (L).



(a)



(b)



(c)

Fig. 10.6 CT of postoperative intraperitoneal abscesses in three different patients. (a) Large abscess in the right side of the abdomen at the level of the umbilicus. Note the large air-fluid collection with a thin enhancing wall. The abscess displaces adjacent bowel loops (containing air and oral contrast). (b) A typical thick-walled abscess (arrows) containing both air and fluid. (c) A pelvic abscess (arrows) containing fluid (pus).

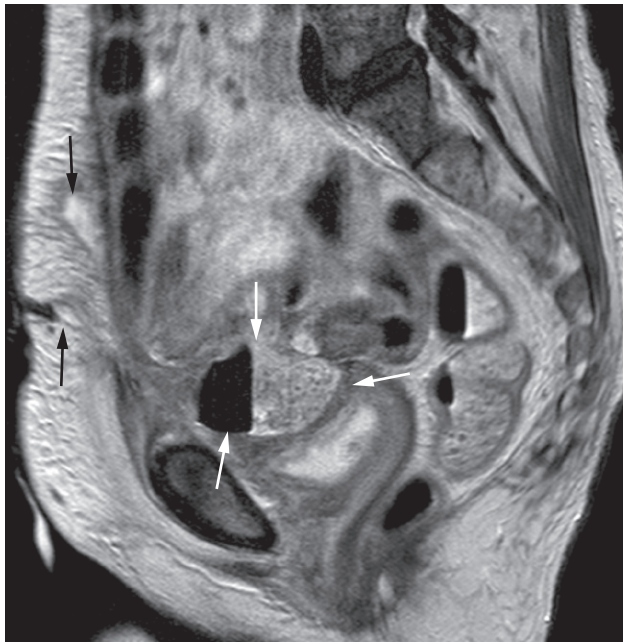


Fig. 10.7 T2-weighted MRI scan in the sagittal plane demonstrating a pelvic abscess (white arrows) containing faecal material and air, which has formed a fistula with the anterior abdominal wall (black arrows).

- Distinguishing between infected and uninfected fluid loculations; needle aspiration may have to be performed.

Magnetic resonance imaging appearances

Pelvic abscesses are occasionally assessed on MRI, and usually have the appearance of a complex septate cyst with a thick enhancing wall. MRI may be helpful in delineating fistulous connections between the abscess and other organs, such as the bladder, bowel or vagina (Fig. 10.7).

Radionuclide examination

If CT and ultrasound have been unsuccessful in locating an abscess, then some of the patient's own white blood cells can be labelled with technetium-99m or with indium-111, which will accumulate in an abscess (Fig. 10.8).



Fig. 10.8 Indium-111-labelled leucocyte scan of an intraperitoneal abscess. This abscess (arrow) followed small bowel surgery with subsequent anastomotic leak. Normal uptake is seen in the liver (L) and spleen (S).

RETROPERITONEUM

Computed tomography, MRI and ultrasound all provide information about retroperitoneal structures. Plain films are limited to showing: very large masses or calcification within a mass; the occasional case where gas is seen in an abscess; and the curvilinear calcification of an aortic aneurysm. Some of the differentials for retroperitoneal masses are given in Box 10. 2.

Box 10.2 Differential diagnoses in retroperitoneal masses

- Nodal (lymphoma, germ cell tumours, metastases)
- Retroperitoneal fibrosis
- Neurogenic (paraganglioma, schwannoma, ganglioneuroma)
- Soft tissue sarcoma (liposarcoma, fibrosarcoma)
- Haematoma (following interventional procedure, trauma or ruptured aortic aneurysm)
- Infection (psoas abscess, retroperitoneal abscess)
- Vascular (aneurysm)

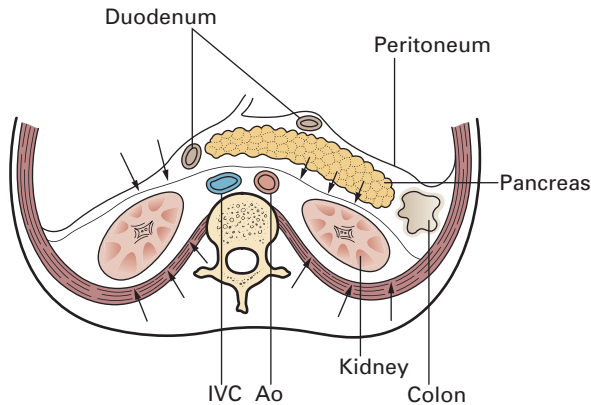


Fig. 10.9 Diagram of anterior (downward pointing arrows) and posterior (upward pointing arrows) renal fascia. Ao, aorta; IVC, inferior vena cava.

When considering the retroperitoneum it is useful to appreciate the anatomy of the anterior and posterior renal fascia (Fig. 10.9) which divide the retroperitoneum into three compartments: the anterior pararenal, the perinephric and the posterior pararenal spaces. Infection in one of these compartments tends to be limited to that compartment. Note that the urinary tract and pancreas are covered in other chapters.

Imaging techniques

Computed tomography

The following normal features should be looked for (Figs 10.9 and 10.10a):

- The complete outline of the aorta and inferior vena cava (IVC) should be clearly visible throughout their lengths. The aorta is round in cross-section and normally measures 2.0–2.5 cm in diameter. CT angiography may be performed, providing three-dimensional views of the aorta and renal vessels, which help to plan vascular interventions. The IVC varies in shape from round to oval. Superiorly, the IVC passes through the liver (known as the intrahepatic IVC) before draining into the right atrium.
- There is usually a fat-containing space to the left of the aorta, which is a good area in which to look for lymphaden-

opathy (Fig. 10.10b). The only structures other than lymph nodes to be seen in this space are the left renal vein and, rarely, a loop of small bowel or an aberrant vessel.

- The psoas muscles are seen as symmetrical, rounded structures outlined anteriorly by fat.
- Both adrenals are well seen in most subjects.

Ultrasound

Retroperitoneal fat, which is very echo-reflective, surrounds the various retroperitoneal structures. The aorta and inferior vena cava are easily identified as hypoechoic tubular structures. Normal adrenal glands are rarely visible in adults. Enlarged lymph nodes can be identified.

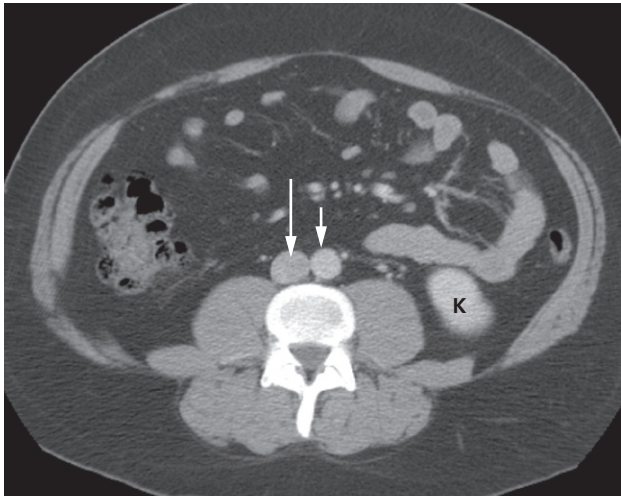
Magnetic resonance imaging

Magnetic resonance imaging plays a small part in diagnosing retroperitoneal disorders as it provides few advantages over CT or ultrasound. The ability to display the body in any plane can be an advantage, for example in helping decide whether a mass has arisen in a kidney or in an adrenal gland. However, with the development of multi-slice CT, excellent multiplanar CT reformats are now available. Characterization of adrenal nodules is often performed on MRI. The ability of MRI to display intravascular spread of tumour can be of value in showing the spread of renal carcinoma into the renal vein, IVC and heart (Fig. 10.11).

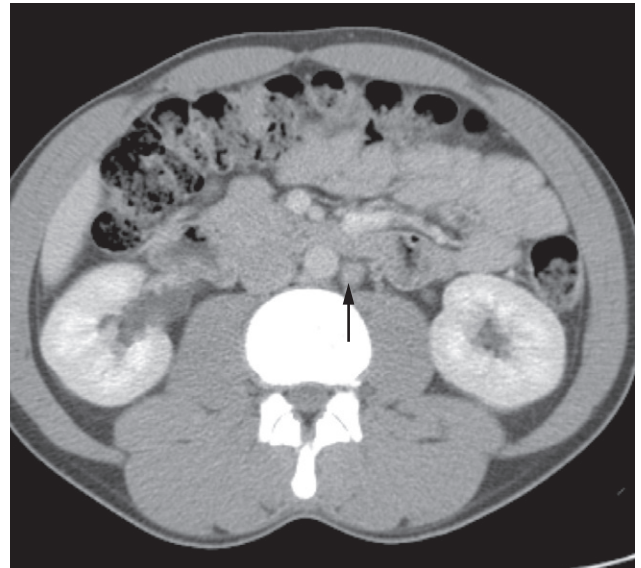
Retroperitoneal disorders

Retroperitoneal lymphadenopathy

The normal para-aortic lymph nodes vary in size from invisible up to a short axis diameter of 1 cm. In the retrocrural area, a diameter of 6 mm is the upper limit of normal. Nodal enlargement may occur secondary to inflammatory disease, metastatic tumour deposits and lymphoma. It is often not possible to reliably diagnose the cause of mild nodal enlargement on cross-sectional imaging, as the nodes have the same features and texture, regardless of the cause of enlargement. New techniques such as FDG-PET/CT can be used to identify metastatic nodal tumour deposits. FDG-PET/CT is of particular importance in the follow-up of patients being treated for lymphoma.

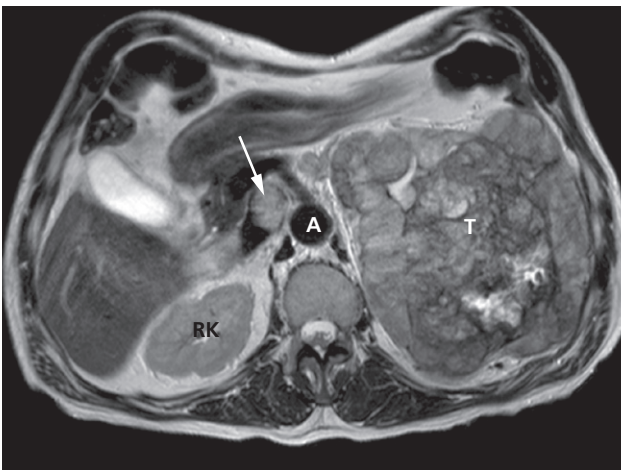


(a)



(b)

Fig. 10.10 (a) CT scan of normal retroperitoneum. Note that the aorta (short arrow) and IVC (long arrow) are clearly outlined by fat and that there is a fat-containing space around the vessels. K, kidney. (b) There is a node at the upper limit of normal size in the left para-aortic space (arrow).

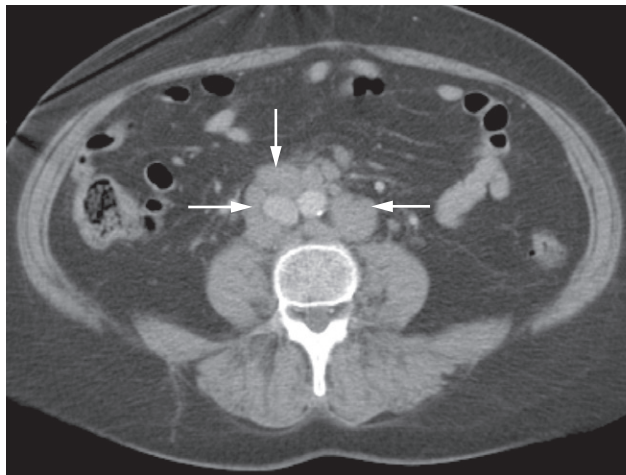


(a)

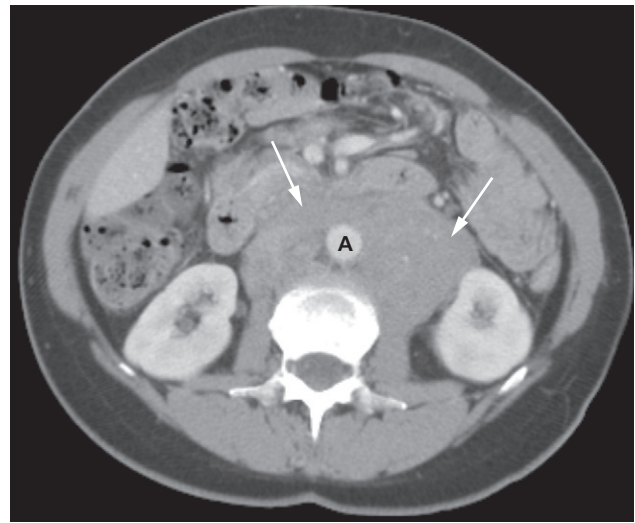


(b)

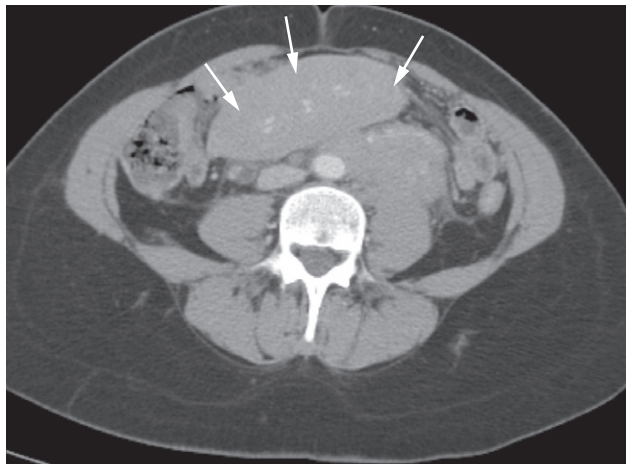
Fig. 10.11 Renal cell carcinoma invading the IVC. (a) T2-weighted MRI demonstrating a very large left renal tumour. The tumour has extended along the left renal vein (not shown) and into the IVC (arrow). (b) Coronal magnetic resonance venogram following gadolinium demonstrating the tongue of tumour tissue (arrow) in the IVC. A, aorta; RK, right kidney; T, tumour.



(a)



(b)



(c)

Fig. 10.12 Lymphoma. (a) Several enlarged lymph nodes (arrows) are shown surrounding the contrast-enhanced aorta and IVC. (b) In this case, the para-aortic nodes have become confluent (arrows), forming a lobulated mass around the aorta (A). (c) Extensive nodal disease is seen infiltrating the small bowel mesentery (arrows).

Nodal enlargement of over 2 cm almost always indicates neoplasm, notably lymphoma. Individually enlarged lymphomatous nodes may be seen (Fig. 10.12a), but not infrequently several nodes are matted together to form a lobular mass engulfing the aorta or IVC (Fig. 10.12b) and may involve the small bowel mesentery (Fig. 10.12c). One of the differential diagnoses for soft tissues adjacent to the IVC and aorta is retroperitoneal fibrosis, which is described in Chapter 8.

Adrenal gland disorders

Normal adrenal glands are thin, bilobed structures surrounded by fat (Fig. 10.13). The right adrenal gland is situated above the upper pole of the right kidney. The left adrenal gland is usually situated just anterior to the upper pole of the left kidney.

Calcification of the adrenal glands (Fig. 10.14) may follow old intra-adrenal haemorrhage or old healed tuberculosis.

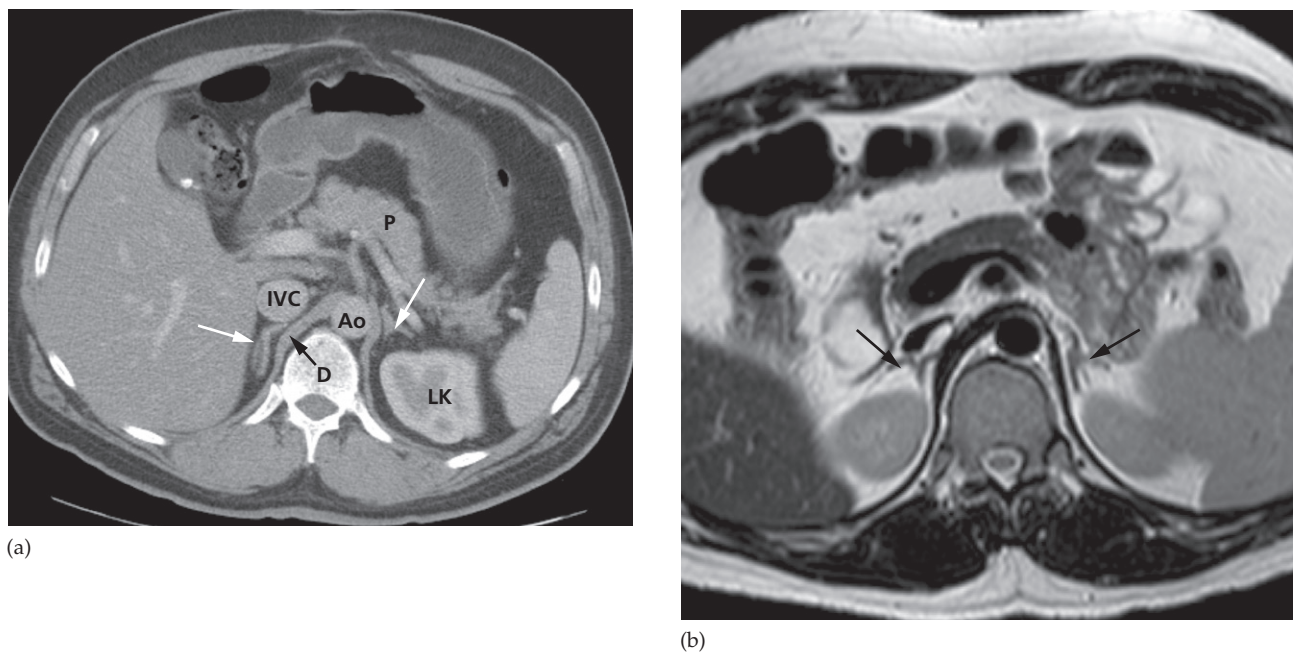


Fig. 10.13 Normal adrenal glands. (a) CT scan. Both adrenal glands (white arrows) are visible in this section. Note the different shape of the two glands. Ao, aorta; D, diaphragmatic crus; IVC, inferior vena cava; LK, left kidney; P, pancreas. (b) MRI scan showing the right and left adrenal glands (arrows), which have an intermediate signal intensity on these T2-weighted images.

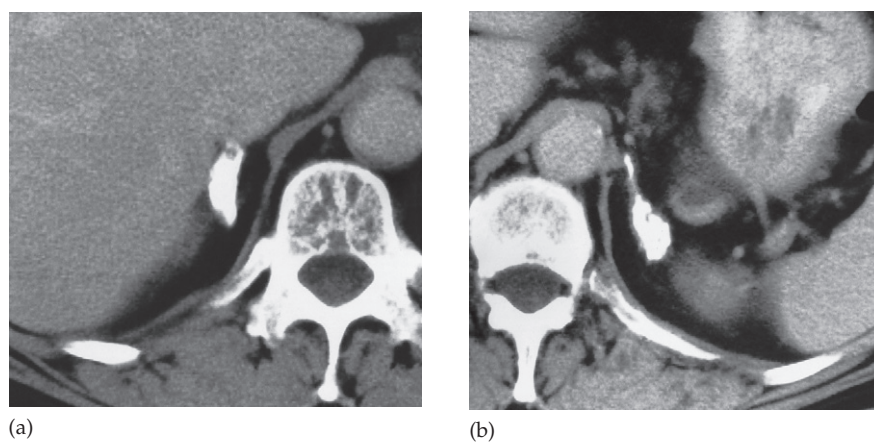


Fig. 10.14 Adrenal calcification shown by CT. (a) Heavily calcified right adrenal gland. (b) Heavily calcified left adrenal gland.

Box 10.3 Causes of adrenal enlargement

- Hyperplasia
- Cortical adenoma:
 - non-functioning
 - functioning (Conn's or Cushing's syndrome)
- Pheochromocytoma:
 - benign
 - malignant
- Primary adrenal carcinoma
- Metastasis
- Haemorrhage
- Cyst
- Abscess

Severe destruction and calcification of the adrenal glands may lead to Addison's disease.

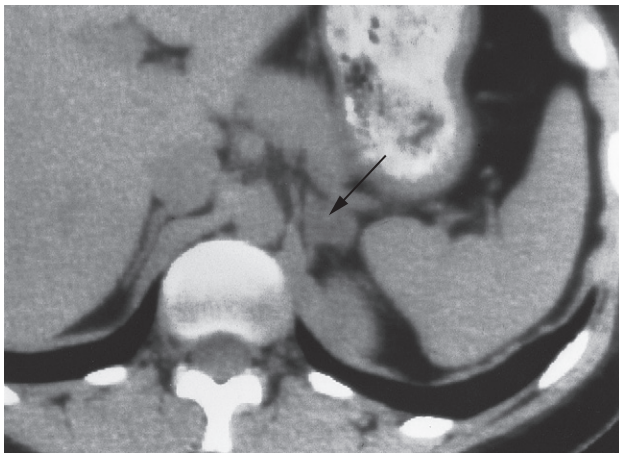
Enlargement of the adrenal glands can be recognized at CT and MRI and occasionally on ultrasound. Enlargement may be due to several different pathologies (Box 10.3). CT is the best technique for diagnosing adrenal enlargement because it consistently shows the size and shape of the glands.

Functioning adrenal tumours

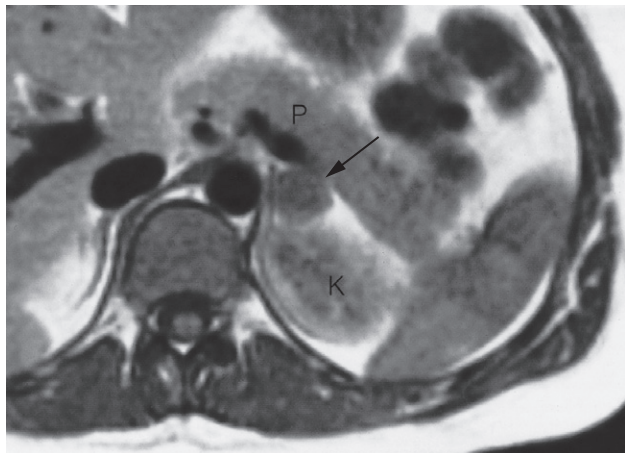
Patients with tumours producing an excess of hormones will usually have had their endocrine disorder diagnosed

clinically and biochemically prior to the imaging examination. CT, or occasionally MRI, is used in this group primarily to localize any tumour. The responsible tumours are usually benign adenomas, but may be carcinomas. An adrenal adenoma appears as a spherical mass arising from one of the adrenal glands. The distinction between pituitary tumour, adrenal adenoma and adrenal hyperplasia as a cause of Cushing's syndrome is usually based on biochemical findings but, on occasion, the precise diagnosis can be in doubt. Adrenal adenomas giving rise to Cushing's syndrome are unilateral and nearly always larger than 2cm, and can virtually always be localized with CT (Fig. 10.15). Most hyperplastic glands in pituitary-dependent Cushing's syndrome appear normal or are slightly enlarged bilaterally at CT. Aldosteronomas (Conn's tumour) are usually unilateral and usually less than 1cm in size and may, on occasion, be difficult to identify at imaging.

Pheochromocytomas are virtually all demonstrable at CT or MRI (Fig. 10.16). Ten per cent are bilateral and, therefore, the opposite adrenal gland must be looked at carefully. They typically enhance avidly following administration of intravenous contrast medium. It should also be remembered that 10% of pheochromocytomas arise outside the adrenal gland, usually in another retroperitoneal site. Extra-adrenal pheochromocytomas are usually called paragangliomas.

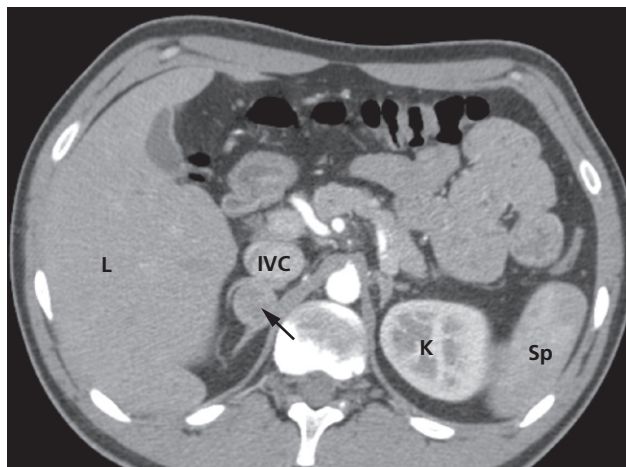


(a)

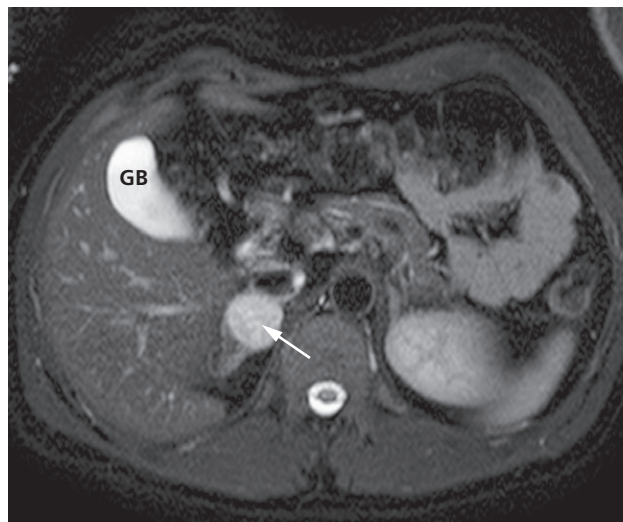


(b)

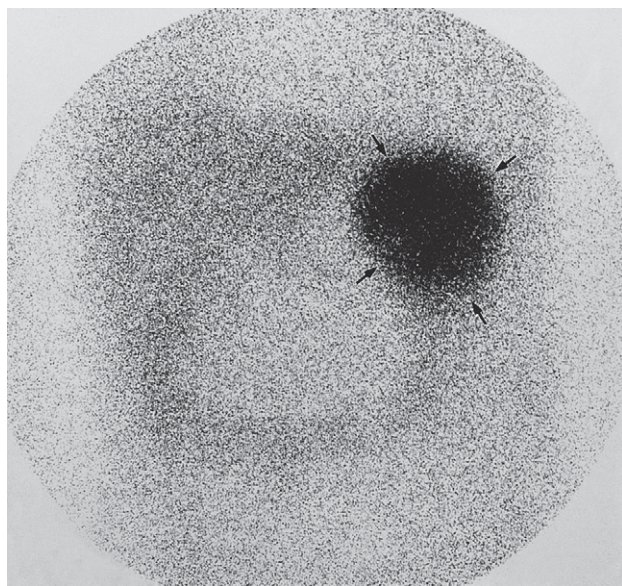
Fig. 10.15 Functioning adrenal adenoma causing Cushing's syndrome. (a) CT scan showing a 2cm mass in the left adrenal gland with a density of <10 Hounsfield units (arrow). (b) T1-weighted MRI scan also showing the lesion (arrow). K, kidney; P, pancreas.



(a)



(b)



(c)

Fig. 10.16 Phaeochromocytoma. (a) CT scan showing a phaeochromocytoma (arrow) arising in the medial limb of the right adrenal gland. The inferior vena cava (IVC) lies anteriorly. K, kidney; L, liver; Sp, spleen. (b) T2-weighted MRI with fat saturation showing the same phaeochromocytoma (arrow) as in (a). GB, gall bladder. (c) Radioiodine-labelled MIBG scan of a phaeochromocytoma (arrows) in the left adrenal gland.

Radionuclide scans can be used to localize functioning adrenal tumours. The only radionuclide in widespread use is iodine-123-labelled MIBG (meta-iodobenzylguanidine), an agent which is concentrated by phaeochromocytomas (Fig. 10.16c). Although the great majority of phaeochromocytomas are single, a few are multiple, either in both adrenal glands or extra-adrenal in location, and radioiodine-

labelled MIBG is an excellent survey technique for finding all sites of phaeochromocytoma.

Non-functioning adrenal masses

In patients with a known underlying malignancy, it is important to distinguish between a small non-functioning

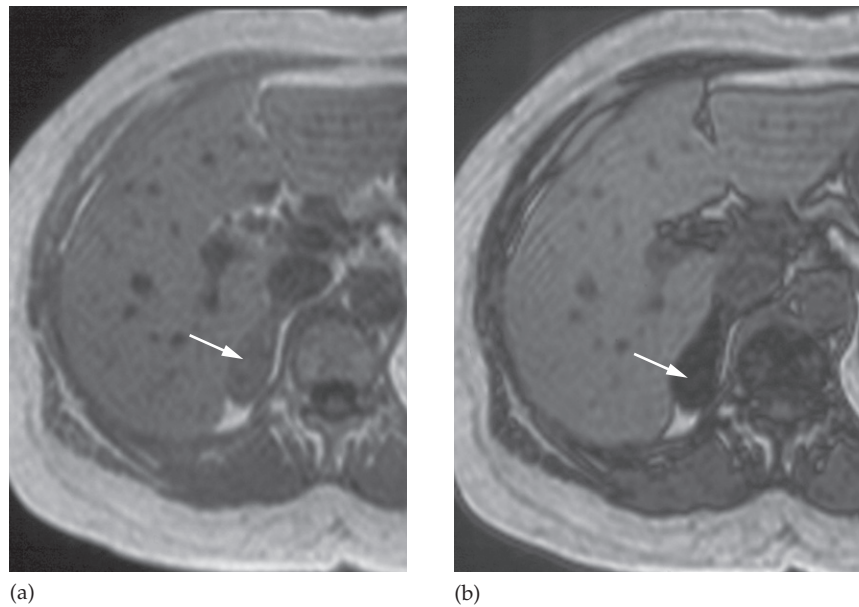


Fig. 10.17 Adrenal cortical adenoma shown by chemical shift MRI. (a) An adrenal mass is demonstrated on the 'in-phase' image (arrow). (b) There is a marked drop in the signal intensity of the adrenal mass on the 'out-of-phase' image, confirming a benign cortical adenoma (arrow).

adenoma and an adrenal metastasis. This can pose a major dilemma for patients being staged for a cancer in whom a small adrenal mass (up to 3 cm in diameter) is discovered. The distinction can be made with reasonable specificity on fine-section non-contrast CT, as benign cortical adenomas are typically of low density (less than 10 Hounsfield units) due to the presence of intracellular lipid, whereas metastases have a density of more than 10 Hounsfield units. Further characterization is possible by evaluating changes in the density of an adrenal lesion at portal venous phase and delayed phase imaging following intravenous contrast administration. Special MRI sequences designed to demonstrate intracellular lipid may also be used to make this distinction between adenomas and metastases. Using an MRI sequence called 'chemical shift imaging', a diagnosis of a benign cortical adenoma may be made with a high specificity (Fig. 10.17).

Metastases to the adrenal gland are relatively common (Fig. 10.18) and may be bilateral. Many different tumours metastasize to the adrenal glands; it is a particular feature

of lung carcinoma, and therefore the adrenals are included in CT scans of the chest in patients being staged for bronchial carcinoma.

Non-functioning benign cortical adenomas larger than 3 cm are very rare, and, therefore, larger adrenal masses in adults are likely to be metastases or, rarely, primary adrenal carcinoma. Adrenocortical carcinoma is rare and usually presents at a late stage, with a large primary tumour mass and metastatic disease (Fig. 10.19). The malignant adrenal tumour of early childhood is *neuroblastoma*.

Adrenal abscesses and haemorrhage are usually bilateral and are indistinguishable from one another at CT and ultrasound. The clinical features usually suggest the correct diagnosis. Adrenal haemorrhage may be seen following significant trauma.

Retroperitoneal tumours

The term retroperitoneal tumour covers tumours arising primarily in retroperitoneal muscles, fat or connective

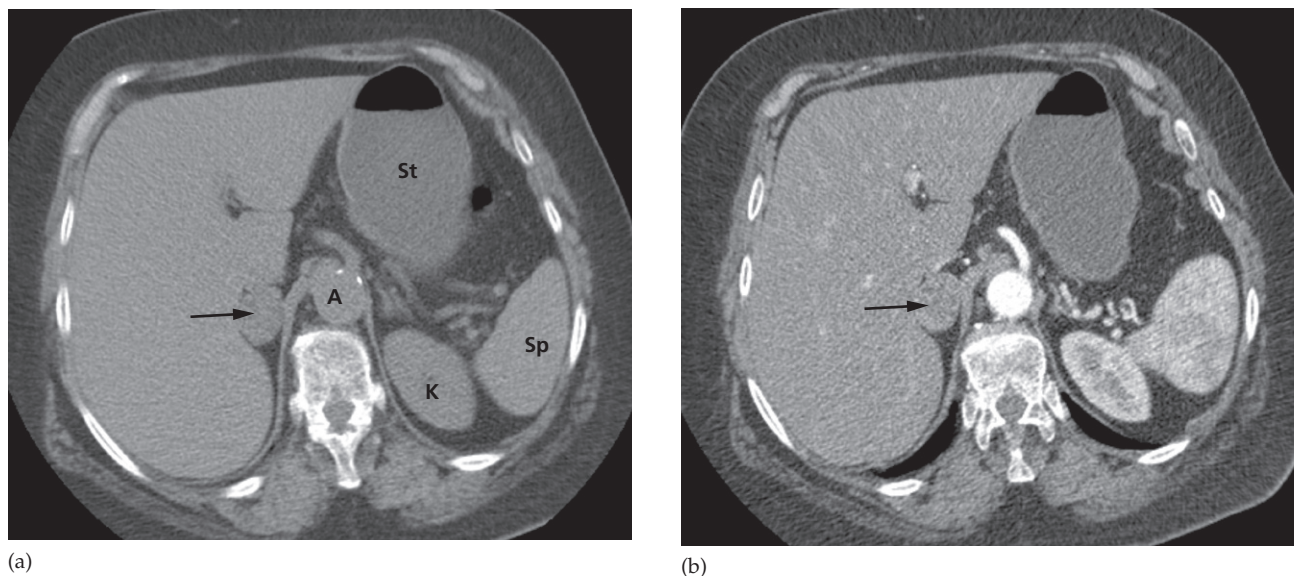


Fig. 10.18 CT scan showing a right adrenal metastasis (arrow). (a) Non-contrast-enhanced study confirmed a density of 35 Hounsfield units. A, aorta; K, kidney; Sp, spleen; St, stomach. (b) Post contrast enhancement characteristics confirmed the presence of a non-adenomatous lesion.

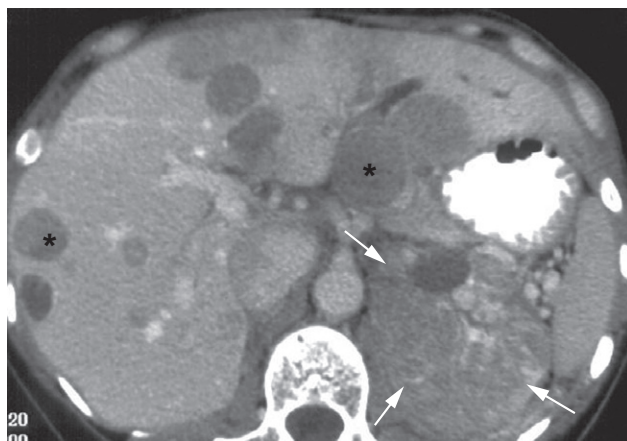
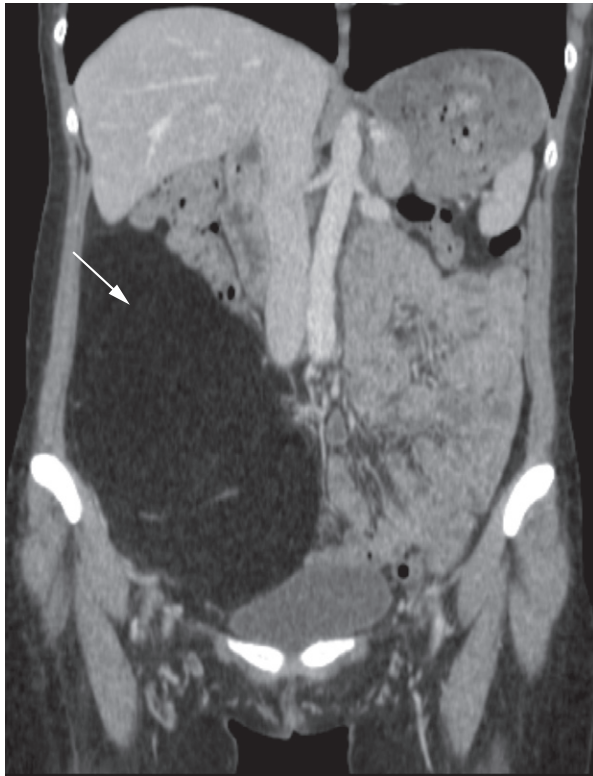


Fig. 10.19 Adrenocortical carcinoma. CT demonstrating a large heterogeneous mass arising in the left adrenal gland (between the arrows). Multiple liver and nodal metastases are also present (*).

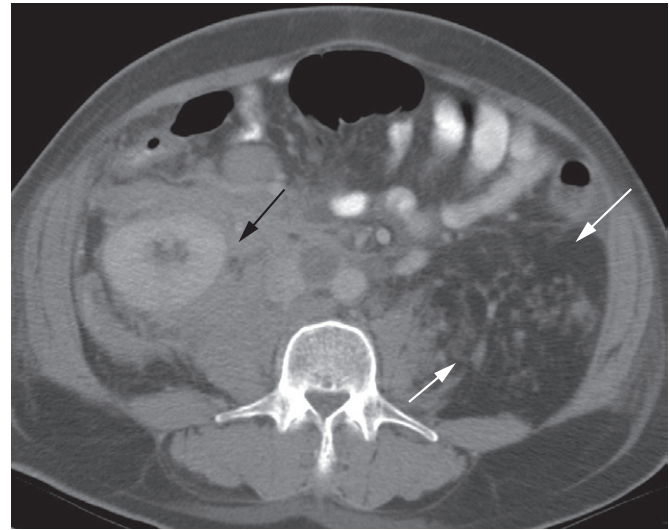
tissue, the commonest being liposarcoma and fibrosarcoma. All these tumours appear as masses on CT, ultrasound or MRI. Sometimes, the edge of the mass is well defined, but sometimes there is invasion of the adjacent tissue. A liposarcoma (Fig. 10.20) almost always contains significant amounts of recognizable fat interspersed between strands of soft tissue density; a combination that permits a specific diagnosis to be made at CT. Tumours of lymphatic or neural origin (Fig. 10.21) may also arise in the retroperitoneum. It is often not possible to determine the histological nature of the tumour by imaging, unless the mass contains significant amounts of fat. CT-guided biopsy is often used to obtain tissue for histological diagnosis.

Aortic aneurysm

Abdominal aortic aneurysms are readily diagnosed at ultrasound, CT and MRI, although MRI is rarely used for this purpose (Fig. 10.22). Ultrasound is used increasingly as a screening examination to find asymptomatic aortic aneurysms in older men.



(a)



(b)

Fig. 10.20 Retroperitoneal liposarcoma. (a) Coronal CT scan showing a large fatty tumour (arrow) with minimal soft tissue and arising in the right retroperitoneum, consistent with a low grade liposarcoma. (b) Axial CT in a different patient demonstrating a left retroperitoneal liposarcoma with more soft tissue (between the white arrows). The patient also had a lymphoma in the right retroperitoneum, surrounding the right kidney (black arrow).

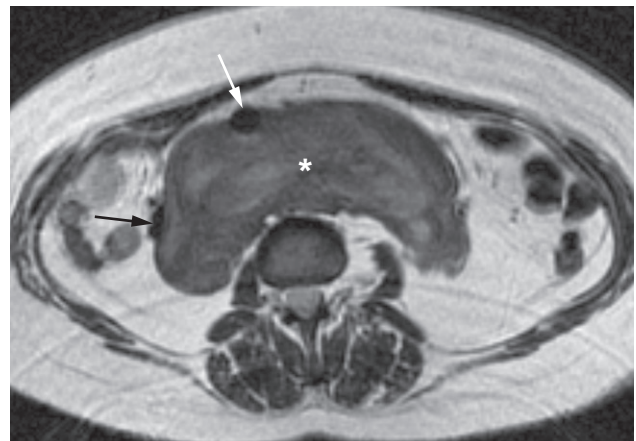
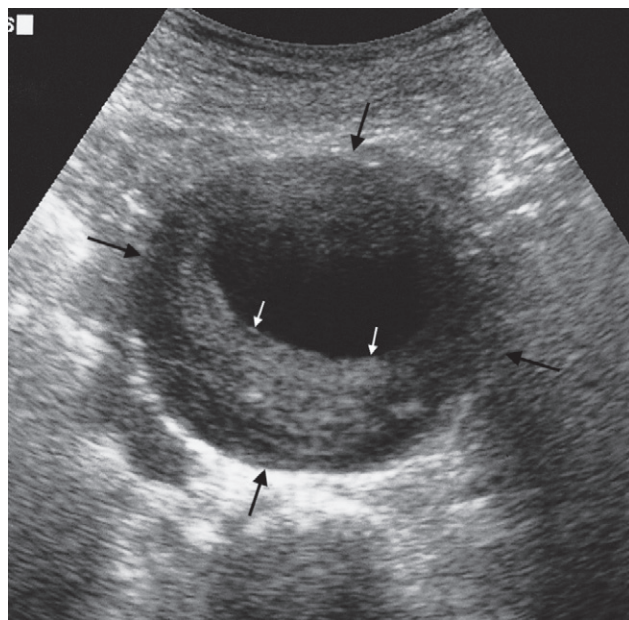
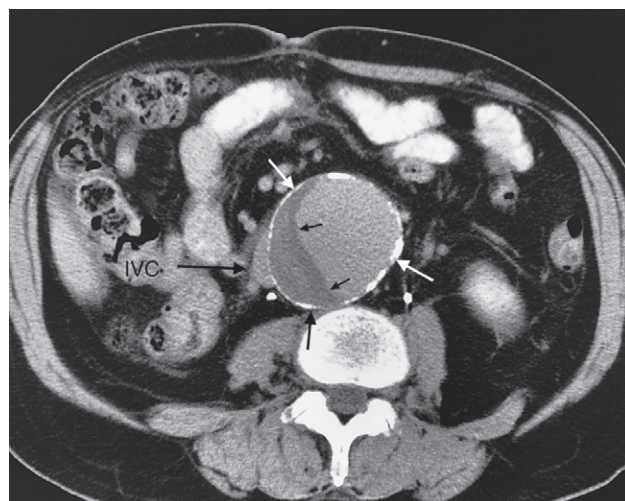


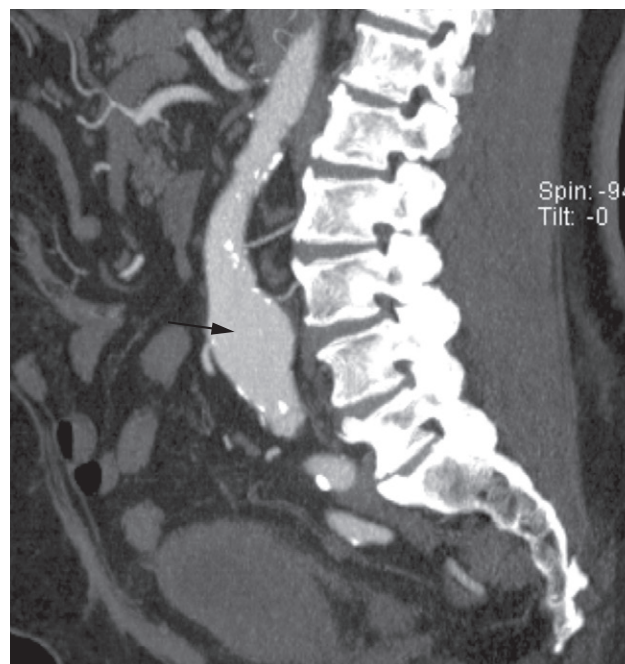
Fig. 10.21 T2-weighted MRI demonstrating an intermediate signal intensity mass arising in the retroperitoneum (*), which is displacing the aorta (white arrow) and inferior vena cava (black arrow). A CT-guided percutaneous biopsy confirmed a benign ganglioneuroma.



(a)



(b)



(c)

Fig. 10.22 Abdominal aortic aneurysm. (a) Ultrasound. Transverse scan showing a blood clot lining the wall (white arrows) within the aneurysm (black arrows). (b) CT scan with intravenous contrast enhancement. A 7 cm aneurysm (larger black and white arrows) with a lower density blood clot (small black arrows) lining the wall. The wall shows patches of calcification. The inferior vena cava (IVC) is displaced by the aneurysm. (c) CT angiography of the aorta. This sagittal reformat demonstrates a 3.5 cm fusiform aortic aneurysm (arrow).

Both CT and ultrasound allow the true maximum diameter of the aneurysm to be measured and to identify the wall and any lining thrombus. It is also relatively easy to see any retroperitoneal bleeding from an aneurysm at CT (Fig. 10.23). Aneurysms of greater than 5.5 or 6 cm in diam-

eter are in danger of rupture, whether or not the patient has had any demonstrable retroperitoneal bleeding. Contrast-enhanced CT angiography with reformats in the coronal and sagittal planes are often used to plan surgical or endovascular stent treatment (Fig. 10.22c).

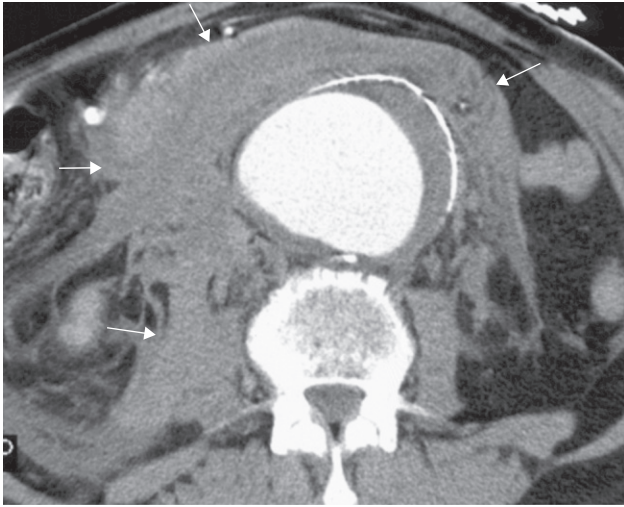


Fig. 10.23 CT scan of a leaking abdominal aortic aneurysm showing the aneurysm and the haemorrhage in the adjacent retroperitoneum (arrows).

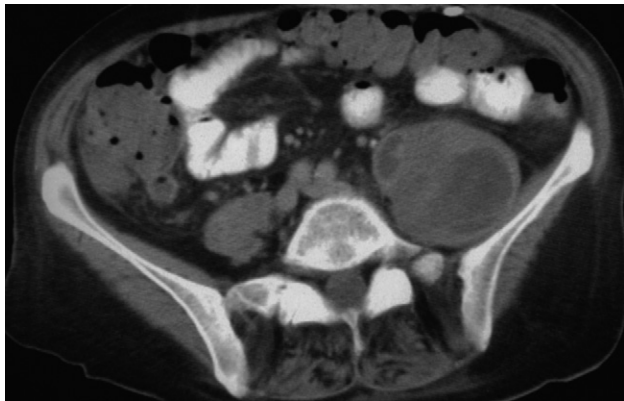


Fig. 10.24 CT scan of a large haematoma in the left iliopsoas muscle. Note the variable density, much of which is of lower density than the normal muscles.

Aortic aneurysms may also be recognizable on plain films of the abdomen (see Chapter 5), but only if substantial calcification is present in the wall.

Retroperitoneal haematoma

Retroperitoneal bleeding is usually due to trauma or to bleeding from an aortic aneurysm (see Fig. 10.23). It may

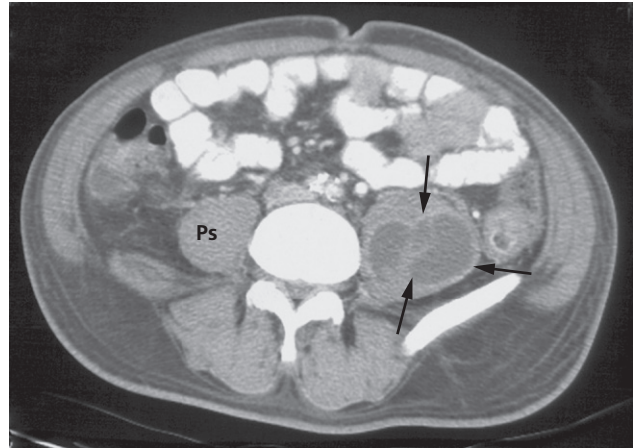


Fig. 10.25 Psoas abscess. CT scan showing a left psoas abscess (arrows). Note the thick wall, which has a rim of enhancement, and low density, fluid-like contents. Ps, normal right psoas muscle.

occur as a complication of an angiographic procedure. It is occasionally spontaneous in patients with bleeding disorders or in those on anticoagulant therapy.

The diagnosis is made by CT (Figs 10.23 and 10.24) or MRI, which show a retroperitoneal mass with the characteristics of haematomas.

Retroperitoneal and psoas abscesses

Retroperitoneal and psoas abscesses (Fig. 10.25) are usually due to spread of infection from the appendix, colon, kidney, pancreas or spine. They are often found close to the organ of origin.

Retroperitoneal abscesses have many similar features to tumours and haematomas at both CT and ultrasound. However, usually the clinical features will point to the presence of infection. There is evidence of a fluid centre and there may be gas within the abscess. The wall of the abscess may enhance with contrast medium, however, this is also a feature that is seen with neoplasms.

Imaging techniques

Plain bone radiographs

The plain radiograph remains a very important investigation in many types of bone disease. It is helpful to understand the anatomical terms used to describe a normal long bone. These are shown in Fig. 11.1.

The radiological responses of bone to pathological process are limited; thus, similar x-ray signs occur in widely different conditions. It should be noted that it takes time for the various signs to develop. For example, in adults, it takes several weeks for a periosteal reaction to be visible after trauma and, in a child with osteomyelitis, the clinical features are present from 7 to 10 days before the first sign is visible on the radiograph. In general, the signs take longer to develop in adults than they do in children.

The signs of bone disease are summarized in Box 11.1.

- A *decrease in bone density* may be focal or generalized. Focal reduction in density is usually referred to as a 'lytic area' or an area of 'bone destruction'. Generalized decrease in bone density is best referred to as 'osteopenia' until a specific diagnosis such as osteomalacia or osteoporosis can be made.
- An *increase in bone density (sclerosis)* may also be focal or generalized.
- The periosteum is not normally visible on a radiograph. The term '*periosteal reaction*' refers to excess bone produced by the periosteum, which occurs in response to such conditions as neoplasm, inflammation or trauma. Several patterns of periosteal reaction are seen (Fig. 11.2), but they do

not correlate with specific diagnoses. At the edge of a very active periosteal reaction there may be a cuff of new bone known as a Codman's triangle (Fig. 11.2d). Although often seen in highly malignant primary bone tumours, e.g. osteosarcoma, a Codman's triangle is also found in other aggressive conditions.

- *Cortical thickening* also involves the laying down of new bone by the periosteum (Fig. 11.3), but here the process is very slow. The result is that the new bone, although it may be thick and irregular, shows the same homogeneous density as does the normal cortex. There are no separate lines or spicules of calcification as seen in a periosteal reaction. The causes include chronic osteomyelitis, healed trauma, response to chronic stress or benign neoplasm. The feature common to all these conditions is that the process is either very slowly progressive or has healed.

- *Alteration in trabecular pattern* is a complex response usually involving a reduction in the number of trabeculae with an alteration in the remaining trabeculae, e.g. in osteoporosis and Paget's disease. In osteoporosis, the cortex is thin and the trabeculae that remain are more prominent than usual, whereas in Paget's disease the trabeculae are thickened and trabeculation is seen in the normal compact bone of the cortex (Fig. 11.4).

- *Alteration in the shape of a bone* is another complex response with many causes. Many cases are congenital in origin; some are acquired, e.g. acromegaly and expanding bone tumours.

- *Alteration in bone age*. The time of appearance of the various epiphyseal centres and their time of fusion depends on the age of the child. For the measurement of 'bone age',

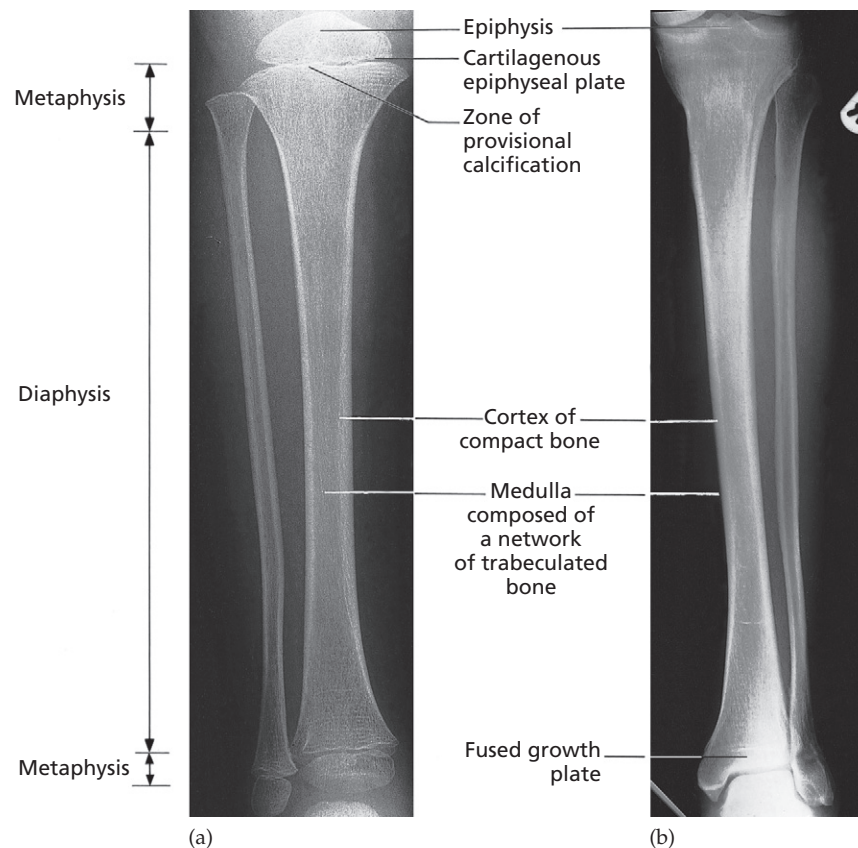


Fig. 11.1 Normal long bones in (a) a child and (b) an adult. Increase in length takes place at the cartilaginous epiphyseal plate. In the growing child, calcification of cartilage occurs at the interface between the radiolucent growing cartilage and the bone to give the zone of provisional calcification, which is seen as a dense white line forming the ends of the shaft and surrounding the bony epiphyses. This calcified cartilage becomes converted to bone. (If there is temporary cessation of growth then the zone of provisional calcification may persist as a thin white line, known as a 'growth line', extending across the shaft of the bone.) As the child grows older the epiphyseal plate becomes thinner until, eventually, there is bony fusion of the epiphysis with the shaft.

Box 11.1 Radiographic signs of bone disease

- Decrease in bone density
- Increase in bone density
- Periosteal reaction
- Cortical thickening
- Alteration in trabecular pattern
- Alteration in the shape of a bone
- Alteration in bone age

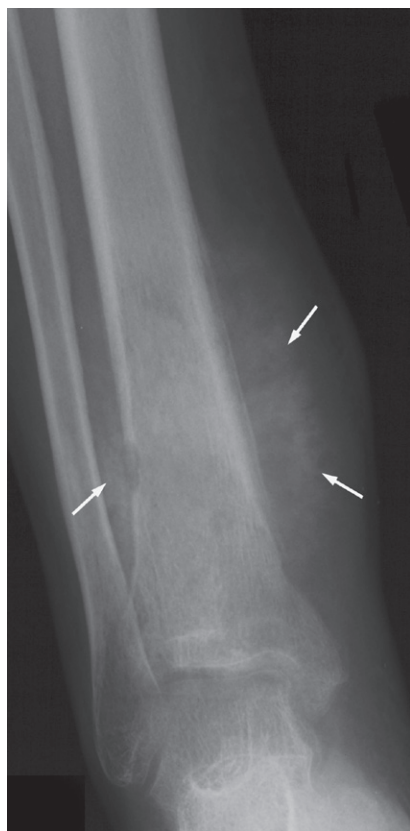
a film of one hand and wrist is taken and compared with a set of standard films, which provides an indication of skeletal maturity.

Ultrasound in musculoskeletal disease

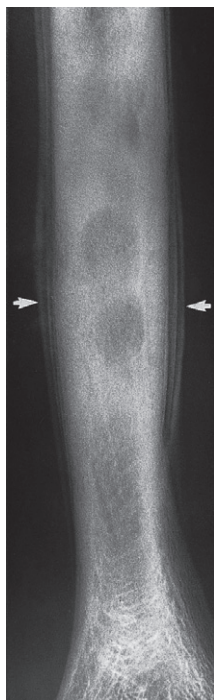
Ultrasound cannot evaluate bone pathology but does have a complementary imaging role in the following:



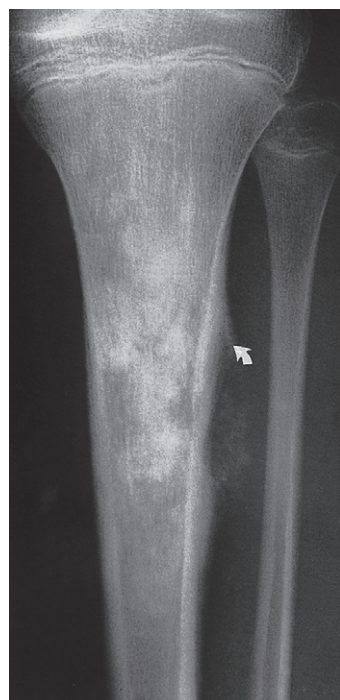
(a)



(b)



(c)



(d)



Fig. 11.3 Cortical thickening. Note the thickened cortex in the midshaft of the tibia from old, healed osteomyelitis. Same patient as in Fig. 11.19a,b taken 1 year later.

Fig. 11.2 Different types of periosteal reactions. (a) Smooth, lamellar, periosteal reaction on the radius and ulna in a case of non-accidental injury. (b) Spiculated (sunray) periosteal reaction in a case of osteogenic sarcoma (arrows). (c) 'Onion skin' periosteal reaction in a case of Ewing's sarcoma (arrows). Here the periosteal new bone consists of several distinct layers. (d) Codman's triangle in a case of osteogenic sarcoma. At the edge of the lesion the periosteal new bone is lifted up to form a cuff (arrow).

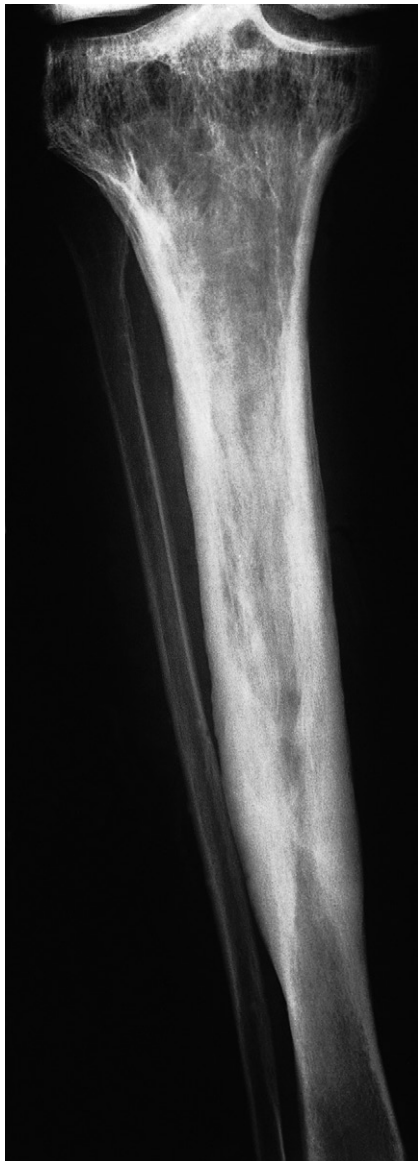
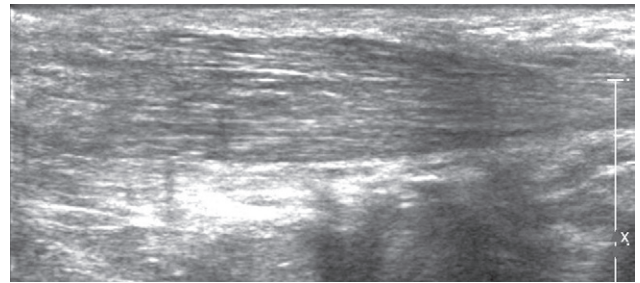
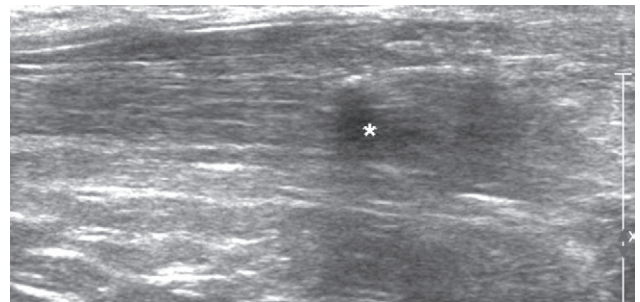


Fig. 11.4 Alteration of trabecular pattern in Paget's disease involving the upper part of the tibia, leaving the lowest part of the tibia and the fibula unaffected. Note the coarse trabeculae. The other features of Paget's disease – thickened cortex and bone expansion – are also present.



(a)



(b)

Fig. 11.5 Achilles tendon rupture. (a) The normal tendon shows a fibrillary pattern. (b) There is disruption of the fibrillary pattern due to a rupture of the tendon. The hypoechoic area (*) is due to a haematoma.

- in detecting tenosynovitis, tendon tears and rupture (Fig. 11.5)
- in the diagnosis of osteomyelitis.

Radionuclide bone imaging

Technetium-99m (^{99m}Tc) labelled phosphate complexes given as an intravenous injection are the agents used for bone scintigraphy. They are taken up selectively by the bones (Fig. 11.6) and are also excreted in the urine. These agents may be concentrated by certain soft tissue tumours, by soft tissue calcifications and by sites of tissue damage.

Increased uptake on the radionuclide bone scan is seen in conditions where there is an increased blood supply and high bone turnover with new bone formation. Many bone abnormalities – including fractures, benign or malignant tumours, infection, infarction and Paget's disease – give positive scans, so correlation with plain radiographs is

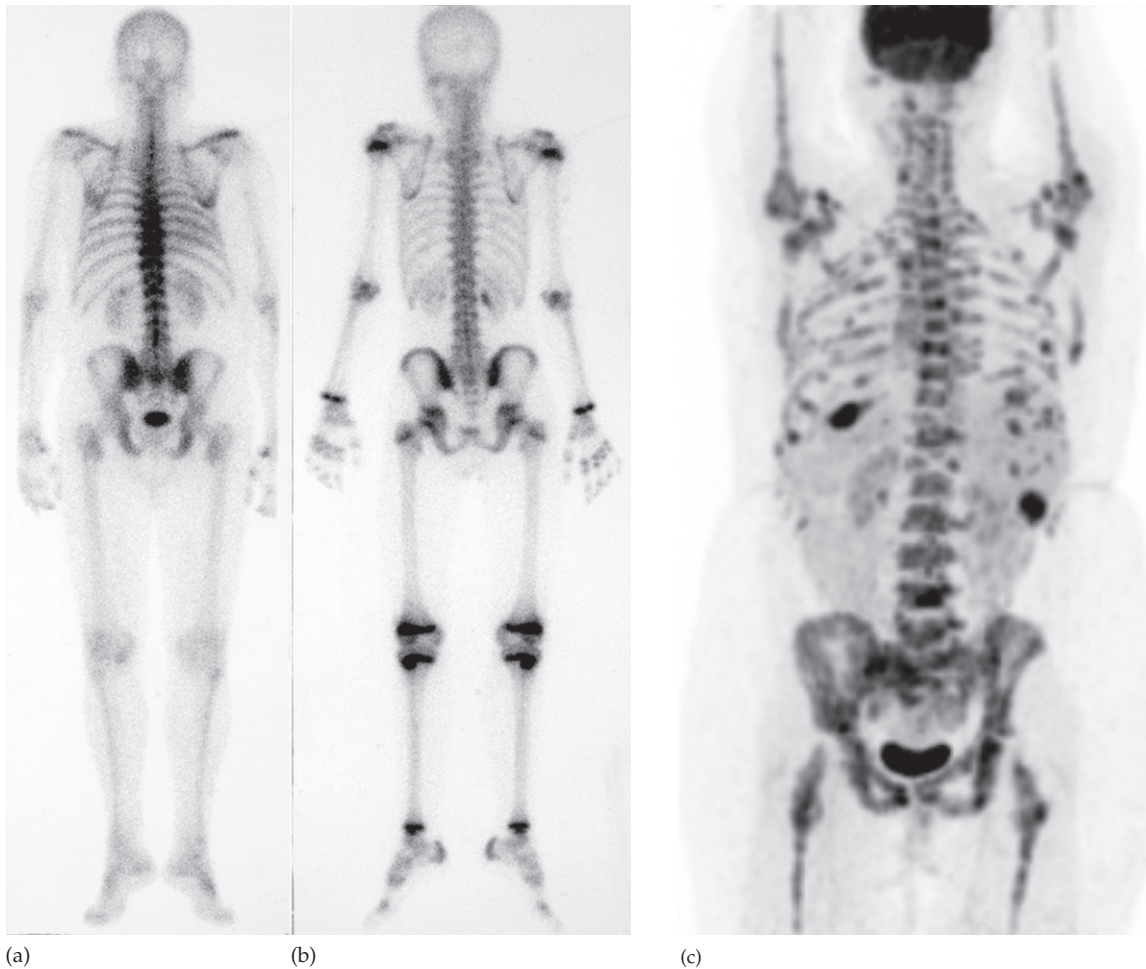


Fig. 11.6 (a,b) Normal radionuclide bone scan. (a) Adult. Note the radionuclide in the bladder. (b) Child. Note the bands of increased uptake in the epiphyseal plates where bone growth is occurring. (c) FDG-PET/CT demonstrates multiple, metabolically active bone metastases in a patient with breast cancer.

usually essential. The indications for technetium bone scanning are given in Box 11.2.

Fluorodeoxyglucose positron emission tomography (FDG-PET) with computed tomography (CT) may be used to demonstrate bone metastases (Fig. 11.6c). However, this would normally only be done in preference to technetium bone scan if other sites of disease were being evaluated. It is recognized that some benign bone lesions take up FDG

to the same extent as some primary malignant bone tumours.

Computed tomography in bone disease

Plain radiographs are usually very informative, however CT is needed in selected cases, particularly in the detection of subtle fractures or in complex fractures (Box 11.3). Bone

Box 11.2 Indications for technetium bone scanning

- Detection of metastases
- Detection of osteomyelitis
- Determination of whether a lesion is solitary or multifocal
- Investigation of a clinically suspected bone lesion despite a normal radiograph:
 - metastases
 - trauma (particularly stress injury)
 - osteoid osteoma (Fig. 11.7)
 - early osteomyelitis
- Determination, in equivocal cases, of whether an abnormality seen on the radiograph is significant or not (a positive bone scan makes it likely that a true lesion exists and a negative one reduces the probability of disease considerably)
- Investigation of painful joint prostheses

Box 11.3 Indications for bone CT

- Demonstration of abnormalities in the spine, pelvis and hips (Fig. 11.8) where plain films are frequently difficult to interpret
- Three-dimensional reconstructions can be made of fractures, which are particularly useful in showing the fractures and position of the fragments and for planning corrective surgery
- Demonstration of the extent and characterization of bone tumours in selected cases to complement MRI
- As a guide for bone biopsy

window settings (see Chapter 1) should always be viewed when reporting CT of the brain, chest and abdomen.

Magnetic resonance imaging in bone disease

Magnetic resonance imaging (MRI) has come to play a vitally important role in musculoskeletal disorders (Box 11.4). Calcified tissues such as bone produce no signal with MRI, but MRI can demonstrate the bone marrow, making it possible to see the extent of disease such as metastases, other tumours and infections, even in areas where bone destruction is not yet evident on plain films or CT (Fig. 11.9). MRI is also particularly good for showing soft tissue abnormalities.

Bone disease diagnosis

When considering the diagnosis and differential diagnosis of bone diseases, it is convenient to divide disorders into four main groups:

Box 11.4 Major indications for musculoskeletal MRI

- Demonstration of disc herniation and spinal cord or nerve root compression
- Diagnosis of bone metastases
- To show the extent of primary bone tumours
- Demonstration of myeloma and lymphoma (Fig. 11.9)
- To image soft tissue masses (Fig. 11.10)
- Diagnosis of osteomyelitis and to show any soft tissue abscess
- Diagnosis of avascular necrosis and other joint pathologies
- To image both acute and chronic injury to joint cartilages, ligaments and other intra-articular soft tissues

- 1 Those that cause solitary lytic or sclerotic lesions.
- 2 Those that produce multiple focal lesions, i.e. several discrete lytic or sclerotic lesions or periosteal reactions in one or more bones.
- 3 Those that cause generalized lesions where all the bones show diffuse increase or decrease in bone density.
- 4 Those that alter the trabecular pattern or change its shape.

Fractures are dealt with separately in Chapter 14.

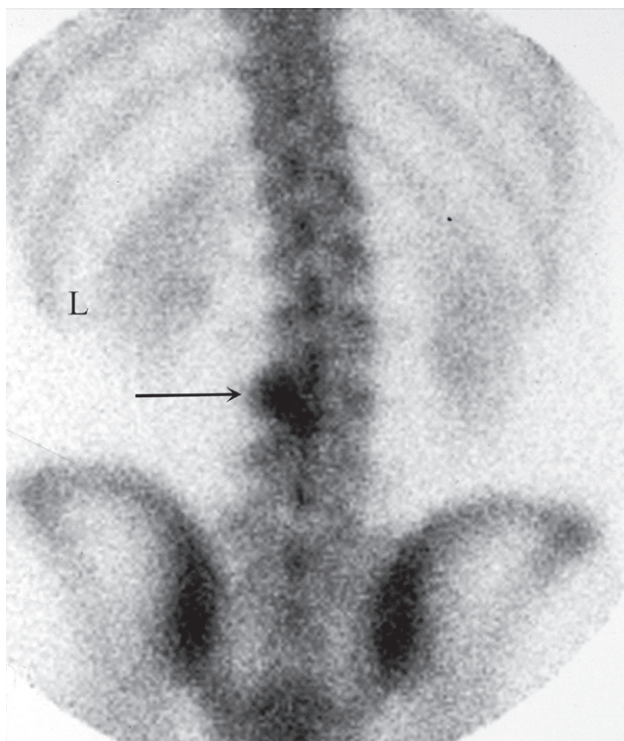
Solitary lesions

Solitary areas of lysis, sclerosis or a combination of the two, are usually one of the following:

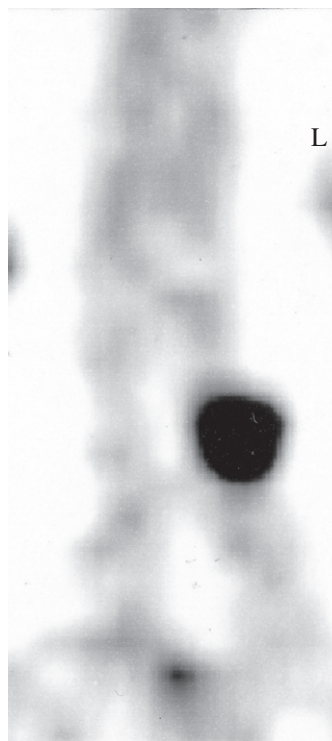
- bone tumour:
 - malignant (primary or secondary)
 - benign
- osteomyelitis
- bone cyst, fibrous dysplasia or other non-neoplastic defect of bone
- conditions of uncertain nature such as Langerhans' histiocytosis and osteoid osteoma.

Primary malignant bone tumours and osteomyelitis are usually accompanied by periosteal reaction. Pathological fractures may be seen through benign and malignant bone tumours and through bone cysts.

The radiological diagnosis of a localized bone lesion can be difficult. Some conditions are readily diagnosed but, in others, even establishing which broad category of disease is present can be difficult. The initial radiological decision is usually to try and decide whether the lesion is benign



(a)



(b)

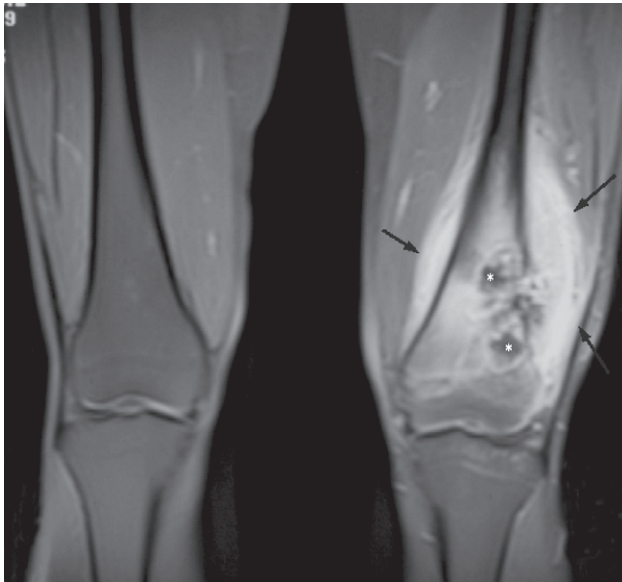


(c)

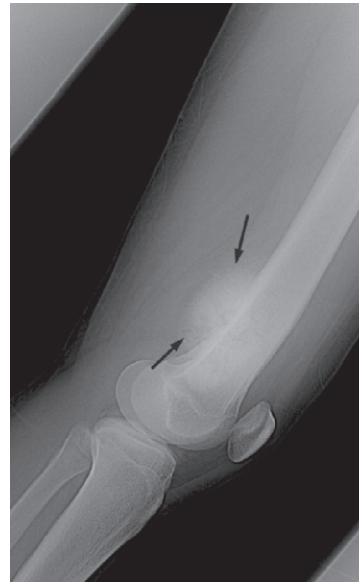
Fig. 11.7 Osteoid osteoma that was not visible on plain films. (a) Bone scan (posterior view) showing a focal area of intense increased uptake in L3 (arrow). L, left. (b) Single photon emission computed tomography (SPECT) scan showing the increased uptake more clearly. (c) CT demonstrating the tumour arising in the pedicle (arrow).



Fig. 11.8 CT scan of a pelvis showing a large mass (arrows) due to a metastasis destroying the medial half of the right iliac bone with extension into the adjacent soft tissues.



(a)

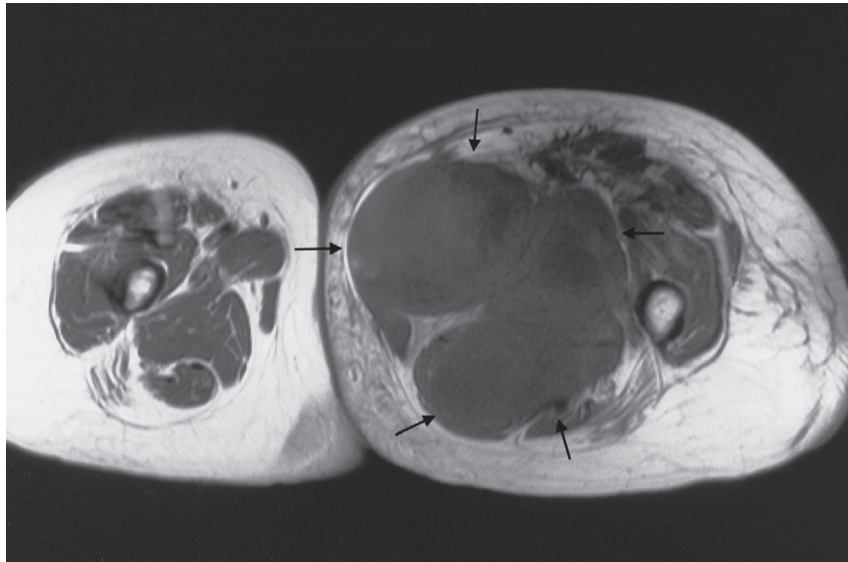


(b)

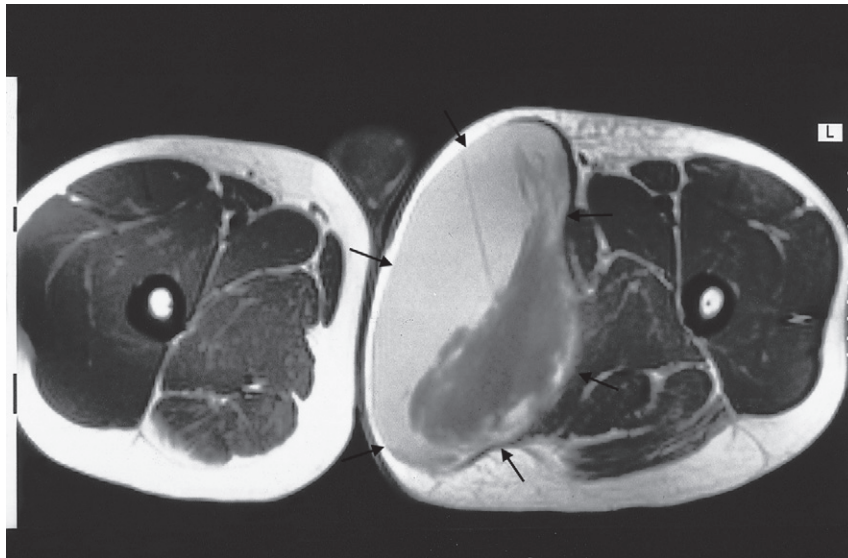


(c)

Fig. 11.9 MRI of bone tumours. (a) T1-weighted post contrast scan of osteosarcoma in the lower shaft and metaphysis of the left femur. The extent of tumour (arrows) within the bone and the soft tissue extension are both very well shown. The low signal in the medulla (*) is due to the calcified osteogenic component of the tumour. (b) The true extent of the tumour cannot be assessed from a plain film, although the plain film provides a more specific diagnosis, because the bone formation within the soft tissue extension (arrows) is obvious. (c) T2-weighted scan of lymphoma in the T10 vertebral body (arrow). The very high signal of the neoplastic tissue is evident even though there is no deformity of shape of the vertebral body.



(a)



(b)

Fig. 11.10 T1-weighted MRI of soft tissue masses. (a) Soft tissue sarcoma producing an obvious soft tissue mass (arrows) in the medial compartment of the left thigh. (b) Large haematoma (arrows) in the medial compartment of the left thigh showing a mixed signal, including the characteristic high signal of recent haemorrhage on a T1-weighted sequence.

(i.e. stable or very slow growing) or whether it is aggressive (i.e. a malignant tumour or an infection). It is also important to know the age of the patient, as certain lesions tend to occur in a specific age range.

The following features should be looked for on plain radiographs and CT when trying to decide the nature of a localized bone lesion.

1 Zone of transition. The edge of any lytic or sclerotic lesion should be examined carefully to see whether it is well demarcated or whether there is a wide zone of transition between the normal and abnormal bone. There are two extremes: a lesion with a well-defined sclerotic edge is almost certainly benign, e.g. a fibrous cortical defect (Fig. 11.11a) or a bone island (Fig. 11.11b), whereas a lytic area with an ill-defined edge is likely to be aggressive. Aggressive lesions are fast changing ones and include both tumour and infection (Fig. 11.11c). In the middle of this spectrum lies the lytic area with no sclerotic rim, which may be a benign or malignant lesion. Metastases and myeloma (Fig. 11.11d) are a frequent cause of this pattern.

2 The adjacent cortex. Any destruction of the adjacent cortex indicates an aggressive lesion such as a malignant tumour or osteomyelitis (Fig. 11.11e).

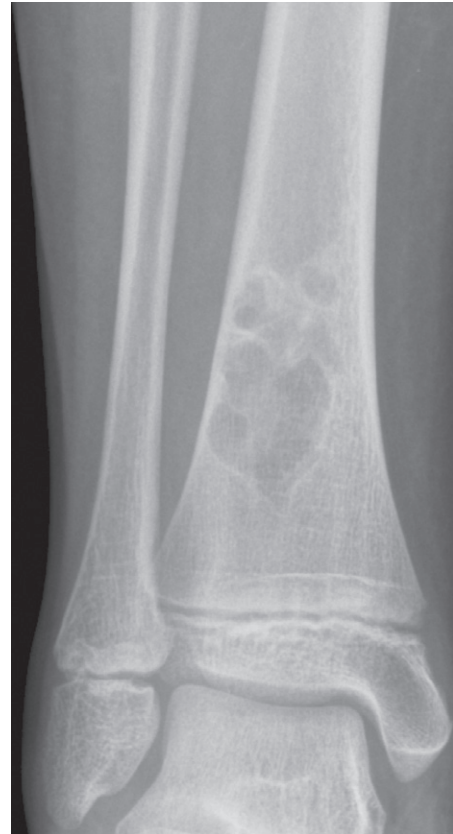
3 Expansion. Bone expansion with an intact, well-formed cortex usually indicates a slow growing lesion such as an enchondroma or fibrous dysplasia (Fig. 11.11f).

4 Periosteal reaction. The presence of an active periosteal reaction (Box 11.5) in the absence of trauma usually indicates an aggressive lesion (Fig. 11.11g). A traumatic fracture causes periosteal reaction but there is no underlying bone destruction.

5 Calcific densities within the lesion. Calcification within an area of bone destruction occurs in specific conditions. Patchy calcification of a popcorn type usually indicates a cartilage tumour (Fig. 11.11h), whereas diffuse, ill-defined

calcification suggests osteoid formation and indicates an osteosarcoma.

6 Soft tissue swelling. The presence of a soft tissue mass suggests an aggressive lesion; the better defined it is, the



(a)

Fig. 11.11 Localized lesions. (a) A well-defined sclerotic edge can be seen indicating a benign lesion – a fibrous cortical defect.

(b) (*Opposite*) Bone island. There is a small, well-defined area of compact bone in the neck of the femur (arrow). This common finding is without significance. (c) An ill-defined edge – in this case a metastasis. This type of bone destruction is known as permeative. (d) A well-defined edge – in this case a metastasis in the shaft of the femur. (e) Destruction of the cortex indicating an aggressive lesion – another metastasis. (f) Expansion of the cortex due to fibrous dysplasia. (g) Periosteal reaction (arrow) – in this case osteomyelitis. (h) A lesion containing calcium (arrow) due to a cartilage tumour – in this case a chondrosarcoma.

Box 11.5 Causes of a localized periosteal reaction adjacent to a lytic or sclerotic lesion

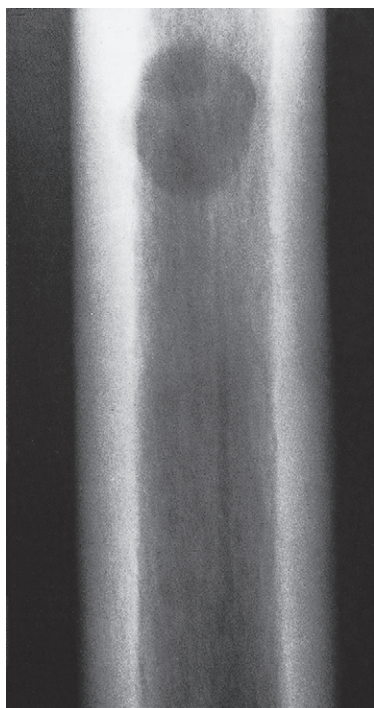
- Osteomyelitis
- Malignant bone tumour, particularly Ewing's sarcoma and osteosarcoma
- Occasionally metastasis, particularly neuroblastoma
- Langerhans' histiocytosis



(b)



(c)



(d)

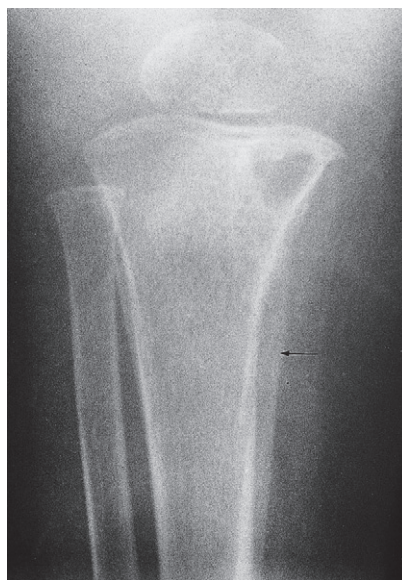


(e)

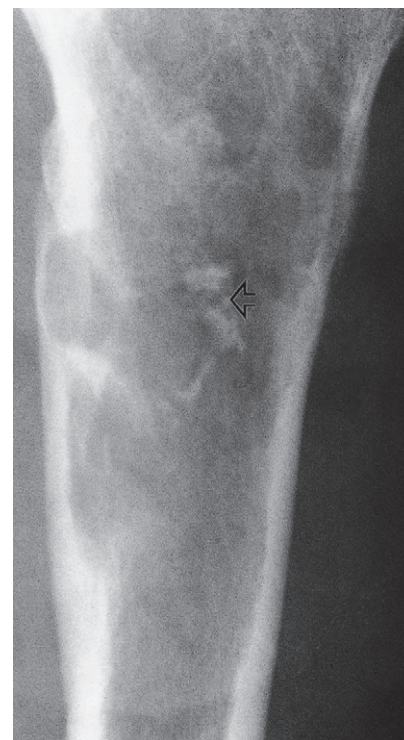
Fig. 11.11 *Continued*



(f)



(g)



(h)

Fig. 11.11 Continued

more likely it is that the lesion is a neoplasm. Ill-defined soft tissue swelling adjacent to a focal destructive lesion suggests infection. Sometimes a tumour arising primarily in the soft tissues may destroy bone by pressure erosion or direct invasion.

7 Site. The site of a lesion is important as certain lesions tend to occur at certain sites, for example osteomyelitis characteristically occurs in the metaphyseal areas, particularly of the knee and lower tibia, whereas giant cell tumours are subarticular in position.

Bone tumours

The precise diagnosis of a bone tumour can be notoriously difficult both for the radiologist and the pathologist. Accurate histological diagnosis is essential for all malignant lesions and it is important to realize that separate

portions of a tumour may show different histological appearances. In general, plain film radiography is the best imaging technique for making a diagnosis, whereas MRI or CT delineate the full extent of a tumour to advantage and show the effects on surrounding structures and the relationship to the neurovascular bundle. The main role for radionuclide bone scanning is to diagnose metastatic bone disease. Metastatic malignant tumours are by far the commonest bone neoplasm, outnumbering by many times primary malignant tumours. They are discussed later in the chapter.

Primary malignant tumours

On plain films, primary malignant tumours usually have poorly defined margins, often with a wide zone of transition between the normal and abnormal bone. The lesion

may destroy the cortex of the bone. A periosteal reaction is often present and a soft tissue mass may be seen.

Radionuclide bone scans show substantially increased activity in the lesion.

MRI is the most accurate technique for showing the local extent of the tumour using multiplanar views. Extension into both the medullary cavity and the soft tissues can be accurately defined, as can the relationship to important nerves and blood vessels.

Osteosarcoma (osteogenic sarcoma) (see Fig. 11.9) occurs mainly in the 5–20-year-old age group, but is also seen in the elderly following malignant change in Paget's disease. The tumour often arises in a metaphysis, most commonly around the knee. There is usually bone destruction with new bone formation, and typically a florid, spiculated periosteal reaction is present, the so-called 'sunray appearance' (see Fig. 11.2b). The tumour may elevate the periosteum to form a Codman's triangle (see Fig. 11.2d).

Chondrosarcoma occurs mainly in the 30–50-year-old age group, most commonly in the pelvic bones, scapulae, humeri and femora. A chondrosarcoma produces a lytic expanding lesion containing flecks of calcium, a sign that indicates its origin from cartilage cells. It can be difficult to distinguish from its benign counterpart, the enchondroma, but a chondrosarcoma is usually less well defined in at least one portion of its outline and it may show a periosteal reaction (Fig. 11.11h). Pelvic chondrosarcomas often have large extraosseous soft tissue components best seen with CT or MRI (Fig. 11.12). A chondrosarcoma may arise from malignant degeneration of a benign cartilaginous tumour.

Fibrosarcoma and malignant fibrous histiocytoma are rare bone tumours with similar histological and radiological features. They most often present in young and middle-aged adults, usually around the knee. Plain radiographs demonstrate an ill-defined area of lysis with periosteal reaction. Frequently the cortex is breached.

Ewing's sarcoma is a highly malignant tumour, commonest in children, arising in the shaft of long bones. It produces ill-defined bone destruction with periosteal reaction that is typically 'onion skin' in type (see Fig. 11.2c).

A *giant cell tumour* has features of both malignant and benign tumours. It is locally invasive but rarely metastasizes. It occurs most commonly around the knee or wrist after the epiphyses have fused. It is an expanding, destructive lesion, which is subarticular in position (Fig. 11.13).

The margin is fairly well defined but the cortex is thin and may in places be completely destroyed.

Primary lymphoma of bone is rare; most osseous malignant lymphoma is associated with generalized lymph node disease. When solitary primary lymphomas are encountered they may produce sclerotic bone lesions or they may cause destruction of bone, indistinguishable on imaging grounds from fibrosarcoma/malignant fibrous histiocytoma.

Benign tumours and tumour-like conditions

Included under this heading are benign tumours such as enchondroma, certain benign conditions similar to tumours, such as fibrous dysplasia, and some abnormalities which are difficult to classify, such as osteoid osteoma and Langerhans' histiocytosis. In general, benign lesions have an edge that is well demarcated from the normal bone by a sclerotic rim. They cause expansion but rarely breach the cortex. There is no soft tissue mass and a periosteal reaction is unusual unless there has been a fracture through the lesion.

Radionuclide scans in benign tumours usually show little or no increase in activity, unless a fracture has occurred. CT and MRI are infrequently needed in the evaluation of benign tumours.

Enchondromas are seen as lytic expanding lesions, most commonly in the bones of the hand (Fig. 11.14). They often contain a few flecks of calcium and frequently present as a pathological fracture.

Fibrous cortical defects (non-ossifying fibromas) are common chance findings in children and young adults. They produce well-defined lucent areas in the cortex of the long bones (see Fig. 11.11a).

Fibrous dysplasia may affect one or several bones. It occurs most commonly in the long bones and ribs as a lucent area with a well-defined edge and may expand the bone (see Fig. 11.11f). There may be a sclerotic rim around the lesion.

A *simple bone cyst* has a wall of fibrous tissue and is filled with fluid. It occurs in children and young adults, most commonly in the humerus and femur. Bone cysts form a lucency across the width of the bone shaft, with a well-defined edge. The cortex may be thin and the bone expanded (Fig. 11.15). Often, the first clinical feature is a pathological fracture.

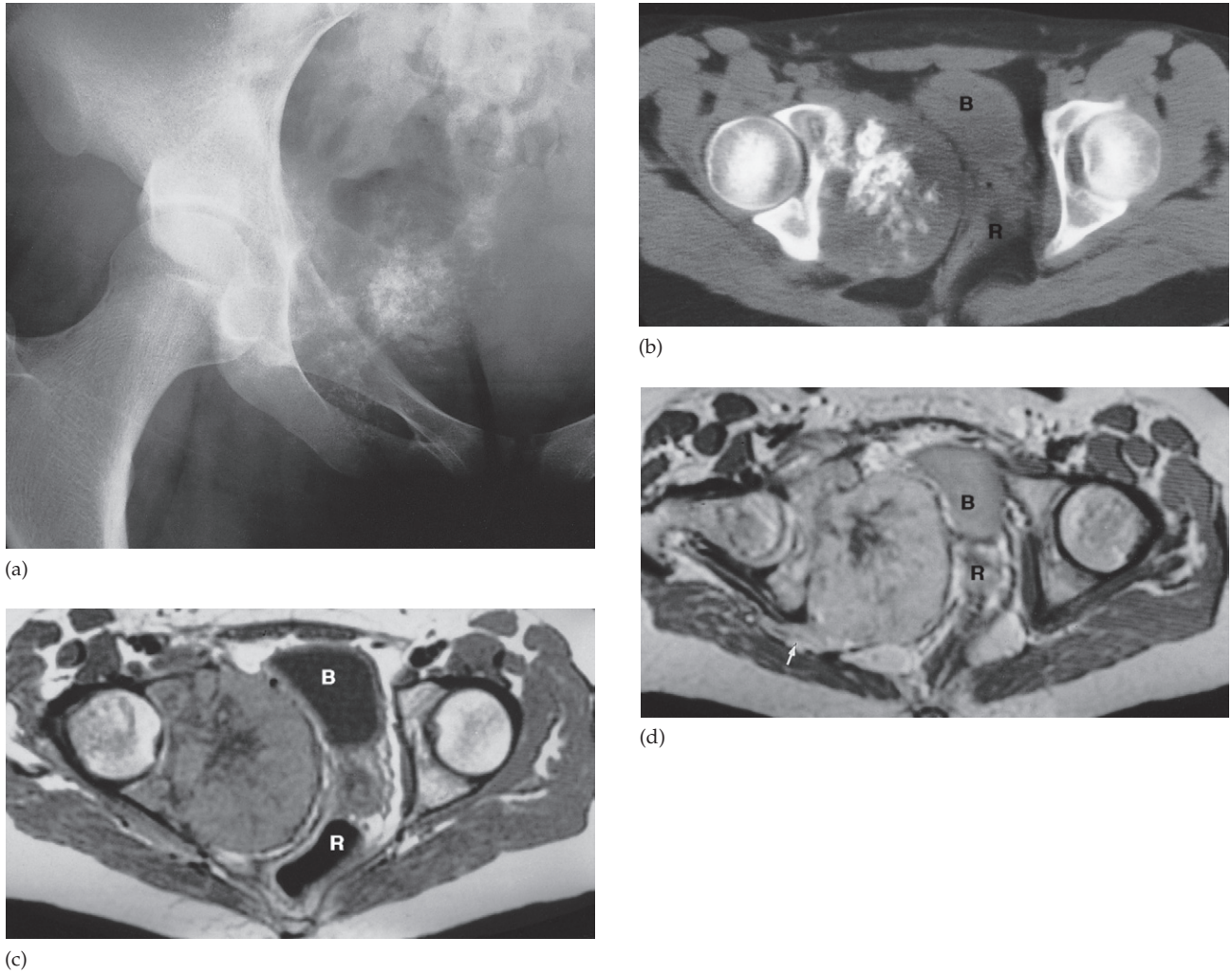


Fig. 11.12 Chondrosarcoma. (a) Plain film showing a large mass containing calcification arising from the pubic ramus. (b) CT showing the large mass containing calcium. There is also displacement of the bladder and rectum. (c) Axial MRI scan at the same level. Note that the calcification gives no signal. (d) MRI scan at a lower level showing the tumour extending into the gluteal muscles (arrow). B, bladder; R, rectum.



Fig. 11.13 Giant cell tumour. An eccentric expanding lytic lesion has thinned the cortex crossed by strands of bone. The subarticular position is characteristic of this tumour.

Aneurysmal bone cysts are not true neoplasms, but they probably form secondarily to an underlying primary tumour. Mostly they are seen in children and young adults in the spine, long bones or pelvis. These lesions are purely lytic and cause massive expansion of the cortex, hence the name 'aneurysmal'. They may grow quickly and appear very aggressive but are, nevertheless, benign lesions. CT and MRI may show the blood pools within the cyst. The major differential diagnosis is from giant cell tumour.

An *osteoid osteoma* is a painful condition found most commonly in the femur and tibia in young adults. It has a characteristic radiological appearance: a small lucency, sometimes with central specks of calcification, known as a



Fig. 11.14 Enchondromas in the metacarpal, proximal and middle phalanges showing lytic areas that expand but do not breach the cortex.

'nidus', surrounded by a dense sclerotic rim. A periosteal reaction may also be present (Fig. 11.16). CT shows these features to advantage and osteoid osteomas can also be shown by MRI. An important imaging investigation is radionuclide bone scanning, which shows marked focal increased activity. Radionuclide bone scanning is particularly useful when the osteoid osteoma is difficult to see on plain film (see Fig. 11.7) and is helpful in locating the tumour during surgery by using a small probe which detects gamma-rays.

An *osteoma* is a benign tumour consisting of dense bone (Fig. 11.17). They may occur in the paranasal sinuses.

Eosinophil granuloma is the mildest and most frequent form of Langerhans' histiocytosis (previously referred to as histiocytosis X). It occurs in children and young adults and produces lytic lesions that may be single or multiple, most frequently in the skull, pelvis, femur and ribs. Extensive



Fig. 11.15 Bone cyst. There is an expanding lesion crossed by strands of bone in the upper end of the humerus in a child. The lesion extends to, but does not cross, the epiphyseal plate.

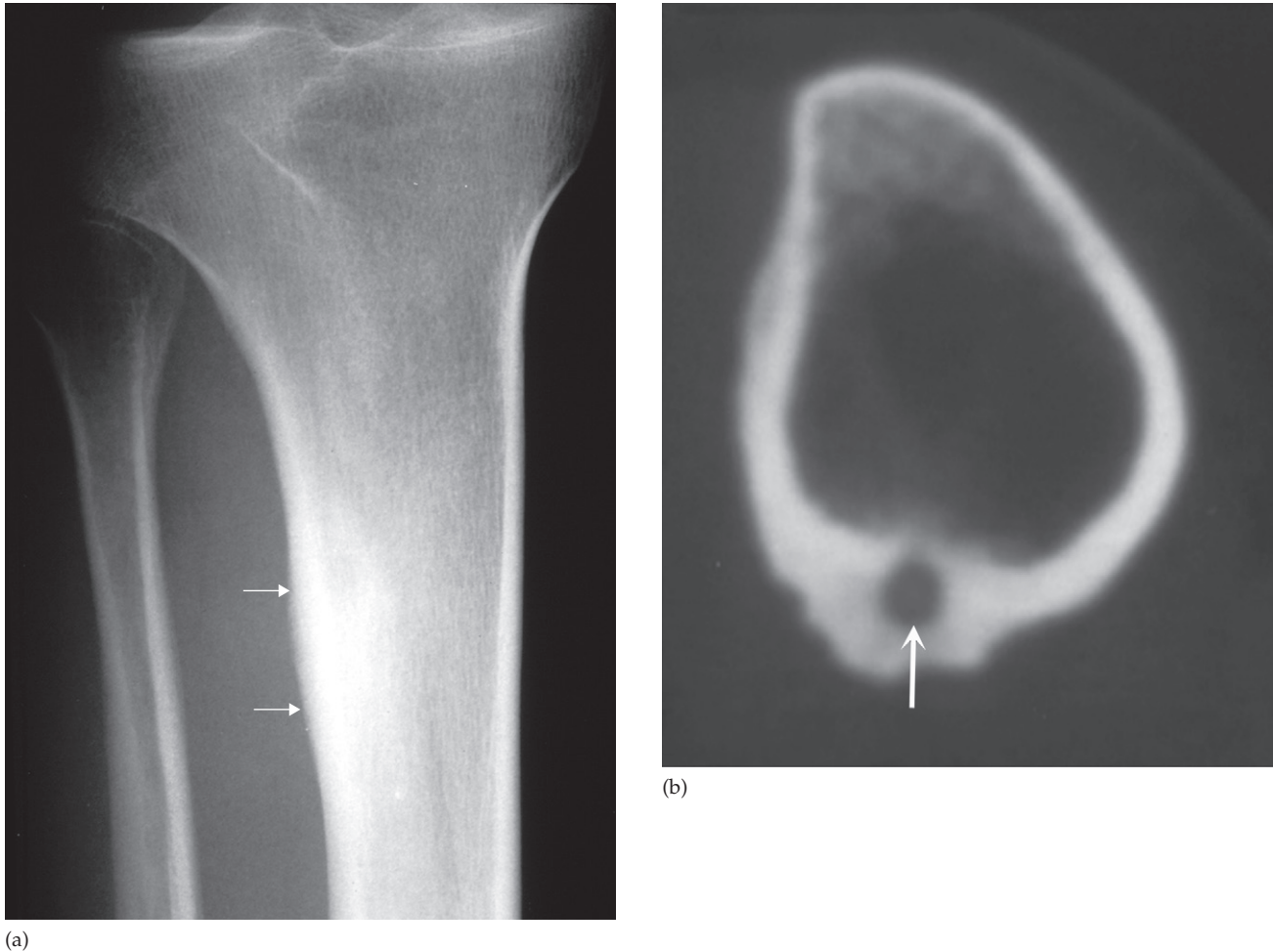


Fig. 11.16 Osteoid osteoma. (a) Plain film showing an area of sclerosis at the upper end of the tibia (arrows). (b) CT scan showing sclerosis with a central lucency known as a nidus (arrow).

lesions may be seen giving rise to the so-called 'geographic skull'. Long bone lesions show bone destruction which may be ill defined, having the features of an aggressive lesion, or well defined and may have a sclerotic rim. A periosteal reaction is sometimes seen.

Osteomyelitis

Osteomyelitis is most often caused by *Staphylococcus aureus* and usually affects infants and children. The initial radio-

graphs are normal as bone changes are not visible until 10–14 days after the onset of infection, but the ^{99m}Tc radio-nuclide bone scan and MRI show changes within a day or two of the disease (Fig. 11.18).

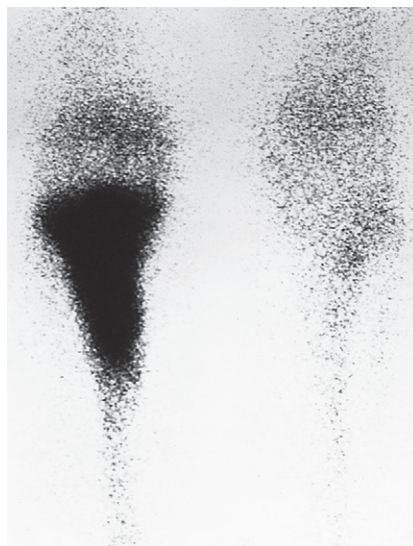
Typically, acute osteomyelitis affects the metaphysis of a long bone, usually the femur or tibia. The earliest signs on plain radiographs are soft tissue swelling and bone destruction in the metaphysis, with a periosteal reaction that eventually may become very extensive and surround the bone to form an involucrum (Fig. 11.19). A part of the original



Fig. 11.17 Osteoma. A well-defined area of dense cortical bone is present below the right acetabulum.



(a)



(b)

Fig. 11.18 Osteomyelitis; radionuclide scans of knees. (a) A blood pool scan taken 1 minute after injection of radionuclide showing increased uptake in the upper part of the leg due to hyperaemia. (b) The delayed scan taken 3 hours later shows substantially increased uptake in the bone itself.

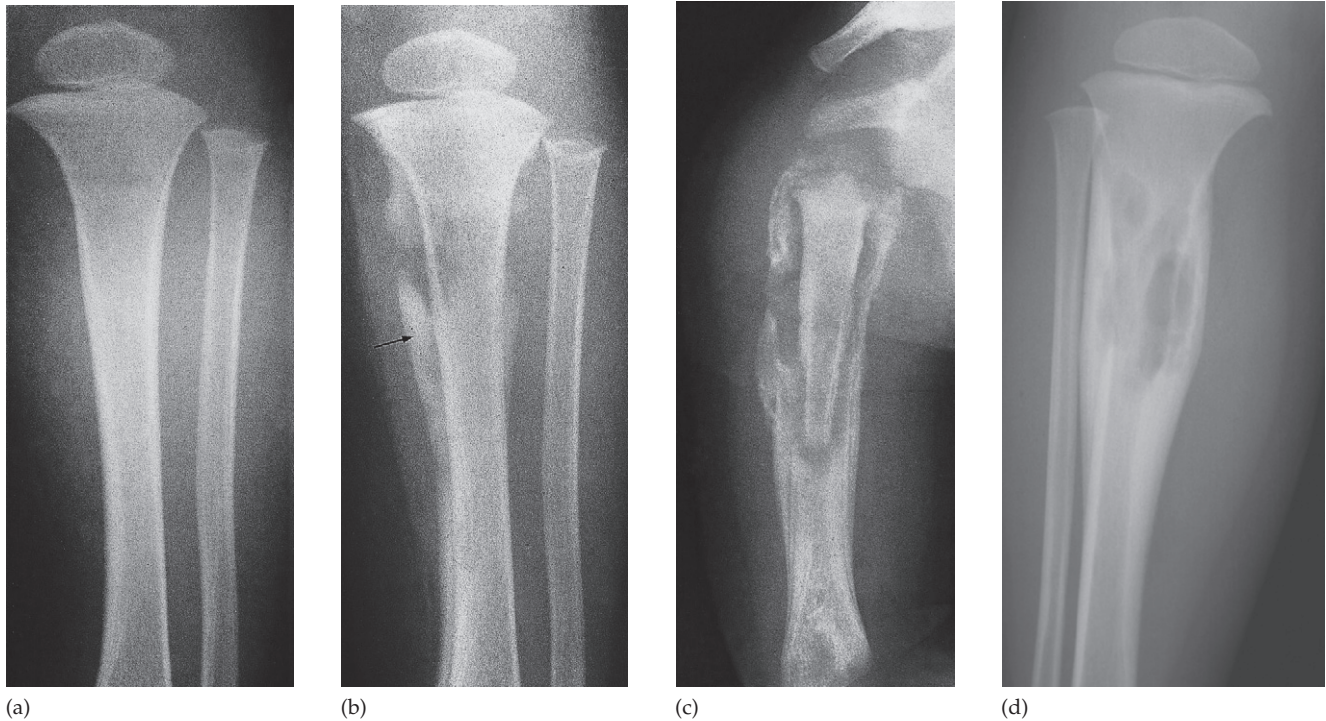


Fig. 11.19 Osteomyelitis. (a) An initial films reveals no abnormality. (b) A film taken 3 weeks later shows some destruction of the upper end of the tibia and an extensive periosteal reaction along the tibia, particularly the medial side (arrow). (c) Late acute osteomyelitis in another young child. The upper part of the humerus has separated to form a sequestrum. It is surrounded by an extensive periosteal reaction to form an involucrum. (d) Chronic osteomyelitis (Brodie's abscess) showing a lucency in the tibia surrounded by substantial sclerosis.

bone may die and form a separate dense fragment known as a sequestrum (Fig. 11.19c). A radionuclide bone scan will show increased activity both on the early (blood pool) images reflecting hyperaemia and on the delayed bone phase images. Ultrasound can demonstrate subperiosteal collections of pus well before bone changes are evident on plain film. MRI is the imaging investigation of choice and shows evidence of bone oedema and pus accumulation in the bone and soft tissues (Fig. 11.20).

In chronic osteomyelitis, the bone becomes thickened and sclerotic with loss of differentiation between the cortex and the medulla. Within the bone there may be sequestra and areas of bone destruction. This type of lesion is known as a Brodie's abscess (see Fig. 11.19d). CT can be used in selected cases to show sequestra and sinus tracks. MRI may be useful in assessing activity by identifying medullary inflammation.

Tuberculous osteomyelitis is a particular problem in African and Asian populations and is seen with increased frequency in patients with acquired immune deficiency syndrome (AIDS). The spine is the most frequent site of infection, followed by the large joints, but any bone may be affected. The disease is relatively indolent and produces large areas of bone destruction which, unlike pyogenic osteomyelitis, may be relatively asymptomatic in the early stages.

Distinction of neoplasm from osteomyelitis

It is not always possible to distinguish osteomyelitis from a bone tumour on imaging so biopsy is then needed. The clinical history is clearly important. With malignant bone tumours, the radiographs are usually abnormal when the patient first presents, whereas with osteomyelitis the initial

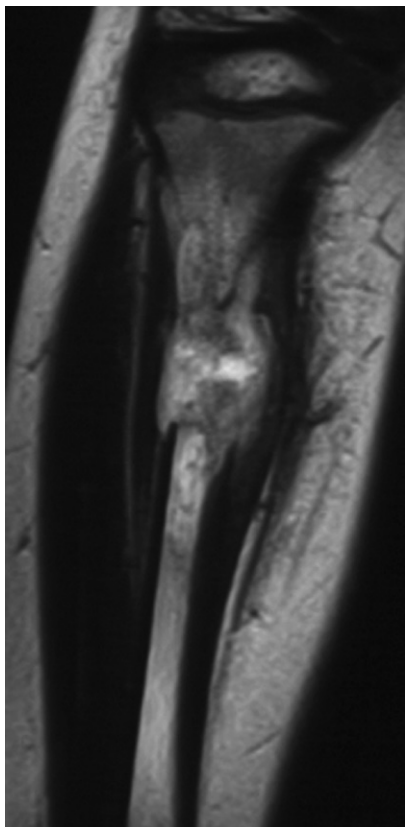


Fig. 11.20 Osteomyelitis. T2-weighted MRI scan showing a high signal in the medulla of the tibia extending into the cortex and soft tissues. Same patient as Fig. 11.19d.

films are often normal. If early films are not available, difficulties may arise in distinguishing acute osteomyelitis from a highly malignant tumour such as Ewing's sarcoma or osteosarcoma. Chronic osteomyelitis may simulate a benign bone tumour on imaging examinations, but the presence of fever, and sometimes of discharging sinuses, usually helps to diagnose an infective lesion. CT and MRI are more informative, but even with these imaging modalities there can be considerable difficulty deciding between infection and neoplasm.

The ^{99m}Tc bone scan is positive in both osteomyelitis and malignant tumours and cannot be used in differentiation.



Fig. 11.21 Bone infarct. There is calcification in the medulla of the lower end of the femur.

Bone infarction

Bone infarction (avascular necrosis) occurs most often in the intra-articular portions of the bones and is therefore described in the chapter on joint disease (see Chapter 12). However, infarcts can occur in the shaft of a bone in several diseases including caisson disease, sickle cell disease or following radiation therapy. Sometimes, they are found incidentally in older people with no known cause. In the acute phase no abnormality is visible, other than a very occasional periosteal reaction. Once healed, they appear as irregular calcification in the medulla of a long bone (Fig. 11.21).

Multiple focal lesions

Metastases

Metastases are by far the commonest malignant bone tumour, outnumbering by many times primary tumours. Metastases may be sclerotic, lytic or a mixture of lysis and sclerosis. Those bones containing red marrow are the ones most frequently affected, namely the spine, skull, ribs, pelvis, humeri and femora.

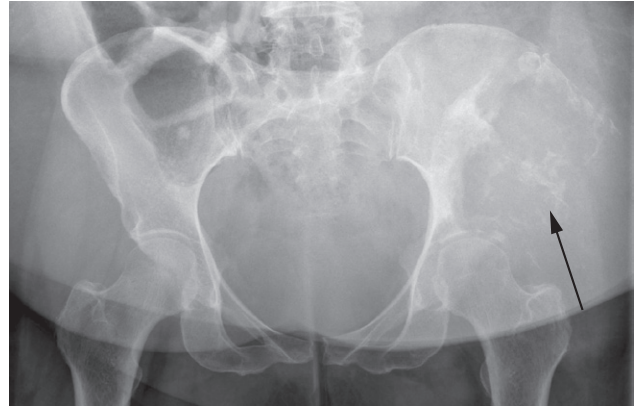
Many tumours metastasize to bone but lytic metastases in adults most commonly arise from a carcinoma of the breast and bronchus, less commonly from carcinoma of the thyroid, kidney or colon, and in children from neuroblastoma or leukaemia. Lytic metastases give rise to well-defined or ill-defined areas of bone destruction without a sclerotic rim. The lesions vary from small holes to large areas of bone destruction (Fig. 11.22). In the long bones, metastases usually arise in the medulla and as they grow they enlarge and destroy the cortex. Metastases and myeloma are virtually the only causes of multiple obvious lytic lesions in bone.

Sclerotic metastases appear as ill-defined areas of increased density of varying size with ill-defined margins. In men, they are most commonly due to metastases from carcinoma of the prostate (Fig. 11.23), and in women from carcinoma of the breast. Metastases with bone expansion occur in primary tumours of the kidney and thyroid.

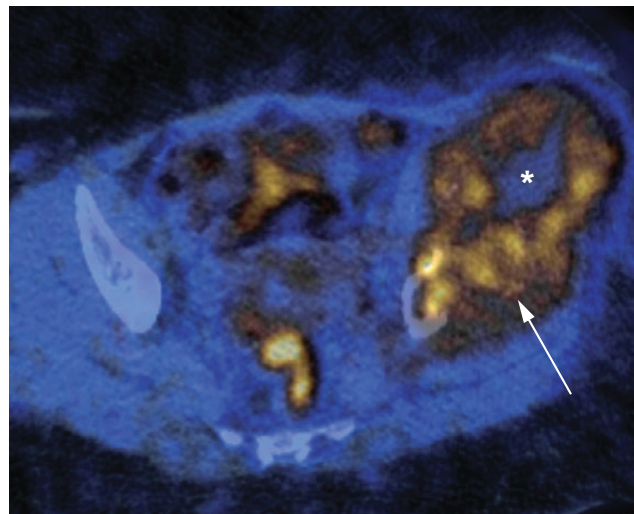
Mixed lytic and sclerotic metastases are not uncommon. They are often seen with carcinoma of the breast (Fig. 11.24).

A periosteal reaction is uncommon with metastases, except in neuroblastoma (Fig. 11.25).

A radionuclide bone scan is much more sensitive for detecting metastases than plain films. Not only are more lesions detected, but it is also an easier examination for the patient than a radiographic skeletal survey, which involves taking numerous films. Approximately 30% of metastases seen on a bone scan will not be visible on plain films. Increased radionuclide uptake in a patient with a known primary tumour but normal bone radiographs suggests metastases. If numerous areas of increased activity are seen in a patient with a known primary carcinoma, then the diagnosis of metastases is virtually certain (Fig. 11.26). If only one or a few areas of increased activity are present,



(a)



(b)

Fig. 11.22 (a) Metastasis from a carcinoma of the kidney causing a large area of bone destruction with an ill-defined edge in the left iliac blade (arrow). (b) Fused FDG-PET/CT demonstrating the large soft tissue mass with peripheral FDG uptake (arrow) and central necrosis (*).

radiographs will be needed to exclude the possibility of a benign condition such as degenerative change or fracture being responsible for the increased uptake of the radionuclide. If the bone scan is normal, it is most unlikely that radiographs will show metastases.

Magnetic resonance imaging is better than radionuclide scanning for the detection of metastases and shows more



Fig. 11.23 Sclerotic metastases showing scattered areas of increased density.



Fig. 11.24 Multiple metastases from carcinoma of the breast showing both lytic and sclerotic areas.



Fig. 11.25 Neuroblastoma. In this child's humerus there are several lytic areas and a florid periosteal reaction.

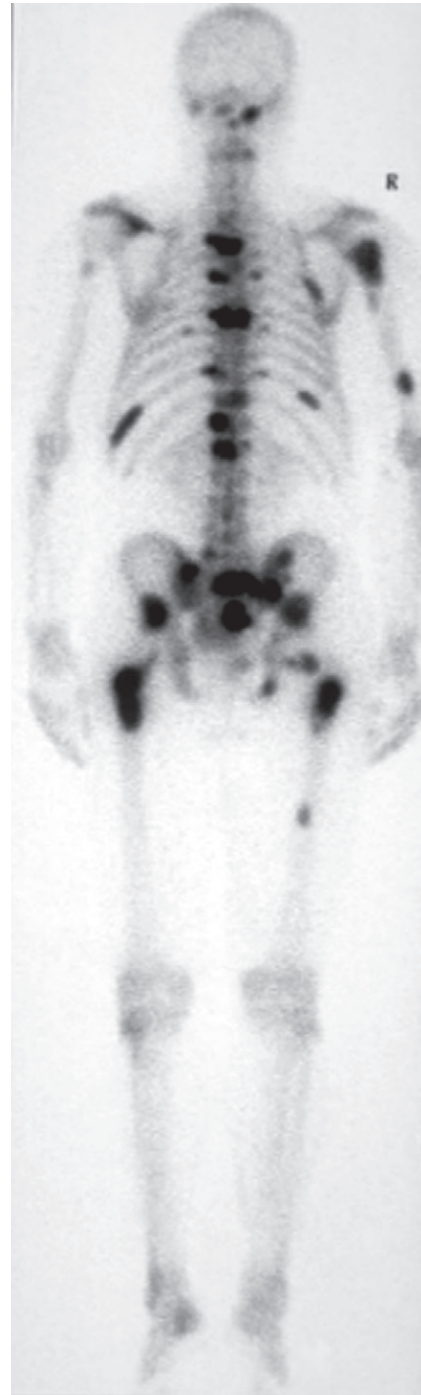


Fig. 11.26 Metastases. Radionuclide bone scan showing numerous discrete areas of increased uptake in the bones in a patient with carcinoma of the prostate.

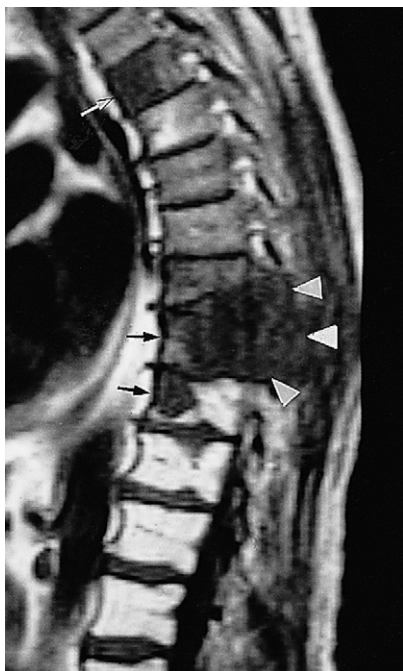


Fig. 11.27 Metastases from carcinoma of the prostate. Sagittal whole spine MRI scan showing low signal intensity in several vertebral bodies (arrows). Note the metastases also involve the posterior elements of two adjacent vertebrae (arrowheads).

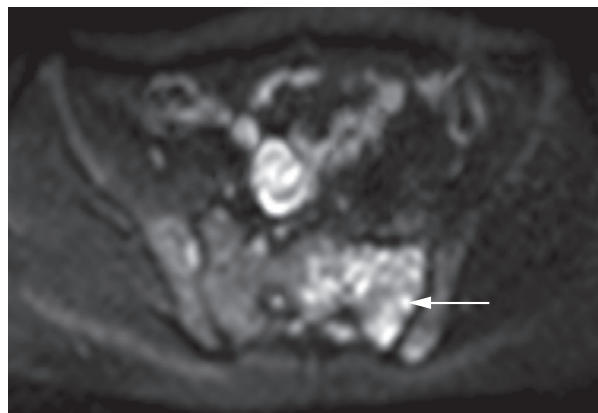
metastases. Whole spine MRI is well established as an imaging survey for metastatic disease or myeloma (Fig. 11.27). Diffusion-weighted sequences may be used for the detection of bone metastases (Fig. 11.28) and whole body MRI is a promising technique that is under evaluation for detection of bone deposits. MRI has an important role to play when the bone scan is normal or equivocal in the face of strong clinical suspicion of metastases. MRI is used if there is a possibility of metastases causing spinal cord compression (Fig. 11.27). CT is less sensitive than MRI for detecting metastases, but can demonstrate lytic and sclerotic metastases, and images should be reviewed on bone windows on all staging scans (Fig. 11.29). Bone metastases may also be demonstrated on FDG-PET/CT when this is used in staging cancer or for the detection of recurrent disease.

Multiple myeloma

Although myeloma deposits may be found in any bone, they are most frequently seen in bones with active haemopoiesis. The bone lesions may resemble lytic metastases in every way (Fig. 11.30), but are often better defined and may cause expansion of the bone. Diffuse marrow involvement may give rise to generalized loss of bone density, producing



(a)



(b)

Fig. 11.28 Metastatic bone disease in a patient with breast cancer. (a) T1-weighted MRI and (b) diffusion-weighted MRI, with b value 1000, demonstrating a large area of metastatic bone disease in the left side of the sacrum (arrows).

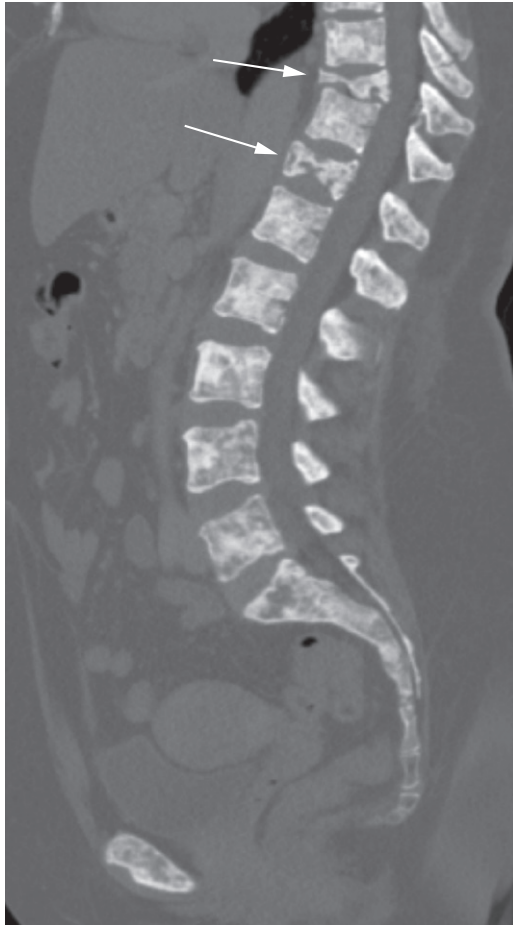


Fig. 11.29 Metastases. CT sagittal reconstruction in a patient with carcinoma of the breast showing multiple mixed, but mainly sclerotic, metastases in the thoracic and lumbar spine. There are pathological wedge fractures in two of the lower thoracic vertebrae (arrows).

a picture similar to that of osteoporosis. A full skeletal survey using plain radiography remains one of the standard staging tools in patients with myeloma.

Myeloma deposits may show increased activity on radio-nuclide bone scans but in some instances, even in large areas of bone destruction visible on plain radiographs, show no abnormality on the scan. MRI is a very effective modality for the detection of myeloma deposits, and MRI

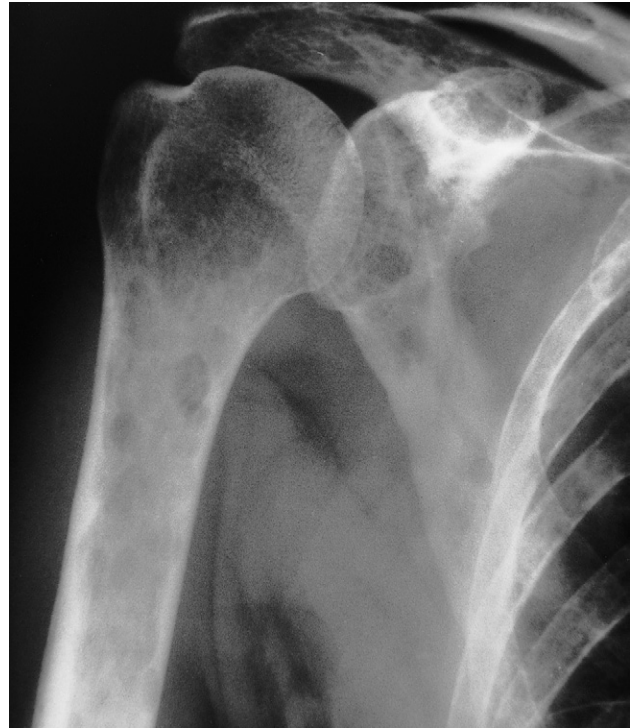


Fig. 11.30 Myeloma deposits causing multiple, well-defined lytic lesions.

of the spine or whole body MRI is often undertaken to evaluate the extent of myeloma deposits.

Lymphoma and leukaemia

Malignant lymphoma involving bone may give rise to lesions closely resembling metastases on all imaging modalities (see Fig. 11.9c).

Bone involvement in acute leukaemia in children is not uncommon. Leukaemic deposits produce ill-defined permeative bone destruction, mostly in the metaphyseal regions. Bone lesions are very rare in adult leukaemias.

Multiple periosteal reactions

Multiple periosteal reactions are seen in conjunction with other signs in several conditions, listed in Box 11.6. In cases

Box 11.6 Causes of multiple periosteal reactions

- Non-accidental injury
- Widespread bone infection:
 - congenital syphilis
 - neonates with infected intravenous catheters
- Venous stasis and ulceration of the legs
- Hypertrophic pulmonary osteoarthropathy
- Scurvy

of venous stasis and ulceration, low grade periosteal reaction and cortical thickening of the tibia and fibula may be encountered. In hypertrophic pulmonary osteoarthropathy there is widespread periosteal reaction around the bones of the forearms and lower legs which, when severe, extends to involve the hands and feet (Fig. 11.31). Finger clubbing is invariably present. Hypertrophic pulmonary osteoarthropathy is seen in a number of conditions, mostly intrathoracic, of which carcinoma of the bronchus is by far the commonest.

Generalized decrease in bone density (osteopenia)

The radiographic density of bone is dependent on the amount of calcium present in the bones. Calcium content may be reduced due to a disorder of calcium metabolism, as in osteomalacia or hyperparathyroidism, or to a reduction in protein matrix, as in osteoporosis. The radiological diagnosis of decreased bone density is often difficult, especially as the appearances of the bones are markedly affected by radiographic exposure factors.

The main causes of generalized decrease in bone density are:

- osteoporosis
 - osteomalacia
 - hyperparathyroidism
 - multiple myeloma, which may cause generalized loss of bone density, with or without focal bone destruction.
- Each of these conditions may have other radiological features that enable the diagnosis to be made, but when they are lacking, as they frequently are in osteoporosis and osteomalacia, it becomes very difficult to distinguish between them radiologically.



Fig. 11.31 Hypertrophic pulmonary osteoarthropathy. There is a periosteal reaction which is present bilaterally along the shafts of the radius and ulna and the metacarpals. In this case, it was associated with a bronchial carcinoma.

Box 11.7 Causes of osteoporosis

- Idiopathic:
 - juvenile
 - postmenopausal
 - senile
- Cushing's syndrome
- Steroid therapy
- Disuse

Osteoporosis

Osteoporosis is the consequence of a deficiency of protein matrix (osteoid). The remaining bone is normally mineralized and appears normal histologically, but because the matrix is reduced in quantity there is necessarily a reduction in calcium content. Osteoporosis predisposes to fractures, particularly of the vertebral bodies and hips. The most common causes of osteoporosis are listed in Box 11.7. Postmenopausal and senile osteoporosis are the commonest forms: up to 50% of women over 60 years of age have osteoporosis.

A radiological diagnosis of osteoporosis is only made after other diseases have been excluded. Bone destruction, which could indicate metastatic carcinoma or myeloma, and evidence of hyperparathyroidism and osteomalacia should be sought, because these conditions can closely resemble osteoporosis.

The changes of osteoporosis are best seen in the spine (Fig. 11.32). Although there is an overall decrease in bone density, the cortex stands out clearly, as if pencilled in. An important feature is collapse of the vertebral bodies, representing compression fractures, which result in the vertebral bodies appearing wedged or biconcave. Several vertebrae may be involved and the disc spaces often appear widened.

The long bones have thin cortices. Many of the trabeculae are resorbed but those that remain stand out clearly.

Disuse osteoporosis can be caused by localized pain or immobilization of a fracture (Fig. 11.33). Besides a reduction in density and thinning of the cortex, the bone may sometimes have a spotty appearance (Fig. 11.33c).

Reflex sympathetic dystrophy syndrome (Sudeck's atrophy) is a disorder of the sympathetic nervous system, comprising severe osteoporosis and oedema of the soft tissues following a fracture. The degree of osteoporosis is disproportionate to the trauma or the degree of disuse.



Fig. 11.32 Senile osteoporosis. There is decreased bone density but the edge of the vertebral bodies are well demarcated. Note the partial collapse of several of the vertebral bodies and the widening of the disc spaces.

Screening for osteoporosis

Because osteoporosis is such a prevalent problem and, once established, is difficult to treat, attempts have been made to develop screening tests for the at-risk population in order to institute preventative treatment. Bone mass is usually measured by dual-energy x-ray absorption, often



Fig. 11.33 (a) Disuse osteoporosis due to osteomyelitis of the right calcaneum. The calcaneum is partly destroyed by infection. The remaining bones of the right foot show a marked reduction in bone density with well-defined cortex. Compare these bones with those in the normal left foot (b). (c) In this patient with paraplegia the osteoporosis has a spotty appearance.

abbreviated to DEXA. Bone mineral density is expressed as a T score, which is the number of standard deviations above or below the mean for a young, healthy adult population. Osteoporosis is defined as a T score ≤ -2.5 . Although bone density can be accurately and reproducibly measured, bone mineral density is a poor predictor of an individual's fracture risk and it has not been possible to use bone densitometry to select patients for preventative therapy on a population-wide basis.

Rickets and osteomalacia

In these conditions there is poor mineralization of osteoid. If this occurs before epiphyseal closure, the condition is known as rickets; in adults the condition is known as osteomalacia. The main causes for osteomalacia are given in Box 11.8.

Regardless of the cause of the osteomalacia or rickets, the bone changes are similar. When it is due to chronic renal

Box 11.8 Causes of rickets and osteomalacia

- Decreased production of endogenous vitamin D:
 - dietary deficiency
 - lack of exposure to sunlight
- Impaired absorption of calcium or vitamin D:
 - malabsorption
- Renal disease, causing vitamin D-resistant rickets, despite normal amounts of vitamin D in diet:
 - tubular defects: hypophosphataemia, Fanconi's syndrome and renal tubular acidosis
 - chronic renal failure: impaired ability to activate vitamin D

failure, the changes of hyperparathyroidism may also be present.

In *rickets* the changes are maximal where bone growth is occurring, so they are best seen at the knees, wrists and ankles. The zone of provisional calcification is deficient and the metaphyses are irregularly mineralized, widened and cupped (Fig. 11.34). This results in an increased distance between the visible epiphysis and the calcified portion of the metaphysis. The generalized decrease in bone density, however, may not be very obvious. Deformities of the bones occur because the undermineralized bone is soft. Greenstick fractures are common.

In *osteomalacia* the characteristic features are loss of bone density, thinning of the trabeculae and cortex, and Looser's zones (pseudofractures) (Fig. 11.35a). Looser's zones are short lucent bands running through the cortex at right angles, usually going only part way across the bone, and are thought to be insufficiency fractures. They may have a sclerotic margin making them more obvious. They are commonest in the scapulae, medial aspects of the femoral necks and in the pubic rami. Bone deformity, due to bone softening, is an important feature. In the spine, the vertebral bodies are biconcave (Fig. 11.35b), the femora may be bowed and in severe cases the side walls of the pelvis may bend inwards, giving the so-called 'tri-radiate pelvis'.

Hyperparathyroidism

Excess parathyroid hormone secretion mobilizes calcium from the bones, resulting in a decrease in bone density. Hyperparathyroidism may be primary, from hyperplasia or a tumour of the parathyroid glands, or secondary,

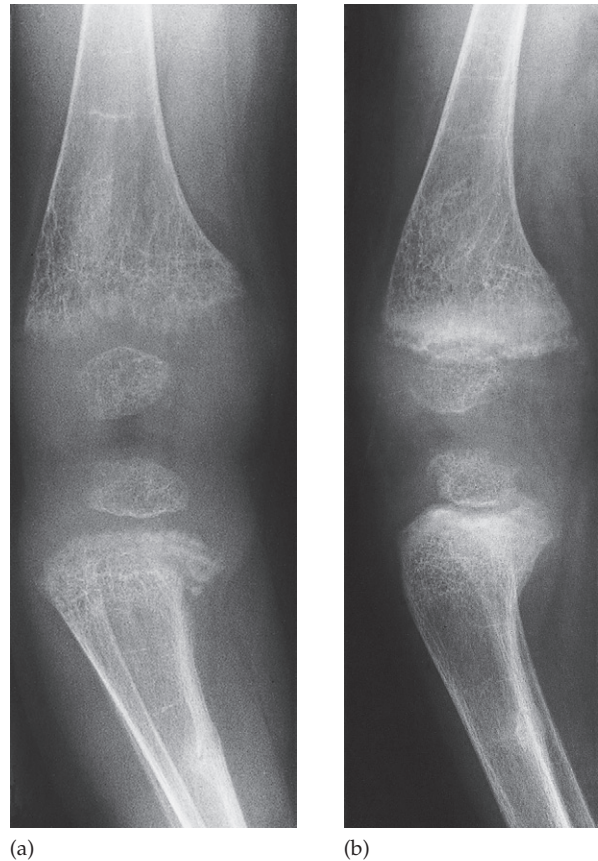


Fig. 11.34 (a) Dietary rickets showing widening and irregular mineralization of the metaphyses, which have a frayed appearance. There is reduced bone density and bowing of the limbs. (b) After commencement of vitamin D treatment, mineralization of the metaphyses has occurred.

due to chronic renal failure (see next section on renal osteodystrophy).

Many patients with primary hyperparathyroidism present with renal stones and only a small minority have radiological bone changes.

The signs of hyperparathyroidism in the bones are:

- A *generalized loss of bone density*, with loss of differentiation between the cortex and medulla. The trabecular pattern may have a fine lacework appearance. With advanced disease there may be marked deformity of the skeleton.

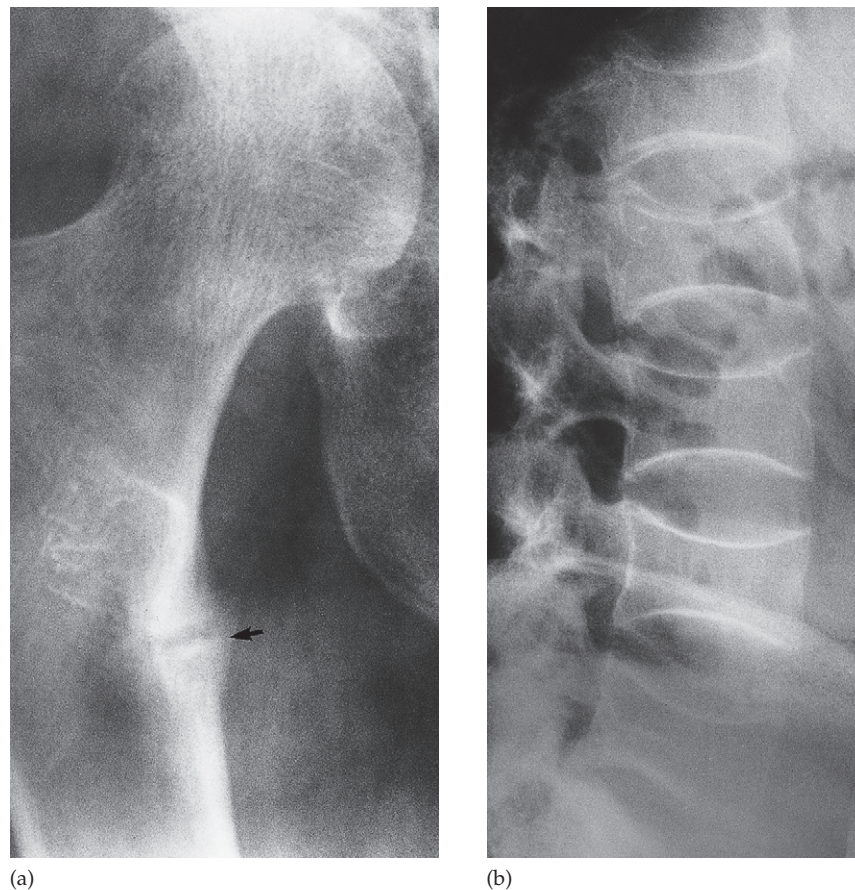


Fig. 11.35 Osteomalacia. (a) Looser's zone showing the horizontal lucent band with sclerotic margins running through the cortex of the medial side of the upper femur (arrow). (b) There is decreased bone density and partial collapse of all the vertebral bodies to approximately the same extent.

- The hallmark of hyperparathyroidism is *subperiosteal bone resorption* (Fig. 11.36a), which occurs particularly in the hands on the radial side of the middle phalanges and at the tips of the terminal phalanges. There may also be resorption of the outer ends of the clavicles.
- *Soft tissue calcification, vascular calcification and chondrocalcinosis* sometimes occur.
- *Brown tumours* are occasionally present. These are lytic lesions, which may be single or multiple, vary in size and may expand the bone. They occur most commonly in the mandible and pelvis but any bone may be involved (Fig. 11.36b).

The bone changes in primary and secondary hyperparathyroidism are similar except that brown tumours are much rarer and vascular calcification is commoner in secondary hyperparathyroidism.

Renal osteodystrophy

Three distinct bone lesions can occur, often together, in patients with chronic renal failure:

- Osteomalacia in adults and rickets in children.
- Hyperparathyroidism.

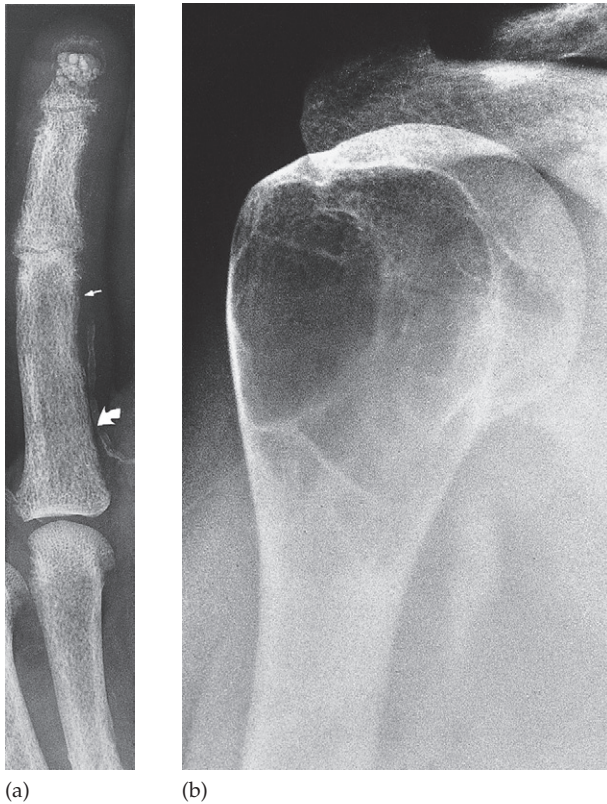


Fig. 11.36 Hyperparathyroidism. (a) Note the characteristic features of subperiosteal bone resorption (straight arrow), resorption of the tip of the terminal phalanx and the altered bone architecture. Arterial calcification is also present (curved arrow). (b) Brown tumour. There is a lytic area in the upper end of the humerus with a well-defined edge.

- Sclerosis, which is an infrequent feature. It may be seen in the spine as bands across the upper and lower ends of the vertebral bodies, giving the so-called 'rugger jersey spine' (Fig. 11.37) or at the metaphyses of the long bones.

Generalized increase in bone density

Several conditions can cause a generalized increase in bone density, including:

- *Sclerotic metastases* are by far the commonest cause, particularly from prostatic or breast carcinoma. These may affect the skeleton diffusely (Fig. 11.38).



Fig. 11.37 'Rugger jersey spine' (renal osteodystrophy). There are sclerotic bands running across the upper and lower ends of the vertebral bodies of the lumbar spine (arrows).



Fig. 11.38 Metastases from carcinoma of the prostate causing a widespread increase in bone density.

- *Osteopetrosis (marble bone disease)*. In this congenital disorder of bone formation the bones are densely sclerotic (Fig. 11.39). The bones are brittle and may fracture readily, but if fractured they heal easily.
- *Myelosclerosis* is a form of myelofibrosis in which, in addition to the replacement of bone marrow by fibrous tissue, the process extends to lay down extratrabecular bone, usually in a rather patchy fashion (Fig. 11.40). The spleen is invariably enlarged because it becomes the site of haemopoiesis. It may reach a very large size and forms an important sign on abdominal radiographs.

Alteration of trabecular pattern and change in shape

Paget's disease

The incidence of Paget's disease varies greatly from country to country, being common in the UK but rare in the USA and Asia. It is usually a chance finding in an elderly patient. One or more bones may be affected, the usual sites being the pelvis, spine, skull and long bones. Bone softening causes bowing and deformity of the bones and pathological fractures may occur (see Fig. 14.54).

Although there is a rare lytic form of Paget's disease, e.g. osteoporosis circumscripta of the skull, the cardinal features are thickening of the trabeculae and of the cortex,



Fig. 11.39 Osteopetrosis. There is a marked generalized increased bone density affecting all bones. There are multiple healed fractures, with a pin and plate in the left femur.

leading to loss of corticomedullary differentiation and increased bone density, together with enlargement of the affected bone (Fig. 11.41).

In the skull, there are many circumscribed areas of sclerosis scattered in the skull vault, giving a mottled appearance which has been likened to cotton wool. An increased thickness of the calvarium is a particularly obvious feature.

These changes of sclerosis, cortical thickening, coarse trabeculae and, most particularly, increase in the size of the bone, distinguish Paget's disease from metastases due to prostatic or breast carcinoma, which are also common in the elderly.

Malignant degeneration, with development of an osteosarcoma in abnormal bone, is an occasional occurrence (Fig. 11.42).

There is a greatly increased uptake of radionuclide at bone scanning in bones affected by Paget's disease (see Fig. 1.11), which can be useful in defining the extent of disease and response to treatment. It should be realized that Paget's disease may mimic tumours on radionuclide bone scans as well as on plain radiographs.



Fig. 11.40 Myelosclerosis. A patchy increase in bone density in the humerus is seen. In this condition the bone marrow becomes replaced with bone.

Haemolytic anaemia

There are several types of haemolytic anaemia, but radiological changes are seen in two main types: thalassaemia and sickle cell disease. Both show changes of marrow hyperplasia, but sickle cell anaemia may also show evidence of bone infarction and infection.

Marrow hyperplasia

Overactivity and expansion of the bone marrow causes thinning of the cortex and resorption of some of the trabeculae so that those that remain are thickened and stand out more clearly. There is usually a generalized decrease in bone density. In the skull, there is widening of the diploë and there may be perpendicular striations giving an appearance known as 'hair-on-end' (Fig. 11.43a). The ribs may enlarge and the phalanges may become rectangular (Fig. 11.43b).

Infarction and infection

Infarction at bone ends causes flattening and sclerosis of the humeral and femoral heads. Areas of bone destruction with periosteal new bone formation, or just a periosteal reaction, may be seen in the shafts of the bones. These signs are due to bone infarction. It is not possible to determine from the radiographs whether or not these infarcts are infected.

Sarcoidosis

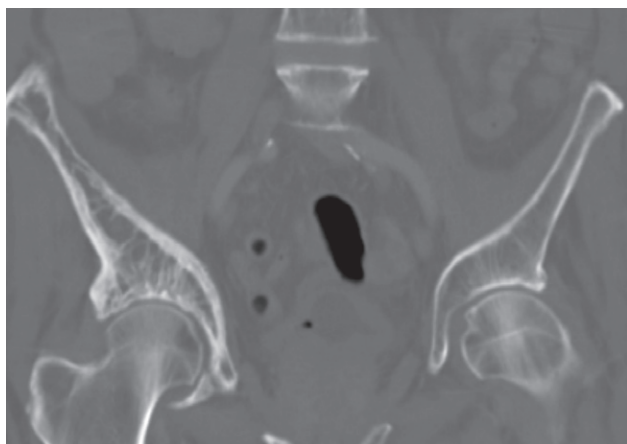
Sarcoidosis occasionally involves the bones. The phalanges of the hands and feet are virtually the only bones affected. The signs are either small cysts with a well-defined edge or areas of bone destruction showing a lace-like pattern (Fig. 11.44). If the bones are involved, there is invariably evidence of sarcoidosis in the chest and sarcoid skin lesions are usually present.

Radiation-induced disease of bone

Radiotherapy may damage bones in the radiation field. Early change may be limited to osteoporosis. In severe cases, the bone thins and shows patchy increased density with small lytic areas – an appearance known as osteonecrosis.



(a)



(b)

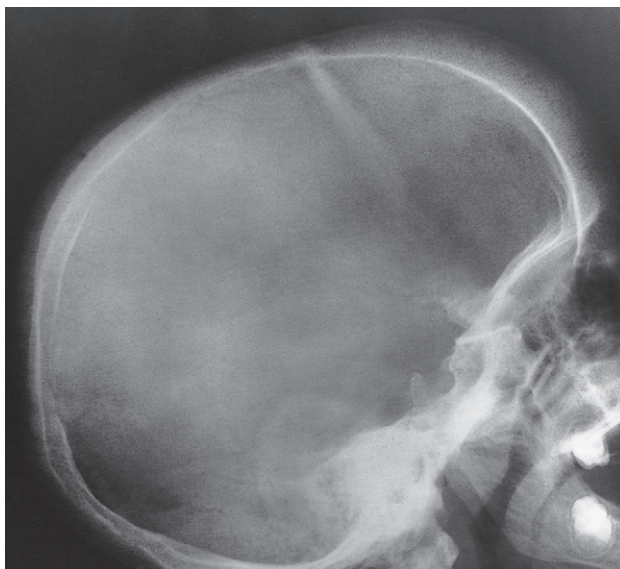


(c)

Fig. 11.41 (a) Paget's disease showing typical sclerosis with coarse trabeculae in the right side of the pelvis. Note that the width of the affected bones is increased. The pelvis is deformed consequent upon the bone softening. (b) Coronal reformat of CT in the same patient demonstrating coarse trabeculae, a thickened cortex and enlargement of the iliac blade. (c) Similar signs in the tibia of another patient. Note the bowing of the bone from softening.



Fig. 11.42 Sarcoma in Paget's disease. There is extensive bone destruction in the humeral head and shaft. Evidence of the underlying Paget's disease can be seen.



(a)



(b)

Fig. 11.43 Thalassaemia haemolytic anaemia. (a) Skull showing thickened diploë. (b) Hand; due to marrow expansion the bones are expanded and those trabeculae that remain are very thickened.



Fig. 11.44 Sarcoidosis, showing the characteristic lace-like trabecular pattern in the middle phalanx.



Fig. 11.45 Diaphyseal aclasia. Several bony projections (exostoses) are seen arising around the knee, directed away from the joint. The opposite knee was similarly affected.

Pathological fracture is a serious complication. The commonest sites are in the ribs following radiotherapy for breast cancer and in the pelvis or femora following treatment for cervical carcinoma.

Occasionally, radiation may induce sarcomatous change, usually an osteosarcoma that occurs several years after the radiation therapy.

Changes in bone shape

Bone dysplasias

Bone dysplasias are congenital disorders resulting in abnormalities in the size and shape of the bones. There are a large number of different dysplasias; many of them are

hereditary and all of them are rare. Only diaphyseal aclasia will be mentioned here. Osteopetrosis has been described earlier in the chapter.

Diaphyseal aclasia is a congenital disorder resulting in abnormalities of the size and shape of the bones. In diaphyseal aclasia (multiple exostoses), there are multiple bony projections known as osteochondromas or exostoses. They have a cartilagenous cap, which may contain calcification. When osteochondromas occur on the long bones they are near the metaphyses and are directed away from the joint (Fig. 11.45).

Occasionally, a chondrosarcoma may develop in the cartilage cap. This should be suspected if there is either rapid growth, an ill-defined edge to the bone, or extensive calcification extending into the soft tissues.

Imaging techniques

Plain film radiographs

The plain film examination remains important for imaging joint disease (Fig. 12.1). On plain film, synovial joints have articular surfaces covered by hyaline cartilage. Both articular and intra-articular cartilage (such as the menisci in the knee) are of the same radiodensity on plain films as the soft tissues, and, therefore, are not visualized as such. Only the space between the adjacent articular cortices can be appreciated, which is referred to as the 'joint space' (Fig. 12.1). The synovium, synovial fluid and capsule also have the same radiodensity as the surrounding soft tissues and, unless outlined by a plane of fat, cannot be identified as discrete structures. The articular cortex forms a thin, well-defined line that merges smoothly with the remainder of the cortex of the bone. The plain film imaging signs of the arthropathies and specific joint abnormalities are described in each section below.

Magnetic resonance imaging

Magnetic resonance imaging (MRI) is widely used for joint imaging, allowing clear definition of the joint anatomy and the detection of abnormal fluid, change in signal intensity or enhancement. It is widely used for

- meniscal and ligamentous tears (e.g. in the knee)
- rotator cuff tears of the shoulder
- avascular necrosis of the hip
- septic arthritis.

Normal tendons are clearly defined, smooth and return no signal and therefore appear black on MRI sequences. In tendon degeneration or ligament sprain, the tendon may have increased signal intensity, altered size (usually increased), irregular margins or abnormal shape. There may be fluid around the ligaments or the fibres may be disrupted. In the knee, the normal menisci appear as black triangles on MRI. A meniscal tear can be seen when either the normal shape of the meniscus is disrupted by an abnormal signal, or if a portion of the meniscus is missing.

The normal synovium is only a thin membrane, and it is therefore invisible to MRI. Synovial proliferation is the hallmark of rheumatoid arthritis. Enhancement of thickened, inflamed synovium following intravenous contrast is the key to an early diagnosis of non-invasive rheumatoid arthritis.

Arthrography

Arthrography involves injecting contrast medium into the joint space directly and then performing a magnetic resonance scan. Magnetic resonance arthrography has a role in the shoulder and wrist.

Ultrasound

Ultrasound is used to image the soft tissues of joints and is also used to inject local anaesthetic and steroid solutions to treat inflammatory conditions. Several joints are amenable to imaging on ultrasound, including the shoulder and joints of the arm, wrist and hand, knee, ankle and foot.

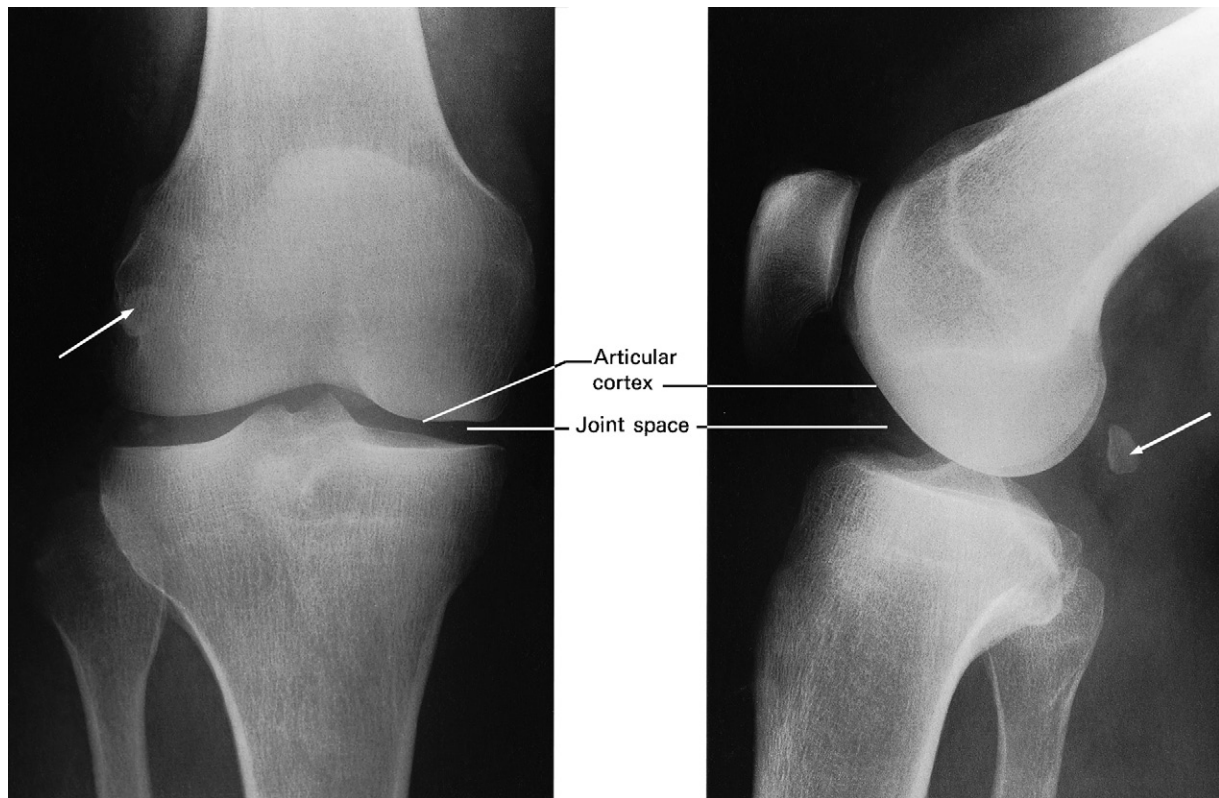


Fig. 12.1 Normal knee joint. Note the fabella (arrow), a sesamoid bone in the gastrocnemius. The 'joint space' consists of articular cartilage and synovial fluid.

On ultrasound, a normal tendon or ligament is a bright/echogenic linear band of varying thickness depending on its location. Normally, the collagen fibres are continuous and intact. The possible findings one should look for are: changes in echogenicity, increase in size of tendon, fluid in the joint and irregularity of bone surface.

When interruptions in ligament or tendon fibres exist, they are visualized as anechoic/black areas within the tendon. Partial thickness tears reveal fibrous disruption, while full thickness tears demonstrate tendon gaps. High grade, partial thickness tearing is imaged as tendon thinning. Enlarged, hypoechoic tendons with normal echotexture may be due to low grade injuries, intratendinous oedema or tendinopathy. In a normal joint, the bursa is a

thin, black/anechoic line which is less than 2 mm thick. The bursa fills with fluid when irritated or infected.

Arthritis

Signs indicating the presence of arthritis

Joint space narrowing is due to destruction of articular cartilage. It occurs in practically all forms of joint disease except avascular necrosis.

Soft tissue swelling around a joint may be seen in any arthritis accompanied by a joint effusion and whenever periarticular inflammation is present. It is, therefore, a feature of inflammatory, and particularly infective, arthri-



Fig. 12.2 Erosions. Areas of bone destruction are seen affecting the articular cortex of the metacarpophalangeal joint. A typical erosion is arrowed. The joint space is also narrowed.

tis. Discrete soft tissue swelling around the joints can be seen in gout due to gouty tophi.

Osteoporosis of the bones adjacent to joints occurs in many painful conditions. Underuse of the bones seems to be an important mechanism, but is not the only factor. Osteoporosis is particularly severe in rheumatoid and tuberculous arthritis.

Signs that point to the cause of arthritis

An *articular erosion* is an area of destruction of the articular cortex and the adjacent trabecular bone (Fig. 12.2), usually accompanied by destruction of the articular cartilage. Erosions are easily recognized when seen in profile, but when viewed *en face* the appearances can be confused with a cyst. Oblique views designed to show erosions in profile are often taken.

There are several causes of erosions (Box 12.1).

Box 12.1 Causes of erosions

- Inflammatory overgrowth of the synovium (pannus), which occurs in:
 - rheumatoid arthritis, by far the commonest cause of an erosive arthropathy
 - juvenile rheumatoid arthritis (Still's disease)
 - psoriasis
 - Reiter's disease
 - ankylosing spondylitis
 - tuberculosis
- Response to the deposition of urate crystals in gout
- Destruction caused by infection:
 - pyogenic arthritis
 - tuberculosis
- Synovial overgrowth caused by repeated haemorrhage in haemophilia and related bleeding disorders
- Neoplastic overgrowth of synovium, e.g. synovial sarcoma

Osteophytes, *subchondral sclerosis* and *cysts* are all features of osteoarthritis. A characteristic increase in the density of subchondral bone is seen in avascular necrosis (see Figs 12.15 and 12.16).

Several conditions lead to characteristic *alterations in the shape of the joint* or relationship of the bone ends, e.g. slipped epiphysis, developmental dysplasia of the hip, osteochondritis dissecans and avascular necrosis in its later stages.

Diagnosis of arthritis

When considering an arthritis it is important to have the following information:

1 Is more than one joint involved? Certain diseases typically involve several joints, e.g. rheumatoid arthritis, while others rarely do, e.g. infections and synovial tumours.

2 Which joints are involved? Many arthropathies have a predilection for certain joints and spare others:

- Rheumatoid arthritis virtually always involves the hands and feet, principally the metacarpo- and metatarsophalangeal joints, the proximal interphalangeal joints and the wrist joints. Psoriatic arthritis usually affects the terminal interphalangeal joints.
- Gout characteristically involves the metatarsophalangeal joint of the big toe.
- When osteoarthritis is seen in the hands it almost always involves the terminal interphalangeal joints and often

affects the carpometacarpal joint of the thumb. In the feet, it is almost always the first metatarsophalangeal joint that is affected. In the large joints, osteoarthritis is common in the hips and knees but relatively rare in the ankle, shoulders and elbows unless there is some underlying deformity or disease.

- The distribution of neuropathic arthritis depends on the neurological deficit; for example, diabetes affects the ankles and feet, whereas syringomyelia affects the shoulders, elbows and hands.

3 Is a known disease present? Sometimes an arthritis is part of a known disease, e.g. haemophilia or diabetes.

Rheumatoid arthritis

Rheumatoid arthritis is a polyarthritis caused by inflammatory overgrowth of synovium known as pannus.

The earliest change is periarticular soft tissue swelling and osteoporosis. This osteoporosis is believed to be due to a combination of disuse and synovial hyperaemia. Destruction of the articular cartilage by pannus leads to joint space narrowing and to small bony erosions which occur, initially, at the joint margins (Fig. 12.3). These erosions are often seen first around the metatarso- or metacarpophalangeal joints, proximal interphalangeal joints and on the styloid process of the ulna. Later, extensive erosions may disrupt the joint surfaces. Ulnar deviation is usually present at this stage. With very severe destruction, the condition is referred to as arthritis mutilans (Fig. 12.4).

Similar changes are seen in the large joints (Fig. 12.5). In such cases, osteoarthritis may be superimposed on the rheumatoid arthritis and may dominate the picture.

With severe disease, there may be subluxation at the atlantoaxial joint (Fig. 12.6) due to laxity of the transverse ligament, which holds the odontoid peg against the anterior arch of the atlas. Atlantoaxial subluxation may only be demonstrable in a film taken with the neck flexed. Even though it is frequently asymptomatic, there is always the possibility of neurological symptoms from compression of the spinal cord by the odontoid process and it is important



Fig. 12.3 Early rheumatoid arthritis. Small erosions are present in the articular cortex (arrows) and there is soft tissue swelling around the proximal interphalangeal joints.



Fig. 12.4 Advanced rheumatoid arthritis (arthritis mutilans). There is extensive destruction of the articular cortex of the metacarpophalangeal joints with ulnar deviation of the fingers. Fusion of the carpal bones and wrist joint has occurred.



Fig. 12.5 Rheumatoid arthritis. Uniform loss of joint space is seen in this hip joint. Sclerosis is also present due to associated osteoarthritis.

to be aware of its existence if the patient is to have a general anaesthetic. Atlantoaxial instability can be well demonstrated with MRI.

Role of radiology in rheumatoid arthritis

Radiographs assist in the diagnosis of doubtful cases. To this end, the detection of erosions is extremely helpful. A widespread erosive arthropathy is almost diagnostic of

rheumatoid arthritis. Radiographs are also useful in assessing the extent of the disease and in observing the response to treatment.

Other erosive arthropathies

A number of other arthropathies, such as juvenile rheumatoid arthritis and the HLA-B27 spondyloarthropathies, which include psoriasis and Reiter's disease, produce articular erosions.



Fig. 12.6 Rheumatoid arthritis – atlantoaxial subluxation. C1 is displaced anteriorly upon C2. The distance between the arch of the atlas and the odontoid peg (arrow) is increased from the normal value (2mm) to 8mm. This is the same patient whose hand is illustrated in Fig. 12.4.



Fig. 12.7 Psoriatic arthropathy. There are extensive erosive changes affecting the interphalangeal joints but sparing the metacarpophalangeal joints.

Juvenile rheumatoid arthritis (Still's disease, juvenile chronic polyarthritis) shows many features similar to rheumatoid arthritis but erosions are less prominent. The knee, ankle and wrist are the joints most commonly affected. Hyperaemia from joint inflammation causes epiphyseal enlargement and premature fusion.

In *psoriasis*, there is an erosive arthropathy with predominant involvement of the terminal interphalangeal joints (Fig. 12.7).

Gout

In gout, the deposition of urate crystals in the joint and in the adjacent bone gives rise to an arthritis that most commonly affects the metatarsophalangeal joint of the big toe.

The earliest change is soft tissue swelling. At a later stage, erosions occur that, unlike rheumatoid arthritis, may be at a distance from the articular cortex. These erosions have a well-defined, often sclerotic, edge and frequently have overhanging edges (Fig. 12.8a). They are due to urate deposits in the bone. These deposits may be very large,

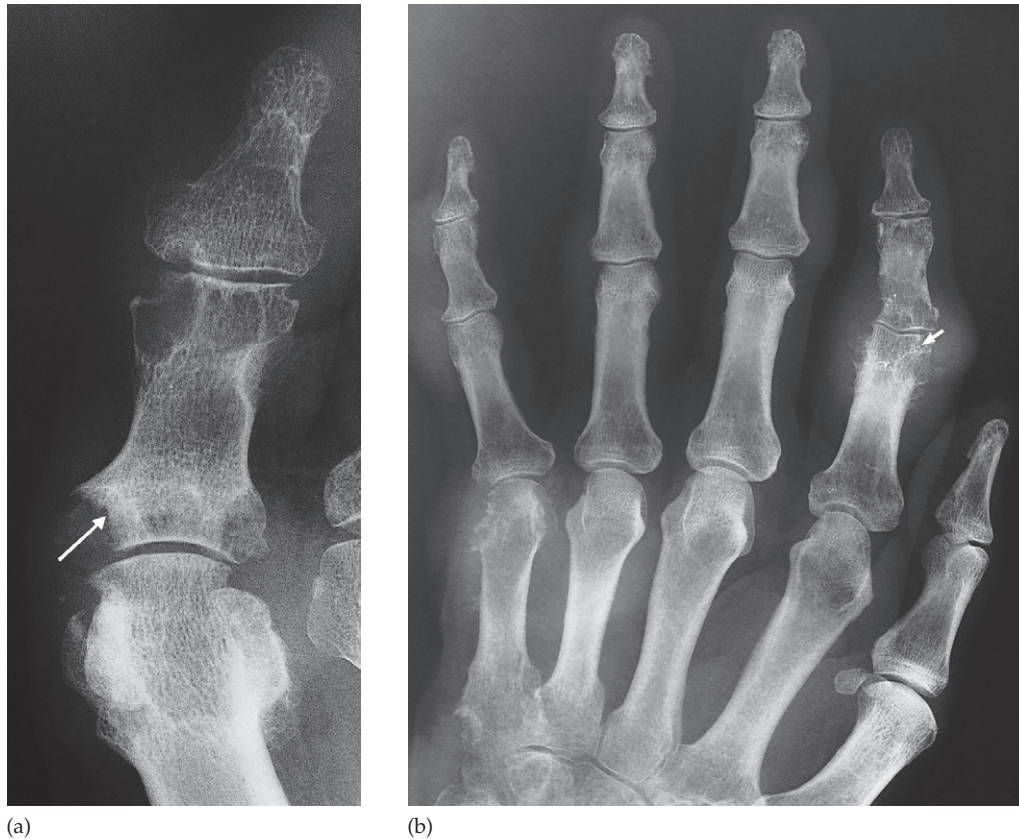


Fig. 12.8 Gout. (a) Erosion: there is a typical well-defined erosion with an overhanging edge (arrow) at the metatarsophalangeal joint of the big toe. (b) Tophi: these are large soft tissue swellings. A good example is seen around the proximal interphalangeal joint of the index finger. Several erosions are present (one is arrowed).

causing extensive bony destruction. There is usually no osteoporosis.

Localized soft tissue lumps caused by collections of sodium urate, known as tophi, may occur in the periarticular tissues (Fig. 12.8b). These swellings can be large and occasionally show calcification.

Calcium pyrophosphate dihydrate crystal deposition disease

In this condition there is deposition of calcium pyrophosphate dihydrate (CPPD) crystals in the joint manifested as chondrocalcinosis, which is a descriptive term for calcifica-

tion occurring in articular cartilage. In the knee, which is the most frequently affected joint, calcification may occur in the fibrocartilage of the menisci (Fig. 12.9) as well as the articular cartilage. CPPD disease may give rise to an arthritis clinically simulating gout, hence the alternative name 'pseudogout'. A severe arthritis resembling degenerative osteoarthritis may follow. Chondrocalcinosis is, however, often an incidental asymptomatic finding.

Osteoarthritis

Osteoarthritis is the commonest form of arthritis. It is due to degenerative changes resulting from wear and tear of the



Fig. 12.9 Chondrocalcinosis. Calcification can be seen in the menisci in the knee (arrows).

articular cartilage. The hip and knee are frequently involved but, despite being a weight-bearing joint, the ankle is infrequently affected. The wrist, joints of the hand and the metatarsophalangeal joint of the big toe are also frequently involved.

In osteoarthritis, a number of features can usually be seen (Fig. 12.10):

- *Joint space narrowing.* The loss of joint space is maximal in the weight-bearing portion of the joint; for example, in the hip it is often maximal in the superior part of the joint, whereas in the knee it is the medial compartment that usually narrows the most. Even when the joint space is very narrow it is usually possible to trace out the articular cortex.
- *Osteophytes* are bony spurs, often quite large, which occur at the articular margins.
- *Subchondral sclerosis* usually occurs on both sides of the joint; it is often worse on one side.

Table 12.1 Comparison of osteoarthritis and rheumatoid arthritis

Osteoarthritis	Rheumatoid arthritis
Joint space narrowing is maximal at weight-bearing sites	Joint space narrowing is uniform
Erosions do not occur but crumbling of the joint surfaces may mimic erosions	Erosions are a characteristic feature
Subchondral sclerosis and cysts may be seen	Not a feature but erosions <i>en face</i> may mimic cysts
Sclerosis is a prominent feature	Sclerosis is not a feature unless there is secondary osteoarthritis
No osteoporosis	Osteoporosis is often present

- *Subchondral cysts* may be seen beneath the articular cortex, often in association with subchondral sclerosis. Normally, the cysts are easily distinguished from an erosion as they are beneath the intact cortex and have a sclerotic rim but, occasionally, if there is crumbling of the joint surfaces, the differentiation becomes difficult.
- *Loose bodies* are discrete pieces of calcified cartilage or bone lying free within the joint, most frequently seen in the knee. It is important not to call the fabella, a sesamoid bone in the gastrocnemius, a loose body in the knee joint (see Fig. 12.1).

Osteoarthritis and rheumatoid arthritis are the two types of arthritis most commonly encountered. They show many distinguishing features, which are listed in Table 12.1.

Haemophilia and bleeding disorders

In haemophilia and Christmas disease, repeated haemorrhages into the joints result in soft tissue swelling, erosions and cysts in the subchondral bone (Fig. 12.11). The epiphyses may enlarge and fuse prematurely.

Joint infections

Joint infection is most often due to pyogenic bacterial infection or tuberculosis. Usually only one joint is affected. Synovial biopsy or examination of the joint fluid is necessary in order to identify the infecting organism.



(a)



(b)

Fig. 12.10 Advanced osteoarthritis. (a) Note the narrowed superior part of the joint space of the hip, subchondral sclerosis and cyst formation and osteophytes. (b) Similar changes are seen in the metatarsophalangeal joint of the big toe, which is known as hallux rigidus.



Fig. 12.11 Haemophilia. Subchondral cysts have formed, caused by repeated haemorrhages into the joint. Note the soft tissue swelling around the joint and the deep intercondylar notch – a characteristic feature of haemophilia.

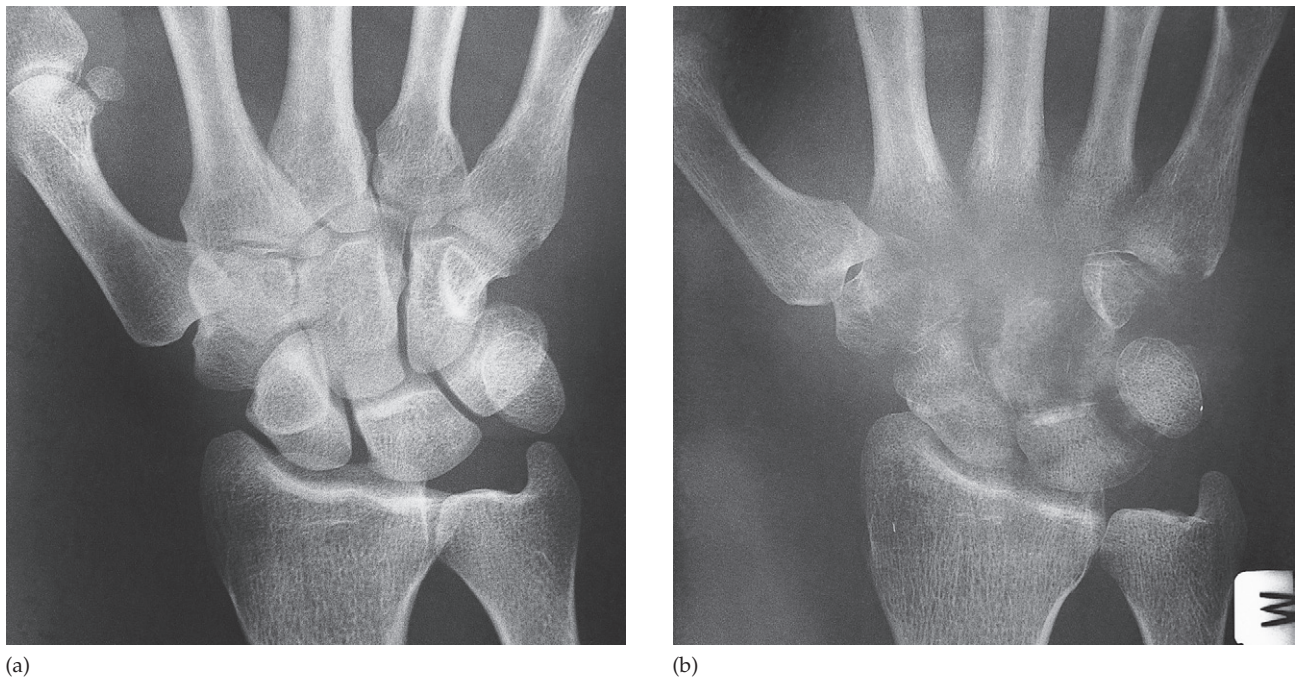


Fig. 12.12 Pyogenic arthritis. (a) The initial film of the wrist was normal. (b) Film taken 3 weeks later showing destruction of the carpal bones and bases of the metacarpals.

Pyogenic arthritis

In pyogenic arthritis, which is usually due to *Staphylococcus aureus*, there is rapid destruction of the articular cartilage followed by destruction of the subchondral bone (Fig. 12.12); a soft tissue swelling around the joint may be visible. A pyogenic arthritis may occasionally be due to spread of osteomyelitis from the metaphysis into the adjacent joint. A joint effusion is the earliest finding, and is readily detected with ultrasound, which can also be used to guide aspiration of the fluid. If the diagnosis is still in doubt then MRI is often performed.

Tuberculous arthritis

An early pathological change is the formation of pannus, which explains why tuberculous arthritis may be radiologically indistinguishable from rheumatoid arthritis. The hip and knee are the most commonly affected peripheral joints.

The features to look for are joint space narrowing and erosions, which may lead to extensive destruction of the articular cortex. A very important sign is a striking osteoporosis, which may be seen before any destructive changes are visible (Fig. 12.13).

At a late stage, there may be gross disorganization of the joint with calcified debris near the joint.

Avascular (aseptic) necrosis

Avascular necrosis, also known as osteonecrosis, is where there is death of bone due to interruption of the blood supply. It occurs most commonly in the intra-articular portions of bones and is associated with numerous underlying conditions (Box 12.2).

The plain radiographic features of avascular necrosis are increased density of the subchondral bone with irregularity of the articular contour or even fragmentation of the bone (Fig. 12.14). A characteristic crescentic lucent line may be

seen just beneath the articular cortex. The cartilage space is preserved until secondary degenerative changes supervene. MRI has now become the imaging modality of choice for demonstrating avascular necrosis and may show changes at a time when the radiographs may be normal. The appearances at MRI depend on the stage of disease, but the typical site of involvement and signal pattern allows a specific diagnosis to be made (Fig. 12.15).

Box 12.2 Causes of avascular necrosis

- Steroid therapy
- Collagen vascular diseases
- Radiation therapy
- Sick cell anaemia
- Exposure to high pressure environments, e.g. tunnel workers and deep-sea divers (caisson disease)
- Fractures



Fig. 12.13 Tuberculous arthritis of the shoulder. Note the striking osteoporosis and erosion of the humeral head.

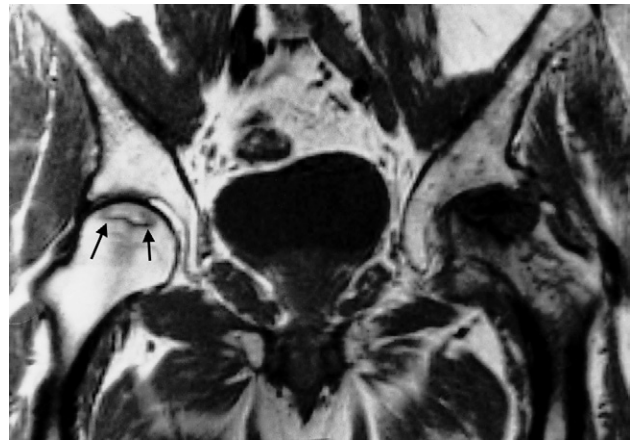


Fig. 12.15 Coronal MRI scan showing avascular necrosis of both femoral heads. The changes on the left are very severe and advanced. The changes in the right hip are relatively early and show a rim of low signal demarcating the ischaemic area (arrows).



Fig. 12.14 Avascular necrosis. There is fragmentation with some sclerosis of both femoral heads.



Fig. 12.16 Post-traumatic avascular necrosis. A pin has been inserted because of a subcapital fracture of the femoral neck (arrow), which occurred 10 months before this film was taken. Avascular necrosis has occurred in the head of the femur, which has become sclerotic.

After a *fracture*, the blood supply may become interrupted and avascular necrosis may then supervene, particularly in subcapital fractures of the femoral neck (Fig. 12.16) and fractures through the waist of the scaphoid. The femoral head and proximal pole of the scaphoid become fragmented and dense due to the ischaemia (Fig. 12.17).

Osteochondritis

There is also a group of conditions, some of which are called osteochondritis, in which no associated cause for avascular necrosis can be found. The osteochondrites are now regarded as being due to impaired blood supply associated with repeated trauma.

Perthe's disease, an avascular necrosis of the femoral head in children, is the most important example. The earliest plain radiographic change is an increase in density and

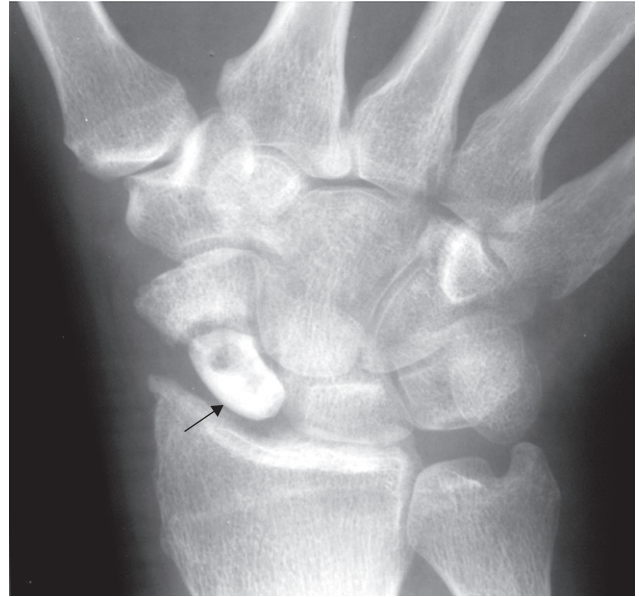


Fig. 12.17 Post-traumatic avascular necrosis. The ununited scaphoid fracture shows a sclerotic proximal pole (arrow) due to avascular necrosis of this part of the bone.

flattening of the femoral epiphysis which later may progress to collapse and fragmentation (Fig. 12.18). The epiphysis may widen and, in consequence, the femoral neck enlarges and may contain small cysts. The joint space is widened but the acetabulum is not affected. With healing, the femoral head reforms but may remain permanently flattened and, therefore, be responsible for osteoarthritis in later life.

Other forms of avascular necrosis are: *Freiberg's disease*, which affects the metatarsal heads; *Kohler's disease*, which affects the navicular bone of the foot; *Osgood-Schlatter disease* of the tibial tuberosity; and *Kienböck's disease* of lunate bone in the wrist.

Osteochondritis dissecans is thought to be a localized form of avascular necrosis. A small fragment of bone becomes separated from the articular surface of a joint leaving a defect, and the bony fragment can often be detected lying free within the joint. It occurs most frequently in the knee and ankle. The diagnosis can be established with plain film radiography (Fig. 12.19). Computed tomography (CT) and MRI are excellent imaging methods to diagnose small



Fig. 12.18 Perthe's disease. The right femoral epiphysis (arrow) in this child is sclerotic and flattened. Compare it with the normal left side.

lesions or osteochondritis dissecans in portions of the articular bone that are difficult to see in standard plain film projections.

Internal derangement of the knee

Most knee injuries produce soft tissue damage, notably meniscal or ligamentous tears, either alone or in conjunction with bony fracture. Plain film examination can only demonstrate the state of the bones and show an effusion. MRI is the best imaging modality for detecting internal derangement, with some investigators believing that MRI is more accurate than arthroscopy.

Menisci

The menisci, which are composed of fibrocartilage, are well demonstrated on MRI as they have a different signal intensity from the hyaline cartilage covering the adjacent femoral condyles and tibial plateau. The normal menisci are of uniform low signal on all sequences and have the appearance on sagittal images described as a 'bow tie'. A meniscal tear (Fig. 12.20) can be recognized as a break in the meniscus disrupting the articular surface and allowing synovial fluid, which has a higher signal intensity, to enter the substance of the meniscus. Meniscal high signal not disrupting the articular surface are caused by intrasubstance degeneration as a result of wear and tear due to ageing.

Some surgeons proceed directly to arthroscopy in patients with clear-cut clinical features of internal derangement, reserving MRI for those patients with suspicious but

not definite clinical signs or symptoms, although many surgeons prefer to have preliminary MRI. MRI can show bone bruises and other pathology adjacent to, but not within, the joint, entities that cannot be diagnosed at arthroscopy. MRI can also, on occasion, show meniscal tears not seen at arthroscopy.

Cruciate ligaments

The anterior cruciate ligament is seen as a low signal linear structure in the intercondylar notch. A torn ligament may either not be visible or a disruption of the ligament may be identified (Fig. 12.21). Partial tears may be seen as high signal within the ligament. Demonstration of the posterior cruciate ligament is not so important as these are rarely repaired even if torn.

Collateral ligaments

The medial and lateral collateral ligaments are of low signal on all sequences, and damage to the ligaments can be recognized by high signal in or around the ligaments.

Shoulder and rotator cuff disorders

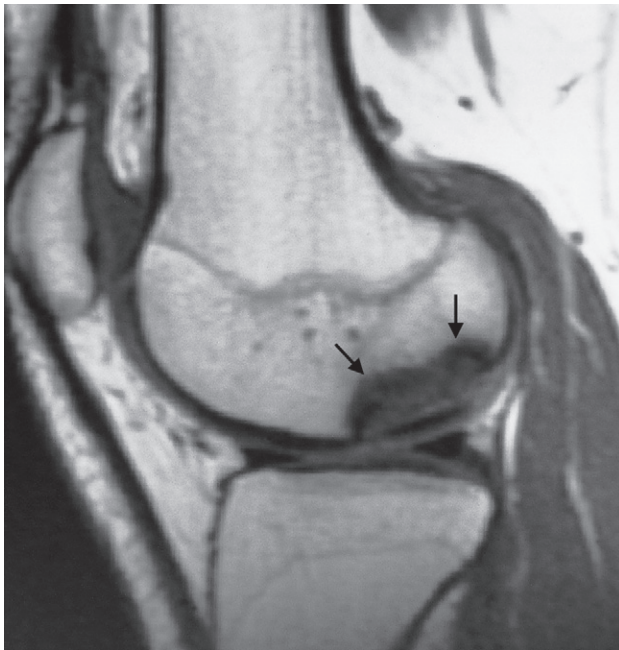
The rotator cuff of the shoulder consists of the supraspinatus, infraspinatus, teres minor and subscapularis muscles together with their tendons, and they provide dynamic stability of the glenohumeral joint allowing the shoulder to perform a wide range of movements.



(a)



(b)



(c)

Fig. 12.19 Osteochondritis dissecans. (a) A fragment (arrow) has become separated from the articular cortex of the medial femoral condyle. (b) Coronal CT scan through an ankle showing a small osteochondritis dissecans fragment (horizontal arrow) separated from the rest of the talus with a well-corticated defect in the underlying bone (vertical arrow). (c) MRI scan of the knee showing an osteochondritis defect (arrows) of the medial femoral condyle.

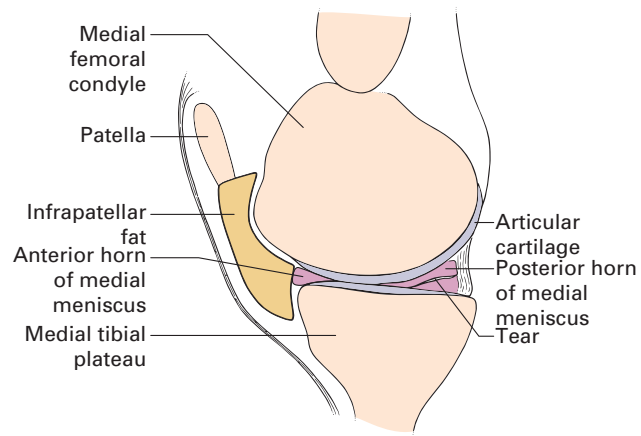


Fig. 12.20 Tear of the medial meniscus. Sagittal MRI through the medial part of the knee joint showing a tear in the posterior horn of the medial meniscus. The anterior horn appears normal.

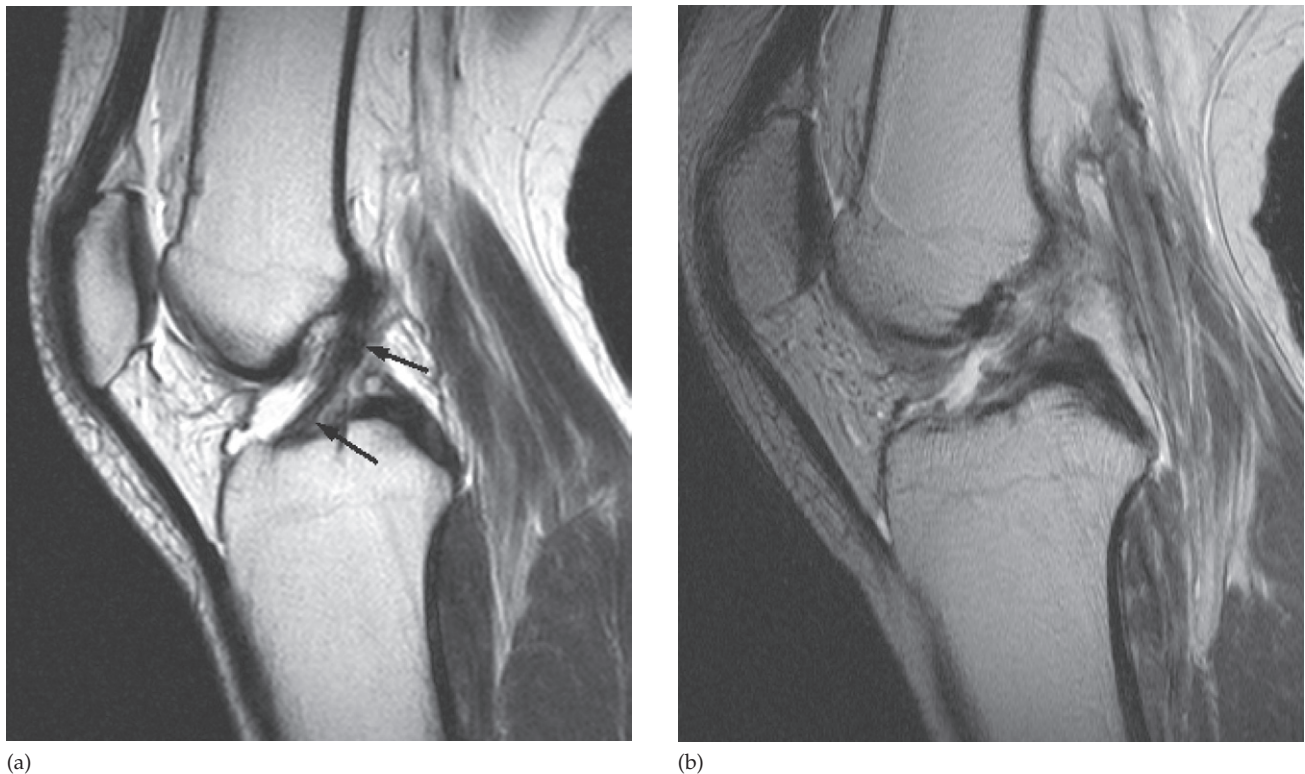


Fig. 12.21 (a) Normal anterior cruciate ligament is shown as a low signal band in the intercondylar notch (arrows) on this MRI scan. (b) With a tear the ligament is disrupted.

Supraspinatus tendon tears

Of the four muscles, the supraspinatus is the one that most commonly causes significant clinical problems. Tears of the supraspinatus tendon are thought to be due to impingement between the acromium and greater tuberosity of the humerus, and can lead to acute or chronic symptoms. MRI and/or ultrasound (Fig. 12.22) can be useful in selected patients when corrective surgery is being considered. On MRI, the normal low signal of the supraspinatus tendon is interrupted by the higher signal of fluid, and in complete tears it may be possible to see the retracted ends of the torn tendon-muscle junction (Fig. 12.23). The added advantage of ultrasound is that subtle tears that are not visualized in MRI are better detected on ultrasound and impingement may be demonstrated due to the dynamic nature of the procedure.

Tears of the supraspinatus tendon may be associated with tears or detachment of the glenoid labrum, which is a fibrocartilaginous ring surrounding the glenoid of the scapula.

Calcific tendonitis

Calcification occurs in the periarticular regions and is most commonly seen in the shoulder, in the supraspinatus tendon, as amorphous calcification adjacent to the greater tuberosity of the humerus (Fig. 12.24). This may be demonstrated on ultrasound of the shoulder and may also be treated by sonographically guided needle injection of local anaesthetic into the region of the calcium deposit followed by flushing and aspiration. Currently, platelet-rich plasma injections are used in some centres to treat tendon calcification.

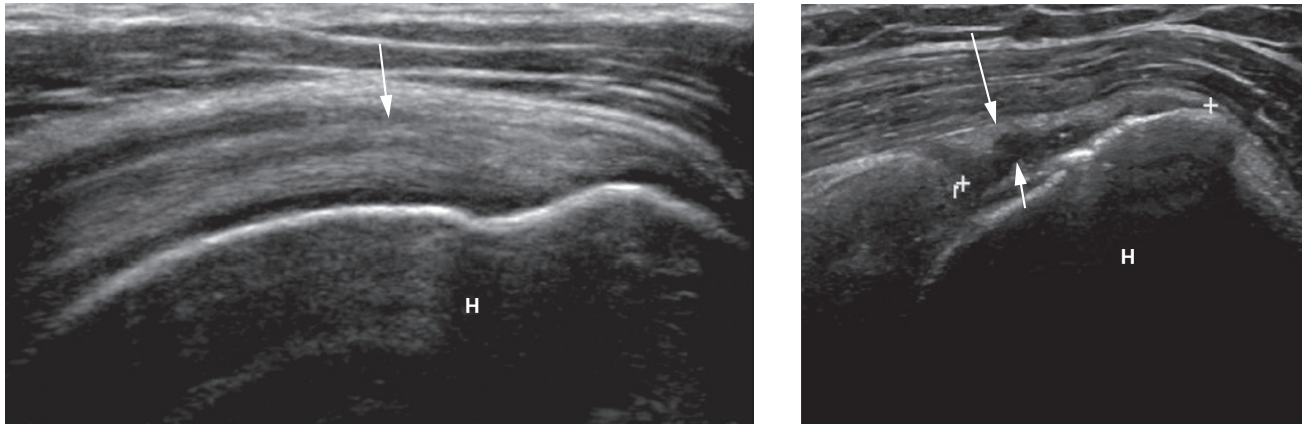


Fig. 12.22 Ultrasound of the supraspinatus tendon. (a) Normal tendon (arrow) demonstrated at the level of insertion into the greater tuberosity of humerus (H). (b) The supraspinatus tendon is thin (long arrow) and there is a tear (short arrow) shown as low echogenicity, between the two caliper crosses. H, head of humerus.

Miscellaneous joint conditions

Neuropathic joint

Changes are seen in the feet of patients with diabetes with peripheral neuropathy. The predominant feature is resorption of the bone ends, and calcification of the arteries in the feet is often present. There may also be bone destruction due to infection (Fig. 12.25). Diagnosing osteomyelitis in the bones of the feet in patients with diabetes can be difficult because bone destruction can be due to neuropathy or infection, or to a combination of the two.

Synovial sarcoma (synovioma)

This tumour appears as a soft tissue mass adjacent to a joint. Bone destruction on one or both sides of the joint occurs at a later stage. The soft tissue mass may contain visible calcification. The diagnosis is most readily made by MRI, which can demonstrate the full extent of the soft tissue mass.

Slipped femoral epiphysis

Slipped femoral epiphysis occurs between the ages of 9 and 17 years, and may present with pain in the hip or pain

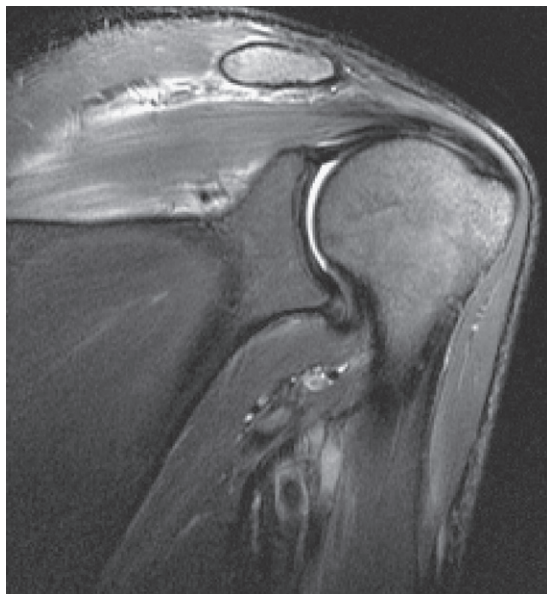
referred to the knee. The epiphysis slips posteriorly from its normal position: this is best appreciated on a lateral film of the hip (Fig. 12.26). With a greater degree of slip, the condition can be recognized on the frontal view as a downward displacement of the epiphysis.

The films of the hip must be very carefully evaluated if the diagnosis is suspected clinically, because the diagnosis is easy to miss in the early stage at a time when further slip can be prevented surgically.

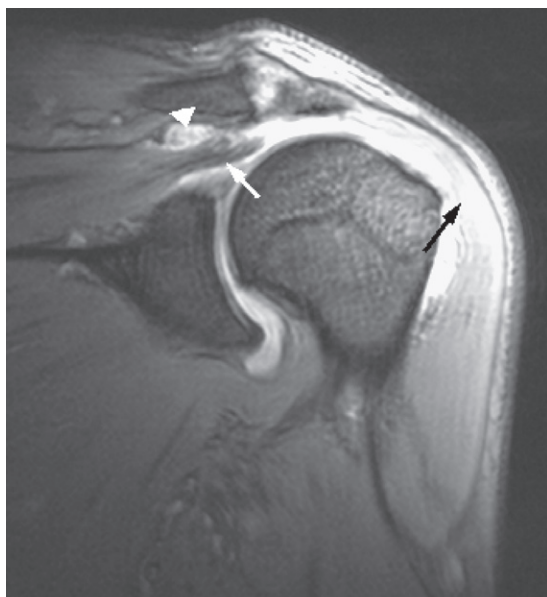
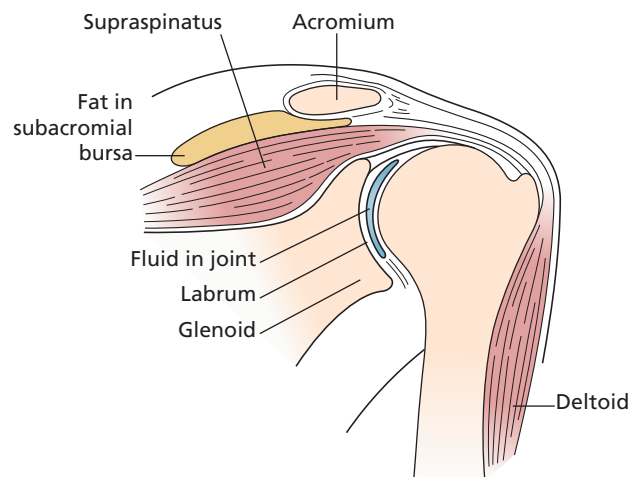
Developmental dysplasia of the hip

Ultrasound has now replaced x-rays for detecting dislocation or subluxation of the hip in the infant in whom clinical examination is suspicious but not diagnostic. Ultrasound allows visualization of cartilagenous structures that are not seen on x-ray films, so the relationship of the cartilagenous femoral head and acetabulum can be determined.

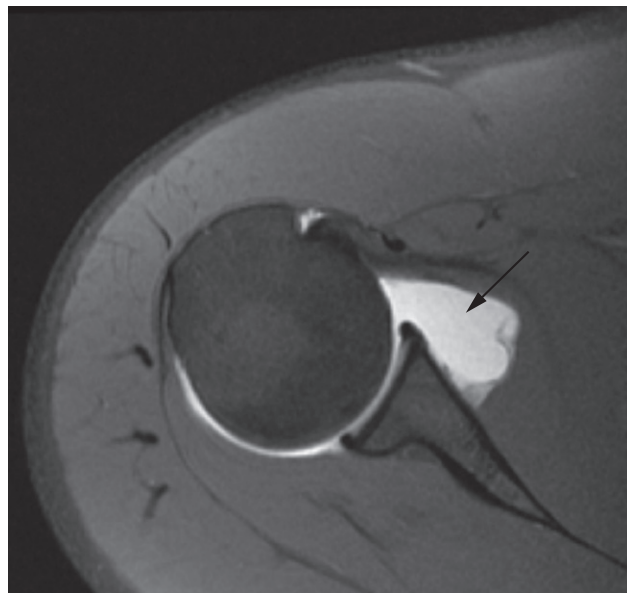
Later in life, the condition is easier to diagnose on plain radiographs, but fortunately such cases are now rare, as the condition is usually treated in the neonatal period, the diagnosis having been made clinically. The features to look for are lateral and upper displacement of the head of the femur (Fig. 12.27). Increased slope to the acetabular roof is sometimes present.



(a)

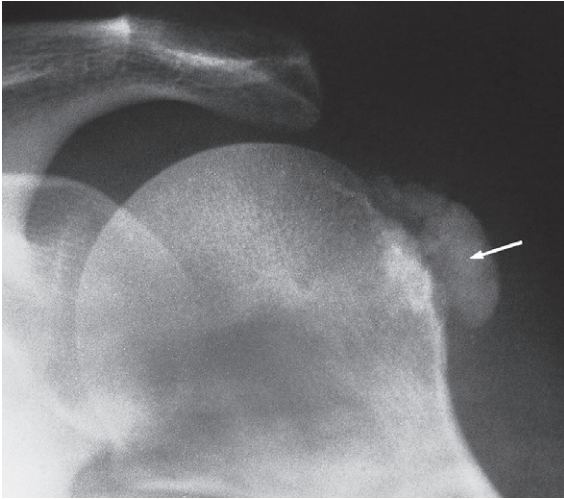


(b)

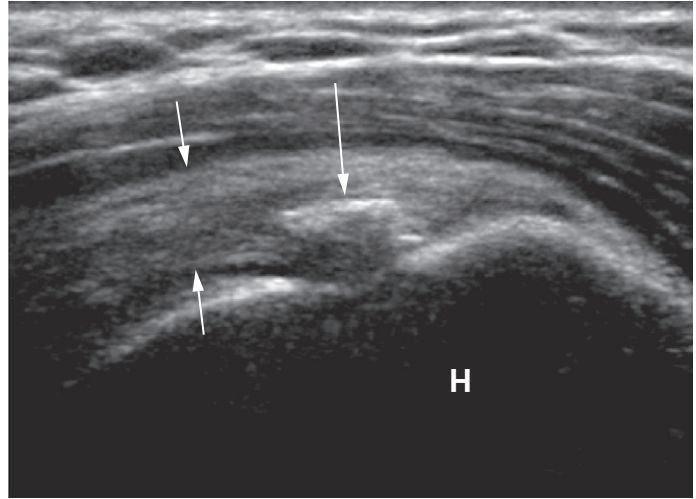


(c)

Fig. 12.23 (a) Normal shoulder MRI showing the supraspinatus tendon inserting into the greater tuberosity of the humerus. (b) Supraspinatus tendon tear. MRI showing complete disruption of the supraspinatus tendon (white arrow) with fluid in the subacromial bursa (arrowhead) and oedema of the adjacent deltoid muscle (black arrow). (c) MRI arthrogram demonstrating the high signal intensity of gadolinium injected into the joint space (arrow).



(a)



(b)

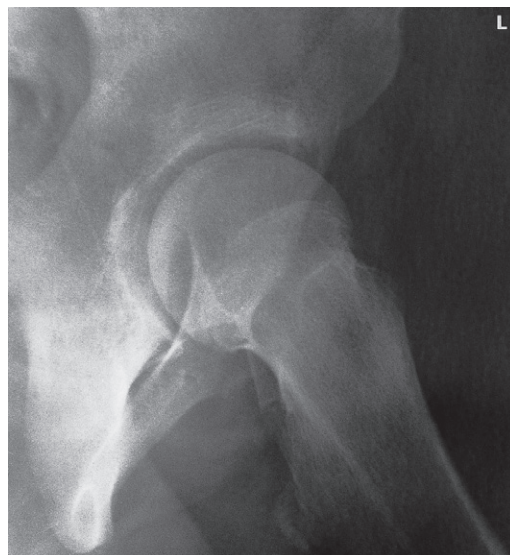
Fig. 12.24 (a) Supraspinatus tendinitis. Calcification is present in the supraspinatus tendon (arrow). (b) Ultrasound image demonstrates focal calcification (long arrow) near the insertion of the supraspinatus tendon (which is shown between the two short arrows). H, head of humerus.



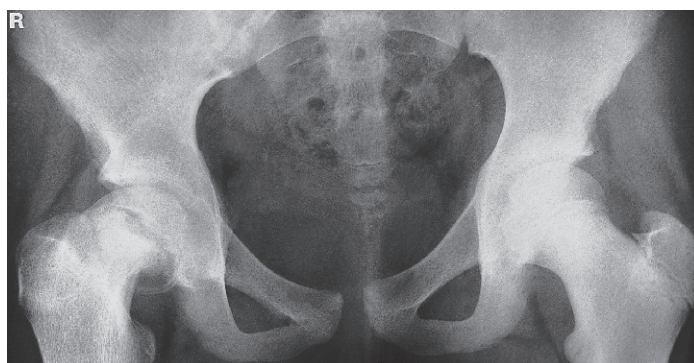
Fig. 12.25 Diabetic foot. There is resorption of the heads of the second and third metatarsals and bases of the proximal phalanges causing disorganization of the metatarsophalangeal joints. The patient had a peripheral neuropathy with an anaesthetic foot.



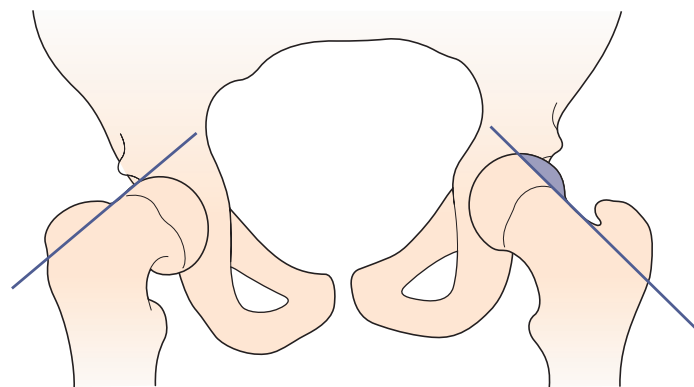
(a)



(b)



(c)



(d) Slipped capital epiphysis

Normal

Fig. 12.26 Slipped femoral epiphysis. (a, b) Lateral views of the hips showing the right femoral epiphysis displaced posteriorly (compare with the normal left side). (c) Frontal view of the same patient showing the right femoral epiphysis displaced downwards. (d) A line drawn along the lateral border of the femoral neck normally intersects a portion of the capital epiphysis whereas this does not occur on the side with slip.

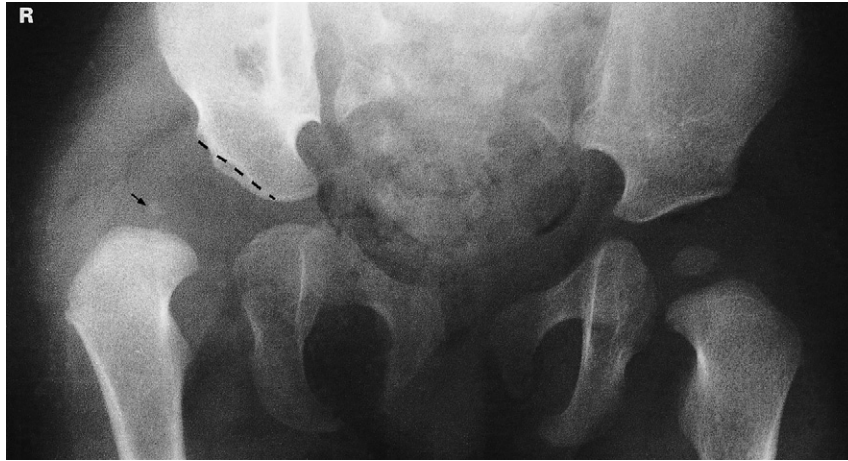


Fig. 12.27 Developmental dysplasia of the right hip. The right femoral epiphysis (arrow) is smaller than on the normal left side and it does not lie within the acetabulum. Note the sloping roof of the right acetabulum (dashed line).



Fig. 12.28 Osteitis condensans ilii, anteroposterior view. Sclerosis is seen in both iliac bones just adjacent to the sacroiliac joints. The joints themselves, however, are normal. The patient was a young woman who had borne children.



Fig. 12.29 Scleroderma. Extensive soft tissue calcification is present as well as atrophy of soft tissues at the ends of the fingers.

Osteitis condensans ilii

Osteitis condensans ilii occurs almost exclusively in women who have borne children. The condition is thought to be a stress phenomenon associated with childbearing and is usually asymptomatic. There is a zone of sclerosis on the iliac side of the sacroiliac joints, but the sacroiliac joints themselves are normal (Fig. 12.28).

Scleroderma

Scleroderma may cause calcification and atrophy of soft tissues of the hands with loss of the tips of the terminal phalanges (Fig. 12.29).

13

Spine

Imaging techniques

Magnetic resonance imaging (MRI) is the gold standard imaging method of the spine as it is able to visualize the spinal cord, nerve roots and intervertebral discs, which are invisible on plain films and poorly seen on computed tomography (CT). It is therefore the preferred examination for most degenerative, inflammatory and malignant conditions of the spine, cord or nerve roots. Plain films do have a role in spinal disorders, particularly in trauma, although their use in simple back pain is questionable. CT will show the bony anatomy in greater detail than radiographs and is therefore useful in trauma, bone tumours and for operative planning.

Myelography, which entails radiographs following the injection of contrast into the subarachnoid space by lumbar puncture to opacify the cerebrospinal fluid (CSF) and visualize the cord and nerve roots, has now been replaced by MRI. However, it can be useful if combined with a CT scan following the intraspinal contrast injection as it produces high resolution images in patients who have contraindications for MRI or contain metallic spinal prostheses which would cause significant magnetic resonance artefact. Other imaging methods for examining the spine are *radionuclide bone scans*, which are particularly useful for the detection of bony metastases or recent fractures and can be combined with CT (single photon emission computed tomography or SPECT) for improved spatial resolution.

The detailed bone anatomy of the vertebrae differs slightly in the cervical, thoracic and lumbar regions, but the general components are similar, as illustrated in Fig. 13.1

and corresponding radiographs in Fig. 13.2. Anteriorly, there is a cylindrical vertebral body and posteriorly a bony ring (neural arch) surrounding the spinal canal formed by the pedicles and laminae. Where the pedicles and laminae meet, the transverse processes project laterally and contain the vertebral arteries in the cervical spine and articulate with ribs in the thoracic spine. Where the laminae meet in the midline posteriorly, the spinous process extends posteriorly and often inferiorly. There are several joints at each intervertebral level which contribute to the stability of the spine. Anteriorly, between each vertebral body is the intervertebral disc and, in the cervical spine only, horn-like projections extend from the lateral vertebral bodies to form the uncovertebral joints. Articular processes extend superiorly and inferiorly from the junction of the pedicles and laminae to form the apophyseal or facet joints with the bone between the processes called the pars interarticularis. For each vertebral body, the superior facet surface is directed dorsally and the inferior facet surface is directed ventrally, which together make up a facet joint. The C1 (atlas) and C2 (axis) vertebral bodies are different in morphology, with the ring-like C1 supporting the skull and articulating with a post of bone (dens) that extends superiorly from C2.

The appearances of a normal spine on MRI are illustrated in Fig. 13.3a–c. On both T1- and T2-weighted sequences, the signal from normal vertebrae is bright due to the fat content of bone marrow. Vertebral marrow should be of higher signal than the disc on a T1-weighted sequence otherwise it could indicate marrow replacement such as by metastatic disease (Fig. 13.3d). The intervertebral disc is

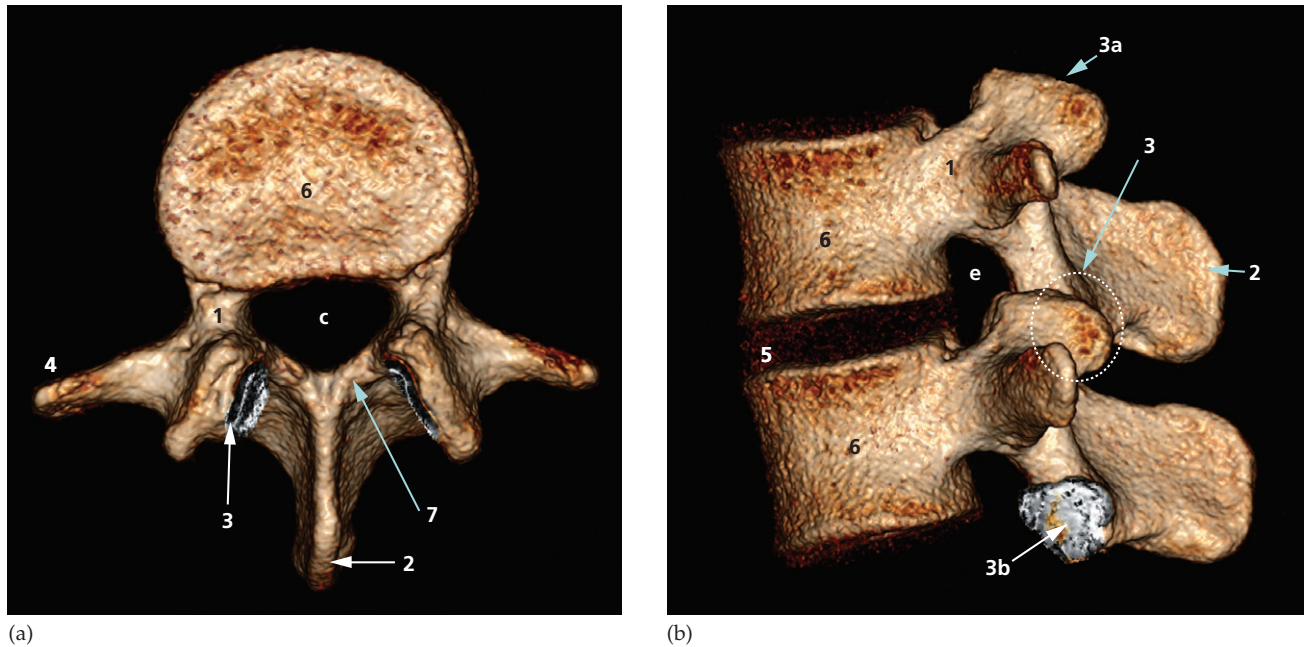


Fig. 13.1 Normal vertebral anatomy. Surface-shaded CT reconstructions of lumbar vertebrae in (a) axial and (b) sagittal views. 1, pedicles; 2, spinous process; 3, facet joint made up of superior (3a) and inferior (3b) articular facets; 4, transverse process; 5, disc space; 6, vertebral body; 7, lamina; c, central canal; e, exit foramen.

composed of three main parts: the annulus fibrosus, which surrounds the central nucleus pulposus, and the cartilaginous endplates. On a T2-weighted scan, the CSF is of high signal with the spinal cord and nerve roots seen to pass to the exit foramina. The spinal cord extends from the cervicomedullary junction at the foramen magnum, and tapers inferiorly to become the conus medularis, which should be located no lower than the inferior border of L2. Extending inferiorly from the conus are the lumbar and sacral nerve roots which make up the cauda equina.

At each level in the cervical region (C3–C7), the anterior and posterior roots extend laterally from the cord and pass into the anterolateral-orientated exit foramina and are named according to the pedicle they pass over (i.e. the C5 nerve exits the spine through the C4/C5 intervertebral foramen). Due to the presence of C8 nerves, beyond C7/T1 the nerves are named according to the pedicle they pass under (i.e. the T4 nerve exits the spine through the T4/T5

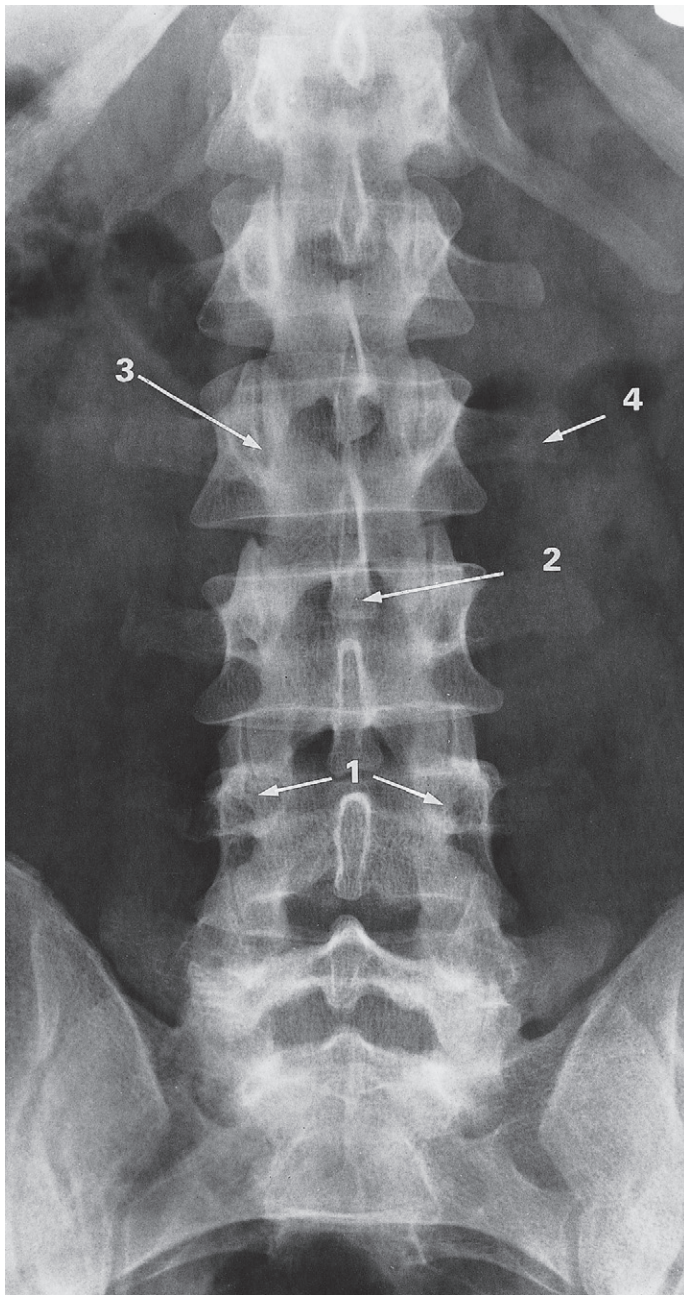
exit foramen). In the lumbar spine, the nerve roots run in the lateral recess of the lumbar canal across a disc level before exiting under the corresponding pedicle.

Radiographic signs of spinal abnormality

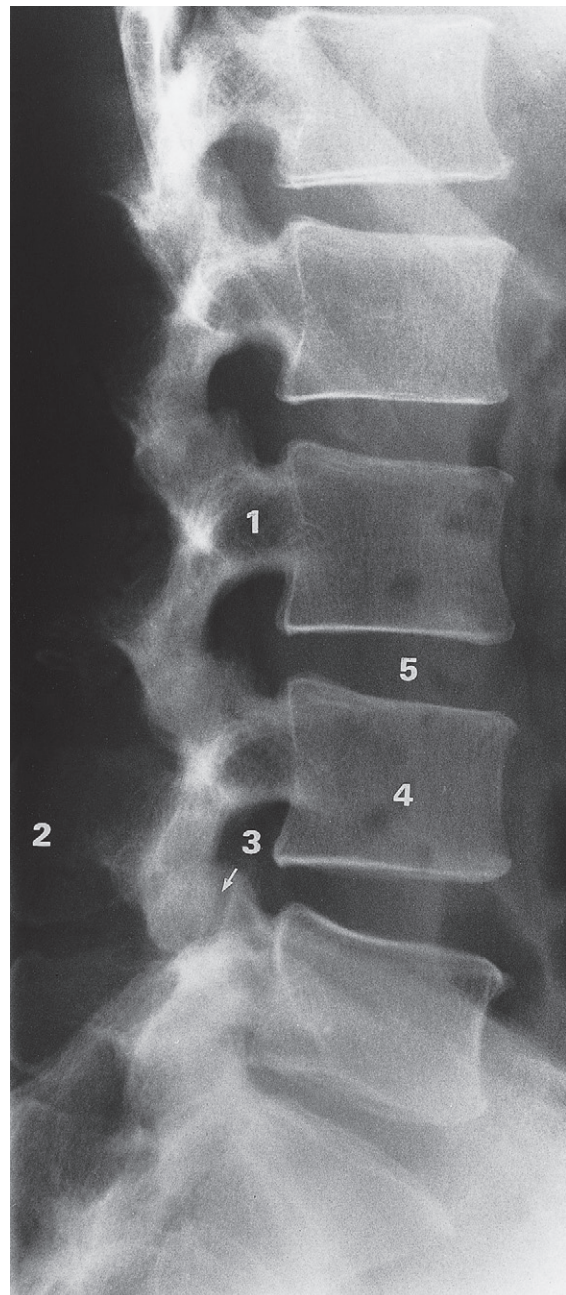
There are some abnormalities detected on plain radiographs that often permit a diagnosis to be made, although other imaging will often be required for confirmation.

Disc space narrowing

Normally, the disc spaces are the same height at all levels in the cervical and thoracic spine. In the lumbar spine, the disc spaces increase slightly in height going down the spine. A reduction in intervertebral height usually implies degenerative disc disease and may be associated with endplate sclerosis and osteophytes around the endplate



(a)



(b)

Fig. 13.2 Plain films of normal lumbar spine. (a) Frontal view. 1, pedicles; 2, spinous process; 3, facet joint; 4, transverse process. (b) Lateral view. 1, pedicles; 2, spinous process; 3, facet joint; 4, vertebral body; 5, disc space. Note how the height of the disc spaces increases from L1 to L5 with the exception of the L5/S1 disc space which is normally narrower than the one above.

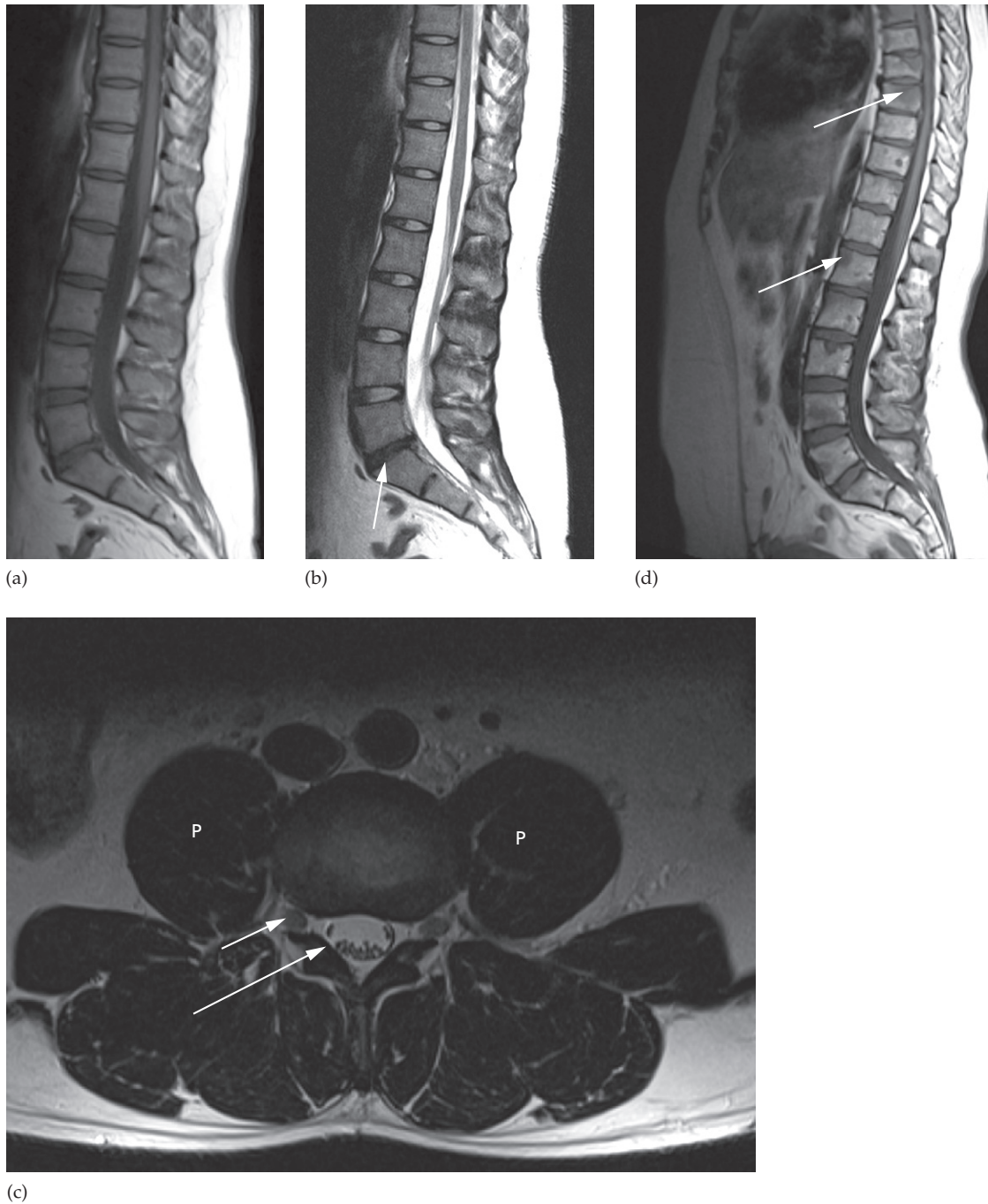


Fig. 13.3 MRI of the lumbar spine. (a) Normal T1-weighted scan. The discs and spinal cord are of intermediate signal. (b) Normal T2-weighted scan. The discs and CSF appear as high signal. The L5/S1 disc has lost height and is reduced in signal compared to the other discs, in keeping with degenerative changes (arrow). (c) Axial T2-weighted scan through the L3/L4 disc space. At this level, the L3 nerve roots are in the exit foramina (short arrow) and the L4 nerve roots have moved to the edge of the dural sac (long arrow) in the lateral recesses prior to exiting the spinal canal at the level below. p, psoas muscle. (d) Sagittal T1-weighted scan showing focal areas of low signal within multiple vertebral bodies (some marked with arrows) due to metastatic breast cancer.

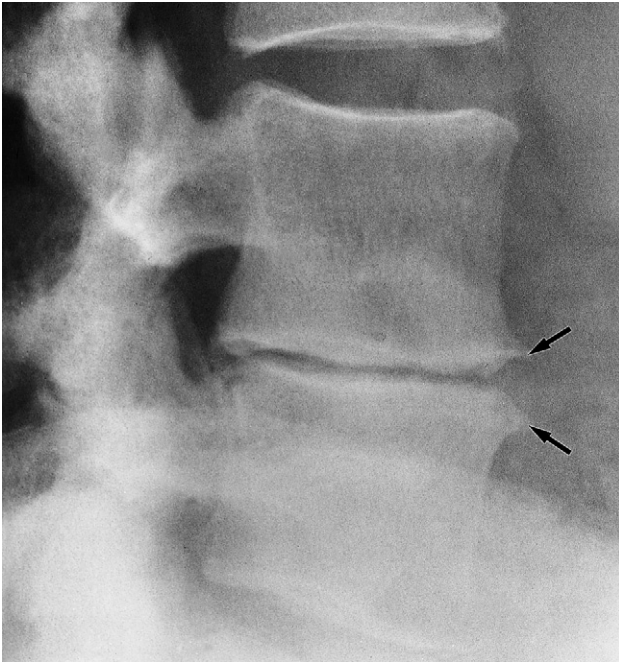


Fig. 13.4 Disc space narrowing caused by disc degenerative changes between L3 and L4. Note the osteophytes (arrows) and sclerosis of the adjoining surfaces of the vertebral bodies.

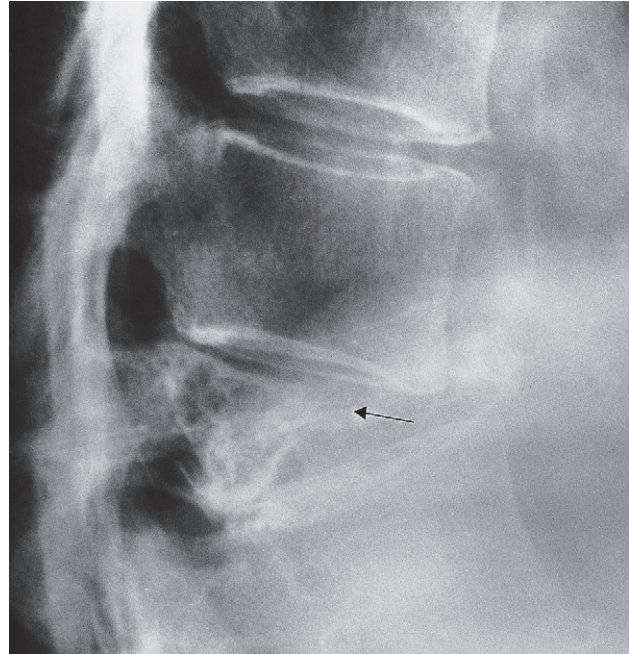
margins (Fig. 13.4). A reduction in intervertebral space associated with poor visualization of the endplates may be seen in disc space infection.

Collapse of vertebral bodies

A collapsed vertebral body is one that has lost height. This could be a normal bone subjected to abnormal stress such as in trauma or an abnormal weakened bone subjected to normal stress such as in metastases or myeloma. If any collapse is present, it is essential to look at the adjacent disc to see if it is narrowed, to check if part of any pedicle or cortical margin is destroyed and to assess the posterior vertebral wall to ensure that there is no compromise of the central spinal canal containing the cord or cauda equina.

Causes of vertebral collapse (Box 13.1) include:

- *Metastases and myeloma.* Bone destruction, or replacement of normal marrow by a lytic tumour, may be visible.



(a)

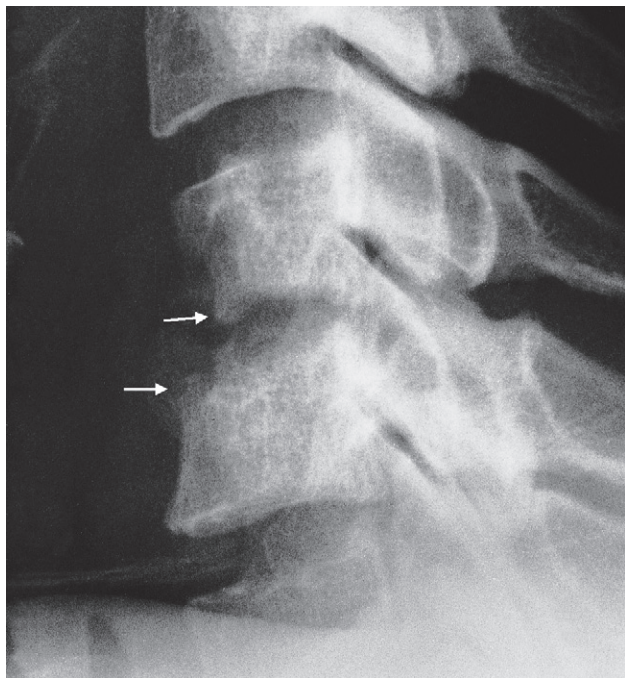
Fig. 13.5 Collapsed vertebra. (a) Metastasis (arrow) causing complete collapse of the vertebral body. The adjacent vertebral discs are unaffected. (Continued on following page)

(b) Osteomyelitis. The disc space is narrowed and there is destruction of the surfaces of the adjacent vertebral bodies (arrows). (c) Traumatic collapse. Note the concave superior surface of the collapsed vertebral body. Some fragments have been extruded anteriorly (arrow). (d) Osteoporotic collapse. There is decreased bone density with a collapse of a vertebral body due to a compression fracture. (e) Collapse due to eosinophil granuloma. In this child the vertebral body is so collapsed that it resembles a thin disc (arrow).

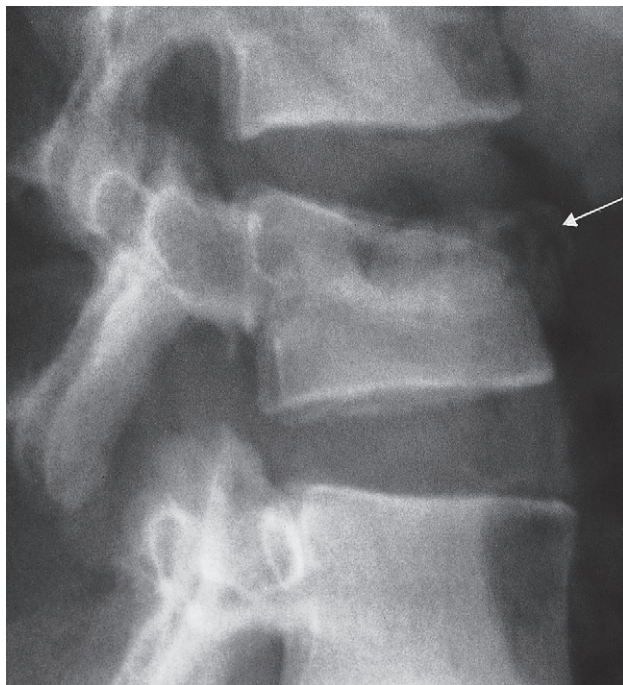
Box 13.1 Causes of collapsed vertebral bodies

- Neoplasm (metastases and myeloma)
- Osteoporosis
- Trauma
- Infection
- Eosinophilic granuloma

The pedicles are a good place to look for evidence of bone destruction on plain film examination. The disc spaces are usually normal (Fig. 13.5a).



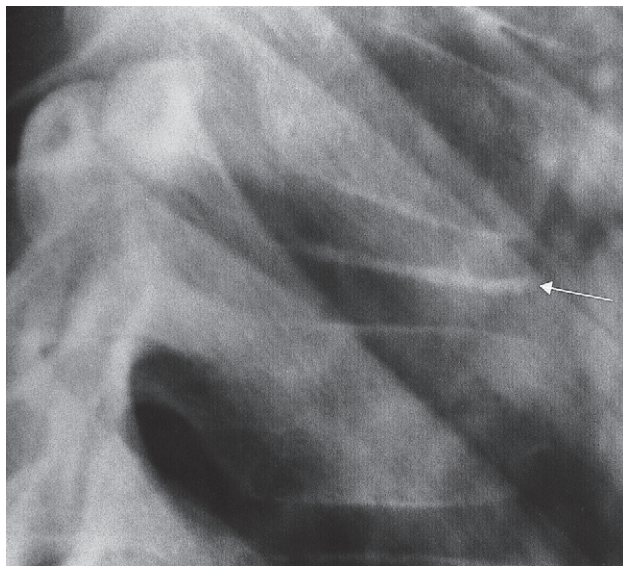
(b)



(c)



(d)



(e)

Fig. 13.5 *Continued*

- *Infection.* The adjacent disc space is nearly always narrow or obliterated. There may be bone destruction next to the affected disc but the pedicles are usually intact (Fig. 13.5b).
- *Osteoporosis.* There is generalized reduction in bone density leading to compression fractures. The disc spaces are normal or even slightly increased in height and the pedicles are intact (Fig. 13.5d).
- *Trauma.* A compression fracture is commonly due to hyperflexion of the spine, causing the vertebral body to become wedge-shaped (Fig. 13.5c, d). The discs are normal but may be impacted into the fractured bone. Associated fractures may be seen in the pedicles or neural arch, but otherwise the bone and discs are normal.
- *Eosinophil granuloma.* Complete collapse of one or more vertebral bodies may occur in children or young adults with a solitary site of Langerhans' cell histiocytosis (eosinophil granuloma). The vertebral body is flattened and sometimes referred to as a 'vertebra plana' (Fig. 13.5e).

Pedicle abnormalities

On plain films, the pedicles are best assessed in the frontal view and are very well demonstrated on CT scans. Destruction or sclerosis of one or more of the pedicles (Fig. 13.6, and see Fig. 13.29b) is a sign of spinal metastases.

Dense vertebrae

Sclerosis, which is demonstrated on plain films or CT, may affect just one vertebra or may be part of a generalized process involving many bones. Common causes (Box 13.2) include the following:

- *Metastases*, particularly from primary tumours of the prostate or breast (Fig. 13.7).
- *Malignant lymphoma.*
- *Paget's disease.* This may be difficult to distinguish from neoplastic disease, but a useful diagnostic feature is expansion of the overall size of the vertebra with coarsening of the trabecular pattern in Paget's disease (Fig. 13.8).
- *Haemangioma*, a benign vascular abnormality that gives rise to characteristic vertical striations in a vertebra that is normal in size (Fig. 13.9).

Spinal abnormalities

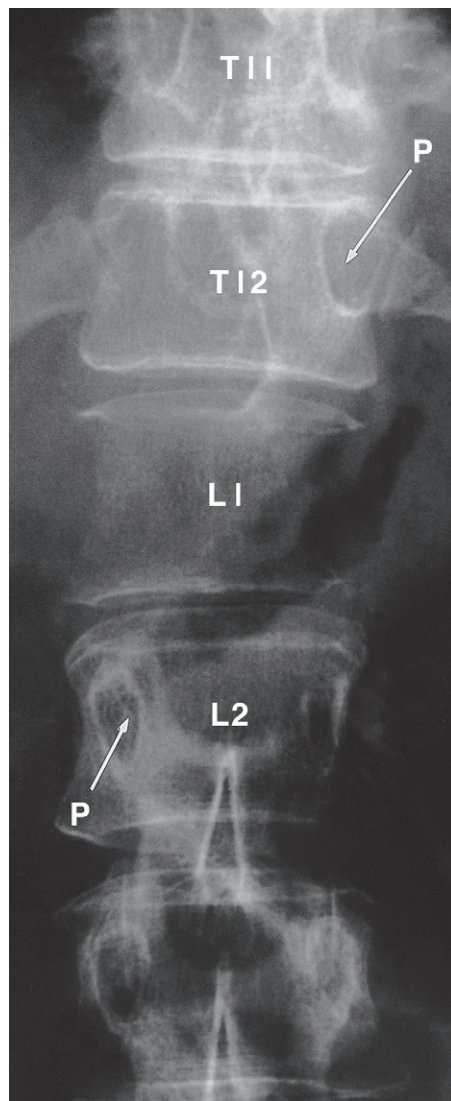
Spinal trauma

Cervical spine injuries are important to identify as significant neurological damage can occur if an unstable injury is unrecognized. Plain films are the commonest initial investigation for trauma to the spine and will usually comprise a lateral, anteroposterior and open mouth or peg view (Fig. 13.10). The following should be looked for:

- Alignment of the vertebral bodies and facet joints.
- Fractures of the vertebral bodies, pedicles, laminae and spinous processes.
- Indirect signs of fracture such as prevertebral soft tissue swelling.

It is important that the entire cervical spine from the craniocervical to the cervicothoracic junction has been imaged otherwise a low unstable injury may be missed. Adequate imaging of the C7/T1 junction on the lateral film may be facilitated by gentle traction on the arms to depress the shoulders or by obtaining a view through the axilla (swimmer's view). However, it may remain difficult to obtain satisfactory films, particularly in severely ill patients, and then a CT is indicated so the entire spine segment can be imaged. CT is also indicated as the primary imaging for patients with high risk of spinal injury, unexplained soft tissue swelling or if a fracture is seen on the radiographs. MRI is indicated in any patient where a potential spinal cord injury is suspected clinically or there are progressive neurological defects such as due to a contusion of the cord (Fig. 13.11). Children may suffer a significant ligamentous injury without evidence of any fractures on radiographs or CT, called SCIWORA (spinal cord injury without radiological abnormality), and are best imaged with MRI.

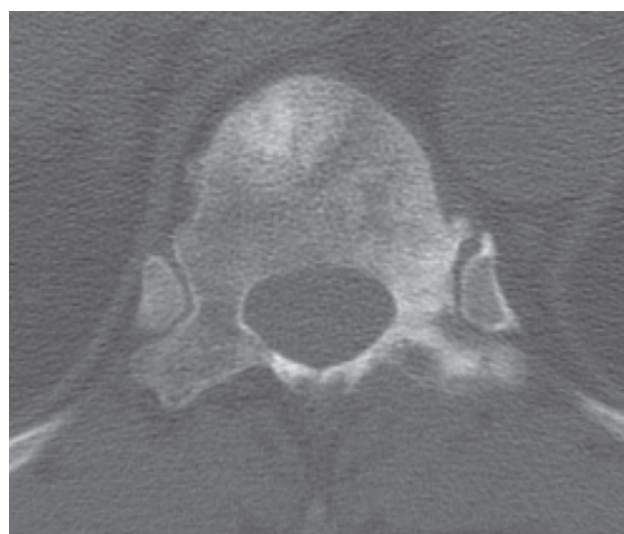
After ensuring the entire cervical spine has been adequately imaged it is important to first assess the alignment of the vertebral bodies by drawing lines on the lateral film along the anterior and posterior surface of the vertebral bodies (which equates to the anterior and posterior longitudinal ligaments, respectively). A line drawn at the junction of the lamina and spinous process indicates the posterior border of the spinal canal (Fig. 13.12) and represents the ligamentum flavum. Any interruption of these lines or significant angulation between endplates indicates



(a)



(b)



(c)

Fig. 13.6 Destruction of the pedicles due to metastatic renal cell carcinoma. (a) The pedicles of L1 have both been destroyed, as has the right pedicle of T12. Arrows point to representative normal pedicles (P). (b) MRI scan in the same patient showing extensive tumour in the vertebral body and a posterior mass of tumour (arrows) which is compressing the dural sac. (c) CT scan in a different patient with prostatic metastases showing sclerosis of the left pedicle of a lower thoracic vertebra together with sclerosis in the vertebral body and transverse process.

Box 13.2 Causes of dense vertebrae

- Metastases
- Lymphoma
- Paget's disease
- Haemangioma
- Healing fracture

there may be serious injury (Fig. 13.13). A line drawn along the tips of the spinous processes may not be smooth due to the presence of bifid spinous processes; it is more useful to ensure the spinous processes are approximately equally

spaced, indicating intact interspinous ligaments. The vertebral bodies should be approximately equal in height with no visible fracture lines. The prevertebral soft tissue is usually outlined by air in the nasopharynx and trachea and parallels the anterior border of the vertebrae. Excessive thickening of the prevertebral tissue may indicate an underlying haematoma secondary to a fracture but is unreliable if the patient is intubated.

The distance between the odontoid peg and the posterior border of the anterior arch of the atlas (atlantodens interval) is a marker of the integrity of the transverse ligament and should be ≤ 3 mm in adults or 5 mm in children. It may



Fig. 13.7 Dense vertebra (arrow) due to metastases from carcinoma of the breast.

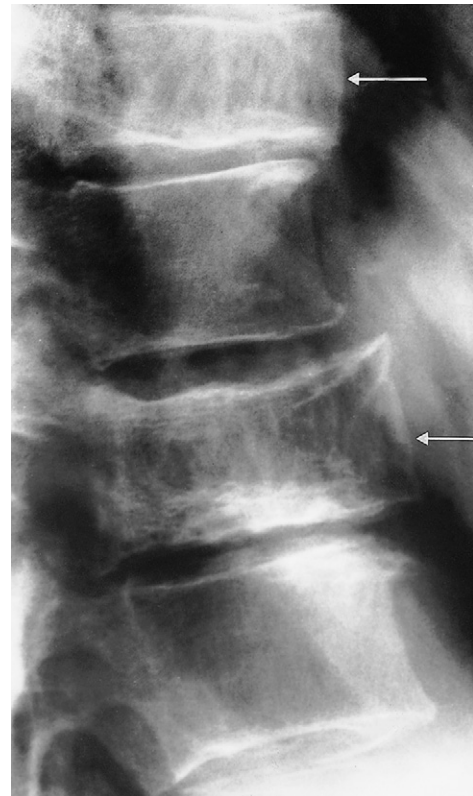


Fig. 13.8 Paget's disease. Note the increased density and coarse trabeculae in the vertebral bodies (arrows). They are also wider than the normal ones.



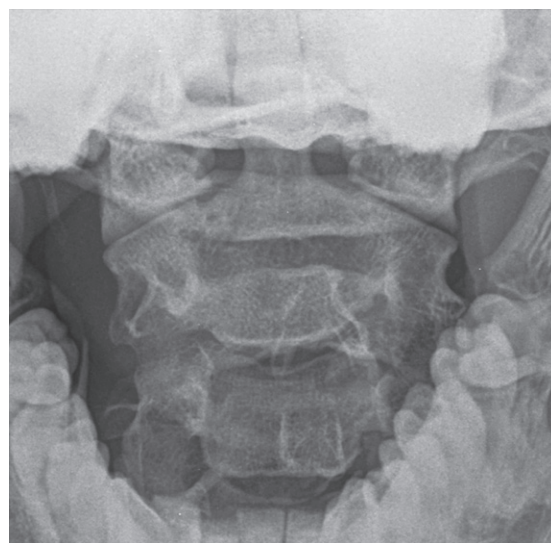
Fig. 13.9 Haemangioma. Vertical striations are present in this normal-sized vertebra (arrowhead).



(a)



(b)



(c)

Fig. 13.10 Normal cervical spine radiographs. (a) Anteroposterior, (b) lateral and (c) open mouth (peg) views. Note the lateral view includes the C7/T1 junction.



Fig. 13.11 Spinal cord injury. T2-weighted MRI showing high signal in the spinal cord due to oedema and haemorrhage (arrow).

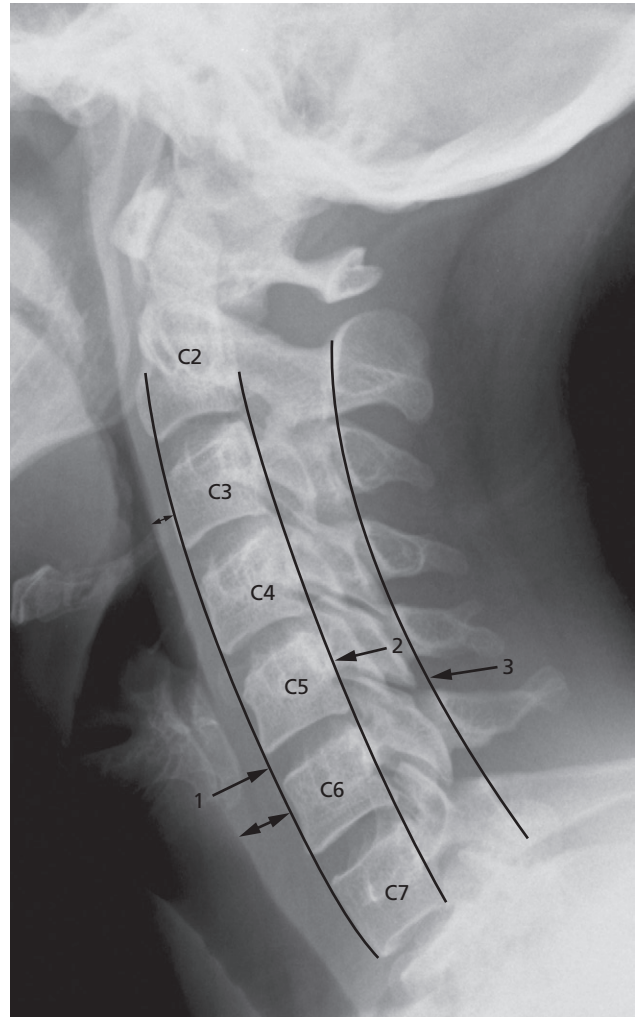


Fig. 13.12 Normal cervical spine showing lines to check alignment. Line 1 runs along the anterior border of the vertebral bodies and corresponds to the anterior longitudinal ligament. Line 2 runs along the posterior border of the vertebral bodies (posterior longitudinal ligament). Line 3 runs along the junction of the laminae and spinous processes (ligamentum flavum). Line 2 indicates the anterior extent and line 3 the posterior extent of the spinal canal. There is a normal soft tissue distance between the anterior border of the spine and the posterior border of the airway (double-headed arrows).

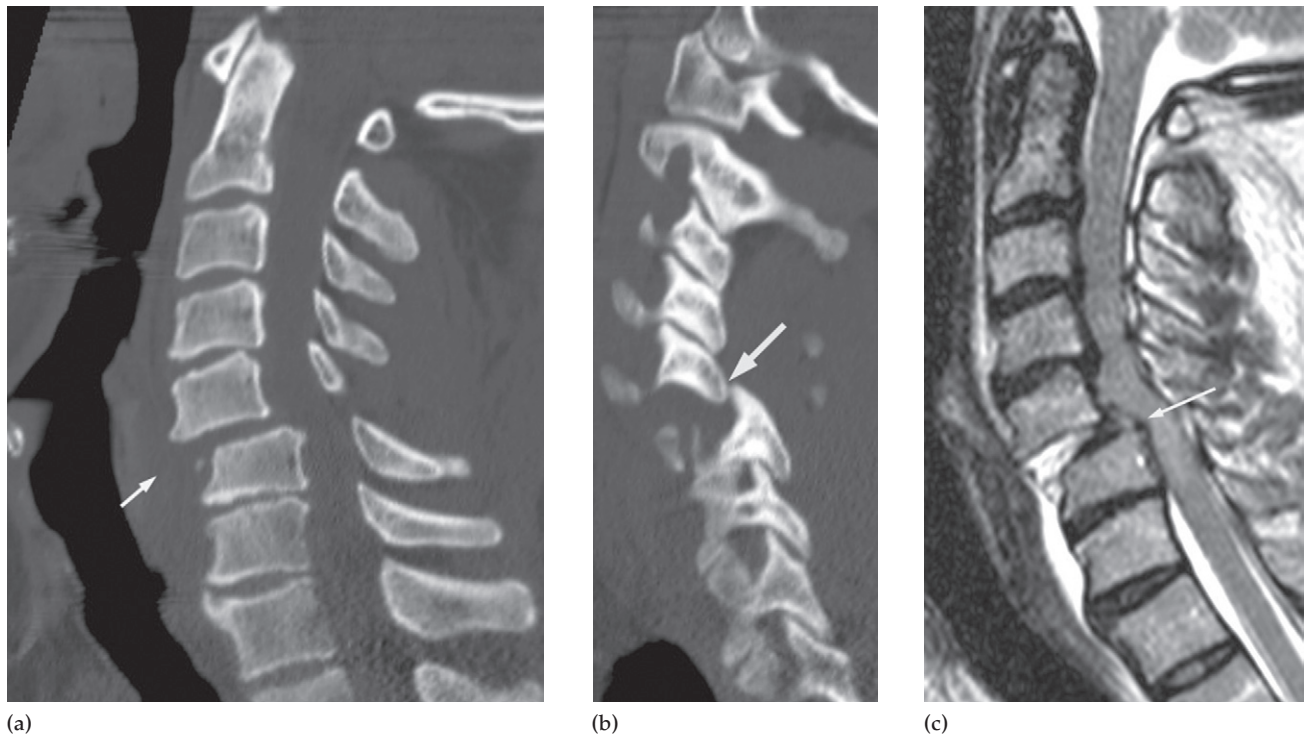


Fig. 13.13 Cervical spine injury. (a) On this midline CT scan there is a step in the alignment at the C5/C6 level. Soft tissue swelling is seen anteriorly at this level (arrow). (b) A section more laterally showing facet dislocation with overlap of the facets (arrow). (c) T2-weighted MRI showing injury to the intervertebral disc and displacement at the C6 level which has caused some spinal cord compression and oedema (arrow). High signal haemorrhage is seen anteriorly.

be widened in trauma but is more commonly subluxed in chronic conditions such as rheumatoid arthritis (Fig. 13.14).

If a fracture or ligamentous disruption is identified it is helpful to localize it by dividing the spine into the anterior, middle and posterior columns (Fig. 13.15), as spinal stability depends on the integrity of at least two of these osteo-ligamentous columns. The middle column is key and acts like a hinge between the anterior and posterior columns during flexion and extension. Injuries confined only to the anterior or posterior columns are generally considered stable whereas those where the middle column is involved are normally unstable injuries and may predict neurological injury.

After looking for the direct and indirect signs of fracture above, the mechanism of injury can aid in the type of fracture that may be encountered. Hyperflexion is the com-

monest mechanism of injury, where the anterior structures are in compression and the posterior elements are distracted, and the severity of injury will depend of the degree of force and structures injured. If relatively mild, there may be an anterior wedge fracture of the vertebral body only. If severe, there may be a fracture through the antero-inferior vertebral body with a fragment that is forced posteriorly into the neural canal and tears of the posterior element ligaments, producing an unstable flexion teardrop injury which is highly associated with cord injury (Fig. 13.16). Hyperflexion may also result in dislocation of the facet joints, which is usually associated with anterolisthesis of one vertebral body on another. Hyperextension injuries may also result in teardrop-shaped fragments of bone arising from the anterior vertebral body due to avulsion by the anterior longitudinal ligament but is not usually associ-

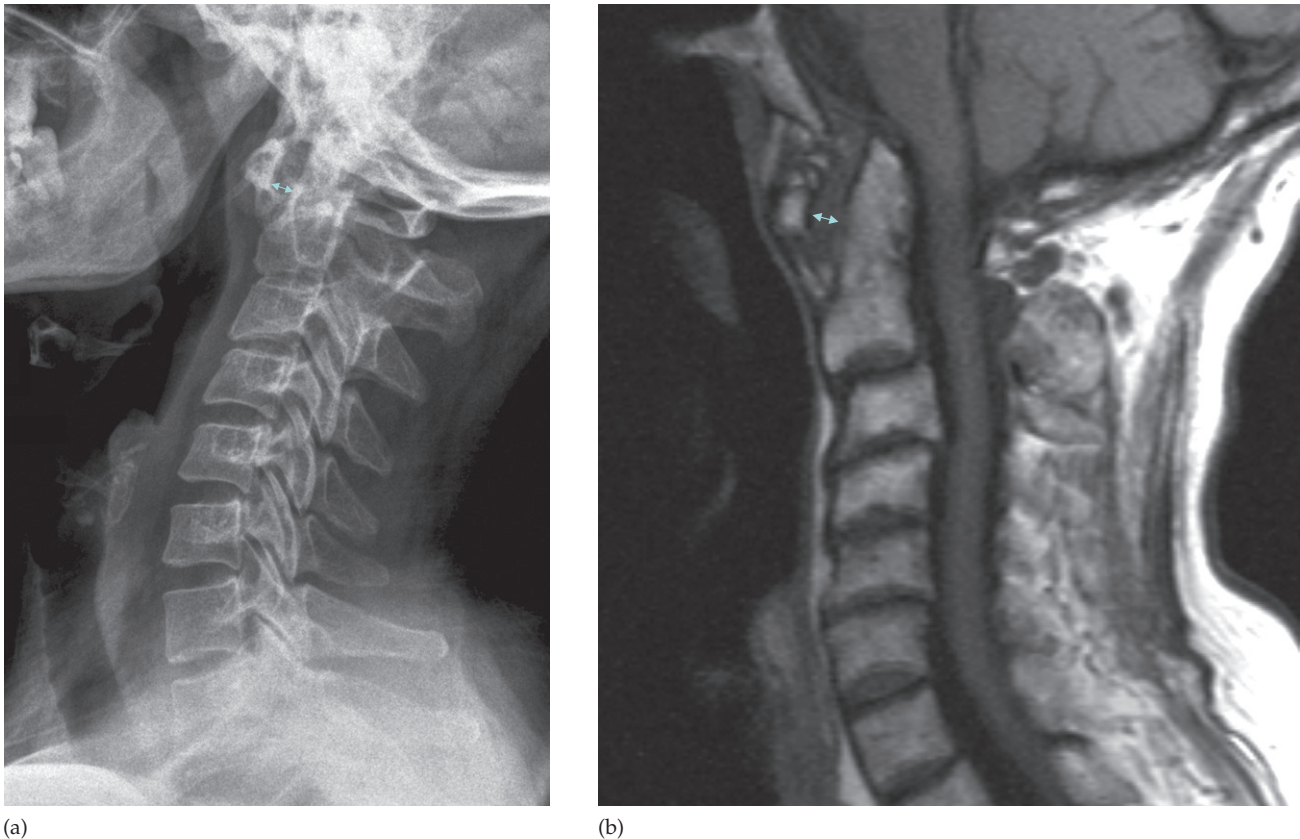


Fig. 13.14 Atlanto-axial subluxation. (a) Plain film taken with the neck flexed showing widening of the space between the dens of C2 and the anterior aspect of C1 (double arrow) in a patient with rheumatoid arthritis. (b) T1-weighted MRI showing widening of the atlanto-axial space in the same patient even when supine in the scanner.

ated with cord injuries (Fig. 13.17a). A more severe hyper-extension injury can result in a fracture involving the pars interarticularis of C2, which is known as a 'hangman's fracture' (Fig. 13.17b).

Blows to the top of the head (axial force) can result in fractures of the lateral masses of C1 – a fracture known as Jefferson's fracture. On the open mouth view, this fracture is suspected if the C1 lateral masses do not line up with the lateral borders of the C2 vertebral body (Fig. 13.18). A high energy injury, particularly with axial compression, may be transmitted to the remainder of the spine and result in a burst fracture with fragments extending radially, including posteriorly into the spinal canal (Fig. 13.19).

Degenerative spinal disease

Degenerative spine disease or spondylosis results primarily from degeneration of the intervertebral disc and occurs maximally in the lower cervical and lower lumbar regions. The nucleus pulposus is a non-compressible structure that is composed almost completely of water at birth and is therefore T2-hyperintense on MRI. With normal ageing, the water content will reduce and the T2 high signal diminish, but this process is accelerated with degenerative disease when it may be associated with reduced disc height and secondary bone changes of osteoarthritis such as osteophytes, which are detectable on all modes of imaging. The

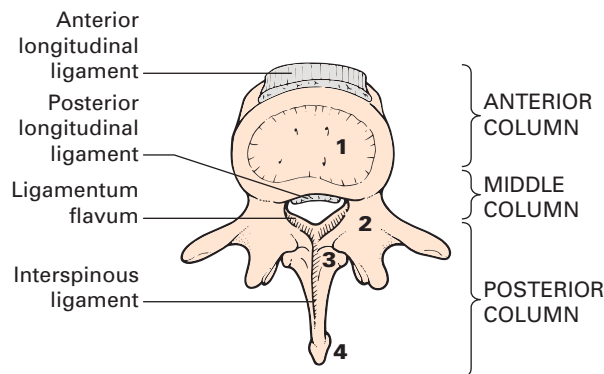


Fig. 13.15 Diagram to show the three columns of the spine. The anterior column includes the anterior longitudinal ligament and anterior two-thirds of the vertebral body (1). The middle column includes the posterior third of the vertebral body and the posterior longitudinal ligament. The posterior column includes the pedicles (2), laminae (3) and spinous processes (4). Redrawn from Dr T. Jaspan, with permission.

annulus, which is attached to the anterior and posterior longitudinal ligaments, loses its lamellar configuration of fibres and may develop high T2 signal fissures which can be associated with pain. Another feature of degenerative spinal disease is facet joint arthropathy. These joints may become inflamed, giving rise to pain and secondary joint hypertrophy and osteophyte formation. In the cervical spine, the abnormal stresses produced by disc and facet joint disease promotes the formation of osteophytes arising from the uncovertebral joints. This may cause compression of the nerve root sheath in the exit foramina. On MRI the calcified disc and uncovertebral osteophytes can be indistinguishable and are termed disc-osteophyte bars (Fig. 13.20).

Disc herniation

Degenerative annulus fissures may allow herniation of disc material beyond the normal margins of the intervertebral space and can be seen on CT but is best identified on MRI. In younger people, a herniation may also occur post-traumatically in the absence of any degenerative disc changes. Disc protrusions vary in size from small, focal herniations (less than 25% of disc circumference on an axial image) to broad-based (25–50%). If the herniated disc



Fig. 13.16 Flexion teardrop. Sagittal reformat of a CT scan showing a hyperflexion teardrop fracture at C6. The anterior column was in compression causing the fracture and the posterior part of the vertebral body is retropulsed (note disrupted posterior vertebral body line) into the canal with potential cord injury.

travels behind a vertebral body it is described as migrated and if a piece breaks off from the main herniation it is termed a sequestered fragment. Any disc herniations are also described in terms of location in relation to the spinal canal and vertebral structures (central, paracentral, subarticular, foraminal or far lateral) and any structures it may be compressing (thecal sac, spinal cord or nerve root depending on location).

Lumbar disc herniation. The majority of disc herniations occur posterolaterally due to the strong posterior longitu-

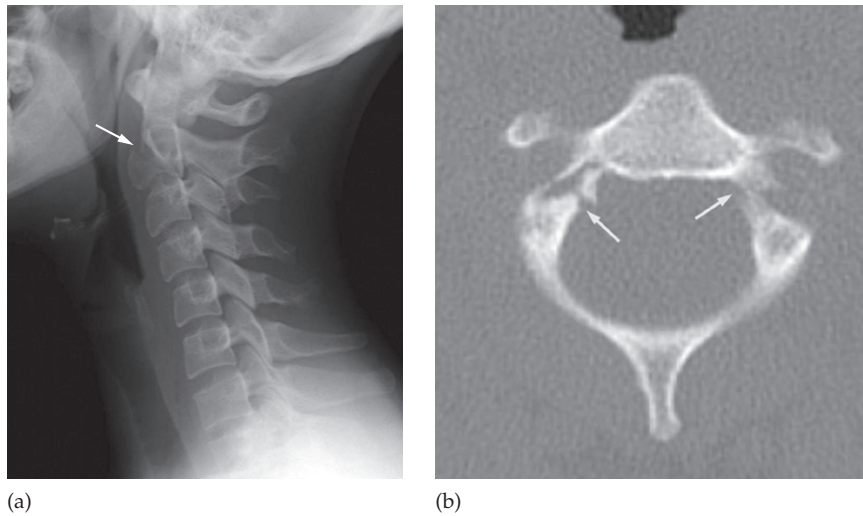


Fig. 13.17 Hyperextension injuries. (a) Radiograph showing an extension teardrop fracture of C2 (arrow) with minimal associated prevertebral swelling (haematoma). (b) 'Hangman's fracture': axial CT showing the bilateral pars interarticularis fractures (arrows).

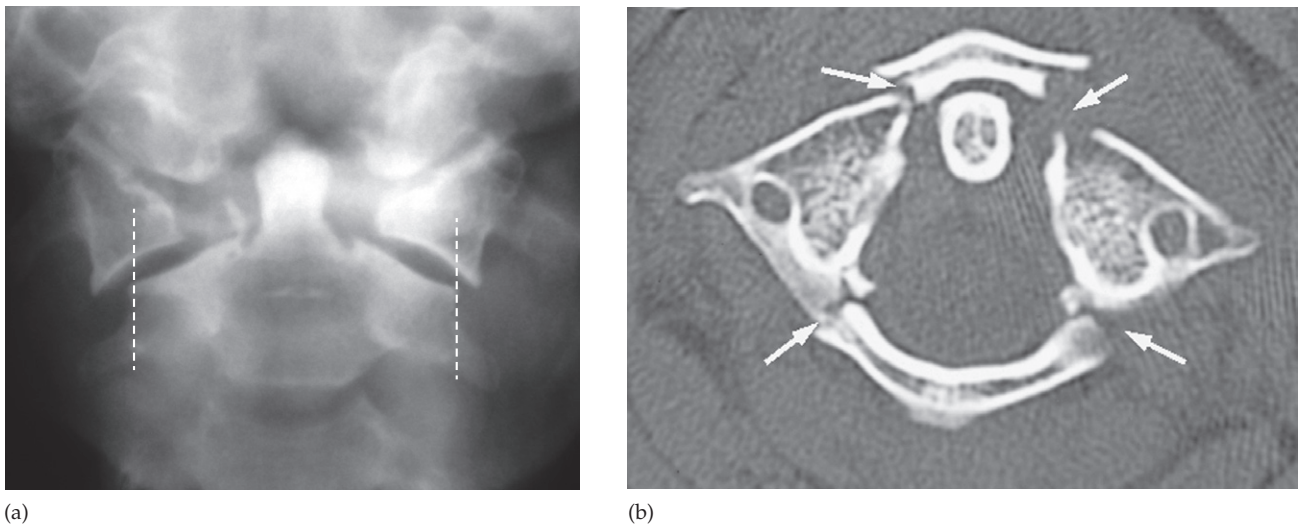


Fig. 13.18 Jefferson's fracture. (a) Plain film showing overlap of the articular pillars of C1 beyond the margins of the C2 vertebral body (dashed lines) due to a burst fracture of C1 (compare with the normal radiograph in Fig. 13.10). (b) Axial CT showing the fractures of the posterior arch more clearly together with fractures of the anterior arch (arrows).

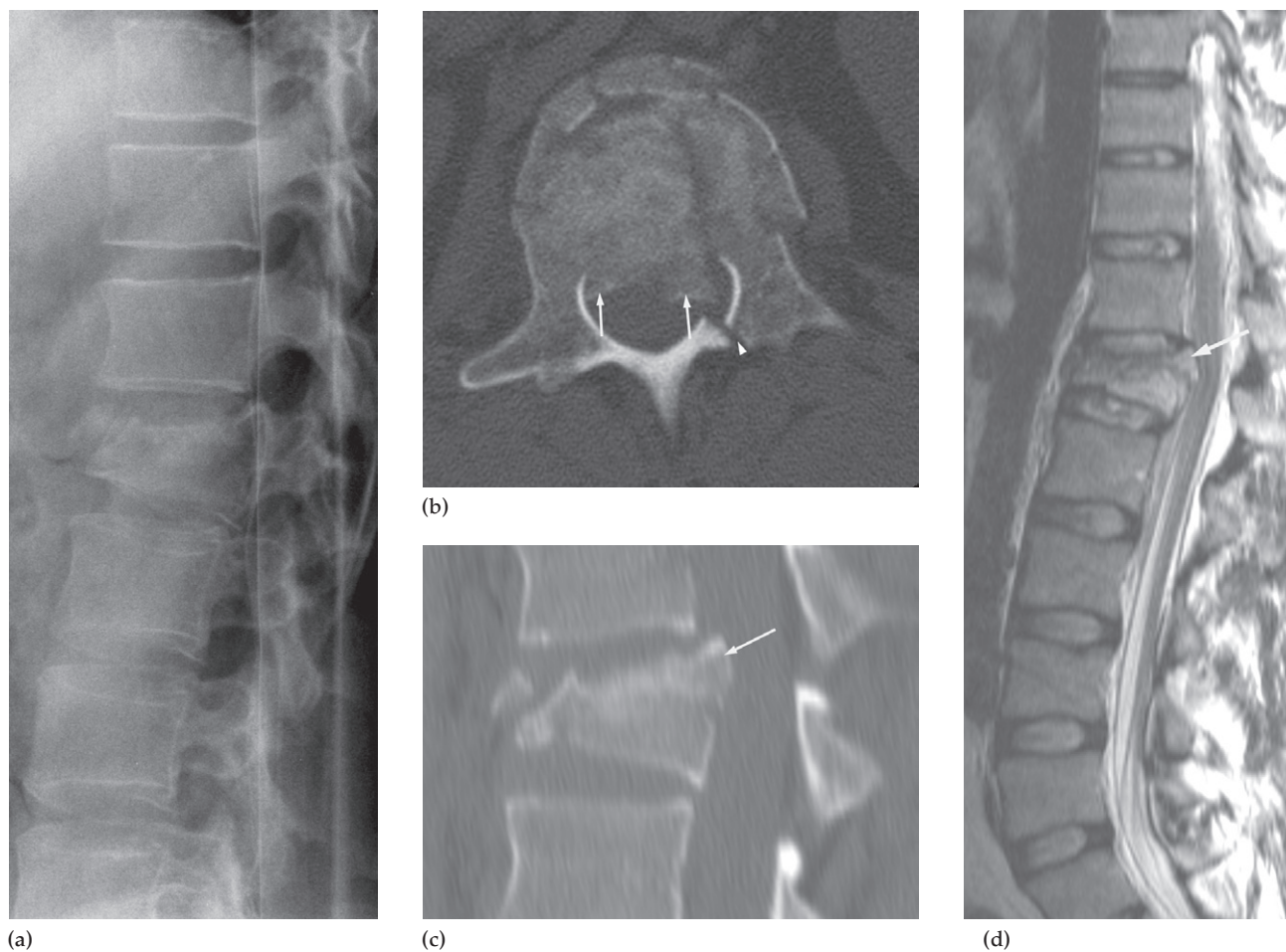


Fig. 13.19 Burst fracture of L1 caused by falling 6m from a ladder. (a) Plain film showing a compression fracture of the body of L1. (b) Axial CT and (c) sagittal CT showing more clearly fragments displaced into the spinal canal (arrows). The arrowhead points to a fracture of the lamina. All three spinal columns are fractured. (d) T2-weighted MRI showing the posterior fragments causing cord compression (arrow).

dinal ligament centrally which narrows the lateral recess of the spinal canal containing the traversing nerve roots (Fig. 13.21). Less commonly, a disc will herniate along the lateral margins of the spine (far lateral disc herniation) and impinge the nerve root as it is leaving the spine in the exit foramen. Loss of visualization of the fat that normally surrounds the nerve roots and root sheaths is a helpful indication of nerve root compression by a herniated disc. It should be appreciated that many demonstrable degenerative disc changes, annular fissures and herniated discs are

asymptomatic, so the criteria for surgery or other interventions must include clinical evidence of compression of the affected nerve root.

Magnetic resonance imaging is also useful in patients who continue to have symptoms following surgery for back pain. Symptomatic postoperative scarring impinging a nerve root can be distinguished from disc herniation if contrast-enhanced images are obtained. Scarring enhances following contrast administration in contradiction to recurrent disc herniation, which does not enhance (Fig. 13.22).

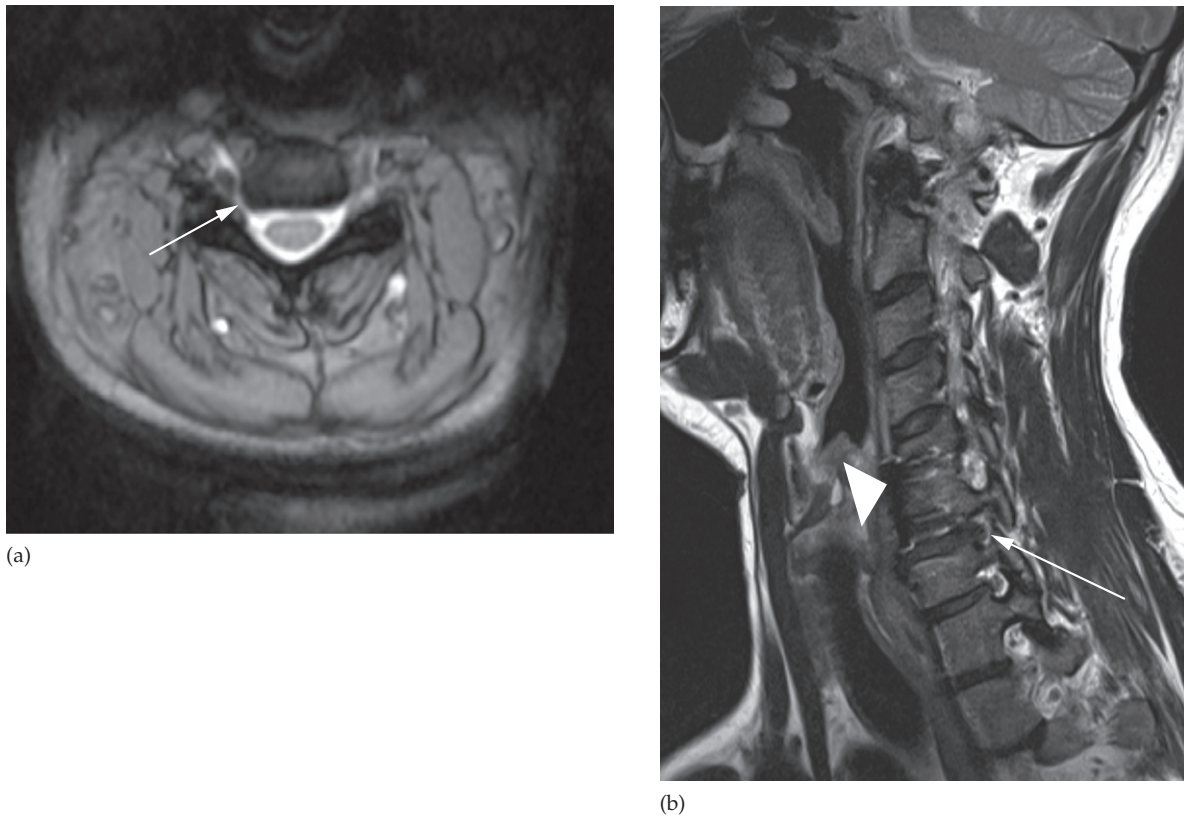


Fig. 13.20 Cervical spondylosis. (a) Axial T2-weighted MRI of the cervical spine showing a combination of disc protrusion and osteophytes causing narrowing of the right exit foramen (arrow). (b) Sagittal oblique T2-weighted MRI of a different patient with a previous anterior spinal fusion (arrowhead) and a disc protrusion causing narrowing of the C6/C7 exit foramen (arrow).

The effects of inflammatory arachnoiditis, which may be secondary to previous haemorrhage, infection or surgery, may also be identified with thickened nerve roots clumped together in the central canal.

Spondylolisthesis

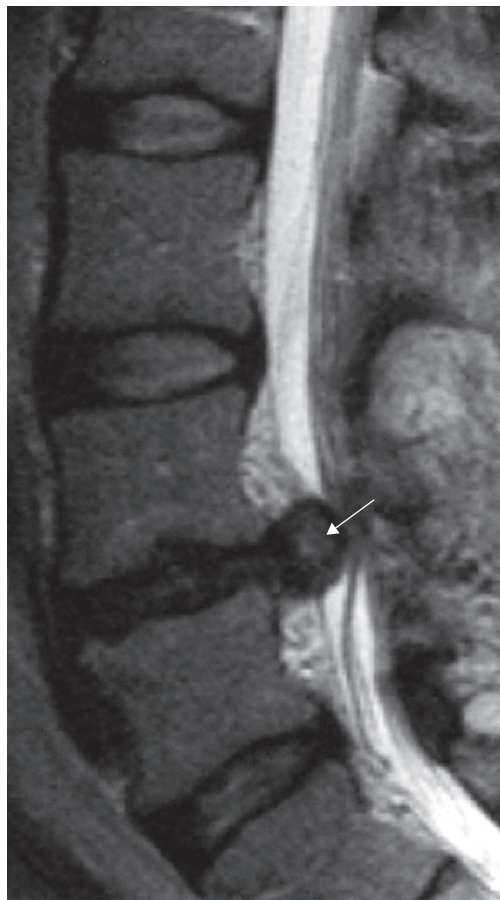
The term spondylolisthesis refers to forward slip of one vertebral body on the one below it, a condition which occurs most frequently at L5/S1. It may be congenital or the result of a stress fracture of the pars interarticularis. Minor degrees of slip can also occur without a break in the pars interarticularis if there is degenerative disc disease with osteoarthritis in the apophyseal joints. *Spondylolysis* is the term given to a defect in the pars interarticularis without

a forward slip of one vertebral body on the other. Stress fractures of the pars interarticularis are a particular problem in people performing active sports.

Defects in the pars interarticularis are readily identified with CT (Fig. 13.23b) or MRI but plain film examination often suffices (Fig. 13.23a). Radionuclide scanning may show increased uptake before the defect is visible on plain films or CT.

Infection

The spread of infection to the spine is usually via the haematogenous route. In children, there are small end vessels where bacteria are deposited which extend through the vertebral endplates into the disc, and thus infection may



(a)



(b)

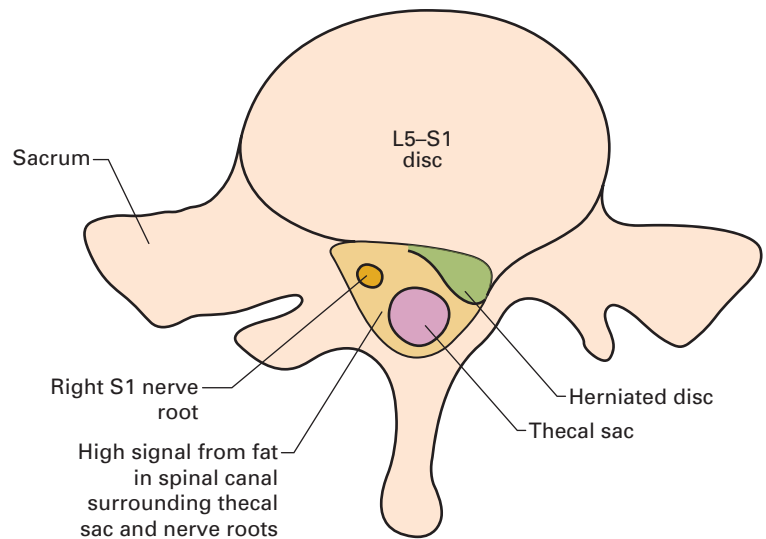


Fig. 13.21 MRI scans of disc herniation. (a) Sagittal T2-weighted scan showing a large posterior herniation of the L4/L5 disc (arrow). (b) Axial T1-weighted scan of an L5/S1 disc showing a disc herniation compressing the adjacent nerve root. The opposite equivalent nerve root can be clearly seen.



(a)

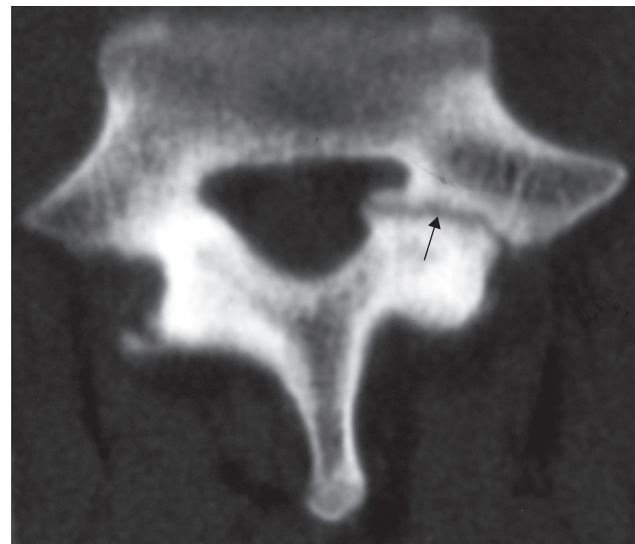


(b)

Fig.13.22 Postoperative fibrosis. T1-weighted MRI scans at the L5/S1 level in a patient with sciatica following L5/S1 laminectomy 6 months previously. (a) The scan shows a normal right S1 nerve root (curved arrow), but around the left S1 nerve root there is a mass (arrows) which could be either fibrosis or recurrent disc herniation. (b) After gadolinium the mass enhances, indicating that it is fibrosis. A disc herniation would not enhance.



(a)



(b)

Fig. 13.23 Spondylolisthesis. (a) Lateral view. There is forward slip of L5 upon S1. The dashed lines that mark the posterior aspects of the vertebral bodies should form a smooth curve. The defect in the pars interarticularis is arrowed. (b) CT scan showing a defect in the pars interarticularis (arrow) in another patient.

originate purely within the disc (discitis). Beyond childhood, the end vessels are confined by the now ossified endplates and hence any infection in the disc is due to local spread of infection from the bony endplate and is termed discitis osteomyelitis. The hallmark of pyogenic infection (often *Staphylococcus aureus*) is destruction of the intervertebral disc and adjacent vertebral bodies. Early in the course of the disease, there is narrowing of the disc space with erosion of the adjoining vertebral endplate. Later,

bone destruction may lead to collapse of the vertebral body and eventually sclerosis. Tuberculous infection can be more insidious as it lacks proteolytic enzymes, which may allow preservation of the disc space, and instead may present with complications such as bone collapse resulting in a sharp angulation (focal kyphosis) known as a gibbus (Fig. 13.24). Involvement of local soft tissue can be seen in both, such as a paravertebral abscess which, in the lumbar spine, may spread into the adjacent psoas muscles. In severe

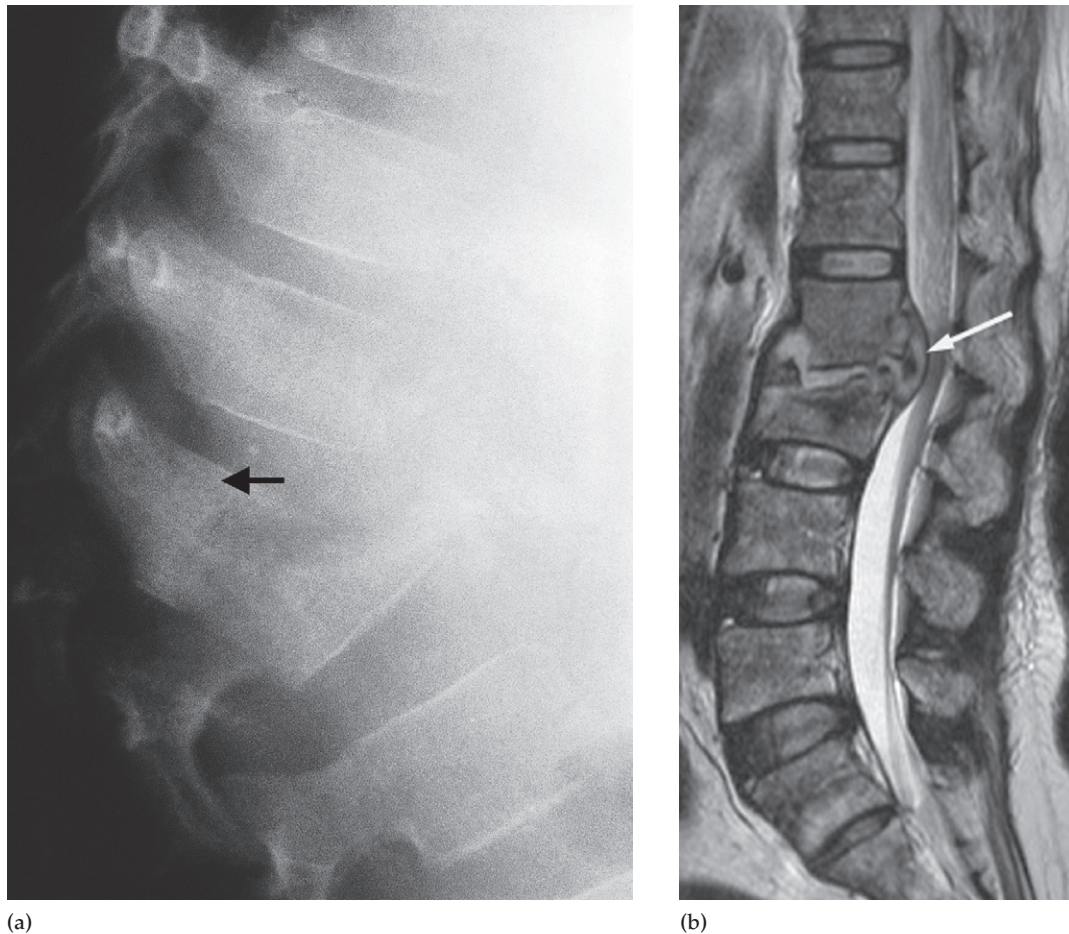


Fig. 13.24 Tuberculosis of the spine. (a) Plain film showing destruction of the vertebral bodies and the intervening discs with the formation of a sharp angulation (gibbus). One vertebral body is almost completely destroyed (arrow) and there is destruction of the upper part of the one below it. (b) T2-weighted MRI in another patient showing destruction of the intervertebral disc and part of the vertebral body below it. A large inflammatory mass is protruding into the spinal canal causing compression of the cauda equina (arrow).

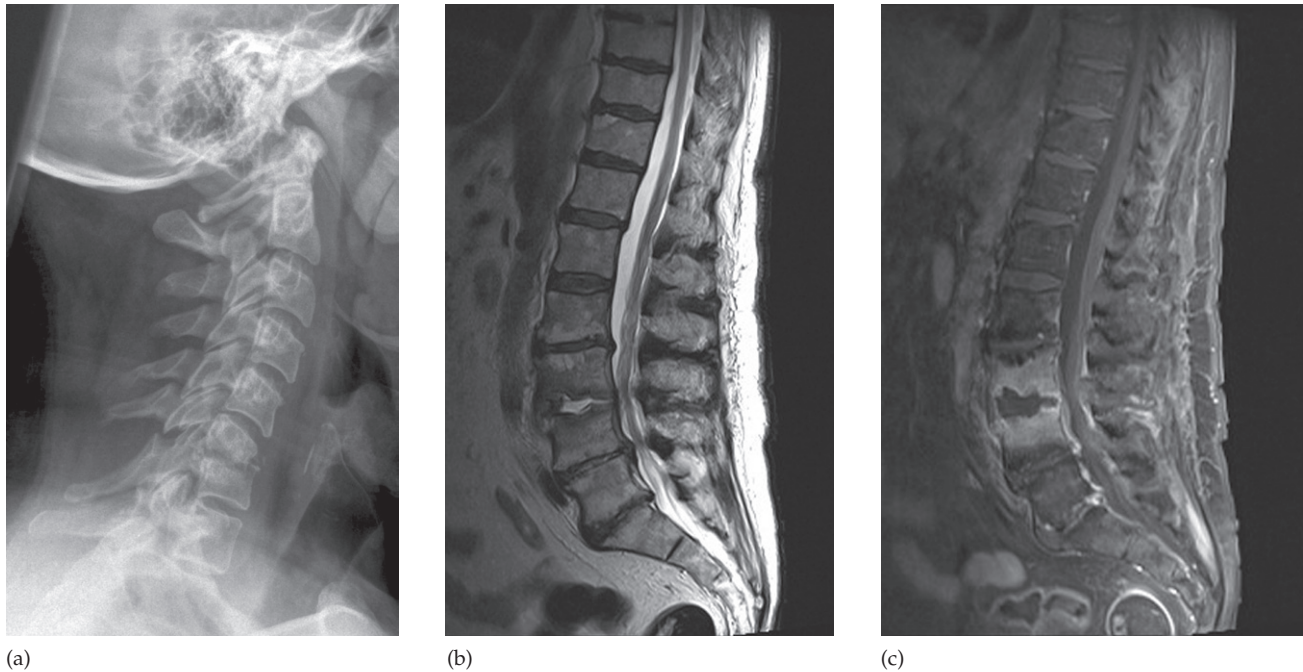


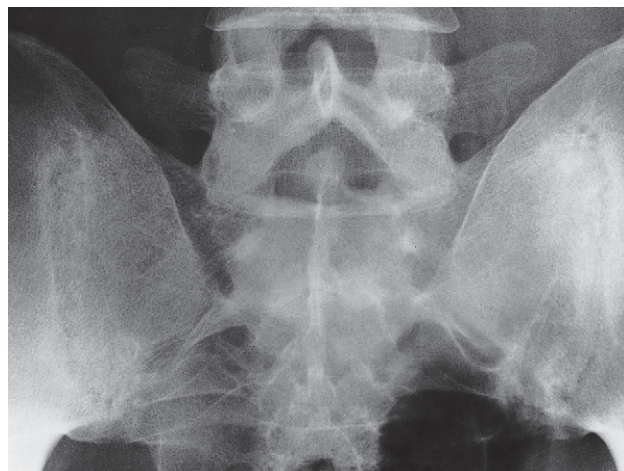
Fig. 13.25 Bacterial discitis. (a) Plain film of discitis at C6/C7 with loss of intervertebral height and non-visualization of the normally corticated adjacent endplate. (b) Sagittal T2-weighted MRI of a different patient with high signal pus in the L3/L4 disc space. (c) Sagittal T1-weighted MRI, post contrast, with intense enhancement of the adjacent vertebral bodies and also between the spinous processes posteriorly.

cases, the infection can spread inside the neural canal and compress the cord or nerve roots, which is a neurosurgical emergency.

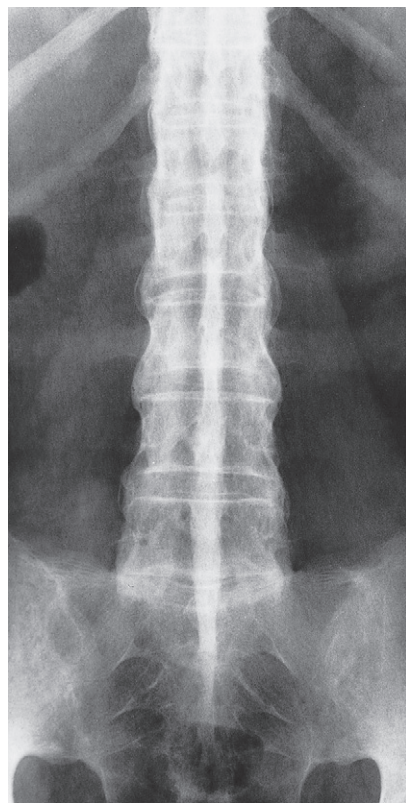
Radiographs or CT can show the bone destruction, paravertebral abscesses and disc space narrowing. However, MRI is the preferred investigation as it can demonstrate disc space narrowing with fluid (pus) in the disc, altered signal in the adjacent vertebral body (infection or oedema), adjacent soft tissue swelling and any spinal cord or nerve root compression (Fig. 13.25). Needle biopsy/aspiration of the infected disc or adjacent vertebral body under fluoroscopic or CT control is useful to confirm the diagnosis and identify the responsible organism, although positive cultures are rare once antibiotics have been commenced. Bony fusion of the vertebral bodies across the obliterated disc spaces occurs with healing and tuberculous paravertebral abscesses may eventually calcify.

Inflammatory spondylarthropathy

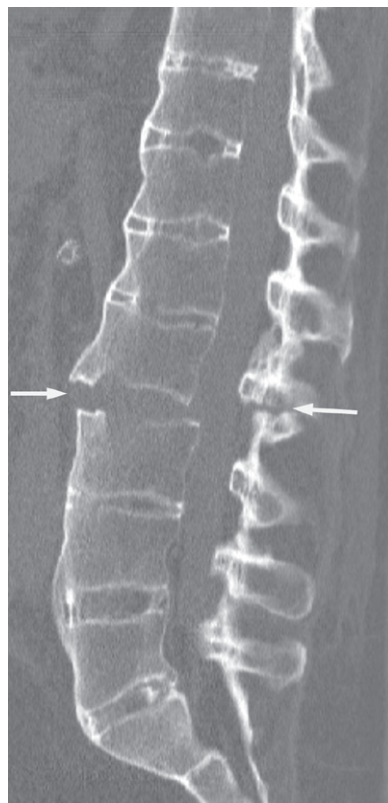
There are some forms of inflammatory arthritides that have a predilection for the spine. Ankylosing spondylitis, psoriatic arthropathy and Reiter's syndrome (a reactive arthritis following genitourinary or gastrointestinal infection) are termed seronegative arthropathies (rheumatoid factor negative and often HLA-B27 positive). They share common findings of sacroiliitis and spine arthropathy. Sacroiliitis is a hallmark of ankylosing spondylitis when it is often symmetrical, whereas the other seronegative spondylarthropathies may be asymmetrical. The earliest radiographic change is fuzziness of the joint margins, followed by erosions which often start on the iliac side of the joint (Fig. 13.26a). Eventually, the process leads to juxta-articular sclerosis, obliteration of the joint space and ankylosis. MRI can identify signs of sacroiliitis earlier than radiographs by



(a)



(b)



(c)

Fig. 13.26 Ankylosing spondylitis. (a) The sacroiliac joints have an irregular fuzzy outline. (b) With advanced disease the whole spine becomes fused ('bamboo spine'). Note that the sacroiliac joints are also fused. (c) CT in another patient showing a transverse fracture through the disc space in the midlumbar spine (arrows). The spine above and below the fracture is fused.

demonstrating periarticular bone oedema (high T2 signal) and erosions in addition to joint effusions. Later, there is fat accumulation adjacent to the joint (bright on T1 and T2 sequences) and eventually a bone marrow signal is seen across the ankylosed joint.

In the spine, there are often syndesmophytes, which are a result of ossification of Sharpey's fibres – the outer fibres of the annulus that pass vertically between the vertebral bodies – giving them a 'squared off' appearance. They can be distinguished from degenerative osteophytes as the latter usually extend horizontally from the vertebral margins before extending vertically. If multiple intervertebral joints are affected it may produce a 'bamboo spine' appearance on radiographs (Fig. 13.26b). Erosive arthropathy may affect other joints of the spine (facet, uncovertebral and costovertebral) and the attachment of ligaments to the bone (enthesopathy) which eventually ossify and fuse (ankylose). This results in restricted movement and progressive deformity, with an increased risk of fracture with minor trauma. A typical fracture involves all three columns and may pass through the vertebral body or disc space (Fig. 13.26c), resembling Chance's fracture usually seen in lap-belt hyperflexion injuries.

Congenital abnormalities

Spina bifida is a result of an *in utero* incomplete closure of the embryological neural tube, usually in the lumbosacral region, and may be associated with neurological complications. It varies in severity from asymptomatic spina bifida occulta, where there is failure of fusion of a posterior bony neural arch but with intact overlying soft tissues and skin (seen in approximately 25% of the population), to severe cases, where there may be protrusion of the neural elements (meningomyelocele) or just the membranes (meningocele) from the spinal canal which require corrective surgery soon after birth. In these cases, the laminae of several vertebrae will be absent and the distance between the pedicles will be increased on radiographs. MRI can provide useful information in cases of complex spinal dysraphisms about the degree of neural involvement and associated anomalies that can occur such as the presence of intraspinal fat (lipomas) or tethered cord where the conus is located caudal to L2/L3 (Fig. 13.27a). Nowadays, the diagnosis is often made antenatally by ultrasound.

There are various types of congenital vertebral body anomalies which can be identified on radiographs or cross-sectional imaging, such as hemivertebrae (Fig. 13.27b), butterfly vertebrae or segmentation anomalies where there is failure of disc formation. These are often associated with varying degrees of focal spine deformities such as kyphosis or scoliosis.

Spinal cord and cauda equine compression

Although the level of cord or cauda equina compression can be suggested by clinical examination, MRI of the spine can demonstrate the site and often the cause and extent of the abnormality and any other sites involved. This information is important should surgery be necessary.

The causes of intraspinal compression can be divided according to the site of origin of the responsible space-occupying lesion (Fig. 13.28):

- *Extradural lesions*: myeloma, lymphoma and metastases are the commonest malignant spinal tumours that can compress the dural sac and its contents, potentially at multiple sites (Fig. 13.29). Infection and degenerative disc protrusions may also cause extrinsic compression of the cord or cauda equina.
- *Intradural extramedullary lesions* (i.e. within the dural sac but not within the spinal cord): meningioma and nerve sheath tumours such as neurofibromas (Fig. 13.30) or schwannomas.
- *Intradural intramedullary lesions* (i.e. within the spinal cord): primary spinal cord tumour such as ependymoma astrocytoma or metastases (Fig. 13.31).

Intrinsic disorders of the spinal cord

Magnetic resonance imaging is the only modality that is able to give an excellent demonstration of the whole of the spinal cord. Conditions such as tumours are readily diagnosed by a combination of altered signal within the cord and expansion of its outline. Syringomyelia is a condition where a CSF-contained cavity forms within the middle of the cord due to local damage or mass. In the cervical region, a syringomyelic cavity (syrinx) is often associated with a Chiari I malformation (Fig. 13.32) where the cerebellar tonsils lie below the level of the foramen magnum and it

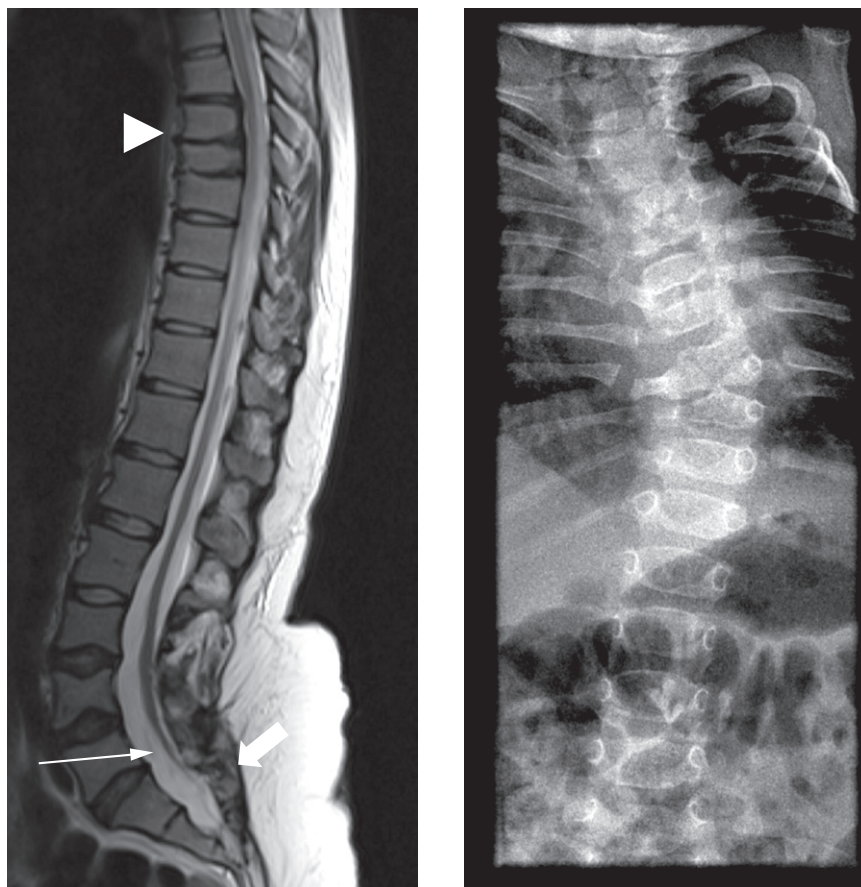


Fig. 13.27 Congenital spinal anomalies. (a) Sagittal T2-weighted MRI showing the conus is located abnormally low at approximately L5/S1 (long arrow) with incomplete formation of the low lumbosacral posterior elements (wide arrow). There is also a segmentation anomaly at T7–T9 with poorly formed intervertebral discs (arrowhead). (b) Frontal radiograph of an infant showing an early scoliosis due to a left hemivertebra at T8 – note the number of ribs compared to pedicles.

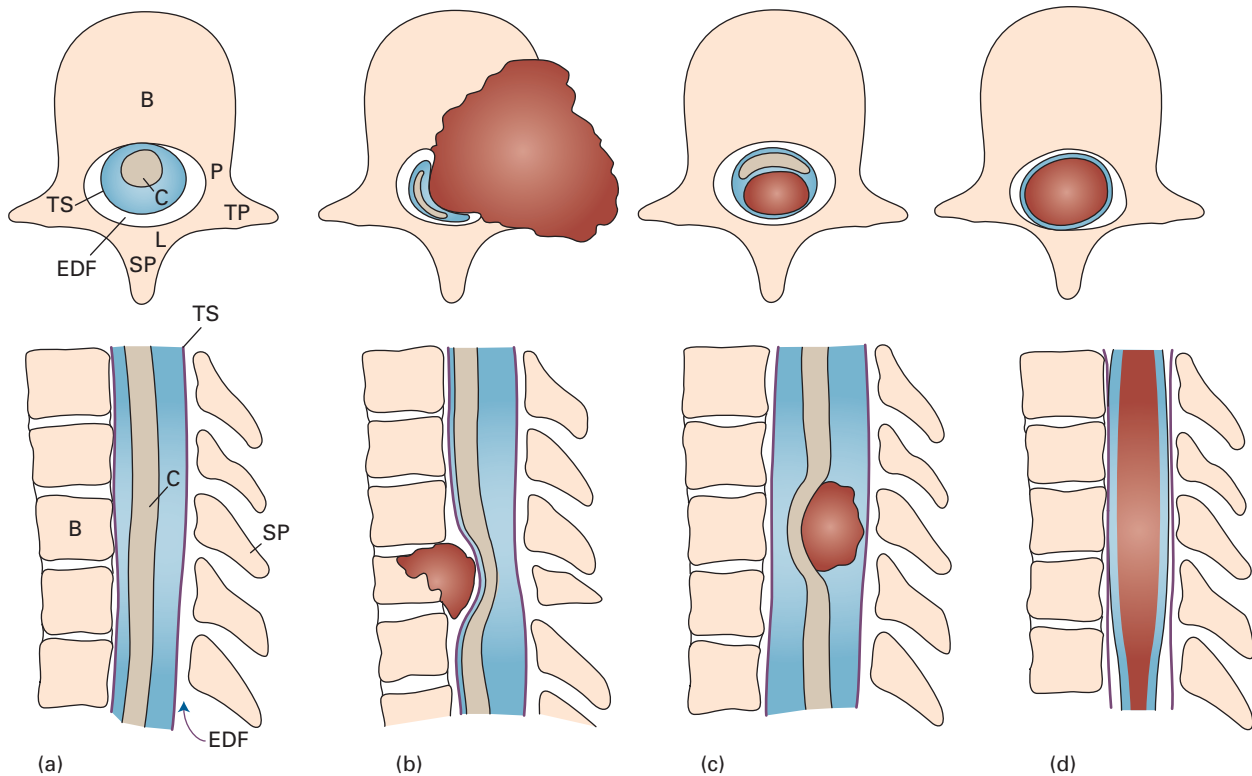


Fig. 13.28 Spinal cord compression; schematic axial and sagittal sections. (a) Normal view. B, vertebral body; C, spinal cord; EDF, extradural fat; L, lamina; P, pedicle; SP, spinous process; TP, transverse process; TS, thecal sac. (b) Extradural metastatic tumour. Extrinsic compression of the thecal sac and spinal cord, which are compressed and displaced away from the tumour. (c) Intradural extramedullary tumour. The tumour is contained within the undisplaced thecal sac but compresses and displaces the spinal cord. (d) Intradural intramedullary tumour. The spinal cord is expanded but undisplaced with little or no visualization of the CSF in the thecal sac around the spinal cord. Redrawn from Dr T. Jaspan with permission.

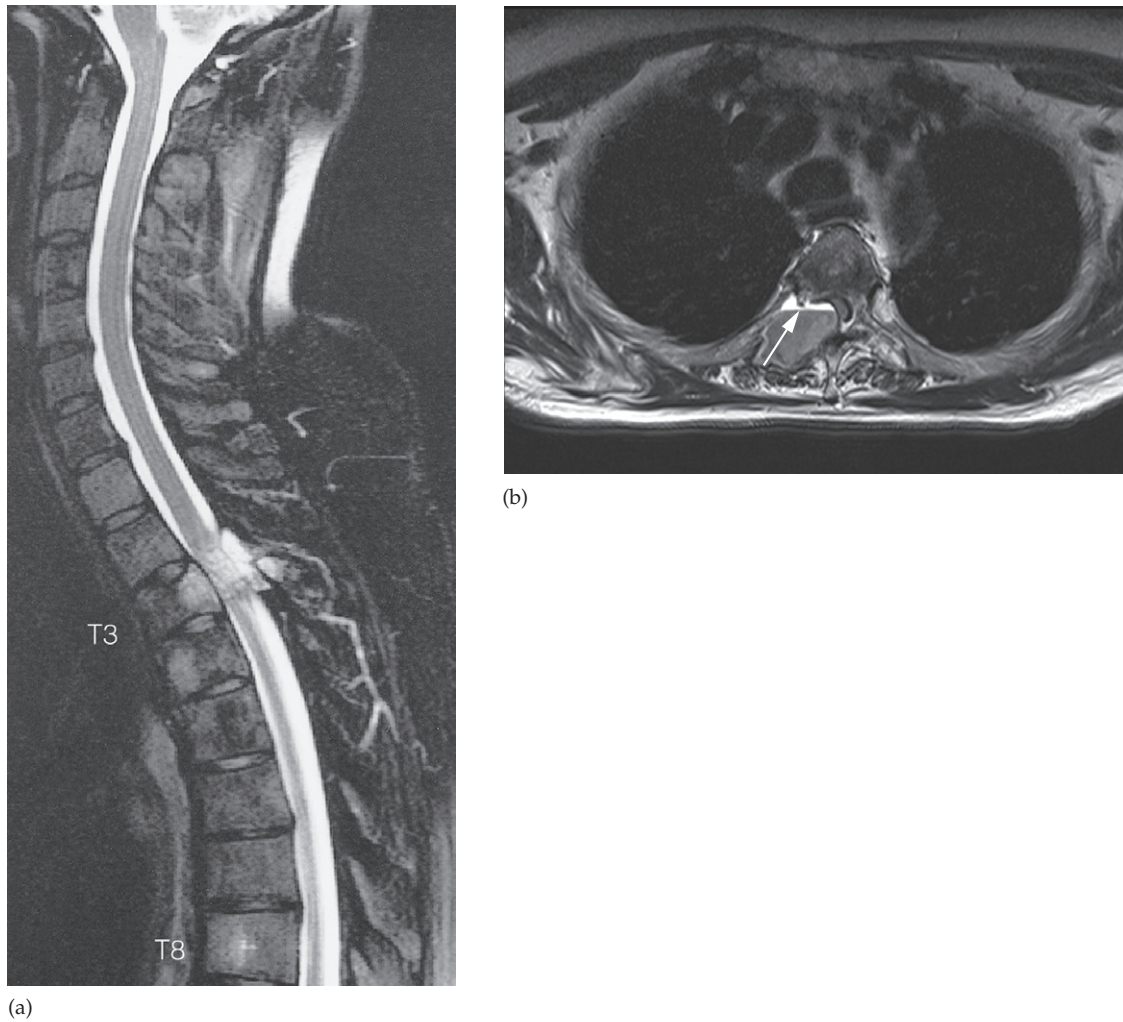
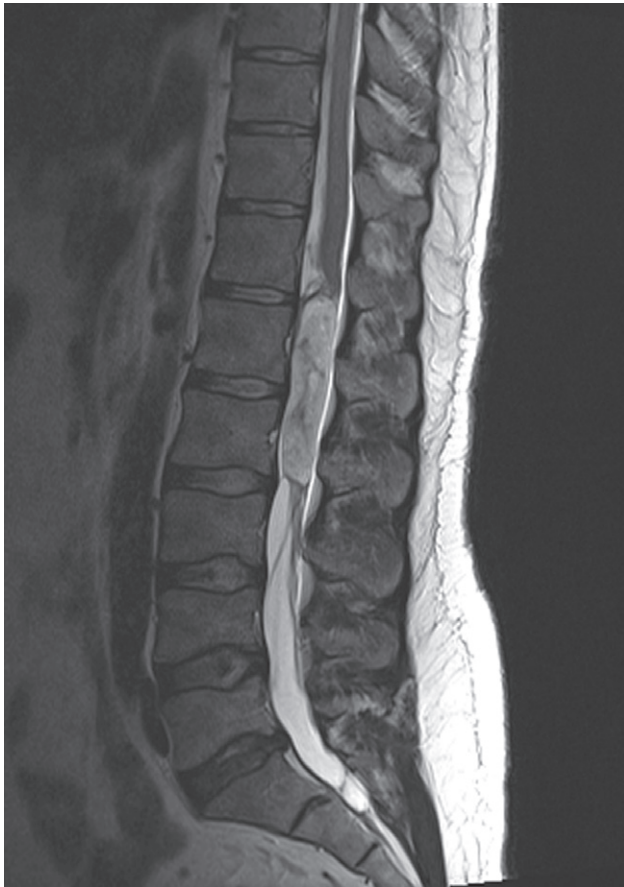


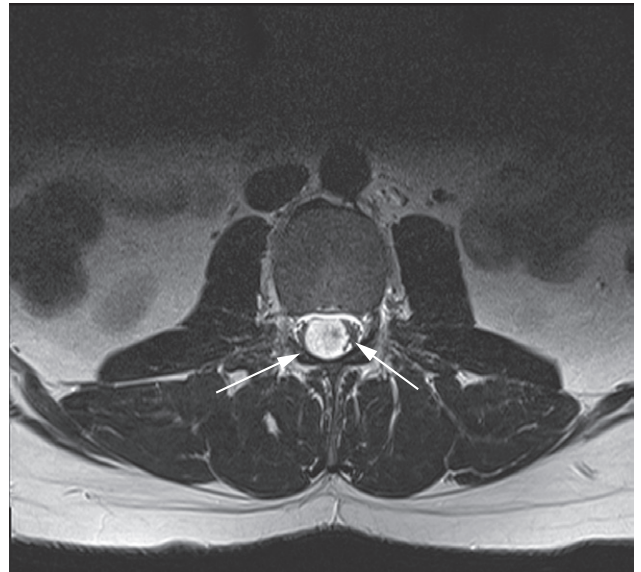
Fig. 13.29 Spinal cord compression. (a) T2-weighted MRI scan showing metastases from a breast carcinoma in the body and pedicle of T3 causing compression of the spinal cord. (b) Axial T1-weighted image of a different patient showing a breast cancer metastasis arising from the right pedicle and causing extradural compression of the cord. There is a fluid–fluid level (arrow) in the metastasis due to bleeding within the tumour.



Fig. 13.30 Intradural neurofibroma. T2-weighted MRI scan showing the tumour at the T6/T7 level compressing and displacing the spinal cord anteriorly (arrows).



(a)



(b)

Fig. 13.31 Intradural intramedullary lesion. (a) Sagittal T2-weighted MRI scan showing an ovoid mass (ependyoma) at the level of the conus. (b) Axial T2-weighted MRI scan below the level of the conus showing the mass within the intradural space surrounded by the cauda equina nerve roots (arrows).

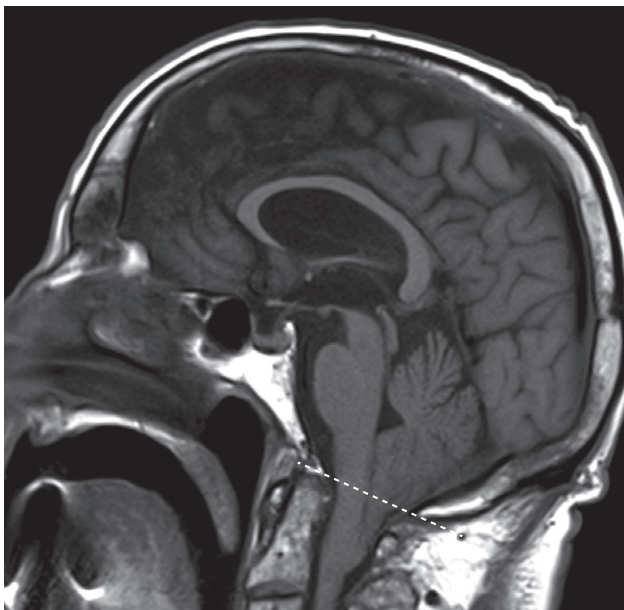


Fig. 13.32 Chiari I malformation. The tips of the cerebellar tonsils extend through the foramen magnum (dashed line) to reach the level of C2.



Fig. 13.33 T2-weighted MRI showing a plaque of demyelination (arrow) in a patient with multiple sclerosis.

can present with upper limb sensory disturbance and lower limb weakness.

Transverse myelitis and multiple sclerosis

Transverse myelitis is an inflammatory condition of the spinal cord which is usually associated with progressive neurological dysfunction depending on the tracts affected in the cord. It is often seen in multiple sclerosis (Fig. 13.33) but other inflammatory conditions such as connective tissue diseases, vasculitis and infection can produce a similar appearance. It can only be identified on MRI with T2-hyperintense lesions which typically do not involve the entire cross-section of the cord and do not respect the grey-white junction. In multiple sclerosis, cord lesions will often be associated with white matter plaques in the brain.

Skeletal Trauma

Imaging techniques

Plain radiographs

Plain radiography in skeletal trauma is invaluable in order to:

- diagnose the presence of a fracture
- assess the type of fracture (Box 14.1)
- show displacement and/or angulation of the bone ends before and after treatment
- diagnose dislocation or subluxation with or without a fracture
- assess healing and complications of fractures
- determine whether the fracture has occurred through abnormal bone (pathological fracture)
- assess soft tissue injury and locate any foreign bodies.

In any case of trauma it is essential to take at least two views, preferably at right angles to one another. Sometimes a fracture or dislocation will be seen on only one view and

so may be missed unless two views are taken. Similarly, the position of a fracture should never be assessed from a single view (Fig. 14.1).

Computed tomography

The major advantages of multidetector computed tomography (MDCT) over plain films are:

- Better assessment of fractures in bones of complex shape, such as the spine and pelvis (Fig. 14.2) which can be aided by three-dimensional reformation of the CT images. Reconstructions to any desired plane (Fig. 14.3) or three-dimensional images (Fig. 14.4) are easily obtained on modern equipment. In the spine, fractures of the pedicles, laminae and articular facets as well as fragments displaced into the spinal canal are particularly well seen (see Fig. 14.3). In fractures of the pelvis, especially those around the hip joints, CT shows the relationship of the fractures to the joint as well as loose fragments within the joint (see Fig. 14.2). CT is invariably performed in acetabular fractures and fracture dislocations of the hip. It is also very helpful in tibial plateau fractures and fractures of the ankle, calcaneum and midfoot.
- Assessment of the extent of soft tissue damage, haematomas and of internal visceral injuries.
- In general, less manipulation of the patient is required, so that the examination of the severely injured individual is more comfortable and often safer. The examination is quick, an important factor in patients with serious internal injuries.

Box 14.1 Types of fracture

- Comminuted
- Transverse/oblique/spiral
- Impacted
- Greenstick
- Avulsion
- Burst/crush
- Insufficiency

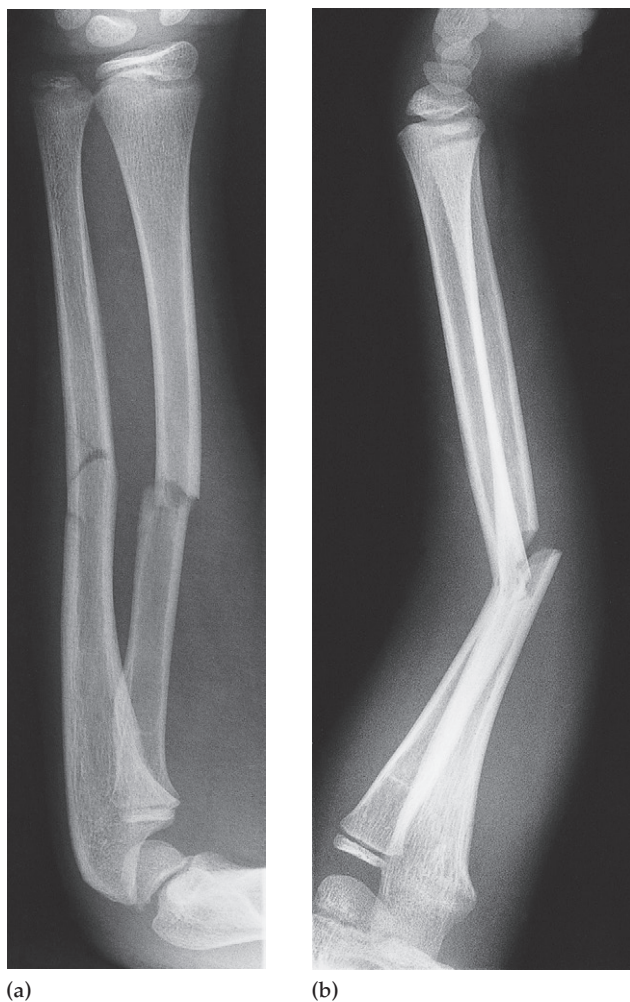


Fig. 14.1 Value of two views for demonstrating the position of fractures. (a) The fractures of the radius and ulna show little displacement on the frontal projection. (b) The lateral view, however, shows a marked angulation.

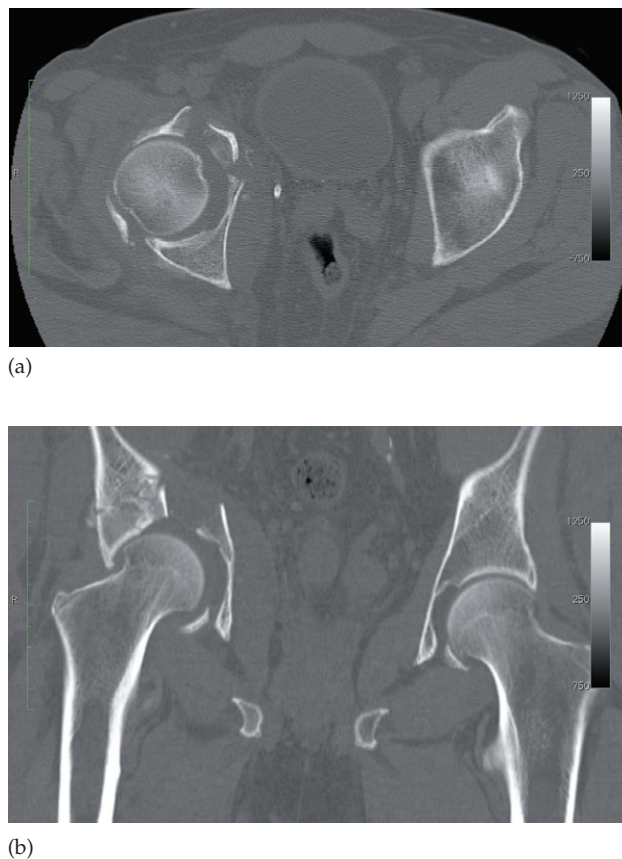
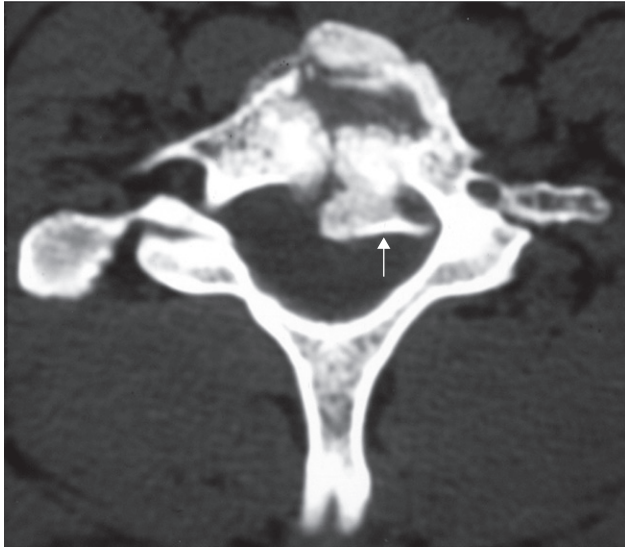
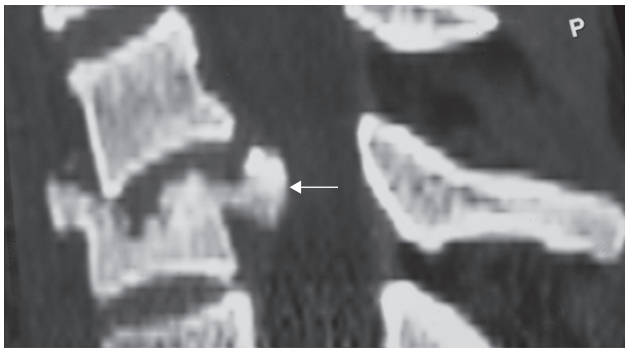


Fig. 14.2 Fracture of the pelvis. (a) A section through the acetabular roof demonstrating an anterior column injury with displaced bony fragments. (b) A coronal section showing the fracture of the acetabulum extending to the iliac bone superiorly. The fractures and their displacement were much better demonstrated with CT than with radiographs of the pelvis.



(a)



(b)

Fig. 14.3 CT scanning in a spinal fracture. (a) A comminuted fracture of C7 with displacement of a large bone fragment (arrow) into the spinal canal. (b) Sagittal reconstruction also shows the fractured vertebra and displaced fragment (arrow).

Magnetic resonance imaging

Even though cortical bone does not produce a magnetic resonance signal, a fracture can be seen as a dark line across the bright signal of the fat in the marrow on a T1-weighted magnetic resonance imaging (MRI) scan (Fig. 14.5a). Increased signal intensity is seen within the bone, represent-

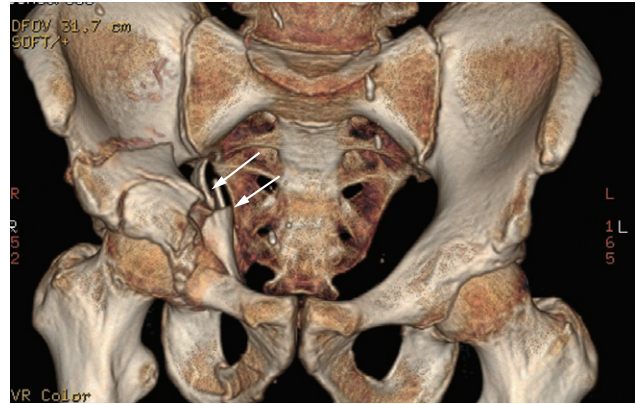


Fig. 14.4 Multiple fractures. Three-dimensional MDCT reformat demonstrating a complex pelvic fracture (arrows), useful in aiding operative planning.

ing haemorrhage and/or oedema on a T2-weighted scan; a STIR sequence has a T2-weighted appearance with saturation of the fat signal intensity (Fig. 14.5b). Sometimes a bone bruise may be visible on MRI (Fig. 14.6) even though there is no discernible fracture on a conventional radiograph.

Magnetic resonance imaging is also very useful for demonstrating injury to soft tissues such as muscle, tendons and ligaments and is particularly useful in knee injuries (Fig. 14.7). MRI is the best examination for sports injury and repetitive strain injuries.

It is also the best method for demonstrating scaphoid fractures and its use has been advocated as the initial investigation.

Radionuclide bone scanning

Fractures may not be visible on plain films, and, in these instances, radionuclide bone scanning may be helpful (Fig. 14.8), although increasingly MRI is often used in these circumstances. The bone scans show increased activity at injured sites within 2–3 days. Increased activity persists for as long as the fractures are healing, often lasting several months. Multiple fractures occasionally give a picture resembling metastases, but usually the distribution suggests injury.

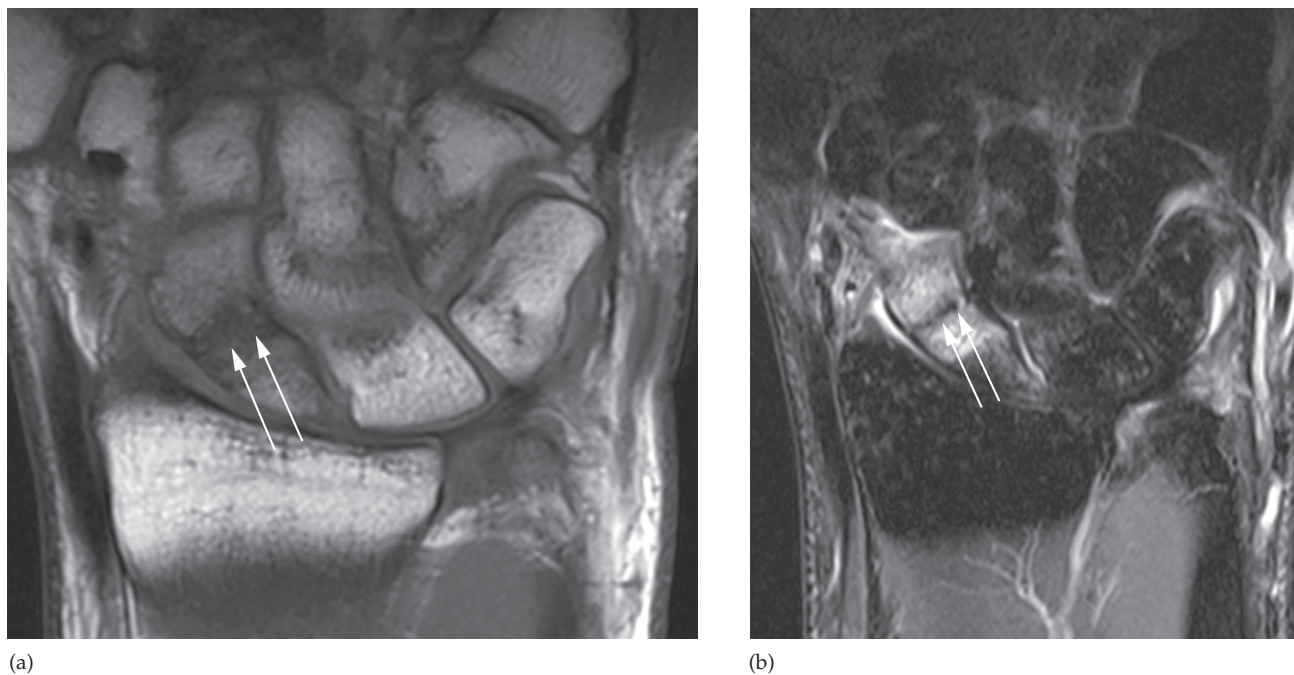


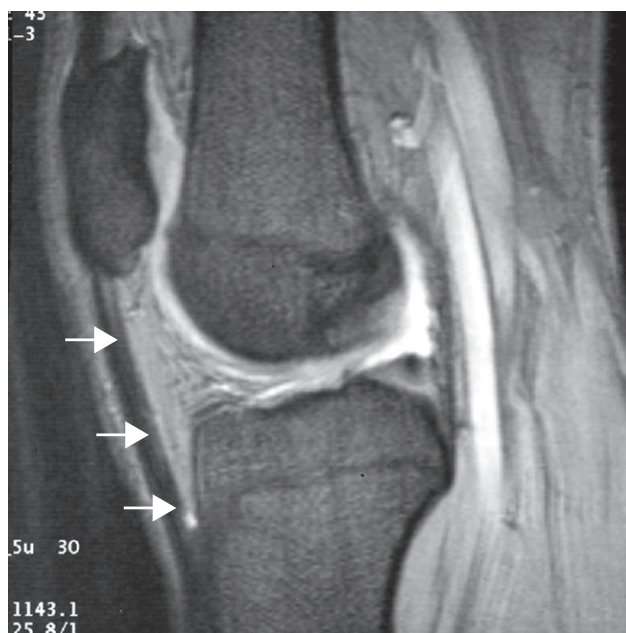
Fig. 14.5 Coronal MRI of the wrist. (a) T1-weighted image and (b) STIR image, showing a low signal intensity fracture line in the waist of the scaphoid (arrows). The STIR image shows surrounding haemorrhage and oedema as high signal either side of the fracture.



Fig. 14.6 Bone bruise. MRI in a patient who suffered severe soft tissue damage to the lateral side of his knee. The high signal in the medial femoral condyle (arrows) is due to a bone bruise. The plain films of the knee showed no bony injury.



(a)



(b)

Fig. 14.7 Rupture of patella tendon. (a) MRI showing diffuse high signal in the region of the patella tendon. (b) Normal patella tendon (arrows) for comparison.

Imaging fractures

Frequently, a fracture is very obvious but in some cases the changes are more subtle. Fractures may be recognized or suspected by several signs (Box 14.2). A *fracture line* may be seen as a lucent line. This may be very thin and easily overlooked (Fig. 14.9). Occasionally, the fracture appears as a dense line from the overlap of the fragments (Fig. 14.10). A *step in the cortex* may be the only evidence of a fracture (Fig. 14.11). *Interruption of bony trabeculae* is of use in impacted fractures where there is no visible lucent line. This is, however, a difficult sign to evaluate (Fig. 14.11). *Bulging or buckling of the cortex* is a particularly important sign in children, where fractures are frequently of the greenstick type (Fig. 14.12). *Soft tissue swelling* may be a valuable guide to the presence of an underlying fracture. A *joint effusion* may become visible following trauma, and, as in elbow fractures, displaced fat pads may indicate an occult radial head fracture (Fig. 14.13).

Some injuries are likely to produce fractures in more than one site. With tibial fractures, for example, the fibula is frequently also broken but the fractures may be a considerable distance apart. Certain bones (e.g. the pelvis and mandible) often fracture in two sites, only one producing severe symptoms. In these situations, all likely fracture sites should be included on the films.

Imaging dislocations

The joint surfaces no longer maintain their normal relationship to each other. Careful evaluation for an associated fracture should be performed.

Further plain film views

Injuries may sometimes be invisible even with two views taken at right angles to each other. If the radiographic findings are equivocal, or if there is clinical suspicion of bony injury with normal radiographs, then further films should be taken as follows:

- *Different projections*, e.g. oblique views (Fig. 14.14).
- *Stress films*. A film taken with a joint under stress may show that it is unstable due to ligamentous damage. Stress films are helpful in ankle injuries when forced inversion and eversion may show movement of the talus (Fig. 14.15).

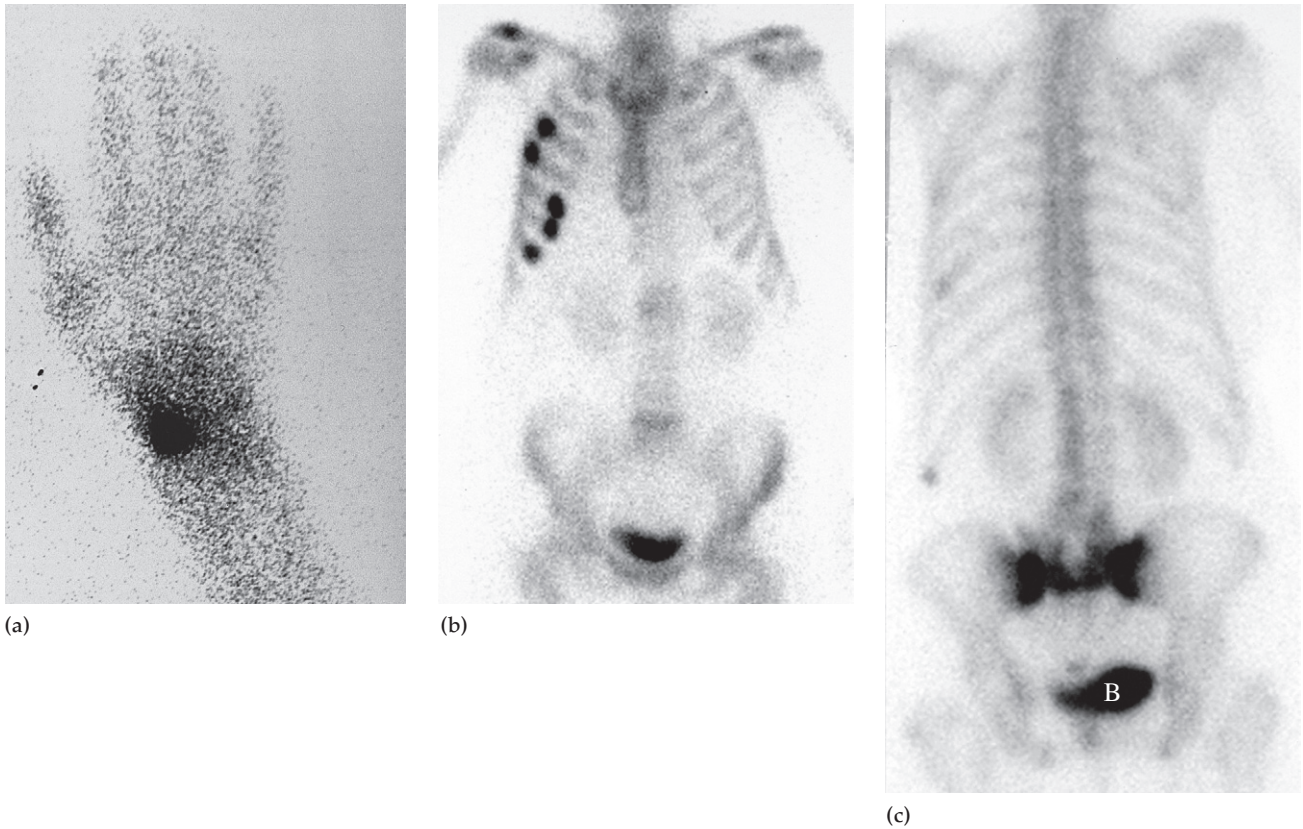


Fig. 14.8 Radionuclide bone scans in trauma. (a) Fracture of the scaphoid. There is increased activity in the scaphoid in this patient who suffered continuing pain after trauma to the wrist. In spite of normal x-rays, the bone scan indicates there is a fracture that was not visible on the radiographs. (b) Fractures in five of the ribs on the right. The distribution of increased uptake is diagnostic of injury. (c) Insufficiency fracture. There is increased uptake in the sacrum in this elderly woman who had a normal pelvic x-ray. B, isotope in the bladder.

Box 14.2 Radiographic signs of fracture

- Fracture line (lucent or dense)
- Step in the cortex
- Interruption of bony trabeculae
- Bulging or buckling of the cortex
- Soft tissue swelling
- Joint effusion

• *Flexion and extension views.* In the cervical spine, injury may cause alteration in the alignment of the posterior borders of the vertebral bodies. This is usually much more obvious on a film taken with the neck flexed (Fig. 14.16). In

the conscious patient, without an obvious subluxation, pain will prevent damage to the spinal cord from instability of the cervical spine, providing the movement is carried out by the patient him- or herself. Flexion and extension views should not be carried out on the unconscious patient.

• *X-ray of the other side.* Comparison with the normal side can be useful in the problem case, particularly if expert help is not available. This applies largely in children where epiphyseal lines and unusual patterns of ossification may simulate a fracture.

• *Delayed films.* If films are taken about 2 weeks after injury, resorption of the bone at the fracture site may then reveal the fracture line. This is particularly useful in detect-



Fig. 14.9 Fracture of the head of the radius appearing as a lucent line.



Fig. 14.10 Fracture of the lower ulnar metaphysis appearing as a sclerotic line (small black arrow).



Fig. 14.11 Step in cortex and interruption of bony trabeculae (arrow) in a Colles' fracture.



Fig. 14.12 Greenstick fracture of the lower end of the radius in a child. There is buckling of the cortex (arrows).

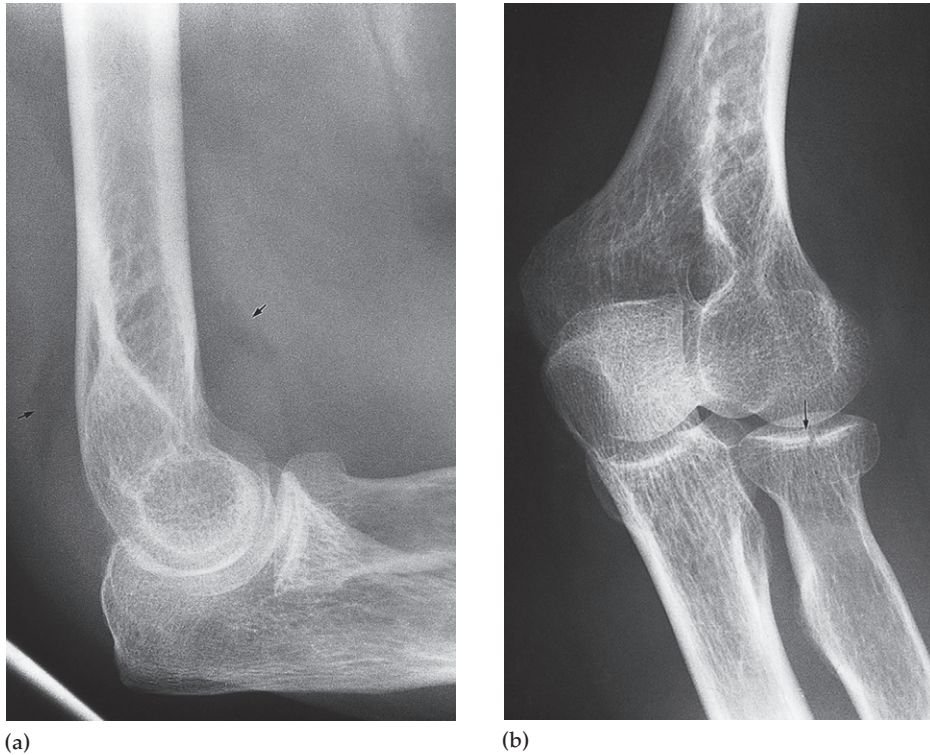


Fig. 14.13 Elbow effusion with fracture of the radial head. (a) The anterior and posterior fat pads (arrows) are displaced away from the humerus, which almost invariably means a fracture is present. (b) Oblique view in this patient showing the fracture of the radial head (arrow) which was only demonstrated on the oblique view.

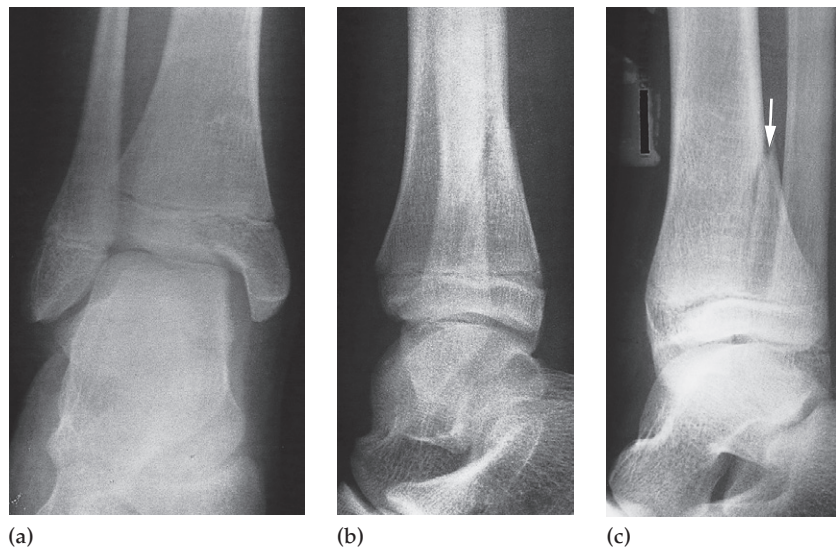


Fig. 14.14 Oblique view demonstrating a fracture. (a) Anteroposterior and (b) lateral views in this child's ankle do not show an obvious fracture. (c) Oblique view clearly demonstrating the fracture (arrow).



Fig. 14.15 Stress view demonstrating ligamentous rupture. Inversion stress on the ankle opens up the lateral joint indicating rupture of the lateral ligaments.

ing scaphoid fractures, which may be invisible immediately after the injury (Fig. 14.17).

Although plain films suffice in almost all patients who have undergone trauma, in certain instances other imaging modalities such as MDCT or MRI are employed.

Specific injuries

Numerous types of fractures and dislocations may be encountered and it is not practical to describe and illustrate them all in this book. The following section is an atlas illustrating a selection of the more common and important injuries.

Salter–Harris classification

Fractures of an epiphysis, growth plate or metaphysis of the long bones often occur in children and may lead to subsequent growth deformities because of damage to a growth plate. Five types are recognized in the Salter–Harris classification (Fig. 14.18a). Types I and II (Fig. 14.18b, c) usually have favourable outcomes. Types III, IV and V require more complex treatment.

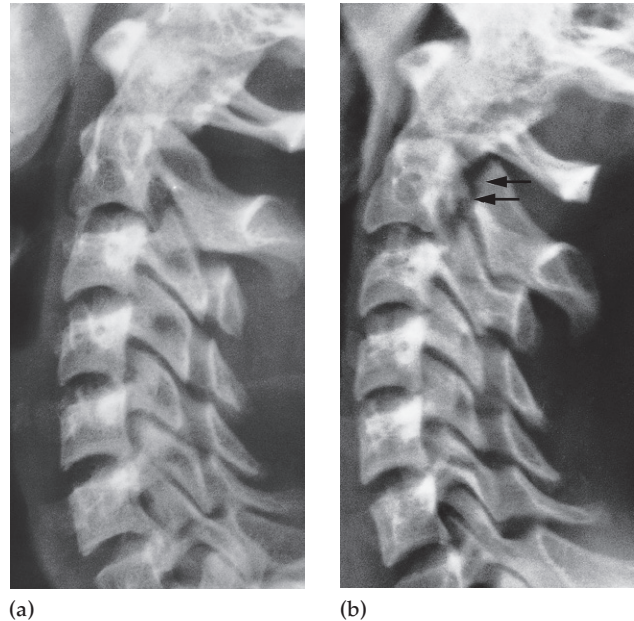


Fig. 14.16 Flexion and extension views demonstrating a fracture. (a) An extension view of the cervical spine does not reveal a fracture. (b) A flexion view clearly shows the fracture of the arch of C2 (arrows).

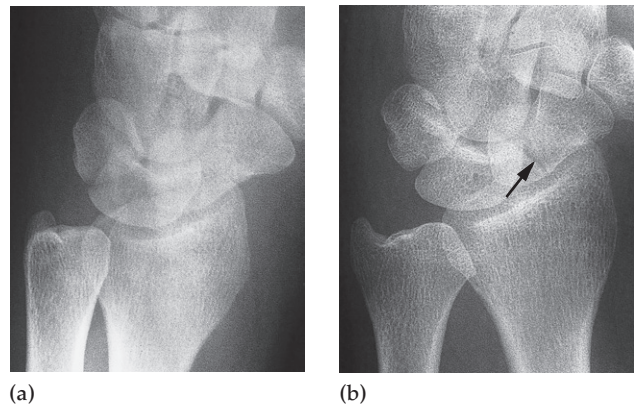


Fig. 14.17 Delayed films demonstrating a fracture. (a) Films taken immediately after the injury did not show a fracture. (b) Films taken 2 weeks after the injury show a fracture through the scaphoid (arrow).

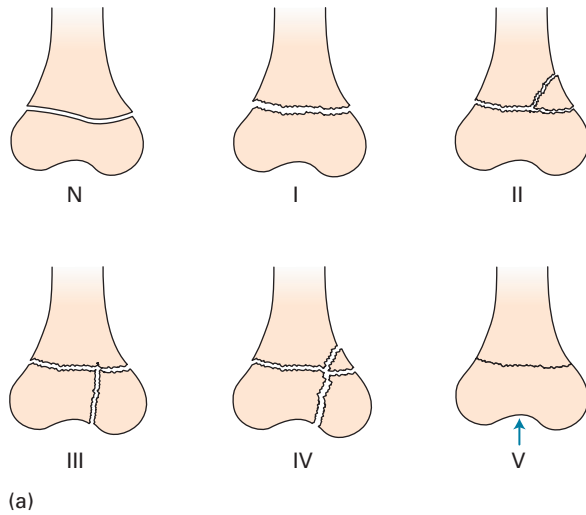


Fig. 14.18 (a) Salter-Harris classification (N, normal):

- Type I: epiphyseal separation by a fracture through the growth plate.
- Type II (the commonest): a fragment of the metaphysis accompanies the displaced epiphysis.
- Type III: a fracture through the epiphysis and growth plate.
- Type IV: a fracture through the epiphysis, growth plate and metaphysis.
- Type V: a crush injury of the growth plate; usually no changes are seen on the radiograph.



(b)



(c)

Fig. 14.18 (b, c) Two examples of Salter-Harris type II fractures. Note that in both examples the fracture runs through the metaphysis as well as through the epiphyseal plate (arrows).



Fig. 14.19 Fracture of the clavicle. This common fracture usually occurs in the outer half of the clavicle. Upward displacement of the medial fragment is frequently seen, as in this example.

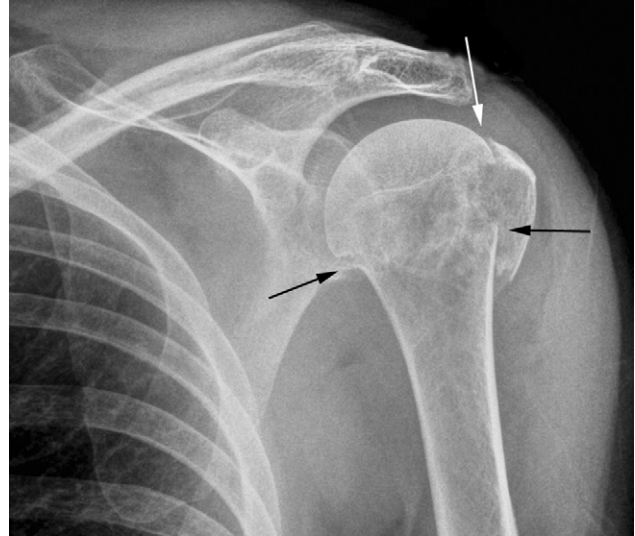


Fig. 14.21 Fracture of the neck of the humerus (black arrows) is a common fracture in the elderly and may be overlooked clinically if it is impacted. The greater tuberosity is also fractured (white arrow) in this example.



Fig. 14.20 Acromioclavicular dislocation. Capsular and ligamentous tears of the acromioclavicular ligaments allow the outer end of the clavicle to be displaced upward relative to the medial aspect of the acromion process (arrow).



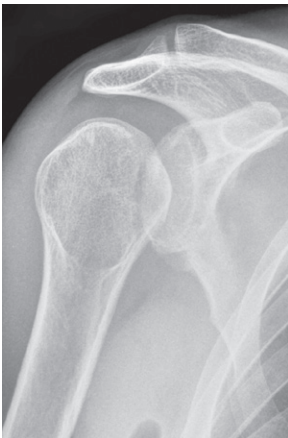
Fig. 14.22 Anterior dislocation of the shoulder. The head of the humerus is displaced inferior and anterior to the glenoid fossa to lie beneath the coracoid process.



Fig. 14.23 Anterior dislocation of the shoulder may be associated with a fracture of the greater tuberosity.



Fig. 14.25 Dislocation of the elbow. The common form is backward and lateral displacement of the radius and ulna.



(a)



(b)

Fig. 14.24 Posterior dislocation of the shoulder is often a consequence of an electric shock or epileptic seizure. (a) The dislocation may be difficult to see on the frontal view. Note the internal rotation of the humerus and lack of congruity of the humeral head with the glenoid. Note the 'lightbulb' appearance of the humeral head. (b) Lateral view showing the humeral head behind the posterior rim of the glenoid fossa beneath the spine of the scapula.

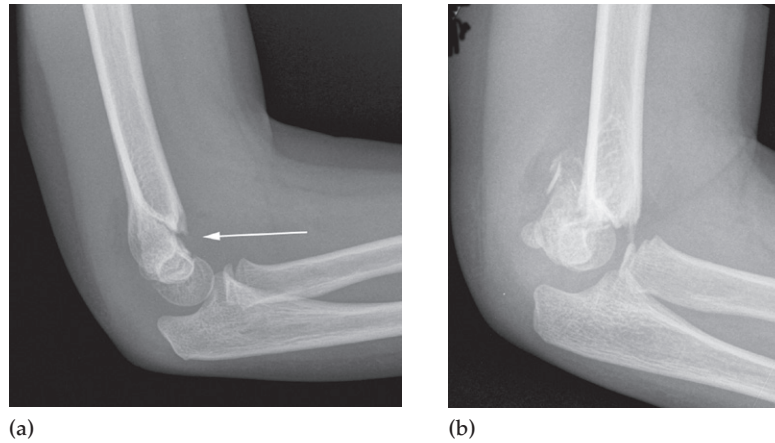


Fig. 14.26 Supracondylar fractures. (a) With minor displacement and (b) with severe displacement. These fractures occur in children and are potentially dangerous because of possible injury to the brachial artery and nerve damage.



Fig. 14.27 Epicondylar fracture showing medial epicondyle separation. Fractures of the epicondyles occur in children before the epiphyses fuse fully.

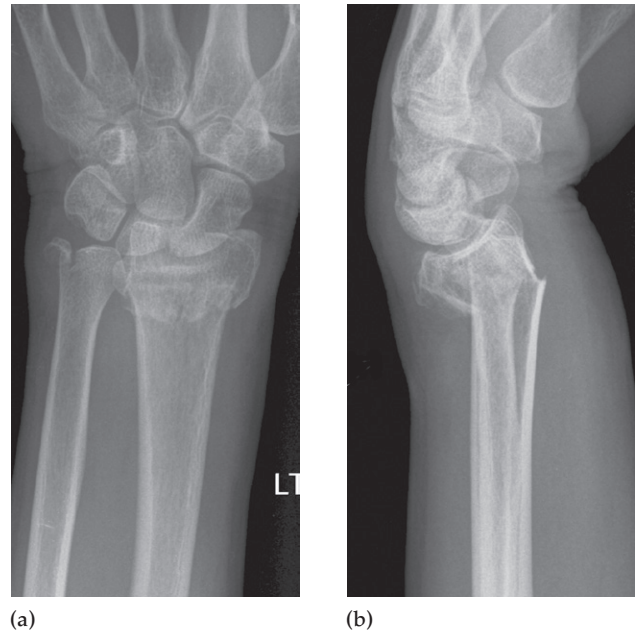


Fig. 14.28 Colles' fracture is common, especially in the elderly. It is a fracture through the lower end of the radius and sometimes the ulnar styloid is avulsed in addition, as in this example. (a) Anteroposterior view. (b) Lateral view showing posterior displacement and angulation giving rise to the 'dinner fork' deformity.



(a)



(b)

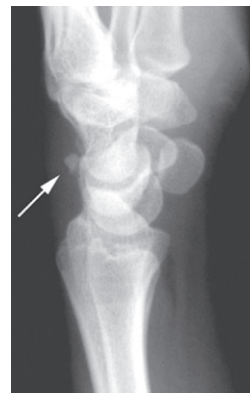
Fig. 14.29 Smith's fracture is a fracture of the lower radius with the reverse deformity to a Colles' fracture. It has anterior displacement and angulation. (a) Anteroposterior view. (b) Lateral view.



Fig. 14.30 Fracture through the lower radial epiphysis resulting in separation of the epiphysis (Salter–Harris I fracture).



(a)



(b)

Fig. 14.31 Fractures of wrist bones. (a) Scaphoid fractures occur in young adults following a fall on the outstretched hand. They are serious injuries because if missed non-union or avascular necrosis may supervene. The fracture (arrow), as in this example, is usually across the waist of the scaphoid. (b) Triquetral fracture – a flake fracture detached from the posterior aspect of the triquetrum (arrow) is seen only on the lateral view.

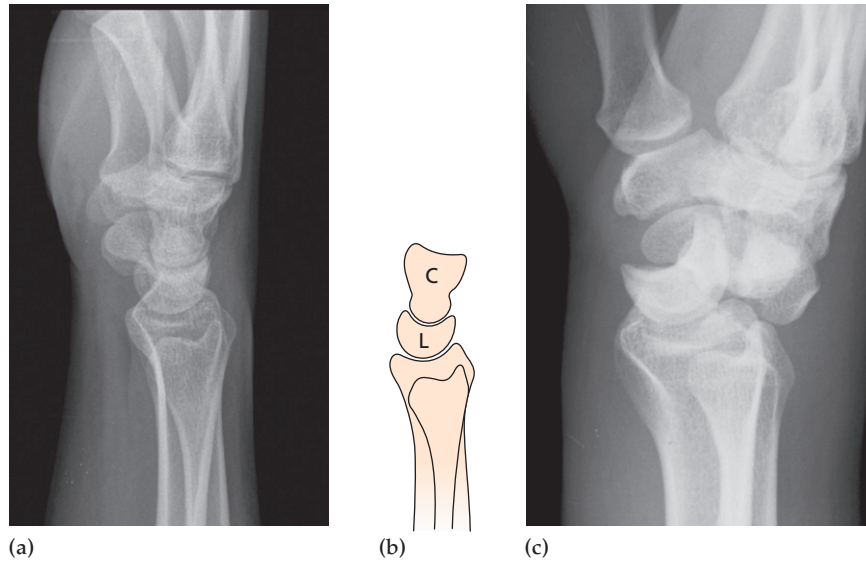


Fig. 14.32 Dislocation of carpal bones. (a, b) The lower end of the radius, lunate (L) and capitate (C) are normally in a straight line. (c) If wrist ligaments are ruptured, the carpal bones, as in this case, may be dislocated posterior to the lunate and the lower radius. Alternatively, and often difficult to differentiate, is anterior dislocation of the lunate.

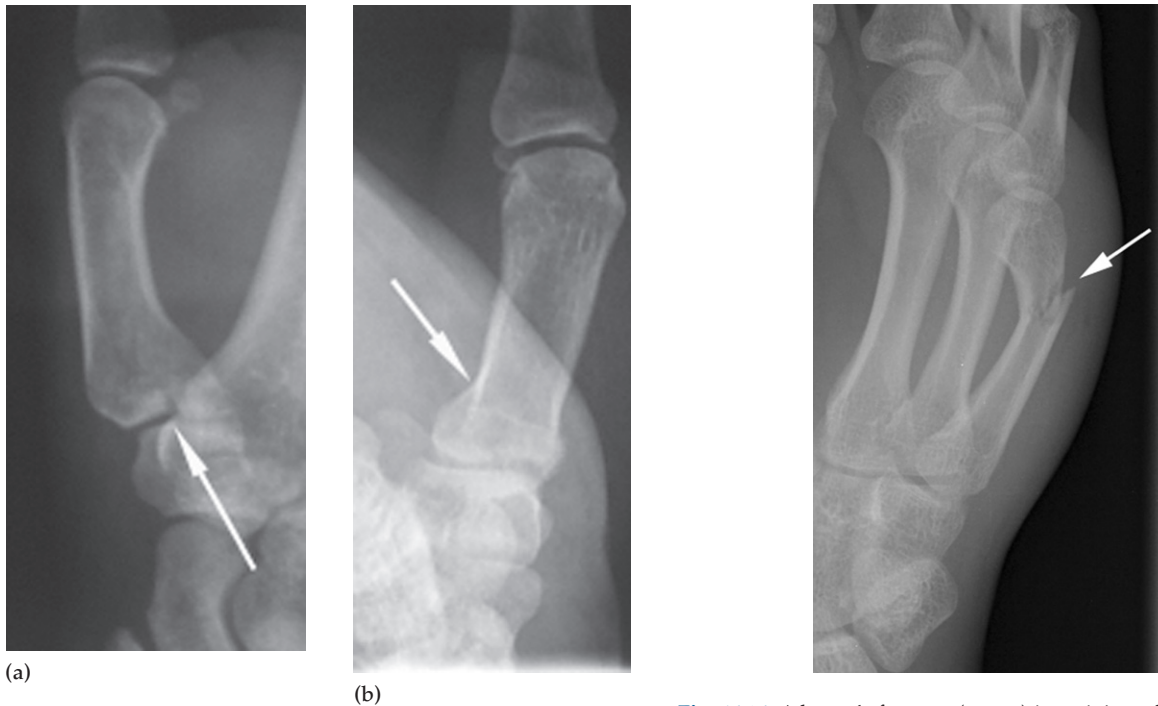


Fig. 14.33 Bennett's fracture is a fracture through the base of the thumb metacarpal. (a, b) Two views showing a fracture (arrow) which, as in this example, often involves the articular surface of the carpometacarpal joint. It invariably requires internal fixation.

Fig. 14.34 A boxer's fracture (arrow) is an injury due to punching. It is a fracture through the shaft of the little finger metacarpal and is often angulated.



Fig. 14.35 Finger injuries. Various fractures and dislocations occur. This patient, who suffered an industrial accident, has a dislocation of the proximal interphalangeal joint of the ring finger with a fracture through the base of the middle phalanx (upward arrow). There is also a fracture through the posterior aspect of the base of the terminal phalanx of the little finger (downward arrow). Such fractures may need special treatment.



Fig. 14.36 Fractures through the pubic rami (arrows) are common in the elderly.



Fig. 14.37 Fractures through the pelvic ring occur with severe trauma. In this example, there is obvious separation of the pubic symphysis. The inevitably accompanying further fractures/dislocations of the pelvic bones and sacroiliac joints often require CT for their demonstration.

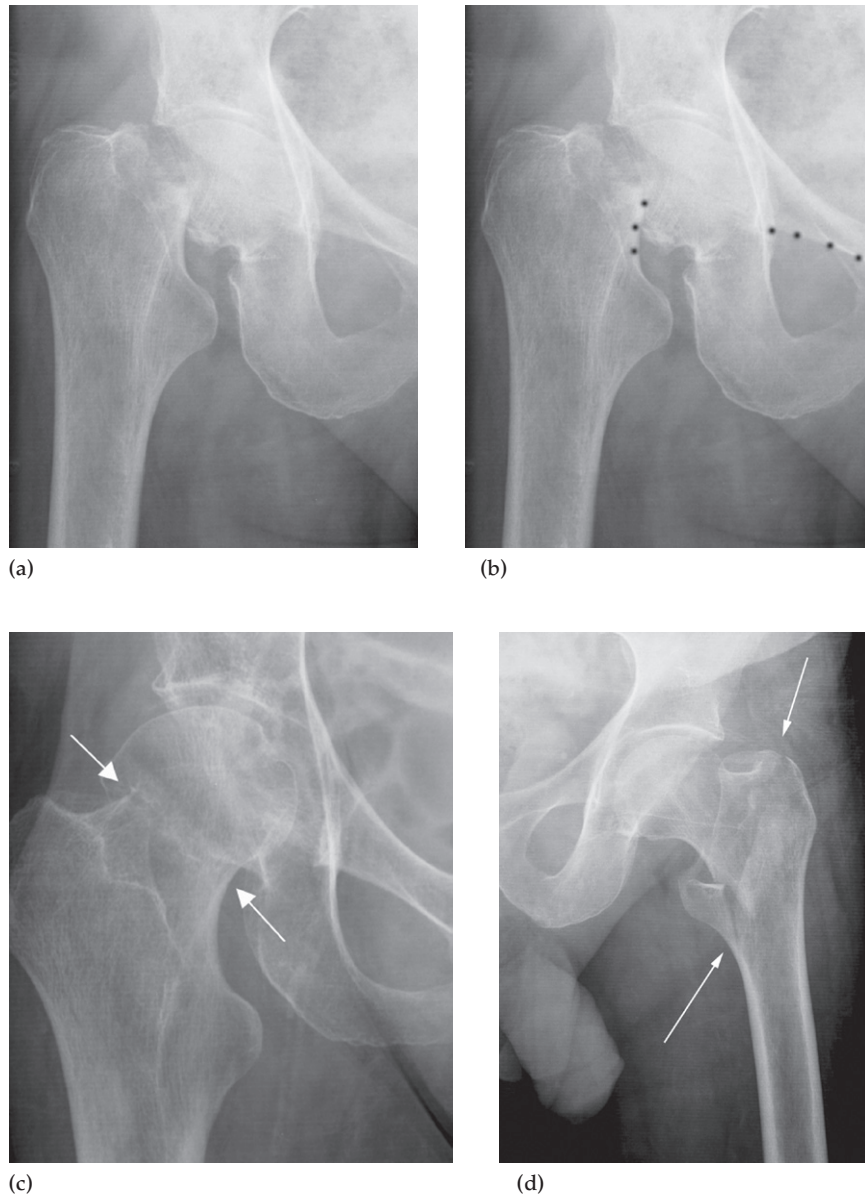


Fig. 14.38 Fractures through the femoral neck are common in the elderly and may result from minor trauma. The radiographic signs in some instances may be subtle. (a) A fracture through the femoral neck interrupts Shenton's line. (b) Shenton's line is a curved line formed by the top of the obturator ring and the medial aspect of the neck of the femur (the interruption of Shenton's line is shown by the dots). (c) Impacted fracture (arrows) causing only a sclerotic line and disruption of the trabecular architecture. (d) Intertrochanteric fracture (arrows) between the greater and lesser trochanters. Intertrochanteric fractures are less prone to subsequent complications than other femoral neck fractures.



Fig. 14.39 Fracture of the patella. There is separation of the fragments and an effusion is present, seen as an opacity in the suprapatellar pouch.



Fig. 14.40 Dislocation of the patella. The patella is dislocated laterally out of the intercondylar groove.



Fig. 14.41 Fat in haemarthrosis. With a knee fracture, fat is often released from the bone marrow and a fat–fluid level may be seen in the suprapatella pouch (black arrows). There is a fracture of the tibial plateau seen as a sclerotic band (white arrow).

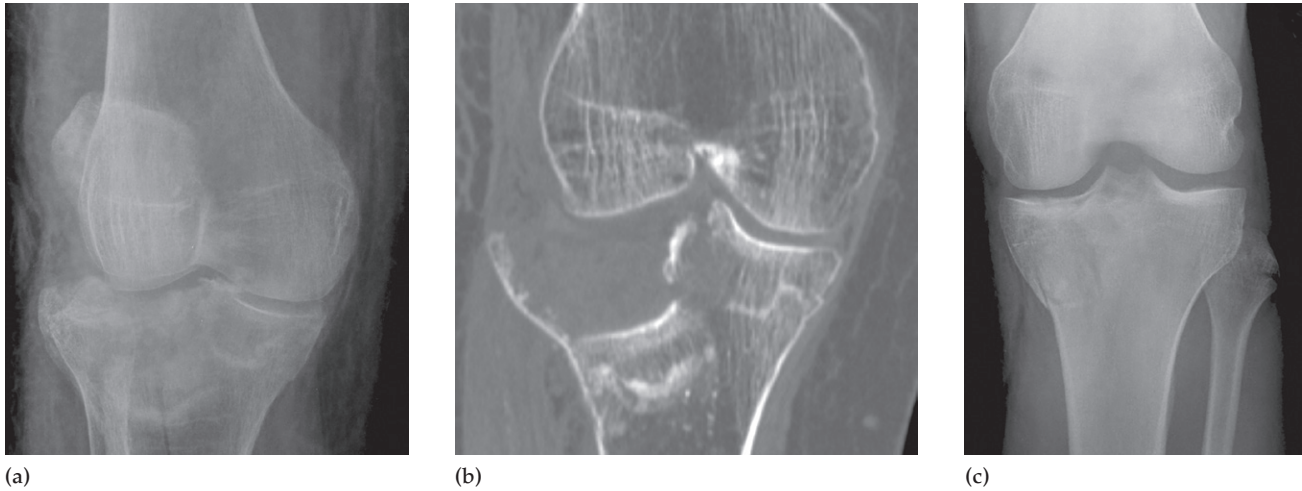


Fig. 14.42 Tibial plateau fractures. A lateral tibial plateau fracture can occur when a car strikes the outer side of the knee ('bumper fracture'). (a) The tibial plateau is fragmented and is driven down into the tibia. (b) CT showing the depression, which requires surgical treatment. (c) A similar injury can occur to the medial tibial plateau.

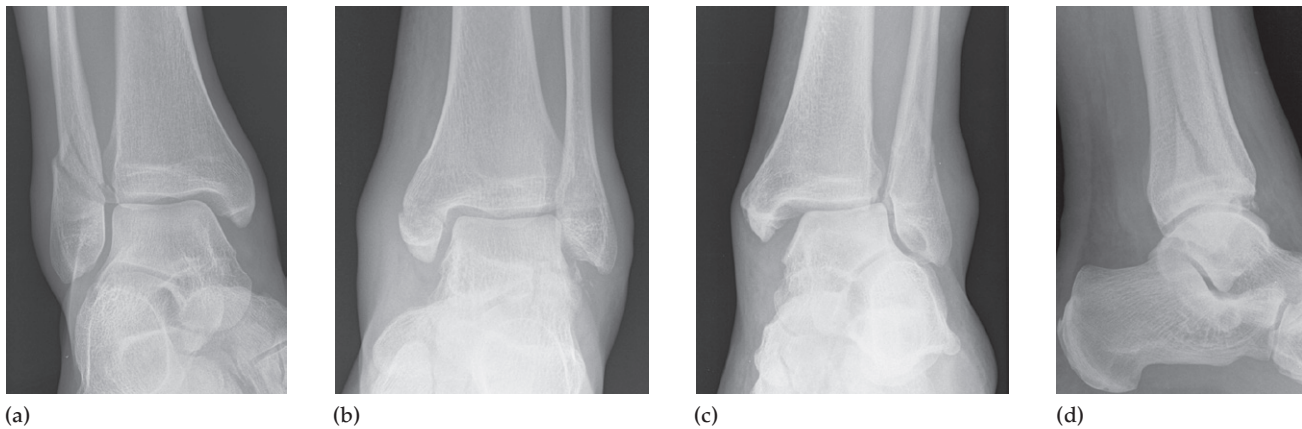


Fig. 14.43 Ankle fractures. Various fractures occur involving the lateral, medial or both malleoli, with or without disruption of the talus in the ankle mortise (see also Fig. 14.15). Soft tissue swelling is usually seen in association with ankle fractures. (a) Fracture of lateral malleolus without displacement of talus. (b) Fracture of the medial malleolus. (c) Anteroposterior and (d) lateral views of a fracture of the lateral malleolus with a lateral shift of the talus indicating ligamentous damage. Note the soft tissue swelling associated with all these fractures.



Fig. 14.44 Fracture of the lateral and medial malleoli with a lateral shift of the talus.

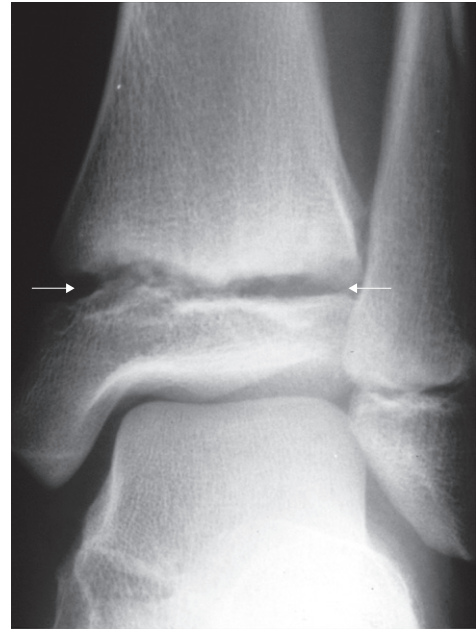
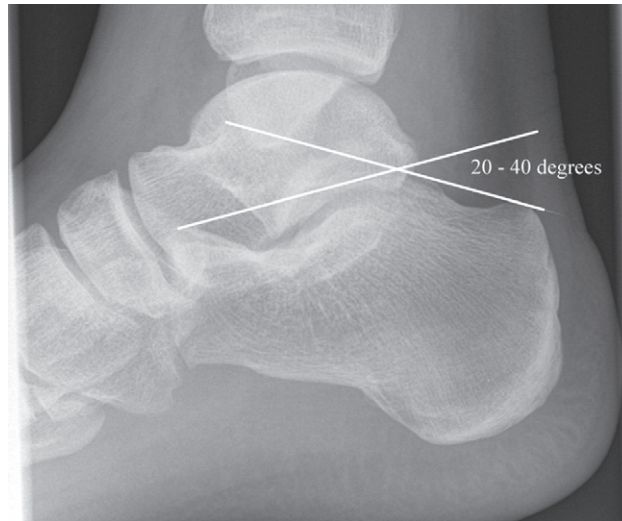


Fig. 14.45 Salter–Harris type I fracture of the ankle (arrows) showing widening of the growth (epiphyseal) plate.



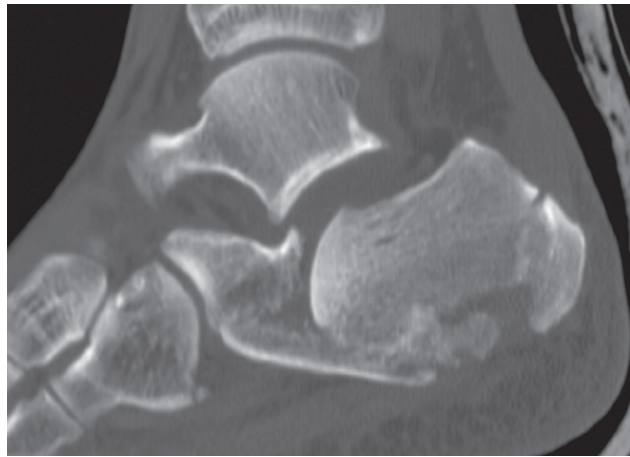
Fig. 14.46 Fracture through the neck of the talus.



(a)



(b)



(c)

Fig. 14.47 Calcaneal fractures are jumping injuries and may be undisplaced or result in compression, causing flattening of the calcaneum. This can be appreciated by a reduction in Bohler's angle to less than 20° . (a) Bohler's angle, shown here in a normal subject, is the angle made by a line across the anterior process of the calcaneum intersecting with a line parallel to the axis of the posterior portion of the calcaneum. (b) Fracture causing flattening and fragmentation of the calcaneum. (c) CT in the same patient showing depressed fragments and complete disruption of the subtalar joint and the fracture involving the calcaneocuboid joint.



Fig. 14.48 Tarsometatarsal dislocation. Lateral dislocation of the metatarsals through the tarsometatarsal joint is known as Lisfranc's fracture. There is a step between the medial border of the medial cuneiform and the medial border of the base of the second metatarsal (arrows point to these two landmarks). The second to fifth metatarsals are dislocated laterally.

Stress fracture

Stress fractures are due to repeated, often minor, trauma. They occur in athletes, particularly in the tibia and fibula. Another example is the so-called 'march fracture' occurring in the shafts of the metatarsals (Fig. 14.50). Initially, despite the presence of pain, a radiograph will show no evidence of a fracture, but if a further film is taken after 10–14 days a periosteal reaction may draw attention to the fracture site, where a thin crack may be visible (Fig. 14.50, Fig. 14.51). A stress fracture may appear as a sclerotic band across the bone and a fracture line may not necessarily be visible.



(a)

(b)

Fig. 14.49 (a) Fractures of the base of the fifth metatarsal appear as a horizontal line across the base of the metatarsal (arrow). (b) They should not be confused with a normal apophysis (arrow) which is seen as a sliver of bone parallel to the axis of the metatarsal.

Radionuclide bone scanning can be helpful in distinguishing stress fractures from other causes of pain, because a stress fracture will appear as an area of increased uptake before any changes are visible on the radiographs (Fig. 14.52). Increasingly, MRI is used to evaluate bone stress injuries and can be a useful tool in the evaluation of pain in athletes.

Insufficiency fracture

An insufficiency fracture results from normal activity or minimal trauma in weakened bone, commonly from osteoporosis or osteomalacia. Compression fractures of the vertebral bodies are the commonest insufficiency fractures but they also characteristically occur in the sacrum, pubic rami and femoral necks, though other bones may be involved.

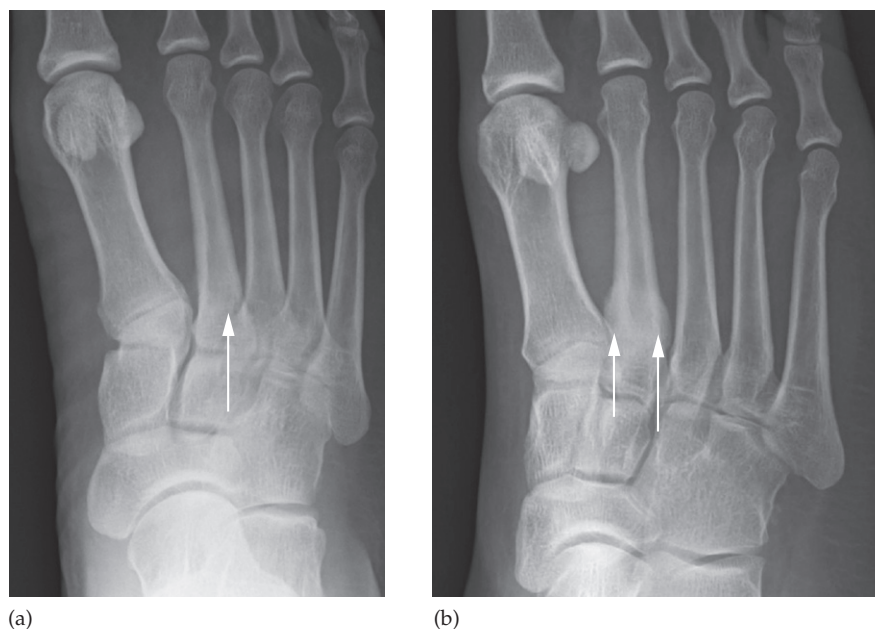


Fig. 14.50 'March fracture'. (a) The initial film at the time of injury showing a faint lucent line at the base of the second metatarsal (arrow). (b) Follow-up film at 2 weeks showing a marked periosteal reaction and callus formation at the site of the stress fracture (arrows).

Pathological fracture

A pathological fracture is one that occurs through abnormal bone. Pathological fractures may be the presenting feature of both primary and secondary bone tumours (Fig. 14.53). Often, the causative lesion is obvious. Sometimes, particularly in the ribs, metastases responsible for fractures are ill defined and difficult to see. In such cases, the diagnosis rests on recognizing the irregularity of the margins of the fracture. If there is doubt about the diagnosis it is helpful to look elsewhere in the skeleton for other metastases, using a radionuclide bone scan.

Transverse fractures occur through abnormal bone, particularly in Paget's disease. In these instances, the Paget's disease is always obvious (Fig. 14.54).

Non-accidental injury

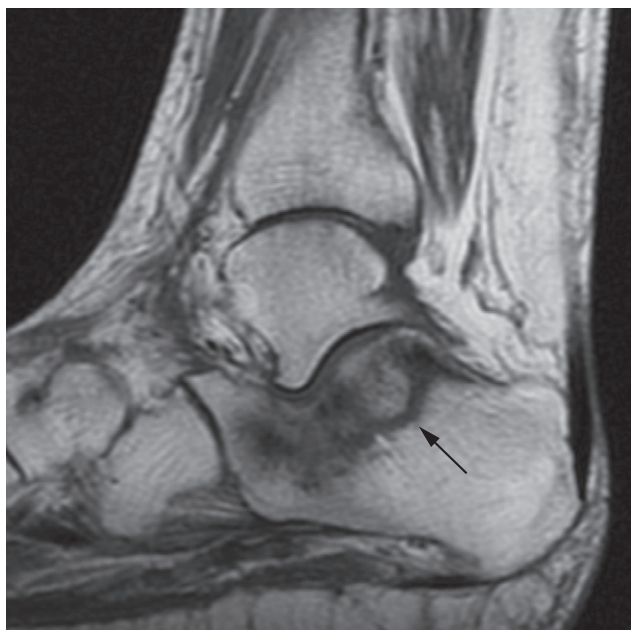
Non-accidental injury was previously known as the battered baby syndrome and it is essential that everyone

looking at radiographs should be fully aware of this condition as the radiological findings may suggest the diagnosis in otherwise unsuspected cases. If child abuse is suspected, the whole skeleton including the skull should be x-rayed, as clinically unsuspected injuries may be detected. Increasingly, a CT head is also performed in the examination. This enables assessment for subdural haemorrhage. Most patients are less than 3 years old and half are younger than 1 year; an age when accidental fractures are uncommon.

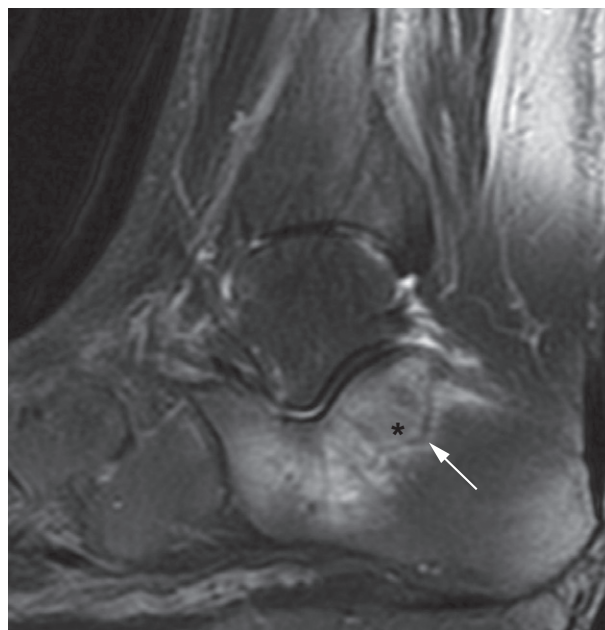
Certain patterns suggest that the injury is not accidental (Figs 14.55 and 14.56), listed in Box 14.3. *Multiplicity of fractures* is an important sign, particularly if the fractures are of different ages, because the injuries often take place on separate occasions. Some fractures appear recent, while others show periosteal reaction, indicating healing. *Metaphyseal fractures* frequently appear as small chips from the metaphyses of the long bones, known as corner fractures. They most probably result from twisting and pulling the limbs of a struggling baby (Fig. 14.56).



(a)



(b)



(c)

Fig. 14.51 Stress fractures. (a) In this calcaneum there is sclerosis adjacent to the stress fracture (arrow). (b, c) MRI of a calcaneal stress fracture in a different patient. (b) T1-weighted image demonstrating a low signal intensity sclerotic stress fracture (arrow). (c) STIR sequence demonstrating bright oedema (*) surrounding the fracture (arrow).

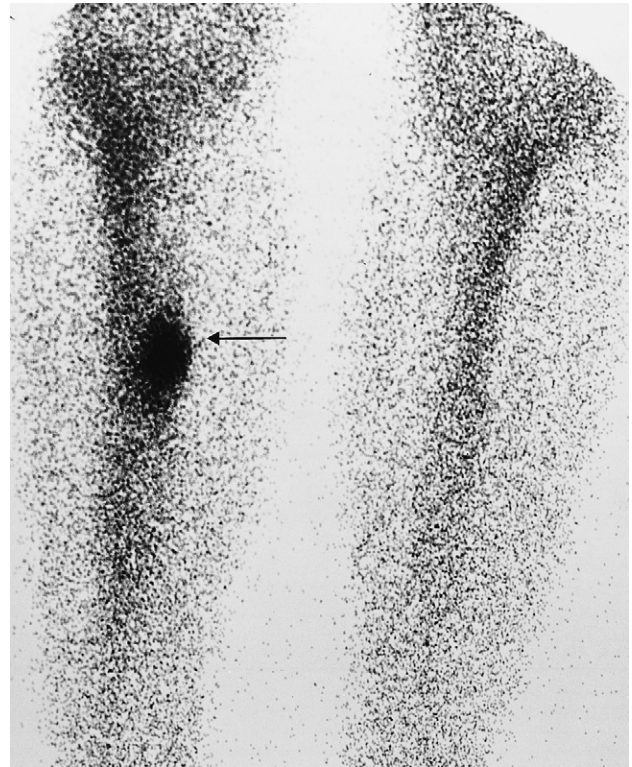


Fig. 14.52 Stress fracture. Radionuclide bone scan showing increased uptake in the tibia (arrow) of this athlete with pain in the leg. The radiographs at the time of the scan were normal.



Fig. 14.53 Pathological fracture. (a) A fracture has occurred through one of many lytic metastases from a carcinoma of the breast. (b) This fracture, in another patient, has occurred through an area of bone destruction due to myeloma.



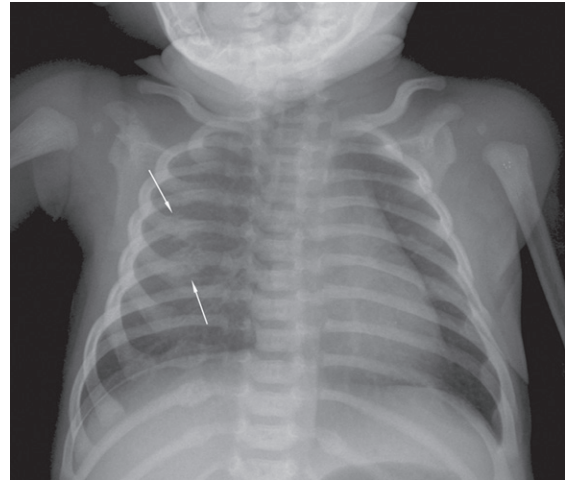
(b)



Fig. 14.54 Paget's disease showing incomplete fractures, known as infracctions, of the lateral aspect of the femur. Note the marked thickening of the cortex and bowing of the femur.



(a)



(b)

Fig. 14.55 Non-accidental injury. (a) The fracture through the humerus is recent and, apart from the young age of the baby, is an unremarkable spiral fracture. (b) However the chest x-ray taken at the same time shows healing posterior rib fractures (arrows).

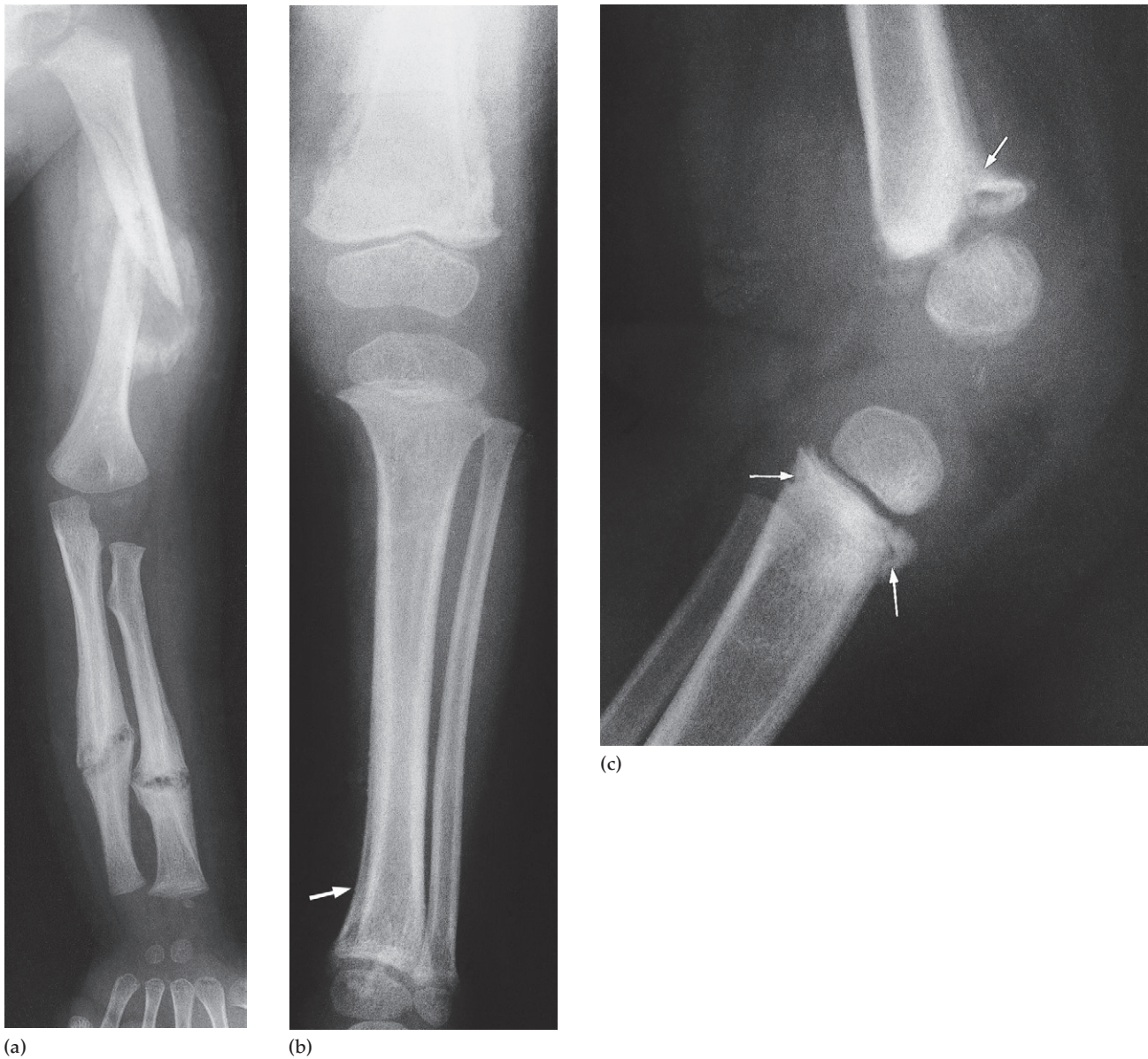


Fig. 14.56 Non-accidental injury. (a) Multiplicity of fractures. There is a recent fracture of the humerus with florid callus formation. The fractures of the radius and ulna are of longer duration and show healing with organized callus. (b) Periosteal reaction along the shaft of the tibia (arrow) from previous trauma with haemorrhage under the periosteum. There has been recent trauma to the lower end of the femur with marked periosteal reaction. (c) Metaphyseal fractures (arrows) and sclerosis around the knee.

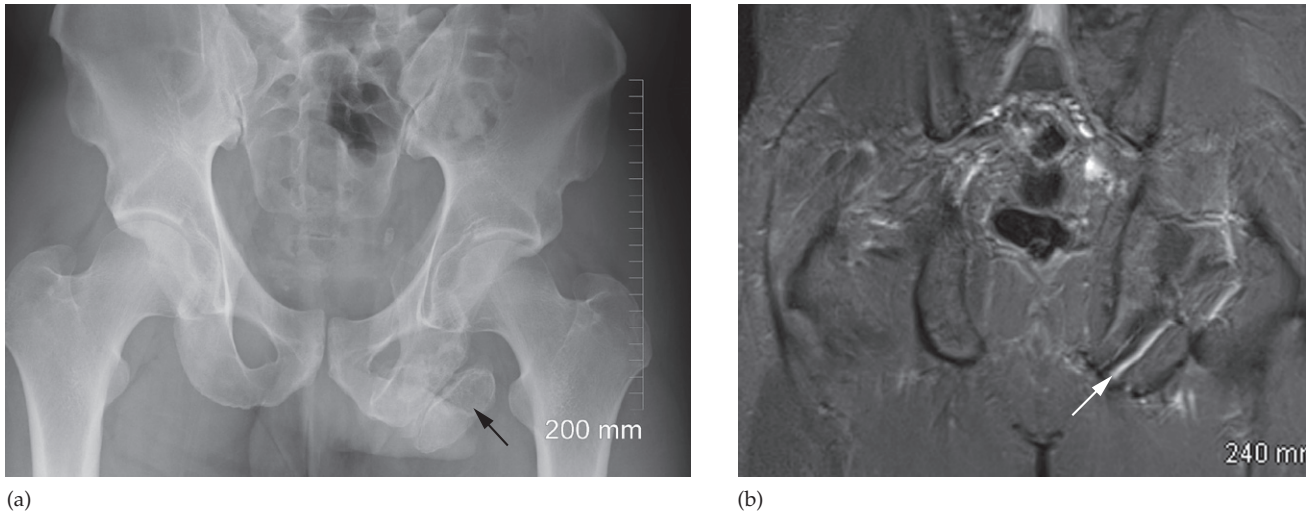


Fig. 14.57 Avulsion fracture. (a) In this example, the avulsed ischial spine appears as a bone fragment adjacent to the ischium (black arrow). (b) MRI showing the non-union of the avulsed fragment (arrow).

Box 14.3 Signs of non-accidental injury in children

- Multiple fractures of different ages
- Rib fractures, particularly axillary and posterior ribs
- Metaphyseal fractures
- Metaphyseal sclerosis
- Epiphyseal separation
- Periosteal reactions

Rib fractures are an important finding as they are rarely seen, even in severe accidental trauma. The fractures are caused by squeezing the baby and are thus usually seen in the axillary and posterior portions of the ribs. *Epiphyseal*

separation is frequently associated with a metaphyseal fracture. *Metaphyseal sclerosis* is probably due to repeated injury and repair. Haemorrhage under the periosteum occurs easily in children. The elevated periosteum lays down new bone, which may be so extensive that it envelops the shaft, forming *periosteal reactions*.

Avulsion fractures

Avulsion fractures occur in sports people and are found in recognized sites such as the inferior iliac spine from avulsion of the rectus femoris muscle or the ischium from avulsion of the hamstring muscles (Fig. 14.57).

Imaging techniques

In most neurological disorders, plain films are either normal or the abnormalities are too non-specific for the diagnosis to be made. Skull radiographs are rarely performed except as part of skeletal surveys in suspected non-accidental injury or myeloma (Fig. 15.1). Computed tomography (CT) and magnetic resonance imaging (MRI) give vastly more information and one or the other investigation is indicated in practically all patients with intracranial disease.

Computed tomography

A routine CT examination of the brain involves making 20–30 axial sections. The axial plane is also the routine viewing projection but, if sufficiently thin, reconstructions can be made from the axial sections, which then provide images in any other plane (Fig. 15.2). However, to enable good differentiation of grey and white matter, a slice thickness of 3–5 mm is needed. The window settings are selected for brain tissue or bone, depending on the structure being assessed (see Fig. 15.33).

Contrast enhancement for computed tomography

The brain parenchyma does not normally enhance following an intravenous injection of contrast medium due to the blood–brain barrier (BBB) – the endothelial lining of cerebral vessels preventing passage of solutes. Contrast enhancement of a brain lesion is therefore a consequence of breakdown of the BBB such as with ischaemia, inflam-

mation and neoplasms (Box 15.1). Intracranial lesions (such as meningiomas) supplied by the external carotid artery, which lacks a BBB, will often enhance avidly. There is also no BBB in the pituitary, pineal and choroid plexuses, which will normally enhance. Contrast is therefore only used routinely to evaluate vessels and extra-axial lesions or to increase the conspicuity of brain lesions.

Computed tomography angiography

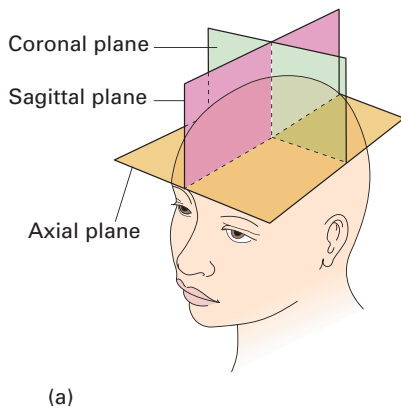
If thin slices are acquired following contrast administration, detailed reconstructions of the vessels can be created in multiple planes and with surface-shaded three-dimensional images (Fig. 15.3). CT angiography has replaced conventional angiography for the initial diagnosis of arterial occlusions, aneurysms and arteriovenous malformations (AVMs). The venous phase of the angiogram can give information on the venous sinuses of the brain such as when looking for thrombosis. Perfusion CT is a new technique that can quantify the passage of contrast through the brain to evaluate the presence and extent of infarction and ischaemia in stroke patients who may be candidates for thrombolysis treatment.

Normal head computed tomography

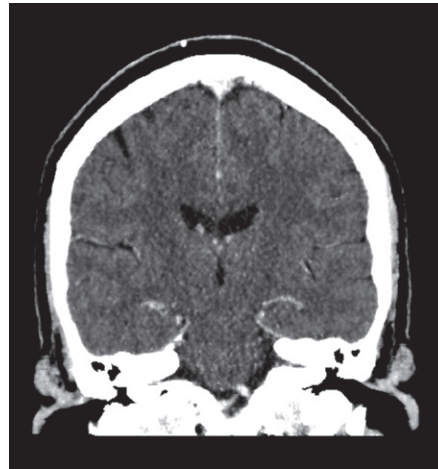
A normal CT scan of the head is illustrated in Fig. 15.4. The cerebrospinal fluid (CSF) is seen as water density within the ventricular system and subarachnoid space surrounding the brain. It is possible to distinguish the white and grey matter of the brain due to the higher fat content within



Fig. 15.1 Myeloma. Multiple well-defined lytic lesions of various sizes are seen in all areas of the skull vault.



(a)



(b)

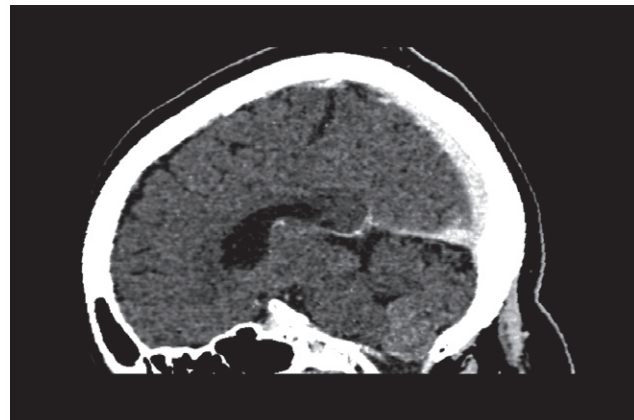
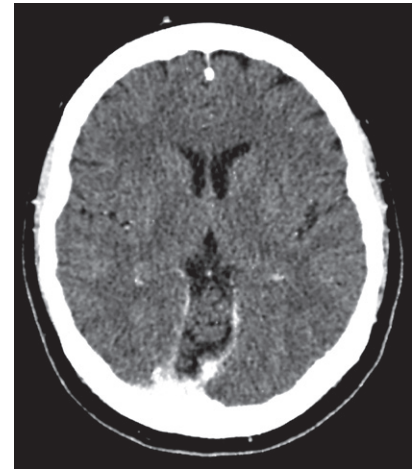


Fig. 15.2 (a) Diagram of the axial, coronal and sagittal planes. (b) Corresponding CT images of a normal brain.

Box 15.1 Intracranial enhancement on computed tomography and magnetic resonance imaging

Physiological

- Choroid
- Anterior pituitary gland
- Arteries
- Dural venous sinuses

Pathological

- Metastases
- Some primary gliomas
- Meningiomas
- Abscess
- Acute demyelination

myelinated white matter, which is therefore of lower attenuation. The larger arteries at the base of the brain can usually be identified within the CSF-containing basal cisterns. Calcification is normally seen in the pineal gland and choroid plexus particularly in the lateral ventricles. Pathological calcification can be seen in abnormal vessels such as an AVM or aneurysm and some types of brain tumour. The supratentorial regions are usually well shown, but details of the posterior fossa may be obscured by artefact from the surrounding bone.

Abnormal head computed tomography

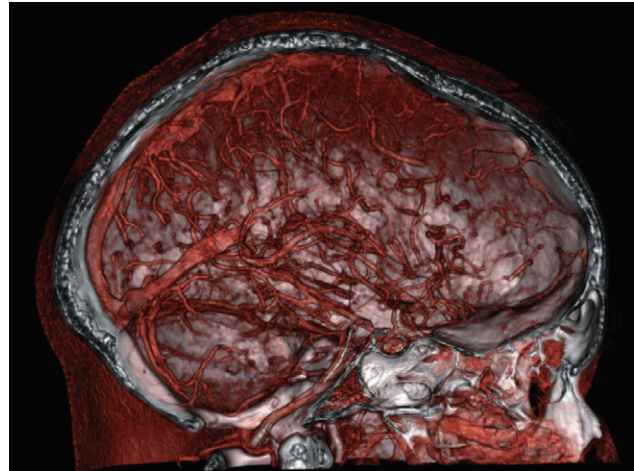
When an abnormality is seen, it is important to decide whether it has an intra-axial or extra-axial location as the pathologies and therefore the differential diagnosis are very different. Intra-axial lesions can involve the white and grey matter structures of the brain parenchyma, while extra-axial lesions may involve the meninges, extracerebral spaces and skull vault. Specific diagnoses are suggested by combining the clinical features with information about multiplicity, size, position and density of the lesion.

The key signs of an abnormality on a CT scan are:

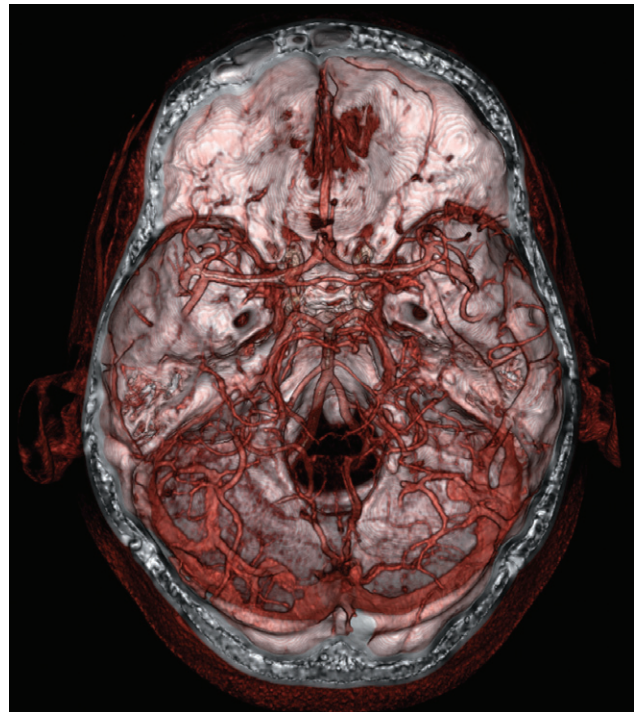
- abnormal tissue density
- mass effect
- enlargement of the ventricles.

Abnormal tissue density

Abnormal tissue may be of higher or lower density than the normal surrounding brain. High density is seen with



(a)



(b)

Fig. 15.3 Surface-shaded CT angiograms. (a) Sagittal and (b) axial images created from a contrast-enhanced CT scan showing the normal arteries and veins of the brain.

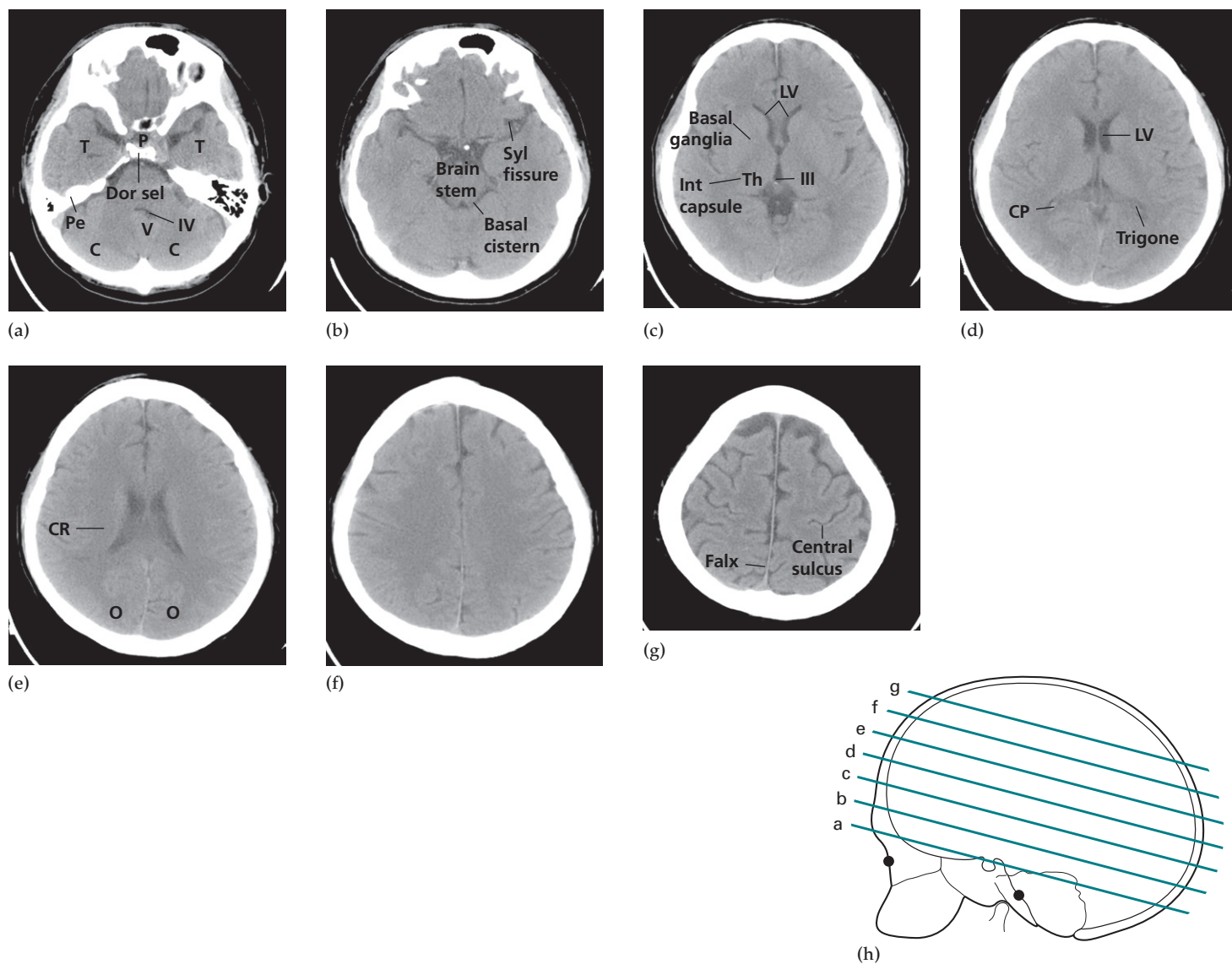
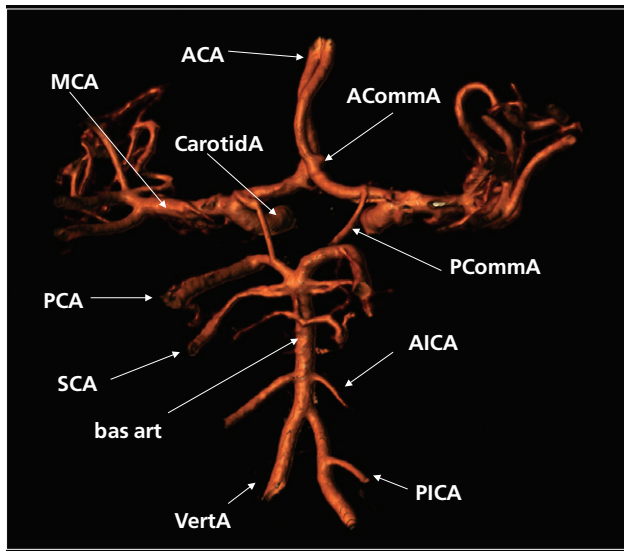


Fig. 15.4 (a–g) Normal head CT images. The levels at which the sections were taken are indicated in the diagram (h). C, cerebellar hemisphere; CP, choroid plexus; CR, corona radiata; Dor sel, dorsum sellae; III, third ventricle; Int capsule, internal capsule; LV, lateral ventricle; O, occipital lobe; P, pituitary gland; Pe, petrous bone; Syl fissure, Sylvian fissure; T, temporal lobe; Th, thalamus; V, vermis. (i) (*Opposite*) Surface-shaded CT angiogram with the major intracranial arteries labelled. ACA, anterior cerebral artery; AComMA, anterior communicating artery; AICA, anterior inferior cerebellar artery; bas art, basilar artery; CarotidA, carotid artery; MCA, middle cerebral artery; PCA, posterior cerebral artery; PComMA, posterior communicating artery; PICA, posterior inferior cerebellar artery; SCA, superior cerebellar artery; VertA, vertebral artery.



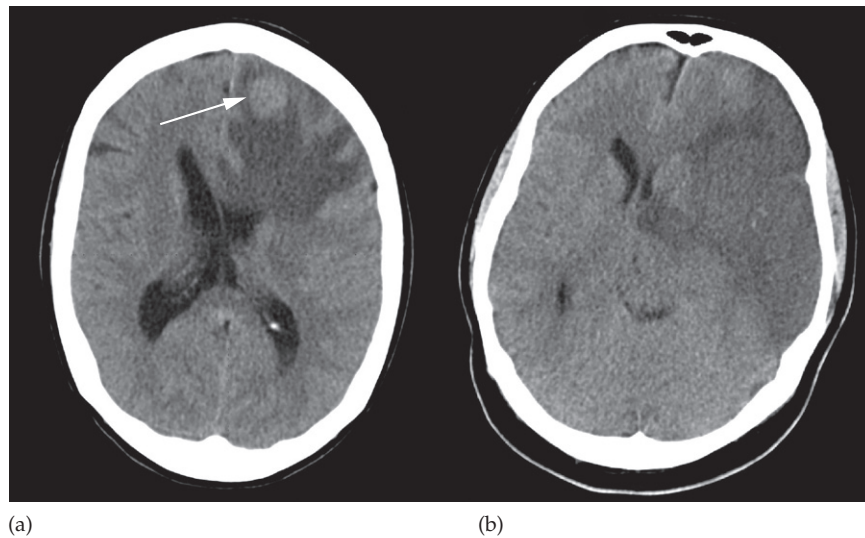
(i)

Fig. 15.4 Continued

acute haemorrhage (see Figs 15.21 and 15.22), calcification and areas of contrast enhancement (see Fig. 15.25). Low density can be due to cytotoxic oedema associated with infarcts, or to vasogenic oedema, which commonly surrounds neoplasms, abscesses and other areas of inflammation. Cytotoxic oedema will involve both the white and grey matter structures (Fig. 15.5b), whereas vasogenic oedema is limited to the white matter and characteristically shows finger-like projections into the subcortical white matter in the gyri. (Fig. 15.5a).

Mass effect

The normally symmetrical lateral ventricles should be examined to see if they are displaced or compressed. Shift of midline structures, such as the septum pellucidum, the third ventricle or the pineal gland away from a lesion indicates a significant mass effect (Fig. 15.6a). Ventricular dilatation will occur if the mass obstructs the flow of CSF. A



(a)

(b)

Fig. 15.5 Types of oedema. (a) Unenhanced CT image demonstrating vasogenic oedema around a hyperdense brain metastasis (arrow). Note how the oedema extends through the white matter but spares the overlying grey matter cortex. (b) Unenhanced CT demonstrating a wedge-shaped area of cytotoxic oedema from an ischaemic stroke involving the middle cerebral artery territory and both the grey matter cortex and the underlying white matter. Both are associated with mass effect causing distortion of the lateral ventricles.

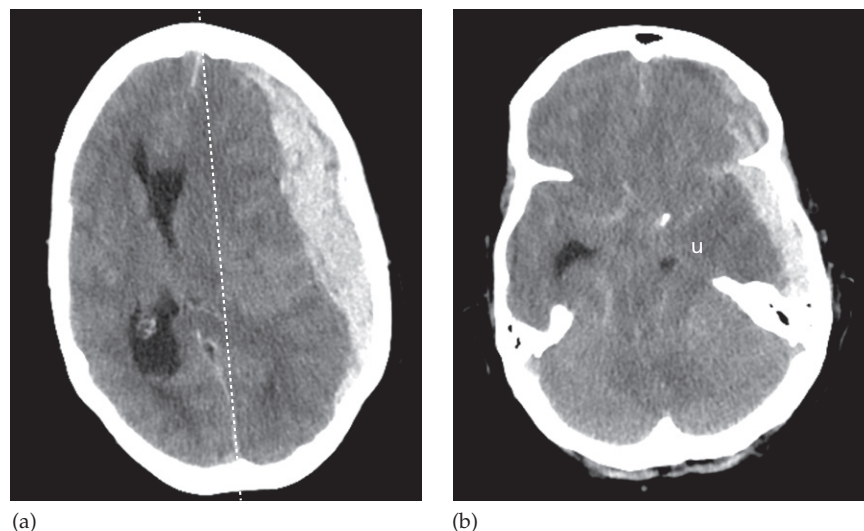


Fig. 15.6 Brain herniation. Unenhanced CT scans showing subfalcine and downward transtentorial herniation due to an acute subdural haematoma. (a) In subfalcine herniation there is a shift of brain and ventricles across the midline (dashed line). (b) In downward transtentorial herniation there is obliteration of the normal CSF-containing basal cisterns and herniation of the medial temporal lobe over the tentorium cerebellum. u, uncus.

mass effect may also show itself by effacing the basal cisterns, such as when the suprasellar cistern is obscured by downward movement of the medial temporal lobes over the tentorium cerebellum (uncal herniation – Fig. 15.6b) or the cerebellar tonsils through the foramen magnum.

Enlargement of the ventricles

There are two basic mechanisms that cause the cerebral ventricles to enlarge:

- Obstruction to the CSF pathway, either within the ventricular system (obstructive hydrocephalus) or over the surface of the brain (Fig. 15.7).
- Secondary to atrophy of the surrounding brain tissue (see Fig. 15.29a).

Magnetic resonance imaging

The advantage of brain MRI is its superior spatial and contrast resolution without the artifact problems associated with local bone structures on CT. Therefore, the anatomy

of the brain can be exquisitely displayed and enables much better visualization of brain pathologies, particularly in areas such as around the skull base for the pituitary gland and the posterior fossa which are poorly seen by CT. The routine sequences used for MRI vary but usually include T1- and T2-weighted sequences in orthogonal planes (Fig. 15.8). A FLAIR (fluid attenuated inversion recovery) sequence is useful as the pulse sequence nulls the bright signal from CSF, making brain pathology (usually T2 bright) more visible. Magnetic resonance can also recognize flowing blood within larger arteries and veins, which can be examined without the need for contrast medium to create intracranial angiograms (Fig. 15.9).

The diffusion-weighted imaging (DWI) sequence looks at the normally random movement of water molecules in brain tissue and is extremely useful, particularly when the patient is suspected of having an acute stroke. Within areas of cytotoxic oedema such as an infarct, the movement of water molecules in the extracellular space is limited by the swollen, dying cells and this produces bright signal, whereas the movement of water within vasogenic oedema is not limited (free) and does not produce any signal

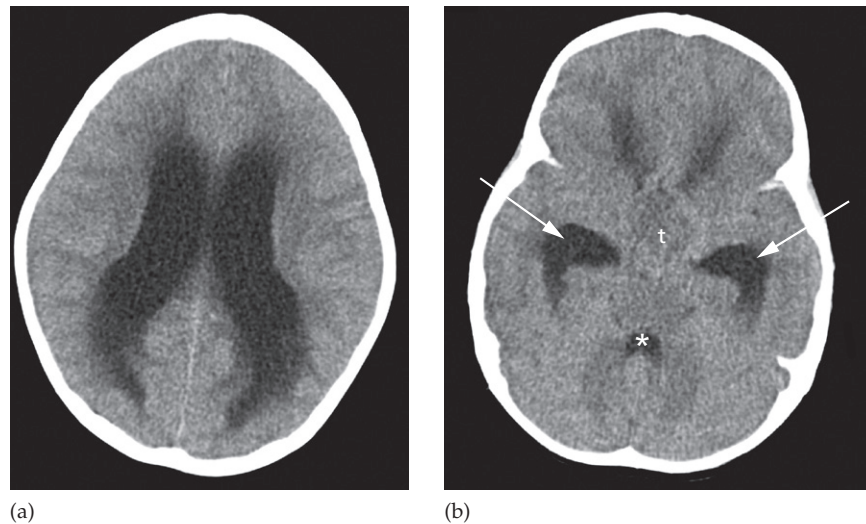


Fig. 15.7 Obstructive hydrocephalus. Axial CT images performed at the level of the lateral ventricles (a) and more inferiorly at the level of the temporal horns (b). The lateral ventricles including the temporal horns (arrows) are dilated but the fourth ventricle (*) is normal in size. The CSF-filled sulci normally seen along the convexities of the cerebral hemispheres are also effaced. The hydrocephalus was due to a tumour (t) obstructing the aqueduct, which connects the third and fourth ventricles.

change. The DWI scan becomes positive within minutes of an acute stroke (Fig. 15.10) whereas CT abnormalities can take hours and will miss very small infarcts. Restricted diffusion within a cystic mass is also relatively specific for pus within a pyogenic abscess.

The water molecules in normal axons making up the white matter are unlikely to traverse the myelin sheath and therefore flow more rapidly in the direction of the axon bundle. An advance in diffusion imaging uses this feature to demonstrate the location and orientation of the tracts connecting various parts of the brain: an investigation known as diffusion tensor imaging or tractography, which may be helpful for studying white matter pathways in disease (Fig. 15.11) and for surgical planning.

Functional MRI utilizes different techniques to measure the blood flow to parts of the brain which changes depending on the neuronal activity in that location at the time of scanning. The patient is usually scanned whilst performing various tasks such as memory recall and the scan produces a map of brain activity superimposed on the anatomical location. The technique may be useful in understanding brain function, particularly in psychiatric disorders.

The disadvantages of MRI compared with CT include the limited visualization of calcification and lack of bone detail. Each sequence has to be acquired separately so the overall scan time is much longer, during which the patient has to lie still, and monitoring seriously ill patients within the scanner can be difficult. If intubated, the life support and monitoring equipment must be MRI compatible. Any intracranial ferrous metal present such as aneurysm clips or cochlear implants are absolute contraindications.

Contrast enhancement for magnetic resonance imaging

Although the natural differences in MRI signal intensity are great, contrast agents can be used to give additional information. Like the intravenous iodinated agents used for CT, the gadolinium compounds used for MRI enhancement are excluded from the normal brain substance by the BBB. Breakdown of the BBB, such as by tumours or abscesses, means that contrast will accumulate within these pathological processes and show high signal intensity (i.e. they appear white) on T1-weighted images (see Box 15.1 and Fig. 15.15b).

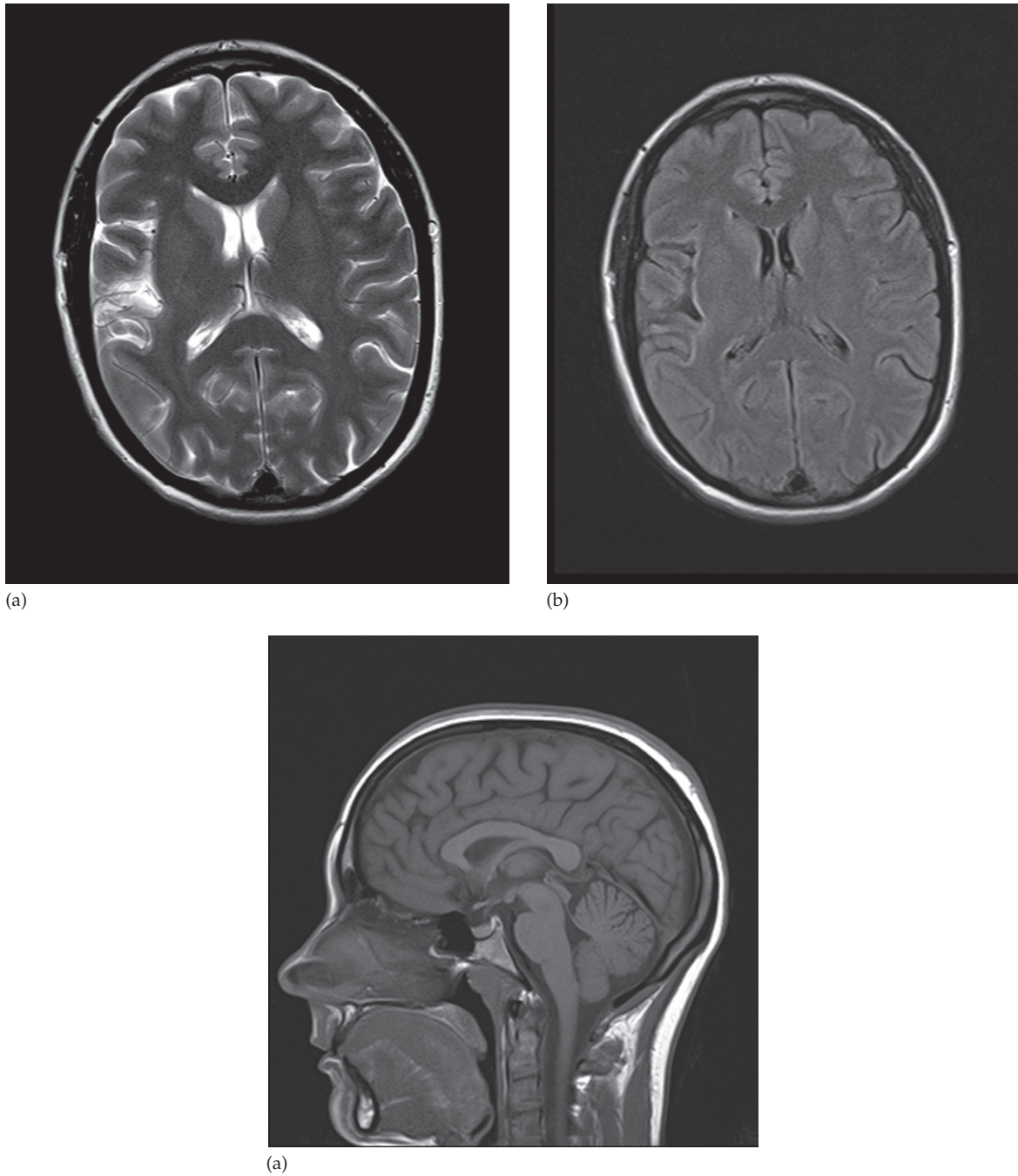


Fig. 15.8 Normal brain MRI. The images are axial sections at the level of the lateral ventricles. (a) T2-weighted image. (b) FLAIR image. (c) A midline sagittal section (T1-weighted).

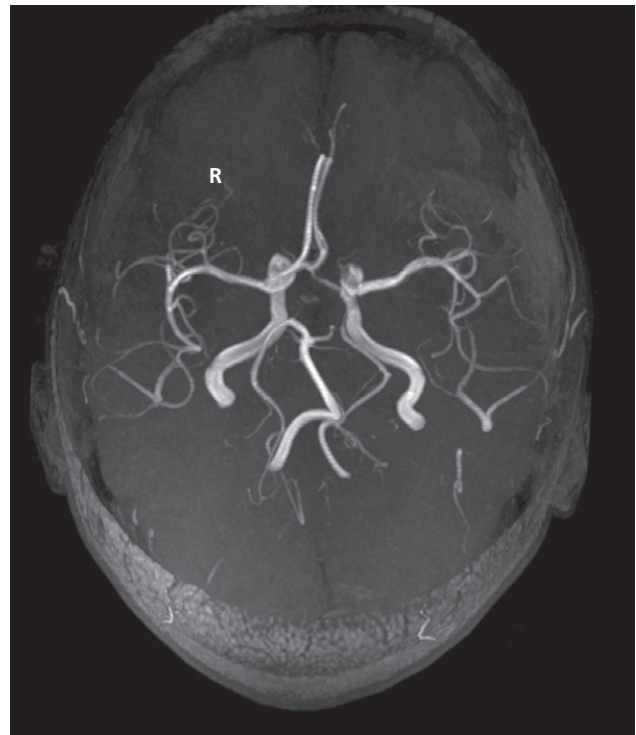
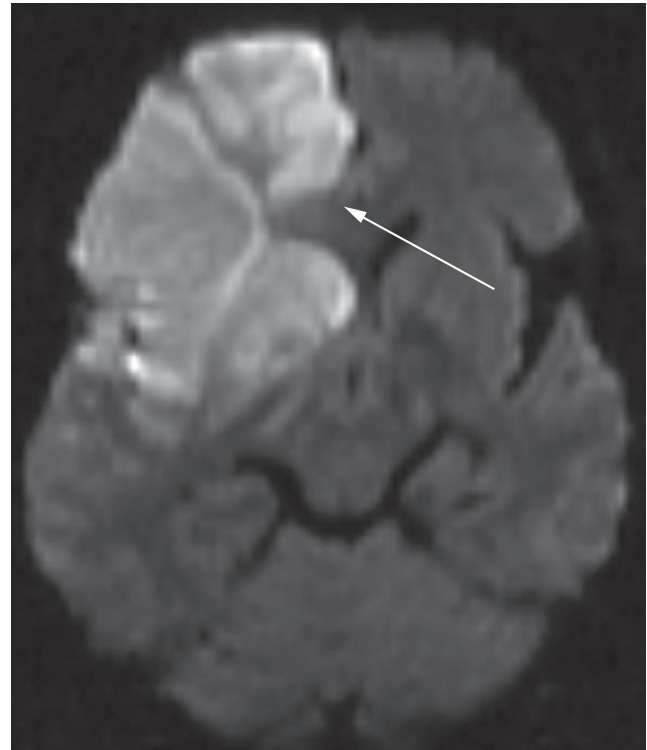


Fig. 15.9 Magnetic resonance angiography (MRA). The arteries at the base of the brain, the circle of Willis, are very well shown by MRA without the use of any contrast agent.



(a)



(b)

Fig. 15.10 DWI in stroke. (a) An unenhanced CT image showing low attenuation in the right frontal lobe and basal ganglia (arrow). (b) Diffusion-weighted MRI showing bright signal indicating the extent of restricted diffusion due to an acute infarct; it is more extensive anteriorly (arrow).

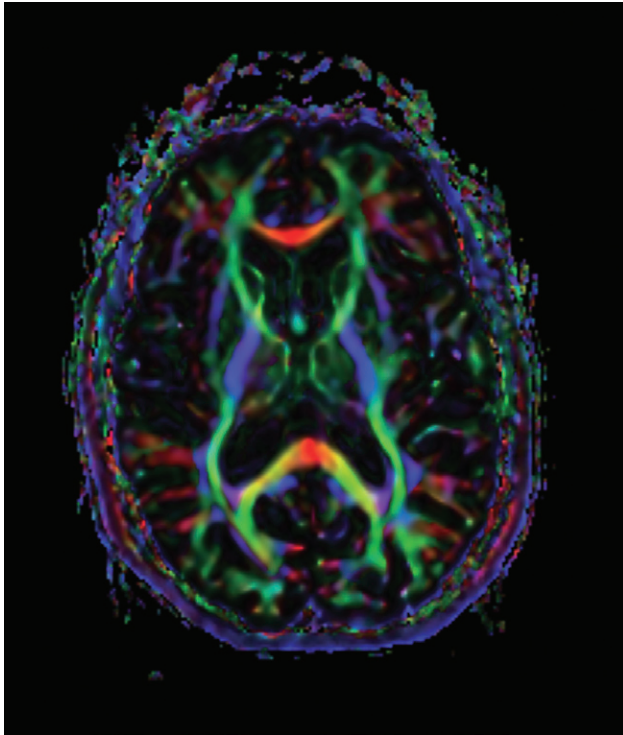


Fig. 15.11 Diffusion tractography image derived from diffusion data showing the structural connectivity of the brain where white matter fibres running in the same orientation are ascribed the same colour. Courtesy of Dr Maddigan, St George's Hospital, London.

Abnormal magnetic resonance imaging of the brain

The range of normal anatomy and abnormalities that can be shown by MRI is very great. Fat, haemorrhage, oedema, CSF and flowing blood all have characteristic signal intensities. Thus, it is more often possible to make a specific diagnosis of an intracranial disorder with MRI than with CT. MRI is the preferred investigation in intracranial sepsis, tumours, inflammatory diseases, epilepsy and congenital malformations.

Haemorrhage can be seen on MRI and the blood can be aged as haematomas develop a specific signal pattern owing to the breakdown products of haemoglobin, such as methaemoglobin or hemosiderin. These have different

paramagnetic effects that profoundly alter the MR signal in a way that can be recognized on T1- and T2-weighted scans (Fig. 15.12).

Neurosonography

It is relatively simple to scan the heads of neonates using ultrasound to obtain images of the ventricular system and brain (Fig. 15.13a). Scanning is done through the open fontanelle where there is no bone to impede the transmission of the ultrasonic waves. No sedation is required and the procedure is readily carried out even on intensive care units. Neurosonography has proved particularly useful in detecting intracranial haemorrhage, which premature babies are more prone to (Fig. 15.13b) and the hydrocephalus that may follow. It has also been used to demonstrate the presence of congenital abnormalities of the brain. When the fontanelle closes it is still possible to perform Doppler studies through the thin pterygion region of the skull to assess the flow of blood through the major intracranial arteries such as in intracranial stenosis.

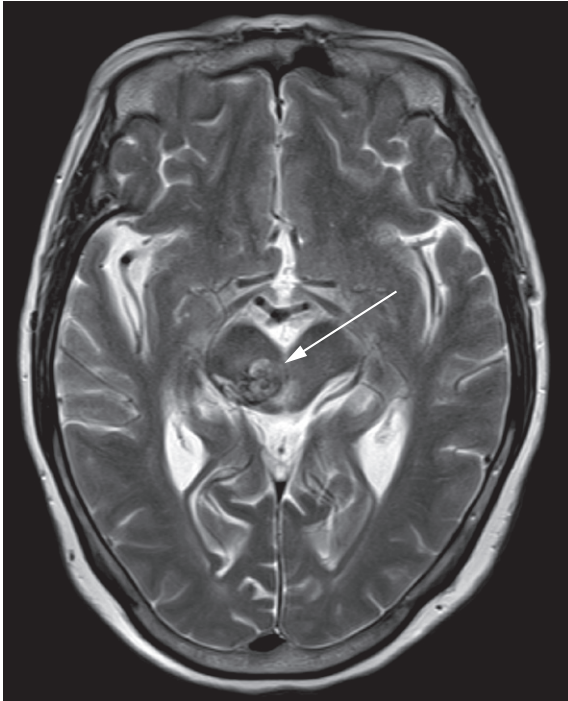
Specific brain disorders

Brain tumours

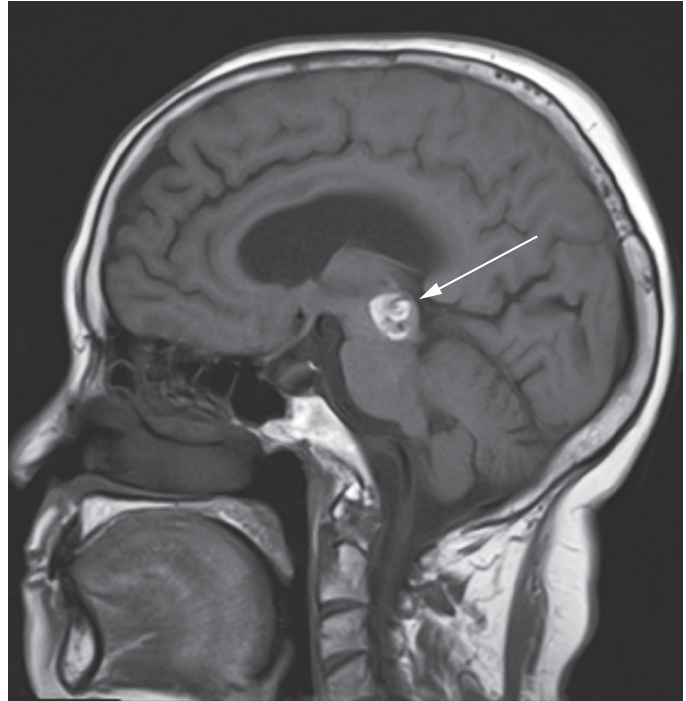
Of all brain tumours, approximately one-third are gliomas, one-third metastases and one-third non-glial tumours. Important features to narrow the differential are the patient's age, the location of the lesion (intra- versus extra-axial and site in brain), density or signal characteristics and the enhancement pattern.

Glioma

Glioma is a non-specific term used to describe a group of tumours that arise from glial cells, which normally support the brain neurons, such as astrocytes (astrocytoma is the commonest tumour type). They range from low grade (e.g. childhood pilocytic astrocytoma) to high grade (e.g. glioblastoma multiforme). At CT, a glioma typically appears as a solitary, irregular, low attenuation lesion (Fig. 15.14a). Local mass effect can usually be demonstrated although this can be minimal as the glioma is replacing rather than expanding brain tissue. Gliomas may calcify – particularly

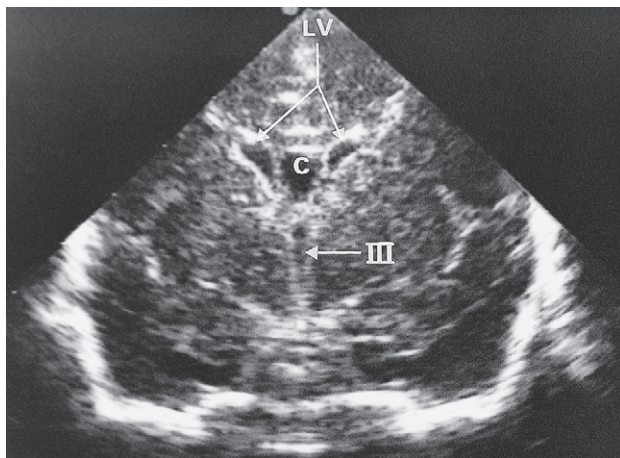


(a)

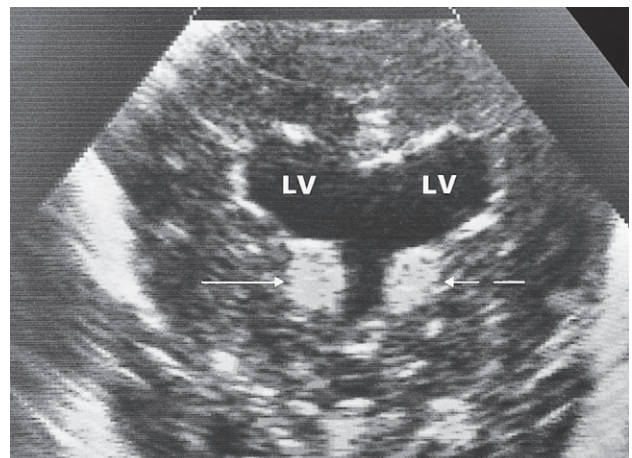


(b)

Fig. 15.12 Cerebral haemorrhage on MRI. A mixed signal haemorrhage in the midbrain on (a) axial T2-weighted and (b) sagittal T1-weighted sequences due to acute blood and chronic blood products (haemosiderin) in a cavernous haemangioma (arrows).



(a)



(b)

Fig. 15.13 Neurosonography. (a) Normal coronal section taken through the anterior fontanelle in a neonate. (b) Coronal section showing bilateral subependymal haemorrhages (arrows). The lateral ventricles are dilated. C, cavum septum pellucidum; III, third ventricle; LV, lateral ventricle.

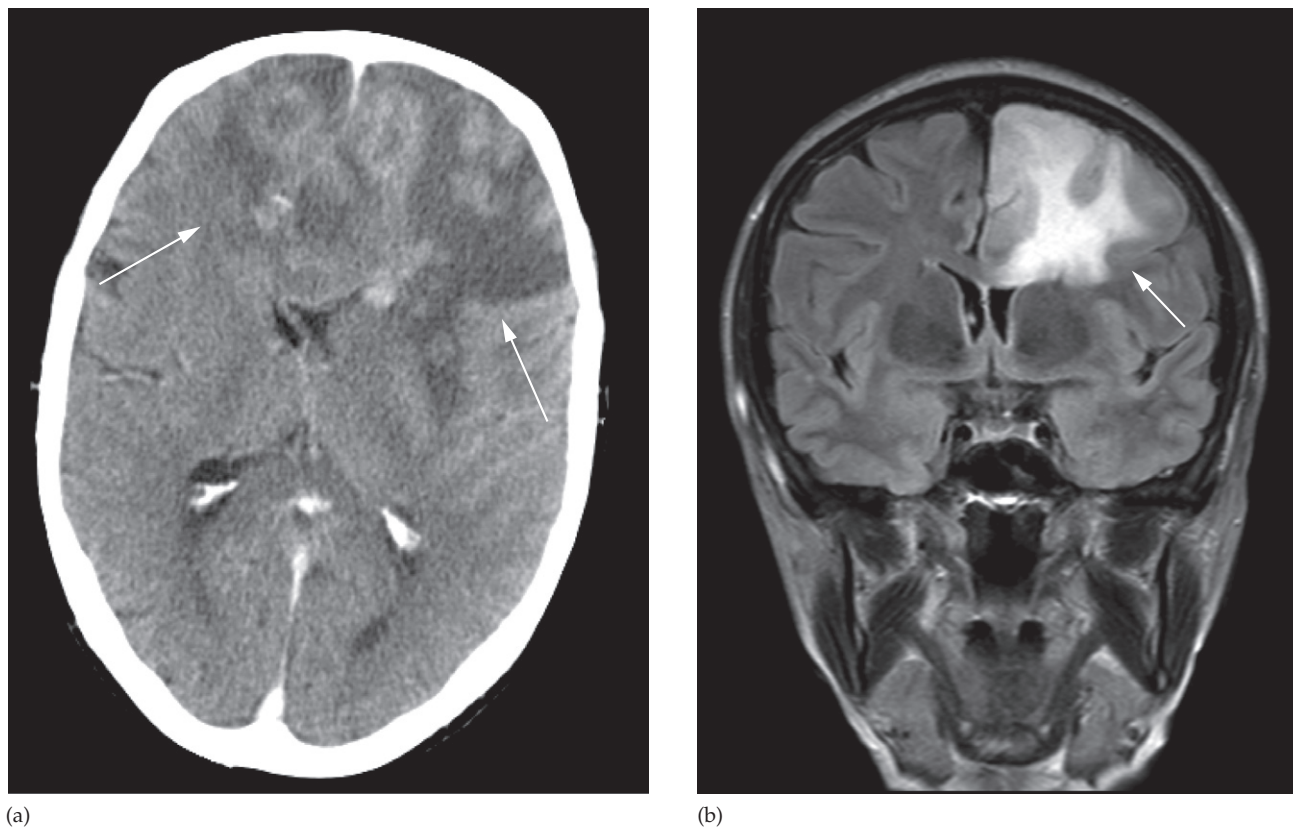


Fig. 15.14 Glioma. (a) CT scan, post intravenous contrast, showing an irregular enhancing mass (arrows) with surrounding low attenuation involving both frontal lobes and the corpus callosum, in keeping with a high grade glioma (glioblastoma multiforme). (b) MRI scan (coronal FLAIR sequence) in a different patient, showing signal change in both the grey and white matter (arrow) with mild mass effect in a glioma (anaplastic astrocytoma).

oligodendrogliomas. For accurate assessment of gliomas, both pre and post contrast scans should be performed as enhancement can be associated with a higher grade of malignancy.

The MRI features are similar to those of a mass, often with adjacent signal change. However, it is important to realize that tumour cells will be present beyond the margin of any signal change seen around a glioma. The mass may show a variety of signal intensities but, in general, the tumour is lower in signal intensity than the normal brain on the T1-weighted images and higher in signal intensity on the T2-weighted images (Fig. 15.14b). Calcification,

though sometimes recognizable as absence of signal, is less evident than it is with CT.

Brain metastases

Metastases in the brain are often low density on CT unless they are haemorrhagic. On CT and MRI, they usually show contrast enhancement and are often surrounded by substantial oedema (Fig. 15.15). Metastases are typically multiple but a solitary metastasis can be indistinguishable from a primary intracerebral brain tumour with either technique. A parenchymal lesion in the posterior fossa of an adult

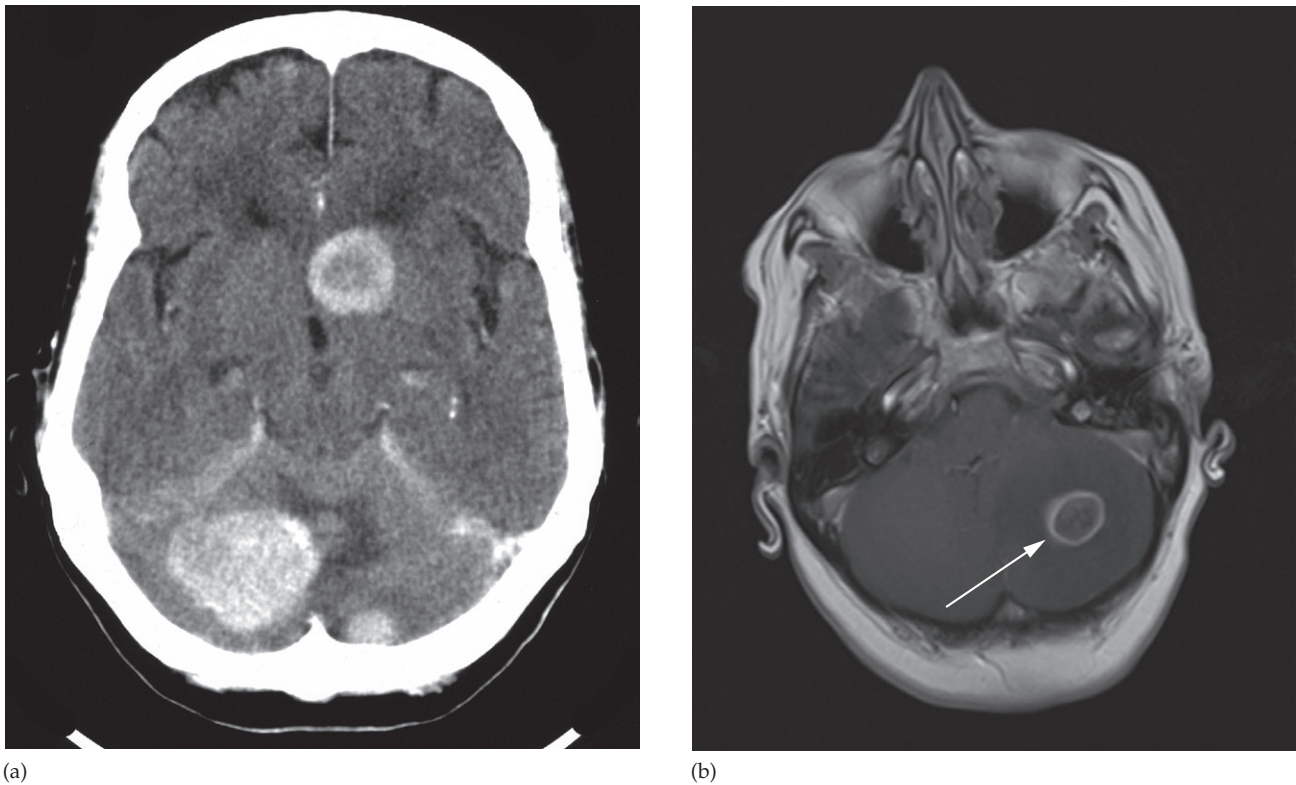


Fig. 15.15 Metastases. (a) Enhanced CT scan showing several metastases as rounded areas of increased density in the cerebral and cerebellar hemispheres. (b) Enhanced T1-weighted MRI scan showing a ring-enhancing cerebellar metastasis (arrow).

should be considered to be a metastasis until proven otherwise.

Meningioma

Meningiomas are the commonest non-glial intracranial tumour and arise from the meninges of the vault, falx or tentorium. The commonest sites are the parasagittal region, over the cerebral convexities and the sphenoid ridges. On an unenhanced CT scan, a meningioma is often denser than the brain because of calcium within the lesion (Fig. 15.16a). Following intravenous contrast, the tumour shows marked homogeneous enhancement (Fig. 15.16b). Reactive sclerosis and blistering of the adjacent bone with thickening and enhancement of the local dura may also be seen.

The multiplanar imaging capability of MRI makes it possible to predict the site of origin of the tumour with greater confidence than is usually possible with CT. Once it can be ascertained that an enhancing tumour is extra-axial, by compressing the brain from outside, the diagnosis of meningioma becomes highly likely.

Acoustic neuroma

The term 'acoustic neuroma' is a misnomer as they are schwannomas that arise from the vestibular branch of the vestibulocochlear nerve. Vestibular schwannomas typically arise on the nerve within the internal auditory canal and may extend out medially into the cerebellopontine angle (Fig. 15.17). When large, they can be recognized at CT or

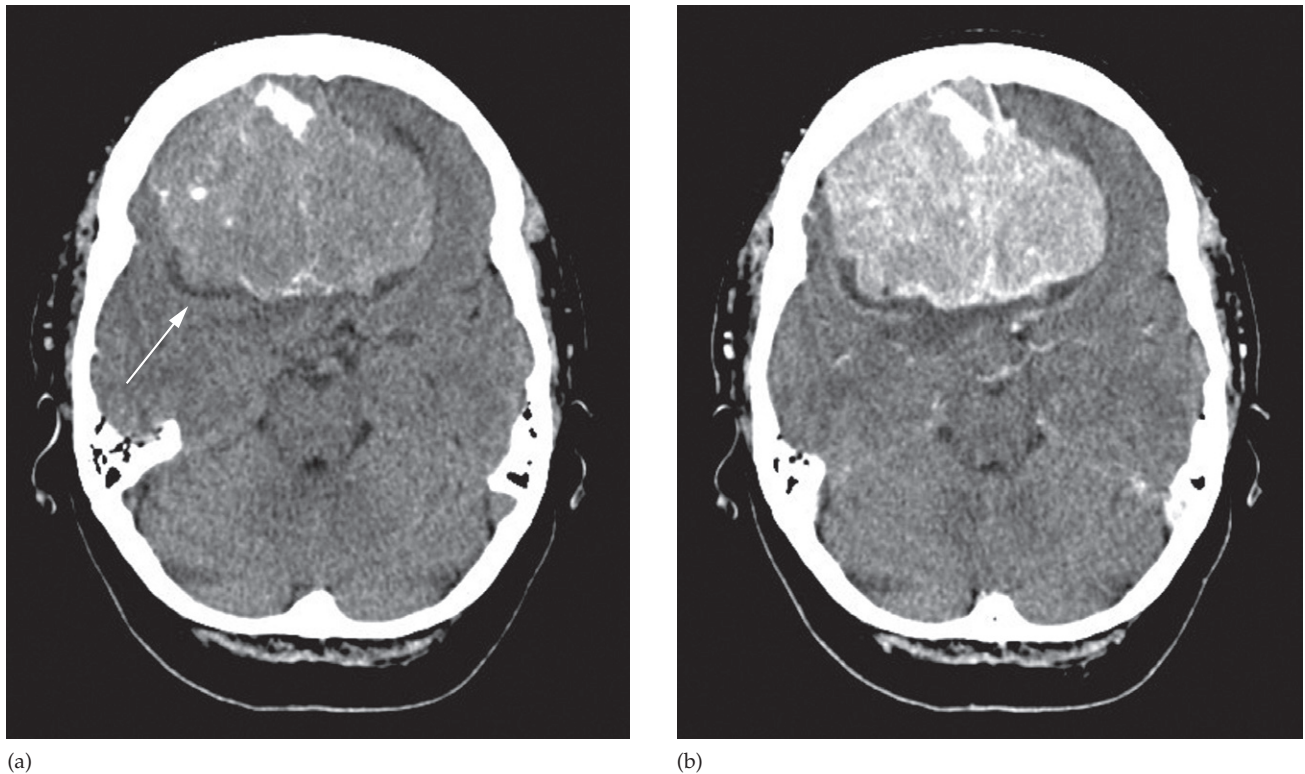


Fig. 15.16 Meningioma. (a) CT scan pre contrast showing a partially calcified mass in the anterior cranial fossa. There is low density CSF between the mass and the displaced grey matter cortex (arrow) indicating the tumour is extra-axial in location. (b) CT post contrast showing prominent enhancement of the mass typical of a meningioma. Also note the normally enhancing vessels which are also extra-axial and between the mass and brain.

MRI. When small, they may only be identifiable with high resolution MRI. As schwann cells are not glial in origin, they enhance avidly.

Pituitary tumours

Pituitary tumours are divided into macroadenomas (>1 cm) and microadenomas (<1 cm). Macroadenomas may cause enlargement of the pituitary fossa and may also extend superiorly into the suprasellar cistern – where they may compress the optic chiasm – and also laterally into the cavernous sinuses.

Computed tomography can show a pituitary tumour (Fig. 15.18a), but MRI is the investigation of choice to demonstrate the presence and extent of a pituitary tumour and

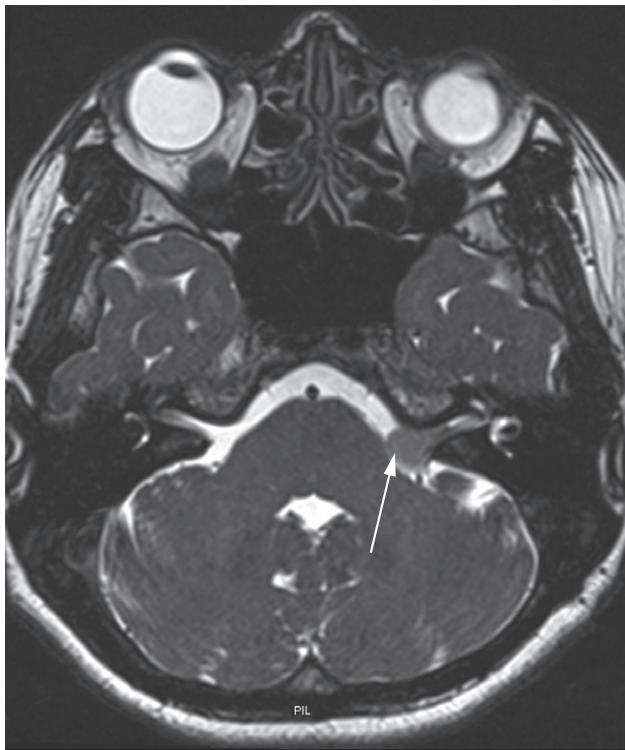
can readily demonstrate its relationship to local structures, which may be compressed (Fig. 15.18b, c).

Stroke

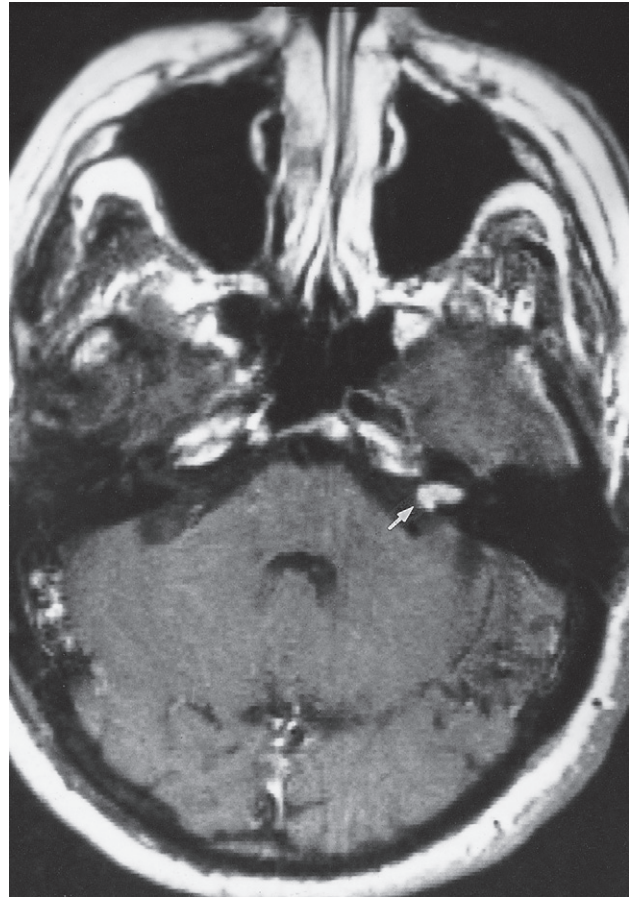
Stroke is defined as a sudden, focal neurological deterioration due to a disturbance in the blood supply to the brain. It is a common cause of hospital admission and has a high morbidity. The important causes of stroke are:

- Cerebral infarction, which may be due to *in situ* thrombus or embolus from the proximal artery or heart.
- Intracerebral haemorrhage.
- Subarachnoid haemorrhage.

Acute cerebral infarction and haemorrhage are often clinically similar, but it is important to distinguish between



(a)



(b)

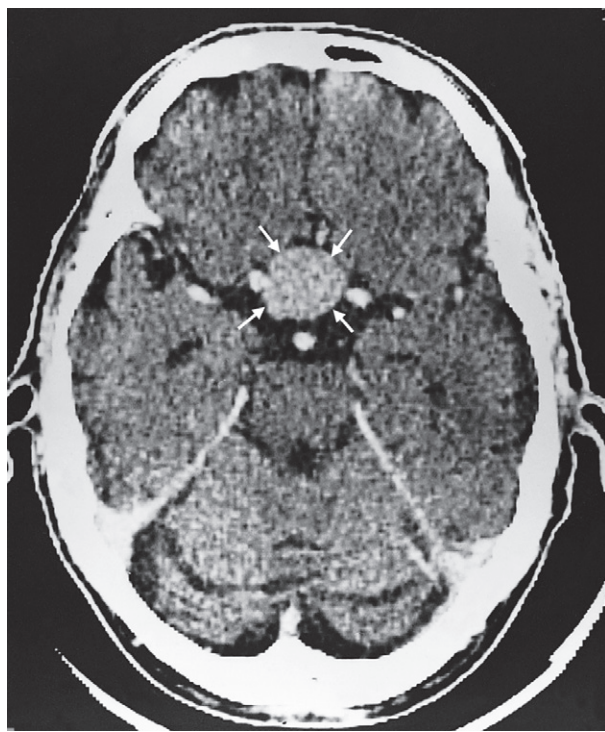
Fig. 15.17 Vestibular schwannoma. (a) High resolution T2-weighted sequence through the internal auditory meati showing a soft tissue mass on the left (arrow) extending into the cerebellopontine cistern. (b) Post gadolinium enhancement; the small schwannoma (arrow) in the left internal auditory canal is clearly demonstrated.

these two conditions as subsequent investigation and treatment differ greatly. The acute management of thromboembolic infarct is aimed at destroying the clot with thrombolysis, but this is contraindicated in the presence of haemorrhage – therefore CT is the best first test.

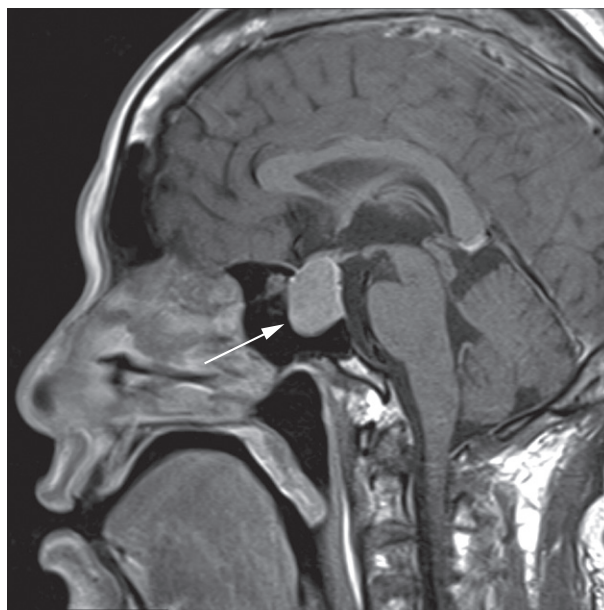
Cerebral infarction

There are four main outcomes of CT performed for an acute stroke:

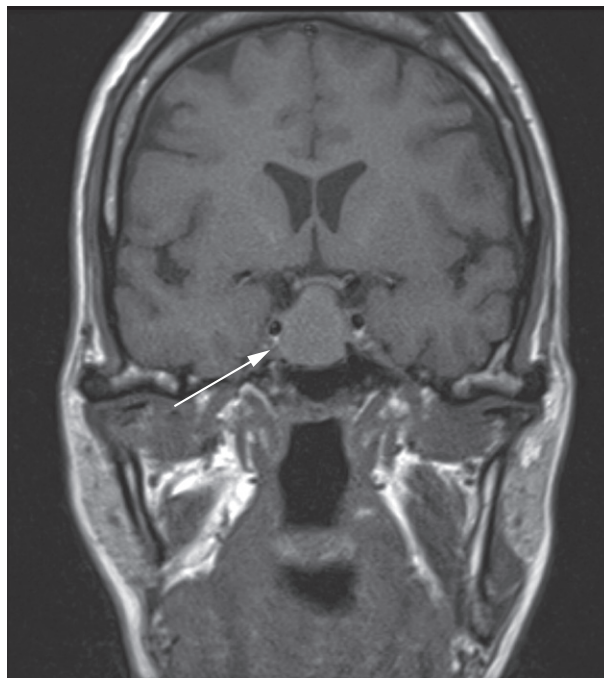
- The presence of haemorrhage precludes thrombolysis treatment and is described below.
- Stroke mimics are conditions that present like stroke, such as a subdural haematoma or brain tumour, for which different treatments are required.
- A normal scan either means the patient is not having a stroke (stroke mimic not identifiable by imaging, such as hemiplegic migraine) or is at the very early stages of a stroke before the CT becomes abnormal and therefore is an ideal candidate for thrombolysis.



(a)



(b)



(c)

Fig. 15.18 Pituitary tumour. (a) CT scan after contrast showing a mass in the pituitary fossa which enhances vividly (small arrows). (b) Sagittal T1 post contrast MRI and (c) coronal T1 MRI showing a macroadenoma (arrows) expanding the pituitary fossa and extending superiorly to touch the optic chiasm in the suprasellar cistern.

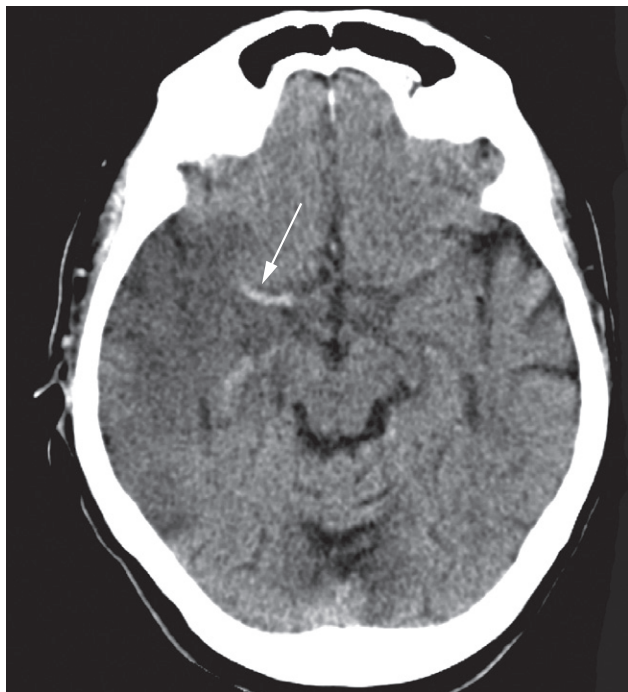


Fig. 15.19 Dense artery sign. Unenhanced CT showing acute thrombus in the right middle cerebral artery (arrow).

- Then there are the early signs of a stroke seen on CT. The dense artery sign (Fig. 15.19) is high density clot visualized within a major intracranial artery. Later, infarcted brain becomes lower attenuation which is initially best seen in areas such as the lentiform nucleus and later may involve the whole vascular territory. The infarct will gradually resolve, leaving an atrophic area of low attenuation gliosis (Fig. 15.20). Diffusion-weighted imaging is the most sensitive method for the early detection of an infarct and will show changes within minutes of the onset (see Fig. 15.10). However, its use acutely is limited by scanning time, availability and problems obtaining safety clearance.

Intracerebral haemorrhage

Acute haemorrhage is seen on CT as high attenuation, frequently causing a mass effect (Fig. 15.21). The initial high density lessens over time, leaving a low density area indistinguishable from an infarct. MRI is useful in the follow-up

of intracerebral haemorrhages to exclude underlying vascular malformation or occult metastasis, which may be obscured by the presence of blood. If no cause is identified, formal cerebral angiography may be required to exclude a subtle vascular anomaly.

Subarachnoid haemorrhage

Spontaneous subarachnoid haemorrhage is usually due to a ruptured intracranial aneurysm or vascular malformation. CT is the best initial investigation to diagnose a subarachnoid haemorrhage and to demonstrate the site of bleeding.

A subarachnoid haemorrhage is recognized by high density blood outside the brain in the sulci, Sylvian fissures and basal cisterns (Fig. 15.22). Subarachnoid haemorrhage on CT will obviate the need for lumbar puncture and CSF examination, but sensitivity of CT decreases with time after a haemorrhage and a normal examination does not exclude the diagnosis. CT angiography can be used to demonstrate the aneurysm and to plan treatment by neurosurgical clipping or by interventional radiological microcatheter techniques which occlude the aneurysm with metal coils (see Fig. 17.14). Ateriovenous malformations may be coiled or embolized to reduce the size and risk of haemorrhage (Fig. 15.23).

Infection

In acute *meningitis* CT and MRI are usually normal and antibiotics should start immediately and not await the result of a scan. A lumbar puncture is frequently performed to obtain CSF to confirm the diagnosis. A CT scan prior to lumbar puncture is only essential if there is evidence of raised intracranial pressure, focal neurological signs or change in conscious level.

Encephalitis is caused by infection, usually viral. CT and MRI show unilateral or asymmetrical bilateral, focal abnormal areas, often in a characteristic distribution appearing as low attenuation on CT and high signal on a T2-weighted MRI scan (Fig. 15.24). The commonest cause of viral encephalitis is herpes simplex, which typically produces abnormalities in the medial temporal lobe, insular cortex and inferior frontal lobes. These areas may contain areas of haemorrhage and enhancement.

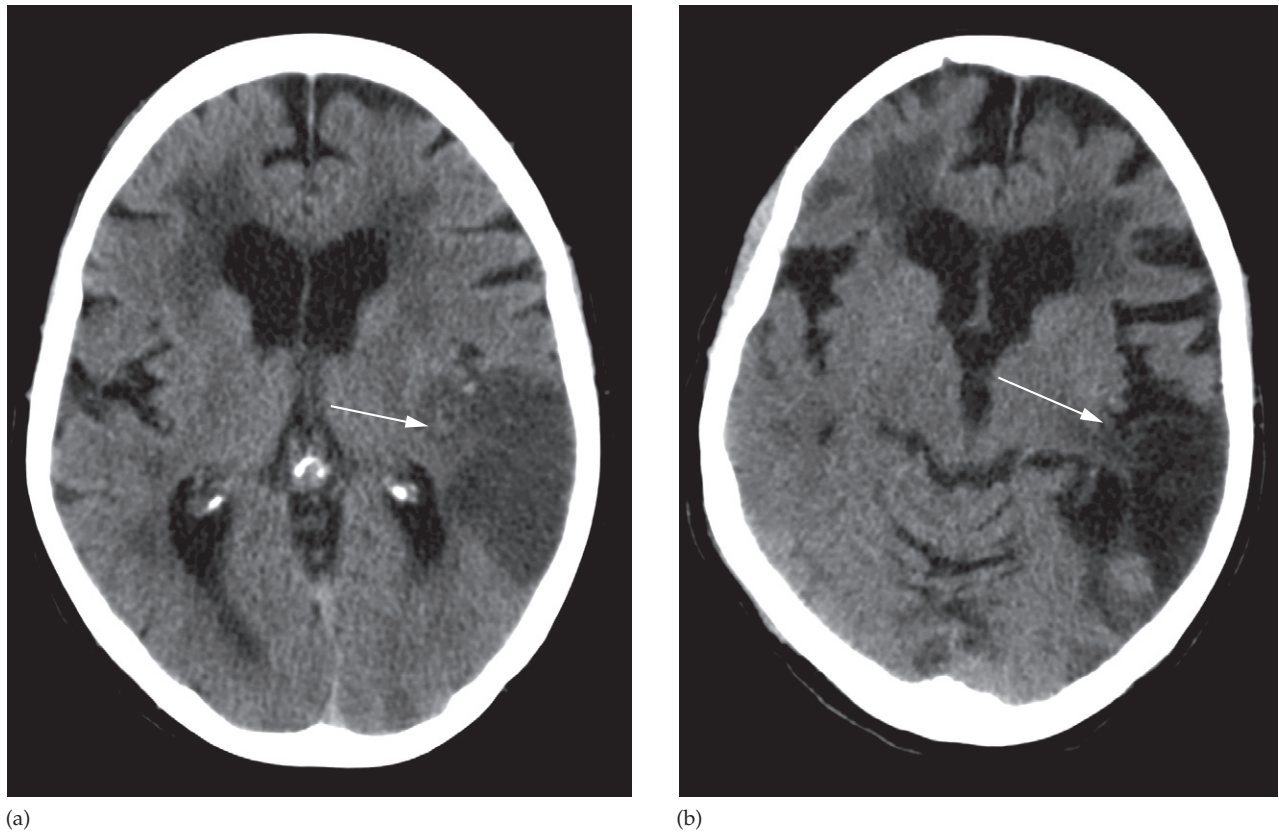


Fig. 15.20 Cerebral infarction. (a) Initial CT scan a few hours after the onset of symptoms showing low attenuation in the posterior cerebral artery territory with swelling causing effacement of the local sulci (arrow). (b) CT scan a month later showing low attenuation gliotic change in the same territory and atrophy causing localized expansion of the lateral ventricle and widening of the sulci (arrow).



Fig. 15.21 Acute parenchymal haemorrhage. CT scan showing the haematoma as a high density area with local mass effect (H) in the left frontal lobe.

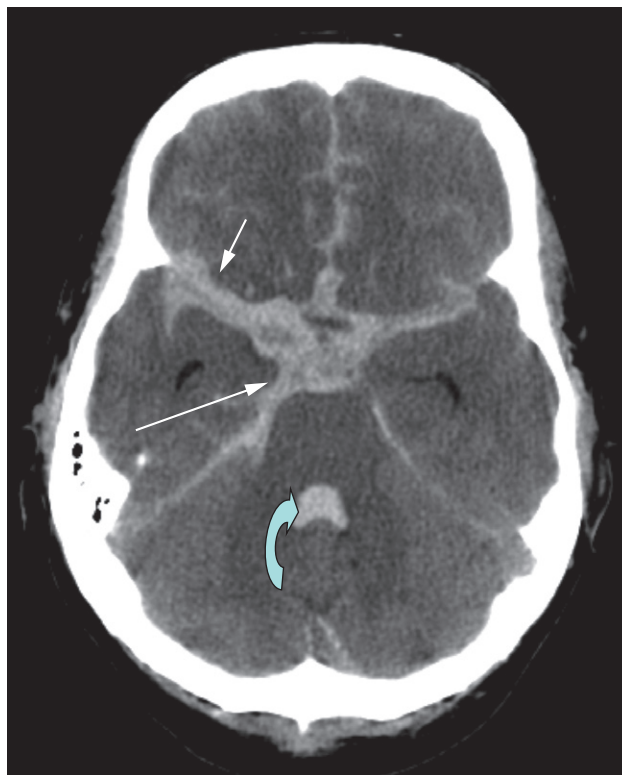
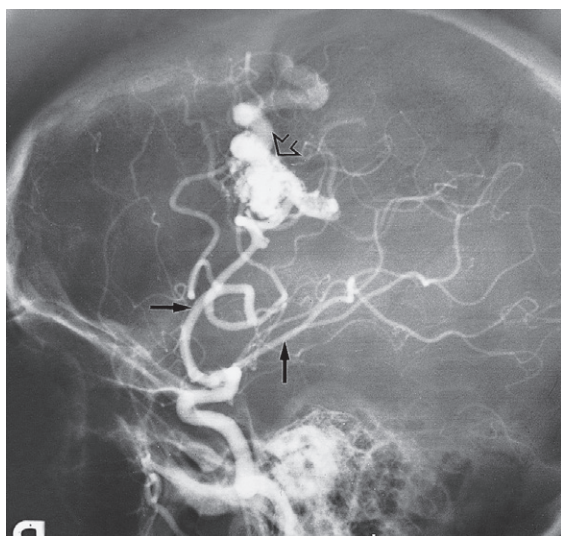
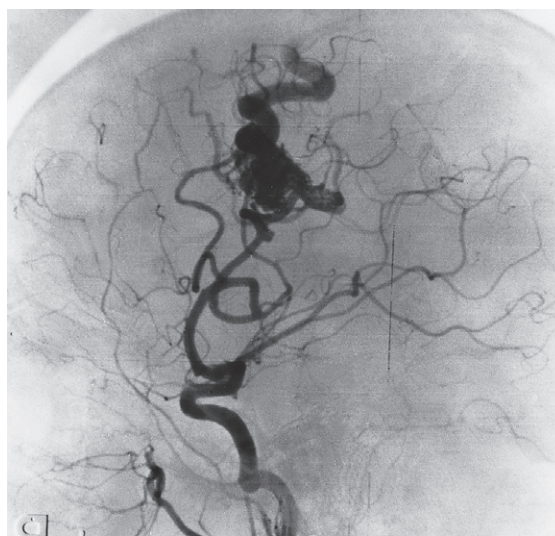


Fig. 15.22 Subarachnoid haemorrhage. (a) High density subarachnoid blood can be seen in the basal cisterns outlining the brain stem (long arrow), the Sylvian fissures (short arrow) and within the fourth ventricle (curved arrow).



(a)



(b)

Fig. 15.23 Arteriovenous malformation. (a) Carotid angiogram showing a collection of large abnormal vessels (large open arrow) supplied by the middle cerebral artery (horizontal arrow). On this injection the posterior cerebral artery (vertical arrow), but not the anterior cerebral artery, has filled. (b) Subtraction. With this technique the shadowing due to the bones has almost been eliminated so that the contrast-filled vessels stand out more clearly.

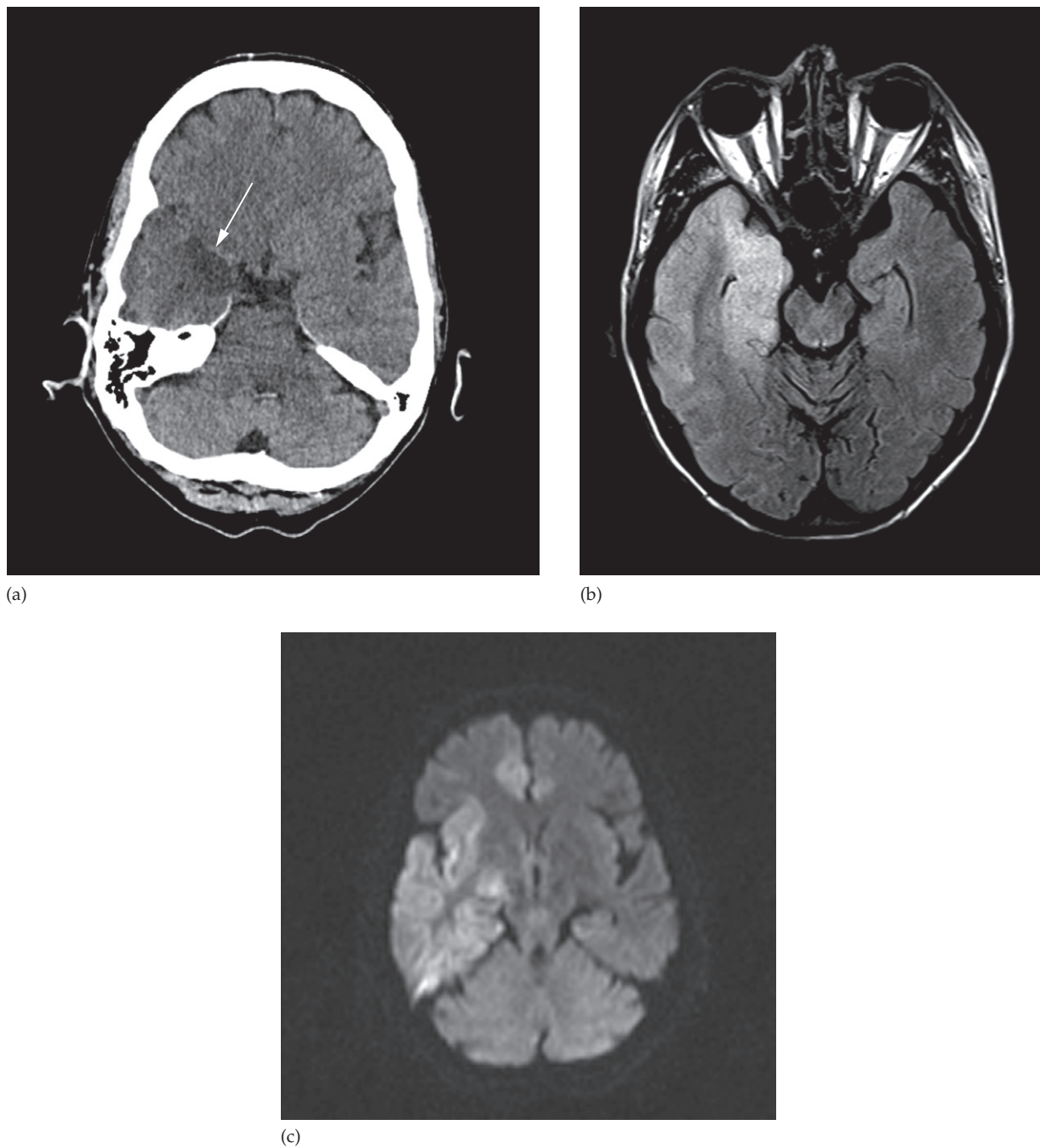


Fig. 15.24 Acute viral encephalitis. (a) Unenhanced CT showing low density in the right temporal lobe (arrow) in a distribution unusual for an acute infarct. (b) Axial FLAIR sequence showing high signal oedema and swelling in the medial temporal lobe and hippocampus. (c) DWI showing acute restricted diffusion of acute encephalitis in the right temporal lobe and inferior frontal lobe.

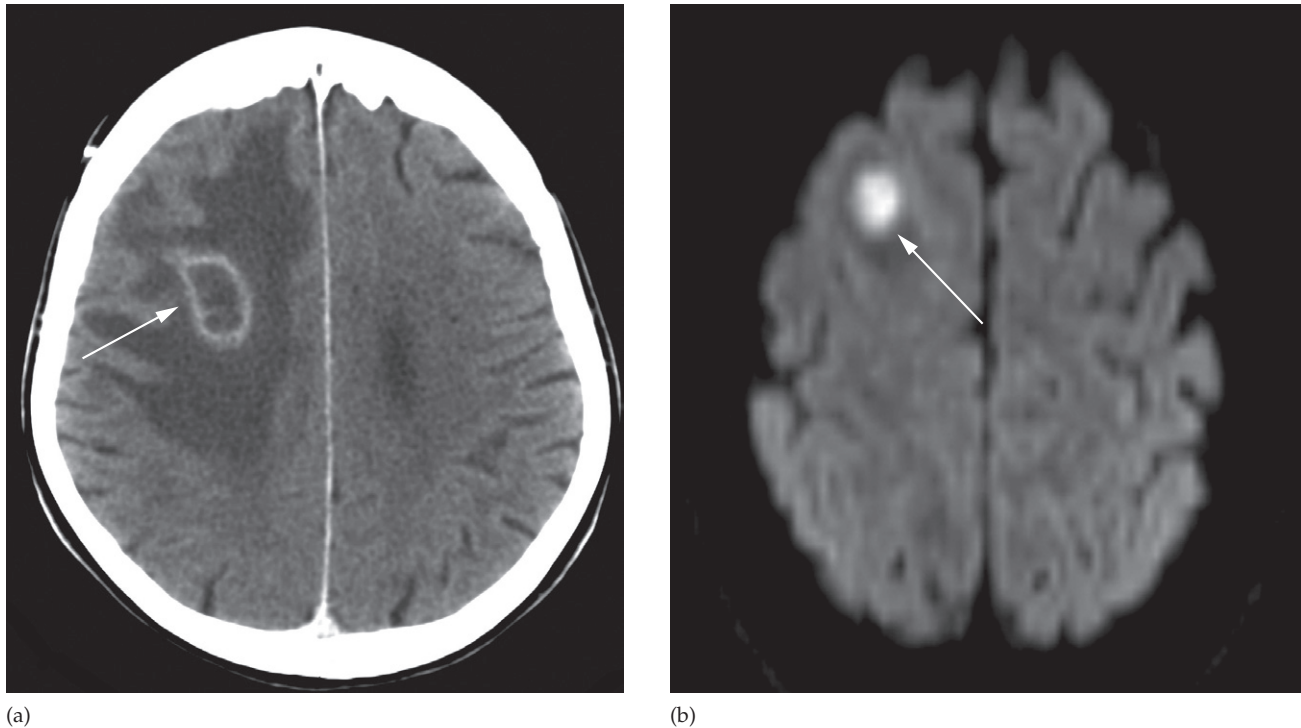


Fig. 15.25 Cerebral abscess. (a) Post contrast CT scan showing a right frontal ring-enhancing lesion with surrounding vasogenic oedema (arrow). (b) DWI showing the contents of an abscess (arrow) with restricted diffusion in keeping with pus.

An *abscess* can be caused by bacterial, tuberculous, fungal or parasitic organisms. Necrosis and pus formation occur in the centre of the abscess, which appears as low density on CT or fluid on MRI. The wall of the abscess enhances with intravenous contrast and may be surrounded by oedema, giving an appearance known as ‘ring enhancement’ (Fig. 15.25). The pus within the centre of a pyogenic abscess will typically demonstrate restricted diffusion.

Cysticercosis is the commonest parasitic infection of the brain (*neurocysticercosis*) and the commonest cause of epilepsy in the developing world. It is due to the migration of ingested *Taenia solium* or pork tapeworm organisms, which form larval cysts located anywhere in the brain, within the ventricles or in the subarachnoid space. Depending on the immune reaction of the patient to the cyst (which can secrete anticytokines), the appearances vary from multiple cysts (Fig. 15.26) containing a dot (larvae) to cysts with local inflammation and enhancement

indicating breakdown of the BBB and more likely to be symptomatic with seizures. Eventually the organism will die and the cyst calcifies.

Patients with acquired immune deficiency syndrome (AIDS) or other causes of immunosuppression have a higher incidence of opportunistic brain infection. Multiple ring-enhancing round lesions on CT or MRI are typical of toxoplasmosis or other cerebral abscesses. Progressive multifocal leucoencephalopathy is due to reactivation of the JC virus, which causes regions of demyelination. These are seen as oedematous areas of brain with no abnormal enhancement. Fungal infections such as cryptococcosis or mycobacterial infections are also more common.

Multiple sclerosis

Magnetic resonance imaging is the key imaging modality for multiple sclerosis. It is useful in demonstrating multiple

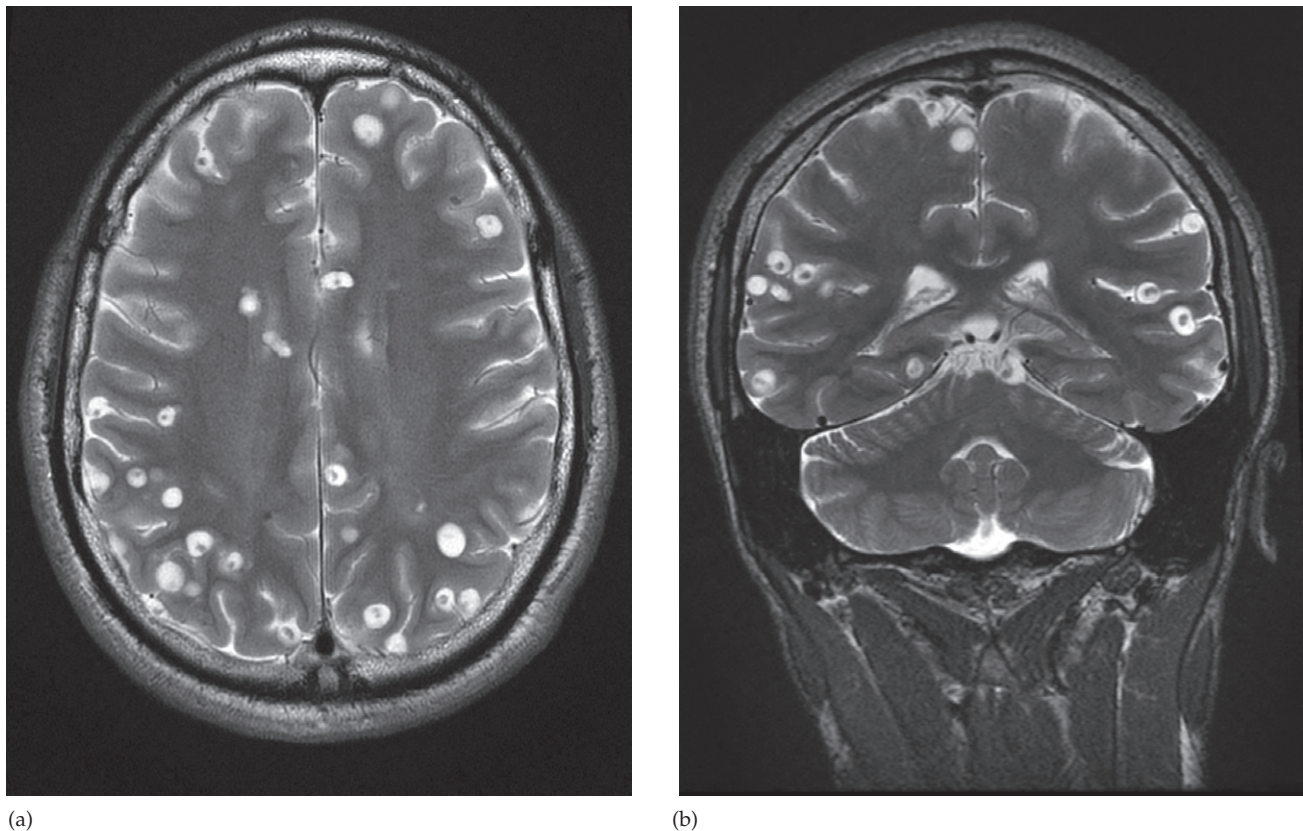


Fig. 15.26 Neurocysticercosis. (a) Axial and (b) coronal T2-weighted MRI showing multiple cysts in the brain and subarachnoid space. Several of the cysts contain a low signal dot which is the headpart (scolex) of the parasite.

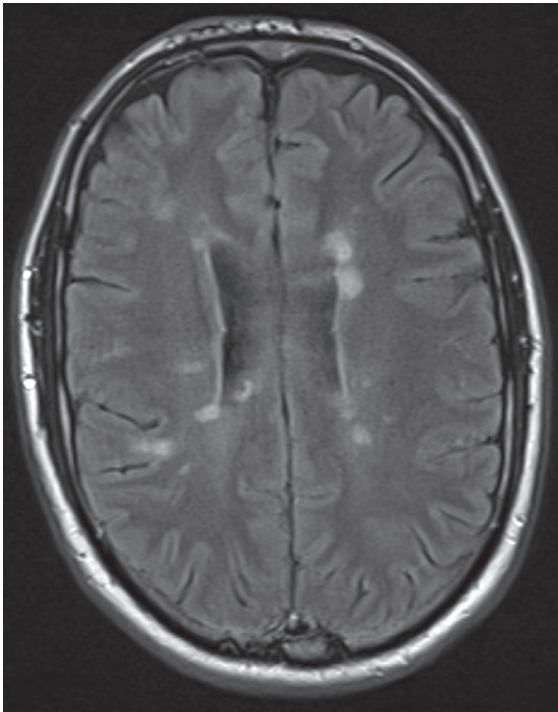
white matter lesions in a typical distribution (dissemination in space) and also the waxing and waning pattern of plaques on follow-up imaging (dissemination in time), which are both diagnostic criteria.

Plaques of demyelination can be seen anywhere in the white matter but are typically seen extending perpendicularly from the margins of the lateral ventricles including the temporal lobes, in the white matter immediately adjacent to the cortex, in the corpus callosum and in the posterior fossa structures (Fig. 15.27). This pattern helps to differentiate it from the white matter lesions seen in small vessel disease and as part of normal ageing. Contrast enhancement may occur with acute plaques but is not seen with

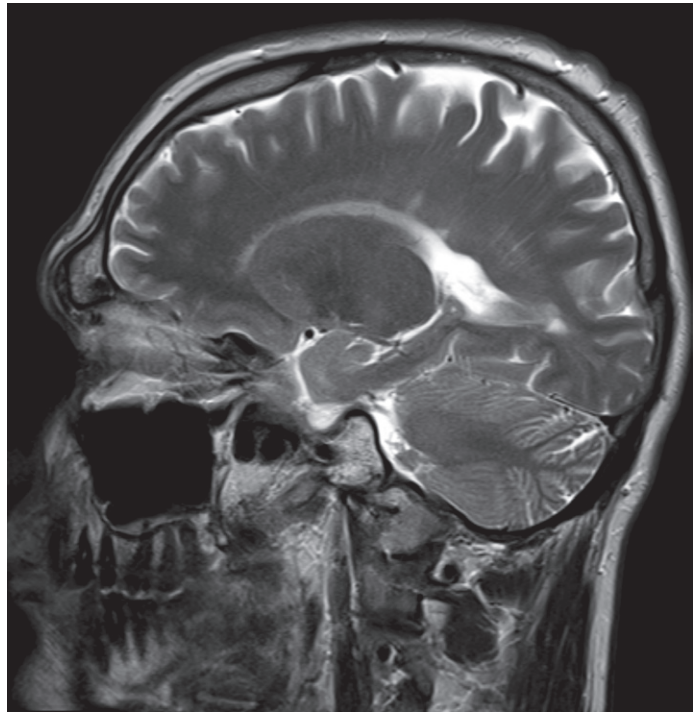
subacute or chronic lesions and the enhancement often comprises an incomplete (broken) ring.

Ageing

Various changes can be seen on CT and MRI in elderly patients that often bear little correlation with the clinical state of the patient. Atrophy of the brain occurs, resulting in dilatation of the ventricles and widening of the cortical sulci (Fig. 15.28). Small vessel atherosclerotic ischaemia can produce low attenuation areas in the deep white matter on CT, normally seen in the periventricular regions, which are T2-hyperintense on MRI.

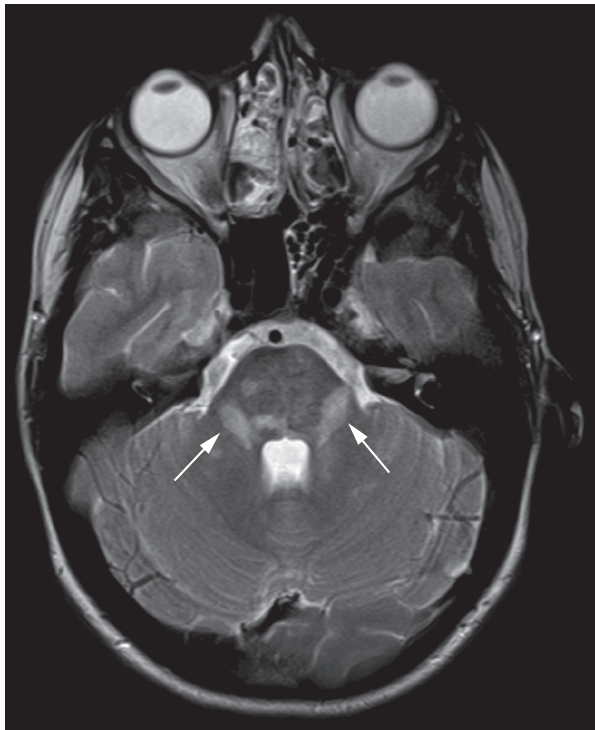


(a)

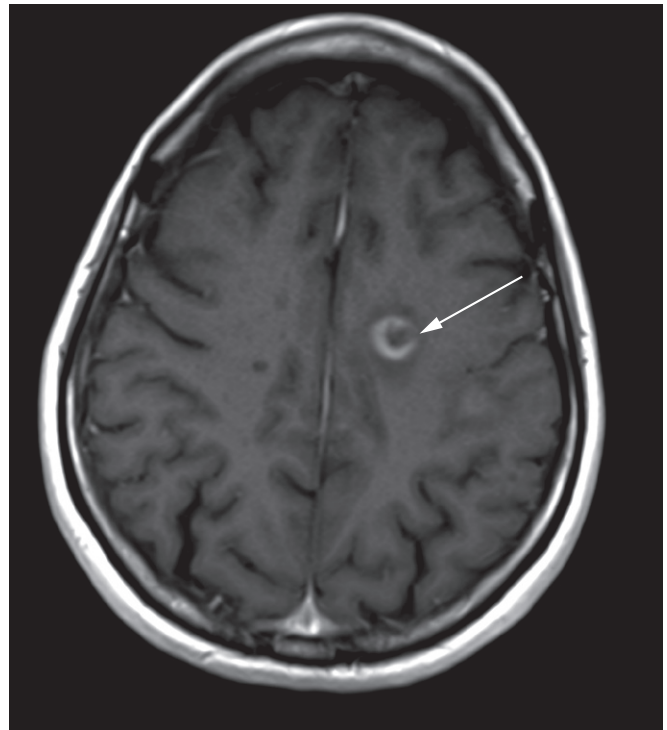


(b)

Fig. 15.27 Multiple sclerosis. (a) Axial FLAIR sequence at the level of the lateral ventricles. (b) Parasagittal T2-weighted MRI and (continued on following page) (c) axial T2-weighted MRI through the posterior fossa. The T2-weighted MRI scans show plaques of demyelination as high signal in the white matter, particularly along the margins of the lateral ventricles and immediately next to cortical grey matter. Bilateral plaques also seen in the middle cerebellar peduncles (arrows). (d) Post contrast T1 sequence showing a broken ring of enhancement (arrow) typical of demyelination.



(c)



(d)

Fig. 15.27 *Continued*

Dementia

Patients with dementia are imaged to exclude a treatable lesion such as hydrocephalus, tumour or subdural haematoma; imaging may also indicate a specific cause of cognitive impairment.

In Alzheimer's disease, the commonest form of dementia, both CT and MRI show generalized cerebral volume loss with dilated ventricles and widened cortical sulci with white matter abnormalities (Fig. 15.29a), although these are common findings in many end-stage dementias. Atrophy of the hippocampi or parietal lobe atrophy are more specific findings in Alzheimer's disease, especially if shown to be progressive over time. Striking frontal lobe atrophy is a feature of Pick's disease (Fig. 15.29b). In vascular dementia there is often more extensive small vessel disease and/or strategic infarcts in areas such as the hip-

pocampi or bilateral thalami which may also lead to cognitive impairment.

Head injury

The aim of imaging is to identify those patients with brain injury and particularly with intracranial haematomas that require urgent neurosurgical treatment. Unenhanced CT is the standard method of investigation as it is most sensitive to acute haemorrhage and bone fractures. In an unconscious patient with a traumatic head injury with a high risk of a cervical spine injury and other injuries, the rest of the body can also be examined.

In the rare event of CT being unavailable and in a skeletal survey for non-accidental injury, a fracture may be demonstrated on a skull x-ray as a translucent line with straight edges. Fractures must be distinguished from lines due to

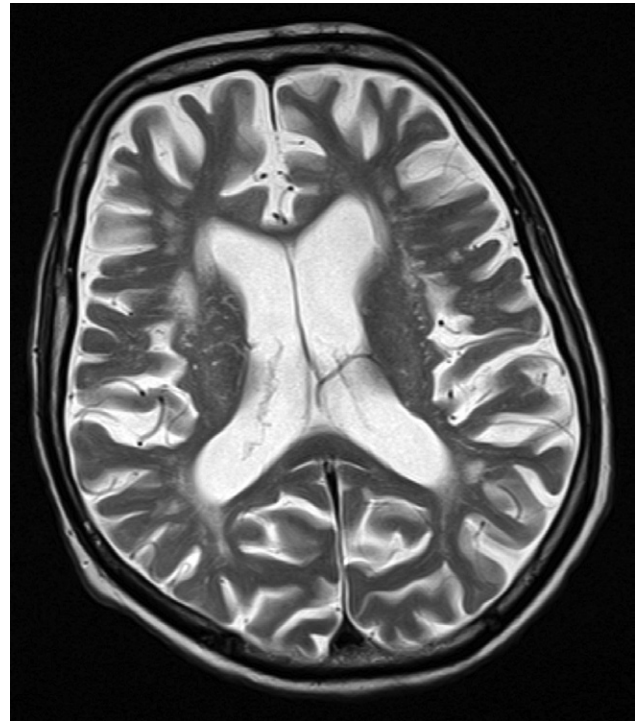
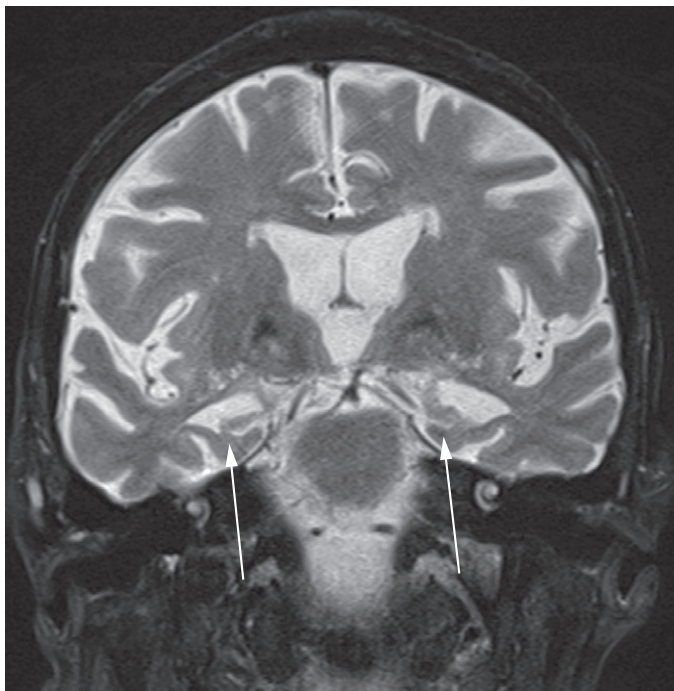
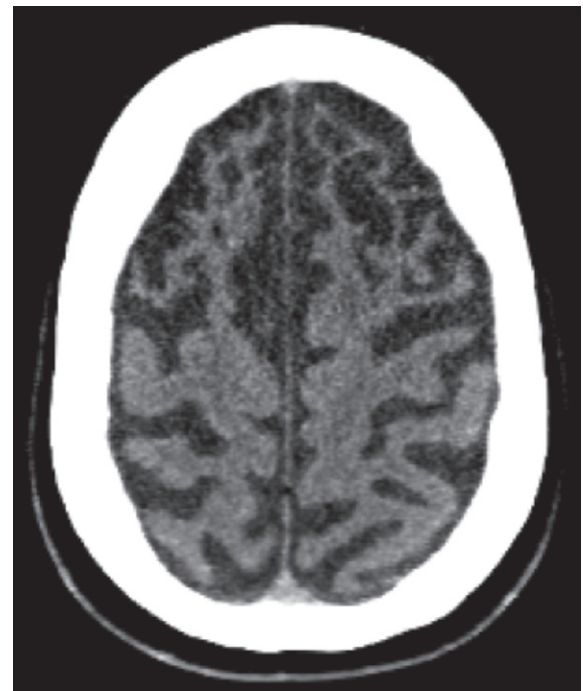


Fig. 15.28 Cerebral atrophy. Axial T2-weighted MRI showing prominence of the ventricles and generalized widening of the cerebral sulci in keeping with age-related atrophy.



(a)



(b)

Fig. 15.29 Dementia imaging. (a) Coronal T2-weighted scan showing generalized cerebral atrophy with widening of the sulci and more advanced atrophy of both hippocampi (arrows) secondary to Alzheimer's disease. (b) CT scan showing severe atrophy of the frontal lobes anteriorly compared to the parietal lobes posteriorly due to Pick's disease.

normal vascular markings or sutures. MRI is rarely used in acute head injury due to the longer scan times and problems in monitoring potentially unstable patients.

Extracerebral haematoma

Extracerebral haematomas comprise extradural and subdural haematomas, depending on the location of the blood in relation to the dura mater layer of the meninges.

An *extradural haematoma* is seen as a lens-shaped, high density area situated over the surface of the cerebral hemisphere that does not cross sutures as it lies below the periosteal layer of the skull (Fig. 15.30). It is normally an arterial



Fig. 15.30 Extracerebral haematoma. CT scan showing a high density lentiform-shaped extra-axial collection.

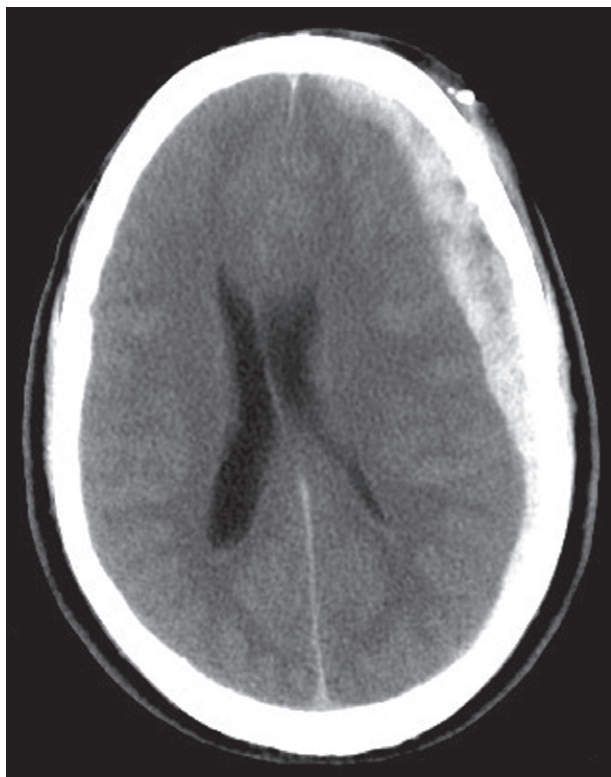
bleed from a meningeal artery which was damaged by a skull fracture – a common associated finding – and therefore occurs at the site of head impact (coup injury). As it is an arterial bleed, an initial period of lucidity is followed by rapid loss of consciousness as the intracranial pressure increases, requiring emergency surgical evacuation.

A *subdural haematoma* is seen as a crescentic collection of blood that conforms to the shape of the underlying brain and occurs most commonly over the convexity of the brain where it is not limited by any of the skull sutures, but can also extend along the falx and tentorium (Fig. 15.31a). It is normally a venous bleed from the bridging veins which cross the subdural space and therefore is more commonly seen in patients who have cerebral atrophy, making the veins more prone to injury. They often occur on the side opposite to the head impact (contracoup injury) or may be bilateral following a shaking injury (as seen in non-accidental injury). Acutely, the blood is high density for 1–2 weeks following injury; however, as the feeding system is low pressure, the haematoma may be clinically occult and become chronic and consequently low (CSF) density after several weeks (Fig. 15.31c). In the intervening period, haematomas pass through a phase of being isodense with the brain and are, therefore, less obvious on CT scans. They should be suspected if there is any midline displacement or ventricular compression. The displacement may not be obvious if the haematomas are bilateral, when effacement of the sulci may be the only clue to their presence (Fig. 15.31b).

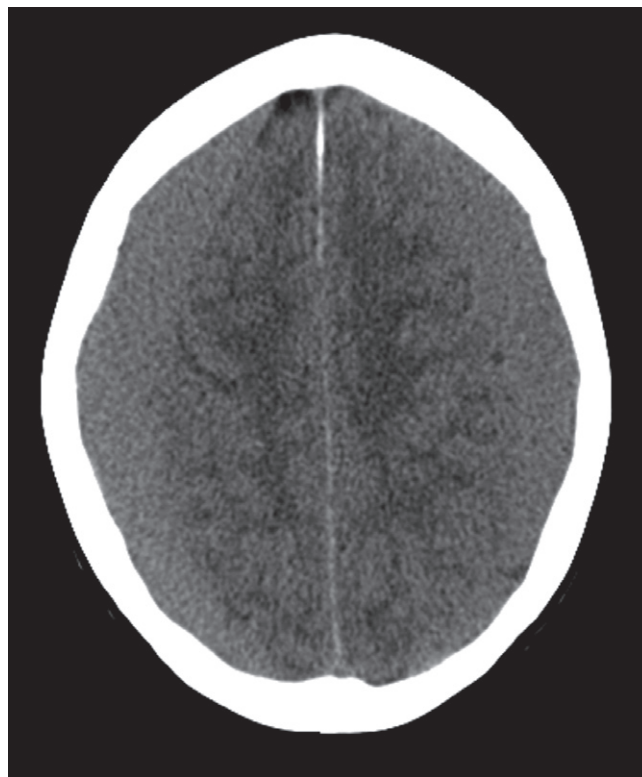
Intracerebral lesion

Haemorrhagic contusions are bruises of the brain which comprise hyperdense haemorrhagic foci with surrounding low attenuation oedema. The swelling associated with the oedema may be significant, raising intracranial pressure and leading to further brain damage. Contusions typically occur in areas of the brain that impact along bony ridges on the inner surface of the skull vault, such as the anterior poles of the temporal lobes and the anterior and undersurface of the frontal lobes bilaterally (Fig. 15.32).

Diffuse axonal injury occurs when deceleration or rotational forces cause shearing injury to axons and capillaries in the brain. The brain injury is more widespread, with microhaemorrhages and oedema typically located at the



(a)



(b)



(c)

Fig. 15.31 Subdural haematomas on CT. (a) High density extra-axial collection paralleling the surface of the brain due to acute subdural haematoma. (b) Bilateral isodense subdural haematomas causing mass effect and effacement of the sulci from the subacute subdural haematomas. (c) Bilateral low density extra-axial collections causing mass effect from chronic subdural haematomas.

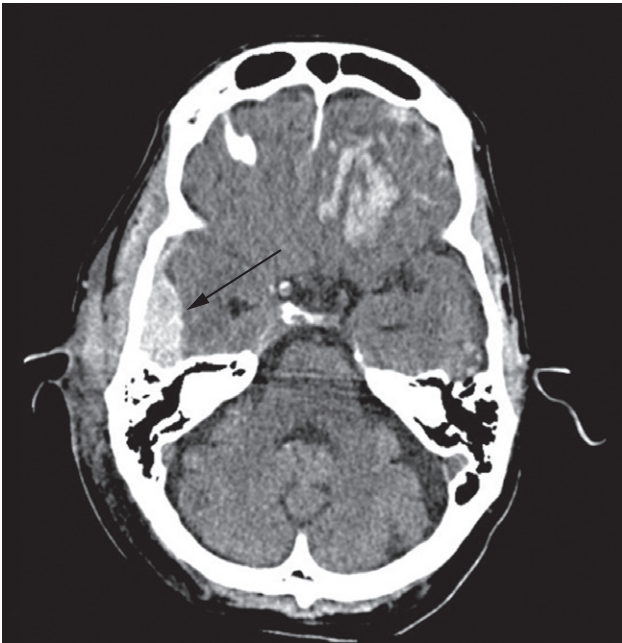
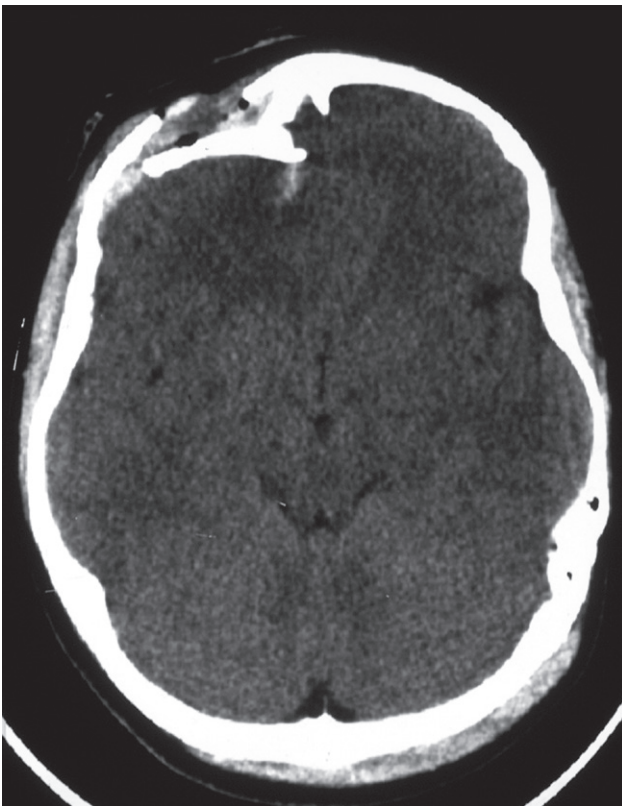
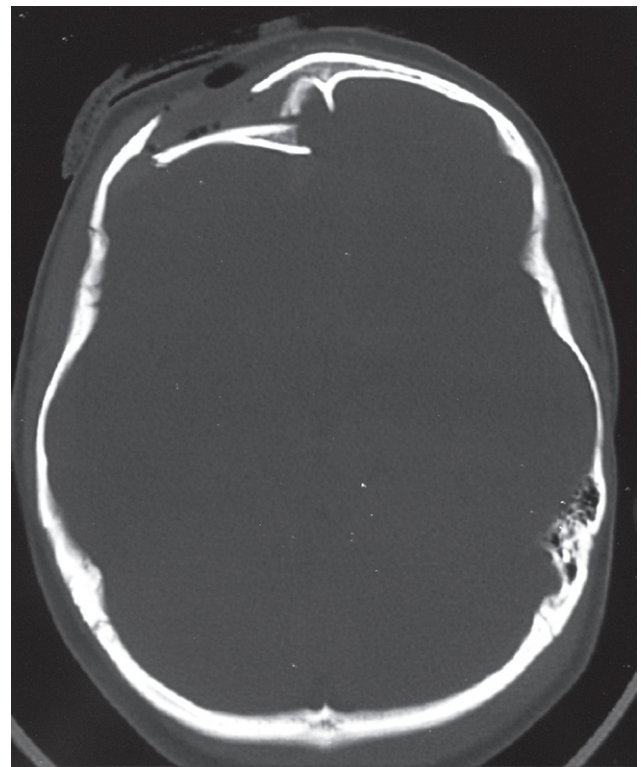


Fig. 15.32 Contusion. CT scan showing irregular high density blood in the inferior left frontal lobe due to contusions. There is also a right-sided extradural haematoma (arrow).



(a)



(b)

Fig. 15.33 Depressed fracture. Axial unenhanced CT on (a) brain and (b) bone window settings. The depressed fracture and bone fragments are more clearly seen on the bone window settings. Such fractures may require surgical elevation.



Fig. 15.34 Pneumocephalus. CT scan showing low density air in the sulci of the brain from a basal skull fracture involving the sinuses.

grey–white junction of the cerebral cortex and basal ganglia, the brain stem and the corpus callosum. The extent of injuries may be underestimated by CT and is more reliably seen on MRI scans, particularly if a blood sensitive (T2* gradient echo) sequence is used.

Fracture

Fractures of the skull base or vault should be looked for on bone window settings (Fig. 15.33). Fractures of the skull vault should not be confused with normal sutures or vascular markings. Assessment should be made of any significant depression of the fracture as these may require surgical elevation and are more likely to be associated with underlying brain injury. If there is a penetrating skull injury or a fracture involves the normally pneumatized paranasal sinuses, middle ears or mastoids, air may enter the cranium and be seen on CT as locules of very low density gas (Fig. 15.34). CT can also demonstrate fluid (blood) in the sinuses and mastoid air cells or air in the orbits, suggesting a facial or skull base fracture.

Orbits, Head and Neck

Sinuses

On plain radiographs the normal sinuses are transradiant because they contain air. Imaging of the sinuses is indicated when simple treatment measures for inflammatory symptoms have failed or in the acute setting of facial trauma. Plain films have a role in showing mucosal thickening, fluid levels and fractures. However, in most sinus disease, low dose computed tomography (CT) is the preferred technique. Magnetic resonance imaging (MRI) also demonstrates the sinuses well, but is rarely required as the primary investigation.

Thickened mucosa can be recognized providing there is some air in the sinus (Figs 16.1 and 16.2) by noting the soft tissue interface between the air in the sinus and the bony wall. The mucosal thickening may be smooth in outline or it may be polypoid. Polyps may be sufficiently large to extend into the nasopharynx.

Allergy and infection both cause mucosal thickening and it is often impossible to say radiologically which condition is responsible. Such changes are often seen in asymptomatic people.

Acute sinusitis is usually diagnosed and treated clinically, but CT is recommended if symptoms persist. Both CT and MRI can elegantly demonstrate mucosal thickening and fluid levels as well as displaying the bony walls of the sinuses. Sinus anatomy is ideally demonstrated with multiplanar reformatted CT in order to assess the drainage sites of the frontal, ethmoid and maxillary sinuses and is a

great aid for the surgeon planning endoscopic sinus surgery (Fig. 16.2).

Opaque sinus

The sinus becomes opaque when all the air is replaced. The causes of an opaque sinus (Box 16.1) are:

- *Infection or allergy.* The air in the sinus is replaced by fluid, or a grossly thickened mucosa, or a combination of the two.
- *Mucocele.* Mucoceles are obstructed sinuses. Secretions accumulate and the sinus becomes expanded. A frontal sinus mucocele may erode the roof of the orbit and cause exophthalmos. CT clearly shows the size and extent of a mucocele.
- *Antrochoanal polyp.* These typically arise from the maxillary antrum mucosa and prolapse through an ostium in the medial antral wall into the nasal cavity and sometimes back into the nasopharynx. This results in unilateral opacification of the maxillary antrum and the frontal and anterior ethmoid sinuses due to obstruction of their drainage pathways.
- *Trauma.* A fracture of the sinus wall may result in haemorrhage and opacification of the sinus.
- *Carcinoma of the sinus or nasal cavity.* In all opaque sinuses, particularly the antra, special attention should be paid to the bony margins on CT, because if these are destroyed a diagnosis of carcinoma needs exclusion (Fig. 16.3). CT is superb at visualizing bone destruction, but MRI

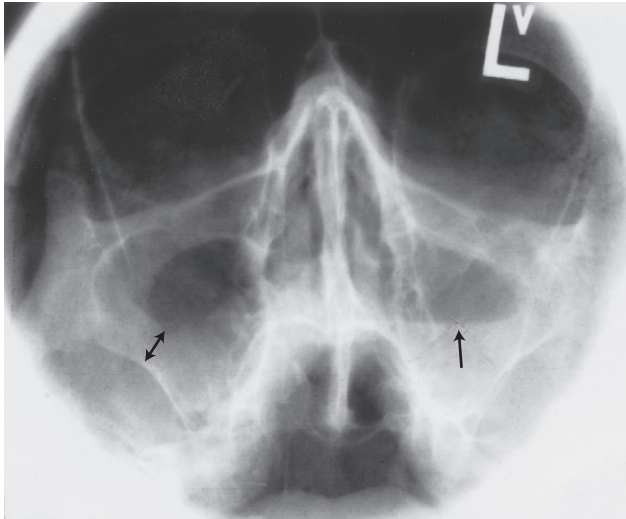


Fig. 16.1 Mucosal thickening and a fluid level. In the right antrum, thickening of the mucosa (double-headed arrow) results in the sinus no longer having a thin outline. The horizontal line in the left antrum on this erect film (arrow) indicates a fluid level that remains horizontal even when the patient's head is tilted.

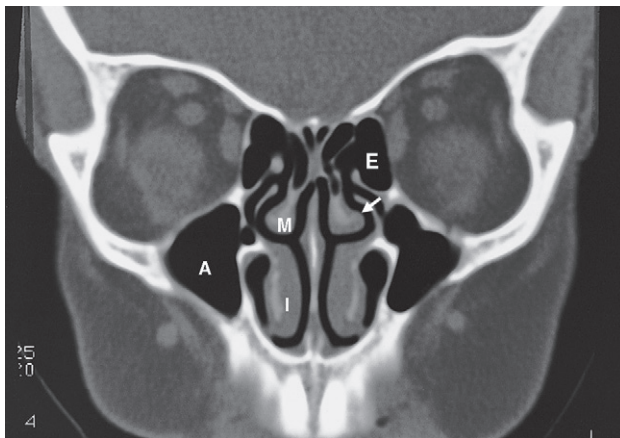
Box 16.1 Causes of opaque sinus

- Infection
- Allergy
- Mucocele
- Antrochoanal polyp
- Trauma with haemorrhage
- Carcinoma of the sinus or nasal cavity

is preferred for demonstrating tumour invasion by showing the extent of any soft tissue mass beyond the sinus cavity. Both CT and MRI have an important role in treatment planning and in assessing response to treatment.

Nasopharynx

Computed tomography and especially MRI give excellent visualization of the nasopharynx and can demonstrate the presence of tumour as a mass disrupting the symmetry of the nasopharynx. The most common type of tumour is nasopharyngeal carcinoma (Fig. 16.4), a type of squamous



(a)



(b)

Fig. 16.2 Coronal CT scan. (a) Normal sinuses. Note the excellent demonstration of the bony margins. The arrow points to the middle meatus into which the maxillary antrum and frontal, anterior and middle ethmoid sinuses drain. The region where all these sinuses drain is known as the osteomeatal complex. A, maxillary antrum; E, ethmoid sinus; I, inferior turbinate; M, middle turbinate. (b) Sinusitis. Mucosal thickening prevents drainage of the sinuses. Both antra are almost opaque. The arrows indicate mucosal thickening in the antra.

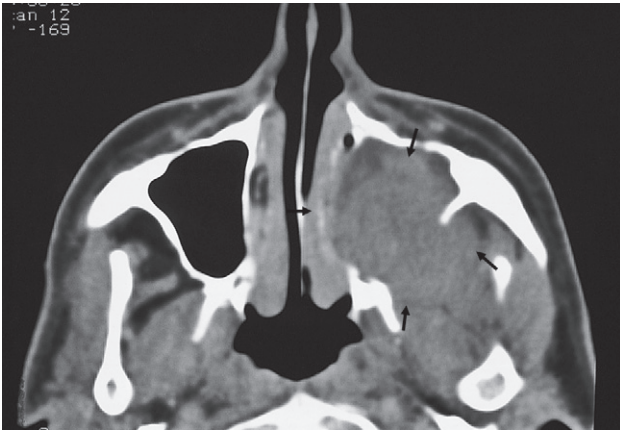


Fig. 16.3 Carcinoma of the antrum. CT scan showing a large mass arising from the left antrum destroying its bony walls and extending into the adjacent soft tissues. The arrows point to the extent of the tumour. The opposite antrum is normal.

cell carcinoma that usually presents late with local invasion and necrotic lymph node metastases. Imaging is required to detect spread into the skull base, perineural extension and lymphadenopathy in the neck (see Fig. 16.13).

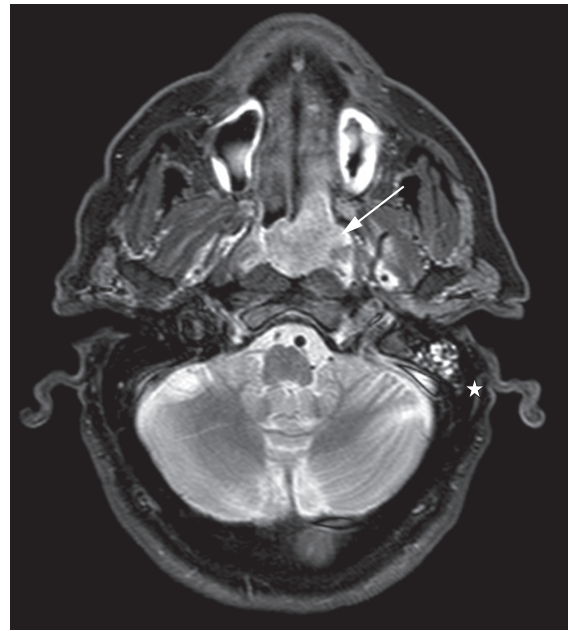
Orbits

Computed tomography and MRI clearly demonstrate the anatomy of the orbits. Imaging is indicated in all patients with exophthalmos because it is important to distinguish between masses arising within the orbit, masses arising outside the orbit and thyroid eye disease. With an intra-orbital mass, its relationship to the optic nerve can be determined.

The main causes of intra-orbital masses include various tumours, such as lymphoma and optic nerve tumours (Fig. 16.5), and vascular malformations. The most common



(a)



(b)

Fig. 16.4 Nasopharyngeal carcinoma. (a) CT scan showing a mass (M) in the nasopharynx on the left extending into the soft tissues of the postnasal space and eroding the skull base (black arrows). Note how the tumour obliterates the fossa of Rosenmuller and eustachian recess, which are shown on the normal right side (white arrows). (b) MRI scan in another patient clearly showing the extent of the tumour (arrow). The tumour is blocking the left eustachian tube and fluid is accumulating in the mastoid (*).

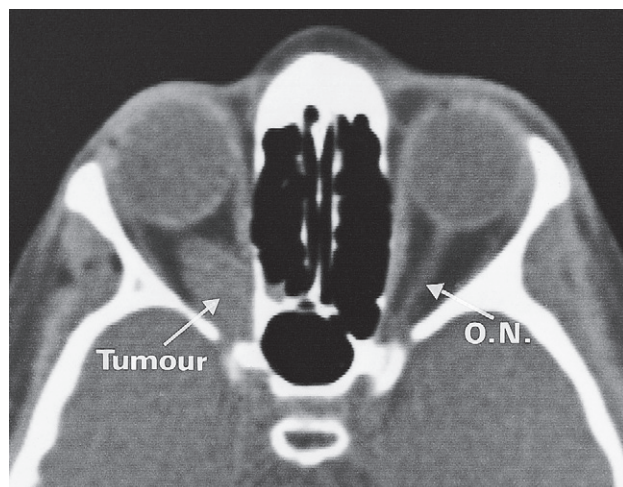


Fig. 16.5 Optic nerve glioma. CT scan showing a soft tissue mass arising from the optic nerve (O.N.). The opposite orbit demonstrates the normal anatomy.

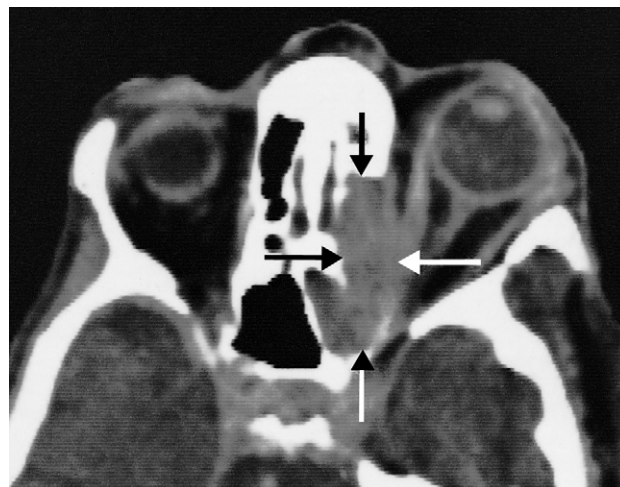


Fig. 16.6 Carcinoma of the ethmoid sinus invading the orbit and causing proptosis. The tumour is arrowed.

orbital masses originating outside the orbit, which often present with exophthalmos, are infection secondary to sinusitis, mucocoeles of the frontal or ethmoid sinuses, tumours (Fig. 16.6) and a meningioma arising from the sphenoid ridge.

In thyroid eye disease, there is enlargement of the extraocular muscles (Fig. 16.7) which is frequently bilateral and may affect one, several or all the eye muscles. There is also hypertrophy and oedema of the fat behind the eye which adds to the exophthalmos. When severe, these changes can lead to compression of the optic nerve in the apex of the orbit.

Blowout fracture

A direct blow to the eye raises the intraorbital pressure and can result in a fracture of the orbital floor, which is the weakest part of the orbit. The break in the orbital floor allows herniation of orbital contents into the antrum, which may result in diplopia. Imaging is best performed by CT with coronal reconstructions, which show a crescentic soft tissue mass in the roof of the antrum (Fig. 16.8a); this should not be confused with mucosal thickening. A fracture of the orbital floor may also be visible.

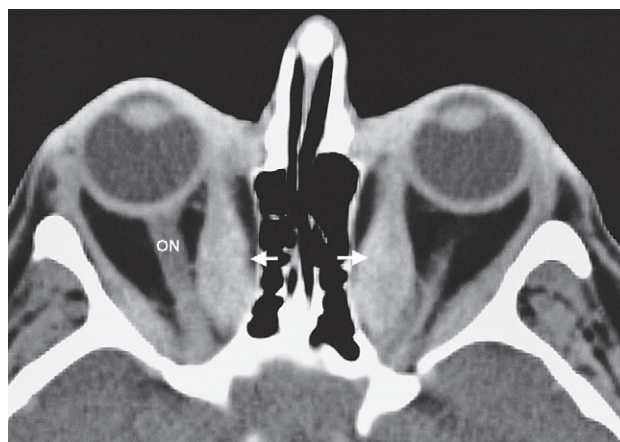


Fig. 16.7 Thyroid eye disease. CT scan through the orbits showing enlargement of the extraocular muscles, particularly the medial rectus (arrows). ON; optic nerve.

Orbital floor fractures also occur with trauma to the side of the face when there may be other fractures of the medial wall of the orbit, the lateral wall of the antrum and the zygomatic arch. Bleeding into the antrum may result in a fluid level or complete opacification of the antrum (Fig. 16.8b).

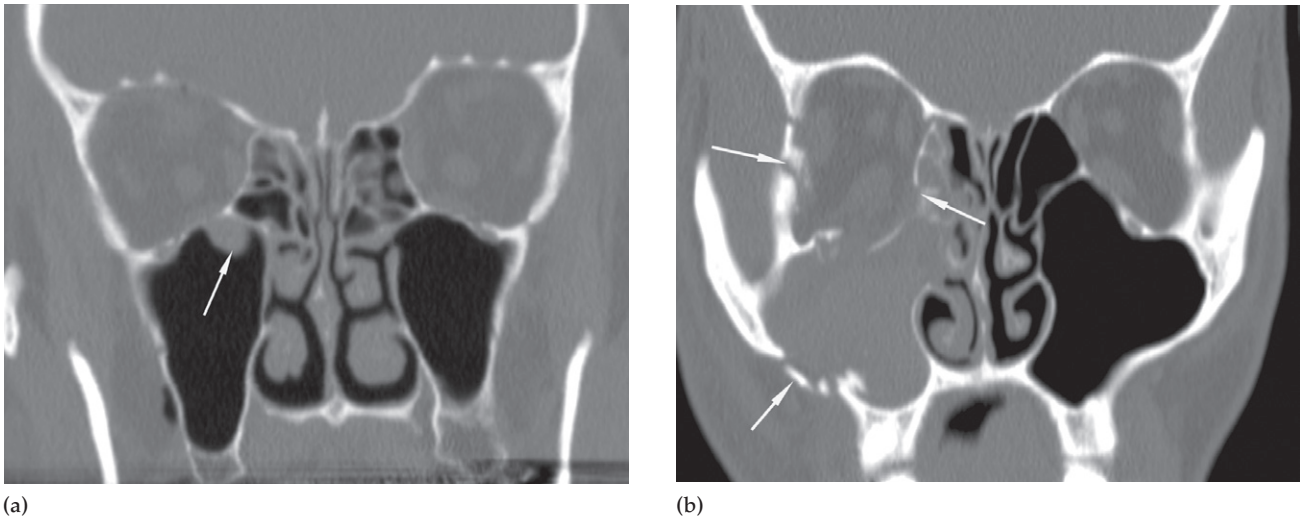


Fig. 16.8 Blowout fracture of the orbit; CT coronal reconstruction. (a) A patient with a blow to the eye showing a soft tissue opacity in the roof of the antrum (arrow). It is difficult to appreciate the fracture of the orbital floor. (b) A patient with trauma to the side of the face showing disruption of the floor of the orbit and fractures of the lateral and medial walls of the orbit, as well as the lateral wall of the antrum (arrows). There is herniation of orbital contents into the antrum, which is opaque.

Salivary glands

Salivary glands disorders, including masses, diffuse enlargement or symptoms of dry mouth, are all first investigated with ultrasound and their nature can be confirmed with fine needle aspiration (FNA). The commonest salivary gland tumour of the parotid gland is a benign pleomorphic adenoma (Fig. 16.9a). MRI is used for the further investigation of FNA-proven tumours that either lie close to the neurovascular bundle or are malignant (Fig. 16.9b). The signal intensity of masses on MRI is often very different to normal salivary tissue and it allows for better delineation of the extent of disease and its anatomical relationships (e.g. to the facial nerve). This is important for surgical planning.

Sialography

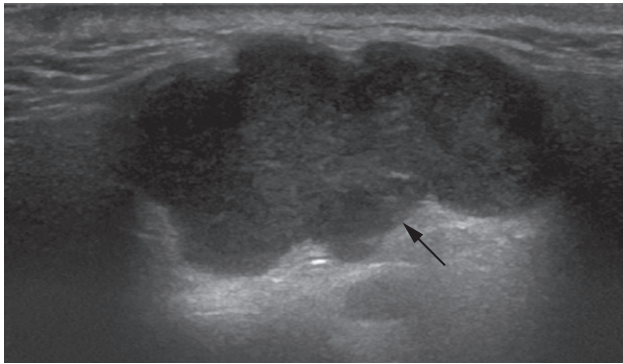
Calculi, which occur most commonly in the submandibular duct or gland, normally contain calcium and can often be seen on plain films, although ultrasound has now taken over as the first line of investigation. Ultrasound is used to

demonstrate sialectasis (dilatation of small intra-glandular ducts or the main duct) and can usually show the calculus. A sialogogue may be used to stimulate secretion of saliva to improve visualization.

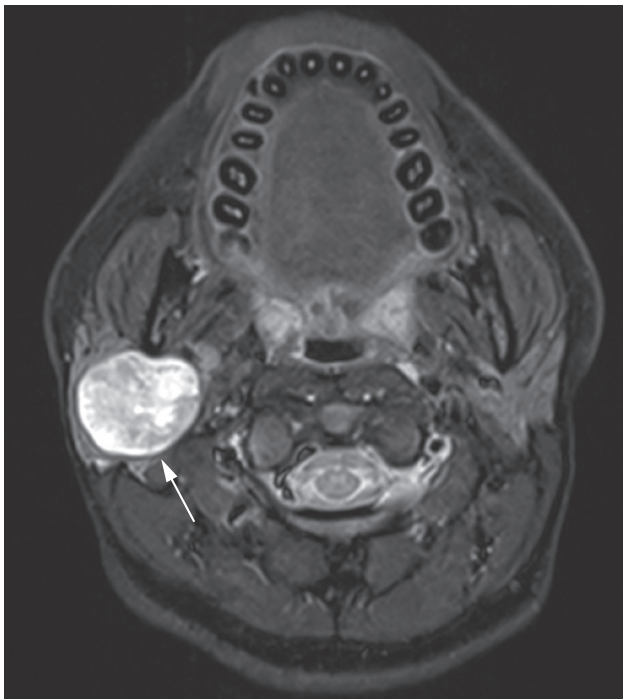
To show the duct system more clearly, a sialogram may be performed by injecting contrast into the ducts of the salivary glands. Only the submandibular and parotid glands have ducts that can be cannulated (Fig. 16.10). Stones and strictures in the ducts can be identified (Fig. 16.11). The main salivary gland ducts are less well visualized by MRI.

Neck

Computed tomography, MRI and ultrasound are all used to investigate a mass in the neck. Ultrasound is recommended as the first line investigation. It confirms the presence of the mass and differentiates solid from cystic lesions. Doppler studies will demonstrate its vascularity, and although ultrasound cannot always predict the cause of a mass, when combined with FNA it is usually possible to obtain a diagnosis (Fig. 16.12).



(a)



(b)

Fig. 16.9 Pleomorphic adenoma of the parotid gland. (a) Ultrasound showing a lobulated parotid mass (arrow). (b) MRI scan showing a high signal intensity mass in the right parotid (arrow), which proved to be a pleomorphic adenoma.

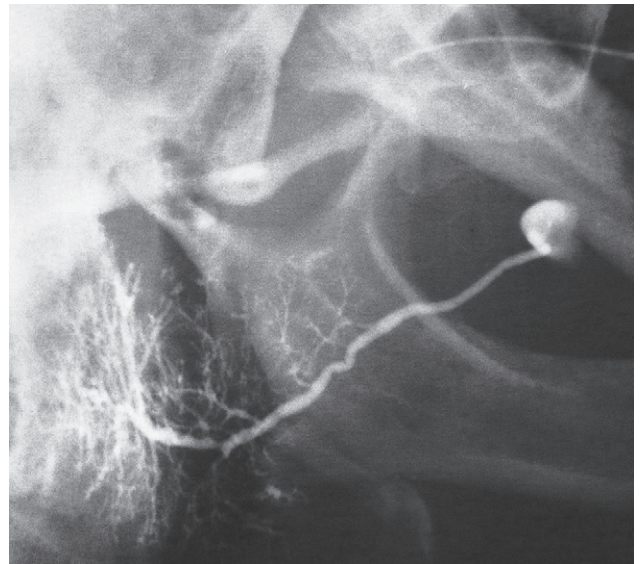


Fig. 16.10 Normal parotid sialogram. Note the long duct of even calibre and the fine branching of the ducts within the gland.

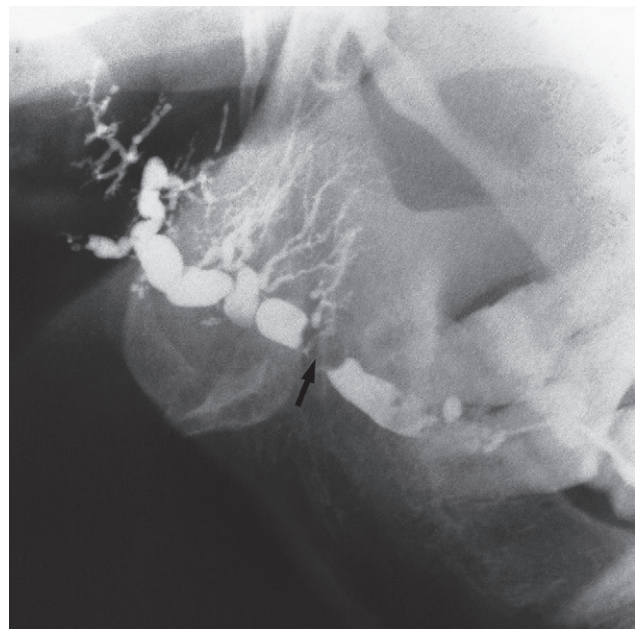


Fig. 16.11 Sialiectasis. There is dilatation of the ducts due to a stone (arrow) in the main parotid duct.

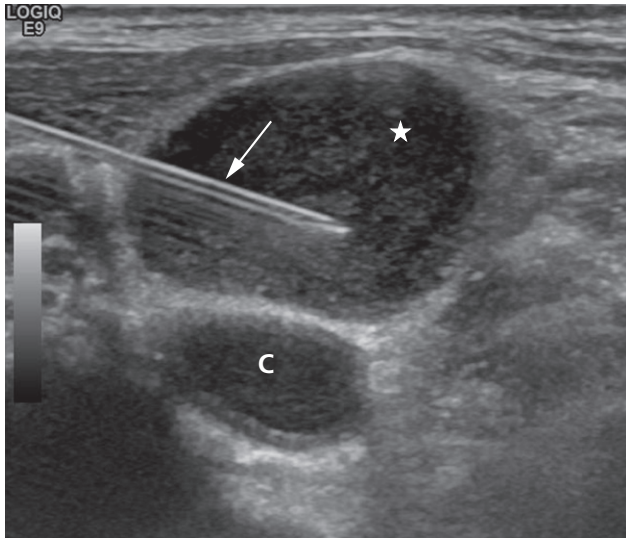


Fig. 16.12 Ultrasound-guided FNA of a cervical lymph node showing the aspiration needle (arrow) within a necrotic lymph node (*). The carotid artery (C) is also visualized.

For CT, intravenous contrast enhancement is necessary to opacify the major vessels that might otherwise be mistaken for small lymph nodes. The thyroid gland, which is situated on either side of the trachea, normally enhances quite markedly after intravenous contrast administration. CT is the first choice for acute infection and inflammation, particularly when abscess formation is suspected.

Magnetic resonance imaging is the best method of delineating the extent of most tumours in the neck because of the superior soft tissue contrast. Both CT and MRI enable characterization of masses (e.g. cystic, in a branchial cleft cyst or cystic hygroma) and can accurately define the site of origin, which influences the differential diagnosis.

Computed tomography, MRI and ultrasound can all demonstrate pathological lymph nodes in the neck that are too small to palpate or are in sites not amenable to clinical examination. Enlarged nodes may be due to lymphoma, metastases or infection (Fig. 16.13), but their appearance on CT and MRI is often similar irrespective of the cause. Ultrasound is more able to accurately predict the underlying

ing pathology but ultimately FNA is required in almost all cases to confirm.

Larynx

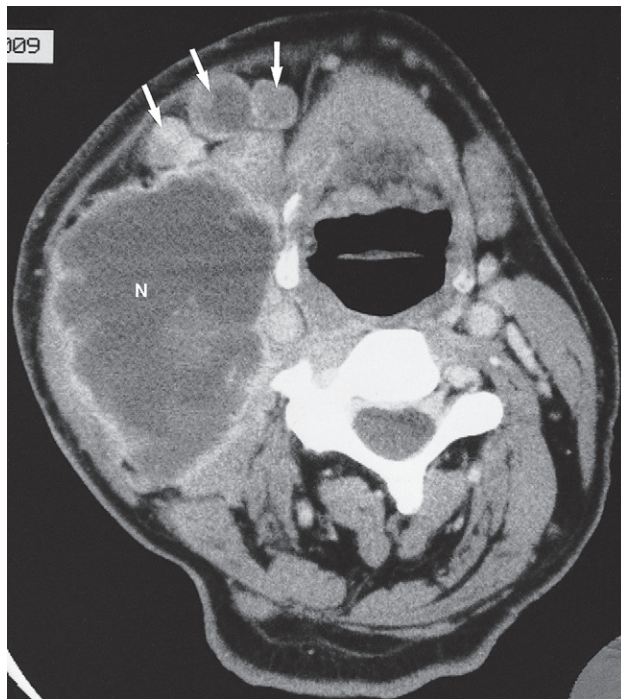
The larynx is best examined with CT, which has less movement artefact than MRI. The CT images can be viewed with multiplanar reformats. Targeted MRI may also be used because of the excellent demonstration of soft tissues, and provides useful additional information concerning the cartilage in laryngeal carcinoma. Direct inspection by laryngoscopy reveals a great deal of information about the larynx, particularly in regard to the vocal cords. However, imaging can provide additional information regarding the extent of the tumour and its spread outside the larynx (Fig. 16.14), particularly into the subglottic space which cannot be inspected directly.

Thyroid imaging

The thyroid is normally imaged by ultrasound (Fig. 16.15), which has largely superseded nuclear medicine techniques using technetium-99m (^{99m}Tc) pertechnetate or iodine-123 (^{123}I). The use of FNA with cytological examination of the aspirate has become the mainstay of diagnosis of thyroid cancer; scintigraphy now has a limited role, reserved for the investigation of abnormal thyroid function and in patients with known thyroid carcinoma.

Computed tomography is not often used to examine the thyroid except to demonstrate the extent of a retrosternal goitre and for the assessment of any local mass effect, such as tracheal compression (Fig. 16.16). It is important to note that iodinated contrast should be avoided in those patients who will require radio-active iodine diagnostic studies or treatment.

The commonest reason for imaging the thyroid is to determine the nature of a thyroid nodule, and in particular to select those nodules that require further evaluation with FNA in order to identify malignancy. Ultrasound determines whether a nodule is cystic or solid or a mixture of both. Simple cysts are invariably benign. Complex solid/cystic lesions are usually benign. A solid mass could be a carcinoma or an adenoma (Fig. 16.17a). Ultrasound may show that the nodule is part of a multinodular goitre by



(a)



(b)

Fig. 16.13 Lymphadenopathy. (a) There is a large lymph node (N) and several additional enlarged nodes (arrows) caused by metastases from a carcinoma of the floor of the mouth. (b) The lymph node mass (M) in this patient was due to infection.



Fig. 16.14 Carcinoma of the larynx. CT scan showing a large tumour (T) in the larynx that has destroyed the vocal cords and invaded the thyroid cartilage (arrow). A lymph node metastasis is present (L). C, carotid artery; V, jugular vein.

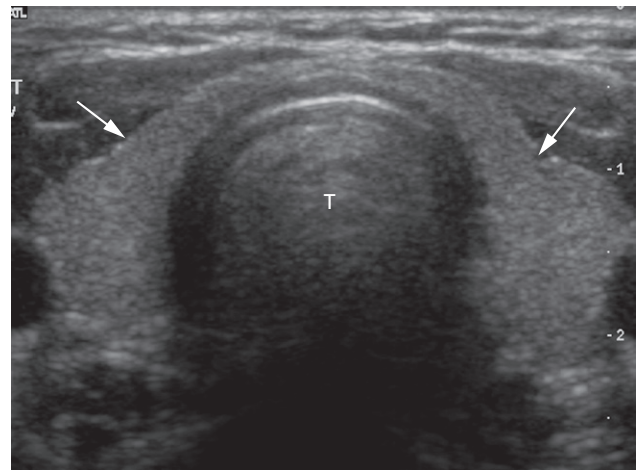


Fig. 16.15 Normal ultrasound of thyroid. The two lobes of the thyroid (arrows) lie on either side of the trachea (T).

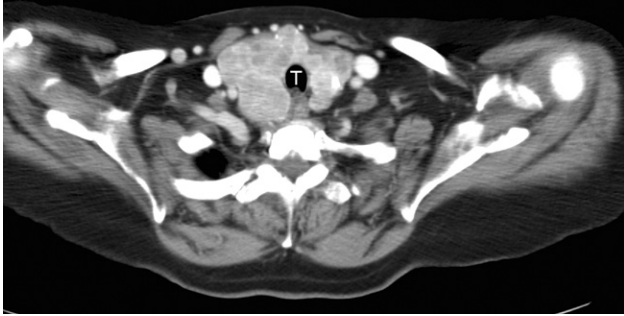


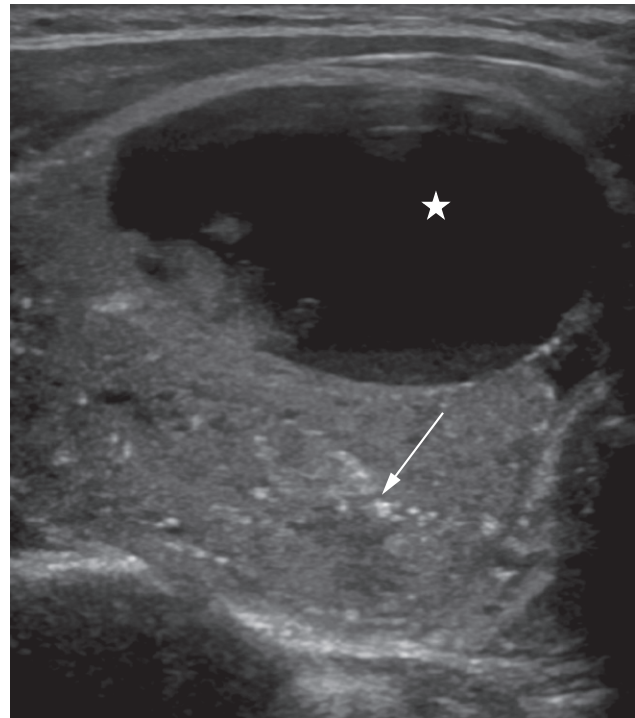
Fig. 16.16 Multinodular goitre. The enlarged thyroid almost surrounds the trachea (T) and enhances avidly after intravenous contrast showing many nodules of varying size.

demonstrating an enlarged gland with several nodules of varying size (Fig. 16.17b).

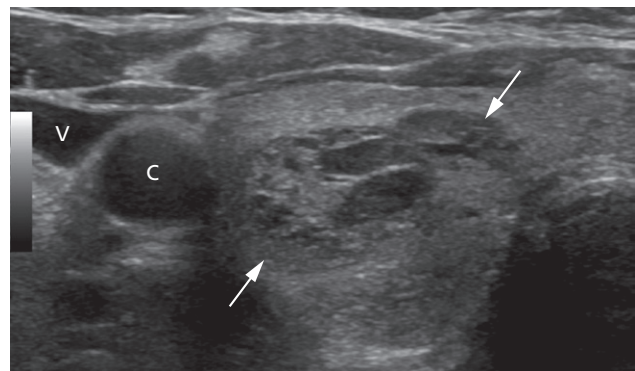
Scintigraphy (with ^{123}I or ^{131}I) for metastatic spread at presentation is usually to no avail as the metastases do not take up sufficient radionuclide. However, after the thyroid tissue has been ablated by surgery or by a therapeutic dose of ^{131}I , thyroid-stimulating hormone (TSH) levels rise and stimulate any functioning metastatic or recurrent tumour which may then be identified by radionuclide imaging (Fig. 16.18). ^{123}I imaging is used after thyroidectomy for cancer to identify any residual or metastatic sites of disease. Any metastases, recurrent tumour or residual thyroid tissue may subsequently be treated with a therapeutic dose of ^{131}I . In poorly differentiated thyroid cancer, fluorodeoxyglucose positron emission tomography (FDG-PET)/CT may be used to delineate the extent of disease.

Parathyroid imaging

Localization of a parathyroid adenoma prior to surgery for hyperparathyroidism is important because about 10% of adenomas are multiple or occur in an ectopic position. Parathyroid adenomas may be detected on ultrasound as a mass lying behind the thyroid (Fig. 16.19). Scintigraphy allows functional localization of abnormal parathyroid glands. Normal parathyroid glands are too small to be visualized, but even a small adenoma can be detected. The most widely used technique is to use two radio-isotopes, one that visualizes the thyroid and parathyroid glands ($^{99\text{m}}\text{Tc}$



(a)



(b)

Fig. 16.17 Ultrasound of thyroid nodules. (a) Ultrasound of a complex malignant thyroid nodule with cystic areas (*) and bright foci that indicate punctate calcification (arrow), which is associated with papillary and medullary thyroid cancer. (b) Ultrasound showing several hyperplastic nodules in the right lobe of the thyroid with a typical spongiform texture (arrows). The common carotid artery (C) and internal jugular vein (V) are also demonstrated.

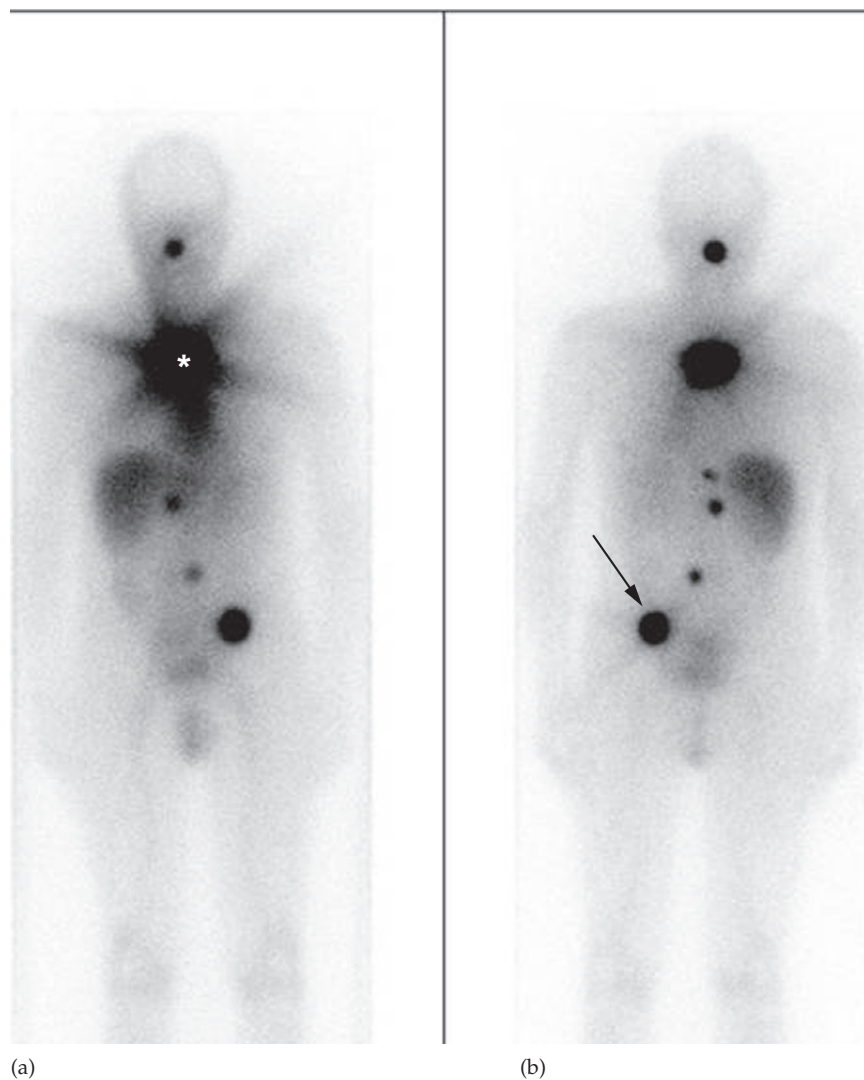
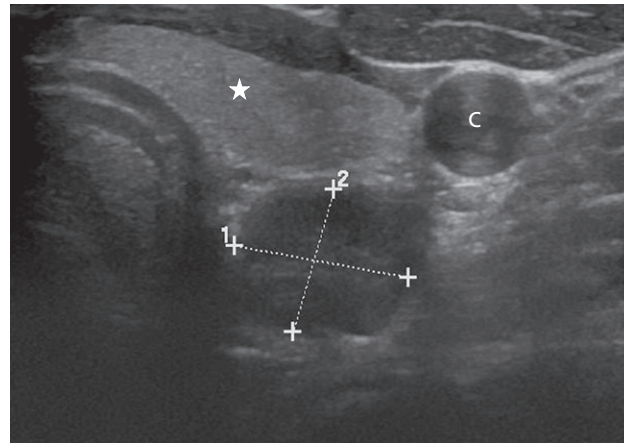
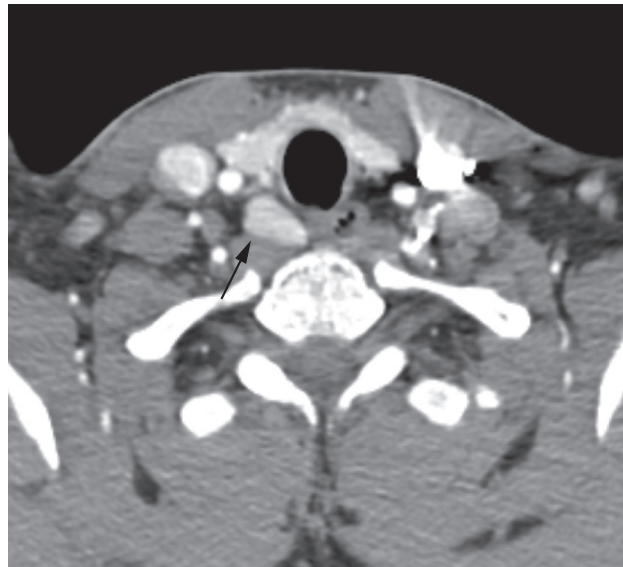


Fig. 16.18 Carcinoma of the thyroid. ^{131}I scan in a patient who had undergone thyroidectomy for carcinoma of the thyroid and then developed bone metastases. (a) Anterior and (b) posterior view. This image was acquired during a therapeutic dose of ^{131}I and shows residual uptake in the thyroid bed (*) as well as multiple bone metastases (one of which is shown with an arrow).



(a)



(b)

Fig. 16.19 Parathyroid adenoma. (a) Transverse ultrasound of a parathyroid adenoma (calipers) seen behind the left lobe of the thyroid gland (*). The common carotid artery (C) is also demonstrated. (b) CT of another patient showing an avidly enhancing right parathyroid adenoma (arrow).

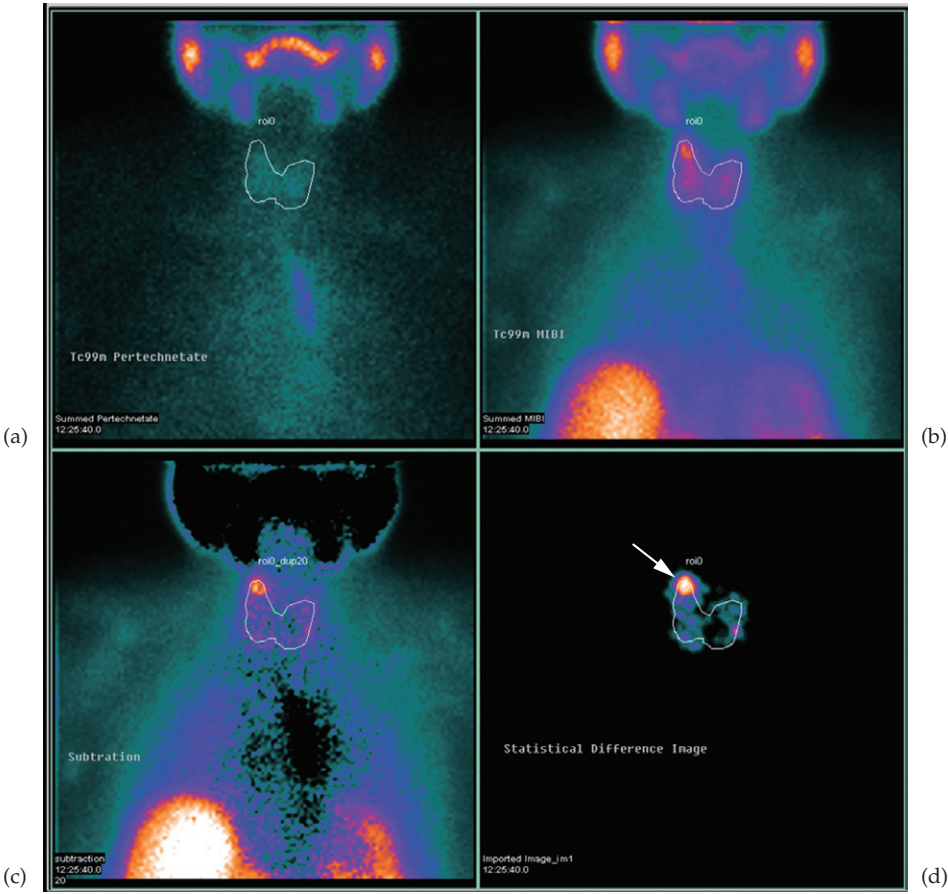


Fig. 16.20 Subtraction scintigraphy showing a single right upper pole adenoma (arrow). (a) ^{99m}Tc Pertechnetate acquisition. (b) ^{99m}Tc Sestimibi acquisition. (c) Subtraction image. (d) Statistical difference image.

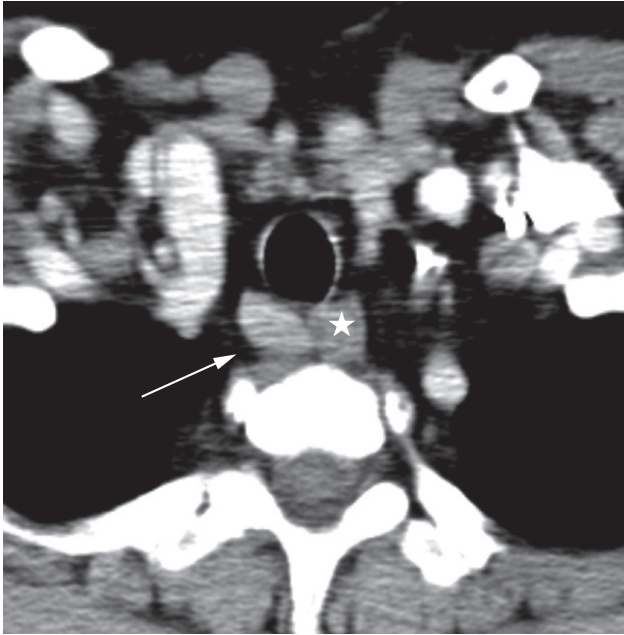


Fig. 16.21 CT of the neck showing an ectopic right retrotracheal adenoma (arrow) lying next to the esophagus (*).

sestamibi) and one that visualizes the parathyroid glands only (^{123}I or $^{99\text{m}}\text{Tc}$ pertechnetate). The two sets of images are digitally subtracted from one another and residual radioactivity on the subtraction image represents a hyperfunctioning parathyroid tissue (Fig. 16.20). Occasionally, when there is discordance between the ultrasound image and scintigraphy, further assessment with CT or MRI is required, particularly when an ectopic gland is suspected (Fig. 16.21).

Vascular and Interventional Radiology

Vascular radiology encompasses the diagnostic and therapeutic interventions that involve the arterial and venous system. Interventional radiology is a subspecialty of radiology in which minimally invasive procedures are carried out under image guidance.

Diagnostic vascular angiography

Prior to undertaking any intervention, it is important to have an accurate assessment of the extent and distribution of disease whether in the venous or, more commonly, the arterial system. In the past this could be obtained with a diagnostic angiogram, though increasingly non-invasive techniques such as Doppler, computed tomography (CT) and magnetic resonance angiography (MRA) are being used.

Arteriography

Arteriograms are performed via a catheter, which is introduced into the blood vessel using the Seldinger technique illustrated in Fig. 17.1. Contrast (usually iodinated contrast but occasionally carbon dioxide) is injected through the catheter, which opacifies the target vessel. Accurate images are obtained by digitally subtracting the background image prior to injection, from the image obtained during injection (digital subtraction arteriography). The result is a road map of the vascular tree without distortion by bones, bowel gas or soft tissues, which would normally appear on a plain x-ray (Fig. 17.2). At the end of the procedure, the catheter

is pulled out. A few minutes compressing the puncture site with the fingers is enough to stop the bleeding in most patients. The advantages of the Seldinger technique are that it is easy and quick to perform, that the hole in the artery is no bigger than the catheter, and that catheters of any length may be used. There are several indications for arteriography, listed in Box 17.1.

Magnetic resonance angiography

Magnetic resonance angiography is a very useful non-invasive technique, which can demonstrate both arteries and veins. Images of the vascular system can be obtained using special sequences that depend on the signal obtained from flowing blood or via an injection of a contrast agent (gadolinium DTPA (diethylene triamine pentacetic acid)) into a peripheral vein (Fig. 17.3).

Magnetic resonance angiography is particularly useful for showing the aorta and its branches (Fig. 17.4a), aortic dissection, the portal vein (Fig. 17.4b) and for demonstrating carotid artery disease, peripheral vascular disease and renal and mesenteric artery stenosis. Aneurysms and vascular malformations can also be detected in the intracranial circulation.

Computed tomography angiography

Spiral CT, particularly multidetector CT, enables large areas of the body to be scanned quickly. After an intravenous injection of contrast, many thin sections can be obtained so

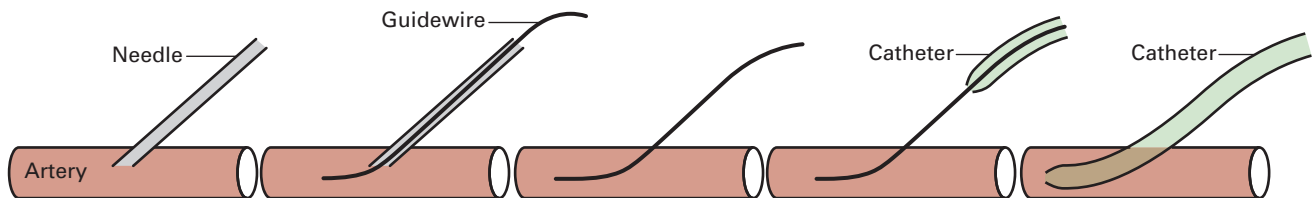


Fig. 17.1 Seldinger technique for catheterizing blood vessels. The femoral artery or vein are the usual vessels used. (a) A needle is inserted through the skin into the blood vessel. (b) A guidewire is passed through the needle into the lumen of the vessel. (c) The needle is withdrawn, leaving the guidewire in the lumen of the vessel. (d) A catheter is threaded over the guidewire and passed into the lumen of the vessel. (e) The guidewire is withdrawn, leaving the catheter in position in the lumen of the vessel.

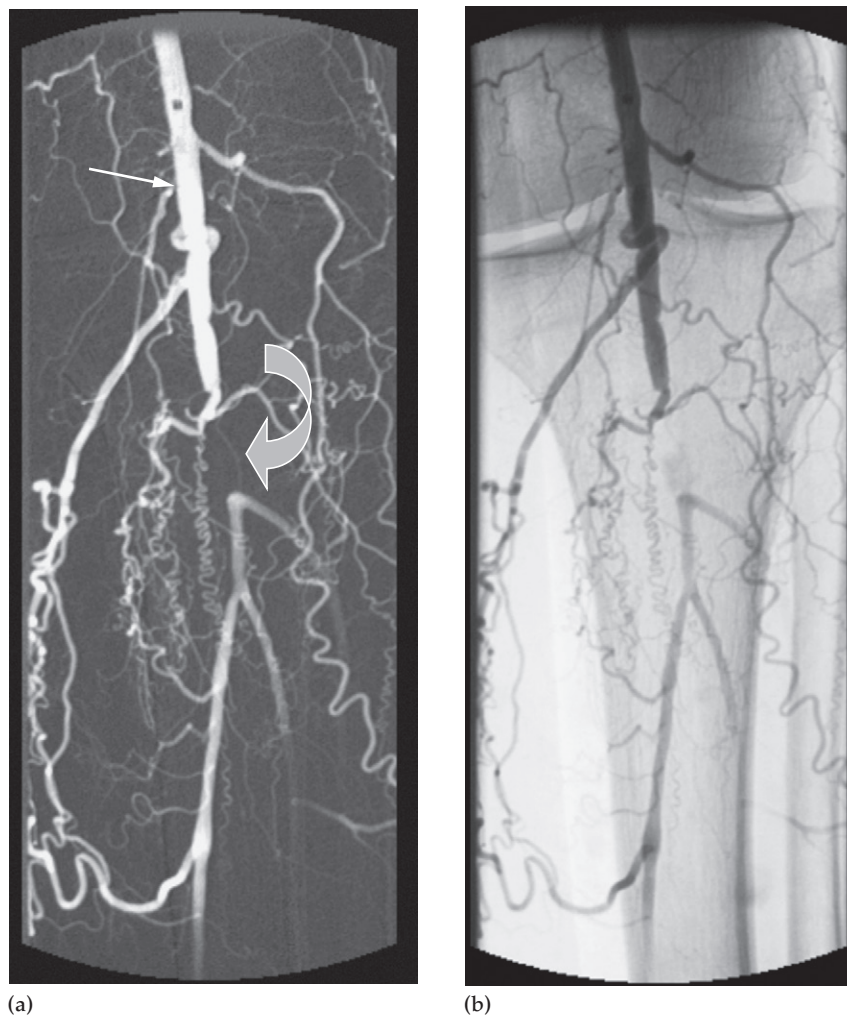


Fig. 17.2 Digital subtraction arteriogram following an intra-arterial injection of contrast medium. On the subtracted image (a) the bones and soft tissues are barely visible compared to the unsubtracted image (b). The angiogram shows a patent popliteal artery (thin arrow) with a short segment occlusion proximal to the trifurcation (curved arrow).

Box 17.1 Major indications for arteriography

- Diagnosis of vascular diseases (e.g. vascular occlusive disease, aneurysm, arteriovenous fistula, arteriovenous malformation)
- Diagnosis or localization of vascular tumours (e.g. insulinoma, parathyroid adenoma)
- Preoperative definition of vascular anatomy (e.g. organ transplant, local tumour resection, revascularization)
- Diagnosis and treatment of vascular complications of disease, trauma or surgery
- Performance of vascular interventional procedures (e.g. percutaneous transluminal angioplasty, stenting, embolization, transcatheter infusional therapy)

reconstruction in the coronal and sagittal planes can be performed to give optimum visualization of the vessels.

Computed tomography angiography is particularly useful for visualizing the aorta and its branches for suspected aneurysms (Fig. 17.5) including any rupture or leakage. CT pulmonary angiography demonstrates the pulmonary arteries and can detect pulmonary emboli (see Chapter 2, Fig. 2.102c). The peripheral arteries can also be visualized by CT angiography, as can the cerebral vessels.

Ultrasound of the arterial system

Ultrasound has an important role to play in diagnosing arterial disease, both in the carotid arteries and peripheral vessels, and is commonly the primary imaging modality used in assessment. The common, internal and external carotid arteries can be readily visualized in the neck. The location or size of any atheromatous plaques and the severity of any luminal narrowing can be determined. With colour Doppler imaging, a stenosis in the artery can be visualized and an occlusion will show as an absence of flow. Because a stenosis disrupts the normal flow pattern, analysis of the flow-velocity waveform can give further information regarding the degree of stenosis. Imaging of the iliac vessels may be difficult due to overlying bowel gas, but evaluation of the abdominal aorta is invariably successful and can easily be performed during an outpatient assessment.

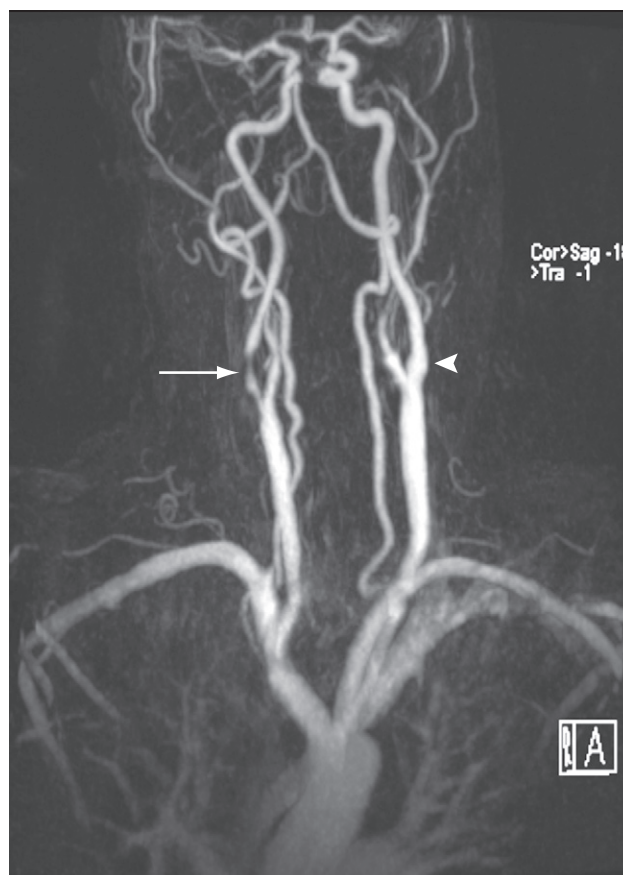


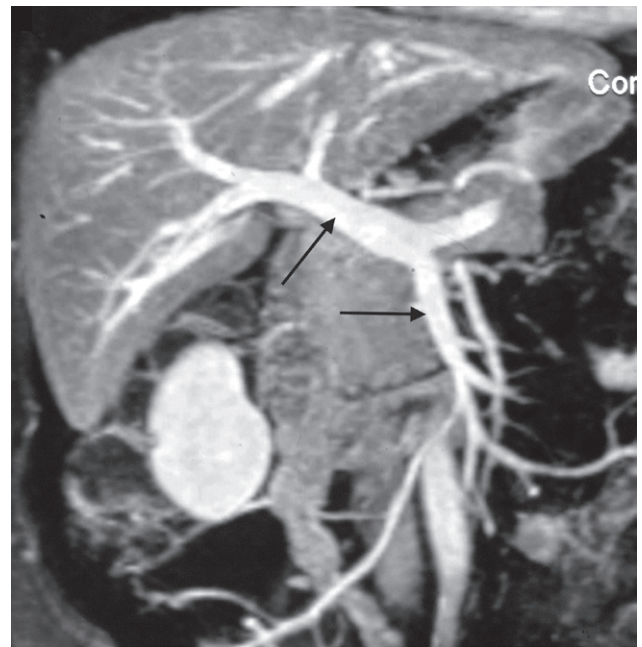
Fig. 17.3 MRA of the carotid arteries showing a short stenosis in the right internal carotid artery (long arrow). A normal internal carotid artery is seen on the left (arrowhead).

Ultrasound venography

Duplex ultrasound has now largely replaced contrast venography for the detection of venous thrombosis. With a venous thrombosis, intraluminal echogenic material is visible and the veins lose their normal compressibility; thrombus-free veins should be compressible by direct pressure using the ultrasound transducer. Colour Doppler scanning shows that there is a lack of spontaneous flow in the affected veins. Ultrasound can readily visualize the external iliac, common femoral and popliteal veins,



(a)



(b)

Fig. 17.4 MRA. (a) Contrast angiogram showing a normal abdominal aorta and its branches. (b) Contrast angiogram showing the superior mesenteric (horizontal arrow) and portal (upward pointing arrow) veins.

although it can be sometimes difficult to visualize the calf veins. In practice, this is often not clinically significant as calf vein (i.e. below knee) thrombosis may not be treated.

Contrast venography

Contrast venography is routinely used for the evaluation of the upper limb veins, as it enables imaging of the central veins with the arm in a neutral and abducted posi-

tion and allows a functional evaluation. A large volume of contrast medium is injected into a vein on the arm or the hand. The contrast is forced into the deep venous system of the upper limb by means of a tourniquet. Thrombi may be seen as filling defects in the opacified veins, and any stenosis or occlusion in the central veins is well demonstrated.

Venography in the lower limb is seldom used, having been superseded by ultrasound.

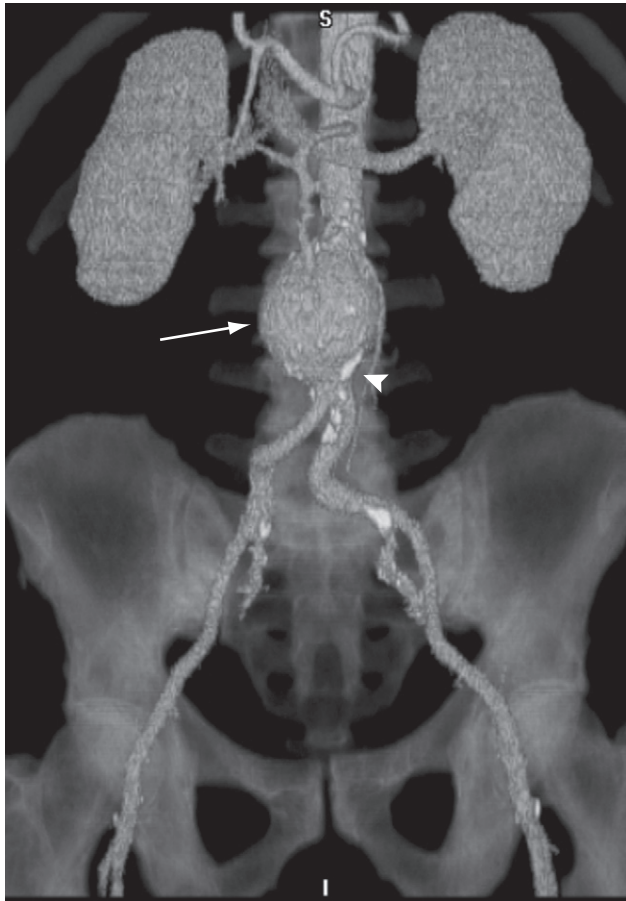


Fig. 17.5 CT angiogram. Reconstruction from many thin axial sections following an intravenous injection of contrast demonstrating an aortic aneurysm (arrow). Calcification is seen in the wall of the arteries (arrowhead).

Interventional radiology

Radiologists carry out various percutaneous techniques under imaging control, including dilating stenoses, occluding vessels, draining abscesses and other fluid collections, and obtaining biopsy samples. These procedures greatly assist and may modify surgery, or even replace it altogether. They are carried out with the help of a variety of imaging modalities, notably fluoroscopy, angiography, ultrasound, CT and, more recently, magnetic resonance imaging (MRI). Interventional radiology is usually performed

under local anaesthesia, causing only relatively minor discomfort to the patient, allowing many procedures to be performed as 'day cases'. Only the basic principles of the interventional techniques in widespread use will be described here.

Angioplasty and stents

Arterial stenoses and even occlusions may be traversed with a guidewire. A balloon catheter can be passed through the abnormal site, which has been previously determined by arteriography (Fig. 17.6). The stenosis is then dilated by inflating the balloon (angioplasty) (Fig. 17.7). This percutaneous technique, which usually uses the femoral artery as an access route, has been widely employed in peripheral vascular disease and gives results as good as bypass surgery, particularly for iliac and superficial femoral artery disease. Short stenoses are the ideal lesions to treat with angioplasty.

Stents are balloon expandable or self-expanding metal cylinders that can be embedded in plastic and collapsed to enable them to be inserted through an artery or vein (Fig. 17.8). As they 'reinforce' the vessel at the site of angioplasty, they have a more durable result. Stents are commonly used in the treatment of arterial stenosis and occlusion in coronary disease, in peripheral vascular disease, and in patients with mesenteric ischaemia secondary to atherosclerotic stenoses in the mesenteric arteries. Their role in the management of renal artery stenosis is debatable following several recent trials, but is still indicated to treat patients with deteriorating renal function, flash pulmonary oedema and occasionally renal vascular hypertension.

Covered metal stents can be used to 'exclude' aneurysms, either in small vessels or, increasingly, in the thoracic or infrarenal aorta, a technique known as endovascular aneurysm repair or EVAR (Fig. 17.9). Due to the size of the deployment system of these large stent grafts, they are normally introduced through a femoral arteriotomy. Stents can also be introduced through the femoral vein and placed across a stricture in the superior vena cava to overcome the distressing symptoms of superior vena caval obstruction, which is usually caused by a malignant tumour in the mediastinum.

Complete occlusions (as opposed to stenoses in a patent vessel) in peripheral vessels of the lower limb can also be

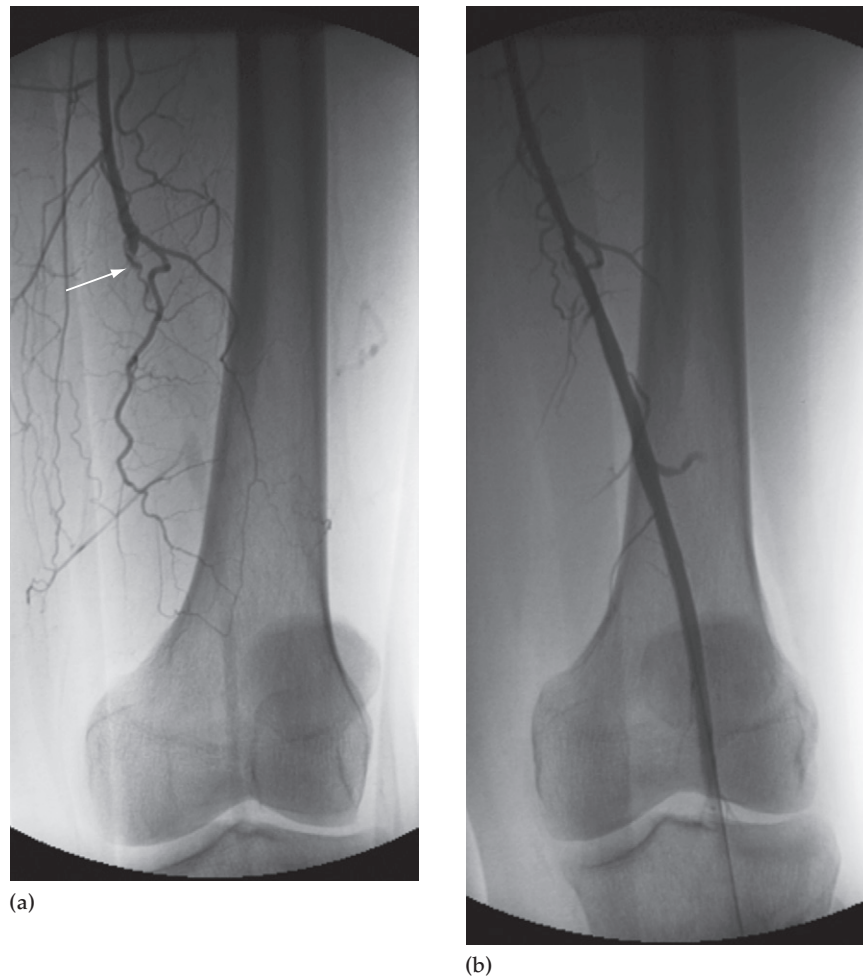


Fig. 17.6 Percutaneous transluminal angioplasty. (a) Preliminary arteriogram showing an occlusion in the left superficial femoral artery (arrow). (b) Following the angioplasty, the lumen has been restored.

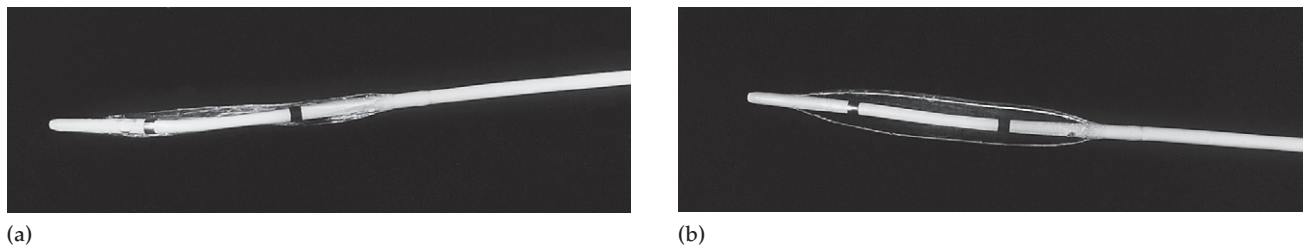


Fig. 17.7 Percutaneous angioplasty balloon catheters. (a) The catheter prior to inflating the balloon. (b) The catheter with the balloon distended as it would be if it were inside the artery.

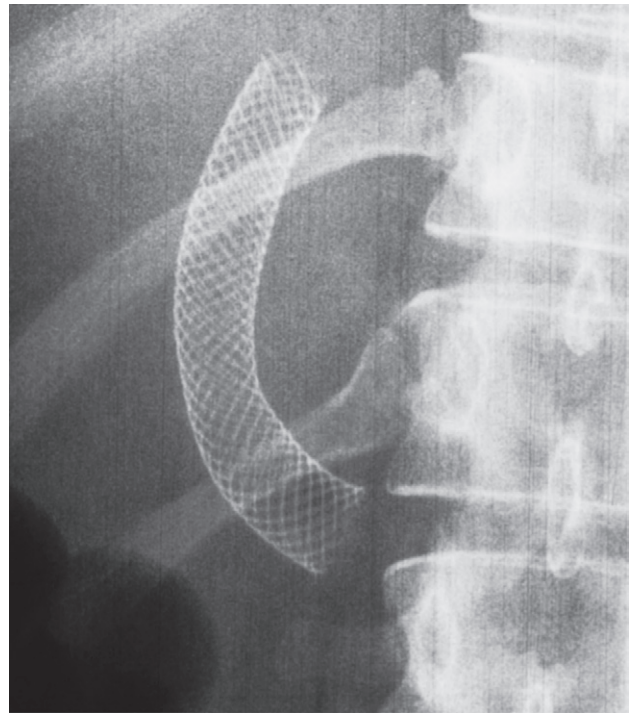
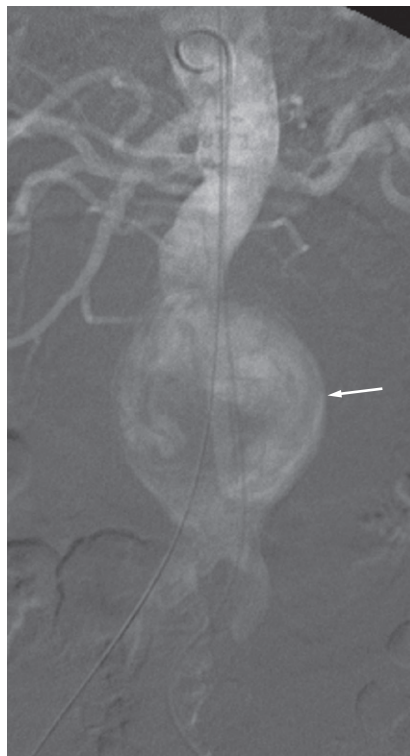


Fig. 17.8 Stent which has been placed in the liver to make a connection between the portal and systemic venous systems in the transjugular intrahepatic portosystemic shunt procedure.



(a)



(b)

Fig. 17.9 (a) Digital subtraction arteriogram (DSA) of the abdominal aorta showing a large aneurysm (arrow). (b) DSA post stent graft. The covered stent (short arrows), acting as an endoskeleton, has excluded the aneurysm from the circulation by creating a seal proximally below the renal arteries (long arrows) and distally in the iliacs. This depressurizes the aneurysmal sac and reduces the risk of rupture.

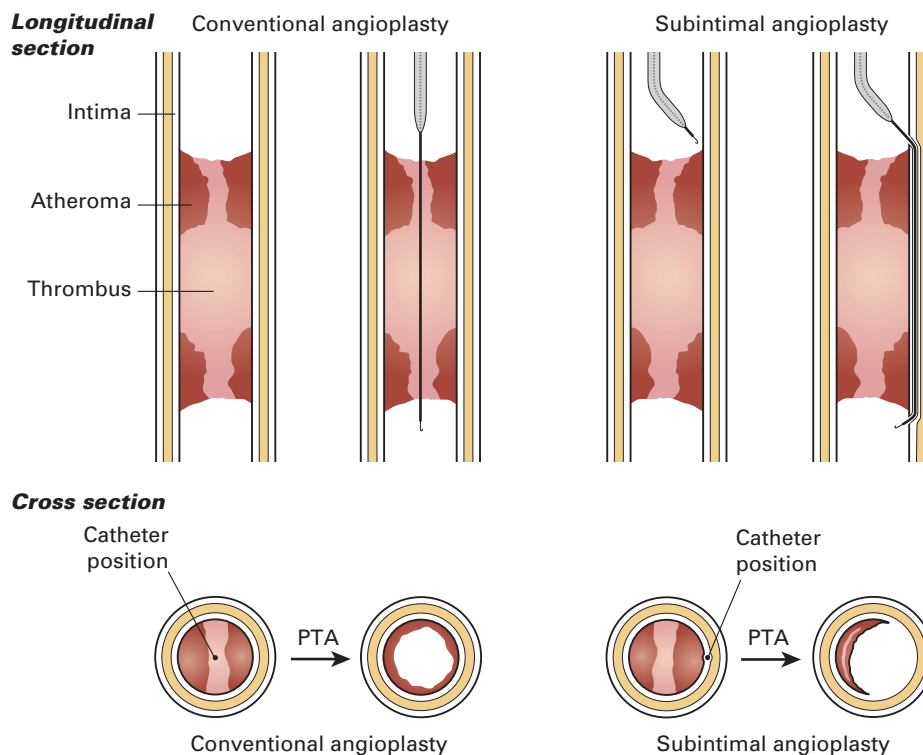


Fig. 17.10 Diagram demonstrating the techniques of conventional and subintimal angioplasty. In subintimal angioplasty, the catheter is passed into the subintimal plane of the vessel, not in the lumen of the vessel. The balloon is then inflated. The principle is to create a new lumen in the subintimal plane rather than re-open the native lumen. PTA, percutaneous transluminal angioplasty.

treated by a technique known as subintimal angioplasty, the principle being to create a new channel through the diseased segment in the subintimal plane (i.e. within the wall of the vessel) rather than to re-cannalize the original lumen (Fig. 17.10).

Therapeutic embolization

Arteries can be occluded by introducing a variety of materials through a catheter selectively placed in the vessel. Metal coils covered with thrombogenic filaments, gelatin foam, small particles made of polyvinyl alcohol and cyanoacrylate glues that solidify on contact with blood, have all been used for therapeutic embolization. These techniques have been used primarily to control bleeding. Once arteriography has demonstrated the bleeding site, the offending

vessel can then be embolized. Arterial embolization is also of use in patients with tumours (e.g. renal cell carcinoma) to reduce tumour vascularity prior to surgery, or with inoperable tumours to treat intractable pain and bleeding (Figs 17.11 and 17.12). Vascular occlusion has also been successfully used in treating arteriovenous malformations in various organs, most notably the brain and the lungs (Fig. 17.13). Embolization of aneurysms on the intracranial arteries is being increasingly undertaken, thus avoiding craniotomy (Fig. 17.14).

Therapeutic ablation

In some cases, metastatic liver lesions and certain other primary tumours (e.g. renal tumours) can be ablated percutaneously using a variety of physical techniques such as

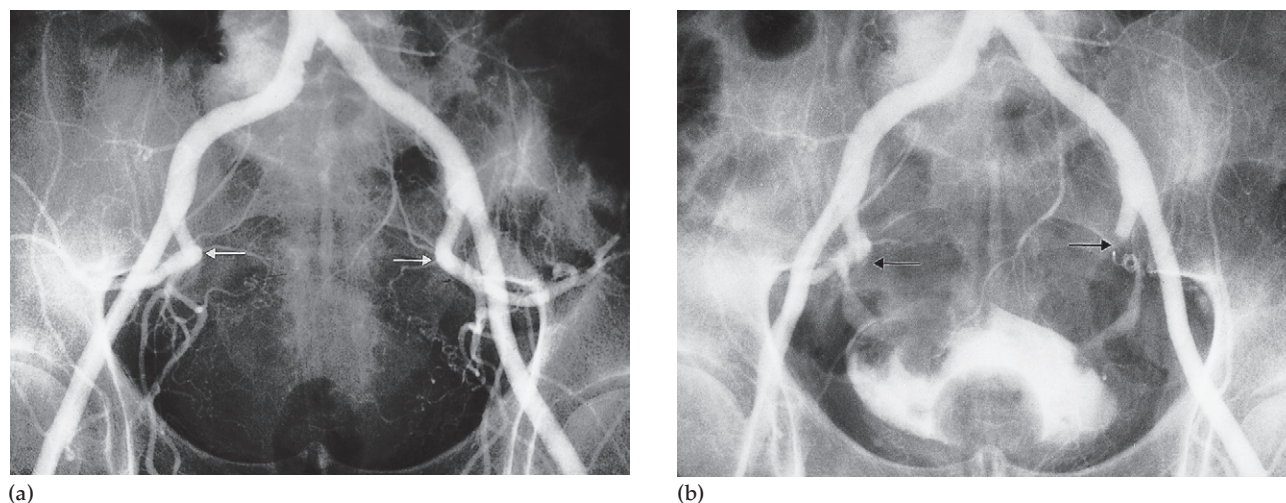


Fig. 17.11 Therapeutic embolization. (a) Arteriogram prior to embolization showing patent internal iliac arteries (arrows) in a patient with uncontrollable bleeding from a large bladder tumour. (b) Following embolization, both iliac arteries are occluded. The arrows point to the level of occlusion.

heating (using radiofrequency, microwave, laser or electrocautery), freezing (cryotherapy) or injecting a noxious agent such as ethanol into the tumour. The size and location of the tumour help to determine which method may be appropriate. The treatment is performed under image guidance using ultrasound, CT or MRI. One of the most frequently used of these techniques is thermal ablation of hepatic metastases.

Vascular catheterization for infusion

Arterial catheters can be accurately placed for the infusion of cytotoxic or radioactive agents directly into malignant tumours (e.g. hepatocellular carcinoma in the liver), a technique known as transarterial chemoembolization, and for the infusion of fibrinolytic agents to dissolve fresh clots from the vascular system, a technique known as thrombolysis.

Inferior vena cava filters

Inferior vena cava filters can be introduced percutaneously through the femoral vein. The filters trap emboli originat-

ing from leg or pelvic vein thrombi (Fig. 17.15). They are used in patients who are at risk of pulmonary embolism that cannot be managed satisfactorily with anticoagulation or where anticoagulation is contraindicated.

Percutaneous needle biopsy

Needle biopsy techniques are particularly useful for the non-operative confirmation of suspected malignancy. Under fluoroscopic, ultrasound or CT guidance (Fig. 17.16), a needle is passed to the desired site and a small amount of tissue is removed. Most intrathoracic or intra-abdominal sites can be sampled. With a fine aspiration needle (20–22 gauge), material can be obtained for cytology. This needle can pass through blood vessels, vascular masses, loops of bowel and solid organs with only minimal risk of infection or bleeding. Apart from a small pneumothorax with intrathoracic biopsy, complications are extremely rare. To obtain material for histological study a larger needle (14–18 gauge for soft tissues, 10–13 gauge for bone) is used. The larger needles require specific approaches to avoid damage to intervening structures and require stricter indications than fine needle aspiration.

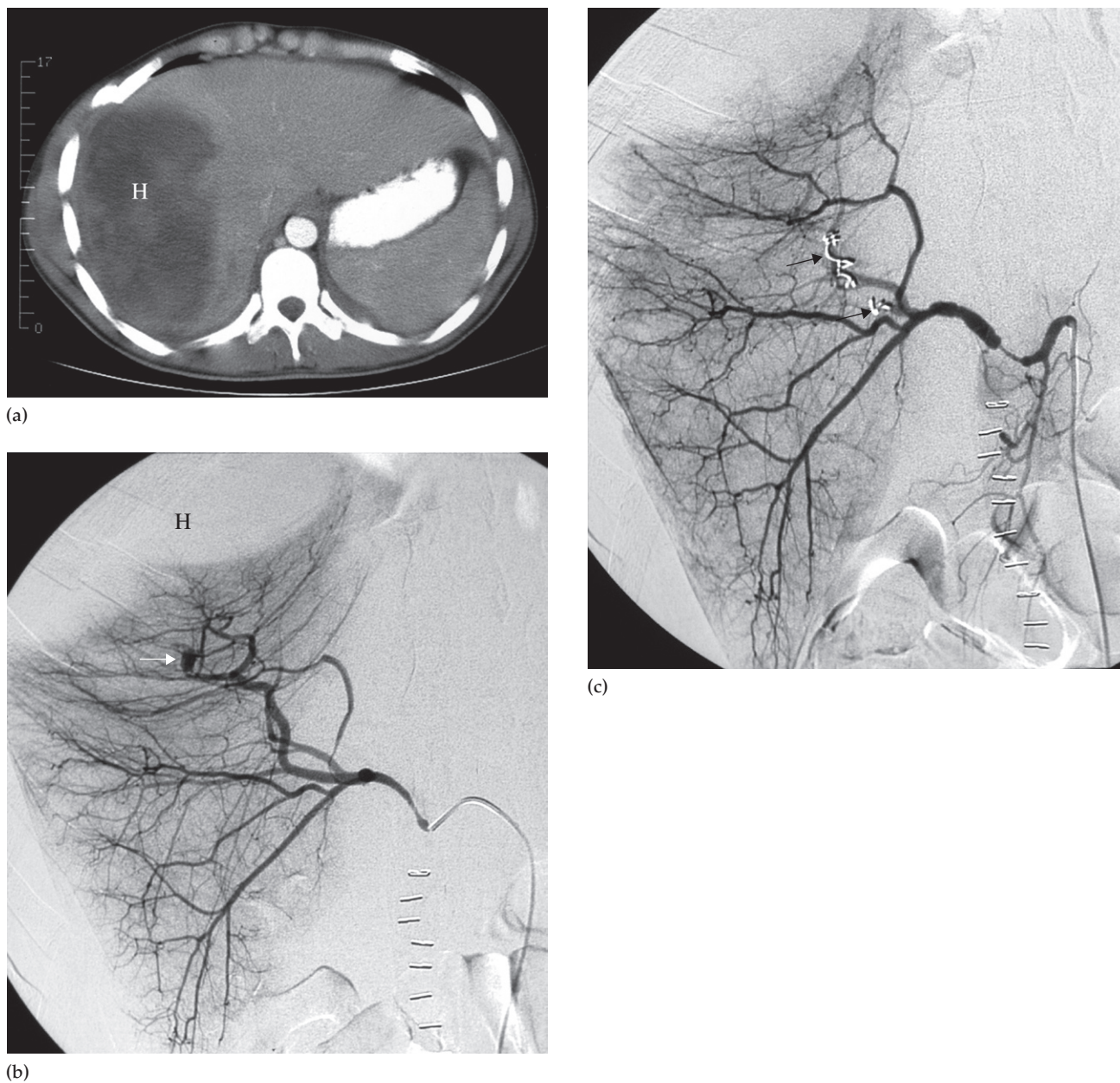


Fig. 17.12 Therapeutic embolization. (a) CT scan in a patient with a large intrahepatic haematoma (H) following a road traffic accident. (b) Selective hepatic arteriogram showing a false aneurysm (arrow) which was the site of bleeding. Note the haematoma (H) compressing the liver substance. (c) A branch of the hepatic artery supplying the aneurysm has been occluded with coils (arrows) and the aneurysm no longer fills.

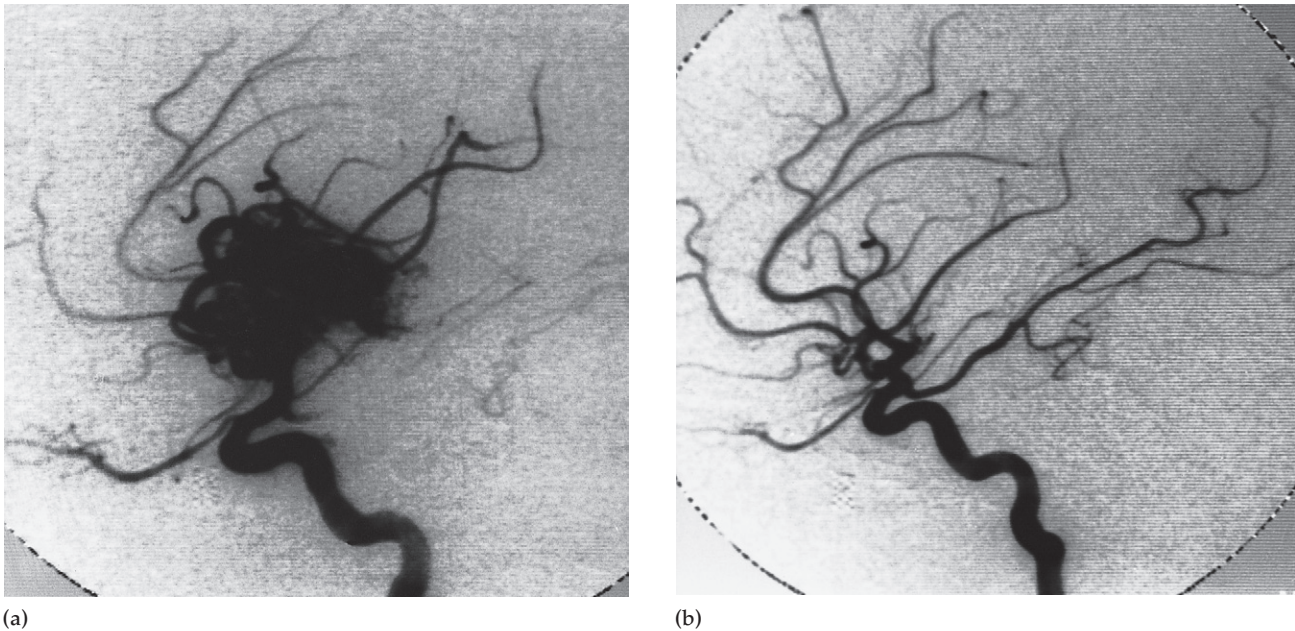


Fig. 17.13 Arteriovenous malformation occlusion. (a) Carotid angiogram showing a large arteriovenous malformation. (b) After occlusion of the feeding vessels with cyanoacrylate glue the malformation is obliterated.

Percutaneous drainage of abscesses and other fluid collections

Specially designed drainage catheters can be introduced percutaneously into abscesses or other fluid collections. The catheters vary in diameter from 6 to 14 French depending on the nature of the fluid to be drained. The larger catheters may have a double lumen to assist with irrigation of an abscess cavity. They are introduced under the control of whichever imaging modality is most convenient; the essential feature is that the operator must know exactly the location of the abscess and must know that the route chosen for introduction of the catheter will be safe (Fig. 17.17). Ultrasound, CT and fluoroscopy are the usual methods.

Once the catheter has been placed in an abscess, it is usually necessary to allow the pus to drain for several days. Irrigation of the tube and the abscess cavity is often essential for continued effective drainage. Thus, the placement of the tube may be only the first step in successful percutaneous abscess drainage.

The technique is suitable for most abdominal abscesses, though the success with some forms of abscess is considerably greater than with others. For example, percutaneous drainage is usually successful for liver and intraperitoneal abscesses, but often less satisfactory for pancreatic abscesses (Fig. 17.18), particularly if they follow pancreatitis and if the abscesses are multiple or multiloculated. A similar technique can be employed to insert a chest tube to drain a pleural effusion or empyema.

Transjugular liver biopsy

In patients with diffuse liver disease, particularly cirrhosis, there may be problems with blood coagulation, with a risk of uncontrolled bleeding after a percutaneous biopsy. To overcome this problem, a biopsy is performed via the hepatic veins so if bleeding occurs it enters the vascular system. The jugular vein is punctured in the neck and, under fluoroscopic guidance, a special biopsy catheter is passed through the superior and inferior vena cavae and

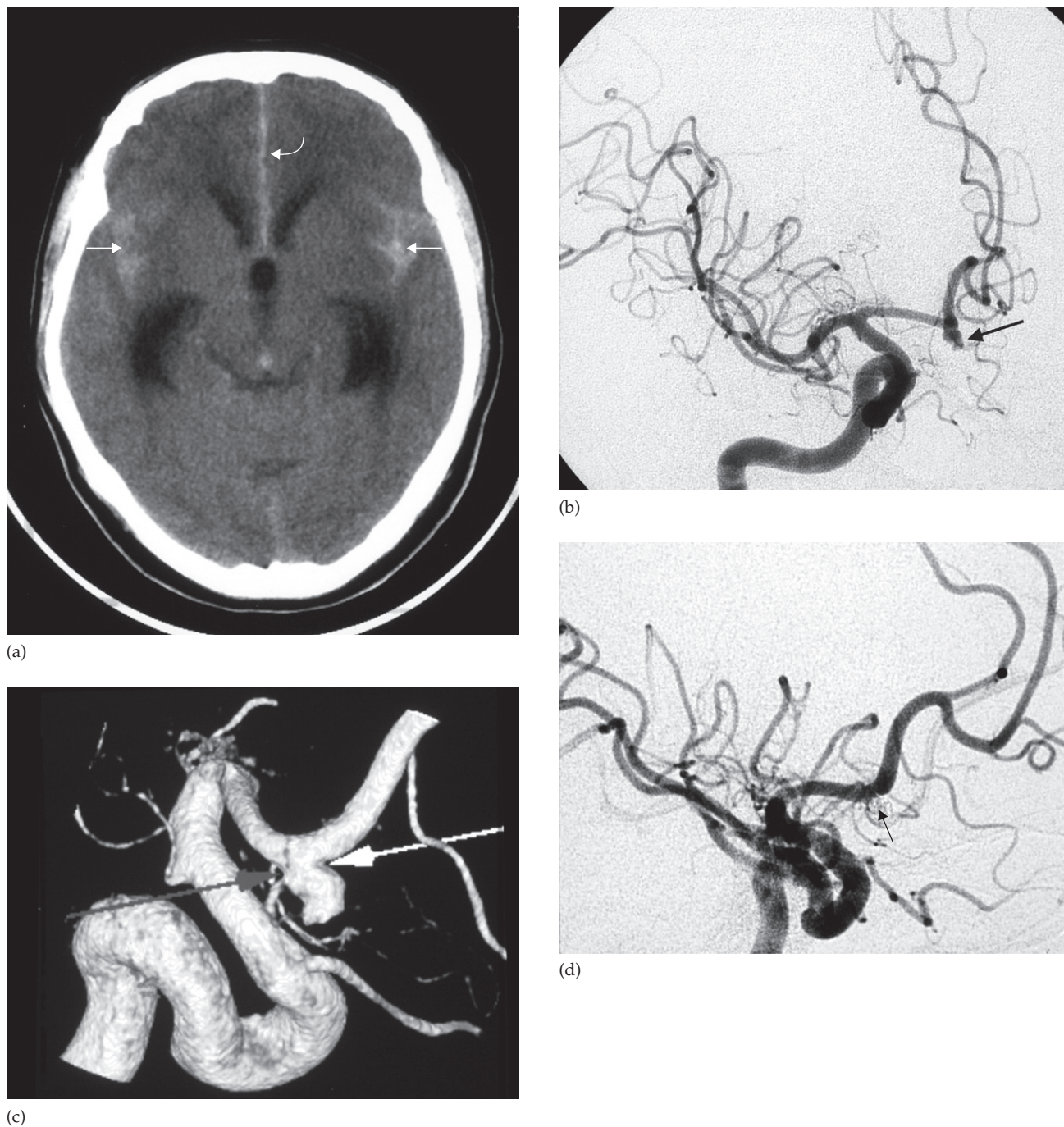


Fig. 17.14 Embolization. (a) CT scan in a patient with a subarachnoid haemorrhage showing high density blood in the Sylvian fissures (arrows) and anterior hemispheric fissure (curved arrow). There is also hydrocephalus. (b) Right internal carotid angiogram showing an anterior communicating artery aneurysm (arrow). (c) The arrows on the three-dimensional formatted image point to the neck of the aneurysm. (d) The aneurysm is obliterated after it is occluded with metal coils (arrow).

Fig. 17.15 Inferior vena cava filter. (a) Plain film showing the bird's nest filter in place. (b) An inferior vena cavogram showing a large thrombus (arrows) trapped by the filter.

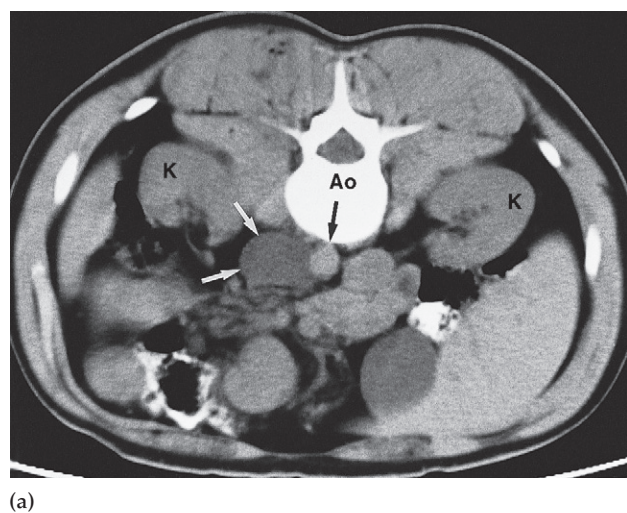
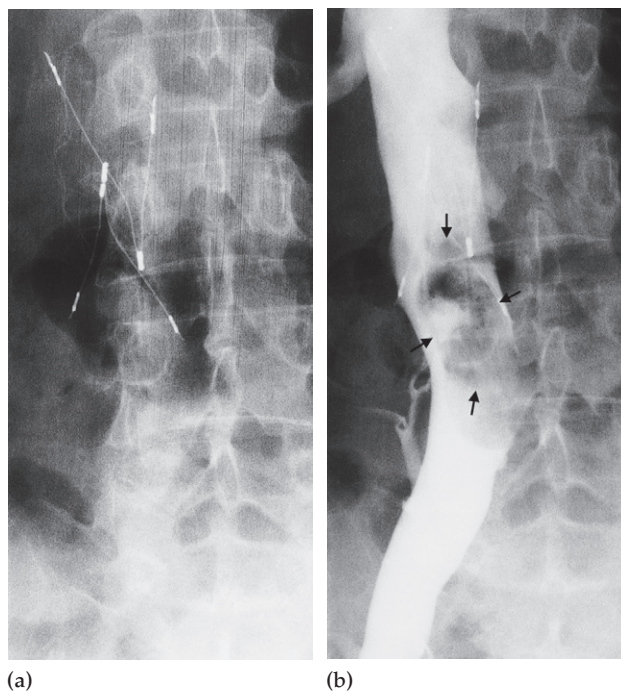


Fig. 17.16 Needle biopsy of an enlarged para-aortic lymph node under CT control with the patient prone. (a) An enlarged lymph node (arrows) is seen to the left of the abdominal aorta (Ao) at the level of the kidneys (K). (b) The tip of an 18-gauge cutting needle has been placed in the enlarged lymph node. The tissue obtained confirmed that the lesion was a metastasis from a germ cell tumour of the testis.

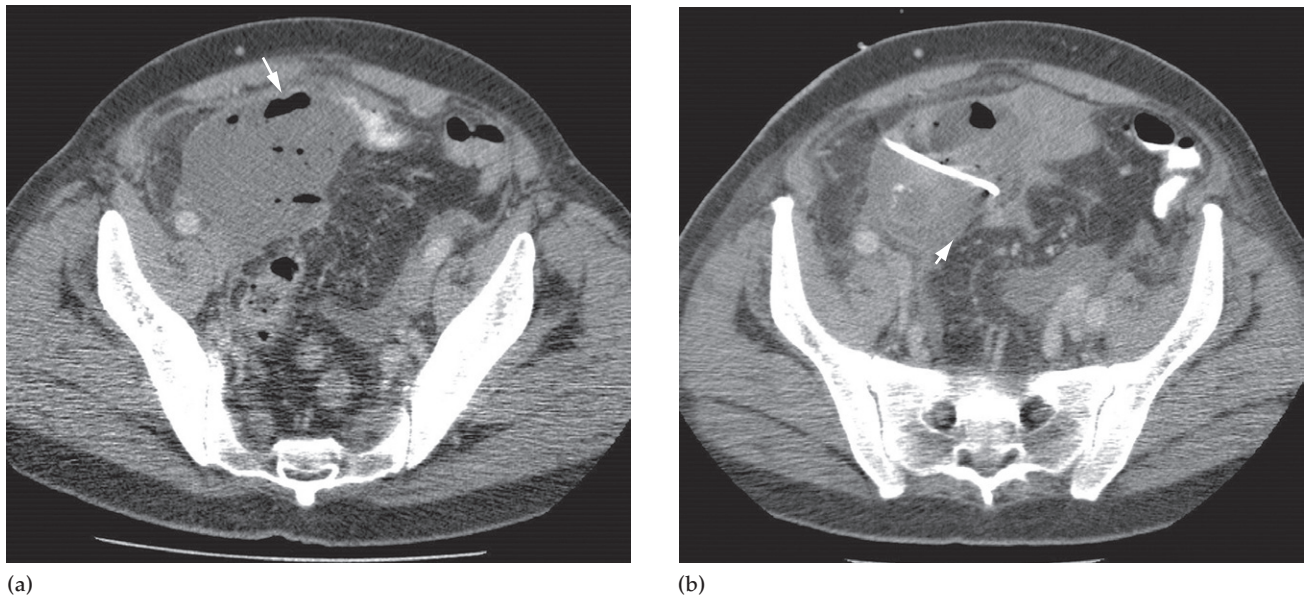


Fig. 17.17 (a) An abdominal abscess in the right iliac fossa secondary to appendicitis. Small pockets of air are seen in the collection (arrow). (b) A percutaneous drainage catheter (partially seen) has been inserted into the collection (arrowhead) which is decreasing in size.

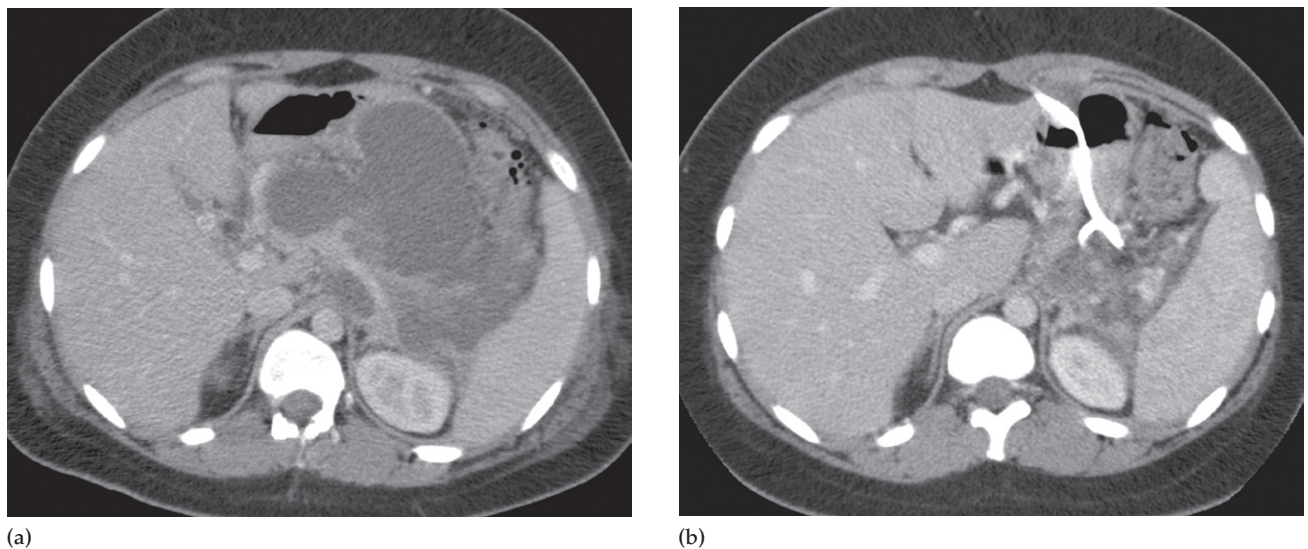


Fig. 17.18 Pancreatic pseudocyst drainage. (a) CT scan showing a collection involving the body of the pancreas, which developed following acute pancreatitis. (b) A drainage catheter has deliberately been inserted through the stomach into the collection (to encourage the development of an internal rather than a cutaneous fistula), which has decreased significantly in size.

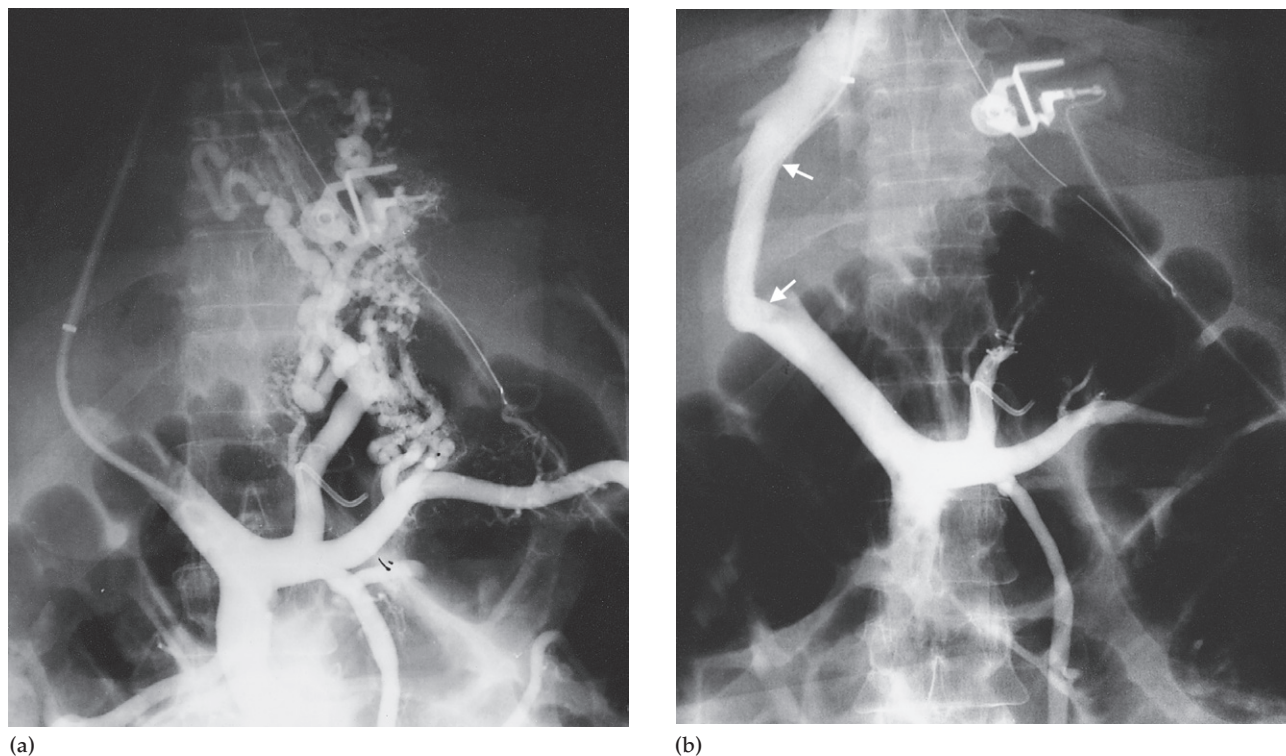


Fig. 17.19 Transjugular intrahepatic portosystemic shunt (TIPSS). (a) A catheter has been passed from the jugular vein in the neck through the heart into a hepatic vein and then pushed through the liver parenchyma into a portal vein. A retrograde injection is made outlining the portal vein and its tributaries. Note the gastro-oesophageal varices. (b) A connection between the portal vein and a large hepatic vein has been established and a stent inserted. Its position is shown by the arrows. Note the varices no longer fill (in part due to deliberate occlusion).

advanced into a hepatic vein where a biopsy of the liver parenchyma is taken.

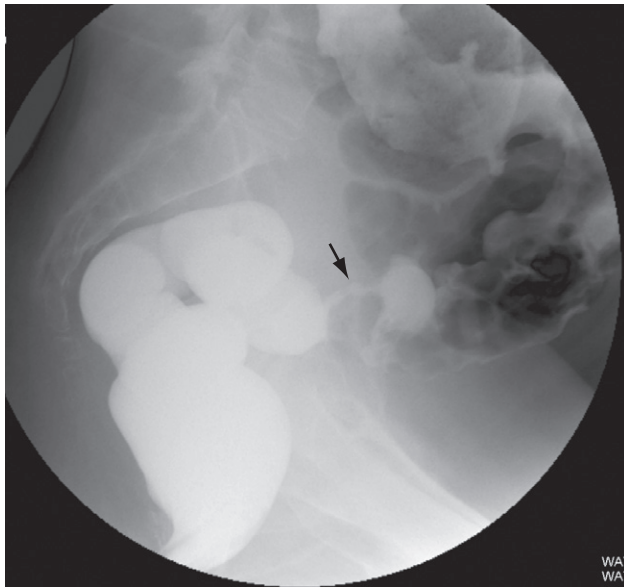
Transjugular intrahepatic portosystemic shunt

Patients who have portal hypertension with bleeding gastro-oesophageal varices or intractable ascites may benefit from the creation of a communication between the portal and systemic venous systems to lower the portal pressure when other attempts to treat the varices, such as sclerotherapy or banding, have failed. This communication may be conveniently performed percutaneously under ultrasound guidance. The internal jugular vein is punctured and a catheter passed through the heart into a hepatic

vein. Using a special needle introduced through the lumen of the catheter, the catheter can be passed from a hepatic vein into a portal vein. Once this portosystemic connection has been established, it is kept open with a permanent stent (Fig. 17.19, and see Fig.17.8).

Interventional radiology of the gastrointestinal tract

Oesophageal, duodenal or colonic stent placement and percutaneous gastrostomy may be performed endoscopically, radiologically or as a combined procedure (Fig. 17.20). Expanding metal stents are usually placed across malignant strictures but newer, removable, covered stents are increasingly used in the treatment of benign strictures.



(a)



(b)

Fig. 17.20 (a) A single-contrast, water-soluble enema, demonstrating a stricture in the distal sigmoid colon (arrow). (b) The stricture has been crossed using endoscopic and fluoroscopic guidance, and stented (arrowheads). This allows decompression of the bowel, allowing the patient to undergo elective rather than emergency surgery.

Radiologically inserted gastrostomy (RIG, as opposed to PEG (percutaneous endoscopic gastrostomy)) is carried out to avoid long-term nasogastric or parenteral feeding. The stomach is distended by gas delivered through a nasogastric tube to make it an easier target. Under fluoroscopy, the anterior abdominal wall is punctured and a special gastrostomy tube introduced, which is then anchored in the stomach.

Interventional radiology of the urinary tract

Internal drainage of an obstructed urinary system is undertaken by the insertion of double-J stents with the proximal end placed into the pelvicalyceal system and the distal end in the bladder, thus bypassing the obstruction. These stents are usually placed via a cystoscopy, the catheters being passed into the ureteric orifice under direct vision. Alternatively, the double-J stents for long-term internal drainage may be introduced percutaneously via the loin under ultrasound and fluoroscopic control.

Short-term drainage (24–48 hours) can be achieved by simply puncturing an obstructed kidney under ultrasound or fluoroscopic control, passing a guidewire through the needle, and exchanging the needle for a small catheter in order to establish temporary external drainage. This procedure, known as percutaneous nephrostomy, is used almost exclusively to establish drainage in such emergency situations as acute obstruction following extracorporeal shock-wave lithotripsy or to drain an acute pyonephrosis.

Interventional radiology of the biliary tract

The last decade has seen an explosion of techniques designed to drain an obstructed biliary system. The methods used can be broadly divided into those in which the drainage tube is introduced endoscopically, which is the common approach, and those in which it is introduced percutaneously, usually when the endoscopic route has failed.

The two most common causes of bile duct obstruction are tumours, notably carcinoma of the pancreas or cholangiocarcinoma, and stones in the common bile duct. If the obstruction is due to stones, then endoscopic removal of the stones and sphincterotomy of the papilla of Vater is a frequently chosen procedure (Fig. 17.21).

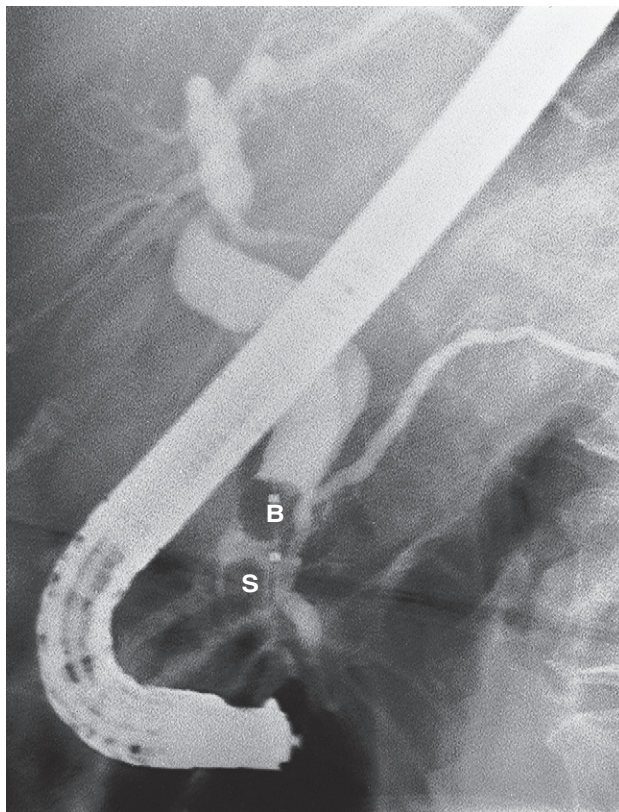
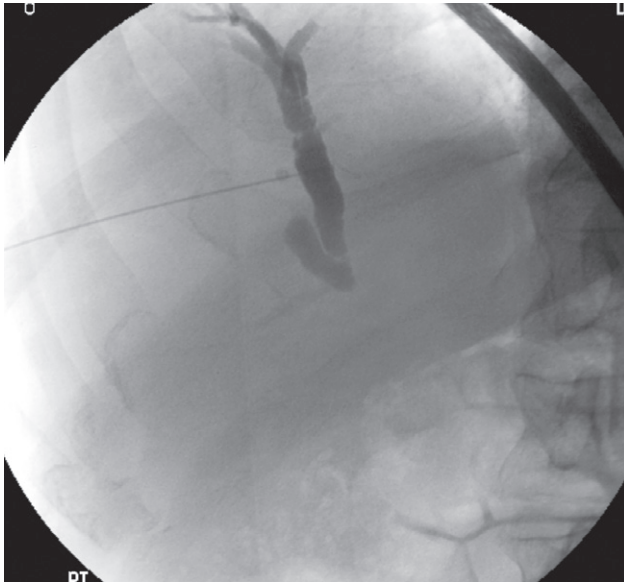
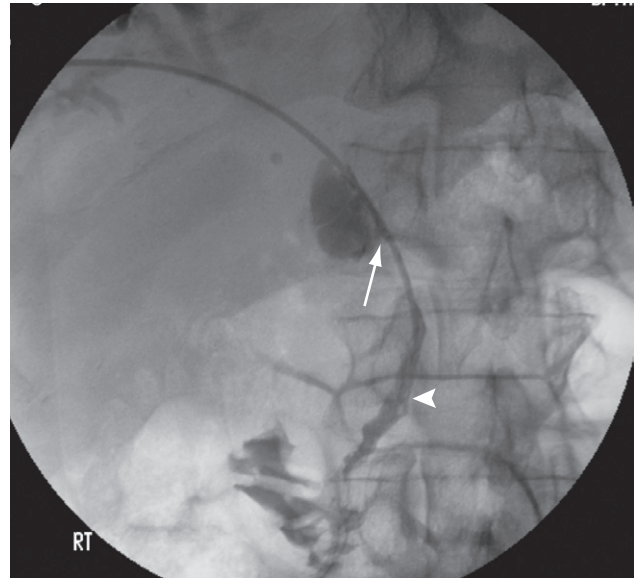


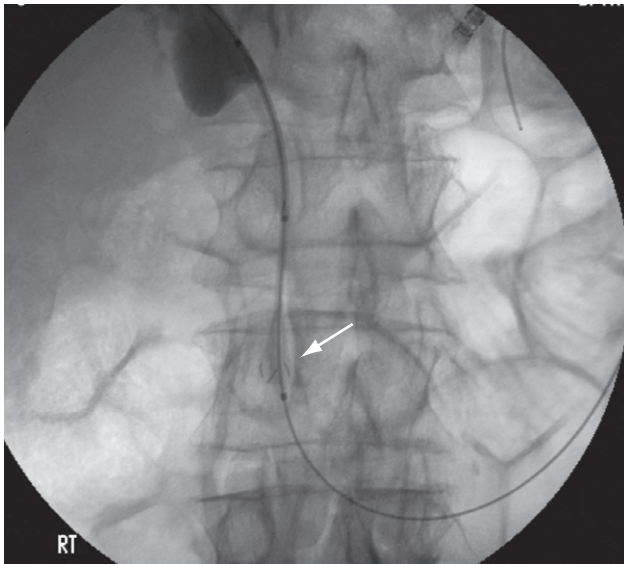
Fig. 17.21 Endoscopic removal of stones in the common bile duct (CBD). A balloon catheter has been passed into the CBD after endoscopic intubation of the papilla of Vater. The stones were then pulled out of the CBD. B, balloon; S, stone.



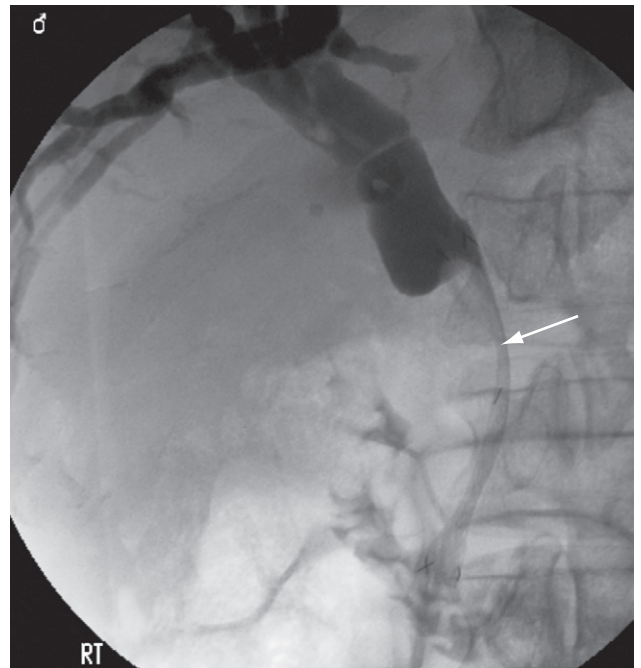
(a)



(b)



(c)



(d)

Fig. 17.22 Percutaneous insertion of a stent to bypass an obstruction in the common bile duct (CBD). (a) A biliary duct has been punctured in the liver and contrast injected to delineate the biliary tree. (b) A guidewire is inserted through the needle over which a catheter is passed to cross the stricture (arrow) and thence through the ampulla into the bowel. Note the decompressed CBD distal to the stricture (arrowhead). (c) A self-expanding metal stent is then inserted over the guidewire (arrow) and deployed across the stricture. Note the radio-opaque marker delineating the distal end of the stent. (d) Completion cholangiogram demonstrating free flow of bile through the stent (arrow) into the duodenum.

Many patients who present with malignant bile duct obstruction cannot be offered a surgical cure. Non-operative stenting and drainage procedures for patients in whom curative surgery is impossible have, therefore, become far more frequent in recent years. Patients may live for a considerable time with biliary stents in place, particularly if the responsible tumour is slow growing, as is the case with many cholangiocarcinomas. Usually the stent is introduced at endoscopic retrograde cholangiopancreatography

(ERCP) by cannulation of the papilla of Vater. The stent is passed retrogradely up the common bile duct through the tumour so that bile from the obstructed biliary tree drains into the duodenum. If this approach is not successful, the stent can be placed over a guidewire that has been introduced percutaneously through the liver into a dilated bile duct. The guidewire can be manipulated through the tumour into the duodenum via the common bile duct and the stent can then be passed over the guidewire (Fig. 17.22).

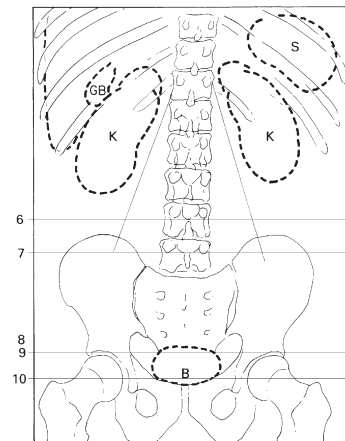
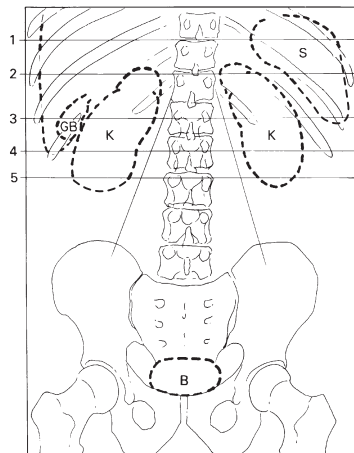
Appendix

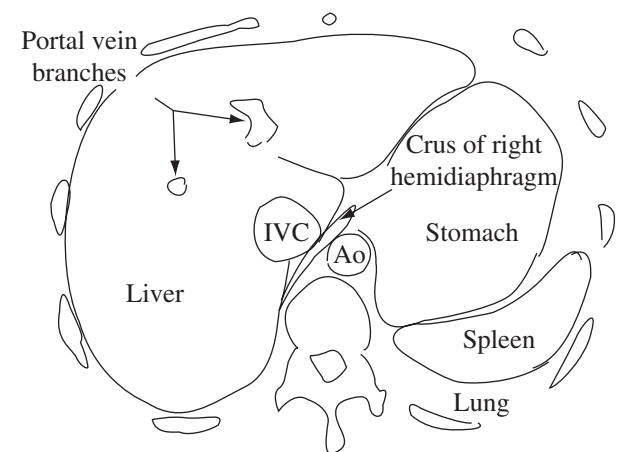
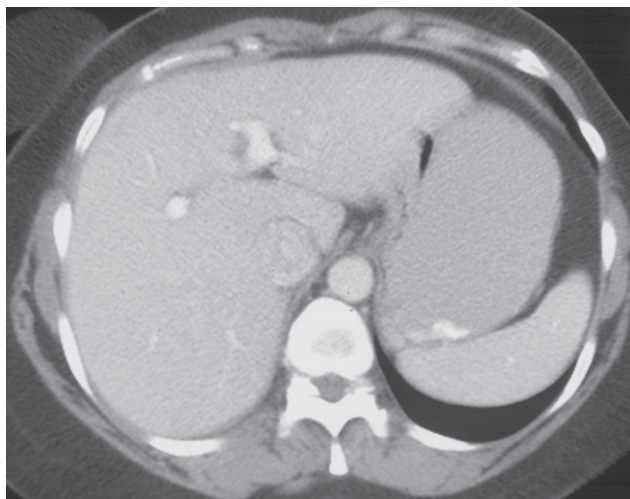
Computed Tomography Anatomy of the Abdomen

The normal appearances of the abdomen and pelvis of an adult female are shown in this appendix. The levels of the sections chosen are illustrated in the two diagrams. Each section is 5 mm thick. Gastrografin was given orally twice: 15 minutes and 1.5 hours beforehand. Intravenous contrast was injected during the examination.

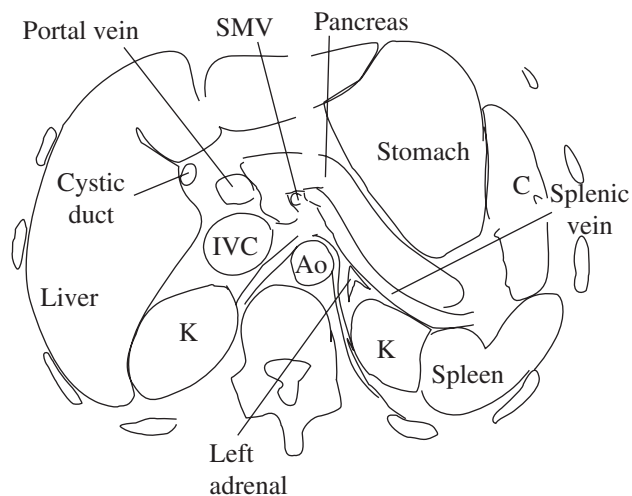
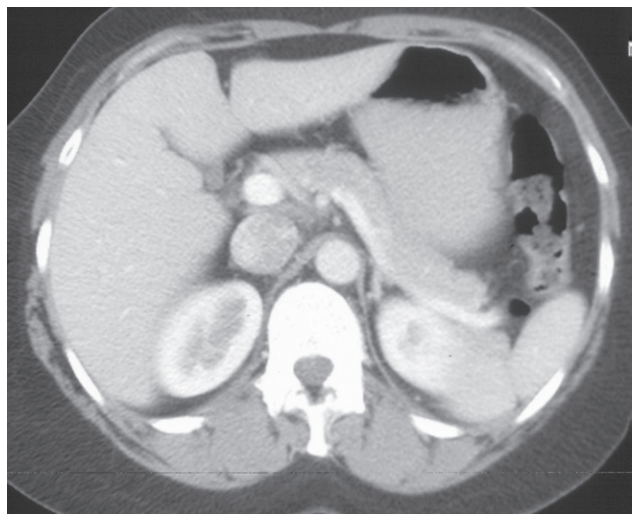
Ao	Aorta
B	Bladder
C	Colon
Duo	Duodenum

Duo III	Third part of duodenum
GB	Gall bladder
IVC	Inferior vena cava
K	Kidney
Ps	Psoas muscle
SB	Small bowel
SMA	Superior mesenteric artery
SMV	Superior mesenteric vein
S	Spleen
U	Uterus

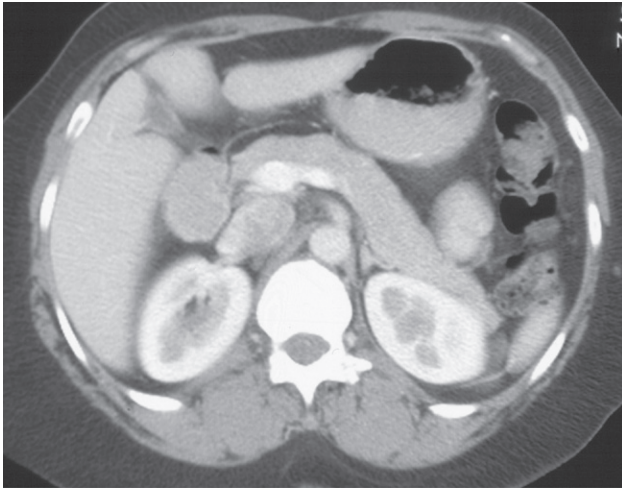




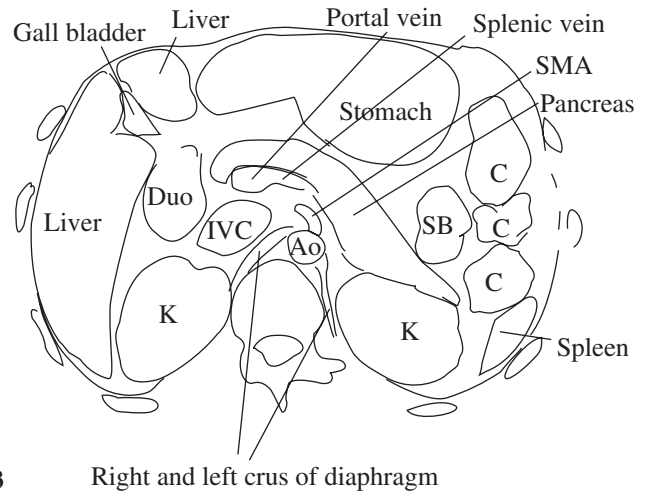
1



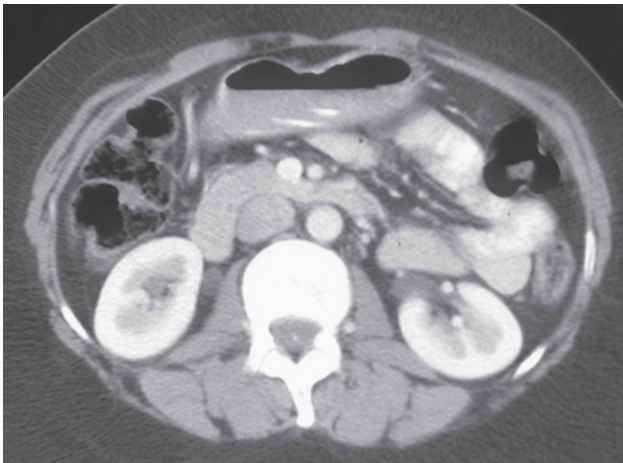
2



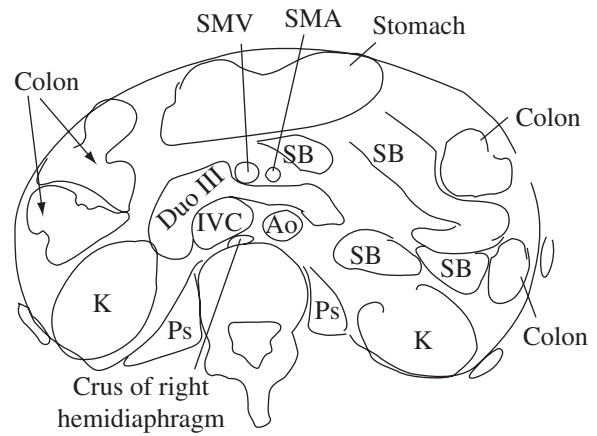
3

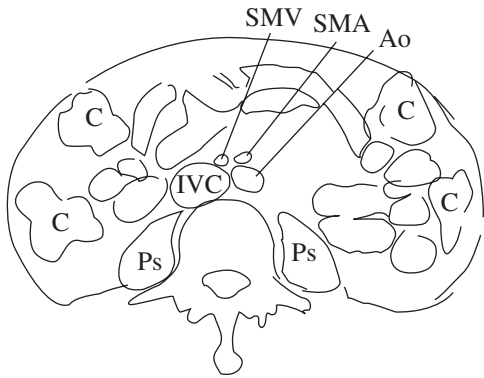
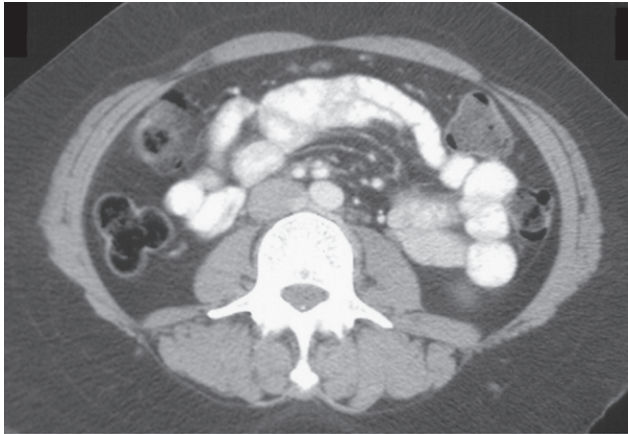
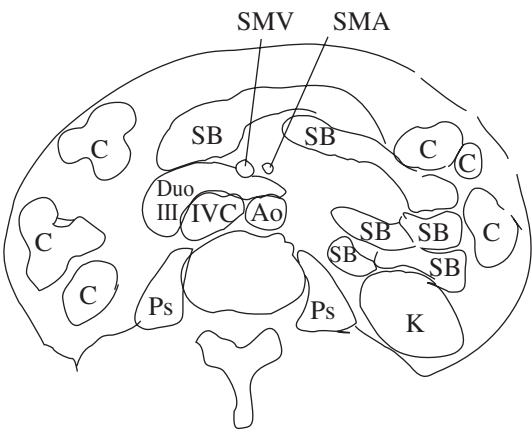
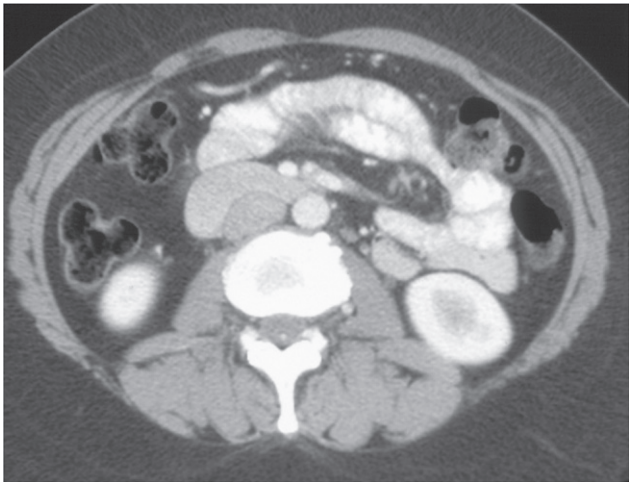


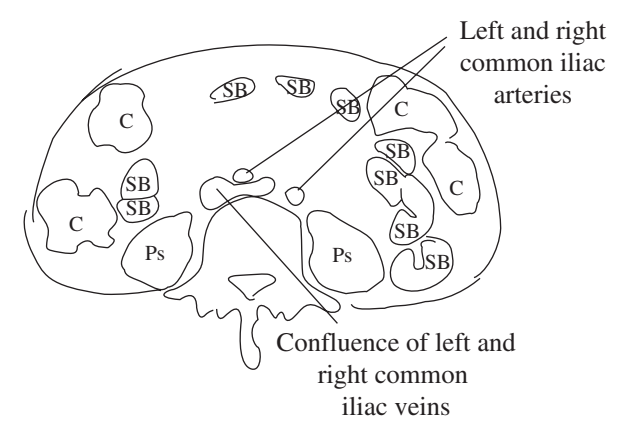
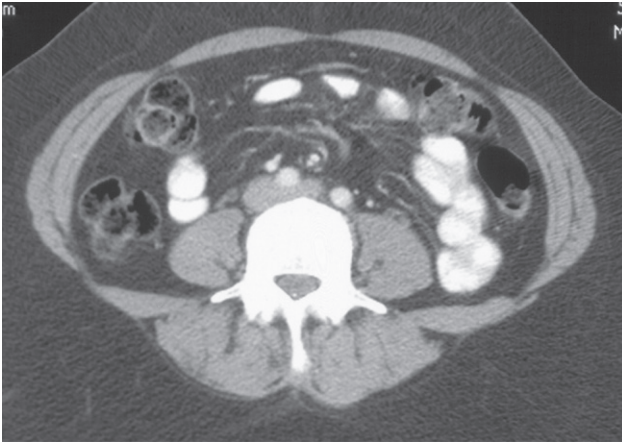
Right and left crus of diaphragm



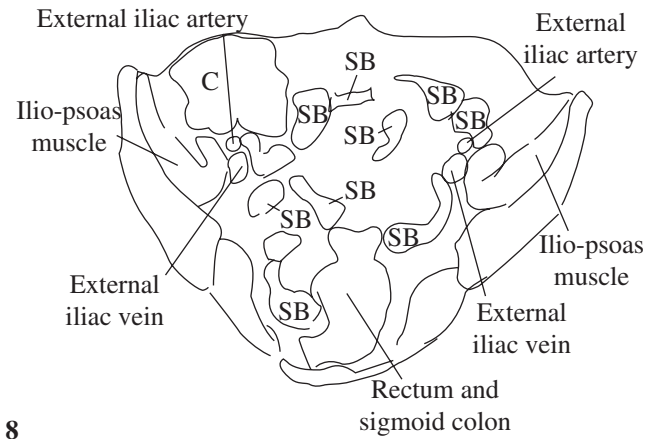
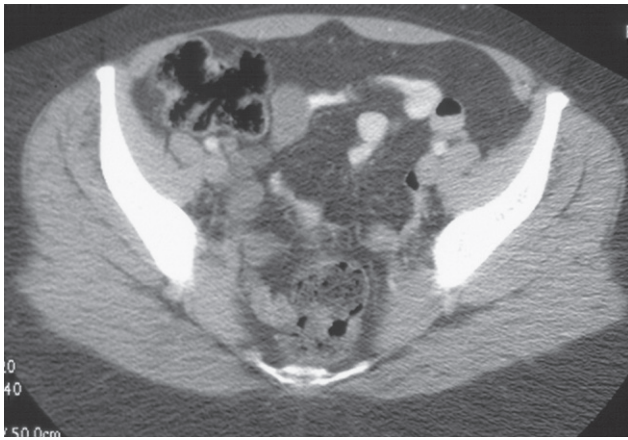
4



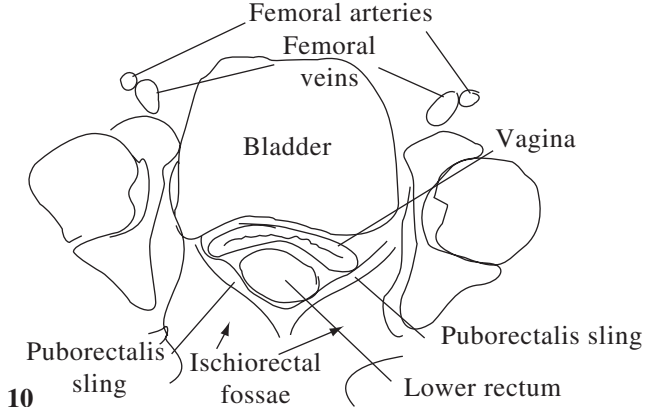
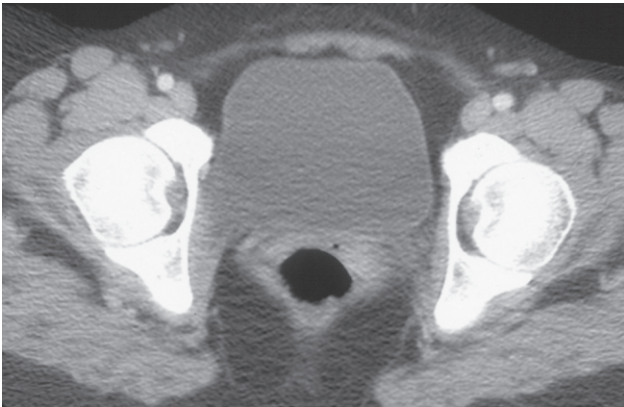
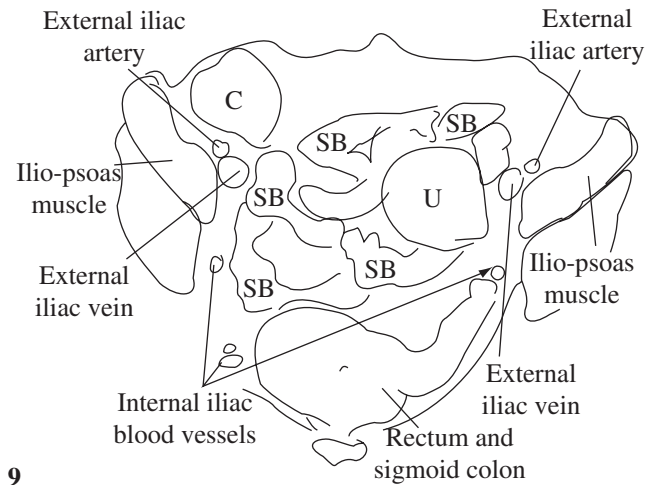
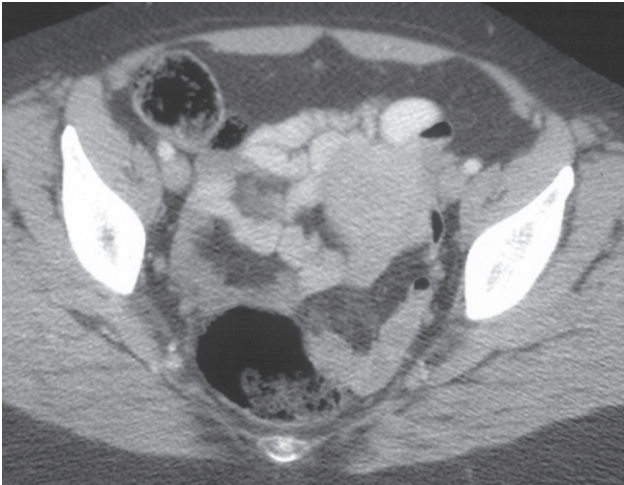




7



8



Index

Note: page numbers in *italics* refer to figures; those in **bold** to tables.

- abdomen
 - acute 189–92
 - calcification 136–8, 137–9
 - CT anatomy 491–6
 - masses 139, 139
 - trauma 194, 206–7, 207
 - see also* peritoneal cavity
- abdominal aortic aneurysms 304–7, 306, 475
 - calcification 136, 137
 - endovascular repair (EVAR) 475, 477
 - leaking 306, 307
- abdominal films, plain 129–39, 130
 - abdominal and pelvic masses 139, 139
 - abdominal calcification 136–8, 137–9
 - acute abdomen 190
 - ascites 136, 136
 - intestinal gas pattern 129–36, 131–5
 - liver and spleen 138–9
 - trauma 194
- ablation, therapeutic 478–9
- abscesses
 - adrenal 303
 - appendix 180, 181
 - brain 447, 447
 - Brodie's 327, 327
 - diverticular disease 180
 - intraperitoneal 132, 293–6, 295–6
 - liver 205, 206
 - lung 31, 33, 34, 72–3
 - pancreas 218
 - paravertebral 388–9
 - pelvic 132, 282, 284, 294, 295–6, 296
 - percutaneous drainage 481, 484
 - perianal 189
 - psoas 307, 307
 - renal and perinephric 255, 255–6
 - retroperitoneal 307
 - subphrenic 50, 132, 135, 294
- acetabular fractures 399, 400
- achalasia 148, 151
- Achilles tendon rupture 312
- acoustic enhancement 5
- acoustic neuroma 439–40, 441
- acoustic shadow 6, 6
- acromioclavicular dislocation 409
- acute abdomen 189–92
- acute tubular necrosis 261
- adenomatous polyps, large intestine 184–7, 186
- adenomyosis, uterine 281, 282
- adrenal glands 299–303
 - abscesses 303
 - adenomas 301, 301, 303, 303
 - calcification 138, 138, 299–301, 300
 - carcinoma 303, 304
 - enlargement 301
 - functioning tumours 301–2, 301–2
 - haemorrhage 303
 - metastases 303, 304
 - non-functioning masses 302–3
 - normal 299, 300
- adult respiratory distress syndrome (ARDS) 86–7, 87, 90
- ageing, brain 448, 451
- AIDS/HIV infection
 - opportunistic brain infections 447
 - Pneumocystis carinii* pneumonia 78, 78
 - tuberculous osteomyelitis 327
- air bronchogram 30, 31
- air-space opacification, intrapulmonary 30, 30–1
- air-trapping 49
- airway diseases 82–4
- ALARA principle 18
- albumin particles, ^{99m}Tc-labelled 9–10
- allergic bronchopulmonary aspergillosis 83
- Alzheimer's disease 450, 451
- amniocentesis 288
- amyloidosis, kidney enlargement 225
- anal fistula 189
- aneurysms
 - therapeutic embolization 478, 480, 482
 - see also* aortic aneurysms
- angiodysplasia, colonic 192
- angiomyolipomas, renal 246, 248, 249, 250
- angioplasty, percutaneous
 - transluminal 475–8, 476
 - subintimal 478, 478
- ankle injuries
 - fractures 417–18
 - oblique views 406
 - stress films 403, 407
- ankylosing spondylitis 389–91, 390
- antegrade pyelography 237
- anterior communicating artery aneurysm 482
- anterior longitudinal ligament 375, 379
- antrochoanal polyp 457
- aorta
 - abdominal 297, 298, 474
 - dilatation of ascending 67
 - dissection 67–8
 - traumatic rupture 90–1
- aortic aneurysms
 - abdominal *see* abdominal aortic aneurysms
 - thoracic 67–8, 67–8
- aortic regurgitation 110, 116
- aortic stenosis 116
- apophyseal joints *see* facet joints
- appendiceal faecoliths (appendoliths) 138, 139, 180, 181
- appendicitis 180, 181
- appendix abscess 180, 181
- AP (anteroposterior) view 2
- arachnoiditis, inflammatory 385
- arteries
 - angioplasty and stenting 475–8, 476–8
 - therapeutic embolization 478, 479–82
 - ultrasound 473
- arteriography 471, 472, 473
- arteriovenous malformations
 - intracerebral 443, 445
 - therapeutic embolization 478, 481
- arthritis 348–54
 - neuropathic 350
 - psoriatic 349, 352, 352
 - pyogenic 356, 356
 - seronegative arthropathies 389–91

- arthritis (*cont.*)
 tuberculous 356, 357
see also osteoarthritis; rheumatoid arthritis
- arthritis mutilans 350, 351
- arthrography 347
- articular erosions 349, 349
- asbestosis 49, 79
- asbestos-related disease 82
 pleura 52, 55, 56, 57, 82, 83
- Ascaris* infestation 170, 170
- ascites 291, 292
 plain films 136, 136
 pleural effusion 51
- aspergillosis, allergic
 bronchopulmonary 83
- Aspergillus fumigatus* 75, 76–7, 83
- asthma 26, 82–3
- astrocytoma 436, 438
- atelectasis *see* pulmonary collapse
- atlantoaxial subluxation, rheumatoid arthritis 350–1, 352, 381
- atlantodens interval 377–80
- atrial septal defects 103–6, 111
- avascular necrosis (osteonecrosis) 356–9, 357
 causes 357
 post-traumatic 358, 358
 radiation-induced 341–6
- avulsion fractures 426, 426
- azygos lobe fissure 21, 22
- back surgery, postoperative
 fibrosis 384–5, 387
- bamboo spine 390, 391
- barium 3, 141
- barium enema 171–2, 172
- barium follow-through 161–2, 162
 acute abdomen 191
- barium meal 153, 154, 154
- barium swallow 143–6, 145–6
- battered baby syndrome *see* non-accidental injury
- Bennet's fracture 412
- bezoar 157, 158
- biliary system 208–13
 dilatation 212, 214
 gas in 135, 135–6
 imaging techniques 208–9, 208–11
 interventional radiology 486–9, 487–8
 obstruction 209, 210–11, 212–13
- biopsy
 needle *see* needle biopsy
 transjugular liver 481–5
see also fine needle aspiration
- bladder (urinary)
 calcification 264
 CT urography 232, 232
 disorders 263–6
 diverticula 264, 266
 intravenous urography 227, 228
 magnetic resonance imaging 234
 neurogenic 264–6, 267
 outflow obstruction 268–9, 270
 stones 239, 240, 264
- trauma 266, 267
- tuberculosis 256–7
- tumours 244, 263–4, 265
- ultrasound 224, 225
- wall, trabeculation 264–6, 267
- blastomycosis 76, 77
- bleeding/haemorrhage
 acute gastrointestinal 192, 193
- adrenal 303
- mediastinal widening 91
- therapeutic embolization 478, 479–82
see also haematoma; intracerebral haemorrhage
- blood–brain barrier (BBB) 427, 433
- Boerhaave's syndrome 68
- Bohler's angle 419
- bone 309–46
 altered trabecular pattern 309, 312, 340–6
 avascular necrosis *see* avascular necrosis
- bruise 401, 402
- change in shape 309, 346
- classification of disease 314
- computed tomography 313–14, 315–16
- cortical thickening 309, 311
- cysts 321–3
 aneurysmal 323
 simple 321, 324
- density
 decreased 309, 334–9
 increased (sclerosis) 309, 339–40
 measurement 335–6
- dysplasias 345, 346
- expansion 318
- growth 310
- imaging techniques 309–14
- infarction 328, 328, 341
- infractures 424
- island 318
- magnetic resonance imaging 314, 316
- metastases 316, 318, 329–32, 329–33
 lytic 329, 329
 mixed lytic and sclerotic 329, 330
 sclerotic 329, 330, 339, 340
see also under spine
- multiple focal lesions 329–34
- plain radiographs 309–10, 310–12
- radiation-induced disease 341–6
- radiographic signs of disease 309–10, 311–12
- sequestrum 327, 327
- solitary lesions 314–28, 318–20
- trauma *see* skeletal trauma
- tumours 316, 320–5
 benign 321–5
 pathological fractures 421, 423
 primary malignant 320–1
 vs. osteomyelitis 327–8
 zone of transition 318
- bone age, altered 309–10
- bone marrow hyperplasia 341, 344
- bone scans, radionuclide 9, 10, 312–13, 313
 indications 314, 315
 metastases 329, 331
 skeletal trauma 401, 404
 spine 369
 stress fractures 420, 423
- bowel *see* intestine
- boxer's fracture 413
- brain 427–55
 abscess 447, 447
 ageing 448, 451
 arteriovenous malformations 443, 445
 atrophy 448, 451
 calcification 429
 computed tomography *see* head
 computed tomography
 contrecoup injury 452
 coup injury 452
 diffuse axonal injury 452–5
 haemorrhage *see* intracerebral haemorrhage
 haemorrhagic contusions 452, 454
 herniation 432, 432
 imaging techniques 427–36
 infarction 440, 441–3, 443–4
 infections 443–7, 446–8
 injury 450–5, 452–5
 magnetic resonance imaging 433–6, 434–7
 mass effect 431–2, 431–2
 metastases 431, 438–9, 439
 oedema 431, 431
 sonography 436, 437
 tumours 436–40, 438–42
- breast 123–8
 benign masses 123, 125, 126
 cancer 123–7, 124, 126–8
 bone metastases 329, 330, 332–3
 pathological fracture 423
 spinal metastases 377, 394
- implants 64
- magnetic resonance imaging 127, 127
- mammography 123, 124–5
- plain chest films 21–3
- screening 127–8, 128
- ultrasound 123–7, 126
- Brodie's abscess 327, 327
- bronchial carcinoid 41
- bronchial carcinoma 91–4
 asbestos-related 82
 cavitation 43, 43, 91, 92
 central tumours 91, 91, 94
 hilar enlargement 70, 91, 91
 peripheral tumours 91, 92–3
 PET 44, 45
 solitary pulmonary nodule 40–2, 41, 43, 43–4
 spread 91–4, 93–5
- bronchial obstruction
 pneumonia secondary to 72
 pulmonary collapse with 31–4
- bronchiectasis 84, 85
 normal chest films 26
 ring opacities 48, 50

- bronchiolitis 26, 83
- bronchitis
 - acute 26, 83
 - chronic 26, 83
- bronchogenic cyst 60, 64
- bronchopneumonia
 - bacterial 72, 72
 - tuberculous 73, 74
- brown tumours 338, 339
- bullae, emphysematous 46, 47, 83, 84
- bumper fractures 417
- calcaneal fractures 419, 422
- calcification
 - abdominal 136–8, 137–9
 - acoustic shadowing 5–6, 6
 - adrenal 138, 138, 299–301, 300
 - bladder 264
 - brain 429
 - heart valve 103, 116, 118
 - hyperparathyroidism 338, 339
 - liver 138
 - mediastinal 65, 67, 67
 - old tuberculous lesions 75, 75, 136, 137
 - ovarian masses 138, 279, 280
 - pancreas 138, 138, 218
 - pleural 56–7, 57
 - prostate 268, 270
 - pulmonary 40, 42, 48
 - renal masses 249, 249
 - spleen 138
 - urinary tract 226, 226, 256, 256
- calcific tendonitis, shoulder 362, 365
- calcium pyrophosphate dihydrate
 - crystal deposition disease 353, 354
- calices, renal *see* renal calices
- cancer
 - percutaneous needle biopsy 479, 483
 - radiation-induced 18
 - therapeutic ablation 478–9
 - therapeutic embolization 478
 - ureteric obstruction 245
 - vascular infusions 479
 - see also specific types*
- Candida albicans*, lung infections 76–7
- capsule endoscopy 160, 161
- carcinoid tumours
 - bronchial 41
 - metastatic small bowel 293, 294
 - see also* neuroendocrine tumours
- cardiac catheterization 112
- cardiac imaging 101–21
 - see also* heart; heart disease
- cardiomyopathies, primary 115
- cardiophrenic angle masses 65, 66, 66
- cardiothoracic ratio (CTR) 101, 103
- carotid artery stenosis 473, 473
- carpal bones
 - dislocation 413
 - fractures 412
 - see also* scaphoid
- cauda equina compression 391
- cavitation, pulmonary
 - bronchial carcinoma 43, 43, 91, 92
 - within consolidated areas 31, 33, 34
 - within masses 42–3, 43
 - tuberculosis 73–5, 74
- cerebral *see* brain
- cervical lymphadenopathy 463, 463–4
- cervical spine
 - degenerative disease (spondylosis) 382, 385
 - injuries 375–81, 380–3
 - flexion and extension views 404, 407
 - flexion teardrop 380, 382
 - hyperflexion 380–1, 383
 - nerve roots 370
 - normal plain films 378, 379
- cervix
 - carcinoma 281–2, 283
 - imaging techniques 274
- chemoembolization, transarterial 479
- chest 19–99
 - abnormal signs 28–49
 - computed tomography (CT) 23, 23–4
 - indications 24, 25
 - maximum intensity projections (MIPs) 24, 25
 - mediastinum 23, 59–60, 61–2
 - normal 24
 - signs of lung disease 30–49
 - diseases *see* thoracic diseases
 - extrapleural mass 28, 28
 - magnetic resonance imaging 24
 - metastatic neoplasms 94–9
 - positron emission tomography (PET) 24, 27
 - radionuclide scanning 24, 26
 - trauma 88–91, 90
 - ultrasound 24–6
- chest radiography, plain (CXR) 19–23
 - acute abdomen 190
 - assessing technical quality 23
 - bronchial carcinoma 91, 91–2
 - cardiac disorders 101–7, 102–7
 - chest diseases with normal 26–7
 - effects of expiration 19, 21
 - interpretation 19–23
 - lateral view 19, 20
 - mediastinal masses 60, 60–7, 64–6
 - oesophagus 143, 144
 - pleural effusion 50–1, 51–2, 53–4
 - pneumoperitoneum 132, 134
 - posteroanterior (PA) view 19, 20
 - pulmonary embolism 87–8
 - pulmonary vasculature 103–7, 105–6
 - signs of lung disease 30–49
 - silhouette sign 28–30, 29
- chest wall 71, 71
 - invasion, bronchial carcinoma 94, 95
 - localizing lesions to 28, 28
 - pulmonary masses involving 40, 43
 - surgical emphysema 90
- Chiari I malformation 391–7, 396
- child abuse *see* non-accidental injury
- cholangiocarcinoma 200, 210
- cholecystitis 212, 213
- chondrocalcinosis 353, 354
- chondrosarcoma 318, 321, 322, 346
- chorionic villus sampling 288
- Christmas disease 354
- chronic obstructive pulmonary disease 83–4
- cirrhosis of liver 205–6
- clavicles
 - fracture 409
 - plain chest films 23
- closed loop obstruction (of bowel) 133, 134
- coal workers' pneumoconiosis 79, 82
- cobblestone appearance, Crohn's disease 178, 178
- coccidioidomycosis 76
- Codman's triangle 309, 311
- collagen vascular diseases
 - diffuse pulmonary fibrosis 79
 - pleural effusion 51
 - thoracic imaging 81–2
- Colles' fracture 405, 411
- colon
 - acute bleeding 192
 - angiodysplasia 192
 - dilatation 173–4
 - idiopathic (functional) 189
 - toxic 133, 134, 175–8, 177
 - diverticula 174, 175
 - filling defects 174, 174
 - imaging techniques 170–1
 - muscle hypertrophy 174, 175
 - narrowing of lumen 172–3, 173
 - normal appearance 171–2, 172
 - plain films 129, 131
 - pseudopolyps 175
 - skip lesions 178, 179
 - strictures 172–3
 - Crohn's disease 178, 179
 - diverticular disease 173, 180, 180
 - ischaemic colitis 182, 182
 - malignant 172, 173, 187
 - ulceration 172, 174
 - Crohn's disease 178, 178–9
 - ulcerative colitis 175, 176
 - see also* large intestine
- colonoscopy 170–1
 - lower GI bleeding 192
 - virtual 171
- colorectal carcinoma 187–8, 187–9
 - staging 188, 189
 - strictures 172, 173, 187, 187
 - ulcerative colitis 175
- colorectal polyps 184–7, 186
- colour Doppler 7, 9
- column of Bertin 232, 245
- common bile duct (CBD)
 - dilatation 212–13, 214
 - imaging 208, 208–9
 - interventional radiology 486–9, 487–8
 - stones 209, 213, 214
- computed tomography (CT) 2–3, 3, 4
 - abdominal anatomy 491–6
 - abdominal trauma 194

- computed tomography (CT) (*cont.*)
 acute abdomen 191–2
 artefacts 3
 bone disease 313–14, 315–16
 brain *see* head computed tomography
 cardiac 112, 114, 115
 chest *see* chest, computed tomography
 contrast agents 3–4
 dual source (dual energy) 2
 female genital tract 273–4, 276
 gastrointestinal tract 142
 high resolution *see* high resolution
 computed tomography
 liver 197–9, 198–9
 multidetector (multislice) 2
 neck 463
 oesophagus 146, 147, 148–9
 pancreas 213, 214–16, 215
 PET combined with 12, 12
 planes 2, 4
 pneumocolon 171
 radiation hazards 17–18
 renal parenchymal masses 249–51,
 250–2
 retroperitoneum 297, 297
 skeletal trauma 399, 400–1
 small intestine 161, 163, 163
 stomach and duodenum 153–4, 155
 three-dimensional 2, 5
 vs. magnetic resonance imaging 13
 window levels (centres) 2, 3, 23
 window width 2, 3, 5
 computed tomography (CT)
 angiography 3, 471–3, 475
 acute lower GI bleeding 192, 193
 brain 427, 429, 431
 pulmonary 88, 89, 473
 computed tomography (CT)
 urography 224–5, 228–32
 indications 225
 non-contrast (KUB) 224, 229–30, 231–2
 post-contrast 230–2, 231–3
 technique 228–9
 urinary tract obstruction 243, 244
 congenital aganglionosis 188–9, 189
 congenital heart disease 121
 Conn's tumour 301
 contrast agents
 magnetic 16–17
 radiographic 3–4
 safety 4, 17
 ultrasound 7
 urinary excretion 225
 contrast studies, gastrointestinal 141
 conus medullaris 370
 cordocentesis 288
 coronary angiography
 computed tomography (CT) 112, 114,
 115
 conventional 112, 114–15, 116
 coronary artery calcium score 112
 coronary artery disease 114–15, 115–16
 see also ischaemic heart disease
- Crohn's disease
 large intestine 178, 178–9
 small intestine 164–6, 165–7
 cruciate ligament injuries 359, 362
 cryptogenic fibrosing alveolitis *see* usual
 interstitial pneumonia
 Cushing's syndrome 301, 301
 cysticercosis, brain 447, 448
 cystic fibrosis 84, 86
 cystogram, micturating 237
 cystourethrogram, voiding 237
 cysts
 bone 321–3, 324, 349
 bronchogenic 60, 64
 dermoid *see* dermoid cysts
 hydatid 77
 kidney *see* renal cysts
 liver 195, 197, 200–3, 203
 mediastinal 67
 ovarian 275–7, 277
 subchondral 349, 354, 355
 ultrasound imaging 5
- dementia 450, 451
 dense artery sign 443, 443
 dermatomyositis 82
 dermoid cysts
 mediastinal 65, 66
 ovarian 138, 139, 279, 280
 developmental dysplasia of hip 363, 367
 diabetic foot 363, 365
 diabetic nephropathy 260, 261
 diaphragm 70–1
 eventration 71, 71
 plain chest films 19, 20
 traumatic rupture 90, 90
 unilateral elevation 70–1
 diaphyseal aclasia 345, 346
 diaphysis 310
 diethylene triamine pentacetic acid
 (DTPA) scan 233–7, 236
 diffuse axonal injury 452–5
 diffusion tensor imaging
 (tractography) 433, 436
 diffusion-weighted imaging (DWI) 13,
 15
 brain 432–3, 435
 digital images 17
 digital subtraction arteriography 471,
 472
 dimercaptosuccinic acid (DMSA)
 scan 233
 discitis 388, 388–9
 dislocations, radiographic signs 403
 diuretic renogram 245, 246
 diverticular disease 173, 178–80, 180
 diverticulitis 179
 DMSA (dimercaptosuccinic acid)
 scan 233
 Doppler angle 7, 8
 Doppler echocardiography 109, 110–11
 Doppler ultrasound 7–8, 8, 9
 vascular disease 473–4
- double contour sign, left atrial
 enlargement 104
 double-contrast technique 141
 DTPA (diethylene triamine pentacetic
 acid) scan 233–7, 236
 dual-energy x-ray absorption
 (DEXA) 335–6
 duodenum 153–9
 contrast studies 153, 154, 154
 diverticula 153, 154
 neuroendocrine tumours 157, 157
 dysphagia 146
- Echinococcus granulosus* 77
 echocardiography 107–9, 108–9
 Doppler 109, 110–11
 stress 113
 transoesophageal 109
 ectopic pregnancy 288–9, 288–9
 elbow
 dislocation 410
 fractures 405, 406, 411
 embolization, therapeutic 478, 479–82
 emphysema 83, 84, 88
 bullae 46, 47, 83, 84
 compensatory 49
 plain chest films 26
 surgical, chest wall 90
 empyema, pleural 49–50, 53–5
 encephalitis 443, 446
 enchondromas 321, 323
 endocarditis, subacute bacterial 120, 121
 endometrial carcinoma 281, 282, 284
 endometriosis 282, 284–5
 endoscopic retrograde
 cholangiopancreatography
 (ERCP) 209, 210, 215, 221,
 489
 endoscopic ultrasound (EUS) 142
 oesophageal carcinoma 147, 147
 pancreas 213–14, 215
 endoscopy 141
 acute GI bleeding 192
 capsule 160, 161
 upper GI 154, 155
 endovascular aneurysm repair
 (EVAR) 475, 477
 enteroclysis 161, 163
 enteroscopy 160
 eosinophilic granuloma 323–5
 vertebral collapse 373, 375
 ependymoma 391, 396
 epicondylar fractures 411
 epiphyseal injuries 407, 408, 412
 non-accidental 426
 epiphyseal plate (growth plate) 310
 injuries 407, 408
 epiphysis 310
 erosive arthropathies 350–2
 Ewing's sarcoma 311, 321
 exophthalmos 459, 460, 460
 extracerebral haematoma 452, 452
 extradural haematoma 452, 452, 454

- facet joints 369, 370–1
 - arthropathy 382
 - dislocation 380, 380
- faeces, colonic filling defects 174, 174
- faecoliths 138, 139, 180, 181
- fallopian tubes 273, 282–5, 286
- familial adenomatous polyposis 187
- FAST scan (focused assessment with sonography for trauma) 206–7
- fat embolism 90
- fat pads, cardiophrenic angle 65, 66, 66
- fatty liver disease 207, 207–8
- FDG-PET *see* fluorodeoxyglucose positron emission tomography
- female genital tract 273–89
 - gynaecological pathology 274–82
 - normal appearances 273–4
 - obstetric ultrasound 285–8
- femoral epiphysis, slipped 363, 366
- femoral head, avascular necrosis 357–8, 358
- femoral neck fractures 415
- fetus
 - death 288
 - karyotyping 288
 - radiation hazards 18
 - small for dates 288
 - ultrasound evaluation 286, 286–7
- fibrolamellar carcinoma, liver 200
- fibrosarcoma 321
- fibrosing alveolitis, cryptogenic *see* usual interstitial pneumonia
- fibrous cortical defects 321
- fibrous dysplasia 318, 321
- fifth metatarsal base fracture 420
- fine needle aspiration (FNA) 479, 483
 - neck masses 461, 463
- finger injuries 414
- fistulae, Crohn's disease 166, 166–7, 178, 179
- Fleishner guidelines 44
- fluid collections, percutaneous drainage 481, 484
- fluorodeoxyglucose positron emission tomography (FDG-PET) 11, 12, 12
 - bone disease 313, 313
 - oesophagus 146, 147–8, 150
- thoracic disease 24, 27
- fluoroscopy 141
- focal nodular hyperplasia 205, 205
- focused assessment with sonography for trauma (FAST scan) 206–7
- foreign bodies
 - inhaled 49, 50
 - oesophagus 143, 144
- fractures
 - avascular necrosis after 358, 358
 - avulsion 426, 426
 - greenstick 403, 405
 - insufficiency 404, 420
 - multiple, non-accidental injury 421, 425
 - pathological 421, 423–4
 - plain radiographs 399, 400
 - radiographic signs 403, 404, 405–6
 - Salter–Harris classification 407, 408
 - specific examples 409–21
 - stress 420, 421–3
 - types 399
- Freiberg's disease 358
- functional magnetic resonance imaging 433
- fungal lung diseases 76–7, 77
- gadolinium-based contrast agents 14, 16–17, 433
- gall bladder
 - imaging techniques 208, 208–9
 - polyps 212, 212
 - wall thickening 208, 212, 213
- gall stones 208, 210–12, 211–12
 - acoustic shadowing 5–6, 6, 211–12, 212
- gamma camera 10–11
- gamma-rays 8
- ganglioneuroma, retroperitoneal 305
- gas
 - in abdominal/pelvic abscess 132, 135, 294
 - in biliary system 135, 135–6
 - in bowel wall 132–5, 135
 - intestinal patterns 129–32, 130–4
 - in peritoneal cavity 132–6, 134–5
- gastric *see* stomach
- gastrinoma 157, 157
- gastroenteritis 133
- Gastrografin studies 141, 191
- gastrointestinal stromal tumours (GISTs) 157, 157
- gastrointestinal (GI) tract 141–94
 - basic descriptive terms 142–3, 142–3
 - bleeding, acute 192, 193
 - contrast examinations 141
 - filling defects 142, 142–3
 - gas pattern 129–32, 130–4
 - imaging principles 141–3
 - interventional radiology 485–6, 486
 - mucosal pattern 142
 - perforation 132, 134, 190, 293–4
 - strictures 143, 143
 - ulceration 142, 142
 - see also* duodenum; intestine; large intestine; small intestine; stomach
- gastrostomy, radiologically inserted (RIG) 486
- giant cell tumour 321, 323
- gibbus 388, 388
- glioblastoma multiforme 436, 438
- gliomas 436–8, 438
- glomerulonephritis
 - acute 225
 - chronic 260, 261
- goitre 463, 465
 - intrathoracic 60, 64, 66
- gout 349, 352–3, 353
- greater tuberosity fracture 410
- greenstick fractures 403, 405
- gynaecological pathology 274–82
- haemangiomas
 - liver 203, 204
 - vertebral 375, 378
- haemarthrosis, knee 416
- haematoma
 - extracerebral 452, 452
 - intracerebral *see* intracerebral haemorrhage
 - muscle 317
 - retroperitoneal 307, 307
- haemolytic anaemia 341, 344
- haemophilia 354, 355
- haemopneumothorax 58–9
- haemorrhage *see* bleeding/haemorrhage
- hallux rigidus 355
- hangman's fracture 380, 383
- haustra, colonic 131
- head 457–61
- head computed tomography (CT) 427–32
 - acute head injury 450–5, 452–5
 - angiography 427, 429
 - contrast enhancement 427, 429
 - imaging planes 427, 428
 - normal images 427–9, 430–1
 - signs of abnormality 429–32, 431–3
 - sinuses 457–8, 458–9
- head injury 450–5, 452–5
- heart 101–21
 - angiography 112
 - imaging techniques 101–12
 - plain chest films 19, 20, 101–7, 102–7
 - size and shape 101–3, 103–4
 - tumours 120, 121
- heart disease 101–21
 - congenital 121
 - hypertensive and myocardial 115–16, 117
 - ischaemic *see* ischaemic heart disease
 - valvular 103, 116–19, 118
- heart failure 51, 112–13, 113
 - pulmonary oedema 107
- hemivertebrae 391, 392
- hepatobiliary radionuclide scanning 209, 211
- hepatobiliary system 195–213
- hepatocellular carcinoma (hepatoma) 200, 203
- herpes simplex encephalitis 443
- hiatus hernia 65, 65, 158–9, 159–60
- high resolution computed tomography (HRCT) 24
 - bronchiectasis 84, 85
 - diffuse pulmonary opacification 48, 48, 49
 - usual interstitial pneumonia 79, 80
- hila, pulmonary 19–21, 68
- hilar enlargement 68–70, 69–70
 - bronchial carcinoma 70, 91, 91

- hilar lymphadenopathy 70
 - bronchial carcinoma 69, 70, 93
 - sarcoidosis 70, 70, 78
 - tuberculosis 70, 73
 - hip
 - developmental dysplasia 363, 367
 - fractures 415
 - slipped femoral epiphysis 363, 366
 - Hirschsprung's disease 188–9, 189
 - histoplasmosis 76, 77
 - HIV infection *see* AIDS/HIV infection
 - honeycomb lung 79, 80
 - horseshoe kidney 262, 263
 - Hounsfield units 2, 4
 - humeral neck fracture 409
 - hyaline membrane disease 86, 86
 - hydatid disease (cysts)
 - liver 203, 203
 - pulmonary 77
 - spleen 221, 221
 - hydrocele 271
 - hydrocephalus, obstructive 432, 433
 - hydronephrosis 225, 240
 - hydropneumothorax 58, 58–9
 - hyperparathyroidism 337–8, 339, 465
 - hypertension
 - heart disease 115–16
 - renal disease 259–60
 - hypertrophic obstructive cardiomyopathy (HOCM) 115, 117
 - hypertrophic pulmonary
 - osteodystrophy 334, 334
 - hysterosalpingography 282–5, 286
 - imaging investigations, requesting 1
 - iminodiacetic acid (IDA) scans 209, 211
 - immunocompromised host
 - fungal lung infections 76–7
 - pneumonia 77–8, 78
 - see also* AIDS/HIV infection
 - indirect voiding cystography 233, 235
 - infections
 - bone *see* osteomyelitis
 - intracranial 443–7, 446–8
 - joint 354–6
 - lung 72–8
 - spine 385–9, 388–9
 - see also* abscesses; *specific diseases*
 - infective endocarditis 120, 121
 - inferior vena cava (IVC) 297, 298
 - filters 479, 483
 - inflammatory bowel disease 174–8, 176–9
 - see also* Crohn's disease; ulcerative colitis
 - inflammatory polyps, large intestine 187
 - inflammatory
 - spondylarthropathy 389–91
 - insulinoma 217, 218
 - interventional radiology 475–89
 - intervertebral disc
 - degeneration 381–2, 385
 - herniation 382–5, 386–7
 - infections (discitis) 388–9, 389
 - magnetic resonance imaging 369–70, 372
 - spaces, narrowing 370–3, 373
 - intestine
 - closed loop obstruction 133, 134
 - dilatation 129–32, 131–4, 133
 - gas pattern 129–32, 130–4
 - intramural gas 132–5, 135
 - obstruction 129–32, 131–2, 133, 190
 - transit time 171
 - see also* large intestine; small intestine
 - intracerebral haemorrhage 443, 445
 - magnetic resonance imaging 436, 437
 - neurosonography 436, 437
 - traumatic 452, 454
 - intracranial aneurysms, therapeutic
 - embolization 478, 482
 - intrauterine contraceptive devices (IUCDs) 282, 285
 - intrauterine growth retardation 288
 - intravenous urography (IVU) 224–8
 - contrast medium 225
 - indications 225
 - plain film 226, 226
 - post-contrast films 226–7, 226–8, 229–30
 - renal parenchymal masses 247–9, 249
 - urinary tract obstruction 230, 242, 243
 - see also* computed tomography (CT) urography
 - intussusception 183–4, 184–5
 - involucrum 325, 327
 - iodine-123 (¹²³I) imaging 465
 - iodine-131 (¹³¹I) imaging 465, 466
 - iodine-containing contrast agents 3–4
 - ischaemic colitis 180–2, 182
 - ischaemic heart disease 113–15, 113–16
 - myocardial perfusion scintigraphy 109, 111, 113–14
 - see also* coronary artery disease
 - jaundice 212–13
 - JC virus 447
 - Jefferson's fracture 381, 383
 - joints 347–68
 - altered shape 349
 - effusions, traumatic 403
 - erosions 349, 349
 - imaging techniques 347–8, 348
 - infections 354–6
 - loose bodies 354
 - neuropathic 363, 365
 - space narrowing 348, 349, 354
 - see also* arthritis
 - juvenile polyps, large intestine 187
 - juvenile rheumatoid arthritis 352
 - karyotyping, fetal 288
 - Kerley B lines 44–6, 46, 96, 107, 107
 - kidneys
 - abscesses 255, 255–6
 - agenesis 263
 - compensatory hypertrophy 225
 - cystic disease, inherited 262–3, 264
 - ectopic 240, 262
 - enlarged 225
 - fetal lobulation 227, 228, 232
 - horseshoe 262, 263
 - infarction/scars 226–7, 228, 257
 - intravenous urography 226–7, 227–8
 - length, measurement 223, 227
 - magnetic resonance imaging 232, 234
 - small 224, 257, 260, 260–1, 261
 - splenic hump 227, 229
 - stones 238–40, 239
 - trauma 258–9, 259
 - ultrasound 223–4, 224
 - see also* entries beginning with renal
- Kienböck's disease 358
- knee
 - collateral ligaments 359
 - cruciate ligament injuries 359, 362
 - haemarthrosis 416
 - internal derangement 359
 - meniscal injuries 359, 361
 - traumatic injuries 401, 403, 416–17
- Kohler's disease 358
- Langerhans' histiocytosis 323–5, 375
- large intestine 170–90
 - dilatation 173–4
 - extrinsic compression 173
 - filling defects 174, 174
 - gas pattern 129, 130
 - imaging techniques 170–1
 - intramural gas 132–5, 135
 - narrowing of lumen 172–3, 173
 - obstruction 131, 132, 133, 134, 173
 - spasm 172
 - transit time 171
 - see also* colon
- larynx 463, 464
- left atrium
 - enlargement 103, 104
 - myxoma 120, 121
- left to right shunts, plain chest
 - films 103–6, 105
- left ventricular aneurysm 113
- leiomyomas
 - gastric 157
 - uterus (fibroids) 136–8, 137, 281, 281
- leukaemia, bone involvement 333
- ligaments 348
- ligamentum flavum 375, 379
- liposarcoma, retroperitoneal 304, 305
- Lisfranc's fracture 420
- liver 195–208
 - abscesses 205, 206
 - adenoma 205
 - benign masses 200–5
 - calcification 138
 - computed tomography 197–9, 198–9
 - cysts 195, 197, 200–3, 203
 - diffuse parenchymal diseases 197
 - fatty infiltration 207, 207–8

- focal nodular hyperplasia 205, 205
- haemangiomas 203, 204
- magnetic resonance imaging 199, 199
- malignant neoplasms 200, 201–3
- masses 195–7, 197–8, 199–205, 201–5
- metastases 197, 200, 201–2
- plain abdominal films 138–9
- segments 198, 198–9
- therapeutic embolization 480
- transjugular biopsy 481–5
- trauma 206–7, 207
- ultrasound 195–7, 196–8
- loose bodies, intra-articular 354
- Looser's zones 337, 338
- lumbar spine
 - disc herniation 382–5
 - injuries 381, 384
 - nerve roots 370
 - normal plain films 371
 - postoperative scarring 384–5, 387
- lung
 - abscess 31, 33, 34, 72–3
 - cavitated lesions *see* cavitation, pulmonary
 - chest CT 23, 24
 - contusion 90, 90
 - disease 71–82
 - with normal plain chest films 26–7
 - radiological signs 30–49
 - fissures 21, 22, 24
 - hamartoma 40, 42
 - increased transradiancy 21–3, 48–9, 50
 - infarction 51, 87–8
 - lobes 21, 22
 - lymphoma 98, 99
 - masses *see* pulmonary nodules
 - opacities *see* pulmonary opacities
 - parasitic diseases 76–7
 - plain chest films 21–3
 - small lesions 27
 - see also* entries beginning with *pulmonary*
- lung scanning, radionuclide 24, 26, 88, 88
 - perfusion scans 24, 26, 88
 - pulmonary embolism 88, 89
 - ventilation scans 24, 26, 88
- lymphadenopathy
 - cervical 463, 463–4
 - hilar *see* hilar lymphadenopathy
 - mediastinal *see* mediastinal lymphadenopathy
 - needle biopsy 483
 - retroperitoneal 297–9, 299
- lymphangitis carcinomatosa 49, 94, 96
- lymphoma
 - bone 316, 321, 333
 - gastric 158, 158
 - kidney 225
 - pulmonary 98, 99
 - retroperitoneal 299, 299
 - small intestine 168, 168
 - spine 375
 - spleen 221, 221
- MAG-3 (mercaptoacetyl triglycine) scan 233–7
- magnetic resonance angiography (MRA) 16, 17, 471, 473–4
 - brain 432, 435
 - kidney 232–3, 235
- magnetic resonance
 - cholangiopancreatography (MRCP) 209, 209
- magnetic resonance imaging (MRI) 12–17
 - bone metastases 329–32, 332
 - brain 433–6, 434–7
 - breast 127, 127
 - cardiac 15, 112, 113–14
 - chemical shift imaging 13
 - contrast agents 16–17
 - diffusion weighted imaging *see* diffusion-weighted imaging
 - dynamic contrast-enhanced (DCE-MRI) 13
 - fat suppression (STIR) sequence 13
 - female genital tract 274, 276
 - functional 433
 - gastrointestinal tract 142
 - HASTE sequence 13
 - joints 347
 - large intestine 171
 - liver 199, 199
 - machine 13, 15
 - mediastinal masses 66, 66
 - mediastinum 59–60, 63
 - musculoskeletal disease 314, 316–17
 - neck 463
 - renal parenchymal masses 249–51, 250, 252
 - retroperitoneum 297, 298
 - skeletal trauma 401, 402–3
 - small bowel 161
 - spine 369–70, 372
 - T1-weighted 13, 13, 14, 16
 - T2-weighted 13, 13, 14, 16, 17
 - thoracic disease 24
 - urinary tract 232–3, 234–5
- magnetic resonance spectroscopy 13
- malabsorption 168–9, 169
- malignant fibrous histiocytoma 321
- malrotation 170
- mammography 123, 124–5
 - screening 128, 128
- marble bone disease 340, 340
- march fracture 420, 421
- mastectomy, plain chest films after 23, 56
- maximum intensity projections (MIPs) 24, 25
- Meckel's diverticulum 192, 193
- meconium aspiration 86, 87
- mediastinal lymphadenopathy 60–5, 65, 66
 - bronchial carcinoma 93, 93
 - sarcoidosis 78, 78
 - tuberculosis 73, 75
- mediastinal masses 60–7
 - classification 59, 59
 - computed tomography 64, 66–7, 66–7
 - magnetic resonance imaging 66, 66
 - oesophageal compression 148
 - plain chest films 27, 60, 60–5, 64–6
- mediastinum 59–68
 - computed tomography 23, 59–60, 61–2
 - invasion, bronchial carcinoma 93, 94
 - magnetic resonance imaging 59–60, 63
 - plain chest films 19, 20
 - widening due to bleeding 91
- megacolon
 - idiopathic (functional) 189
 - toxic 133, 134, 175–8, 177
- meningiomas 439, 440
- meningitis 443
- meningocele 391
- meningomyelocele 391
- meniscal tears 359, 361
- mercaptoacetyl triglycine (MAG-3) scan 233–7
- mesenteric lymph nodes, calcified 136, 137
- mesothelioma, malignant 55, 82
- meta-iodobenzylguanidine (MIBG) scans 302, 302
- metaphysis 310
 - fractures 405, 407, 408
 - non-accidental 421, 425
 - sclerosis 426
- MIBG (meta-iodobenzylguanidine scans) scans 302, 302
- micturating cystogram 237
- mitral regurgitation 116
- mitral stenosis 107, 116, 118
- mitral valve
 - calcification 103, 116, 118
 - disease 104, 106, 116, 118
- MRA *see* magnetic resonance angiography
- MRI *see* magnetic resonance imaging
- mucocoele, sinus 457, 460
- mucosal pattern, gastrointestinal 142
- multiple sclerosis 447–8, 449–50
 - transverse myelitis 397, 397
- muscle haematoma 317
- musculoskeletal disease
 - magnetic resonance imaging 314, 316–17
 - ultrasound 310–12, 312
 - see also* bone; joints
- mycetoma 75, 76
- mycoplasma pneumonia 72
- myelography 369
- myeloma, multiple 332–3, 333
 - pathological fracture 423
 - skull radiograph 428
 - vertebral collapse 373
- myelosclerosis 340, 341
- myocardial disorders 115–16, 117

- myocardial infarction (MI) 113–14,
113–14
- myocardial perfusion scintigraphy 109,
111, 113–14
- myocarditis 115–16, 117
- nasal carcinoma 457–8
- nasogastric tube 143, 144
- nasopharynx 458–9
carcinoma 458–9, 459
- neck 461–9
masses 461, 463, 463
- necrotizing enterocolitis 135, 135
- needle biopsy
percutaneous 479, 483
transthoracic, lung nodules 44
see also fine needle aspiration
- neonates
neurosonography 436, 437
respiratory distress syndrome 86, 86
- nephrocalcinosis 241, 241
- nephrostomy, percutaneous 486
- nephrotic syndrome 51
- nerve roots, spinal 370
compression 384–5, 386–7
- neuroblastoma 329, 331
- neurocysticercosis 447, 448
- neuroendocrine tumours
pancreas 217, 218
stomach and duodenum 157, 157
see also carcinoid tumours
- neurofibroma
mediastinal 66
spinal cord compression 391, 395
- neurogenic bladder 264–6, 267
- neuropathic arthritis 350
- neuropathic joints 363, 365
- neurosonography 436, 437
- nipples, plain chest films 23
- non-accidental injury
skeletal signs 311, 421–6, 424–5
subdural haematoma 452
- nuclear medicine techniques *see*
radionuclide imaging
- obstetric ultrasound 285–9, 286–8
- obstructive airways disease, plain chest
films 26
- obstructive uropathy *see* urinary tract,
obstruction
- octreoscan 217
- oesophagus 143–51
atresia 151, 153
benign tumours 148
carcinoma 146–8, 147–50
computed tomography 146, 147,
148–9
contrast studies 143–6, 145–6
corkscrew (tertiary
contractions) 143–6, 146
dilatation 148–50
diverticula 150–1, 153
plain films 143, 144
pouch 143, 144
- strictures 146–8
corrosive 148, 151
malignant 146–8, 147
peptic 148, 150
varices *see* varices, gastro-oesophageal
web 150, 152
- oligohydramnios 288
- omental cake 292, 293
- optic nerve glioma 460
- orbits 459–60
blowout fractures 460, 461
masses 459–60, 460
- Osgood–Schlatter disease 358
- osteitis condensans ilii 367, 368
- osteoarthritis 349–50, 353–4, 355
rheumatoid arthritis with 350, 351
vs. rheumatoid arthritis 354
- osteochondritis 358–9, 359
- osteochondritis dissecans 358–9, 360
- osteoid osteoma 315, 323, 325
- osteoma 323, 326
- osteomalacia 336–7, 338
- osteomyelitis 318, 325–8, 326–8
chronic 327, 327
distinction from neoplasm 327–8
old healed 311
vertebral collapse 373, 375
- osteonecrosis *see* avascular necrosis
- osteopenia 334–9
- osteopetrosis 340, 340
- osteophytes 349, 354, 355
spinal 381–2, 385
- osteoporosis 335–6
disuse 335, 336
near arthritic joints 349
rheumatoid arthritis 350
screening 335–6
senile 335
tuberculous arthritis 356, 357
vertebral collapse 373, 375
- osteosarcoma (osteogenic sarcoma) 311,
316, 321
in Paget's disease 340, 343
radiation-induced 346
- ovaries
carcinoma 278–9, 279
disseminated 293, 294
cysts 275–7, 277
masses 275–9
calcified 138, 279, 280
plain abdominal films 139, 139
polycystic 277, 277
tumours 277–9, 278–80
ultrasound 273, 275
- Paget's disease 10, 312, 340, 342–3
pathological fractures 421, 424
spine 375, 377
- Pancoast's tumour 40, 95
- pancreas 213–21
calcification 138, 138, 218
(aden)carcinoma 216–17, 217
computed tomography 213, 214–16,
215
- cystic tumours 217
- endoscopic ultrasound 213–14, 215
- masses 215, 216–17
- neuroendocrine tumours 217, 218
- pseudocysts 218, 220
percutaneous drainage 481, 484
- trauma 221
- ultrasound 216, 216
- pancreatitis
acute 217–18, 219
chronic 218–21, 220
- pannus 350, 356
- papilla of Vater, sphincterotomy 486,
487
- para-aortic lymph nodes
enlarged 297–9, 299
percutaneous needle biopsy 483
- paralytic ileus 132, 133, 133, 173–4
- paranasal sinuses *see* sinuses, paranasal
- parasitic diseases
brain 447, 448
lungs 76–7
small bowel 170, 170
see also hydatid disease
- parathyroid gland 465–9
adenomas 465–9, 467–9
- parotid gland
pleomorphic adenoma 461, 462
sialography 461, 462
- pars interarticularis defects 385, 387
- patella
dislocation 416
fractures 416
- patella tendon, ruptured 403
- PA (posteroanterior) view 2
- pectus excavatum 101–3, 104
- pelvic/iceal system, renal *see* renal
collecting system
- pelvic inflammatory disease 282, 284
- pelvis
abscesses 132, 284, 294, 295–6, 296
female, imaging 273–4, 274–6
fractures 399, 400, 401, 414
masses 139, 139, 274–5
phleboliths 136, 137
- pelviureteric junction (PUJ), congenital
intrinsic obstruction 245, 245,
246
- peptic ulcer 155, 155–6
perforated 132
- percutaneous transhepatic cholangiogram
(PTC) 209
- perianal abscess 189
- perianal fistulae 189
Crohn's disease 166, 169
- pericardial calcification 103
- pericardial effusion 103, 105, 119, 119–21
- perinephric abscesses 255, 255–6
- periosteal reactions 309, 311, 318, 318
- bone metastases 329, 331
multiple 333–4, 334
non-accidental injury 311, 425, 426
stress fractures 420, 421
- peripheral vascular disease 475–8, 476

- peritoneal cavity 291–6
 abscesses 132, 293–6, 295–6
 gas in 132–6, 134–5
 tumours 291–3, 293–4, 294
 peritonitis, localized 133
 Perthe's disease 358, 359
 PET *see* positron emission tomography
 phaeochromocytomas 301–2, 302
 pharyngeal pouch 150–1, 153
 phleboliths, pelvic vein 136, 137
 Pick's disease 450, 451
 picture archiving and communication systems 17
 pituitary tumours 440, 442
 placental imaging 287, 287
 plain radiography *see* radiography, conventional
 pleura 49–59
 calcification 56–7, 57
 edge, in pneumothorax 46, 57, 58
 metastases 50–1, 56, 95
 plaques 56, 82, 83
 thickening (fibrosis) 52, 56, 82
 tumours 55, 56
 pleural effusions 49–52, 50–2
 loculated 49–50, 53–5
 malignant 50–1, 93
 pulmonary collapse and 34, 40
 small 27
 tuberculosis 50, 73
 pleurisy, dry 27
 pleuropulmonary scars 46
 Plummer–Vinson syndrome 150
 pneumatosis coli 132, 183, 183
 pneumocephalus 455, 455
 pneumoconiosis 82
Pneumocystis carinii pneumonia 27, 78, 78
 pneumomediastinum 68, 69
 pneumonia
 bacterial 72, 72
 fungal 76–7, 77
 immunocompromised host 77–8, 78
 mycoplasma 72
 normal plain chest films 27
 pleural effusions 50
 usual interstitial (UIP) *see* usual interstitial pneumonia
 viral 72, 73
 pneumonitis, radiation 81, 81
 pneumoperitoneum 132–6, 134–5, 190
 pneumothorax 49, 57–8, 57–9
 chest trauma 90
 pleural edge 46, 57, 58
 pulmonary collapse 34, 58, 58
 tension 58, 58
 polyarteritis nodosa 260
 polycystic kidney disease 225, 262–3, 264
 polycystic ovaries 277, 277
 polyhydramnios 287
 popcorn calcification, pulmonary nodule 40, 42
 popliteal artery occlusion 472
 portable x-ray machines 2
 portal hypertension 205–6, 207
 transjugular intrahepatic portosystemic shunt 206, 485, 485
 portal vein 474
 positron emission tomography (PET) 11, 11–12, 12
 cardiac disease 112
 female genital tract 274, 278
 solitary pulmonary nodule 44, 45
 thoracic disease 24, 27
see also fluorodeoxyglucose positron emission tomography (FDG-PET)
 posterior longitudinal ligament 375, 379
 posterior urethral valves 268–9, 270
 pregnancy
 ectopic 288–9, 288–9
 large for dates 287
 small for dates 288
 ultrasound evaluation 285–7, 286–7
 progressive multifocal leucoencephalopathy 447
 proptosis 460
 prostate 267–9
 calcification 268, 270
 cancer 267–8, 268–70
 bone metastases 329, 331–2, 340
 enlargement 267–8
 pseudogout 353
 pseudomyxoma peritonei 291
 psoas abscess 307, 307
 psoriatic arthritis 349, 352, 352
 pulmonary angiography, computed tomography 88, 89, 473
 pulmonary arterial hypertension 69, 106, 106
 pulmonary artery, main 103–6
 enlarged 69, 103–6, 105–6
 pulmonary blood flow, increased 103–6
 pulmonary collapse (atelectasis) 31–40
 bronchial carcinoma 91, 94
 bronchial obstruction (lobar) 31–4, 35–9
 linear (discoid) 34–40, 46, 46
 pleural effusion 34, 40
 pneumothorax 34, 58, 58
 whole lung 34, 39
 pulmonary consolidation 30, 30–1
 bacterial pneumonia 72, 72
 cavitation 31, 33, 34
 chest trauma 90, 90
 lobar 30, 32
 patchy 30–1, 32
 tuberculosis 73–5, 74
 pulmonary contusion 90, 90
 pulmonary embolism 27, 87–8, 89
 inferior vena cava filters 479
 pulmonary fibrosis
 asbestos-related 82
 diagnosis of cause 79–81
 diffuse interstitial 27, 49, 79–81
 idiopathic *see* usual interstitial pneumonia
 postirradiation 81, 81
 progressive massive 82, 82
 sarcoidosis 79, 79
 pulmonary infarction 51, 87–8
 pulmonary metastases 94–5, 97–8
 bronchial carcinoma 94
 multiple opacities 44, 97
 pulmonary nodules (or masses) 40–4
 multiple 44
 solitary 40–4, 41
 assessing growth rate 40
 calcification 40, 42
 cavitation 42–3, 43
 chest wall involvement 40, 43
 follow-up 44, 44
 needle biopsy 44
 role of CT 43–4, 44
 role of PET 44, 45
 shape 42, 43
 size 43
 pulmonary oedema
 alveolar 107, 107
 cardiogenic 107, 107
 interstitial 107, 107
 non-cardiogenic 87
 pulmonary opacities 21–3
 air-space opacification 30, 30–1
 line or band-like 44–6, 46–7
 multiple ring 48, 50
 nodular 46, 47, 49
 reticular 46, 49
 reticulonodular 46, 48
 spherical 40–4, 41–3
 widespread small 46–8, 47–9
 pulmonary plethora 105, 106
 pulmonary translucencies (increased transradiancy) 21–3, 48–9, 50
 pulmonary valve stenosis 105
 pulmonary vasculature 103–7, 105
 pulmonary venous hypertension 106, 106–7
 pyelography, retrograde and antegrade 237
 pyelonephritis
 acute 252–5
 chronic 230, 257, 257–8, 260, 260
 pyloric stenosis 158, 159
 pyogenic arthritis 356, 356
 pyonephrosis 256
 pyopneumothorax 58–9
 radial head fractures 405, 406
 radiation hazards 17–18
 radiation-induced bone disease 341–6
 radiation pneumonitis 81, 81
 radiography, conventional 1–2
 bone 309–10, 310–12
 contrast agents 3–4
 joints 347, 348
 radiation hazards 17–18
 skeletal trauma 399, 400, 403–7, 405–7
 skull 427, 428
 spine 370–5, 371
see also abdominal films, plain; chest radiography, plain

- radiology department 1
- radionuclide imaging 8–12, 10
 - adrenal tumours 302, 302
 - bone *see* bone scans, radionuclide
 - cardiac disease 109–12
 - gastrointestinal bleeding 192
 - gastrointestinal tract 142
 - hepatobiliary 209, 211
 - intraperitoneal abscesses 296, 296
 - kidney/urinary tract 233–7, 235–6
 - large intestine 171
 - lungs *see* lung scanning, radionuclide
 - Meckel's diverticulum 192, 193
 - parathyroid glands 465–9, 468
 - small bowel 161
 - thyroid 465, 466
- rectal carcinoma 188, 189
- rectovaginal fistula 179
- red blood cells, radiolabelled 192
- reflex sympathetic dystrophy 335
- reflux nephropathy 257, 257–8
- Reidl's lobe 139
- renal agenesis 263
- renal arteries, MR angiography 232–3, 235
- renal arteriography 237, 237
- renal artery stenosis 260, 260, 475
- renal calices
 - clubbed 230
 - CT urography 232
 - dilatation 227, 230, 241–2, 242
 - intravenous urography 227, 230
 - see also* renal collecting system
- renal cell carcinoma 249, 249–51, 251, 298
 - staging 249–51, 251–2
- renal collecting system (pelvic/iceal system)
 - bifid 224, 225, 261–2, 261–2
 - blood clots 244, 252, 254
 - causes of obstruction 243–5
 - CT urography 231, 232
 - dilatation 241–2, 242
 - filling defects 228, 238, 251–2, 253–4
 - infective strictures 244–5
 - pyelography 237
 - tuberculosis 256, 256
 - urothelial tumours 251–2, 253–4
 - see also* renal calices; renal pelvis
- renal cysts 245
 - computed tomography 249, 250
 - inherited 262–3, 264
 - magnetic resonance imaging 234, 249
 - ultrasound 246, 248
- renal disease
 - hypertension in 259–60
 - intrinsic, renal failure 261, 261
- renal failure 51, 260–1
- renal fascia 297, 297
- renal (parenchymal) masses 225, 245–51
 - computed tomography 249–51, 250–1
 - intravenous urography 247–9, 249
- magnetic resonance imaging 249–51, 250, 252
 - plain abdominal films 139
 - ultrasound 246–7, 248
- renal osteodystrophy 338–9, 339
- renal papillary necrosis 243–4, 258, 258
- renal pelvis
 - 'baggy' 245, 246
 - CT urography 231, 232
 - intravenous urography 227, 228
 - see also* renal collecting system
- renal pseudotumour (column of Bertin) 232, 245
- renal sinus (central echo complex) 223, 224
- renal tumours 245
 - computed tomography 249–51, 250–1
 - magnetic resonance imaging 249–51, 250, 252
 - ultrasound 246–7, 248
- renal vein thrombosis 225
- renogram 233–7, 236
 - diuretic 245, 246
- respiratory distress in newborn 86, 86
- retrograde pyelography 237
- retroperitoneum 296–307
 - abscesses 307
 - anatomy 297, 297
 - fibrosis 245, 247
 - haematoma 307, 307
 - imaging 297, 298
 - lymphadenopathy 297–9, 299
 - masses 139, 296
 - tumours 303–4, 305
- rheumatoid arthritis 350–2, 350–2
 - atlantoaxial subluxation 350–1, 352, 381
 - joints involved 349
 - juvenile 352
 - pulmonary involvement 79, 80, 81
 - role of radiology 351
 - vs. osteoarthritis 354
- ribs
 - detection of abnormalities 71, 71
 - fractures 88–90, 404
 - non-accidental injury 421–6, 424
 - metastases 94, 95–9
 - plain chest films 23
- rickets 336–7, 337
- right atrial enlargement 103
- right subclavian artery, anomalous 148, 152
- rotator cuff disorders 359–62, 363–5
- roundworms 170, 170
- rugger jersey spine 339, 339
- sacroiliitis 389–91, 390
- salivary glands 461
 - calculi 461, 462
 - tumours 461, 462
- Salter–Harris classification 407, 408
- sarcoidosis 78–9, 78–9
 - bone 341, 345
 - lymphadenopathy 70, 70, 78, 78
 - reticulonodular lung opacities 49, 78–9, 79
- scaphoid
 - avascular necrosis 358, 358
 - fractures 401, 402, 404, 407, 407, 411
- schistosomiasis 244–5
- schwannoma, vestibular 439–40, 441
- scintigraphy *see* radionuclide imaging
- scleroderma
 - chest imaging 79, 80, 82
 - oesophageal dilatation 150
 - soft tissue changes 368, 368
- scrotal swelling/pain 269–71, 271
- Seldinger technique 471, 472
- seminoma, testicular 271
- septal lines 44–6, 46, 96
- sequestrum, bone 327, 327
- seronegative arthropathies 389–91
- Shenton's line 415
- shoulder
 - dislocation 409–10
 - disorders 359–62, 363–5
- sialectasis 462
- sialography 461, 462
- sickle cell disease 341
- sigmoidoscopy 171
- silhouette sign 28–30, 29
 - pulmonary consolidation 30, 32
 - pulmonary lobar collapse 34
- silicosis 79
- single photon emission computed tomography (SPECT) 11, 315
- sinuses, paranasal 457–8, 458
 - carcinoma 457–8, 459, 460
 - mucocoele 457, 460
 - mucosal thickening 457, 458
 - opaque 457–8, 458
- sinusitis 457, 458
- skeletal trauma 399–426
 - computed tomography 399, 400–1
 - magnetic resonance imaging 401, 402–3
 - plain radiographs 399, 400, 403–7, 405–7
 - further views 403–7, 407
 - signs of dislocations 403
 - signs of fractures 403, 404, 405–6
 - radionuclide bone scanning 401, 404
 - specific injuries 407–26, 408–26
 - see also* fractures
- skip lesions, Crohn's disease 178, 179
- skull
 - fractures 450–2, 454–5, 455
 - radiographs 427, 428, 450
- slipped femoral epiphysis 363, 366
- small bowel enema 161, 163
- small bowel follow-through (small bowel meal) 161–2, 162

- small intestine 159–70
 bleeding 192
 computed tomography 161, 163, 163
 dilatation 129–31, 131, 163, 164
 diverticulosis 169, 169
 gas pattern 129, 130
 imaging techniques 161
 infarction 133, 167
 ischaemia 167, 167
 lymphoma 168, 168
 malrotation 170
 mucosal abnormality 163, 164
 narrowing 163, 165
 normal appearances 161–3, 162
 obstruction 169–70, 170
 dilatation from 129–31, 131, 133, 164
 tuberculosis 167–8
 ulceration 163–4, 165
 worm infestation 170, 170
 Smith's fracture 412
 soft tissue
 calcification 138, 338
 injuries 401
 sarcoma 317
 scleroderma 368, 368
 swelling
 arthritis 348–9
 fractures 403
 near bone lesions 318–20
 somatostatin receptor radionuclide scan 217
 spina bifida 391
 spinal cord
 compression 391, 393–6
 injuries 375, 379, 380–1, 382–4
 injury without radiological abnormality (SCIWORA) 375
 intrinsic disorders 391–7
 magnetic resonance imaging 370, 372
 tethered 391, 392
 tumours 391, 393, 396
 spinal nerve roots *see* nerve roots, spinal
 spine 369–97
 abnormalities 375–97
 columns 380, 382
 congenital abnormalities 391, 392
 degenerative disease
 (spondylosis) 381–2, 385
 imaging techniques 369–70
 infections 385–9, 388–9
 inflammatory
 spondylarthropathy 389–91
 metastases
 cord compression 391, 393–4
 dense vertebrae 375, 377
 pedicle abnormalities 375, 376
 vertebral collapse 373, 373
 plain chest films 23
 radiographic signs of
 abnormality 370–5
 rugger jersey 339, 339
 trauma 373, 375–81, 379–84
 tumours 391, 393, 395
 spleen 221–2
 calcification 138
 enlargement 207, 221
 infarction 221, 222
 masses 221, 221
 plain abdominal films 139
 trauma 221–2, 222
 spondylolisthesis 385, 387
 spondylolysis 385
 stack of coins appearance 131, 131
 staghorn calculi 239, 239
 stents
 biliary 488, 489
 gastrointestinal 485, 486
 urinary tract 486
 vascular 475, 477
 sternum, depressed (pectus excavatum) 101–3, 104
 Still's disease 352
 stomach 153–9
 carcinoma 156, 156–7
 computed tomography 153–4, 155
 contrast studies 153, 154, 154
 intraluminal defects 157, 158
 lymphoma 158, 158
 outlet obstruction 158, 159
 plain films 129
 polyps 157
 tumours 156–7, 156–7, 158, 158
 ulcers 155, 155–6
Streptococcus pneumoniae pneumonia 72
 stress echocardiography 113
 stress films, skeletal trauma 403, 407
 stress fractures 420, 421–3
 string sign, Crohn's disease 164
 stroke 440–3
 computed tomography 431, 441–3, 443–5
 diffusion-weighted imaging 432–3, 434
 subarachnoid haemorrhage 443, 445, 482
 subchondral cysts 349, 354, 355
 subchondral sclerosis 349, 354, 355
 subclavian artery, anomalous right 148, 152
 subdural haematoma 432, 452, 453
 subperiosteal resorption 338, 339
 subphrenic abscess 50, 132, 135, 294
 subpulmonary effusion 51, 51–2, 70
 Sudeck's atrophy 335
 superior mesenteric artery
 occlusion 167, 167
 superior mesenteric vein 474
 supracondylar fractures 411
 supraspinatus tendon
 calcific tendonitis 362, 365
 tears 362, 363–4
 syndesmophytes 391
 synovial sarcoma (synovioma) 363
 syringomyelia 391
 systemic lupus erythematosus (SLE) 81
 talus neck fracture 418
 target lesions, liver metastases 200, 201
 tarsometatarsal dislocation 420
 technetium-99m (^{99m}Tc) 8, 9–10, 10
 bone scans *see* bone scans, radionuclide
 tendons, imaging 347, 348
 testes 269–71
 acute pain and/or swelling 271
 ectopic/undescended 271, 271
 tethered cord 391, 392
 thalassaemia 341, 344
 thallium-201 myocardial perfusion scan
 see myocardial perfusion
 scintigraphy
 therapeutic ablation 478–9
 therapeutic embolization 478, 479–82
 thoracic diseases 19–99
 diaphragm 70–1
 hilar enlargement 68–70
 imaging techniques 19–26
 mediastinum 59–68
 with normal chest radiograph 26–7
 pleura 49–59
 radiological signs 28–49
 specific 71–99
 see also lung
 thrombolysis 479
 thumb injury 413
 thymoma 65, 67
 thymus 19, 21
 thyroid 463–5, 464–5
 carcinoma 465, 465, 466
 nodules 463, 465
 tissue, intrathoracic 60, 64, 66
 thyroid eye disease 460, 460
 tibial plateau fractures 416–17
 tophi, gouty 353, 353
 toxoplasmosis 447
 tracheobronchial tree, traumatic
 rupture 91
 tractography (diffusion tensor imaging) 433, 436
 transarterial chemoembolization 479
 transitional cell carcinoma (TCC)
 bladder 263–4, 265
 renal collecting system 251–2, 253–4
 urinary tract obstruction 244
 transjugular intrahepatic portosystemic shunt (TIPSS) 206, 477, 485, 485
 transjugular liver biopsy 481–5
 transrectal ultrasound (TRUS) 267, 268
 transtentorial herniation 432, 432
 transvaginal ultrasound 273, 275, 286
 transverse myelitis 397, 397
 trauma
 abdomen 194, 206–7, 207
 bladder and urethra 266, 267
 chest 88–91, 90
 head 450–5, 452–5

- trauma (*cont.*)
- kidney 258–9, 259
 - liver 206–7, 207
 - orbital blowout fractures 460, 461
 - pancreas 221
 - paranasal sinus 457
 - skeletal *see* skeletal trauma
 - spine 373, 375–81, 379–84
 - spleen 221–2, 222
- tricuspid regurgitation 116–19
- tricuspid stenosis 116–19
- triquetral fracture 411
- tuberculoma 75
- tuberculosis
- bone 327
 - hilar lymphadenopathy 70, 73
 - joints 356, 357
 - mediastinal lymphadenopathy 73, 75
 - miliary 47, 49, 73, 74
 - old, calcification 75, 75, 136, 137
 - pleural effusions 50, 73
 - postprimary 73–5, 74
 - primary 73, 74
 - pulmonary 73–6
 - signs of active disease 75–6
 - small intestine 167–8
 - spine 388, 388–9
 - urinary tract 244–5, 256, 256–7
- ulcerative colitis 134, 174–8, 176–7
- ultrasound 5–7, 6, 7
- abdominal trauma (FAST) 194, 206–7
 - acute abdomen 191
 - arterial system 473
 - biliary system 208, 208
 - breast 123–7, 126
 - cardiac *see* echocardiography
 - contrast agents 7
 - Doppler 7–8, 8
 - endoscopic *see* endoscopic ultrasound
 - female genital tract 273, 274–5
 - gastrointestinal 142
 - hysterosalpingography 285
 - intracranial 436, 437
 - joints 347–8
 - liver 195–7, 196–8
 - musculoskeletal disease 310–12, 312
 - neck 461, 463, 463
 - obstetric 285–9, 286–8
 - pancreas 216, 216
 - pleural effusion 52, 52, 54
 - prostatic 267, 268
 - renal masses 246–7, 248
 - retroperitoneum 297
 - small bowel 161
 - thoracic disease 24–6
 - three-dimensional 7
 - thyroid 463, 464
 - urinary tract 223–4, 224–5
 - urinary tract obstruction 242, 242
 - venography 473–4
- uncal herniation 432, 432
- upper gastrointestinal (GI)
- endoscopy 154, 155
- ureterocele 262
- ureters
- calculi 239–41, 240
 - CT urography 231, 232, 233
 - dilatation 242
 - duplication 261, 261–2
 - ectopic 262, 262
 - intravenous urography 227, 228
 - magnetic resonance imaging 235
 - obstruction 230, 242, 243
 - causes 243–5
 - tumours 252, 254
 - stenting 486
 - tumours 244
- urethra 267–9
- strictures 268, 270
 - trauma 266
- urethrography 237
- urinary calculi 237–41, 238–40
- causing obstruction 242, 243, 243
 - radiolucent 237, 238, 252
- urinary tract 223–71
- calcification 226, 226, 256, 256
 - congenital anomalies 261–3, 261–4
 - imaging techniques 223–37
 - infections, acute upper 252–6
 - magnetic resonance imaging 232–3, 234–5
 - obstruction 241–5
 - bladder outflow 268–9, 270
 - causes 227, 243–5
 - computed tomography 243, 244
 - interventional radiology 486
 - intravenous urogram 230, 242, 243
 - renal failure 260–1
 - ultrasound 242, 242
 - radionuclide studies 233–7, 235–6
 - tuberculosis 244–5, 256, 256–7
 - ultrasound 223–4, 224–5
- urography 224–32
- contrast media 225
 - CT *see* computed tomography (CT)
 - urography
 - plain film 226–8
- urothelial tumours 251–2, 253–4
- usual interstitial pneumonia (UIP)
- (cryptogenic fibrosing alveolitis) 48, 49, 79, 80
- uterus
- adenomyosis 281, 282
 - bicornuate 276
 - carcinoma of body of 281–2, 284
 - computed tomography 274, 276
 - fibroids 136–8, 137, 281, 281
 - magnetic resonance imaging 274, 276
 - masses 281–2
 - septate 276
 - small for dates 288
 - ultrasound 273, 274–5
- vagina
- computed tomography 274
 - ultrasound 273, 274
- valvulae conniventes 129–31, 131, 162
- valvular heart disease 103, 116–19, 118
- varices, gastro-oesophageal
- portal hypertension 205–6, 207
 - transjugular intrahepatic portosystemic shunt 206, 485, 485
- vascular calcification 136, 137, 338
- vascular catheterization, for
- infusion 479
- vascular radiology 471–9
- diagnostic 471–4
 - therapeutic 475–9
- venography
- contrast 474
 - ultrasound 473–4
- ventricular dilatation (cardiac) 103, 115
- ventricular enlargement (cerebral) 432, 433
- ventricular hypertrophy (cardiac) 103, 115
- ventricular septal defects 103–6, 105
- vertebrae
- anatomy 369, 370–1
 - collapsed 373–4, 373–5
 - congenital anomalies 391, 392
 - dense 375, 377, 377
 - fractures 373, 375
 - ankylosing spondylitis 390, 391
 - burst 381, 384
 - cervical spine 380–1, 382–3
 - computed tomography 399, 401
 - haemangiomas 375, 378
 - magnetic resonance imaging 369, 372
 - pedicle abnormalities 375, 376
- vertebral column *see* spine
- vesicoureteric reflux
- indirect voiding cystography 233, 235
 - reflux nephropathy 257, 257–8
- vestibular schwannoma 439–40, 441
- videourodynamics 237
- villous adenomas, large intestine 187
- viral encephalitis 443, 446
- viral pneumonia 72, 73
- virtual colonoscopy 171
- voiding cystography, indirect 233, 235
- voiding cystourethrogram 237
- volvulus 133, 134, 183, 184
- Wegener's granulomatosis 82
- white blood cells, radiolabelled 296, 296
- Wilms' tumour 251, 252
- worm infestation, small bowel 170, 170
- wrist injuries 411–13
- X-rays 1–2
- radiation hazards 17–18
 - see also* radiography, conventional
- Zenker's diverticulum 150–1, 153